Billy L. Edge

COASTAL ENGINEERING

PROCEEDINGS OF NINTH CONFERENCE

ON

COASTAL ENGINEERING

LISBON, PORTUGAL

JUNE 1964

PUBLISHED BY
AMERICAN SOCIETY OF CIVIL ENGINEERS
UNITED ENGINEERING CENTER
345 EAST 47TH STREET
NEW YORK, N.Y. 10017

1964

ACKNOWLEDGMENTS

At the suggestion of the late Professor Boris A Bakhmeteff, the Council on Wave Research was formed in 1950 under the Engineering Foundation. At intervals thereafter the Council has cosponsored with various societies, universities, and governmental agencies throughout the world several international conferences on coastal engineering. The purpose of these conferences has been to bring together both engineers and scientists of many disciplines for an exchange of information and thereby delineate fruitful research areas in the general field of coastal engineering. In 1964 the Council on Wave Research transferred its activities to the American Society of Civil Engineers and became the Coastal Engineering Research Council. Thus, the Ninth Conference on Coastal Engineering was cosponsored by this new Council and the Laboratorio Nacional de Engenharia Civil in Lisbon, Portugal.

The following engineers from Portugal served as the Organizing Committee for the conference:

President/Président

CARLOS KRUS ABECASIS	President, Junta de Investigações do Ultramar (Overseas Scientific Research Board—Bureau de Recherches Scientifiques d'Outre-Mer)

Members/Membres

AFONSO J. FERNANDES	Head, General Technical Department, Laboratório Nacional de Engenharia Civil (National Laboratory of Civil Engineering—Laboratoire National du Génie Civil)
ARMANDO DA PALMA CARLOS	Director-General, Direcção-Geral dos Servicos Hidraulicos (Directorate-General of Hydraulic Services—Direction Generale des Services Hydrauliques)
FERNANDO M. ABECASIS	Head, Department of Hydraulics, Laboratório Nacional de Engenharia Civil (National Laboratory of Civil Engineering—Laboratoire National du Génie Civil)
FERNANDO R. DA SILVA AMORIM	Representing Junta Central de Portos (Central Department of Ports—Bureau Central des Ports)
HENRIQUE SCHRECK	Director-General, Direcção-Geral dos Portos do Douro e Leixoes (Douro and Leixoes Port Authority—Direction Générale des Ports du Douro et Leixões)
MANUEL ANTUNES DA MOTA	Representing Instituto Hidrográfico (Hydrographic Institute—Institut Hydrographique)
MANUEL FERNANDES MATIAS	Director, Serviços Marítimos (Maritime Services—Services Maritimes)
MANUEL ROCHA	Director, Laboratório Nacional de Engenharia Civil (National Laboratory of Civil Engineering—Laboratoire National du Génie Civil)
PEDRO ARSÉNIO NUNES	Director-General, Administração Geral do Porto de Lisboa (Port of Lisbon Authority—Administration Générale du Port de Lisbonne)

CONTENTS

PART 1

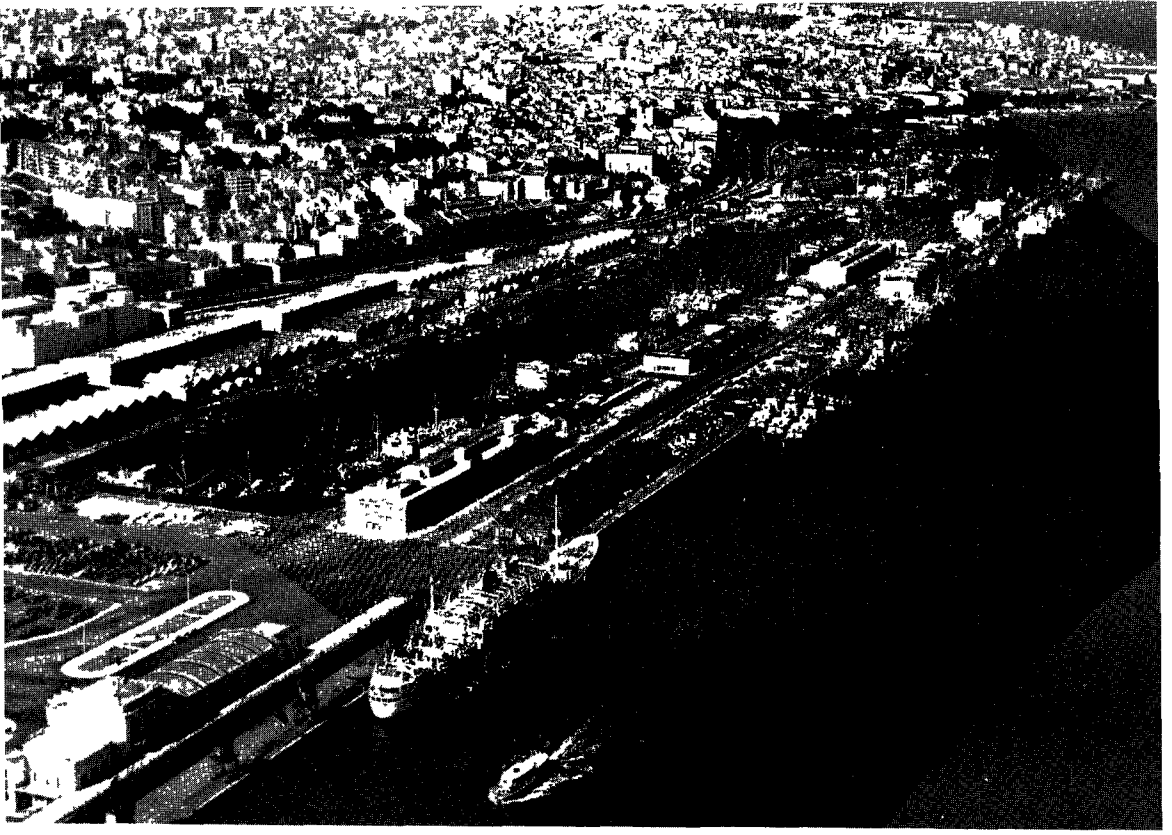

Lisbon Harbor

Part 1
THEORETICAL AND OBSERVED WAVE CHARACTERISTICS

Lisbon Harbor

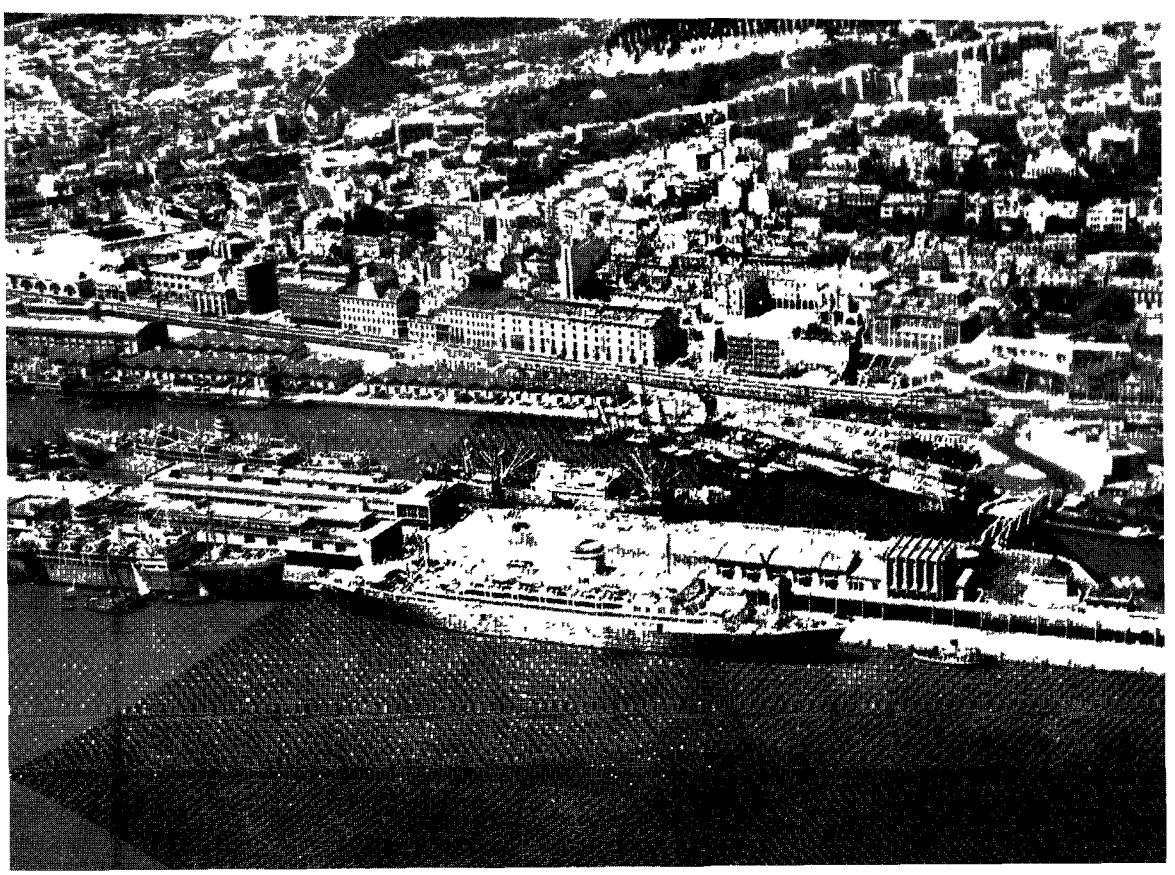

Chapter 1

CNOIDAL WAVES IN SHALLOW WATER

Frank D. Masch
Associate Professor of Civil Engineering
The University of Texas, Austin, Texas

ABSTRACT

The propagation of long waves of finite amplitude in water with depth to wavelength ratios less than about one-tenth and greater than about one-fiftieth can be described by cnoidal wave theory. To date little use has been made of the theory because of the difficulties involved in practical application. This paper presents the theory necessary for predicting the transforming characteristics of long waves based on cnoidal theory. Basically the method involves calculating the power transmission for a wave train in shallow water from cnoidal theory and equating this to the deep water power transmission assuming no reflections or loss of energy as the waves move into shoaling water. The equations for wave power have been programmed for the range of cnoidal waves, and the results are plotted in non-dimensional form.

INTRODUCTION

The cnoidal wave theory developed in 1895 by Korteweg and deVries describes a class of permanent type long waves of finite amplitude. This theory which yields the solitary wave and the sinusoidal wave as its two limiting cases is useful for describing the propagation of periodic waves in shallow water with depths less than about 1/10 the wave length. The theory for cnoidal waves is based on the assumption that the square of the slope of the water surface is small in relation to unity. The properties of the waves are given in terms of the Jacobian elliptic functions and the complete elliptic integrals of the first and second kind.

The cnoidal wave theory has been studied more recently by Benjamin and Lighthill (1945), Patterson (1948), Keulegan and Patterson (1949), Littman (1957), Wehausen and Laitone (1960), Laitone (1960), (1961), (1962), (1963), and Sandover and Taylor (1962). Although this class of waves has received rather extensive theoretical study, little use has been made of the theory. Wiegel (1960) summarized much of the existing work on cnoidal waves and presented the leading results of Korteweg and deVries and Keulegan and Patterson in a more useable form. However, solutions of Wiegel's equations for the wave characteristics are still complex and involve either trial and error type computations or require extensive use of graphs of the cnoidal functions. To further facilitate the application of cnoidal wave theory, Masch and Wiegel (1961) computed several of the cnoidal wave characteristics such as celerity, wave length, and wave period based on the results of Korteweg and deVries, and presented these results in tabular form over a range applicable to water waves.

WAVE TRANSFORMATION

As waves propagate from deep water into shallow water ($d/L < 1/2$), the geometric properties of the waves such as height and length change with decreasing depth. It is customary to assume that as a wave train moves into shallow water, the wave period as defined under deep water conditions remains essentially constant. Generally speaking as the bottom begins to affect the wave motion, the phase velocity is reduced. Since the period for the shoaling waves remains nearly constant, the wave length is reduced and in shallow water the waves can be thought of as stacking up behind one another.

If the waves move perpendicular to the shoreline with their crests parallel to the bottom contours and it is further assumed that energy dissipation and reflections are negligible, then the power transmitted per unit crest width is constant at all points along the path the wave follows. If the waves refract as they move into shallow water, it can be assumed that the power is constant between adjacent orthogonals drawn normal to successive wave crests.

If such deep water wave characteristics as height, period, or length are known, it is possible to compute the rate of energy transmission or power transmission per unit width of the wave crest in deep water. Equating the deep water power transmission to that in shallow water as computed from a suitable finite amplitude wave theory and by making use of the fact that the period remains constant as the waves move into shallow water, the wave characteristics in the shallow water can be determined.

When evaluated for deep water conditions, small amplitude wave theory reduces to the following well known equations:

$$C_o = (gL_o/2\pi)^{1/2} \tag{1}$$

$$L_o = gT^2/2\pi \tag{2}$$

and

$$P_o = \frac{1}{16}\frac{\gamma H_o^2 L_o}{T} \tag{3}$$

where C_o, L_o, H_o, P_o are the deep water wave velocity, length, height and power respectively. Based on trochoidal theory, the deep water wave power given by Mason (1951) is

$$P_o = \frac{\gamma H_o^2}{16}\sqrt{gL_o/2\pi}\left(1 - 4.93\,\frac{H_o^2}{L_o}\right) \tag{4}$$

The zero subscript is the conventional notation for deep water wave conditions.

Using the concepts of Rayleigh (1877) the power or rate of energy transmission in deep water can be equated to that in shallow water to give

$$P_o = (nEC)_o = (nEC) = P \tag{5}$$

where E is the wave energy, and n is the ratio of group velocity to phase velocity and has a value approaching one-half in deep water and unity in shallow water. For waves of small steepness, energy is directly proportional to the square of the wave height. Using eq. (5), the wave height is then given by

$$\frac{H}{H_o} = \left(\frac{1}{2} \cdot \frac{1}{n} \cdot \frac{C_o}{C}\right) \tag{6}$$

where

$$n = \frac{1}{2}\left[1 + \frac{4\pi d/L}{\sinh(4\pi d/L)}\right] \tag{7}$$

If it is assumed that the phase velocity of waves propagating over a sloping bottom is the same as that for waves moving over a horizontal bottom at the corresponding depth, then for waves of small steepness, eq. (6) becomes

$$\frac{H}{H_o} = \left[\frac{2\cosh^2(2\pi d/L)}{4\pi d/L + \sinh(4\pi d/L)}\right]^{1/2} \tag{8}$$

Similarly it can be shown that

$$\frac{L}{L_o} = \tanh\left(2\pi d/L\right) \tag{9}$$

The variability of wave height and length as given by eqs. (8) and (9) is usually related to the relative depth d/L_o, and these equations are shown graphically in Fig. 1. It is seen from eqs. (8) and (9) that shallow water wave characteristics can be predicted theoretically at any depth from a knowledge of specified deep water wave conditions.

Wiegel (1950), Iverson (1952), (1953), Eagleson (1956) and others have performed experiments on shoaling waves and have made comparisons of measured wave characteristics with those computed from small amplitude wave theory. They have found the small amplitude theory satisfactorily predicts the phase velocity of shoaling waves. This is as one would anticipate since the wave velocity changes only slightly when the effect of finite amplitude is taken into account. On the other hand, predicted wave heights were usually found to be smaller than measured heights when compared on the basis of small amplitude theory.

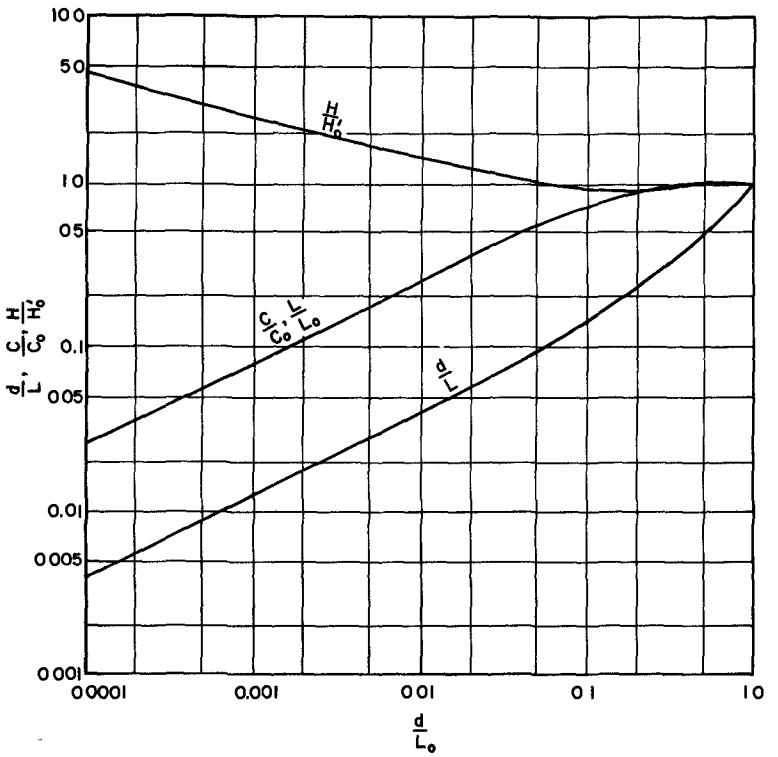

FIG 1. WAVE TRANSFORMATION
(after Wiegel, 1959)

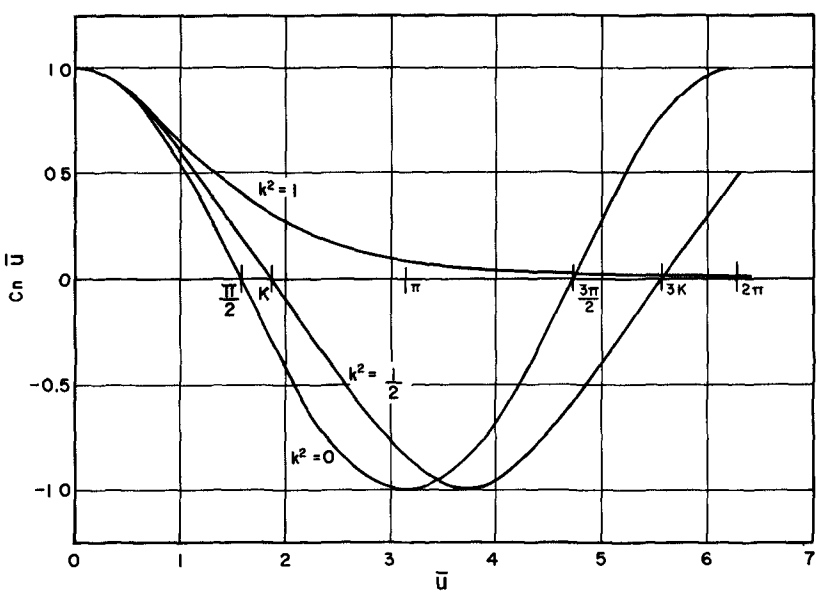

FIG 2 CNOIDAL FUNTION
(after Milne-Thompson)

In order to determine a useable expression for the transformation of waves in shallow water which takes into account the effect of finite amplitude waves, it remains to determine the power transmission in terms of the wave properties from a suitable shallow water wave theory. The following sections of this paper are devoted to this end in which the power transmission for shallow water waves is computed according to the cnoidal theory. Before computing the actual power transmission, a brief resume of cnoidal wave theory is included.

RESUME OF CNOIDAL WAVE THEORY

In shallow water where cnoidal wave theory is applicable, the wave profile, y_s, measured above the bottom is given by

$$y_s = y_t + H\,cn^2(\bar{u}, k) \tag{10}$$

where y_t is the distance from the bottom to the trough, H is the wave height, and $\bar{u}$ and k are the argument and parameter respectively of the elliptic cosine denoted hereafter as cn. The elliptic cosine is a periodic function of $\bar{u}$ whose amplitude is equal to unity. However the period is not a fixed constant as in the case of the circular functions but rather depends on the modulus, k, where k is defined over the range $0 \leq k < 1$. The argument, $\bar{u}$, is defined by the definite integral

$$\bar{u} = \int_0^{\phi} \frac{d\phi}{\sqrt{1 - k^2 \sin^2\phi}} \tag{11}$$

which is an elliptic integral of the first kind, and is a function of k and the upper limit, ϕ. When evaluated over a quarter period, eq. (11) becomes

$$\int_0^{\pi/2} \frac{d\phi}{\sqrt{1 - k^2 \sin^2\phi}} = K\left(\frac{\pi}{2}, k\right) \tag{12}$$

which is the complete elliptic integral of the first kind. This is analogous to defining the quarter period of the circular functions by the complete circular integral.

Thus the period of the cn function is $4K(k)$ and the cn^2 function is $2K(k)$. It can be noted that when $k = 0$, $cn(\bar{u}, 0) = \cos(\bar{u})$ and $K = \frac{\pi}{2}$, so that the elliptic cosine reduces to the circular cosine with a fixed quarter period of $\pi/2$ and a fixed period of 2π. Similarly when $k = 1$, the elliptic cosine degenerates to the sech $(\bar{u})$, the quarter period, $k(1) = \infty$, and the wave profile becomes essentially that of a solitary wave. The cn function is plotted in Fig. 2 for several values of k.

Equation (10) is often written in the form

$$y_s = y_t + H\,cn^2(\ ) \tag{13}$$

where $cn^2(\ )$ denotes $cn^2\left[2K(k)\,(x/L - t/T),\ k\right]$ where $\bar{u}$ has been repla by the more conventional notation of $2K(k)\,(x/L - t/T)$. Values of the cn function have been tabulated over limited ranges of k by Spenceley and Spenceley (1947), Milne-Thompson, (1950), and Schuler and Gabelein (1955 Masch and Wiegel (1961) have extended the range by tabulating values of the sn, cn, and dn functions for $1\text{-}10^{-2} \leq k^2 \leq 1\text{-}10^{-40}$.

The distance from the bottom to the wave trough as used in eq. (13) is defined by the relation

$$\frac{y_t}{d} = \left(\frac{y_c}{d} - \frac{H}{d}\right) = \frac{16}{3}\frac{d^2}{L^2}\left\{K(k)\left[K(k) - E(k)\right]\right\} + 1 - \frac{H}{d} \tag{14}$$

where y_c is the distance from the bottom to the wave crest, d is the still water depth, L is the wave length, and K(k) and E(k) are the complete elliptic integrals of the first and second kind respectively. The wave length is given by the equation

$$L = \sqrt{\frac{16\,d^3}{3\,H}}\ k\,K(k) \tag{15}$$

Based on the work of Korteweg and deVries, the wave period is defined by the equation

$$T\sqrt{g/d} = \sqrt{\frac{16\,d}{3\,H}}\left[\frac{k\,K(k)}{1 + \left(\frac{H}{d}\right)\left(\frac{1}{k^2}\right)\left(\frac{1}{2} - \frac{E(k)}{K(k)}\right)}\right] \tag{16}$$

and the phase or propagation velocity is given by

$$\frac{C}{\sqrt{g\,d}} = \left[1 + \frac{H}{d}\cdot\frac{1}{k^2}\left(\frac{1}{2} - \frac{E(k)}{K(k)}\right)\right] \tag{17}$$

These equations are in the form given by Wiegel (1961) and are the relat used by Masch and Wiegel for computing their Tables of Cnoidal Wave Func tions.

If it is further assumed as an approximation that the pressure dist bution is linear, then the pressure at any point, y, above the bottom is

$$p = \rho g\,(y_s - y) \tag{18}$$

where y_s is defined by eq. (13).

The horizontal and vertical components of water particle velocity based on the equations of Keulegan and Patterson (1948) are

$$\frac{u}{\sqrt{gd}} = \left[\frac{h}{d} - \frac{h^2}{4d^2} + \left(\frac{d}{3} - \frac{y^2}{2d}\right)\frac{\partial^2 h}{\partial x^2}\right] \tag{19}$$

and

$$\frac{v}{\sqrt{gd}} = -y\left[\left(\frac{1}{d} - \frac{h}{2d^2}\right)\frac{\partial h}{\partial x} + \frac{1}{3}\left(d - \frac{y^2}{2d}\right)\frac{\partial^3 h}{\partial x^3}\right] \tag{20}$$

where u and v are the horizontal and vertical components of water particle velocity and h is defined by

$$h = y_s - d = -d + y_t + H\,cn^2(\ ) \tag{21}$$

POWER TRANSMISSION IN CNOIDAL WAVES

In considering power or the rate at which energy is transmitted across a vertical plane in the direction of wave propagation, it is convenient to define power as the product of energy per unit volume of fluid and the volume rate of movement. Using the bottom as a datum for y = o, and defining terms as in Fig. 3, the energy per unit volume with respect to the still water level is

$$E_v = p + \rho g y - \rho g d \tag{22}$$

Substituting the approximate pressure distribution relation of eq. (18) gives

$$E_v = \rho g (y_s - d) \tag{23}$$

The instantaneous rate, P, at which work is done across a section of unit width is

$$P = \int_0^{y_s} \rho g (y_s - d)\, u\, dA \tag{24}$$

The average power over one wave period is

$$\overline{P} = \frac{1}{T}\int_0^T P\,dt = \frac{1}{T}\int_0^T \int_0^{y_s} \rho g (y_s - d)\, u\, dA \tag{25}$$

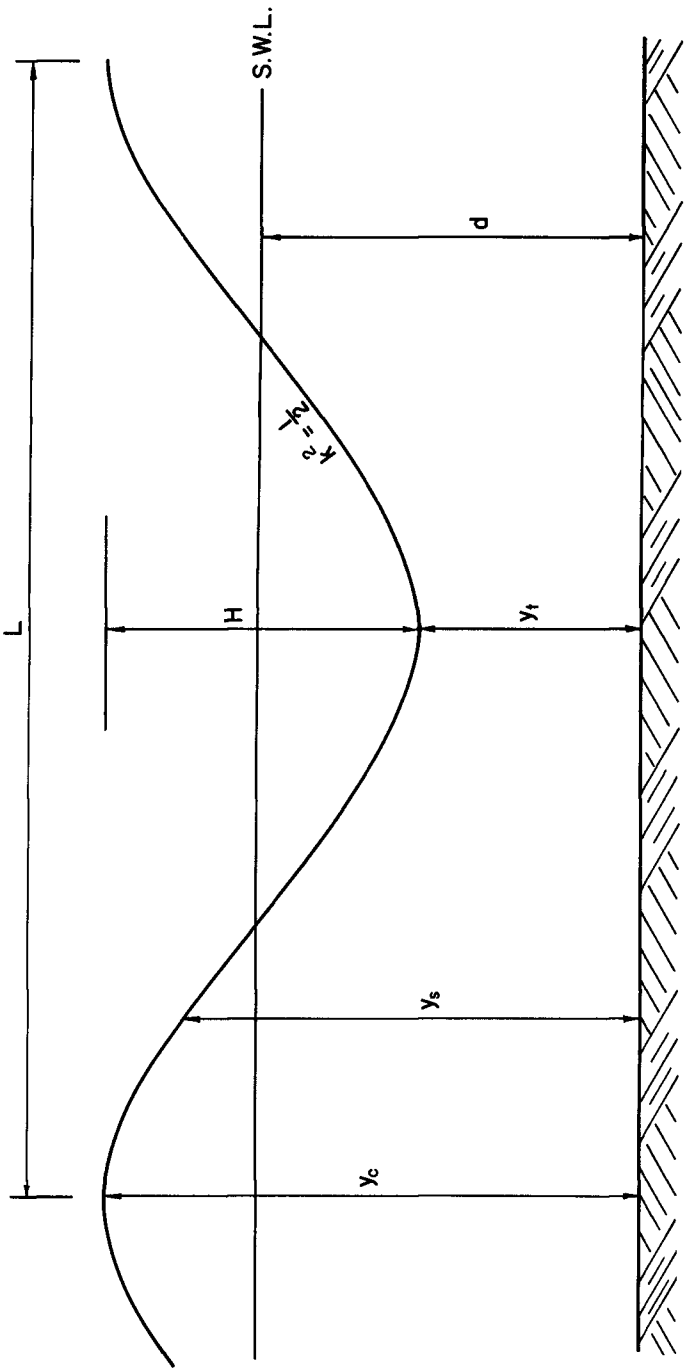

FIG. 3. DEFINITION SKETCH

Substituting the expressions of eqs. (13) and (19) for cnoidal waves into eq. (25) the average power is given by

$$\overline{P} = \frac{1}{T}\int_0^T \int_0^{y_t + H\,cn^2(\,)} \rho g \left[-d + y_t + H\,cn^2(\,)\right] u \, dy \, dt \qquad (26)$$

where

$$u = \sqrt{gd}\left[-\frac{5}{4} + \frac{3}{2}\frac{y_t}{d} - \frac{y_t^2}{4d^2} + \left(\frac{3H}{2d} - \frac{y_t H}{2d^2}\right) cn^2(\,) - \frac{H^2}{4d^2} cn^4(\,) - \frac{8H}{L^2} K^2(k)\left(\frac{d}{3} - \frac{y_t}{2d}\right)\left(k^2 sn^2(\,) cn^2(\,) + cn^2(\,) dn^2(\,) - sn^2(\,) dn^2(\,)\right)\right]$$

Now integrating first with respect to y, substituting the limits, and rearranging, the average power can be written as

$$\frac{\overline{P}}{(\rho g)(gd)^{1/2}} = \frac{1}{T}\int_0^T \left\{\left(\frac{5dy_t}{4} - \frac{11}{4}y_t^2 + \frac{7}{4}\frac{y_t^3}{d} - \frac{y_t^4}{4d^2}\right) + cn^2(\,)\left(\frac{5dH}{4} - \frac{11}{2}Hy_t + \frac{21}{4}\frac{Hy_t^2}{d} - \frac{y_t^3 H}{d^2}\right) + cn^4(\,)\left(-\frac{11H^2}{4} + \frac{21}{4}\frac{H^2 y_t}{d} - \frac{3}{2}\frac{y_t^2 H}{d^2}\right) + cn^6(\,)\left(\frac{7H^3}{4d} - \frac{H^3 y_t}{4d^2}\right) + cn^8(\,)\frac{H^4}{4d^2} + \frac{8HK^2(k)}{L^2}\Omega\left[\left(\frac{d^2 y_t}{3} - \frac{dy_t^2}{3} - \frac{y_t^3}{6} + \frac{y_t^4}{6d}\right) + cn^2(\,)\left(\frac{d^2 H}{3} - \frac{y_t^2 H}{2} - \frac{2dHy_t}{3} + \frac{2Hy_t^3}{3d}\right) + cn^4(\,)\left(-\frac{dH^2}{3} + \frac{y_t^2 H^2}{d} - \frac{y_t H^2}{2}\right) + cn^6(\,)\left(\frac{2y_t H^3}{3d} - \frac{H^3}{6}\right) + cn^8(\,)\left(\frac{H^4}{6d}\right)\right]\right\} \qquad (2$$

where $\Omega = -k^2\, sn^2(\,)\, cn^2(\,) + cn^2(\,)\, dn^2(\,) - sn^2(\,)\, dn^2(\,) \neq \Omega(y)$.

Before performing the integration of the various even powers of the cn( ) function with respect to time, the elliptic cosines were expanded in terms of the elliptic integrals to determine the value of the integrals, and to prove that the elliptic integrals become complete elliptic integrals when integrated over a cnoidal wave period. Masch (1964) gives the details of these expansions as well as the evaluation of the various integral formulas. When evaluating the integrals with respect to time, it is also important to recognize that the period of the $cn^2( )$ function is equal to 2K(k), i.e., two times the first complete elliptic integrals. Since only tables of K(k) and E(k) are available, it becomes expedient to make use of the symmetry of the cnoidal function, and to write the identity

$$\int_{\bar{u}=0}^{\bar{u}=2K} cn^2(\bar{u}, k)\, d\bar{u} = 2\int_{\bar{u}=0}^{\bar{u}=K} cn^2(\bar{u}, k)\, d\bar{u} \qquad (28)$$

Integrating eq. (27) and after some rearrangement and collecting of terms, the average power transmission of a cnoidal wave over one wave period is

$$\frac{\bar{P}}{(\rho g)\sqrt{gd}} = \frac{1}{T}\left\{\left[A_0 T + \frac{A_2 T}{k^2}\left[\frac{E(k)}{K(k)} + k^2 - 1\right] + \frac{A_4 T}{3k^4}\left[(4k^2-2)\frac{E(k)}{K(k)}\right.\right.\right.$$

$$\left. + 3k^4 - 5k^2 + 2\right] + \frac{A_6 T}{15k^6}\left[(23k^4 - 23k^2 + 8)\frac{E(k)}{K(k)} + 15k^6 - 23k^4\right.$$

$$\left. + 27k^2 - 8\right] + \frac{A_8 T}{105k^8}\left[(176k^6 - 264k^4 + 184k^2 - 48)\frac{E(k)}{K(k)} + 105k^8\right.$$

$$\left. - 298k^6 + 353k^4 - 208k^2 + 48\right] + 8H/L^2 (K(k))^2 \left\{\frac{B_0 T}{k^2}\left[(4k^2\right.\right.$$

$$\left. -2)\frac{E(k)}{K(k)} + 3k^4 - 5k^2 + 2\right] + \frac{2B_0 T(1-2k^2)}{k^2}\left[\frac{E(k)}{K(k)} + k^2 - 1\right]$$

$$+ B_0 T(k^2-1) + \frac{2B_2 T}{3k^4}\left[(4k^2-2)\frac{E(k)}{K(k)} + 3k^4 + 27k^2 - 8\right] + \frac{B_2 T}{k^2}(k^2-1)$$

$$\left[\frac{E(k)}{K(k)} + k^2 - 1\right] + \frac{B_2 T}{5k^4}\left[(23k^4 - 23k^2 + 8)\frac{E(k)}{K(k)} + 15k^6 - 34k^4\right.$$

$$\left. + 27k^2 - 8\right] + \frac{B_4 T}{3k^6}\left[(176k^6 - 264k^4 + 184k^2 - 48)\frac{E(k)}{K(k)} + 105k^8\right.$$

$$\left. - 298k^6 + 353k^4 - 208k^2 + 48\right] + \frac{2B_4 T}{15k^6}(1-2k^2)\left[(23k^4 - 23k^2\right.$$

$$\left. + 8)\frac{E(k)}{K(k)} + 15k^6 - 34k^4 + 27k^2 - 8\right] + \frac{B_4 T}{3k^4}(k^2-1)\left[(4k^2-2)\frac{E(k)}{K(k)}\right.$$

$$\left. + 3k^4 - 5k^2 + 2\right] + \frac{B_6 T}{315k^8}\left[(1689k^8 - 3378k^6 + 3537k^4 - 1848k^2\right.$$

$$+384)\frac{E(k)}{K(k)}+945k^{10}-3207k^8+5043k^6-4437k^4+2040k^2$$
$$-384\Big]+\frac{2B_6T(1-2k^2)}{105k^8}\Big[(176k^6-264k^4+184k^2-48)\frac{E(k)}{K(k)}$$
$$+105k^8-298k^6+353k^4-208k^2+48\Big]+\frac{B_6T(k^2-1)}{15k^6}\Big[(23k^4$$
$$-23k^2+8)\frac{E(k)}{K(k)}+15k^6-34k^4+27k^2-8\Big]+\frac{B_8T}{3465k^{10}}\Big[(19524k^{10}$$
$$-48810k^8+68232k^6-53538k^4+22272k^2-3840)\frac{E(k)}{K(k)}$$
$$+10395k^{12}-40947k^{10}+80199k^8-93729k^6+64434k^4-24192k^2$$
$$+3840\Big]+\frac{2B_8T(1-2k^2)}{945k^{10}}\Big[(1689k^8-3378k^6+3537k^4-1848k^2$$
$$-3840)\frac{E(k)}{K(k)}+945k^{10}-3207k^8+5043k^6-4437k^4+2040k^2$$
$$-384\Big]+\frac{B_8T(k^2-1)}{105k^8}\Big[(176k^6-264k^4+184k^2-48)\frac{E(k)}{K(k)}+105k^8$$
$$-298k^6+353k^4-208k^2+48\Big]\Big\}\Big\} \tag{29}$$

where

$$A_0=\left(\frac{5dy_t}{4}-\frac{11y_t^2}{4}+\frac{7y_t^3}{4d}-\frac{y_t^4}{4d^2}\right)$$

$$A_2=\left(\frac{5dH}{4}-\frac{11Hy_t}{2}+\frac{21Hy_t^2}{4d}-\frac{y_t^3H}{d^2}\right)$$

$$A_4=\left(-\frac{11H^2}{4}+\frac{21H^2y_t}{4d}-\frac{3y_t^2H^2}{2d^2}\right)$$

$$A_6=\left(\frac{7H^3}{4d}-\frac{H^3y_t}{4d^2}\right)$$

$$A_8=\left(\frac{H^4}{4d^2}\right)$$

$$B_0=\left(\frac{d^2y_t}{3}-\frac{dy_t^2}{3}-\frac{y_t^3}{6}+\frac{y_t^4}{6d}\right)$$

$$B_2 = \left(\frac{d^2H}{3} - \frac{Y_t^2 H}{2} - \frac{2dHY_t}{3} + \frac{2HY_t^3}{3d}\right.$$

$$B_4 = \left(-\frac{dH}{3} + \frac{Y_t^2 H^2}{d} - \frac{Y_t H^2}{2}\right)$$

$$B_6 = \left(\frac{2Y_t H^3}{3d} - \frac{H^3}{6}\right)$$

$$B_8 = \left(\frac{H^4}{6d}\right)$$

For any given value of the modulus, k, the groups of terms which resulted from the integrations of the cn( ) functions and involve k, K(k), and E(k) can be evaluated. These terms are dimensionless and will be denoted by $\bar{c}_{A2}$, $\bar{c}_{A4}$, ... and $\bar{c}_{B2}$, $\bar{c}_{B4}$, ... Equation (29) for the average power can also be put into a more convenient non-dimensional form by dividing through by the square of the still water depth to give

$$\begin{aligned}
\frac{\bar{P}}{(\rho g)\sqrt{gd}\, d^2} = &\left[\frac{5}{4}\left(\frac{Y_t}{d}\right) - \frac{11}{4}\left(\frac{Y_t}{d}\right)^2 + \frac{7}{4}\left(\frac{Y_t}{d}\right)^3 - \frac{1}{4}\left(\frac{Y_t}{d}\right)^4\right] \\
&+\left(\frac{H}{d}\right)\left[\frac{5}{4} - \frac{11}{2}\left(\frac{Y_t}{d}\right) + \frac{21}{4}\left(\frac{Y_t}{d}\right)^2 - \left(\frac{Y_t}{d}\right)^3\right]\bar{c}_{A2} \\
&+\left(\frac{H}{d}\right)^2\left[-\frac{11}{4} + \frac{21}{4}\left(\frac{Y_t}{d}\right) - \frac{3}{2}\left(\frac{Y_t}{d}\right)^2\right]\bar{c}_{A4} \\
&+\left(\frac{H}{d}\right)^3\left[\frac{7}{4} - \frac{1}{4}\left(\frac{Y_t}{d}\right)\right]c_{A6} + \left(\frac{H}{d}\right)^4\left(\frac{1}{4}\right)\bar{c}_{A8} \\
&+\frac{3}{16}\frac{1}{k^2}\left\{\left(\frac{H}{d}\right)^2\left[\frac{8}{3}\left(\frac{Y_t}{d}\right) - \frac{8}{3}\left(\frac{Y_t}{d}\right)^2 - \frac{4}{3}\left(\frac{Y_t}{d}\right)^3 + \frac{4}{3}\left(\frac{Y_t}{d}\right)^4\right]\bar{c}_{B0}\right. \\
&+\left(\frac{H}{d}\right)^3\left[\frac{8}{3} - \frac{16}{3}\left(\frac{Y_t}{d}\right) - 4\left(\frac{Y_t}{d}\right)^2 + \frac{16}{3}\left(\frac{Y_t}{d}\right)^3\right]\bar{c}_{B2} \\
&+\left(\frac{H}{d}\right)^4\left[-\frac{8}{3} - 4\left(\frac{Y_t}{d}\right) + 8\left(\frac{Y_t}{d}\right)^2\right]\bar{c}_{B4} \\
&+\left(\frac{H}{d}\right)^5\left[-\frac{4}{3} + \frac{16}{3}\left(\frac{Y_t}{d}\right)\right]\bar{c}_{B6} \\
&\left.+\left(\frac{H}{d}\right)^6\left[\frac{4}{3}\right]\bar{c}_{B8}\right. \qquad (3.
\end{aligned}$$

Using a functional notation, the average power transmission thus becomes

$$\frac{\overline{P}}{(\rho g)\sqrt{gd}\,d^2} = f_1\left(\frac{H}{d}, \frac{Y_t}{d}, k\right) \tag{31}$$

The number of parameters in eq. (31) may be reduced by substituting eq. (15) into eq. (14) which gives

$$\frac{Y_t}{d} = \left(\frac{H}{d}\right)\frac{1}{k^2K^2(k)}\left[K(k) - E(k) + 1 - \frac{H}{d}\right] \tag{32}$$

Since Y_t/d can be written in terms of H/d and k, eq. (32) can be substituted into eq. (30) giving the dimensionless power relation in terms of two parameters

$$\frac{\overline{P}}{(\rho g)\sqrt{gd}\,d^2} = f_2\left(\frac{H}{d}, k\right) \tag{33}$$

While the power remains constant as the wave propagates into shallow water, the period also remains essentially constant. For cnoidal waves, the period is as given by eq. (16) or again using a functional notation

$$T\sqrt{g/d} = f_3\left(\frac{H}{d}, k\right) \tag{34}$$

Assuming then that the specific wave characteristics, $\overline{P}$ and T, are known or can be calculated in deep water, the left-hand side of eqs. (33) and (34) are known for any shallow water depth, d. This leaves two equations with two unknowns which can be solved simultaneously for k and H/d.

COMPUTATION OF CNOIDAL WAVE POWER

In order to evaluate the functional relationship of eq. (33) for application to shallow water waves, the terms involving k, K(k) and E(k) (i.e., $\overline{c}_{A2}, \ldots$ and $\overline{c}_{B2}, \ldots$) must be evaluated for the range $0.05 \leq k^2 \leq 1\text{-}10^{-40}$, the range of modulus applicable to water waves. Because of the repetitive nature of the somewhat complex expressions involving k, these calculations can best be done by digital computer. Still other repeated computations are necessary. For example, the parameter H/d has a range extending from about 0.01 to 0.78 such that

for each value of H/d, a range of k's may exist. To enable the dimensionless power term to be written in terms of two parameters, use must also be made of eq. (14) for y_t/d, the value of which also depends upon k and H/d.

Equations related to the power transmission of cnoidal waves were computed on a CDC 1604 digital computer. Because it was desirable to check various parts of the calculations, the computer program was divided into two parts. In the first part of the program, those terms involving k, K(k), and E(k) were computed for values of k^2 up to $1\text{-}10^{-40}$. The coefficients evaluated from this program were checked and used as input for the second part of the program which computed the actual power.

The second part of the overall computer program involves the calculation of eqs. (14), (33), and (34) for the range of cnoidal waves. For each value of H/d, the computations have been truncated to include only those values for C^2/gd (as computed from eq. (17)) greater than 0.8200. This is the same range of computations used by Masch and Wiegel (1961). Since the values of C^2/gd have already been computed and given in tabular form, these values were not printed out in the program for power.

CNOIDAL WAVE CHARACTERISTICS

Using the computed values for eqs. (33) and (34), the simultaneous solution for these two equations is given in Fig. 4 with the non-dimensic power transmission term plotted against the ratio, H/d. This graph covers the range of power calculations and utilizes $T\sqrt{g/d}$, which is a function of the modulus of the elliptic integrals, as a parameter. The parametric values of $T\sqrt{g/d}$ have been selected to be representative of the range applicable to cnoidal waves. The solution of eqs. (33) and (34) have als been plotted in Fig. 5 with the non-dimensional power term plotted agains $T\sqrt{g/d}$ for different values of H/d up to the limiting value of 0.78.

The simultaneous solution of eqs. (33) and (34) enables the ratio H/d to be determined from which it is possible to compute the transformin wave height. Assuming that either deep water wave conditions are known or can be predicted so that the period and the deep water power are speci fically known or that the wave power transmission is known at some depth, then for any other shallow water depth, the left hand sides of eqs. (33) and (34) are known, and the wave height at the specified shallow water depth can be determined. These calculations can be carried out with the aid of either Fig. 4 or 5. On the basis of deep water conditions, an initial point may be located for example on Fig. 5. As the wave progress into shallow water, the average power and period are assumed to remain constant, while the depth decreases. For a depth $d_1 < d_o$, the depth used to locate the initial point, the ordinate of Fig. 5 increases defining a new level for the non-dimensional power term. Similarly, for $d_1 < d_o$, the period parameter increases, and defines the horizontal position on the ne power level. From this newly defined point, the value of H_1/d_1 can be re from the graph, and the wave height, H_1 can be obtained from the depth d_1

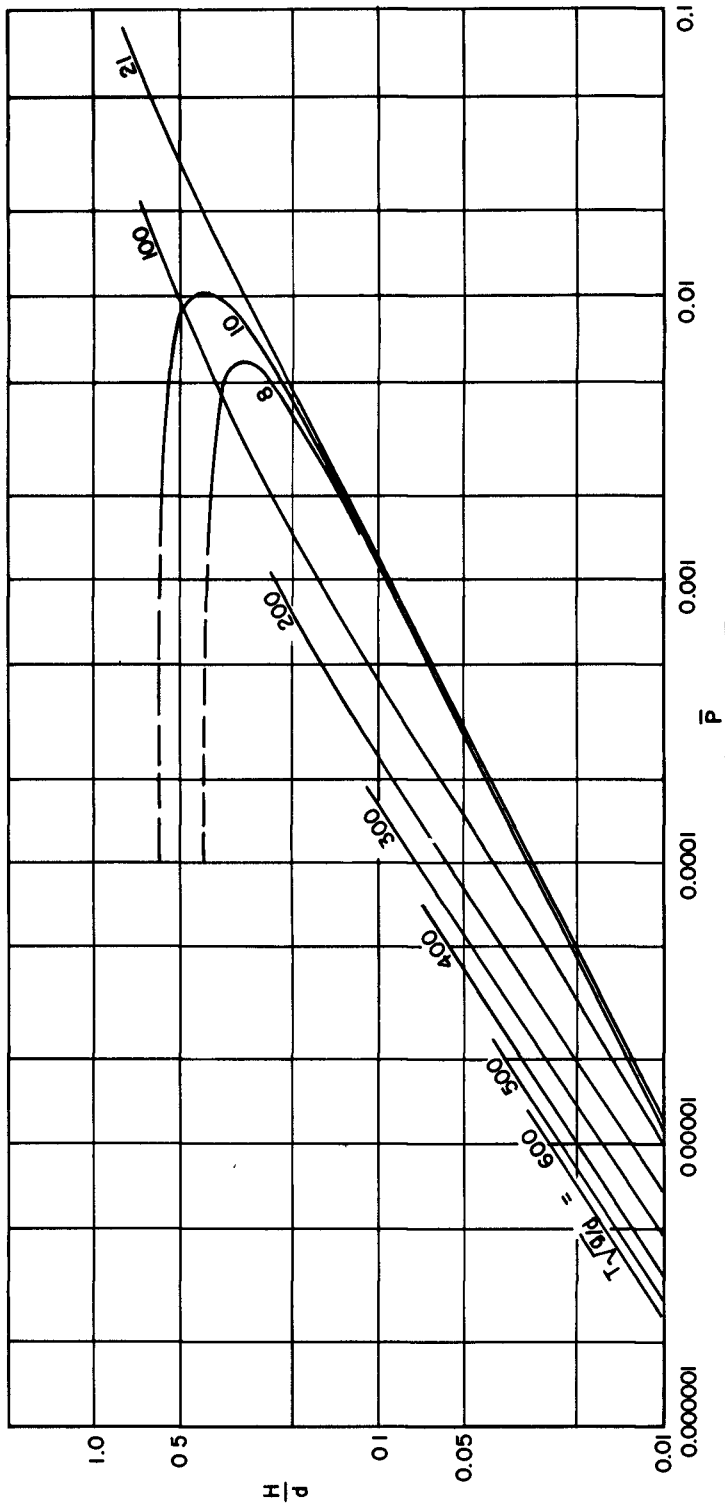

FIG. 4. $\frac{H}{D}$ vs. $\frac{\bar{P}}{(\rho g)(gd)^{1/2}(d)^2}$

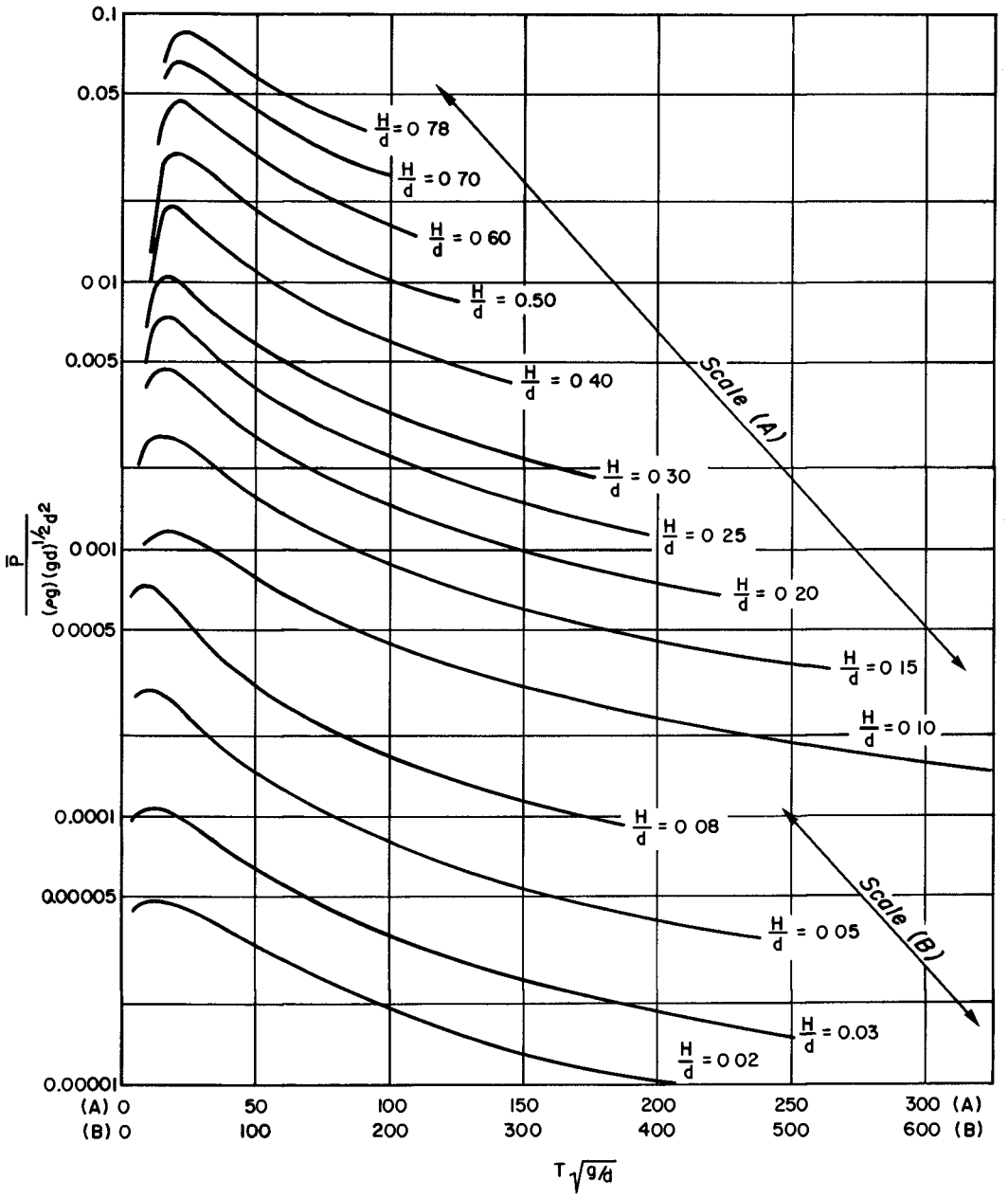

FIG. 5. $\frac{\bar{P}}{(\rho g)(gd)^{1/2}d^2}$ vs $T\sqrt{g/d}$

Figure 6 is a plot showing the relation of y_t/d to $T\sqrt{g/d}$ for several different values of H/d. This plot clearly shows the steepening of the crests and the flattening of the troughs. Since an increase in the value of $T\sqrt{g/d}$ reflects an increase in the modulus, k, then as the depth becomes smaller, the modulus, k, approaches unity and the wave form approaches that of the solitary wave. Thus as $T\sqrt{g/d}$ increases, the distance from the bottom to the wave trough, y_t, approaches the still water depth, d, and the ratio, y_t/d approaches unity.

The transformation of wave length as cnoidal waves move into shallow water can be determined directly from wave steepness considerations. Equation (15) which defines cnoidal wave length can be rearranged to the form

$$\frac{H}{L} = \left[\left(\frac{H}{d}\right)^3 \cdot \frac{3}{16}\right]^{1/2} \frac{1}{k K(k)} \qquad (35)$$

which is an expression for the conventional wave steepness. Using the Tables of Cnoidal Wave Functions by Masch and Wiegel (1961), eq. (35) has been evaluated and the steepness has been plotted against $T\sqrt{g/d}$ for different values of H/d in Fig. 7. As the wave moves into shoaling water, it has been assumed that the period remains constant, so that the quantity $T\sqrt{g/d}$ increases. At the same time, it can be seen from Figs. 4 and 5 that for a fixed period, the wave height also increases as the depth becomes shallower, and the ratio H/d increases up to the limiting value of 0.78. Thus from Fig. 7, the wave steepness is seen to increase as the wave propagates into shallow water. It can also be seen from eq. (35) that for the range of cnoidal wave theory, the wave length decreases as the wave moves into shallower water.

From Fig. 7, it can be noted that cnoidal waves are not very steep. In general the value of wave steepness is less than 0.1, and for the greater part of the range of cnoidal waves, the shallow water steepness is actually less than 0.01. These values of steepness are considerably less than most of those reported in laboratory studies on shoaling waves. However this is not unexpected since the theory is limited to a class of long waves in water with depths less than about one-tenth the wave length.

SUMMARY

The study described in this paper has been devoted to the application of cnoidal wave theory to the transformation of long waves in shoaling water. The method used involved the calculation of the power transmission of cnoidal waves in terms of the geometric wave characteristics and the complete elliptic integrals of the first and second kind. The power and wave period equations were evaluated on a digital computer for the range of cnoidal waves assuming no loss of energy and no reflections as the waves propagate into shallow water. Variations of wave parameters such as height length and steepness were determined from theoretical considerations. It was found that both the wave height and steepness increases as the depth becomes shallower, whereas the wave length decreases with decreasing water

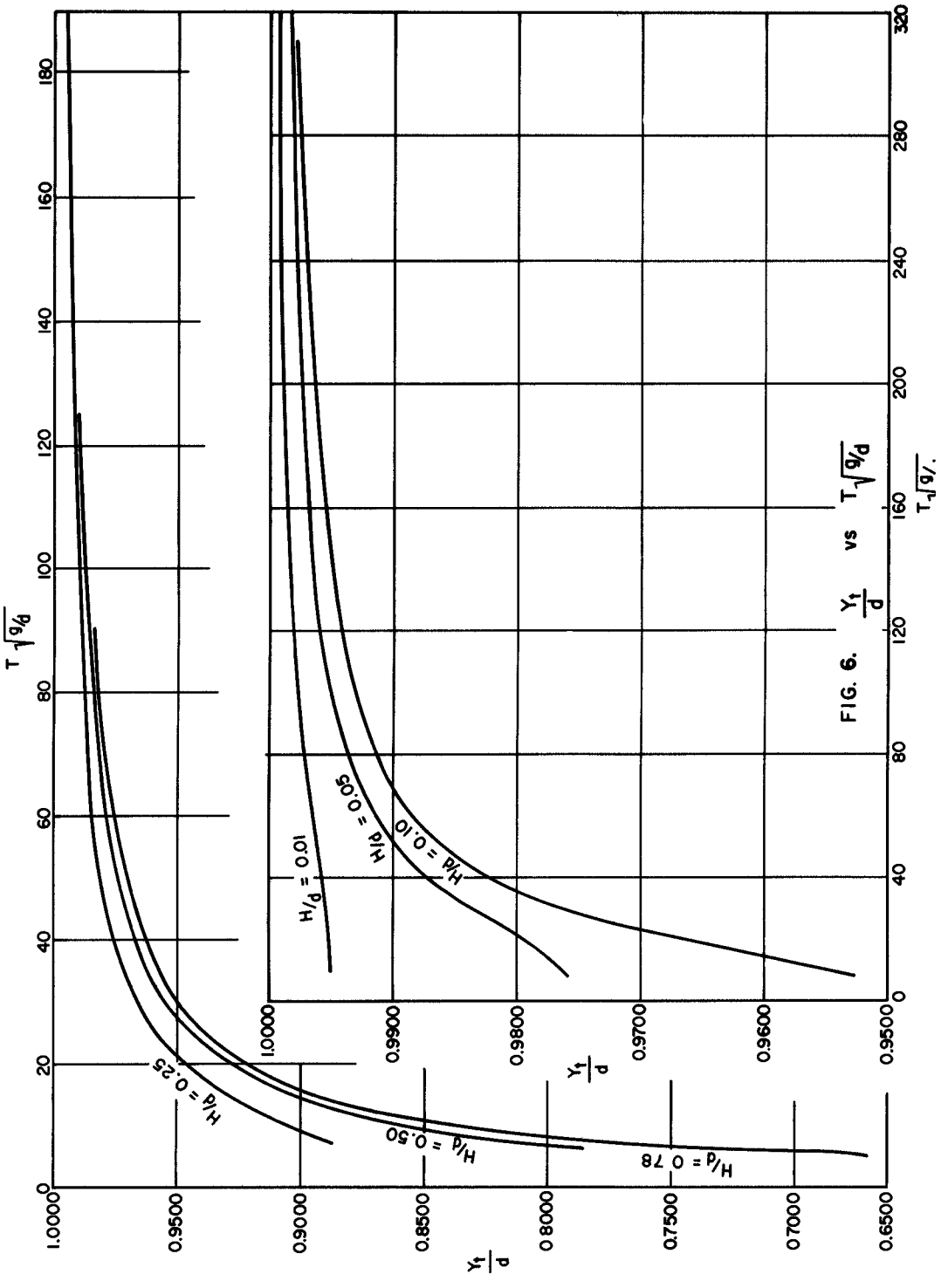

FIG. 6. $\frac{Y_t}{d}$ vs $T\sqrt{\frac{g}{d}}$

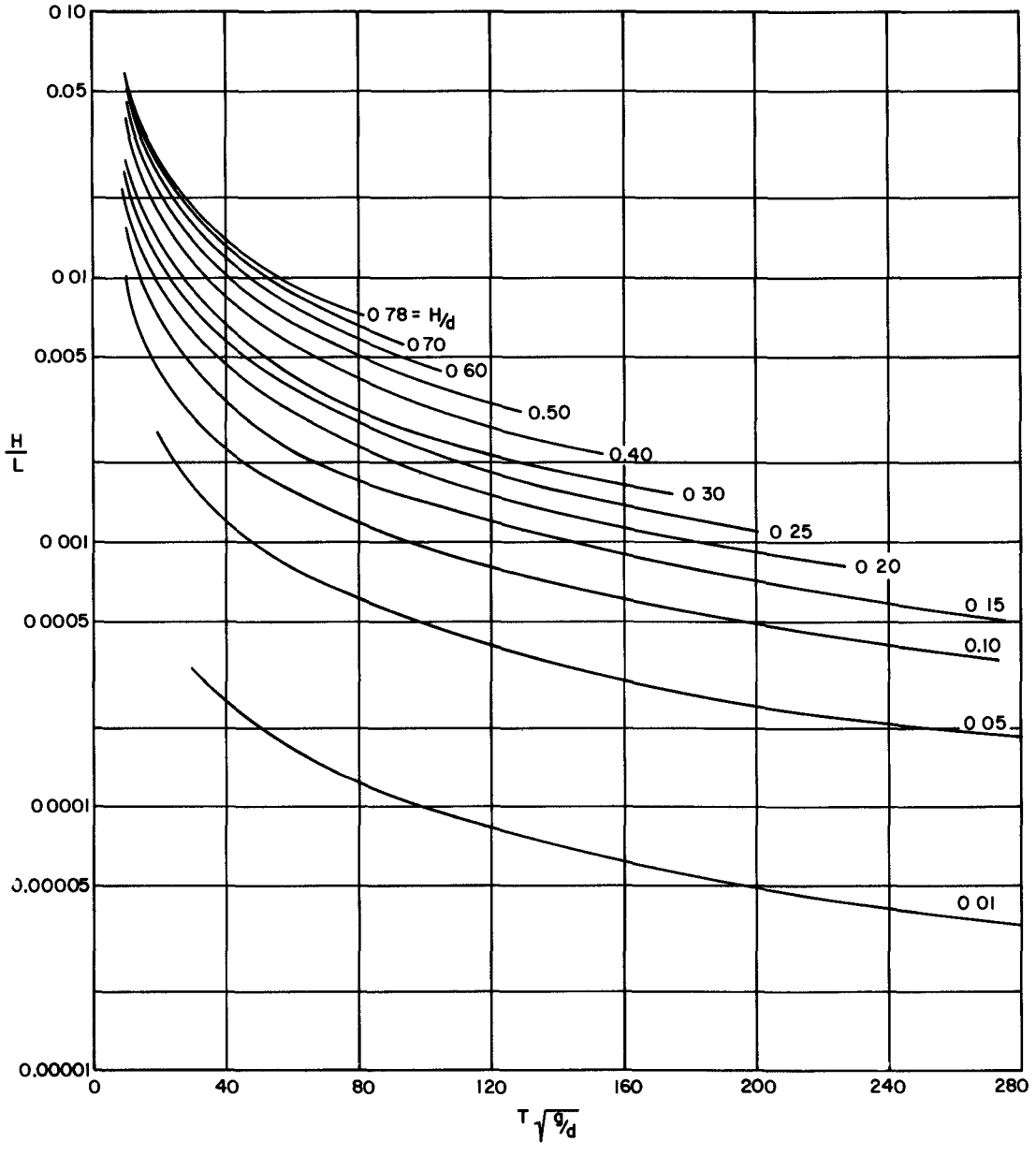

FIG. 7. $\frac{H}{L}$ vs $T\sqrt{\frac{g}{d}}$

depth. These results are compatible with those found by other wave theories although the range of steepnesses for cnoidal waves is much lower than that for other finite amplitude waves.

Generally speaking cnoidal wave characteristics cannot be represented as neatly as can the properties of waves determined by other theories. According to linear wave theory, the phase velocity, wave length, and wave period are independent of the wave height. Even to the second order Stokes theory, the phase velocity, wave length and steepnes are still independent of the wave height. On the other hand, the relati ships for cnoidal wave properties, eqs. (15), (16), (17), and (35) all involve the wave height in addition to the still water depth. Hence sin graphs such as Fig. 1 which show wave height, phase velocity, steepness, etc. related directly to d/L_o cannot be constructed. Since most cnoidal wave equations are three variable equations, families of curves are necessary to represent the results.

It still remains to apply the theoretical computations of this stu to experimental or field data. Although a thorough search of the litera has not been completed, there appears to be only meager data reported fo shoaling waves in water with d/L less than 0.1. Of the data available f d/L less than 0.1, wave steepnesses are relatively large and wave period are short so that the waves are out of the range of cnoidal theory.

ACKNOWLEDGMENT

Work presented in this paper was carried out under contract with the Coastal Engineering Research Center, U. S. Army, Corps of Engineers. The author wishes to express his appreciation to them for their support of the investigation.

REFERENCES

Benjamin, T. B. and Lighthill, M. M., On cnoidal waves and bores, Proc. Roy. Soc. A., 224, 1954 pp. 448-60.

Eagleson, P. S., Properties of shoaling waves by theory and experiment, Trans. Am. Geophys. Union, 37, No. 5, 1956, pp. 565-72.

Eckart, C., The propagation of gravity waves from deep to shallow water, Gravity Waves, Cir. 521, Nat'l Bur. Studs., U. S. Dept. Commerce, Chap. 19, 1951, pp. 165-173.

Iverson, H. W., Laboratory study of breakers, Gravity Waves, Circular 52 Nat'l Bur. Studs., U. S. Dept. Commerce, Chap. 3, 1952.

Iverson, H. W., Waves and breakers in shoaling water, Chap. 1, Proc., Third Conf. on Coastal Engineering, Council on Wave Research, The Engineering Foundation, 1952, pp. 1-12.

Iwasa, Y., Analytical considerations on cnoidal and solitary waves, Mem. Fac. Engr., Kyoto Univ., Japan, 17, No. 4, 1955.

Keulegan, G. H. and Patterson, G. W., Mathematical theory of irrotational translatory waves, Jour. Res., Nat'l. Bur. Studs., U. S. Dept. Commerce, 24, 1940, pp. 47-101.

Korteweg, D. J. and deVries, G., On the change of form of long waves advancing in a rectangular canal and on a new type of long stationary wave, Phil. Mag. 5th Series 39, 1895, pp. 422-43.

Laitone, E. V., The second approximation to cnoidal and solitary waves, Jour. Fluid Mech., Vol. 9, Part 3, pp. 430-444, 1960.

Laitone, E. V., Higher approximations to nonlinear water waves and the heights of cnoidal and solitary waves, Inst. Engr. Res. Tech. Rep., Ser. 89, Iss. 6, Univ. Calif. 1961, 130 pp.

Laitone, E. V., Limiting conditions for cnoidal and Stokes waves, Jour. Geoph. Res., 67, No. 4, 1962, pp. 1555-64.

Laitone, E. V., Higher approximation to nonlinear water waves and the limiting heights of cnoidal, solitary and Stokes' waves., Tech. Memo. No. 133, Beach Erosion Board, U. S. Army Corps of Engineers, 1963, 106 pp.

Littman, W., On the existence of periodic waves near critical speed., Com. Pure & Appl. Math., 10, 1957, pp. 241-269.

Masch, F. D. and Wiegel, R. L., Cnoidal Waves - Tables of Functions, Council on Wave Research, The Engineering Foundation, Richmond, California, 1961, 129 pp.

Masch, F. D., Application of cnoidal wave theory to the transformation of long waves, Hydr. Engr. Lab., Tech. Rep. No. HYD 05-6401, The University of Texas, June 1964, 62 pp.

Mason, M. A., The transformation of waves in shallow water, Proc. First Conf. Coastal Engr., Engr. Found., 1951, Chap. 3, pgs. 22-32.

Milne-Thompson, L. M., Jacobian Elliptic Function Tables, Dover Pub. Inc., New York, 1950, 123 pp.

Rayleigh, Lord, On progressive waves, Proc. London Math. Soc., Vol. 9, Nov. 1877, pp. 21-26.

Sandover, J. A. and Taylor, C., Cnoidal waves and bones, La Houille Blanche, No. 3, 1963, pps. 443-55.

Schuler, M. and Gabelein, H., Eight and Nine Place Tables of Elliptic Functions, Springer, Berlin, 1955.

Spenceley, G. W., and Spenceley, R. M., Smithsonian Elliptic Functions Tables, Smithsonian Institute, Washington, D. C., 1955.

Wehausen, J. V. and Laitone, E. V., Surface Waves: Handbuch der Physik, Vol. 9, Springer-Verlag, Berlin, 1960, pp. 446-778.

Wiegel, R. L., Experimental study of surface waves in shoaling water, Trans. Am. Geoph. Union, Vol. 31, 1950 pp. 377-85.

Wiegel, R. L., A presentation of cnoidal wave theory for practical application, Jour. Fluid Mech., Vol. 7, Part 2, 1960, pp. 273-286

Wiegel, R. L., Theory of periodic waves, Unpublished notes, Univ. Calif 1959.

Chapter 2

PERIODIC GRAVITY WAVES OVER A GENTLE SLOPE AT A THIRD ORDER OF APPROXIMATION

by

B. Le Méhauté and L M. Webb

National Engineering Science Company, Pasadena, California

The concepts of energy flux and group velocity for nonlinear periodic gravity waves are discussed The average energy flux, average energy per wavelength and "group velocity" are calculated for irrotational periodic gravity waves at a third order of approximation. Then the principle of conservation of transmitted energy between wave orthogonals is applied to the same order of approximation for determining the variation of wave height in decreasing depth.

The results are presented as nomographs. It is seen that the "shoaling coefficient" needs to be expressed at least at a third order of approximation to account for experimental results.

Les concepts de flux d'énergie et de vitesse de groupe sont étudiés en vue de leur application a la théorie non lineaire des ondes de gravité periodiques Le flux d'énergie moyen, l'énergie moyenne par longueur dónde et la vitesse de groupe sont calculés au troisième ordre d'approximation La variation d'amplitude d'une onde en profondeur variable est calculée au même ordre d'approximation en applicant le principe de conservation d'energie transmise entre orthogonales.

Les résultats sont presentés sous forme d'abaques, et comparés avec quelques resultats expérimentaux Il est conclus que la méthode présentée est encourageante, et reclamerait d'être travaillée à un ordre d'approximation plusélevée que le troisième ordre.

INTRODUCTION

The present study is a theoretical contribution to the problem of periodic gravity waves traveling in water of decreasing depth. It is remembered that this problem can be treated by two different methods: the analytical method and the energy method.

The analytical method consists of finding a potential function ϕ (x, y, t) for a progressive wave, as a solution of $\nabla^2 \phi = 0$ and which satisfies the usual boundary condition including that of a sloped bottom: $\phi_x - s\,\phi_y = 0$ for $y = -d(x)$ (d is the depth and oy is positive upwards, s is the bottom slope).

The general solution in form of power series can be expected to be of the following form:

$$\phi = H\phi_{10} + SH\phi_{11} + S^2 H\phi_{12} + \cdots + H^2\phi_{20} + SH^2\phi_{21} + \cdots + H^3\phi_{30} + \cdots \quad (1)$$

The terms in $(\phi_{10}, s\phi_{11}, s^2\phi_{12} \cdots)$ are obtained from the linear theory, i.e. by taking: $\phi_{tt} - g\phi_y = 0$ as free-surface condition. (2)
Actually $H\phi_{10}$ is the classical Airy solution valid for a horizontal bottom. It has been shown (Biesel, 1951), that $H = H_1$ and

$$H_1 = \frac{H_0}{\left\{\left[1 + \frac{4\pi d/L}{\sinh 4\pi d/L}\right]\tanh\frac{2\pi d}{L}\right\}^{1/2}} \quad (3)$$

where H_0 is the deep water wave height and L the wave length.

The terms in successive powers of H $(H^2\phi_{20}, H^3\phi_{30} \cdots)$ are obtained from the Stokes Theory, i.e by taking for free-surface condition.

$$\phi_x \eta_x - \phi_y + \eta_t = 0 \quad \text{FOR } y = \eta(x,t) \quad (4)$$

$$g\eta + \phi_t + \tfrac{1}{2}(\phi_x^2 + \phi_y^2) = F(x,t) \text{ ON } y = \eta(x,t) \quad (5)$$

On a very gentle slope such as encountered on the continental shelf and for relatively steep waves, it is easily realized that these non-linear terms are far more important than the terms in S, (linear or nonlinear).

It is recalled that the energy method consists of assuming first that for a short distance, the wave motion on a sloped bottom is the same as on a horizontal bottom. Then when the wave motion has been so

determined, it is assumed that the rate of transmission of energy is constant over a varying depth. The use of the energy method instead of the analytical method permits to take into account a number of phenomena such as bottom friction and variation of distance between wave orthogonals, which are often more important than the flow pattern deformation due to the bottom slope as given by the analytical method and represented by the terms in S. The definition of average flux

$$F_{av} = \frac{\rho}{T} \int_{t}^{t+T} \int_{-d}^{\eta} \phi_x \phi_t \, dt \, dy \tag{6}$$

is independent of the order of approximation for ϕ. Hence, writing F_{av} = constant should give the variation of wave height as function of depth at an order of approximation corresponding to the order of approximation for ϕ.

It is recalled that the application of this principle where ϕ is taken as the Airy solution gives also the relationship (3) above. It is realized that the analytical method merges with the energy method, based on the conservation of transmitted energy flux, when S tends to zero. This confirms the validity of the energy method for small values of S. Then it can be assumed that the principle of conservation of energy flux also applies to a nonlinear wave.

It is recalled also (Stoker, 1957) that the rate of propagation of energy G is given by

$$G = \frac{F_{av}}{E_{av}} \tag{7}$$

where the average energy E_{av} is:

$$E_{av} = \frac{\rho}{L} \int_{0}^{L} \left[\frac{1}{2} \int_{-d}^{\eta} (\phi_x^2 + \phi_y^2) \, dy + g \int_{-d}^{\eta} \eta \, d\eta \right] dx \tag{8}$$

The speed of propagation of energy happens to be also the "group velocity" G' if F_{av} and E_{av} are calculated to the first order of approximation: $G = G'$, where

$$G' = C - L \frac{dC}{dL} \tag{9}$$

This result is consistent with the fact that there is no energy passing through the nodes of a wave train and that the energy travels at the speed of the wave train, the so called group-velocity. This statement does not hold true in the case of nonlinear waves (Biesel 1952). In this case only formula (7) is valid. In fact, it is immaterial whether or not this happens to coincide with the classical group velocity formula (9) since the study

of the modification of wave shoaling involves the use of the flux of energy given by formula (6) only However, in the following, the two values G and G', given by formulas (7) and (9) respectively, have also been calculated for the sake of academic interest and to conform to tradition. It will be seen that the results given by these two procedures are different if the calculations are carried out at a third or higher order of approximation.

ENERGY FLUX, AVERAGE ENERGY AND "GROUP VELOCITY" AT A THIRD ORDER OF APPROXIMATION

In the following, these notations are used:

- H_3 - wave height at a third order of approximation
- H_1 - wave height at a first order of approximation
- H_o - wave height in deep water
- L - wave length at a third order of approximation
- T - wave period
- C_1 - phase velocity at a first order of approximation
- C_3 - phase velocity at a third order of approximation
  $\Big\} = \frac{L}{T}$
- d - water depth
- g - acceleration of gravity
- ϕ - potential function
- t - time
- x - horizontal coordinate
- η - free-surface elevation around the S. W. L.
- y - vertical coordinate from the mud line
- κ - wave number $= 2\pi/L$
- σ - angular frequency $= 2\pi/T$
- ρ - fluid density
- θ - phase angle $= 2\pi\left(\frac{x}{L} - \frac{t}{T}\right)$

Subscripts

- o - refers to deep water
- 1 - refers to linear wave theory
- 3 - refers to third order wave theory

Other notations are defined as they appear in the text.

The Stokes third order wave theory as extracted from the theory at the fifth order developed by Skjelbreia and Hendrickson (1961) is defined by the following set of equations: the potential function ϕ is given by

$$\phi = \frac{L^2}{2\pi}\left[(A_{11}\lambda + A_{13}\lambda^3)\cosh \kappa y \sin\theta + \lambda^2 A_{22}\cosh 2\kappa y \sin 2\theta + \lambda^3 A_{33}\cosh 3\kappa y \sin 3\theta\right] \tag{10}$$

The free-surface elevation η is given by:

$$\eta = \kappa\left(\lambda\cos\theta + \lambda B_{22}\cos 2\theta + \lambda^3 B_{33}\cos 3\theta\right) \tag{11}$$

and the phase velocity C_3 is given by:

$$\left(\frac{L}{T}\right)^2 = C_3^2 = C_1(1 + B\lambda^2), \qquad C_1 = \frac{g}{\kappa}\tanh \kappa d \tag{12}$$

where λ is the real positive root of

$$\lambda^3 B_{33} + \lambda = \frac{\pi H}{L} \tag{13}$$

and with $S_* = \sinh kd$
$C_* = \cosh kd$ (14)

$$\left.\begin{aligned} A_{11} &= \frac{1}{S_*}, \quad A_{13} = -\frac{C_1^2(5C_*^2+1)}{8S_*^5}, \quad A_{22} = \frac{3}{8S_*^4} \\ A_{33} &= \frac{13-4C_*^2}{64S_*^7}, \quad B_{22} = \frac{C_1(2C_*^2+1)}{4S_*^3}, \\ B_{33} &= \frac{3(8C_*^6+1)}{64S_*^6}, \quad B = \frac{8C_*^4-8C_*^2+9}{8S_*^4} \end{aligned}\right\} \tag{15}$$

It is pointed out that most often, C_3^2 given in technical literature and as presented above by formula (13) is wrongly taken at a third order of approximation with $\lambda = \frac{\pi H}{L}$. In fact λ calculated from formula (13) gives a very different value for shallow water due to the fact that the term B_{33} tends to infinity when $d \to 0$. Hence in very shallow water λ should be taken as a third order of approximation as:

$$\lambda = \left[\frac{1}{B_{33}} \frac{\pi H}{L}\right]^{1/3} \tag{16}$$

In the following the full formula (13) is used, and it has been verified that due to that third order term, the correction on the wave height variation by shoaling with respect to the linear theory appears to be in the opposite direction of what it would be if λ were taken as $\frac{\pi H}{L}$. Hence, it has been judged important to emphasize this discrepancy with other papers, making use of the third order wave theory. It is easily seen that, in deep water, equation (14) becomes

$$\frac{3}{8}\lambda_o^3 + \lambda_o = \frac{\pi H_o}{L_o} \tag{17}$$

and equation (12)

$$\left(\frac{L_o}{T}\right)^2 = \frac{g}{k}\left(1+\lambda_o^2\right) \tag{18}$$

in which case $\lambda_o = \frac{\pi H_o}{L_o}$ is a reasonable approximation.

It is recalled that this set of equations gives λ, L and C_3, simultaneously for given values of d, T and H. The corresponding value of $\frac{C_3}{C_1}$ vs. $\frac{d}{L}$, for various values of $\frac{H}{L}$ is presented in Figure 1.

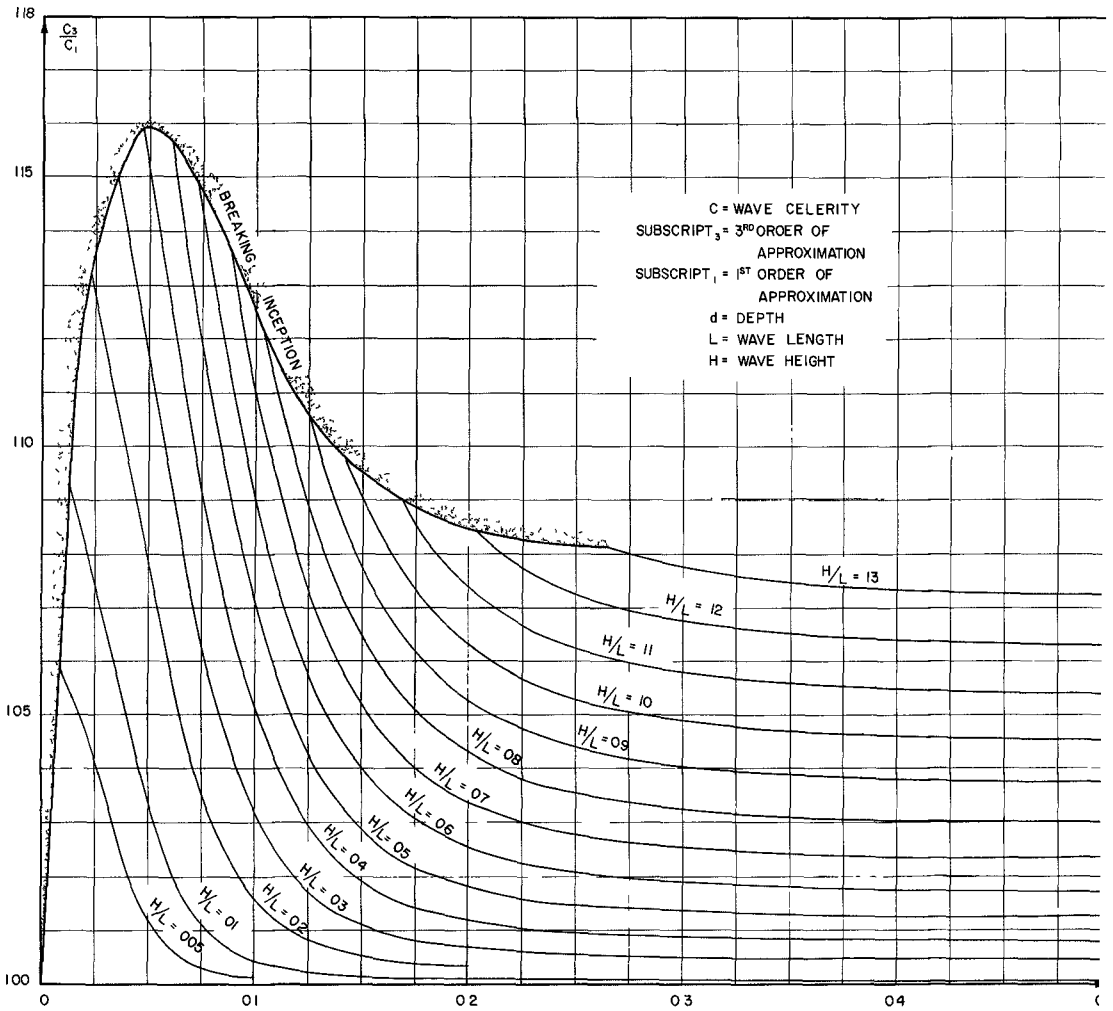
C = WAVE CELERITY
SUBSCRIPT 3 = 3RD ORDER OF APPROXIMATION
SUBSCRIPT 1 = 1ST ORDER OF APPROXIMATION
d = DEPTH
L = WAVE LENGTH
H = WAVE HEIGHT
BREAKING INCEPTION
H/L = 13
H/L = 12
H/L = 11
H/L = 10
H/L = 09
H/L = 08
H/L = 07
H/L = 06
H/L = 05
H/L = 04
H/L = 03
H/L = 02
H/L = 01
H/L = 005
118
115
110
105
100
0
01
02
03
04

FIG 1

Now, by inserting the value of φ given by (10) into (6), (8) and integrating, one obtains after lengthy but straightfoward calculations.

$$F_{av} = \frac{\pi \rho C_3^2 \lambda^2}{8 k^2 T} \cdot \frac{1}{S_*^2} \left\{ 4(S_* C_* + kd) + \lambda^2 \left[\frac{(S_* C_* + kd)}{4 S_*^6} (-20 C_*^6 + 16 C_*^4 + 4 C_*^2 + 9) + \frac{S_* C_*}{2 S_*^4} (16 C_*^4 + 2 C_*^2 + 9) \right] \right\} + O(\lambda^6) + \cdots \quad (19)$$

and

$$E_{av} = \frac{\pi \rho C_3^2 \lambda^2}{L k^2} \frac{C_*}{S_*} \left\{ 1 + \frac{\lambda^2}{32 S_*^6} (-16 C_*^6 + 56 C_*^4 - 49 C_*^2 + 27) \right\} + O(\lambda^6) + \cdots \quad (20)$$

Then the rate of energy propagation $G = \frac{F_{av}}{E_{av}}$ is found to be.

$$G = G_3 = \frac{C_1}{2} \left\{ 1 + \frac{2kd}{\sinh 2kd} + \frac{\lambda^2}{32 \sinh^4 kd} \left[5(8 \cosh^4 kd - 8 \cosh^2 kd + 9) - \frac{6kd}{\sinh 2kd} (8 \cosh^4 kd + 16 \cosh^2 kd - 3) \right] \right\} \quad (21)$$

which is quite different from

$$G = \frac{C_3}{2} \left[1 + 2kd / \sinh 2kd \right]$$

as sometimes is proposed.

If one applies the formula (9)

$$G' = G_3' = \frac{C_1}{2} \left\{ 1 + \frac{2kd}{\sinh 2kd} + \frac{\lambda^2}{8 \sinh^4 kd} \left[-(8 \cosh^4 kd - 8 \cosh^2 kd + 9) - \frac{2kd}{\sinh 2kd} (8 \cosh^4 kd + 28 \cosh^2 kd - 9) \right] \right\} \quad (22)$$

It can easily be seen that only the first terms of (21) and (22) are alike. The value of $\frac{G_3}{C_1}$, $\frac{G_3}{C_3}$ vs $\frac{d}{L}$, for various values of $\frac{H}{L}$ is presented on Figures 2 and 3 respectively. The transformation of these

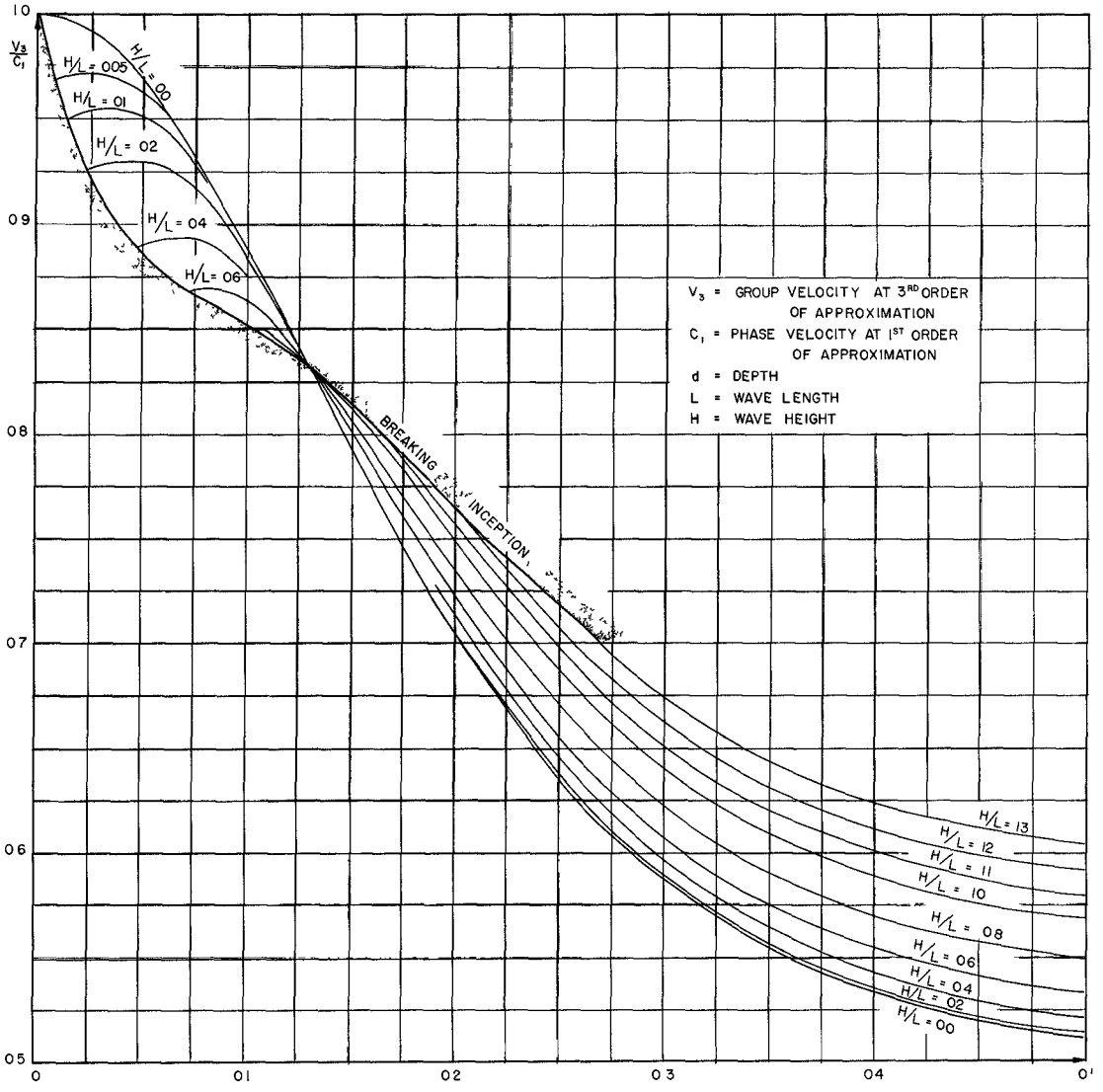
1.0
$\frac{V_3}{C_1}$
0.9
0.8
0.7
0.6
0.5
0
0.1
0.2
0.3
0.4
0.5
H/L = 005
H/L = 00
H/L = 01
H/L = 02
H/L = 04
H/L = 06
BREAKING INCEPTION
V_3 = GROUP VELOCITY AT 3RD ORDER OF APPROXIMATION
C_1 = PHASE VELOCITY AT 1ST ORDER OF APPROXIMATION
d = DEPTH
L = WAVE LENGTH
H = WAVE HEIGHT
H/L = 13
H/L = 12
H/L = 11
H/L = 10
H/L = 08
H/L = 06
H/L = 04
H/L = 02
H/L = 00

FIG 2

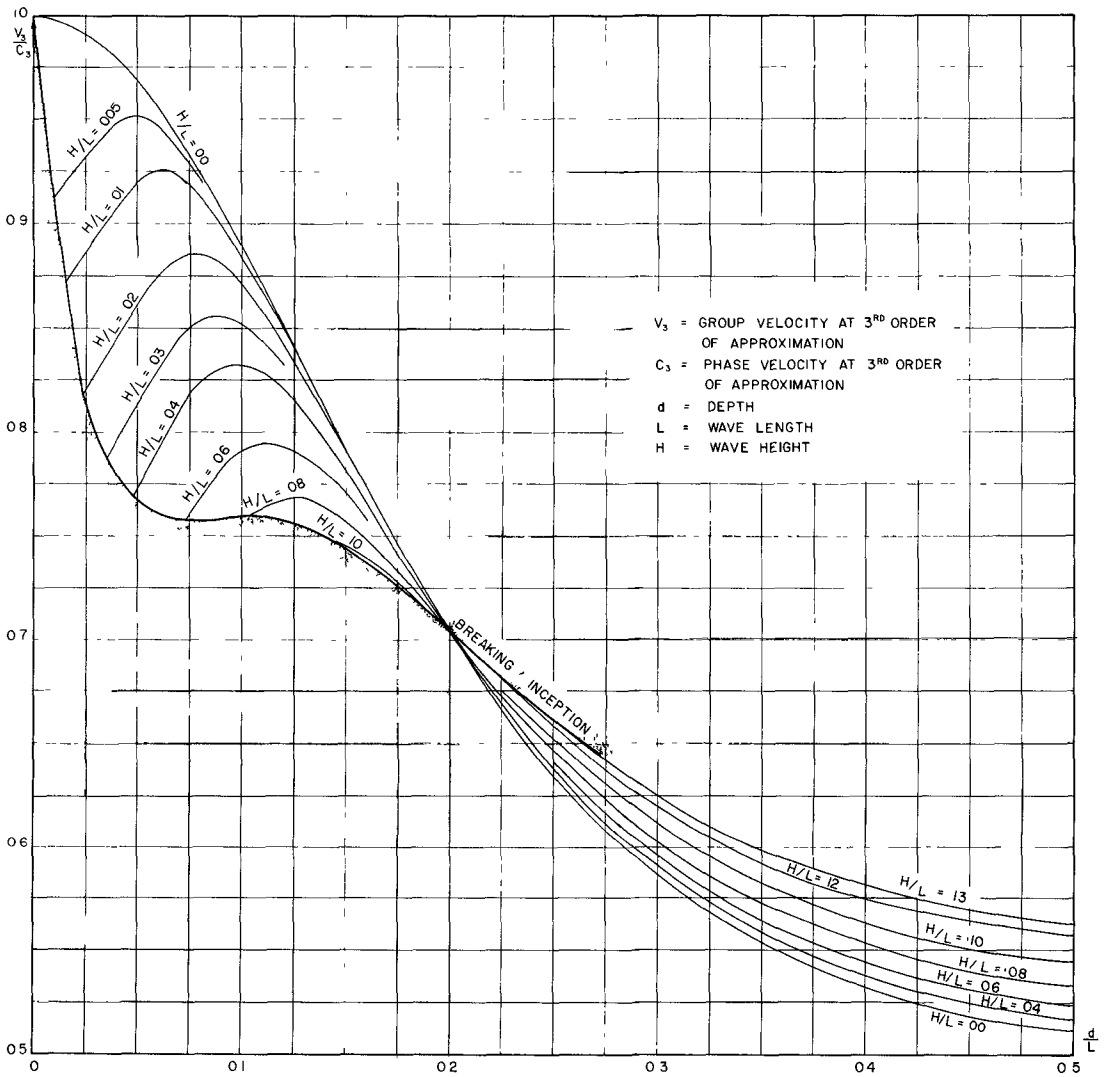
1.0
$\frac{V_3}{C_3}$
0.9
0.8
0.7
0.6
0.5
0
0.1
0.2
0.3
0.4
0.5
$\frac{d}{L}$
H/L = 005
H/L = 00
H/L = 01
H/L = 02
H/L = 03
H/L = 04
H/L = 06
H/L = 08
H/L = 10
BREAKING , INCEPTION
H/L = 12
H/L = 13
H/L = 10
H/L = 08
H/L = 06
H/L = 04
H/L = 00
V_3 = GROUP VELOCITY AT 3RD ORDER OF APPROXIMATION
C_3 = PHASE VELOCITY AT 3RD ORDER OF APPROXIMATION
d = DEPTH
L = WAVE LENGTH
H = WAVE HEIGHT

FIG 3

results as functions of H/T^2 and d/T^2 for practical purposes has not been carried out because the primary purpose of the study is the wave shoaling

It is interesting to note that G for nonlinear waves decreases relatively as $\frac{H}{L}$ increases in shallow water, while it increases with $\frac{H}{L}$ in deep water It can easily be verified that the results of the first order wave theory are found provided λ is taken to be equal to $\pi H/L$ in formulas (18) and (20), and in formulas (20) and (21) . Then

$$F_{av} = \frac{1}{2}\rho g\left(\frac{H}{2}\right)^2 \frac{C_1}{2}\left[1 + \frac{2\kappa d}{\sinh 2\kappa d}\right] \tag{23}$$

$$E_{av} = \frac{1}{2}\rho g\left(\frac{H}{2}\right)^2 \tag{24}$$

and

$$G = G_1 = \frac{C_1}{2}\left[1 + \frac{2\kappa d}{\sinh 2\kappa d}\right] \tag{25}$$

WAVE SHOALING

Now multiplying F_{av} given in (19) by the constant value $K = \frac{32\pi}{\rho T^5}$ and taking the corresponding limit for $\frac{d}{L} \to \infty$ and writing the conservation of energy flux $K F_{av}\big|_{d=d} = K F_{av}\big|_{d\to\infty}$ gives

$$\left(\frac{L}{T^2}\right)^4 \frac{\lambda^2}{5^2_\kappa}\left\{A\left(\lambda, \frac{d}{L}\right)\right\} = \left(\frac{L_o}{T^2}\right)^4 \lambda_o^2\left[4\left(1 + \frac{3}{4}\lambda_o^2\right)\right] \tag{26}$$

Where A is the expression between bracket of formula (19) the subscript o refers to deep water. Equation (26), combined with equations (12), (13), (17) and (18) forms a system of 5 simultaneous equations which permits calculation of L_o , λ_o , L , λ and H , i e. the shoaling coefficient $\frac{H}{H_o}$ as function of $\frac{d}{T^2}$ and $\frac{H_o}{T^2}$ once H_o , T and d are given.

An outline of the method of solution is given now:

Given $\frac{d}{L}$ and $\frac{H}{L}$, λ is calculated from formula (13). Also $\frac{L}{T^2}$ is calculated from formula (12) divided by L, as function of λ , $\frac{d}{L}$ and $\frac{H}{L}$

Consequently, $\frac{d}{T^2}$ and $\frac{H}{T^2}$ are obtained. Then $\frac{32\pi F_{av}}{\rho T^3}$ is calculated from formula (26) at a depth d

By eliminating λ_o between (18) and the following equations

$$F = \left(\frac{L_o}{T^2}\right)^4 \lambda_o^2 \left[4\left(1 + \frac{3}{4}\lambda_o^2\right)\right] \tag{27}$$

and defining X as follows

$$\frac{L_o}{T^2} = \frac{g}{2\pi}(1+X) \tag{28}$$

and

$$B = F\left(g/2\pi\right)^{-4} \tag{29}$$

gives

$$4X + 19X^2 + 36X^3 + 34X^4 + 16X^5 + 3X^6 = B \tag{30}$$

X in the correction due to the nonlinear terms Hence X remains small, as does B Consequently by inverting the polynomial we have

$$X = \frac{1}{4}B - \frac{19}{64}B^2 + \frac{573}{1024}B^3 - \frac{21,159}{16,384}B^4 + \cdots \tag{31}$$

at a very good approximation Because this calculation has been done by computer, the solution (30) has been obtained by successive approximations around $X = \frac{C}{4}$ by the Newton-Raphson method. $\frac{L_o}{T^2}$ is obtained from equation (28), then λ_o from equation (18) and $\frac{H_o}{L_o}$ from equation (17) Finally $\frac{H_o}{T^2}$ and $\frac{H}{H_o}$ are obtained by simple operation. The curve $\frac{H_o}{T^2}$ = constant for various value of $\frac{d}{T^2}$ have been obtained by linear interpolation between the values found for H_o/T^2

Finally the correction $\frac{\Delta H}{H_1} = \frac{H_2 - H_1}{H_1}$ due to the third order of approximation, H_1 being the value which is obtained by the linear theory (formula 3) has also been calculated as function of $\frac{d}{T^2}$ and $\frac{H_o}{T^2}$ for a given value of $\frac{d}{L}$ and $\frac{H}{L}$, by a similar process.

These results are presented on Figure (4) and (5) on which the limit for breaking criteria has been added. The complete set of tables is published in a NESCO Report SN-134.

Wilson (1964) has determined the limit after which the ratio of the fourth order term to the third order is larger than 1/100, which may be considered from an academic new point, the limit of validity of the third order wave theory It has been found that this limit is defined in shallow water by the condition ($kd < \pi/10$)

$$\frac{H}{L_o} < 0.725\left(\frac{kd}{L}\right)^2 \frac{d}{L_o} \tag{32}$$

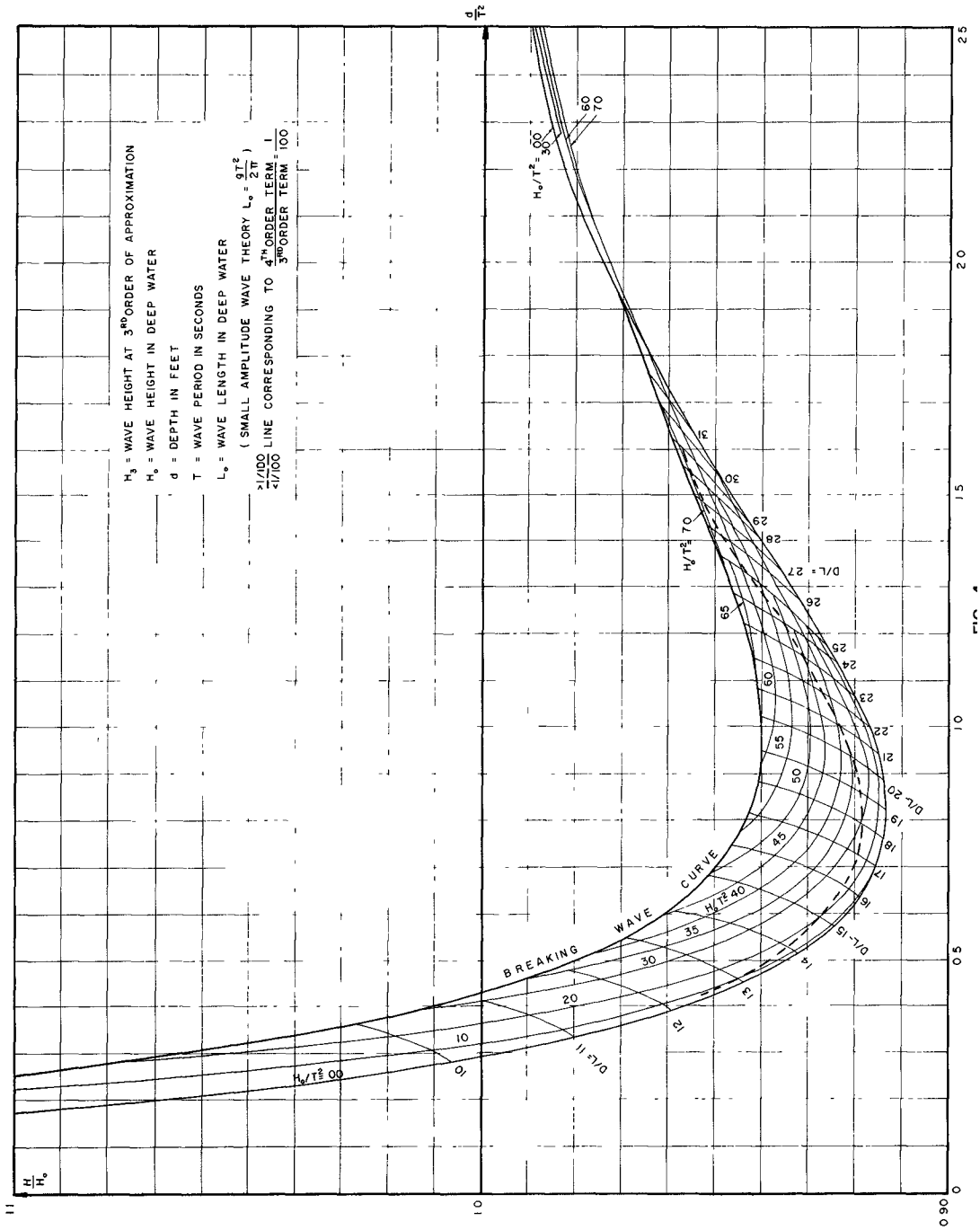
H₀ = WAVE HEIGHT IN DEEP WATER
d = DEPTH IN FEET
T = WAVE PERIOD IN SECONDS
L₀ = WAVE LENGTH IN DEEP WATER
(SMALL AMPLITUDE WAVE THEORY $L_0 = \frac{gT^2}{2\pi}$)
>1/100 LINE CORRESPONDING TO 4TH ORDER TERM = 1/100
<1/100 3RD ORDER TERM = 1/100
BREAKING WAVE CURVE
d/L = 27
d/L = 20
d/L = 15
d/L = 11
d/L = 10
H₀/T² = 70
H₀/T² = 40
H₀/T² = 00
H/H₀
d/T²

FIG. 4

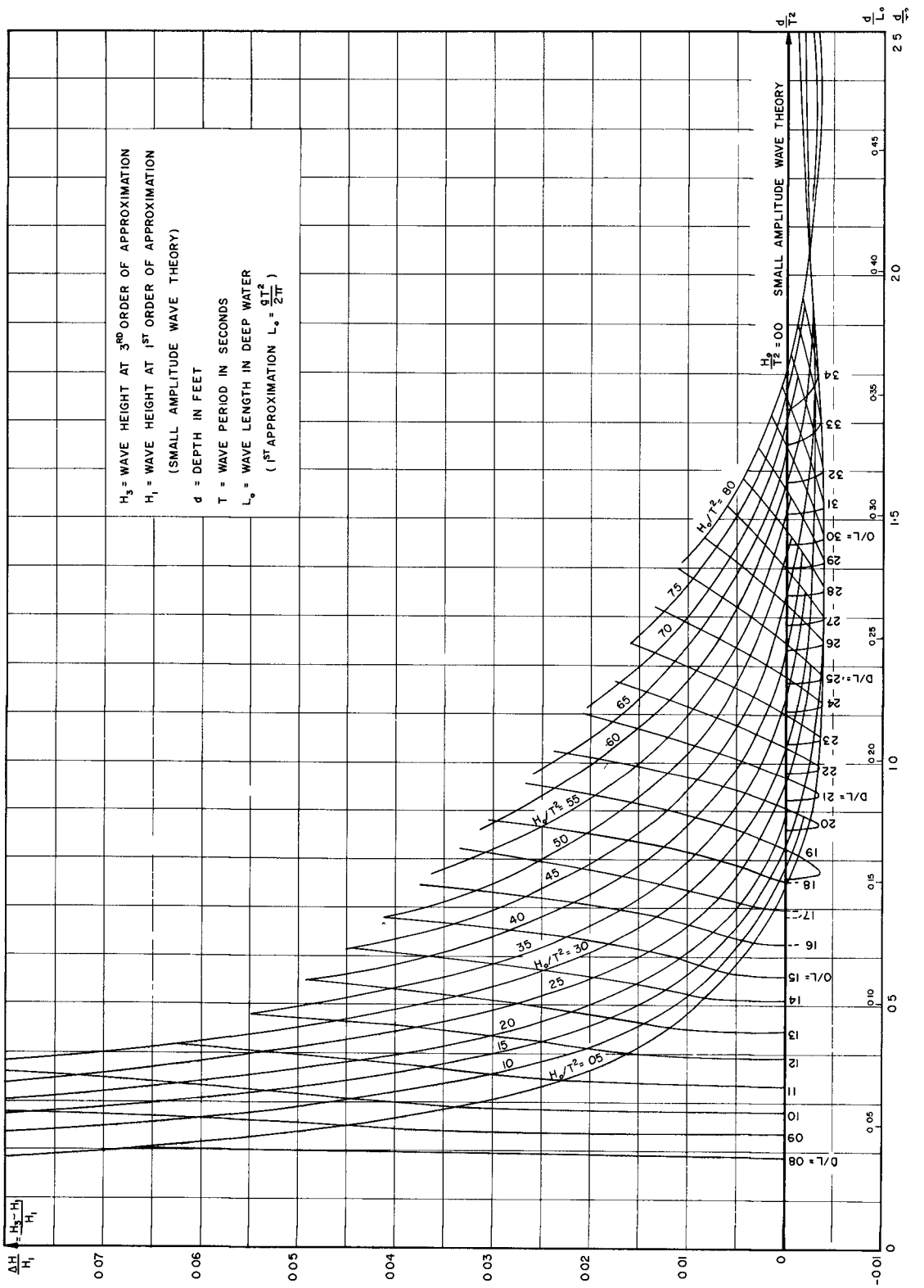
H_3 = WAVE HEIGHT AT 3RD ORDER OF APPROXIMATION
H_1 = WAVE HEIGHT AT 1ST ORDER OF APPROXIMATION
(SMALL AMPLITUDE WAVE THEORY)
d = DEPTH IN FEET
T = WAVE PERIOD IN SECONDS
L_o = WAVE LENGTH IN DEEP WATER
(1ST APPROXIMATION $L_o = \frac{gT^2}{2\pi}$)
$\frac{\Delta H}{H_1} = \frac{H_3 - H_1}{H_1}$
$\frac{H_o}{T^2} = .00$ SMALL AMPLITUDE WAVE THEORY
$\frac{d}{T^2}$
$\frac{d}{L_o}$
$H_o/T^2 = .05$
$H_o/T^2 = .10$
$H_o/T^2 = .15$
$H_o/T^2 = .20$
$H_o/T^2 = .25$
$H_o/T^2 = .30$
$H_o/T^2 = .35$
$H_o/T^2 = .40$
$H_o/T^2 = .45$
$H_o/T^2 = .50$
$H_o/T^2 = .55$
$H_o/T^2 = .60$
$H_o/T^2 = .65$
$H_o/T^2 = .70$
$H_o/T^2 = .75$
$H_o/T^2 = .80$
d/L = .08
d/L = .09
d/L = .10
d/L = .11
d/L = .12
d/L = .13
d/L = .14
d/L = .15
d/L = .16
d/L = .17
d/L = .18
d/L = .19
d/L = .20
d/L = .21
d/L = .22
d/L = .23
d/L = .24
d/L = .25
d/L = .26
d/L = .27
d/L = .28
d/L = .29
d/L = .30
d/L = .31
d/L = .32
d/L = .33
d/L = .34
-.01
0
.01
.02
.03
.04
.05
.06
.07
.05
.10
.15
.20
.25
.30
.35
.40
.45
.5
1.0
1.5
2.0
2.5

and in deep water

$$\frac{H_o}{L_o} < 0.10 \tag{33}$$

The corresponding line has also been drawn on Figure 4.

It is theoretically necessary to use a higher order of approximation or the cnoidal wave theory, if one wants an error smaller than 1/100.

It is evident that Figures (4) and (5) permit also the calculation of $H(d, X)$ after insertion of a term for bottom friction and a correcting term for taking into account the variation of width of orthogonals. In this case, the calculation has to be done step by step over an interval ΔX, by going from one line $\frac{H_o}{T^2}$ = constant to another.

THEORY VS. EXPERIMENTS

The comparison of theoretical curves $\frac{H}{H_o}$ vs. d/T^2 for various $\frac{H_o}{T^2}$ = constant with the experimental results published by Iversen (1951) where actually $L_o (= 5.12T^2)$ replaces T^2 is encouraging Figure (6) . If one excepts a general tendency for the experimental points to be shifted down, a fact which can be explained by bottom friction, the following facts are found both by theory and experiments:

The steepest is the wave, the smaller is the value H/H_o in relatively deep water and the highest is the value H/H_o in relatively shallow water. The crossing of the curve obtained by linear theory with the third order wave theory curves on one hand and experimental curves on the other hand happens for increasing value of $\frac{d}{T^2}$ as $\frac{H_o}{T^2}$ increases . Also the scattering of isolines $\frac{H_o}{T^2}$ = constant increases as $\frac{d}{T^2}$ decreases. Due to the bottom friction, a quantitive comparison does not present a good agreement. On the other hand, the scattering of the isolines $\frac{H_o}{T^2}$ = constant is wider in the experiments of Iversen than in the theoretical curves. It can be expected that a better agreement will be obtained if the above calculations were performed at a fifth order of approximation. This task has been achieved partially only. The relationships between $\frac{L}{T^2}$, $\frac{H}{d}$ and $\frac{d}{T^2}$ are readily available from the tables developed by Skjelbreia and Hendrickso (1961). The corresponding graph is presented Figure (7) . The correspondi fifth order relationship has been inserted numerically in the calculation and the corresponding shoaling effect has been calculated by hand. The results are presented in Figure (8) . It should be realized that these results being a combination of third order wave theory for the energy flux with a fifth order wave theory for the wave length are not consistent. Moreover, they have been obtained by curve reading and hand calculation, i. e. with less accuracy than the previous results presented in Figures (4) and (5) obtained by computer. However, by comparing the curves of Figures (4) and (8) with the experimental results of Figure (6), it is seen that the agreement tends to increase as one uses a higher order of approximation. Consequently, it

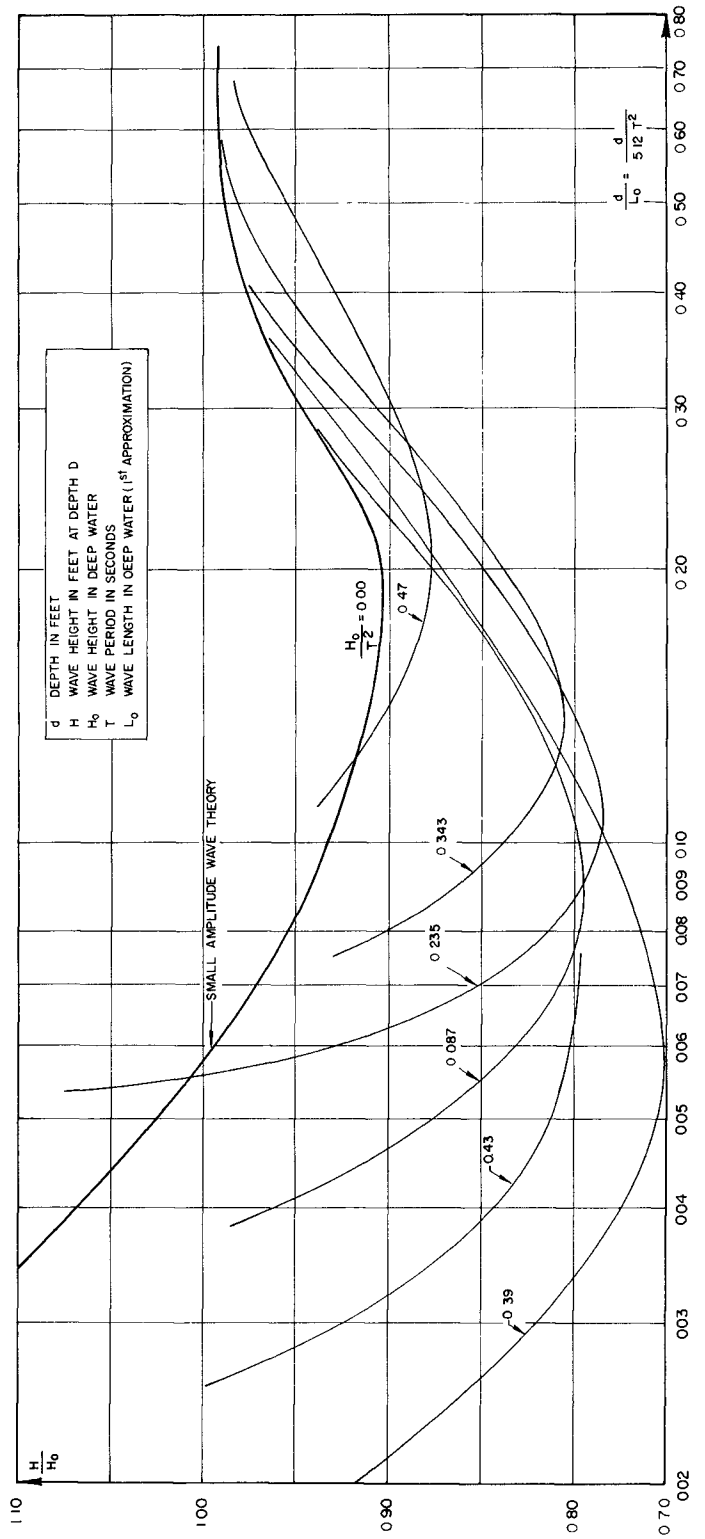
d DEPTH IN FEET
H WAVE HEIGHT IN FEET AT DEPTH D
H_o WAVE HEIGHT IN DEEP WATER
T WAVE PERIOD IN SECONDS
L_o WAVE LENGTH IN DEEP WATER (1st APPROXIMATION)
SMALL AMPLITUDE WAVE THEORY
$\frac{H_o}{T^2} = 0.00$
0.47
0.343
0.235
0.087
0.43
0.39
$\frac{d}{L_o} = \frac{d}{5.12\,T^2}$
$\frac{H}{H_o}$
1.10
1.00
0.90
0.80
0.70
0.02
0.03
0.04
0.05
0.06
0.07
0.08
0.09
0.10
0.20
0.30
0.40
0.50
0.60
0.70
0.80

FIG 6

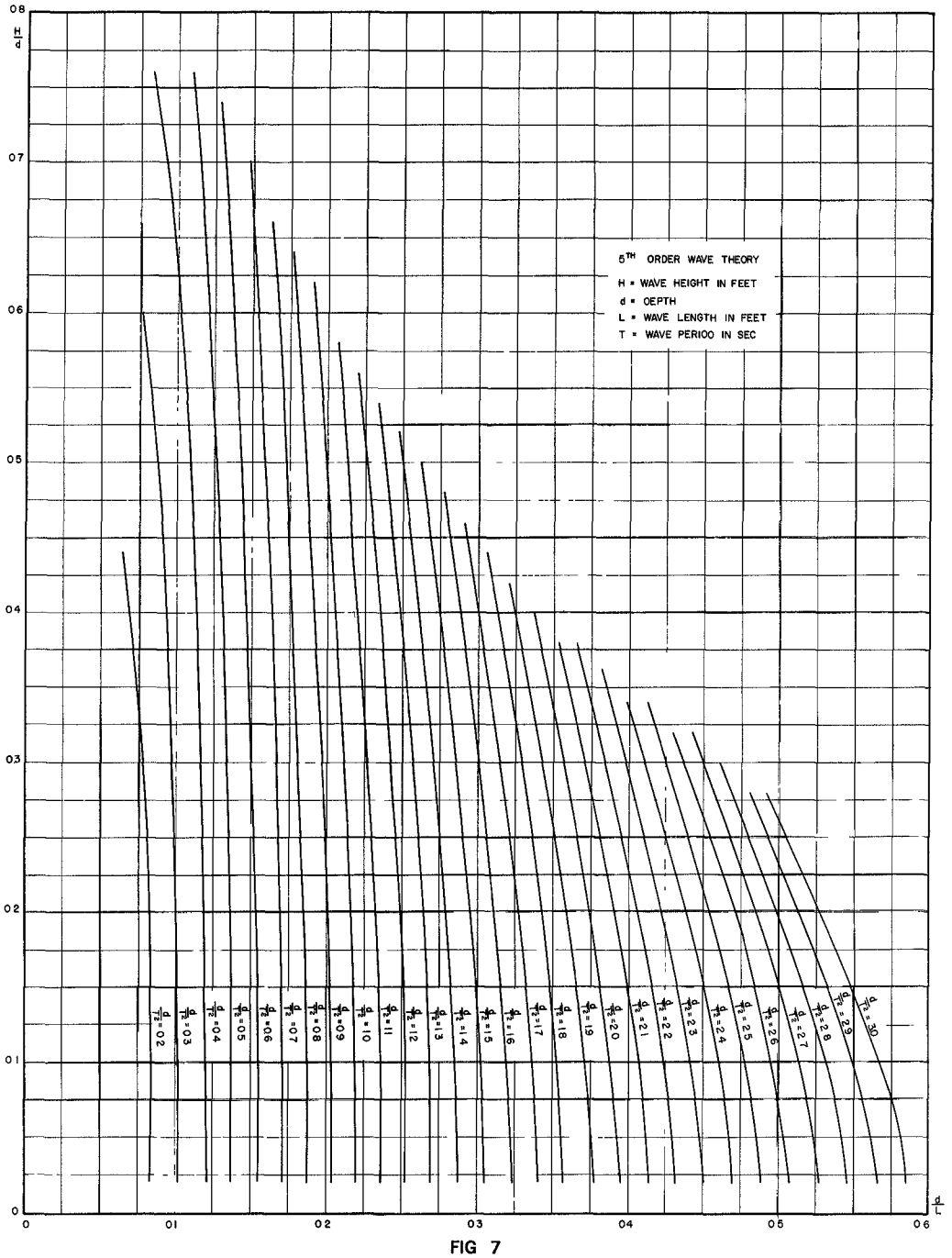
5TH ORDER WAVE THEORY
H = WAVE HEIGHT IN FEET
d = DEPTH
L = WAVE LENGTH IN FEET
T = WAVE PERIOD IN SEC
H/d
d/L
d/gT² = .02
d/gT² = .03
d/gT² = .04
d/gT² = .05
d/gT² = .06
d/gT² = .07
d/gT² = .08
d/gT² = .09
d/gT² = .10
d/gT² = .11
d/gT² = .12
d/gT² = .13
d/gT² = .14
d/gT² = .15
d/gT² = .16
d/gT² = .17
d/gT² = .18
d/gT² = .19
d/gT² = .20
d/gT² = .21
d/gT² = .22
d/gT² = .23
d/gT² = .24
d/gT² = .25
d/gT² = .26
d/gT² = .27
d/gT² = .28
d/gT² = .29
d/gT² = .30

FIG 7

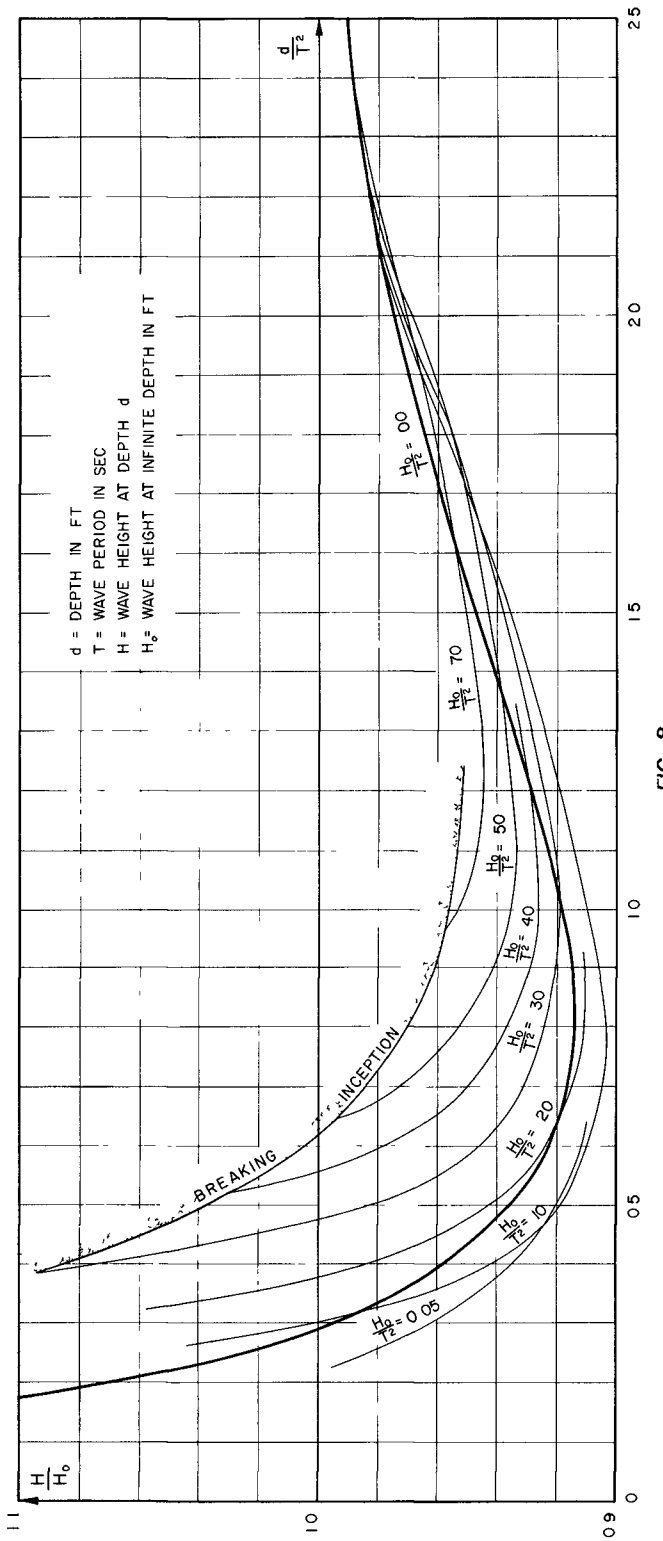
d = DEPTH IN FT
T = WAVE PERIOD IN SEC
H = WAVE HEIGHT AT DEPTH d
H_o = WAVE HEIGHT AT INFINITE DEPTH IN FT
$\frac{d}{T^2}$
$\frac{H}{H_o}$
$\frac{H_o}{T^2}$ = 00
$\frac{H_o}{T^2}$ = 70
$\frac{H_o}{T^2}$ = 50
$\frac{H_o}{T^2}$ = 40
$\frac{H_o}{T^2}$ = 30
$\frac{H_o}{T^2}$ = 20
$\frac{H_o}{T^2}$ = 10
$\frac{H_o}{T^2}$ = 0 05
INCEPTION
BREAKING
25
20
15
10
05
0
11
10
09

FIG 8

would be desirable to perform the calculation which is presently developed at a higher order of approximation. The length of the calculation is discouraging. The calculation of the shoaling coefficient by application of a similar formulation to cnoidal wave theory is probably a better method when the Ursell coefficient $\frac{H}{L}\left(\frac{L}{d}\right)^3$ reaches the value 10 or above the limit previously presented on Figure (4) .

ACKNOWLEDGEMENTS

This work was sponsored by the Office of Naval Research under contract No. Nonr. 4177(00) . Paul Gilon was the computer programmer and Mrs. Lya Kauk did the nomographs.

REFERENCES

Biesel, F. (1951). Study of Wave Propagation in Water of Gradually Varying Depth; Gravity Waves: Nat. Bureau of Standards, Circular 521, paper no. 28, pp. 243-253.

Biesel, F. (1952). Equatons Générales an Second Ordre de la Houle Irrégulière: La Houille Blanche, No. 3, May - June, pp. 372-376.

Iversen, H. W. (1951). Laboratory Study of Breakers; Gravity Waves: Nat. Bureau of Standards, Circular 521, paper No. 3, pp. 9-32.

Skjelbreia, L. and Hendrickson, J. (1961). Fifth Order Gravity Wave Theory Coastal Engineering, Proceedings of Seventh Conference: The Hague 1960, Vol. I, pp. 184-196.

Stoker, J. J. (1957). Water Waves: Interscience Publishers, pp. 13-15 and pp. 47-54.

Wilson, B. (1964). Publication Pending.

Chapter 3

EXEMPLE DE REALISATIONS DE MODELES MATHEMATIQUES A SOGREAH POUR DES ETUDES DE PROPAGATION DE HOULE

L. BARAILLER et P. GAILLARD*

INTRODUCTION

Cet article présente des applications du calcul sur ordinateur électronique à l'étude de la propagation de la houle dans les zones côtières. Cette propagation peut mettre en jeu deux phénomènes :

- l'effet de la variation des fonds sur la célérité de propagation et en conséquence sur la courbure des fronts d'ondes, phénomène dit de "réfraction" par analogie avec l'optique géométrique.
- le rayonnement de l'énergie de la houle en arrière d'obstacles naturels ou artificiels, phénomène dit de "diffraction".

Jusqu'à ces dernières années, seule la réfraction faisait l'objet de méthodes de calcul relativement simples, consistant à tracer, soit des fronts d'ondes par application du principe de Huygens, soit les orthogonales à ces fronts par application de la loi de réfraction de Descartes.

En dehors de cas schématiques simples où des solutions théoriques rigoureuses ou approchées sont applicables - tels que la diffraction par une passe dans une jetée rectiligne Cf. [1] ou celle observée en arrière d'une jetée semi-indéfinie Cf. [2] - la pénétration de la houle dans les ports était étudiée sur un modèle physique à échelle réduite.

Mettant à profit les performances des ordinateurs électroniques, la SOGREAH a élaboré trois programmes généraux destinés à calculer les caractéristiques de la houle pour une configuration quelconque des fonds et des ouvrages portuaires.

---

* Ingénieurs à la SOGREAH - Grenoble - FRANCE.

Ces programmes sont relatifs à trois cas distincts :

1. Celui où seule la réfraction entre en jeu, ainsi que les réflexions éventuelles de la houle sur des ouvrages. Ce programme permet d'étudier la plupart des problèmes de propagation dans les zones d'approche des installations côtières.

2. Celui où la profondeur étant pratiquement constante, seule la diffraction et la réflexion de la houle sont à considérer. Ce programme permet d'étudier essentiellement les conditions d'abri dans les bassins portuaires.

3. Celui où les phénomènes de réfraction et de diffraction interviennent simultanément. Ce programme peut servir dans des conditions particulières de propagation, telles que le franchissement local de hauts fonds ou le contournement d'une presqu'île.

Le dernier de ces programmes est actuellement en cours de mise au point. Les deux premiers ont déjà donné lieu à des nombreuses applications pratiques dans le domaine du génie côtier. Après une brève description du principe de calcul utilisé, on donnera de celles-ci quelques exemples simples sur lesquels les résultats d'autres méthodes de calcul seront comparés.

REFRACTION PURE

La méthode de calcul consiste à tracer point par point le réseau d'orthogonales aux fronts d'onde de la houle connaissant le rayon de courbure local :

$$\rho = \frac{h}{|\overrightarrow{\text{Grad}}\, h \wedge \vec{t}|} \left(1 + \frac{\text{sh}\, 2\pi h/L}{2\pi h/L}\right) \qquad (1)$$

où :

h désigne la profondeur d'eau locale, considérée comme une fonction des coordonnées géographiques.

$\vec{t}$ le vecteur unitaire tangent à l'orthogonale considérée.

L la longueur d'onde locale déduite de la période de la houle et de la profondeur au moyen de la formule classique d'Airy.

Cette relation résulte de l'application de la relation de Descartes à la réfraction dans un milieu où la variation des fonds est progressive.

Le pas de progression adopté dans ce calcul correspond à un intervalle de temps constant de sorte que les points calculés représentent les noeuds du réseau des fronts d'ondes et des orthogonales. Une table traçante associée à l'ordinateur électronique reporte automatiquement ces points sur une épure où il est ensuite aisé de tracer ce réseau.

L'amplitude de la houle est calculée à partir de l'écartement de deux orthogonales voisines en admettant la conservation du flux d'énergie transmis entre celles-ci.

Sur le modèle mathématique, les fonds marins sont définis aux noeuds d'un réseau maillé au moyen d'un programme d'interpolation annexe exploitant les données relevées suivant des lignes parallèles sur les cartes marines.

La profondeur h et son gradient, qui interviennent dans la relation (1), sont déterminés par une formule d'interpolation appropriée des valeurs de h aux neuf points du réseau qui encadrent le point considéré. La dimension des mailles de ce réseau dépend de la pente des fonds à représenter : elle est généralement de l'ordre de 100 à 250 m. Dans les calculs pratiques, on peut décomposer la zone côtière étudiée en zones où la dimension des mailles est différente suivant la distance à la côte, ou la configuration locale des fonds ; le programme enchaîne automatiquement le calcul au passage d'une zone à une autre.

Le programme actuel permet également de tenir compte des réflexions éventuelles sur des ouvrages côtiers de forme simple se ramenant à une succession d'éléments de forme rectiligne ou circulaire.

Ce procédé de calcul a sur la méthode purement graphique l'avantage :

- d'une rapidité plus grande du tracé des épures de propagation grâce à l'association ordinateur-table traçante.
- d'une précision plus grande du tracé des orthogonales et du calcul des amplitudes.
- de déterminer l'amplitude sur toute la zone de propagation étudiée.

En contre partie, il exige un relevé des fonds et une mise en forme de ces données sur ordinateur qui peut demander beaucoup de temps dans certains cas. Le procédé est cependant particulièrement intéressant lorsque l'on doit, pour une topographie des fonds donnée, étudier successivement la propagation de plusieurs houles de périodes et de directions distinctes.

Les expériences de calcul faites avec la présente méthode dans des cas théoriques où les orthogonales sont connues à priori, ont permis d'apprécier l'influence des divers facteurs sur la précision des résultats obtenus. Ceux-ci font également l'objet d'une confrontation avec des mesures en cours d'exécution à l'échelle nature.

Pour illustrer cette méthode nous présentons sur la figure 1 un cas concret de pénétration de la houle dans un golfe pour lequel on a établi une comparaison avec le tracé à la main des fronts d'onde par application du principe de Huygens. L'accord entre les deux méthodes est très satisfaisant. On peut en particulier vérifier sur la figure 2 que les répartitions de l'amplitude sur le dernier front d'onde fournies par ces méthodes concordent avec une bonne approximation.

DIFFRACTION PURE

La méthode de calcul utilisée, décrite par F. BIESEL et B. RANSON dans [3] sera ici rappelée brièvement. Elle repose sur l'emploi d'une des formules de Kirchoff valables en profondeur constante :

$$\zeta_o = \frac{1}{4\pi}\int_\Gamma \frac{\partial \zeta}{\partial n}(M)\, G_2\,(OM)\, ds \qquad (2)$$

$$\zeta_o = -\frac{1}{4\pi}\int_\Gamma \zeta(M)\, \frac{\partial G_1}{\partial n}(OM)\, ds \qquad (3)$$

Γ désigne le contour fermé limitant un domaine arbitraire défini dans la zone de propagation étudiée,

$\zeta_o = a_o e^{i\varphi_o}$ l'amplitude sous forme complexe de la houle en un point O intérieur,

a_o l'amplitude de la houle au point O,

φ_o sa phase en ce point,

ζ l'amplitude complexe supposée connue en tout point M de Γ

$\frac{\partial \zeta}{\partial n}$ la dérivée de ζ suivant la normale intérieure à Γ,

ds la longueur d'un élément de Γ

a. G_1 et G_2 satisfont à l'équation d'onde :

$$\frac{\partial^2 \zeta}{\partial x^2} + \frac{\partial^2 \zeta}{\partial y^2} + m^2 \zeta = 0 \qquad (4)$$

où :

$$m = \frac{2\pi}{L}$$

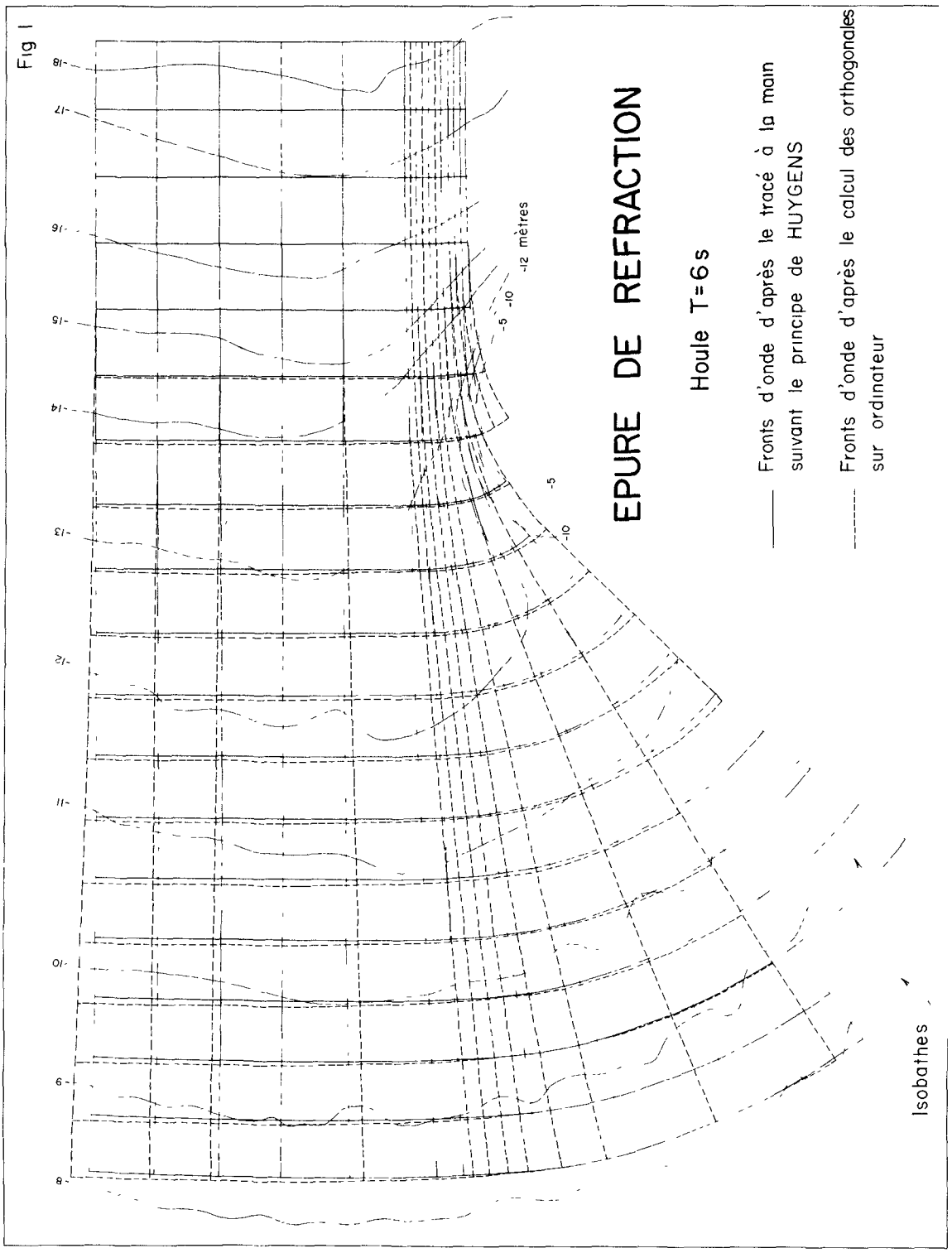
Fig 1
EPURE DE REFRACTION
Houle T=6 s
Fronts d'onde d'après le tracé à la main suivant le principe de HUYGENS
Fronts d'onde d'après le calcul des orthogonales sur ordinateur
Isobathes
-12 mètres
-10
-5
-18
-17
-16
-15
-14
-13
-12
-11
-10
-9
-8

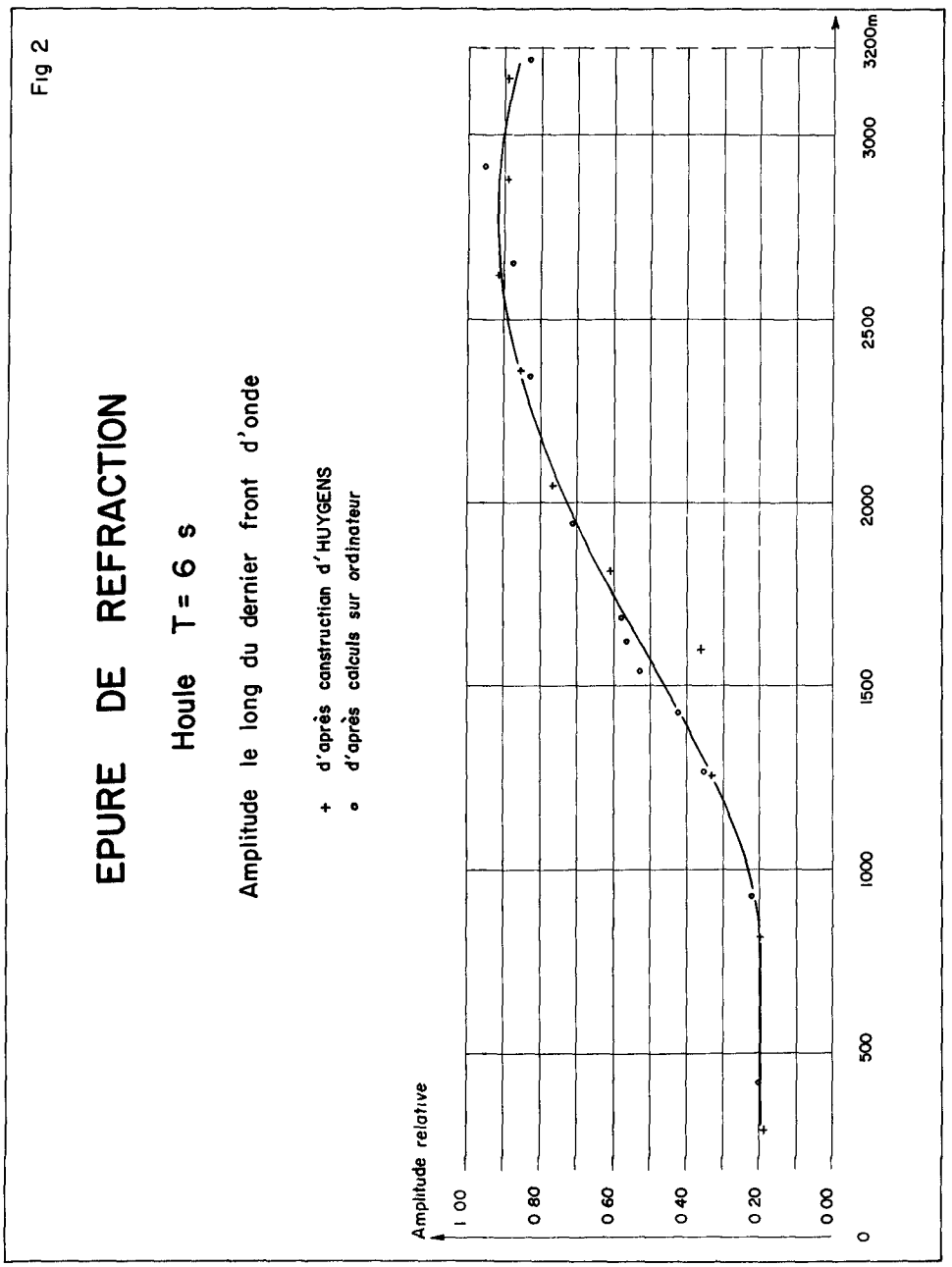
Fig 2
EPURE DE REFRACTION
Houle T= 6 s
Amplitude le long du dernier front d'onde
+ d'après construction d'HUYGENS
• d'après calculs sur ordinateur
Amplitude relative
1 00
0 80
0 60
0 40
0 20
0 00
0
500
1000
1500
2000
2500
3000
3200m

b. elles ont au voisinage de O un comportement logarithmique.

c. elles sont continues dans le domaine D sauf au point O et possèdent des dérivées partielles secondes.

d. elles satisfont aux conditions suivantes sur Γ :

$$G_1 (OM) = 0$$
$$\frac{\delta G_2}{\delta n} (OM) = 0 \qquad (5)$$

Ces fonctions n'ont d'expression simple que dans un petit nombre de cas et en particulier dans celui d'un domaine D constitué d'un demi-plan où l'on a :

$$G_2 = 2H_o^{(1)} (mr)$$
$$\frac{dG_1}{dn} = 2m\, H_1^{(1)} (mr) \cos\Theta \qquad (6)$$

où :

$H_o^{(1)}$ et $H_1^{(1)}$ désignent les fonctions de Hankel de première espèce d'ordre 0 et 1 respectivement,

r la distance OM,

Θ l'angle de $\vec{MO}$ avec la normale intérieure à Γ au point M.

Les expressions (6) sont applicables à un domaine D de forme quelconque à condition de :

- Décomposer, si cela est nécessaire, le domaine réel considéré en plusieurs domaines partiels de forme convexe,
- De ne considérer comme données que les ondes pénétrant dans chaque domaine partiel considéré. Les ondes éventuellement réfléchies par les parois entrent évidemment dans cette catégorie au même titre que les ondes incidentes transmises directement dans ce domaine (par des passes entre bassins communiquants par exemple).

Moyennant ces précautions, il est possible de superposer (puisque l'on se limite à la théorie linéaire de la propagation de la houle) les solutions théoriques relatives aux différents demi-plans limités par les tangentes au contour Γ de chaque domaine partiel et contenant ce domaine. En d'autres termes, le calcul sur ordinateur remplace les intégrales (2) et (3) par des sommations finies où

chaque élément du contour, de longueur ds, joue le rôle d'une brèche dans une jetée rectiligne de longueur indéfinie et à travers laquelle la houle incidente pénètre dans le domaine partiel considéré.

Après une étude comparative des formules (2) et (3), la préférence a été donnée à la première, pour laquelle l'hypothèse à formuler le long d'une paroi réfléchissante à savoir :

$$\left(\frac{\partial \zeta}{\partial n}\right)_{\substack{\text{onde} \\ \text{réfléchie}}} = -\left(\frac{\partial \zeta}{\partial n}\right)_{\substack{\text{onde} \\ \text{incidente}}} \qquad (7)$$

est plus conforme à la réalité qu'une condition arbitraire imposée à ζ (la plus simple étant $\zeta = 0$ à l'abri d'une jetée).

Dans le cas d'une paroi partiellement absorbante la relation (7) est remplacée par :

$$\left(\frac{\partial \zeta}{\partial n}\right)_{\substack{\text{onde} \\ \text{réfléchie}}} = -\alpha \left(\frac{\partial \zeta}{\partial n}\right)_{\substack{\text{onde} \\ \text{incidente}}} \qquad (8)$$

où :

α est le coefficient de réflexion de l'ouvrage qui peut être fonction de l'incidence connue lors du calcul de l'onde incidente.

Le calcul de la valeur de $\left(\frac{\partial \zeta}{\partial n}\right)$ correspondant à l'onde pénétrant dans chaque domaine partiel considéré est donc nécessaire à partir des valeurs correspondantes connues sur la frontière du domaine réel :

- sur toutes les parois partiellement ou totalement réfléchissantes qui font partie du contour Γ. (La valeur de $\frac{\partial \zeta}{\partial n}$ relative à l'onde incidente joue le rôle d'inconnue et $\frac{\partial \zeta}{\partial n}$ celle relative à l'onde réfléchie le rôle de donnée),
- sur toutes les parties du contour Γ communes à deux domaines partiels adjacents (la valeur de $\partial\zeta/\partial n$ qui joue le rôle de donnée dans l'un des bassins joue le rôle d'inconnue dans l'autre).

On utilise pour cela la formule suivante déduite de (2) par dérivation au point O, qui en l'occurence se trouve sur Γ :

$$\left(\frac{\partial \zeta}{\partial n}\right)_O = \frac{1}{4i}\int_\Gamma \frac{\partial \zeta}{\partial n}(M)\,\frac{\partial G_2}{\partial n}(OM)\,ds \qquad (9)$$

avec :

$$\frac{\partial G_2}{\partial n} = 2m\,H_1^{(1)}(mr)\cos\psi \qquad (10)$$

où ψ est l'angle entre la normale intérieure au contour Γ et le vecteur $\overrightarrow{OM}$.

Le calcul de l'amplitude dans un domaine portuaire de forme quelconque comporte ainsi :

- dans une première phase le calcul éventuel des $\frac{\partial \zeta}{\partial n}$ inconnus. Ce calcul est effectué par itérations successives, la convergence des résultats obtenus étant contrôlée d'un tour de calcul au suivant,
- dans une deuxième phase, le calcul de ζ_o proprement dit.

Si l'on considère à titre d'exemple l'avant-port dont la configuration est indiquée sur la figure 3, le domaine D situé à droite de aa' peut être décomposé en deux domaines partiels D1 et D2 présentant une frontière commune B1b. La connaissance des caractéristiques de la houle incidente dans la passe A1 A2 permet de déterminer :

- en vue du calcul de ζ dans le domaine D1, la valeur de $\frac{\partial \zeta}{\partial n}$ sur les parois A1a, B1A2 et B1B2 si celles-ci ne sont pas totalement absorbantes.
- en vue du calcul de ζ dans le domaine D2, la valeur de $\frac{\partial \zeta}{\partial n}$ sur la limite fictive B2b. Si l'on admet l'absence totale de réflexions sur la partie droite de D2, il n'y a aucune réflexion à considérer sur les éléments a'B1 et B1B2, il n'y a également aucune transmission de houle réfléchie de D2 vers D1 et la valeur de $\frac{\partial \zeta}{\partial n}$ à prendre en considération le long de B2b lors du calcul de ζ dans D1 est nulle.

La méthode exposée permet d'étudier les conditions d'abri des bassins portuaires, quelles que soient le pouvoir réfléchissant des ouvrages et la complexité de leur disposition. Elle fait actuellement l'objet à la SOGREAH d'une confrontation avec les résultats d'une étude sur modèle réduit de quelques dispositions types, afin de déterminer la meilleure façon de schématiser sur un modèle mathématique des ouvrages réels tels qu'une jetée à talus ou une jetée verticale de largeur non négligeable vis à vis de la longueur d'onde de la houle. Le lecteur trouvera dans la communication de M. MONTAZ à ce même congrès Cf. [4] les principaux résultats obtenus à ce jour.

Pour illustrer ce qui précède, nous indiquons ici un résultat fragmentaire obtenu au cours d'une étude effectuée pour guider le choix de l'implantation d'un nouveau bassin portuaire. Sur la figure 3 sont esquissés deux éléments de projets étudiés et sur la figure 4 sont indiquées les valeurs de l'amplitude relative de la houle à l'abri de la jetée en fonction de la distance au musoir. Pour la disposition (a) on présente également les valeurs calculées par la solution théorique de SOMMERFELD [2] pour une jetée rectiligne,

Fig 3

CALCULS DE DIFFRACTION

Exemple schématique d'application

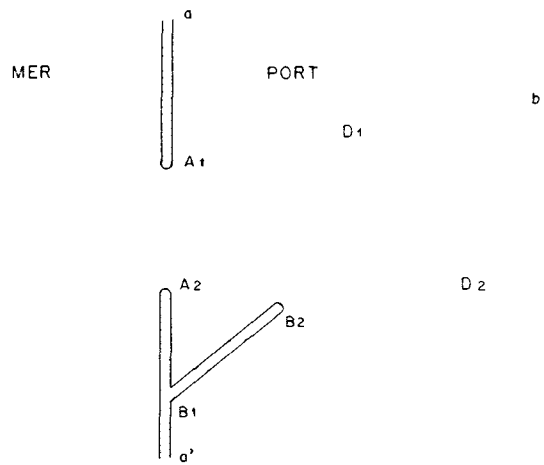

Fig 4

CALCULS DE DIFFRACTION

Dispositions étudiees

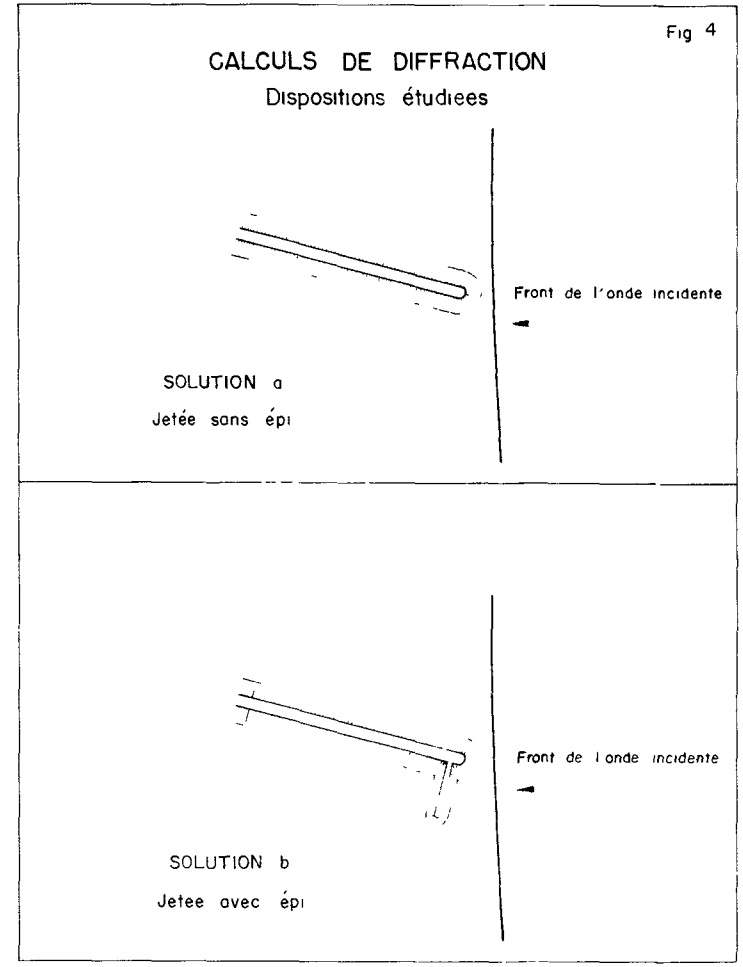

semi-indéfinie et celles déduites d'une formule asymptotique proposée par CARRY et CHAPUS Cf. [5]:

$$2a = \frac{1}{2\pi (r/L)^{\frac{1}{2}} \sin \Theta_0} \qquad (11)$$

où :

2a est l'amplitude de la houle,
r la distance au musoir,
L la longueur d'onde de la houle,
Θ_0 l'angle d'incidence de la houle par rapport à la jetée.

REFRACTION ET DIFFRACTION SIMULTANEES

La formule (2) traduit en profondeur constante et sous une forme mathématique précise le fait que l'effet de la houle au point O est identique à celui de sources ponctuelles fluctuantes réparties le long du contour Γ, conformément au principe de Huygens. Dans un domaine D de profondeur variable, le calcul de l'agitation observée en O consiste à appliquer des formules analogues à (2) et (9), où les fonctions G2 et dG2/dn sont liées au flux d'énergie connu émis par les sources ponctuelles équivalentes. La formule (2) en particulier est remplacée par :

$$\zeta_o = \int_\Gamma \frac{\partial \zeta}{\partial n}(M)\, I(OM)\, e^{i\Theta(OM)}\, ds$$

où :

$$I(OM) = \left(\frac{\Theta}{2\pi m \sigma_o} \frac{c_g}{c_{go}}\right)^{\frac{1}{2}} \qquad (12)$$

$$\phi(OM) = \int_0^M m(r)\, dr - 3\pi/4$$

c_g et c_{go} désignent les célérités de groupes de la houle en M et O,

σ_o l'écartement de 2 rayons d'onde voisins issus de la source M et formant en ce point un petit angle Θ,

r l'abscisse curviligne le long du rayon d'onde issu de M et passant par O,

$m = 2\pi/L$ la valeur du nombre d'onde en un point courant de ce rayon.

Le calcul pratique de l'amplitude et de la phase de la houle en un point comporte :

- d'une part le tracé des rayons d'ondes parvenant en ce point à partir des sources ponctuelles fictives réparties sur Γ .

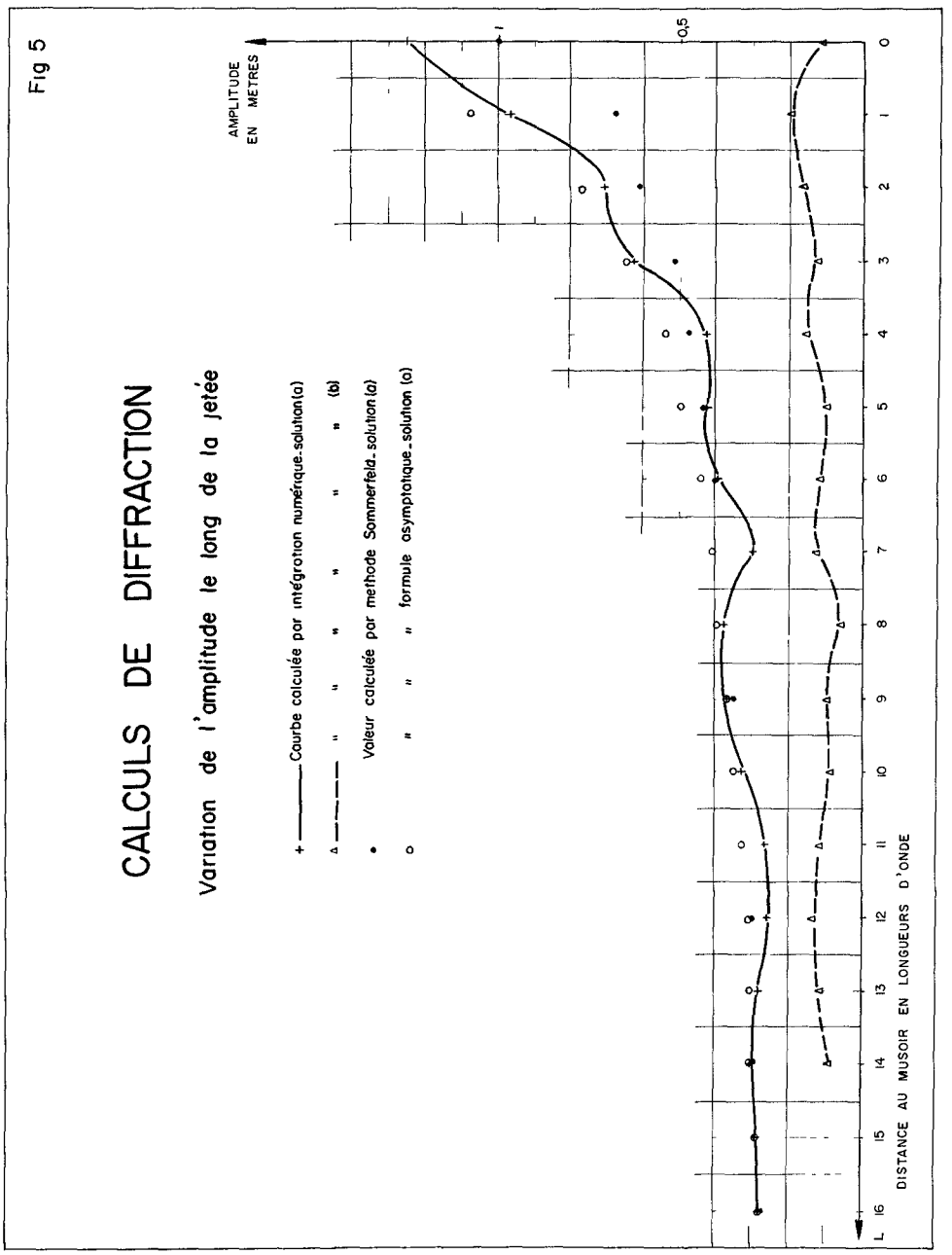
Fig 5
CALCULS DE DIFFRACTION
Variation de l'amplitude le long de la jetée
Courbe calculée par intégration numérique-solution (a)
" " " " " " (b)
Valeur calculée par methode Sommerfeld-solution (a)
" " " formule asymptotique-solution (a)
AMPLITUDE EN METRES
1
0,5
0 1 2 3 4 5 6 7 8 9 10 11 12 13 14 15 16 L
DISTANCE AU MUSOIR EN LONGUEURS D'ONDE

- d'autre part le calcul de $I(OM)$ et $\phi(OM)$. La détermination de σ_o en particulier s'effectue par intégration de l'équation différentielle régissant l'évolution de l'écartement de deux rayons d'onde voisins :

$$\frac{d^2\sigma}{dr^2} + p(r)\frac{d\sigma}{dr} + q(r)\sigma = 0$$

avec : (13)

$$p(r) = -\frac{1}{c}\frac{\partial c}{\partial r}$$

$$q(r) = \frac{1}{c}\frac{\partial^2 c}{\partial n^2}$$

où :

c désigne la célérité de phase de la houle au point courant,
r l'abscisse curviligne le long d'un rayon d'onde,
n l'ordonnée suivant la normale à ce rayon au point courant Cf. [6]

Les conditions d'applications de (12) et l'organisation des calculs, hormis les points qui viennent d'être soulignés, sont les mêmes que dans le cas de la diffraction pure.

Le processus de calcul est, comme on peut s'en rendre compte d'après le principe exposé, beaucoup plus long à exécuter que les deux précédents programmes. C'est pourquoi, bien que ce dernier programme soit en principe applicable aux phénomènes spécifiques aux précédents, il convient de ne l'utiliser que si les phénomènes de réfraction et de diffraction risquent d'entrer en jeu simultanément. Ceci peut être le cas par exemple :

- lors du contournement par la houle d'une presqu'île ou d'une jetée dans une zone où les fonds varient notablement.

- lors du franchissement d'un haut fond (sans toutefois que le déferlement entre en jeu). Dans ce dernier cas, une épure de réfraction fait apparaître une forte convergence du faisceau d'orthogonales aux fronts d'ondes et localement le croisement de certaines d'entre elles, de sorte que le calcul de l'amplitude par le premier programme décrit perd beaucoup de son intérêt à cet endroit.

Une étude est actuellement en cours pour déterminer les modalités d'application de ce dernier procédé, notamment par comparaison avec des mesures sur modèle réduit dans des cas particuliers appartenant aux types cités.

CONCLUSION

La rapidité d'exécution des calculs et la précision des résultats obtenus au moyen d'ordinateurs électroniques permettent d'envisager l'étude sur modèle mathématique de la propagation de la houle même par des procédés aussi complexes que le dernier décrit.

L'ensemble des programmes de calcul décrits ici vise à déterminer les caractéristiques de la houle dans les zones côtières et dans les bassins portuaires, quelle que soit la configuration des fonds et la disposition des ouvrages étudiés.

REFERENCES

(1) MORSE P.M. et RUBENSTEIN P.J. "The diffraction of waves by ribbons and by slits" Physical Review 54, 1938.

(2) SOMMERFELD A. "Vorlesungen über theoretische Physic", Band IV, Optik 1950.

(3) F. BIESEL et B. RAUSON "Calculs de diffraction de la houle" A.I.R.H. Dubrovnik 1961.

(4) J.P. MONTAZ "Etude expérimentale systématique en vue de l'utilisation de modèles mathématiques pour l'étude de la diffraction pure de la houle" Congrès Coastal Engineering, Lisbonne 1964.

(5) CARRY et CHAPUS "Calcul pratique de l'amplitude de la houle diffractée derrière une jetée semi-indéfinie", la houille blanche n° 1, 1951.

(6) MUNK W.H. et ARTHUR R.S. "Wave intensity along a refracted ray" Gravity waves, Nat. Bur, Standards. Circular 521, 1952.

Chapter 4

EQUATIONS APPROCHEES DE LA REFRACTION DE LA HOULE

F. BIESEL
Directeur Scientifique à la SOGREAH

INTRODUCTION

En 1951, au Symposium sur les ondes de gravité, organisé par le National Bureau of Standards, j'ai présenté une étude sur les équations approchées de la houle en profondeur variable [1]. Cette étude était limitée aux problèmes plans (houles cylindriques) mais j'indiquais que la méthode pouvait être étendue aux cas tridimensionnels. Les formules auxquelles on aboutissait alors pour ces cas, justifiaient à titre de première approximation, la pratique usuelle de construction et d'interprétation des plans de vagues ; elle introduisait néanmoins un certain nombre de corrections qui pouvaient en gros se grouper en trois catégories :

- des déformations des houles identiques en substance à celles obtenues pour le cas bi-dimensionnel,

- des corrections d'amplitude,

- des corrections de longueur d'onde.

Les effets de la première catégorie ont été étudiés dans l'article cité plus haut. Ceux de la deuxième catégorie ne sont pas significatifs à l'ordre de précision retenu. Par contre, les effets de la troisième catégorie peuvent avoir une certaine importance pratique du fait de leur aspect "cumulatif". En effet, des variations de longueur d'onde, même petites n'ont pas uniquement un effet local mais sont susceptibles de déformer l'ensemble d'un diagramme de réfraction. Cependant, la précision que l'on pouvait atteindre par le tracé *graphique* des épures de réfraction ne permettait guère l'utilisation pratique de ces résultats. Ceci est la raison pour laquelle je m'étais jusqu'ici, abstenu de les publier, leur intérêt semblant d'autant plus lointain que l'aspect mathématique pur de ces formules est sans intérêt théorique.

Par contre, maintenant, étant donné les extraordinaires progrès de rapidité et d'économie des calculatrices électroniques, il est possible d'exécuter économiquement des calculs de réfraction très précis utilisant

au besoin des formules théoriques complexes. Il devient donc possible d'utiliser les corrections de longueur d'onde présentées ici ; elles permettent d'augmenter encore la précision et la sécurité des calculs électroniques de propagation d'onde de gravité.

DEFINITION DU PROBLEME ET NOTATIONS

Nous considérons la propagation d'ondes de gravité "monochromatiques" sur un plan d'eau de profondeur variable d'un point à un autre. Nous nous limitons à la théorie irrotationnelle, en fluide parfait et incompressible ; par ailleurs, nous négligeons les termes de l'ordre du carré de la cambrure.

La méthode que nous employons est du type "calcul des perturbations", le phénomène de référence (non perturbé) étant la houle monochromatique cylindrique en profondeur constante.

D'une façon plus précise, les ondes étudiées devront être *localement* peu différentes d'une houle de référence ; par contre, par suite des effets cumulatifs de diverses déformations, une houle de référence donnée n'aura qu'une valeur locale. Ces hypothèses sont d'ailleurs parmi celles que l'on fait implicitement pour justifier la théorie usuelle du tracé des épures de réfraction. On peut ainsi définir des fronts d'onde, des orthogonales, des amplitudes locales, etc...

En chaque point, la houle de référence locale, ou houle "tangente", aura par définition des fronts d'onde et des orthogonales rectilignes, une amplitude constante ainsi qu'une profondeur de référence également constante et égale à la profondeur réelle locale. Notre hypothèse suivant laquelle le mouvement réel diffère localement peu de la houle de référence entraîne donc la petitesse :

- de la courbure des fronts d'ondes,
- de la courbure des orthogonales,
- des pentes de fond,
- des dérivées de l'amplitude.

Ces quantités seront considérées comme des infiniment petits dont certaines puissances ou produits seront négligés suivant des règles que nous préciserons plus loin.

Les notations utilisées sont les suivantes :

x, y, z, coordonnées dans un système cartésien $OXYZ$ dont l'origine est sur la surface libre moyenne, l'axe OZ etant vertical ascendant.

ξ, η, z, coordonnées dans un système curviligne tri-orthogonal, z étant défini comme précédemment, ξ et η étant tels que les lignes $\xi = c^{te}$ correspondent aux fronts d'onde et les lignes $\eta = c^{te}$, aux orthogonales, le sens de la propagation étant celui des ξ croissants et deux lignes de crête consécutives ayant des coordonnées ξ différant de 2π.

$\varphi(\xi, \eta, z, t)$: potentiel des vitesses du mouvement,

k, fréquence angulaire de la houle $(k = \frac{2\pi}{T})$,

T, période de la houle,

$h(\xi, \eta)$, profondeur locale ($z = -h$ sur le fond),

m_o, nombre d'ondes de référence ($k^2 = g m_o \text{th}\, m_o h$),

m, nombre d'ondes corrigé $m \sqrt{(\frac{\partial \xi}{\partial x})^2 + (\frac{\partial \xi}{\partial y})^2}$

m', défini dans le texte,

l, défini par $l = \sqrt{(\frac{\partial \eta}{\partial x})^2 + (\frac{\partial \eta}{\partial y})^2}$

γ_1, courbure des fronts d'onde (positif lorsque les ondes convergent),

γ_2, courbure des orthogonales (positif lorsque la concavité est vers les η croissants),

α, pente du fond le long des orthogonales, positive lorsque le fond remonte (la profondeur diminue), dans le sens de la propagation :

$$\alpha = - m \frac{\partial h}{\partial \xi},$$

β, pente transversale du fond le long des fronts d'onde, positive lorsque le fond remonte dans le sens des η croissants

$$\beta = -\frac{1}{l}\frac{\partial h}{\partial \eta},$$

a, demi-amplitude locale de la houle.

EQUATIONS ET ORDRE D'APPROXIMATION

Nous définirons le mouvement par son potentiel des vitesses $\varphi(\xi, \eta, z, t)$. Nous nous limitons aux théories linéaires par rapport à l'amplitude φ qui devra donc satisfaire aux conditions classiques suivantes :

Incompressibilité :

$$\Delta\varphi = ml\left\{\frac{\partial}{\partial\xi}\left(\frac{m}{l}\frac{\partial\varphi}{\partial\xi}\right) + \frac{\partial}{\partial\eta}\left(\frac{l}{m}\frac{\partial\varphi}{\partial\eta}\right)\right\} + \frac{\partial^2\varphi}{\partial z^2} = 0$$

Δ désignant le laplacien.

Condition sur le fond :

$$\frac{\partial\varphi}{\partial z} = m\alpha\frac{\partial\varphi}{\partial\xi} + l\beta\frac{\partial\varphi}{\partial\eta} \quad \text{pour} \quad z = -h$$

Condition de pression constante en surface :

$$g\frac{\partial\varphi}{\partial z} = -k^2\varphi = 0 \quad \text{pour } z = 0$$

Nous savons déjà que ces équations ne sont justes qu'à des termes de l'ordre du carré de l'amplitude près. Mais de plus, nous considérons comme petites les quantités γ_1 et γ_2, ainsi que les dérivées de h et de a.

Plusieurs de ces infiniment petits sont a priori indépendants si bien que la définition de l'ordre d'approximation auquel on pousse les calculs est assez complexe. La façon la plus directe de l'exprimer est de faire la liste des quantités non négligées, cependant, pour rendre cette liste moins arbitraire et abréger l'énoncé des approximations faites, nous introduisons un infiniment petit de référence ε et convenons que :

α et β sont de l'ordre de ε^3.

Toutes les autres dérivées de h sont d'ordre supérieur au 5ème :

γ_1 est de l'ordre de ε^2.

$\frac{1}{a}\frac{\partial a}{\partial y}$ est de l'ordre de ε^2.

$\frac{1}{a}\frac{\partial^2 a}{\partial y^2}$ est de l'ordre de ε^4.

Les dérivées supérieures de a, divisées par a, sont d'ordre supérieur au 5ème ; les autres quantités infiniment petites (γ_2, $\frac{1}{a}\frac{\partial a}{\partial \xi}$, etc...) ne sont pas indépendantes des précédentes.

Nous convenons alors que toutes les équations du problème telles qu'elles sont écrites ci-dessus doivent être satisfaites à des quantités du sixième ordre (multipliées par a) près.

Au facteur a près qui intervient partout au 1er degré, nous conservons donc toutes les quantités du même ordre que :

$$\gamma_1,\ \frac{1}{a}\frac{\partial a}{\partial \eta},\ \alpha,\ \beta,\ \frac{1}{a}\frac{\partial^2 a}{\partial \eta^2}$$

ainsi que les produits deux à deux des quatre premières ($\alpha\beta$ excepté) et les carrés des deux premières.

Ainsi que nous l'avons indiqué dans l'introduction, la recherche de la solution ne met pas en jeu de méthodes mathématiques originales ou intéressantes en elles-mêmes. En résumé, elles consistent à partir d'une première approximation qui revient à admettre que localement le potentiel a la même expression que celui de la houle de référence locale :

$$\varphi_o = f \operatorname{ch} m(z+h) \sin(kt-\xi)$$

expression dans laquelle f, m et h sont des fonctions de ξ et de η et ξ etant une ordonnée curviligne convenable.

Les équations du problème imposent alors :

- de donner une forme précise aux fonctions f et m,
- de définir différentiellement le système de coordonnées ξ,η,
- d'introduire un certain nombre de termes correctifs.

Les formules essentielles auxquelles on aboutit ainsi, sont réunies sur le tableau p.7.

Elles appellent les remarques suivantes :

a) - Dans un but de simplification, nous n'avons pas fait apparaître directement l'amplitude dans l'expression de φ mais une fonction f qui lui est liée en première approximation par la relation (12).

b) - La relation (3) définit les positions relatives des lignes $\xi = c^{te}$, la construction usuelle des épures de réfraction (à partir d'un front d'onde origine) n'est autre que l'intégration graphique de ces équations — de même que le calcul sur ordinateur en est l'intégration numérique.

Notre résultat justifie donc le procédé de construction ou de calcul des épures de réfraction, cependant, il apporte une correction du fait que m est légèrement différent de m_o. Autrement dit, la longueur d'onde locale dont il faut tenir compte pour ces épures est :

$$L = \frac{2\pi}{m} \text{ et non } L_o = \frac{2\pi}{m_o}$$

Nous étudierons plus en détail, cette correction qui constitue l'essentiel du résultat obtenu, en ce qui concerne les applications.

c) - De même que m est inversement proportionnel à l'écartement des lignes $\xi = c^{te}$, l est inversement proportionnel à l'écartement des orthogonales. La relation (2) correspond à la loi de

TABLEAU DE FORMULES

$$\varphi = f \left\{ [\mathrm{ch}\ m'(z+h)]\ \sin(kt-\xi) + \alpha[Qm(z+h)\mathrm{sh}\ m(z+h) + G]\ \cos(kt-\xi) \right.$$
$$\left. + \frac{1}{m}\left[\alpha\frac{\gamma_1}{2}\mathrm{sh}\ m(z+h) - \beta bG + \theta \mathrm{ch}\ m(z+h)\right]\ \sin(kt-\xi) \right\} \qquad (1)$$

$$f = K(\eta)\sqrt{\frac{l}{E}} \qquad (2)$$

$$\sqrt{\left(\frac{\partial\xi}{\partial x}\right)^2 + \left(\frac{\partial\xi}{\partial y}\right)^2} = m \qquad (3)$$

$$l = \sqrt{\left(\frac{\partial\eta}{\partial x}\right)^2 + \left(\frac{\partial\eta}{\partial y}\right)^2} \qquad (4)$$

$$m = m_o - \frac{\alpha\gamma_1}{2E} + \frac{\gamma_1^2}{8m} + \frac{1}{2K(\eta)\sqrt{l}}\ \frac{\partial^2}{\partial\tau^2}\ \left[\frac{K(\eta)\sqrt{l}}{m}\right] \qquad (5)$$

où : $\dfrac{\partial}{\partial\tau} = l\dfrac{\partial}{\partial\eta}$; $\dfrac{\partial^2}{\partial\tau^2} = l\dfrac{\partial}{\partial\eta}\left(l\dfrac{\partial}{\partial\eta}\right)$

$$m' = m_o - \frac{\alpha\gamma_1}{2E} - \beta bQ \qquad (6)$$

$$gm_o\ \mathrm{th}\ m_o h = k^2 \qquad (7)$$

$$E = \mathrm{ch}\ m\ h\ .\ \mathrm{sh}\ m\ h + m\ h \qquad Q = \frac{\mathrm{sh}\ m\ h\ \mathrm{ch}^3\ m\ h}{E^2} \qquad (8)$$

$$G = \left[\frac{m(z+h)}{2E} - 1\right]\ m(z+h)\ \mathrm{ch}\ m(z+h) \qquad (9)$$

$$b = \frac{1}{f}\frac{\partial f}{\partial\tau} = \frac{1}{f}\frac{\partial f}{\partial\eta} \qquad (10)$$

$$\gamma_1 = \frac{m}{l}\frac{\partial l}{\partial\xi} = \frac{1}{R}\ (R = \text{rayon de courbure des fronts d'onde}) \qquad (11)$$

θ = fonction arbitraire de ξ et η d'ordre de grandeur ε^4 ou ε^5 et dont toutes les dérivées sont négligeables.

$K(\eta)$ = fonction arbitraire de η satisfaisant aux conditions d'ordre de grandeur indiquées pour a. On a d'ailleurs en première approximation :

$$a = -\frac{m'\ \mathrm{sh}\ m'h}{k} f \qquad (12)$$

la valeur absolue de a étant la demi-amplitude.

NB - Sauf dans l'équation (3) m peut partout être remplacé par m' ou m_o sans que l'ordre d'approximation choisi cesse d'être respecté.

conservation des énergies transmises entre deux orthogonales (en fait, il faudrait dire, des énergies de référence car on admet dans cet énoncé que la formule de transmission d'énergie est celle de la houle de référence locale).

Le débit moyen d'énergie par unité de temps et par unité de largeur de front est en effet pour une houle cylindrique en profondeur constante :

$$\frac{\rho g\, a^2\, k}{4m_o}\,\frac{E_o}{\operatorname{sh} m_o h \operatorname{ch} m_o h} \qquad (E_o = \operatorname{sh} m_o h \operatorname{ch} m_o h + m_o h)$$

ce qui, compte tenu des formules (2) et (12) et (7) où en première approximation, nous confondrons m, m' et m_o, peut s'écrire :

$$\frac{\rho k}{4} 1 K^2(\eta)$$

Le débit d'énergie par unité de temps entre deux orthogonales η et $\eta+d\eta$ est, toujours en première approximation :

$$\frac{\rho k}{4} K^2(\eta) d\eta$$

La fonction "arbitraire" $K(\eta)$ représente donc à un facteur constant près et en première approximation la racine carrée (positive ou négative) de la densité d'énergie par rapport à la variable η. Cette densité ne dépend pas de ξ, elle se conserve donc le long des orthogonales, ce qui est bien le principe appliqué pour le calcul classique des amplitudes réfractées.

d) - Ce qui précède n'est vrai qu'en première approximation car, en fait, m, m_o et m' ne sont pas rigoureusement égaux et d'autre part, le troisième crochet de la formule (1) apporte une certaine modification à l'amplitude qui n'est donc pas rigoureusement donnée par l'expression (12).

L'existence de la fonction arbitraire θ dans ce crochet montre que la théorie, *au degré d'approximation où elle est poussée*, ne peut déterminer les lois de variation des amplitudes mieux qu'au quatrième ordre près - par conséquent, les "premières approximations"

établies plus haut, sont les seules que cette théorie nous permette d'atteindre. Elles sont en plein accord avec la règle de non-transfert de l'énergie à travers les orthogonales.

APPLICATION AUX CALCULS DE REFRACTION

La formule (5) permet d'apporter une correction aux calculs ou de réfraction. Celles-ci doivent être établies comme si la longueur d'onde locale, ou la vitesse de phase, était proportionnelle à $\frac{1}{m}$ et non à $\frac{1}{m_o}$.

Posons, pour simplifier :

$$\Delta m = m - m_o = - \frac{\alpha \gamma_1}{2E} + \frac{\gamma_1^2}{8m_o} + \frac{1}{2K(\eta)\sqrt{1}} \frac{\partial^2}{\partial t^2} \left[\frac{K(\eta)\sqrt{1}}{m_o}\right]$$

où nous avons, à droite, remplacé les m par des m_o comme il est licite de le faire.

La longueur d'onde à prendre en compte dans les épures de réfraction est :

$$L = \frac{2\pi}{m} = \frac{2\pi}{m_o}\left(1 - \frac{\Delta m}{m_o}\right)$$

Autrement dit, la correction relative sur les longueurs d'onde sera : $- \frac{\Delta m}{m_o}$. Si cette correction était partout la même, la forme du plan de vagues ne serait pas changée et la correction resterait purement locale et sans intérêt pratique vu sa petitesse. Mais, en fait, cette correction relative varie d'un point à un autre et peut provoquer ainsi des déviations des orthogonales qui se répercutent sur l'ensemble du plan de vagues.

ORDRE DE GRANDEUR DES CORRECTIONS

Il est évidemment utile de se rendre compte de l'ordre de grandeur pratique des corrections $\frac{\Delta m}{m_o}$ ainsi introduites. Pour cela, nous examinerons quelques cas numériques.

a) - *Terme* : $-\frac{\alpha\gamma_1}{2Em_o}$

Un rayon de courbure des crêtes égal à la longueur d'onde est déjà relativement petit ; nous pouvons donc considérer que $\frac{1}{L}$ est une valeur forte pour γ_1 ; il en resulterait :

$$\frac{\gamma_1}{m_o} = \frac{1}{2\pi}$$

E croît très vite avec la profondeur mais par fonds faibles il vaut environ $2m_o h$. Pour des profondeurs relatives faibles $\frac{L}{h} = 20$, par exemple, on aurait :

$$E \not= 2mh = \frac{4\pi}{20}$$

Enfin α est rarement de plus de quelques pour-cent. Pour un fond naturel très raide, 10 % par exemple serait déjà très élevé. En définitive, on aurait donc :

$$-0,1 \times \frac{1}{2\pi} \times \frac{20}{4\pi} \not= -0,025$$

Des conditions extrêmement favorables étant réunies, on voit que la correction reste néanmoins assez minime (2,5 %).

On peut ajouter que les profondeurs relatives très faibles ne se rencontreront vraisemblablement que vers la fin de la course des houles, sur les plages où elles déferleront. Les modifications du plan de vagues n'ont plus alors pratiquement qu'un effet local puisque les changements d'orientation des orthogonales n'auront plus d'effets lointains.

En résumé, ce terme est vraisemblablement toujours négligeable.

b) - *Terme* : $\frac{\gamma_1^2}{8m_o^2}$

Dans l'hypothèse de courbure ci-dessus ($\gamma_1 = \frac{1}{L}$), ce terme vaut :

$$\frac{1}{8(2\pi)^2} = 0,003$$

Il est donc également très faible et sauf dans des travaux de grande précision, pourra aussi être le plus souvent négligé.

c) - *Terme* : $\frac{1}{2m_o K(\eta)\sqrt{1}} \frac{\partial^2}{\partial t^2} \left[\frac{K(\eta)\sqrt{1}}{m_o}\right]$

Si, pour simplifier l'étude de ce terme, nous supposons m_o (donc h) constant (ou au moins indépendant de η), nous savons que le crochet est proportionnel a un facteur constant (ou indépendant de η) près, à la demi-amplitude a [Cf. formules (2) et (12)]. Ce terme peut donc s'écrire :

$$\frac{1}{2m_o^2 a} \frac{\partial^2 a}{\partial \tau^2}$$

$m_o^2 a$ représente la courbure maximum de la surface libre de la houle de référence, le terme correctif peut donc s'ecrire :

$$-\frac{1}{2}\frac{\gamma_t}{\gamma_n}$$

γ_n et γ_t désignant les courbures de la surface libre des crêtes dans les directions de propagation et de front d'onde.

Ce rapport peut ne pas être négligeable car la réfraction peut provoquer le long d'un front d'onde des variations d'amplitude relativement brutales. γ_t pourra aussi prendre des valeurs relativement importantes au voisinage de points de diffraction ainsi que le montre l'exemple suivant.

Il s'agit en fait de l'étude expérimentale de la diffraction d'une houle en profondeur constante au passage d'une brèche de trois longueurs d'onde de large, pratiquée dans une jetée rectiligne indéfinie perpendiculaire à la direction de propagation incidente.

La figure 2a) représente schématiquement la disposition de l'essai. Par suite des phénomènes de diffraction, l'amplitude n'est pas

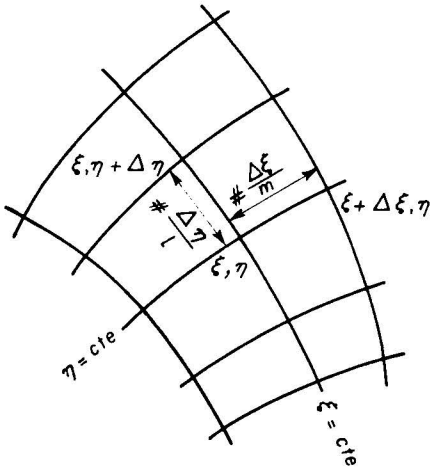

— Fig. 1 —

Signification géométrique de l et n dans le système de coordonnées ξ, η

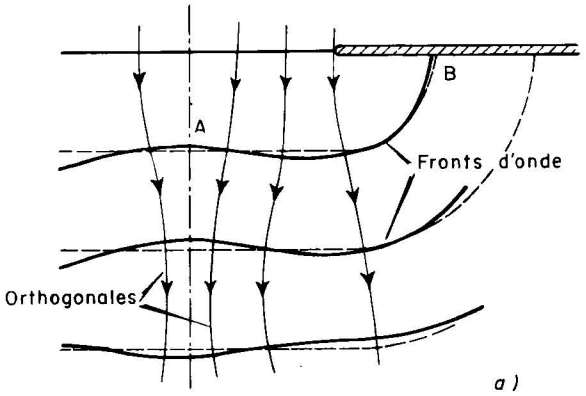

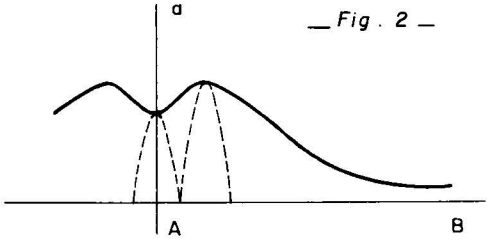

— Fig. 2 —

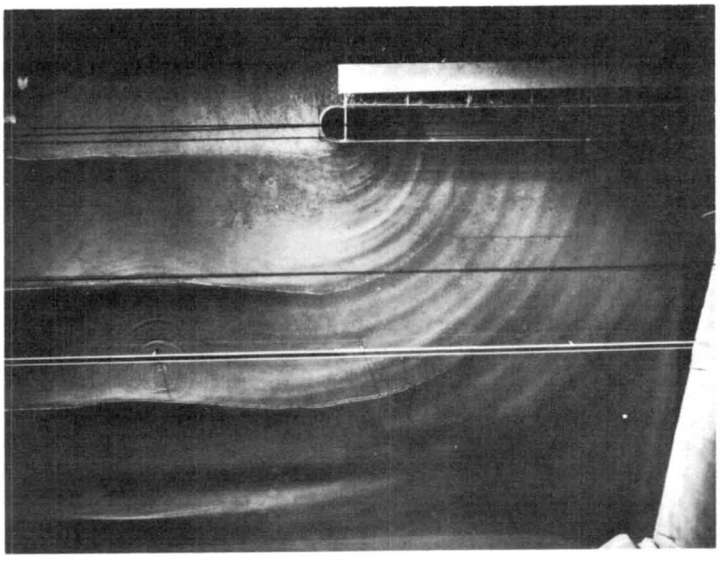

— Fig. 3 —

répartie uniformément le long des crêtes. Au contraire, au voisinage de la brèche, l'amplitude marque une diminution sensible au voisinage de l'axe et bien entendu des diminutions importantes vers les zones abritées. La répartition de l'amplitude mesurée le long de la crête AB (ayant parcouru une longueur d'onde depuis la brèche) est donnée à titre d'exemple dans la figure 2b).

Sur cette figure, sont également indiquées en pointillés, aux mêmes échelles verticales exagérées, les allures des sections de la houle par des plans verticaux perpendiculaires à la crête. On voit que les courbures γ_t quoique plus faibles que les courbures γ_n ne sont cependant pas d'un ordre de grandeur très différent si bien que l'on peut s'attendre à des corrections $\frac{\Delta m}{m_o}$ atteignant par exemple l'ordre de grandeur de 10 %.

Ainsi, les longueurs d'onde seront sensiblement plus faibles sur l'axe que de part et d'autre de celui-ci et les orthogonales convergeront vers l'axe ainsi que le montre la figure. Cette convergence aura pour effet de reconcentrer de l'énergie vers la zone axiale et ainsi, d'y augmenter l'amplitude aux dépens des zones voisines. Ainsi, une longueur d'onde plus loin, par exemple, l'amplitude aura au contraire un maximum local sur l'axe au lieu d'un minimum. L'inversion des courbures γ_t qui en résultera fera d'ailleurs également s'inverser la courbure des orthogonales.

Ainsi, l'introduction de la correction de longueur d'onde dans les calculs de diffraction permet, pour cet exemple, de prévoir des modifications de répartition d'énergie le long de la crête alors que la théorie usuelle n'aurait pu le faire. Ces modifications se font d'ailleurs sans enfreindre la loi de non-transfert d'énergie à travers les orthogonales mais celles-ci, au lieu d'être rectilignes comme la théorie usuelle le prévoit en profondeur constante, deviennent en fait des lignes plus ou moins sinueuses.

La photographie de l'essai, figure 3, permet de voir clairement l'essentiel des phénomènes décrits, y compris le renforcement d'amplitude dans l'axe à quelque distance de la brèche et l'inversion de la variation de la longueur d'onde le long du front.

LIMITES DE VALIDITE, COMPLEMENTS

Il importe de rappeler que toute cette théorie est basée sur la petitesse des éléments qui distinguent localement la houle réfractée de la houle de référence, soit α, β, γ_1, etc..., son domaine de validité sera donc celui où ces quantités seront faibles, c'est-à-dire au fond les cas que l'on pourrait appeler de réfraction modérée. Il faut exclure en particulier, les voisinages des croisements et accumulations d'orthogonales (focales, caustiques, etc...) qui, d'ailleurs, cesseraient de satisfaire à nos conditions qui excluent en fait toute anomalie de la transformation $\xi(x,y)$, $\eta(x,y)$.

D'une façon générale, tous les accidents "brusques" (voire discontinuités) de la propagation entrent dans le domaine de la diffraction et il est certain que l'ensemble du phénomène de diffraction à travers une brèche par exemple, ne saurait être *entièrement* étudié par une théorie de la réfraction telle que celle-ci. Il suffit de remarquer par exemple, qu'au voisinage des extrémités de la brèche, notre infiniment petit γ_1, par exemple, deviendrait infiniment grand.

En résumé, les corrections proposées ne nous permettent pas de traiter tous les cas de propagation et en particulier, pas ceux qui relèvent foncièrement de la théorie de la diffraction, mais elles permettent néanmoins d'étendre le domaine de validité des calculs de réfraction et d'augmenter la précision de certains résultats.

Il est peut-être utile de rappeler également que nous nous sommes limités à des théories du premier ordre par rapport aux amplitudes a de la houle. Nous avons donc la possibilité, au même degré de précision de "superposer" un nombre quelconque de houles de fréquences identiques ou différentes. Par contre, nous n'utilisons qu'une théorie approchée. En particulier, pour les applications aux calculs de réfraction, il pourrait être souhaitable d'ajouter aux corrections données ici celles qui résultent de l'importance de la courbure - Cf. référence [2]. La discussion complète de cette nouvelle "correction" nous entraînerait trop loin pour le cadre de la présente étude.

REFERENCES

[1] STUDY OF WAVE PROPAGATION IN WATER OF GRADUALLY VARYING DEPTH — F.BIESEL — GRAVITY WAVES — NAT.BUREAU OF STANDARDS — CIRCULAR 521, pp.243-253.

[2] REMARQUES SUR LA CELERITE DE LA HOULE IRROTATIONNELLE EXACTE AU TROISIEME ORDRE — F.BIESEL — LA HOUILLE BLANCHE N° 3 — MAI-JUIN 1951, pp.414-416.

Chapter 5

BORE INCEPTION AND PROPAGATION BY THE NONLINEAR WAVE THEORY

Michael Amein
Assistant Professor of Civil Engineering
North Carolina State of the University
of North Carolina at Raleigh

ABSTRACT

The integration of the equations of the nonlinear shallow-water theory by a finite difference scheme based on the method of characteristics is programmed for digital computers. In the program, the equations of the bore propagation are coupled to the equations of the nonlinear theory, and thus a procedure for predicting the motion of the entire wave, including the bore, is established. Waves of irregular shape and experimental data are treated by an iterative method. Laboratory experiments on the inception and propagation of bores also are presented.

INTRODUCTION

The theory of waves of small amplitude, which has been the basis for the classical studies of ocean waves, predicts an infinite wave amplitude at the shoreline. The shallow-water theory, on the other hand, presents no such difficulty, and is more appropriate for the study of waves near the coast. However, before a strong case for the shallow-water theory can be established, it is desirable that (a) a method of solution for its routine application be developed and (b) fairly good agreement between the theory and observation be shown. The purpose of this paper is to present the results of an effort made to achieve these objectives. The principles for obtaining the solutions of the equations of the nonlinear shallow-water theory on a digital computer are described. It is shown that by using an iterative method, it is feasible to feed experimental and field data into the computer program. Finally, experiments of an exploratory nature are described and the results of the computed and experimental values are compared.

THEORY

The equations of the nonlinear shallow-water theory in two-dimensional flow are

$$(\partial/\partial x)[u(h + \eta)] + (\partial\eta/\partial t) = 0 \qquad (1)$$

$$(\partial u/\partial t) + (u\partial u/\partial x) = -(g\partial\eta/\partial x) + (1/\rho)(\partial\tau/\partial x) \qquad (2)$$

In these equations, the x-axis is taken along the bottom, h is the depth of water, η is the water surface elevation above the steady-state position, ρ is the water density, and τ is the shear stress along the bottom. The derivation of these equations is given by Stoker (1957). In (2), the last term on the right is added to the corresponding inviscid equation to take care of the friction effects. In the terms of the friction slope S_f, $(1/\rho)(\partial\tau/\partial x) = gS_f$. (1) and (2) are the equations of the first-order shallow-water theory in which it is assumed that the pressure distribution is hydrostatic or that the vertical component of the acceleration has a negligible effect on the pressure. Friedrichs (1948) has shown that by using a perturbation scheme higher-order theories may be developed from the hydrodynamical equations. In a higher-order theory, the vertical acceleration may not be neglected and the pressure distribution need not be hydrostatic. This presentation, however, is only concerned with the first-order nonlinear theory.

Equations (1) and (2) constitute a system of first-order hyperbolic equations. In such systems, smooth solutions do not necessarily exist for all time; after a finite time a smooth solution may cease to be smooth and later tend to a discontinuity that may behave quite differently from the smooth solution (Jeffrey and Taniuti, 1964). Physically, it is implied that the wave may develop a bore and the propagation of the bore will not be given by the system of equations (1) and (2). The bore speed, however, can be determined by the application of the momentum principle.

METHODS OF SOLUTION

Analytical solutions of the nonlinear equations are seldom known. Finite difference methods are therefore used to obtain numerical solutions. A survey of these methods is given by Forsythe and Wasow (1960). The numerical methods for the solution of hyperbolic equations may be classified broadly into (a) finite difference schemes using regular networks and (b) the method of characteristics. The first method employs fixed space and time intervals. It has been applied by Stoker and his associates to the movement of floods in rivers (Stoker, 1957) and by Keller et al. (1960) for determining the change in bore height and speed as it advances into nonuniform flow. However, as yet, no way has been found to predict the development of a bore by this method.

The second method is based on the characteristics of the differential equations (1) and (2). Because these equations are hyperbolic, the characteristics are real and numerical methods utilizing the characteristics have been developed.

METHOD OF CHARACTERISTICS

The solution of equations (1) and (2) may be given by the intersection of the two sets of positive and negative characteristic curves. The slope of the positive characteristic is given by

$$dx/dt = u + c \tag{3}$$

where c is the wave clerity given by $c = g\sqrt{h + \eta}$. The slope of the negative characteristic is given by

$$dx/dt = u - c \tag{4}$$

Furthermore,

$$d(u + 2c - mt) = 0 \tag{5}$$

on a positive characteristic, and

$$d(u - 2c - mt) = 0 \tag{6}$$

on a negative characteristic, where $m = -gS - gS_f$ and S is the rate of change of depth with distance x. The derivation of equations (3) through (6) and a description of the underlying principles are given by Stoker (1957). A critical analysis of the method of characteristics is given by Le Mehaute (1963). Wave transformation in shoaling water has been investigated by an approximate analytical method based on characteristics by Kishi (1963). Equations (3) through (6) serve as the basis for numerical computations by the method of characteristics. These four ordinary differential equations replace the system of partial differential equations (1) and (2). Once the initial values are known, solutions may be obtained step by step.

The required initial values may be prescribed in several ways. But for free surface flows, it is recommended that the initial values be given as (a) the values of u and c as functions of x at time $t = t_0$ and (b) the values of c as functions of time t at a, given $x = X_0$. The first set is known from the steady-state conditions prior to the arrival of the wave and the second set is known from a knowledge of the variation of the water surface elevation with time at $x = X_0$.

The values of u, the particle velocity, need not be prescribed at $x = x_0$ as a function of time. This is a fortuitous circumstance so far as experimental data are concerned, because the particle velocity is difficult to measure. But the choice of initial values in the manner described above rests on a deeper principle, the choice being influenced by the role of the negative characteristics. The negative characteristics issued from the leading wave elements interact with and modify the original wave (Ho, 1962). Stoker (1957) has suggested, in this context, that the values of either u or c, but not both, should be prescribed as initial values. An analogous situation has been observed in flood waves in rivers where the stage discharge curve may have a loop. At a given location, for the same surface elevation, the water velocity at the wave front may be different from that at the rear of the wave. The water velocity at the rear is subjected to modification by the negative characteristic issued from the wave front. This may be called the "backwater effect." With the choice of the initial values in the recommended manner, the "backwater effect" is taken into consideration.

The method of characteristics has an inherent advantage in that it provides insight into the physical phenomenon under study. Thus, the inception of a bore is predicted by the intersection of adjacent positive characteristics. The bore speed is given by (Stoker, 1957)

$$V = \sqrt{g(h + \eta)(2h + \eta)/2h} \tag{7}$$

The bore propagation is determined by coupling the bore equation (7) to the equations of the shallow-water theory. In terms of the bore strength defined by

$$M = V/\sqrt{g(h + \eta)} \tag{8}$$

it is found that (Keller et al., 1960)

$$V/\sqrt{gh} = M(2M^2 - 1) \tag{9}$$

$$c/\sqrt{gh} = \sqrt{2M^2 - 1} \tag{10}$$

and

$$\frac{1}{h}\frac{dh}{dM} = \frac{-4(M + 1)(M - 0.5)^2(M^3 + M^2 - M - 0.5)}{(M - 1)(M^2 - 0.5)(M^4 + 3M^3 + M^2 - 1.5M - 1)} \tag{11}$$

The changes in bore height and speed as the bore advances into nonuniform flow are calculated from (11). If a positive characteristic should meet the boreline at a later time, then a new value for the bore strength M should be calculated. The new value of M should be taken from the characteristic that intersects the boreline.

An alternate method for the calculation of the bore propagation based on the continuity and momentum, as used in hydraulics, is given by Freeman and Le Mehaute (1964).

NUMERICAL PROCEDURE

The integration of the equations of the shallow-water theory by the method of characteristics may be performed very efficiently on a digital computer. In this method, the shallow-water theory is represented by the ordinary characteristic differential equations (3) through (6), rather than the original partial differential equations (1) and (2). The numerical solutions of equations (3) through (6) are obtained by replacing the differential equations by the corresponding difference equations. Only the procedure for the investigation of irregular waves that develop a bore at the wave front and whose profiles are given by discrete point functions of the time will be described. An iterative method, perhaps feasible only in machine calculations, constitutes a key element of the computational procedure. A study on regular waves and waves developing bores at intermediate points on their profiles and the wave runup is currently under way for the U.S. Naval Civil Engineering Laboratory and will be reported on at a later date.

The solution of the equations of the shallow-water theory may be presented in the form of sets of values of flow quantities from which a network of characteristics could be plotted on the x,t plane. The procedure for the determination of the network, in accordance with the discussion on the initial values, is patterned after de Prima (Stoker, 1948). Essentially, it consists of first establishing the initial characteristic depicting the motion of the wave front and then issuing the negative characteristics from it. The values of c on the t-axis are given at discrete points as input data. By introducing these values at appropriate points in the computations, the network is extended to cover the pertinent portion of the x,t plane. Brief descriptions of the various phases of the procedure are given as follows.

INITIAL CHARACTERISTIC

From (X_0,t_0) (Fig. 1), the initial characteristic C_0 is drawn first. This is a positive characteristic, and the values of u and c for C_0 are known from the steady-state flow

conditions. If an appropriate time interval, δt, is chosen on the characteristic segment P_1P_2, then

$$t(P_2) = t(P_1) + \delta t \tag{12}$$

The value of x at P_2 is calculated from equation (13), which in turn is obtained from the finite difference forms of (3) and (5):

$$x(P_2) = x(P_1) + [u(P_1) + c(P_1) - 0.5m(P_1)\cdot\delta t]\cdot\delta t \tag{13}$$

INTERIOR CHARACTERISTICS

For purposes of illustration, let it be assumed that the calculation has progressed to the line P_1J_1, with all the characteristics to the left of this line being known. Therefore, at each of the node points $P_1,Q_1,R_1,\cdots,J_1$, the slopes of the positive characteristics are given by (3). The values of x, u, and c are also known at P_2, since it lies on the initial characteristic. Then a negative characteristic can be drawn from P_2 to intersect a positive characteristic drawn from Q_1, the point of intersection being Q_2. The finite difference forms of (3) through (6) provide four simultaneous algebraic equations from which the four unknown quantities u, c, t, and x at Q_2 can be calculated. The computation then proceeds to R_2, S_2, and on up to K'. If K' coincides with K, one of the discrete points on the t-axis given as input data, then one chain of operation is completed. To advance the computations to the right, storage locations in the machine occupied by $P_1,Q_1,R_1,\cdots,J_1$ will be taken over by $P_2,Q_2,R_2,\cdots,J_2$, and the storage locations occupied by $P_2,Q_2,R_2,\cdots,J_2$ will be vacated and reserved for the results of the next chain. The maximum number of storage locations required to handle this part of the program is that which can accommodate the computations for a single chain. By conducting the computations in a sequence of chains and recording the results after each chain, large outputs may be obtained from a relatively small computer.

If K' does not correspond to a discrete point K given by the input data, an iterative method will be used to pass a negative characteristic through K.

ITERATIVE METHOD

Let it be assumed that the difference between the values of t(K') and t(K), where K is in the neighborhood of K' and

its position is fixed by the input data, is larger than a prescribed tolerance interval. Then, the value of δt in (12) will be adjusted, and the chain of operations on $P_2, Q_2, R_2, \cdots, K'$ will be resumed. The operation will be repeated as many times as necessary until the difference between the values of t(K') and t(K) lies within the prescribed tolerance interval.

BORE PROPAGATION

From a computational viewpoint, the inception of the bore is indicated when two adjacent points on a negative characteristic coincide with each other. The slope of the boreline on the x,t plane is given by

$$dx/dt = V + u_0 \qquad (14)$$

where u_0 is the water velocity in the water ahead of the bore. The bore path is then determined step by step, using a procedure similar to Freeman and Le Mehaute's (1964). The changes in the bore speed between the consecutive intersections of the positive characteristics with the bore path are taken from the numerical solution of (11).

COMPUTER PROGRAM

The integration of the equations of the nonlinear shallow-water theory by the method of characteristics, together with the determination of the inception and propagation of the bore, has been programmed in FORTRAN. The program includes the iterative method for the treatment of experimental data for irregular waves. A conceptual flow diagram is given in Fig. 2.

The following input data are required for each run:

h_1, the initial steady-state depth at X_0
N, the number of points taken on the wave on the t-axis
n, the coefficient of friction in Manning's formula
S, the rate of change of depth in the x-direction
T, the final value of time on the t-axis
t_0, the initial value of time on the t-axis
u_1, the initial steady-state velocity at X_0
X_f, the value of x at the downstream station
X_0, the value of x at the upstream station
Δ, the time interval between sonsecutive points on the t-axis
Values of c at X_0 as functions of time.

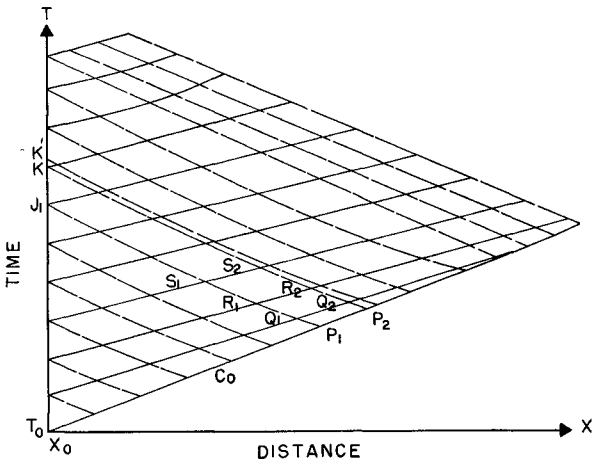

FIG. 1 --NETWORK OF CHARACTERISTICS

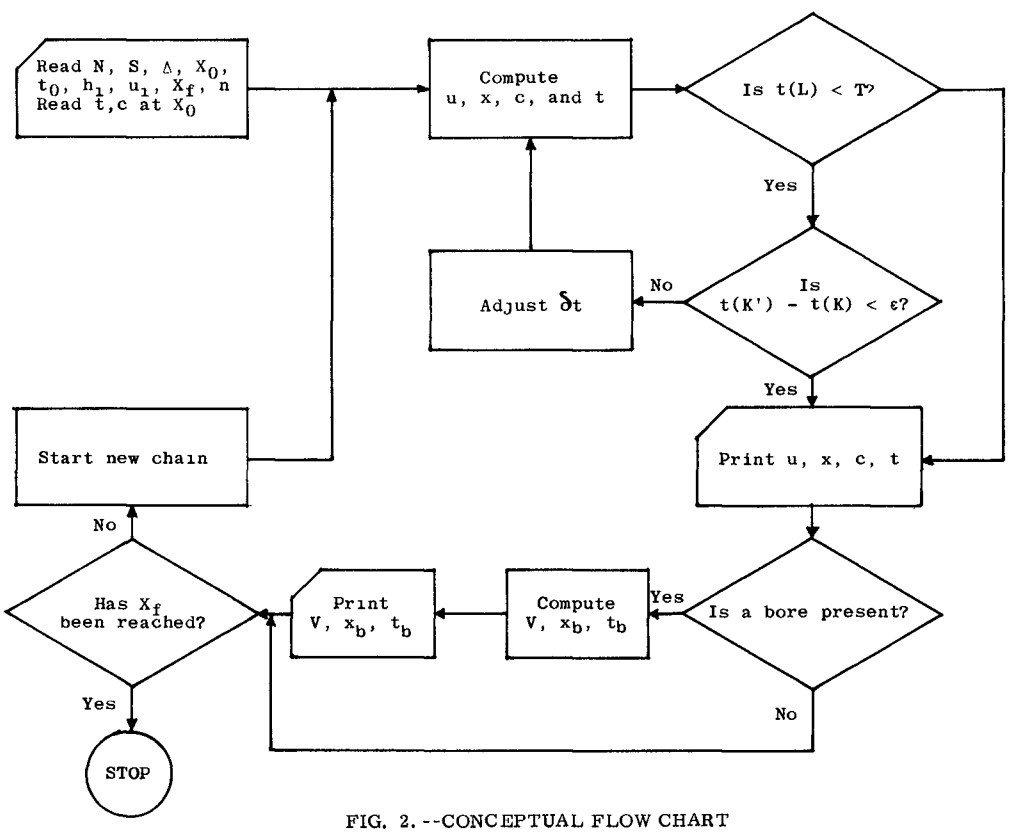

FIG. 2. --CONCEPTUAL FLOW CHART

The output information is printed out in the form of tables of values of depth, distance, time, water velocity, wave celerity, bore speed, and bore position.

EXPERIMENTS

Experiments of an exploratory nature involving waves of irregular shape were performed in a glass-walled rectangular channel. The disturbances were generated by manipulating the valve controlling the flow into the channel. Two resistance probes, one near the upstream end and the other farther downstream, were installed in the channel. The probes operate on the principle that the resistance across two wires immersed in water is a function of the depth of immersion. The probe outputs, representing the variation of the water surface elevation with time, were amplified and recorded on oscillograph recorders. The principles and details for this type of instrumentation are described by Wiegel (1955).

To obtain a comparison of the experimental and computed values, the surface elevation data as recorded at the upstream probe were fed into the computer program, from which the theoretical data at the downstream probe could be obtained. Some of these results are shown in Figs. 3, 4, and 5. In Figs. 3 and 4, the water is initially at rest. In Fig. 5, the flow is initially steady but nonuniform and accelerating in the x-direction. An examination of these figures indicates that there is excellent agreement between the computed and experimental values for the time of arrival of the bore. Perhaps the conditions at the bore front caused by the pile-up of the water there may not be faithfully represented by the theory in its present form. The computed wave behind the bore is seen to conform in general outline to the recorded wave. Because of the difficulty of maintaining constant calibration curves for the probes, the experimental results should be considered to be providing qualitative evidence in support of the theory for the portion of the wave behind the bore. It is felt that more extensive experiments will favor the establishment of the nonlinear shallow-water theory as a powerful tool for the study of wave processes near the coast.

CONCLUSION

A finite difference scheme for the solutions of the equations of the nonlinear shallow-water theory by the method of characteristics for digital computer applications is described. The significance of the proper method for choosing the initial values is discussed. The computer program includes the test for the inception of bores and methods for the calculation of bore speed and height. The use of an iterative method makes it possible to treat waves of irregular arbitrary shape. Exploratory experiments on the inception and propagation of bores are also presented.

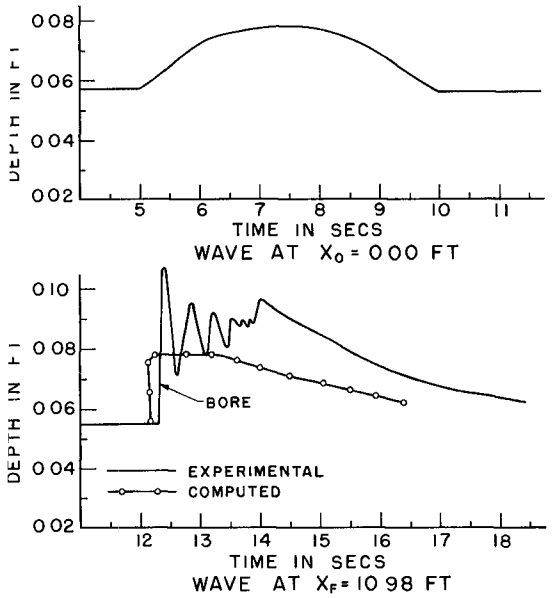

FIG 3 --BORE PROPAGATION IN WATER OF CONSTANT DEPTH TYPE A

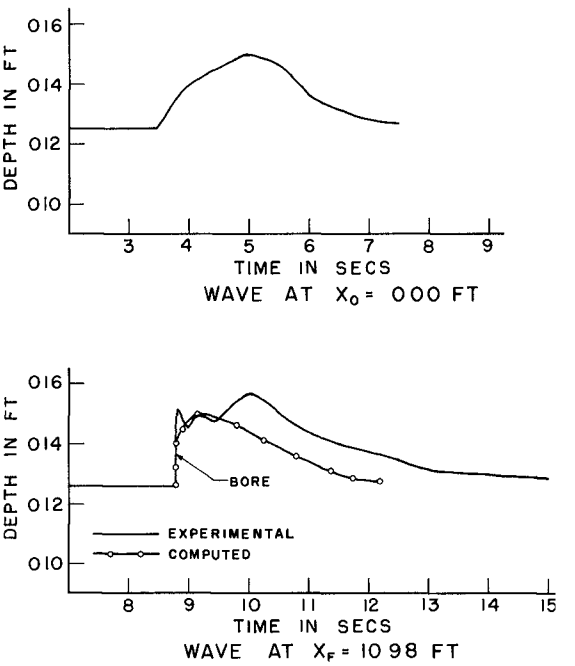

FIG 4 --BORE PROPAGATION IN WATER OF CONSTANT DEPTH TYPE B

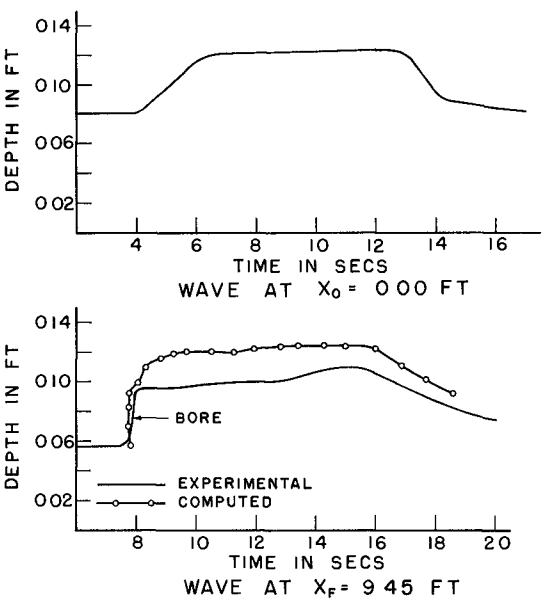

FIG 5 --BORE PROPAGATION IN NONUNIFORM FLOW

The accuracy, economy, and speed of the digital computer have eliminated the extensive calculations involved in integrating the equations of the nonlinear shallow-water theory. It is hoped that the feasibility of successful computer programming will encourage the greater use of the nonlinear theory by the coastal engineer. However, further research, with improved equipment and instrumentation, is needed to establish the range of validity of the theory so that it could be applied with confidence to predict the wave motion near the coast.

ACKNOWLEDGEMENTS

This research was initiated by a grant from the Ford Foundation. Portions of the computer program were developed in conjunction with a study on long-period waves for the U.S. Naval Civil Engineering Laboratory, Bureau of Yards and Docks, under Contract NBy-32236. Recorders were supplied by the Department of Engineering Research at North Carolina State. The experimental work was performed by J. G. Howe.

REFERENCES

Forsythe, G. E., and Wasow, W. R. (1960). Finite-difference methods for partial differential equations: John Wiley & Sons, New York.

Freeman, J. C., and Le Mehaute, B. (1964). Wave breakers on a beach and surges on a dry bed: J. Hydraulics Div., Proc. Am. Soc. Civ. Eng., vol. 90, No. HY2, pp. 187-216.

Friedrichs, K. O. (1948). On the derivation of the shallow water theory: Communications on Appl. Math., vol. 1, pp. 81-85.

Ho, D. V. (1962). On problems of non-uniform bore and shock propagation: Unpublished doctoral thesis, Brown University, Providence, Rhode Island.

Jeffrey, A., and Taniuti, T. (1964). Non-linear wave propagation: Academic Press, New York.

Keller, H. B., Levine, D. A., and Whitham, G. B. (1960). Motion of a bore on a sloping beach: J. Fluid Mech., vol. 7, pp. 302-316.

Kishi, T. (1963). Transformation, breaking and run-up of a long wave of finite height: Proc. 8th Conf. Coastal Eng., pp. 60-76.

Le Mehaute, B. (1963). On non-saturated breakers and the wave run-up: Proc. 8th Conf. Coastal Eng., pp. 77-92.

Stoker, J. J. (1948). The formation of breakers and bores: Communications on Appl. Math., vol. 1, pp. 1-87.

Stoker, J. J. (1957). Water waves: Interscience, New York.

Wiegel, R. L. (1955). Parallel wire resistance wave meter: Proc. First Conf. Coastal Eng. Instruments, pp. 39-43.

Chapter 6

WATER WAVE EQUIVALENT OF MACH-REFLECTION

R. L. Wiegel
Professor of Civil Engineering
University of California
Berkeley, California

SUMMARY

Periodic (shallow water and transitional water) and solitary water gravity waves do not reflect from a wall in the manner commonly supposed, when the angle between the direction of wave advance and the wall is less than about 35 to 45 degrees. The wave front bends near the wall, becoming normal to the wall, with a small reflected wave. For angles less than about 20 degrees the reflected wave becomes almost negligible. The portion of the wave near the wall (called the Mach-stem in air blast waves) increases in height as the wave continues to move along the wall. Once the Mach-stem is formed, it will continue to grow even when the wall is bent around through almost 90 degrees; for periodic waves a Mach-reflected wave also develops. The Mach-stem is insensitive to undulation of the wall. Results of studies of this phenomenon in the laboratory are presented, together with some observation of its occurrence in the ocean. The importance of this phenomenon to the study of tsunami action at Hilo, Hawaii, is presented.

INTRODUCTION

On occasions, tsunamis in certain coastal regions have exhibited characteristics which do not seem to be accounted for when they are studied by means of the commonly used types of refraction drawings, diffraction calculations and run-up theory and measurements. It was suggested to the author by Professor John D. Isaacs in 1956 that this might be due to something analogous to the Mach-reflection phenomenon in acoustics. A number of aspects of this phenomenon have been investigated experimentally by several graduate students under the author's direction (Perroud, 1957; Chen, 1961; Sigurdsson and Wiegel, 1962; Nielsen, 1962). The first tests were made using a solitary wave, as it was believed that this was most nearly the water wave equivalent of a shock wave in compressible flow.

The first experiments were performed with a solitary wave incident to an oblique, vertical, impervious, smooth barrier; it was found that the phenomenon did exist. Later, tests were performed with periodic waves, and the Mach-reflection also occurred for these for values of $L/d >$ about 2 (where L is the wave length and d is the water depth). Several experiments were performed with types of models which were of importance to coastal engineering problems. One of these was an undulating vertical wall, which was found to affect only the small details of

the wave motion. A second model consisted of a curved, vertical impervious barrier (similar to curved vertical wall jetties or breakwaters). Experiments in the laboratory showed that once the Mach-stem formed, it became so strong that it ultimately became independent of the incident wave.

Finally, experiments were made with an undistorted model of the bay at Hilo, Hawaii, and a phenomenon was found to exist which had the appearance of a Mach-reflection.

The only theory available on the Mach-reflection, to the author's knowledge, is due to Lighthill (1949), and it is not useful in its present form in the solution of water gravity wave problems.

MACH-REFLECTION, SOLITARY WAVE

It is usually assumed that a wave which encounters an obstacle will either reflect from it, be dissipated, or both. In certain cases, however, a third possibility exists: the crest of the wave near the wall may bend, becoming normal to it, with the energy density adjacent to the wall increasing as the wave moves along. This phenomenon is known as a Mach-reflection.

Perroud (1957) made a series of tests in the laboratory of the reflection of a solitary wave from a straight, vertical, impervious wall. He found that three types of patterns occurred, with one of the patterns being a special case of one of the others. The critical angle of incidence, i, separating these two types of patterns appeared to be 45 degrees (Chen, 1961, found the critical angle to be between 35 and 40 degrees).

For incident angles (the angle between the direction of wave advance and the wall) greater than 35 to 45 degrees the reflection pattern is "normal" (Fig. 1). The incident and reflected waves are slightly disturbed near the wall, but the angle of reflection is equal to the angle of incidence, and the reflected wave height is only slightly less than the incident wave height. However, the reflected wave is followed by a trough, except for the case in which the angle of incidence is 90 degrees. It is interesting to note that in the latter case the wave height at the wall was 20 percent higher than twice the incident wave height.

For angles of incidence less than about 35 to 45 degrees the reflection appears to be of the type called a Mach-reflection in acoustics. When the angles of incidence are less than about 20 degrees, the wave crest bends, becoming normal to the wall, and no reflected wave appears. When the angle of incidence is greater than 20 degrees but less than 40 to 45 degrees, three waves are present, the incident wave I, a Mach-reflected wave R, and the Mach-stem wave M, the width of which grows as the wave moves along the wall. The angle δ ($\delta = r - i$) depends upon the angle of incidence in the manner shown in Fig. 2. The reflected wave height is smaller than the incident wave height, and the angle of reflection (r) is greater than the angle of incidence. The height of the Mach-stem portion is greater than the incident wave height and is at its maximum at the wall. The Mach-reflected and Mach-stem waves are followed by a trough.

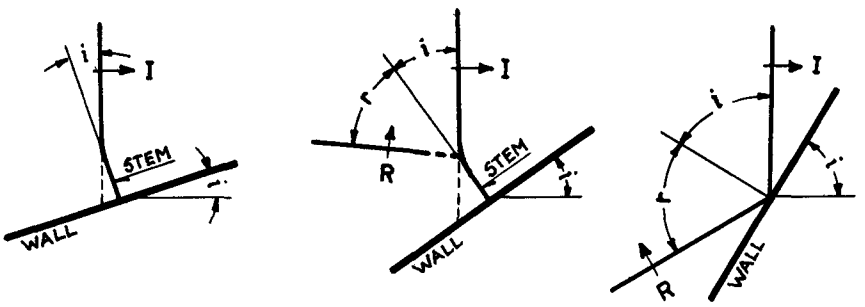

(A) $i < 20°$ — Mach-stem without reflection

(B) $20° < i < 45°$ — Mach-stem with reflection

(C) $i > 45°$ — Regular reflection

FIG 1. REFLECTION OF A SOLITARY WAVE WITH VERTICAL BREAKWATER.

I : Incident wave
R : Reflected wave

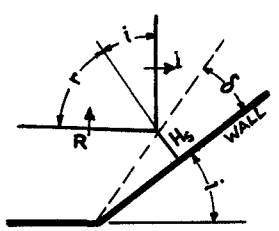

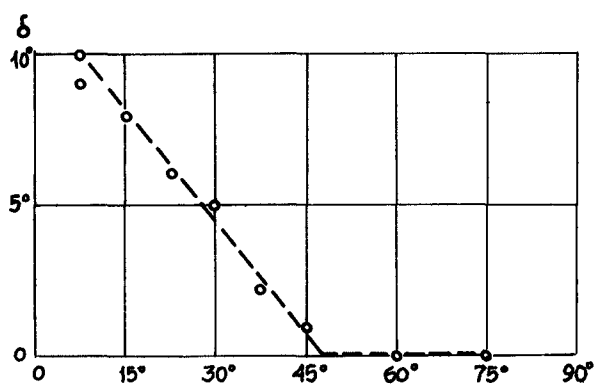

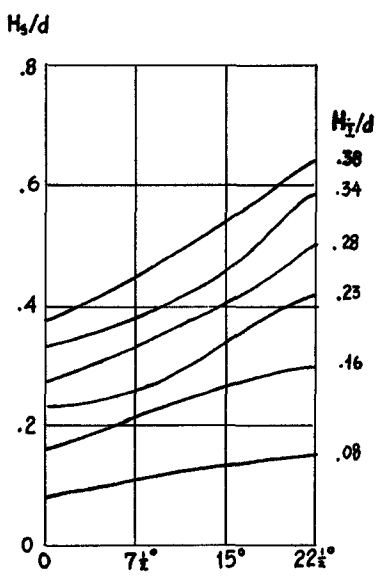

Angle of incidence i

FIG 2a. STEM-ANGLE δ FOR SOLITARY WAVE. EACH PLOT IS AN AVERAGE VALUE FOR 6 DIFFERENT WAVE HEIGHTS. (H_I/d: .05-.43). Water depth d = 0.132 ft.

FIG 2b. HEIGHT OF STEM-WAVE FOR SOLITARY WAVE. Water depth d = 0.132 ft

(From Perroud, 1957)

In practice, most structures and coastal areas have slopes. Experiments made with smooth impermeable slopes (Chen, 1961) showed that for nearly vertical walls the phenomenon looked the same as for the case of a vertical wall (β = 90 degrees). As the wall slope (β) was decreased a large horizontal eddy formed over the slope, and as the slope was decreased further, the wave broke along the slope (Fig. 3); the slope angle at which this occurred was found to be dependent upon the angle of incidence. The values of i and β which determine whether or not the wave breaks over the slope are shown in Fig. 4, for a specific value of H/d. For small values of H/d (where H is the incident wave height and d is the water depth) no break occurred when $\beta \approx 90$ degrees. For intermediate values of H/d it was not possible to determine whether or not a wave would break because of the small size of the tank. In regard to this, Friedlander (1946) has shown theoretically for a sound pulse incident to a wedge (less than 90 degree wedge) that the pulse has to travel a considerable distance along the wedge before the pressure at the wedge builds up to its maximum value of twice the pressure of the incidence pulse, and that the smaller the wedge angle (hence, the smaller i) the greater this distance will be. For example, for a 30-degree wedge the pulse must travel nearly 60 pulse lengths to build up to about 90 percent of its final value.

Waves incident to an overhanging wall ($\beta > 90$ degrees) behaved in a manner similar to a vertical wall except that the stem did not grow with distance from the start as was found by Perroud for the vertical wall. At least, the width of the Mach-stem did not appear to grow within the limits of the experimental facilities.

The region of i and β for which various types of reflections occur are shown in Fig. 5.

The author (Wiegel, 1963) has observed ocean waves with the appearance of a Mach-stem occurring along a curved structure, and this led to another series of laboratory studies. A vertical wall breakwater was made of a piece of sheet metal. A 2 ft long straight section, starting at one wall of the tank, was placed at a 12 degree angle with the wall (Sigurdsson and Wiegel, 1962). This straight section was connected tangentially to a 66 degree segment of a circle of 3.33 ft radius, to make a total change in direction of 78 degrees (Fig. 6). Tests made with a barrier with a smooth wavy surface (corrugated aluminum, with corrugations 0.021 ft deep by 0.135 ft long, about 1/2 and 3 times the incident wave height, respectively) and with a rough barrier showed similar results (Fig. 7). It was observed that the amplitudes at the barrier were greater in the hollows than in the ridges of the corrugations.

The essential feature that was determined from the series of tests just described is that once the Mach-reflection starts, with an angle of incidence less than the required value, the non-linear Mach-stem becomes so strong that it continues to move around the curved barrier, normal to the barrier, and near the end of the barrier becomes independent of the incident wave. In this region there were essentially two separate waves, the "incident wave" and the Mach-stem advancing at an appreciable angle (up to 90 degrees) to the "incident wave." These two waves were connected

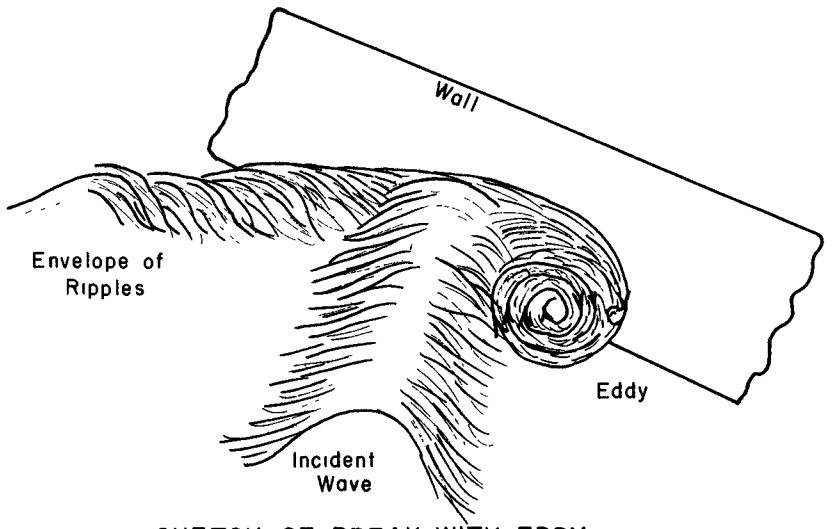

SKETCH OF BREAK WITH EDDY
FIGURE 3a

FIGURE 3b– WAVE BREAK

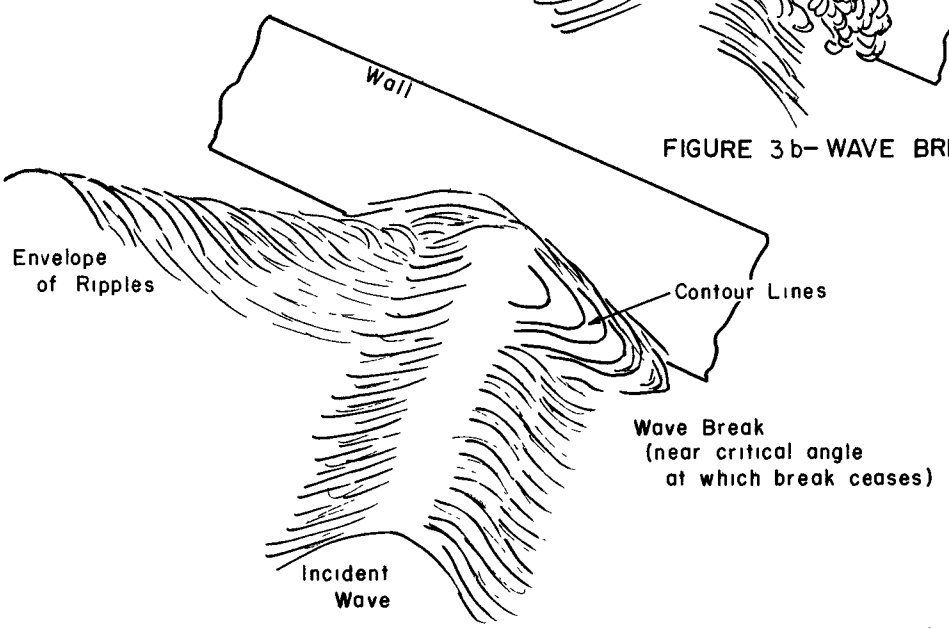

SKETCH OF BREAK WITHOUT EDDY
FIGURE 3c

(After Chen, 1961)

FIGURE 3 a,b,c

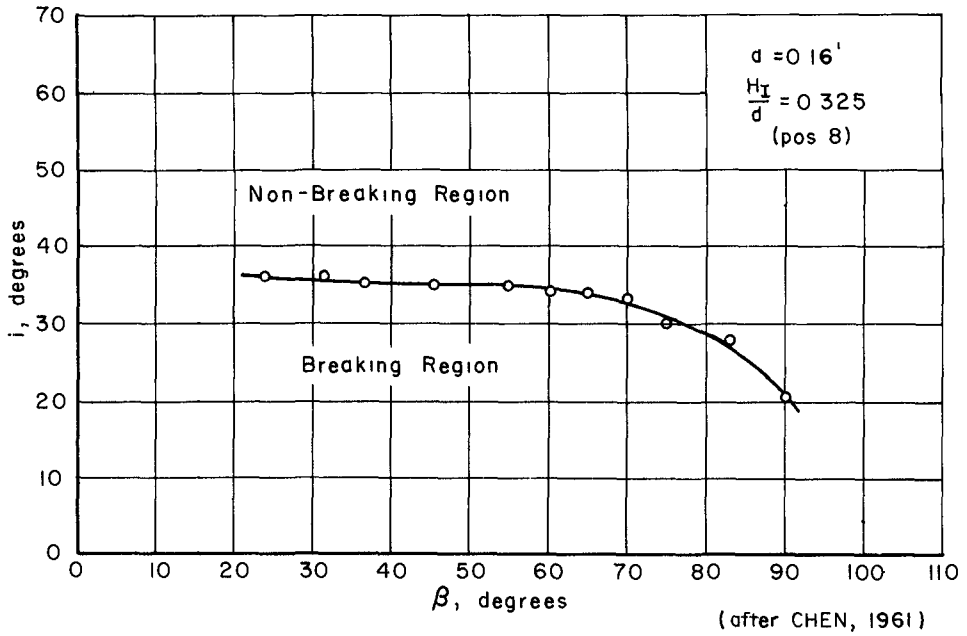

FIGURE 4 ANGLE OF INCIDENCE SEPARATING BREAKING AND NON-BREAKING REGIONS

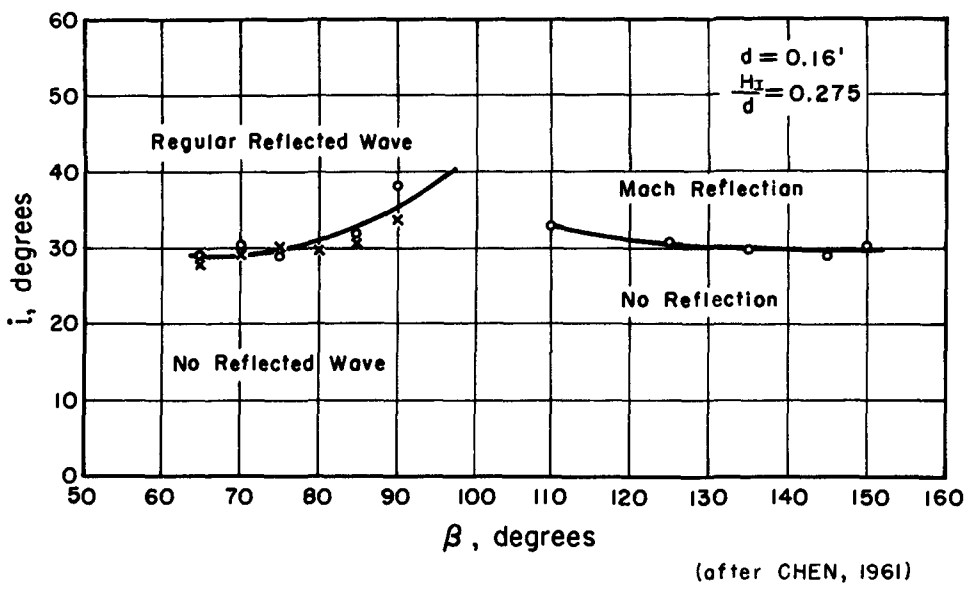

FIGURE 5 INCIDENT ANGLE i BEYOND WHICH REGULAR REFLECTED WAVE OCCURS FOR DIFFERENT SLOPES β, AND ι AT WHICH MACH REFLECTION STARTS FOR EACH NEGATIVE SLOPE ($\beta > 90°$).

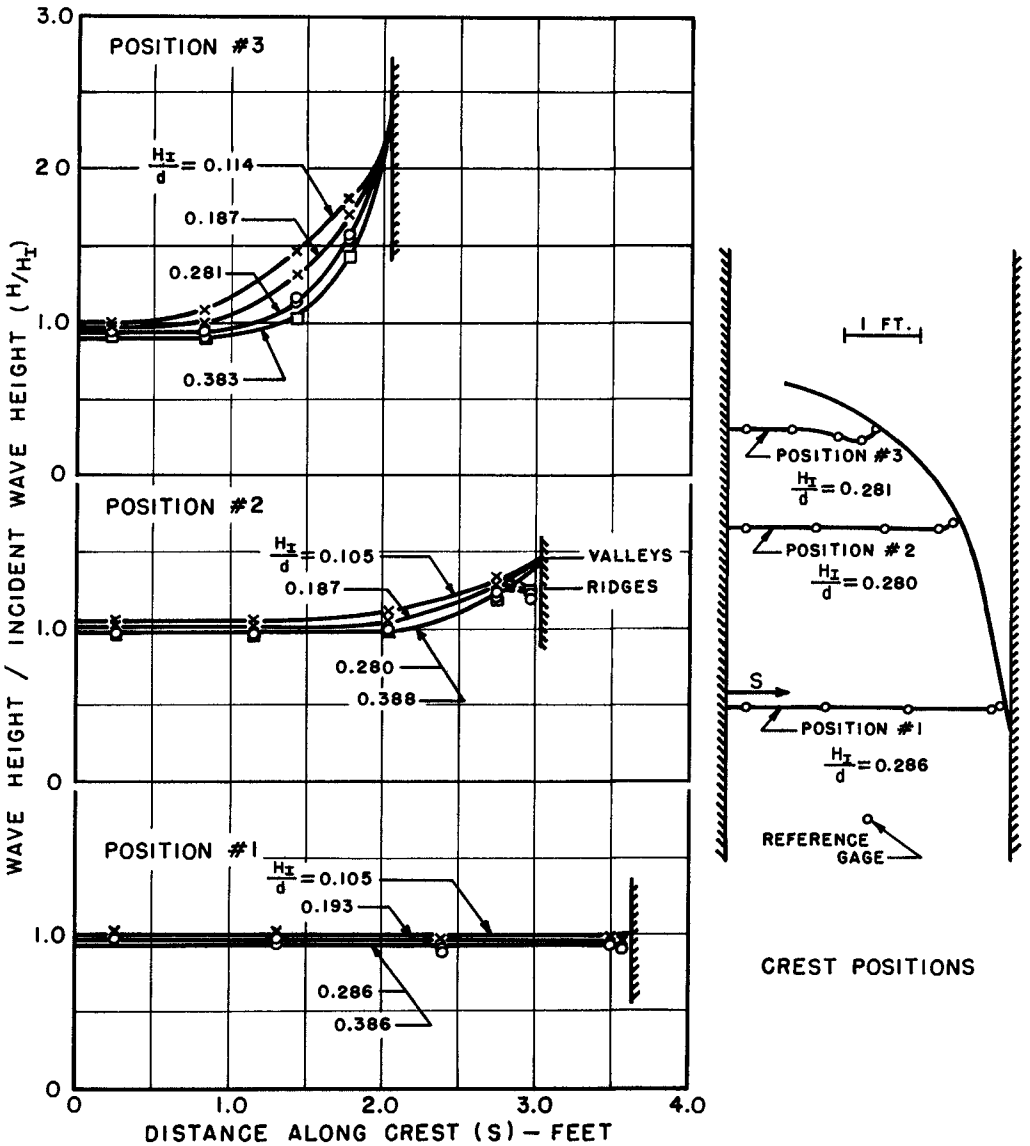

FIGURE 6. CREST POSITION AND CREST ELEVATION SERIES E

(From Sigurdsson and Wiegel, 1962)

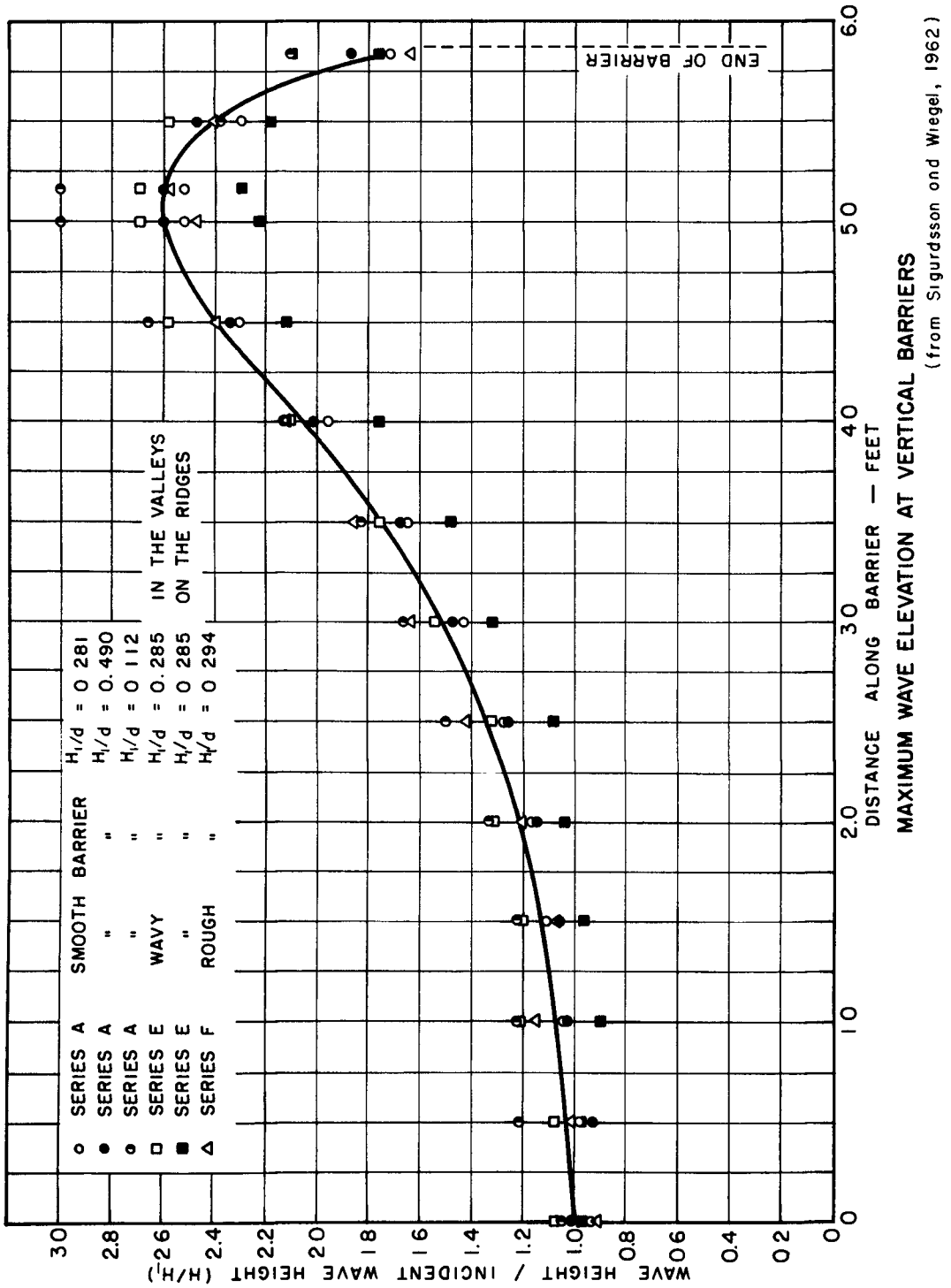
MAXIMUM WAVE ELEVATION AT VERTICAL BARRIERS
(from Sigurdsson and Wiegel, 1962)
WAVE HEIGHT / INCIDENT WAVE HEIGHT (H/H_I)
DISTANCE ALONG BARRIER — FEET
END OF BARRIER
SERIES A SMOOTH BARRIER H_I/d = 0.281
SERIES A " H_I/d = 0.490
SERIES A " H_I/d = 0.112
SERIES E WAVY " H_I/d = 0.285 IN THE VALLEYS
SERIES E " H_I/d = 0.285 ON THE RIDGES
SERIES F ROUGH " H_I/d = 0.294

FIGURE 7

by a transition zone, and in this zone the incident and stem waves were superimposed, and there was a considerable variation in the profile.

When a barrier was made of 3/8 inch gravel to the same plan as the impervious barrier, but with a 36 degree side slope, there was no indication of either a build up of wave amplitude at the barrier, or of a reflected wave.

MACH-REFLECTION, PERIODIC WAVES

The experiments described so far were for solitary waves, as the solitary wave is analogous to the single pressure impulse in acoustic waves in air. The phenomenon had been observed for periodic waves in some coastal areas, so it was known that it did exist in actual conditions for nearly periodic waves. In order to see whether or not it existed for deep water as well as for shallow water waves, a program of laboratory studies was undertaken (Nielsen, 1962).

The first series of tests were made in the same tank as the one used in the various tests described in the previous section. Most of the tests were made using the same water depth, 0.160 ft, but some tests were made in deeper water, 0.240 ft. It was found that for shallow water waves a Mach-stem formed which was similar to the one formed by the solitary wave. This was true even for waves in the transitional region, as can be seen in Fig. 8a in which the phenomenon is shown for an L/d of 4.9 for angles of incidence of 5, 10, 15, and 20 degrees. In these shadow photographs the dark lines are the wave crest, and the wider the "line" the higher the wave. In deep water a type of Mach-stem forms, but it occurs to the rear of the incident wave and is connected to the incident wave by a crest with a compound curve, as can be seen in Fig. 8b. In addition, a curved Mach-reflected type of wave also occurs which is similar in appearance to the Mach-reflected wave of a solitary wave when 20 degrees $< i <$ 35 to 45 degrees. It is different in that it locks in with the intersection of the Mach-stem and incident wave of the following wave. For deeper water waves, $L/d < 2$, it appears that the reflected wave gradually develops into something similar to a normal type of reflection pattern, except that there appears to be a small Mach-stem adjacent to the barrier. For example, as can be seen in Fig. 8c for $i > 5$ to 10 degrees, the more or less regular reflection pattern seems to be emerging, while for $i = 5$ degrees only the Mach-stem occurs.

It was found that the width of the Mach-stem increased as the wave moved along the barrier, as was the case for the solitary wave. It was found that the longer the wave length the greater the width for a given distance along the barrier; however, it was found that the solitary wave had the minimum width for a given distance, which is quite surprising as one normally thinks of a solitary wave having a long "length."

The ratio of wave height of the stem at the barrier to the incident wave height, H/H_I, was a complicated function of distance along the barrier, water depth and wave length. In general, for a given angle of incidence it increased up to a certain distance along the barrier, and

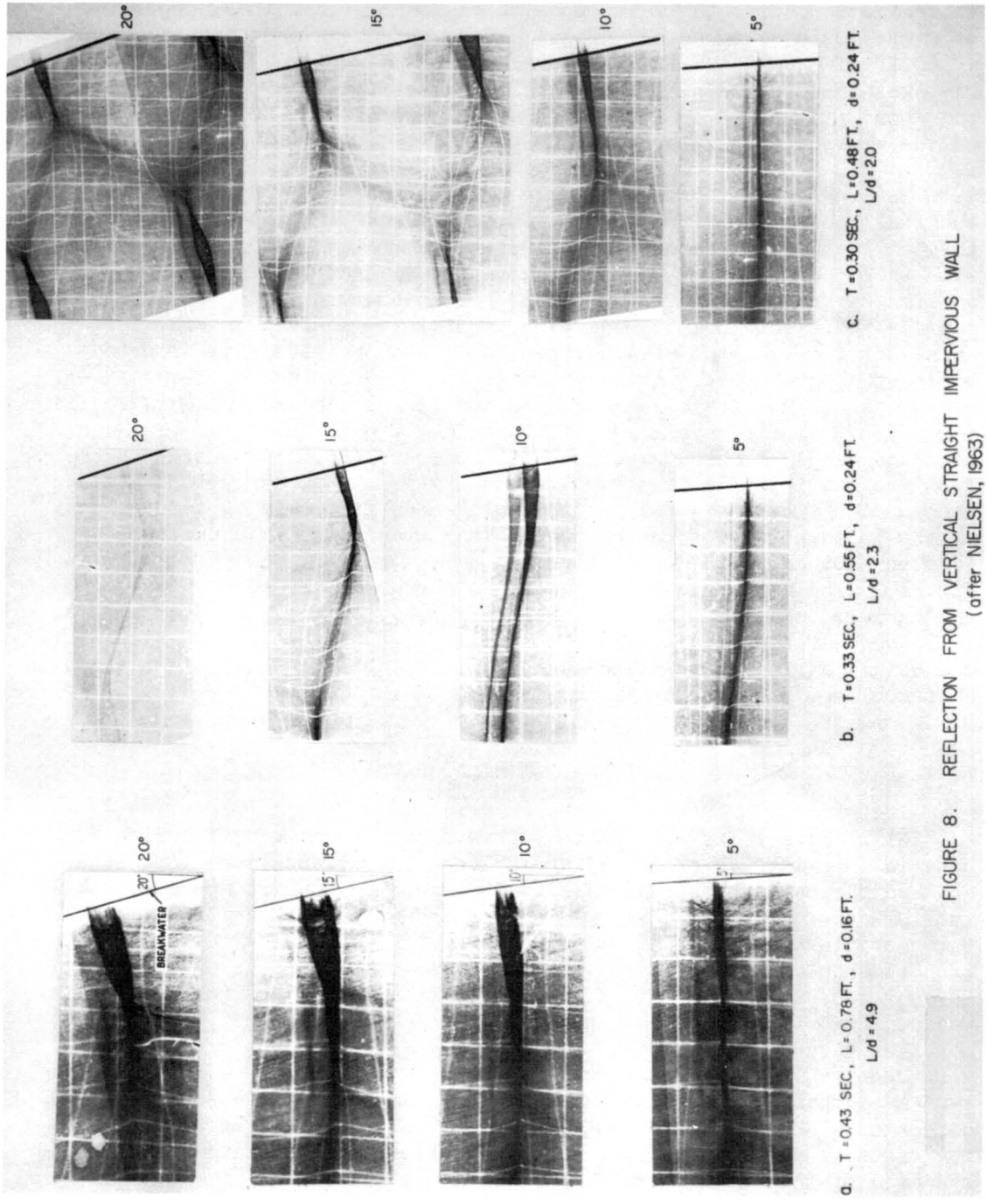

FIGURE 8. REFLECTION FROM VERTICAL STRAIGHT IMPERVIOUS WALL (after NIELSEN, 1963)

then remained nearly constant, and in some instances started to decrease. The effect of the angle of incidence upon H/H_I was similar to the case for the solitary wave, as can be seen in Fig. 9.

In order to study the phenomenon near the end of a curved breakwater, it was necessary to use a larger facility so that there would be no reflections from the wall opposite the barrier until a large number of waves could be measured. These experiments were made in a 150 ft long by 64 ft wide by 2 1/2 ft deep model basin. A vertical impervious barrier was constructed similar to the one described in a previous section, but about five times as large, as can be seen in Fig. 10. A photograph of the waves that were observed is given in Fig. 11.

The results were similar to the results obtained through the use of the small model basin. Color motion pictures were taken (16 mm), and they were studied thoroughly. Use of these motion pictures, together with the other types of results, permitted Nielsen to determine the details of the motion of a system of periodic waves moving along a curved barrier. His conclusions, in graphical form, are given in Fig. 12. The Mach-stem forms on the straight portion of the barrier (A), dropping behind the wave crest (which is different from the case of the solitary wave). As it moves along the curved section, a Mach-reflected wave also forms (B). As the wave moves still farther along the curve, the Mach-stem and Mach-reflected waves seem to coalesce (C), and then separate from the barrier as a free wave (D) moving nearly normally to the direction of the incident wave. At this stage the free wave is independent of the incident wave. The effect of this transition from one type of wave to another on the wave height along the barrier can be seen in Fig. 13. The amplitude increases in height gradually as it moves along the barrier, and then increases rather rapidly as the Mach-stem and Mach-reflected waves coalesce. Then, as the wave "separates" from the barrier the height at the barrier decreases rapidly, although the height a short distance from the barrier is still high.

TSUNAMI AT HILO, HAWAII

Hilo, Hawaii, is subject to severe damage from tsunamis which originate in the vicinity of Alaska and Chile. The orientation, topography and hydrography of the region (Fig. 14) are such that it appeared likely that a Mach-stem might have been associated with the 1 April 1946 tsunami which originated in the Aleutian Islands of Alaska. The height of the tsunami should increase by a factor of 4 to 5 as it moves onto the shallow portion of the reef off Hilo, due to shoaling effects alone, and it was believed that this, together with the Mach-stem effect, could account for the characteristics of several of the waves of the tsunami as they were observed. It was observed (M. L. Child of Hilo, Hawaii) that the two waves that did the most damage came in as a bore in a southerly direction along the cliff that forms the west border of the bay, swinging easterly and running up through the streets of the town and into the lee area of the breakwater, and waves also came over the top of the breakwater. A photograph taken at the time shows a wave that looks remarkably

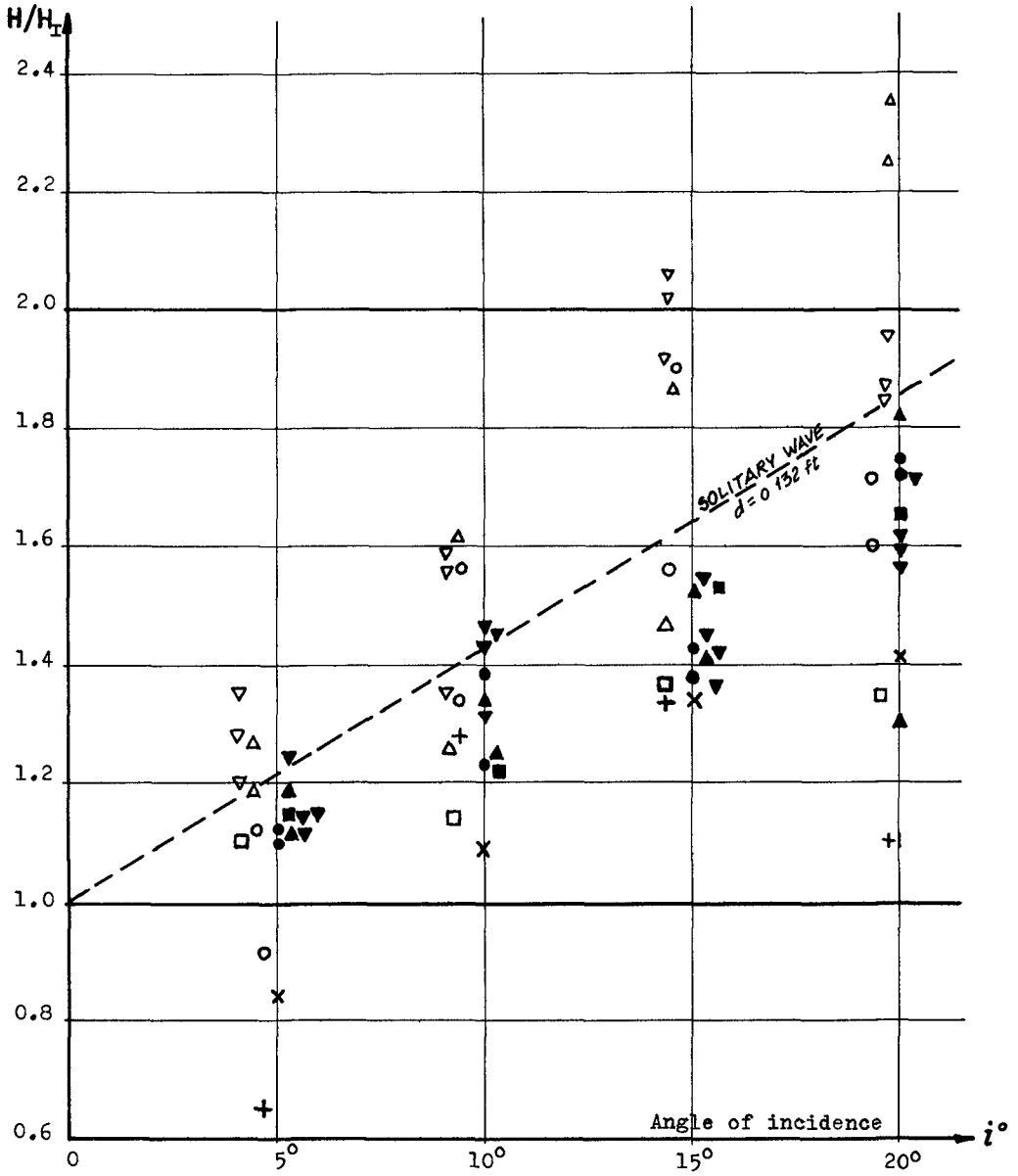

LEGEND:

Wave length L ft	Period T sec	Water depth d ft	Distance X along breakwater $2\frac{1}{2}$ ft	$5\frac{1}{2}$ ft
0.45	.30	.160	×	+
0.68	.38	.160	●	○
1.20	.58	.160	▲	△
1.46	.58	.240	▼	▽
1.50	.71	.160	■	□

FIGURE 9 INCREASE OF WAVE HEIGHT WITH ANGLE OF INCIDENCE.
H_I/d varies from 0.09 to 0.19
(from Nielsen, 1962)

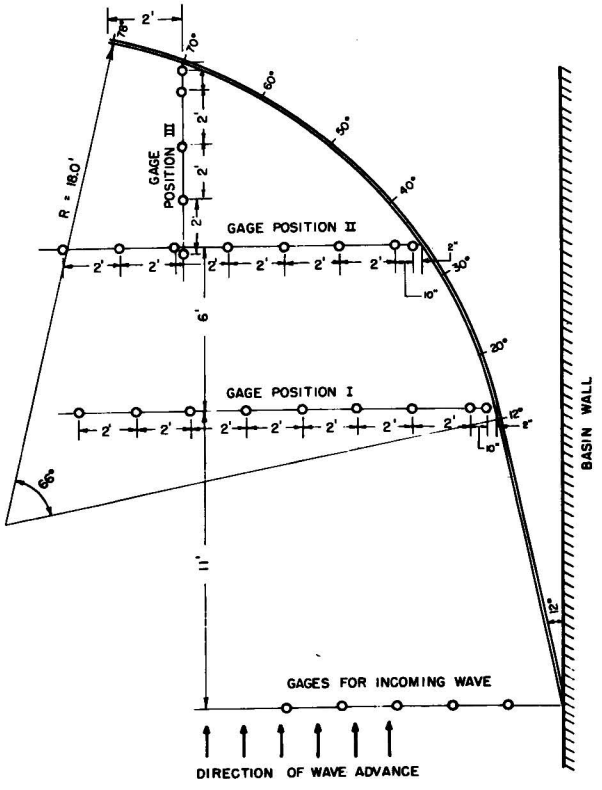

FIGURE 10 EXPERIMENTAL SET-UP IN THE MODEL BASIN IN RICHMOND

FIGURE 11 WAVE PATTERNS AT CURVED SECTION OF BREAKWATER. $L/d=6.3$, $H_I/d=0.25$, $d=1.0$ ft.

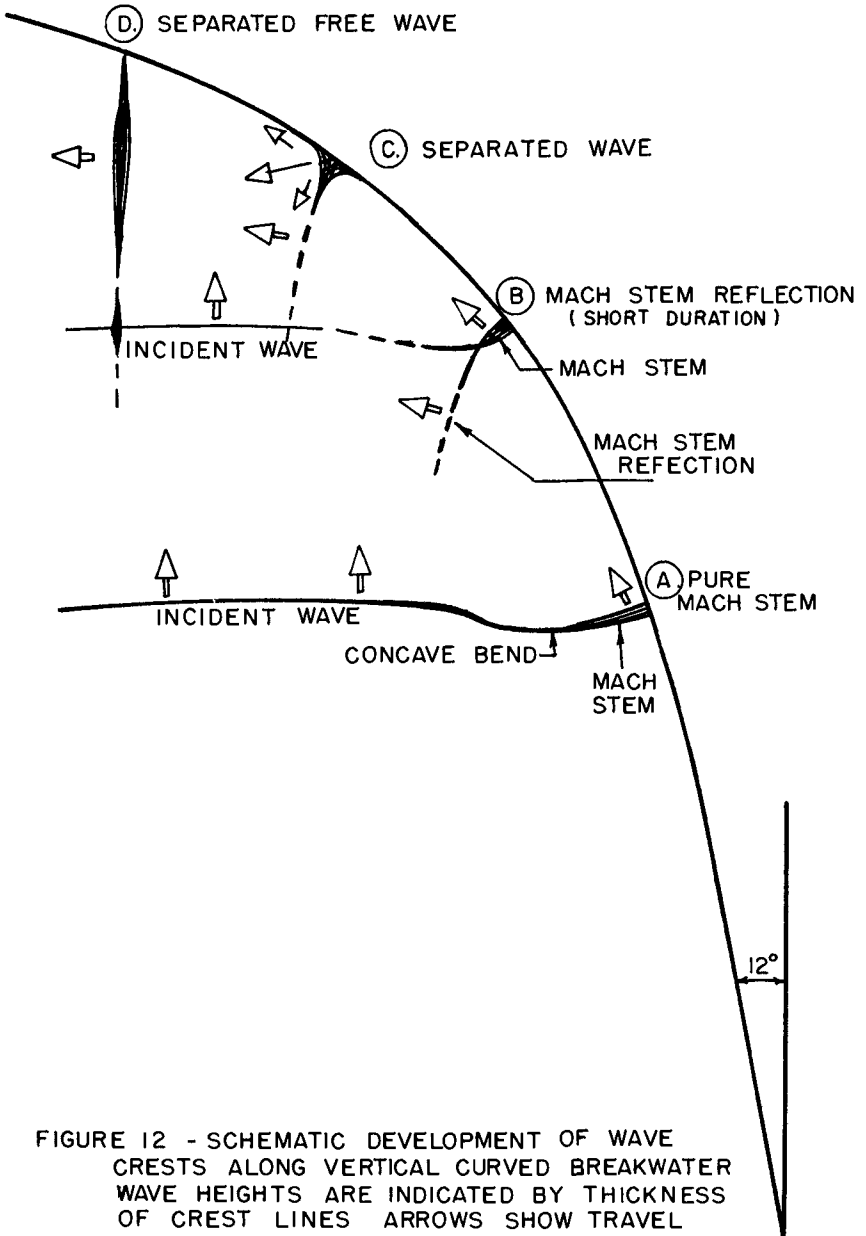

FIGURE 12 - SCHEMATIC DEVELOPMENT OF WAVE CRESTS ALONG VERTICAL CURVED BREAKWATER WAVE HEIGHTS ARE INDICATED BY THICKNESS OF CREST LINES ARROWS SHOW TRAVEL DIRECTIONS (from Nielsen, 1962)

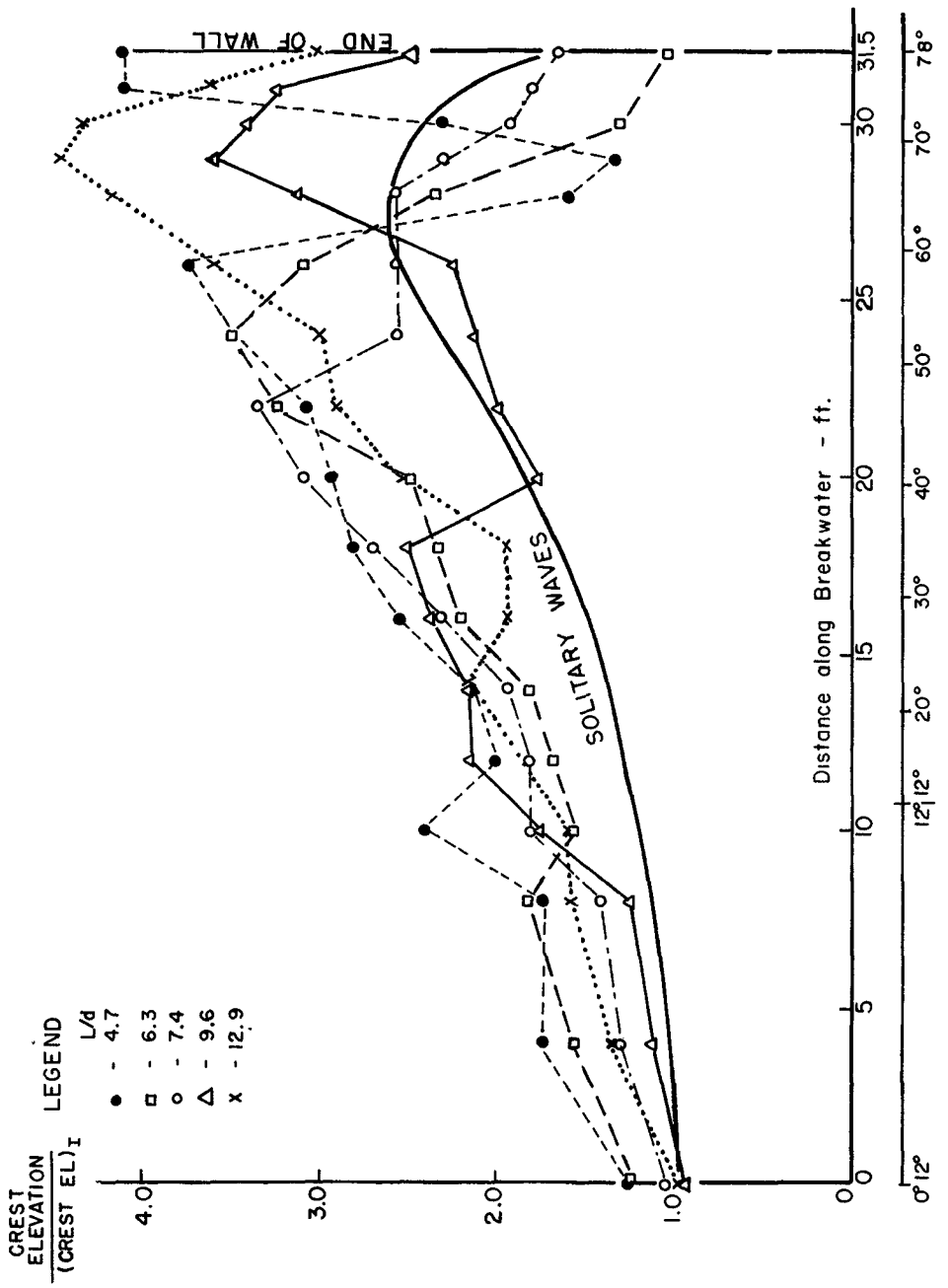

FIGURE 13 - MAXIMUM WAVE ELEVATION ALONG CURVED VERTICAL BREAKWATER FOR DIFFERENT WAVE LENGTHS (RICHMOND MODEL) $H_I/d \cong 0.14$, d = 1.0 ft
(from Nielsen, 1962)

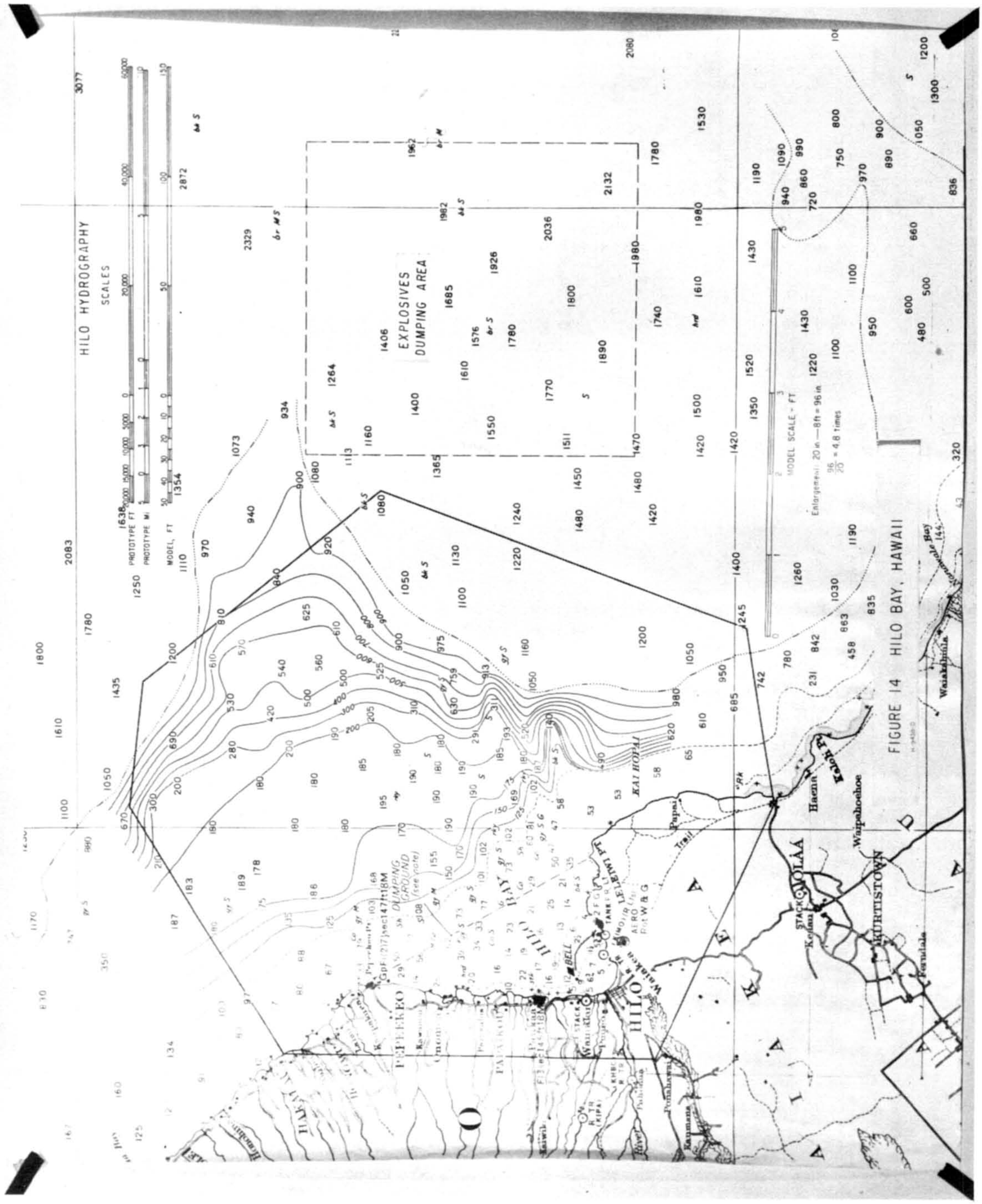

FIGURE 14 HILO BAY, HAWAII

like a Mach-stem (Fig. 15). Another photograph, showing the wave rolling into the town, is shown in Fig. 16.

From some of the observations of the tsunami of 22 May 1960, originating in Chile, it appeared as if something similar must have happened, but the author could not visualize how it could have occurred.

In order to study the gross characteristics of tsunamis at Hilo, a 1:15,000 ($1:\sqrt{15,000}$ = 1:122 time and velocity scale) undistorted model was constructed of fiberglass. The model was approximately 8 ft on a side, so that the entire bay could be included, as well as the reef. A portion of the ocean was included, to a depth of 6,000 to 7,000 ft, prototype. The model was placed at one end of an 8-ft wide by 6-ft deep by 200-ft long tank so that a number of waves could be measured before reflections could be of importance. A series of runs were made with periods ranging from 8 to 24 minutes, prototype, and with waves from the N, E, and SE directions.

It was found, for waves from the north, that a wave which had the appearance of a Mach-stem was generated along the west cliff and rolled into the town of Hilo in a manner that was similar to observations. It was also found that the shoaling effect was about as theory predicted; that is, the wave height increased by a factor of about 4 over the reef, with respect to the wave height in the deep water portion of the tank.

After the tests had been run, it was brought to the investigator's attention that due to refraction in the ocean, the tsunamis generated off Chile would most likely approach Hilo Bay from an easterly direction, rather than from a southeasterly direction as was originally supposed. Because of this, the results of the model tests for the waves from the east will be described herein. A remarkable phenomenon was observed in the 12 to 20 minute (prototype) period range. Referring to Fig. 17a, the initial wave refracted to about the position shown as (1)-(1). The northerly portion started to reflect from the coast while the southerly portion continued to move towards shore. This resulted in the pattern (2A)-(2A) as the reflected portion and (2)-(2) as the continuing portion. As the reflected portion (2A)-(2A) moved down the coast, it became independent of (2)-(2). At the same time the southerly tip of (2)-(2) diffracted into the harbor, raising the water level. About at the same time (2A)-(2A) progressed to position (3)-(3) with the portion near the coast being considerably higher than the portion offshore. The portion near the coast ran right along the coast, reaching positions (4)-(4) and (5)-(5) as a high wave running on top of the water which had diffracted into the harbor from (2)-(2). It then ran into the town of Hilo. The author believes that something similar to this must have happened during the actual tsunami.

The transformation of (2A)-(2A) to (3)-(3) was probably caused by a combination of refraction and reflection, together with some non-linear effects because of the relatively large wave height to water depth ratio along the coast, and the height of the tsunami at Hilo was probably due to this combined with the diffracted wave. At some place between

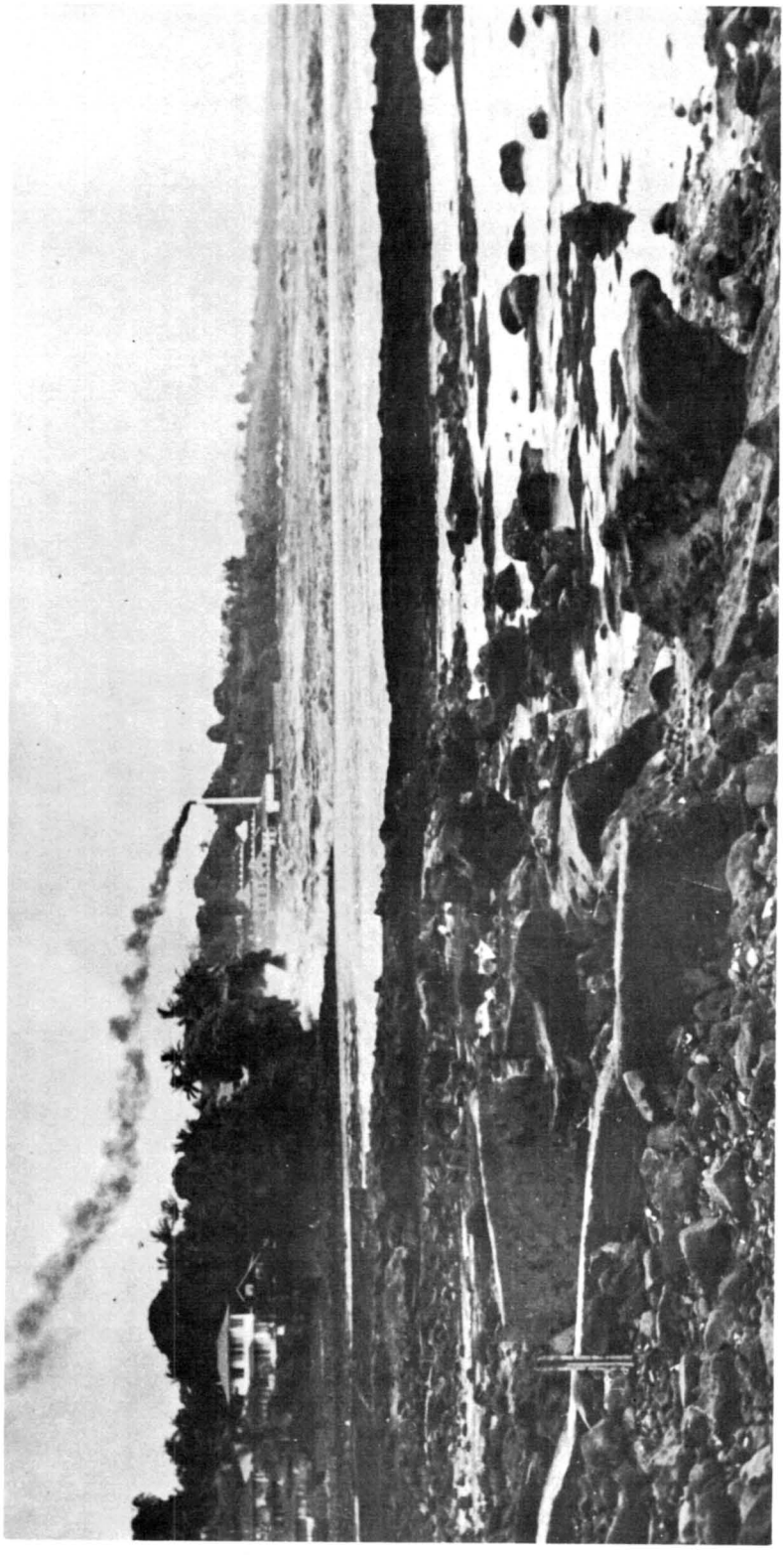

1946 TSUNAMI - HILO

FIGURE 15 WAVE IN THE FORM OF A BORE APPROACHING MOUTH OF WAILUKU RIVER.
NOTE: MACH-STEM EFFECT INCREASED WAVE HEIGHT ALONG COASTAL BLUFF.
WATER IN FOREGROUND HAS RECEDED SEVERAL FEET.
(COURTESY, MODERN CAMERA CENTER, HILO)

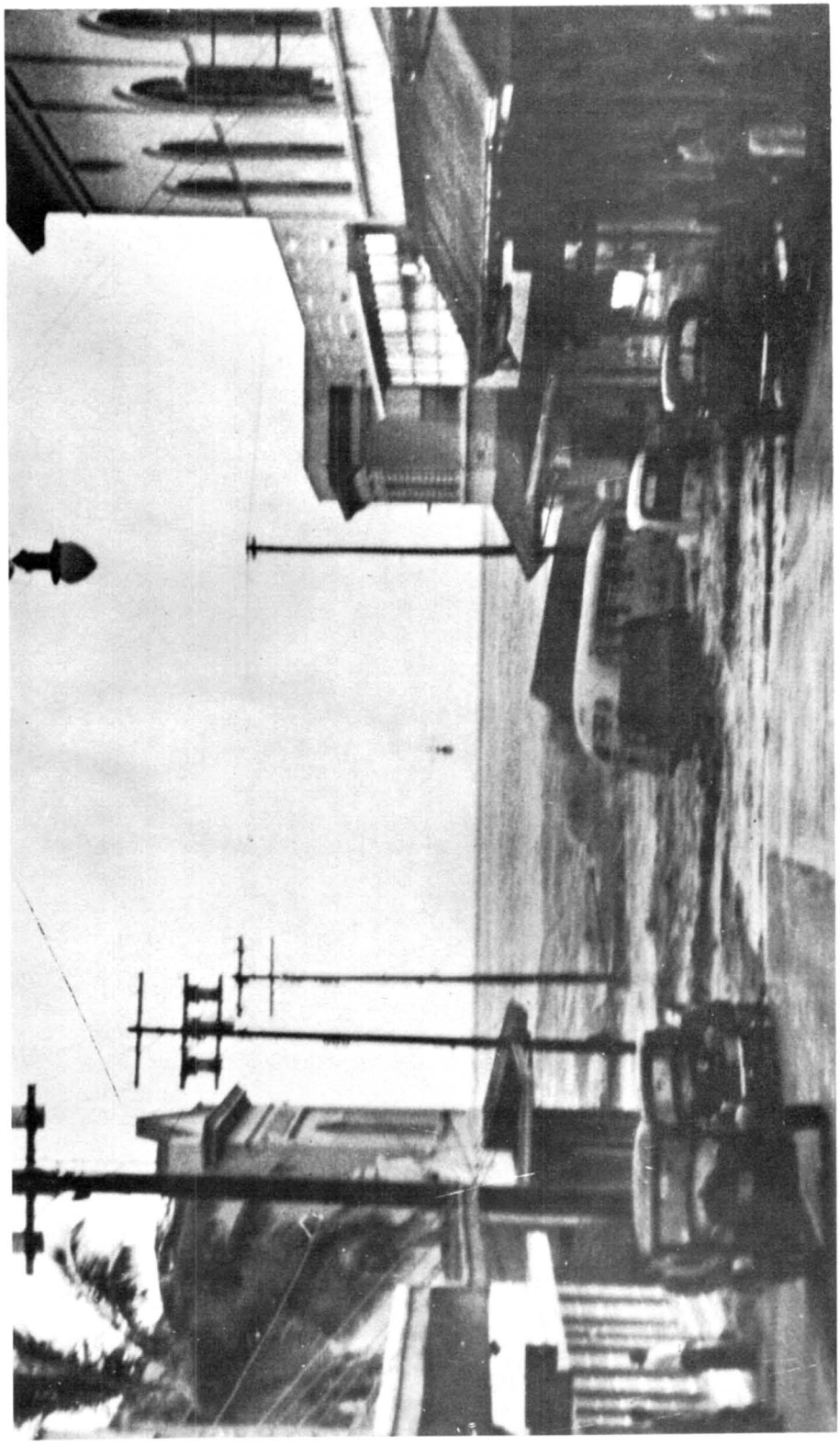

1946 TSUNAMI – HILO

FIGURE 16 VIEW DOWN WAIANUENUE STREET. THIS WAS SECOND WAVE ACCORDING TO MR. YOSHIO SHIGENAGA, EMPLOYEE OF AMERICAN TRADING CO., LTD., WHICH WAS THEN LOCATED IN GROUND FLOOR OF TWO STORY BUILDING ON RIGHT AT END OF STREET. BUS WAS AT INTERSECTION OF KAMEHAMEHA STREET. BREAKWATER IN DISTANCE WAS BREACHED BY 3rd OR 4th WAVE.
(COURTESY, MODERN CAMERA CENTER, HILO)

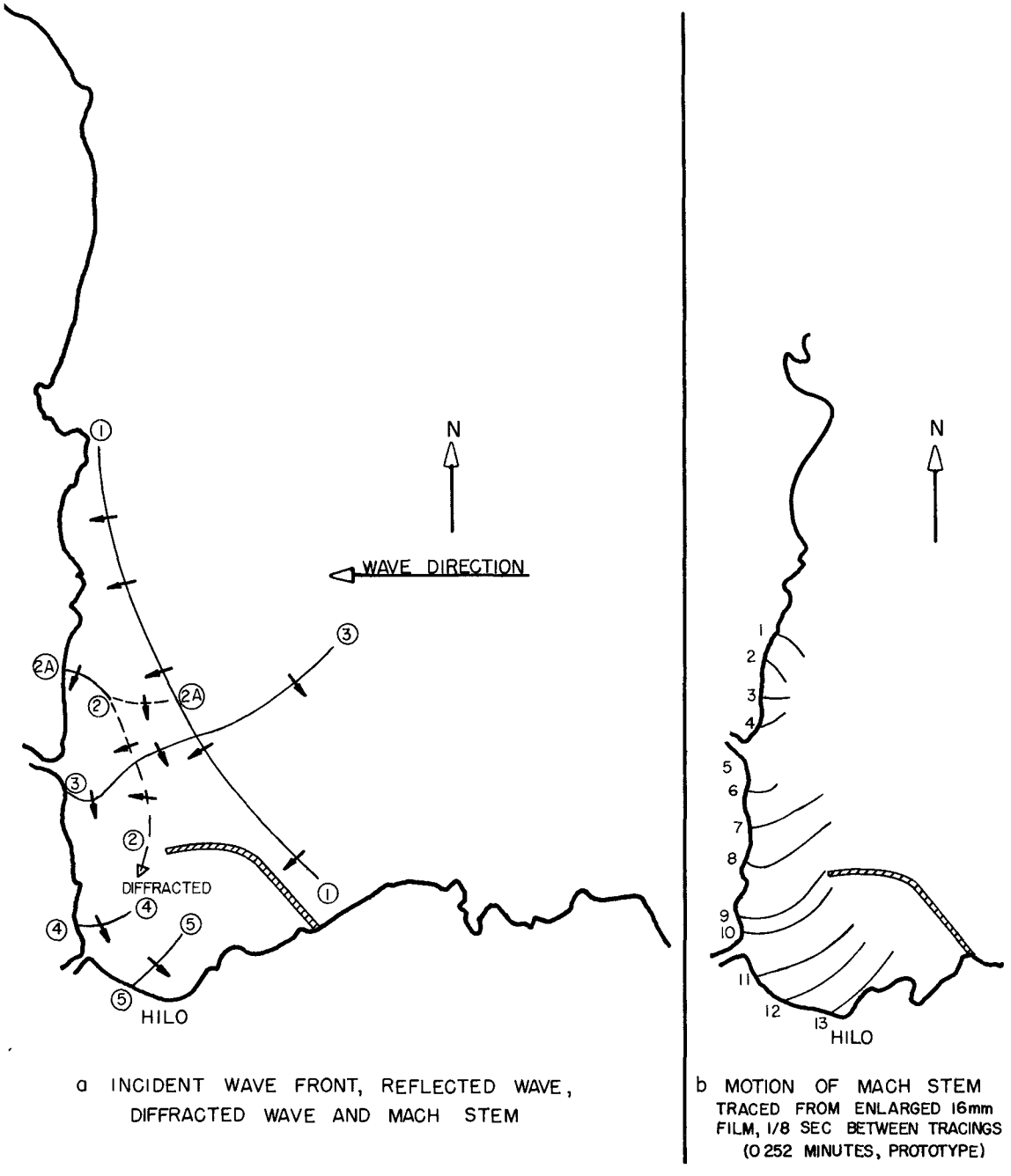

a INCIDENT WAVE FRONT, REFLECTED WAVE, DIFFRACTED WAVE AND MACH STEM

b MOTION OF MACH STEM TRACED FROM ENLARGED 16mm FILM, 1/8 SEC BETWEEN TRACINGS (0 252 MINUTES, PROTOTYPE)

FIGURE 17, SOME RESULTS FROM A 1:15,000 SCALE MODEL STUDY OF TSUNAMIS (16 MINUTE, PROTOTYPE) AT HILO HAWAII. RUN X, 8 FEB 1963, WAVE FROM THE EAST (IN 7,000 FT OF WATER, PROTOTYPE)

(2A)-(2A) and (3)-(3) a Mach-stem type of phenomenon evolved and because of its strength o came independent of the normally reflected portion of the wave. In Fig. 17b are shown the successive positions of this Mach-stem type of wave a. it moves along the coast. These positions were traced from enlargements of a 16 mm motion picture taken during the model study, for a wave of 8 second period (16 minute period in the prototype).

ACKNOWLEDGMENTS

The author wishes to acknowledge the valuable help of James D. Cumming and Arne H. Nielsen for taking the data in the Hilo model tests, and to W. J. Ferguson and Arne H. Nielsen for constructing the model.

REFERENCES

Chen, T. C., Experimental study on the solitary wave reflection along a straight sloped wall at oblique angle of incidence, U. S. Army, Corps of Engineers, Beach Erosion Board, Tech. Memo. No. 124, 24 pp., March 1961.

Friedlander, F. G., The diffraction of sound pulses, Proc. Roy. Soc. (London), Ser. A, Vol. 186, No. 1006, pp. 322-367, 24 Sept. 1946.

Lighthill, M. J., The diffraction of blast. I, Proc. Roy. Soc. (London), Ser. A, Vol. 198, No. 1055, pp. 454-470, 7 Sept. 1949.

Nielsen, Arne Hasle, Diffraction of periodic waves along a vertical breakwater for small angles of incidence, Univ. of Calif., Berkeley, IER Tech. Rept. HEL-1-2, 83 pp., Dec. 1962.

Perroud, Paul Henri, The solitary wave reflection along a straight vertical wall at oblique incidence, Univ. of Calif., Berkeley, IER Tech. Rept. 99-3, 93 pp., Sept. 1957.

Sigurdsson, Gunnar, and R. L. Wiegel, Solitary wave behavior at concave barriers, The Port Engineer (Calcutta), pp. 4-8, Oct. 1962.

Wiegel, R. L., Research related to tsunamis performed at the Hydraulic Laboratory, Univ. of Calif., Berkeley, Proceedings of the Tsunami Meetings associated with the Tenth Pacific Science Congress, Aug.-Sept. 1961, Internat. Union of Geodesy and Geophysics, Monograph No. 24, pp. 174-197, July 1963.

Wiegel, R. L., Oceanographical Engineering, Prentice-Hall, Inc., 535 pp., 1964.

Chapter 7

THE INTERNAL VELOCITY FIELD IN BREAKING WAVES

Robert L. Miller
Department of Geophysical Sciences
University of Chicago, Chicago, Illinois

John M. Zeigler
Woods Hole Oceanographic Institution
Woods Hole, Massachusetts

INTRODUCTION

As far as is known, the results presented here are the first detailed measurements of the horizontal velocity component inside breaking waves. The field study was originally undertaken in 1960 to determine the presence and strength of mid-depth return flow under shoaling waves (Miller and Zeigler, 1961, 1964). In the course of the experiment, a series of measurements was made very close to the shore. During one tidal cycle, the instruments became exposed to breakers, and continued to operate. A study of the resulting data convinced us that detailed velocity measurements could be made within the natural breaker in the field. Accordingly, a series of runs was made and velocity data collected on breakers ranging from very small to storm size. This data will be presented and discussed in detail in a later portion of this paper.

A number of laboratory studies have been made on breakers. These may be placed in three categories for our purposes. The first group includes detailed discussion of observations and sequential figures illustratin the development of breakers. An example is Mason (1951). The second group of papers gives some detail on the structure of breakers and presents, either by direct photograph or sketch of, the trajectory inside the breakers. Examples are Hamada (1951) and Morison and Crooke (1953). The third group of papers presents, in addition to most of the material referred to above, a series of vector maps of the internal velocity under various types of breakers, including both sinusoidal and solitary wave generated breakers. Papers in the third category include Iversen (1951), Larras (1952), and Ippen and Kulin (1955). The latter were of most direct interest to us within the context of the present study.

Several qualitative studies made either directly or in part on breakers in the field were found particularly useful. These include O'Brien (1949) and Hayami, Ishihara, and Iwagaki (1953). Finally the work of Inman and Nasu (1956) includes observations of both horizontal and vertical velocity

components at a fixed point near the bottom as well as the surface trace, for several breakers, taken during the course of a study of shoaling waves. These were found to be particularly useful, and served as the only available check on our data.

FIELD TECHNIQUE

To make measurements in very shallow water and in breakers, a reasonably mobile system was developed. This was necessary in order to take advantage of suitable tide, weather and bottom configurations. Details are illustrated in Figure 1. Three towers were employed consistin of 1-1/2 inch pipe driven approximately 5 feet into the sand. The overall pipe lengths were about 20 feet. Two guy wires held by mushroom anchors were used to steady each tower. The entire system was put in at low tide on a section of coast on the eastern side of Cape Cod. The tide range at this location is approximately 8 feet. The large tide range was a critical factor in the technique and served two purposes. First it allowed proper and unhurried mounting and re-mounting of velocity meters at low tide, when the entire test area was above water. Second, the rise of tide brough the breaker line in past the outer to the innermost tower on the rising tide and in the reverse order on the falling tide. In this way it was possibl to consider any tower as sampling sequentially the front, middle, or rear of the breaker, and during higher tide stages, as sampling simultaneously the breaker on the innermost tower and the near-breaking and shoaling wave at the middle and outer towers respectively.

The data consisted of the following:

1. The tide level (short term still-water level)
2. The surface time-history of the water level, (the wave trace)
3. Up to four continuous recordings of the horizontal velocity component on any one tower, depending on the sampling scheme

All the above data were recorded simultaneously on Sanborn records for visual analysis. Several of the runs were also recorded on magnetic tape as a pilot study for future work in which high speed computer facilitie will be used.

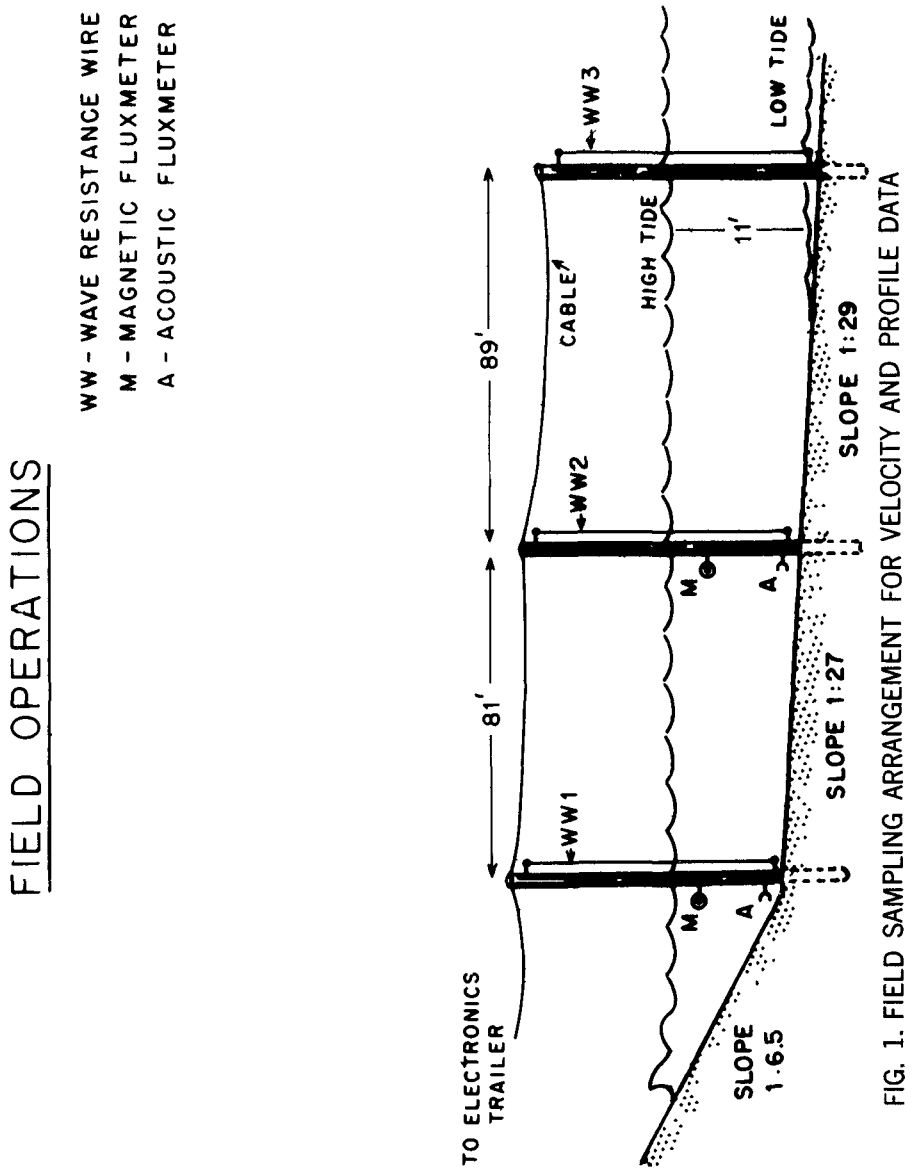

FIG. 1. FIELD SAMPLING ARRANGEMENT FOR VELOCITY AND PROFILE DATA

The velocity meters and resistance wave wires received power from a portable gasoline powered generator on the shore through cable strung from top to top of the towers as shown in Figure 1. The returning signals utilized the same cable and were carried to an enclosed trailer on the beach about 170 feet from the inner tower. The Sanborn recorder, tape recording system, and necessary electronics for the velocity meters and wave wires were all housed in the trailer. Figure 2 shows the system at early rising tide before the breakers have arrived at the inner tower. As soon as the breakers arrived at the inner tower, all systems were switched on and recording began.

Additional field activity included a detailed bathymetric survey of the area from the shore to well beyond the outer tower. Measurements were confined to those periods where local wind effect was negligible and refraction at a minimum. Thus, relatively uncomplicated, swell-generated breakers were studied.

INSTRUMENTATION

Details of the instruments used cannot be given sufficient space here, and will be described fully in a forthcoming paper.

SURFACE WAVE RECORD

Each tower was equipped with two stainless steel resistance wires .015 inch diameter with a resistance of 1.01 ohms per linear foot. One wire was suspended inside the pipe. A 1/8 inch hole drilled through the pipe served as a low pass filter so that essentially short term still-water level was recorded. The external wire served as the wave sensor. It was tightly mounted on a pair of brackets attached to the pipe (see Figure 1). The system follows that described by Farmer and Ketchum (1961). Critical factors include equality of length of internal and external resistance wires the relative distance of both from the center of the pipe cross-section and from the pipe itself, and the length of wetted to exposed wire. Excellent results were obtained with this system.

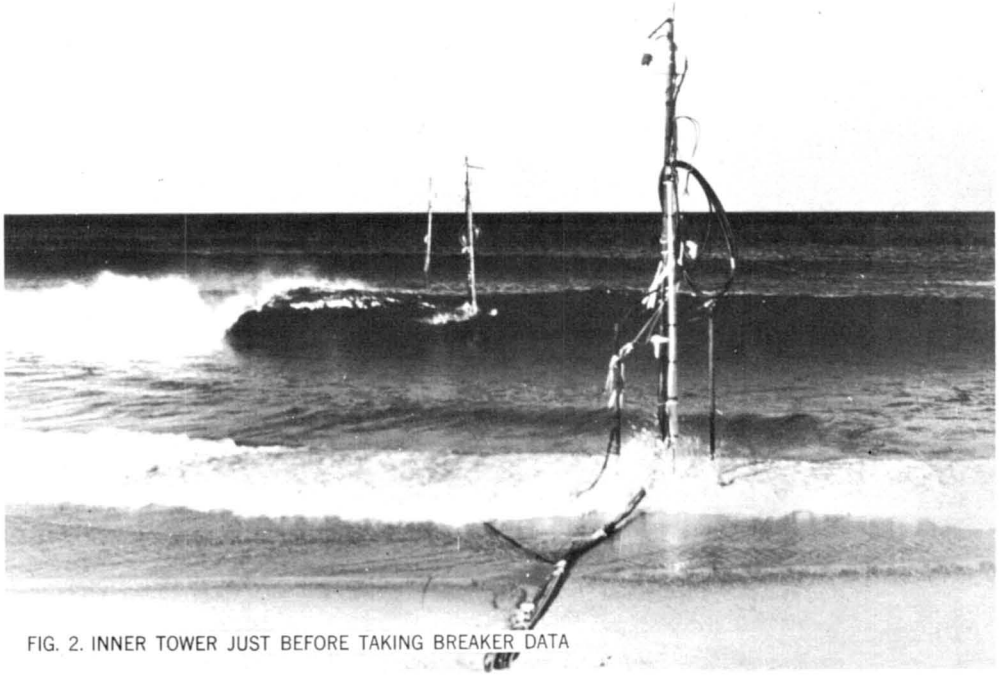

FIG. 2. INNER TOWER JUST BEFORE TAKING BREAKER DATA

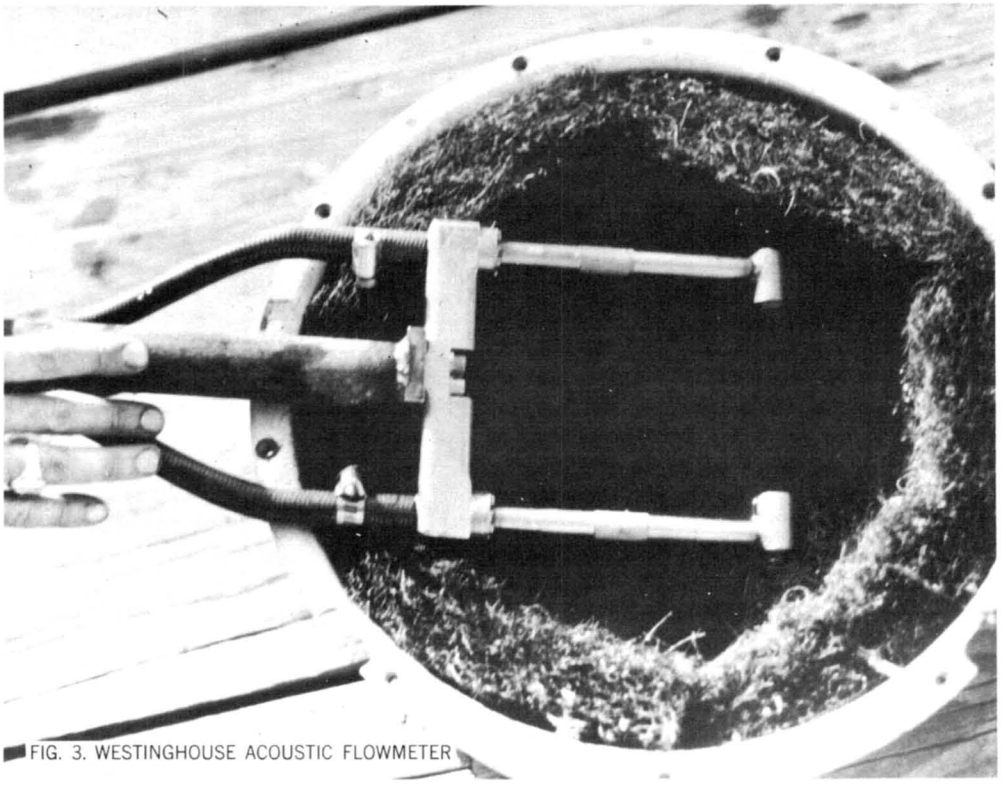

FIG. 3. WESTINGHOUSE ACOUSTIC FLOWMETER

VELOCITY METERS

Two types of meters were used in collecting the data used in this paper. Each type was independently calibrated under both linear flow and in wave tanks. The output of the two meter types was found to be quite comparable within the velocity ranges experienced under field conditi

1. Acoustic Flowmeter

The instrument is made by Westinghouse. The basic operation consi of two simultaneous acoustic signals sent in opposite directions between a pair of probes spaced 8 inches apart. The meter itself is roughly in the sh of a tuning fork with a flat base (see Figure 3). The instrument is position so that an imaginary line between the tips of the probes is parallel to the velocity component to be measured. When the fluid is in motion, the acous signal traveling in the direction of fluid flow will be out of phase with the acoustic signal traveling against the flow. The resulting phase angle is directly related to velocity and the signal identification gives the instantaneous direction of flow.

2. Magnetic Flowmeter

The basic components for this meter consist of a Foxboro Magnetic Flow Meter housed in a fiberglas sphere 8 inches in diameter. During flo from left to right, the fluid acting as a moving conductor, enters the apert ture on the left and then passes through a straight tube containing two electrodes and around which is a pair of saddle-shaped magnets. The magnets create a constant magnetic field at right angles to the moving flui The result is a change in voltage directly proportional to the velocity of the fluid through the tube. The fluid then leaves the spherical housing through the aperature at the right. For operation the tube is aligned with the velocity component which is to be measured.

DISCUSSION

Details of calibration and tests made for direction sensitivity, and c the degree to which the external shapes of the two types of meters interfe with the flow will be given in a later paper. However, as a result of thes tests and our field experience, we are, at present, using the acoustic me in preference to the magnetic type.

DATA ANALYSIS

The data was received in the form of continuous records on a 10-channel Sanborn recorder, in which the horizontal axis represents time (t) with 1 second time marks for scale. The vertical axis gave magnitude in terms of voltage output calibrated against velocity for the meters, or height for the resistance wires. An optimum record included three surface wave traces and their associated still-water levels, and four velocity traces directional in the seaward or shoreward sense as the trace crossed above and below zero.

The velocity field maps were constructed in the following way:

1. Approximately 200 breaker traces were selected from the many thousands recorded. These were chosen on the basis of clarity of pen trace, and were intended to represent as wide a spectrum of breaker sizes as was available. The actual breaker heights varied from two feet to about 12 feet.

2. Using a magnifying glass and templates, the breaker traces were then digitized and each separate breaker plotted on a dimensionless graph. The absicissa consists of zero at the center of the graph and units of t/T_B increasing both to the left and to the right of zero; t is time and T_B is defined as the breaker period and is equivalent to the period of the following breaker T_f, plus the period of the preceding breaker T_p, divided by two, following the method of Inman and Nasu (1956). The ordinate consists of units of Z/B_d where Z is the observed water height above the bottom and B_d is the height of the breaker crest above the bottom. The crest is placed at zero on the horizontal reading and $Z/B_d = 1$ on the vertical. By comparing the breaker profiles plotted on the dimensionless graph described above, it was noted that the breaker forms fell into three major categories. These are referred to as "symmetric", "asymmetric", and "very asymmetric", in the

remainder of the paper, and serve as a useful classification. It seemed possible to spend a good deal of time in considering the classification of breaker shapes and in erecting subdivisions within the three major classes. However, we felt that much more data on a wide variety of bottom configurations and wave conditions would be needed before useful results could be expected.

3. The individual breaker traces for each class were then averaged, resulting in a single trace. The single breaker profile for each class was then transferred to large graph paper with ordinate z/B_d and absicissa t/T_B as before.

4. Corresponding to a given breaker trace, velocity data in the form of both magnitude and direction was available from one to four points on the vertical. Since the tower is fixed as the breaker passes, velocity data was thus available in continuous form from the front to the back of the breaker under scrutiny. Thus our data is on an Eulerian coordinate system with fixed x and varying time. Due to the changing tide level, the relative vertical position on a line from surface to bottom of the velocity input for a given meter changed accordingly. By utilizing this fact, and by choosing a sufficiently wide array of absolute breaker sizes, fairly close control on the vertical scale was achieved. This, together with the continuous recording on the horizontal scale, gave us a closely spaced grid of velocity points from front to back and top to bottom of the breaker. The locations of the velocity values were finally plotted on a single graph (referred to in Step 3 above), for each of the three breaker classes.

5. The velocity value was entered in the form of $u/u_{max.}$ where u is the observed velocity and $u_{max.}$ is the maximum velocity for the individual breaker. In addition, a plus or minus sign is entered to indicate either seaward or shoreward direction, (plus represents shoreward, and minus represents seaward).

6. Finally, the velocity entries were contoured in feet per second intervals and the velocity field-breaker shape map was completed.

RESULTS

DISCUSSION

In the work described in this paper, we focus attention on that region in which the shoaling wave begins to deform to a marked degree, becomes unstable, and finally breaks. Before presenting our results, some discussion on relevant literature and related areas of investigation seems appropriate.

A considerable number of papers have been devoted to investigation of the various properties of Stokes' finite amplitude (non-linear) waves, and of Cnoidal waves including solitary waves. Summaries are given in Stokes (1957), Laitone (1961) and Ippen et al. (1963). An example is Biesel (1951) whose solutions include a wave shoaling over a sloping bottom and finally breaking. Recently, interest has been shown in the properties of long waves and surges as they break on a beach, for example, Freeman and Le Mehaute (1964). A non-linear model has been developed by Meyer and his colleagues in which the entire sequency of shoaling, breaker formation and collapse, and subsequent uprush and backwash is described. (See Ho and Meyer, 1962; Meyer and Taylor, 1963; and Ho, Meyer, and Shen, 1963)

Papers specifically devoted to breaking wave criteria in addition to those referred to in the introduction include Michell (1893) and a summary by Reid and Bretschneider (1953). For the solitary wave in particular, a summary is given by Ippen and Kulin (1955).

The concensus of opinion seems to be at the present time that in the very shoal region, but not including the breaker, Stokes' finite amplitude theory holds reasonably well to an inner limit of $d/L \cong 0.10$, Cnoidal wave theory in general, in the region $0.10 \geq d/L \geq 0.02$ and solitary wave theory in particular in the region $d/L < 0.02$. (See Ippen et al, 1963; Keulegan, 1950; Morison and Crooke, 1963; and Inman and Nasu, 1956.) It would appear, therefore, that information on the internal velocity field in near-breaking waves and breakers, would be of considerable interest in the theoretical investigations of the shallow water and breaking properties of waves, and indeed, may serve as an additional boundary condition for a successful theory of the complete phenomenon.

The general problem of sediment transport is also directly related. For example, a sandy coastline is almost always under direct attack by breakers. Under certain conditions, the net result is transportation of sediment from the sea through the breaker, with ultimate deposition on the shore. Under other conditions, the sediment is ultimately transported seaward through the breaker. The phenomenon of erosion and deposition on coastlines are under active investigation both in the laboratory and in the field. However, the internal structure of the natural breaker, itself a basic aspect of this whole area of investigation, is not well understood.

RESULTS OF THIS STUDY: THE NEAR-BREAKING WAVE:

The near-breaking wave average profile and internal horizontal velocity field map was constructed according to the method described in the previous section. It is shown in Figure 4. The profile is quite asymmetric with a well defined break in slope on the shoreward side just above still-water level. Maximum velocity is in the shoreward direction throughout the crest and extending well into the body of the breaker. Comparison with the analogous theoretical profiles and velocity fields can be made by inspection of Figure 5 for the finite amplitude Stokes' wave and Figure 6 for the Cnoidal wave. These calculations were facilitated by using tables from Masch and Wiegel (1961), and Skjelbreia (1959). In profile, the near-breaking Cnoidal wave most nearly resembles the natural wave, although the asymmetry is not present in the theoretical wave. The internal velocity field of the Cnoidal wave, although much more regular in appearance, again more nearly resembles the natural wave, in the consideration of shoreward velocity in a "chimney" under the crest, flanked both in front and behind by regions of seaward motion. Considerable differences are apparent however, in that asymmetry of the velocity field does not appear in the Cnoidal wave, nor the well-defined increase in shoreward velocity toward the bottom under the crest. Also of note is the presence of significant seaward motion on the back slope of the wave, well above still-water level.

RESULTS OF THIS STUDY: THE BREAKERS:

Theory is presently not available for calculation of internal velocity fields under breakers. Therefore, the results of the field observations will be presented and discussed for each class in turn.

Class I, "Symmetric" Breaker (Figure 7)

Transition from the profile and velocity field of the near-breaking wave to the symmetric breaker does not appear to be easily made in this case. It is apparent that in further work care must be

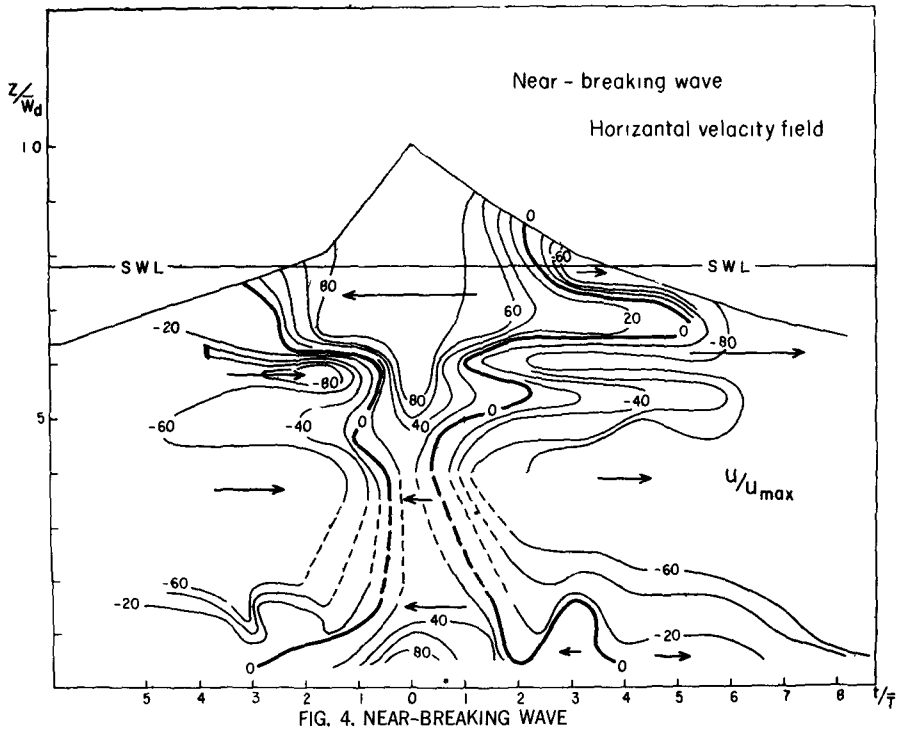

FIG. 4. NEAR-BREAKING WAVE

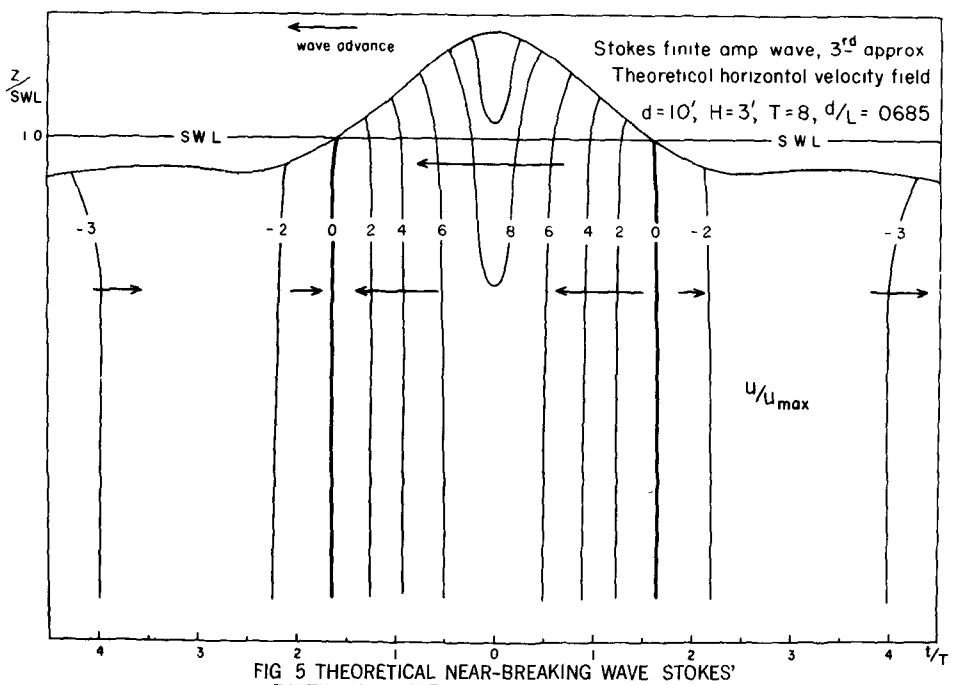

FIG 5 THEORETICAL NEAR-BREAKING WAVE STOKES' FINITE AMPLITUDE WAVE, THIRD APPROXIMATION

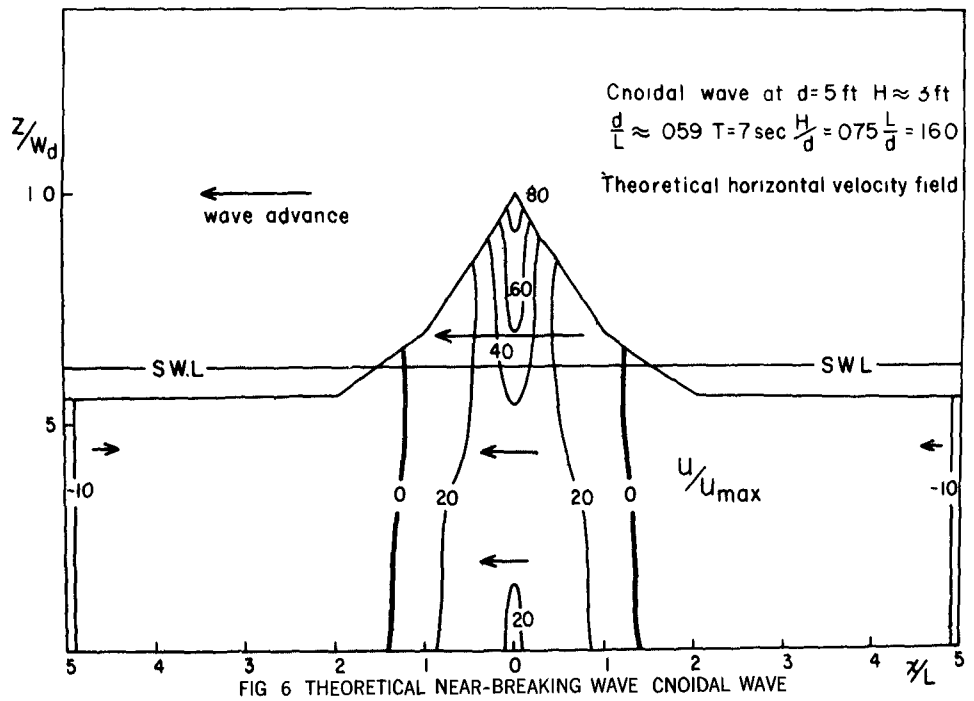

FIG 6 THEORETICAL NEAR-BREAKING WAVE CNOIDAL WAVE

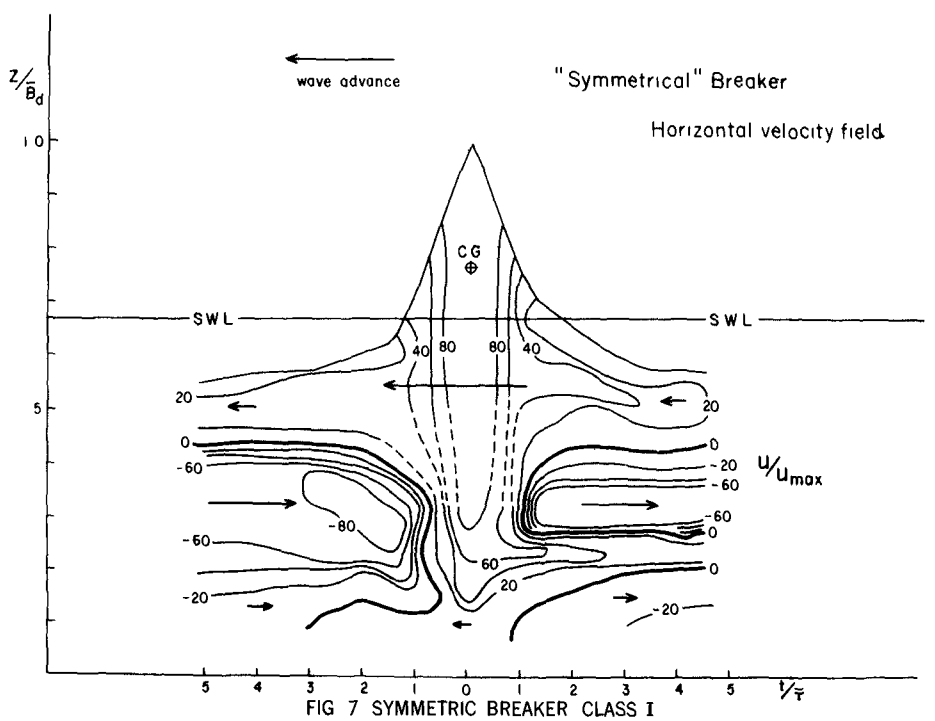

FIG 7 SYMMETRIC BREAKER CLASS I

taken to identify each near-breaking wave with its breaker in order to avoid ambiguity. Fortunately, this is not difficult with the system we are now using.

Particularly notable in this breaker class are the following features:

1. The close approach to symmetry in the average breaker profile, which closely resembles the theoretical profile for a Cnoidal wave in very shallow water, see Figure 6.

2. The lack of symmetry in the velocity field of the lower portion of the breaker.

3. The absence of seaward movement in the upper half of the breaker.

4. The persistence of the "chimney" of shoreward movement from crest to bottom.

Class II, "Asymmetric" Breaker (Figure 8)

This class of breakers as well as Class III appears to complete the transistion from the near-breaking wave (Figure 4) in both profile and velocity field, the difference being a matter of degree. In comparison with the near-breaking wave profile, the profile of the "Asymmetric" breaker is more peaked and the asymmetry greater. With respect to the internal velocity field, the following is noted:

1. The distribution of magnitudes and direction is less complicated than in the Class I "Symmetric" Breaker (Figure 7).

2. The seaward motion on the high back slope of the near-breaking wave (Figure 4) has now become an isolated pocket, but remains in about the same location.

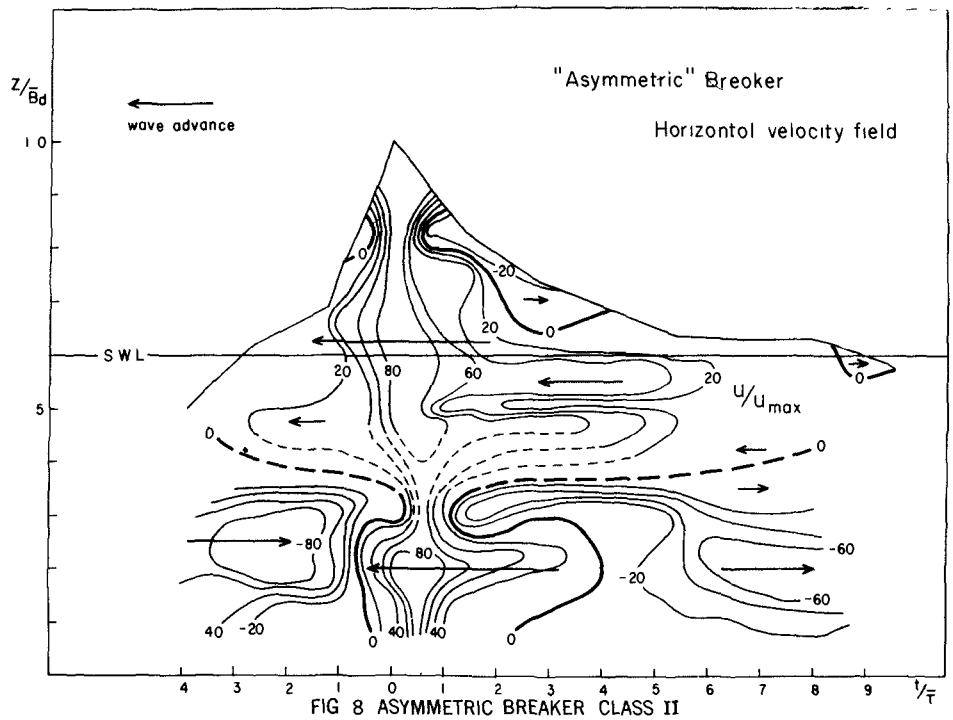

FIG 8 ASYMMETRIC BREAKER CLASS II

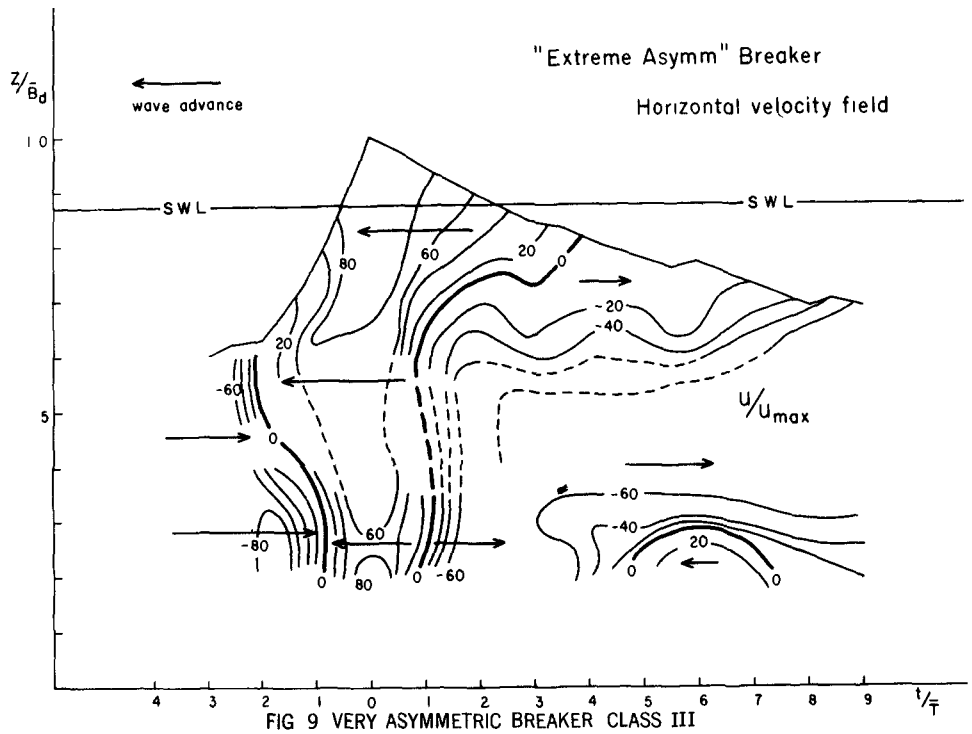

FIG 9 VERY ASYMMETRIC BREAKER CLASS III

3. The "chimney" of shoreward movement from crest to bottom still persists, but the margins are quite indented and distorted.

4. The regions of near-bottom seaward movement are enlarged and the magnitudes increased in comparison with both the "Symmetric" breaker and the near-breaking wave.

5. An anomolous region of seaward movement or at least of zero motion, appears on the front slope of the breaker just below the crest.

Class III, "Extreme Asymmetry" Breaker (Figure 9)

This breaker class is the least complicated of the three categories. Transition from the near-breaking wave (Figure 4) may be easily visualized with asymmetry of profile more strongly developed than in the "Asymmetric" breaker, and with a corresponding lowering of the profile and reduction of the crest. The internal velocity structure appears to present a smoothing and coalescing of velocity regions in the transition from the near-breaking wave field and in contrast to the "Asymmetric" and "Symmetric" breakers.

The following features seem of particular interest:

1. The persistence of the "chimney" of shoreward movement crest to bottom, in this case, with relatively straight margins.

2. The correspondence of the sharp break in slope in the forward face with the reversal in fluid direction.

3. The presence of an isolated subsidiary pocket of shoreward movement near the bottom at the back end of the breaker.

CONCLUSIONS: FURTHER INVESTIGATION

Further measurements under a variety of bottom topographies are needed before we attempt anything more than tentative conclusions. At the present time it is felt that particular effort is needed to establish both uniqueness and generality of our results. However, the data thus far suggests the following:

1. The three breaker classes appear to be well established. In comparison to classification now in general use, our "Symmetric" breaker is possibly analogous to the plunging type, the "Very Asymmetric" breaker is similar to the spilling type and the "Asymmetric" breaker somewhat intermediate between plunging and spilling. However, the three classes given here were developed directly from the field data breaker profiles by the method described in an earlier portion of this paper, and no effort was made to use visual classification of breakers as they occurred in the field.

It is of interest to note that all three classes were measured from the same tower, with single bottom slope! This seems to suggest that, in nature, in addition to the importance of bottom and of foreshore slopes, breaker shapes are affected by interaction of approaching waves and wave trains, and also by the timing and magnitude of the backwash, forming a complex system. This is in contrast to laboratory studies, where for a given simple wave form, the bottom slope is the dominant factor in breaker shape.

2. The results very strongly suggest that different breaker shapes have different internal velocity fields. This corraborates the qualitative field conclusions of Hayami, Ishihara, and Iwagaki (1953), as well as the laboratory studies referred to earlier. It would seem that observation of the direction and magnitude of sediment transit through the three contrasting velocity fields would be of considerable interest in the erosion-deposition phenomenon on coasts. This aspect is now in progress at the University of Chicago sediment transport laboratory by R. L. Miller. The

laboratory work of Eagleson and his colleagues is of particular interest here. See, for example, Ippen and Eagleson (1955), and Eagleson and Dean (1959).

3. The velocity fields under breakers appear to be less complicated than we had thought. It is possible that the initiation of instability and the subsequent development of the breaker may be characterized by one or several vortex systems, as suggested by the velocity field patterns. However, it is necessary to measure simultaneously both vertical and horizontal components before pursuing this aspect. We are engaged in these measurements at the present time.

4. The breakers studied were of the type that break directly on the shore and include within the sequence, the runup and backwash from the foreshore. We feel that the internal velocity fields under two quite different conditions deserves similar investigation:

a. breakers over bars and shoals, where the foreshore effect is absent

b. breakers in open water where both foreshore and bottom effects are removed.

ACKNOWLEDGEMENTS

We are indebted to a very large number of colleagues and co-workers, for aid and advice on this project. Particular thanks go to the members of our group at the Woods Hole Oceanographic Institution; Carl Hayes, Herman Tasha and Graham Geise. The electronics has been under the supervision of Robert Foley, with the complete cooperation of James Allen of Westinghouse Corporation, Baltimore, and Robert Cushman of the Foxboro Instrument Company, Foxboro, Massachusetts. Without the help of the people named above, this project could not have been undertaken.

We are also indebted to Fred Hotchkiss and George Chappel for their aid in the field program and to David Owen for photography both in design of equipment and field operation, to David Ketchum and Robert Walden, for advice and assistance in design and construction of instruments and electronic systems, and to Dan Clark for advice on the towers.

This project was supported by grants from the National Science Foundation and the Office of Naval Research under contracts, N. S. F. G. P. 1194, Nonr-2196(00) at the Woods Hole Oceanographic Institution and Nonr-2121-26 at the University of Chicago.

Contribution Number 1542 from the Woods Hole Oceanographic Institution, Woods Hole, Massachusetts.

REFERENCES

Biesel, F. (1951). Study of wave propagation in water of gradually varying depth: Gravity Waves Circular No. 521, Nat. Bureau of Standards, Washington, D. C.

Eagleson, P. S. and Dean, R. G. (1959). Wave induced motion of bottom sediment particles: Jour. Hydraulics Div. Proc. A. S. C. E. 2202, pp. 53-79.

Farmer, H. G. and Ketchum, D. C. (1961). An instrumentation system for wave measurements, recording, and analysis: Proc. 7th Conf. on Coastal Eng., The Hague, pp. 77-99.

Freeman, J. C. and Le Mehaute, B. (1964). Wave breakers on a beach and surges on a dry bed: Proc. A. S. C. E. Jour. of Hydraulics Div., Vol. 90, No. HY2, Proc. Paper 3834, pp. 187-216.

Hamada, T. (1951). Breakers and beach erosion: Rept. No. 1, Transporta Technical Research Institute, Tokyo.

Hayami, S. T., Ishihara, and Iwagaki, Y. (1953). Some studies on beach erosions: Bull. No. 5, Disaster Prevention Research Inst., Kyoto Univ., Kyoto, Japan.

Ho, D. V. and Meyer, R. E. (1962). Climb of a bore on a beach: Part I, Uniform beach slope: J. Fluid Mech. 14, pp. 305-318.

Ho, D. V., Meyer, R. E. and Shen, M. C. (1963). Long surf: Jour. Marine Res., Vol. 21, No. 3, pp. 219-230.

Inman, D. L. and Nasu, N. (1956). Orbital velocity associated with wave action near the breaker zone: Beach Erosion Board, Tech. Memo. No. 79, Washington, D. C.

Ippen, et al. (1963). Estuary and Coastline Hydrodynamics: Hydrodynamics Laboratory, M. I. T., Cambridge, Mass. Chap. B., Finite amplitude waves: by Dean, R. G. and Eagleson, P. S.

Ippen, A. T. and Eagleson, P. S. (1955). A study of sediment sorting by waves shoaling on a plane beach: M. I. T., Hydrodyn. Lab., Tech. Rept. 18.

Ippen, A. T. and Kulin, G. (1955). Shoaling and breaking characteristics of the solitary wave: M. I. T. Hydrodyn. Lab., Tech. Rept. No. 15.

Iversen, H. W. (1951). Laboratory study of breakers: Gravity Waves, Cir. No. 521, Nat. Bureau of Standards, Washington, D. C.

Keulegan, G. H. (1950). Wave motion: Engineering hydraulich, H. Rouse, Editor, John Wiley, New York, pp. 711-768.

Laitone, E. V. (1961). Higher approximations to non-linear water waves and the limiting heights of Cnoidal, solitary and Stokes' waves: Univ. of Calif. Inst. of Eng. Res. Tech. Rept. Series 89, Issue 6. Berkeley, Calif.

Larras, J. (1952). Experimental research on breaking of waves: Annales des Ponts et Chaussees, v. 122, p. 525, ff.

Masch, F. D. and Wiegel, R. L. (1961). Cnoidal waves; tables of functions: Council on Wave Research, Univ. of Calif., Richmond, Calif.

Mason, M. A. (1951). Some observations of breaking waves: Gravity Waves Cir. No. 521. Nat. Bureau of Standards, Washington, D. C.

Meyer, R. E., and Taylor, A. D. (1963). On the equations of waves on beaches: Brown Univ. Tech. Rept. Nonr-562(34)/5.

Michell, J. G. (1893). On the highest waves in water: Philosophical Magazine vol. 36, No. 5, 430-435.

Miller, R. L. and Zeigler, J. B. (1961). A field and laboratory program for study of shoal waves and sediment transport: Proc. of the1st. Nat. Coastal and Shallow Water Res. Conf., Los Angles, p. 65.

Miller, R. L. and Zeigler, J. M. (1964). A study of sediment distribution in the zone of shoaling waves over complicated topography: Chap. 8 in Papers in Marine Geology, R. L. Miller, Editor; John Wiley and Sons, New York.

Morison, J. R. and Crooke, R. C. (1953). The mechanics of deep-water, shallow water, and breaking waves: Beach Erosion Board, Tech. Memo. No. 40, Washington, D. C.

O'Brien, M. P. (1949). The causes of spilling and plunging breakers: Bull. Beach Erosion Board, V. 3, No. 3, Washington, D. C.

Reid, R. O. and Bretschneider, C. L. (1953). Surface waves and offshore structures: Texas A & M Res. Foundation, Tech. Rept. Oct.

Skjelbreia, L. (1959). Gravity waves, Stokes' third order of approximation, tables of functions: Council on Wave Research, Eng. Foundation, Univ. of Calif., Berkeley, Calif.

Stokes, J. J. (1957). Water waves: Interscience Publishers, Inc., New York.

Chapter 8

STATISTICAL DISTRIBUTION OF WAVE HEIGHTS IN CORRELATION WITH ENERGY SPECTRUM AND WATER DEPTH

by

*L.A. Koelé and *P.A. de Bruyn

Wave motion has been studied at various places in the south western part of the Netherlands (the Delta area) as part of a study on coastal morphology and the design of coastal structures.

The main part of this study deals with the statistical distribution of wave heights in relation to:

a. the height of the sea surface at fixed points, as a function of time;
b. the water depth;
c. the energy spectrum of the wave motion.

The results of theoretical studies by D.E.Cartwright and M.S.Longuet Higgins (lit. 1) and data on wave measurements obtained by Rijkswaterstaat in the North Sea were used. These measurements were taken by means of an electrical step-capacity gauge, with wireless transmission of the data to shore . Three gauges, fastened to fixed poles (named E, K and T) were placed at points at depths of 5, 10 and 15 meters respectively. (fig. 1).

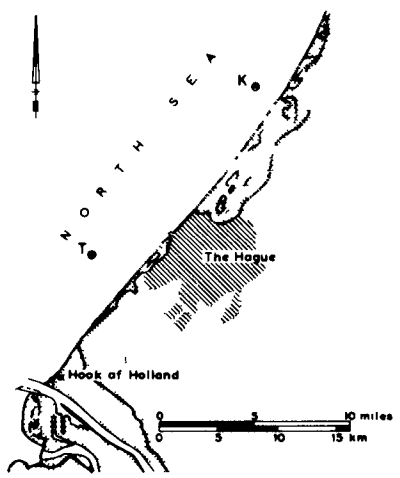

Fig 1 Situation of measuring stations

The theoretical frequency distributions of the wave heights, derived by Cartwright and Longuet Higgins for the "lineair model", are based on the assumption that the distribution of the ordinates

* Hydraulics Division, Delta Project, Rijkswaterstaat, The Hague, Holland.

of the sea surface as a function of time is Gaussian. From the data of wave records, it appeared that in relatively shallow water (depths varying from 3.5 to 17.0 meters) Gaussian as well as non-Gaussian distributions occur.

In § 1 a brief description is given of the "lineair model" and its limitations. The deviations of frequency distributions of the sea surface from those of the lineair model are studied in § 2.

Four parameters are used to describe the wave heights. In § 3 the distributions of these four wave height parameters are considered as a function of three variables:
the standard deviation $\sqrt{m_o}$, the skewness α_3 of the sea surface distribution and ε , the relative width of the energy spectrum.
From the frequency distributions obtained from observations the quotients of the significant wave heights $H_{1/10}$, $H_{1/3}$ and H_m are determined as a function of ε and α_3 in § 4 . In § 5 the wave height parameters are further discussed.

§ 1. The lineair model of the wave motion and its limitations

Let $z=f(t)$ denote a continuous function of the time t, representing the ordinate of the sea surface above the mean water level; z is measured at a fixed point and it is assumed that $f(t)$ is a statistically stationary function during a limited time interval T_o.

Any function $f(t)$ thus defined can be represented by the sum of a large number of sine-waves:

$$z = \sum_n a_n \sin(\omega_n t + \varepsilon_n) \tag{1}$$

a_n = amplitude, ω_n = angle-frequency and ε_n = phase-angle.

In the "lineair model" the ordinates z measured from the mean sea level, z=o, are assumed to be Gaussian distributed during the time interval T_o.

Let the function for which this is valid be represented by:

$$z_a = f_a(t) \tag{2}$$

Analogous to (1) we thus obtain:

$$z_* = \sum_n a_n \sin(\omega_n t + \varepsilon_n) \tag{3}$$

But now the phases ε_n are random and distributed uniformly between 0 and 2π and the frequencies ω_n are distributed densely in the interval $(0, \infty)$; (lit.2).

Furthermore it is assumed that for every sine-wave, according to the classic wave theory:

$$\omega = \frac{2\pi}{T} = \sqrt{\frac{2\pi g}{L} \operatorname{tgh} \frac{2\pi D}{L}} \tag{4}$$

where T and L represent the wave period and length respectively, D is the water depth and g the gravitational acceleration.

Function (4) is valid when (lit.3):

$$\frac{2\pi a}{L} \ll 1 \text{ and } \frac{2\pi a}{L} \ll \left(\frac{2\pi D}{L}\right)^5 \tag{5}$$

Furthermore for every very small interval $d\omega$ the sum of the squares of the amplitudes is a continuous function of the frequency ω or:

$$E(\omega)\, d\omega = \Sigma \tfrac{1}{2} a_n^2 \tag{6}$$

The function $E(\omega)$ is called the energy spectrum. The moments of $E(\omega)$ about the origin are defined as:

$$m_p = \int_0^\infty E(\omega)\, \omega^p\, d\omega \tag{7}$$

The relations (3), (4) and (5) define the "lineair model" of the wave motion and it has been found that it is possible to compute the distribution of the maxima and minima of $f_*(t)$. (lit.1).

The energy-spectrum $E(\omega)$ of a continuous, statistically stationary function f (t) can be determined by means of: (lit.4)

$$E(\omega) = \frac{1}{\pi} \int_0^\infty R(\tau) \cos \omega\tau\, d\tau \tag{8}$$

where $R(\tau)$ is the auto-correlation function of f(t), defined as:

$$R(\tau) = \frac{1}{T_0} \int_0^{T_0} f(t+\tau) f(t)\, dt \tag{9}$$

From (8) and (9) it follows that if $\tau = 0$,

$$R(0) = \overline{z^2} = \int_0^\infty E(\omega)\, d\omega \tag{10}$$

in which $\overline{z^2}$ is the variance of f(t) and $\int_0^\infty E(\omega) d\omega$ is the area m_0 of the energy spectrum.

Thus: $\overline{z^2} = m_o$ (11)

Let E_p denote the mean potential energy per unit of surface $(E_p = \frac{1}{2}\rho g z^2)$**, then:

$$m_o = \int_0^\infty E(\omega)\, d\omega = 2E_p \tag{12}$$

For the "lineair model", in which E_p is half of the total energy E_{tot}, it follows from (12) that: $m_o = E_{tot}$ (13)

Equation (10) may also be computed by integration of (1) and (6).

To check in how far agreement between the "lineair model" and the measured wave motion could be expected, the distribution of the ordinates of the sea surface was examined.

§2. Distribution of the ordinates of the sea surface.

In the following pages the probability distribution of the ordinates z of the sea surface will be indicated by the symbol p(z). The ordinates, measured from the mean sea level, are computed from a wave record obtained at a fixed point in the sea; $\sqrt{m_o}$ is the standard deviation of p(z).

The distribution p(z) has been determined by a computer from 35 wave records using a continuous measuring period of 10 minutes from each record. The intervals ΔZ were kept constant for a specific record, but they varied for the different records from 10 to 25 cm., depending upon the wave height.

To obtain sufficient variations in the water depths, wave heights and wave lengths, a selection has been made from the available wave records. The relation between wind force and wave height has not been considered.

It appeared that in the relatively shallow water, Gaussian as well as non-Gaussian distributions occur. Some examples are given in fig. 2.

**Introducing specific units, ρg can always be made 1.

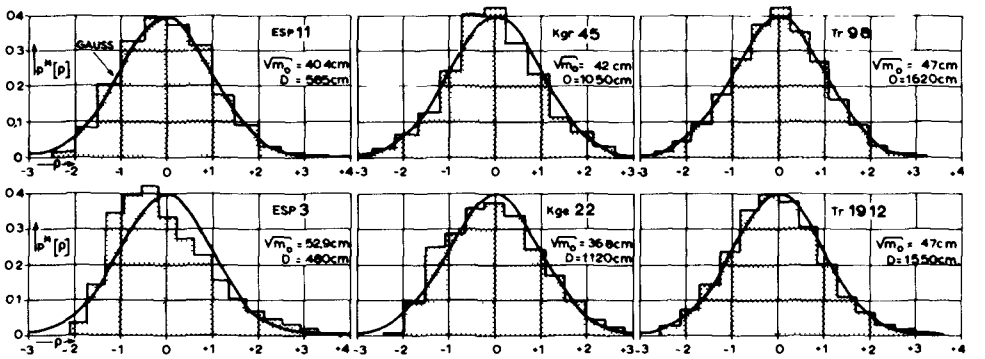

Fig 2 Probability distributions p[ρ] obtained from measurements, compared with the Gauss distribution

To facilitate comparison these distributions have been expressed in terms of $p^*\left(\frac{z}{\sqrt{m_o}}\right)$ where:

$$p^*\left(\frac{z}{\sqrt{m_o}}\right) = \sqrt{m_o} \cdot p(z) \tag{14}$$

Every distribution has been compared with the normal distribution. The deviation of a distribution $p^*\left(\frac{z}{\sqrt{m_o}}\right)$ from the Gaussian distribution, may be defined by the coefficient of skewness $\alpha = M_3 / M_2^{3/2}$.

The factors M_2 and M_3 represent the second and third moment about the mean value of the distribution p^*.

The deviation between both distributions was also defined by an emperical parameter:

$$\alpha_* = \frac{q(\rho=0) - q(\rho=1)}{q_1(\rho=0) - q_1(\rho=1)} \tag{15}$$

where: $\rho = \frac{z}{\sqrt{m_o}}$,

$q(\rho=0)$ and $q(\rho=1)$ are the values of the cumulative distribution $q(\rho)$ for the values $\rho = 0$ and $\rho = 1$,

$q_1(\rho=0)$ and $q_1(\rho=1)$ are the corresponding values for the Gaussian distribution.

Consequently in the parameter α_* the areas between the values $\rho = 0$ and $\rho = 1$ are compared for the distribution $p(\rho)$ and the Gaussian distribution.

It also follows that for a Gaussian distribution: $q(\rho=0) = 0{,}5$ and $q(\rho=1) = 0{,}159$, so that the considered area is $0{,}341$. If the distribution $p^*\left(\frac{z}{\sqrt{m_o}}\right)$ is Gaussian, then $\alpha_* = 1$ and $\alpha = 0$.

The coefficients α and α_* computed from the records appeared to be correlated with the factor: $L_m^2\sqrt{m_o}/D^3$ (fig.3), where D is the water depth; L_m is a value for the wave length, computed by means of equation (4) using the mean period T_m. The value T_m is defined as twice the average time interval between two successive zero-crossings of z=f(t).

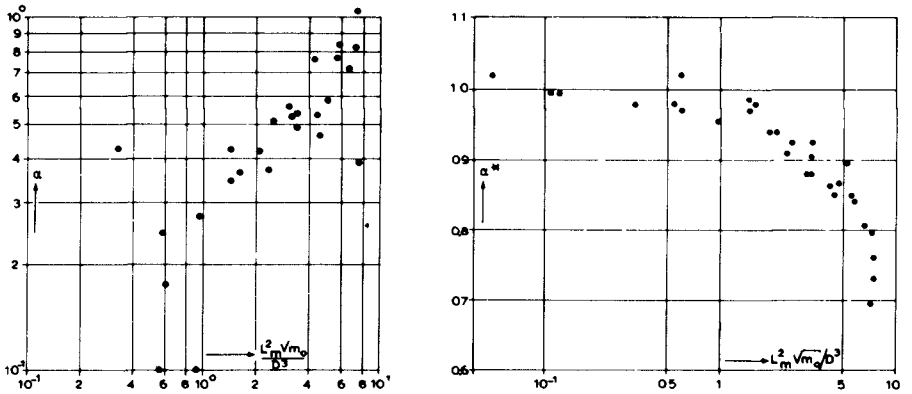

Fig 3 Relation between $L_m^2\sqrt{m_o}/D^3$ and α c q α*

The parameters obtained from the records studied, varied as follows:

$\sqrt{m_o}$ from 0,15 m up to 0,80 m. ($H_{1/3}$ from 0,60 m up to 3,50 m).

L_m from 18,0 m up to 60,0 m.

D from 3,50 m up to 17,0 m.

The scattering of the points in figure 3 may be due to the fact that an interval of only 10 minutes was taken from each record in order to obtain a statistically stationary process; a longer time interval may result in a significant change in water depth (tidal motion) or wind force. Furthermore, the smaller the wave energy spectrum, the better L_m will represent the average wave length.

For most p(z) distributions, the high values of z show a significant departure from the Gaussian curve. It is not clear wether these deviations can be fully explained by statistical variations. This phenomen has not been studied in detail.

From the correlations of fig.3 it appears that α_* shows a better correlation than the description of the skewness by means of α. The scatter in the results of α may also be due to the fact

that M_3 does not give an unambigious interpretation of the skewness.

In the following pages only the values of α_* will be considered; the results, however, are based on separate computations with α as well as α_*

§ 3. Distribution of the wave heights.

Four parameters (fig.4) have been used to describe the wave heights as fully as possible.

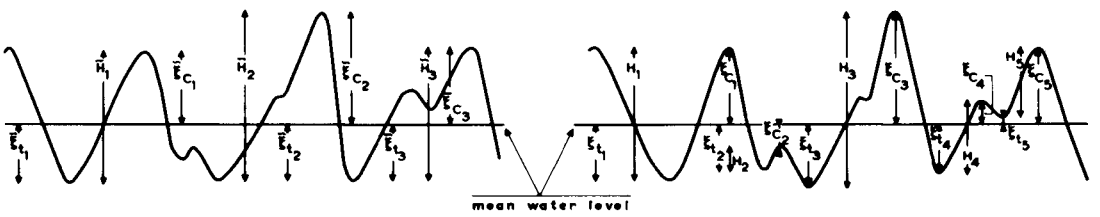

Fig 4 Wave height parameters

The wave heights $\tilde{\tilde{H}}$, measured from trough to crest and $\tilde{\tilde{\zeta}}$ measured from mean level to crest or trough, are defined for those waves which have exactly one zero crossing between crest and the predeeding trough. Between two successive zero crossings the highest crest and the lowest trough are considered.

The wave heights H and ζ are defined for all waves irrespective of the zero crossings.

When determing the wave heights, H and ζ, the sensitivity of the measuring instrument is important. The more sensitive the instrument, the more detailed the surface movement recorded. Waves less than 5 cm high and those between 5 and 10 cm with a period less than 1 second, were not included in this study. The measuring steps of the gauge were 4 cm. It was evident from the energy spectra of the records that waves with a period less than 1 sec contribute very little to the total wave energy.

Furthermore the distribution of ζ_c (measured from mean level to crest) and the distribution of ζ_T (measured from mean level to trough) will be considered separately.

The statistical distributions of the heights H, $\tilde{\tilde{H}}$, ζ_c, $\tilde{\tilde{\zeta}}_c$, ζ_T, and $\tilde{\tilde{\zeta}}_T$ show remarkable differences. The cumulative distribution of the

several parameters obtained from a 10 minute record are shown in fig.5 (wave height interval 10 cm.).

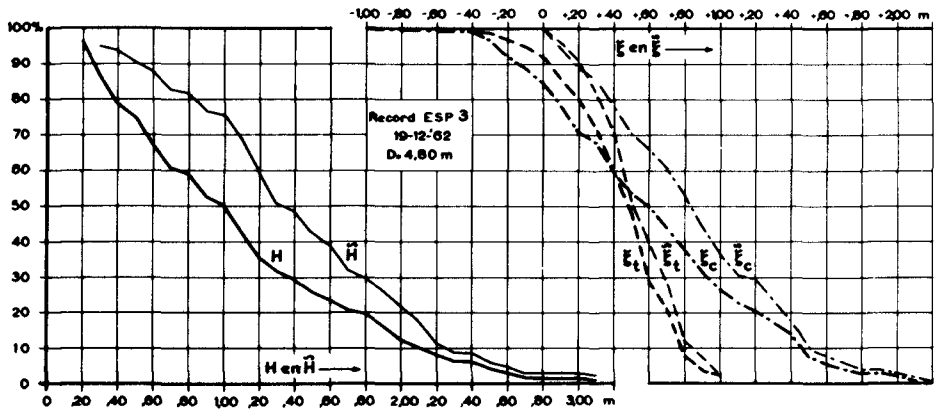

Fig 5 Example of a cumulative probability distribution q[H],q[H̃],q[ξ] and q[ξ̃]

The factors which influence these distributions will be discussed first.

In the lineair case (§§ 1, 2 and lit.1), probability distributions of ξ are derived by Cartwright and Longuet Higgins (assuming that the distribution of the ordinates of the sea surface should be Gaussian.) Then the probability distribution $p(\xi)$ is a function of $\sqrt{m_o}$ and ε ; $\sqrt{m_o}$ is the area of the energy spectrum and ε defines the relative width of the energy spectrum :

$$\varepsilon^2 = \frac{m_o m_4 - m_2^2}{m_o m_4} \tag{16}$$

where m_n is the n^{th} moment about the origin of the energy spectrum (see equation (7))

A general assumption of the distributions of H, $\tilde{H}$, ξ and $\tilde{\xi}$ may be

$$p(H;\xi;\tilde{H} \text{ or } \tilde{\xi}) = f\left[p(z), \sqrt{m_o}, \varepsilon\right] \tag{17}$$

or

$$p(H;\xi;\tilde{H} \text{ or } \tilde{\xi}) = f\left[\alpha_4 , \sqrt{m_o}, \varepsilon\right] \tag{18}$$

By means of (18) the wave height distributions for general cases $\alpha_4 = 1$ and $\alpha_4 \neq 1$ are studied in comparison with those derived from the lineair model.

a. Distributions of the values ξ_c and ξ_T

When $\alpha_4 \approx 1$ (distribution of sea surface is nearly Gaussian), the

distributions derived from the wave records correspond to a great extent with the theoretical curves given by Cartwright and Longuet Higgins. After application of the χ^2 test, no significant deviation was found. Three examples are given in table 1. The records with $\alpha_* < 1$ have been divided into three groups in which α_* is 0,9 - 0,8 and 0,7 respectively.

For each group a comparison has been made between the cumulative distributions of ξ_c and ξ_T obtained from observations and the corresponding theoretical distributions with the same values of $\sqrt{m_o}$ and ε. Correction factors, by which the theoretical values must be multiplied to obtain the measured ones, have been derived from this comparison. It was found that these factors are not influenced by ε. From the result in fig. 6 it is seen that ξ_c increases and ξ_T decreases when α_* decreases.

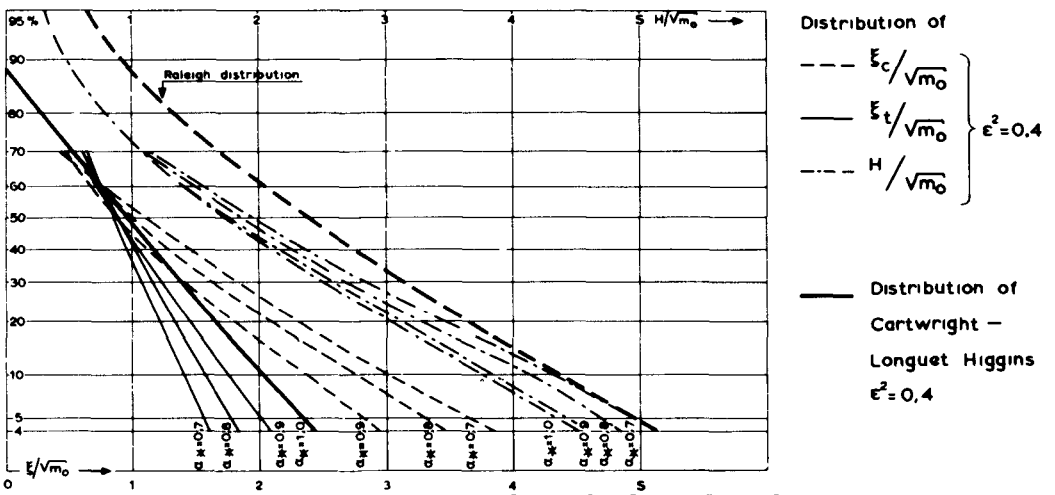

Fig 6 The cumulative probability distributions $q\left[\xi_c/\sqrt{m_o}\right]$, $q\left[\xi_t/\sqrt{m_o}\right]$ and $q\left[H/\sqrt{m_o}\right]$ for different values of α_*

b. Distribution of the wave height H. (measured from trough to crest).

When $\alpha_* \simeq 1$, the probability distribution of H can be represented by the formula:

$$p(\varphi) = \tfrac{1}{4} r^{1/2} \cdot \varphi \cdot e^{-\frac{1}{8}\varphi^2/r^{1/4}} + a^2\left(1 - r^{3/4}\right)\varphi \cdot e^{-a\varphi} \qquad (19)$$

where $\varphi = H/\sqrt{m_o}$, $r = 1 - \varepsilon^2$ and $a = 2\left(1 + r^{3/8}\right)/(2\pi r)^{1/2}$

The first term in the right member of (19) represents a Raleigh distribution, multiplied by a factor; the additional term is

derived empirically.

Formula (19) has been verified for about 100 wave records, for which $\alpha_* \approx 1$, while different values of $\sqrt{m_o}$ and ε were considered. Furthermore ε has been computed from:

$$1 - \varepsilon^2 = (a/2n)^2 \qquad \text{(lit.1)} \qquad (20)$$

where a is the number of zero crossings for a specific record and n is the number of waves occuring in the record; $\sqrt{m_o}$ is the area of the energy spectrum.

These spectra have been computed by a computer.

The limiting case of (19), $\varepsilon \to 0$, corresponds with the distribution for a very narrow spectrum: then

$$p(\varphi) \to \tfrac{1}{4}\varphi e^{-\frac{1}{8}\varphi^2} \qquad \text{(Raleigh distribution)} \quad (21)$$

The limiting case $\varepsilon \to 1$ gives the distribution for a very broad spectrum, then $p(\varphi) \to 0$ This case can occur when a wave of high frequency and small amplitude is superimposed on another wave of lower frequency (lit.1). The high frequency wave forms a ripple in the base wave and the distribution of the maxima $p(\xi/\sqrt{m_o})$ of the composed wave tends to the assumed Gaussian distribution of the ordenates of the sea surface $p(z/\sqrt{m_o})$

The cumulative probability $q(\varphi)$ is defined as the probability of φ exceeding a given value:

$$q(\varphi) = \int_{\varphi}^{\infty} p(\varphi)\, d\varphi \qquad (22)$$

Substituting from (19) it is found:

$$q(\varphi) = r^{3/4} \cdot e^{-\frac{1}{8}\varphi^2/r^{1/4}} + (1-r)^{3/4}(1+a\varphi)\cdot e^{-a\varphi} \qquad (23)$$

Graphs of $p(\varphi)$ and $q(\varphi)$ for various values of ε^2 are shown in fig.7.

In those wave records where $\alpha_* < 1$, correction factors have been computed analogous to those for ξ. The corrected graphs $q(\varphi)$ for various values of α_* and for $\varepsilon^2 = 0.4$ are given in fig.6. Examples of the application of the χ^2 test are given in table 1.

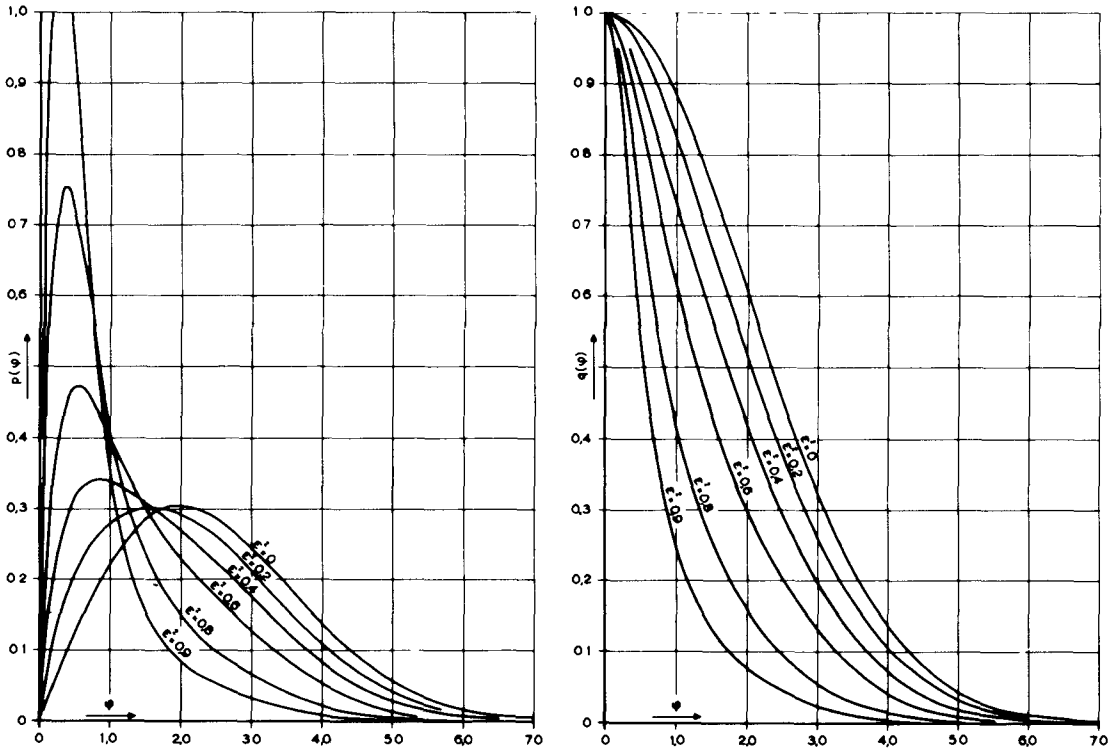

Fig 7 Probability distribution $p[\varphi]$ and cumulative distribution $q[\varphi]$, for $\alpha_x = 1$ and different values of ε^2

c. Distribution of $\tilde{\xi}$ and $\tilde{H}$.

The distributions of $\tilde{\xi}_c$ and $\tilde{\xi}_t$ obtained from the records, correspond sufficiently with the Raleigh distribution when $\alpha_x \approx 1$ The distribution of $\tilde{H}$, where $\alpha_x \approx 1$, deviates from the Raleigh distribution. The graphs for the cumulative probabilities

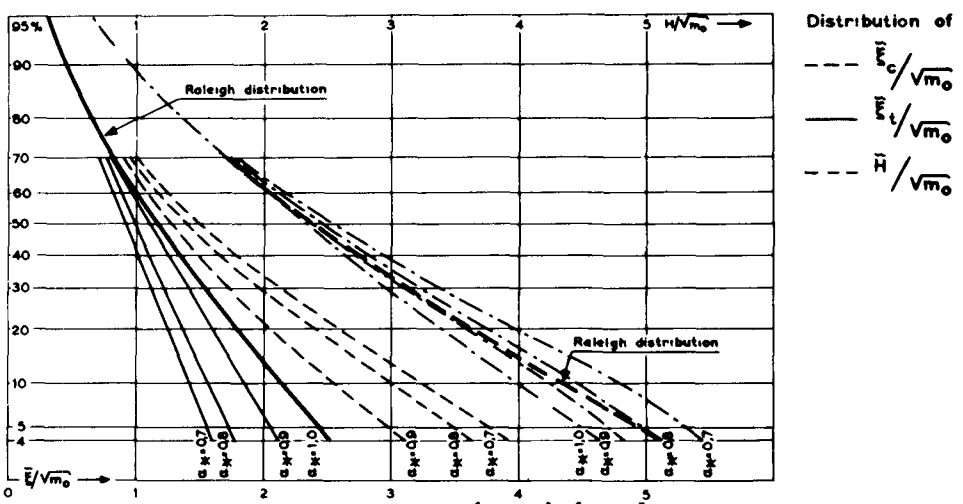

Fig 8 The cumulative probability distributions $q\left[\tilde{\xi}_c/\sqrt{m_0}\right]$, $q\left[\tilde{\xi}_t/\sqrt{m_0}\right]$ and $q\left[\tilde{H}/\sqrt{m_0}\right]$ for different values of α_x

record	$\sqrt{m_o}$ [cm]	ε^2	α_*	$p(\zeta_c)$		$p(\zeta_t)$		$p(H)$		$p(\tilde{\zeta}_c)$		$p(\tilde{\zeta}_t)$		$p(\tilde{H})$	
				χ^2	$p(\chi^2)$	χ^2	$p(\chi^2)$	χ^2	$p(\chi^2)$	χ^2	$p(\chi^2)$	χ^2	$p(\chi^2)$	χ^2	$p(\chi^2)$
Tr 98a	41	0.441	1.00	5.51	40%	9.96	8%	11.99	10%	7.28	20%	11.0	5%	9.60	20%
Tr 24.7	28	0.202	1.02	8.54	28	13.23	7	6.95	79	13.97	6	12.70	8	21.05	3
Tr 9.8	47	0.370	0.998	8.86	29	4.52	73	14.22	15	7.82	18	7.75	17	4.72	85
ESP 2	57	0.412	0.88	16.64	4	12.00	15	18.27	5	32.29	< 1	15.39	4	19.61	5
ESP 15	56	0.391	0.765	46.03	< 1	57.66	< 1	15.59	21	65.30	< 1	54.45	< 1	12.12	21
ESP 3	53	0.412	0.82	49.16	< 1	24.21	1	15.03	15	71.29	< 1	20.82	< 1	9.20	55
						I		II				III			

I. comparison with frequency distributions of Cartwright and Longuet Higgins ($\alpha_* = 1$).

II. comparison with frequency distributions according to equation (19); ($\alpha_* = 1$).

III. comparison with Raleigh distribution.

table 1

$q(\tilde{H}/\sqrt{m_o})$ and $q(\tilde{\zeta}/\sqrt{m_o})$ for $\alpha_* \approx 1$ and the corrected graphs for various values of α_* are shown in fig. 8. See also table 1. and § 3a.

The results shown in fig. 8, correspond on the whole with those obtained from the measurements by Goodknight and Russel (lit.6). These measurements were taken during hurricanes in the Gulf of Mexico and off the Pacific Coast of the U.S.A.

§ 4. Significant wave heights.

Irregular wave motion can be conveniently described by taking the highest $1/n^{th}$ waves of the total number in a sample. In practice the average value of the highest waves $H_{1/3}$ or $H_{1/10}$ is often used, as is the mean wave height H_m. For practical purposes the relations between these quantities have been studied by several investigators using theoretical formula (lit.5) as well as measurements taken in nature and in a laboratory. The relations can be computed from the formula given in § 3. This has been done only for the wave heights H and $\tilde{H}$; (for § see lit.1).

The $1/n^{th}$ highest waves correspond to the values of $\varphi(=H/\sqrt{m_o})$ greater than φ', which is defined by

$$q(\varphi') = \int_{\varphi'}^{\infty} p(\varphi)\, d\varphi = 1/n \qquad (24)$$

The average value of φ for these maxima, denoted by $\varphi_{1/n}$ is:

$$\varphi_{1/n} = n \int_{\varphi'}^{\infty} p(\varphi) \cdot \varphi \, d\varphi \qquad (25)$$

The mean wave height φ_m is found from:

$$\varphi_m = \varphi_1 = \int_{0}^{\infty} p(\varphi) \cdot \varphi \cdot d\varphi \qquad (26)$$

For the lineair case ($\alpha_* \approx 1$), $\varphi_{1/n}$ can be computed from (19) and (25). The values of $\varphi_{1/n}$ (n=1, 3 and 10) have been computed for different values of ε, as have the ratios $H_{1/10}/H_{1/3}$, $H_{1/10}/H_m$ and $H_{1/3}/H_m$; they are given in table 2 (see also fig.9).

A formula of $p(\varphi)$ for the non-lineair cases ($\alpha_* < 1$) has not yet been derived. In order to dertermine the relation between $H_{1/10}$, $H_{1/3}$ and H_m for such cases, use has been made of the fact that $H_{1/3}$ almost always corresponds to $H_{13,5\%}$ and $H_{1/10}$ with $H_{4\%}$. The values of $H_{13,5\%}$ and $H_{4\%}$ are exceeded by resp. 13,5 and 4% of the total number of wave heights in the sample. From the 100 records with different values of ε and α_* it was found that on the average $H_{1/3} = 0,996\ H_{13,5\%}$ and $H_{1/10} = 1,027\ H_{4\%}$; only a slight scattering of the points in the correlation occurs. By means of these relations the ratios $H_{1/10}/H_{1/3}$ $H_{1/10}/H_m$ and $H_{1/3}/H_m$ for $\alpha_* = 0,9 - 0,8$ and 0,7 have been determined (table 2) from the distributions $p(H)$ and $p(\tilde{H})$, given in §3.

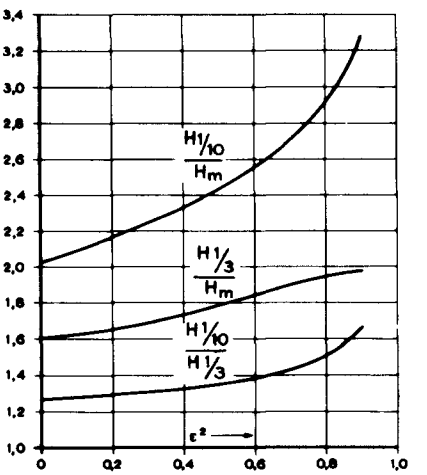

Fig 9 The quotients of $H_{1/10}$, $H_{1/3}$ and H_m [for $\alpha_* = 1$] as a function of ε^2

	$\alpha_* = 1$			$\alpha_* = 0,9$			$\alpha_* = 0,8$			$\alpha_* = 0,7$		
	$\varepsilon^2=0$	0.4	0.6	$\varepsilon^2=0$	0.4	0.6	$\varepsilon^2=0$	0.4	0.6	$\varepsilon^2=0$	0.4	0.6
$H_{1/10}$ / H_m	2.03	2.53	2.56	2.03	2.29	2.55	2.03	2.31	2.56	2.05	2.30	2.58
$H_{1/3}$ / H_m	1.60	1.74	1.85	1.61	1.77	1.86	1.62	1.79	1.87	1.62	1.79	1.88
$H_{1/10}$ / $H_{1/3}$	1.27	1.33	1.38	1.26	1.31	1.37	1.26	1.29	1.37	1.26	1.30	1.37

table 2

When the distribution $p(\bar{\varphi})$ approximates to a Raleigh distribution, $\bar{\varphi}_{1/10}$, $\bar{\varphi}_{1/3}$ and $\bar{\varphi}_m$ can also be computed from (25). From these values it was found that:

$$\bar{H}_{1/10}/\bar{H}_m = 2{,}00, \quad \bar{H}_{1/3}/\bar{H}_m = 1{,}60 \text{ and } \bar{H}_{1/10}/\bar{H}_{1/3} = 1{,}27.$$

It has been found that average values of ε and of the various ratios $H_{1/3}/H_m$ etc. may be applied along the Dutch North Sea Coast. The value of ε^2 is almost always found in the interval 0,4 -0,6.

The average ratios have been determined for different values of α_* from 100 records. It was found that the deviation of α_* from unity is not important (table 3).

	$H_{1/10}/H_m$	$H_{1/3}/H_m$	$H_{1/10}/H_{1/3}$	$\bar{H}_{1/10}/\bar{H}_m$	$\bar{H}_{1/3}/\bar{H}_m$	$\bar{H}_{1/10}/\bar{H}_{1/3}$
$\alpha_* \sim 1$	2,45	1 72	1 54			
$\alpha_* < 1$	2,34	1 75	1,30	2 04	1,58	1 24

table 3

However the value of ε greatly affects the distribution of the wave height H. The value of ε is largely determined by the sensitivity of the measuring instrument. When an instrument is used which damps out high frequency waves (for example a pressure meter) the energy spectrum is narrowed artificially and the values of ε will decrease. Thus the kind of instrument with which the records have been made must be taken into account. Wiegel (lit.7) reviewed the ratios between certain values of $H_{1/n}$ measured in various seas. Most of these measurements were taken with a pressure meter. When ε is zero, the values correspond on the whole with the values given in table 1.

Some results of measurements by Piest and Walden (lit.8) in the German Bight are given, which also deals with the relation between $\bar{H}_{1/10}$, $\bar{H}_{1/3}$ and $\bar{H}_m$. These ratios correspond well enough with the above mentioned values.

§5. Choice of a significant wave height.

In the foregoing the parameters H, ζ, $\overset{\frown}{H}$ or $\overset{\frown}{\zeta}$ were used to describe the wave motion for practical purposes. It appears however, that the parameters ζ and $\overset{\frown}{\zeta}$ are preferable to H and $\overset{\frown}{H}$ when the difference between deep water and shallow water waves is important. The distribution of H or $\overset{\frown}{H}$ is not greatly affected by the difference between deep and shallow water wave motion but the distribution of ζ, (and especially ζ_c and ζ_T) is. This can be expressed in terms of α_* which depends on the factor $L_m^2 \sqrt{m_o}/D^3$

In the preceeding pages it has been demonstrated that high waves in shallow water show an increasing eccentricity relative to the mean level if the water depth decreases. It is evident that the movement of the water particles in shallow water waves differs considerably from that in deep water waves. Therefore, when a wave motion is described by means of the parameters H or $\overset{\frown}{H}$, the factor $L_m^2 \sqrt{m_o}/D^3$ must also be taken into account.

In the second place we have seen that the distributions of $\overset{\frown}{H}$ and $\overset{\frown}{\zeta}$ are independent of the width of the energy spectrum (expressed in terms of ε). The distributions $p(\overset{\frown}{H})$ and $p(\overset{\frown}{\zeta})$ correspond to a great extent with the formula of the Raleigh distribution, which occurs when the energy spectrum of a wave motion is very narrow. Thus, by using the parameters $\overset{\frown}{H}$ or $\overset{\frown}{\zeta}$ (by which usually only the higher waves are described), a rather rough picture of the actual wave motion can be given. The cumulative distribution of $\overset{\frown}{H}/\sqrt{m_o}$ and $\overset{\frown}{\zeta}/\sqrt{m_o}$ have the shape of a Raleigh distribution with the same m_o as the energy spectrum of the actual wave motion.

Finally, it should be noted that for shallow water wave research in the laboratory, the influence of α_* and thus of $L_m^2 \sqrt{m_o}/D^3$ cannot be neglected.

Conclusions and discussion.

In the case of wave motion in relatively shallow water, the distribution of the "trough to crest" wave heights H or $\tilde{H}$, do not differ much from those in deep water. However, the heights from mean level to crest ζ_c or $\tilde{\zeta}_c$, and to trough, ζ_T or $\tilde{\zeta}_T$, may differ greatly. It appeared that the statistical distribution of wave heights in relatively shallow water depends on:

a. The standard deviation $\sqrt{m_o}$ of the distribution of the sea surface ordinates z(m_o is also the area of the energy spectrum)
b. The relative width of the energy spectrum (denoted by ε);
c. The relation between the wave length L_m, the mean energy m_o and the water depth. This relation can be expressed by $L_m^2 \sqrt{m_o}/D$ Transition from deep water into shallow water wave distributio also results in a skewness of the distribution of the ordinate of the sea surface. This skewness is defined by α or α_*; especially α_* is closely correlated with the factor $L_m^2 \sqrt{m_o}/D^3$

In this study the statistical variation of m_o has not been examined, nor has the problem of how far the wave motion can be considered as a statistically stationary process. This condition has been satisfied as well as possible by taking at least one hundred waves during the measuring time under which conditions depths and wind forces did not change significantly during the measurement. The maximum time interval of records was 30 minutes; the minimum was 10 minutes.

In some cases very broad energy spectra were found; it appeared that in those cases the wave motion was composed of two or more separate wave trains from different directions. Such spectra have not been used for this study, as a mean wave length cannot be defined.

References.

1. D.E. Cartwright and M.S. Longuet Higgins.
"The statistical distribution of the maxima of a random function".
Proceedings of the Royal Society, A, volume 237, 1956.

2. S.O. Rice.
"The mathematical analysis of random noise".
Bell Syst. Techn. Journ. nr. 23 and nr. 24, 1944-'45.

3. G.G. Stokes.
"On the theory of oscillatory waves".
Trans. Comb. Phil. Soc., 8. 441-55, 1847.

4. M.G. Kendall.
"The advanced theory of statistics".
London 1948.

5. M.S. Longuet Higgins.
"On the statistical distribution of the heights of sea waves".
Journal of Marine Research Vol. XI, 1952 nr. 3.

6. R.C. Goodknight and T.L. Russel.
"Investigations of the statistics of wave heights".
Journal of Waterways and Harbours Division. Volume 89, May 1963.

7. R.L. Wiegel.
"Wind, waves and swell".
Proceedings on the 7 th Conference on Coastal Engineering,
The Hague, The Netherlands 1960.

8. H. Walden und J. Piest.
"Vergleichsmessungen des Seeganges".
Deutscher Wetterdienst, Einzelveroff. Nr. 30, Hamburg 1961.

Chapter 9

CARACTERISTIQUES DE L'AGITATION MARITIME DAN LA CÔTE OUEST DU PORTUGAL METROPOLITAIN

Júlio Patriarca Barceló
Ingénieur du Service d'Hydraulique
Laboratório Nacional de Engenharia Civil, Lisboa, Portugal

RESUME

Dans cette communication on présente les caractéristiqu générales de l'agitation maritime au large du port de Figueira Foz dans la période comprise entre 1954 et 1960 et les rappor entre les paramètres qui caractérisent les trains d'ondes obse vés près de la côte, en ce port. La présente étude est un appo à la connaissance du régime général de l'agitation à la côte oue du Portugal metropolitain et, faute d'autres études complètes actualisées dans ce domaine, on la présente comme une approx mation pouvant avoir une large application pratique.

INTRODUCTION

L'agitation maritime se caractérise, à proximité des côt par l'existence de trains d'ondes qui, em général, présentent d caractéristiques bien définies (voir Fig.1), à l'opposé de ce q se passe dans les zones de génération où l'agitation est extrên ment irrégulière. La nature aléatoire des trains d'ondes réell fait que soient définies, par des méthodes statistiques, des v leurs de hauteur et période se rapportant à des ondes sinusoïdal equivalentes dont l'analyse peut se faire facilement par l'applic tion de la théorie mathématique de la houle.

L'observation des caractéristiques de l'agitation maritin est fondamentale et est faite d'après des méthodes différent telles que les observations tachéométriques et les enregistrement pris au moyen d'ondographes. Les valeurs obtenues permettent définir, pour les trains d'ondes, des paramètres caractéristiqu dont les rapports ont fait l'objet d'étude et de comparaison av des valeurs théoriques et expérimentales.

Dans cette ligne et en prenant comme base les observatio réalisées au port de Figueira da Foz* (voir Fig.2) dans la pér de 1954 - 1960, qui montent à 3000 à peu près, on a fait l'étu

---

* Observations réalisées par la "Junta Autónoma do Porto Figueira da Foz"

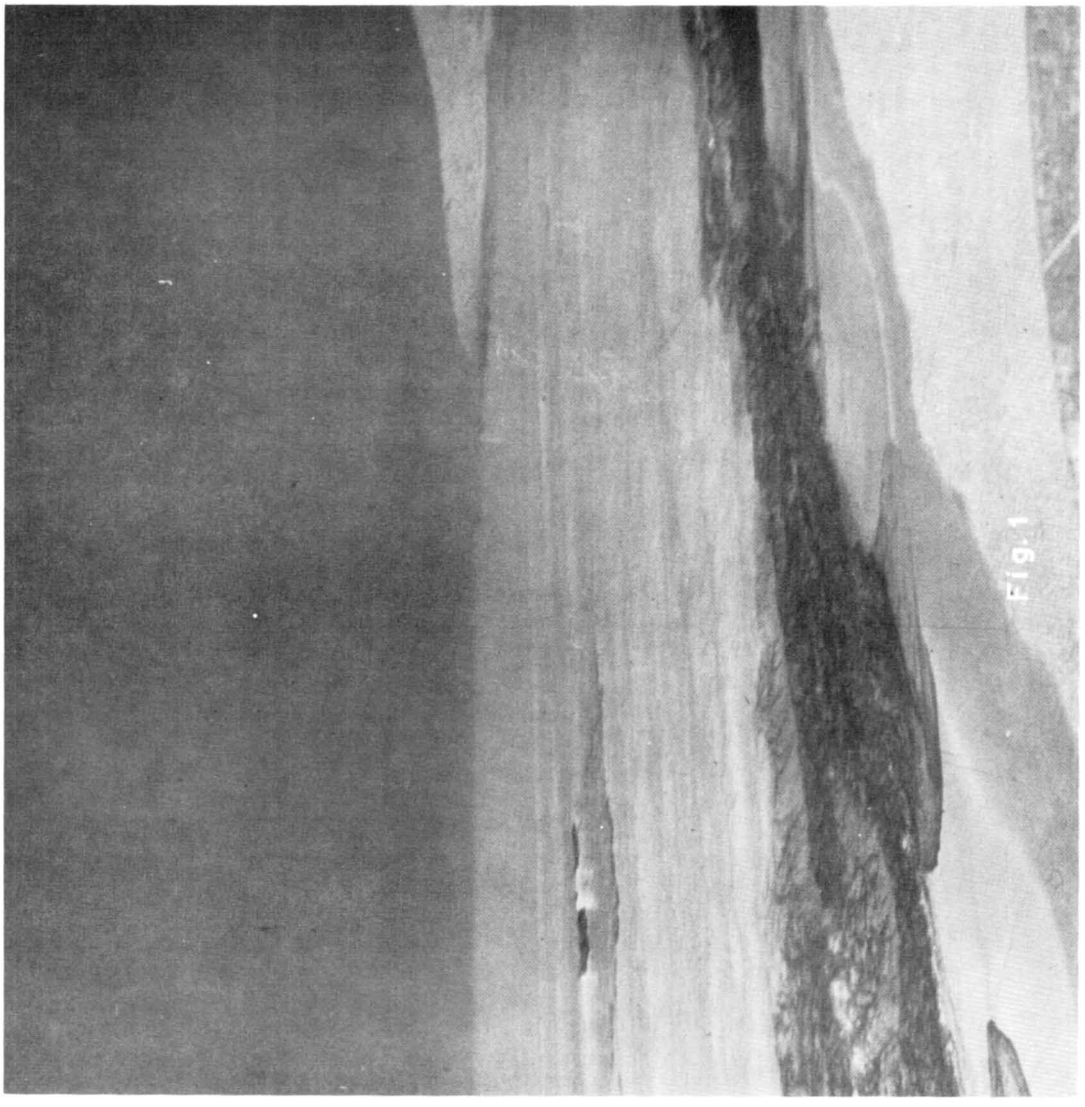
Fig. 1

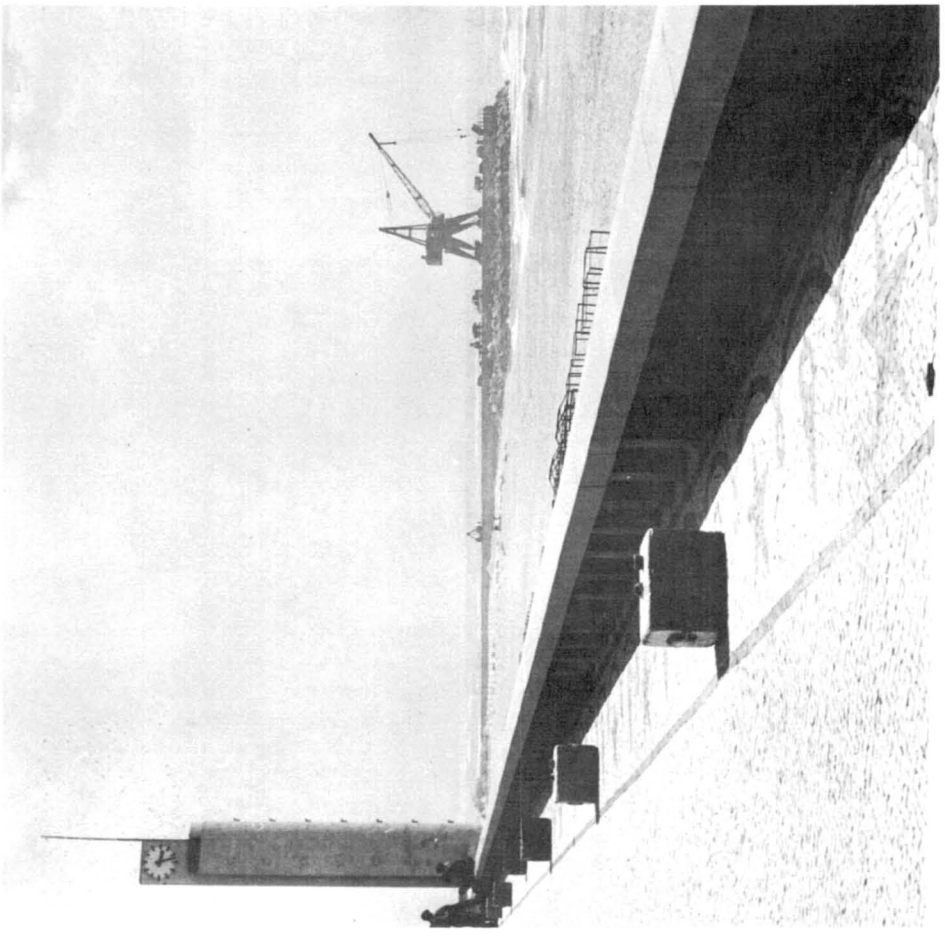

Fig. 3

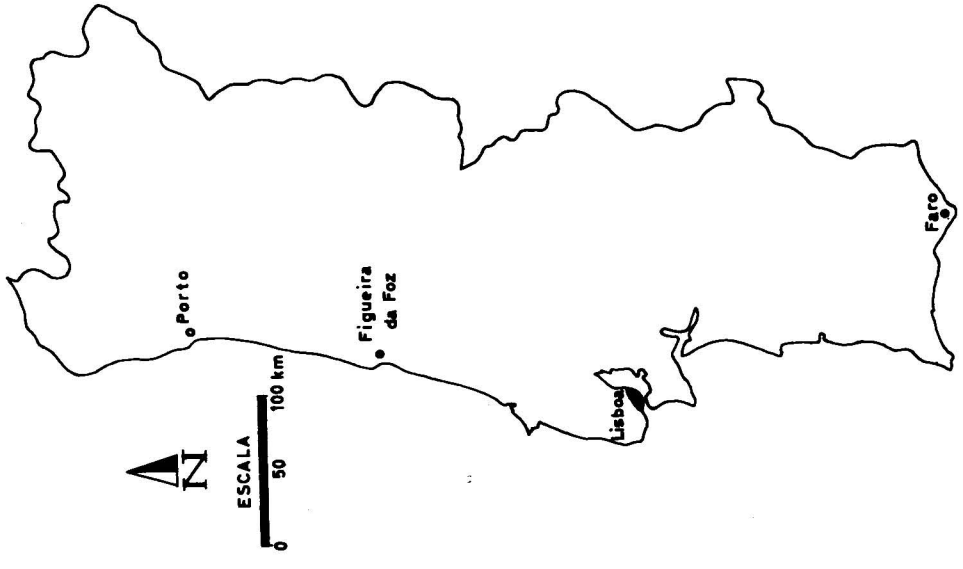

Fig. 2

statistique des trains d'ondes observés dans le dessein de contribuer pour la connaissance des caractéristiques générales du régime de l'agitation et aussi des rapports entre les paramètres indiqués.

Les observations de l'agitation à Figueira da Foz sont faites trois fois par jour, au moyen d'un tachéomètre installé dans une tour à la cote environ 25 m (voir Fig.3) qui permet d'accompagner les mouvements d'une bouée placée à la profondeur d'environ 14 m et à la distance 1 400 mètres de la station. Les caractéristiques de l'agitation mesurées sur la bouée sont la période et la hauteur des ondes qui composaient les trains observés; la direction de l'ondulation est mesurée par l'ajustement d'un tronçon horizontal de référence aux crêtes des ondes. Chaque période d'observation comprend des lectures correspondant au passage de 22 crêtes successives, pour la détermination de hauteurs et périodes, suivies de lectures de direction pour trois zones distinctes: au large, immédiatement avant la zone de déferlement, entre cette zone et la côte (voir Fig.4).

Prenant pour base ces observations, moyennant le tracé de plans de l'ondulation, on a fait l'extrapolation des caractéristiques de l'agitation près de la côte vers des profondeurs supérieures à une demi-longueur d'onde (caractéristiques au large). Pour le but en cause, on a reconnu des défauts dans ces observations, qui dérivent de la localisation de la zone d'observation dans une baie et devant l'embouchure d'un fleuve (baie de Buarcos et fleuve Mondego) (Fig.5). Les défauts principaux sont l'influence des courants du Mondego et la grande refraction que subissent certaines ondes actuantes du quadrant nord, ce qui conduit à l'indétermination dans l'extrapolation. L'erreur introduite par les courants de marée est due à ce que leur influence n'est pas prise en considération lors du tracé des plans d'ondulation par méconnaissance des caractéristiques du champ des courants; on peut dire, en face des plans d'ondulation tracés dans ce but, que cette influence peut être de quelques degrés dans la zone d'observation. La grande refraction subie par les ondes du quadrant nord fait que certaines ondes ayant des directions différentes au large, aient la même direction près de la côte. Il s'ensuit que l'extrapolation basée sur les directions observées conduit à l'indétermination. En plus de ces deux défauts, d'autres existent tels que: l'inertie et les mouvements secondaires de la bouée, la perte de la bouée par rupture de la chaîne lors de violentes tempêtes et l'impossibilité d'observation en des jours de brouillard ou de grosse pluie.

Pour le tracé des plans d'ondulation, on a adopté la technique courante se basant sur la propagation d' ondes sinusoïdales

JUNTA AUTÓNOMA DO PORTO DA FIGUEIRA DA FOZ

779

Coordenadas (H/G-P. C.)
DA ESTAÇÃO DE OBSERVAÇÃO
M = – 6[illegible] m.
P = + 53.7[illegible] m.
DO SINAL (BOIA)
M = – 63.848.00 m.
P = + 53.[illegible].00 m.

OBSERVAÇÃO DA ONDULAÇÃO

ANO 1958 MÊS DEZEMBRO DIA 1o

HORA 12 h 15 m

—VENTO À HORA DA OBSERVAÇÃO: D ___ V ___

—PM. DIURNO NA ESTAÇÃO MAREGRÁFICA DE normal: H 15.25 A 3.o2

Nº de ordem das passagens das cristas e cavas	Ângulos de depressão: Cristas (b)	Cava (a)	(a–b)'	Amplitude da onda H (a–b)' H = (a–b)' × .21	Determinação do período: Períodos acumulados (Tseg)	Período de cada onda (Tseg)	Comprimento da onda para 13.4 m (44 pés) (L)	Declividade da onda (H/L)
1	1o	14	4	.84	00	1o	1o4	.81
2	1o	15	5	1.05	1o	11	116	.91
3	9	14	5	1.05	21	9	91	1.15
4	11	16	5	1.05	3o	13	141	.75
5	9	15	6	1.26	43	9	91	1.39
6	1o	16	6	1.2[illegible]	52	12	128	.93
7	11	14	3	.63	64	1o	1o4	.61
8	1o	15	5	1.05	74	14	153	.6[illegible]
9	9	14	5	1.05	88	11	116	.91
10	1o	15	5	1.05	99	11	116	.91
11	12	15	3	.63	11o	12	128	.49
12	11	14	3	.63	122	1o	1o4	.61
13	11	15	4	.84	132	1o	1o4	.81
14	11	15	4	.84	142	8	78	1.o8
15	1o	15	5	1.05	15o	12	128	.82
16	1o	15	5	1.05	162	13	141	.75
17	12	14	2	.42	175	15	165	.25
18	1o	15	5	1.05	19o	8	78	1.35
19	1o	13	3	.63	198	11	116	.54
20	1o	14	4	.84	2o9	11	116	.72
21	1o	15	5	1.o5	22o	1o	1o4	1.o1
22	11				23o			
SOMAS				19.32		23o	2422	17.53
MÉDIAS							11[illegible].3	
				7.77		79	836	6.77

Ca=119.4

Direcção de propagação da ondulação: Grados	Mil.	Ângulo vertical
86	4o	Zona A Av= 1o1.8o
88	9o	
87	8o	
89	6o	
89	5o	
MÉDIA: 88.44		
Const. 18o.81		
Rumo 269.25		
85	2o	Zona B Av= 1o4.8o
87	oo	
87	1o	
87	7o	
88	9o	
MÉDIA: 87.18		
Const. 18o.81		
Rumo 267.99		
88	6o	Zona C Av= 111.68
88	6o	
88	2o	
89	6o	
88	2o	
MÉDIA: 88.4o		
Const. 18o.81		
Rumo 269.21		

Cota à hora da observação 2.2o

CONSTANTES E ELEMENTOS DEDUZIDOS

1. Distância da estação de observação à boia .... 1.4o2.5om.
2. Azimute da direcção origem dos ângulos horizontais, catavento o anemógrafo .... 18o.81gr.
3. Correspondente azimute da boia .... 278.79gr.
4. Cota da estação de observação .... 2[illegible].53(ZH)
5. Altura do aparelho .... 1.55 m.
6. Cota do fundo, no local da boia .... 11.18(ZH)
7. Direcção de propagação de ondulação
7. 1-Ao largo, a .951 Kms, Zona A .... W 3o.8 S
   2-Imediatamente antes da rebentação, a .384 Kms. Zona B .... W 32.0 S
   3-Entre a rebentação e a costa a .163 Kms. Zona C .... W 3o.8 S
8. Elementos da onda

H médio	.92	Hs =	1.11
T médio	11.o	Ts =	11.[illegible]
(H/L) médio	.83	(H/L)s =	.[illegible]7

O OBSERVADOR: .... O CALCULADOR: ....

Mod F. M 101

Fig. 4

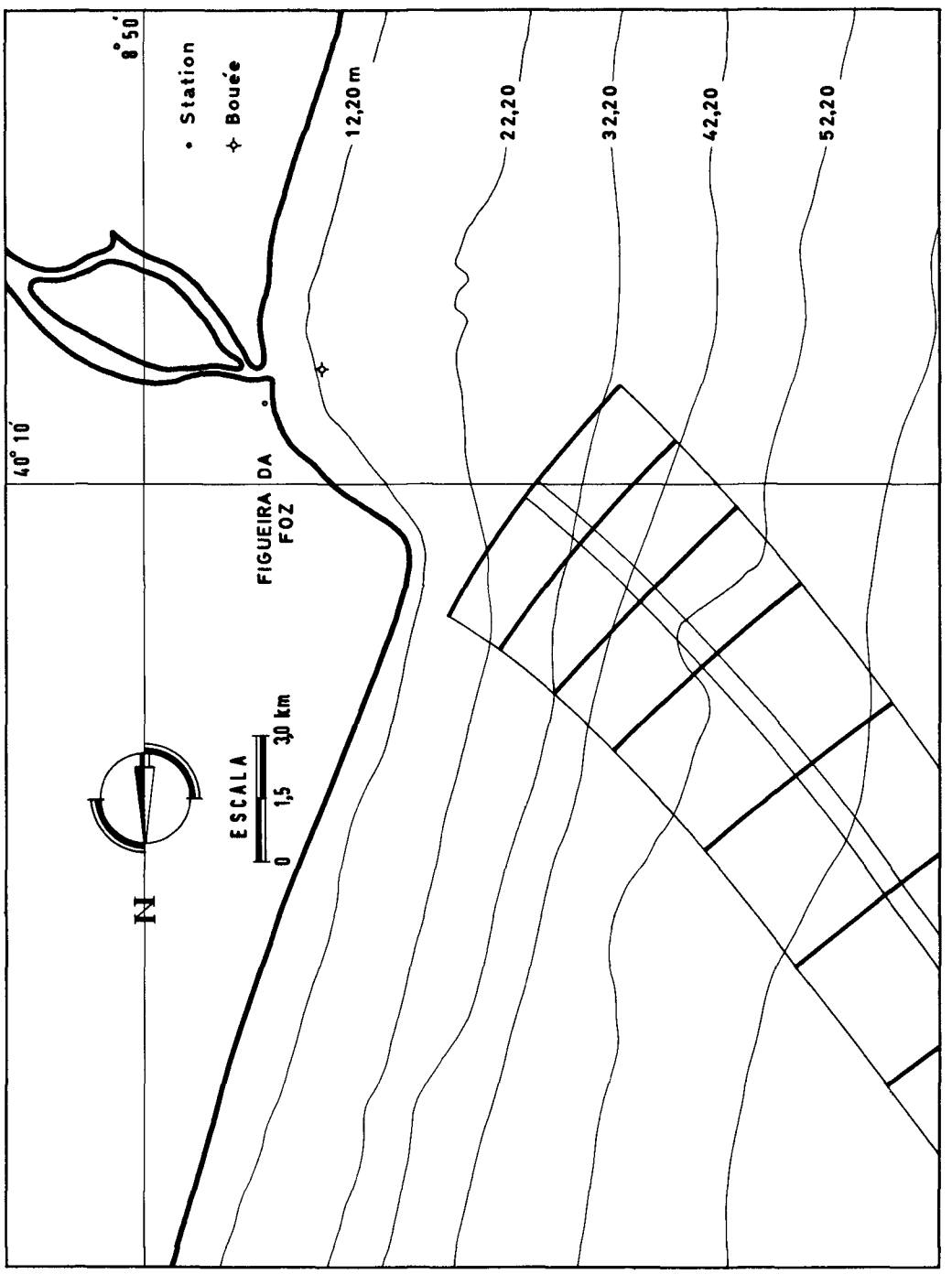
8°50'
40°10'
• Station
✧ Bouée
12,20 m
22,20
32,20
42,20
52,20
FIGUEIRA DA FOZ
ESCALA
0
1,5
3,0 km
N

Fig.5

aux hauteurs et périodes correspondant aux valeurs significatives des trains observés; la méthode utilisée a été celle des crêtes, établie d'après la théorie de Stokes.

CARACTERISTIQUES GENERALES DE L'AGITATION AU LARGE DE FIGUEIRA DA FOZ

Le régime de l'agitation dans la période allant de 1954 à 1960 a été étudié dans le but de connaître:

1 - les distributions des valeurs significatives de la hauteur et de la période de l'onde ($H_{1/3}$ et $T_{H1/3}$) et encore la distribution des valeurs de la direction.

2 - les courbes de fréquence, par corrélation des directions et des hauteurs significatives, des directions et des périodes significatives, des périodes significatives et des hauteurs significatives.

Ces distributions sont présentées à la Fig.6 et on y remarque ces traits fondamentaux:

a) Distribution des périodes significatives:

- valeurs comprises entre 6 et 20 sec.
- fréquence maximale entre 10 et 12 sec.
- 90% des ondes ont des périodes significatives inférieures à 14 sec.

b) Distribution des hauteurs significatives:

- valeur maximale de l'ordre des 11 m.
- fréquence maximale entre 1 et 2 m.
- 90% des ondes ont des hauteurs significatives inférieures à 3,5 m.
- le pourcentage des calmes est de l'ordre de 6%.

c) Distribution des directions: on remarque l'existence d'une vaste gamme de directions dans les quadrants NW et WS, aux caractéristiques suivantes:

- seulement 20% des ondes ont des directions dans le quadrant WS.
- la fréquence maximale se trouve entre W - 10° - N et W - 20° - N.

Les courbes de fréquence mentionnées à l'alinéa 2 sont caractérisées par:

a) Directions et hauteurs significatives (Fig.7): on a défini les courbes d'égale densité de fréquence (pourmillage

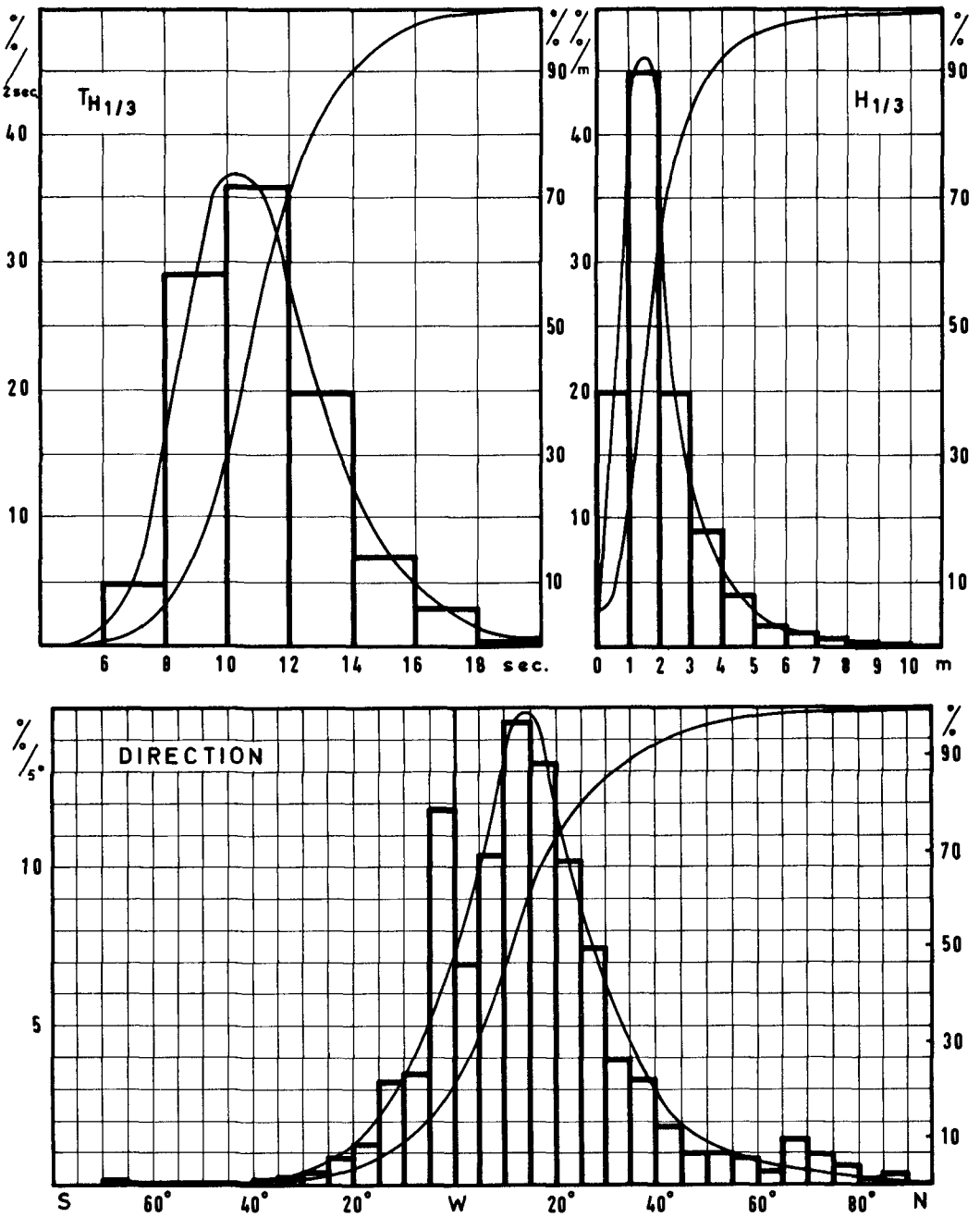
%/2sec
$T_{H1/3}$
40
30
20
10
6 8 10 12 14 16 18 sec.
%
90
70
50
30
10
%/m
$H_{1/3}$
0 1 2 3 4 5 6 7 8 9 10 m
%/5°
DIRECTION
10
5
S 60° 40° 20° W 20° 40° 60° 80° N

Fig. 6

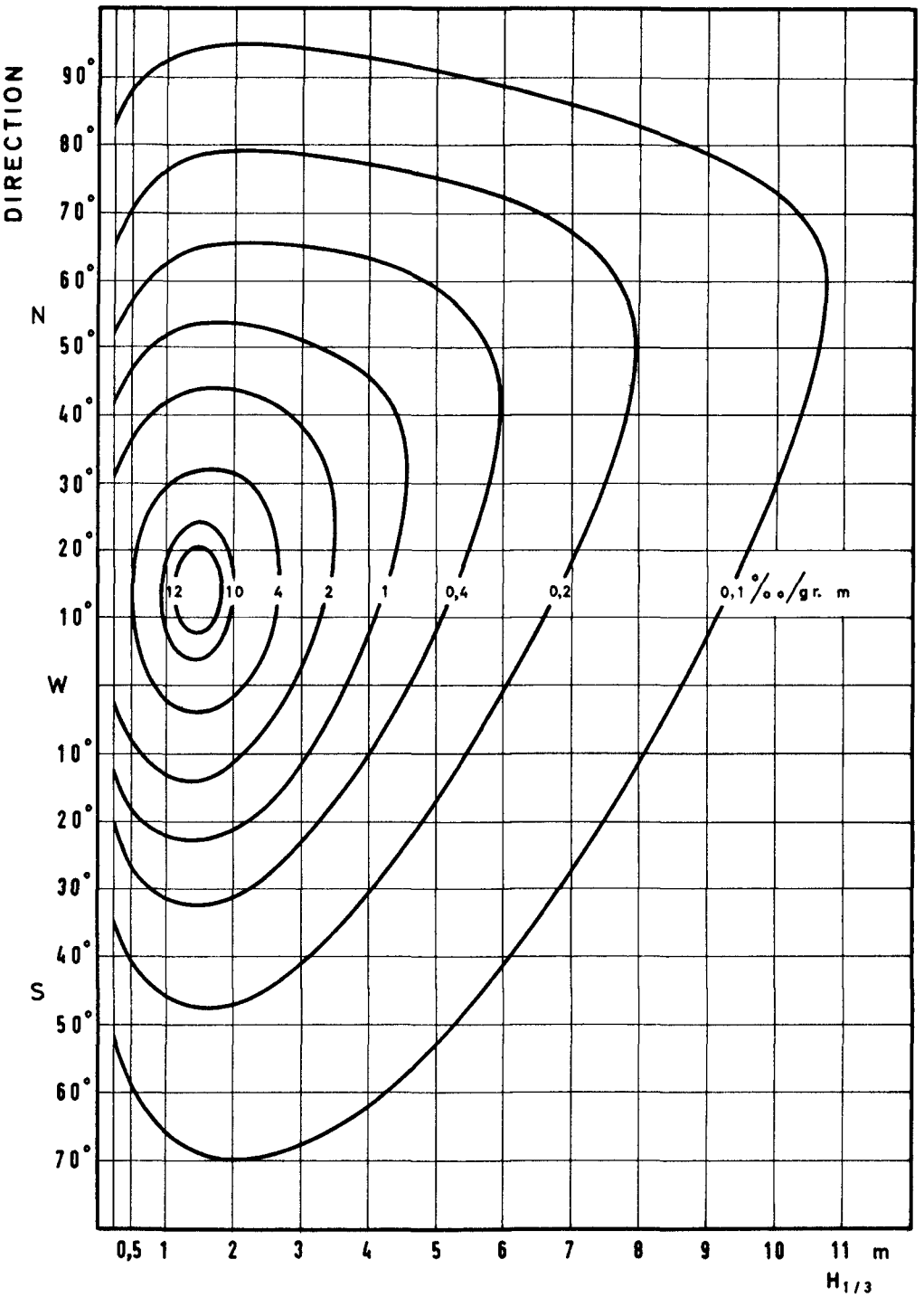
DIRECTION
N
W
S
90°
80°
70°
60°
50°
40°
30°
20°
10°
10°
20°
30°
40°
50°
60°
70°
12
10
4
2
1
0,4
0,2
0,1 ‰ e/gr. m
0,5 1 2 3 4 5 6 7 8 9 10 11 m
H1/3

Fig. 7

par unité du produit degré par mètre).

- la densité de fréquence maximale correspond à des directions comprises entre W - 10° - N et W - 20° - N associées à des hauteurs significatives comprises entre 1 et 2 m.
- les hauteurs significatives maximales sont associées à des directions de l'ordre de W - 60° - N.

b) Directions et périodes significatives (Fig.8) : on a défini les courbes d'égale densité de fréquence (pourmillage par unité du produit degré par seconde).

- la densité de fréquence maximale correspond à des directions comprises entre W - 10° - N et W - 20° - N associées à des périodes significatives comprises entre 10 et 11 sec.
- les valeurs les plus élevées de la période significative sont associées à des ondes du quadrant NW.

c) Périodes significatives et hauteurs significatives (Fig.9) : on a défini les courbes d'égale densité de fréquence (pourmillage par unité du produit seconde par mètre).

- la densité de fréquence maximale correspond à des périodes significatives de 10 sec. et à des hauteurs significatives de l'ordre de 1,5 m.
- les valeurs les plus grandes de la hauteur significative sont associées à des périodes significatives de l'ordre des 17 sec.

Ces trois types de courbes permettent de définir les caractéristiques des ondes de calcul à considérer dans les problèmes de l'agitation et de la stabilité des ouvrages maritimes.

Toutefois, les conclusions de cette étude doivent être prises comme des approximations car, comme on lessait d'après les missions des bateaux océanographiques à l'Atlantique Nord, les caractéristiques de l'ondulation sont assez variables le long de la côte. De ce fait, le régime de l'agitation étudié ne pourra être bien défini qu'après installation de diverses stations d'observation en des points convénients de la côte.

RAPPORTS ENTRE LES PARAMETRES CARACTERISTIQUES DES TRAINS D'ONDES OBSERVES A FIGUEIRA DA FOZ

À partir des valeurs fournies par les observations, on a pu définir les paramètres suivants, caractéristiques de l'agitation:

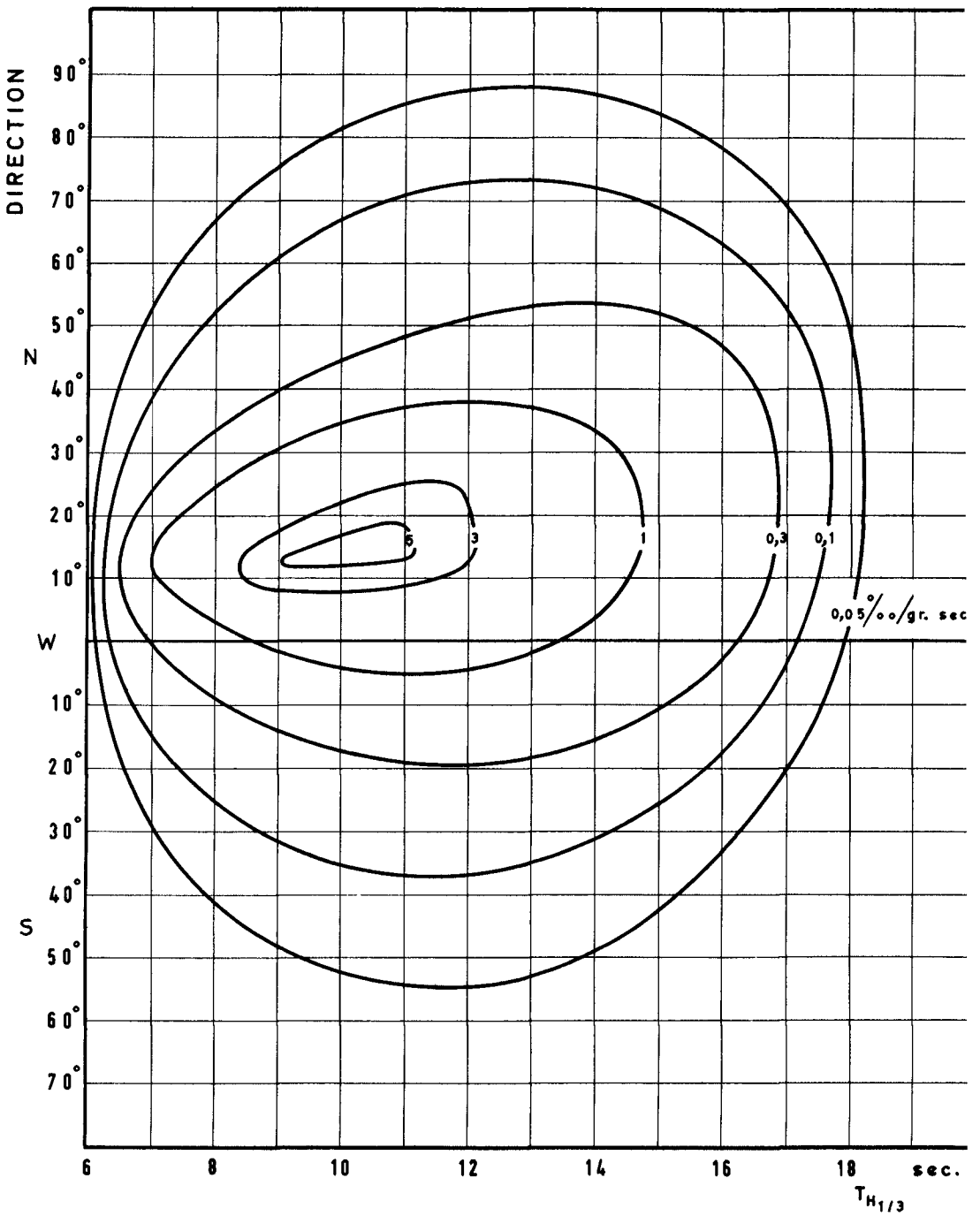
DIRECTION
90°
80°
70°
60°
50°
N
40°
30°
20°
10°
W
10°
20°
30°
40°
S
50°
60°
70°
6
3
1
0,3
0,1
0,05 °/oo/gr. sec
6
8
10
12
14
16
18
sec.
$T_{H_{1/3}}$

Fig. 8

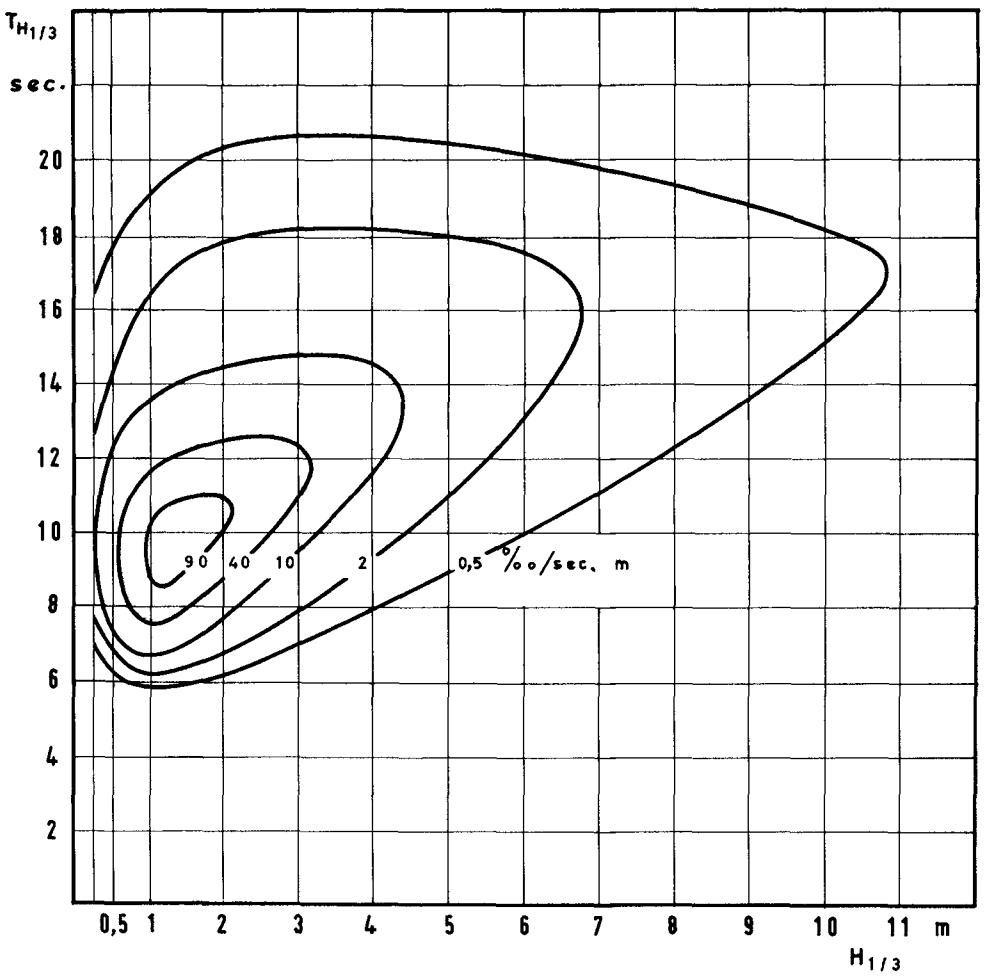
$T_{H1/3}$
sec.
20
18
16
14
12
10
8
6
4
2
90
40
10
2
0,5 ‰/sec. m
0,5
1
2
3
4
5
6
7
8
9
10
11 m
$H_{1/3}$

Fig. 9

$H_{1/3}$ - hauteur significative: hauteur moyenne du tier des ondes les plus élevées.

$T_{H1/3}$ - période significative: valeur moyenne correspon dant à la moyenne des périodes associées a u hauteurs qui déterminent $H_{1/3}$.

H_{max} - hauteur maximale.

T_{max} - période maximale.

$H_{1/10}$ - hauteur moyenne du dixième des ondes les plu élevées.

H_m - hauteur moyenne.

T_m - période moyenne.

$T_{H_{max}}$ - période associée à la hauteur maximale.

$T_{1/3}$ - valeur moyenne du tiers des ondes à la périod la plus élevée.

Les différents rapports que l'on peut établir entre ces p ramètres ont fait l'objet de l'étude présentée par le Prof.R.L Wiegel au"Coastal Engineering" de 1961; dans le but de compare les valeurs de ce travail avec celles présentées par cet auteur on a défini ces mêmes rapports et l'on a déterminé les valeur moyennes des distributions respectives. Les rapports étudiés e leurs distributions sont représentés aux Figs.10 et 11.

Les rapports entre les valeurs significatives et moyenne des hauteurs et périodes méritent une attention spéciale, ce qu justifie que l'on présente les histogrames respectifs avec une di tribution plus détaillée (Fig.12), ainsi que les deux graphiques d la Fig.13 où l'on établit la corrélation entre ces valeurs.

L'examen des histogrames de la Fig.12 rend évident que:

- la valeur de plus grande fréquence du rapport $\frac{H_{1/3}}{H_m}$ es comprise entre 1,25 et 1,30; ce rapport présente u pourcentage très réduit de valeurs supérieures à 1,60.
- la valeur de plus grande fréquence du rapport $\frac{T_{H1/3}}{T_m}$ es comprise entre 0,95 et 1,00; les valeurs limites de ce rapport sont 0,65 et 1,30.

On a calculé la valeur moyenne et l'écart, concernant ces distributions, selon les expressions:

$$m = \sum_k x_k p_k \qquad \sigma = \sqrt{\sum_k (x_k - m)^2 p_k}$$

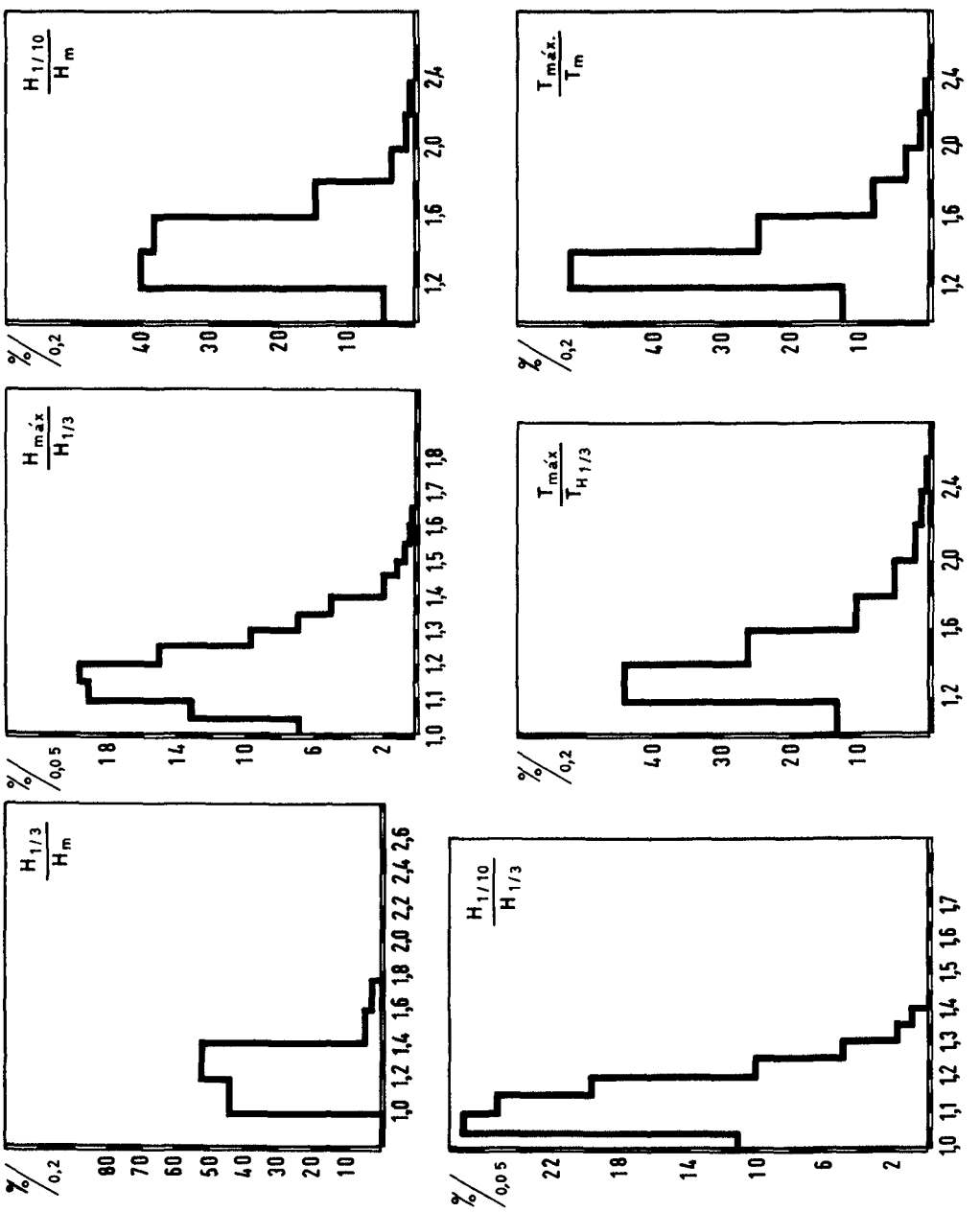
$\frac{H_{1/10}}{H_m}$
$\frac{H_{máx}}{H_{1/3}}$
$\frac{T_{máx.}}{T_m}$
$\frac{H_{1/3}}{H_m}$
$\frac{T_{máx}}{T_{H\,1/3}}$
$\frac{H_{1/10}}{H_{1/3}}$
%/0,2
%/0,05

Fig. 10

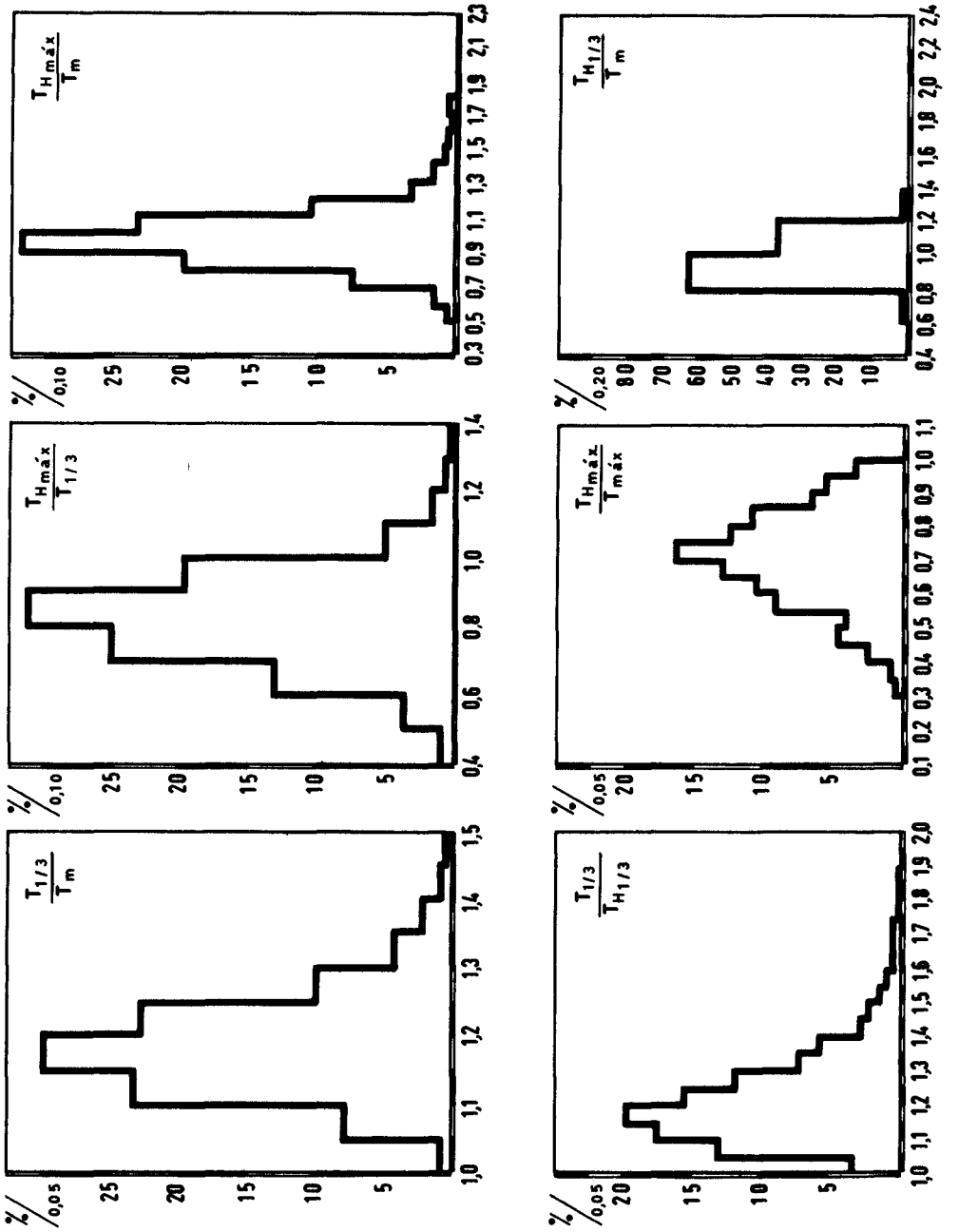
$\frac{T_{1/3}}{T_m}$
$\frac{T_{H\,máx}}{T_{1/3}}$
$\frac{T_{H\,máx}}{T_m}$
$\frac{T_{1/3}}{T_{H1/3}}$
$\frac{T_{H\,máx}}{T_{máx}}$
$\frac{T_{H1/3}}{T_m}$
%

Fig.11

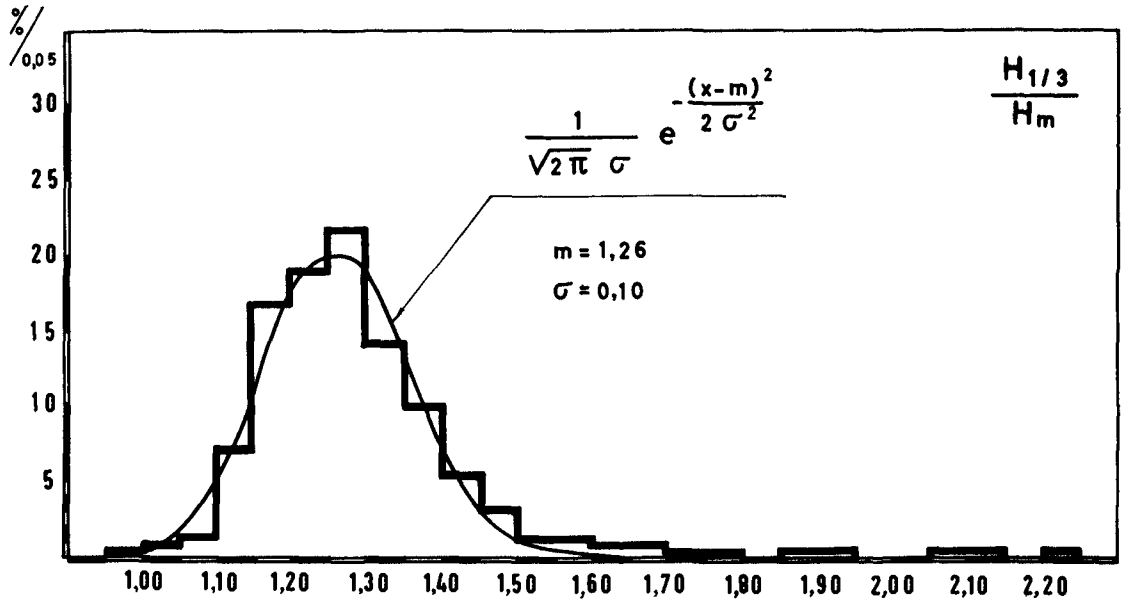
%/0,05
30
25
20
15
10
5
$\frac{1}{\sqrt{2\pi}\,\sigma}\, e^{-\frac{(x-m)^2}{2\sigma^2}}$
$\frac{H_{1/3}}{H_m}$
m = 1,26
σ = 0,10
1,00 1,10 1,20 1,30 1,40 1,50 1,60 1,70 1,80 1,90 2,00 2,10 2,20

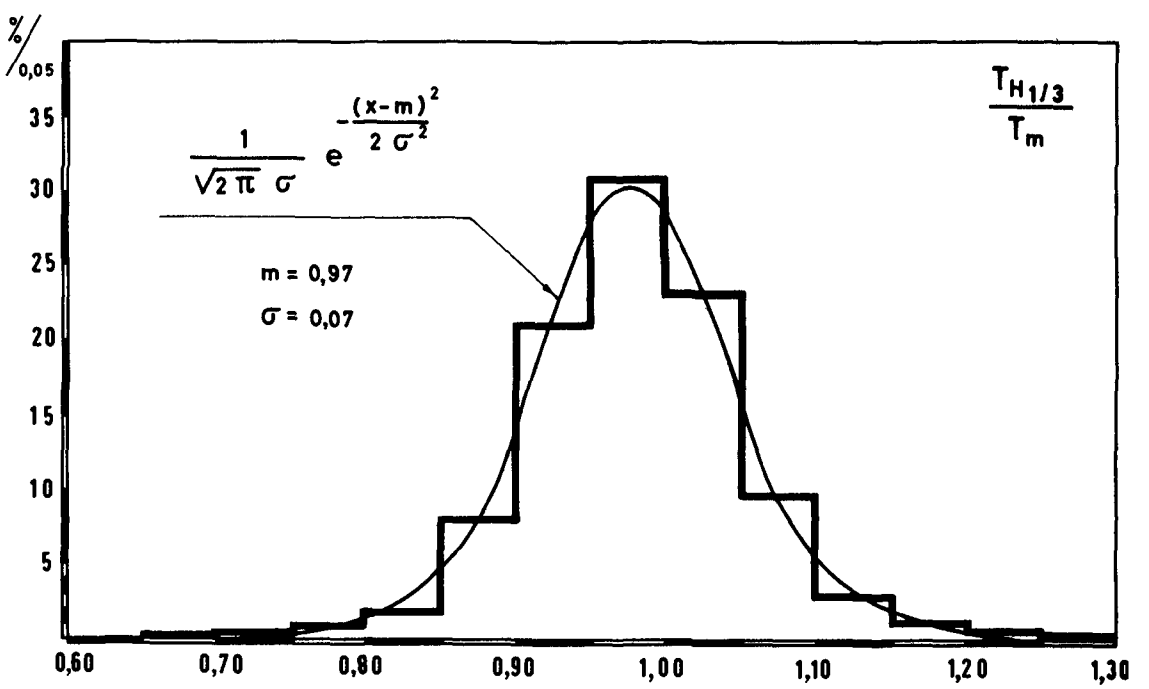
%/0,05
35
30
25
20
15
10
5
$\frac{1}{\sqrt{2\pi}\,\sigma}\, e^{-\frac{(x-m)^2}{2\sigma^2}}$
$\frac{T_{H1/3}}{T_m}$
m = 0,97
σ = 0,07
0,60 0,70 0,80 0,90 1,00 1,10 1,20 1,30

Fig. 12

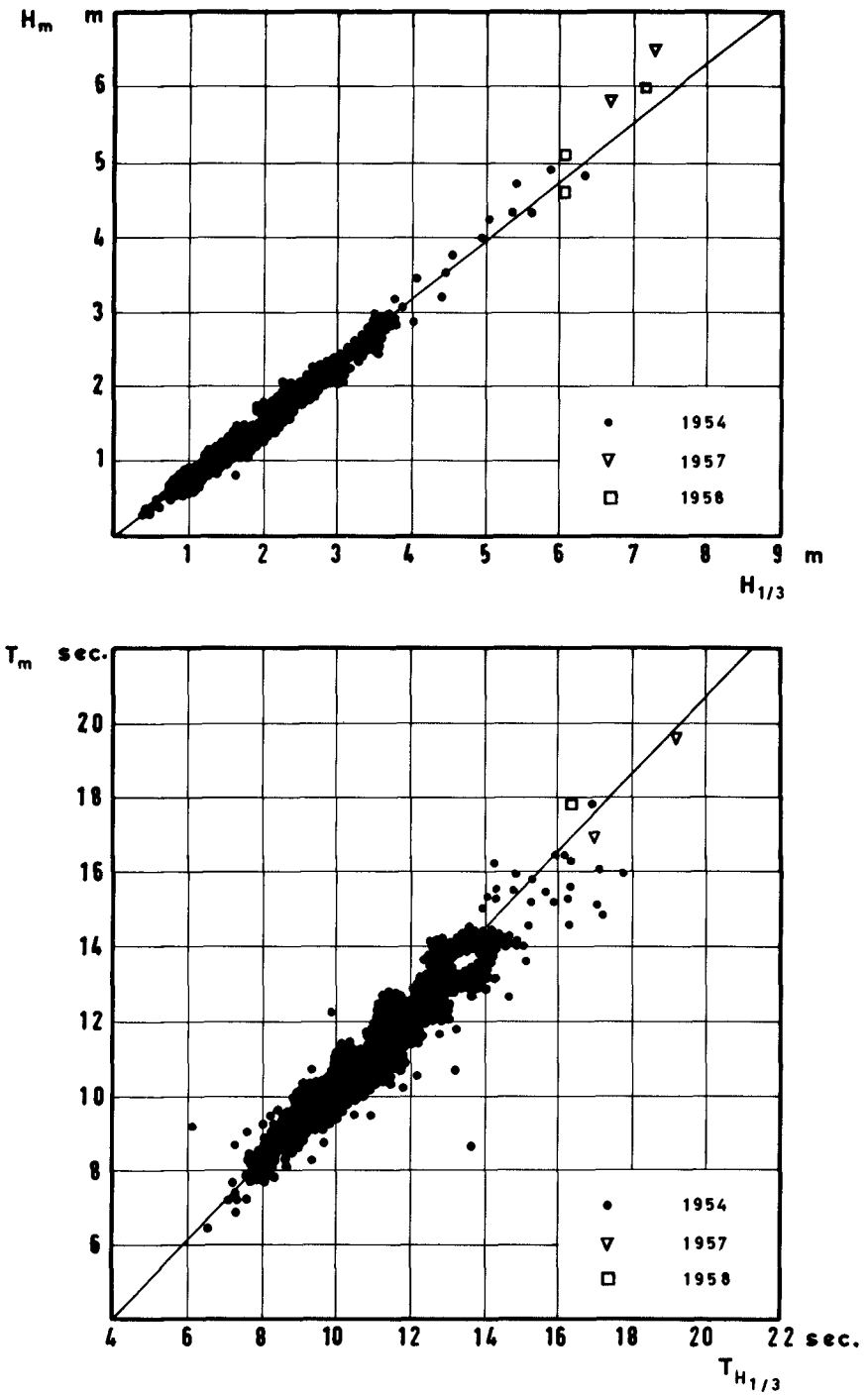
H_m m
6
5
4
3
2
1
1 2 3 4 5 6 7 8 9 m
$H_{1/3}$
• 1954
▽ 1957
□ 1958
T_m sec.
20
18
16
14
12
10
8
6
4 6 8 10 12 14 16 18 20 22 sec.
$T_{H_{1/3}}$
• 1954
▽ 1957
□ 1958

Fig. 13

où

m est la valeur moyenne.
σ est l'écart.
x_k est une valeur du rapport étudié.
p_k est la fréquence de la valeur x_k

Pour le rapport $\frac{H_{1/3}}{H_m}$ on détermina $m = 1,26$ et $\sigma = 0,10$.

Pour le rapport $\frac{T_{H1/3}}{T_m}$ on détermina $m = 0,97$ et $\sigma = 0,10$.

Les distributions de ces rapports suivent d'assez près la loi de Gauss - Laplace; le rapport $\frac{H_{1/3}}{H_m}$ a une distribution qui s'accorde avec cette loi pour une valeur de $\sigma = 0,10$ tandis que le rapport $\frac{T_{H1/3}}{T_m}$ a une distribution qui suit la loi Gauss - Laplace avec $\sigma = 0,07$.

À la Fig.13 on présente deux graphiques où l'on fait la comparaison entre les valeurs moyennes et significatives des hauteurs et des périodes, en établissant la corrélation entre les valeurs de ces paramètres. Tant pour les hauteurs que pour les périodes, on remarque une approximation satisfaisante en ce qui concerne les droites correspondant aux valeurs moyennes des rapports; les écarts les plus importants sont en général liés à des valeurs élevées de la hauteur ou de la période. Les valeurs significatives maximales correspondant aux fréquences maximales sont de l'ordre des 4 m pour les hauteurs et 14 sec. pour les périodes; les valeurs moyennes correspondantes sont de l'ordre de 3 m et 14 sec. respectivement.

Parmi les rapports que l'on peut établir entre les paramètres caractéristiques des trains d'ondes, le rapport $\frac{H_{1/3}}{T_m}$, dont l'étude a été faite par Sibul en canal à vent en 1955, prend un intérêt tout spécial. Dans le travail que le Prof. Wiegel présenta au Congrès de 1960, on trouve indiqués les résultats de ces essais ainsi que des valeurs obtenues en des observations réalisées en plusieurs lieux. La loi que Sibul a énoncée pour de petites perturbations, d'après ses études expérimentales, est du type:

$$H_{1/3} \simeq 1,4 \times 10^{-1} \times T_m^2 \qquad (H_{1/3} \text{ en mètres et } T_m \text{ en sec.})$$

Dans le travail sus-mentionné on s'aperçoit que les grandes perturbations océaniques s'écartent assez de cette loi; en effet, au cas de Figueira da Foz, cet écart est un fait comme

l' indique la Fig. 14. Il faut remarquer qu' une loi quadratique qui définisse une valeur moyenne de la distribution, présente une grande dispersion comme on le peut voir à la Fig.15.

Avec une approximation assez grande, on peut définir pour le cas de Figueira da Foz, dans la zone d'observation, une lo du type:

$$H_{1/3} \simeq 3{,}3 \times 10^{-4} \times T_m^{3,5} \qquad (H_{1/3} \text{ en mètres et } T_m \text{ en sec})$$

On a fait aussi l'étude de ce rapport, pour les valeurs au large, et on a obtenu le graphique de la Fig.16; dans ce cas on peut établir avec approximation la loi suivante:

$$H_{1/3} \simeq 5{,}6 \times 10^{-4} \times T_m^{3,5} \qquad (H_{1/3} \text{ en mètres et } T_m \text{ en sec.})$$

Les rapports presentés dans ce travail - ci peuvent soulever quelques doutes. En réalité, la méthode d'observation présente, en plus des imprécisions déjà mentionnées, l'inconvénient de se baser sur l'observation d'un nombre limité de crêtes, ce qui conduit en essence à ce que la valeur $H_{1/10}$ ne soit pas tellement significative, vu que seulement deux valeurs maximales de la hauteur sont utilisées dans la détermination de cette valeur - - là qui, donc, reste proche de H_{max}.

Dans le tableau de la Fig.17 on trouve systematisées toutes les valeurs moyennes des rapports étudiés. En analysant ce tableau on est porté à conclure que les rapports des hauteurs présentent des différences très marquées par égard aux valeurs théoriques et aux valeurs observées en d'autres stations. En ce qui concerne les rapports entre les valeurs de la période, les différences sont moins importantes, il s'y trouvant des valeurs égales ou très proches de celles obtenues expérimentalement.

Les différences dans les rapports de hauteurs, 15% au maximum, peuvent être imputables à la méthode tachéométrique qui est moins rigoureuse, évidemment, que les méthodes d'observation se servant d'ondographes. Dans les déterminations de la valeur de la période faites par chronométrage, il est effectivement possible d'admettre une moindre erreur.

DISCUSSION

Lors de la présentation de ce travail, l'auteur a eu le plaisir d'entendre deux interventions très avisées dont l'opportunité ne souffre pas de doute.

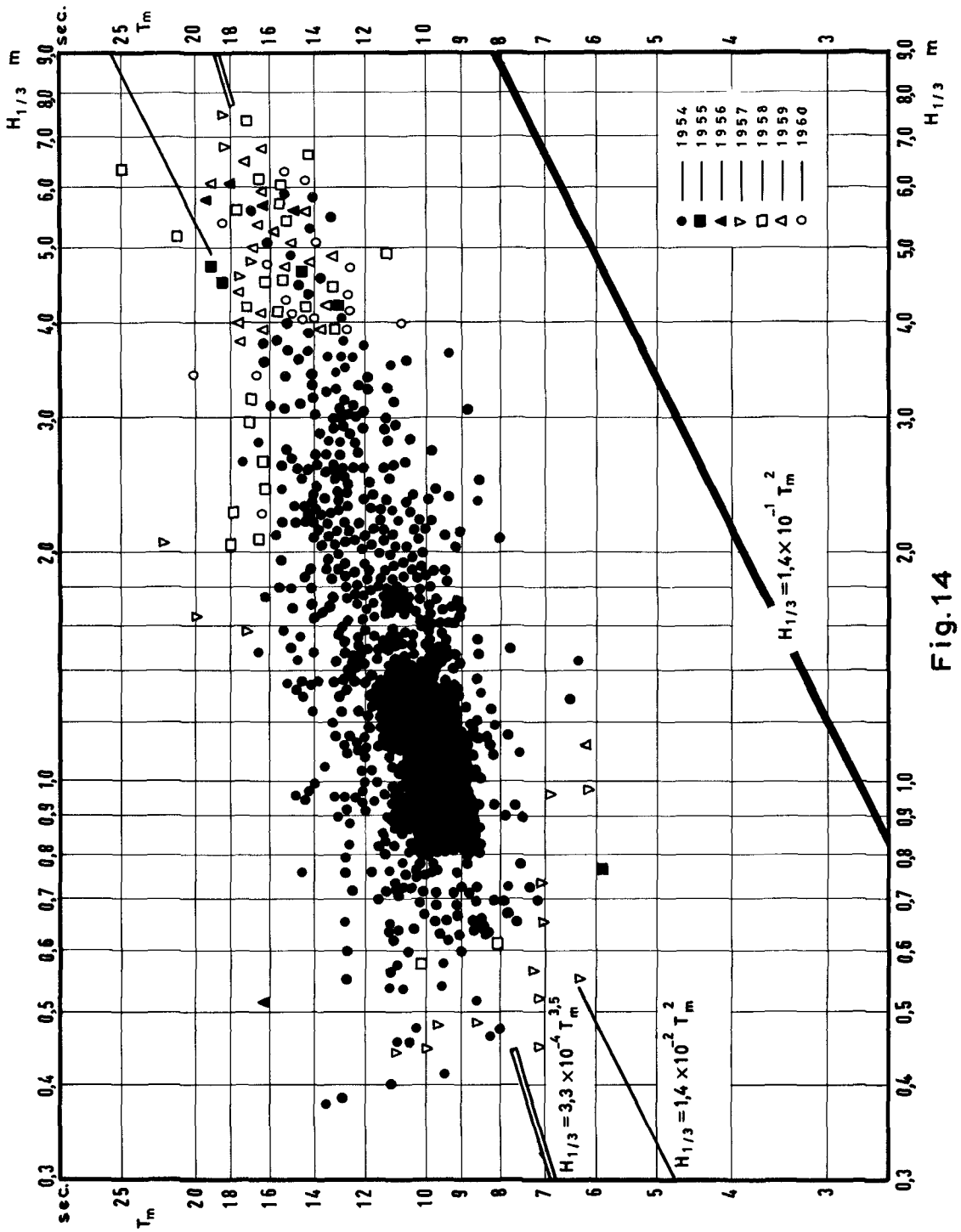
$H_{1/3}$ m
sec.
T_m
1954
1955
1956
1957
1958
1959
1960
$H_{1/3} = 1{,}4 \times 10^{-1} T_m^2$
$H_{1/3} = 3{,}3 \times 10^{-4} T_m^{3,5}$
$H_{1/3} = 1{,}4 \times 10^{-2} T_m^2$

Fig. 14

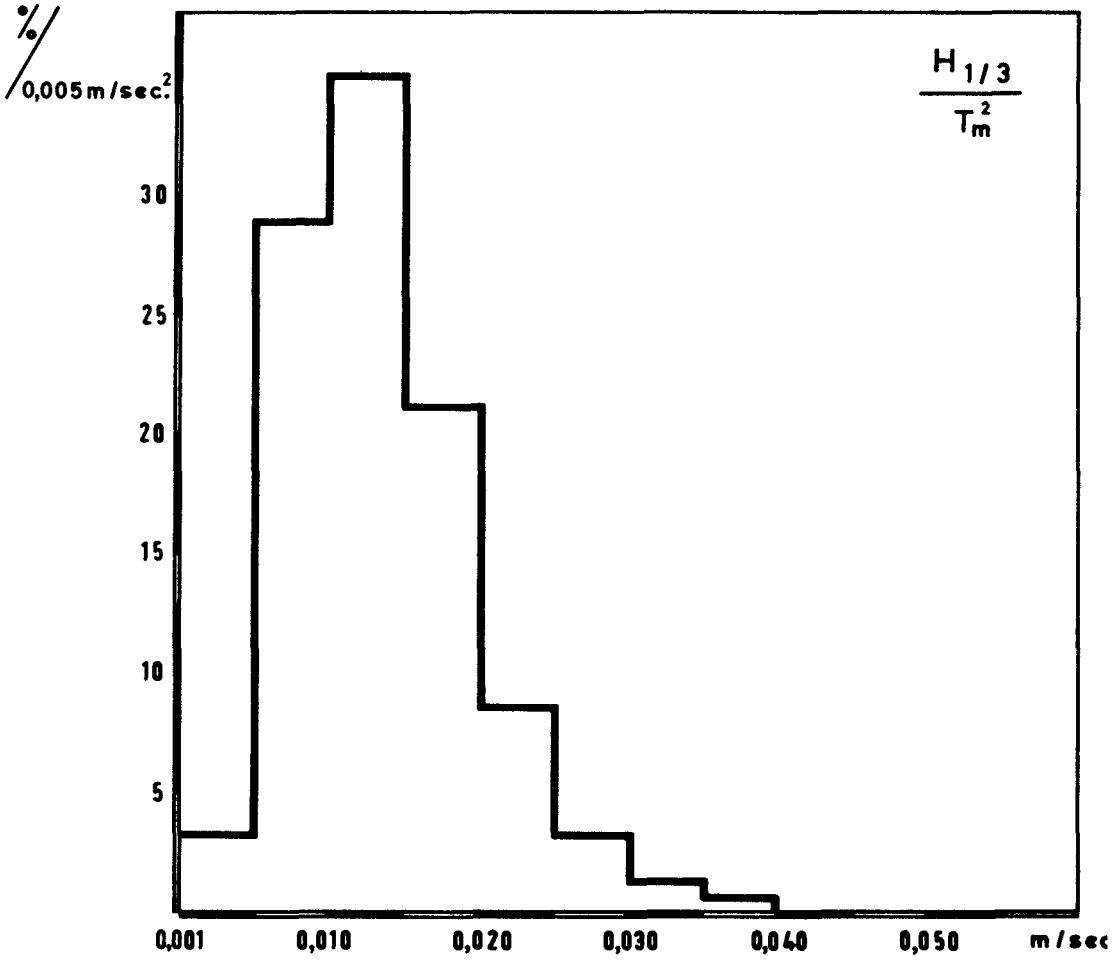
%/0,005 m/sec.²
$\frac{H_{1/3}}{T_m^2}$
30
25
20
15
10
5
0,001
0,010
0,020
0,030
0,040
0,050
m/sec

Fig.15

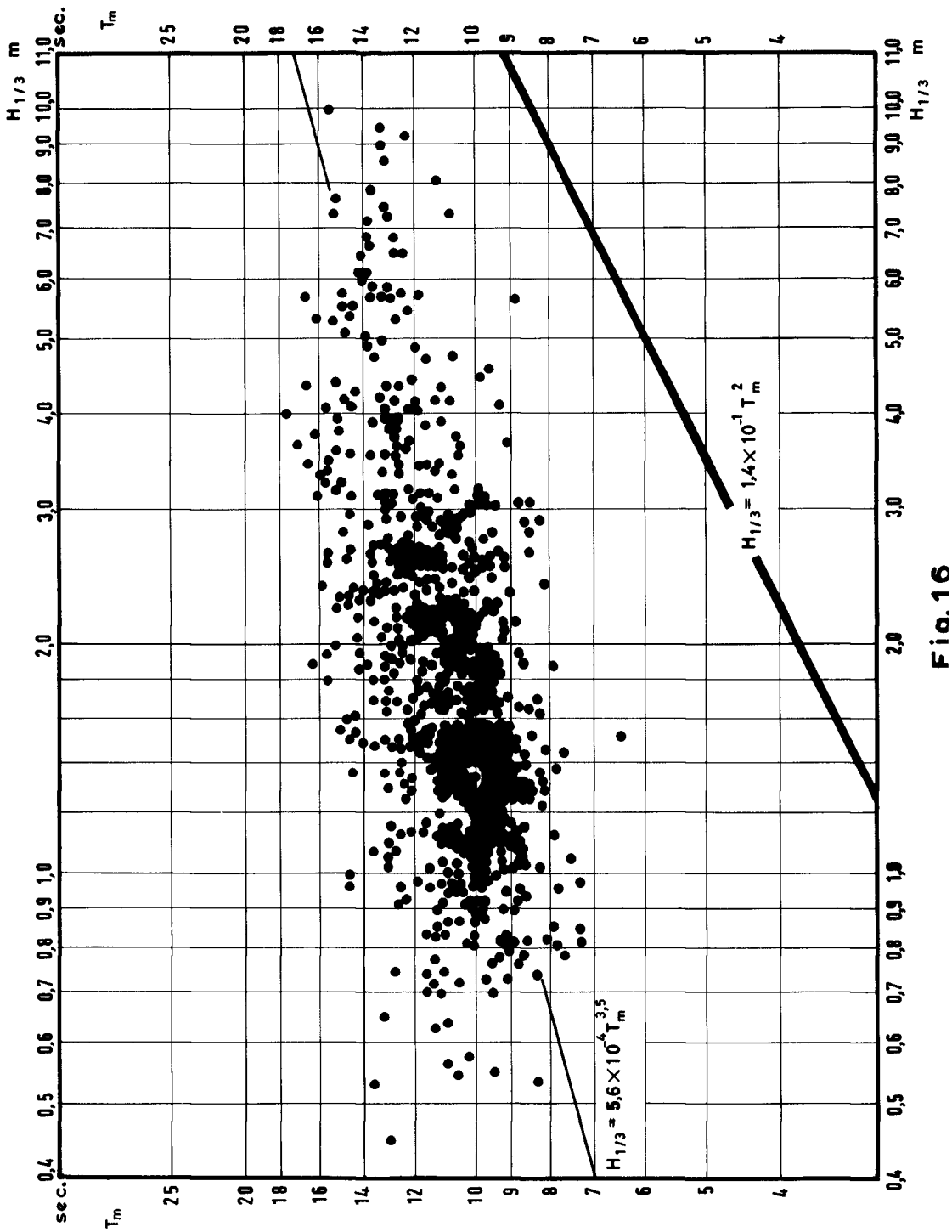

Fig. 16

Rapports	Valeur moyen			Obs.	
	Prof. Wiegel Coastal Engineering (1961)		Figueira da Foz (1954 - 1960)		
$\frac{H_{1/3}}{H_m}$	1,37	*	1,27	Valeur théorique 1,61	Atlantique Nord 1,60
$\frac{H_{máx.}}{H_{1/3}}$	1,40		1,19	——	* Valeurs de ondographes de surface
$\frac{H_{1/10}}{H_m}$	1,63		1,46	——	
$\frac{H_{1/10}}{H_{1/3}}$	1,19		1,13	Valeur théorique 1,27	(Davenport Calif.
$\frac{T_{máx.}}{T_{H_{1/3}}}$	1,29	**	1,42	** Valeur expérimental. Sibul (1955)	
$\frac{T_{máx.}}{T_m}$	1,42		1,38		
$\frac{T_{1/3}}{T_m}$	1,24		1,19		
$\frac{T_{Hmáx.}}{T_{1/3}}$	0,89		0,91		
$\frac{T_{Hmáx.}}{T_m}$	1,10		0,98		
$\frac{T_{1/3}}{T_{H_{1/3}}}$	1,12		1,22		
$\frac{T_{H máx.}}{T_{máx.}}$	0,71		0,71		
$\frac{T_{H_{1/3}}}{T_m}$	1,10		0,97		

Fig.17

Ces interventions, dues aux ingénieurs néerlandais MM.A. PAAPE et J.SVAŠEK, ont mérité toute l'attention de l'auteur qui tient à exprimer ici sa reconnaissance pour l'intérêt porté au problème.

Les questions soulevées se rapportent au nombre limité de crêtes observées en chaque période d'enregistrement et à la possibilité d'erreur dans la détermination de $H_{1/3}$.

On a reconnu le besoin de comparer les valeurs des observations réalisées avec d'autres, données par l'observation d'un nombre supérieur de crêtes.

Vraiment on a déjà dit que l'on considère assez imparfaites les conditions d'observation, notamment en ce qui concerne les valeurs de $H_{1/10}$; pour ce qui est des valeurs de $H_{1/3}$, on a calculé un rapport $\frac{H_{1/3}}{H_m}$ où la valeur moyenne est de l'ordre de grandeur de celle que l'on obtient avec des ondographes, comme l'on peut voir à la Fig.17.

On doit remarquer, cependant, que toutes ces valeurs s'éloignent assez de la valeur théorique et aussi de valeurs obtenues à l'Atlantique Nord.

On doit encore dire que les observations avaient déjà été réalisées lorsque cette étude commença et aussi que la "Junta Autónoma do Porto da Figueira da Foz" n'avait pas en vue une étude de cette nature lorsqu'elle installa la station d'observation.

Quand le "Laboratório Nacional de Engenharia Civil" décida d'entreprendre une étude en partant de ces observations, a naturellement admis que ses résultats seraient une approximation valable et pourvue d'intérêt pratique. D'un autre côté, vu que l'on reconnaissait les défauts ci-avant mentionnés, on entreprit, à la fin 1962, les démarches nécessaires à l'installation d'une station d'observation de l'ondulation au port de Leixões, équipée d'ondographes et tachéomètres pour l'observation de la direction.

Pour finir, il faut dire que l'on reconnait le plus grand intérêt à réaliser des observations sur un nombre supérieur de crêtes, à fin d'évaluer l'erreur introduite dans cette étude. Dans ce but, on a déjà pris contact avec la "Junta Autónoma do Porto da Figueira da Foz" et seulement des difficultés actuelles nous ont empêchés de recevoir déjà des résultats.

------- x -------

------- x -------

L'auteur tient à remercier l'ingénieur M.J.J. REIS DE CARVALHO dont le concours lui a permis de mener à bien ce travail, aussi que les calculateurs MM. L.CARIA DA SILVA et PLATINO CUNHA et les dessinateurs MM.J. CARROGIO et F.SANTOS PEREIRA qui ont prêté leur meilleure collaboratior

BIBLIOGRAPHIE

LONGUETT - HIGGINS - "On the statistical distribution of the heigts of sea waves "Journal Marine Research",Vol.XI,pages 245-246.

ABECASIS, F.MANZANARES; CASTANHO, J.PIRES;CARVALHO, J.J.REIS DE - "A previsão das características das ondas do mar". Memória nº. 114 du LNEC. Lisboa, 1957.

WIEGEL,R.L. - "Wind waves and swell" Coastal Engineering, 1961, Vol.1, pages 1 - 40.

MICHE, M.ROBERT - "Propriétés des trains d'ondes océaniques". Paris, 1954.

TABLE DES FIGURES

Chapter 10

SOURCE MECHANISM OF THE TSUNAMI OF MARCH 28, 1964 IN ALASKA

WM. G. VAN DORN
University of California
Scripps Institution of Oceanography
La Jolla, California

ABSTRACT

The distribution of permanent, vertical crustal dislocations, the times and directions of early water motion in and around the generation area, and the unusual low-frequency character of the tsunami record obtained from Wake Island, all suggest that the tsunami associated with the great Alaskan earthquake of March 28, 1964 was produced by a dipolar movement of the earth's crust, centered along a line running from Hinchinbrook Island (Prince William Sound) southwesterly to the Trinity Islands. The positive pole of this disturbance encompassed most of the shallow shelf bordering the Gulf of Alaska, while the negative pole lay mostly under land. Thus, the early effect was the drainage of water from the shelf into the Gulf, thus generating a long solitary wave, which radiated out over the Pacific with very little dispersion.

Tilting of Prince William Sound to the northwest produced strong seiching action in the deep, narrow adjacent fjords, thus inundating inhabited places already suffering from earth shock and slumping of the deltas on which they were situated.

Preliminary calculations indicate that the initial positive phase of the tsunami contained about 2.3×10^{21} ergs of energy, as compared with 2.7×10^{22} ergs computed for the tsunami of March 9, 1957 in the Andreanof Islands.

The dipolar dislocation also produced a 'tsunami' in the atmosphere, which was recorded in La Jolla, indicating that the dislocations must have occurred during the period (circa 2-6 min.) of strong ground motion near the epicenter.

INTRODUCTION

On March 28 at 0336 GMT the largest North American earthquake of this century occurred in Southeastern Alaska. The epicentral coordinates for the principal shock (Richter magnitude 8.4) are currently taken as 61.05N, 147.5W, focal depth less than 20 km, although these coordinates may be subject to later revision, owing to the long-continuing nature of the seismic signals, and the fact that lesser shocks occurred as much as two hours earlier in the same vicinity. The great strength and shallow depth of this quake were visibly manifested by violent dynamic earth motions over a radius of more than 200 km in all directions. The duration of these motions, during which time it was difficult or impossible for people to run or even stand erect, was reported to be from three to eight minutes in various localities. Deep ground fissures, snow and rock avalanches, and permanent changes in land elevations relative to sea level also occurred in most of the areas of strong ground motion, and, presumably, over a similar period of time. Closely following the principal shocks, tsunami waves were reported in many areas of the Gulf of Alaska and adjacent Prince William Sound. The tsunami which subsequently spread out over the Pacific Ocean, appears to have been of rather moderate intensity, generating oscillations in bays and harbors around the Pacific of

several feet in amplitude, but causing relatively little damage beyond the immediate area of generation.*

There is no question that the severity of this tsunami was substantially mitigated because it occurred near the time of low tide in all areas where the waves were largest.

This great natural catastrophe, which may well have jeopardized the future of the state of Alaska, was the immediate focus of attention of earth scientists from all over the world. To the author, it represented an unprecedented opportunity to reconstruct the generation mechanism for a tsunami, because the earthquake epicenter was located in a region where fairly precise geodetic control has existed for some decades, and because of the likelihood that enough local eyewitness accounts of the water wave chronology might be obtained to put together a systematic picture of the generation process. Although it is apparent at this writing that many months will elapse before the land elevation changes relative to sea level will be known in detail, obvious vertical displacements occurred in many places along the sea coast and islands in the Gulf of Alaska of sufficient magnitude to be easily distinguishable from the normal tide range by the trained eye. Thus, it is already possible to draw some fairly firm qualitative conclusions regarding the generation process, although its quantitative aspects must await more accurate data. An essential feature of this reconstruction is the wave record for the tsunami obtained at Wake Island, at a special

---

* "Some damage to waterfront establishments occurred along the coast of southeastern Alaska, British Columbia, and as far south as Crescent City, California."

recording station installed there in 1960 (Van Dorn, 1960). Because this record can be used within limits as an indicator of the deep water nature of this tsunami, it serves as a check on the mode of generation hypothesized from other considerations.

BACKGROUND

There have been several attempts to estimate the generation mechanism of tsunamis. Most of these are inconclusive for lack of specific evidence of the seafloor readjustment, although Nagata (1950) has shown in the case of the great Nankaido earthquake of December 21, 1946 near Shikoku that the dislocations on land can be quite complex. Miyabe (1934) attempted to compute the size of the tsunami generation area for the Sanriku earthquake (March 3, 1933) by projecting wave fronts back towards the epicenter from observation stations along the shore. According to Takahasi (personal communication) the generation areas determined by such constructions generally agree with those delimiting the areas of earthquake aftershocks obtained from seismic evidence. Van Dorn (1963) computed the equivalent axisymmetric source which could have produced the wave spectrum observed for the tsunami of March 1957 at Wake Island. Kajiura (1963) has pointed out that, aside from explosions, seismic sources cannot be expected to be axisymmetric, and has given solutions for asymmetric sources of various types. Never before, however, has a sufficiently detailed knowledge been obtained of seafloor motion, type of wave action, and the deep-water spectrum offshore, to permit a convincing reconstruction of the generation mechanism.

GEOMORPHOLOGY

According to the U. S. Coast and Geodetic Survey (1964), the substructure of the region affected by the earthquake is underlain by a blanket of cretaceous sediments which have subsequently been uplifted and deformed into a series of geanticlines and geosynclines, having a vertical relief as great as 10,000 ft. The axes of this accordian-like structure have been mapped from the Trinity Islands through Kodiak, up the Kenai Peninsula, and identified as outcrops at elevations as high as five or six thousand feet in the Chugak Mountains (Figure 1). The entire structure is bent in an arc around the Gulf of Alaska, essentially paralleling the coast. Although the old tectonic history of this region appears to have been very complex, its present general appearance gives the impression that it is a coastline of submergence (Twenhofel, 1951) which has undergone recent, gradual uplift, except for small areas in the Prince William Sound and Copper River delta areas. Figure 2 shows the general pattern of uplift as evidenced by a series of exposed marine terraces. Twenhofel reports that such secular changes have, in fact, been observed since the turn of the century in several areas where geodetic control exists, and rates of uplift as high as seven or eight feet per century have been recorded.

SEISMOLOGICAL HISTORY

The Gulf of Alaska, in common with the Aleutian Arc and the entire western border of North America, has a long history of repeated seismic activity and associated volcanism. The epicenters of earthquakes larger than magnitude 6 which have occurred since 1900 are shown in Figure 3, and it is apparent that several of the largest quakes

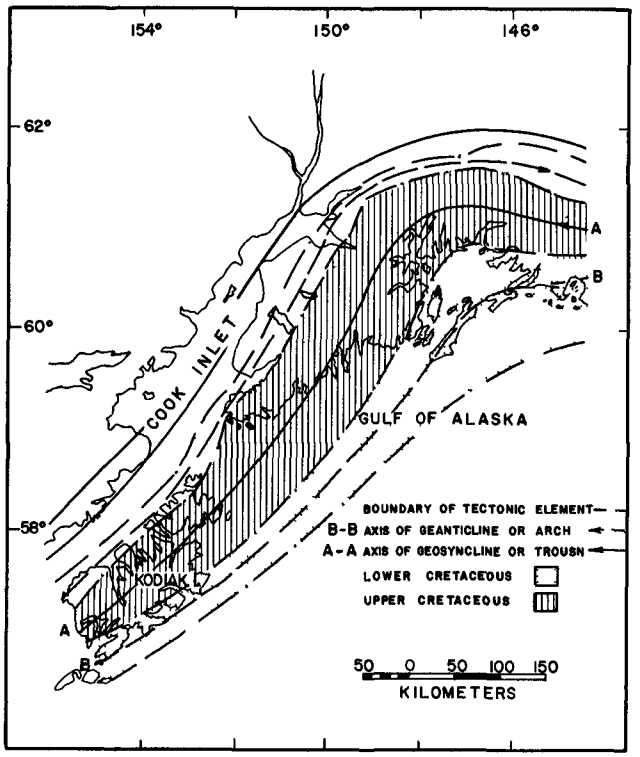

FIG 1 --TECTONIC MAP OF EPICENTRAL AREA (USC & GS)

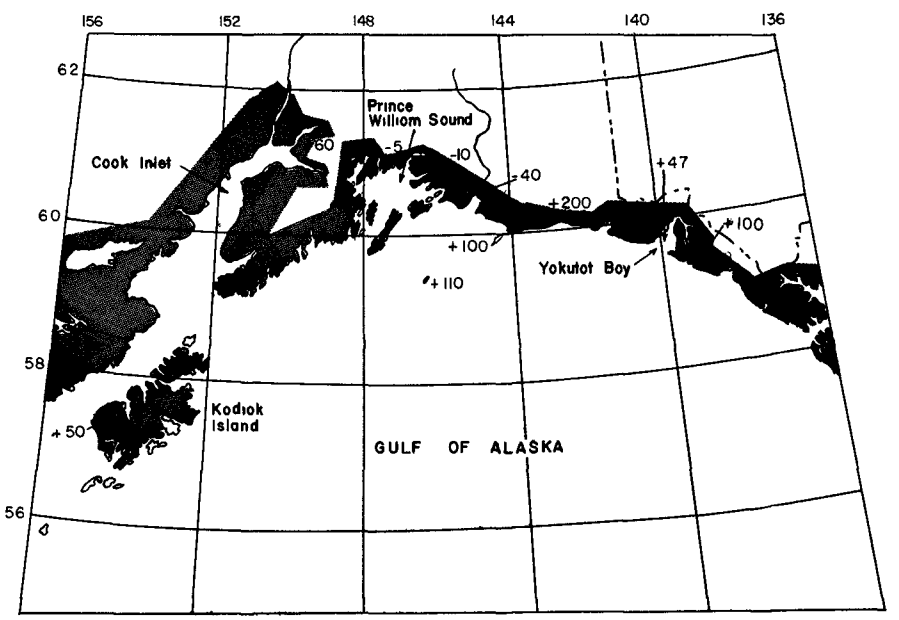

FIG 2 --RECENT LAND ELEVATION CHANGES IN GULF OF ALASKA (AFTER TWENHOFEL)

occurred in the immediate region of Prince William Sound. Thus, the present quake was not particularly anomalous, either from the standpoint of magnitude or frequency of occurrence, since the most recent previous quake of this magnitude (8.4) occurred in nearby Yakutat Bay in 1899.

St. Amand (1957) has probably made the most thorough study of the fault system of this region, which tends to follow the synclinal substructure parallel to the coast. Aftershocks from the present quake, however, (Figure 4) are clustered in two loci; one in the vicinity of Hinchinbrook Island (A) and the other southeast of Kodiak (B), and these loci are connected by scattered aftershocks in the region between them. It appears as if the aftershock activity was essentially confined to the region of the westerly geanticline of the cretaceous substructure, being mostly underwater beneath the shallow coastal shelf, and bounded to the southeast by the Aleutian Trench.

NATURE OF THE GROUND MOTION

A remarkable feature of this earthquake, which became apparent very early during the field survey, was the enormous extent of the areas which have undergone relatively large vertical changes in elevation relative to sea level. Virtually the entire Kenai Peninsula, from the Turnagain Arm of Cook Inlet, including the Kenai-Kodiak Ridge, and Kodiak Island itself, appears to have subsided by two to six feet. At the same time most of the land areas along the seacoast from the Yakutat area to the center of Prince William Sound have been elevated by similar amounts. The time rates of these displacements are unknown, but appear to have been of the same order as that of the intense ground motion (2-6 min.), since many observers reported immediate

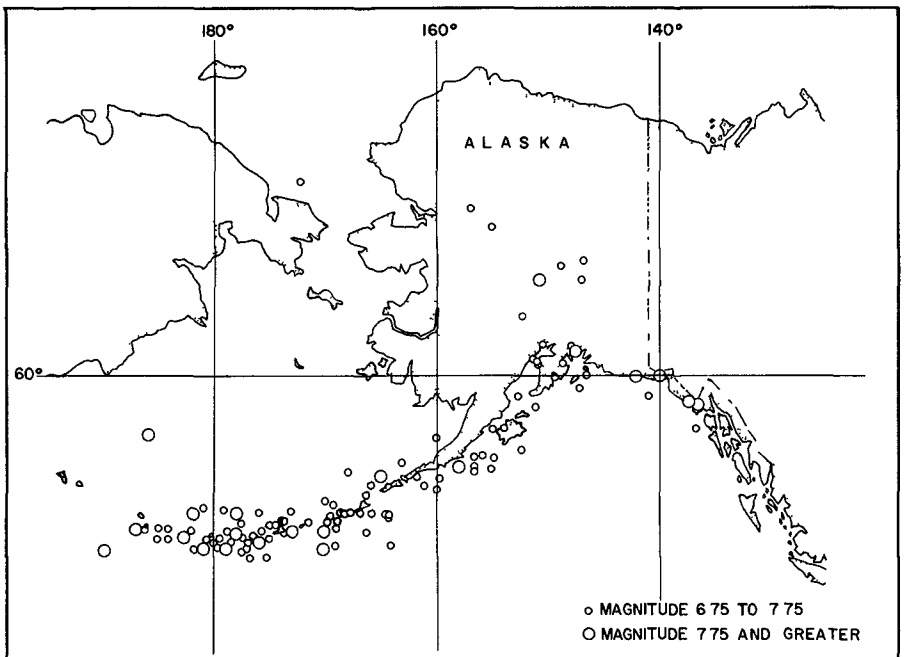

FIG 3 --DISTRIBUTION OF LARGE EARTHQUAKES IN GULF OF ALASKA SINCE 1899 (USC ¢ GS)

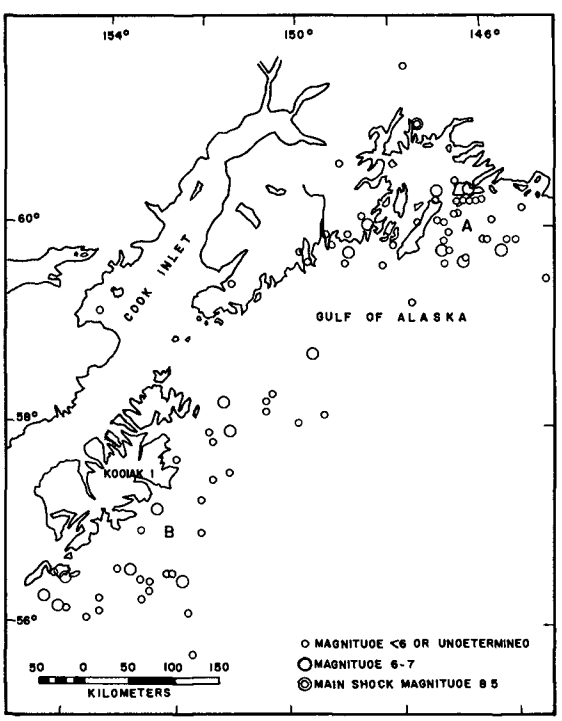

FIG 4 --DISTRIBUTION OF AFTERSHOCKS OCCURRING DURING FIRST 9 DAYS FOLLOWING EARTHQUAKE OF MARCH 28, 1964 (USC & GS)

water withdrawal from the elevated regions. Additionally, an atmospheric gravity wave transient was recorded on a special microbarograph at the Scripps Institution of Oceanography, beginning at 280655Z, (Figure 5). Such atmospheric pulsations are a common feature associated with the detonation of large nuclear explosions, but, to the authors knowledge, have not previously been observed in connection with earthquake motions. Pressure pulses from the explosions outside of the region of hypercompression, propagate at acoustic velocity in the lower atmosphere (about 1050 ft/sec ± 30 ft/sec). Therefore, the initiating disturbance - if it originated in the vicinity of the reported epicenter - occurred at about the same time as the principal shock. Such a pressure disturbance in this case could only have been produced by vertical motions of the earth over a very large area, and in a time of the order of that required for an acoustic wave to propagate across dimensions of the generator. Thus, a substantial fraction of the net motion inferred from relative sea level changes must have occurred very rapidly.

The present picture of the areas of permanent dislocation which is now emerging is shown in Figure 6. It should be born in mind that most of these figures are tentative, some being obtained on the basis of preliminary surveys by the U. S. Coast and Geodetic Survey, while others are only estimated by measurements to local sea level at some later time, and are largely based on the long-term experience of local inhabitants. Such observations as these, carried on over a period of several weeks, are probably accurate to about 1 foot, although smaller changes are readily apparent to fishermen and mariners, who have had long experience with the tides in a particular area. The tentative distribution of these dislocations is included,

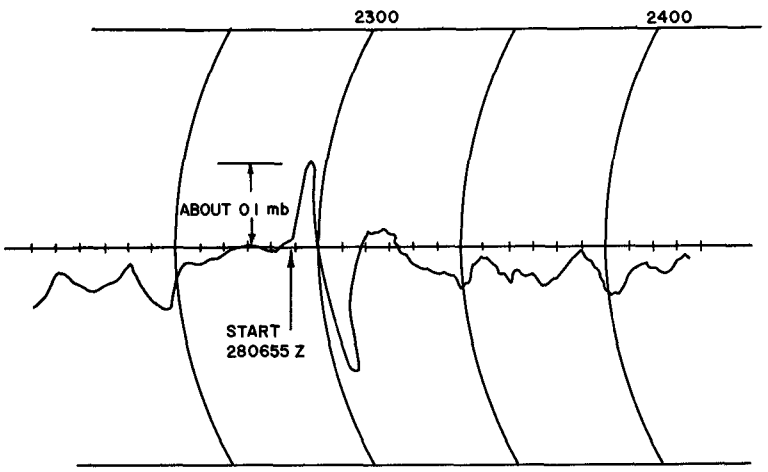

FIG 5 --MICROBAROGRAPH RECORD FROM LA JOLLA, SHOWING ATMOSPHERIC TSUNAMI FROM ALASKAN EARTHQUAKE (SIGNATURE IS TYPICAL OF THAT FOR LARGE DIPOLE SOURCE)

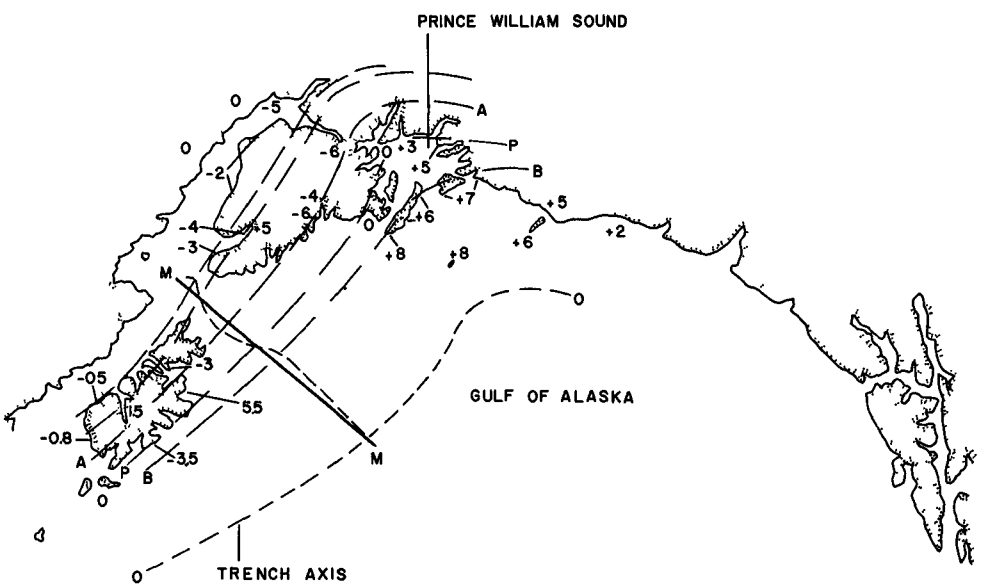

FIG 6 --TENTATIVE DISTRIBUTION OF LAND DISLOCATIONS (IN FEET) RELATIVE TO SEA LEVEL IN GULF OF ALASKA FOLLOWING EARTHQUAKE OF MARCH 28, 1964

for the most part, within the same perimeter which circumscribes the earthquake aftershocks. Also shown in this figure are the axes of the synclinal ridges and troughs of the cretaceous substructure, transferred from Figure 1, and a schematic profile section M-M. Significantly, perhaps, the general trend of surface dislocations is well mapped by the "contour lines" of the substructure; negative elevation changes lying to the west and north of the line P-P dividing the Kodiak geosyncline from the shelf geanticline, and all of the areas of positive elevation lying to the south and east of this line. It almost appears as if the observed dislocations could have been produced by slight increase in the subsurface deformation. It is certainly beyond the author's training and experience to comment on this seeming coincidence, but, as will be shown, this interpretation permits an extrapolation of the pattern of surface dislocations out under the sea, which is quite consistent with that obtained from interpretation of the surface wave history.

THE PATTERN OF EARLY WATER MOTION

A strenuous attempt was made during the field survey to obtain information on the chronology and direction of early water motion, particularly in Prince William Sound, since it was felt that the key to the tsunami generation problem might hinge on the decision as to whether the tsunami originated close to the reported epicenter, or in some other region outside the Sound. As it turned out, the region of wave generation was very much larger than the Sound, encompassing most of the shelf bordering the Gulf of Alaska.

The hydrodynamic situation in Prince William Sound at early times following the principal shock is shown in Figure 7. The land elevation changes in feet are shown by the large numerals in this figure. As already mentioned, the positive changes and negative changes are separated into two regions by a line of zero change in elevation. Within the Sound, this line runs through Pt. Elrington, up the Knight Island Passage, through Perry Island, and curves away towards the east - possibly through Port Valdez. So far, no specific data is available on change of elevation at Valdez. The reported subsidence there was most probably due to the settling of the alluvial delta on which the town is built. The pattern of earthquake and wave damage at Valdez is typical of what occurred also at Seward, Whittier and at numerous other uninhabited areas of the Sound. Such glacial deltas possess very steep angles of repose (approximately 45°) beneath the water level. During the violent earthquake motion, the edges of these deltas simply slumped into the fjords, carrying with them any indigenous waterfront structures. Alluvial slumping also precipated local seiche action which, in turn, was large enough in some cases to cause inundation of waterfront areas.

The pattern of elevation changes indicates that the entire Prince William Sound region was tilted about the axis (P-P) of zero elevation change. This tilting action caused an immediate flux of water in the direction of the tilt gradient. Prince William Sound is a very deep basin (200-300 fathoms), compared with the broad continental shelf outside (50-100 fathoms). It is also of complex shape, containing many mountainous islands, and radiating into numerous deep fjord-like inlets, some of which are more than 100-miles in length. The hydrodynamic motions of this body of water were extremely complicated, and it

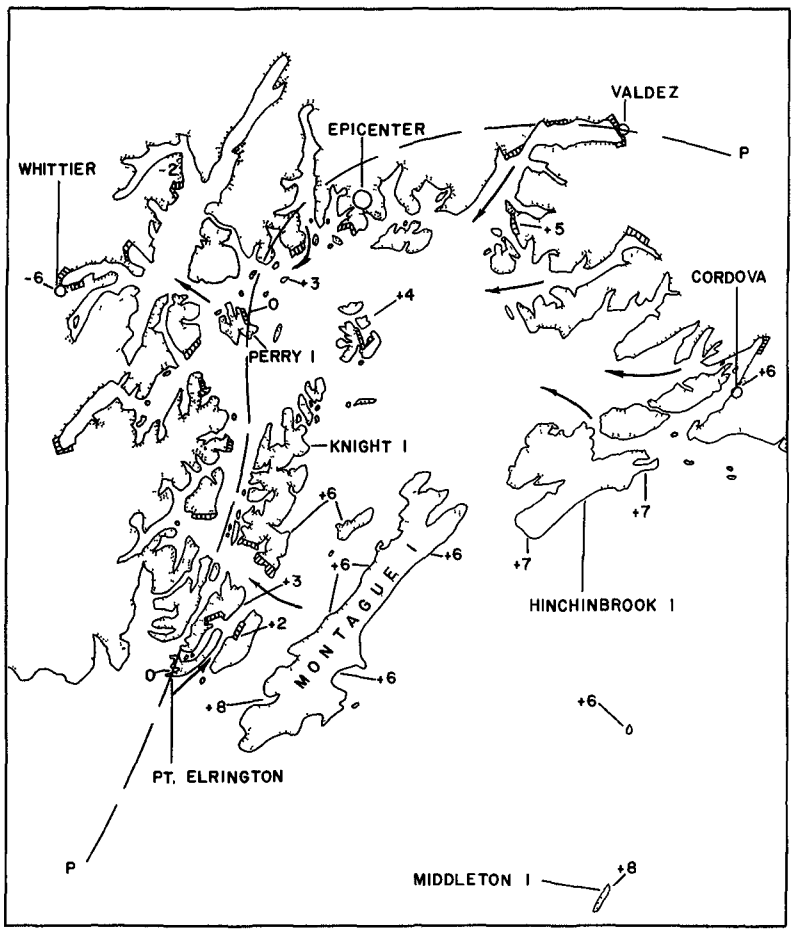

FIG 7 --LAND ELEVATION CHANGES WITHIN PRINCE WILLIAM SOUND

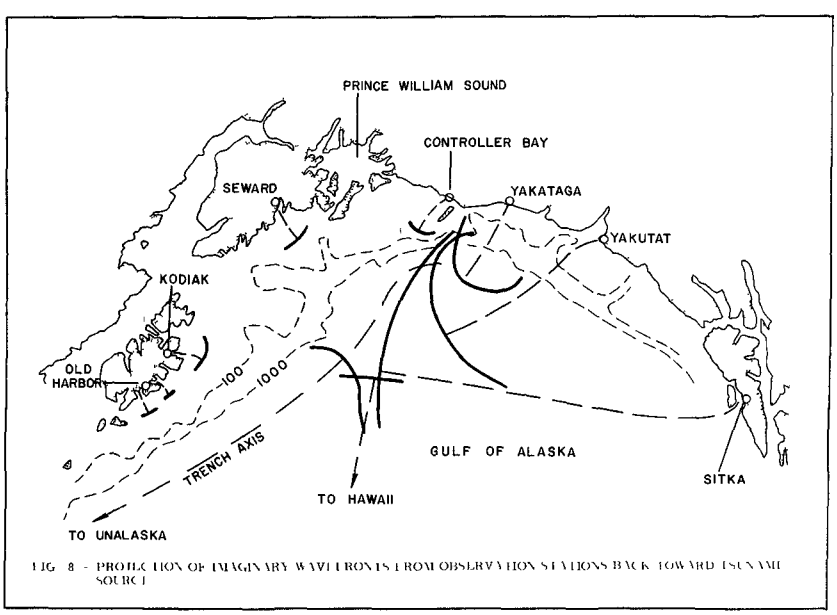

FIG 8 - PROJECTION OF IMAGINARY WAVE FRONTS FROM OBSERVATION STATIONS BACK TOWARD TSUNAMI SOURCE

is not always easy to predict details of the initial motion, except to state that the water withdrew from elevated areas almost immediately, and began to rise in depressed areas very soon after the earthquake. Large seiches were set up in the main basin and the adjacent fjords, although it appears that there was relatively little exchange of energy between Prince William Sound and the Gulf of Alaska. The Sound is virtually cut off from the Gulf by a cluster of islands, the largest of which are Montague Island and Hinchinbrook Island, as well as by the extreme shoalness of the shelf outside. The general early flow of water within the Sound was northwest as indicated by the heavy arrows in Figure 7. Strong northerly currents and violent seiching action were observed immediately in the Knight Island Passage. Water was observed to drain southerly and easterly out of Unakwik Inlet. A large wave was observed to propagate out of Valdez Narrows into the Sound immediately after the principal shock. Strong seiching action within the Sound continued for at least twelve hours after the earthquake. In many regions the greatest inundation damage occurred about five to six hours after the earthquake, at the time of high tide.

Although the details of the wave activity within Prince William Sound are of great practical interest because of the extensive damage to habitation, it is apparent that this activity is of only secondary importance to the tsunami generated outside of the Sound.

In the Gulf of Alaska (Figure 6), the general picture is the same, except that much less specific detail is available: Immediate water withdrawals were reported at Boswell Bay (Hinchinbrook Island), Cape St. Elias, and Middleton Island, all of which were regions of uplift; while similar

withdrawals were reported at Rocky Bay and Nuka Bay, at the end of the Kenai Peninsula, and in Marmot Bay, Afognak Island, all of which are located on the northwest side of the axis of major depression. No early water motion was reported from regions on the synclinal axis running from Chiniak Bay, Kodiak Island, to just easterly of Resurrection Bay on the Kenai Peninsula. Aside from local turbulence and seiching generated by the earthquake motions, no wave action or water motions were reported anywhere within the Cook Inlet until several hours after the earthquake. This pattern of water motion is again consistent with the concept of uplift along the shelf geanticline and subsidence along the Kodiak geosyncline, and suggests that the tsunami was produced by drainage of water away from the anticlinal ridge running from the Trinity Islands southeast of Kodiak through Montague and Hinchinbrook Islands in Prince William Sound. As will be shown, this view is also supported by the wave observations.

WATERWAVE OBSERVATIONS

Reproductions of tide gage records were obtained from the U. S. Coast and Geodetic Survey for tide stations at Sitka, Yakutat, Hilo Hawaii, and Unalaska. Additionally, fairly complete early chronologies of wave motion were available from Cape Yakutaga and Chiniak Bay, Kodiak (U. S. Naval Station). Less reliable, but useful information of the time of arrival and sense of first wave motion were also reconstructed from eyewitness accounts at numerous places along the Gulf of Alaska. Pertinent data on initial wave motion are given in Table 1. It is significant that, outside of the immediate area of tsunami generation, the sense of the initial wave motion was everywhere positive, being strongly upwards at all points in the southeasterly quadrant, and weakly positive westerly along the Aleutian Chain.

TABLE I

TSUNAMI TRAVEL TIMES TO OBSERVATION STATIONS

Station	Arrival Time of First Motion (GMT)	Sense of First Motion	Travel Time (min)	Travel Distance (n.min)	Effective Depth	Travel Time Correction (min)	Corrected Travel Time (min)
Old Harbor	0424*	UP	48	29	117	0	48
Chiniak Bay	0420	UP	44	26	111	0	44
Seward	0411*	UP	35	45	510	0	35
Controller Bay	0415	UP	39	51	530	0	39
Cape Yakataga	0425	UP	45	78	930	1	44
Yakutat	0450	UP	74	169	1630	2	72
Sitka	0508	UP	92	347	4420	3	89
Unalaska	0903	UP	157	840	8900	5	152
Hilo Hawaii	0900	UP	324	2440	17600	8	316

* These times are average of 2 or more estimates

In order to obtain some concept of the size of the tsunami generation area, imaginary wave fronts were projected according to Huygen's principle back towards the epicenter at velocity $c = \sqrt{gh}$ (h=depth) from each of the several points of wave observations over time intervals equal, respectively, to the time intervals between the main shock and the observed times of arrival of the first wave motion at these stations. The most recent analysis of the nature of the leading wave of a tsunami (Kajiura, 1963) points out that the toe of the leading wave actually precedes the wave 'front', which travels at $\sqrt{gh}$ velocity. The correction term is given by, approximately

$$\left(\frac{6}{t\sqrt{gh}}\right)^{1/3}\left(\frac{r}{h} - t\sqrt{g/h}\right) = 4$$

where $h = \frac{1}{g}\left(\frac{r}{t}\right)^2$, r = distance, g = gravitational acceleration, and t = time of arrival of first disturbance. These corrections increase as the cube root of travel time, and were subtracted from the observed arrival times for first motion at all stations The corrections are also listed in Table 1.

In order to maintain accuracy these graphical - numerical constructions were commenced on very small scale charts in the immediate vicinity of each station, and the coordinates successively transfered to larger scale charts, until deep water was reached. Such constructions are carried out routinely by Japanese scientists in tracking tsunamis, and can be considered accurate to about 2% in time. The results are shown in Figure 8 by the heavy curves, each of which is connected to its source station by dashed lines. The best representation of the area of tsunami generation is

construed to be the region which is circumscribed by an envelope which touches each of these heavy curves. It seems clear from the distribution of these curves that the origin of the tsunami was a broad region of uplift somewhere near the central part of the continental shelf in the Gulf of Alaska; the waves which radiated to the northwest appear to have originated from a line source which coincides with the presumed axis of the geanticline, while the wave system traveling towards the south and east seems to have originated along the northeasterly end of the Aleutian Trench itself.

Since the wave front constructions depend on the assumption that the ground motion took place instantaneously at the time of the principal shock, it is apparent that any finite time required for this action would modify this picture somewhat, pushing back the constructed wave fronts towards their sources by distances corresponding to travel times equal to the appropriate time delay in each case. For example, the time of the principal shock is listed by the U. S. Coast and Geodetic Survey as 0336Z, while the inception of strong ground shocks in Kodiak (Navy Weather Central) is given as 0342Z, or about six minutes after the first shock.

THE TSUNAMI IN THE OPEN SEA

The tsunami generated by the earthquake of March 28 was recorded at Wake Island, 3050 nautical miles from the source region, at a station specifically constructed for this purpose in 1960. A portion of this record showing the first two hours of this tsunami is shown in Figure 9. The recording element of this station is an absolute pressure transducer on the bottom in fifty feet of water, and connected to a plastic garden hose extending to a depth of

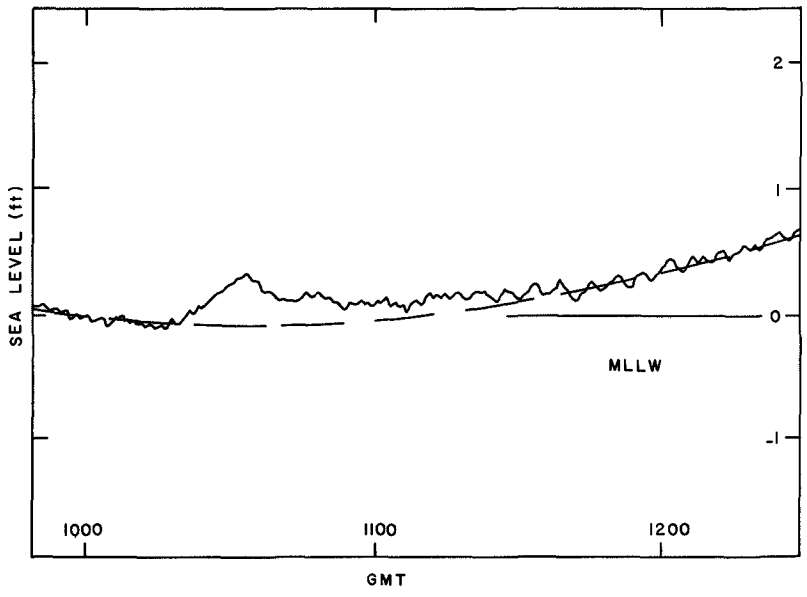

FIG 9 --WAVE RECORD FROM WAKE ISLAND, SHOWING ARRIVAL OF TSUNAMI (INITIAL MOTION IS POSITIVE AND REMAINS ABOVE NORMAL TIDE CURVE FOR OVER AN HOUR)

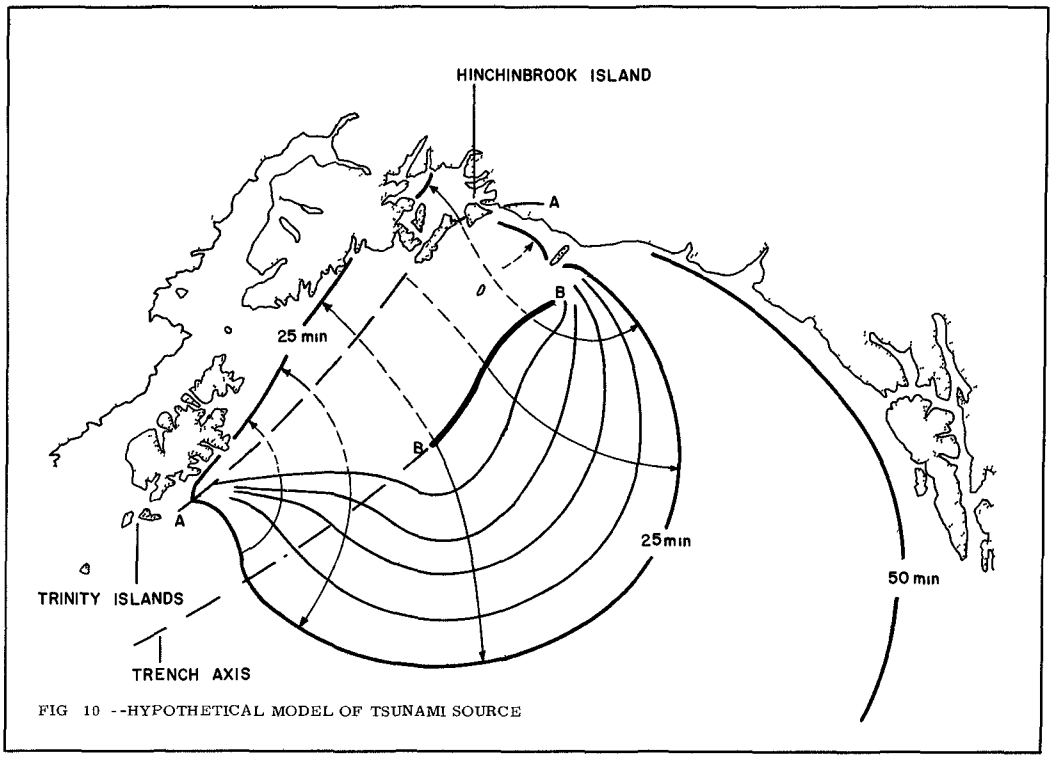

FIG 10 --HYPOTHETICAL MODEL OF TSUNAMI SOURCE

800 feet off shore on the south side of Wake Island. The hose depth, together with an electrical low-pass filter, restrict the excursions of ordinary wind waves to negligible amplitudes. For wave periods longer than about forty seconds the response is unity, and the resolution of the record is about .02 ft of water. The tsunami begins with a slow increase in sea level to a height of about 4 in. over a period of fifteen minutes, followed by a normal dispersive wave train of rather small amplitude. The remarkable feature of this record is that it does not return to normal tide level - as indicated by the dashed line in this figure - for more than an hour. At the time of the tsunami the local wind velocity was about 7 knots and extremely steady, and therefore the record obtained can be considered to be a reasonably accurate representation of the actual tsunami characteristics in deep water.

From the general appearance of this record, one has the impression that a large fraction of the energy of the tsunami was contained in a single, long solitary wave, formed in the Gulf of Alaska by drainage of water from the coastal shelf. The small amplitude of the dispersive signature attests to the lack of sudden or discontinuous variations in the rate of drainage. Kajiura (1963) has investigated in some detail the theoretical aspects of the leading wave of a tsunami for a variety of source conditions. But the theory applies only to tsunamis generated and propagating in water of uniform depth, and thus it cannot be applied directly to the present situation without some suitable modification of the initial conditions, and consideration of the effect of depth variations along the travel path. Some speculations in this connection, and the results of model tests in the author's wave channel at the Scripps Institution, will be reported later.

A broad solitary wave of the type observed at Wake can only be produced by the net (albeit temporary) addition of water to the ocean. The nature of the tsunami source described above appears to fulfil this condition, if the gross ground motion is considered to be dipolar, as evidenced by the signature of the barometric wave recorded at La Jolla. Judging by the pattern of ground dislocations, the positive pole was mostly on the shelf, under water, while the negative pole was largely on land. This circumstance would not be expected to influence the barometric wave, which was fairly symmetric, but implies that the net signature in the Gulf was strongly positive, as shown by the initial motion at all coastal observation stations. The later stages of the Wake record (not shown in Figure 6) exhibit slow, lesser oscillations of both above and below the local tide stage, which are probably due to readjustments of sea level in the Gulf to the initial outflow of water from the shelf, and reflection from the Kenai-Kodiak Ridge produced by subsidence of the Kodiak geosyncline.

RECONSTRUCTION OF THE TSUNAMI ORIGIN - AN HYPOTHESIS

The tsunami of March 28, 1964 is construed to have originated from a dipolar dislocation of the earth's crust centered about the axis P-P in Figure 6. The dipole appears to have had positive and negative extrema along the axes B-B and A-A, respectively, along which severe bending or ground rupture occurred. The dislocations probably took place within six minutes following the initial shock, beginning in the region of maximum dislocation, in the vicinity of Hinchinbrook Island, and propagating southwesterly along these axes to a point of zero dislocation southeast of Kodiak.

An hypothetical reconstruction of the early wave motion is given in Figure 10. The entire, quasi-rectangular area of the coastal shelf between the lines A-A and B-B is considere

to have been uplifted in a pattern indicated by the dotted gradients between these lines. Water motion towards the south and east commenced concurrently with the uplift at all points within this region, and parallel to the direction of the gradients. Successive wave fronts, constructed from the topography, are shown for five minute intervals out to 25 minutes, as is the wave front at 50 minutes, which encompasses most of the Gulf of Alaska. Also shown in this figure is a positive front propagating northwest 25 minutes after the earthquake. The negative wave, which was presumably generated within the small negative dipole region over the subsiding geosyncline, would not be observed within the generation area, and was probably immediately reflected by the shallow ridge connecting Kodiak with the Kenai Peninsula.

Within Prince William Sound, no negative phase was generated, and the local tsunami was caused by tilting of the entire region of the Sound towards the northwest, followed by extensive seiching in the deep, complex basin, with little exchange of energy with the Gulf.

Outside the region of generation, the tsunami radiated into the Pacific basin, principally as a solitary wave, followed, some hours later, by lesser slow oscillations, as described above. Judging by the circumpacific distribution of reported tide gage heights, the tsunami source was somewhat directional, radiating energy preferentially towards the southeast. Local shoreline wave heights were larger at similar distances all along the coast of North America than along the Aleutian Islands. A maximum height of four feet was reported from the Palmer Peninsula in Antartica, while heights in Japan were only a foot or so. Despite the long-continuing nature of the disturbance observed at Wake, tide records around the Pacific exhibited their usual strong perodicities, characteristic of the

local environment, showing that such records cannot be depended upon to give much information about the nature of a tsunami in the open sea.

A preliminary estimate of the total energy for this tsunami can be obtained by consideration of the potential energy of the dipole uplift over the shelf. Taking the source dimensions as 240n miles x 100n miles, and the uplift as six feet at the northeasterly end of the long axis and zero at the southwesterly end, the total energy E_t is

$$E_t = \tfrac{1}{2}pgh^2A = \frac{35 \times 36 \times 100 \times 240 \times 6080^2}{2 \times 6} = 1.7 \times 10^{14} \text{ft-lbs} =$$

$$2.3 \times 10^{21} \text{ergs}$$

which is about 10% of that (2.7×10^{22}ergs) computed for the tsunami of March 9, 1957 in the Andreanof Islands (Van Dorn, 1963). This calculation, of course, ignores the energy of wave motion within Prince William Sound, but is consistent with the general magnitude of shoreline heights reported around the Pacific, relative to those from the previous tsunami.

ACKNOWLEDGEMENT

Much of the data presented here was collected by the author in person, in the course of ten days following the earthquake, either by direct observation, or by conversations with eye-witnesses - many of whom were contacted through the courtesy of the extensive military communication network of the Alaskan Headquarters Command. Contributors to the fund of information available are too numerous to mention here, but particular

advice and assistance was provided by Dr. Pierre St. Amand, Navy Ordnance Test Station, China Lake, California, and by Lt. Delmer L. Brown, U. S. Army Engineers, who cooperated with the author during his survey, and later remained for some weeks to collect additional data under the terms of his temporary assignment for this purpose. The tide gage data and the bulk of the seismic evidence presented herein was obtained through the auspices of the U. S. Coast and Geodetic Survey, whose representatives were among the earliest scientific personnel to appear after the earthquake. Most of the data thus collected has yet to appear in print, although the Coast Survey (1964) has issued a special publication intended as an early information advisory. The author was considerably impressed by the number of people who, without any official concern for the collection of data, had the initiative and interest to keep detailed logs of all available information as it occurred. Among these should be mentioned Lt. Barney, U. S. Fleet Weather Central, Kodiak, Mr. Jim Reardon, Area Biologist, Alaskan Fish and Wildlife Service, Homer, Alaska, and Mr. C. R. Bilderbock, fisherman and ten-year resident of remote Cape Yakataga. Upon just such detailed information, the conclusions drawn herein heavily depend.

REFERENCES

Kajiura, Kinjiro (1963). The leading wave of a tsunami: Bul. Earthquake Res. Inst., vol. 41, pp. 535-571.

Miyabe, Naomi (1934). An investigation of the Sanriku tunami based on mareogram data: The earthquake Res. Inst., Supp. vol. 1, pp. 112-126.

Nagata, Takesi (1950). Summary of the geophysical investigations on the great earthquake in southwestern Japan on December 21, 1946: Trans. Amer. Geophys. Union, vol. 31, No. 1, pp. 1-6.

St. Amand, Pierre (1957). Geological and geophysical synthesis of the tectonics of portions of British Columbia, the Yukon Territory, and Alaska: Bul. Geol. Soc. of Amer., vol. 68, pp. 1343-1370.

Takahasi, Ryutaro. Director Earthquake Research Institute, Tokyo University.

Twenhofel, W. S. (1951). Recent shore-line changes along the Pacific coast of Alaska: Amer. J. of Sci., vol.250, pp. 523-548.

U. S. Coast and Geodetic Survey (1964). Preliminary report; Prince William Sound, Alaskan earthquakes: Washington D. C.

Van Dorn, Wm. G. (1960). A new long-period wave recorder: J. Geophys. Res., vol. 65, No. 3, pp. 1007-1012.

Van Dorn, Wm. G. (1963). The source motion of the tsunami of March 9, 1957 as deduced from wave measurements at Wake Island: Int. Union of Geodesy and Geophys.; Proceedings of the Tsunami Meetings; Tenth Pacific Science Congress, Univ. of Hawaii, pp. 39-48.

Chapter 11

MODEL TESTS ON THE RELATIONSHIP BETWEEN DEEP-WATER WAVE CHARACTERISTICS AND LONGSHORE CURRENTS

Arthur Brebner
Chairman, Department of Civil Engineering
Queen's University at Kingston, Ontario

and

J.W. Kamphuis
Research Fellow, Department of Civil Engineering
Queen's University at Kingston, Ontario

INTRODUCTION

It has long been recognized that the movement of littoral material takes place, in the main, in the onshore regions of a beach where breaking of waves occurs. Waves whose crests in deep water make an angle α_o with the shoreline, and which break at an angle α_B, are the main source of energy for the generation of the forces which manifest themselves in long-shore currents and the resulting littoral transport. This littoral material is put into motion before, during and after breaking but it is extremely difficult to separate the effects of the forces and currents in these three zones. In what follows the authors have attempted to measure the intensity of the current around the breaking zone in a highly idealized beach model in which the shoreline is straight, has a constant beach slope, θ, and is attacked by waves of constant deep-water wave-height, H_o, and period, T.

During refraction and shoaling the angle of the wave-crests with the shore-line is reduced from α_o to α_B and during this process some of the deep-water energy being transmitted shorewards may be dissipated by friction. The exact value of α_B is a function of α_o, H_o/L_o, and the friction loss, but will increase, both theoretically and experimentally, with increasing H_o/L_o, as shown by Brebner and Kamphuis (1963).

Based on the angle of breaking, α_B, the wave-steepness at breaking, H_B/L_B, the depth of breaking d_B, and the beach slope, θ, it is possible to formulate relationships for the long-shore current, v_L, using the principle of conservation of energy and momentum and the principle of continuity.

Using energy considerations, $$v_L = K_1 \left[\theta \cdot \frac{H_B^2}{T} \cdot \sin 2\alpha_B \right]^{1/3}$$

and using momentum considerations,

$$v_L = K_2 \left[\theta \cdot \frac{H_B^{3/2}}{T} \cdot \sin 2\alpha_B \right]^{1/2}$$

where K_1 and K_2 are empirical "constants" depending on the friction energy offered to the longshore current, the amount of energy dissipated in the breaking process, and the amount used in maintaining on-shore

off-shore motion at right angles to the longshore current.

Using continuity considerations and a random-walk distribution of wave-heights Chiu and Per Bruun (1964) arrive at a value of v_L which is apparently in reasonable agreement with field observations. However, since wave-forecasting methods give H_o, T, and α_o the authors deem it preferable in this instance to express v_L in terms of the deep-water characteristics instead of breaking characteristics, and also to deal with regular waves since these are normally used in laboratory models simulating prototype installations.

MODEL TESTS OF LONGSHORE CURRENTS

a) Procedure:- The tests were carried out in a basin approximately 2 ft. deep with a plan area of 100 ft. x 50 ft. Sixteen differing wave periods ranging from 0.78 to 1.13 seconds, five differing wave-heights from 0.075 to 0.258 feet, six differing values of α_o from 10° to 60°, and two differing impermeable fixed-bed beach slopes, 1:10 and 1:20 were used. The longshore velocities in and around the breaking zone were measured by timing coloured neutral density bubbles of trichloroethylene and benzene over known distances. About 50 such readings were taken per incident wave and a mean value of v_L established. In all about 500 values of v_L were obtained.

b) Presentation of Results:- The variables in the tests were θ, α_o, H_o and L_o (or T). In view of the form of the theoretical relationship for v_L it was decided to put v_L in the form

$$v_L = K \theta^a H_o^b T^{-c} \quad (\text{Function } \alpha_o)$$

For given values of α_o it was possible, using a 1620 IBM computer, to perform regression analyses using values of a varying from 0.33 to 1, b from 0.5 to 1 and c from 0.33 to 1. Further, since T remains constant during refraction and the breaking height H_B is of the same order as H_o, it is possible to carry out a Fourier analysis on α_o to give (Function α_o) as a sine series.

In keeping with the theoretical results it was possible to produce two expressions for v_L, namely,

$$v_L = 2.5 \left[\frac{g\theta H_o^2}{T}\right]^{1/3} \left[\sin(1.65\alpha_o) + 0.1 \sin(3.30\alpha_o)\right] \qquad (1)$$

and

$$v_L = 6 \left[\frac{g\theta^2 H_o^3}{T^2}\right]^{1/4} \left[\sin(1.65\alpha_o) + 0.1 \sin(3.30\alpha_o)\right] \qquad (2)$$

In both these expressions the constant is dimensionless. The experimental values are shown on Figures 1 and 2. Of the total energy available prior to breaking only about 8% is used in maintaining the long-

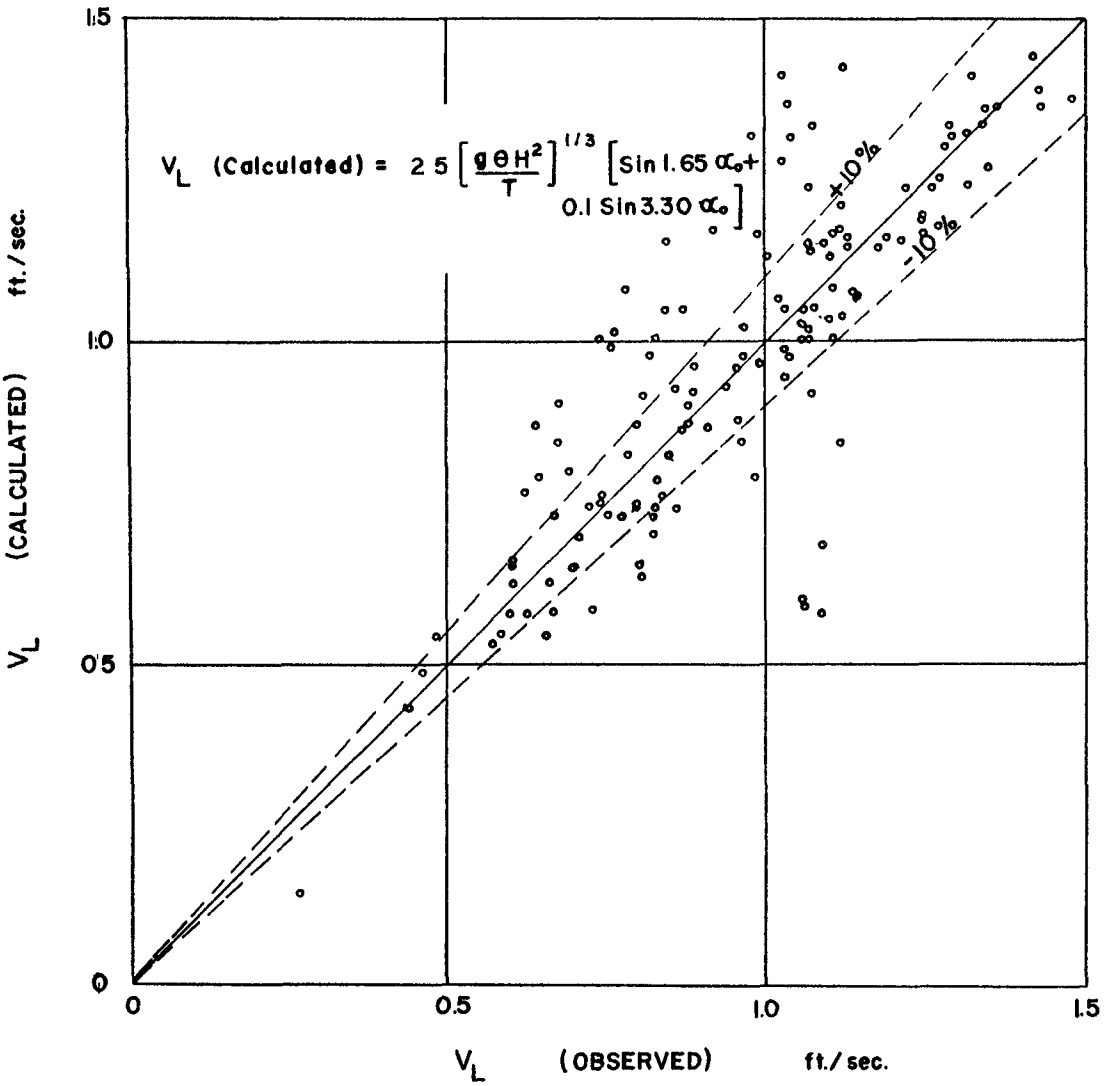
V_L (Calculated) = $2.5\left[\frac{g\Theta H^2}{T}\right]^{1/3}\left[\text{Sin } 1.65\,\alpha_o + 0.1\,\text{Sin } 3.30\,\alpha_o\right]$
+10%
-10%
1.5
1.0
0.5
0
0
0.5
1.0
1.5
V_L (CALCULATED) ft./sec.
V_L (OBSERVED) ft./sec.

FIGURE 1

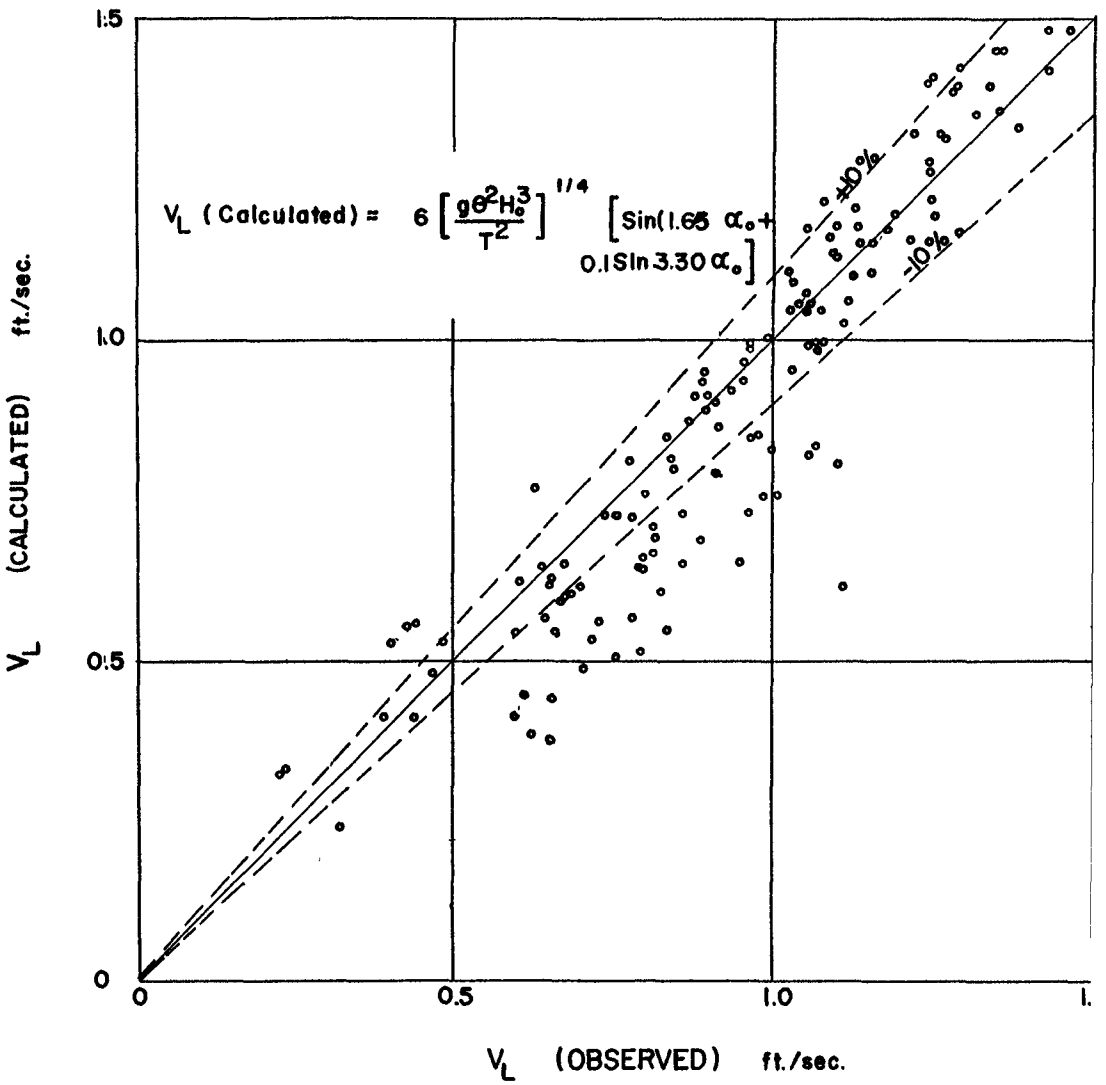
1.5
1.0
0.5
0
0
0.5
1.0
1.
V_L (CALCULATED) ft./sec.
V_L (OBSERVED) ft./sec.
V_L (Calculated) = $6\left[\frac{g\theta^2 H_o^3}{T^2}\right]^{1/4}\left[\text{Sin}(1.65\ \alpha_o + 0.1\text{Sin}3.30\ \alpha_o\right]$
+10%
-10%

FIGURE 2

shore current at the intensity given by either equations 1 or 2, indicating the high energy loss in the breaking phenomenon itself and in maintaining on-shore off-shore movement of water, normal to the longshore current.

The (Function α_o) term reveals that the maximum value of v_L occurs when α_o is about 55°, which is in good agreement with Bruun's value of 54° and Sauvage and Vincent's value of 53°.

DISCUSSION OF RESULTS

The model may be considered distorted or undistorted. If undistorted the Froude scale is about 1:100 for linear dimensions and at this scale the "Reynolds Number" damping effect, using Eagleson's (1962) theory of damping of oscillatory waves, is not marked.

If n_d is the ratio $\frac{\text{prototype depth}}{\text{model depth}}$ and if the suffix L refers to wave-length, H to wave-heights, and c to wave-speed, then for such a refraction model as this which demands homologous angles of breaking, homologous shoaling, and homologous breaking depths,

$$n_c = n_T = n_L^{1/2} = n_d^{1/2} = n_H^{1/2}$$

Referring to equations 1 and 2, if n_x is the plan length scale,

$$\text{Longshore current scale} = n_{vL} = \frac{v_{Lp}}{v_{Lm}} = \left[\frac{\frac{n_d \cdot n_H^2}{n_x}}{n_T}\right]^{1/3} = n_d^{1/2}\left[\frac{n_d}{n_x}\right]^{1/2}$$

$$\text{or} \qquad n_{vL} = \frac{v_{Lp}}{v_{Lm}} = \left[\frac{\frac{n_d^2 \cdot n_H^3}{n_x}}{n_T^2}\right]^{1/4} = n_d^{1/2}\left[\frac{n_d}{n_x}\right]^{1/2}$$

If the model is considered undistorted, $n_d = n_x$ and $n_{vL} = n_x^{1/2}$, as in a simple Froude model.

In effect equations 1 and 2 should be universally applicable if one assumes that

a) the model beach slopes are not so steep as to excessively deform the orbital paths compared with the prototype.

b) the prototype slopes are neither so flat, rough, nor permeable as to cause excessive attentuation due to friction compared with the model.

c) the exponent of the slope Θ is to be trusted in view of the fact only 2 differing slopes were used in the tests.

In conclusion, equations 1 and 2 probably give a maximum attainable envelope value of v_L when extrapolated to a prototype situation since, in nature,

a) beaches are not straight and uniform,

b) rip currents are set up which limit the longshore current,

c) due to the presence of longshore bars, energy and momentum are transferred to the longshore process at various locations,

d) waves are not regular and thus the breaking zone is not too well defined.

For use on prototype situations with non-regular waves the authors' suggest that H_o be replaced by $\frac{H_s}{1.6}$ on the argument that the mean height of all waves in a random-walk sample is the significant wave-height divided by 1.6. Thus, on a one-bar beach having a slope Θ of 0.017 radians, wave-period 8 secs., $\alpha_o = 45°$, and $H_s = 5.5$ metres, the longshore current is 1.4 m/sec. by equation 1 and 1.2 m/sec. by equation 2. A typical prototype value is about 1 m/sec. under such conditions, indicating as suggested previously that the authors' relationships probably give limiting values of the maximum longshore current for any particular situation.

REFERENCES

Brebner and Kamphuis, "Model Tests on the Breaking of Waves at an Angle with a Shoreline", 10th I.A.H.R. Congress, London, September 1963.

Chiu and Per Bruun, "Computation of Longshore Currents by Breaking Waves", Engineering Progress at the University of Florida, Vol. XVIII, No. 3, March 1964.

Eagleson, "Laminar Damping of Oscillatory Waves", Proc. A.S.C.E., Vol. 88, No. HY 3, May 1962.

ACKNOWLEDGEMENT

The authors are grateful to the National Research Council of Canada under whose sponsorship the investigation was carried out.

Chapter 12

COMPUTATIONS OF LONGSHORE CURRENTS

by

Tsao-Yi Chiu and Per Bruun
Coastal Engineering Laboratory
University of Florida

ABSTRACT

This article introduces the longshore current computations based on theories published under the title "Longshore Currents and Longshore Troughs" (Bruun, 1963). Two approaches are used to formulate the longshore current velocities for a beach profile with one bar under the following assumptions: (1) that longshore current is evenly distributed (or a mean can be taken) along the depth; (2) that the solitary wave theory is applicable for waves in the surf zone; (3) that the statistical wave-height distribution for a deep water wave spectrum with a single narrow band of frequencies can be used near the shore, and (4) that the depth over the bar crest, D_{cr}, equal $0.8H_{b(1/3)}$. Breaking wave height $H_{b(1/3)}$ is designated to be the actual height equal to $H_{1/3}$ (significant wave height).

Diagrams have been constructed for both approaches for beach profiles with one bar, from which longshore current velocities caused by various wave-breaking conditions can be read directly. As for longshore currents along the beach with a multibar system, fifteen diagrams covering a great variety of wave-breaking conditions are provided for obtaining longshore current velocities in different troughs.

This paper is printed as "Computation of Longshore Currents by Breaking Waves", Technical Paper No. 279, Vol. XVIII, No. 3, March, 1964, by the Florida Engineering and Industrial Experiment Station and may be requested by letter addressed to "The Editor, The Florida Engineering and Industrial Experiment Station, University of Florida, Gainesville, Florida".

Launda, Angola

Part 2
COASTAL SEDIMENT PROBLEMS

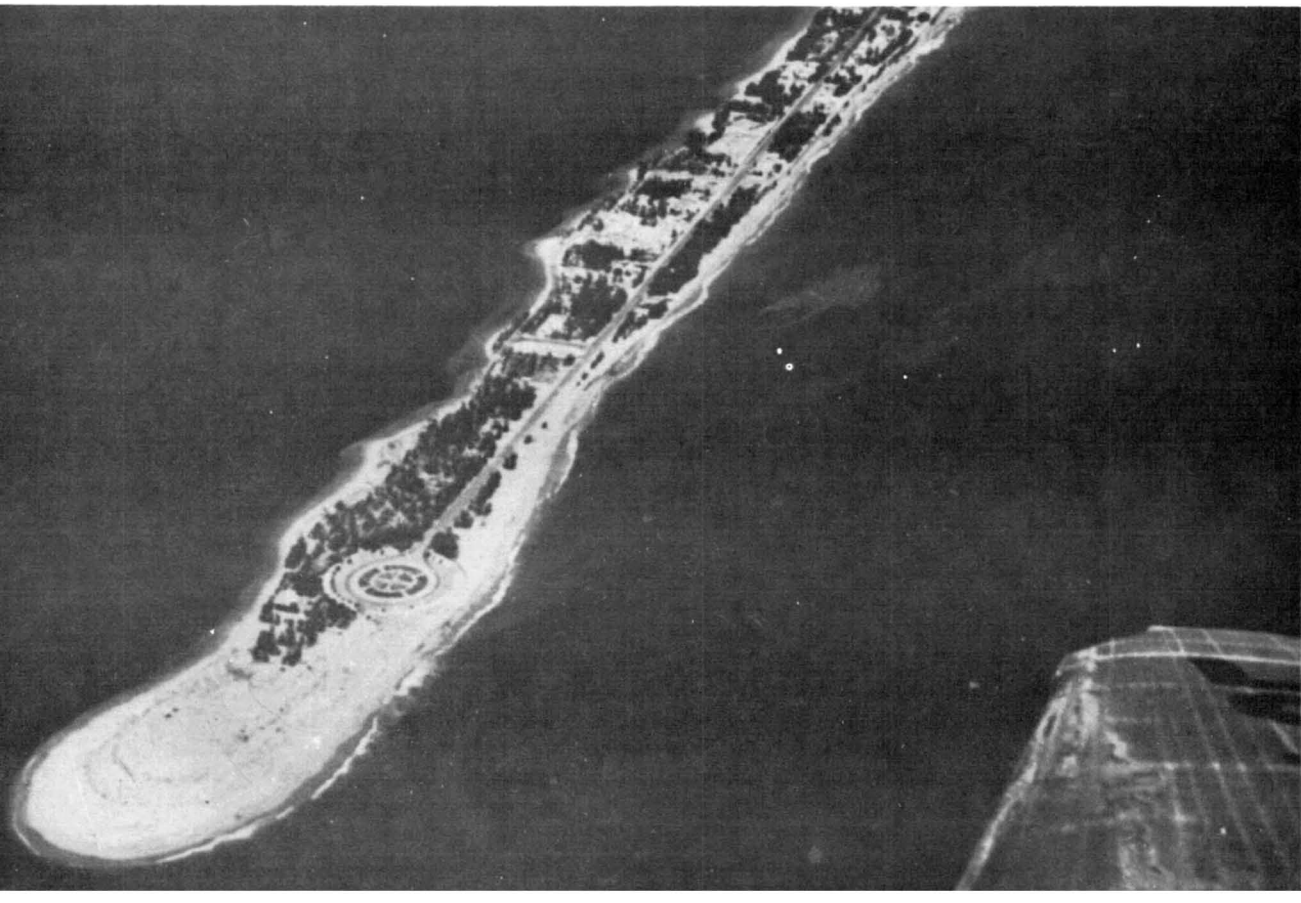

Lobito, Angola

Chapter 13

THE COASTLINE OF RIVER-DELTAS

by W.T.J.N.P. Bakker and T. Edelman
Coastal Research Department of the
Rijkswaterstaat. The Hague, Netherlands.

INTRODUCTION.

The purpose of this paper is to investigate the shape of the coastline of a river delta on a coast, along which sediment is transported by waves only. In order to make the problem suitable to a mathematical treatment it is necessary to simplify to a large extend the processes occurring in nature. We assumed:

1e. There are no tides and no tidal currents.
2e. The influence of currents on the sedimenttransport will be neglected.
3e. In the beginning the coastline is a straight line (x -axis).
4e. The fore shore has a constant slope until a depth D; the influence of the waves reaches until this depth D; further seawards the waterdepth has a constant value D.
5e. The mouth of the river lies in the origin of the system of coördinates, and stays there.
6e. The river continually brings a constant quantity of sediment into the sea.
7e. Waves with a constant height and a constant wave lenght are approaching the coast continually under a angle β with the x - axis.
8e. Refraction, diffraction and reflexion of the waves are neglected.
9e. The relation between the quantity of sediment Q, transported by the waves along the coast, and the angle α between the wave crests and the coastline, will be simplified in such a way, that an analytical solution of the partial differential equation will be possible. The next paragraph deals with this problem.

THE TRANSPORT FUNCTION

The sediment transport along shore, caused by oblique waves, is often represented by the formula:

$$Q = Q_m \sin 2\alpha$$

in which Q_m is the maximum value of Q, occuring when $\alpha = 45^\circ$. EDELMAN (1963) showed, that this formula is a fair approximation of the transport in the breaker zone. GRIJM (1960) showed, that an application of this formula to the delta problem leads to a very complicated partial differential equation, the solution of which seems to be possible only by means of a computer or a graphical method (GRIJM 1964).

LARRAS (1957) produced experimental data on the relation between Q/Q_m and α (Table I), that are not in agreement with the formula: $Q = Q_m \sin 2\alpha$

TABLE I

α =	0	10	20	30	40	50	60	70	80	90 degrees
$\frac{Q}{Q_m}$ =	0	0,30	0,57	0,70	0,83	0,98	0,70	0,28	?	?

Considering the problem from a theoretical point of view, however, it seems to be unprobably, that any single formula or any single series of data on this topic could be correct. Since refraction of waves depends on wave-height and wave-lenght, it seems to be impossible to set up a simple formula, covering the transport by all types of waves occuring.

The formulae and data, proposed by investigators in this field, until now, have, however, some things in common. Transport is increasing from zero at $\alpha = 0$ towards a maximum at a value of α lying somewhere between 40 and 65 degrees. At greater values of α the transport decreases and perhaps becomes zero at $\alpha = 90^{\circ}$.

Since we want a solution of the delta problem only in a general way, in order to obtain a general insight into the behaviour of the coastline in the neighbourhood of a river mouth, it seems to be admissible to make use of a new transport equation, provided, that this equation covers the above mentione characteristics in a general way. Moreover, the new equation must lead to a delta-equation of which the solution can be obtained along a analytical way.

The authors believe to have succeeded in finding an equation which sufficiently satisfies these conditions. For that purpose the range of α was split up into two areas. The transpo within the first area, in which $0 < \tan\alpha < 1.23$ is described by the formula:

$$Q = Q_m K_1 \tan\alpha$$

In the second area, in which $1.23 < \tan\alpha < \infty$ the formula

$$Q = Q_m \frac{K_2}{\tan\alpha}$$

will sufficiently cover the few data known about wave-transport in this area.

$$\frac{1}{K_1} = K_2 = 1.23.$$

The maximum wave transport according to this formula would occur at $\tan\alpha = 1.23$ or $\alpha \approx 51^{\circ}$.

The data and formulae given in this paragraph are plotted in figure 1.

THE DELTA EQUATION

From the continuity equation it follows that:

$$\frac{\partial Q}{\partial x} + \frac{\partial y}{\partial t} \cdot D = 0$$

If ρ is the angle between the coastline and the x - axis, and β is the angle between the wave crests and the x - axis, figure 2 shows that $\alpha = \beta - \rho$

Therefore:

$$\tan\alpha = \tan(\beta-\rho) = \frac{\tan\beta - \tan\rho}{1 + \tan\beta \cdot \tan\rho} = \frac{\tan\beta - \frac{\partial y}{\partial x}}{1 + \tan\beta \cdot \frac{\partial y}{\partial x}}$$

Area I

$$Q = K_1 Q_m \tan\alpha$$

$$Q = K_1 Q_m \frac{\tan\beta - \frac{\partial y}{\partial x}}{1 + \tan\beta \frac{\partial y}{\partial x}}$$

$$\frac{\partial Q}{\partial x} = -K_1 Q_m (1+\tan^2\beta) \frac{\frac{\partial^2 y}{\partial x^2}}{\left(1+\tan\beta\frac{\partial y}{\partial x}\right)^2}$$

thus

$$K_1 Q_m (1+\tan^2\beta) \frac{\frac{\partial^2 y^2}{\partial x^2}}{\left(1+\tan\beta\frac{\partial y}{\partial x}\right)^2} = \frac{\partial y}{\partial T} \cdot D$$

Area II

$$Q = K_2 \frac{Q_m}{\tan\alpha}$$

$$Q = K_2 Q_m \frac{1 + \tan\beta \frac{\partial y}{\partial x}}{\tan\beta - \frac{\partial y}{\partial x}}$$

$$\frac{\partial Q}{\partial x} = K_2 Q_m (1+\tan^2\beta) \frac{\frac{\partial^2 y}{\partial x^2}}{\left(\tan\beta - \frac{\partial y}{\partial x}\right)^2}$$

thus

$$-K_2 Q_m (1+\tan^2\beta) \frac{\frac{\partial^2 y}{\partial x^2}}{\left(\tan\beta - \frac{\partial y}{\partial x}\right)^2} = \frac{\partial y}{\partial T} D$$

Putting $t = \frac{Q_m}{D}(1 + \tan^2\beta)\, T$, we obtain

$$K_1 \frac{\frac{\partial^2 y}{\partial x^2}}{\left(1+\tan\beta\cdot\frac{\partial y}{\partial x}\right)^2} = \frac{\partial y}{\partial t}$$

$$-K_2 \cdot \frac{\frac{\partial^2 y}{\partial x^2}}{\left(\tan\beta - \frac{\partial y}{\partial x}\right)^2} = \frac{\partial y}{\partial t}$$

FIGURE 1

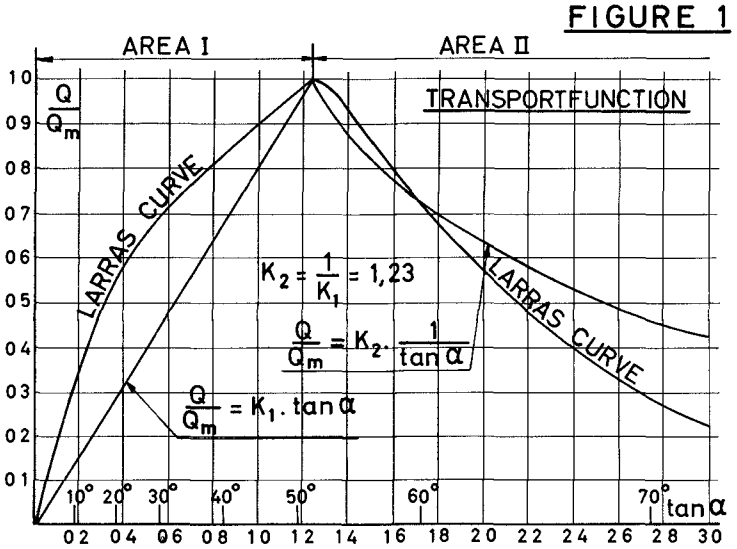

FIGURE 2

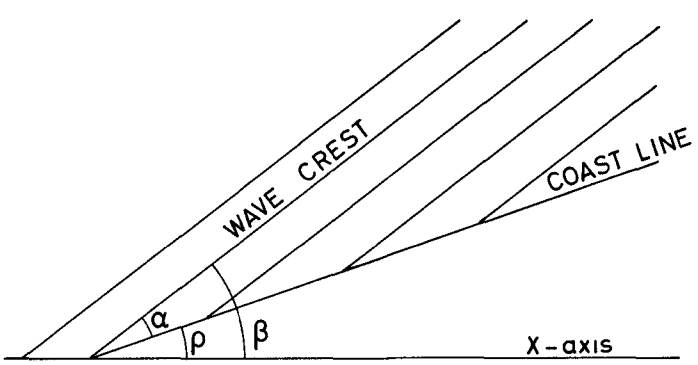

If Q_m is expressed as a volume per time-unit, t possesses the dimension of a surface.

SOLUTION OF THE DELTA EQUATION

If we put: $y = t^n f(u)$ and $x = ut^m$ we obtain:

Area I

$$K_1 \frac{t^{n-2m} \cdot \frac{d^2f}{du^2}}{\left(1+\tan\beta \cdot t^{n-m}\frac{df}{du}\right)^2} = t^{n-1}\left(nf - mu\frac{df}{du}\right)$$

Area II

$$-K_1 \frac{t^{n-2m}\frac{d^2f}{du^2}}{\left(\tan\beta - t^{n-m}\frac{df}{du}\right)^2} = t^{n-1}\left(nf - mu\frac{df}{du}\right)$$

t disappears, if we put: $n = m = \frac{1}{2}$ and we obtain:

$$y = f\sqrt{t}, \quad x = u\sqrt{t}, \quad \frac{\partial y}{\partial x} = \frac{df}{du} \text{ and } \frac{\partial y}{\partial t} = \frac{1}{2\sqrt{t}}\left(f - u\frac{df}{du}\right)$$

The delta equations become

$$2K_1 \frac{\frac{d^2f}{du^2}}{\left(1+\tan\beta\frac{df}{du}\right)^2} = f - u\frac{df}{du}$$

$$-2K_2 \frac{\frac{d^2f}{du^2}}{\left(\tan\beta - \frac{df}{du}\right)^2} = f - u\frac{df}{du}$$

The solutions of these non-partial differential equations are:

$$u = -A\left[e^{-v^2} + v\sqrt{\pi}\left\{E(v)+a\right\}\right]$$

$$\frac{df}{du} = -\frac{1}{\tan\beta}\cdot\left[\frac{2\sqrt{K_1}}{A\sqrt{\pi}\left\{E(v)+a\right\}} + 1\right]$$

in which

$$v = \frac{u + f\tan\beta}{2\sqrt{K_1}}$$

$$E(v) = \frac{2}{\sqrt{\pi}}\int_0^v e^{-v^2}dv$$

A and a are integration constants.

$$u = -B\left[e^{w^2} - 2w\left\{\varphi(w)+b\right\}\right]$$

$$\frac{df}{du} = \tan\beta - \frac{2\sqrt{K_2}}{2B\left\{\varphi(w)+b\right\}}$$

in which

$$w = \frac{u\cdot\tan\beta - f}{2\sqrt{K_2}}$$

$$\varphi(w) = \int_0^w e^{w^2}dw.$$

B and b are integration constants.

The curve f(u) is the basic curve of the deltaproblem; a function $y = f(x)$ at any time T can be obtained from the basic curve by central projection from the origin of the system of coordinates, multiplying with the factor $\sqrt{t}$.

The basic curve of area I has a hyperbolic shape; it possesses two asymptots running through the origin.

The basic curve of area II has a parabolic shape; it does not possess asymptots.

INVESTIGATION ABOUT THE STABILITY

Introducing the new coördinates $\bar{x}$ and $\bar{y}$ of which the $\bar{x}$ - axis is taken parallel to the wave crests, we obtain

Area I

$$K_1 \frac{\partial^2 \bar{y}}{\partial \bar{x}^2} = \left(1 + \tan^2\beta\right) \frac{\partial \bar{y}}{\partial t}$$

Area II

$$-K_2 \frac{\partial^2 \bar{y}}{\left(\frac{\partial \bar{y}}{\partial \bar{x}}\right)^2} = \left(1 + \tan^2\beta\right) \frac{\partial \bar{y}}{\partial t}$$

or, changing the variables:

$$-K_2 \frac{\partial^2 \bar{x}}{\partial \bar{y}^2} = \left(1 + \tan^2\beta\right) \frac{\partial \bar{x}}{\partial t}$$

The solution with separated variables is:

$$\bar{y} = e^{-\left(K_1 a^2 \cos^2\beta\right)t} \left\{C_1 \sin a\bar{x} + C_2 \cos a\bar{x}\right\}$$

$$\bar{x} = e^{\left(K_2 a^2 \cos^2\beta\right)t} \left\{C_3 \sin a\bar{y} + C_4 \cos a\bar{y}\right\}$$

In area I the amplitude decreases with t. In area II, however, the amplitude increases with t.

If we understand these solutions to be disturbances, superimposed upon the solutions of the foregoing paragraph, we see, that in area I such a disturbance will decrease with time and, at last, will disappear. In area II, however, such a disturbance will grow larger and larger with time (fig. 3). The original curve grows with $\sqrt{t}$, but the disturbance grows with $e^{\frac{t}{T}}$. Therefore, in area II the disturbance will supersede the original curve after some time.

Obviously, the original solution (the basic curve) is stable in area I, but unstable in area II.

This is an important conclusion. It may be seen from figure 1, that two different values of $\tan\alpha$ are associated with every value of $\frac{q}{q_m}$. That means that in every point of a

FIGURE 3

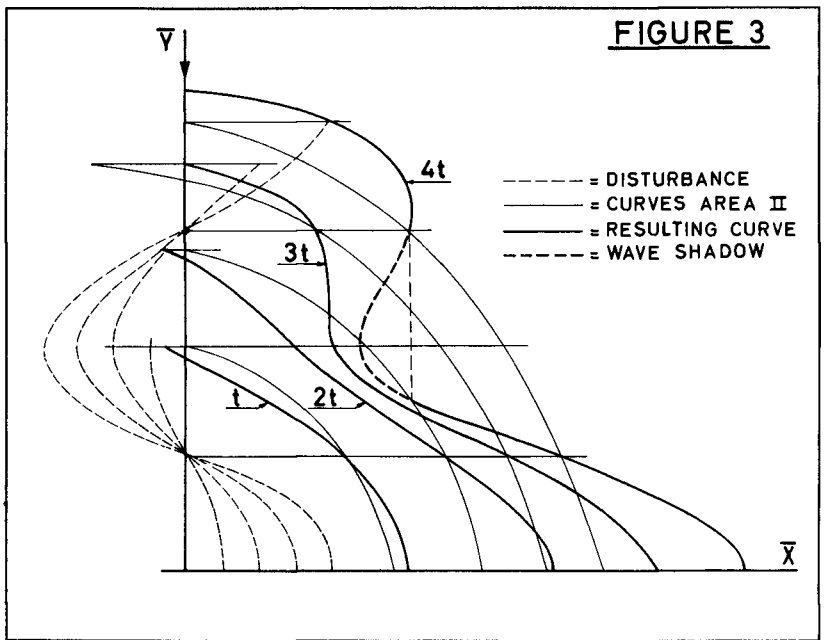

FIGURE 4

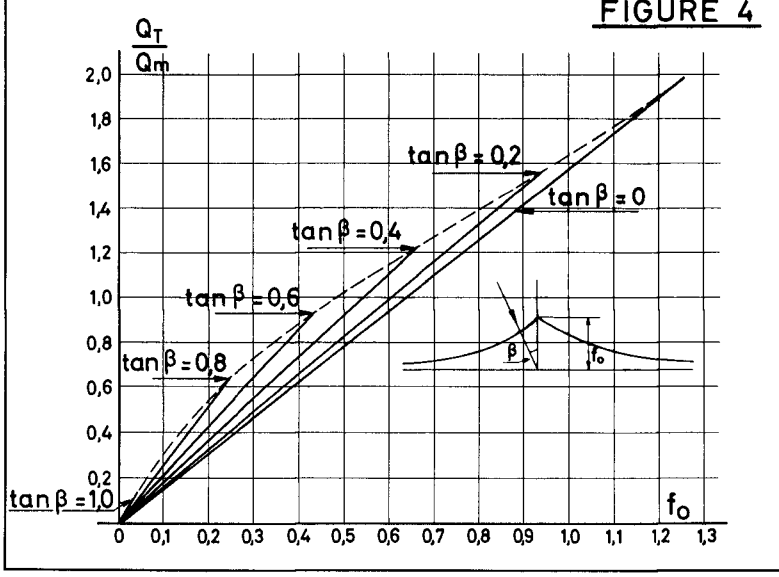

coastline two different directions can be found, along which an equal quantity of sediment can be transported by the waves. Since we have found that one of these directions is unstable, this ambiguity is eliminated from the problem.

Secondly, the problem of the delta shape can now be restricted to the cases in which $\tan\beta$ has values between zero and K_2, because a straight coastline is already unstable in itself if $\tan\beta > K_2$.

If $\tan\beta < K_2$, stable solutions can be obtained only if the coastal curves are in accordance with the formula of area I. This solution is an asymptotic one. In a stable delta, therefore, the influence of the river will be always perceptible, at both sides, towards infinite distance.

SHAPE OF THE POINTED DELTA

Using the foregoing formulae, we calculated f_o as a function of the quotient $\frac{Qt}{Qm}$ ($f = f_o$ when $u = o$; Q_t is the quantity of sediment, transported by the river) the result of which may be seen from figure 4. In figure 5 we show some basic curves of stable deltas if $\frac{Qt}{Qm}$ has the maximum value associated with distinct values of β. If $\frac{Qt}{Qm}$ exceeds this maximum value, the right hand side of the delta becomes unstable. (Area II).

Presumably, this type of instability means, that in nature spits will occur at the lee side of the delta.

The quantity Qt is related to Qm by the angle between the two tangents in the point of the delta. It can easily be seen, that the ratio $\xi = \frac{Qt}{Qm}$ can never exceed the value 2.

If $\xi > 2$, no solution at all can be obtained from our formula. It seems therefore, that the method in which the problem has been approximated until now, is not quite satisfactory; because we want to know the shape of a delta for the whole range of ξ between zero and infinity. Moreover, our pointed deltas possess the pecularity, that always a distance from the origin to the sea exists, which is shorter than the distance between the origin and the point of the delta. A better approximation of nature may be obtained if we alter some of our basic assumptions.

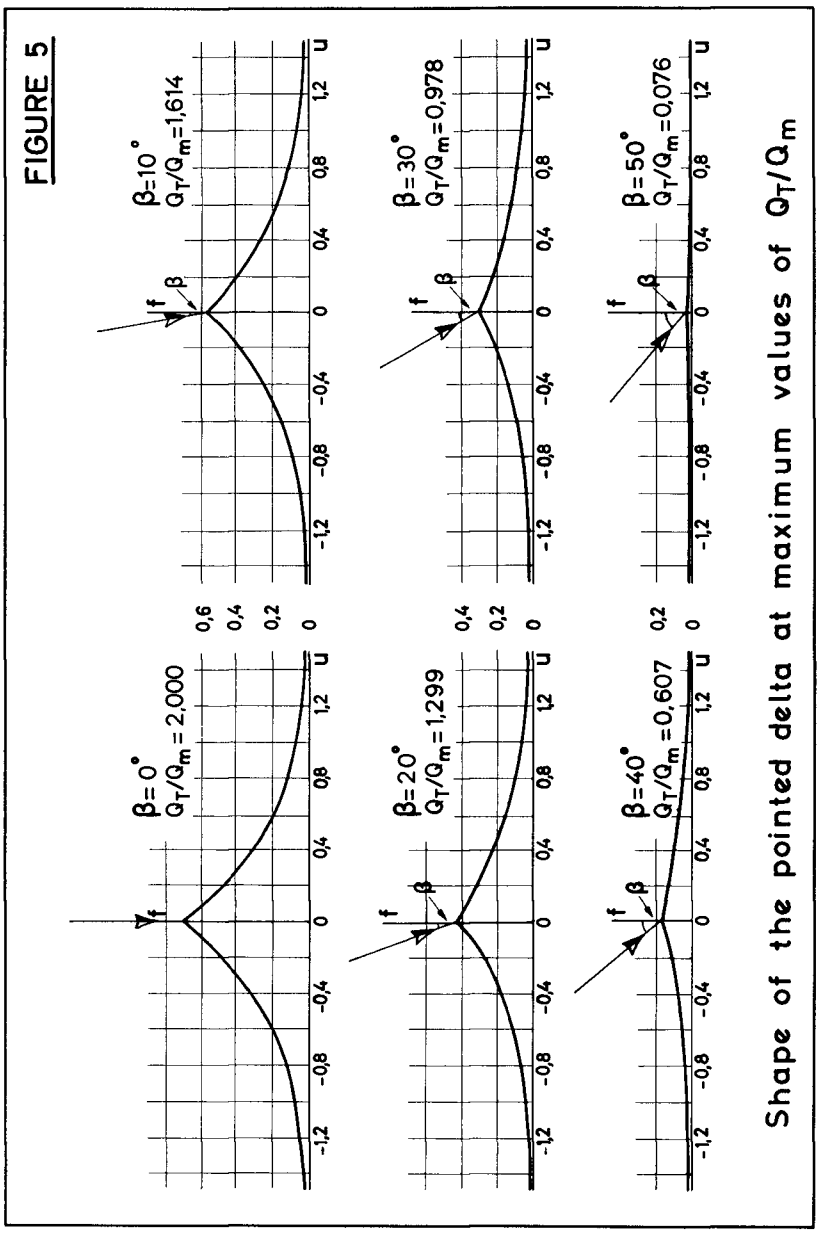
FIGURE 5
β=0°
Q_T/Q_m = 2,000
β=10°
Q_T/Q_m=1,614
β=20°
Q_T/Q_m=1,299
β=30°
Q_T/Q_m=0,978
β=40°
Q_T/Q_m=0,607
β=50°
Q_T/Q_m=0,076
f
β
u
0,6
0,4
0,2
0
-0,4
-0,8
-1,2
0,8
1,2
Shape of the pointed delta at maximum values of Q_T/Q_m

THE BEHAVIOUR OF THE RIVER WITHIN THE DELTA

In nature, a river will always try to take the shortest way to the sea. In the long run, and as an average, this will result in a delta with a more or less circular central part. In order to put this behaviour of a river into a mathematically usable shape, we made the following basic assumptions.

1e. The central part of the delta coastline is a circle with its centre in the origin.
2e. The river provides every point of the circle with a quantity q, necessary to maintain the circular coastline.
3e. At both sides the circular coastline is joined by coastal curves of the "pointed"-delta-type, belonging to area I.

From figure 6 it may be seen, that during a time-interval ΔT the circular part of the delta has grown with a quantity:

$$D.R.(\varphi_R + \varphi_L), \Delta R$$

At the right hand side the waves have removed during this time-interval a quantity $K_1 Q_m \tan\varphi_R \Delta T$ and at the left hand side a quantity $K_1 Q_m \tan\varphi_L . \Delta T$.

During the time interval ΔT the river has supplied a quantity: $Q_r . \Delta T$

Obviously: $\Delta T . Q_r = D.R(\varphi_R+\varphi_L)\Delta R + K_1 Q_m (\tan\varphi_R + \tan\varphi_L)\Delta T$

or : $\frac{Q_r}{Q_m} = z = \frac{D}{Q_m} R.\frac{\partial R}{\partial T}(\varphi_R+\varphi_L) + K_1(\tan\varphi_R + \tan\varphi_L)$.

If we put: $R = r\sqrt{t}$, we find $\frac{\partial R}{\partial t} = \frac{1}{2}\frac{r}{\sqrt{t}}$ and $R\frac{dR}{\partial T} = \frac{1}{2}r^2$.

Thus: $z = \frac{1}{2}r^2(1+\tan^2\beta)(\varphi_R+\varphi_L) + K_1(\tan\varphi_R + \tan\varphi_L)$

The circular part of the delta is stable if $\tan\varphi_R \leqq K_2$ and $\tan\varphi_L \leqq K_2$. Further conditions are

$\tan\beta < \tan\varphi_R < K_2$; $-\tan\beta < \tan\varphi_L < \frac{1}{\tan\beta}$

Admitting instability in the circular part of the delta, we see that a coastal curve of area I cannot join the instable circular part tangentially. The condition of joining is

$$K_1 \tan\alpha_1 = \frac{K_2}{\tan\varphi_L}.$$

FIGURE 6

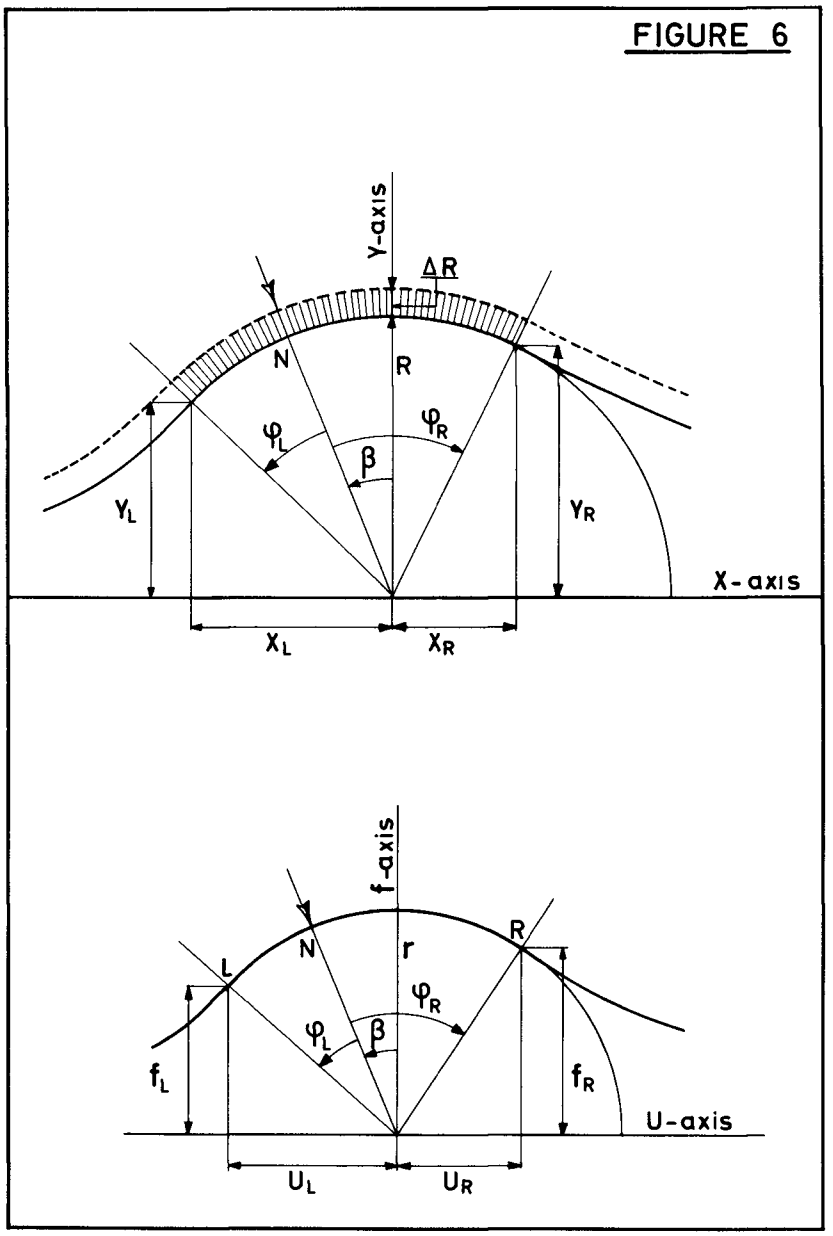
Y-axis
ΔR
N
R
φL
φR
β
YL
YR
X-axis
XL
XR
f-axis
L
N
r
R
φR
φL
β
fL
fR
U-axis
UL
UR

or $K_1 \tan \alpha_L = \dfrac{K_2}{\tan \varphi_R}$.

we find in these cases

$$\Sigma = \tfrac{1}{2} r^2 (1 + \tan^2 \beta)(\varphi_R + \varphi_L) + K_2 \left(\frac{1}{\tan \varphi_L} + \frac{1}{\tan \varphi_R} \right)$$

At the right hand-side another interesting case exists, in which the unstable delta causes erosion of the coast. In this case (figure 7):

$$\Sigma = \tfrac{1}{2} r^2 (1 + \tan^2 \beta)(\varphi_L + \pi - \varphi_R) + \frac{K_2}{\tan \varphi_L}$$

RADIAL DISTRIBUTION OF Q_L

If q = the quantity of river sediment per angle unit, continuity considerations lead to:

$$q = \frac{\partial Q}{\partial \varphi} + D.R. \frac{\partial R}{\partial T}$$

in which

$$D.R. \frac{\partial R}{\partial T} = \tfrac{1}{2} r^2 Q_m (1 + \tan^2 \beta).$$

In area I $(\tan \varphi \leq K_2)$: $Q = K_1 Q_m \tan \varphi$ and thus:

$$\frac{\partial Q}{\partial \varphi} = K_1 Q_m \frac{1}{\cos^2 \varphi}.$$

In area II $(\tan \varphi > K_2)$: $Q = K_2 Q_m \dfrac{1}{\tan \varphi}$ and therefore

$$\frac{\partial Q}{\partial \varphi} = -K_2 Q_m \frac{1}{\sin^2 \varphi}.$$

Thus: in area I : $q = K_1 Q_m (1 + \tan^2 \varphi) + \tfrac{1}{2} r^2 Q_m (1 + \tan^2 \beta)$

in area II: $q = -K_2 Q_m \dfrac{1 + \tan^2 \varphi}{\tan^2 \varphi} + \tfrac{1}{2} r^2 Q_m (1 + \tan^2 \beta)$

In the direction OB, with $\tan \varphi = K_2$, we see that

out of area I: $q_L = K_1 Q_m (1 + K_2^2) + \tfrac{1}{2} r^2 Q_m (1 + \tan^2 \beta)$.

and out of area II: $q_L = -K_2 Q_m \dfrac{1 + K_2^2}{K_2^2} + \tfrac{1}{2} r^2 Q_m (1 + \tan^2 \beta)$.

We see that in the direction OB a jump occurs : $2 Q_m \dfrac{1 + K_2^2}{K_2}$.

(figure 8). This jump has been caused by the discontinuity we introduced in the transport equation. If we choose a continual transport equation no jump occurs. For instance, if we choose

$Q = Q_m \sin 2\varphi$, then

FIGURE 7

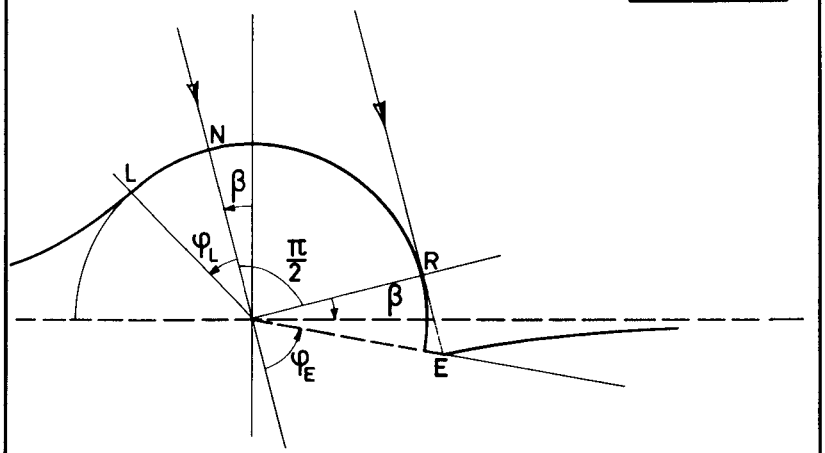

FIGURE 8

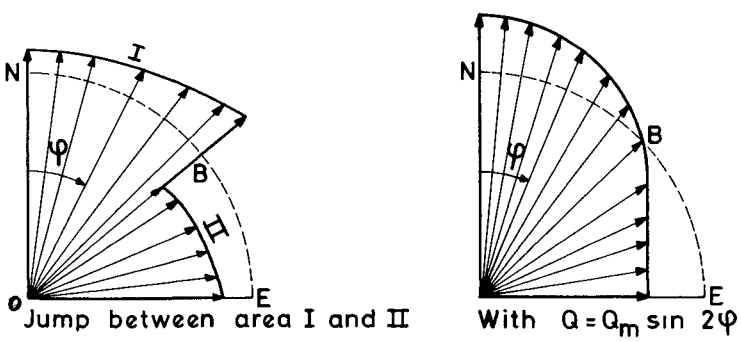

RADIAL DISTRIBUTION OF Q_T

$\frac{\partial q}{\partial \varphi} = 2 q_m \cos 2\varphi$ and $q = \frac{1}{2} r^2 q_m (1+\tan^2\beta) + 2 q_m \cos 2\varphi$

being a curve without a jump (figure 8).

With our discontinual transport equation q may grow negative in area II. This occurs at first in the direction OB, where $\tan\varphi = K_2$ and

$$q_B = \tfrac{1}{2} r^2 q_m (1+\tan^2\beta) - \frac{1+K_2^2}{K_2} \cdot q_m$$

A negative value of q does not make sense. Thus the condition has to be fullfilled:

$$r^2 > \frac{2(1+K_2^2)}{K_2} \cos^2\beta$$

or

$$r > 2.02 \cos\beta$$

If $q = 0$ at $\tan\varphi = 0$ (or $r \leqq 1.57 \cos\beta$) q is negative over the whole range of area II.

With the transportfunction: $Q = Q_m \sin 2\varphi$, the minimum value of q lies at $\varphi = \frac{\pi}{2}$ $q_{min} = \frac{1}{2} r^2 q_m (1+\tan^2\beta) - 2 q_m$

from which follows the same condition: $r > 2 \cos\beta$.

Obviously, a minimum value of r exists in these problems. Roughly we may put the condition:

$$r > 2 \cos\beta .$$

DELTAS WITH PARTLY CIRCULAR COASTLINE

a) Left hand side

There are two cases:

aI: $\tan\varphi_L \leqq K_2$; stable solution

a2: $\tan\varphi_L > K_2$; the circular part of the delta is partly unstable.

Case aI.

The infinity condition provides: $2\sqrt{K_1} = -A\sqrt{\pi}(a-1)$ ... (1)

Point L provides: $2\sqrt{K_1}\, v_L = u_L + f_L \tan\beta$ ..... (2)

$$u_L = -A\left[e^{-v_L^2} + v_L\sqrt{\pi}\{E(v_L)+a\}\right] \text{ ... (3)}$$

$$\tan(\beta+\varphi_L) = -\frac{1}{\tan\beta}\left[\frac{2\sqrt{K_1}}{A\sqrt{\pi}\{E(v_L)+a\}} + 1\right] \text{ .... (4)}$$

$$\tan(\beta+\varphi_L) = -\frac{u_L}{f_L} \text{ ..... (5)}$$

$$u_L^2 + f_L^2 = r^2 \text{ ..... (6)}$$

Eliminating A, a, u_L and f_L from these equations we obtain:

$$\frac{e^{-(-v_L)^2}}{(-v_L)\sqrt{\pi}\{1-E(-v_L)\}} = \frac{1+\tan^2\varphi_L}{\tan\varphi_L(\tan\varphi_L+\tan\beta)} \quad \text{------ I}$$

and $$r^2(1+\tan^2\beta) = 4K_1\frac{1+\tan^2\varphi_L}{\tan^2\varphi_L}v_L^2 \quad \text{------ II}$$

We find r as a function of φ_L by eliminating v_L along a graphical way from I and II. The result is shown in figure 9.

Case a2.

In the same way we find

$$\frac{e^{-(-v_L)^2}}{(-v_L)\sqrt{\pi}\{1-E(-v_L)\}} = \frac{K_2^2+1}{K_2^2+\tan\varphi_L\cdot\tan\beta} \quad \text{------ I}$$

and $$r^2(1+\tan^2\beta) = 4K_1\frac{1+\tan^2\varphi_L}{\tan^2\varphi_L}v_L^2 \quad \text{------ II}$$

from which v_L has to be eliminated in order to find r as a function of φ_L. The result is shown in figure 9.

b) Right hand side.

There are three cases:

b1: $\tan\varphi_R \leq K_2$; stable delta

b2: $\tan\varphi_R > K_2$; the circular part of the delta is partly unstable;

b3: $\tan\varphi_R = \infty$; erosion at the lee side (fig. 7); the circular part of the delta is partly unstable.

Case b1.

In the same way as before we find the two equations

$$\frac{e^{-v_R^2}}{v_R\sqrt{\pi}\{1-E(v_R)\}} = \frac{1+\tan^2\varphi_R}{\tan\varphi_R(\tan\varphi_R-\tan\beta)} \quad \text{---- I}$$

and $$r^2(1+\tan^2\beta) = 4K_1\frac{1+\tan^2\varphi_R}{\tan^2\varphi_R}v_R^2 \quad \text{---- II}$$

from which V_R has to be eliminated in order to find r as a function of φ_R. The resulting curves are shown in figure 9.

Case b2.

We find:

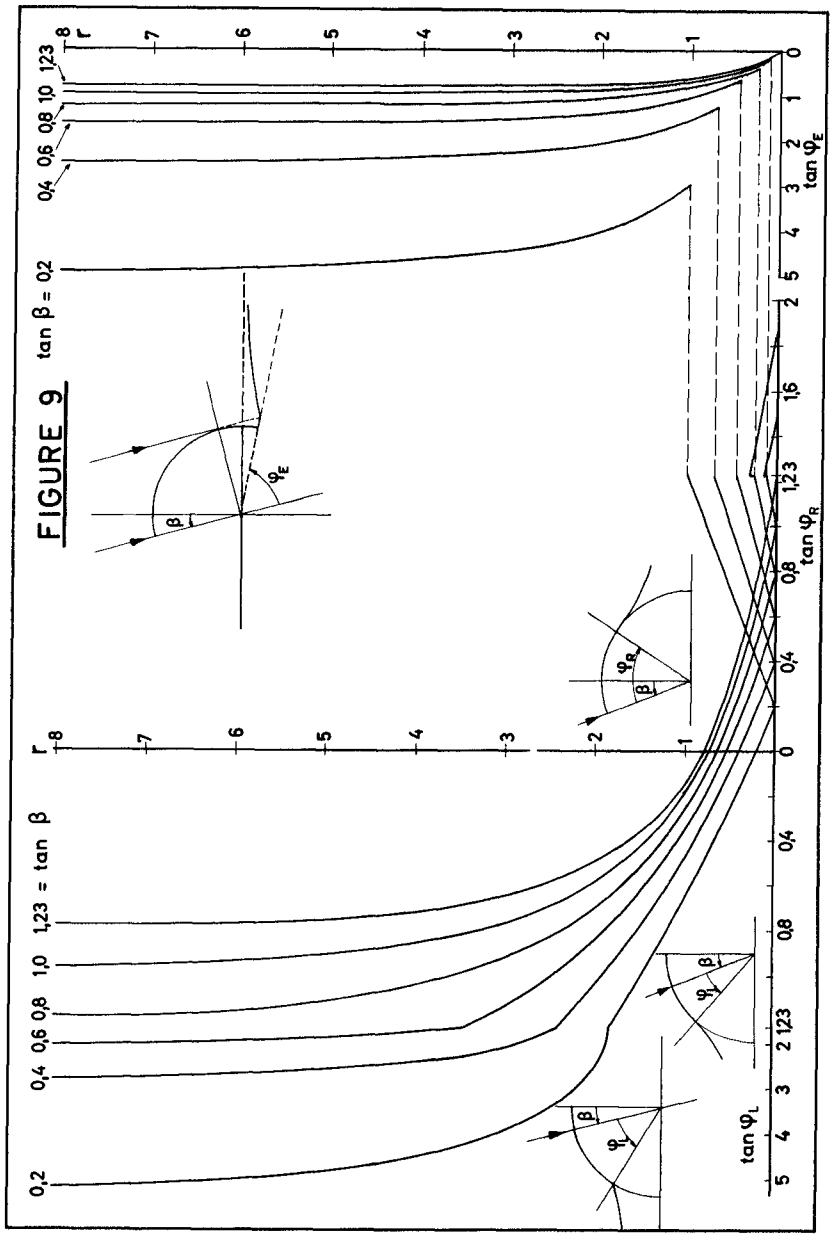
r
tan β = 0,2
0,4 0,6 0,8 1,0 1,23
tan φE
tan φR
tan φL
β
φE
φR
φL
0,2
0,4 0,6 0,8 1,0 1,23 = tan β

FIGURE 9

$$\frac{e^{-v_R^2}}{v_R\sqrt{\pi}\{1-E(v_R)\}} = \frac{K_2^2+1}{K_2^2-\tan\varphi_R\cdot\tan\beta} \quad \text{---- I}$$

$$r^2(1+\tan^2\beta) = 4K_1\frac{1+\tan^2\varphi_R}{\tan^2\varphi_R}\cdot v_R^2 \quad \text{---- II}$$

If we eliminate V_R from I and II, we find in this case, that always $r < 2\cos\beta$. Moreover, we find, that r decreases with increasing values of φ_R. This case, therefore, has to be rejected.

Case b3.

In a similar way we find here:

$$\frac{e^{-v_p^2}}{v_p\sqrt{\pi}\{1-E(v_p)\}} = \frac{1}{\tan\varphi_E\cdot\tan\beta} \quad \text{--- I}$$

$$r = 2\sqrt{K_1}\cdot v_p\cdot\cos\beta \quad \text{---- II}$$

Eliminating graphically V_p from both equations, we find r as a function of $\tan\varphi_E$. The result also is shown in figure 9.

The minimum values of r ($r_{min} = 2\cos\beta$) in this case b3 are higher than the maximum values of r, in the case b1. Therefore, if we maintain our condition: $\zeta \geq 2\cos\beta$, a gap will occur between b1 and b3. However, if we accept a certain disorder in the internal distribution of the river output, we can avoid this gap by calculating in case b3 the values of r between $r = 2\cos\beta$ and the maximum values of case b1.

OUTPUT OF THE RIVER

If we divide the total output of the river: Q_T into two parts, Q_L and Q_R, we are able to calculate r as a function of ζ from the curves of figure 9 by means of the following formulae:

$$\zeta = \frac{Q_T}{Q_m} = \frac{Q_L}{Q_m} + \frac{Q_R}{Q_m} .$$

case a1: $$\frac{Q_L}{Q_m} = \tfrac{1}{2}\zeta^2(1+\tan^2\beta)\cdot\varphi_L + K_1\tan\varphi_L .$$

case a2: $$\frac{Q_L}{Q_m} = \tfrac{1}{2}\zeta^2(1+\tan^2\beta)\varphi_L + \frac{K_2}{\tan\varphi_L} .$$

case b1: $$\frac{Q_R}{Q_m} = \tfrac{1}{2}\zeta^2(1+\tan^2\beta)\varphi_R + K_1\tan\varphi_R .$$

case b3: $$\frac{Q_R}{Q_m} = \tfrac{1}{2}\zeta^2(1+\tan^2\beta)(\pi-\varphi_E) .$$

Our figure 10 shows r as a function of ζ for some values of $\tan\beta$.

We can use the graphs of the figures 10 and 9 in the following way.

Supposing, that the values of ζ and β are given, we find the value of r from figure 10. From figure 9 we find, which values of φ_L and φ_R (resp φ_E) belong to this value of r. Also we can find out from figure 9, whether, at the left hand side, case a1 or case a2 occurs and, whether, case b1 or case b3 exists on the right hand side.

CONCLUSIONS

1. We considered the theoretical shape of a partly circular river delta with $0 < \tan\beta \leq 1.23$. If $\tan\beta > 1.23$ a straight coastline is unstable already in itself and a stable solution for the delta shape cannot be found.

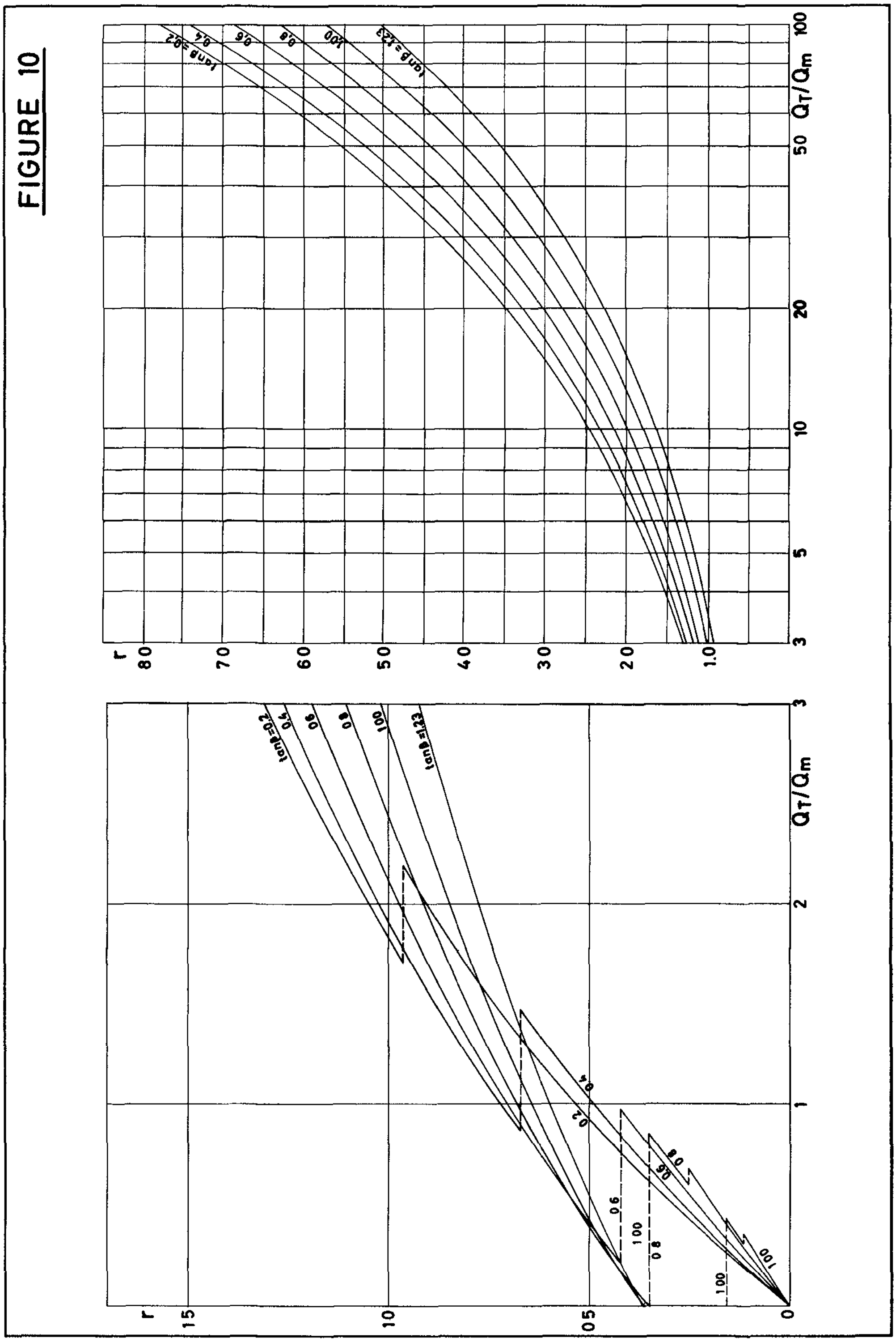
FIGURE 10
r
Q_T/Q_m
tanβ=0.2
0.4
0.6
0.8
1.00
tanβ=1.23

2. With $0 < \tan\beta \leq 1.23$ we found, that a stable delta is possible only if $\xi \leq \xi_1$, in which ξ_1 depends on β. To ξ_1 a distinct maximum value r_1 is associated.
3. If $\xi > \xi_1$, and $r > r_1$, the circular part of the delta becomes partly unstable and the internal distribution of river sediment becomes improbable. Erosion on the right hand coast occurs.
4. If $\xi > \xi_2 > \xi_1$ the improbability of the internal sediment distribution comes to an end, but the circular part of the delta remains partly unstable and the erosion of the coast at the right hand side of the delta goes on.
5. Instability along the circular part of the delta (all other parts are always stable) probably means, that "spits" occur. The shape of spits has not been dealt with in this paper.
6. Speaking in common language, we deduced that if the quantity of river sediment exceeds a certain amount, the delta becomes partly unstable and erosion on the lee side of the delta begins; the delta grows so large, that it is acting as a partly circular "groin" with erosion on its lee side and accretion on the weather side.

REFERENCES

Edelman; T. (1963) Littoral transport in the breaker zone, caused by oblique waves: Proceedings IAHR Congress London 1963, vol. I p.p. 61-67.

Grijm, W. (1960) Theoretical forms of shorelines: Proceedings VIIth conference on coastal engineering. The Hague 1960 vol. I p.p. 197-202.

Grijm, W. (1964) Theoretical forms of shorelines: IXth Conference on coastal engineering, Lisbon 1964. Paper 2.13.

Larras, J. (1957). Plages et côtes de Sable (p.57): Collection du laboratoire national d'hydraulique. Paris 1957.

Chapter 14

THEORETICAL FORMS OF SHORELINES

by

W. Grijm

Engineer Coastal Research Department Rijkswaterstaat

SUMMARY

Laboratory tests say that the littoral transport by waves reaches a maximum value when the waves approach the shore obliquely. In some way this must lead to peculiarities in the forms of shorelines. Therefore we put the question what types of shorelines can mathematically exist assuming the littoral transport is ruled by the function sin 2α where α is the angle between the wave front and the shoreline. This yields some basic types of shorelines. After a brief discription of the mathematical treatment these results will be discussed.

This paper is a continuation of the paper presented on the same subject at the 7^{th} conference on coastal engineering.

INTRODUCTION

The configuration of sandy shores and the changes in it depends completely on the variation in the transport of sand above the seabottom. The sand movement is a consequence of the movement of the water. In its turn the watermovement is a result of the tide and of the wind action. For the coastal engineer it is of importance to know the relations between the stream and wave characteristics on the one side and the intensity of the littoral sand transport on the other side. Therefore several laboratory tests have been made to get an idea about these relations. Knowing how extremely complicated these relations are we have to expect much scatter in the results of these tests. In spite of this scatter however all tests show a similar characteristic. They say that the intensity of the littoral transport is maximum when the waves approach the shore obliquely. Some tests say that this maximum is reached

when the angle α between the wave front and the shoreline is 30°. Other tests say that this happens when this angle is 60°. Whatever the real value may be it seems to be true that the intensity of the littoral transport has a maximum by a value of α which differs much from $\alpha = 0^{\circ}$ and from $\alpha = 90^{\circ}$.

On the supposition that this fact must lead to certain peculiarities in the form of shorelines the coastal research department of the Rijkswaterstaat in the Netherlands has made a study about this. They have put the question what types of shorelines can mathematically exist assuming the littoral transport is ruled by the function $\sin 2\alpha$ which has its maximum value when $\alpha = 45^{\circ}$.

THE MATHEMATICAL TREATMENT

Considering a stretch of shore of an infinite small length we have the condition that the quantity of deposited (or eroded) material must be equal to the difference between the quantities transported by the sea at the beginning and at the end of that stretch of shore. On the basis of figure 1 we put:

$$\frac{\partial q}{\partial \varphi} d\varphi \, dt = ar \, d\varphi \frac{\partial r}{\partial t} dt$$

or

$$\frac{\partial q}{\partial \varphi} = ar \frac{\partial r}{\partial t}$$

in which

r and φ are the polar coordinates of the considered point of the shore

q is the function that determines the quantity of the littoral transport

t is the time

a is the depth of the water which will be a function of r and φ

The magnitude of q depends on the angle α only. So this angle holds a key position. Therefore we take α as the independent variable instead of φ. This has two consequencies. First the form of the equation of continuity must be reduced to:

$$\frac{\partial q}{\partial \alpha} + ar \left(\frac{\partial r}{\partial \alpha} \frac{\partial \varphi}{\partial t} - \frac{\partial r}{\partial t} \frac{\partial \varphi}{\partial \alpha} \right) = 0 \qquad (1)$$

Secondly we need another equation to relate α and φ. On the basis of figure 2 we have:

$$\alpha + \varphi + \psi = \beta \qquad (2)$$

It will be clear that β defines the direction of the wind. But ψ is a new variable also depending on α and t. So we cannot get away from

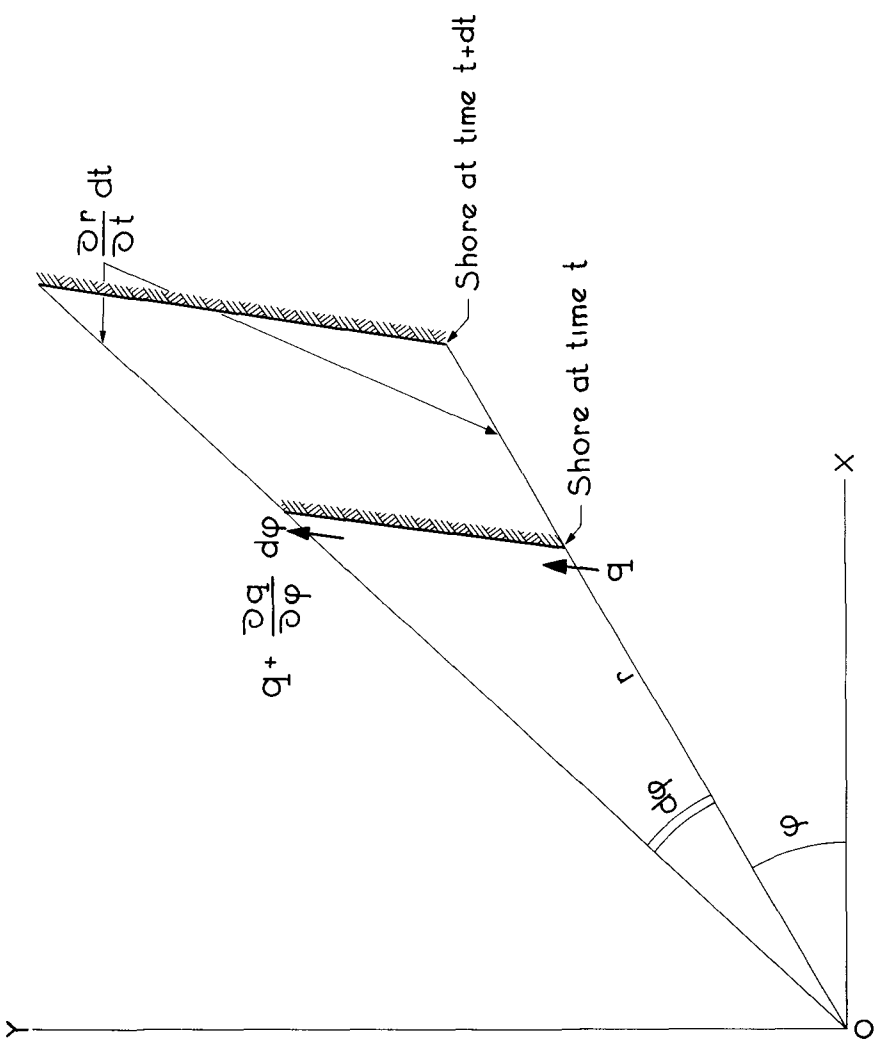
Y
O
X
φ
dφ
r
q
Shore at time t
Shore at time t+dt
$\frac{\partial r}{\partial t} dt$
$q + \frac{\partial q}{\partial \varphi} d\varphi$

FIGURE 1

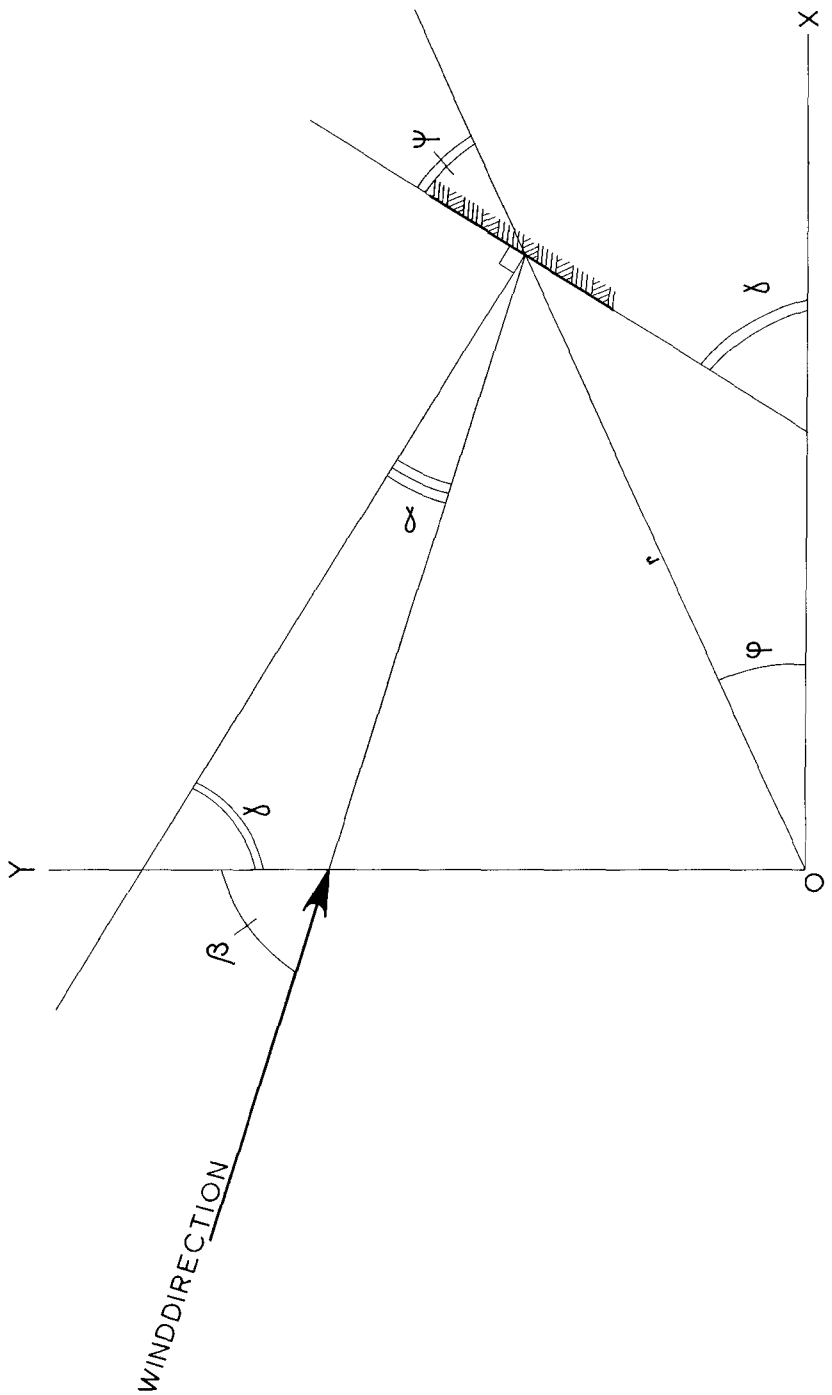

FIGURE 2

another equation that defines ψ. From the well-known formula:

$$\tan \psi = \frac{r}{r'}$$

we derive:

$$\tan \psi \frac{\partial r}{\partial \alpha} = r \frac{\partial \varphi}{\partial \alpha} \tag{3}$$

Now the problem is to find functions which satisfy the three equations (1), (2) and (3). We shall try whether the following combination of functions will do.

$$\begin{aligned} a &= c r^n \phi(\varphi) \\ r &= R(\alpha) T(t) \\ \varphi &= \varphi(\alpha) \\ q &= A Q(\alpha) \end{aligned}$$

where Q, φ and R are functions of α only and T is only a function of the time t.

Substituting these functions in the equation of continuity (1) yields:

$$\frac{\frac{dQ}{d\alpha}}{R^{n+2} \phi \frac{dQ}{d\alpha}} = \frac{c}{A} \cdot T^{n+1} \frac{dT}{dt}$$

On the left hand side of this equation there are expressions of α only, on the right hand side there appears only the time t. This equation can only be satisfied when both parts are equal to a constant k. This yields the two conditions:

$$\begin{aligned} dQ &= k R^{n+2} \phi \, d\varphi \\ T^{n+1} dT &= \frac{kA}{c} \, dt \end{aligned} \tag{4}$$

The second condition offers no problem while it can be integrated to:

$$T = \sqrt[n+2]{(n+2) \frac{kA}{c} (t - t_o)} \tag{5}$$

where t_o is an integration constant. The first condition replaces the original equation of continuity (1). However much simplier we are not able to solve the set of equations (2), (3) and (4) unless we restrict ourselves further. Therefore we assume that the bottom of the sea is horizontal. This means that $n = o$ and that $\phi = 1$.

Finally we have obtained the following set of equations we can manage:

$$dQ = k \, R. \, d\varphi \tag{6}$$

$$\tan \psi \, dR = R. \, d\varphi \tag{7}$$

$$\alpha + \varphi + \psi = \beta \qquad (8)$$

while the function T is:

$$T = \sqrt{\frac{2kA}{c}(t - t_o)}$$

The function Q can have each form. We took for it the function sin 2α. It is usefull to realise that the choosen combination of functions shows a certain character. The matter is that when we divide the radius vector r by T we obtain a value depending on α only. That means that the shoreline at the time $t = t_1$ and the shoreline at the time $t = t_2$ can be reduce to the very same shape by geometrical multiplying out of the origin. So to discuss these shorelines it is sufficient to discuss the curves given by R and φ which satisfy the equations (6), (7) and (8). The constant k can have each value. We took it equal to $\frac{1}{2}$ because then the relation of the area between two radius vectors in the graph of R with the area between the corresponding lines in the prototype is the most simple one.

THE RESULTS

Before discussing the solutions of these equations obtained by means of a computer we shall bring to the fore some general remarks on these solutions. First with respect to the function of sin 2α it can be proved that when the curve a of figure 3 is a solution of the differential equation, the curves b, c and d will also satisfy the equations. Curves a and b and the curves c and d are symmetrical with respect to the wind direction. Curves a and c and the curves b and d are symmetrical with respect to the polar axis.

The second remarkable thing is that straight lines through the origin satisfy the equations but other straight lines do not.

The third point is that only in the octants 0,3, 4 and 7 of figure 4^a these straight lines can be asymptotes of the solutions. This means that we can have bays and capes of a shape as shown in figure 4^b and 4^c, but when the angle δ becomes more than 45^o the bays and capes must be shaped as in the figures 4^d and 4^e while in the points A the condition of continuity must been satisfied. The fourth point which asks attention is the fact that when the littoral transport reaches its maximum value the shore line shows a cusp as will be shown later.

Figure 5 shows the result of a calculation on the computer. The computer was programmed to follow this curve starting from a point A practically in the infinite and stopping in another point B likewise in the in-

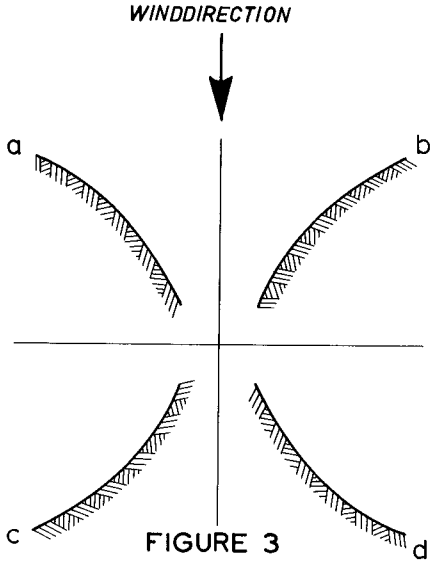

FIGURE 3

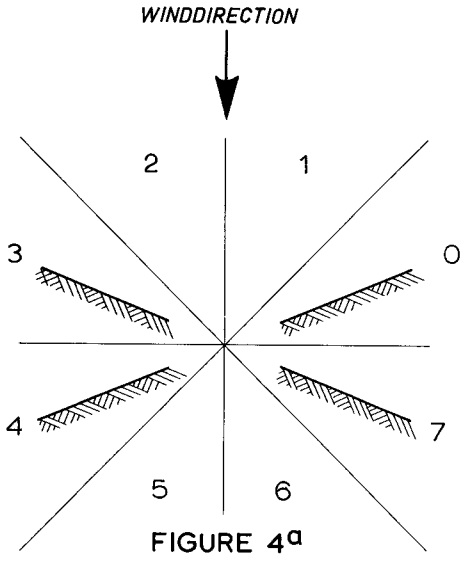

FIGURE 4a

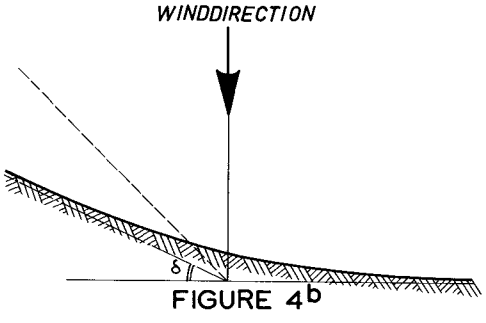

FIGURE 4b

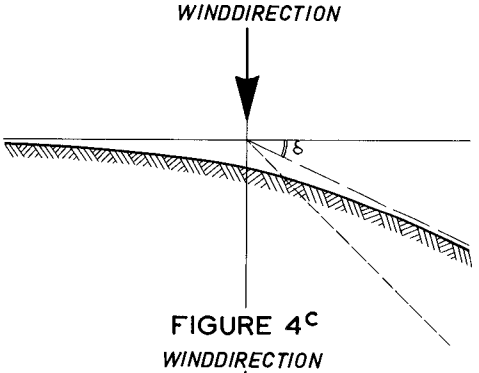

FIGURE 4c

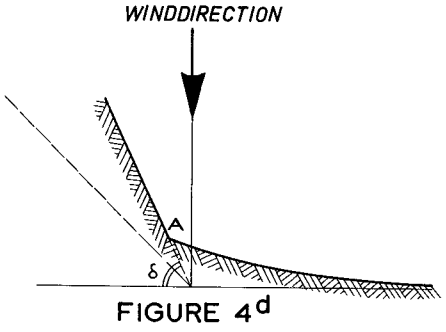

FIGURE 4d

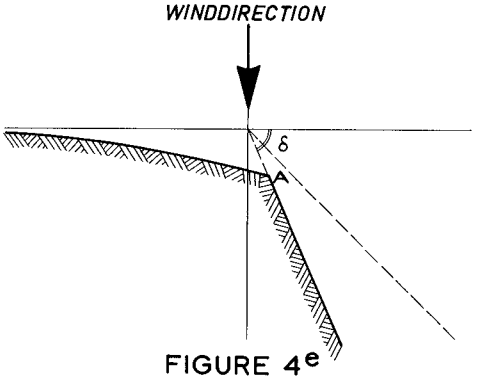

FIGURE 4e

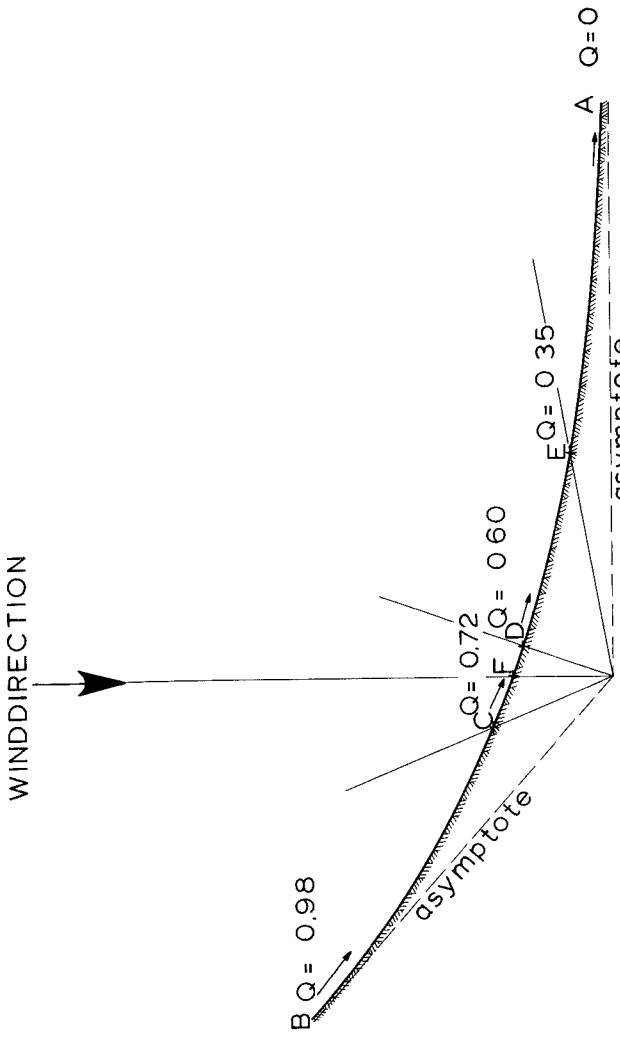
WINDDIRECTION
A Q=0
asymptote
E Q= 0 35
D Q= 0 60
C Q= 0.72
F
asymptote
B Q= 0.98

FIGURE 5

finite.

With this one solution of the differential equations we can construct shorelines of different types. First the curve of figure 5 can be interpreted as the shoreline of a bay or by mirroring with respect to the polar axis as the shoreline of a cape. Besides we can construct with this curve a symmetrical simple delta. Therefore we take only part A - F, mirror it with respect to the wind direction and put a rivermouth in point F. Then the condition is that the river brings a quantity of material to the sea that equals twice the quantity of the littoral transport in point F of the original curve.

But there is still a third way to use this curve. The computer has been programmed in such a way that all points of transition were indicated. A point of transition means that in that point the littoral transport along the curve has the same magnitude as the littoral transport that would take place when the shore would be situated along the radius vector to that point. In the curve of figure 5 there are three of such points C, D and E. At each point there is written down a number. This number gives the ratio between the magnitude of the littoral transport in that point and the quantity of material that the sea is able to transport. The magnitude of the littoral transport will be always expressed in this manner. With point C we can construct four other shorelines. This is not possible with the points D and E. Finally figure 6 shows all the shorelines which can be constructed form the curve of figure 5.

Mathematically there exists another shape of the shoreline for a symmetrical simple delta. This shape is shown in figure 7. The centre of curvature lies at the other side of the shore shown in figure 6. The curve links op the original shore in the finite and just in the point where the littoral transport equals zero.

It is easy to construct deltas with more rivermouths. The only thing we have to do is to link up different curves and to put a rivermouth in each point of connection. There the river must bring to the sea such a quantity of material that the condition of continuity is satisfied. Such composed deltas are shown in figure 8. A mathematical condition in constructing such deltas is that the river arms must be situated along a radius vector. These deltas are still symmetrical ones. It is also very simple to construct non-symmetrical deltas in the same way. The only thing

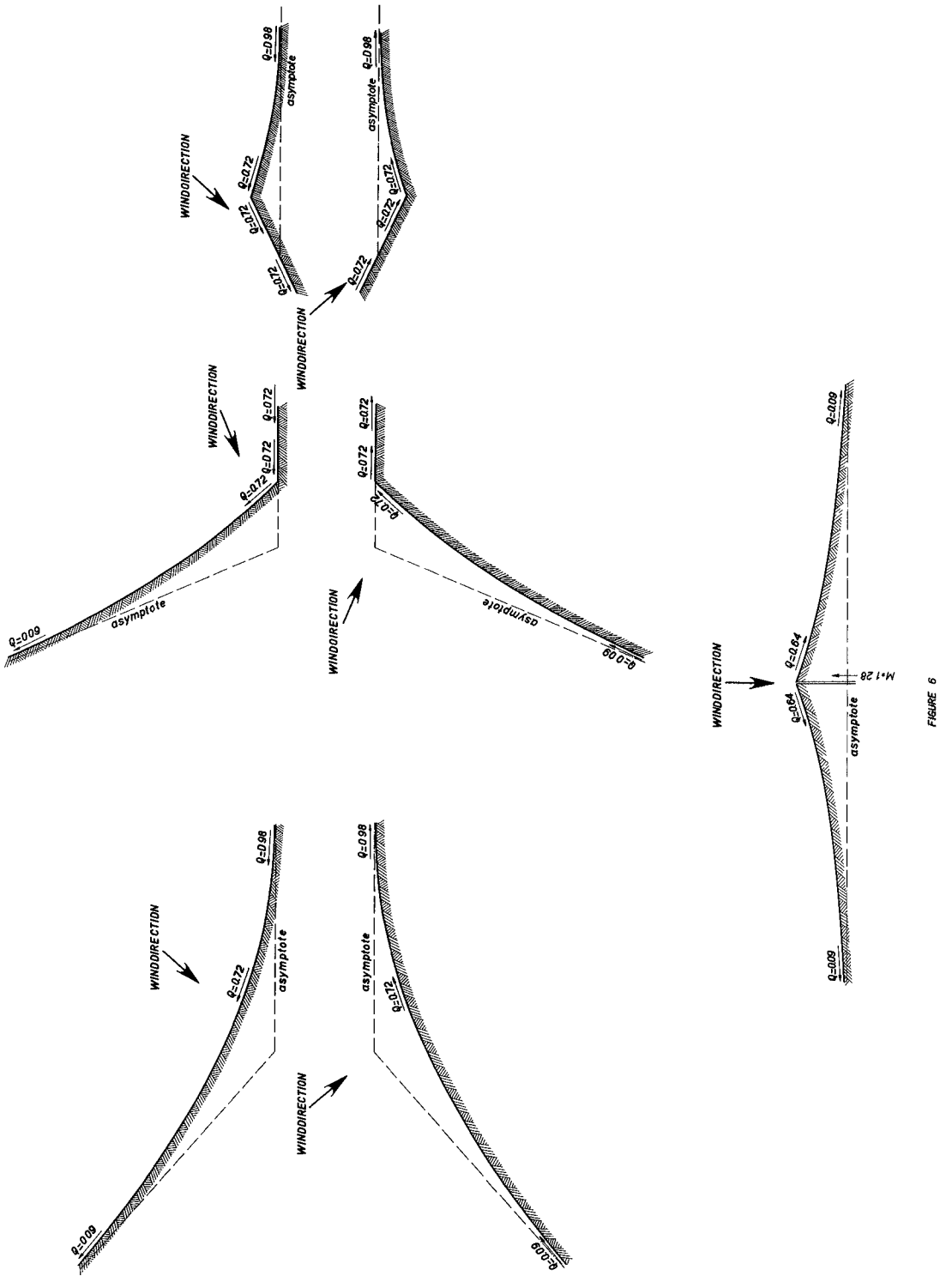

FIGURE 6

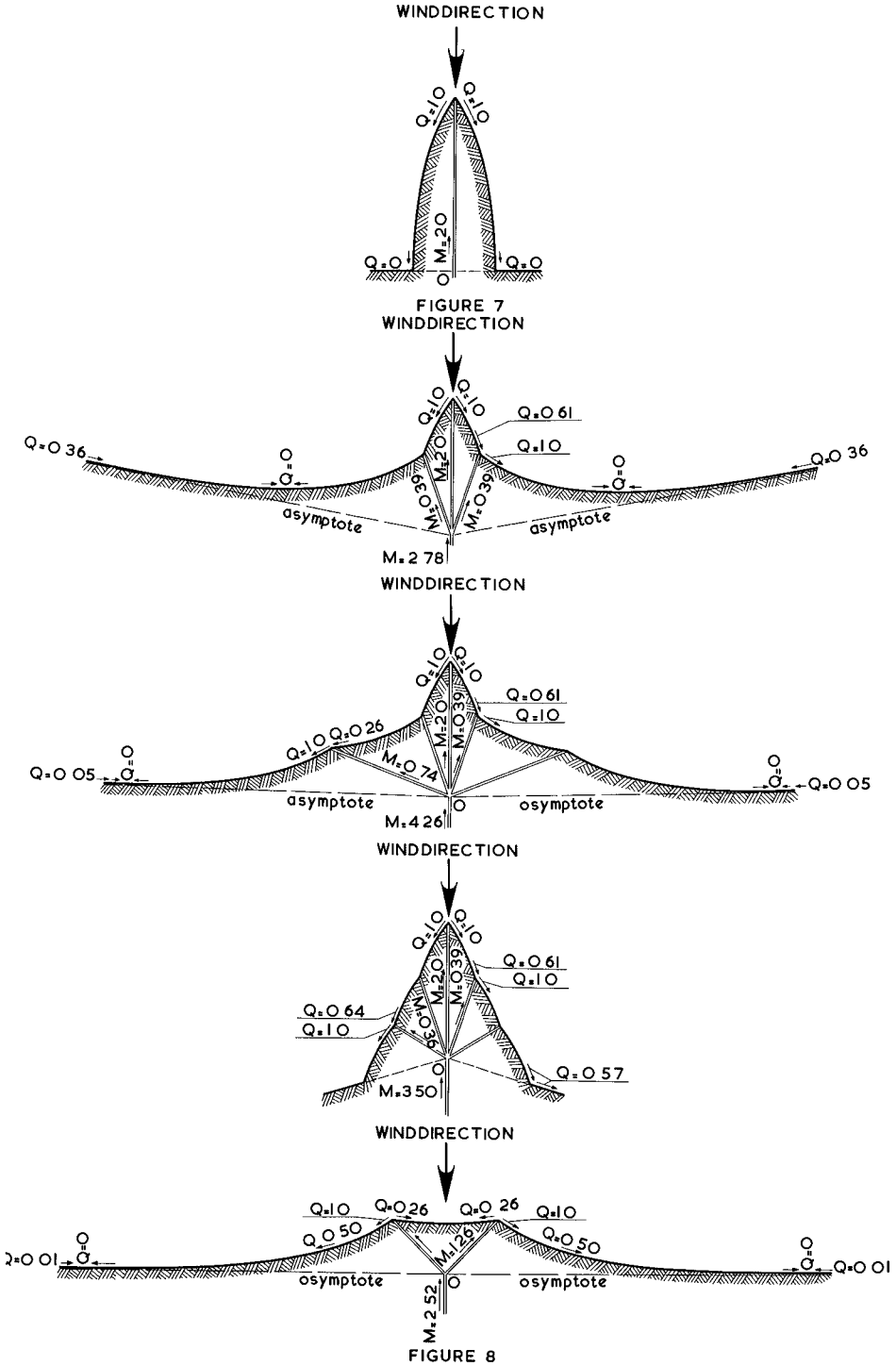
WINDDIRECTION
Q=1.0
Q=1.0
M=2.0
Q=0.0
Q=0.0
FIGURE 7
WINDDIRECTION
Q=1.0
Q=1.0
Q=0.061
Q=1.0
Q=0.36
Q=0.36
M=2.0
M=0.39
M=0.39
asymptote
asymptote
M=2.78
WINDDIRECTION
Q=1.0
Q=1.0
Q=0.061
Q=1.0
M=2.0
M=0.39
Q=1.0
Q=0.26
M=0.74
Q=0.05
Q=0.05
asymptote
osymptote
M=4.26
WINDDIRECTION
Q=1.0
Q=1.0
Q=0.061
Q=1.0
M=2.0
M=0.39
Q=0.64
Q=1.0
M=0.30
Q=0.57
M=3.50
WINDDIRECTION
Q=1.0
Q=0.26
Q=0.26
Q=1.0
Q=0.50
Q=0.50
M=1.26
Q=0.01
Q=0.01
osymptote
osymptote
M=2.52
FIGURE 8

we have to do is to connect on the left hand side other curves as on the right hand side (figure 9). We can construct an infinite number of shorelines. By the way some of the original shores in the figures 8 and 9 have the shape of a bay or of a cape.

But there is still another way to construct non-symmetrical deltas. Till yet we have put β equal to zero. That means that the wind direction has been always perpendicular to the polar axis. When we take $\beta = -20^{\circ}$ we can construct the set of curves shown in figure 10. The curves on the right hand side of the line d have a cusp in the point where the littoral transport reaches its maximum value. At one point A is indicated how the shoreline would continue when the computer was not been stopped in the cusp. With this second part of the curve the symmetrical simple delta form figure 7 has been constructed. On the left hand side of line d the curves have an asymptote with decreasing values of Q according to the flatness of the curve.

When we take $\beta = +20^{\circ}$ we can construct the set of curves of figure 11. Here also exists a locus of cusps. When we mirror the set of figure 11 with respect to the wind direction we can combine this set with that of figure 10 and obtain figure 12. Here we have in principle 32 non-symmetrical deltas. Note that by each value of the quantity of material that the river brings to the sea there exist two different forms of shorelines. The deltas indicated by a letter A and by a letter B are a pair where the ratio between the quantity of material conveyed by the river and the quantity of material the sea is able to transport is about 0,55. The deltas indicated by a letter D and by a letter E are a pair where this ratio is about 1,25. Only when this ratio becomes equal to two (the delta indicated by the letter F) there exist mathematically only one solation. These 5 deltas are drawn in figure 13 seperately.

It will be clear that in this way we can also construct non-symmetrical deltas with more rivermouths combined with bay- or cape shaped original shorelines. But before continuing this stude it seems necessary to investigate whether the results we have obtained can be recognized in nature or not.

ACKNOWLEDGEMENTS

I have to point out that this article would not have been written without the leading of dr. ir. J.C. Schönfeld in the mathematical treat-

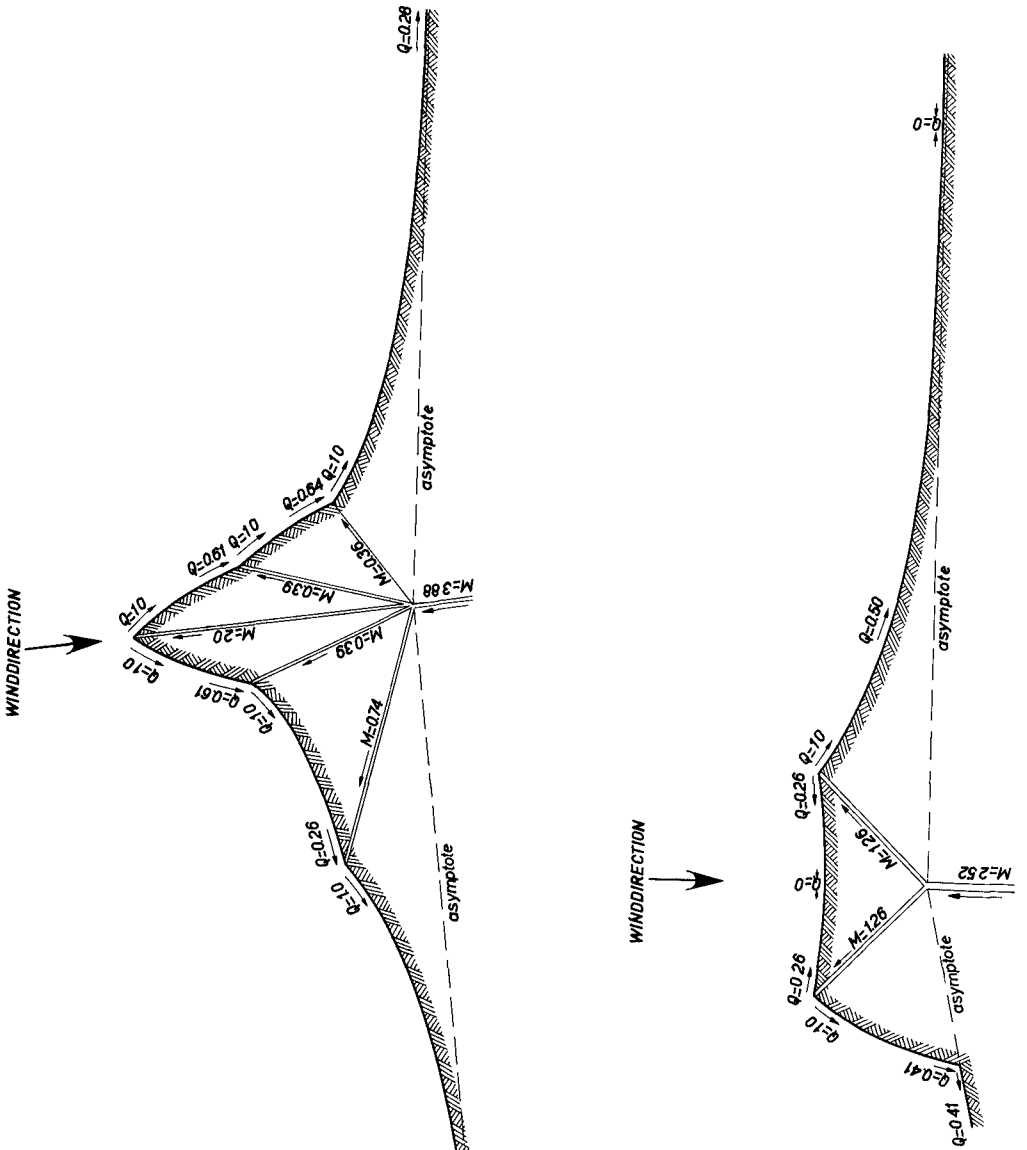
WINDDIRECTION
Q=0.28
asymptote
Q=0.64
Q=10
Q=0.61
Q=10
Q=10
M=0.36
M=0.39
M=3.88
M=2.0
M=0.39
Q=10
Q=0.61
M=0.74
Q=0.26
Q=10
asymptote
Q=0
Q=0.05
WINDDIRECTION
Q=0
Q=0.50
asymptote
Q=10
Q=0.26
M=1.26
M=2.52
Q=0
M=1.26
Q=0.26
asymptote
Q=10
Q=0.41
Q=0.41

FIGURE 9

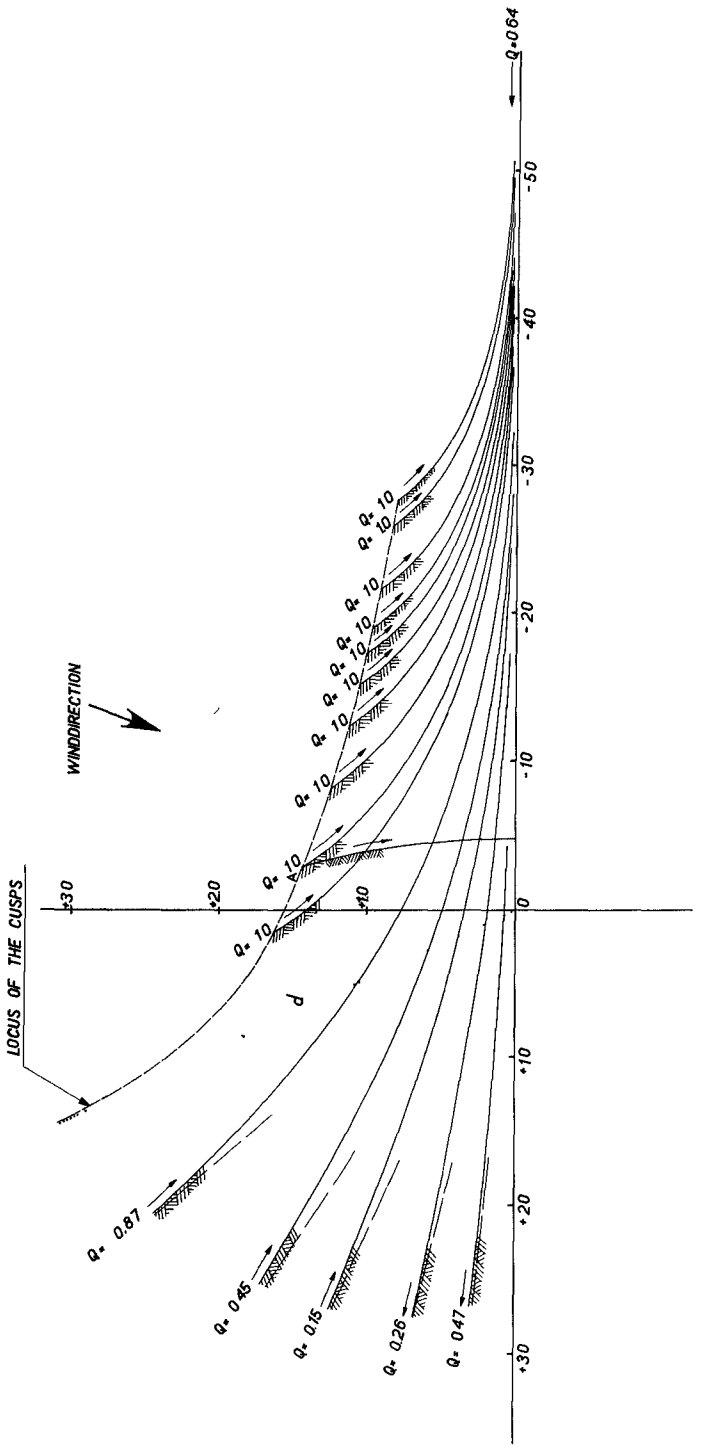
Q=.064
-50
-40
-30
-20
-10
0
+10
+20
+30
WINDDIRECTION
LOCUS OF THE CUSPS
d
Q= 10
Q= 0.87
Q= 0.45
Q= 0.15
Q= 0.26
Q= 0.47

FIGURE 10

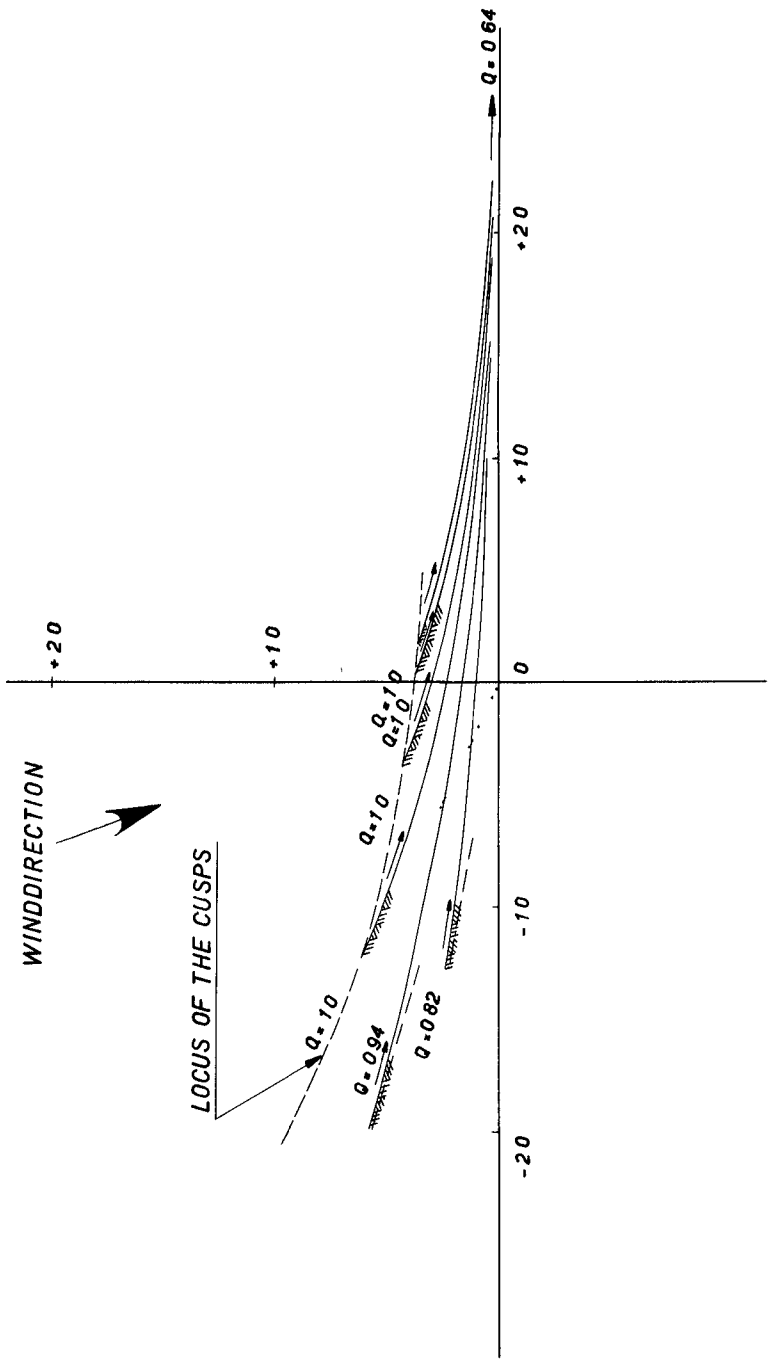
Q = 0.64
+20
+10
0
-10
-20
+20
+10
Q=1.0
Q=1.0
Q=1.0
Q=1.0
Q=1.0
Q=0.94
Q=0.82
WINDDIRECTION
LOCUS OF THE CUSPS

FIGURE 11

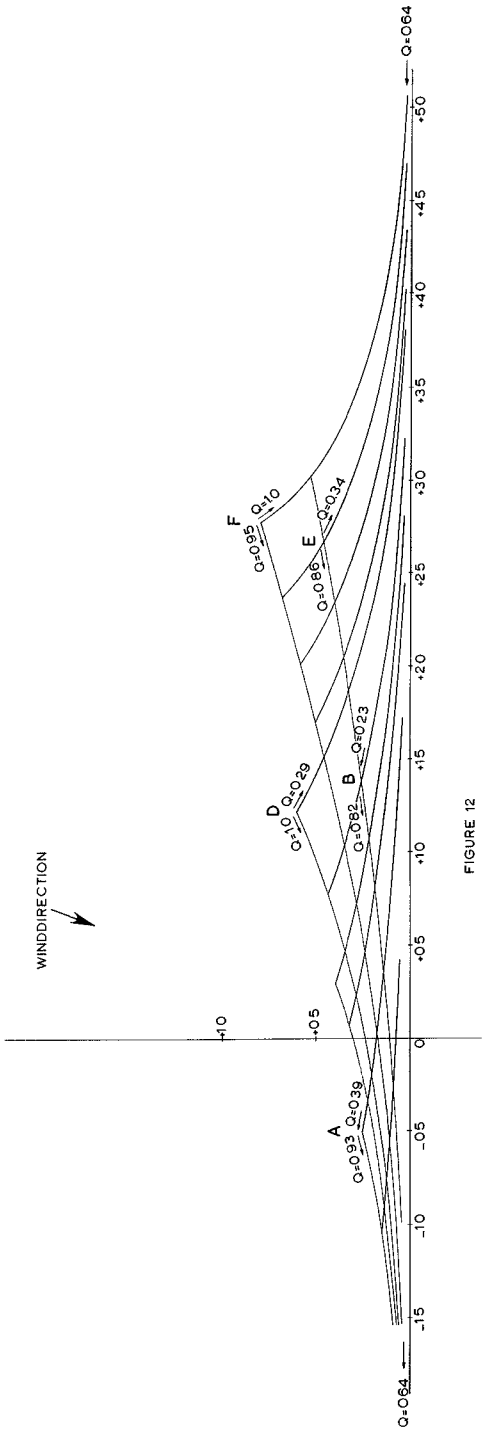
WINDDIRECTION
+10
+05
0
-05
-10
-15
+50
+45
+40
+35
+30
+25
+20
+15
+10
+05
0
-05
-10
-15
Q=064
Q=064
F
Q=095
Q=10
E
Q=086
Q=034
D
Q=10
Q=029
B
Q=082
Q=023
A
Q=093
Q=039
Q=064

FIGURE 12

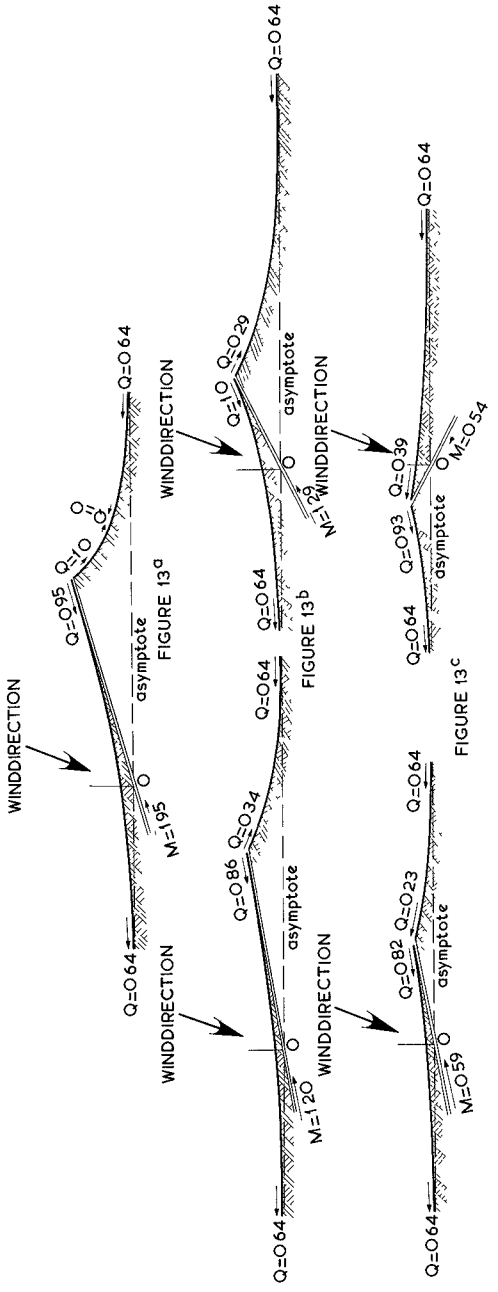
WINDDIRECTION
Q=095
Q=10
Q=064
asymptote
M=1.95
Q=064
WINDDIRECTION
FIGURE 13a
Q=086
Q=034
Q=064
asymptote
M=1.20
Q=064
WINDDIRECTION
FIGURE 13b
Q=082
Q=023
Q=064
asymptote
M=0.59
Q=064
WINDDIRECTION
FIGURE 13c
Q=064
Q=10
Q=029
asymptote
M=1.29
WINDDIRECTION
Q=064
Q=093
Q=039
asymptote
M=0.54
Q=064

ment of the problem. Further I wish to express my thanks to mr. Bruyn, the assistant of dr. ir. Schönfeld, and to mr. Rundberg, my own assistant. Also I could not have dispensed with their dedicated assistance.

***

Chapter 15

SEASONAL CHANGES IN BEACHES OF THE NORTH ATLANTIC COAST OF THE UNITED STATES

By

John M. Darling
Hydraulic Engineer, Research Division
U. S. Army Coastal Engineering Research Center
Corps of Engineers, Washington, D. C.

ABSTRACT

Seasonal changes of eight Atlantic Ocean beaches along the East Coast of the United States from southern New Jersey to Rhode Island have been under study since September 1962. These beaches are surveyed at frequent intervals repeating profile lines perpendicular to the shoreline, spaced to indicate any major changes occurring to the beach shape or dimensions with as much assurance as is reasonably possible. Correlation of changes in beach profile with tide and wave data is being made. Changes in the beach profiles to date indicate variations on a seasonal basis.

INTRODUCTION

The impetus for initiating this study of beaches along the Atlantic Coast stemmed from the disastrous effects of a severe east coast storm which occurred in March 1962. This was an unusual storm because of its great extent and duration. It remained relatively stationary for such a long period that heavy seas battered the coastline at high surge levels through five successive tidal cycles. For this reason this storm has been referred to as "High Five". The wreaking of such extreme havoc along the Atlantic coastline has been attributed to this storm's long duration, which permitted high water and storm waves to reach backshore development after natural and man-made protective features had been swept away.

Protective beaches and dunes were severely eroded along much of the coast from Cape Hatteras, North Carolina to Cape Cod, Massachusetts. This left remaining developments exposed and vulnerable to the damaging forces of storms of lesser magnitude. In order to protect against ordinary storms, emergency restoration of protective features was necessary. Mr. Joseph M. Caldwell of the Coastal Engineering Research Center (formerly Beach Erosion Board) was called upon for advice in this task. An emergency beach and dune section, which became known as the Caldwell section, was designed as protection against a storm of 10-year frequency and was placed along much of the coastline after the storm. This emergency beach section, as shown on Figure 1, has a foreshore slope of 1:20 up to the berm elevation of 10 feet above mean low water, a berm width of 50 feet and a dune slope of 1:5 with a dune crest elevation of 12 feet and width of 20 feet.

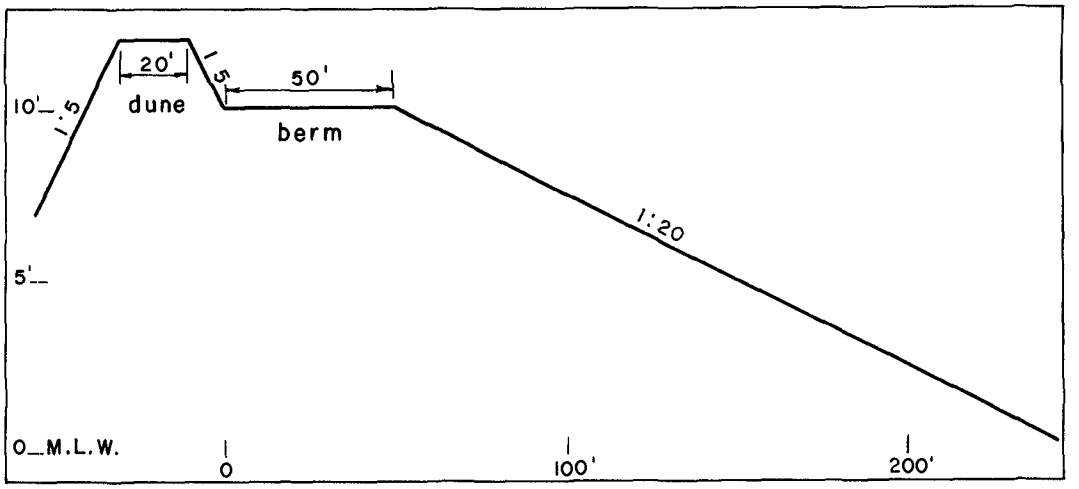

FIGURE 1. EMERGENCY SECTION

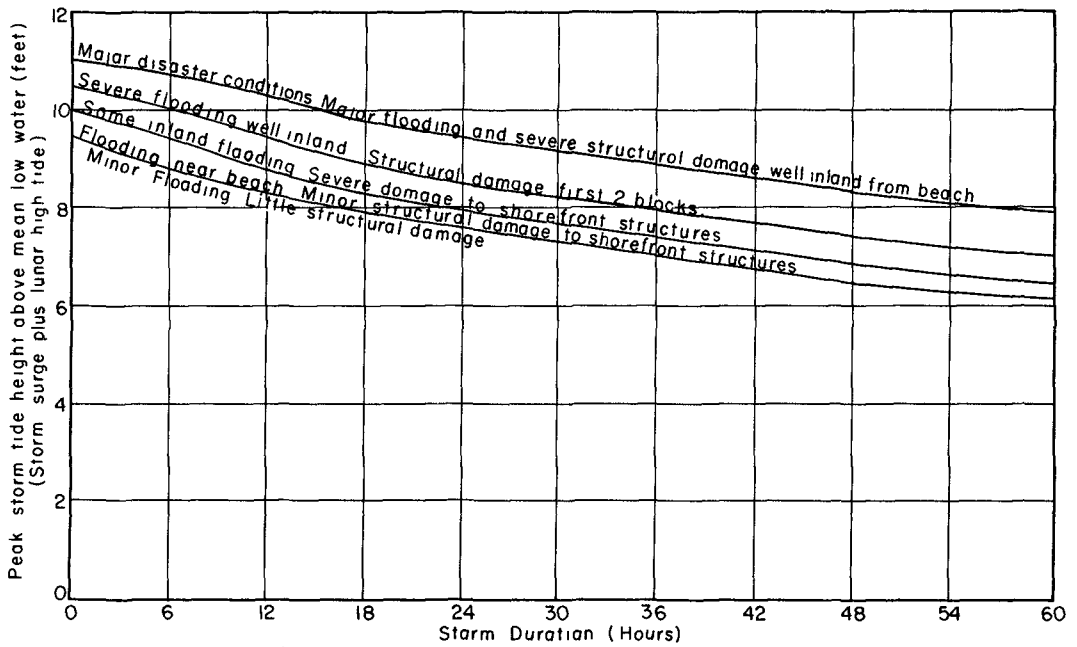

FIGURE 2. VULNERABILTY CONDITION 1 FOR ATLANTIC CITY, N.J.

After the 1962 storm a pilot study was set up to determine the feasibility of a warning system which would forecast effects on the coast for approaching storms through the development of vulnerability curves for individual areas, such as shown in Figure 2. The peak storm tide height above mean low water (storm surge plus astronomical high tide) is plotted along the Y-axis. The storm duration (hours) is plotted along the X-axis. The term storm duration is defined in this case in tidal cycles a particular peak storm tide is present. If a peak storm tide occurs for two successive high tides, this would indicate a storm duration of about 24 hours. These curves are actually limits for determining the extent of damage that might be expected for a particular peak storm tide and storm duration. This set of curves is only applicable for one particular condition of the beach. As the beach condition changes a new set of curves is necessary. The development of the vulnerability curves is being made by correlating beach changes with data on those surge tides and waves responsible for the beach changes. Field surveys for the study are made under the direction of the Division and District offices of the Corps of Engineers in which the pilot beaches are located. Although much of the analysis of data is now being done at the Coastal Engineering Research Center, eventually it will be accomplished in the Division or District offices; the Coastal Engineering Research Center will then act only in an advisory capacity. The seasonal changes in beach conditions along the Atlantic Coast which are discussed in this paper are thus but a part of the continuing study.

STUDY AREA

Eight beaches are under observation for the pilot study located from southern New Jersey to Rhode Island. As shown in Figure 3, three are in New Jersey, two in New York on Long Island, one in Rhode Island, and the other two on Long Island Sound in Connecticut. Although data from all beaches involved in the study are included in this paper, only one or two beaches are discussed in detail.

Tidal and storm surge data are being furnished by the U. S. Weather Bureau and Coast and Geodetic Survey for several places in the study area. Sources of wave information include Fleet Weather Services' charts, surf observations made by the U. S. Coast Guard in cooperation with the Coastal Engineering Research Center, and wave records from stations of the Coastal Engineering Research Center. The tidal records for the following locations are being studied for use in this pilot program: Atlantic City, N. J., Sandy Hook, N. J., Montauk, N. Y., Port Jefferson, N. Y., New London, Conn., and Newport, R.I. Surf observations are available for the following points in the study area: Atlantic City, N. J., Monmouth Beach, N. J., and Point Judith, R. I. These data are subjective in nature as they are actual observations. The Coastal Engineering Research Center has wave gages in the study area at Atlantic City, N. J., and Buzzards Bay, Mass. The wave gage

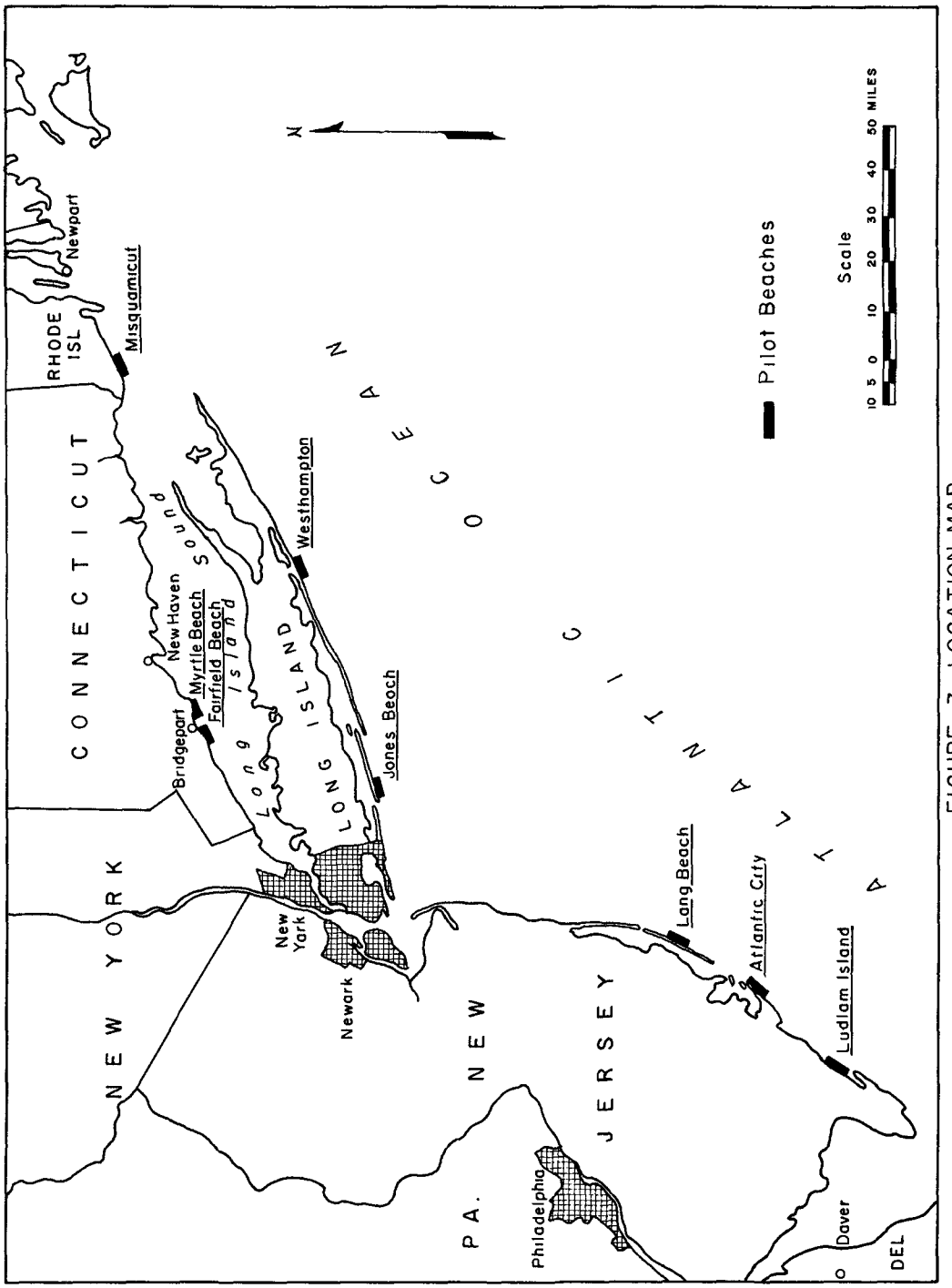

FIGURE 3 LOCATION MAP

at Atlantic City, N. J., is a step-resistance staff located on the seaward end of Steel Pier where the water depth is about 20 feet. Waves at this station are recorded on both paper tape and magnetic tape. The Buzzards Bay recorder is located on the Buzzards Bay light tower operated by the U. S. Coast Guard. The record for this station has been intermittent for various reasons. One is the ice problem in the winter. Originally the only wave gage was a 45-foot step-resistance staff which fouled easily with ice. A pressure-type gage is now in operation which should eliminate the ice problem. These records should be valuable particularly for the pilot study beach at Misquamicut, R. I.

The wave data from Atlantic City for 1963 have been compiled as shown in Table 1. Note that 81% of the waves do not exceed 4 feet in height or rather only 19% are more than 4 feet. During 1963, 46% of the waves had periods between 6-10 seconds and heights of less than 4 feet. High tide elevations at Atlantic City for 1963 relative to MSL were less than +2 feet 35% of the time, 45% were between +2 and +3 feet, 18% between +3 and +4 feet and only 2% above +4 feet. The ordinary mean high tide (astronomical) elevation for Atlantic City is about +2 feet.

The New Jersey beaches under observation are barrier beaches located on the central and southern portions of the New Jersey coast. They are composed of medium to fine sand which is fairly well sorted. Ludlam Island beach, located south of Atlantic City, has a flat foreshore slope of about 1:40 and is quite wide. At Atlantic City, the beach is narrower with a foreshore slope in the order of 1:20. Long Beach is fairly steep, with a foreshore slope of 1:10 to 1:15 with generally a narrow berm.

The study beaches in New York are Jones Beach and Westhampton Beach along the south shore of Long Island. Their characteristics are somewhat different. Jones Beach, located near the west end of Long Island is composed of poorly sorted medium to fine sand. The foreshore slope of the beach, 1:20, is similar to that at Atlantic City, but in general it is accompanied by a wide berm. Westhampton Beach, in the central part of Long Island's southern shore, is fairly steep with a foreshore slope of 1:10 to 1:15. There is little or no berm. Westhampton Beach material is coarse to medium sand, fairly well sorted.

In Connecticut the study areas are Myrtle and Fairfield Beaches, adjacent to Bridgeport Harbor, and Misquamicut Beach in southwest Rhode Island. Myrtle and Fairfield Beaches in Connecticut front on Long Island Sound and are not directly exposed to the Atlantic Ocean. These beaches are fairly flat, foreshore slope of 1:20 to 1:40, and are not exceptionally wide. The materials on these beaches range from medium sand to fine gravel. Misquanicut Beach is relatively narrow and steep with a foreshore slope of 1:10 to 1:15. The beach material consists of coarse to fine sand with some gravel and shingle. Figures 4, 5, and 6 are typical views of beaches in the three major areas under study. They show the general configuration of the beaches in their areas.

Sig. Height (ft)	SIGNIFICANT WAVE PERIOD (SECONDS)								Total %
	Calm	2-4	4-6	6-8	8-10	10-12	12-14	14-16	
0-2	2.7	6.5	6.3	12.0	9.2	2.8	0.5	-	40
2-4	-	3.5	8.6	16.0	9.2	2.6	0.7	-	41
4-6	-	0.3	1.8	4.8	3.2	1.6	0.6	0.1	12
6-8	-	-	0.7	1.3	1.4	0.7	0.2	-	4.3
8-10	-	-	0.2	0.3	0.5	0.2	0.1	-	1.4
10-12	-	-	-	0.1	0.2	0.3	0.05	-	1.4
12-14	-	-	-	-	0.2	0.1	-	-	0.3
14-16	-	-	-	0.05	0.1	-	-	-	0.15
16-18	-	-	-	0.05	-	-	-	-	0.05
18-20	-	-	-	-	-	-	-	-	-
Total (Percent)	2.7	10	18	35	24	8.4	2.2	0.1	

TABLE 1: WAVE STATISTICS FOR ATLANTIC CITY, N. J., 1963 IN PERCENT OCCURRENCE

Sig. Height (ft)	SIGNIFICANT WAVE PERIOD (SECONDS)							Total %
	Calm	2-4	4-6	6-8	8-10	10-12	12-14	
0-2	2.5	5.4	13	15	9.4	4.8	0.4	51
2-4	-	3.6	6.7	6.1	5.0	1.3	0.4	23
4-6	-	0.8	3.3	2.7	2.5	1.7	-	11
6-8	-	-	1.5	3.3	2.7	1.3	0.2	9
8-10	-	-	0.6	2.7	1.1	0.6	-	5
10-12	-	-	-	0.4	0.4	-	-	.8
Total (Percent)	2.5	9.8	25	31	21	9.8	1.0	

TABLE 2: WAVE STATISTICS FOR ATLANTIC CITY, N. J., OCTOBER 1962 to JANUARY 1963 IN PERCENT OCCURRENCE

FIG. 4. MISQUAMICUT, RHODE ISLAND

FIG. 5. WESTHAMPTON, LONG ISLAND

FIG.6. ATLANTIC CITY, NEW JERSEY

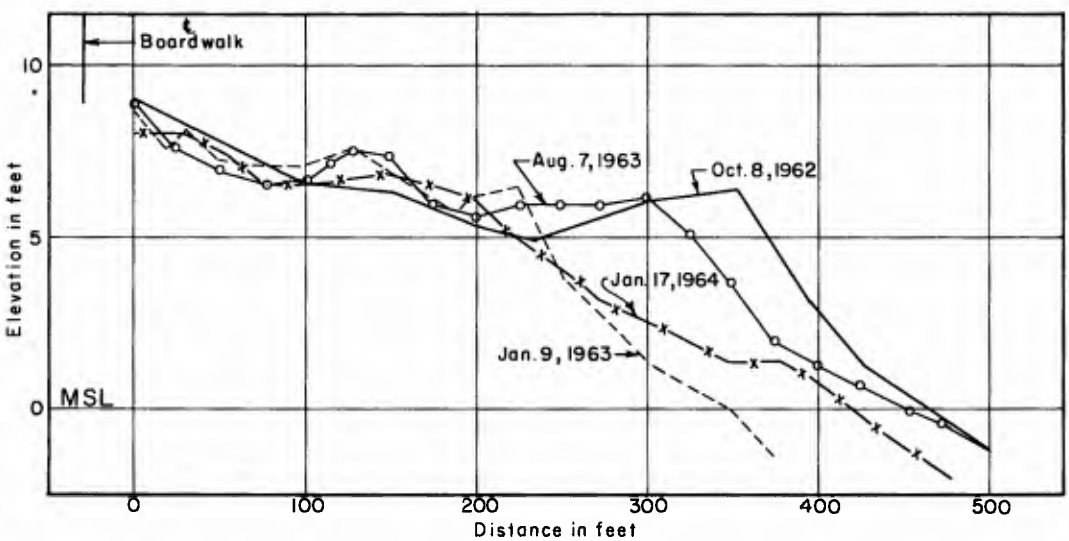

FIGURE 7. PROFILE G - ATLANTIC CITY, N.J.

SEASONAL VARIATIONS VERSUS WAVE AND TIDE STATISTICS

For the purpose of this paper only one beach will be discussed at length. Atlantic City was selected for discussion as wave and tide data are obtained specifically at this point.

At Atlantic City, seven profiles have been surveyed at regular intervals but to simplify matters only one typical profile will be described. It is reasonably representative of conditions at Atlantic City.

The method selected for studying the seasonal changes is a simple one. It is accomplished by recording the distance seaward or landward which certain contours moved from one survey period to the next. Landward movement is an indication of erosion. Similarly, seaward movement should indicate accretion. Mean sea level is used as the reference datum at Atlantic City. This particular study involves only that portion of the beach above mean sea level as very little data were obtained seaward of that shoreline.

Figure 7 shows the changes in the beach shape at Atlantic City at intervals during the period October 1962 through January 1964. Referring to the dates of the actual surveys, between 8 October 1962 and 9 January 1963, contour +3 eroded 134 feet and contour +6 eroded 127 feet. This represents about 27 cubic yards of erosion per linear foot of beach between MSL and +6 feet. In discussing quantity of erosion or accretion, the zone between the MSL and +6-foot contours will be used throughout this paper. The wave characteristics for this period were as shown in Table 2. For this period of erosion 74% of the waves were below 4 feet in height or 26% were above 4 feet. Only 35% had periods between 6-10 seconds and height below 4 feet. The high tides were above +3 feet in elevation 32% of the time for this interval.

The beach accreted between 9 January 1963 and 7 August 1963 to the extent of 96 feet at +3 feet and 75 feet at +6 feet. This is in the order of 19 cubic yards of accretion per linear foot of beach. Concurrent wave characteristics were as shown in Table 3. During this period of accretion 86% of the waves were below 4 feet or only 14% above 4 feet. Fifty-three percent had periods of 6-10 seconds and heights under 4 feet. High tides were above +3 feet elevation for only 17% of the time.

Between 7 August 1963 and 17 January 1964, the beach eroded 84 feet at the +3 level and 104 feet at the +6 level, with erosion amounting to 15.5 cubic yards per linear foot of beach. The wave characteristics were as shown in Table 4. Seventy-two percent of the waves were less than 4 feet, or 28% were greater than 4 feet. Thirty-five percent of the waves had periods from 6 to 10 seconds with heights less than 4 feet. High tides were above +3 feet for 24% of the time.

Sig. Height (ft)	SIGNIFICANT WAVE PERIOD (SECONDS)							Total %
	Calm	2-4	4-6	6-8	8-10	10-12	12-14	
0-2	0.7	6.9	6.3	15	10	3.4	0.8	43
2-4	-	3.6	8.5	20	8.2	1.7	.7	43
4-6	-	.4	1.8	4.7	2.9	.7	.1	11
6-8	-	-	.5	.9	1.0	.2	.1	2.7
8-10	-	-	.1	.4	-	.2	-	.7
Total (Percent	.7	11	17	41	22	6.1	1.7	

TABLE 3: WAVE STATISTICS FOR ATLANTIC CITY, N. J., JANUARY 1963 TO AUGUST 1963 IN PERCENT OCCURRENCE

Sig. Height (ft)	SIGNIFICANT WAVE PERIOD (SECONDS)								Total %
	Calm	2-4	4-6	6-8	8-10	10-12	12-14	14-16	
0-2	5.4	6.7	5.6	6.9	6.9	1.9	0.1	-	34
2-4	-	3.5	9.1	11	10	3.4	0.8	-	38
4-6	-	0.1	2.1	4.4	4.3	2.8	1.0	0.2	15
6-8	-	-	0.9	2.1	2.0	1.5	0.6	-	7.1
8-10	-	-	0.4	1.1	1.0	0.4	0.2	-	3.2
10-12	-	-	-	0.4	0.7	0.9	0.1	-	2.1
12-14	-	-	0.1	0.1	0.7	0.2	-	-	1.1
14-16	-	-	-	0.1	0.2	-	-	-	0.3
16-18	-	-	-	0.1	-	-	-	-	0.1
Total (Percent)	5.4	10	18	26	26	11	2.8	0.2	-

TABLE 4: WAVE STATISTICS FOR ATLANTIC CITY, N. J., AUGUST 1963 TO JANUARY 1964 IN PERCENT OCCURRENCE

Figure 8 depicts the degree of erosion at Atlantic City accompanying the passage of Hurricane Ginny during the latter part of October in 1963. Consecutive surveys were made 28 October and 14 November 1963. One was just before the hurricane passed and the other shortly thereafter. Therefore, the indicated changes were no doubt caused by this storm. Contour +3 eroded 38 feet and +6, 49 feet, or approximately 10.5 cubic yards were removed per linear foot of beach. During the period between surveys the waves were as shown in Table 5. It may be noted that a period of over 24 hours during passage of the hurricane, significant wave height of recorded waves at Atlantic City were of the order of 8 to 10 feet and significant periods were 8 to 10 seconds. Concurrently storm surge levels reached elevations of 3.4 to 3.9 feet above MSL during four consecutive tidal cycles, where ordinary mean high water is about +2 feet.

SUMMARY AND RESULTS

Analysis of the surveys made at Atlantic City from October 1962 to the present, although covering a period of little more than one year, does indicate marked seasonal differences in beach conditions. The beach recedes during the fall or early winter, and recession of the beach seems to have reached a maximum by about January or February. There is a fairly constant beach condition during the remainder of the winter (February and March) once the maximum recession limit is approached. The beach is restored during spring and summer months, reaching its maximum accreted position in July or August; however, the beach is fairly stable during the summer (June through August). It seems significant that during the erosion periods the characteristics of the waves were similar. In both cases 26% to 28% of the significant waves were above 4 feet in height and 17% had 6 to 10-second periods and heights greater than 4 feet. The high tides were above +3 feet for 24% to 32% of the time. During the accretion portion of the cycle only 14% of the significant waves were above 4 feet in height and 10% had periods of 6 to 10 seconds and were above 4 feet. Also, the high tides were above +3 feet only 17% of the time. From the foregoing it will be seen that the waves during the erosion periods were characteristically of greater steepness than those of the accretion period.

The seasonal trend inferred from data for Atlantic City seems to prevail in varying degrees at all the beaches under study, with the possible exception of those fronting on Long Island Sound rather than the Atlantic Ocean. It must be recognized that the actual erosion or accretion does not occur as a continuous pattern, but there are periods which are dominated either by erosion or accretion. These seasonal trends are then the net or resultant behavior pattern.

These observations are based on only a little over one year's record of events, so these are only trends. It is hoped that with additional

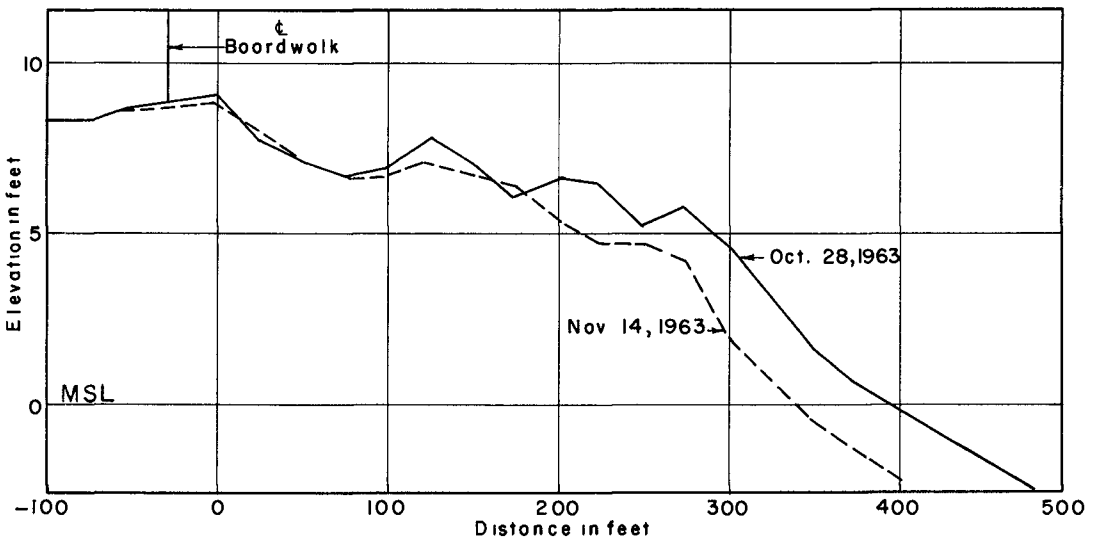

FIGURE 8 PROFILE G-ATLANTIC CITY, N.J.

Sig. Height (ft)	SIGNIFICANT WAVE PERIOD (SECONDS)							Total %
	Calm	2-4	4-6	6-8	8-10	10-12	12-14	
0-2	4	11	-	1.0	5.0	5.0	-	26
2-4	-	2.0	4.0	3.0	12	12	3.0	36
4-6	-	1.0	2.0	4.0	6.0	4.0	5.0	22
6-8	-	-	1.0	3.0	2.0	2.0	-	7.9
8-10	-	-	1.0	1.0	-	-	-	2.0
10-12	-	-	-	1.0	-	2.0	1.0	4.0
12-14	-	-	-	-	2.0	-	-	2.0
14-16	-	-	-	1.0	-	-	-	1.0
Total (Percent)	4.0	14	8.0	14	27	25	9.0	

TABLE 5: WAVE STATISTICS FOR ATLANTIC CITY, OCTOBER 28, 1963 TO NOVEMBER 14, 1963 IN PERCENT OCCURRENCE

years of records we can either confirm or establish the general behavior pattern of this section of coastline, and extend the study to other coastal areas.

ACKNOWLEDGMENTS

The data collected and analysis thereof was made in connection with the general research program of the U. S. Army Coastal Engineering Research Center. Permission of the Chief of Engineers to publish this information is appreciated. Grateful acknowledgment is made to the New England Division, New York and Philadelphis Districts of the Corps of Engineers for their extensive work on this study. Appreciation is extended to those members of the Coastal Engineering Research Center who have been extremely helpful in this study. The conclusions reached and presented herein are those of the author and do not necessarily reflect the policy or views of the Corps of Engineers.

REFERENCES

Taney, N. E. (1961) - Littoral Materials of the South Shore of Long Island, New York: Tech. Memo. No. 129, BEB, Corps of Engineers, Washington, D. C.

U. S. Army Corps of Engineers: South Kingstown & Westerly, Rhode Island, Beach Erosion Control Study, 1958, House Doc. 30, 86th Cong., 1st Sess.

U. S. Army Corps of Engineers: Area 3 - New Haven Harbor to Housatonic River, Connecticut, Beach Erosion Control Study, 1953. House Doc. 203, 83rd Cong. 1st Sess.

U. S. Army Corps of Engineers: South Shore, State of Rhode Island, Beach Erosion Control Study, 1950, House Doc. 490, 81st Cong., 2nd Sess.

Chapter 16

QUASI-WEEKLY AND DAILY PROFILE CHANGES ON A DISTINCTIVE SAND BEACH

John D. Rohrbough and James E. Koehr, Lieutenants, U. S. Navy

and

Warren C. Thompson, Professor of Oceanography
U. S. Naval Postgraduate School, Monterey, California

INTRODUCTION

Casual observations over a period of years of a long sand beach in the southern end of Monterey Bay, California, suggested that the sand elevation, while varying noticeably from one time to another, does not display the well-defined seasonal alternation between build-up in the summer and erosion in the winter that is now widely recognized on the exposed beaches of California. Accordingly, a program was established to measure the beach-profile changes by means of serial observations and to attempt to relate the changes to wave, tide, and beach conditions prevailing during the observation period. The results of the study, covering nine months, are presented herein.

In the course of the study it became evident that quite special conditions of sand, waves, and water circulation exist in the extreme southern end of Monterey Bay which make this small area a natural laboratory where beach profile changes as well as other nearshore phenomena may be investigated under quite simply defined conditions in nature. The characteristics of this beach will be described in some detail, partly because they are distinctive and therefore of more than usual interest, and partly because they are essential to understanding the causes of the profile changes observed.

CHARACTERISTICS OF THE BEACH STUDIED

Monterey Bay is a broad open indentation about 40 km. in width on the central California coast (Figure 1). Its entire inner shoreline, extending approximately between the cities of Santa Cruz on the north and Monterey on the south, is a long sand beach which is continuous except in the middle of the bay where the well-known Monterey Submarine Canyon heads within the entrance of Moss Landing Harbor. The two segments appear to be independent with regard to sand sources and littoral drift because of the barrier offered by the canyon. The beach marks the terminus of the alluvial plain of the Salinas River and is backed along most of its length by coastal dunes of Recent age which are largely inactive. Rocky headlands flank the beach on either end of the bay.

The beach profiles studied are located very near the southern end of the bay on what is known locally as Del Monte Beach (Figure 2). The

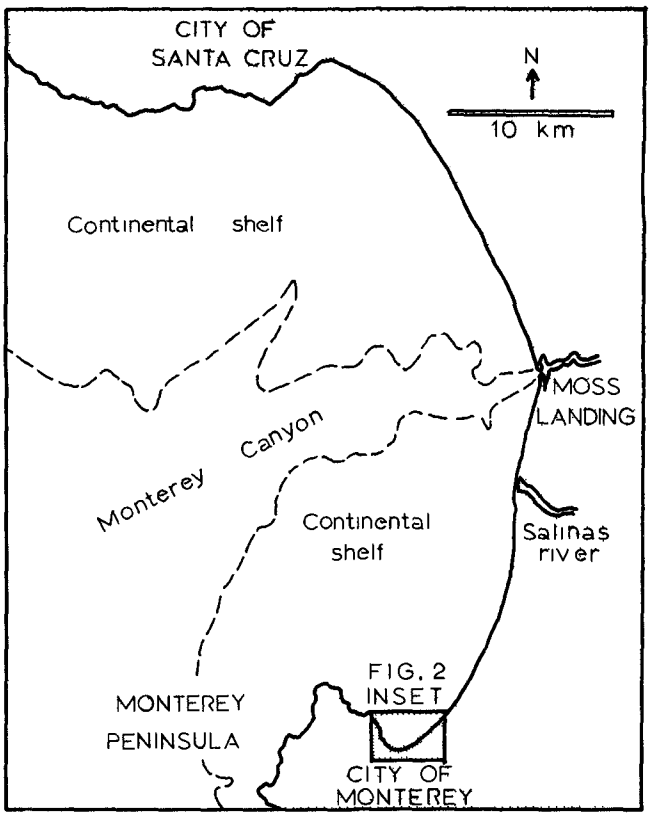

FIG 1 --MAP OF MONTEREY BAY

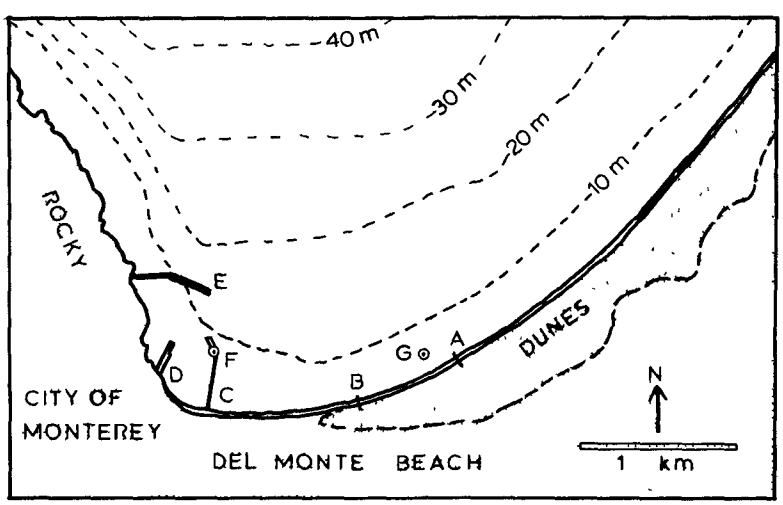

FIG 2 --MAP OF DEL MONTE BEACH A IS PROFILE A, B, IS PROFILE B, C IS A SOLID BULKHEAD, D IS END OF DEL MONTE BEACH, E IS A PERMEABLE BREAKWATER, F IS TIDE GAGE, G IS WAVE GAGE

sand on Del Monte Beach is quartzitic, of fine to medium texture, and very well sorted. A definite gradient in both grain size and beach slope occurs along the beach, with the finest sand and flattest slope occurring at the south end of the beach (Figure 3).

The beach profile, basically very simple, usually displays a fairly uniform gradient from the back of the beach, through the intertidal zone, and into the surf zone. The profile ordinarily lacks a well-defined berm and offshore bar, but a narrow sand flat is sometimes present at the lowest tide level.

The predominant wave type on Del Monte Beach is swell a very large percentage of the time. The extreme southern corner of Monterey Bay, because of its recessed location, is so sheltered from the open ocean that both sea and swell entering the bay from all directions experience extreme refraction in travelling across the broad smooth shelf offshore, and are accordingly reduced to swell of moderate or low steepness upon arrival on Del Monte Beach. With regard to wind waves generated locally within the bay, large waves can arrive only from northerly directions but the frequency of northerly winds is very low. Afternoon sea breezes from westerly directions often generate a white-capped sea to the north of Del Monte Beach but the latter usually enjoys the shelter of the Monterey Peninsula and the sea is typically low or calm.

Associated with the dominance of swell are low breaker heights, which seldom exceed one meter and are usually much less. Due to the marked refraction effects, a noticeable decrease in the breaker height toward the south can nearly always be observed along Del Monte Beach. In view of the wave-height gradient a decision was made to establish two beach profiles, separated by 670 m., in order to study the influence of the gradient on the profile.

Breaker heights, seldom in excess of one meter as mentioned, are superimposed on an astronomical tide of the mixed type having a diurnal range averaging about two meters. Meteorological tides are negligible, the largest noted during the observation period having an amplitude of about 15 cm. according to a study of anomalous water levels at Monterey Harbor by O'Connor (1964). Thus, gravity waves are superimposed on nearly periodic water-level variations, which undoubtedly simplifies the relationship between waves and beach-profile changes.

The significant periods of the wave trains observed on Del Monte Beach vary widely between about 5 and 20 sec., like those measured on the exposed beaches of the Pacific Coast. No wave spectra have been measured, but visual observations indicate that the spectrum is characteristically narrow, even when wind waves enter the bay from the open ocean. Differential refraction of the spectrum probably accounts for the latter situation.

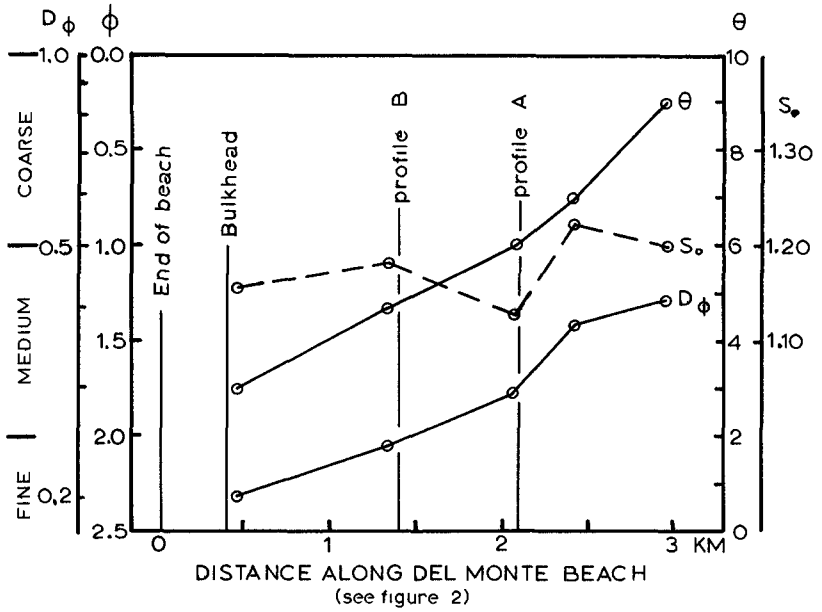

FIG. 3 --DISTRIBUTION OF GRAIN DIAMETER, D_ϕ (IN MM AND PHI UNITS), SAND SORTING S_o (IN TRASK COEFF), AND BEACH SLOPE θ (IN DEG) ALONG DEL MONTE BEACH (DATA FROM McFADDEN, 1964

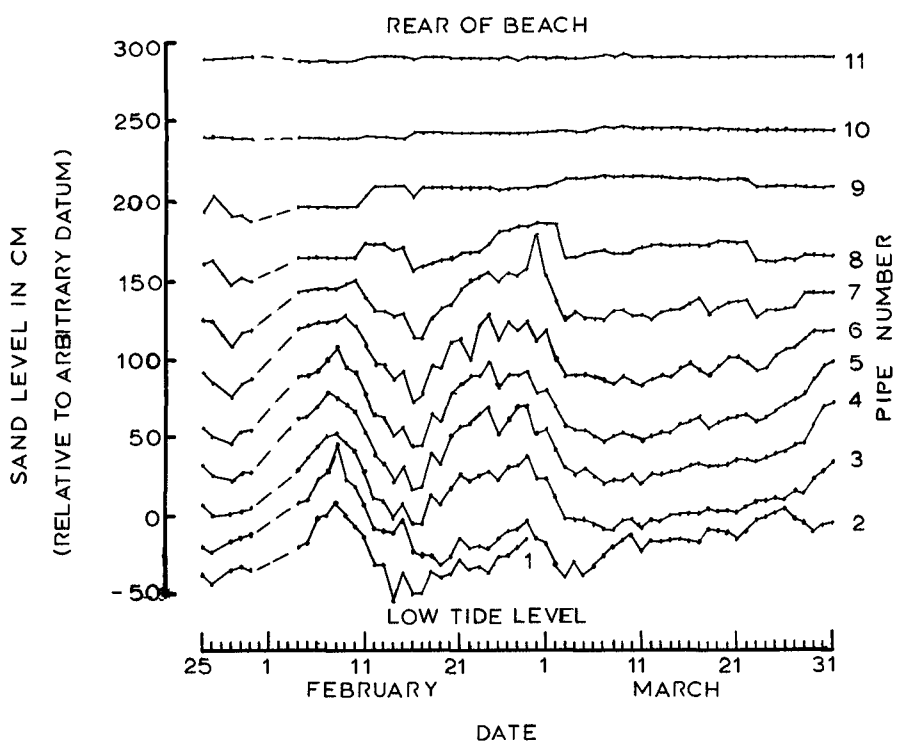

FIG 4 --DAILY SAND LEVEL VARIATION ON PROFILE A

The usual occurrence of low to negligible breaker angles is another consequence of the intense refraction in the southern end of the bay. The accelerating curvature of Del Monte Beach that can be readily seen in Figure 2 undoubtedly owes its adjustment largely to this effect. The beach has remained very nearly fixed in position since the earliest hydrographic survey in 1851 according to comparisons of successive hydrographic surveys by the U. S. Army, Corps of Engineers (1958).

Net littoral drift along Del Monte Beach is very small or non-existent, as indicated by a variety of both direct and indirect evidence. Such evidence includes the absence of any significant net sand accumulation against the solid bulkhead shown in Figure 2 since its construction two years ago, obvious differences that exist between the mineralogical composition and texture of the sand on Del Monte Beach and that on nearby pocket beaches along the rocky shoreline of Monterey Peninsula, occurrence of the gradient in sand texture along Del Monte Beach which would not be expected to persist in the presence of any significant littoral drift, absence of any significant sink for the beach sand (the coastal dunes to the north represent a large potential source), dominance of swell of small breaker height and angle which must produce generally negligible longshore currents, and the common occurrence of subdued cusps on Del Monte Beach which would not ordinarily be expected in the presence of significant longshore currents.

The absence of significant littoral drift indicates that only onshore-offshore transport of sand grains appears to be ordinarily involved in the beach profile changes. In addition, it indicates a long residence time for the sand on Del Monte Beach.

Neither coastal nor tidal currents are known to flow along Del Monte Beach according to local observers. The circulation of water seaward of the surf zone appears to be controlled almost entirely by the wind, as indicated in field observations made by Stevenson (1964). Water circulation within the surf zone on Del Monte Beach has been described by Brennan and Meaux (1964) from field measurements.

BEACH PROFILE MEASUREMENT AND OBSERVATIONS

The two profiles established on Del Monte Beach each consist of a series of 5 cm. pipes driven into the sand at intervals of 3.7 m. (12 feet) along a line perpendicular to the beach. The profiles, each 37 m. in length, extend from the landward limit of the beach, marked by fixed dunes, to the approximate lowest tide level. They are designated A and B.

During the conduct of a survey, the sand elevations against the pipes are measured relative to the tops of the pipes the heights of which are referred to a common datum. This method of profile measurement permits one man to take readings accurately in a matter of minutes, and to make subsequent

profile surveys at precisely the same locations as often as desired.

The sequence of profile measurements collected over a period of time represents a time series at each fixed location which is directly amenable to statistical analysis and is in a form convenient for correlation with waves and other related time-dependent factors. An example of the profile data graphed in the form of a time series at each pipe is shown in Figure 4.

The profile observations to be described herein were made over the period from July 1963 to March 1964, inclusive. The profiles were measured quasi-weekly from July 1963 through January 1964, but a detailed study of continuously recorded wave data for that period showed the quasi-weekly interval to be inadequate for the purpose of relating observed beach changes to the varying wave conditions, and in February and March 1964 the beach profiles were measured daily near the time of low tide. The quasi-weekly profile data are not plotted herein but may be found in Koehr and Rohrbough (1964). The daily observations at Profile A only are presented herein (Figure 4).

During the nine months of observations Profiles A and B experienced an extreme range in sand height of about 100 cm. at the low-tide and mid-tide levels, diminishing to zero at the back of the beach where waves did not reach. The sand-level variations on both profiles were fairly similar in major trend and magnitude and were essentially synchronous, but they often differed considerably in their minor variations. The general similarity in the magnitude of the major fluctuations at the two profiles is interesting in view of the prominant gradient in wave height and other factors that occur between the profiles.

The most pronounced features evident in the data are large cycles of fill and cut, fairly symmetrical in time, averaging about 60 cm. on the lower part of the beach and commonly covering an interval averaging about 20 days. The entire active portion of the beach tended to rise and fall during each cycle. The cycles occurred at irregular intervals throughout the observational period but appeared to be more frequent in autumn and winter. Their cause has not been ascertained. Examples of two prominant cycles may be seen in Figure 4.

Superimposed on the large cycles and on the less active periods between them are continual day-to-day changes in the sand level. During the two-month period of daily observations, these changes exceeded 3 cm. per day about two-thirds of the time on the more active lower part of the beach, and ranged up to 20 cm. per day. The frequency distributions of the daily rates of change were similar for cut and fill.

During approximately half the period the sand level rose or fell in common at all points along the profile from one day to the next, whereas during the

remainder of the period differential cutting and filling on different parts of the profile occurred. Filling on the upper part of the beach and cutting on the lower part occurred more frequently than the reverse situation. An example of the former case may be seen in Figure 4 for the one-day interval of January 25 to 26. The pivotal point in the profile occurred at Pipe 7.

No seasonal alternation between build-up in the summer and erosion in the winter, such as has been commonly observed on the exposed beaches of the California coast, is evident in the nine months of data.

CAUSITIVE FACTORS INFLUENCING THE PROFILE

Factors that were investigated in searching for causes of the observed profile changes were the waves, tides, and beach saturation.

Waves were recorded during the first four months of the study using a pressure sensor located in an average depth of 7.5 m. a short distance seaward of the two profiles (Figure 2). Fast traces were made twice daily and were analysed for the wave characteristics. A summary of the analysed records shows that the wave period ranged widely between 7 and 18 sec., with the most frequent period being 10.8 sec. The maximum significant wave height at the sensor location was 2.0 m., but the height was less than 1.0 m. in 93% of the records analysed. The initial wave steepness (unrefracted), $H_o'/\overline{T}^2$, ranged between 0.001 and 0.034, and averaged about 0.010. Graphs of the wave parameters plotted with time (Koehr and Rohrbough, 1964) display continual daily fluctuations superimposed on longer undulations.

Comparison of the quasi-weekly beach profiles with the semi-diurnal wave data for the four-month period suggests that the sand level rises during periods of generally diminishing initial wave steepness, and falls during periods of increasing steepness, but the relationship is by no means clear-cut. In view of the daily variability of the wave data, the profile sampling interval was much too coarse, even with respect to the major beach cycles, to indicate any more than a very general relationship.

During the period of daily profile observations that followed, when reaction of the sand level to the wave parameters could have been studied more satisfactorily, the wave gage was unfortunately out of operation (visual observations proved to be inadequate). However, the constant change in the profiles from day to day indicate a sensitive reaction of the beach to very subtle changes in the character of the incident waves.

With regard to tidal influences on the profiles, both the quasi-weekly and daily sand elevations were examined for evidence of a possible fortnightly tidal cycle that might be expected in response to spring and neap tide ranges, such as is mentioned by Shepard (1963). Although conditions on Del Monte Beach seemed favorable for detection of such a cycle in view of the fact that the tide range exceeded the breaker height nearly all of the time, no

such cycle was evident. It appears that the effects of variable wave run-up on the beach overshadowed any spring-neap tide effect.

It is of interest to mention here that Strahler (1964), using a profile sampling interval of a half hour on a beach on the New Jersey coast, found a semi-diurnal cycle of cut and fill that is associated with the semi-diurnal tide. The cycle was superimposed on what he termed an equilibrium profile. A cycle of this frequency cannot be detected in our own daily data because of our choice of sampling interval. However, the effect of the daily tides evidences itself indirectly in that the lowest portion of the profile which is covered with water at all tide stages displays a greater degree of daily variation in sand level than the higher parts of the profile which are wetted fewer hours of the day.

Saturation of the beach, which was not measured, was considered as a factor in altering the beach profile through deposition and erosion of sand accompanying the seepage of water into and out of the beach face with changing water levels. It may be presumed that the water table in Del Monte Beach is determined momentarily by the tide, which undoubtedly produces a semi-diurnal fluctuation in the water table (but not one of longer period because of the high permeability of sand), by the superimposed wave run-up, and possibly by heavy rainfall and ground-water discharge from the dune field behind the beach. The effects of the water table on changing the beach profile are undoubtedly complex, and have been accounted for by the authors only indirectly in terms of the wave and tide parameters that were measured and the beach profiles that resulted.

The weather during the nine-month period consisted of dry periods punctuated by a half-dozen storms, during two of which the rainfall exceeded 2.5 cm. in 24 hours. No effects of heavy rainfall were detected in the beach profiles, either immediately following the rainfall or over a longer period of time due to possible ground-water drainage from the dune field behind the beach.

SUMMARY AND CONCLUSIONS

Del Monte Beach, because of its sheltered location in Monterey Bay, California, provides a natural laboratory for the study of beach profile change and other nearshore phenomena by virtue of the relative simplicity of the natural conditions that prevail there.

Extreme wave refraction results in a prevalence of swell of low height and breaker angle, but having a wide range of period. Coastal currents, tidal currents, and meteorological tides are negligible. There is no significant net littoral drift, accordingly, changes in the beach profile appear to involve only onshore-offshore transport of sand grains.

A breaker-height gradient occurs along the beach, so that two beach profiles were established. Gradients also occur along the beach in sand texture, beach slope, and beach curvature.

The two profiles, restricted to the intertidal zone, were measured quasi-weekly and then daily over a period of nine months. The changes in sand level at both were quite similar in magnitude in spite of the wave height gradient along the beach.

Large time-symmetrical cycles of cut and fill commonly averaging about 60 cm. at the low-tide level and covering an interval of roughly 20 days occurred irregularly throughout the period. Superimposed on these were day to day variations in sand elevation ranging up to about 20 cm. Differential cutting and filling on different parts of the profile from one day to the next commonly occured. The low-tide portion of the profiles varied most sensitively with time.

No clear-cut seasonal cycle and no fortnightly spring-neap tidal cycle was detected in the data. The concurrent nature of the daily variations of both sand level and waves recorded immediately off the beach leave no doubt that changing wave conditions were the primary cause of the changes observed in Del Monte Beach, even though no clear-cut relationship between the two factors was apparent.

The authors conclude that further observations should be carried out on Del Monte Beach and on other beaches in order to further elucidate the character of sand changes on natural beaches and determine their causes. The additional conclusion is reached that because of the sensitivity of this beach, and probably all sand beaches, to changing wave conditions, profile measurements should be made at time intervals comparable to or less than the time intervals characteristic of the changing wave conditions, if the measurements are to be used to examine the causes of profile changes. In view of the broad wave regimes occurring in the world oceans, an acceptable observation interval seems to be on the order of one day or less on open coasts.

ACKNOWLEDGMENTS

The authors wish to thank Mr. Robin Loftus, Physical Science Aid, U. S. Naval Postgraduate School, who installed the profile pipes and made the profile measurements during the first half of the survey, and the Engineer's Office of the City of Seaside who surveyed the profiles. This work was performed under the Office of Naval Research Institution Grant to the Postgraduate School.

REFERENCES

Brennan, J. F. and Meaux, R. P. (1964). Observations of the Nearshore Water Circulation off a Sand Beach: M. S. thesis, U. S. Naval Postgraduate School.

Koehr, J. E. and Rohrbough, J. D. (1964). Daily and Quasi-Weekly Beach Profile Changes at Monterey, California: M. S. thesis, U. S. Naval Postgraduate School.

McFadden, G. R. (1964). An Investigation of the Sand Textures of the Monterey Bay Beaches: B. S. thesis, U. S. Naval Postgraduate School.

O'Connor, P. (1964). Short-Term Sea-Level Anomalies at Monterey, California: M. S. thesis, U. S. Naval Postgraduate School.

Padrta, J. C. (1964). Observations of Water Circulation in the Surf Zone: B. S. thesis, U. S. Naval Postgraduate School.

Shepard, F. P. (1963). Submarine Geology (2nd edition): Harper & Row, Publ., New York.

Stevenson, C. D. (1964). A Study of Currents in Southern Monterey Bay: M. S. thesis, U. S. Naval Postgraduate School.

Strahler, A. N. (1964). Tidal Cycle of Changes in an Equilibrium Beach, Sandy Hook, New Jersey: Tech. Report No. 4, Dept. of Geology, Columbia Univ.

U. S. Army, Corps of Engineers (1958). Survey Report on Monterey Bay (Monterey Harbor), California, for Navigation. Appendix V, Shoreline Changes: U. S. Army Engineer District, San Francisco, 30 April 1958.

Chapter 17

WAVE ENERGY AND LITTORAL TRANSPORT

José Castanho

Engineer, Beaches and Harbors Division
Laboratório Nacional de Engenharia Civil, Lisboa, Portugal

1. GENERAL

As is known the breaking of oblique waves generates currents roughly parallel to the shore line usually designated by longshore currents. The intensity of these currents which are present almost exclusively between the breaking line and the shore depends on the characteristics of the waves (angle of approach, height and period) and on the characteristics of the shore (slope and roughness).

A certain amount of energy E is transmitted by the breaking wave along its direction of propagation. As this is a transmitted energy, it is possible to speak about its component parallel to the shoreline which would be indicated by $E \operatorname{sen} \alpha$, being the angle of approach of waves, i.e. the angle that crests make with the shoreline.

Let us consider the breaking line and two near orthogonals distant dx from one another (fig.1).

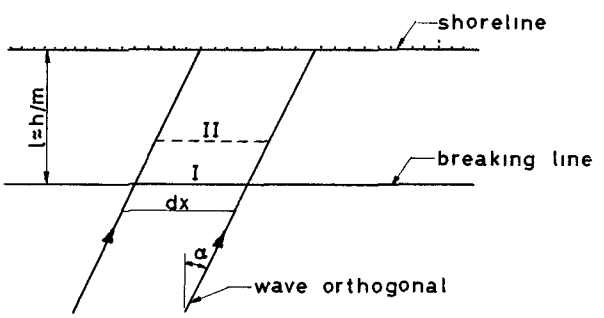

Fig.1 - Sketch of wave attack

A fraction of the energy flowing through the breaking line remains in the longshore current from which it will flow out in a continuous or concentrated form (rip currents); another part is dissipated by friction in the bottom whilst the remaining is lost by breaking (turbulence).

The distribution of the difference between the energy flo ing in at section I and flowing out at section II by these thre fractions depends firstly on the type of breaking (spilling or plun ing) and secondly on the characteristics of the wave and of th shore.

That distribution varies also along the zone where the lon shore current is present, i.e. between the breaking line and th shore.

2. DISTRIBUTION OF TRANSMITTED ENERGY

2.1 Energy dissipated in friction losses - Let us assum that the average velocity V of the longshore current betwee the breaking line and the shore* is known. Denoting by k th friction factor and assuming that the friction force is propor tional to the square of the velocity, the energy dissipated in beach length dx will be proportional to the third power of th velocity and can be written

$$E_d = k \rho V^3 \, dx$$

$$\text{or} \quad E_d = k \rho V^3 \, \frac{h}{m} \, dx \qquad (1$$

where ρ represents the unit mass of water, m being the slope c the beach and h the breaking depth.

Assimilating the breaking waves to solitary waves arriv ing each T seconds (T being the period)** the transmitted er ergy parallel to the shore, per second is

$$E_t = \frac{2{,}2g\,H^3}{T} \operatorname{sen}\alpha \cos\alpha \, dx \qquad (2$$

H being the wave height.

According to some authors it is preferable to consider p riodic waves of which the deep-water characteristics are knowr

---

(*) For the present purpose it is sufficient to consider an ave age value of the velocity of the current. In a more detaile study now under way the variation of the velocity of the long shore current in the surf zone is taken into account.

(**) Munk: "The solitary wave theory and its application to sur problems". Annals of the New York Academy of Sciences Vol.51 - 1949

Anyhow if these characteristics were known, it would always be possible to calculate the solitary wave which each T seconds transmits the same amount of energy than the periodic wave in deep water.

Therefore we shall continue to assimilate breaking waves to solitary waves.

The ratio s of the energy dissipated in friction losses in the bottom (eq.1) and the component of the transmitted energy parallel to the shore (eq.2) is

$$s = \frac{k \rho V^3 h/m \, dx}{2,2 \, gH^3 \operatorname{sen}\alpha \cos\alpha \, dx/T} \tag{3}$$

Writing the velocity of propagation of the breacking solitary wave $C = \sqrt{g(h + H)}$ with $H = 0,78\, h$ and considering the steepness of the wave $\delta = \frac{H}{L} = \frac{H}{CT}$, equation (3)

becomes

$$s = \frac{(V/C)^3}{0.38 \, A \operatorname{sen} 2\alpha} \tag{4}$$

where A is the dimensionless parameter $A = \frac{m\delta}{k}$

2.2 Energy contained in the longshore current - According to the theory of the solitary wave, the volume of water Q leaving the breaking wave in each strip of width dx is

$$Q = 2 h^2 \cos\alpha \, dx \tag{5}$$

V being the mean velocity of this volume of water, its kinetic energy will be

$$E_c = \frac{1}{2} QV^2 \tag{6}$$

The ratio t of the kinetic energy of the longshore current (eq.6) to the component of the transmitted energy parallel to the shore can be written, taking equation (5) into account,

$$t = \frac{(V/C)^2}{0.64 \operatorname{sen}\alpha} \tag{7}$$

2.3 Energy dissipated in wave breaking(turbulence) - Th energy fraction dissipated in breaking is

$$r = 100\% - (s + t)\%$$

3. CALCULATION OF THE MEAN VELOCITY OF THE LONGSHORE CURRENT

Let us apply the momentum method for calculating the mea velocity of the longshore current.

Being Q_b the volume of water carried by the solitary bre ing wave and C_b the velocity of propagation, the component pa allel to the shore of the transmitted rate of momentum will be

$$Q_b \times C_b \ \text{sen}\alpha \cos\alpha \, dx/T$$

V being the mean velocity of the longshore current, the vo ume Q_b keeps a momentum towards the shore equal to

$$Q_b V \cos\alpha \, dx/T$$

According to the momentum theorem, the variation of t rate of momentum is equal to the friction force. Therefore will be

$$\frac{Q_b C_b \ \text{sen}\alpha \cos\alpha}{T} = \frac{Q_b V \cos\alpha}{T} - k\rho V^2 \cdot \frac{h}{m} \qquad ($$

Computing V from equation (8) and substituting its value equations (4) and (7), it is possible to determine the values of and t, i.e. the fractions relative to the ingoing energy respec tively of the energy dissipated in friction losses in the bottom a of the energy contained in the longshore current.

Nevertheless if equation (8) was applied as written abov we should find that for some values of $s + t > 100\%$ which is possible.

This lead us to some considerations on the momentum ac ally available to generate the longshore current.

In the present paper only the case of beaches with a ve gentle slope (say 2 per cent or less) will be considered, it bei

assumed that wave breaking is gradual so that the wave resumes its shape at each moment, remaining practically symmetric. This amounts to assuming that the wave height decreases linearly with depth and that the decrease of transmitted energy corresponds exactly to the energy progressively lost in wave breaking. The wave height thus follows constantly the law $H = 0.78\, h$.

In a study now in progress we have approached the case of a breaking wave giving rise to a bore.

Let us consider then two neighbouring sections I and II (fig.1). The change of momentum between them will be

$$dM = d(QC) = Q\,dC + c\,dQ$$

From $Q = 2\,h^2$ and $C = 1.78\,g\,h\,\frac{1}{2}$ (solitary wave), the expressions $dQ = 4\,h\,dh$ and $dC = \frac{1}{2}\,Ch^{-1}dh$ are obtained. Hence

$$\int_{h_1}^{h_2} C\,dQ = \frac{4}{5}\,(Q_1C_1 - Q_2C_2)$$

$$\int_{h_1}^{h_2} Q\,dC = \frac{1}{5}\,(Q_1C_1 - Q_2C_2)$$

This lead us to suggest that between sections I and II the momentum available to generate the longshore current is only the volume dQ of water available in the section under consideration times the velocity of propagation C, the momentum available between the breaking line and the shore being

$$\int_{h_b}^{o} C\,dQ = \frac{4}{5}\,Q_bC_b$$

The amount $\int_{hb}^{o} Q\,dC = \frac{1}{5}\,Q_bC_b$ would correspond to a lost momentum since the wave flowing out at section II has a velocity of propagation $C + dC$ instead of velocity C which corresponds to the wave flowing in at section I.

The momentum theorem will be written now

$$\frac{4}{5}\,\frac{Q_b C_b \operatorname{sen}\alpha \cos\alpha}{T} - \frac{Q_b V \cos\alpha}{T} = k\,\rho\,V^2\,\frac{h}{m} \qquad (9$$

Solving equation (9) with respect to V and taking into ac count that $Q_b = 2\,h^2$, $C_b = 1.78g\,h^{\frac{1}{2}}$ and $\delta = \frac{H}{C_b T}$, the followin dimensionless equation results

$$\frac{V}{C_b} = 1.30 \cos\alpha\, A \left[\sqrt{1 + \frac{1.22 \tan\alpha}{A}} - 1\right] \qquad (10$$

where $A = \frac{m\delta}{k}$

Thus for a given angle of approach , the relative veloc ity $\frac{V}{C_b}$ is a function of the parameter $A = \frac{m\delta}{k}$ alone.

4. CALCULATION OF THE ENERGY FRACTIONS DISSI PATED IN FRICTION LOSSES AND BREAKING LOSSE

By substituting the value of $\frac{V}{C_b}$ given by equation (10), is possible to obtain s and t from equations (4) and (7).

Figures 2 and 3 show the values of s and t for angles 10°, 30°,45°,60° and 80° in a function of the parameter $A = \frac{m}{k}$

Figure 2 shows that the fraction s of the energy dissipa ed in friction losses in the bottom reaches a maximum for a ce tain value of A which varies in accordance with .

On the other hand, for values of A not exceeding 0.3, th fraction s is a function of the angle α, reaching a maximum nea 45° to 60°.

Figure 3 shows that energy dissipated in breaking losses always important (between 85 and 95%) for angles $\alpha = 10°$. Fo greater angles the fraction r is important for small values of A decreasing regularly as A increases.

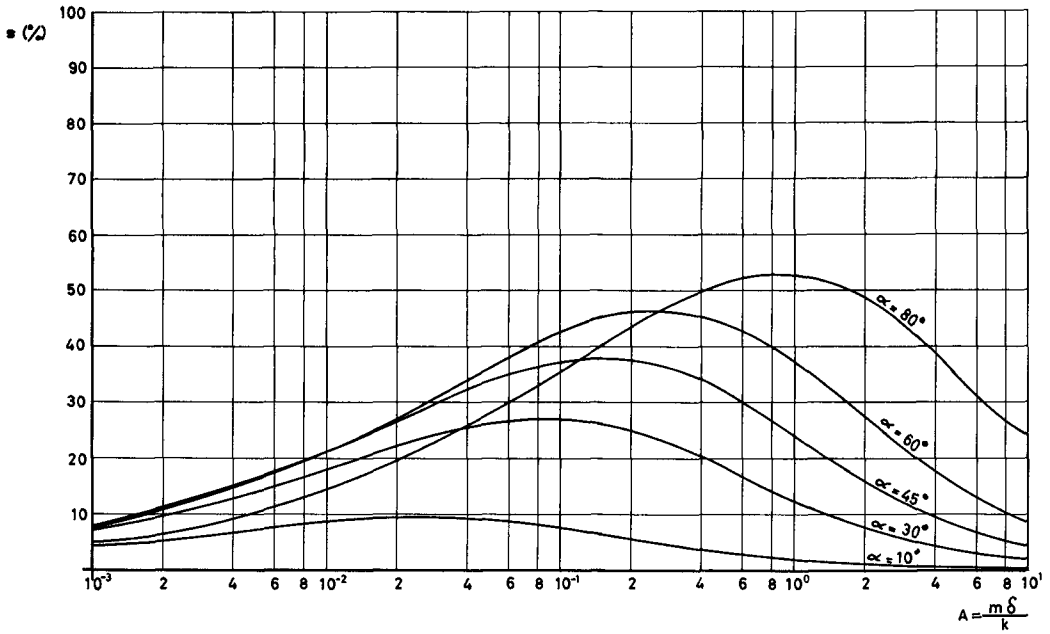

FIG 2 --PERCENTAGE OF ENERGY DISSIPATED BY FRICTION

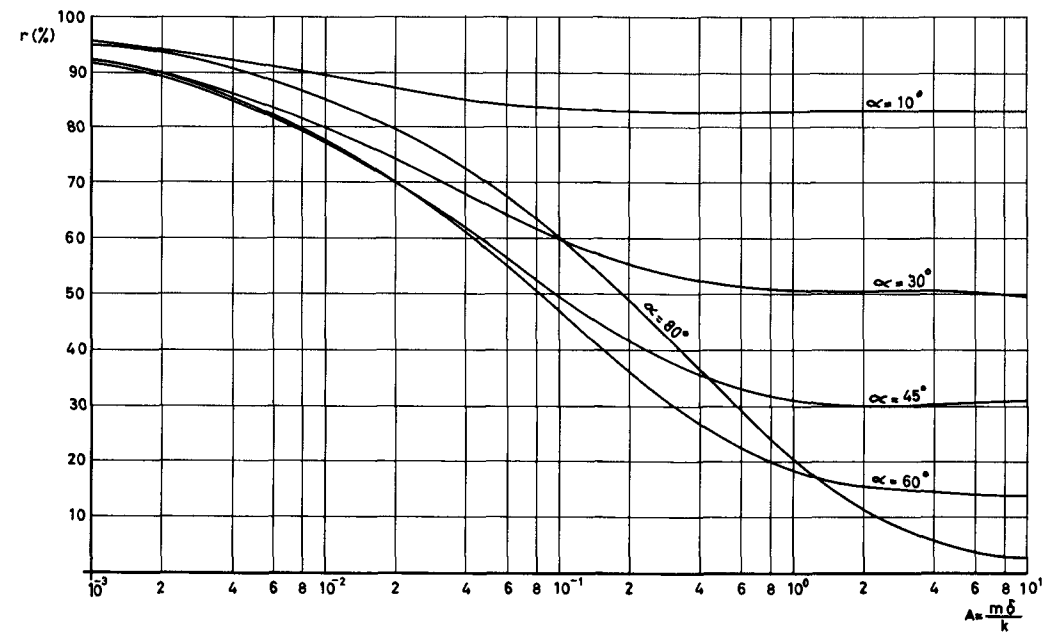

FIG 3 --PERCENTAGE OF ENERGY DISSIPATED BY BREAKING

5. SOLID DISCHARGE

For constant values of $\underline{m}$ and $\underline{k}$ the shape of the curves $s = f(\frac{m\delta}{k})$ or $s = f(\delta)$ is very similar to that of curve $Q_{solid} = f(\delta)$. The same applies to $s = f(\alpha)$, a maximum being reached between $\alpha = 45^{o}$ and $\alpha = 60^{o}$.

This seems to suggest that the solid discharge can be dimensionlessly expressed as a function of $\underline{s}$. In a first attempt Q_{solid} could be considered as proportional to $\underline{s}$.

Chapter 18

QUANTITATIVE RESEARCH ON LITTORAL DRIFT IN FIELD AND LABORATORY

Coastal Engineering Laboratory, University of Florida
Presented by Per Bruun and James Purpura

INTRODUCTION

The Coastal Engineering Laboratory of the University of Florida is at present carrying out a combined field and laboratory research program to gain quantitative information on littoral drift longshore as well as perpendicular to the shore. The laboratory utilizes modern tracing technique by luminophores including a scanning (counting of grains) machine and experiments in a wave tank where a current is passed through waters agitated by waves propagating parallel to or perpendicular to the current action.

FIELD RESEARCH

GENERAL

Sediment transport is caused by a combination of shear stresses by wave and current action. The wave induced shear stresses "break loose" the material from the bottom while the longshore currents transport it longshore. A research program on littoral drift must combine wave and current action. The research procedures described below are based on the philosophy that although it is not possible to understand the complex problems in full unless research penetrates down in the very details (refs. 4, 10, 11, 17, 19), it is still possible to secure results of scientific and practical value by considering an integrated part of the problem, including a variety of details to be looked into when the integrated problem has been analyzed to the extent this is possible. The procedure, therefore, may be said to follow the pattern of penetrating into the problem "from above".

MODES OF TRANSPORT

It is known that bed load transport takes place in two different modes - partly in a fast moving sheet-layer on the surface of the bottom and partly in bulk movements as slowly migrating waves on the bottom, perhaps in a multiwave system with one wave creeping on the top of the other as observed in the Mississippi River (ref. 16). The situation on the seashore may be similar to the situation in rivers although the surf zone has its peculiarities. The existence of migrating waves has been clearly demonstrated, e.g. by surveys on the Danish North Sea Coast (ref. 3), in Florida (ref. 6), in Holland (ref. 23) and in Japan (ref. 22).

Sheet-Layer Movement

The thickness of the sheet-layer depends upon the forces exerted upon the bottom and their variation with time. Under the influence of these stresses, sand particles travel parallel to the wave crests (longshore) when the oscillating water particles are mainly in vertical movement and they

migrate perpendicular to the wave crests (and to the shore) below wave crests and troughs. Tests on sheet-layer movement are now in progress. In the field quantitative research is undertaken using luminescent tracers. Experiments using fluorescent tracers are mentioned in refs. 6, 12, 13, 24 and 25.

With respect to research on sheet-layer movement the following procedure is used at experiments in progress at Fernandina Beach, Florida, for grant by the National Institute of Health, Education and Welfare.

Tracer material is dumped by diver or from helicopter in soluble plastic bags on the updrift side of an 800 ft. long pier extending in the ocean up to 15-20 ft depth at M.S.L. Sampling is undertaken from the pier. Fig. 1 shows a schematic of the instrumentation as installed on the pier. Sampling equipment consists of four bed load traps and four suspended load traps. The bed load traps are raised and lowered from the pier deck to the bottom. The bed load trap is about 3 ft long, 2 ft wide, 8 in high, streamlined (turtle-shaped) box with steel sides and plexiglass top. It has doors controlled from the pier at each end. To avoid excessive scour around the trap and its openings, a steel apron is attached to the bottom of the trap. The trap is placed with open doors parallel to shore. After a few minutes, doors are closed and water jets circulate the water in the trap at the same time as vertically slitted pipe in the middle of the trap sucks up the material to the pier (Fig. 2). Details of this phenomena are explained by the fact that the sand moves along the bottom in a circular path and the pressure gradient directed toward the center causes sand movement toward the center.

The suspended load pump sampler has three vertical intakes pointing upwards. Laboratory tests have proven that vertical intake-samplers are not fully accurate for sediments much coarser than 0.06 mm, but the error experienced for coarser sediment (0.1-0,2 mm) is, on the other hand, less than about 20%, if the velocity in the intake does not deviate much from the actual current velocity. Because of the eddy turbulence at the bottom where concentrations are highest, the actual concentrations are being checked by other sampling methods.

The sampling arrangement on the pier permits four bed load traps and four suspended load samplers to be operated with four electrically powered pumps by an easily assembled, valved pipeline system.

During the test which may run for several hours continuous sampling is carried out by which the "number of grains versus time relationship" is obtained. If n tracer grains are trapped per unit time, one has with v_x = travel velocity of grains, b = thickness of sheet-layer, w = width of trap-opening and k_1 a soils constant:

$$w.b.v_x = n.k_1$$

$$b = \frac{nk_1}{wv_x} = k_2 \frac{n}{v_x} \quad (k_2 = \frac{k_1}{w}) \qquad (1)$$

"b" indicates the thickness of the "imaginary layer" of coated grains and is very small (a fraction of grain size). The corresponding number of non-coated grains coming from the same bottom area as the coated grains is unknc

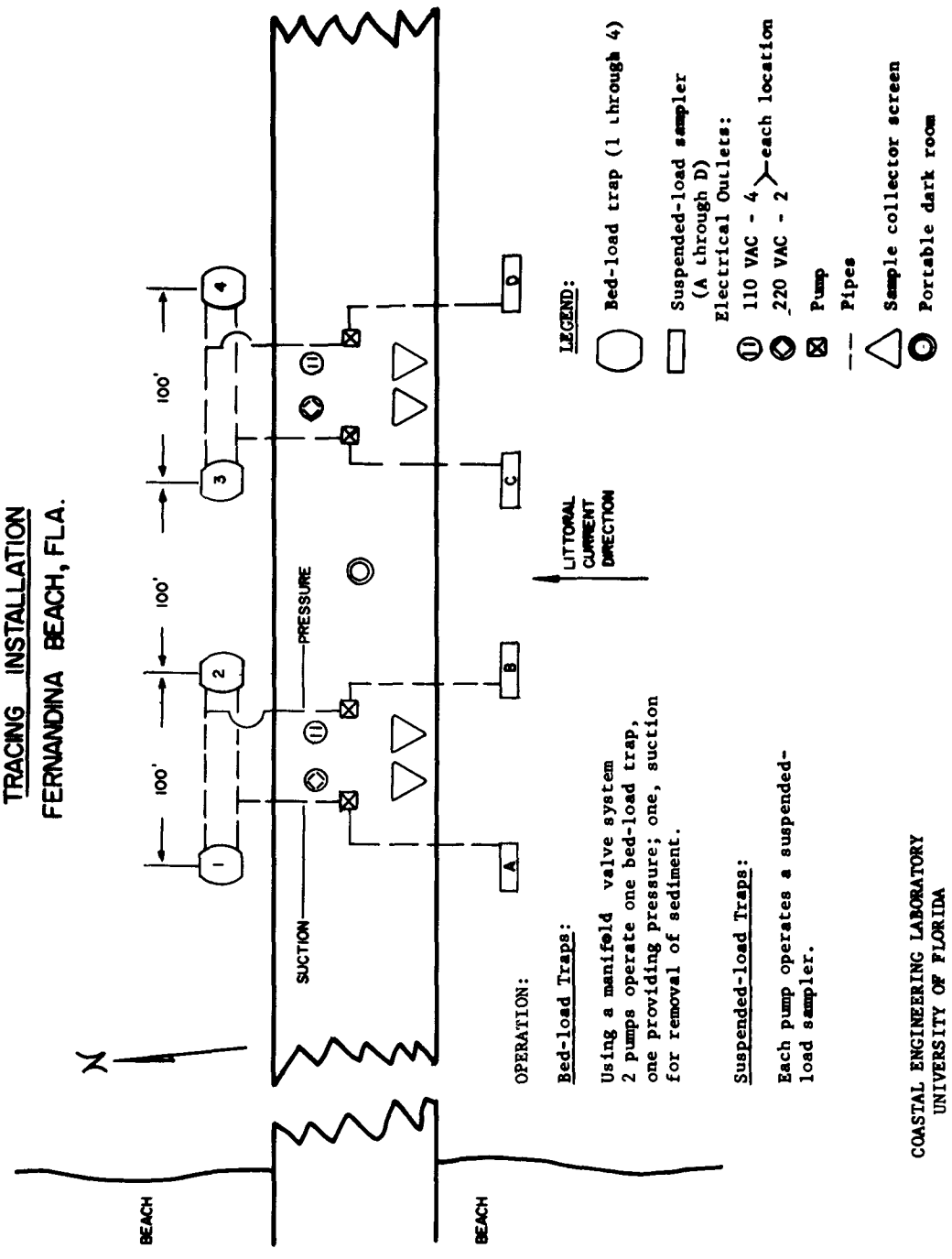

FIG 1 SCHEMATIC INSTRUMENTATION INSTALLED ON FERNANDINA BEACH PIER, NE, FLA.

PLAN VIEW OF BED-LOAD SAND TRAP

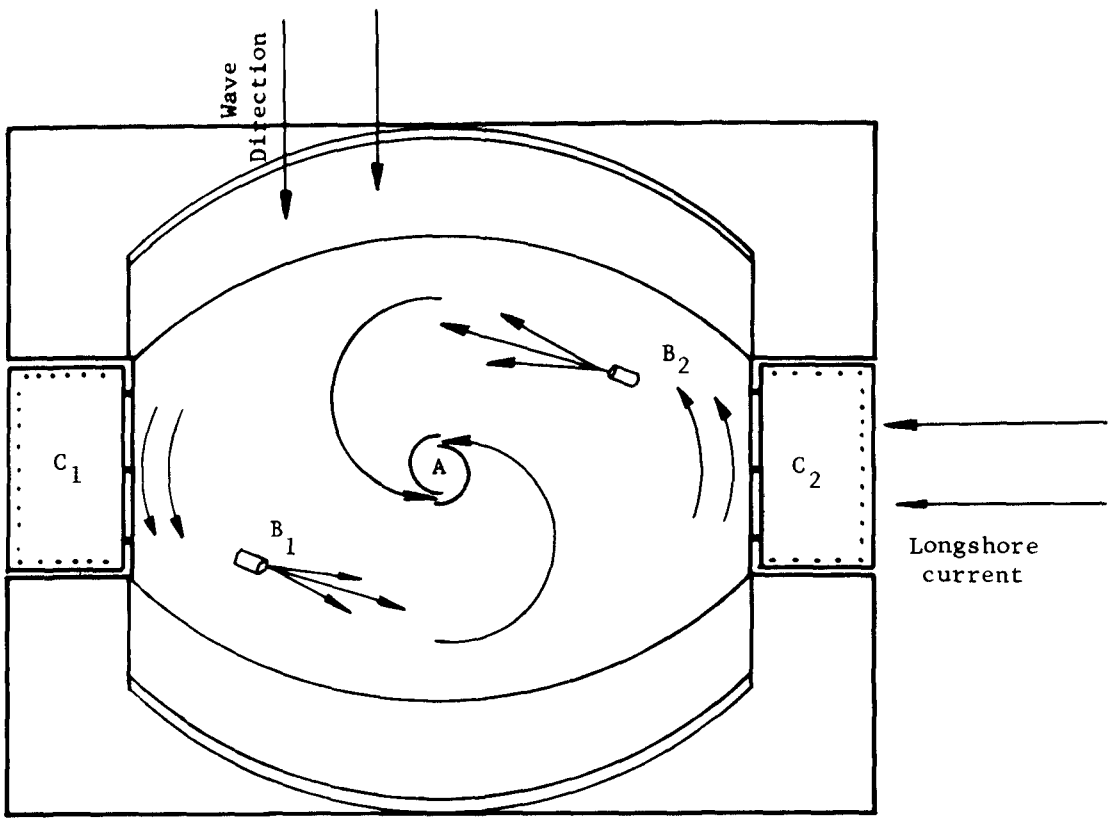

Operation:

Step 1. Close doors C_1 and C_2

2. Inject water at 15 psi at B_1 and B_2

3. Apply suction at A

4. Filter discharge from A for sand sample

FIG. 2. FLOW IN BED-LOAD TRAP

Most grains trapped in the period immediately following the dumping of tracer grains come from the area close to the pier as described below.

Assuming relatively heavy (measurable) concentrations, coated grains wil arrive at the pier in a stream which most likely will increase rather rapidly to a maximum value and then fade out.

When sheet layers of maximum concentration of coated grains have reached the pier, discharge of material from the injection area has its maximum value The corresponding maximum thickness of material arriving from the injection area is:

$$B_{max} = \frac{N}{n_{max}} \cdot \frac{n_{max}}{V_{n_{max}}} \cdot k_2 \qquad (2)$$

when N is the total number of grains trapped per unit time.

Next the assumption is made that the ratio $\frac{N}{n_{max}}$ is a characteristic value for release of material from the injection area valid for the various sheet-layers sliding on the top of each other with different velocities. Considering the fact that the tracer material spreads out on the bottom and mixes with non-coated grains, this assumption seems correct.

The total thickness of the fast moving sheet-layer (up to maximum concentration) may then be found by an integration:

$$B_{total} = \sum_{j=1}^{j=j_{max}} \frac{N}{n_{max}} k_2 \frac{n_j}{v_j} = k \frac{N}{n_{max}} \sum_{j=1}^{j=j_{max}} \frac{n_j}{v_j} \qquad (3)$$

where j refers to the number of sheet layers sliding on the top of each other.

The total quantity of material in all sheet-layers may be found by direct observation of the quantity Q_{total} trapped. The total rate of transport including fast as well as slow moving sheet layers is:

$$Q_{total} = Q_{fast} + (Q_{slow}) = k_2 \frac{N}{n_{max}} \sum_{j=1}^{j=j_{max}} \frac{n_j}{v_j} \cdot v_j + (Q_{slow}) \qquad (4)$$

The characteristics of the "slow" or "slower moving" sheet layer may be determined by continued long range observations beyond maximum concentration and will finally include the migrating humps of material which has erosion slopes updrift and deposit slopes downdrift.

In equation (4), the $\frac{N}{n}$ ratio is independent of the direction of travel of material (or direction of arrival of material to the bed trap) but the design of the trap must assure that the material is derived from the actual longshore movement of sheet-layer only and not from the drift perpendicular to shore. This is secured by exact longshore placement of the trap by the apron bottom protection around it and by its streamlining. Checks on proper functions are made by divers.

The detailed mechanics of the bed transport is complex and it is necessary to accept that records will demonstrate considerable irregularities. Two main factors may be responsible for this - the systems of migrating sand waves and the rip currents. Fig. 3 shows schematically how migrating sand waves on the bottom may interfere with the longshore drift when the instrumer pier is located on a crest and in a trough of a migrating wave (Fig. 3). Assuming that the littoral drift goes from left to right and that tracer material is dumped on the places indicated by A, B, C (crest located at pier) and I, II, III (trough located at pier). Figs. 3-b/c indicate the expected concentration of tracer particles from samples taken at the pier as function of time considering that the sand wave(s) are creeping from left to right and that this process causes higher drift on the updrift side of the wave th on the downdrift side, where some accumulation takes place or where the migrating sheet layer get thinner. The actual quantity of material trapped by the bed load traps on the pier will vary accordingly.

The indicated relative concentrations of tracer material in Fig. 3 are based on modes of transportation in rivers. While tracer material dumped at locations III, B and C may give useful results on the sheet layer movemen material dumped at I, II and A may be clogged or covered up to such extent that results may demonstrate very low concentration in the samples or perhap "no concentration at all" because almost all the tracer grains dumped were buried by the migrating sand waves. Meanwhile, by dumping of various color schemes in strips along the shore, knowledge will be gained about the mechan of movement of the migrating wave and the thickness of the sheet layers whic by-pass the migrating sand waves.

The share of responsibility for movement of bed load transport in sheet layers and in migrating bottom waves may depend greatly upon wave and currer conditions. Under calm or moderate wave conditions, a considerable higher percentage of migration may take place in the slow moving sand wave than unc more severe wave conditions, where the sheet movement may be dominating. I other words, the actual bed load movement will vary in quantity not only wi shifting wave and current conditions but also with the actual situation wit respect to migrating sand waves on the bottom. We may get an idea about th order of magnitude of the net sheet layer drift versus the net bulk drift i migrating waves by considering the situation at Fernandina Beach, Florida, N.E. Atlantic coast. Most likely most of the bed transport takes place inside the 20 ft. contour located approximately 300 yds. from shore. The net quantity moving southward is estimated to be approximately 400,000 cu yds/y or approximately 4 cu yds/yd/day. A migrating wave may move 1-2 yds per da in downdrift direction and its height above the bottom may be 1 yd. This gives quantities of averagely 1-2 cu yds/yd/day which in turn means that up to half of the total net bed transport may take place in migrating waves. Consequently, the irregularity in sheet layer transport may be of the order $\pm$ 50%. Most likely this figure is too high for most conditions in the fiel

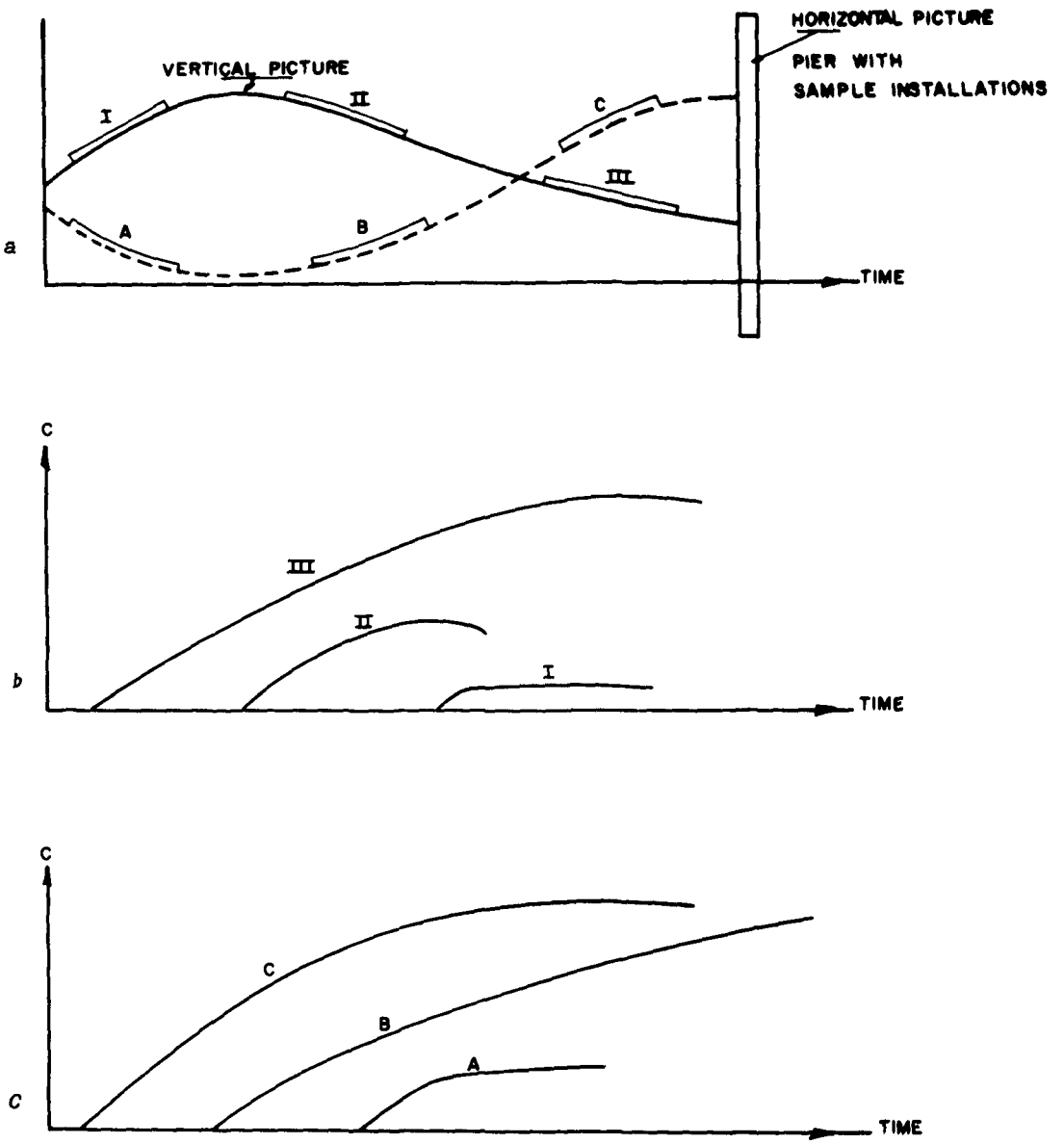

FIG 3 INTERFERENCES BY MIGRATING WAVES WITH LONGSHORE BED-LOAD TRANSPORT
(c=CONCENTRATION OF TRACER MATERIAL)

Another reasons for irregularity is the rip currents. Reference is made to Fig. 4. If no rip current exists at the pier, no difficulty will be encountered because the rip currents will transfer the material downdrift to its full extent. If they did not do so, a headland would be formed in the shore. Meanwhile, if the rip current is located at the pier, the concentration versus time diagram may become very confused and the trap would not give reliable results. This situation, therefore, must be avoided.

The research program in progress concentrates on moderate to heavy wave conditions and, so far, does not include general sampling over the bottom area contaminated by tracer particles. Such procedure would undoubtedly be of value in case of wave and current conditions causing a relatively slow bed load transport which makes it possible to follow the spreading of tracer particles on the bottom by continued sampling. The distribution of tracer particles may then be explored simultaneously. Ref. 21 mentions the so-called p-q statistical approach which proved to be useful for a laboratory channel. Most likely it will not have much bearing to conditions on a sandy seashore bottom. Another interesting theory by the Wallingford Laboratory (ref. 20) utilizes a theoretical approach by which the dispersion of tracer material by diffusion combined with advection is considered. The theory is applied for a shingle beach and the results seem reasonable even though the theoretical explanation so far seems to be of a speculative nature.

Sand particles are moving fast in the top sheet layer, which within a few hours may have traveled some few thousand feet.

Figure 5 demonstrates the results of a preliminary test on tracing from Fernandina Beach pier in N.W. Florida. Fifty pounds of tracer sand was dumped by diver on the updrift side of the pier at each of the depths 2.5 ft, 6 ft, and 6 ft depth (M.L.W.) at distances 50 ft (Station I, 125 ft (Station II) and at 200 ft from the M.L.W. line. Waves were in this case very moderate with $H_{1/3}$ = about 2 ft only. Distance of dumping place from the pier was 250 ft. Bed-load samples were picked up at the pier by scrapers and by a pump (suspended load). From Fig. 5 it may be seen that the samples (bed as well as suspended load) have a rather pronounced peak of concentration. Concentrations of 10^{-2} to 10^{-7} were recorded but after three hours concentrations were negligible or zero which probably is an indication of a very rapid sheet layer drift combined with burial of the tracer material. Initia velocities were highest in the uprush zone (up to about 0.5 ft/sec) and lowest in the trough inside the (not much developed) bar (about 0.1 ft/sec).

Scanning of the results are made by a photoelectric scanner. This instrument was developed for the purpose of accelerating the part of littoral sand transport research known as analyzing of samples.

In essence, the instrument provides a reduction in the time of analysis of fluorescent tracer particles concentration in samples. The scanner, in this process, differentiates for four colors simultaneously counting each and tabulating these counts. The mechanical principle lies in free fall during which the tracer particles mixed well with the uncoated sand are excited for their quality of fluorescence and this is detected by photocells. The resulting signal is decoded by a threshold decision logic circuitry into the proper color and guided for recording into its respective channel.

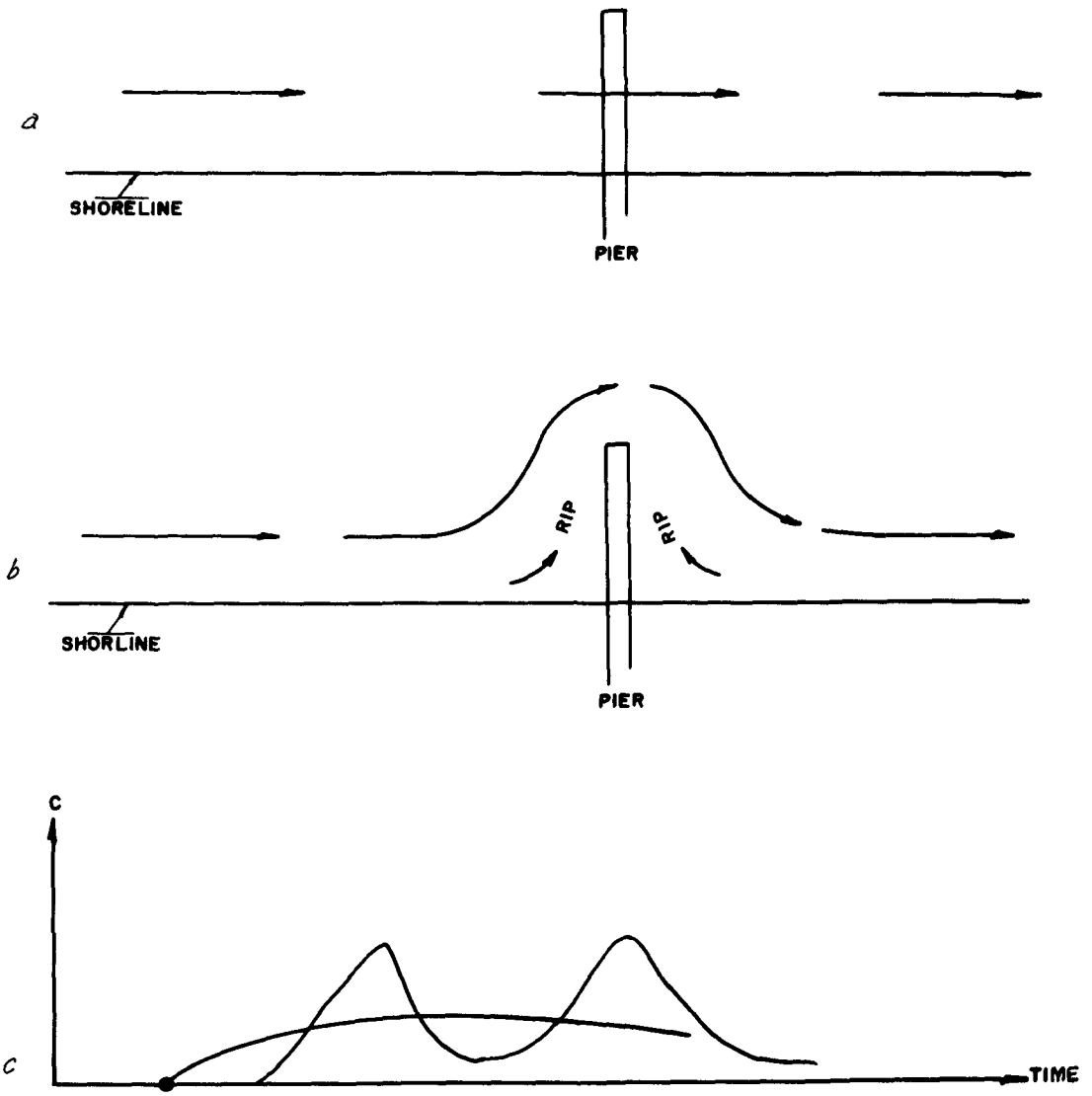

FIG 4 INFLUENCE BY RIP CURRENTS ON LONGSHORE SEDIMENT TRANSPORT

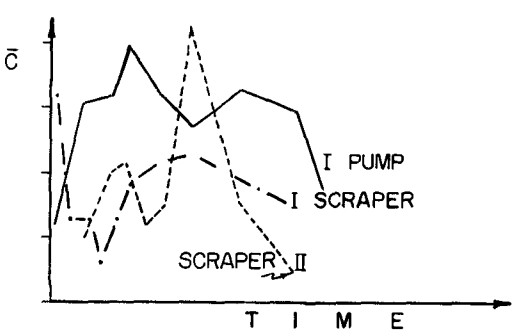

FIG 5 RESULTS OF PRELIMINARY TESTS
ON BED-LOAD TRACING

The rate of fall is variable between 20,000 - 40,000 particles per second.

The detectable colors are spectrally established. A change to another color, however, is possible using slight modification in the detecting assembly.

One difficulty associated with that kind of experiments is that tracers often have a very substantial coating which will not wear off easily. The result is that it may take several months before a tracer experiment can be repeated using the same colors as used at earlier experiments. This problem may be solved by the use of smaller quantities of tracers of a different color mixed up with larger quantities of the "basic tracer", e.g. red, red plus 10% green, red plus 10% yellow and red plus 10% blue; or red, red plus 50% yellow, red plus 50% orange and red plus 50% blue. If concentrations in a certain area are known from detailed sampling, one particular test may also be continued by mixing, e.g. red (concentration c_1) red (concentration c_2) and red (concentration c_3) with an equal amount of a different tracer and this procedure may even be continued by the use of more "indicator tracers". But sampling must be careful and the use of core samplers is necessary. Scanning has to be partly visual if the scanner is only able to handle a few colors.

TRANSVERSAL MOVEMENT OF MATERIAL

Material movements in the bottom profile are partly of long term feature caused by fluctuations of the sea water table and partly a seasonal fluctuation which is the reaction of the bottom profile to the seasonal chnage of wave and current action.

Ref. 5 and paper by Rhodes Fairbridge printed in these proceedings mention the interrelation between rise of sea level and beach erosion (shoreline recession). Ref. 5 explains that even small sea level rises (e.g. the eustatic rise of 1.2 mm per year) may cause shoreline recessions of 100 times the magnitude of the rise in Florida.

TABLE 1

Mean Dimension of Vertical Short-Term Seasonal Fluctuation, Tokai, Japan

0 - 6 meters	0 - 20 ft	0.0 meters
6 - 9 meters	20 - 30 ft	0.15 meters

TABLE 2

Mean Dimension of Vertical Short-Term Seasonal Fluctuation
Bovbjaerg, Danish North Sea Coast

0 - 6 meters	0 - 20 ft	0.40 meters
6 - 9 meters	20 - 30 ft	0.70 meters

Table 1 (Tokai, Japan) explains that seasonal fluctuations of bottom profiles with bar depth 3 meters corresponding to $H_{1/3}$ = 3.75 m (heavy storms) almost entirely takes place inside the 6 m (20 ft) depth contour where erosion and deposit balance each other (ref. 22). Table 2 (Bovbjaerg, Danish North Sea Coast) indicates that profile fluctuations with bar depth 4 m (13 ft) corresponding to $H_{1/3}$ = 5 m (17 ft)(heavy storms) take place beyond the 9 m (30 ft) depth contour. Migrating sand waves on the bottom are, however, in this case interfering with the seasonal fluctuation of the profile (ref. 3). Various research on the Californian shore indicate that although seasonal fluctuations are mianly restricted to the 0-9 m (0-30 ft) area the nearshore littoral drift may extend up to about 20 m (60 to 70 ft) depth.

Fig. 6 shows the bottom profile at Jupiter Island, S.E. Florida where, at present, tests on offshore dredging by dragline scraper are being run. Fluorescent sand material is dumped at various depths in the profile to check on the operation of the drag scraper.

Similar scraper tests have been carried out in England using a "submersible scraper" invented by the Hydraulic Experiment Station in Wallingford. Tests were rather successful but heavy equipment has so far not been put in action. In Florida the following basic equipment is involved: (a) a three-drum Sauerman drag scraper unit powered by a diesel motor; (b) a three cubic yard (2 m^3) bottomless crescent drag bucket; and (c) an offshore anchor arrangement including an anchored barge to which the dragline cables are attached. It is possible to shift the anchor barge from the shore. With the barge located about 300 m (1,000 ft) from shore, the excavation takes place about 200 m (700 ft) from shore at about 3.5 m (12 ft) depth. The production is about 50 m^3 (80 cu yd) per hour but may increase when more experience has been gained. Fig. 7 shows the scraper operation power unit and Fig. 8, the bucket on its way toward the beach filled with sand material scraped up in the offshore borrow area.

So far the tracer tests have shown that the scraper generally picks up its material where it is desired in the borrow pit, but that it may sometimes loose some material on its way to shore and then picks up new material closer to shore. Tracer material is injected in the pile on the beach and the migration of this material is being observed. At the same time the accumulation of material in the borrow area is surveyed in order to see how fast material is accumulated and what kind of material it is. Tracers of various colors are injected at various distances from the borrow hole. Aerial

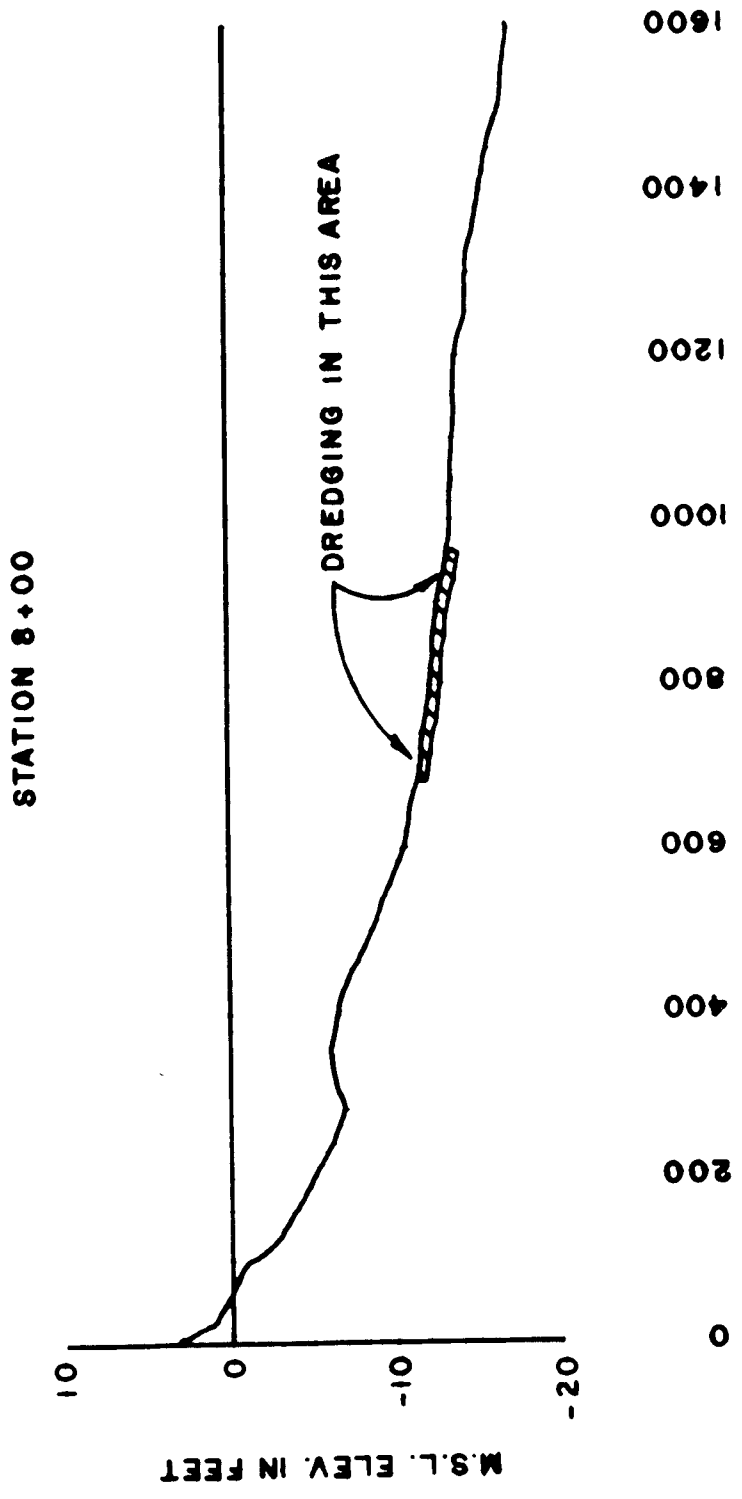

FIG 6 BOTTOM PROFILE AT JUPITER ISLAND, SE FLA.

FIG. 7. DRAG SCRAPER AT JUPITER ISLAND, FLA.: POWER UNIT

FIG. 8. BUCKET OF JUPITER SCRAPER ON WAY BACK TO SHORE LOADED WITH SAND

photography is also being used to observe the operation as well as the development of the borrow area after operation has been shifted to another area. The coastal protection at Jupiter Island is a combination of artificial nourishment by hydraulic dredge from the intracoastal waterway and lagoon behind the barrier, some short adjustable groins and revetments as described in ref. 8.

An evaluation of the efficiency of such scraper operation includes technical as well as economical aspects. Technically, the possibilities for return of material dredged in the offshore bottom and dumped on the beach to the offshore bottom (perhaps in the holes where it came from) must be evaluated. At the same time the cost of the dredging operation must be considered. Even if the possibility for return of material to, say, 8 m (25 ft) depth is only 1/3 of the possibility for return of the material to 5 m (15 ft depth, the price of dredging at 8 m (25 ft) depth (by suction type dredge in offshore waters) may be four times the price of dredging at 5 m (15 ft) depth (by scraper) and, therefore, dredging at 5 m (15 ft) is still to be preferred for dredging at 8 m (25 ft) depth which may be found at much greater distance from shore.

Example - Based on preliminary consideration partly of theoretical nature considering the adjustment of an equilibrium beach and bottom profile to a new and higher water table (ref. 5) and partly based on actual - but still inadequate - field observations, the possibility for return of materia from the beach to a certain depth y is given by the expression:

$$F_1 = e^{\frac{-D}{(D-y)}} \qquad (11$$

in which D is the limiting depth for short term ("seasonal") fluctuations of the bottom profile. The price of bringing the material to the beach is base on preliminary experience given by the expression:

$$F_2 = 0.125\sqrt{y} \qquad (12$$

in which y is the depth in meters. For example the cost at 1 m (3 ft) depth may be \$0.125 per cu yd (bulldozer) and the cost at 4 m depth (13 ft) may be \$0.25 per cu yad (developed drag scraper operation) while the cost at 9 m depth (30 ft) may be about \$0.40 per cu yd (large quantities by hydraulic dredge which may discharge through pipe located on the bottom). My multiplication of expressions (11) and (12):

$$F_1 \times F_2 = 0.125\sqrt{y}\, e^{\frac{-D}{(D-y)}} \qquad (1$$

Equations (11), (12) and (13) are depicted in Fig. 9. Expression (13) indicates the relative benefit of dredging of material for nourishment at vario depth omitting the extremes (0 and D depths). It may be seen that dredging at depth D_y is the most expensive procedure while dredging at depths D_x and D_{xx} are of equal benefit because probability and unit price by multiplicati give the same result.

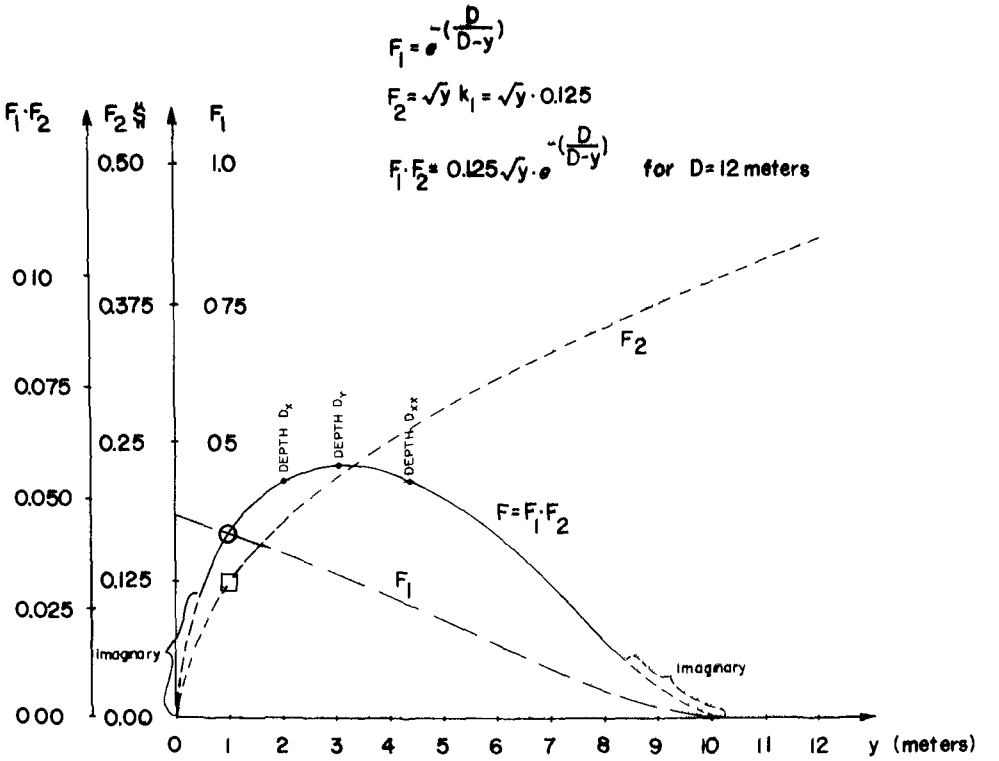

FIG 9 RELATIVE BENEFIT FROM DREDGING OF MATERIAL AT VARIOUS DEPTHS IN A BOTTOM PROFILE

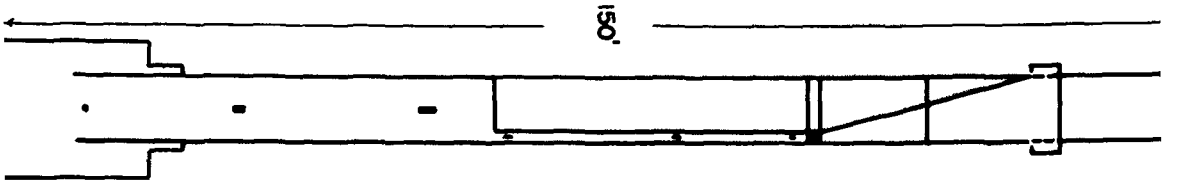

PLAN

FIG. 10. WAVE TANK FOR TESTS ON BED-LOAD TRANSPORT BY WAVES AND CURRENTS

At this time, results available for checking of the validity of equations 11 to 13 are inadequate. It is clear that only average values may be obtained and that results of single extreme storms may deviate considerably from the average. It should be mentioned that the development of a hydraulic dredge for operation in open seas and discharging to shore through submerged pipeline is progressing. So far, tests are being run by the U. S. Army Corps of Engineers using a converted dredge, the U. S. Comver.

LABORATORY RESEARCH

It is clear that the results of field experiments with bed and suspended load are only valid for the (often complex) conditions under which these experiments were run and in order to gain information useful in practice a great many results under a variety of wave and current conditions are needed. These results must link wave and current characteristics to sediment transportation characteristics. Concerning the hydraulic hcaracteristics, reliance should not be placed on generalized wave and flow patterns alone but efforts should be intensified to determine more detailed data, such as bottom velocities, their directions and fluctuations, turbulence in the grand as well as the small scale. This information in detail is difficult to obtain in the field but may be determined in the laboratory by "prototype experiments" as described below.

TRANSPORT BY WAVE ACTION

Several experiments have been made in flumes on transportation of bed material by wave action and on the distribution of velocities including mass transport velocities. Ref. 21 mentions tests in a wave flume. Near the sand bottom within certain limits of steepness, the bottom drift was always in the direction of propagation of wave action. So was the drift in the water surface, while in the middle drift was seaward or against direction of propagation of wave action.

Similar experiments by Lhermitte (ref. 17) consider the formation of ripples and the influence of viscosity in the bottom boundary layers. These tests do not mention specifically the damping effect caused by loss of energy by friction between fluid and bottom. The friction parameter depends partly upon the bottom configuration (ripples, dunes, smooth, etc.) and partly upon whether the undulating boundary is non-movable or movable. Water velocity and particle velocity cannot be measured separately unless the material is very fine (wash-load) in which case the sediment and water particle velociti are identical.

TRANSPORT BY WAVE AND FLOW ACTION

Propagation Unidirectional

Inman and Bowen (ref. 14) mention tank research on waves and currents running over a sand bed using Bagnold's (refs. 1 and 2) transport formula:

$$i_\Theta = kw \frac{u_\Theta}{u_m} \qquad (14)$$

where i_θ is the dynamic transport rate of sand which results when wave stress places sand in motion in the presence of a current, w is the decrement in transmitted power of the waves attributable to bed drag, u_θ is the steady current flowing near the bed in the direction of the wave travel, u_m is the maximum horizontal component of the orbital velocity near the bed and k is the dimensionless coefficient of proportionality. Traps were installed in the sand bottom and the net transport was determined by subtracting the amount of sand trapped at the upwave end of the bed, from that trapped at the downwave end. Estimates of the power expended by the waves was obtained from the decrement in wave height as the wave traveled over the sand bed. The decrement in wave height was found to be about 10^{-3} per unit of distance traveled. Preliminary calculations showed that about one tenth of the total power expended by the waves was in transporting sediments. For low values of the current, a consistent relationship was found between the energy loss of the waves and the work done in transporting the sediment over the bed. Further increases of current velocity created complex flow conditions over the ripples and the theoretical assumptions were no longer valid. Future research was, therefore, recommended to include detailed studies of the current picture.

Wave and Current Action Operating Under An Angle With Each Other

Wave action may be operating under various angles with current activity. Inasmuch as a current running parallel to shore has to turn 90 degrees in order to enter a coastal inlet, angles between current and wave direction of 0 to 90 degrees may occur in the inlet entrance. Longshore currents and wave action responsible for the longshore current activity on the open seashore are not far from being perpendicular to each other.

The relative importance of the two sediment agitating water movements have to be considered. As long as the longshore current movement is predominant it may be expected that it will be associated with friction factors valid for unidirectional flow under similar bottom conditions.

The longshore current theory by Bruun (ref. 7) and by Chiu and Bruun (ref. 9) is based on the statistical distribution of wave heights. It has two approaches. One, "the rip current continuity approach" refers particularly to moderate velocity longshore currents caused by waves of smaller angles of incidence of wave crests.

The other approach is called "the slope continuity approach" and is based on inflow of water from wave breaking under a certain not too small angle with the shoreline which creates a longshore "hydraulic slope" of the water table corresponding to an ideal situation by which the entire cross section of the trough between the bar and the beach has a uniform distributed energy head. The difference between the assumed and actual situation must be expected to reveal itsel in the way that computed currents are on the high side.

With respect to friction factors, it will probably depend upon the relative importance of the longshore current velocity and the velocities of the wave agitated water particles. Both factors are of importance for current and for the littoral drift by action of waves and currents.

With wave action only, the decrement in transmitted power $\frac{dP}{dx}$ may be obtained when the decrement in wave height per unit of distance traveled $\frac{dH}{dx}$ is known. One has:

$$\frac{dP}{dx} = \tfrac{1}{4} \rho g H \frac{dH}{dx} \cdot C_n \tag{15}$$

where C_n is the group velocity. Inman and Bowen (ref. 14) observed that the distribution in wave height was approximately exponential:

$$H = H_i \, e^{-ax} \tag{16}$$

where H_i is the initial wave and e is the attenuation coefficient $\frac{dP}{dx} = w$ in equation (14) which must be a function of $(\tau_{\text{bottom shear}})^{3/2}$. If no suspended load is being transported, Bagnold (ref. 2) writes the bed-load transport relation as follows for unidirectional flow:

$$\Phi_b = A^1 (\theta - \theta_t)\theta^{\frac{1}{2}} \tag{17}$$

in which Φ_b is the bed-load transport function =

$$\frac{Q_b}{6D\sqrt{\gamma/\rho}} \; \frac{(\tan \alpha_o - \tan \beta)}{\tan \alpha} \; \frac{1}{\sqrt{2 \tan \alpha/3\psi}} \tag{18}$$

Q_b = volume transport per unit flow per unit time, ρ = density, D = grain diameter, $\tan \alpha_o$ is the dynamic shear stress ratio just over the bed surface, $\tan \alpha$ is the shear-stress ratio for the grains (friction angle), β = the declination of the bed surface, ψ = the drag coefficient of a single isolated grain, A^1 is a numerical transport-rate coefficient, $\theta = \tau/\gamma$ where τ is the overall (measurable tangential bottom shear stress consisting of a component due to influence of grain on grain and a tangential stress in th grainless fluid, modified by presence of dispersed grains. Quantity θ_t is the general threshold value = τ_t/γ where τ_t is the non-efective applied tangential stress on the stationary bed surface (ref. 4).

Without going into details, equations (14) and (17) demonstrate certain similarity. Adding the shear stresses "tearing loose ability" and taking into consideration the material transport, one gets for quantity of material transport:

$$M = \text{Function} \left(\frac{K_{1tv} \sqrt{\tau_1^2 + \tau_{tv}^2}^{\beta} U_{tv}}{U_{mtot}} \right) \tag{19}$$

where K_{ltv} is a combination of K in equation (14) and a corresponding coefficient for drift by unidirectional flow including soils characteristics as mentioned in Bagnold's bed-load expression. U_{tv} is the velocity of the transversal (transporting) current and U_{mtot} is the maximum vectorial current velocity occurring during one cycle of the wave motion assuming a longshore current of a certain average value. This, in turn, is another "ideal" assumption.

Tests sponsored by the National Science Foundation are now in progress at the Coastal Engineering Laboratory of the University of Florida on littoral drift with a current running parallel to, as well as perpendicular to, the wave action. In all tests the current conditions at the bottom correspond to prototype conditions with water particle velocities of about 0.5 m per sec. maximum.

Figures 10 and 11 show the wave tank. A partition wall separates it in a 2 ft wide and 4 ft wide section. Bed-load traps are installed on the bottom and current velocities are measured partly by a propeller instrument (minimum 2 cm/sec) and partly by photographing buoyant particles (amber). With waves passing down through the tank, currents are run along as well as perpendicular to the direction of wave propagation. The latter is possible because of the T-shaped end of the wave tank where a longshore current is generated by the circulation system indicated in Fig. 11. To avoid eddy formation and dispersion of sand material from the bottom in the upper water layers of the tank, a plastic sheet is put in about 15 to 20 centimeters above the bottom. The longshore current runs below said sheet which does not disturb the general motion of water particles in almost closed paths but hinders the development of free turbulence between the two bodies of water above and below it. This arrangement would be rather fatal to the study of suspended load movement, but inasmuch as the space left between the sheet and the bottom is outside the saltation zone, the sheet will not have much influence, if any at all, on the bed-load transport.

Velocities and velocity profiles close to bottom are measured with fixed (mortared) as well as loose bottom in all the experiments with waves parallel to, as well as in experiments with wave and current action perpendicular to each other. Information on friction parameters are obtained hereby and by measuring head differences.

Bed-load traps and fluorescent tracers are used to detect details of the movement which takes place in sheet layers as well as in sand waves of varying dimensions. Several colors are used injected at different distances from the trap to trace movements in sand waves as bed load. Scanning of the results are made by the photoelectric scanner described earlier in this paper. Results to these tests will be available in the course of 1965 (ref. 15).

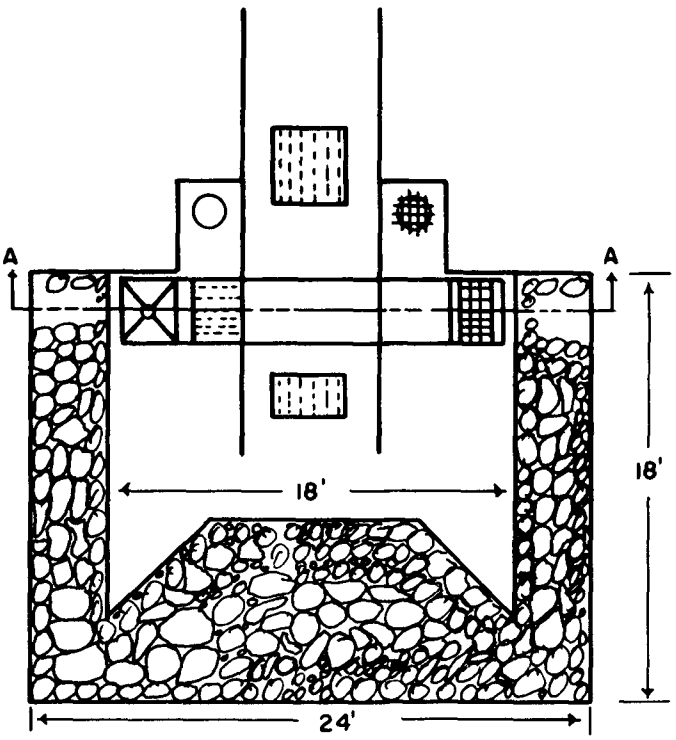

DIFFRACTION BASIN

SEC AA

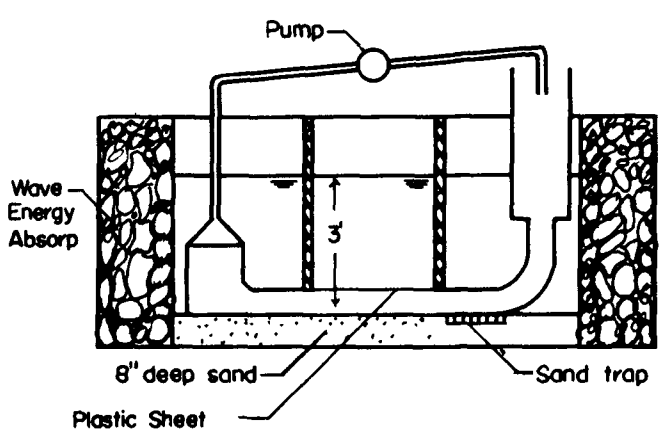

FIG. 11. CROSS SECTION OF WAVE TANK FOR TESTS ON BED-LOAD TRANSPORT BY WAVES PERPENDICULAR TO CURRENTS

REFERENCES

1. Bagnold, R. A. (1956) "The Flow of Cohesionless Grains in Fluids", Royal Soc. London Trans., Ser. A, Vol. 249, pp. 235-297.

2. Bagnold, R. A. (1956) "The Flow of Cohesionless Grains in Fluids", Royal Soc. London Trans., Ser. A, Vol. 245, pp. 235-297.

3. Bruun, P. (1954) "Migrating Sand Waves or Sand Humps, with Special Reference to Investigations on the Danish North Sea Coast", Coastal Engineering No. V, Council on Wave Research, Berkeley, pp. 269-295.

4. Bruun, P. (1962) "Engineering Aspects of Sediment Transport", Reviews in Engineering Geology, Vol. I, pp. 39-103.

5. Bruun, P. (1962) "Sea Level Rise as a Cause of Shore Erosion", Jour. of the Waterways and Harbors Division, Proc. Am. Soc. Civil Engineers, WW1.

6. Bruun, P. and Battjes, J. (1963) "Tidal Inlets and Littoral Drift", IAHR Conference, London, Paper No. 1.17

7. Bruun, P. (1963) "Longshore Currents and Longshore Troughs", Jour. of Geophysical Research, Vol. 68, No. 4.

8. Bruun, P. (1964) "New Trends in Revetment Design", The Dock and Harbour Authority, London, Feb. 1964.

9. Chiu, T. Y. and Bruun, P. (1964) "Computations of Longshore Currents", Florida Engineering and Industrial Experiment Station, Technical Paper No. 279, Vol. XVIII, No. 3, Presented in Lisbon, June, 1964.

10. Einstein, H. A. (1948) "Movement of Beach Sands by Water Waves", Trans. Am. Geophys. Union, Vol. 29, No. 5, pp. 653-655.

11. Einstein, H. A. and Chien, N. K. (1955) "Effects of Heavy Sediment Concentration Near the Bed on Velocity and Sediment Distribution", Univ. of Calif., M. R. D. Sediment Series No. 8.

12. Griesseier, H. (1959) "Uber die Verwendung von Luminoforen beim Studium der litoralen Materialbewegungen", Excerpt from Acta Hydrophysica, Vol. 6, No. 1, Inst. fur Phys. Hydrog. der Deutschen Akad. der Wissenschaften, Berlin.

13. Hydraulics Research Station (1960) "The Production of Fluorescent Tracers for Detecting the Movement of Sand and Shingle", Hydraulics Research Station, Howberry Park, Wallingford, Berkshire, England.

14. Inman, D. L. and Bowen, A. J. (1963) "Flume Experiments on Sand Transport by Waves and Currents", Coastal Engineering No. 8, Proceedings Conference in Mexico, 1962, U. S. Council on Wave Research, Berkeley, Calif.

15. Kamel, A. and Bruun, P. (1965) "Prototype Experiments on Littoral Drift in Wave Tank", (manuscript).

16. Lane, E. and Eden, E. W. (1940) "Sand Waves in the Lower Mississippi River", Jour. Western Soc. of Engrs., Vol. 44-45, No. 6, pp. 281-291.

17. Lhermitte, P. (1958) "Mouvement des Materiaux de fond sous l'action de la houle", Coastal Engineering No. VI, Council on Wave Research, Berkeley, pp. 211-261.

18. Longuet-Higgins, M. S. (1953) "Mass Transport in Water Waves", Phil. Trans. Royal Soc. London, Series A, No. 903, Vol. 245, pp. 553-581.

19. Manohar, Madhav (1955) "Mechanics of Bottom Sediment Movement due to Wave Action", University of California, Ser. 72, Issue a.

20. Rance, P. J. (1963) "The Determination of Quantities of Sediment Transport in Oscillating Motion by Consideration of the Dispersion of Tracer Sediment", IAHR Congress, Longon, Paper No. 1.25

21. Russell, R. C. H. and Osorio, J. D. C. (1958) "An Experimental Investigation of Drift Profiles in a Closed Conduit", Coastal Engineering No. VI, Council on Wave Research, Berkeley, pp. 171-193.

22. Sonu, C. and Hom-ma, M. (1962) "Rhythmic Patterns of Longshore Bars Related to Sediment Characteristics", Proc. 8th Conference on Coastal Engineering, Council on Wave Research, Mexico City.

23. Thierry, J. W. and van der Burgt, J. H. (1949) "Report to the XVIIth International Navigation Congress", S-II, C-I, pp. 135-156.

24. Zenkovitch, V. P. (1960) "Fluorescent Substances as Tracers for Studying the Movements of Sand on the Sea Bed", (Experiment conducted by the U.S.S.R.) "Dock and Harbour Authority", Vol. 40, No. 471, London, January, 1960.

25. Zenkovitch, V. P. (1962) "Application of Luminescent Substances for Sand-Drift Investigations in the Nearshore Zones of the Sea", De Ingenieur, Bouw-en Waterbouwkunde No. 7, March, 1962 (Netherlands), pp. 81-89.

Chapter 19

ATTRITION TESTS OF NATURAL AND REDEPOSITED SHINGLE BEACHES

J. Duvivier
Senior Partner, Lewis & Duvivier, Consulting Engineers,
Westminster, London.

SUMMARY

Administrative difficulties sometimes inhibit the transfer of beach shingle from areas where there is a surplus to areas where there is a shortage and it may be necessary to form an artificial beach of ballast dug from an inland pit or of quarried stone to reinforce the defence works or as a substitute for them.

Coast erosion may be caused by a seasonal reversal of the prevailing drift, or by the protection of a previously eroding frontage up-drift, or by building harbour works, or by attrition of beach material, and the recharging of a beach with imported stone may be a cheaper and more satisfactory all round solution than the progressive underpinning of sea walls.

Nevertheless it can be a costly expedient and it is necessary to be able to compare the resistance of the imported material to loss by attrition with the behaviour of the natural beach material.

The paper describes some simple tests which were carried out in an attempt to evaluate the relative resistance of various quarried stones and natural beaches to attrition.

INTRODUCTION

There is no better protection to a coast against sea erosion than a natural beach of hard shingle or sand, and at places where there is a steady inflow of fresh material to compensate for material that is lost by outward drift or by other causes erosion problems do not exist.

Where the average rate of inflow by littoral drift is on balance less than the outflow it may be necessary to have recourse to coast protection works such as sea walls and groynes, or to artificial beach nourishment, or a combination of the two in order to preserve the status-quo.

Artificial nourishment may involve merely transferring shingle or sand from parts of the coast where there is a surplus to places where there is a shortage; if there is no surplus available within an economical hauling distance, the material for recharging must be quarried, excavated or dredged

from an inland or offshore source and transported and dumped on the shore.

There are difficulties about transferring shingle from one part of a populated coast line to another, even when both places are within the administrative area of one Authority, as people who own properties bordering on the sea usually object to the transfer of what they consider to be their beach to other parts of the coast for the protection of other people's properties.

The outflow of shingle from a beach by littoral drift, and the resulting exposure of the underlying strata to erosion by the sea, is sometimes an intermittent or a seasonal occurrence. For example, the dominant winds and the resultant drift on the Durham Coast are on balance from north, to south but during the three successive winters of 1958, 1959 and 1960 the dominant wind was from south to north with the result that much of the shingle below the cliffs to the north of the harbour was moved northward towards Sunderland and fresh material was unable to move in from the south due to the obstruction caused by the harbour breakwaters.

A state of accretion or of stability may be changed to a state of erosion by the construction of sea defences up-drift. For example, the stabilisation of the coast in front of the town of Aldeburgh, Suffolk, by means of groynes and a sea wall has given rise to an erosion problem to the south which is causing the River Board some concern. The stabilisation of the North Shore of Bathurst, Gambia, by groynes and laterite revetments between 1957 and 1960 has given rise to a state of erosion at the eastern end of the sandspit on which the town was built.

The denudation of a shingle beach may give rise to foundation problems in cases where the exposed substratum consists of soft and easily eroded material such as silty sandy clay.

A few years ago the clay substratum at Hayling Island (Hampshire) and Fleetwood (Lancashire) was eroded during the course of a single storm to depths of 6 to 7 feet and the sea walls at these places were breached.

Even rock can be a deceptive foundation for a sea wall. The new Seaham wall was founded on Magnesian Limestone, yet the limestone seaward of the wall was eroded to such a depth during the period of exposure referred to in an earlier paragraph that it was subsequently necessary to extend the wall foundations down to a substantially lower level by means of sloping concrete aprons and the groynes also had to be underpinned.

However, the long-term solution to a problem of

this nature is not to be found in the progressive underpinning of a sea wall to an ever increasing depth. Apart from the difficulty and expense of building sea defence works under tidal conditions in exposed situations and the difficulty and expense of maintaining them, a narrow beach which is submerged except at low tide is of little use to the public, the strain and wear and tear on the defences is greatly increased, sea front property is drenched with spray and continuous expense is incurred in clearing shingle and weed from promenades and roadways after storms.

A possible solution to such problems is to recharge the beach with imported stone, to contain as much as possible of the recharged material against lateral displacement by means of groynes and to import fresh material from time to time under a maintenance programme to replace shingle that escapes over the groynes, or round their outer ends, or that is ground away and lost by attrition.

An artificial flint beach 6 feet high and 90 feet wide with a slope of 1 in 15 may cost up to £10 per foot of frontage to create. Groynes to contain it would cost about another £12 to £15 a foot.

Artificial replenishment can therefore be a costly expedient and it is necessary to weigh the cost against the probable life of the material which must be tough, chemically inert and of a suitable size for placing on beaches which may be used by the public.

The rate at which shingle is wasted by attrition depends upon the hardness of the material, its size and the extent to which wastage occurs by the impact and attrition of one wave-driven stone upon another, or by the impact of the shingle upon a concrete or granite faced sea wall.

To restore and maintain a shingle beach to its original form by recharging with imported stone it is necessary to compare the properties of the imported material with those of the natural material. If the rate of wastage of the natural beach is known, it is possible to form a rough estimate of the quantity of recharge material that will be required provided the comparative properties of the two materials are known.

Usually the rate at which a shingle beach wears away by attrition is not known although it could probably be determined by a suitable full scale experiment extending over a number of years. However, it is not usually possible to wait upon long-term experiments before prescribing a remedy to a sea defence problem.

In certain cases where the beach as a whole is and has been for many years confined laterally between clearly defined limits (e.g. Aberystwyth, North Shore) and record sections have been taken at intervals for a number of years, the rate of loss by attrition, i.e., the rate at which shingle is reduced to fine sand and silt can be roughly estimated.

Tests were carried out by the author's firm recently to compare the relative rate of wastage of various types of material comprising samples of quarried stone, mine waste and natural beach shingles from various parts of the coast.

Samples were taken from four sites, one on the east coast, two on the west and one on the south coast.

At Site 1, Selsey, Sussex, the beach consists of rounded flint pebbles of varying size from about 3 inches down; the pebbles were derived originally by attrition from large angular flints eroded from the chalk but the recent beaches consist of pebbles eroded from glacial period deposit in the cliffs. Selected samples were tested for comparison with the less durable shingle and stone available elsewhere.

At Site 2, Seaham, Co. Durham, the beach material consists of a mixture of siltstone, limestone and Dolerite pebbles, derived partly from erosion of the Magnesian Limestone of which the cliffs are composed and of the Boulder Clay which overlies them. The Magnesian Limestone pebbles have a short life compared with the Lower Carboniferous Limestone and other stones. Large quantities of shingle were removed several years ago for the construction of breakwaters at Seaham Harbour. Much of the remaining material has been lost by attrition.

The only stone that is available in sufficient quantities at an economical price for recharging the beach consists of Coal-Measure shales and sandstone from local collieries, two of which are situated at a short distance from the coast.

The material from the collieries naturally varies in composition and quality; the best material, known locally as "Post-Stone", is a fairly hard light grey sandstone and is found mainly when cutting drifts from one level to another. The supply of this material is consequently uncertain and the quantity available at the pit heads is small.

Very large quantities of shale, with varying amounts of Post Stone are, however, available from the coal seams and this was found to be the only material which could be obtained at an economic cost. Some of the larger material is sorted below ground before being sent to the surface and is known as "Pit Stone", but the bulk of the waste

material is brought out mixed with the coal and is sorted on the surface, the larger pieces of stone being removed by hand on the picking belts and the remainder in the washing plant.

For nearly a century the mine waste has been tipped indiscriminately on to the shore south of Seaham Harbour and an appreciable area has been reclaimed from the sea by this method, the rate of tipping having been in excess of the rate of loss by attrition which, in the case of shale, is considerable.

At Site 3, Aberystwyth, West Wales, the beach consists of flat elongated fine-grained sandstone pebbles of various sizes from 6" down to sand, together with small quantities of shale. For several years the rate of beach regeneration by littoral drift has been substantially less than the loss by attrition and the sea wall at the north end of the town has had to be reinforced by means of a low level sheet piled granite-paved apron which has been costly to maintain.

Material for replenishing the beach is obtainable in unlimited quantities from the cliffs north of the town and from outcrops situated within the town itself, and consists of alternating bands of fine grained sandstone and shale.

The shale has a short life compared with the sandstone and in calculating the amount of recharge material it is necessary to make allowance for their relative resistance to attrition and to the relative proportions of the two materials at the quarry face.

At Site 4, Fleetwood, Lancashire, the shingle contains a high proportion of hard igneous pebbles derived partly by erosion of the underlying Boulder Clay and partly by erosion of the cliffs north of Blackpool. The latter are now protected by sea walls over the whole of this seven mile stretch of coast and the loss by attrition has in recent years exceeded the rate of regeneration by littoral drift, and erosion of the Boulder Clay and gravel deposits and the quantity of residual material has been insufficient to cover and protect the underlying soft silty sandy clay against erosion. As a result the foreshore has been progressively lowered and it has been necessary to extend the sea wall foundations downward and seaward by stages by building sloping granite aprons in order to prevent the walls from being undermined. Beach loss by attrition has been accelerated since these aprons were built and the aprons themselves have been costly to maintain.

Large quantities of shingle were excavated from places where there was a surplus and redeposited at places where there was nothing but a shifting layer of sand over the underlying clay.

THE TESTS

The tests were carried out by placing weighed and graded samples of each material (between 40 and 50 lbs. of each) in a revolving steel drum and re-weighing and re-sieving the residue at 3, 6 and 9 hour intervals.

A 14/10 Stothert and Pitt concrete mixer was used for the tests. All except two opposite blades were removed and the filling skip and discharge spout were replaced by steel cover plates. A drain plug for washing out fine residue was welded into the perimeter of the drum.

Each sample was weighed, graded and placed in the drum with two gallons of water and the machine was then run for 3 hours at a constant speed of 19 r.p.m. The sample was then removed from the drum, all fine sand and silt below No.14 sieve discarded and the residue weighed and regraded.

The residue above No.14 sieve was then replaced in the drum and the procedure repeated for two further three hour tests. The reason for removing all but two of the blades was to simulate both the rolling and impact forces to which beach shingle is subjected by waves.

The results of the tests are shown in Fig. 1. The percentage weight of the residue above No. 14 sieve is plotted against duration of test in hours.

In each test the samples containing the largest stones showed greater percentage losses than samples of similar materials of smaller size. Presumably the heavy stones fracture more readily than the small ones and the sharp fractured edges are worn away rapidly until the stones acquire the characteristic rounded shape of beach pebbles.

The softer materials which arrived as large broken lumps broke down very quickly into lozenge shaped pebbles up to about 2" long. Until this stage was reached fractured faces could still be seen.

The most resistant of all samples were the fine flint pebbles from Selsey C2. This material which initially was graded from $\frac{3}{4}$" down to 3/16" produced only 10% of fines below No.14 sieve after 9 hours wear. Coarse flint pebbles C1 with an initial grading from $1\frac{1}{2}$" down to $\frac{3}{8}$" produced 45% of fines. The rate of wear of sample C1 was greatest in the first 3 hours. It continued to wear at a faster rate than C2 for the remainder of the test. The behaviour of mixed flint pebbles (sample C3) was intermediate between C1 and C2.

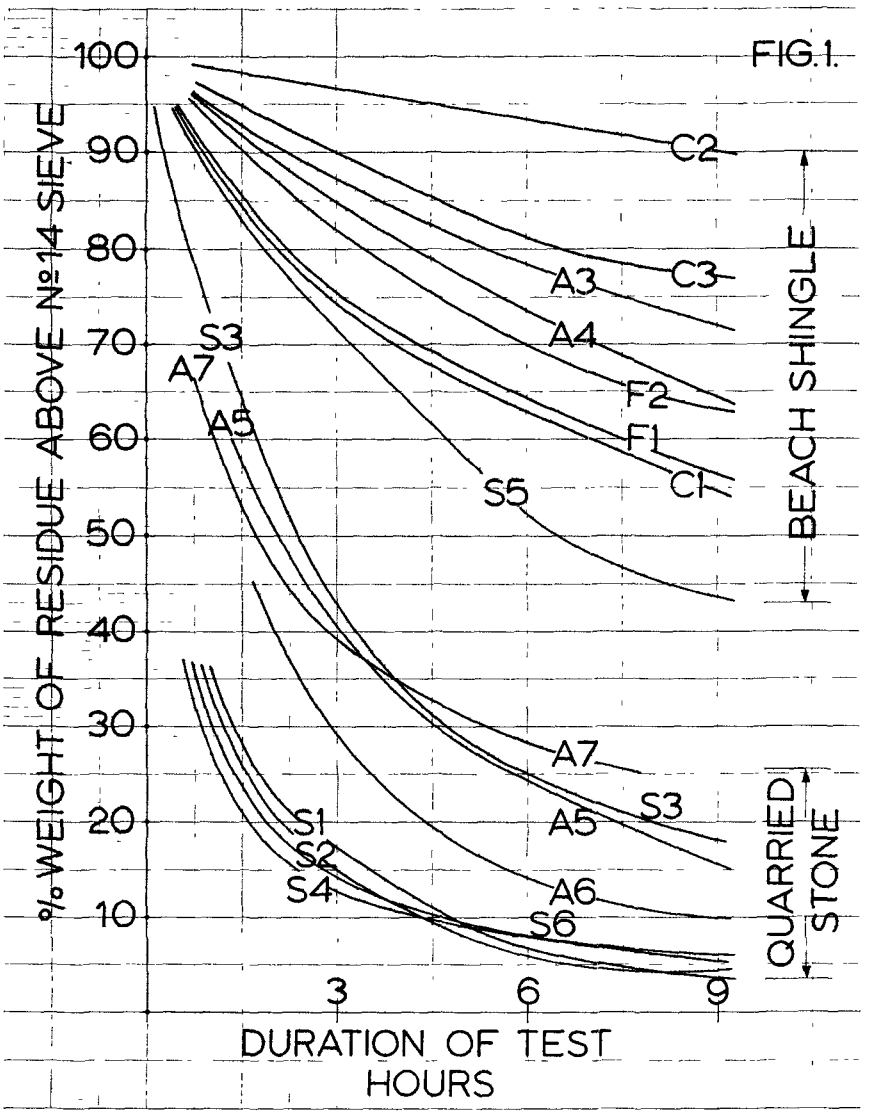
FIG.1.
% WEIGHT OF RESIDUE ABOVE No 14 SIEVE
100
90
80
70
60
50
40
30
20
10
C2
A3
C3
A4
F2
F1
C1
S3
A7
A5
S5
BEACH SHINGLE
A7
S3
A5
S1
S2
S4
A6
S6
QUARRIED STONE
3
6
9
DURATION OF TEST
HOURS

The highest percentage losses occurred with samples of mine waste from the collieries at Seaham and a hand-picked sample of Magnesian Limestone pebbles from the beach north of Seaham Harbour. The results of the Seaham tests were as follows:-

Serial No.	Origin	Description	Composition	Size	% loss after 9 hours
S1	Vane Tempest Colliery	Pit Stone	Mainly grey shale but with some siltstone (Post Stone) fairly clean.	8" down to $1\frac{1}{2}$"	96
S2	"	Picking belt chippings	As above but not so clean	6" down to $1\frac{1}{2}$"	97
S3	"	Wet Shale	Mainly grey oily shale with some coal	3" down to $1\frac{1}{2}$"	82
S4	Dawdon Beach Tip	Pit Stone	As S1 but picked by hand from the Coal Board tip at Dawdon	4" down to $\frac{3}{4}$"	95
S5	Seaham	Average natural shingle	Siltstone, limestone and Dolerite	3" down to $\frac{3}{4}$"	56
S6	Seaham Beach	Selected pebbles	Limestone	6" down to $1\frac{1}{2}$"	94

It will be seen that by comparison with the natural shingle of Seaham Beach (S5), the mine refuse from Vane Tempest and Dawdon has a short life and that some 11,000 tons of this material would have to be placed on the beach to replace every 1000 tons of natural beach shingle worn away by attrition. The limestone pebbles (S6) are seen to be useless as a beach material and as mine refuse is the only material available in large quantities and it costs only 3/- a ton to dig, transport and dump it on the beach,

the local authority was advised to carry out a massive initial recharge of the beach, to contain the tipped material between massive groynes so that it is retained at places on the Seaham coast line where concentrated erosion of the underlying bed rock had occurred and to maintain the beach in a healthy condition by recharging month by month at a rate in excess of the rate at which the material wears away.

Sample (S3), showed 13% less loss than the other mine waste samples, due presumably to the fact that it was composed of finer material than the other Seaham samples.

Somewhat similar results were experienced with comparative tests between natural beach shingle in two sizes and quarry stone and quarry waste from Aberystwyth (Samples A3, A4, A5, A6 and A7).

The natural shingle is flat and rounded and varies from 6" to 8" dia. down to $\frac{1}{4}$" material and sand. Samples A3 and A4 were respectively fine ($1\frac{1}{2}$" down to $\frac{3}{8}$") and coarse (3" down to $\frac{3}{8}$"). Both gave good results under test, the finer material showing less wear than the coarser. The percentage loss after 9 hours testing (28% with A3 and 36% with A4) was of the same order as with mixed flint shingle from Selsey C3 and the finer of the two samples of natural beach shingle from Fleetwood.

Three samples of quarried stone and quarry waste were tested.

A5, selected hard material from one of the tips from 4" down, lost 84% of its bulk. A6, similar to A5 but containing rather more shale and graded from 6" down to sand lost 90%. The third sample A7 consisting exclusively of hard sandstone rubble and containing seven hand-picked stones measuring 11" x 8" x 5" down to 5" x 3" x 3" lost 74% by weight after $7\frac{1}{2}$ hours when the test was discontinued due to the fracture of the drum.

APPLICATION OF THE TEST RESULTS

It hardly needs emphasising that the treatment to which shingle on an open foreshore is subjected by wave action is much more complicated than the treatment given to the samples in the revolving drum. In nature the beach profile is continually changing, being drawn down by short steep waves and built up again by long low waves. Further, in the revolving drum the amount of material above No.14

sieve size was continually being reduced, whereas on an open beach only a relatively thin surface layer is being attacked at any one time and as material is worn away it is replaced in the surface layer by new material from below, i.e., the amount of material being subjected to attrition does not vary in the same way as the material in the experiments although it obviously must vary from time to time with changes in tide level and the severity of wave action. Consequently there is no simple correlation between the scales of the experimental work and the natural scale on an open beach. Nevertheless, it has been found possible to use the results of the experiments to give a comparison of the durability of different types of material and, consequently, to determine the amount of imported material that is needed to maintain the required beach levels relative to the amount that would have been needed if material equal to the natural beach had been available.

Chapter 20

STABILITY OF BEACHES USING GROINS

Tojiro Ishihara
Professor of Hydraulics,
Kyoto University, Kyoto, Japan

and

Toru Sawaragi
Assistant Professor of Hydraulics,
Nagoya University, Nagoya, Japan

SUMMARY

The authors have conducted a field investigation on the stability of beaches, using groins along the Imazu and Sakano Coasts in Tokushima, Japan. Based on the survey of coastal configuration between groins and on the estimation of the amount of littoral sand drift in the case of no structure, the storage capacity of permeable and impermeable groins was determined. It is found that the groins have to be designed in types, length and intervals under the condition that the equal amount of littoral sand drift along the coast may be secured.

INTRODUCTION

The qualitative studies on the effect of the groin to the littoral sand transport have been conducted by many investigators.[1)2)3)] However, no study on how the amount of littoral transport past a groin changes with time after the installation of the groins is yet made.

The scale model test using movable bed in the laboratory is very difficult since the small scale studies in the experiment can not give the exact quantitative evalution under the prototype condition. Therefore, to clarify the storage capacity of the groin to sand drift, the field investigation is carried out along the Imazu and Sakano Coasts in Tokushima, Japan.

Beach process after the installation of groins is discussed and the amount of transport past an impermeable groin made of the cubic concrete blocks is compared with the one of a permeable groin made of hexaleg blocks. It is believed that this quantitative results on the storage capacity of sand drifts by the groins will be valuable when the groin system will be used to stabilize beaches.

GENERAL DESCRIPTION OF TEST AREA

The Imazu and Sakano Coasts are situated about 15 km south-south-east from Tokushima City. The coast is about 8 km in length and the seawalls along the coast have been constructed to protect the coast from the storm wave. The beaches are relatively steep with fine sand (medium grain size= 0.4-0.2 mm). The groin system, in which T-type and peninsular type of groins are used, is installed at the foreshore as shown in Fig. 1.

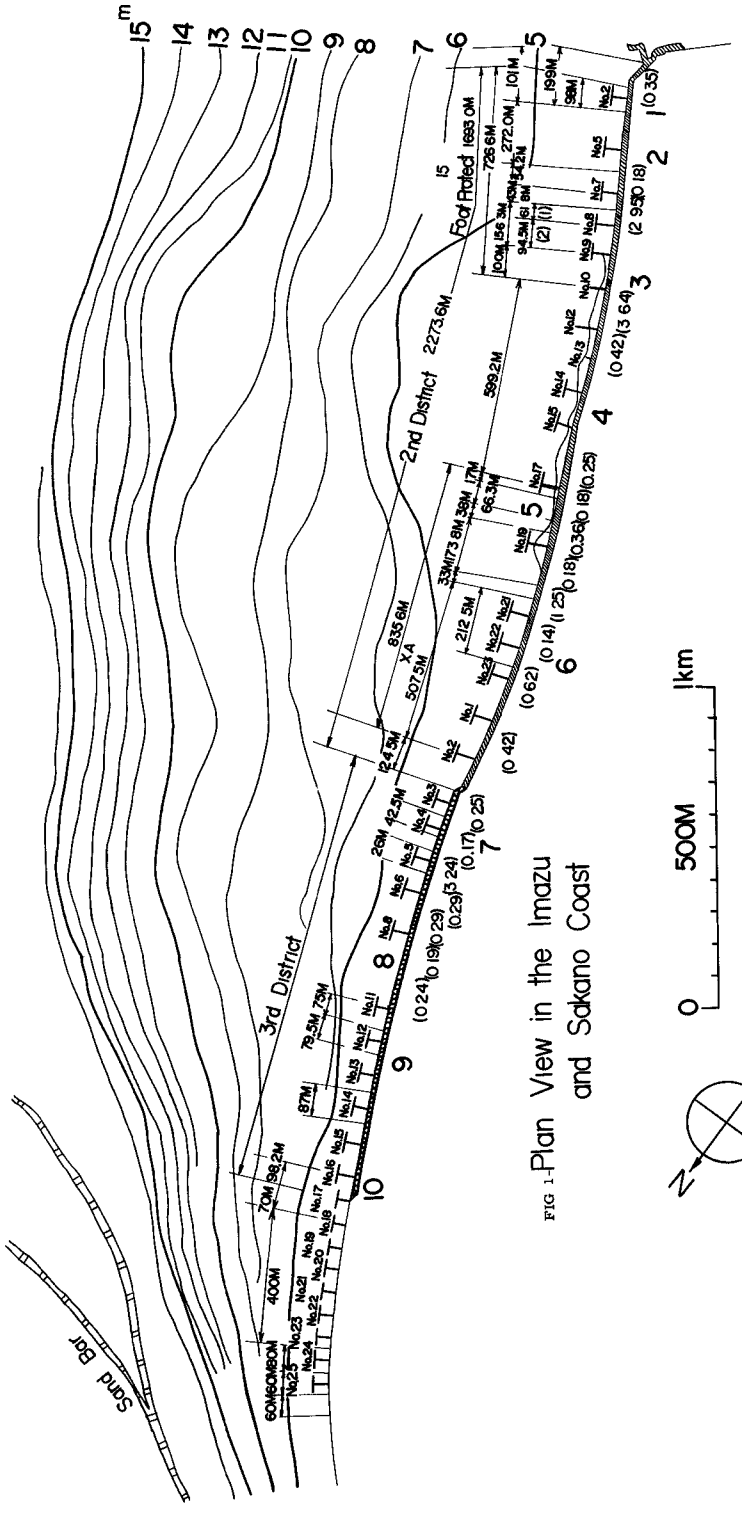

FIG 1. Plan View in the Imazu and Sakano Coast

The T-type groin made of hexaleg blocks is of permeable type, whereas the peninsular groin of cubic concrete blocks is impermeable. Both types of the groins consist of various scale in length and interval. The hexaleg block has six rectangular prisms adhering to the surface of its core cube as shown in Fig. 2, and the interlocking method of blocks and the porosities of accumulated blocks can be changed with the rate of littoral sand drift.

This coast faces the Pacific Ocean in the direction of SE,SSE and S, and the north-east side faces the Osaka Bay and Kii Channel. The fetches in each direction are shown in Table 1. Therefore, the characteristics of incident waves generated from northward are generally steeper than the one of coming wave from southward. Wave heights from southward, however, are remarkably larger than the ones from northward since the coming waves from southward are mainly generated by typhoons.

Then, the predominant direction of littoral sand drift along this coast may be specified from south to north.

INVESTIGATION

The field investigation was conducted twice, in August 1962 and in march 1963, because the directions of waves to this coast indicate the seasonal change.

In the above mentioned periods of investigation, the characteristics of shallow water wave and the hydrographic survey around the groin system were observed at fixed time. Bed materials were also collected at 20 points along the shorline and were sieved by J.I.S.* sieves. The distribution of medium grain size at the shoreline along this coast is indicated numerically in the parentheses in Fig. 1.

The characteristics of wave at deep water during the period of investigation were hindcasted the meteorological data of Tokushima Weather Bureau.

The coming waves from southward during August, 1962 were mainly attributed to typhoons which send large swells from outer ocean or bring extraordinary storm waves. For hindcasting the waves generated by typhoons, the scale as well as the location of typhoon are considered in this study. Fig. 3 indicates the courses of typhoons during this investigation.

When the estimated wave heights are compared with observed wave heights under the consideration of wave refraction, the former comes from SE pretty coincides with the latter, but the coming waves from ESE, SSE and S are diffracted by Shiono Cape and Gamoda Cape and fall into decay about half of an ordinary wave height.

The characteristics of waves generated within several decade km in fetch as shown in Table 1 from northward in March are determined by

---

* J.I.S. abbreviates Japanese Industrial Standards.

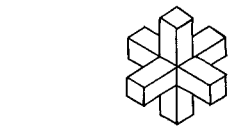

(a) A hexaleg block

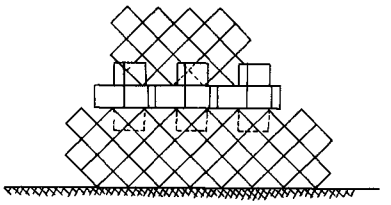

(b) Interlocking hexaleg blocks

FIG 2

TABLE 1

direction	fetch Km
N	90
NE	105
NNE	55
E	40
ESE	85
SE	

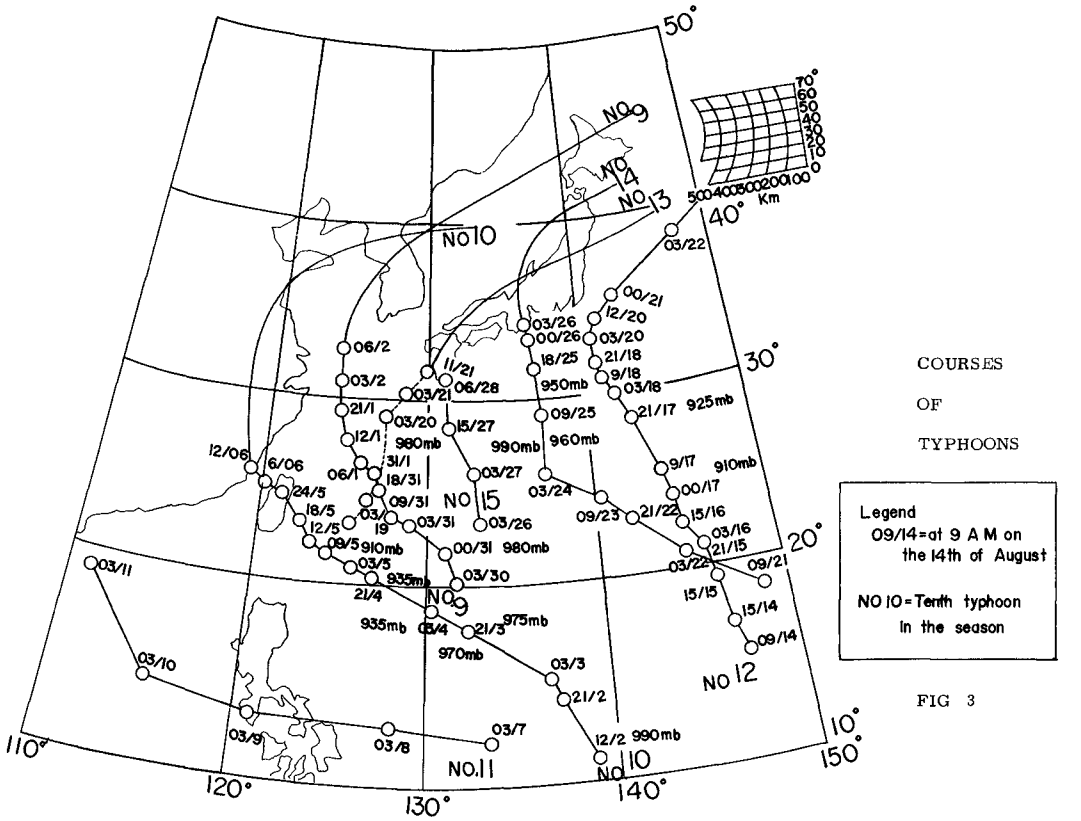

COURSES OF TYPHOONS

Legend
09/14=at 9 A M on the 14th of August
NO 10=Tenth typhoon in the season

FIG 3

and wind velocity.[4] The characteristics of waves in the shallow water are obtained by drawing wave refraction diagram in each direction.

Consequently, the breaker height and incident angle at the breaking point are found.

BEACH PROCESS AFTER THE CONSTRUCTION OF GROINS

The parallel portion to shoreline of T-type groins at this coast is constructed under the mean water level so that it has the identical effect of submerged breakwater. The length of parallel portion of the groin is equal to the longitudinal length of groin, and the intervals between the groins are 1.5-2.0 times the longitudinal length of groins. The groins constructed at this coast have different longitudinal lengths such as 35, 50, 60 and 70 m, respectively.

As a general rule, when the groins of peninsular type are built perpendicular to or at an inclination with the shoreline, the deposition occurs on the updrift side of the groin and the erosion occurs on the downdrift side of the groin. The shoreline furiously fluctuates with the change of the direction of littoral drift as sketched in Fig. 4.

On the other hand, as shown in Fig. 4, the seasonal fluctuation of the shoreline between the T-type groins are almost independent with the seasonal changes of the direction of littoral drift. The beach configuration shows concave in plan and the maximum concave point deviates just a few from the center of interval of the groins with the change of the direction of littoral drift.

In Fig. 5, the observed configuration between the groins in August and March verifies the above description. Each number of the groins corresponds to the groin number as indicated in Fig. 1. The concave configuration due to the T-type groin is caused by the diffraction of waves at the both end of parallel portion of groins.

It is obvious that the longer groin is constructed, the flatter beach configuration results as shown in Fig. 5.

It is concluded from the above mentioned fact that the T-type groin gives the effective results for the stabilization of the beaches where the direction of littoral drift furiously changes.

But if the length of groin becomes shorter, the center of groins recedes. The wave concentrates in this part, and coastal construction there is easy to destructive. Therefore, in order to protect the concentration of the wave, the groin should be at least 60 m in length from the observed results.

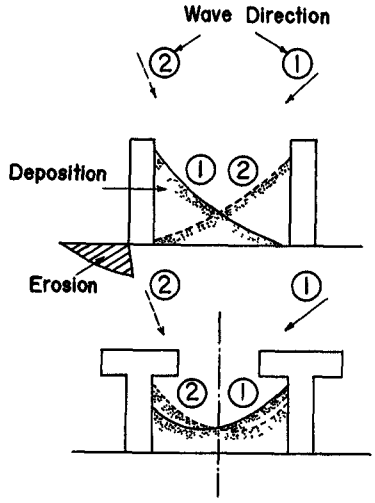

FIG. 4--SKETCH OF BEACH PROCESS AROUND GROINS

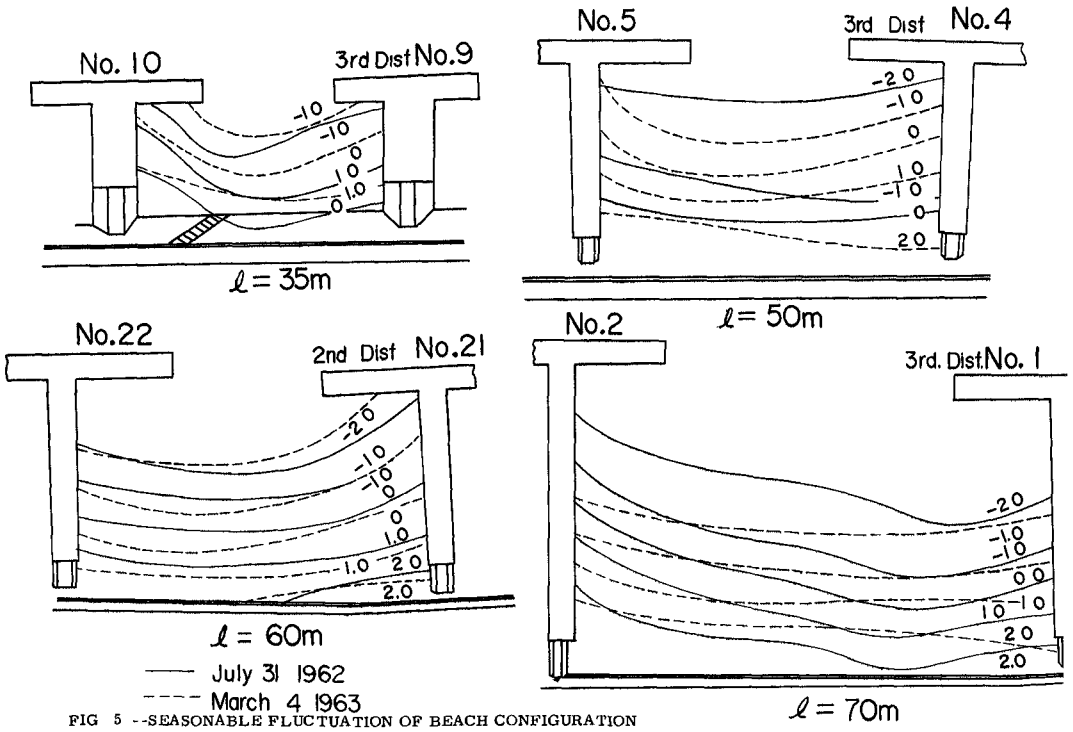

FIG 5 --SEASONABLE FLUCTUATION OF BEACH CONFIGURATION

ESTIMATION ON THE STORAGE CAPACITY OF SAND DRIFT BETWEEN GROINS

The installation of groins has not been designed effectively because the storage capacity of groin to littoral sand drift was not estimated properly.

The amount of sediment eroded or deposited between two groins can be estimated by the hydrographic survey of coastal configuration. Using these field data the authors have estimated the storage capacity to littoral drifts between the groins by the following procedure.

Now, let consider the case in which three adjacent groins are installed as shown in Fig. 6. In this figure, X_1, Y_1 and Z_1 denote the amount of littoral drift per unit time at each location before the installation of groins along the coast, X_i', Y_1' and Z_1' the amount of transport past a groin per unit time after the installation of groins and the amount of sediment between two groins are indicated by V_1' (between No. 1 and No. 2 groins) and V_2' (between No. 2 and No. 3 groins), respectively.

The following relationships are then obtained:

$$\sum_{i=1}^{n} X_1' t_1 - \sum_{i=1}^{n} Y_1' t_1 = V_1' \qquad \cdots\cdots\cdots\cdots(1)$$

$$\sum_{i=1}^{n} Y_i' t_1 - \sum_{i=1}^{n} Z_1' t_1 = V_2' \qquad \cdots\cdots\cdots\cdots(2)$$

where t_1 is the duration time of the wave under the identical conditions. When the ratios of amount of littoral transport past a groin to the amount of littoral transport in the case of no structure are defined by $a=X_i'/X_1$, $b=Y_1'/Y_i$ and $c=Z_1'/Z_1$, the storage capacities of the groin to littoral drift are expressed by (1-a), (1-b) and (1-c), respectively.

In the case when two groins, No. 1 and No. 2, are same in type, length and interval, a and c are obtained by the following equations, if a is assumed equal to b.

$$a=b= V_1'/\left(\sum_{i=1}^{n} X_1 t_i - \sum_{i=1}^{n} Y_1 t_i\right) \qquad \cdots\cdots\cdots\cdots(3)$$

$$c= \left(a \sum_{i=1}^{n} Y_1 t_i - V_2'\right)/\sum_{i=1}^{n} Z_i t_1 \qquad \cdots\cdots\cdots\cdots(4)$$

Also assuming that No. 3 in Fig. 6 is very longer in length compared with No. 1 and No. 2 and it can perfectly catch the littoral transport, then a and b can be determined by Eqs. (5) and (6).

$$b= V_2'/\sum_{i=1}^{n} Y_1 t_1 \qquad \cdots\cdots\cdots\cdots(5)$$

$$a= (V_1'+V_2')/\sum_{i=1}^{n} X_1 t_1 \qquad \cdots\cdots\cdots\cdots(6)$$

In Eqs. (3) to (6), V_1' and V_2' may be estimated from the field observation.

The several empirical formulae[5)6)7)] for the estimation of amount

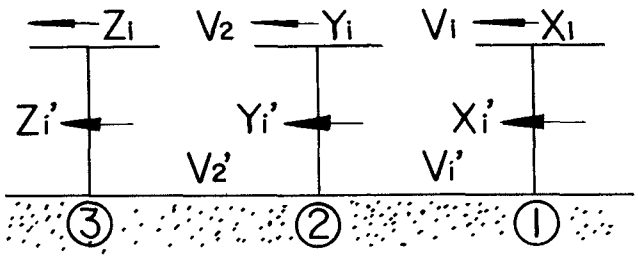

FIG. 6. --SKETCH OF GROIN SYSTEM

TABLE 2. --VALUES OF THE STORAGE CAPACITY OR THE PASSING RATIO OF GROIN

Date	a	1-a	c	1-c
Aug. 1-Aug. 7	0.48	0.52	0.38	0.62
Aug. 7-Aug.10	0.58	0.42	0.57	0.43
Aug.10-Aug.19	0.47	0.53	0.44	0.56
Aug.19-Aug.22	0.62	0.38	0.51	0.49
Aug.22-Aug.23	0.58	0.42	0.18	0.82
Aug.23-Aug.26	0.48	0.52	0.44	0.56
Mar. 7-Mar.14	0.45	0.55	0.43	0.57
Mar.14-Mar.21	0.51	0.49	0.40	0.60

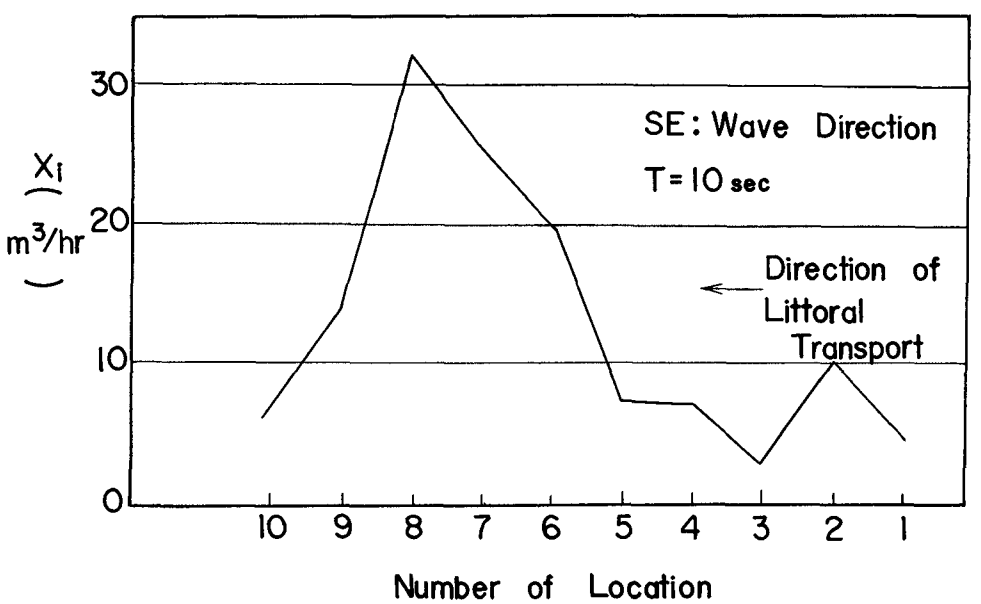

FIG. 7. --DISTRIBUTION OF AMOUNT OF LITTORAL DRIFT ALONG IMAZU COAST

of littoral drift are proposed by many investigators. In this investigation, the empirical formula proposed by Iwagaki and Sawaragi[7] is used. This formula has been derived by modifying the Kalinske-Brown formula for sediment transport in open cannels. The width of littoral sand drift zone may be obtained experimentally. Good agreement is obtained between this formula and the field investigation made at the North of the Akashi Strait between Honshu and Tokushima.

The formula is expressed by the following equation of

$$X_1,\ Y_1 \text{ and } Z_1 = m \cdot H_o'^{15/4} \cdot T^{-3/2} \cdot i^{4/3} \cdot d^{-1/2} \cdot (H_o'/L_o)^{-1/2} \cdot (\sin 2\alpha_b)^{4/3} \cdot \cos\alpha_b \quad \ldots(7)$$

where $m = (31.7) \cdot (1/16)^{3/2} \cdot (\sigma/\rho - 1)^{-3/2} \cdot g^{-1/4}$, $H_o' = K_b H_o$

X_1, Y_1 and Z_1 are the amount of littoral drift per unit time, H_o wave height of deep water, d mean grain size, i beach slope, L_o wave length of deep water, σ and ρ density of the bed material and water, respectively, α_b incident angle of breaker, K_b coefficient of refraction at the breaking point and g acceleration of gravity.

The passing ratio of groin, which is the ratio of the amount of littoral transport past a groin to the amount of littoral transport in the case of no structure, or the storage capacity of a groin may be obtained under the boundary condition mentioned in Eqs. (3) to (6). In the case where the boundary condition may not be satisfied, the storage capacity of groins in Eqs. (3) to (6) may be determined successively from the location where the conditions may be fulfilled.

Table 2 shows the result calculated for the passing ratios, a and c, by Eqs. (3) and (4). In Table 2 the groin having the storage capacity (1-a) is constructed by the hexaleg blocks. Its length is 60 m and the interval 100 m. On the other hand, in case of the storage capacity having (1-c) the half-length of the groin at the inshore side are made of the cubic concrete blocks and the other half the hexaleg blocks. From the table, it is cleared that the former's storage capacity indicates about 50 % and the latter one about 60 %.

The storage capacity of a groin may be influenced by the characteristics of wave and other factors. To clarify the effects of these factors for the storage capacity, however, is still very complicated in this stage.

DESIGN OF GROINS AND STABILITY OF BEACHES

To stabilize beaches by groins, the groins have to be designed to secure that the amount of transport past a groin along the coast should be held constant. In this respect, the distributions of the amount of transport along the coast without structure may be required in advance.

Now, the design of groin system is explained by the following example. Fig. 7 shows the distribution of the amount of littoral sand drift per unit time along the Imazu Coast without structure in the case

when the direction of wave is SE and wave period 10 sec.. The amounts of littoral drift at the locations from No. 1 to No. 10 are expressed as X_1, X_2, ... X_9 and X_{10} , where X_{10} is the amount at the downdrift end. If a_i is the passing ratio of groins, the amounts of littoral drift past the groins at each location are expressed as a_1X_1, a_2X_2, ...a_9X_9, respectively.

To stabilize beaches, the amount of transport past a groin should be satisfied by the following equations,

$$X_{10}-a_9X_9 = 0, \quad a_9X_9-a_8X_8 = 0, \quad \ldots\ldots\ldots \quad a_2X_2-a_1X_1 = 0 \quad \ldots\ldots(8)$$

Using the amounts X_1 as shown in Fig. 7,

$$a_9=0.48, \quad a_8=0.20, \quad a_7=0.25, \quad a_6=0.33 \quad \ldots\ldots$$

are successively obtained by Eqs. (8).

The required passing ratios of the sand drift in groins are changed with length and interval of the groins. However, if the hexaleg block is used for groin, the required passing ratios of groins may be obtained by the change of interlocking method of blocks.

CONCLUSIONS

The following conclusions have been drawn from the results of this study.

(1) The T- type groins give the effective results for the stabilization of the beaches where the direction of littoral drift furiously changes.

(2) The longer T-type groins are constructed the flatter beach configuration results.

(3) Using the results of the field investigation, the method of estimation on the storage capacity of littoral sand drift for the permeable and impermeable groins are proposed.

(4) To stabilize beaches by groins, the storage capacity of the groins has to be changed with the locations such that the amount of transport past a groin is kept constant along the coast.

REFERENCE

1) Savage, R.P.; Laboratory Study of the Effect of Groin on the Rate o Littoral Transport, Equipment Development and Initial Tests, Beach Erosion Board, Tech. Memo. No. 114, 1959.

2) Horikawa, K. and Sonu, C.; An Experimental Study on the Effect of Coastal Groin, Coastal Eng. in Japan, Vol. 1, 1958.

3) Nagai, S.; Arrangement of Groins on a Sandy Beach, Journal of the Waterways and Harbours Division, A.S.C.E. No. WW4, Vol. 82.

4) Ishihara, T., Iwagaki, Y. and Murakami, M.; On the Investigation of Beach Erosion Along the North Coastal of Akashi Strait, Coastal Eng. in Japan, Vol. 1, 1958.

5) Watts, G.M.; A Study of Sand Movement at South Lake Worth Inlet, Florida, Beach Erosion Board, Tech. Memo. No. 49, 1953.

6) Caldwell, J.M.; Wave Action and Sand Movement near Anaheim Bay, California, Beach Erosion Board, Tech. Memo. No. 68, 1956.

7) Iwagaki, Y. and Sawaragi, T.; A New Method for Estimation of the Rate of Littoral Sand Drift, Coastal Eng. in Japan, Vol. 5, 1962.

Chapter 21

EFFECTS OF HYDROGRAPHIC CHANGES DUE TO NEARSHORE DREDGER DUMPING ON WAVE REFRACTION AND LITTORAL SAND BALANCE

Jan M. Jordaan, Jr.
Hydraulic Engineer Research U.S. Naval Civil Eng. Laboratory, formerly Senior Research Officer, S.Afr. Council for Scientific and Industrial Research.

This paper presents a case where, in the development of a harbour, dredged material was dumped in a location where a large accumulation eventually formed. This changed the offshore topography sufficiently to affect the predominant-wave refraction conditions. The wave environment along the principal bathing beaches was changed as a result, and a degree of beach erosion ensued which can be ascribed as partly due to the effects of continued dredger dumping in one area.

In the normal development of any port it must be accepted that some change of the wave environment has to take place due to the change in boundaries. This paper attempts to show that not only visible structural features, such as breakwaters, but also less evident submarine topographical changes can create some change in wave action. This can best be analysed and understood by making wave refraction studies of the conditions at various times.

Considerable hydrographic changes occurred within the port limits of Durban (situated on the southeast coast of Africa) over the period 1850 to the present. This resulted from the development of the harbour through dredging and then dumping the sand a few miles offshore. Figs 1(a) to (e), drawn from hydrographic maps available for five different surveys, show the remarkable build-up of two lens-shaped shoal areas close to the harbour entrance. Fig 2(a) and (b) show that the accretion during the period 1887-1926 occurred ENE of the entrance and in 1926-1961 mostly to the south east. This is due to a change in dumping grounds after 1938 when the larger accretion to the ENE began to assume alarming proportions. This dump contained 19 mill cu yd of dredged sand by 1926 corresponding to the dredging taking place in and around the entrance channel to maintain adequate draft. By 1938 the volume had reached 27 mill cu yd which is approximatel the present volume. Since 1938 accretion of a further 20 mill cu yd occurred due to dumping in the SE area.

The maintenance dredging of sand traveling northwards along the Bluff coast to the south of the harbour entrance has risen to a figure of 800,000 to 1 million cu yd/annum, and over the years a gradual depletion of sand along certain of the northern bathing beaches occurred that was countered by

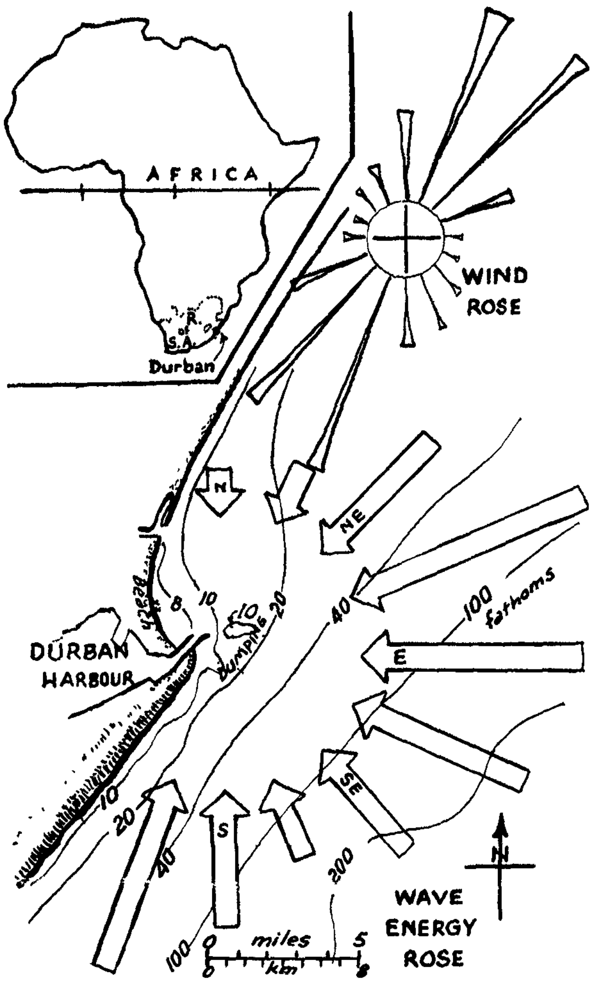
AFRICA
R. of S.A.
Durban
WIND ROSE
DURBAN HARBOUR
Beach
N
NE
E
SE
S
8
10
10
20
40
100 fathoms
Dumping
200
miles
km
WAVE ENERGY ROSE
N

Fig. a

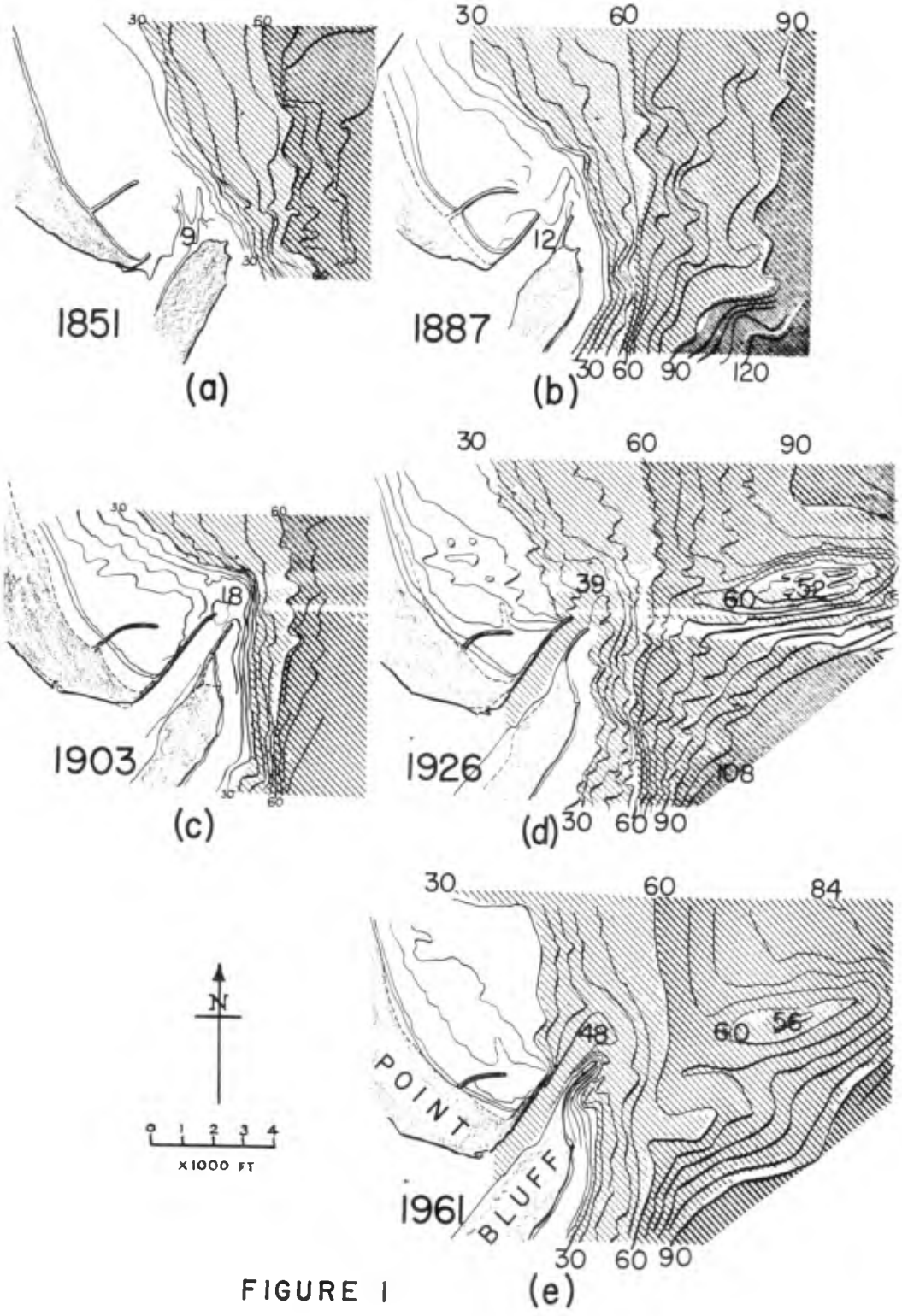
30
60
90
9
30
1851
(a)
30
60
90
12
1887
30 60 90 120
(b)
30
60
18
1903
(c)
30
60
90
39
60
52
1926
108
30 60 90
(d)
30
60
84
48
60
56
POINT
BLUFF
1961
30 60 90
(e)
N
0 1 2 3 4
X1000 FT

FIGURE 1

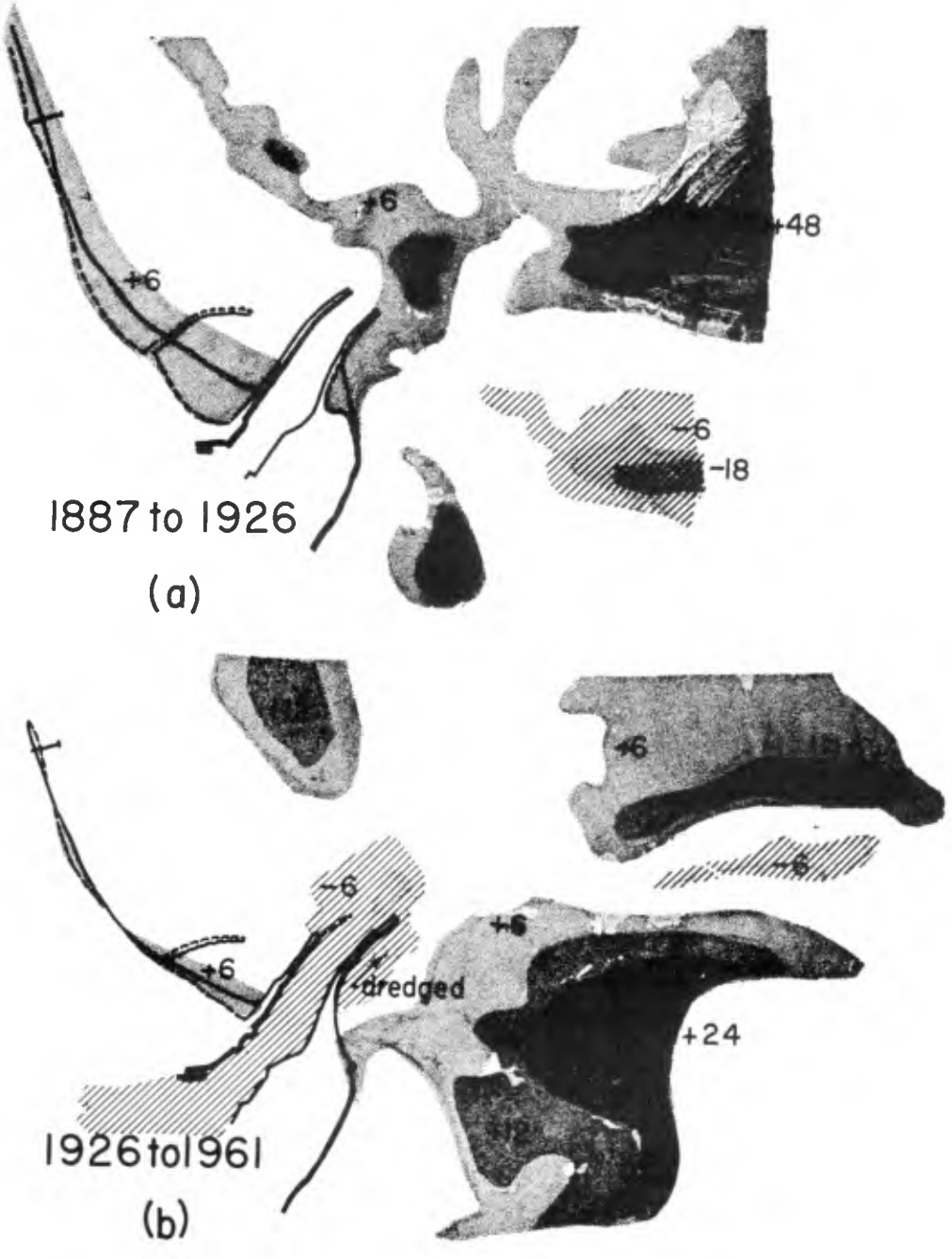

FIGURE 2

partial sand byoassing across the harbour entrance. A-scheme whereby dredging could be reduced and better beaches be maintained was constantly sought leading to a comprehensive scale model investigation of the problem. This study was supnorted by analytical methods and field observations over a period of three years.

WAVE REFRACTION

It was found from model observations and later confirmed by field data taken during storms that the predominant swell waves are markedly higher along a particular stretch of the beach where the greater erosive tendencies were observed. Three sets of wave refraction diagrams were accordingly prepared for each of the three predominant wave approach directions and for the hydrographic conditions both before and after the offshore accretions took place, i.e. ESE, NE and SE wave approach for 1887 and for 1961 conditions. The results are shown in Figs. 3 to 5.

The shallow areas in the underwater topography present in 1961 but nonexistent in 1887 had the effect of changing the wave approach direction and consequently refocusing wave energy on certain parts of the coastline, which formerly was a zone of wave diffraction and gradual beach building. This explains why higher waves and greater erosive capacity were observed in the affected zone in both model and nature. It can be assumed that this region downdrift of the harbour entrance had been in relatively stable state before 1851 although, geologically speaking, slowly accreting. The beaches to the south (updrift) had a practically unlimited supply of sand from a long straight coastline southwards which was fed by many littoral-drift producing rivers. The rocky headland bounding the southern stretch of coastline confined the littoral drift to a narrow breaker zone and originally fed sand to the northern beaches across the shallow tidal inlet to the several square miles of Bay (which later became the harbour). When in recent years the tidal inlet was dredged to 42 ft plus to develop the harbour, all natural bypassing of sand to the north ceased, and it became necessary to maintain the approach depths by continuously dredging a "sand trap" immediately updrift (southeast) of the main breakwater defining the entrance channel.

The wave refraction diagrams for ESE and SSE swell show that a greater degree of sheltering occurred due to the south breakwater construction which, combined with the sand supply being cut off, reduced the northward drift along the northern beaches. Storm waves from NE were focused by the mound caused by dumping offshore onto the updrift coast region (Bluff) causing a likely return of part of the littoral drift southwards at times. The offshore accretions and the entrance dredging together have the net effect therefore of

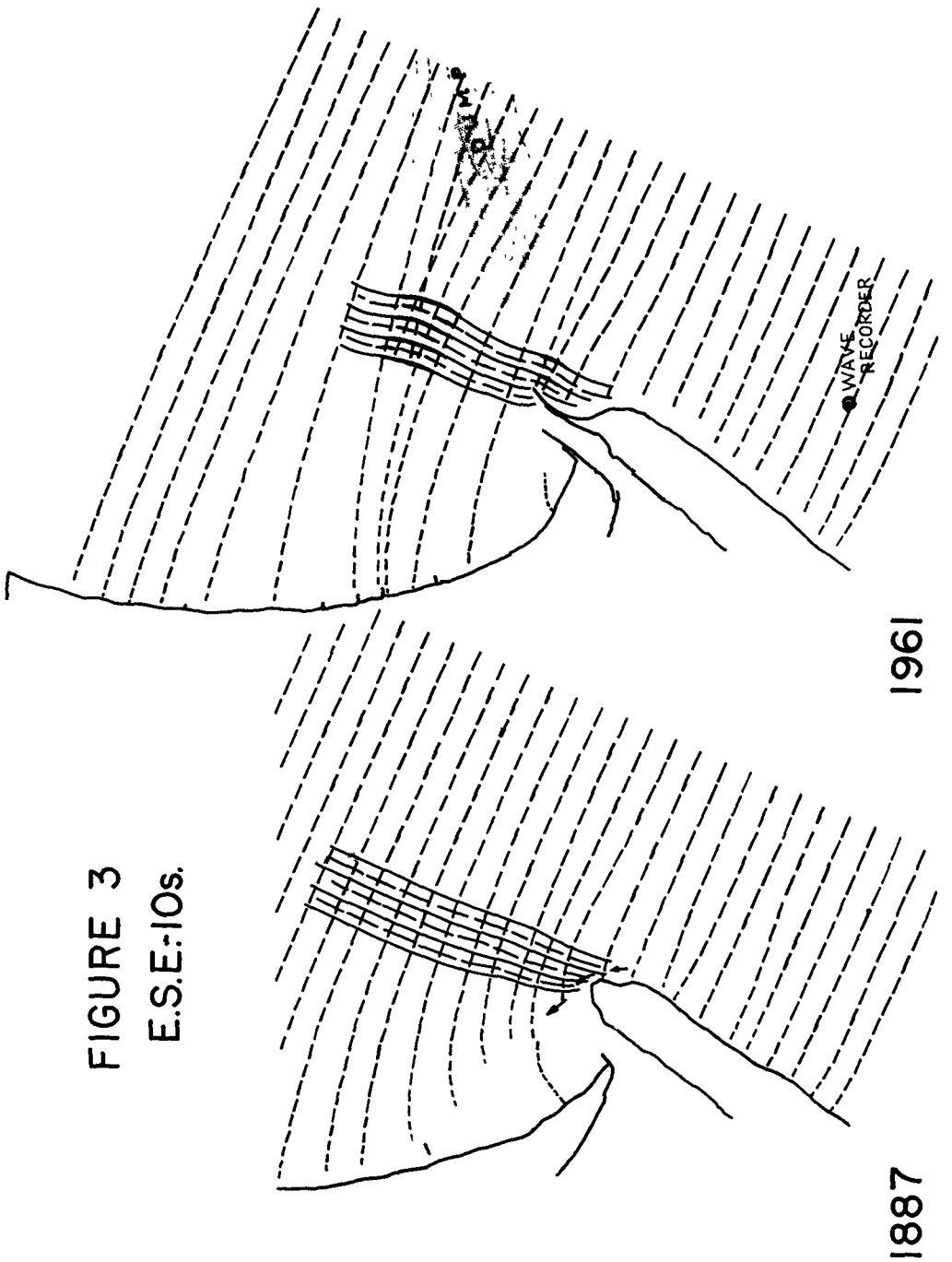

FIGURE 3
E.S.E.-10s.

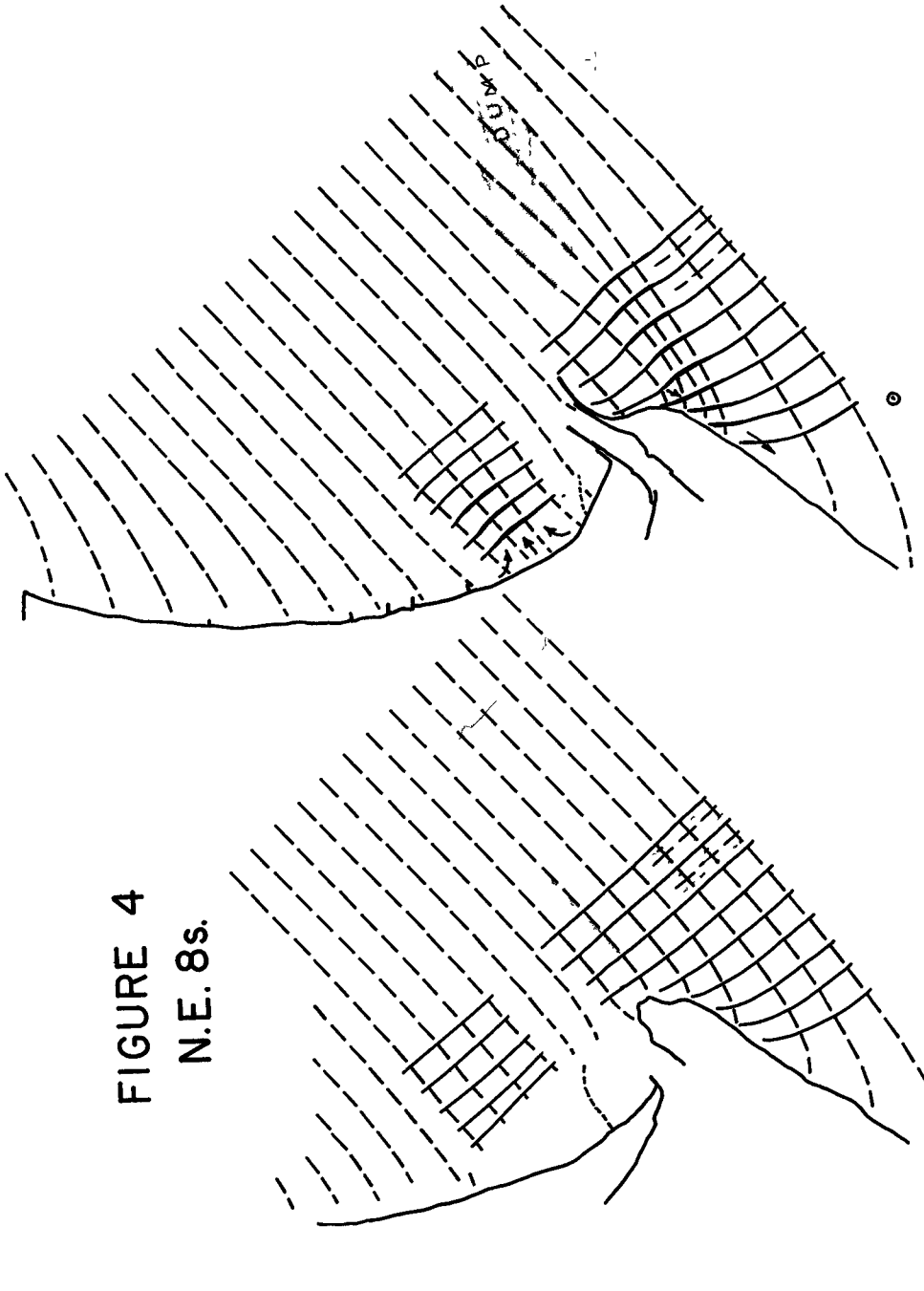

FIGURE 4
N.E. 8s.

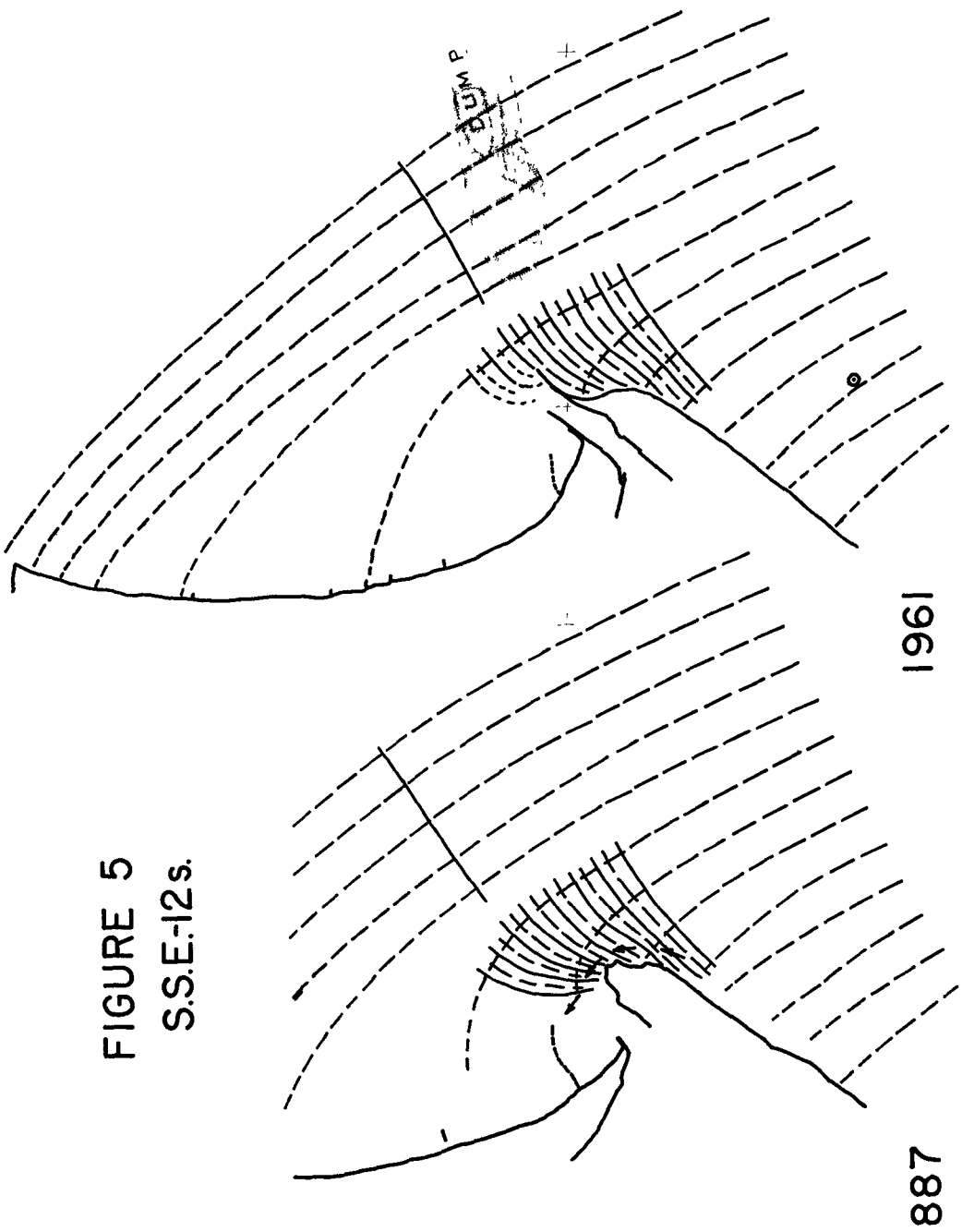

FIGURE 5
S.S.E.-12s.

changing the wave environmental conditions along the coastline. The northern stretch of beach, in response to the changed environment, tends to establish a new equilibrium shore line which is more concave seaward, by virtue of the sheltering of the lower Point area and the increased wave attack on the central area of this crescent-shaped stretch of beach. The two groynes that were built there in 1953 apparently are effective in maintaining present conditions there at a reasonably stable level, but this is inferior to requirements.

This hypothesis was subsequently tested by drawing the wave energy vectors for upcoast and downcoast littoral drift, Fig.6, which were obtained by collecting wave data over a period of over three years, combined from records and observations kept regularly at Stations 2, 3 and 4 and developing a "wave rose" diagram for offshore conditions. By means of the wave refraction studies here presented (and four others for different directions in 1961) the refracted (nearshore) wave roses for points 4 to 12 along the coastline were derived. The funicular diagrams for wave energy were drawn and the net longshore energy component, a relative measure of the net drift, obtained all along the coastline under consideration. Because of currents and wave interaction, the nearshore littoral drift combines with an offshore sand drift to a natural accretion area north of the harbour entrance (shown dot shaded in Fig 7). Along the southern (Bluff) coastline littoral drift is caused principally by an interaction of waves and currents and not by one or the other alone. A yearly influx of about 1 million cu yds sand occurs into the dredged sand trap area adjacent and seaward of the south breakwater, as shown schematically in Fig.7. From this trap sand is continuously dredged and dumped offshore, at present about 3 miles SE of harbour entrance.

CONCLUSIONS

With the aid of wave refraction studies and confirmed by model and field observational data, it was determined that man-made offshore shoal areas had the effect of increasing wave action down-weather thereof. As a result, wave- and wind-induced off-shore circulation in this locale was found to favor a condition of beach erosion. This result was confirmed by a study of the sorting and granulometric distribution of sand samped extensively in the offshore environment and by the diagnosis of the situation. This diagnosis was subsequently used as a basis for testing remedial measures on the model. It was apparent that redredging of the dump or attempts to flatten and spread it would be prohibitive, and possibly not fully effective. Schemes to reduce the wave energy over localized area were investigated, such as parallel-to-shore breakwaters or wave-screens of a semi-permeable nature. These were found hydraulically effective in the model but because

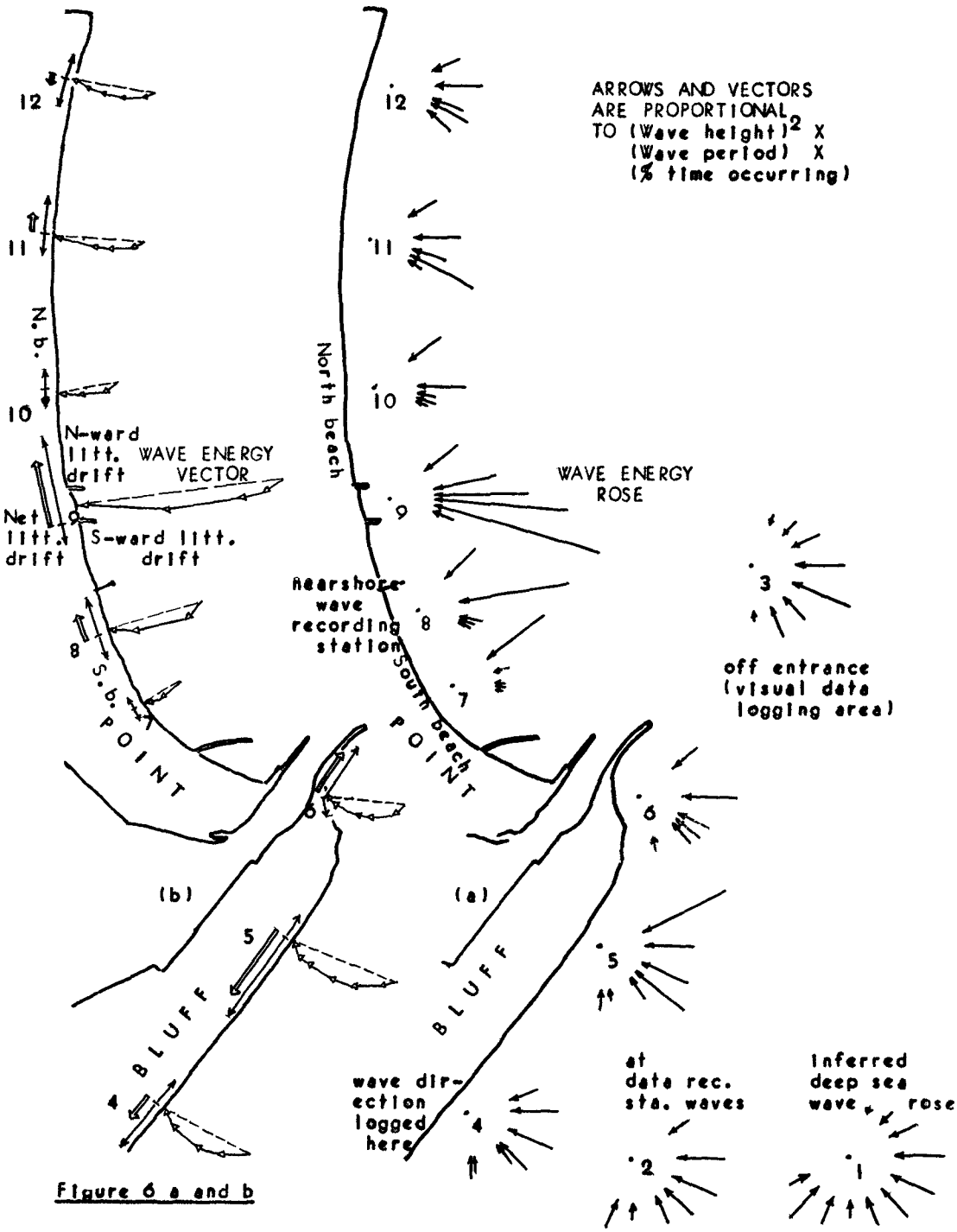

Figure 6 a and b

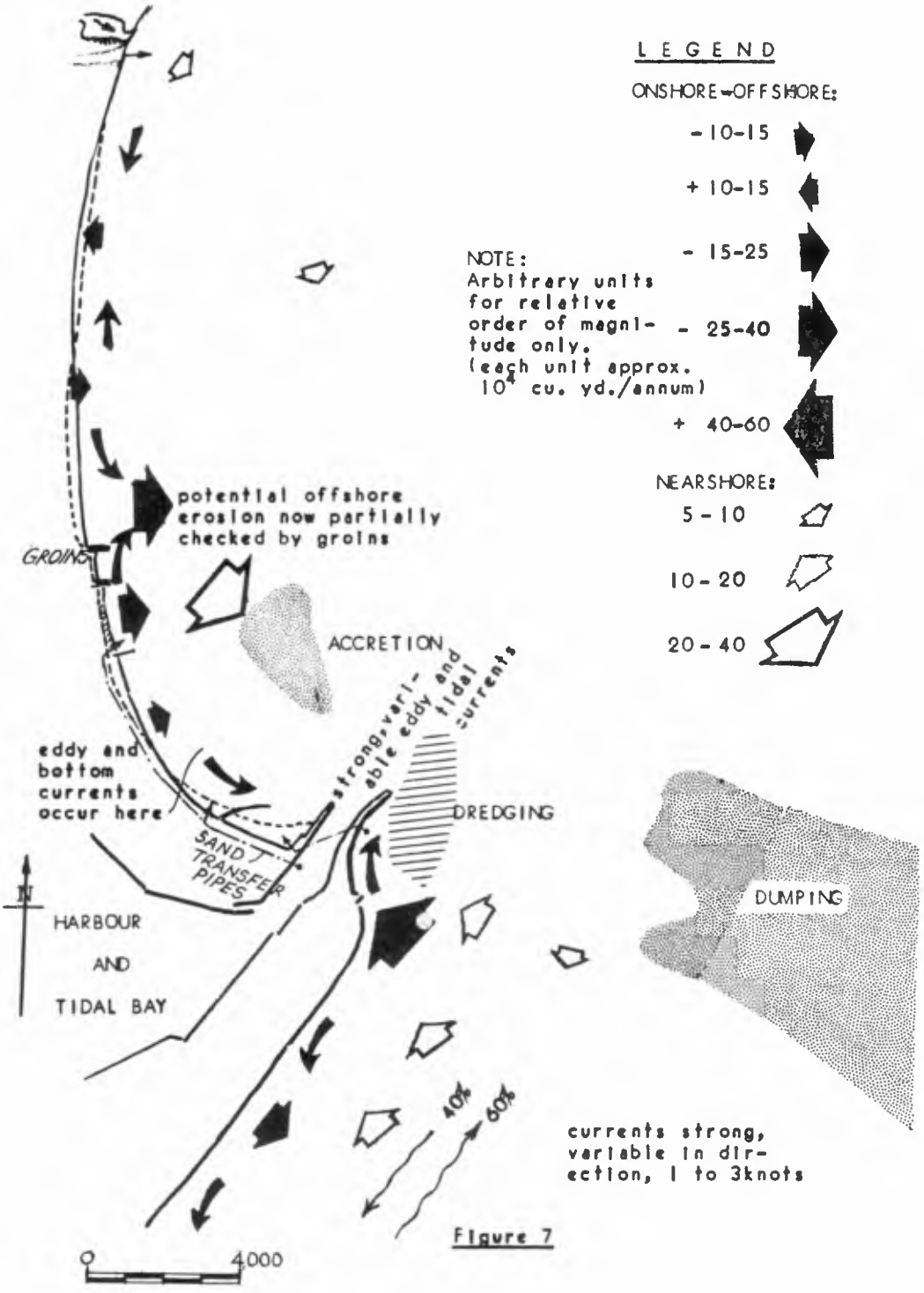
LEGEND
ONSHORE-OFFSHORE:
- 10-15
+ 10-15
- 15-25
- 25-40
+ 40-60
NEARSHORE:
5 - 10
10 - 20
20 - 40
NOTE:
Arbitrary units
for relative
order of magni-
tude only.
(each unit approx.
10⁴ cu. yd./annum)
potential offshore
erosion now partially
checked by groins
GROINS
ACCRETION
strong, variable eddy and tidal currents
eddy and
bottom
currents
occur here
DREDGING
SAND
TRANSFER
PIPES
DUMPING
N
HARBOUR
AND
TIDAL BAY
40%
60%
currents strong,
variable in dir-
ection, 1 to 3knots
0
4000
Scale: 4000ft.

Figure 7

of their large size, of the order of several thousand feet long, would be very expensive to carry out in practice. Floating wave absorbers could not be guaranteed to outlast some of the storms witnessed while the study was conducted. Schemes to reduce the wave energy over the localized affected areas or alternatively, stabilize the beach with shore works and continued sand-bypassing and beach renourishment have been investigated.

ACKNOWLEDGEMENT

Permission to present a paper on this suject has been granted by the authorities on behalf of which the research herein reported was carried out: The South African Railways Administration and the City Council of Durban and by the South African Council for Scientific and Industrial Research. The assistance of members of the staff of the above organizations is gratefully acknowledged.

List of Figure Captions

Figure a — Locality map and detail of problem area.

Figure 1 — Hydrographic changes in the Approaches to Durban harbour 1851 to 1961. Isobaths in feet.

Figure 2 — Isopleths of equal offshore gain or loss in periods 1887 to 1926 and 1926 to 1961. Isolines in feet.

Figure 3 — Wave Refraction diagrams for S.S.E. swell of 10 sec period comparing conditions of 1961 with those of 1887.

Figure 4 — Wave Refraction diagrams for N.E. swell of 8 sec period comparing conditions of 1961 with those of 1887.

Figure 5 — Wave Refraction diagrams for S.S.E. swell of 12 sec period comparing conditions of 1961 with those of 1887.

Figure 6 a, b — Wave energy rose diagram, vector diagram and resultant littoral drift-producing energy vectors.

Figure 7 — Inferrred nearshore redistribution of sand for present time conditions (1962). Sand transport by combined wave and current action shown diagrammatically (based on Fig. 6 results)

Chapter 22

ON THE EFFECT OF AN OFFSHORE BREAKWATER ON THE MAINTENANCE OF A HARBOR CONSTRUCTED ON A SANDY BEACH

Akira Ozaki
Professor of Civil Engineering
Department of Hokkaido University
Sapporo, Japan

INTRODUCTION

In this paper the author describes an experimental attempt to prevent the rapid blocking of a harbor entrance caused by littoral drift in the summer period. This work was conducted at "Seppu", a fishing harbor constructed on a sandy beach in Hokkaido, Japan. This investigation was originally sponsored by the Harbor Section of the Hokkaido Prefectural Office. One of the top priority objectives, at that time, was to determine the efficiency of two jetties constructed on the updrift side for the purpose of countering the sand drift. Detailed observations including preliminary model experiments, were made from 1961 to 1963 on the general aspects (ie condition and phenomena) of the coast in question. Meteorological data were also compiled together with investigations as set forth by the government.

Based on the above, the author finally suggested the utilization of natural forces ie waves, offshore currents etc, by constructing an offshore breakwater to curb the blockage of the harbor mouth.

This idea was shown to be adequate at least qualitatively by model experiment with the exception of the troublesome time scale problem. These findings, however, have not been adopted as yet for actual improvement of the harbor at present.

DESCRIPTION OF THE PROTOTYPE

GENERAL DESCRIPTION

The Hidaka coast, where the above mentioned fishing harbor is located, faces the Pacific Ocean, and its 160 km shoreline is a continuation of gently curved arcs from Point Erimo to Tomakomai harbor, stretching in a south-easterly direction. The general view of the Hidaka coast is shown in Fig.1.

Many rivers from the Hidaka mountains flow into the ocean transporting large quantities of sand and gravel. Moreover eroded cliffs and beaches can be seen in many places along the coast. Accordingly it may be surmised that a large amount of sand is drifting in the vicinity of the shore line extending over many miles of this coast. A rough survey of the coast reveals a general trend of deposits of sand exclusively on the south-eastern side of the water-front structures, for example, jetties or breakwaters, which project at right angles to the coast line. On the other hand it was noted that the north-western side of these structures were more or less eroded. The directions of river mouth are angled in most cases in a westerly direction by littoral current. However, in a few exceptional cases an alternation of river mouths by summer and by winter, according to their geological condition was seen.

Moreover, observations revealed that the complicated problems resulting from the drifting sand occured more frequently along the coast line to the west of Shizunai than along the coast line to the east. Some examples of the difficulties due to drifting sand will be given on the fishing harbors "Seppu", "Atsuga", "Mitsuishi", and "Higashishizunai", and various other sites along the coast line between these fishing harbors.

In Seppu harbor the south-east breakwater was constructed by steps over a period of 10 years adding 20 or 40 meters at a time due to governmental reasons. Immediately after the construction of the first section, progression of the south-eastern beach was observed reaching the head of the constructior by the end of the summer period with a retreat of coresponding lengths in the winter period. This was repeated until the final construction of the breakwater in 1963. It was noted that the progression of the sand in the windward of the breakwater became practical solid ground approximately 1 meter above sea level. This results in a rapid blocking in some cases of the harbor entrance channel, which is reopened in winter, and this was repeated each successive year for each addition of the breakwater construction. On the north western beach adjacent to the harbor, the situation was entirely different. In other words a gradual receding of the coast was noted. In addition during the corresponding summer months there were no sand deposits even in the recess between the groins. Thus, the base of revetment is washed directly by waves approaching obliquely to the coast. At a distance of 500 meters along the coast to the west of the base of the north-west breakwater no sand deposits even in updrift recesses of the groins were seen. Thus, with increase of the random loss of the groins by scouring, the revetments protected by the groins gave way to severe scouring which eventually resulted in the breaking up of the revetments.

A similar state of affairs was seen in the Atsuga harbor. (Fig.1.) Here also the progression of the beach on the south-eastern side, and the recession on the north-western side was observed. Approximately 1 km to the west of this harbor, a large number of groins, consisting of wooden piles and stone rubble were destroyed after the construction of the harbor.

As a result, with the loss of the revetments, the Hidaka railroad running parallel to the coast, became exposed to the direct washing over by waves. According to the inhabitants of this area, this direct exposure to wave damage was not seen before the construction of the harbor.

Next, in regard to the mouth of the Niikappu river, a few miles south-east of Seppu, while a slight swerving to the west was seen, this change did not go any further. This may be attributed to the protective effect of a point of land consisting of hard rocks jutting out into the sea.

Over some distance of the western beach extending to the downdrift side of these projected rocks, a remarkable erosion can be seen at present. There is a place eroded violently, also between Shizunai and Niikappu. At this place there remains an old sand dune of approximately 10 m height, and several hundred meters in length, half of which has already been eroded on the seaside. Thus the railroad and highway formerly passing by the dune was transfered to a more stable location.

Concerning the fishing harbor Higashishizunai which is located 10 km to the east of Shizunai, it is a well known fact that this harbor was once buried almost completely by sand immediately after its completion. Since this incidence, plans for a new harbor were carefully investigated to avoid such conditions and as a result at present the harbor has a new outer breakwater built some distance on the seaside of the previous breakwater. Since then the condition of the harbor has improved considerably. However, the beach to the south of the breakwater of this harbor began to recede, especially in the winter as in the previous case.

Now as an additional situation the Monbetsu river mouth lying close to the west breakwater, began to show a tendency of changing its direction towards the east. This tendency seems to depend largely upon the appearance of the new outer breakwater.

At the Mitsuishi fishing harbor, at present while no annoying problems concerning drifting sand on the harbor itself have been observed, on the western beach adjacent to the west breakwater an increasing recession of the coast line has manifested itself especially in recent years. As a means of prevention solid revetments and permeable groins are now under construction. Although the direction of the mouth of the

Mitsuishi river located close to the harbor is westward in summer season, in winter it turns eastward towards the Erimo point. On the shoreface immediately outside of the south breakwater a considerable amount of sand is deposited in summer. Extending over the entire length of the Hidaka coast waves sweeping in during the winter have a more serious effect upon the coastal erosion than those in summer. The summer waves generally have a longer period or smaller steepness than those in the winter.

The above mentioned facts seem to provide us with some important suggestions in surveying the data already prepared, on the wind, the waves the offshore current and the drifting sand of the Hidaka coast.

WIND, WAVES, AND CURRENT

Wind The windrose shown in Fig.2. is the result of observations performed by the Construction Office of the Seppu harbor in 1961 and 1962. The frequency distribution of the wind direction is also shown in Table 1. A more detailed analysis of the data shows that the directions from ESE to S are most frequent in the summer and in contrast those from W to NNW are dominant in the winter. These tendencies of the wind direction coincides with those of the waves washing the coast of Seppu harbor. Since the coast line of the Hidaka runs in a SE direction the general trend of winds are at oblique angles along the entire coast line. The shoreline is at an angle of 40 to 60 degrees to the direction of the summer wind which sweeps in from the south-eastern seaside. In winter, the shoreline is at an angle of 0 to 30 degrees to the wind from the west.

Waves The observation of waves at Seppu was commenced in 1961 and has been continued ever since. The apparatus used here for the purpose is rather simple and inexpensive. It is an ordinary transit type provided with a handle connected to the horizontal axis and some other transmission mechanisms for recording. The observer of the transit follows the vertical movement of a buoy set beforehand at an adequate position in the sea, and then the recording pen, attached to the end of an arm connected to the horizontal axis at a right angle, runs on a paper rolled on drum, which gives a scaled wave motion. The observation is usually done twice a day throughout the year, at 9:00 in the morning and at 3:00 in the afternoon. By this method, however, it is practically impossible to make observations at night or on snowy or heavy rain days. There were a considerable number of days in which the observations were impossible because the offshore buoy was often washed away in rough weather.

An interesting feature of the incident waves on this coast was noted by reviewing the general tendency of waves

TABLE 1.--WIND DIRECTION (FEB., 1961, to MARCH, 1962)

Wind Direction	S	SE	SW	SSE	SSW	N	NE	NW	NNE	NNW	W	WNW	WSW	E	ESE	ENE	Total
The number of Times	27	54	14	44	7	9	7	47	5	6	61	33	24	11	26	2	377
Frequency (%)	7	14	3	11	1	2	1	12	1	1	16	8	6	2	6	0.5	

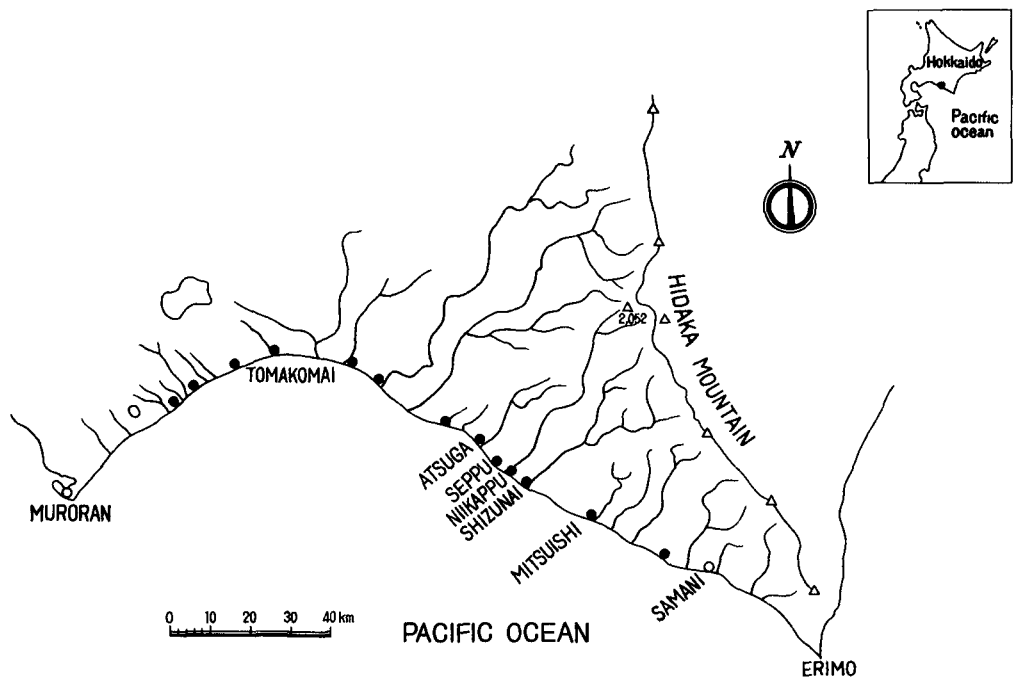

FIG. 1 --LOCATION MAP OF HIDAKA COAST

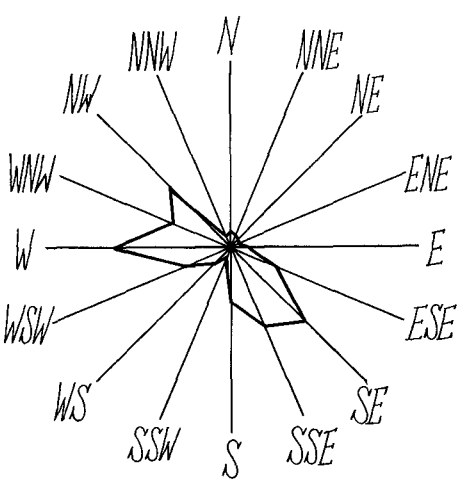

FIG 2

coming to this harbor as a whole and by further more careful observations on details by season and by month.

The diagram shown in Fig.3. is a histogram of wave height and wave period accumulated as a significant wave for the total number of observations from February 1961 to March 1962. From this figure, it can be seen that the most frequent height of the incident waves was from 50 to 60 cm and their most frequent period was 3 seconds throughout a given year. As far as the present data of observation is concerned, the maximum value for wave height and wave period were 310 cm and 8 seconds respectively, and the frequency of occurence of the wave height above 100 cm was 36 % and that of the wave period above 5 seconds was 17 %. Furthermore from April to October, the occurence frequency of the wave period longer than 5 seconds is higher than that from November to the following March.

With regard to the wave height, we do not know at present whether a similar tendency exists or not. However within the limit of the present available data it may probably be said that the occurence frequency of the wave height above 100 cm is higher in both September and October than in others.

With regard to the direction of incident waves which have an important effect on the movement of the drifting sand, those from W to WNW were quite frequent in winter.

Current It is a well known fact that the direction of the incident waves is closely related to that of littoral current, which has also been proved on the Seppu coast. In Fig.4. and Fig.5. the frequency diagrams on the direction of the incident waves and that of the littoral current are shown respectively. It can clearly be seen that a very close correlation exists between them. Some current meters, including a autorecording type, were used for the field observations of offshore currents. As a supplement to these instruments, a simple method of current observation has been used by floating an anchored painted board which shows the direction of current.

CHANGES ON THE BEACH LINE AND ON THE PROFILE OF THE SEA BED ALONG THE COAST

Though the rough outline on the coastal changes occuring in various places along the Hidaka coast was as mentioned above, further detailed information on the changes of the beach line and sea bed in the vicinity of the Seppu are required prior to model experiments for the Seppu investigation.

As mentioned before the present water-front lay approximately 150 m to the seaward in the summer of 1962

FIG. 3.--FREQUENCY DISTRIBUTION ON WAVE HEIGHT

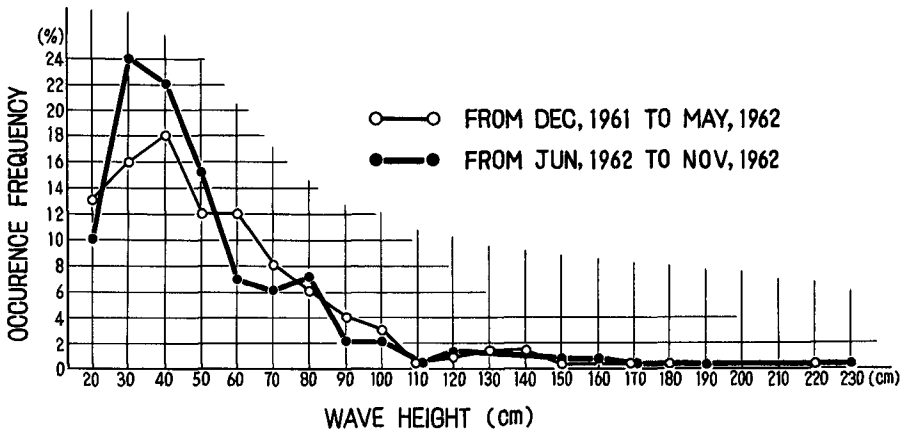

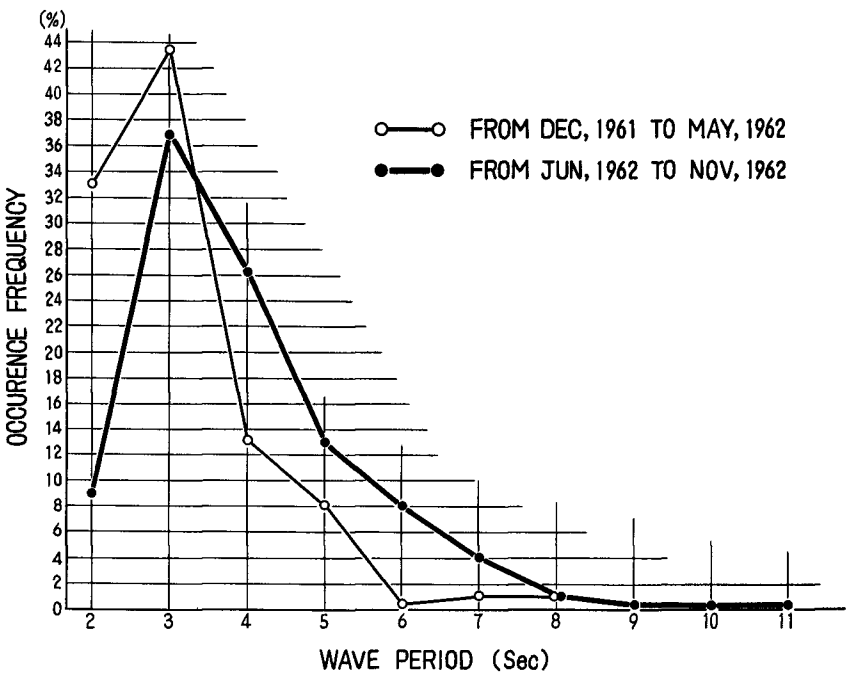

FIG 4.--FREQUENCY DISTRIBUTION ON WAVE PERIOD

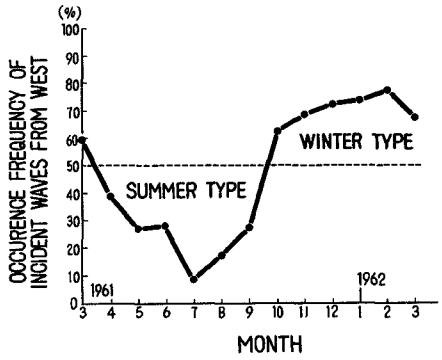

FIG. 5. --FREQUENCY DISTRIBUTION ON DIRECTION OF INCIDENT WAVES

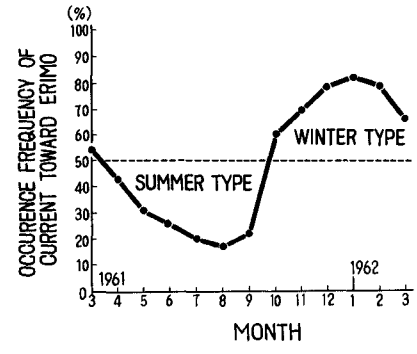

FIG 6 --FREQUENCY DISTRIBUTION ON DIRECTION LITTORAL CURRENT

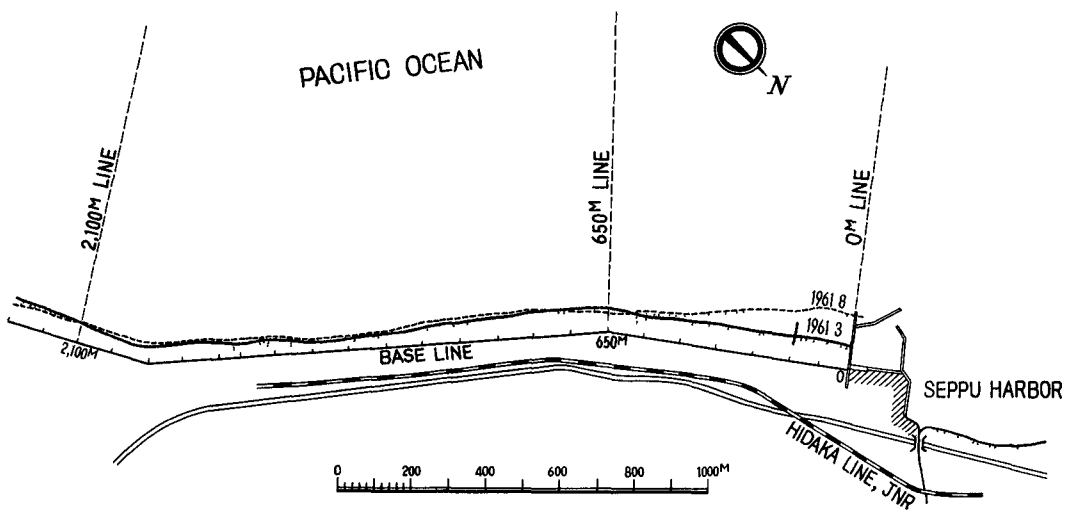

FIG 7 --LOCATION MAP NEAR HARBOR "SEPPU"

as compared to that of 1948, which is the year prior to the construction of the breakwater. The water-front showed a recession of 50 to 80 m usually in winter. The total amount of this recession is, however, decreasing gradually in accordance with the two added jetties, one of which extends from the joint where the south breakwater first turns and another is placed about 150 m apart along the coast to the east side of the breakwater. The two jetties are approximately 40 meters in length and both project at right angles to the coast line. This fact is clearly shown in Fig.8, in which the results of monthly observations are plotted regarding the progression or recession of the beach. In each diagram the distance from the base line to the water-front is plotted in the ordinate and the time is plotted in the abscissa.

In Fig.8, "a", "b", "c", "d",....show respectively the position on the shoreline at 150 meter intervals in a south-easterly direction. Fig."a" shows the position of the water-front at a point close to the south breakwater in the manner as above. Figures "a",...."d" indicate the maximal and minimal line of progression and recession of the shore line during August~September and January~February. It was noted that in accordance with the progressive distance from the harbor as in "e", "f",...the difference between the two decrease.

Now at greater distances from the harbor beyond the 2000 m point the time of the progression and recession show a complete reverse with the maximal recession seen from August to October and the maximal progression seen from February to March. Fig.9. represents the profile of the sea bed at points "0", "650", "2100". As may be seen, similar phenomena as indicated above are apparent. As a result of sounding, it was shown that at depths over 6.0 m no changes were seen on the sea bed. This site is 700 m off shore. As may be seen in this Figure, no sand bars were present which is a special feature of this coast.

From the above findings, the following may be surmised: ie (1) along the gently curving waterline between the south breakwater of Seppu harbor to the Niikappu river mouth a large amount of sand shifts towards the harbor in summer and during the winter this shift reverses its direction. (2) This migrating sand mainly consists of bed load drift which moves along the water line. This may be seen in the size distribution which clearly shows the difference in size of sand particles at the sea bed at a depth over 5.0 m as compared against that along the beach line.

In short, every year in summer during the typhoon season the swells (or waves of long period) sweep in along the coast and cause a massive migration of the comparatively large grained sand which makes up the beach line. This shifting sand moves out to the mouth of the harbor. After the blocking the mouth, at times part of this sand is known to reach the northern beach. It may also be surmised that the smaller sized sand grains are carried off shore composing a suspended drift

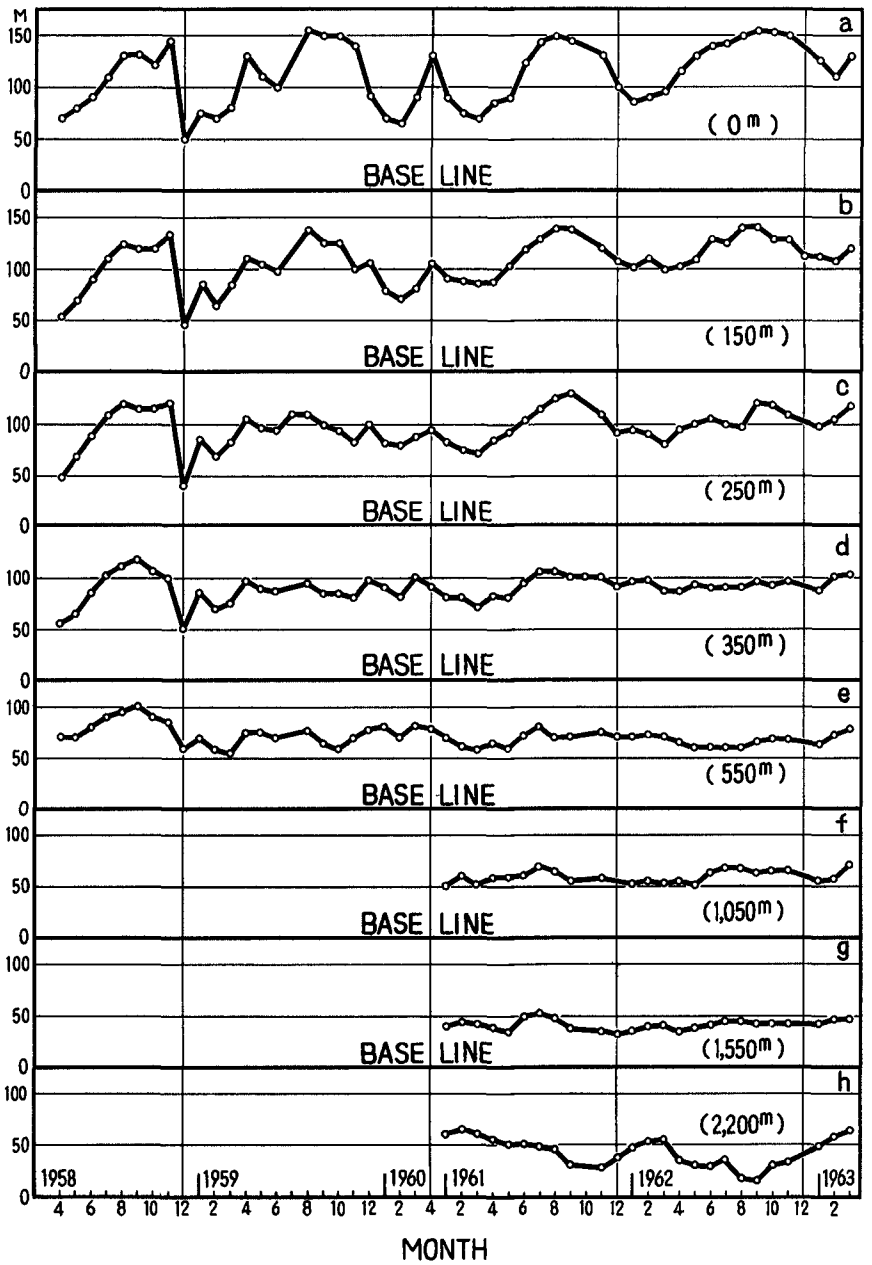

FIG. 8. --CHANGES OF BEACH LINE ON SOUTHEASTERN SIDE OF HARBOR "SEPPU"

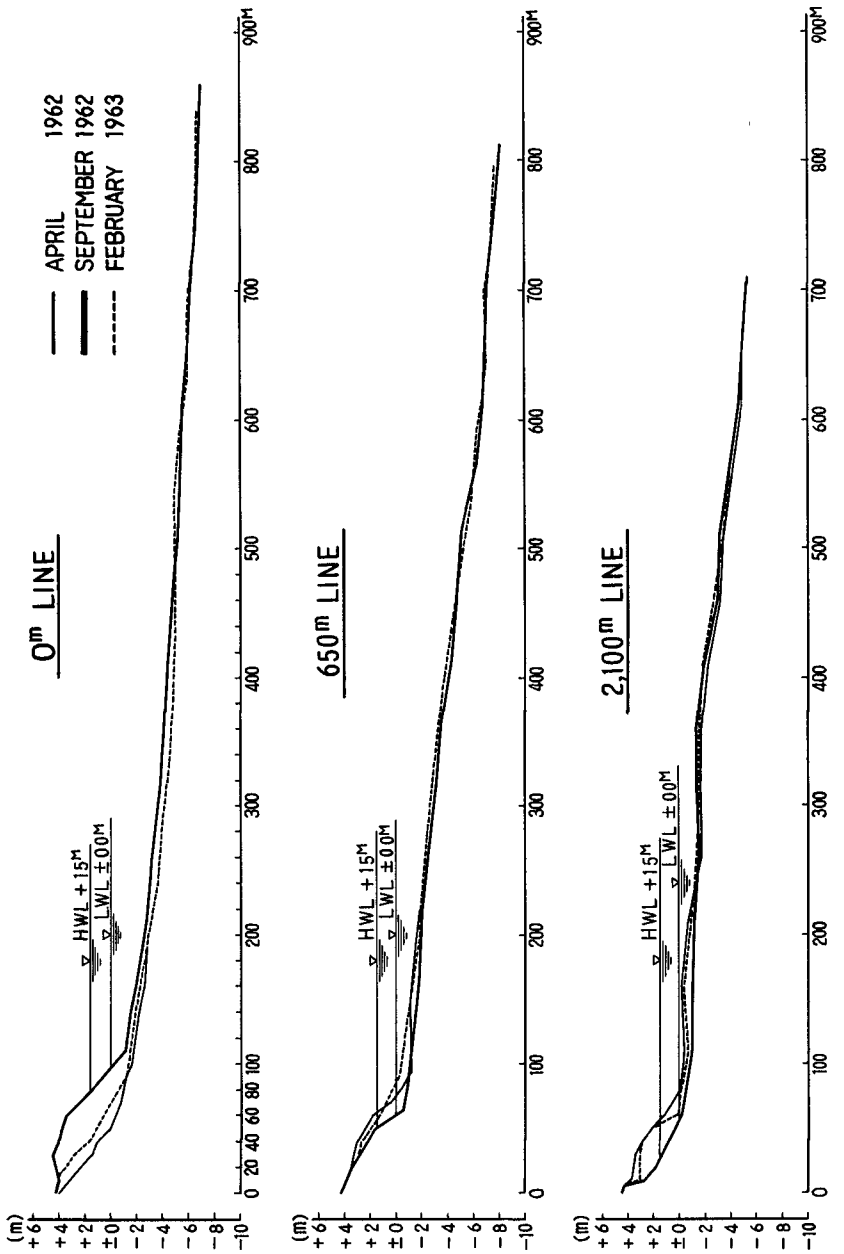

FIG. 9.--PROFILE OF SEA BED NEAR "SEPPU"

and may be carried across the front of the harbor entrance to the west.

However, a complete investigation concerning this has not been carried out. Nevertheless, it may be considered that no significant difference in volume between the amount of sand newly deposited along the entire sloping coast line between Seppu and the Niikappu river mouth, and the sand carried west past the harbor mouth exists. Therefore, it may be said that the blocking of the harbor mouth in summer is caused by a rapid shift of the sand deposited during the short period over the entire length of this section which results in the accumulation of sand on the south-eastern side of the harbor.

Summarizing the above, the following may be said.
(1) The beach line to the south-east of the harbor, when viewed for the entire year, shows an approximately orderly progression and recession.
(2) No remarkable sand bars are seen on the entire bed of the sea in the off shore areas in front of the harbor.
Further, it was observed that the sorting coefficient of the sand at depths over 5.0 m was small and even, showing a remarkable difference as compared against the beach line sand. Still further, in regard to the sand blocking the Seppu harbor, the size was large and generally the size was the same.

THE DRIFTING SAND

In the case of this model experiment no dynamical similarity between the motion of sand particles in the model and in the prototype exists, because the same kind of natural sand as in prototype was used for the movable bed materials. Now, as well known, sand movement on a coast may be divided into the so-called beach drift and suspended drift. However, in such a small scale model as described in the later part of this paper, it is impossible to observe the motion of the suspended drift itself in the model. In spite of this, a satisfactory similarity, at least qualitatively, with regard to the motion of the bed load drift may be expected.

From this point of view, the mean diameter and the sorting coefficient were chosen as the index, which shows the difference between these two types mentioned above. Thus, from the results of sieve analysis on numerous samples collected at various points on the beaches and shorefaces extending around Seppu, it was suggested that a large quantity of drifting sand in the form of beach drift or bed load drift contributed in blocking the harbor mouth. This may be said at least within the extent of the present work.

MODEL EXPERIMENTS

The initial purpose of the present model experiments was in determining experimentally the extent of the effect of the two proposed jetties on the prevention of harbor blockage. The jetties were proposed by the Harbor Section of the Hokkaido Prefectural Office. The dimension of the model basin was 7m x 12m. The depth of the tank was 0.4 m with a movable bed constructed on a 1/100 scale. The prototype represented by this model covers an area of 1060m x 670m. The sea sand used in the movable bed has a mean diameter of 0.4 mm and a specific gravity of 2.7. Since this is an experiment concerning the shifting of sand on the sea bed, as the law of similarity Reynold's law should be applied, however in the present work the calculation made on the wave heights and periods in the model experiment were based on Froude's law. The time scale will be dealt with in a later series of work. In other words, the size of sand used in the present model had no direct relationship with the prototype, and the movement of the sand was caused by the scoring force of the waves.

As for the current pattern since Froude's law was applied in the construction of the model the path of sand migration insofar as the beach drift is concerned, shows a similarity. Here the author considered the fact that the sand of the water line moves by the scoring force of waves on the sea bed, eventually resulting in erosion of the shore or accumulation of sand. However, he decided to ignore the complicated mechanism of the above, and endeavored to reproduce the outward appearance of the end result of the above as seen in the prototype. This was because, he considered that it would be sufficient to achieve the purpose of the preliminary experiment. Further, as seen in the description of the prototype, as a result of sand sampling and observations on shore line changes it was determined that the drift phenomena in the vicinity of Seppu harbor were almost invariably related with beach drift. Thus, in the model experiments qualitatively it was considered sufficient to observe the beach drift alone which greatly simplified the work.

In regard to the incident direction of the waves in the model, the direction was based on data previously described. Namely, the summer waves were from a SSW direction and the winter waves were from a westerly direction and the height and wave period, as described under waves, it was shown that wave heights of 50～60 cm and wave periods of 3～4 sec. had the highest frequency of occurence. However, at the actual site during August and September when the shore line rapidly advances and the harbor mouth is blocked, wave heights of 1.5～2.0 m with periods of 7～10 seconds show the highest frequency of occurence under the influence of typhoons. Now in view of the fact that during this period, the highest

number of no observation days is seen, the accuracy of the data on long wave periods and wave heights may be lacking. This was taken into consideration and the experimental wave heights were set at 2.3 cm with a wave period of 1.0 second in 1/100 scale model. Naturally, comparative studies were made on the most frequent wave heights and periods.

The experiments were conducted as follows. The proposed jetties were placed in their positions in the model. Thereupon, as an initial step, waves from a SSW direction were sent in continuously over a long period and at given intervals, the changes of the beach line and the profile of the sea bed were observed. Thus, in the final stages the experiments were continued until the beach line advanced to the head of the breakwater and blocked up the entrance of the harbor. The time required for the above was used as the criteria for the purpose of comparing the phenomena as seen in the model experiments. As mentioned previously, the above has no similarity with the actual time of the prototype. An example of the experiment is given in Fig.10.

Next, experimentally, following the experimental on the proposed jetties, a plan for an offshore breakwater in parallel to the sea shore, it is well known that on the inland side a tombolo appears. In this particular case wave diffraction is seen at both ends of the offshore breakwater, and the resulting waves are reflected by the south breakwater. This results in a current between the offshore breakwater and the south breakwater which flows in the opposite direction to the normal current of this coast. As a result, the sand drift to the west is strongly inhibited, and a tombolo forms at the east end of the offshore breakwater. One example of this experiment is given in Fig.11.

By this method an extensive sand jetty reaching out to the offshore breakwater is formed by the strength of the waves. This results in a considerable delaying of the arrival of the sand pile to the mouth of the harbor. The location of the offshore breakwater together with its length was varied within reason.

While some difference was seen in the results, in all cases, insofar as the experiments using the same model are concerned, the time required for the tombolo to form was twice as long as that of the time lapse for the harbor mouth to be blocked by sand in the presence of the proposed jetties as set forth in the original plans.

In order to determine still further the effect of this offshore breakwater, the same model was reproduced in 1/50 scale in a 20m x 15m tank. The results of this large scale model experiments are shown in Fig.12....Fig.16. While the scale of this second model is twice as large as that of the first model, the sand composing the movable bed in the second case was the same size as the first.

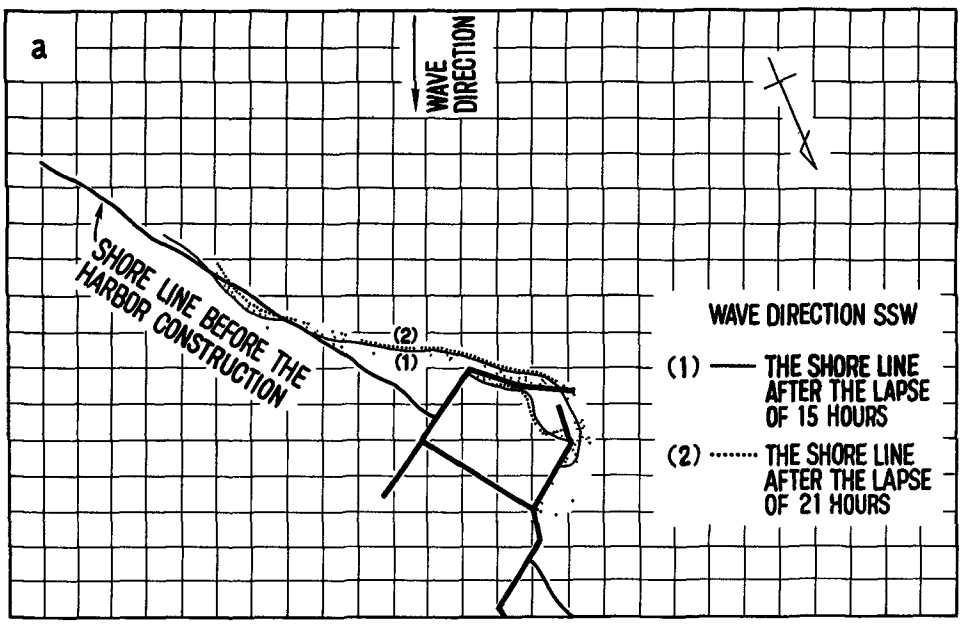

FIG. 10.--RESULTS OF EXPERIMENT IN THE CASE OF JETTIES

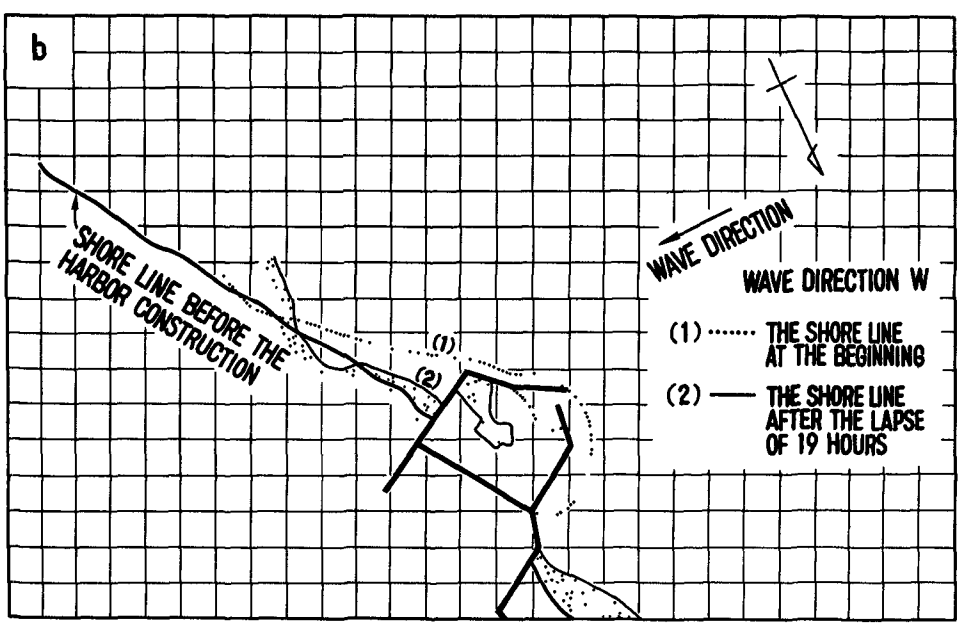

FIG. 10.--CONTINUED

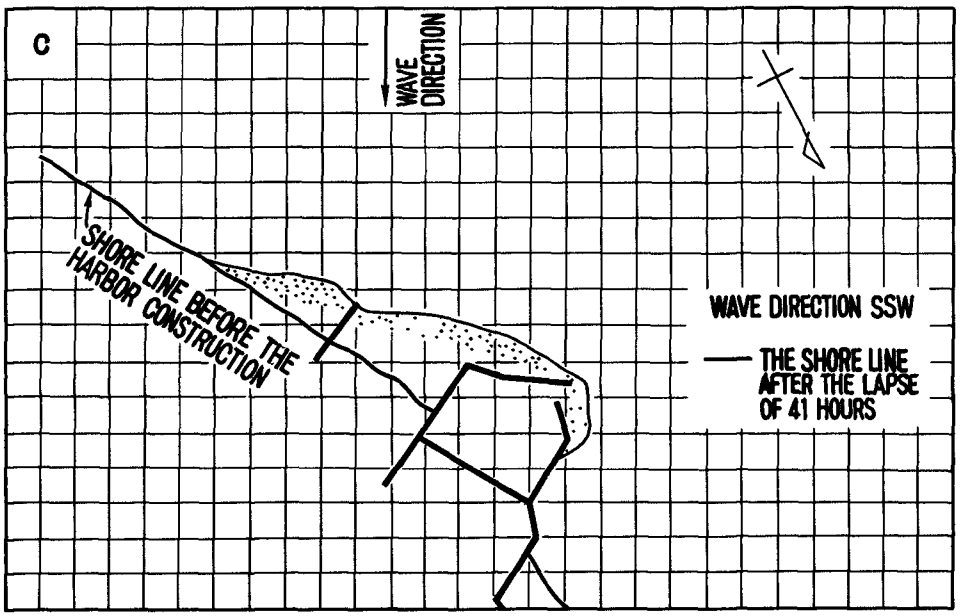

FIG 10.--CONTINUED

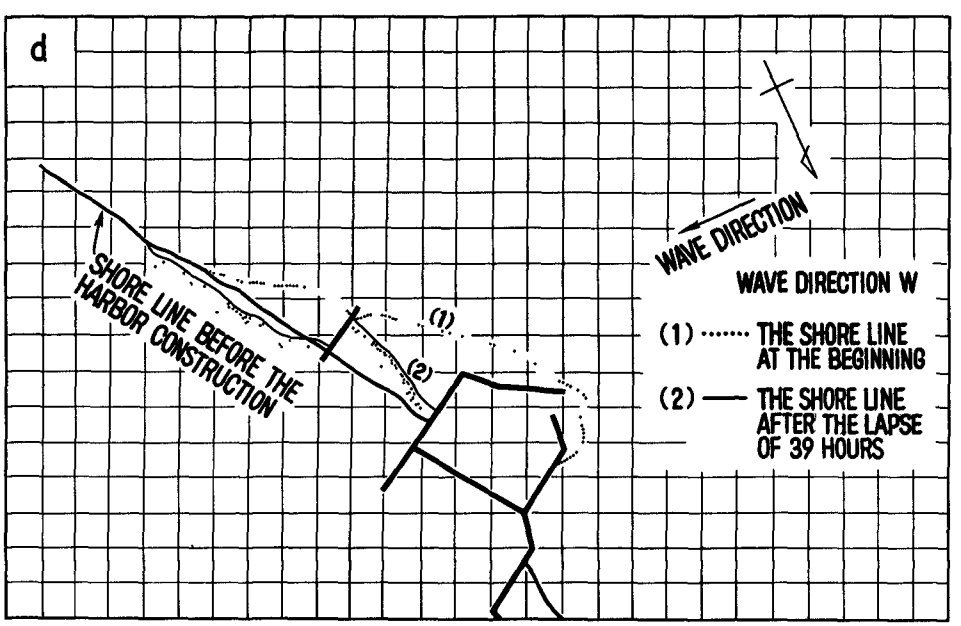

FIG 10 --CONTINUED

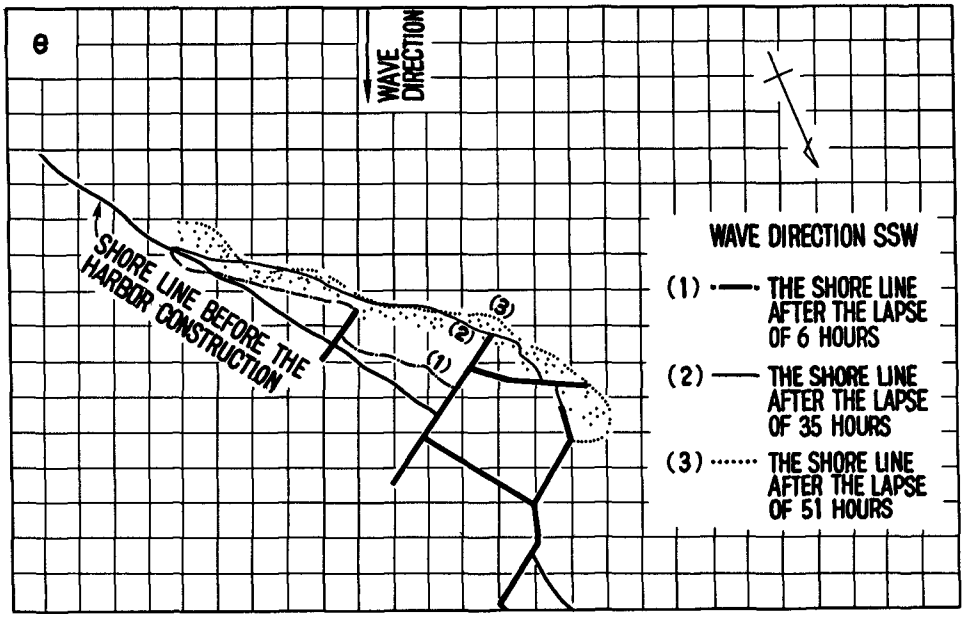

FIG. 10. --CONTINUED

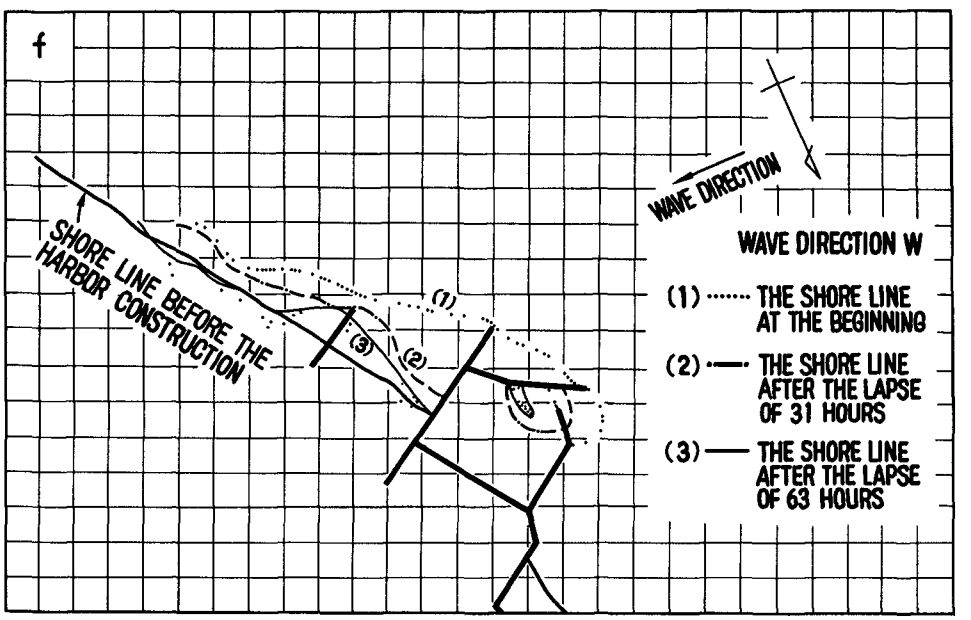

FIG 10 --CONTINUED

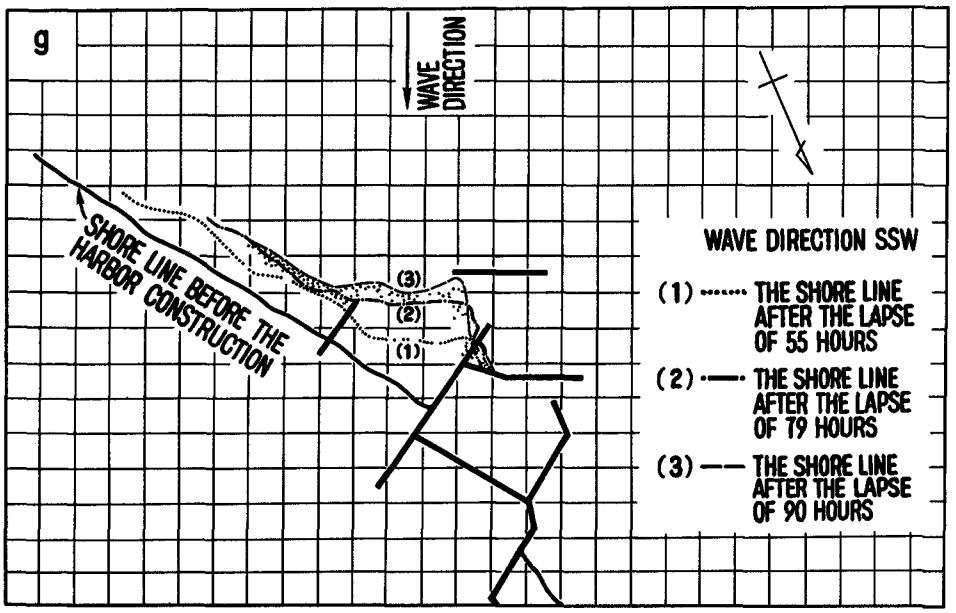

FIG. 11. --RESULTS OF MODEL EXPERIMENT IN THE CASE OF OFFSHORE BREAKWATER (SCALE 1/50)

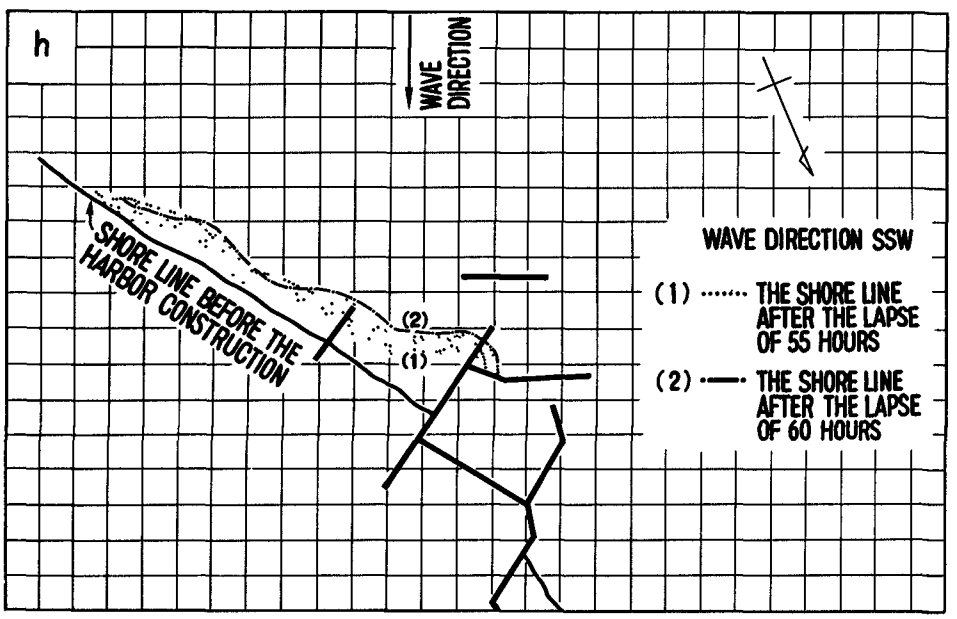

FIG. 11. CONTINUED

FIG 12 --RESULTS OF MODEL EXPERIMENT IN THE CASE OF OFFSHORE BREAKWATER (SCALE 1/100)

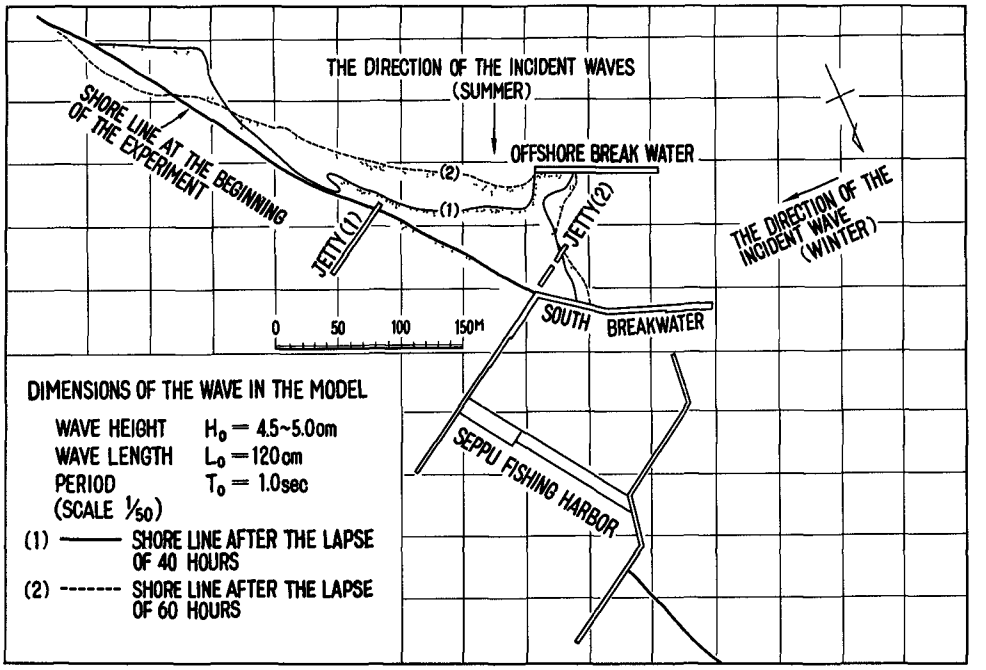

FIG 13 --RESULTS OF MODEL EXPERIMENT IN THE CASE OF OFFSHORE BREAKWATER (SCALE 1/100)

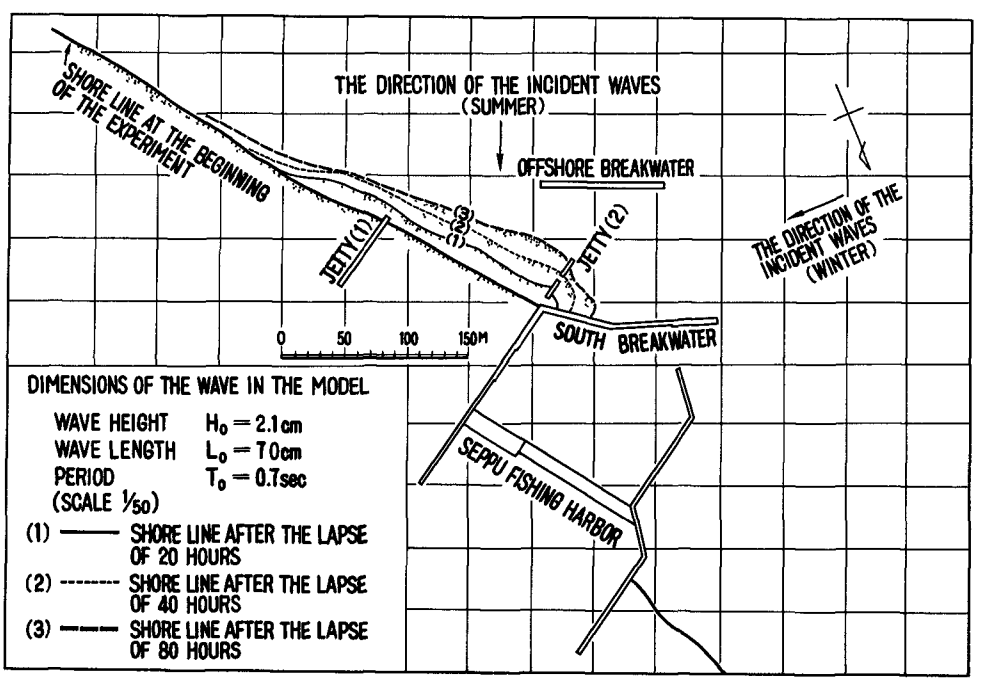

FIG 14 --RESULTS OF MODEL EXPERIMENT IN THE CASE OF OFFSHORE BREAKWATER (SCALE 1/100)

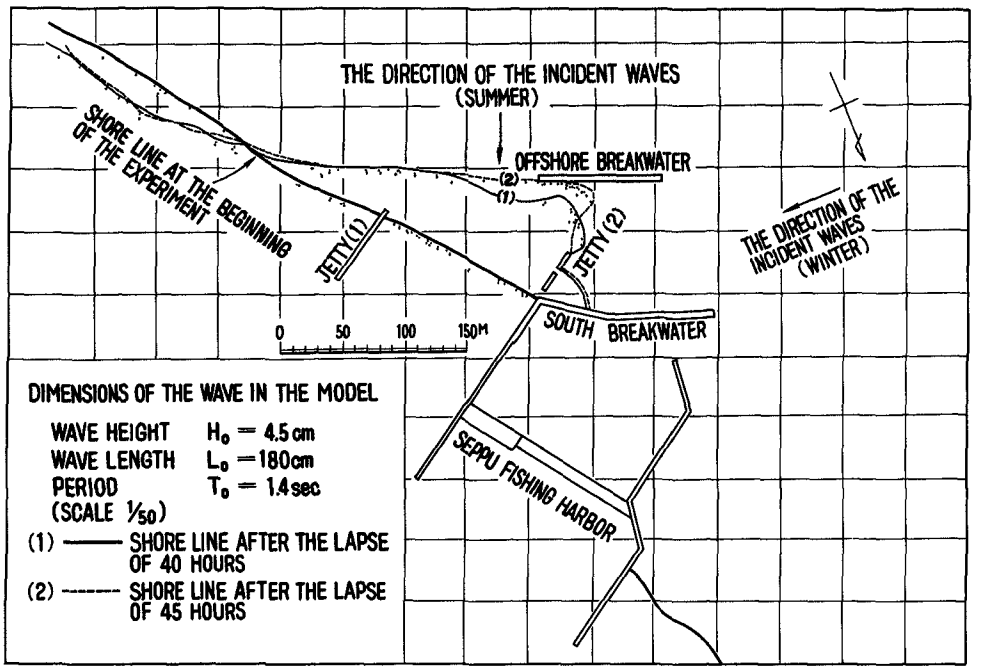

FIG 15 --RESULTS OF MODEL EXPERIMENT IN THE CASE OF OFFSHORE BREAKWATER (SCALE 1/100)

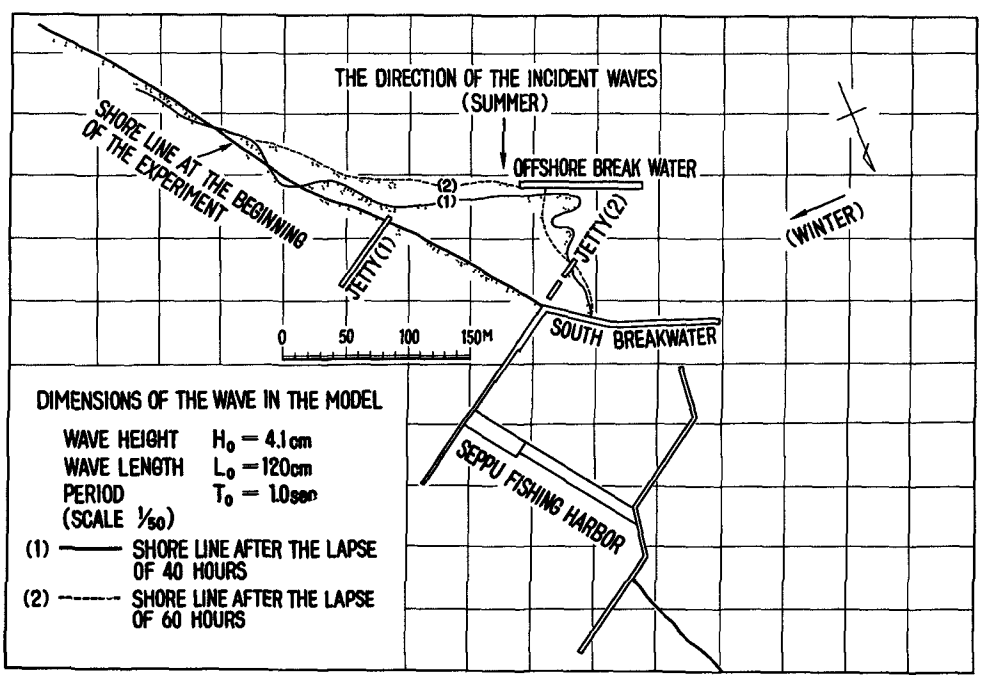

FIG. 16 --RESULTS OF EXPERIMENT IN THE CASE OF OFFSHORE BREAKWATER

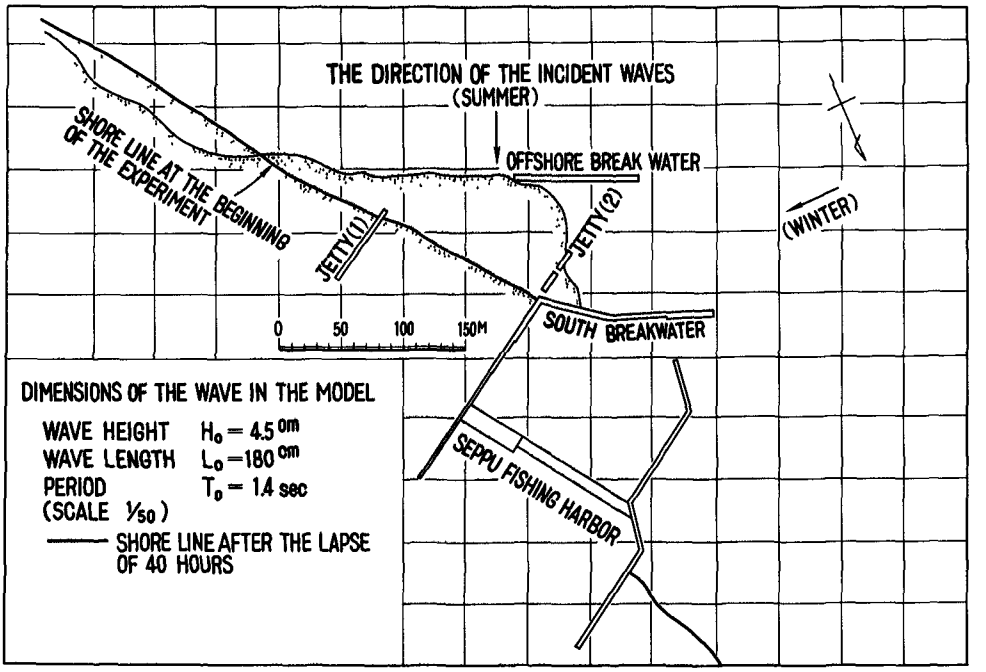

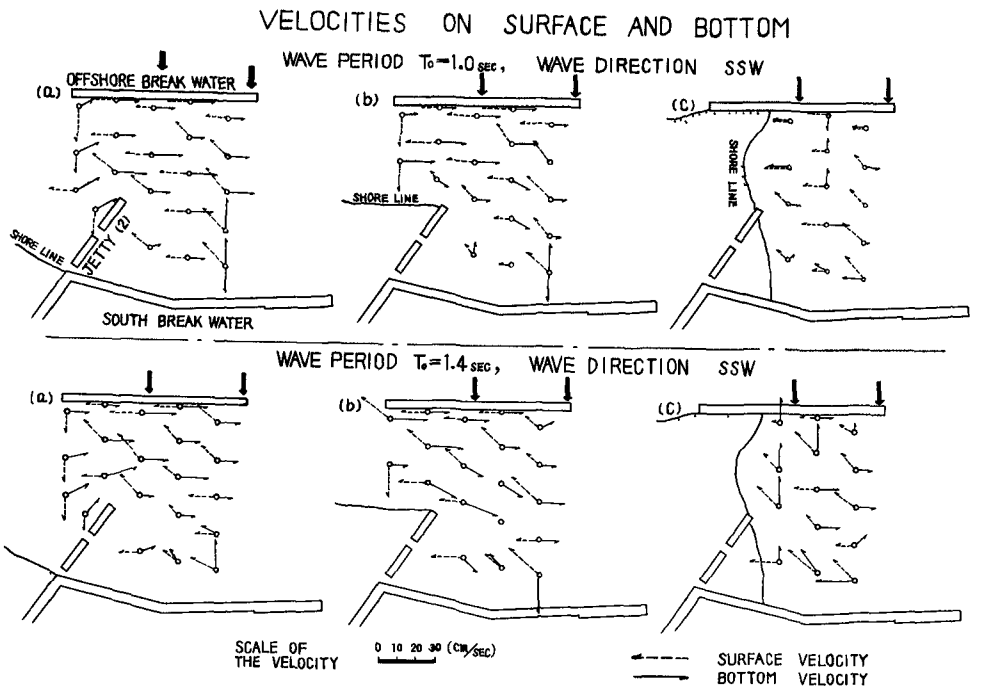

FIG 17 --VELOCITIES MEASURED ON MODEL

Therefore the time standard differed from that in the first model experiment.

As may be seen in Fig.17, in the area between the offshore breakwater and the south breakwater, the direction of the localized currents seen on the sea bed and on the surface change in accordance with the development of the tombolo. Moreover, in all cases the above mentioned currents move in such a way as to prevent the infiltration of the drift sand into this area.

CONCLUSION

Since, all effective methods for the prevention of sand blocking of Seppu harbor, are of such a nature that the balance of summer and winter waves must be taken into consideration, it is imperative that any instalation which may inhibit, even to the slightest extent, the recession of the south-eastern shoreline of the harbor caused by westerly waves in winter must be strictly avoided unless of course the advantages of such an instalation are outstanding in a positive direction.

From this point of view, it may be said that the original plans for the prevention of sand drift along the water line, are in all cases, direct means of preventing sand migration by jetties, while the proposal of an offshore breakwater has its aim on the indirect effects of diffraction and reflection by which it is proposed to inhibit the migration of the sand.

In the case of this particular coast the direction of this offshore breakwater, approximately coincides with the outstanding westerly wave direction in the winter months, and as a result it hardly inhibits the recession of the south-east shore line.

In short it seems obvious that a direct assault on the natural forces would merely result in a tremendous expenditure. Thus, in the case of a small fishing harbor such as Seppu, from a financial point of view alone, methods which directly oppose the natural elements should be avoided, and such forces should rather be diverted and put good use.

As mentioned before the original jetties were aimed at directly blocking the waterline sand drift. In this case, by diverting the direction of the coast current caused by breaking waves in an offshore direction, the migration of the sand along the shore line is swept seawards and the jetties serve as sand accumulation pockets until the sand pile advances to the head of the jetty. However, the effectiveness of this direct blocking jetty method is seen only when the absolute volume of shore line drift sand is small, or when the grade of the sea bed is steep .

Now in the case of Seppu where the drift sand volume from a single direction is extremely large, and moreover since

the sea bed slopes gently away, the sand deposit rapidly reaches the head of the jetty and instead of being swept seawards, the deposit creeps around the jetty and advances.

In place of the above jetty method, by constructing an offshore breakwater in an appropriate position, it would become possible to make the sand deposit pocket much larger and to delay the time of the sand arriving at the harbor mouth at least until the beginning of the recession of the south-east shore line by winter waves.

ACKNOWLEDGEMENT

First of all, the writer is deeply indebted to Dr. H. Fukushima, Dr. M.Kashiwamura, and Dr. I.Yakuwa, the faculty member of school of Engineering, Hokkaido University, for their valuable field data on the coastal condition and phenomena. The writer further wishes to express his gratitude to them for the techniques developed by them in measuring the drifting sand and observing the current. The writer is particularly grateful to Mr. H.Shirakawa, the cheif of the Harbor Section of Hokkaido Prefectural Office and his staffs for their co-operation in the field observation.

REFERENCES

1. Fukushima,H and Mizoguchi,Y
Field Investigation On Suspended Littoral Drift: Coastal Engineering in Japan, Vol.1. 1958

2. Fukushima,H and Kashiwamura,M
Field Investigation On Suspended Sediment by the Use of Bamboo Samplers: Coastal Engineering in Japan Vol.2. 1959

3. Fukushima,H and Kashiwamura,M
Some Experiments on Bomboo Samplers: Coastal Engineering in Japan Vol.4. 1961

4. Maione,A A Study of the Possibility from the Technical and Economic points of View--of Arresting the Erosion of Sea Coast: Bulletin of PIANC Vol.4. 1963

Chapter 23

THE CONSTRUCTION OF A DRIFT-SAND DYKE ON THE ISLAND ROTTUMERPLAAT

K.P.Blumenthal.
Chief engineer Rijkswaterstaat (Public Works),
department for Land Reclamation at
Baflo, Holland.

SUMMARY

In the paper a description is given of the construction of a dyke using drift-sand on a sandy shoal off the Netherlands' Northcoa called "Rottumerplaat", and of the experiences gained hereby. Only where necessary for general understanding reference is made to conditions and experiences in other places in Holland, where dunes or dykes are built using drift-sand.

The object of the dyke under consideration is to obtain a flood-free strip of land in an area, where this may be useful for future hydraulic engineering works. A special circumstance on Rott merplaat is the low level in relation to the tidal curve: it has a ways been assumed that construction of a drift-sand dyke, starting on such a low level, would have no chance of success.

The most important points to which attention is drawn are t following:

a) The choice of the design-plan (layout) and the position of this plan in relation to the winning area and to wind directions;
b) The method of catching sand by windscreens, and the materials used for the construction of these screens;
c) The method of fixing by vegetation the sand once it is caught. The most frequently used species of plants will be discussed in this context.

Compared to all other techniques of constructing seadefenc drift-sand dykes and dunes are very cheap. They cannot be used, however, for important sea defence design, because a driftsand dy cannot be realized in a short time, and also because the influenc

of chance is not to be neglected.

With the exception of the special case of Rottumerplaat drift-sand dykes or dunes are therefore only used to improve or strengthen existing sea-defences.

1. INTRODUCTION.

The knowledge of techniques to construct drift-dykes and drift-dunes is very old in the Netherlands. For this reason, and also because the principles of these techniques are relatively simple, little has been published on this subject. There is evidence, that in other countries there are many, who do not even suspect the existence of these methods. It appeared to be useful, therefore, to give some information on recently gained experiences in this field.

Drift-dykes or dunes have been and are being built or maintained in the Netherlands in several parts of the islands in the south-west, on the westcoast and on the islands bordering the "Waddenzee" in the north. In many parts, by the existence of a belt of dunes the construction of an expensive sea-dyke becomes redundant. In places where the width of the chain of dunes is too small for sufficient security, it is possible when circumstances are favourable, to increase the security by stimulating the growth of dunes by drifting sand on the seaward side of the existing dunes. Also, especially on the "Wadden"-islands, low areas are being protected against the sea by a drift-sand dyke, the construction of which is far less expensive than building a real sea-dyke.

In the following a description will be given of the construction of a drift-sand dyke on the island "Rottumerplaat", the geographic position of which is shown in fig. 1. With respect to its function this dyke occupies a special place. The Rottumerplaat is a somewhat unstable sandy shoal on the northern edge of the area of shallows called the "Waddenzee". Before the building of the drift dyke began, the height of the shoal (with the exception of a small circular dune near the south-eastern end) was such, that it was entirely flooded during storms several times each year. The reason for the construct-

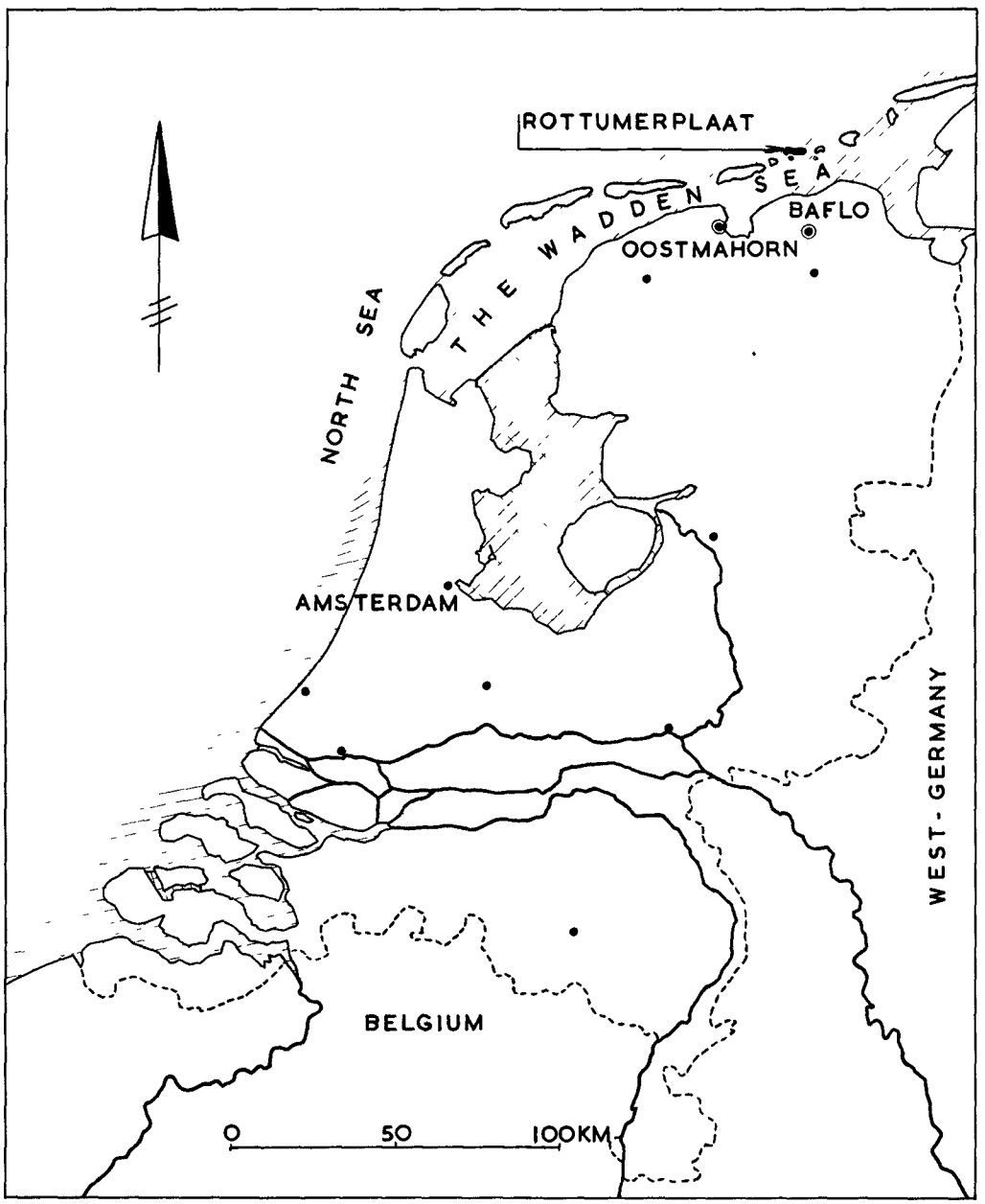

FIG. 1 THE NETHERLANDS, WITH GEOGRAPHIC POSITION OF THE ROTTUMERPLAAT

ion of the dyke was to obtain without great expense a base for possible future damming and reclamation works in the "Waddenzee". Beside other considerations, that will be discussed later, the choice of the layout (fig. 2) was determined by the necessity to keep the sand dyke, if possible, clear of the influence of the instability of the shoal, caused by the tidal currents.

It should be pointed out, that no generally accepted technique exists for the construction of drift-sand dykes or dunes. Beside personal preference or experience, the method is largely determined by local circumstances and by the result that is expected. Although in the following from time to time other possibilities will be pointed out, the argumentation is determined by the experiences on the "Rottumerplaat", and does not claim general validity. The object of the paper is only to show to those who are interested but have not previously heard of it, how, by utilizing drifting sand, it is possible to obtain a sand dyke of considerable size with relatively small expenses.

2. GENERAL OUTLINE OF THE CIRCUMSTANCES AND OF THE RESULTS.

As an illustration of the changes the Rottumerplaat has undergone, fig. 3 gives the positions of the contour-line of mean high tide (MHT) for a number of years between 1900 and the present.Though not very distinct, there is apparently a periodicity of decrease and increase, especially of the northern shoreline. This phenomenon can be explained if it is assumed, that the transportation of sand from west to east along the islands, takes place, at least in part, by the movement of sand-banks. Such a sand-bank unites with the Rottumerplaat causing the shoal to expand. The tidal currents then gradually clear the expansion away, which is a different way of saying that the sand-bank moves on in easterly direction.

In this way the size of the accumulation area, that is the beach situated to windward of the projected drift-dyke, from which beach the material for the dyke is obtained, is constantly changing. To ensure the safety of the drift dyke, the ground-plan has to be designed at sufficient distance from the extreme landward extension

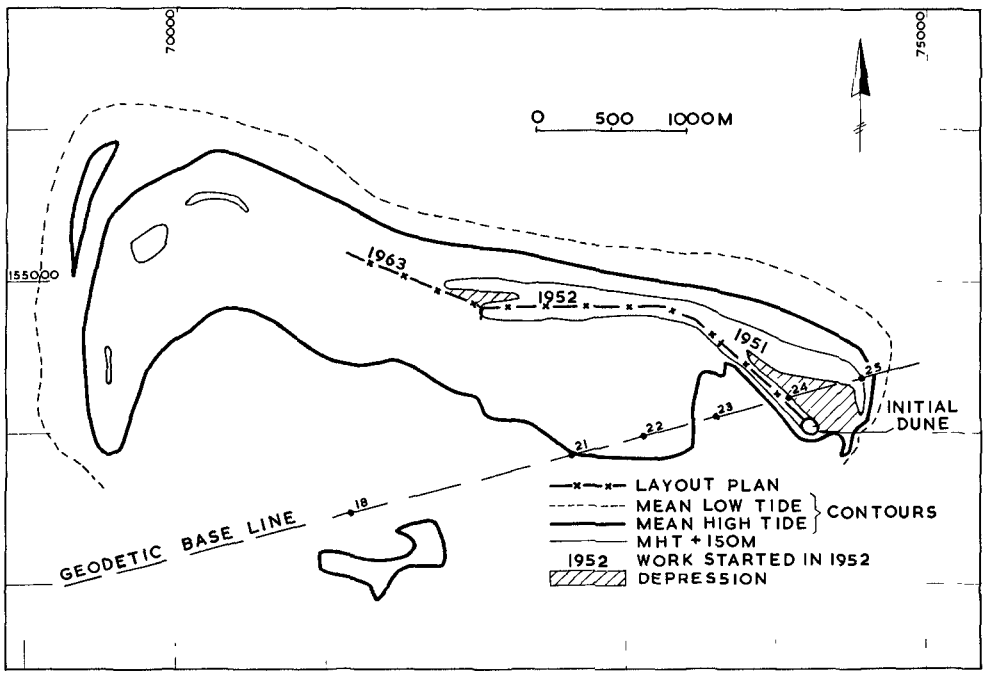

FIG 2 SITUATION OF ROTTUMERPLAAT WITH LAYOUT PLAN OF THE DRIFT-SAND DYKE AND CONTOURS

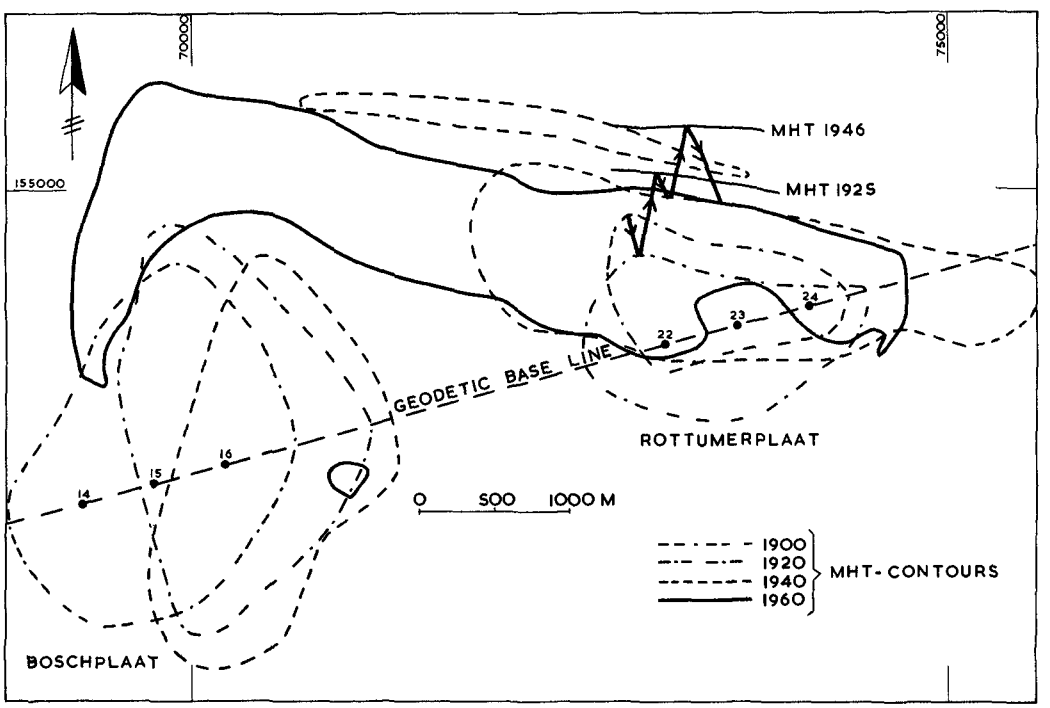

FIG 3 ROTTUMERPLAAT COURSE OF MEAN HIGH TIDE CONTOURS FROM 1900 TO 1960

of the MHT line.

Fig. 4 shows a cross section of the Rottumerplaat that is to be regarded as more or less characteristic. The same cross section is shown for different years, i.e. 1952 (the year in which the work began) and some of the subsequent years to 1962 incl. Naturally the initial situation as shown in the figure is only valid for this one profile, but to put it in a more general sense, before the beginning of the work the height of the shoal in the places covered by the design plan, was between N.A.P. (national zero level) + 1,25 m and N.A.P. + 1,65 m, or roughly between MHT + 0,25 m and MHT + 0,65 m. This is at variance with the general opinion, that the initial height should not be lower than MHT + 1,00 m. In the beginning indeed it looked as if the work yielded little result, especially on rough visual observation.

Fig. 5 shows a graph giving the sums of the acquired quantities of sand (in m^3/m^1 drift-dyke) plotted against the years 1950 to 1963. The quantities have been determined by cubature of annual levelings. From this, as opposed to the superficial impression, it is apparent that the annual gain during the first years has not been less than later on (the depression in the graph relates to a year in which the dyke suffered considerable damage from a storm surge). The course of events during the first years is, that the sand, acquired during the drift season, is flattened to a "pancake" by the water during the winter season. In this way a wide base is formed, that does have a height of 1 m or more above MHT. Only after this stage has been reached, rapid heightening can be pursued. This means that, if the work has to be started at a low level, it is sensible to place the windscreens (to be discussed later) initially in such a way that width is gained rather than height. This makes it possible to adapt the width of the base consciously to the planned height of the drift-dyke. For instance, in the case under consideration, where a height of N.A.P. (national datum) + 7,0 m is pursued, the basic width should be 50 m at a level of N.A.P. + 2,5 m. Evidently these figures are strictly related to the characteristics of the prevailing tidal circumstances.

The graph of fig. 5 shows, that the total profit in a period

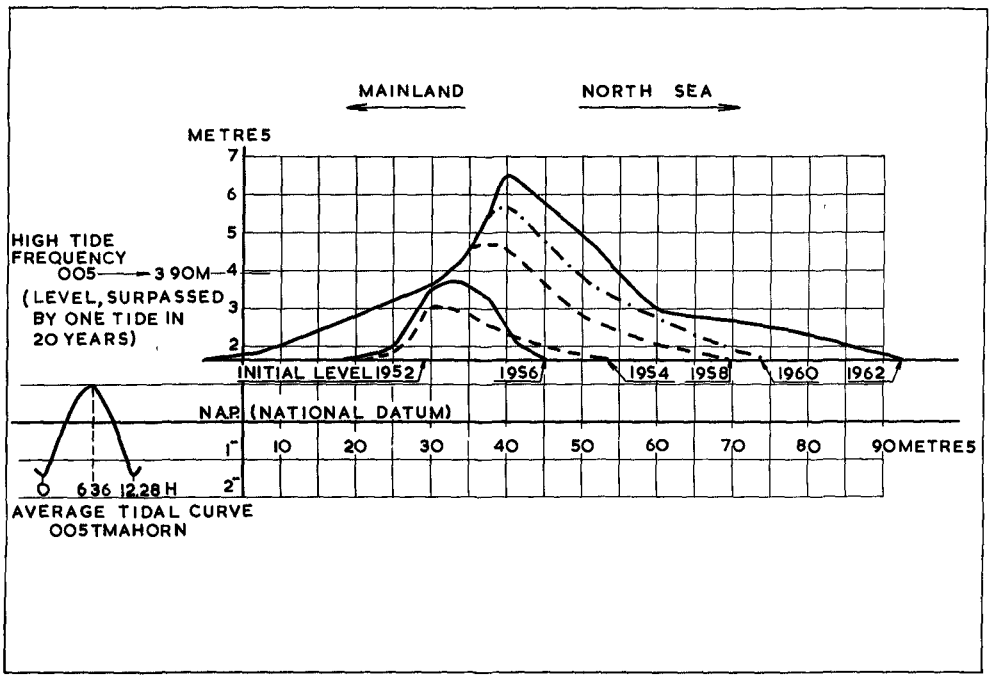

FIG 4 DEVELOPMENT OF THE DRIFT-DYKE LEVELING RESULTS IN A CROSS SECTION FROM 1952 TO 1962

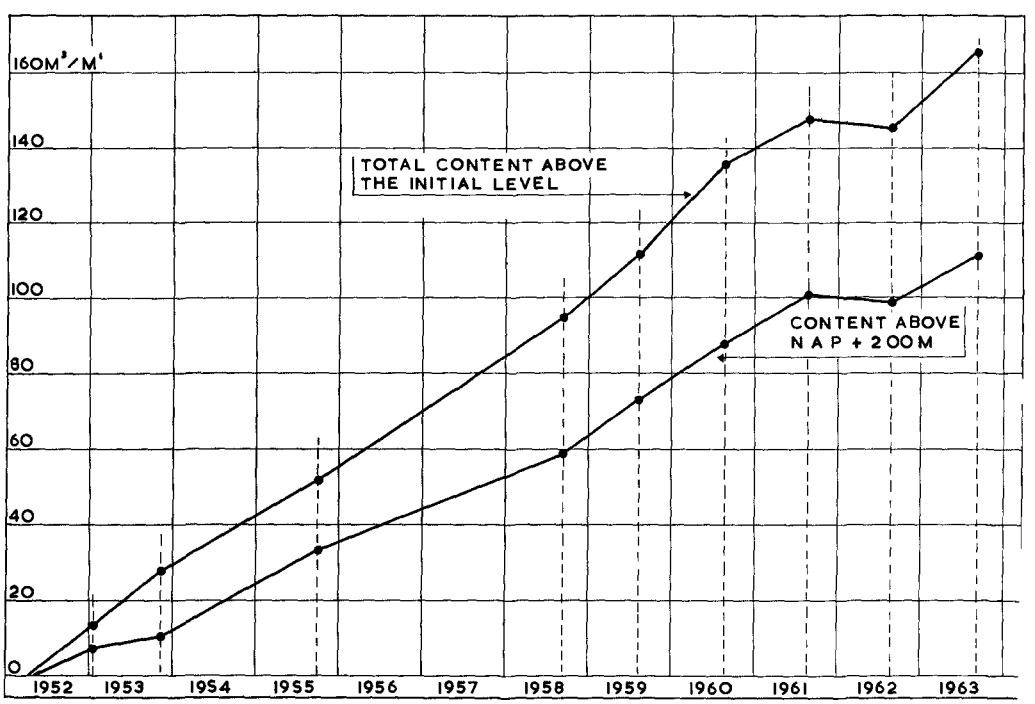

FIG 5 ANNUAL INCREASE OF SAND-CONTENT IN M^3/M' OF THE DRIFT-DYKE ON THE ROTTUMERPLAAT

of 11 years amounted to about 160 m^3 per running metre.

3. TECHNICAL DATA.

For the technique of the construction of a drift-sand dyke two factors are of paramount importance: the determination of the most favourable layout-plan, and the method of catching the sand. Both are largely determined by local circumstances and by the result that is to be obtained.

a). The layout. On the Rottumerplaat two facts were established from the beginning: the ground-plan had to be joined to the existing dune at the south-easterly end of the shoal, and from there it had to run roughly in the longitudinal direction of the shoal, that is west-north-westerly.

To obtain more detailed information on the most favourable design a number of crosses was set up as shown in fig. 6. The crosses were made from brushwood-screens, and their object was to show where and from which quadrant the best catch of sand was to be expected. In the judgement on this, visual observation played an important part. The figures given in the sketch are based on the leveling of a single profile over the cross and are only meant to give rough figures for the ratios. More direct methods to measure the transport of sand across the shoal were unknown in those days, at least in the department in charge of the execution of the work.

The foregoing was regarded to be sufficient to determine the layout as given in fig. 2. Even now it is not to be seen that a different plan would have yielded better results, although experience has shown that favourable and less favourable conditions have played their parts.

Highly favourable is the exposition on the dyke with respect to the accumulation area and to the wind direction. Although winds from the north-east quadrant are not very frequent (they often occur during the spring), they have a strong drying effect and are accompanied with low sea levels. Indeed, an important part of the annual profit is often made during a few days with a strong wind

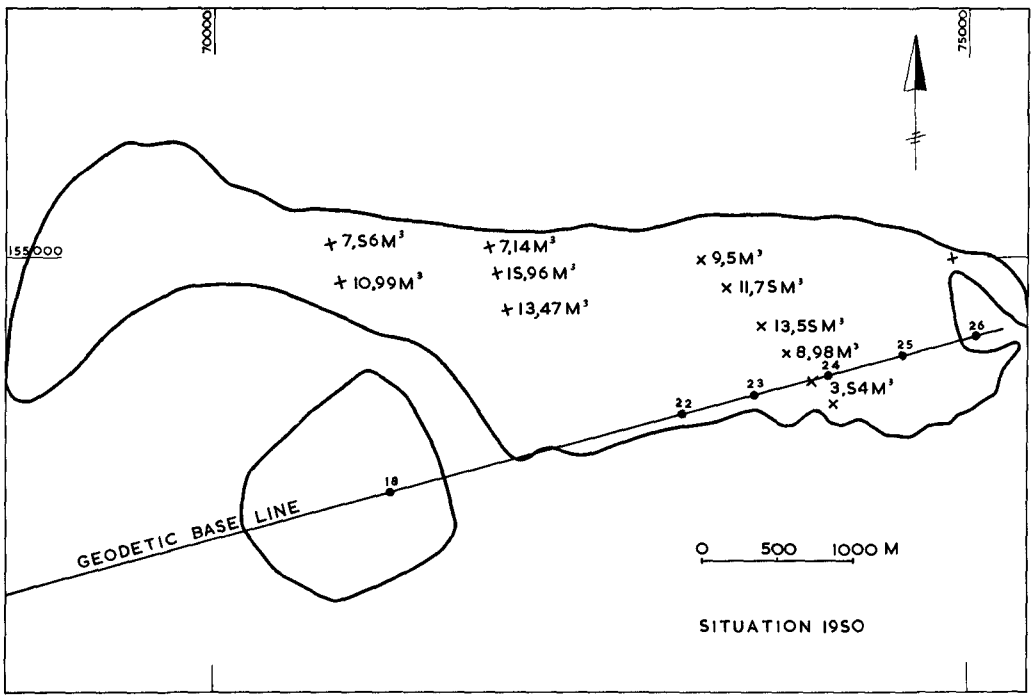

FIG 6 RESULTS OF DRIFT TESTS FOR CHOICE OF LAYOUT

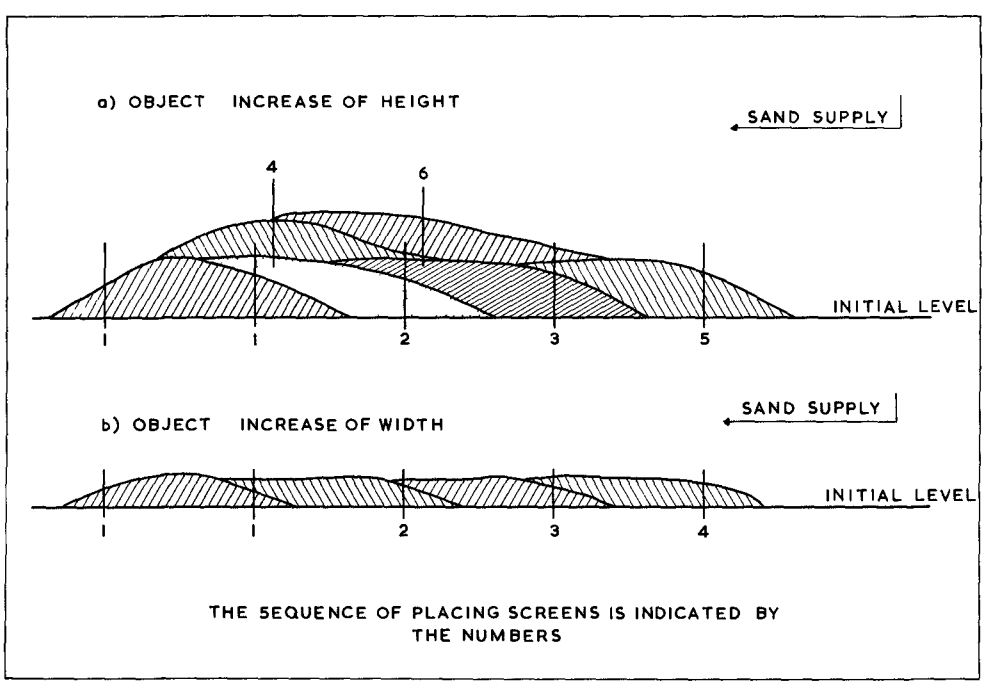

FIG 7 THE PRINCIPLE OF PLACING WIND SCREENS

between north and east.

This is not to say that a different exposition would prevent the possiblities of constructing a drift dyke: although winds from westerly directions are more humid and may, when sufficiently strong to cause drifting, be attended with high sea levels, they occur with much higher frequency in the Netherlands. The only requirement for a drift-sand dyke with orientation towards the west would be, that the level of the foreshore (accumulation area) must be considerably higher with respect to the local MHT than is the case on the Rottumerplaat.

The position of the ground-plan with regard to the accumulation-(production-)area is not equally favourable in all places. The relatively high foreshore, occuring along the entire northern shore, is regarded as accumulation area. The contours given in fig. 2 show, that the foreshore borders the drift dyke in some parts, but in others is dévided from it by a depression. With time, the foreshore varies in width, in keeping with the formerly mentioned sand banks that either unite with the coast or are scoured away. During winter on the foreshore small parabolic dunes are formed, that supply material for the drift dyke during drift-winds in spring. In this way, the small dunes disappear relatively soon, but in favourable circumstances sands from the flat foreshore also drift towards the dyke.

Where the dyke borders the high foreshore, circumstances are generally favourable. Where, in front of the dyke, a depression is found, it appears that part of the drifting sand does not reach the dyke. Apparently this is caused, on the one side, by the fact that the sand is caught away by the depression itself, that is often still wet, on the other side, and especially, by the fact that in the low areas spontaneous growth of sand couch (a g r o p y r o n j u n c e u m) occurs. In this way local dunes are formed, absorbing sand that otherwise might have served to build up the dyke. In these places the height of the dyke is appreciably inferior to that in places where there is no depression.

A general conclusion following from the foregoing is that, in

places where the first signs of growth appear in front of a drift dyke, this growth should be destroyed relentlessly. Once the growth has a firm hold, it is almost impossible to destroy. On the Rottumerplaat, where timely defrayal has been neglected, destruction of the unfavourable growth by mechanical means is now being considered

Even if all this would have been appreciated right from the start, it is doubtful whether this would have resulted in a differe choice of the layout: the width of the foreshore does not only vary with time, but also from place to place. For the following reasons the dyke should not approach the MHT-line too closely: 1. A landwar shifting of the MHT-line (shrinkage of the foreshore) must never result in a threatening, not only of the dyke itself, but also of the accumulation area; 2. As will appear later the method of catchi sand involves, that the gaining of height, which is coupled with t gaining of width, goes in seaward direction; 3. Should it become desirable to build a second dyke or belt of dunes, this has to be done on the seaward side, as the existing dyke would prevent the winning of sand on the landward side (in all probability, this poi will have no bearing on the Rottumerplaat).

b). <u>The catching of sand.</u> The catching of sand is realized using screens made from brushwood (osier) or reed (photographs nr. 1 and In principle two systems are practicable.

1. Utilization of low screens: in case (e.g. in the first stages) width is pursued, or if, later on, the foot of the dyke has to be built forward before a further heightening is realized.

2. Utilization of high screens, which makes it possible to gain height rapidly.

The two systems are schematically shown in fig. 7. It must b stressed, that these sketches are indeed schematical, as for practi purposes it is necessary to judge in the field, in what place a ne screen can be expected to yield the best results. The rather simpl general principle is to set up for instance two rows of screens in longitudinal direction of the dyke, and, as soon as these screens have been almost buried by sand, to set up more rows on top and in

front of the elevation, and so on.

In the Netherlands, brushwood and reed are used, because these materials are easily available, and have the desired properties. On the one side, the screens must be sufficiently close to paralyse the air stream in such a way, that it drops the sand it carries, on the other side they must be sufficiently open to prevent collapse under the load of the sand deposited in front of the screen: an entirely closed screen would result in deposition of sand only in front, and hardly at all behind the screen. Here, the flexibility of the material is also an important factor. The desirable degree of openness might be described by the term "half transmitting wall", The result is, that in front of, as well as behind the screen sand is deposited, thus gradually improving the support to the screen. This will only become completely buried after the placing of new screens on top of the obtained elevation.

As to the materials used: part of the screens are made from so-called "Hollands rijshout", (a name, indicating quality and species of the brushwood branches and twigs, as well as measures of these branches and of the bundles). This material is supplied in lengths between 1,5 and 2,5 m, bound together at the upper and lower ends to form bundles 0,4 m or 1,0 m round. The smaller bundles, after removing the upper band, are put into the ground as they are, the larger ones are taken apart and spread out. Also, on the Rottumerplaat, the so-called "Biesbos" - reed is used, that is supplied in bundles, long about 2,5 m, and 1,25 - 1,5 m round. After having been sawed to lengths of about 1 m, these bundles are taken apart. A groove is dug out, into which the material is placed in a vertical position. For brushwood,the depth of the gully is 0,35 - 0,45 m, for reed 0,25 - 0,30 m. It is important to take care, that the upper edge of the screen is straight and horizontal. Depressions in the screen are reproduced in the dyke, which, at a later stage, may result in wind-erosion.

The mutual distance of the screens and the number of screens to be placed per season, are factors that have to be learned from experience, and that will also depend on circumstances. It is

possible to catch about 5 m^3 of sand per running metre between two brushwood screens at a distance of 5 m. To catch 15 m^3/m^1 it is therefore necessary to place at least 4 screens. When utilizing low (reed-) screens, a larger number has to be placed.

In this context, too, it might be useful to be able to carry out quantitative measurements of the transport of sand. It is doubtful, however, whether their usefulness would be very great, as the result at best would be some knowledge on transport-capacty. This knowledge would not enable to predict anything about the quantities that will actually be transported in any given season. No method of measuring is known at present, suffuciently accurate to determine the ratio between material transported and material caught.

On the Rottumerplaat the quantities of sand caught are being verified by annual levelings.

c). Special features. Because of the function assigned to the drift dyke (base for future damming projects), already mentioned in the introduction, and because the Rottumerplaat is an uninhabited islan this work occupies a special place in the Netherlands. Contrary to the situation in most of the other cases, the sea, at high flood levels, has accessto this drift dyke from all sides. Moreover the dyke, by its very seaward position, is exposed to frequent and dangerous attacks of the sea. This became apparent during the storm surge of 16th and 17th february 1962: a breach was formed at the bend of the dyke to the north-west of the initial dune (fig.2). The storm blew predominantly from westerly directions, resulting in a very exposed position of the bend with respect to the currents caus by the wind. The breach was about 150 m long and was subsequently closed by mechanical means.

The island is not only uninhabited, but it is also, during the winter months, practically inaccessible. Only during the workin season (march to october incl.), workmen are on the island on behal of the drift dyke. Inspection or repairs are impossible during winte For this reason, screens are placed at the end of the season, that run a great risk of being swept away. Their main object is to catch sand during favourable winds in early spring, when work on the

island is still impossible.

In this context it may be useful to state, as a general remark, that it is not practicable to build drift-sand dykes without consciously accepting risks. Beside understanding and experience the factor chance plays a more important part than in other hydraulic engineering works. As however, even if set-backs occur, a drift dyke is considerably cheaper than any other construction, this element can be accepted, on condition, that no narrow time limit is set to the completion of the work.

4. THE STABILIZATION OF SAND ON THE DRIFT DYKE.

One of the subjects discussed in the foregoing was the method used to catch the sand. The sand caught in this way is, however, an incoherent mass and may, in dry weather, be lost owing to an unfavourable wind. It is important, therefore, to take measures as soon as possible to stabilize the sand.

It is conceivable to realize this by artificial means, such as bituminous products or cement. Such a method would, however, raise the expenses to an unnecessarily high level, and would be opposed to the real aim: the creation of a dune, as far as possible by natural means. A temporary fixation can be rapidly obtained by using dead plants or their remnants; seaweed is sometimes used (it is often found in large quantities on the spot), and also straw.

Normal practice, however, on the Rottumerplaat and elsewhere, is to stabilize the sand by means of plantation. Generally speaking, it will be correct to use plant-species, belonging to the surroundings and the climate of the area, where the drift dyke is built. On the Rottumerplaat and elsewhere in the Netherlands the most frequently used species are marram-grass (a m m o p h i l a a r e n a r i a), lyme grass (e l y m u s a r e n a r i u s) and sand couch (a g r o p y r o n j u n c e u m). The suitability of these species mainly depends on the level at which they are planted. Sand couch and lyme grass can endure several floodings by salt water per growing-season, and can be planted at minimum heights of MHT + 0,50m and MHT + 0,75 m, respectively. For their growth they are dependant

FIG. 8 Photograph nr.1
Brushwood screen.

FIG. 9 Photograph nr.2
Reed screen.

on the supply of fresh sand, from which they mainly draw nitrogen. For this reason it is not possible to give a generally applicable highest level at which these plants can still grow. Both species are eagerly sought after by rabbits for their food. Fortunately, these animals do not occur on the Rottumerplaat. As far as possible, rabbits should be kept down in places, where drift dunes or - dykes are being constructed, as they hamper the growth of the dyke, This has, for instance, become apparent on the island of Rottumeroog (to the east of the Rottumerplaat), where rabbits do occur.

For marram grass, requirements with respect to its growing place and to circumstances are less specific. It frequently occurs, therefore, in older dune formations. It is planted in those places, where the previously discussed species do not grow so well, generally on the higher levels. The photographs nr. 3, 4 and 5 may serve to illustrate the various types of growth.

The growth is able to spread by natural means, but, as long as heigtening or lengthening of the dyke is actively pursued, this is not sufficient. The expansion of the vegetaion is promoted by the vegetative or by the generative method. The latter is the cheapest, but the results vary. When using the vegetative method, parts of the plants are cut off and planted again; this is generally successful. Of course the method and time of planting, the density with which the vegetation is planted etc., are factors that influence the result. Local circumstances, experience and biological know-how have to show the way in this respect.

In circumstances as outlined above, and provided the planning is good, the cost of planting is low. In the case of the construction of a new drift dyke in an area without vegetation, however, it is necessary to supply all the plants to the site, which may result in high initial cost of plantation.

It should be mentioned, that plant-diseases and insect-plagues have, as yet, hardly at all influenced the work on the Rottumerplaat. In the first stages, here and there artificial fertilizers were applied, but later this was stopped in order to stimulate the development of a natural plant-association.

FIG. 10

Photograph nr.3
Marram grass
(a m m o p h i l a a r e n a r i a)

FIG. 11

Photograph nr.4
Lyme grass
(e l y m u s a r e n a r i u s)

FIG. 12
Photograph nr.5
Sand couch
(a g r o p y r o n j u n c e u m)

FIG. 13 Photograph nr.6
Shrubbery on the Rottumerplaat
Creeping willow
(s a l i x r e p e n s)

FIG. 14 Photograph nr.7
The oldest part of the drift dyke,
seen in north-westerly direction

The most important aspect regards the question concerning the part of the dyke that should be protected by plantation. One possibility is to plant on the outer talus. A large part of the sand then drifts over the dyke and causes the inner talus to grow, which means, that the growth of width of the dyke takes place on the landward side. Elsewhere, this method is applied succesfully. On the Rottumerplaat, however, the aim is to catch the largest part of the sand on the outer talus, as fig. 7 shows. The growth of width now takes place in seaward direction, and it is indicated to cover the inner talud with plants, up to the top of the dyke or a little further. In this case, planting of the outer talus would have little effect, because the quantities of sand caught are so large, that the vegetation would be smothered.

The reason why this method is applied is the open position of the drift dyke. The "landward" side is exposed to attacks from water and wind, whilst no accumulation area is found on this side.

A third possibility is to cover the entire dyke with plants. If this is done right from the start, wind screens can, at least theoretically, be omitted: this is the principle of organogenic formation of dunes. The quantity of sand caught by the vegetation is such, that the growth of the plants can keep pace with the increase of height. Advantages of this method are, that it is, at least as far as maintenance is concerned, less labour consuming; that the chance of succes is better, and that, to a certain degree, the profile is stronger because of the intricate system of roots. A disadvantage is the considerably slower rate of growth. Moreover, a condition is, that the initial width must be larger than with the other methods. Also, it is necessary that the height at which the work is begun be such, that floodings of the site are rare.

Experiments with organogenic dune formation on the Rottumerplaat have met with little succes. This has been traced to the circumstance, that the experimental sectors were bordered by sectors with wind screens. The idea is, however, to cover the entire surface with vegetation as soon as the dyke will have reached a desired minimum profile. Further growth will then be slower, but it is hoped

that the resistance of the dyke will increase.

With regard to planting the following additional remarks can be made:

a). Implements. A specially designed plant-spade is used, a.o. for the planting of marram. A normal spade, however, is very suitable, for planting as well as for lifting.

b). In addition to the plants that have already been discussed, in recent years also various types of shrubbery have been planted. With this object, a nursery was set up on the mainland. Among the shrubs used are creeping willow (s a l i x r e p e n s) and other types of willow, sea buck-thorn (h i p p ó p h a ë r h a m n o ï d e s), box-thorn (l y c i u m h a l i m i f o l i u m) and abele (p o p u l u s a l b a). The aim is to strengthen the dyke by a close shrubbery and the deep and intricately branched system of roots that goes with it. This type of vegetation, however is as yet nowhere sufficiently close to justify an opinion on the results (see photograph nr. 6).

c). Under the lee of the dyke a spontaneous vegetation develops. The type of vegetation depends on the height of the territory, on the groundwater level, on whether or not the area is cut off from the sea, etc. It would carry too far to discuss this in more detail. Behind the dyke on the Rottumerplaat a reasonably varied flora has developed.

Photograph nr. 7 was added to give a general impression of the oldest part of the dyke on the Rottumerplaat.

5. LABOUR PERFORMANCE AND COST.

Detailed data on achievement per man and cost of the dyke are not available. There are, however, some rough figures that may be worth mentioning.

With regard to the placing of screens, there are many circumstances infuencing the pace of the work. It is, for instance, unfavourable, if on or below the surface wreckage-wood is found, or if the screens have to be placed in freshly accumulated sand, where

the grooves cave in as soon as they are dug. If such circumstances do not occur, and if the material is supplied and distributed in such a way, that unnecessary moving of persons is avoided, it is possible to obtain a mean performance per man per 9-hour work-day of 145 m length of screen put up.

The performance with planting depends on the distances betwee plants. For sand couch these vary from 0,5 x 0,5 m to 0,75 x 0,75 m, for marram grass and lyme grass from 0,3 x 0,3 m to 0,5 x 0,5 m.

As a guide it may be mentioned, that the mean performance per man per day is about 75 m^2 when the plant pattern is 0,3 x 0,3 m, an about 175 m^2 at 0,5 x 0,5 m.

As regards the cost a rough calculation shows, that during th first years fl.1.-- (Dutch guilders) was paid for each m^3 of sand; at present this is about fl. 0.50. Taking the average of these figures, and taking into account that the total gain amounts to 160 m^3 sand per m^1 dyke, the result is that up to the present the dyke has cost about fl.120.-- per m^1. This includes only the cost o wages and material. Owing to the special circumstances on the Rottumerplaat, cost of housing and cost of transport of men and material to and from the shoal have to be added. According to a rough estima this doubles the total expenses, which would mean that a price of fl. 250.-- per m^1 dyke in the present situation may not be far off the truth.

ACKNOWLEGDEMENT.

The author wishes to express his gratitude to Mr.C.T.Bergman and Mr. P.Bouwsema of the Rijkswaterstaat department for Land Recla ation at Baflo for their preparatory work, and for putting at his disposal the results of their vast experience on the subject.

REFERENCES.

1. V.J. Chapman, M.A.Ph.D. "The Stabilization of Sand-dunes by vegetation". The Institution of Civil Engineers, Excerpt from th

proceedings of the Conference on Biology and Civil Engineering, London, 1949, p. 142 - 157.

2. J.H. van der Burgt, Civ. Eng. and L. van Bendegom, Civ. Eng: "The Use of Vegetation to Stabilize Sand-dunes". Inst. of Civ. Eng, Excerpt proc. on conf. on Biology and Civil Engineering, London, 1949, p. 158 - 170.

3. Dr. J.W. van Dieren: "Organogene Dünenbildung", The Hague, Martinus Nijhoff, 1934.

Chapter 24

SAND LOSSES FROM A COAST BY WIND ACTION

J. W. Johnson and A. A. Kadib
College of Engineering
University of California
Berkeley, California

INTRODUCTION

Sand supplied to a coast by streams, cliff erosion, and other sources generally is moved in one particular direction along the shoreline as a littoral drift by the prevailing wave conditions in the area (3). When this drift encounters a partial obstruction, such as a prominent natural headland or a major engineering structure, a condition is realized which is conducive to sediment deposition. Such littoral compartments eventually become filled and some sand is carried past the obstruction. If the topography back of the area of deposition is relatively low and the prevailing winds are onshore, considerable quantities of sand may be moved inland to create a dune system. This loss of material from the coast may affect the stability of the downcoast shoreline. A measure of the annual loss of sand from a particular section of coast by wind action is necessary in many instances. A method of estimating this loss of sand involves the use of a suitable transport equation along with a knowledge of the sand characteristics and the duration and velocity of the wind in the area under study.

SAND TRANSPORT EQUATION

Numerous laboratory investigations on sand transport by wind action have been made over the years. Recently these various studies were critically reviewed and additional laboratory measurements made by Belly (2). The results of these studies indicated that the Bagnold equation (1), when supplemented by data by other investigators, best defined the rate of sand transport by wind action. The basic Bagnold equation for the rate of sand movement, q, per unit width and unit time is

$$q = c\sqrt{\frac{d}{D}}\ \frac{\gamma}{g}\ U_*^3 \qquad (1)$$

where D is the grain diameter of standard 0.25 mm sand; d is the grain diameter of the sand under study; γ is the specific weight of air; g is the acceleration of gravity; U_* is the shear velocity, and c is a coefficient with a value of: 1.5 for nearly uniform sand, 1.8 for a naturally graded sand, and 2.8 for a very wide range of grain diameter.

The shear stress, τ, produced at the sand surface by wind is one of the most important factors in the movement of sand by wind. When the shear stress exceeds a certain critical value, the sand particles start to move. As long as there is no sand movement, the wind velocity distribution is described by the general equation

$$U = c \log \frac{Z}{Z_o} \tag{2}$$

in which U is the velocity at height Z above the sand surface and Z_o is a reference parameter. In experiments where sand movement occurs, it was developed by Zingg (6) that

$$U = 6.13\, U_* \log \frac{Z}{Z'} + U'$$

or

$$U_* = \frac{U - U'}{6.13 \log (Z/Z')} \tag{3}$$

where Z' is the height where the velocity profiles for different wind speeds appear to meet at a point which is termed a "focus" and U' is the wind speed at this elevation. The height of the focus, Z' appears to be associated with the height of the ripples on the surface. Zingg (6) found that the value of Z' and U' is given by the expressions

$$Z' = 10\ d, \text{ in millimeters} \tag{4}$$

$$U' = 20\ d, \text{ in miles/hour} \tag{5}$$

where the grain diameter, d, is expressed in millimeters.

Equation (1) gives the transport in pounds per second per foot width. In a more general way this equation can be written as

$$Q = c \cdot \ell \cdot T \sqrt{\frac{d}{D}}\, \frac{\gamma}{g}\, U_*^3 \tag{6}$$

where

- Q = total transport in pounds per year
- c = Bagnold constant
- ℓ = length of reach in feet perpendicular to direction of wind considered
- d = average grain diameter of sand considered (d_{50} mm)
- D = average grain diameter of standard 0.25 mm sand

γ = specific wt of air = (0.076 lbs/ft^3)
U_* = shear velocity in ft/sec
T = duration of wind of a particular speed in seconds per year
g = acceleration due to gravity = 32.2 ft/sec^2

Now substituting the values of γ, g, and choosing c = 1.8, since the sand considered has a natural grading, we obtain,

$$Q = (1.8) \cdot (\ell) \cdot (t \cdot 3.6 \cdot 10^3) \sqrt{\frac{d}{D}} \cdot \frac{0.076}{32.2} \cdot U_*^3$$

$$Q = 15.20\, t \cdot \ell \sqrt{\frac{d}{D}}\, U_*^3 \text{ in pounds per year} \qquad (7)$$

where t is in hours per year.

ESTIMATES OF TRANSPORT FROM NATURAL BEACHES

As an illustration of the application of the above equations to calculating the annual transport of sand from a beach, Salmon Beach in Northern California was selected (Fig 1) (Kadib, (4). As discussed by Zeller (5), this is a typical condition for the establishment of a major sand dune area--namely, (1) a supply of sand from streams upcoast from the area, (2) a prominent headland where sediment over the centuries has accumulated, and (3) low topography back from the beach where the prevailing onshore winds can easily move the sand inland from the region of accumulation at the beach.

In the calculations to follow it is assumed that the sand size at the mid-tide level on the beach face is a measure of the sand being blown inland from the beach by wind action. Consequently, sand samples were taken at the mid-tide level for eight localities along the coast as shown in Fig. 2. These samples were subjected to mechanical analyses and the 50% grain diameter (d_{50}) determined. These mean diameters are shown in Fig. 2. For calculations the coastline was divided into eight reaches whose characteristics are shown in Table 1.

The wind duration in hours of winds of various speeds from various directions was compiled from wind observations taken nearby at the Pacific Marine Station, Dillon Beach, California. A year of observations (September 1, 1962 to August 31, 1963), in which both wind speed and direction were obtained from an anemometer located at 18 ft above the ground surface, are summarized in Table 2. As indicated in this table, the anemometer recording system was inoperative a portion of the time; consequently, the computed rate as indicated below perhaps is on the low side, but the computation procedure is valid. In Table 2 wind speeds below 10 mph were considered as "calm," since their contribution to transport can be considered as small. The choice of the uneven values

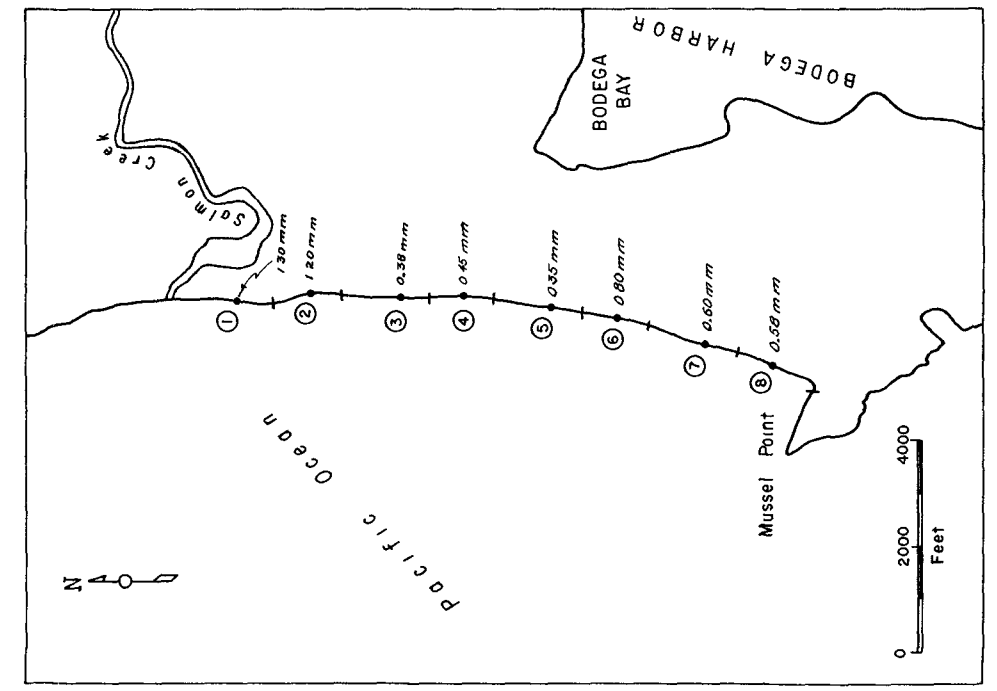

FIG 2 -- NUMBER AND LOCATION OF REACHES AND SAND SAMPLES (SALMON BEACH, CALIF.)

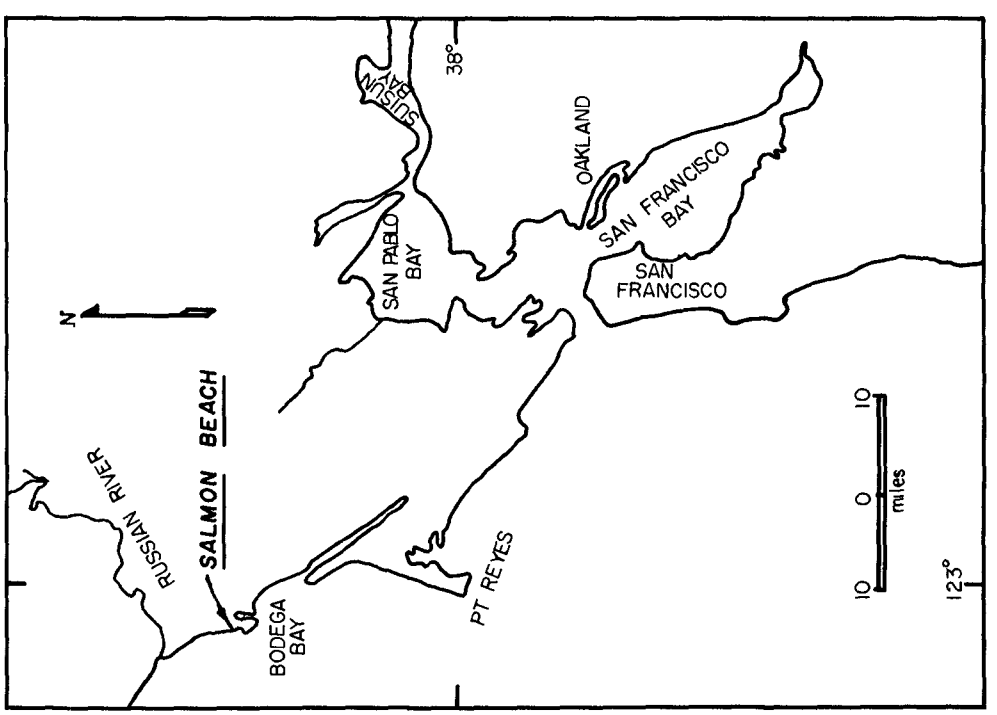

FIG. 1. -- VICINITY MAP: SALMON BEACH NEAR BODEGA BAY, CALIF.

Table 1

Physical Characteristics of Salmon Beach

Reach No.	Length along the coastline (ft)	d_{50} (mm)	$\sqrt{\frac{d_{50}}{D}}$	Remarks
1	2200	1.30	2.29	Naturally graded sand
2	1350	1.20	2.20	"
3	1700	0.380	1.24	"
4	1200	0.450	1.35	"
5	1700	0.355	1.22	"
6	1350	0.800	1.80	"
7	1800	0.600	1.55	"
8	1800	0.580	1.53	"

Table 2

Duration of Wind Per Year for Different Wind Speeds
(Pacific Marine Station)

Speed ft/sec.	Speed mph	Duration of Wind (Hours per Years) N	NW	W	SW	S	SE	E	NE
14.7	10	4	45	3	5	2		1	1
16.5	11.2	20	83	13	12	18	2	38	2
18.2	12.4	3	50	1	7	2		1	2
18.8	12.8	10	23	6	4	5	6	20	
20.	13.6	5	24	1	1	3			2
21.02	14.3	12	39	5	5	6	7	24	
21.8	14.8	1	33	4				1	1
22.9	15.6	14	35	5	5	2	9	10	1
23.2	15.8		28	1		1		1	2
24.7	16.8	10	53	2	3	4	6	8	
26.2	17.8	1	25	1					1
26.6	18.1	4	28			1	5	12	
27.6	18.8		15			1			1
28.4	19.3	6	14	2	2	4	10	5	
29.1	19.8		18	4					
30.3	20.6		14	2	1	4	5	3	
32.	21.7	6	13			3	7	1	1
33.2	22.6	5	8		3	3	8	4	
34.7	23.6	8	10	1	1	2	7		
36.3	24.6	2	14		3	1		2	
37.8	25.7	8	3				4	2	
39.3	26.7	8	5		3		3	1	
40.7	27.7	3	2				5	2	
> 41.2	>28.0	5	1				2	16	

Total hrs - 1135 hrs. of wind > 10 mph
Calm - 3555 hrs.
No records - 4070 hrs.

of wind speeds resulted from the reduction of wind data from the anemometer chart and the calibration curve of the anemometer.

Although it is noted from Table 2 that winds may blow from practically all directions, it is evident from Fig. 2 that winds from only a few directions will cause an inland transport of sand from the beach. Thus, considering the different possible wind directions to give inland transport, it appears that only four directions need be considered at Salmon Beach. These directions are N, NW, W, and SW. The perpendicular projections ℓ_2, ℓ_4, ℓ_1, and ℓ_3, respectively, of these directions (Fig. 3) were measured and presented in Table 3. These lengths represent ℓ in equation 7 for total transport calculations.

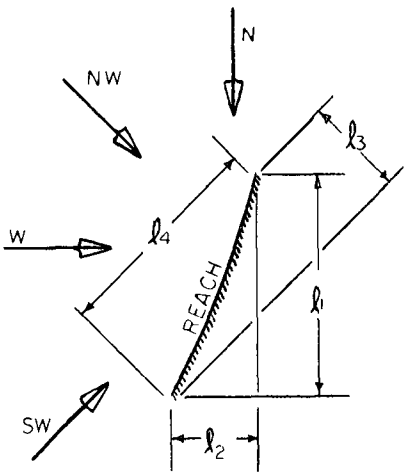

Fig. 3

The shear velocity, U_*, in equation 7 is calculated from equation 3 with the values of Z' and U' being evaluated by equations 4 and 5, respectively, from the mean grain diameter, d, for each reach. Values of Z' and U' for each reach are presented in Table 4. The value of Z in equation 3 was 18 ft, the anemometer height. Using the data in Table 4 the shear velocity for various wind speeds U observed at an elevation Z of 18 ft was calculated for each reach and is summarized in Table 5. A sample calculation for the data summarized in Tables 4 and 5 is as follows:

For Reach (4)

$d_{50} = 0.45$

From equation (4), $Z' = (10)(0.45) = 4.5$ mm or 0.0147 ft. and from equation (5), $U' = (20)(0.45) = 9$ mph or 13.20 ft/sec. Considering a wind speed of 27.7 mph (40.70 ft/sec) the shear velocity from equation (3) is

$$U_* = \frac{U - U'}{6.13 \log(Z/Z')} = \frac{40.70 - 13.20}{6.13 \log (18/0.0147)} = 1.44 \text{ ft/sec}$$

Table 3

Perpendicular Projections for Different Wind Directions*

Reach No.	Length ℓ (ft)	Representing grain dia. d_{50} (mm)	ℓ_1 (ft)	ℓ_2 (ft)	ℓ_3 (ft)	ℓ_4 (ft)
1	2200	1.30	1900	200	1400	1450
2	1500	1.20	1400	200	900	900
3	1700	0.38	1600	150	1150	1300
4	1200	0.45	1150	150	850	800
5	1700	0.355	1500	400	1100	1400
6	1350	0.80	1300	300	700	1000
7	1800	0.60	1700	500	900	1500
8	1800	0.58	1400	900	500	1700

* South, SE, E and NE winds do not contribute to inland movement

Table 4

Calculations for the Focal Point Using the Zingg Formula

Reach No.	d_{50} mm	Z' = 10 d mm	Z' (ft)	U' = 20dm (m/h)	U' ft/sec
1	1.30	13.0	0.0427	26.00	38.00
2	1.20	12.0	0.0394	24.0	35.00
3	0.38	3.8	0.0125	7.6	11.30
4	0.45	4.5	0.0147	9.0	13.20
5	0.355	3.55	0.0116	7.10	10.40
6	0.80	8.0	0.0262	16.00	23.50
7	0.60	6.0	0.0197	12.00	17.60
8	0.58	5.80	0.019	11.60	17.00

Table 5

Calculation of U_* for Different Reaches and Wind Speeds

U_{18} ft/sec	$U_* = \frac{U_{18} - U'}{6.13 \text{ Log } Z/Z'}$ ft/sec							
	Reach No. 1	Reach No. 2	Reach No. 3	Reach No. 4	Reach No. 5	Reach No. 6	Reach No. 7	Reach No. 8
14.70	-	-	0.175	0.079	0.22	-	-	-
16.50	-	-	0.268	0.175	0.310	-	-	-
18.20	-	-	0.356	0.264	0.40	-	0.033	0.065
18.8	-	-	0.385	0.286	0.428	-	0.066	0.098
20.0	-	-	0.45	0.358	0.49	-	0.130	0.164
21.02	-	-	0.50	0.410	0.55	-	0.19	0.22
21.8	-	-	0.54	0.450	0.58	-	0.23	0.26
22.9	-	-	0.61	0.510	0.635	-	0.29	0.32
23.2	-	-	0.615	0.53	0.64	-	0.31	0.34
24.7	-	-	0.690	0.605	0.73	0.069	0.39	0.42
26.2	-	-	0.780	0.695	0.815	0.167	0.48	0.51
26.6	-	-	0.795	0.710	0.825	0.180	0.49	0.525
27.6	-	-	0.840	0.760	0.88	0.235	0.55	0.58
28.4	-	-	0.88	0.800	0.92	0.29	0.59	0.621
29.1	-	-	0.918	0.84	0.954	0.328	0.63	0.66
30.3	-	-	0.98	0.90	0.97	0.40	0.694	0.73
32.0	-	-	1.07	0.99	1.06	0.494	0.73	0.81
33.2	-	-	1.13	1.053	1.12	0.56	0.80	0.882
34.7	-	-	1.15	1.13	1.20	0.65	0.88	0.964
36.3	-	0.074	1.24	1.22	1.28	0.74	0.97	1.05
37.8	-	0.172	1.32	1.29	1.35	0.83	1.05	1.19
39.3	.082	0.265	1.39	1.37	1.43	1.00	1.13	1.27
40.7	0.168	0.31	1.464	1.44	1.50	1.10	1.207	1.35
>41.2								

Using the above equations and the data presented in Tables 1-5, inclusive, the total annual transport can be calculated for each reach for all winds contributing to the movement of sand. The procedure in these calculations is presented in Table 6 where Reach 4 is considered as an example. Winds in excess of 10 mph from the critical directions of N, NW, W, and SW are considered. The application of the various data in the calculation of the annual rate of transport in Reach 4 by equation 7 is self-explanatory. Similar calculations for the other reaches along the beach under investigation show a total estimated annual rate of transport inland of approximately 11,000 cubic yards; however, as previously stated this quantity perhaps is on the low side since the anemometer was inoperative for an appreciable percentage of the time. It should be noted that no

Table 6

Total Transport Per Year, Reach 4

Reach No. 4 $\sqrt{\frac{d}{D}} = 1.35$

U ft/sec	U* ft/sec	U*^{3}	N t hrs	N ℓ^2 ft	N U*^{3}t	NW t hrs	NW ℓ^4 ft	NW U*^{3}t	W t hrs	W ℓ ft	W U*^{3}t	SW t hrs	SW ℓ^3 ft	SW U*^{3}t
14.7	0.079	.0005	4	150.00	.002	45	800.00	.0225	3	1150.00	..0015	5	850	.0025
16.5	0.175	.0053	20	150.00	0.106	83	800.00	0.440	13	1150.00	.069	12	850	.0635
18.20	0.264	0.0185	3	150.00	0.555	50	800.00	.925	1	1150.00	.019	7	850	.1295
18.80	0.286	0.0234	10	150.00	0.234	23	800.00	0.57	6	1150.00	0.140	4	850	0.0935
20.00	0.358	0.046	5	150.00	0.230	24	800.00	1.10	1	1150.00	.046	1	850	.046
21.02	0.410	0.0685	12	150.00	0.820	39	800.00	2.66	5	1150.00	0.342	5	850	0.342
21.80	0.45	0.090	1	150.00	0.090	33	800.00	2.96	4	1150.00	0.360	0	850	0.000
22.90	0.51	0.132	14	150.00	1.850	35	800.00	4.64	5	1150.00	0.650	5	850	0.650
23.20	0.53	0.148	0	150.00	0.000	28	800.00	4.15	1	1150.00	0.148	0	850	0.000
24.70	0.605	0.220	10	150.00	2.200	53	800.00	11.65	2	1150.00	0.440	3	850	0.660
26.20	0.695	0.335	1	150.00	0.335	25	800.00	8.36	1	1150.00	0.335	0	850	0.000
26.60	0.710	0.358	4	150.00	1.432	28	800.00	10.024	0	1150.00	0.000	0	850	0.000
27.60	0.76	0.440	0	150.00	0.000	15	800.00	6.600	0	1150.00	0.000	0	850	0.000
28.40	0.80	0.510	6	150.00	3.060	14	800.00	7.140	2	1150.00	1.020	2	850	1.020
29.10	0.84	0.590	0	150.00	0.000	18	800.00	10.60	4	1150.00	2.360	0	850	0.000
30.30	0.90	0.712	0	150.00	0.000	14	800.00	10.000	2	1150.00	1.424	1	850	0.712
32.00	0.99	0.980	6	150.00	5.880	13	800.00	12.700	0	1150.00	0.000	0	850	0.00
33.20	1.053	1.160	5	150.00	5.80	8	800.00	9.28	0	1150.00	0.000	3	850	3.48
34.70	1.130	1.45	8	150.00	11.60	10	800.00	14.50	1	1150.00	0.145	1	850	0.145
36.30	1.22	1.82	2	150.00	3.64	14	800.00	25.50	0	1150.00	0.000	3	850	5.46
37.80	1.29	2.15	8	150.00	17.20	3	800.00	6.45	0	1150.00	0.000	0	850	0.00
39.30	1.37	2.55	8	150.00	20.40	5	800.00	12.75	0	1150.00	0.000	3	850	7.65
40.70	1.44	2.96	3	150.00	8.88	2	800.00	5.92	0	1150.00	0.000	0	850	0.000
>41.2	1.80	5.80	5	150.00	29.00	1	800.00	5.80	0	1150.00		0		0.000
					112.815			174.742			7.500			20.456
		$\Sigma U^{*3}\ell t$	=		16,930	+		139,793	+		8,625	+		17,368
			=		182,712									
		Q_4	=	1.35 x 15 · 2 x 182,716		=	3,758,000	lb/year						

reduction was made in the calculated rate of transport for sand being in the moist condition--which Belly (2) showed to be an important factor. This factor may be particularly important in localities, such as the section of the California coast discussed above, where high winds may also be accompanied by considerable rain.

SUMMARY

A procedure is outlined for the calculation of the annual rate of transport of sand that might be expected to be carried inland from a natural beach by wind action. The procedure involves the beach composition and alinement, the frequency of winds of various speeds from various directions, and a suitable formula to describe the transport. It is possible that the transport formula may be altered as a result of current research; however, the general procedure as outlined herein should apply.

REFERENCES

1. Bagnold, R. A., The physics of blown sand and desert dunes, William Morrow and Co., New York, 265 pp.

2. Belly, Pierre-Yves, Sand movement by winds, U. S. Army Coastal Engineering Research Center, Tech. Memo. No. 1, Wash., D. C., Jan. 1964.

3. Johnson, J. W., Sand movement on coastal dunes, Federal Inter-Agency Sedimentation Conference, Jackson, Miss., Jan. 1963.

4. Kadib, A. L., Calculation procedure for sand transport by wind on natural beaches, U. S. Army Coastal Engineering Research Center, Misc. Paper 2-64, April 1964, Wash., D. C.

5. Zeller, R. P., A general reconnaissance of coastal dunes of California, Beach Erosion Board Misc. Paper No. 1-62, Wash., D. C., June 1962.

6. Zingg, A. W., Wind-tunnel studies of movement of sedimentary materials, Proc. Fifth Hydraulic Conference, State Univ. of Iowa Studies in Engin., Bull. 34, 1953, pp. 111-135.

Chapter 25

DEVELOPMENT OF HYDRAULIC AND SHOALING CHARACTERISTICS OF SAVANNAH HARBOR, GEORGIA, BY PROTOTYPE STUDIES AND HYDRAULIC MODEL

John W. Harris
Supervisory Hydraulic Engineer
U. S. Army Engineer District, Savannah, Georgia

SUMMARY

Maintenance of Savannah Harbor became progressively more critical as the deepening of the channels caused heavy shoaling concentrations in a highly industrialized section of the harbor where spoil disposal areas are limited. Studies were performed to evaluate the shoaling and develop means of reducing the high cost of maintaining 31 miles of deep-water navigation channels. A hydraulic model investigation substantiated the conclusions reached through analysis of prototype data, greatly expanded the knowledge of hydraulic conditions and shoaling processes, and developed an improvement plan which involved a tide gate to induce the deposit of sediment in an off-channel sediment basin.

THE PROTOTYPE

DESCRIPTION OF THE PROTOTYPE

Savannah Harbor. Savannah Harbor is located on the South Atlantic Coast of the United States in the tidal estuary where the Savannah River empties into the Atlantic Ocean. The Harbor Entrance is about 32° 02' latitude and 80° 55' longitude.

The Port of Savannah is used for importing petroleum products, gypsum rock, raw sugar, fertilizer materials, and many other miscellaneous products. Principal foreign export commodities are wood pulp, paperboard, naval stores, and iron and steel scrap. During 1962 over 4.5 million tons of waterborne commerce was carried by 1611 ships entering and leaving the harbor.

The authorized channels which are maintained by the U. S. Army Corps of Engineers are shown on Figure 1. The project provides for 9.7 miles of channel 36 ft deep at mean low water and 500 ft wide from the 36-ft contour in the ocean to the harbor entrance; thence 18.8 miles, 34 ft deep and generally 400 ft wide; thence 2.5 miles, 30 ft deep and 200 ft wide to the upstream limit of the project. Four turning basins constructed at strategic locations are maintained to the project depth in the adjacent channel. The upper end of the harbor connects with the 9-ft channel in Savannah River which extends about 200 miles to the City of Augusta, Georgia, and the 12-ft Atlantic Intracoastal Waterway crosses the harbor about 8 miles below the City of Savannah. The city and industrial areas are located on the south side of Front River from 12 to 20 miles above the harbor entrance.

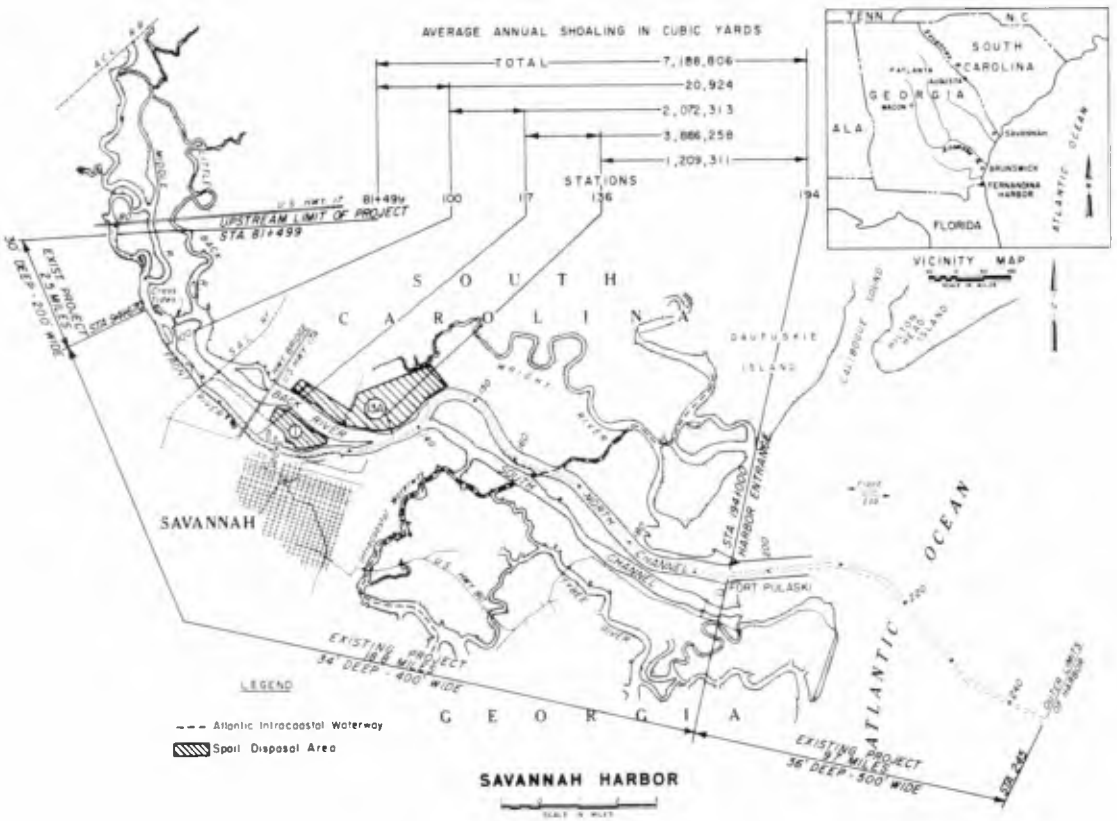

FIG. 1 - EXISTING PROJECT AND ANNUAL SHOALING

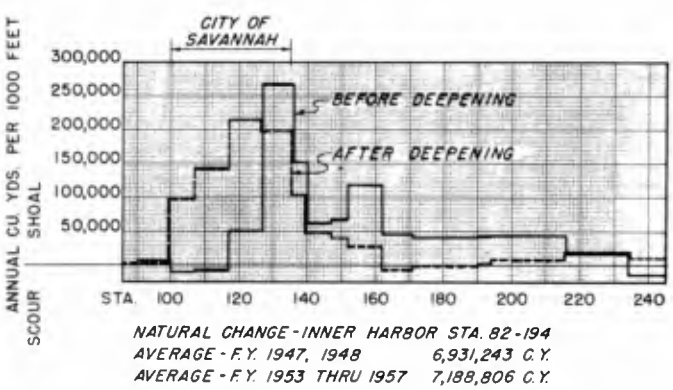

FIG. 2 - ANNUAL SHOAL AND SCOUR (NATURAL CHANGE)
BEFORE AND AFTER
DEEPENING NAVIGATION CHANNELS

Savannah River. The Savannah River, a heavy silt-bearing stream, has its source in the Blue Ridge mountains about 400 miles above the harbor and has a drainage area of 10,579 square miles. The river is tidal for a distance of about 50 miles upstream from the mouth. The index station for the harbor for the measurement of fresh water and sediment inflow is located 65 miles above the mouth. Two major reservoirs, which exercise significant control of the river flows, are located 238 and 305 miles above the mouth Normal fresh water inflow is about 7000 cfs and with regulation of flows by the two reservoirs, 16,000 cfs and 5800 cfs are considered the normal high and low flows to be expected during the year. An average annual sediment load transported into and deposited in the harbor by the Savannah River is equivalent to about 2,000,000 cu yds of shoal material.

EXISTING CONDITIONS

Tides and currents. The tides in Savannah Harbor are the semi-diurnal type with a tidal range of about 6.8 ft at the mouth and 7.4 ft at the City of Savannah. The maximum current velocities encountered in the navigation channels are of the order of 4 ft per second on flood and 5 ft per second on ebb tides.

Salinity. The water in the upper portion of Savannah Harbor is fresh while that near the ocean entrance is essentially sea water. The variation in the density of the water in the tidal reach of Savannah River causes a difference in the magnitude and phase of surface and bottom current velocities. This difference is more pronounced near the entrance, decreasing progressively upstream with decreasing salinities until the water becomes completely fresh. The degree of mixing of salt and fresh water and upstream extent of salt water intrusion in Savannah Harbor vary with the range and elevation of tides and the amount of fresh water discharge. With normal fresh water discharge the upstream limit of the salt water on the bottom extends from about Sta 140 to about Sta 100. (Channel locations refer to 1000-ft stations throughout the harbor).

Shoaling. The annual shoaling rate for the inner harbor, from the harbor entrance to the upstream limit of the project, averages about 7,000,000 cu yds. The greatest concentration occurs in the 3.6 mile reach above the juncture of Back River in the channels along the city and the industrial areas where over half of the total shoaling takes place. The annual shoaling in the bar channels amounts to about 700,000 cu yds.

Maintenance. A Government pipeline dredge is normally assigned to the district to maintain the inner harbor channels. The present maintenance program for the inner harbor costs over $1,000,000 annually.

Disposal of dredge spoil. Dredge spoil is disposed in marsh areas adjacent to the channel. Until recent years these areas were undiked; however, a diking program was initiated and has progressed as funds permitted and will continue whenever needed to prevent runback into the harbor channels. The depletion of spoil areas convenient to the channels especially in the reaches of heavy shoaling, necessitating locating spoil areas considerably more remote and requiring longer dredge discharge lines, has greatly increased the cost of channel maintenance.

Presentation of the problem. Maintenance of Savannah Harbor has become progressively more critical with each successive deepening of the channel which caused heavy shoaling to extend farther upstream into the highly industrialized section of the harbor where spoil areas are limited. The shoaling shifted upstream to its present location after the deepening of the channels to 34 ft in 1947-1948. Figure 2 shows a graphical comparison of the shoaling before and after the deepening. In the most critical City Front channel, not only is the total amount of shoaling serious but also the extremely rapid rate of occurrence. It is almost impossible to maintain the channel to the project depth of 34 ft at all times thereby diminishing effective utilization of the harbor. Due to the seriousness of the problem, extensive prototype investigations and engineering studies supplemented by a hydraulic model at the Waterways Laboratory, Vicksburg, Mississippi, have been made.

PROTOTYPE INVESTIGATIONS AND STUDIES

Purpose of the investigations and studies. The prototype investigations included operation of sediment sampling stations on the Savannah River to ascertain the fresh water contribution of silt, and exhaustive salinity and current velocity measurements at various points in the harbor. Studies were made to determine the shoaling characteristics and rates, composition of the shoal material, and the hydraulic characteristics of flow, and to evaluate dredging equipment and methods, and the utilization of spoil disposal areas.

Sources of shoaling. The studies indicated that the major portion of the shoaling material is supplied by the Savannah River with substantial amounts deriving from the ocean and runback from the spoil areas. The solids content of the industrial wastes, deposited in the harbor by several large industries, is negligible as a source of shoal material. The Savannah River sampling program which has been continuous since 1949 has shown that the annual total load of sediment transported into the harbor by the Savannah River is equivalent to about 2,000,000 cu yds of shoal material. This quantity is based on an average density of 1140 grams per liter (20 percent solids by weight) of the bulk of the material dredged from the rapid shoaling area. Of this quantity approximately 78 percent is suspended sediments which are deposited when velocities are reduced and 22 percent consists of colloidal

clay and organic particles in solution which are flocculated by the electro-chemical action on contact with the sea water and deposited in the harbor.

Shoaling quantity and location. Shoaling is referred to also as natural change. Annual surveys of the entire harbor are used to determine the net change from year to year in total cross section area at each 1000-ft station. Shoaling quantities are derived from the summation of the net change and the gross quantities dredged during the year. The present annual shoaling rate is about 7,000,000 cu yds in the inner harbor and although the shoaling is distributed over all the inner channels, over half of the total concentrated along the city and industrial areas as shown on Figure 1.

The effect of the salt-water wedge on the location of shoaling. The salt water entering the harbor from the ocean, due to its greater density, moves along the bottom and extends into the river above the mouth somewhat in the shape of a wedge with the fresh water of Savannah River flowing downstream above it. This wedge moves upstream and downstream with the tide over a distance of several miles. The extent of travel varies with the range and height of tides and the amount of fresh-water inflow. The area of most severe shoaling coincides with the limit of travel of the salt-water wedge. This is evidence that the salt-water wedge condition is a factor in controlling the location of sediment deposition.

The effect of fresh water inflow on shoaling. The normal fresh water inflow is about 7000 cfs. With the regulation of flows by the two major reservoirs, Clark Hill and Hartwell, 16,000 cfs and 5800 cfs are considered the normal high and low flows to be expected during the year. The runoff from rainfall occurring in the lower Savannah River basin combined with the regulated flows from Clark Hill are expected to produce freshets of 16,000 cfs or greater each year. An inflow of this magnitude tends to shift the concentration of shoaling downstream. In 1964 a fresh water inflow of 20,000 cfs and more for a period of 4 months shifted the shoaling, and the salt-water wedge, as much as 8 miles downstream, and with 80,000 cfs which occurred during this same period, the shoaling moved to near the harbor entrance. This event has not been completely documented, but it can be seen that as the discharge decreased that the shoal material returned upstream to its normal location. Future studies will include determination of the quantity of shoaling which remained downstream.

The effect of the construction of the Clark Hill project on shoaling. The construction and operation of the Clark Hill project, completed in 1952, resulted in an annual decrease of about 400,000 cu yds in the quantity of shoal material transported into Savannah Harbor by the Savannah River. Construction of the dam was commenced 16 December 1946 and partial closure was made prior to commencement of the river sampling program in

October 1949 and may have had a diminishing effect on the quantity of sediment determined.

The effect of spring and neap tides on shoaling. The normal range of spring tides in Savannah Harbor is about 9 ft and for neap tides about 5 ft. During the neap tide periods the fluff, which is an indication of shoaling and will be discussed later, shifts upstream and during the spring tides it shifts downstream, and when a spring tide is accompanied by high fresh water discharge, a more pronounced downstream movement is experienced. This fluctuation of tidal range extends the area over which the shoaling occurs, although the effect on the quantity of shoaling is not apparent.

The effect of deepening of the channel on shoaling. The deepening of the channel from 30 to 34 ft in 1947-1948 caused the concentration of shoaling to shift upstream. An increase in the quantity also was observed at this time. The decrease in quantity contributed by the Savannah River due to the construction of Clark Hill project was countereacted by the increase from other sources. The increase may be only apparent since the principal sources of the shoaling material were not altered appreciably.

Conditions affecting shoaling rates. The annual shoaling rate of about 7,000,000 cu yds may be partially caused by certain operating practices which tend to increase the apparent quantity of shoaling.

a. The shifting of the shoaling upstream by the deepening necessitated the use of spoil disposal areas which have been inadequately diked. When this occurs a portion of the dredge material re-enters the channels and forms shoals.

b. The dredging process, due to the nature of the operation, causes material from the shoal to be placed in suspension and temporarily moved from the area by currents present in the area at the time. Hydraulic characteristics of the channel prevent the material from being carried out to sea and, in time, it consolidates and forms other shoals.

Surveys. Hydrographic surveys which are used as a basis for estimating dredged quantities are made by fathometer. The correlation of density data and the fathometer surveys indicate that generally the fathograms reflect a change in density and record a double bottom in the rapid-shoaling areas. The bottom line interpreted as firm bottom occurs at a density of about 1100 grams per liter. This material is generally stable and, except in extreme conditions, is not shifted by varying flows and tide conditions. The firm bottom material dredged from areas maintained regularly will be as much as 1200 grams per liter and averages about 1144 grams per liter, the density depending on the length of time it is allowed to consolidate. Fluff is the unconsolidated shoal material which overlays the firm bottom material and may be as much as 8 ft thick. The material is unstable and is

shifted to and fro by varying flows and tide conditions. This material increases in density from one dredging operation to the next at a rate that depends on such factors as fresh water inflow and the location and type of dredging being performed in the inner harbor.

Dredging practices. Pipeline dredges are used to maintain the inner harbor. The present maintenance program requires the services of a 24-inch Government plant nearly full time. Dredging requirements are based on present maintenance policy which provides that dredging be performed when an area with authorized project depth of 34 ft has shoaled to about 30 to 32 ft; however, in the two most rapidly shoaling areas an additional 2 ft and 4 ft advanced maintenance is dredged to decrease the frequency of dredging. This has proven to be an effective means of increasing the time during which project depths are available.

Prototype tests made during experimental agitation dredging showed that the agitated material settles rapidly and is not permanently removed from the area. Based on this determination, in order to prevent agitation of the shoal material and the unconsolidated sediments overlaying the shoal, the cutter speed of the dredge has been reduced to 2 rpm and the swing speed controlled.

Numerous slips and wharves located adjacent to the channels experience rapid shoaling and maintenance of adequate depths in these areas is a serious problem to the owners. Required depths are maintained by dragging with a tug and I-beam. Since tests have shown that agitation dredging is not effective in removing the shoal material from the harbor, permits issued for dragging require that the Government be reimbursed for the material dragged into the channel.

Disposal of dredge spoil. Dredge spoil is disposed in marsh areas adjacent to the navigation channel. These areas are diked adjacent to the channel and a program is underway to completely enclose the areas with dikes of adequate height to produce ponding for complete settlement and retention of the solids. Studies have evaluated shoaling patterns and rates and provided means of estimating spoil area requirement so that timely acquisition of required areas is possible. Spoil area Number 1 (Figure 1) has been virtually filled necessitating acquiring and diking Area 13-A which is considerably more remote. Maintenance of some of the channel sections now requires more than 10,000 ft of dredge discharge line. Material dredged from the bar and jetty channels by hopper dredge is dumped at sea except in bad weather when the material is dumped in a previously dredged area adjacent to the channel between Sta 184 and 189, then rehandled by pipeline dredge and pumped ashore.

MODEL STUDY

THE MODEL

Purpose. The model tests were conducted to discover means of reducing or controlling the location of shoaling in the harbor, or otherwise improve navigation conditions and reduce the cost of maintenance.

Description. Approximately 413 square miles of prototype area were reproduced in the Savannah Harbor model including the Atlantic Coast from Hilton Head Island to Wassaw Sound and offshore areas well beyond the 40-ft contour in the ocean; up the Savannah River about 50 miles to the head of tidewater at Ebenezer Landing; the extensive system of tidal tributaries, salt-water creeks, and boundary marshes which affect tidal action throughout the harbor; and the Atlantic Intracoastal Waterway from Calibogue Sound through Skidaway River. Figure 1 shows most of the area reproduced. The model was constructed on scale ratios, model to prototype, of 1:800 horizontally and 1:80 vertically. It was equipped with necessary appurtenances to reproduce and measure all pertinent phenomena such as tidal elevations, salt-water intrusion, current velocities, fresh water inflow, pollution and shoaling. The model was constructed to conform to the prototype conditions that existed in 1950. Hydraulic and salinity verification was based on extensive prototype measurements made in 1950 and 1951. Shoaling verification was based on the quantitative distribution for the years 1953-1954 which is representative of prevailing conditions for the existing 34-ft project depth.

Plan of model tests. The tests conducted include general investigations, fresh water diversions, channel realignments and sediment basin. Significant results of these tests are discussed in this paper with emphasis on the sediment trap-tide gate plan which is considered the most favorable improvement plan developed.

GENERAL INVESTIGATIONS

Purpose. The principal purpose of the general investigations was to provide basic hydraulic, salinity, and shoaling data for use in evaluating the probable effectiveness of proposed improvement plans. As the condition of an estuary is never static, observation at any particular moment shows conditions of salinity, current, pollution, or shoaling that are the end products of a long series of changing tides and fresh-water flows. A static condition can be set up in a model, however, and the effect of a single variable can be studied.

Effects of tidal range and fresh water discharge. Tests to determine the effects of tidal range involved reproducing neap, mean, and spring tides and a fresh water discharge of 7000 cfs. Tests to determine the effects of fresh water discharge involved

reproducing discharges of 7000 cfs and 16,000 cfs for both mean and spring tide conditions. The salinity profile, Figure 3, show that the salt-water penetration upstream was greatest for neap tides and least for spring tides. The high salinity encountered at the entrance to Savannah Harbor gradually diminishes in an upstream direction as the salt water encounters fresh water and is mixed with it by the tidal currents.

The effect of the tidal range on the mixing environment in the harbor is reflected in the predominance of flow in one direction or the other at surface and bottom. "Predominance of flow" is a single expression that combines analyses of velocities, directions, and durations of currents at a specified location and depth (surface, middepth, and bottom). It is expressed in percent of total flow in the direction of flood or ebb. Plots of predominance of flow for neap, mean, and spring tides are show on Figure 4. It is an important factor in determining the location of shoaling that predominance of downstream flow at the bottom extended from the upper harbor to Sta 121 for neap and mean tides and to Sta 130 for spring tides. Similarly the greatest shoaling concentration was found to extend farther upstream for neap tide and farther downstream for spring tide. Increasing the fresh water discharge from 7000 cfs to 16,000 cfs was found to have a marked effect on salinities, predominance of flow and shoaling in that equivalent salinities were shifted downstream, the point of balanced flow was shifted downstream, and shoaling was moved downstream by the higher discharge. These effects were more pronounced when the high discharge was accompanied by spring tide.

The effects of channel deepening. A review of future harbor development and the trend of increased draft of vessels indicate that a channel depth of 40 ft may be required in the foreseeable future. Model tests were, therefore, conducted for the deeper channel, as well as for the 34-ft depth presently authorized. Channel depths of 36 ft and 40 ft were tested initially and later channel depths of 38 ft with widening in the downstream reaches were tested. Emphasis in this paper is placed on the 40-ft channel depths, which at present is considered maximum, and the 38-ft channel depths with widening in the downstream portions which has been justified and recommended in a review report prepared for Savannah Harbor and which probably will be authorized in the near future.

The deepening to 40 ft caused a lowering of the low water plane of about 0.5 ft throughout the harbor. Salinities were increased throughout the harbor, with the principal increases occurring at the upper end. Total shoaling was increased about 5 percent; however, shoaling in the upper harbor above Sta 135 was decreased about 22 percent, and that downstream from Sta 135 was increased about 30 percent. Flow predominance computations indicate that the degree of predominance of upstream flow at the bottom was increased; however, computations of the total flood

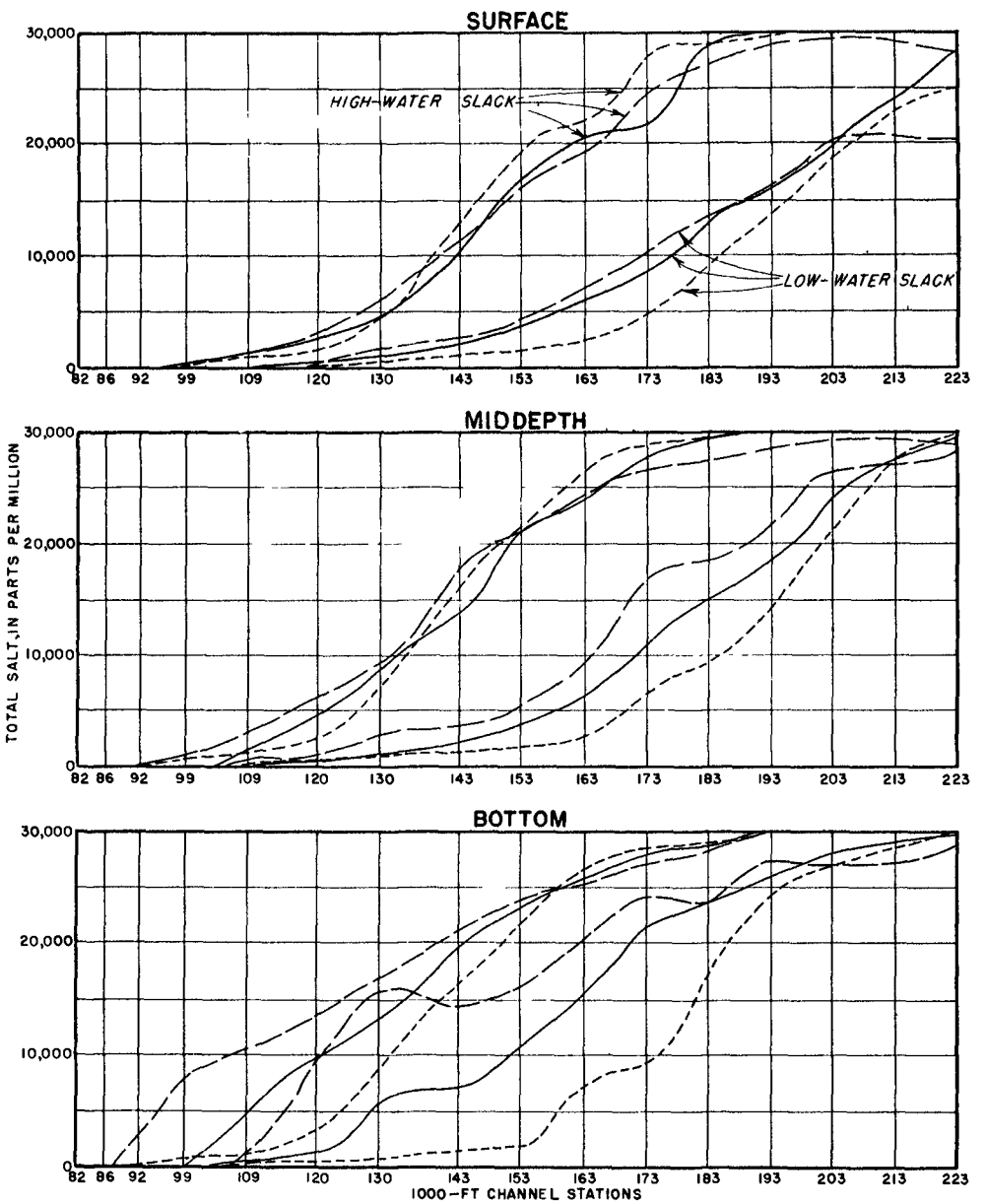

MODEL TEST DATA

TIDE , SEE LEGEND
FRESH-WATER DISCHARGE 7000 CFS
SOURCE SALINITY 30,000 PPM

LEGEND

——— NEAP TIDE
——— MEAN TIDE
- - - - - - SPRING TIDE

FIG. 3
SALINITY PROFILES
PHASE II
EFFECT OF TIDES
PRESENT PROJECT 34 FT

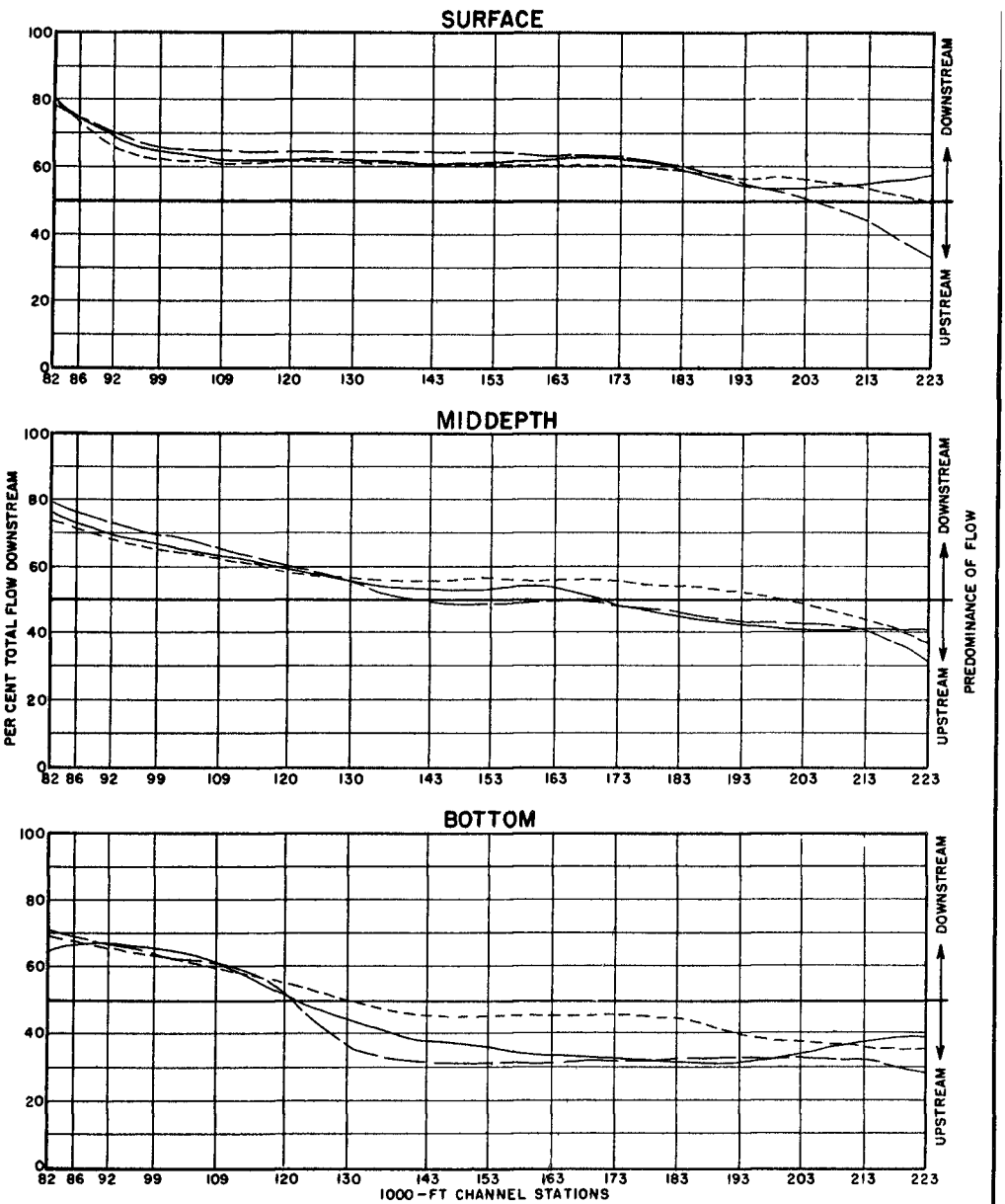

FIG. 4

PREDOMINANCE OF FLOW
PHASE II
EFFECT OF TIDES
PRESENT PROJECT 34 FT

and ebb flows at the bottom indicate that both were reduced appreciably by the deeper channel. The redistribtuion of shoaling observed during this test is attributed to the drastic reduction in the bottom flood currents. The sediments which reach the bottom in North Channel during the flood tides tended to remain there since the reduced flood currents on the bottom were not sufficient to resuspend and move the sediments progressively upstream during subsequent tidal cycles. These model shoaling test results, using gilsonite as the silting agent, might be somewhat different than shoaling in the prototype where even the very low velocities could be sufficient to move the light fluff material.

The deepening of the channel to 38 ft with the recommended widening from 400 ft to 500 ft in the lower reaches and 40 ft deep and 600 ft wide in the entrance channels caused little change in the low water plane and the time of the tidal events; however, salinity was increased greatly in the upper reaches and to a lesser degree near the entrance. The resulting salinities are shown on Figure 5. Predominance of flow is moderated. Resulting data are shown on Figure 6. The significance of the data is that bottom predominance is upstream to the extent that the sediment trap plan will be effective with the deeper channels and also that without this plan critical shoaling will continue in the same general locations as presently encountered. The tests indicate that the quantity of shoaling will be increased by about 20 percent; however since the shoaling sources were not altered by the plan the increase may not be completely valid but some increase can be expected with the wider channels.

FRESH WATER DIVERSION

The effects of fresh water diversion. The concept of complete diversion of fresh water as a means for reducing shoaling in Savannah Harbor, or relocating the major shoal areas, was based on two major factors:

a. Available information indicated that the fresh water flow in the Savannah River is a known source of sediment to the harbor.

b. The fresh water discharge is responsible for the density currents which amass 80 percent of the shoaling in the lower four miles of Front River. It was visualized that complete diversion of fresh water would eliminate the Savannah River source of sediment and at the same time eliminate density effects which are responsible for concentration of sediment in lower Front River. It would also eliminate the bottom density currents near the harbor mouth. The only currents remaining there would be tidal currents which should be approximately the same on flood and ebb. A large portion of the material carried in on the flood tide would most likely be carried out on the ebb. Several plans of diversion were tested, all of which were relatively successful in controlling the shoaling; however, all plans greatly reduced the

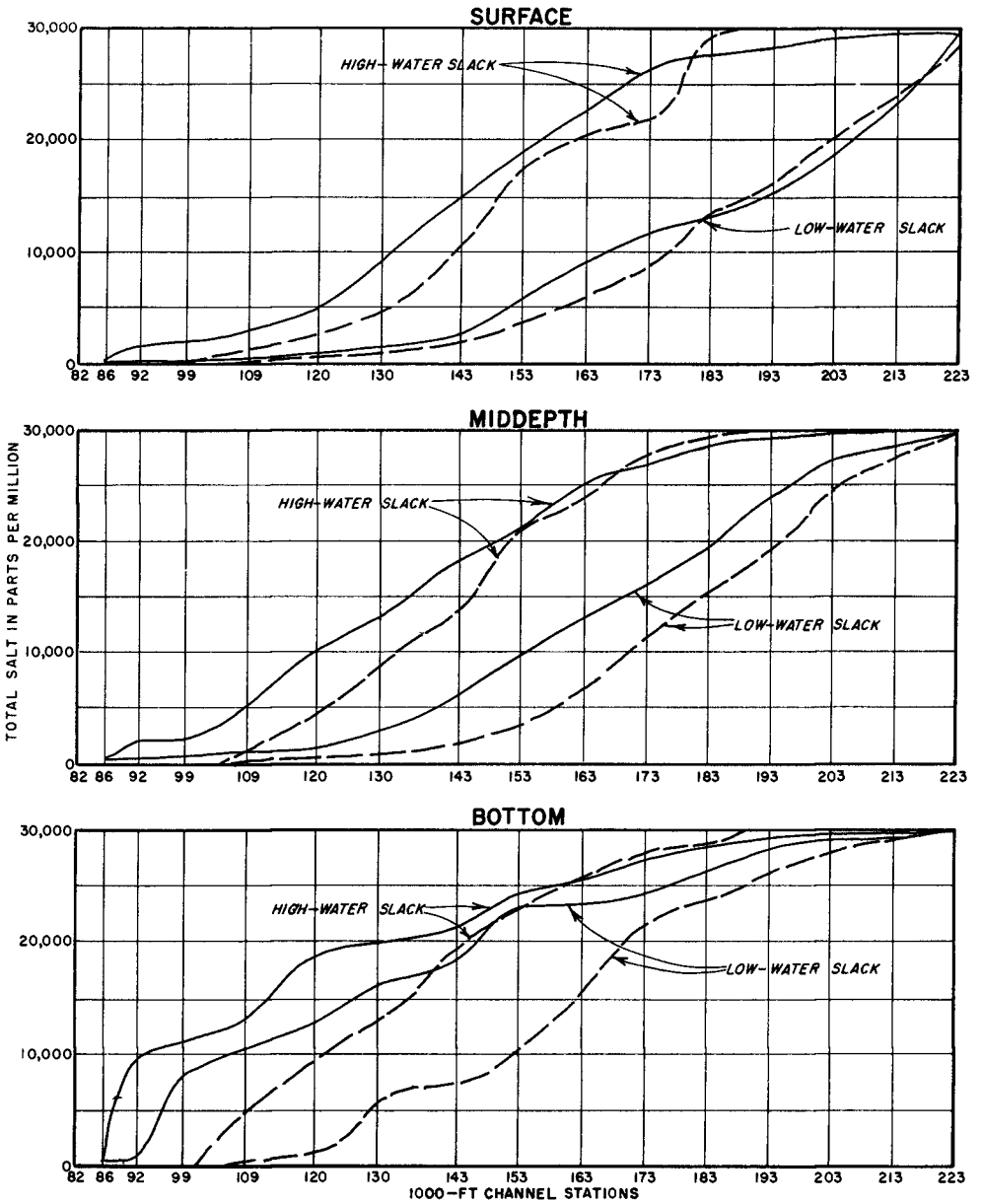

MODEL TEST DATA

TIDE	MEAN
FRESH-WATER DISCHARGE	7,000 CFS
SOURCE SALINITY	30,000 PPM

LEGEND

—— —— BASE TEST
———— PLAN TEST

BASE TEST 34-FT CHANNEL DEPTH
PLAN TEST 38-FT. CHANNEL DEPTH

FIG. 5

SALINITY PROFILES
PHASE IX SCHEME 4
TEST 2

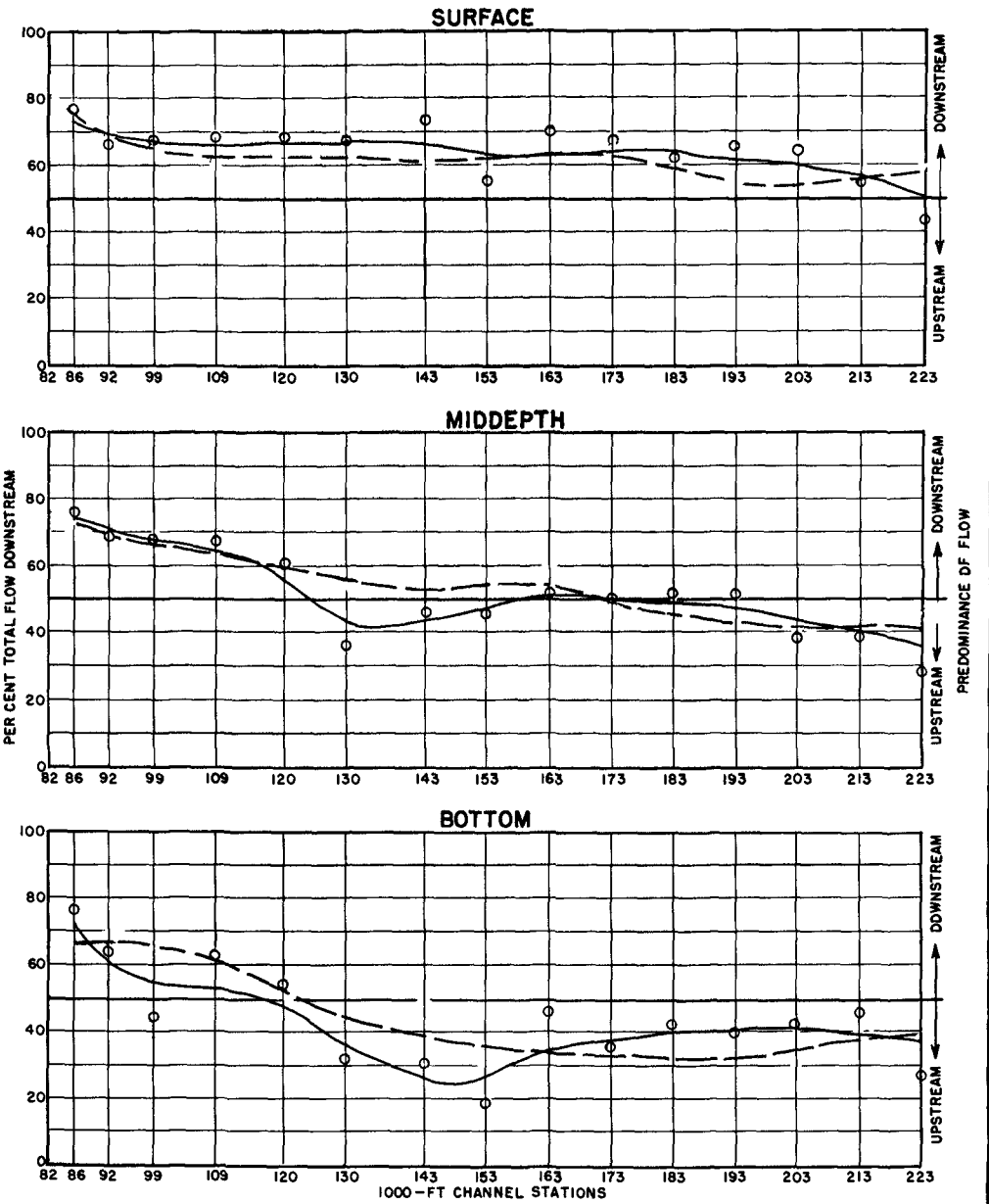

FIG. 6

PREDOMINANCE OF FLOW

PHASE IX SCHEME 4

TEST 2

quantity of available dissolved oxygen in the Front River channel caused by the removal of the fresh water, and caused a reduction in ebb velocities. Under these conditions the industrial wastes and sewage deposited in the harbor would cause an extreme nuisanc condition in the vicinity of the City of Savannah, the prevention of which would be very costly and greatly reduce the overall mone tary benefits of the plan. Since another more favorable plan was developed by later studies, diversion of fresh water has not been adopted.

CHANNEL REALIGNMENT

Effects of channel realignment at Elba Island. This phase of the model study involved investigations to determine the effec of realignment of the navigation channel in the vicinity of the westerly end of South Channel on the hydraulic, salinity, and shoaling regimens of the harbor. The elements of the realigned channels and North Channel sediment basin are shown on Figures 7 and 8. The realignment at Elba Island was designed to improve navigation conditions by eliminating the sharp bend in the existing channel. The realigned navigation channel would connect the present channel at about Sta 160 and Sta 140. Tests were made fo the following purposes:

a. To determine the best alignment and entrance conditions for the new channel.

b. To determine the amount of contraction required in the intercepted reach of North Channel to prevent excessive shoaling in the realignment.

c. To determine the effectiveness of various sizes and shapes of openings into the intercepted reach of North Channel fo trapping and retaining sediment.

Hydraulic characteristics and shoaling were not materially affected by this plan which was envisioned only to benefit navigation. Tests, however, were made utilizing the abandoned portio of North Channel as a sediment basin, which was found to be effective if the entrances were restricted. Economies could be realize in dredging from the basin instead of the navigation channel but the benefits would be negligible since shoaling quantities in the critical channels were not affected and only those in the lower reaches where disposal areas are adequate were reduced.

SEDIMENT BASINS

Back River Sediment Basins. The results of the verification and preliminary tests confirmed the conviction that sediment basin might offer a possible means for reducing maintenance costs if the location, entrance, and hydraulic conditions of such basins could be designed to attain the maximum possible rate of shoaling in the and if the basins could be located adjacent to adequate spoil

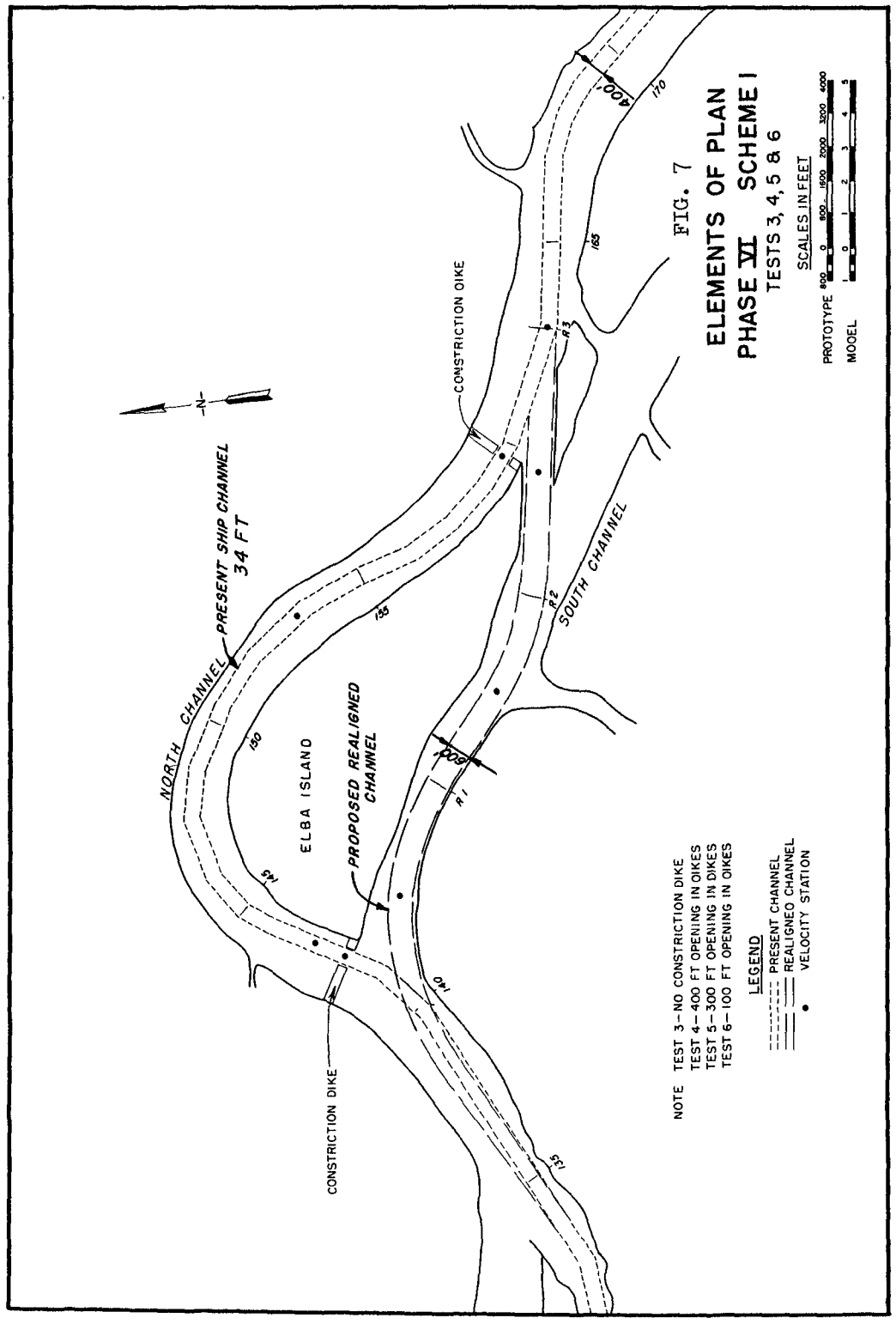
ELEMENTS OF PLAN
PHASE VI SCHEME I
TESTS 3, 4, 5 & 6
SCALES IN FEET
PROTOTYPE
MODEL
NORTH CHANNEL
PRESENT SHIP CHANNEL
34 FT
ELBA ISLAND
PROPOSED REALIGNED CHANNEL
CONSTRICTION DIKE
CONSTRICTION DIKE
SOUTH CHANNEL
R1
R2
R3
LEGEND
PRESENT CHANNEL
REALIGNED CHANNEL
VELOCITY STATION
NOTE TEST 3 - NO CONSTRICTION DIKE
TEST 4 - 400 FT OPENING IN DIKES
TEST 5 - 300 FT OPENING IN DIKES
TEST 6 - 100 FT OPENING IN DIKES

FIG. 7

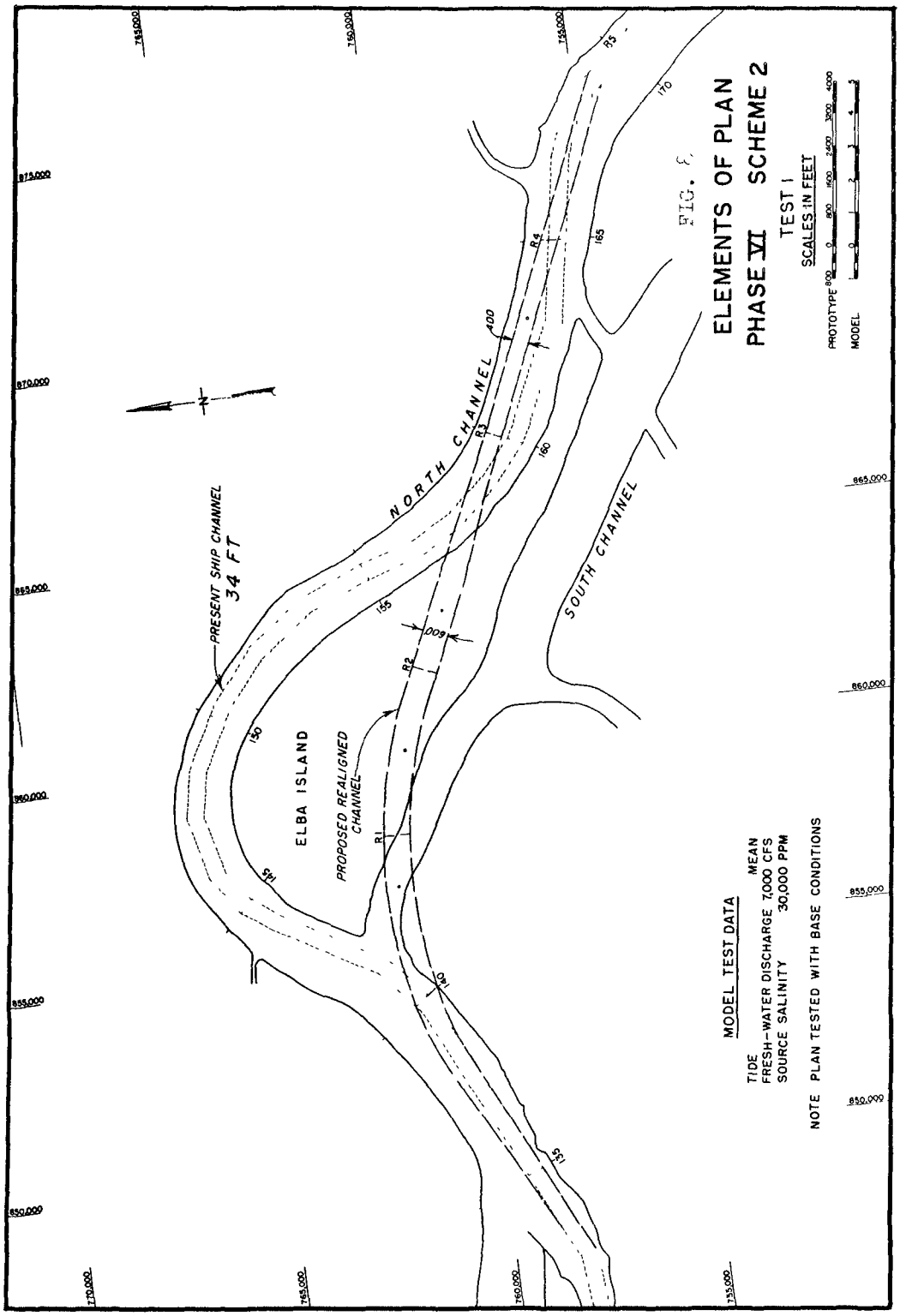
ELEMENTS OF PLAN
PHASE VI SCHEME 2
TEST I
SCALES IN FEET
PROTOTYPE 800 0 800 1600 2400 3200 4000
MODEL 0 1 2 3 4
MODEL TEST DATA
TIDE MEAN
FRESH-WATER DISCHARGE 7,000 CFS
SOURCE SALINITY 30,000 PPM
NOTE PLAN TESTED WITH BASE CONDITIONS
PRESENT SHIP CHANNEL 34 FT
NORTH CHANNEL
SOUTH CHANNEL
ELBA ISLAND
PROPOSED REALIGNED CHANNEL
R1
R2
R3
R4
R5
875,000
870,000
865,000
860,000
855,000
850,000
745,000
750,000
755,000
760,000
765,000
770,000

FIG. 8

disposal areas. Back River is ideally located for construction of a sediment basin. It has no commercial traffic, it is located near the major shoal area, it has no industrial development on either side, and the Government has perpetual spoilage easements on extensive diked areas adjacent to the proposed location for the sediment basin. A series of tests were made to determine the most favorable conditions for a sediment basin, and the effect of such a plan on the hydraulic regimen of the harbor.

Development of a Plan. The effectiveness of each plan was judged primarily by the ability of the plan to reduce shoaling in the Front River navigation channel between Sta 82 and Sta 135 and to concentrate shoaling in the sediment basin. The model tests of a sediment basin, located in the lower portion of Back River, 1500 ft wide and 2 miles long with an entrance channel in the mouth of Back River, reduced the shoaling in the navigation channel by about 20 percent. Since the reduction in channel shoaling occurred downstream from the entrance to Back River instead of in the critical shoaling area upstream from that point, little benefit would be realized.

The tide gate structure. The tide gate structure was provided across Back River at the SAL Bridge to increase the efficiency of the sediment basin by reducing ebb flows through the basin. A 500-ft gated opening was provided in the structure which opened automatically to allow flood flows to pass through but which was closed during the ebb periods. A canal was provided to drain the Back River tidal prism above the tide gate structure into Front River thus increasing ebb flows in Front River to reduce shoaling in that section.

It was determined by further tests that the sediment basin could be reduced to a width of 600 ft and still be reasonably effective. Tests incorporating deepening of the channels to 40 ft showed that ebb velocities in Front River were inadequate to maintain the channel to 40-ft depth. The tide gate was then shifted to the vicinity of the U. S. Highway 17A Bridge. It was found that a 100-ft opening was required in the tide gate to prevent excessive velocities in Front River during spring tides as long as the 34-ft channel was maintained. This reduced the efficiency of the sediment basin; however, the effect could be minimized by a controlled opening to be used only during spring tide periods.

The sediment trap-tide gate plan. The most effective plan was Phase VIII, Scheme 6, Test 4, (Figure 9) which requires a sediment basin in Back River 600 ft wide, 40 ft deep, and about 2 miles long; a tide gate in the vicinity of Highway 17A; and a canal connecting Back River to Front River in the upper portion of the harbor. The entrance channel to the sediment basin is 300 ft wide and 34 ft deep. During the shoaling tests, at the end of the prescribed number of tidal cycles, a stable condition

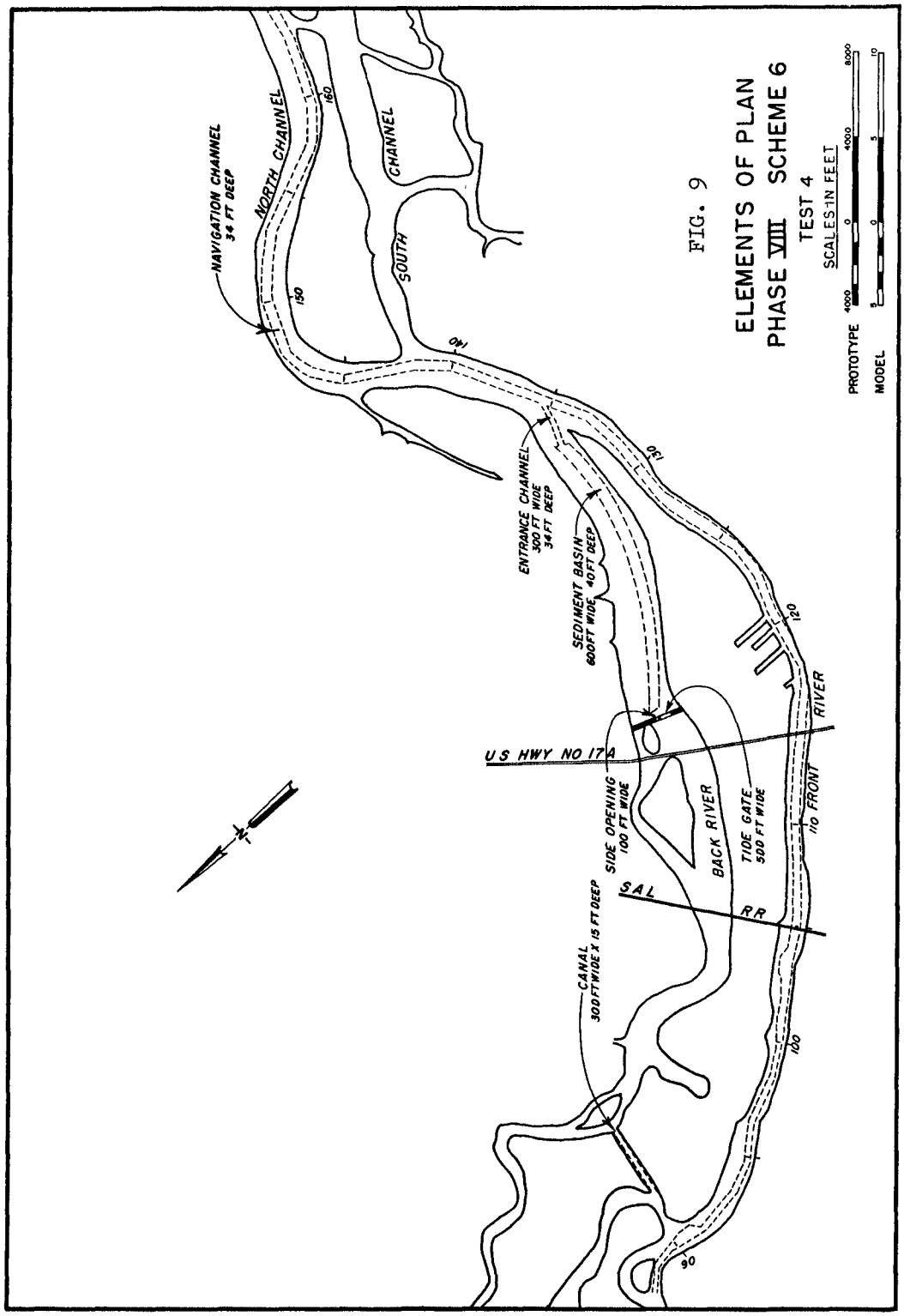
NAVIGATION CHANNEL
34 FT DEEP
NORTH CHANNEL
SOUTH CHANNEL
160
150
140
130
120
110
100
90
ENTRANCE CHANNEL
300 FT WIDE
34 FT DEEP
SEDIMENT BASIN
600 FT WIDE 40 FT DEEP
U S HWY NO 17A
SIDE OPENING
100 FT WIDE
BACK RIVER
TIDE GATE
300 FT WIDE
FRONT RIVER
SAL RR
CANAL
300 FT WIDE X 15 FT DEEP
N
ELEMENTS OF PLAN
PHASE VIII SCHEME 6
TEST 4
SCALES IN FEET
PROTOTYPE 4000 0 4000 8000
MODEL 5 0 5 10

FIG. 9

had not been reached in the navigation channels and sediment was still actively entering the sediment basin, whereas, in other tests the sediment had stabilized. Test 10 was then performed which extended the shoaling test until stability was reached. This plan reduced the shoaling between Sta 82 and Sta 135 from 77 to 5 percent and between Sta 135 and Sta 205 from 23 to 9 percent.

The 38-ft channel - with and without sediment basin. The 38-ft deep 500-ft wide channel which is being recommended for construction was tested with the Back River sediment basin and the results indicate that the plan will be successful. The model test data has been prepared to indicate a comparison of the 38-ft channel with and without the sediment basin.

The effects of the sediment trap on salinity throughout the harbor are shown on Figure 10. The only significant changes occurred in Front River where surface and middepth salinities were increased and bottom salinities were reduced; these changes were caused by the higher current velocities and more intense vertical mixing in Front River associated with the increased ebb discharge created by the plan.

Detailed velocity data were obtained; however, only the predominance of flow is presented. Figure 11 shows that in the bottom strata the predominance of flow is downstream from the upper limit of the harbor to about Sta 132 and upstream in the lower reaches as required to insure the maximum effectiveness of the sediment basin.

The effects of the sediment trap on shoaling are shown by Figure 12. Total shoaling in the navigation channel was increased by about 3 percent; however, shoaling of Front River was reduced to a great extent. This channel accounted for 57 percent of the total shoaling for the base test (without the sediment basin) but only 18 percent of the total shoaling with the sediment basin plan. Shoaling of the channels downstream from the confluence of Back River and Front River was not changed appreciably. The sediment basin retained 36 percent of the total shoaling. As was the case during previous tests of the sediment trap for other channel conditions, sediment was still moving into and depositing in the basin at the end of the test period. Therefore, had the tests been continued for a longer period of time, the results would have shown a much greater reduction in shoaling of the navigation channel. Previous tests indicated that 89 percent of the total shoaling material would be deposited in the basin if the tests were run until stability was reached.

In evaluating the results of this test, it should be kept in mind that the shoaling base test in the model represents the results of introducing a fixed amount of material into the model and operating for a fixed number of tidal cycles after injection

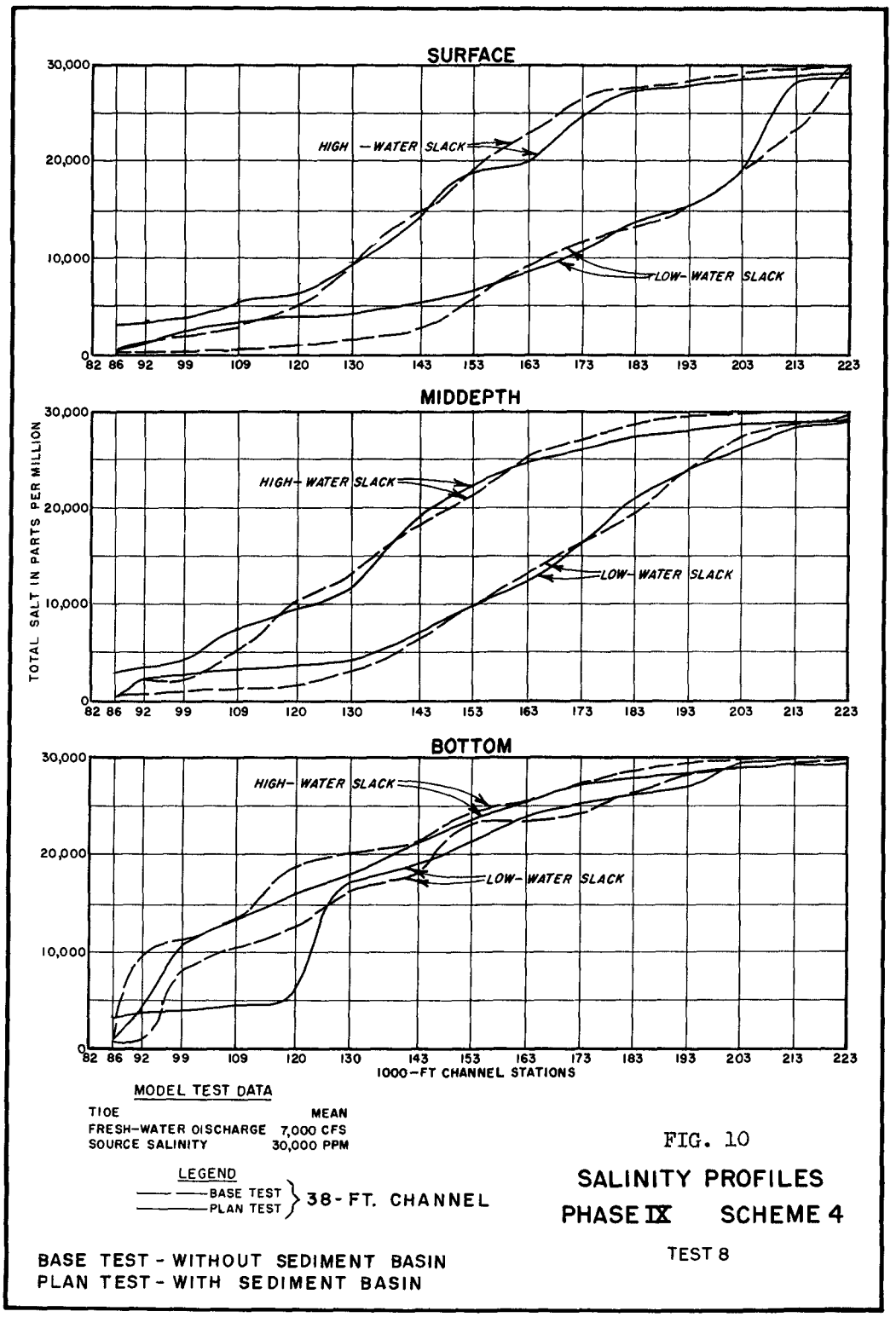

FIG. 10

SALINITY PROFILES

PHASE IX SCHEME 4

TEST 8

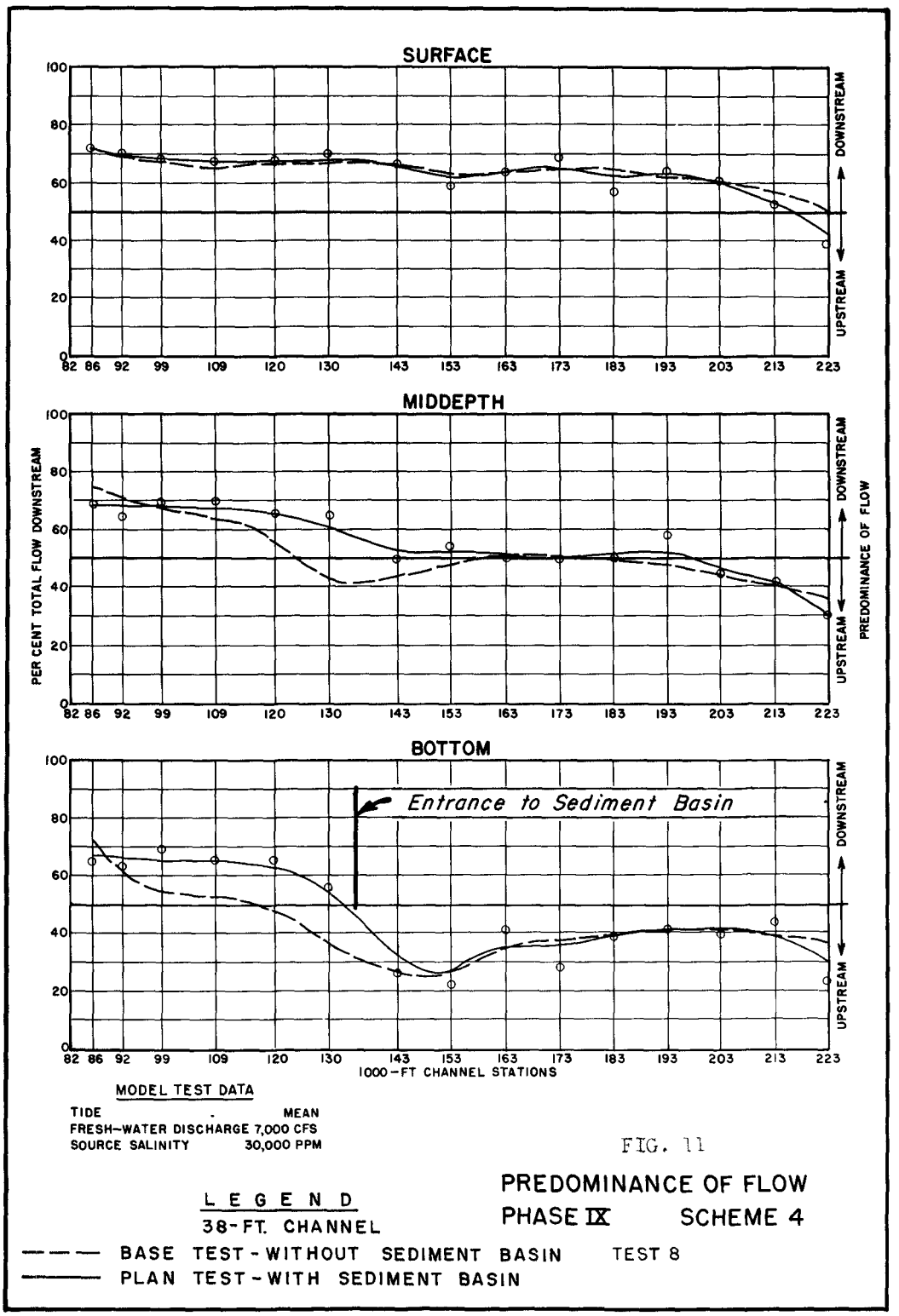

FIG. 11

PREDOMINANCE OF FLOW
PHASE IX SCHEME 4

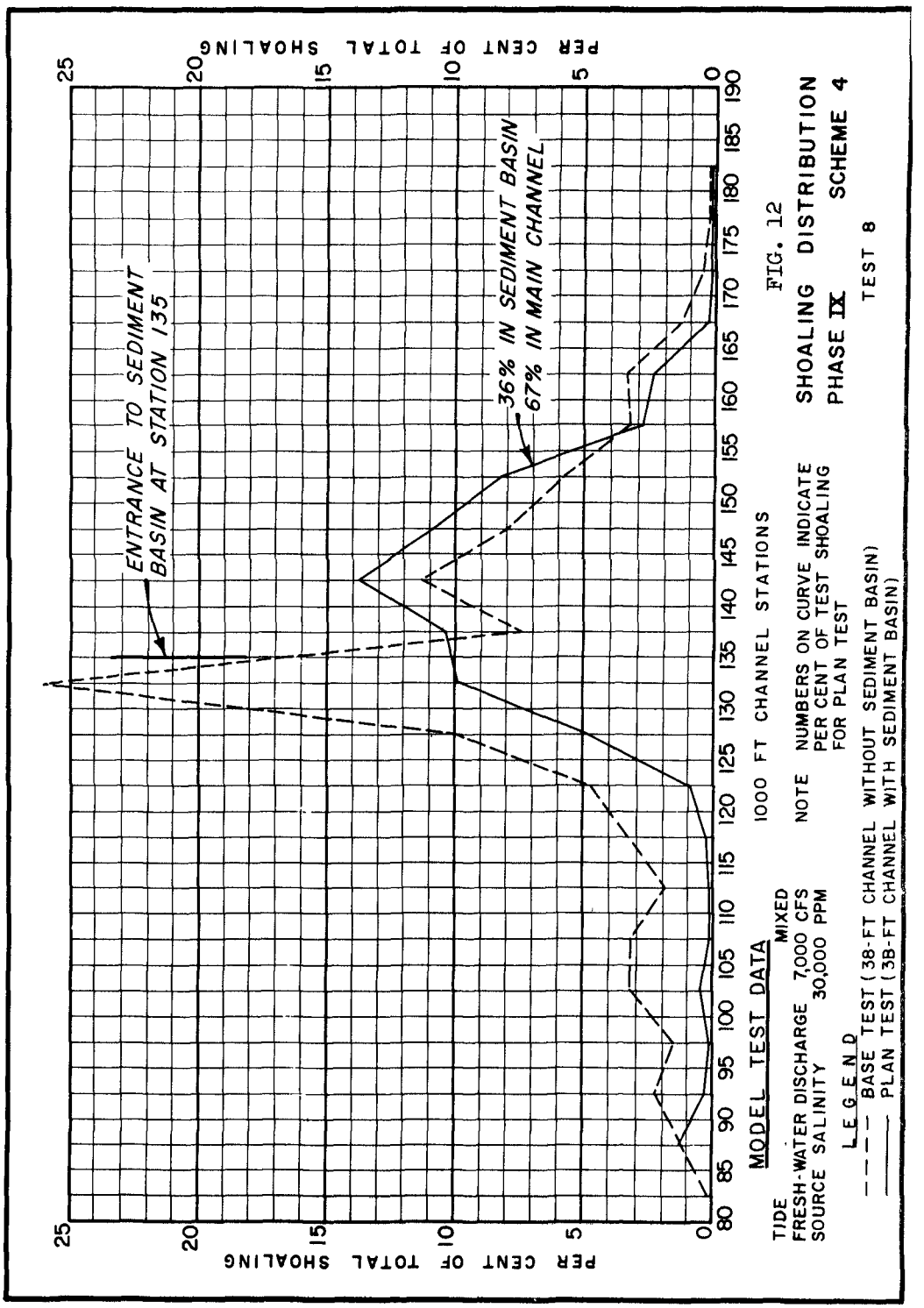
PER CENT OF TOTAL SHOALING
25
20
15
10
5
0
ENTRANCE TO SEDIMENT BASIN AT STATION 135
36% IN SEDIMENT BASIN
67% IN MAIN CHANNEL
80 85 90 95 100 105 110 115 120 125 130 135 140 145 150 155 160 165 170 175 180 185 190
1000 FT CHANNEL STATIONS
MODEL TEST DATA
TIDE MIXED
FRESH-WATER DISCHARGE 7,000 CFS
SOURCE SALINITY 30,000 PPM
NOTE NUMBERS ON CURVE INDICATE PER CENT OF TEST SHOALING FOR PLAN TEST
LEGEND
BASE TEST (38-FT CHANNEL WITHOUT SEDIMENT BASIN)
PLAN TEST (38-FT CHANNEL WITH SEDIMENT BASIN)
SHOALING DISTRIBUTION
PHASE IX SCHEME 4
TEST 8

FIG. 12

of the material. In the prototype, however, it is probable that shoaling material arrives in the problem area more or less continuously, although the rate of supply at certain times may vary. Of special importance is the fact that for higher fresh water discharges the effectiveness of the sediment trap would be temporarily reduced since much of the deposition would probably occur in the navigation channel downstream from the entrance to the sediment basin. For these reasons, it seems likely that the effectiveness of the plan is greater in the model than it would be in the prototype. After evaluation of this shoaling factor and the extended model tests, it was concluded that at least 60 percent of the total shoaling material would be deposited in the sediment basin. This has been used in economic analyses of the plan.

Sediment basin maintenance. Based on the present harbor shoaling rate and the model shoaling tests, it will be necessary to dredge about 6 million cu yds annually from the sediment basin. To retain the effectiveness of the sediment basin, it will be necessary to dredge it annually, or probably continuously, with periodic maintenance dredging in the navigation channels. The redistribution of the shoaling material is expected to produce considerable savings over the present maintenance cost because:

a. If a conventional pipeline dredge is used, reasonably short pipelines would be required since the spoil area is located adjacent to the basin, whereas, long lines are now required to maintain navigation channels.

b. Fixed pipelines could be utilized to eliminate much labor in handling.

c. The dredge would be out of the navigation channel which would eliminate loss of time permitting vessels to pass.

d. The operation of the dredge would be confined to limits of the sediment basin, eliminating the costly movement of the dredge over many miles of navigation channel.

e. It would be possible to let the sediment consolidate to an optimum density for efficient removal from the basin, whereas the present specified depths in the navigation channel which must be maintained often necessitates dredging material which has not consolidated sufficiently for economical removal.

The savings in labor and increased efficiency of dredging the material from the sediment basin would produce appreciable reduction in the maintenance cost. Preliminary economic studies for the plan indicate a favorable benefit-cost ratio. Although no specific plans have been made, it is contemplated that some means other than a conventional pipeline dredge can be devised to maintain the sediment basin, such as a simple arrangement of pumps on barges with drags similar to the hopper dredge or dustpan type intake, or semi-mobile dredge powered by electricity.

Since the preliminary economic studies have been based on the maintenance of the sediment basin with a conventional pipeline dredge, it is almost certain that final studies will indicate a more favorable benefit-cost ratio for the plan.

Review of findings. When the deepening of channels caused shoaling to be shifted to the section of Savannah Harbor where disposal areas are limited, prototype investigations and a model study were undertaken to determine means of reducing the high cost of maintenance.

The prototype studies determined that the Savannah River is a major source of shoaling material and contributes about 2,000,000 cu yds annually; the stratified condition caused by the mixing of the fresh and the salt water produces a hydraulic mechanism that controls the location of shoals, which in turn is affected by the fresh water discharge, tidal range, and dredging methods; the diking of spoil disposal areas is necessary to prevent the runback of spoil into the channel; and the dredging method would be improved by reducing the cutter speed and controlling the rate of swing.

Data and knowledge of existing conditions was obtained from the prototype studies for verification of the hydraulic model of Savannah Harbor. The general investigations in the model confirmed the prototype findings and depicted in detail existing prototype hydraulic, salinity, and shoaling conditions throughout the harbor with random or sporadic factors eliminated.

The model tests of improvement plans showed that plans to reduce shoaling by fresh water diversion were successful, but they created problems of pollution of a scope which would make their adoption questionable. Plans of channel realignment tested in the model proved to be beneficial to navigation but would be of little benefit to harbor maintenance. They also indicated that the deposit of shoal material could be induced in a sediment basin. A sediment basin in Back River with a tide gate to increas its effectiveness was the most desirable improvement plan tested. Tests developed hydraulic and shoaling conditions for proposed harbor deepening and determined that the Back River sediment basin plan would induce about 60 percent of the total shoaling quantity in the basin and that other aspects of the plan would be favorable.

Chapter 26

RESIDENCE TIME OF SAND COMPOSING THE BEACHES AND BARS OF OUTER CAPE COD

John M. Zeigler
Associate Scientist, Woods Hole Oceanographic Institution

Sherwood D. Tuttle
Professor and Chairman, Department of Geology, State University of Iowa

Graham S. Giese
Woods Hole Oceanographic Institution

Herman J. Tasha
Woods Hole Oceanographic Institution

INTRODUCTION AND DEFINITIONS

When a grain of sand is delivered to the sea by erosion it begins a journey being transported along beaches or bars, or offshore by waves and currents. The history of this journey can be extremely complex for the grain might spend a few seconds in one place and many years trapped in another before being released again for travel. It is therefore important at the outset to place some limitations upon our study. Firstly, our time scale is limited to the past seventy years, the time over which data were gathered. Secondly, the geographical position is limited to a strip of the east coast of Cape Cod 29,400 yards in length (Figure 1), extending seaward to where water depth is about forty feet. After a grain of sediment leaves this area we are no longer concerned with it. We define residence time as the average number of years a grain of eroded sediment is likely to spend in this prescribed area before it is transported elsewhere. We will further try to show that sediment takes a preferred path, some of it moving along the beach and some along the bars. It makes no difference to us if specific environments share grains; that is to say, some material will be on the beach one day and on the bar the next. In the end those grains which tend to be more stable in the beach environment will spend more time there and will travel with a characteristic velocity which is different from the velocity of those grains which are in hydrodynamic equilibrium on bars.

The method used to compute residence time involves volume stability. We measured the volume of the beaches and bars in the definition area and assumed that these volumes have not changed within the time limits of our study. We also measured the yearly addition of sediment to the area. In-as-much as there is neither gain nor loss of the average volume of sand -built features, i.e., the beaches and bars, sand must be moving out of the study area at the same rate it is being introduced. Therefore, the residence time in years is the average volume of a beach or bar divided by the yearly volume of sediment added by erosion to the beach or bar.

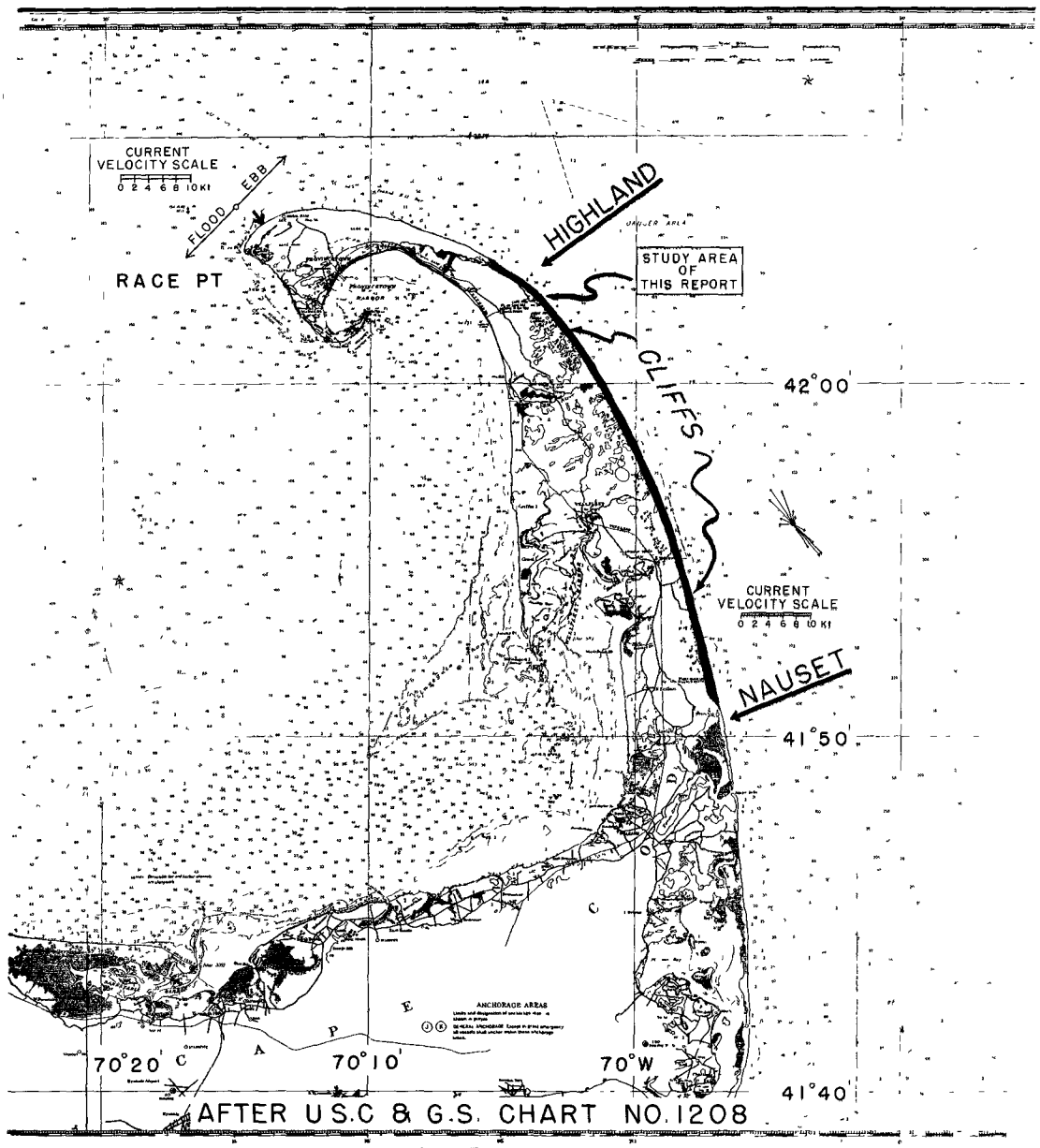

FIG. 1. LOCATION OF STUDY AREAS

The measurements which are needed for this determination are: the volume of sediment supplied each year; the volume of the coastal features within the definition area and the frequency distribution of grain size of the sediments being eroded and of the materials of the beaches and bars.

The east coast of Cape Cod is uniquely situated for a study such as this because sediment is introduced into the definition area only by erosion within the area of the cliffs or sea floor. No sediment or very little of it is introduced into the study area by means of littoral drift. There are no rivers on this coast, the northern end of the Cape is a site of deposition where a hook is building into the deep open water of the Gulf of Maine, and the southern end of the Cape is likewise a site of spits building to the south. The portion of the coast for which residence time is to be computed is therefore defined as that part of the eastern coast of Cape Cod between Highland and Nauset, a distance of 29,400 yards.

RATES OF COASTAL EROSION

Mr. Henry Marindin, an assistant to the Superintendent of the U.S. Coast and Geodetic Survey, conducted a most interesting and worthwhile series of measurements which allowed him to determine the rates of erosion on the cliffs and beaches of Outer Cape Cod (Marindin, 1889, 1891). These were made beginning in August 1887 through 1889. In brief, Marindin established a series of points, 229 in all, approximately 300 meters apart along almost the entire eastern coast of Cape Cod and around the Provincelands Hook. From these points, which he marked in the field by oaken stakes, he published measured distances, azimuths, and elevations over the ground more or less at right angles to the coast. The elevations were established on a mean sea level datum that he derived from tidal observations made at Chatham, in 1887. Marindin located his origins in terms of latitude and longitude but, because of a change in geodetic grid, it is necessary to correct his origins by subtracting 0.6 seconds from each of his latitudes in order to plot the points on present-day charts. This survey, which was carried out under the usual adversities of scrubby vegetation and variable weather, technically was an excellent job.

Marindin simply compared the new position of the cliff base, or cliff top, or high water line with its position on earlier charts that had been surveyed in 1848, 1856, or 1868. He gives the average rate of erosion along the coast as 3.2 feet per year. Marindin published all of the data concerning the location of the points of origin, the azimuths of the lines and the distances along the lines to cliff tops, cliff bases and water lines.

Giese and Tasha, using both plane table and transit surveying methods reoccupied 74 of Marindin's points of origin located between Nauset at the south end of the cliffs, and Pilgrim Lake, north of Highland, in the Provincelands. They marked each of the relocated points of origin with a concrete post which held a circular brass plate. We found none of Marindin's original oak stakes but in a few places our relocated points matched the descriptions of landmarks as given by Marindin.

We compared the profiles measured in 1958 and 1959 with the profiles measured in 1879. Where the profiles crossed cliffs we compared the rate of change of the cliff lip and cliff base and used the average of the two. Where the profiles crossed dunes we chose the base of the foredune on the sea side as a point for comparison, supporting this choice where possible by using mean sea level. This re-surveying information has been placed in a set of tables and graphs (Zeigler, Tasha, Giese 1964).

The major sources of error in determining rates of coastal change in this manner are failure to re-occupy the exact point of origin of the original survey, short term differential erosion of the cliffs and short term changes in the position of high water or beach level The coast of Cape Cod has a smooth outline and so far as old charts can be trusted, it has always had a smooth outline, one might reason therefore that although the rate of erosion or accretion is slightly different from point to point, these differences must even out with time and the variation observed from profile to profile consequently is due to one of the above-mentioned causes. Therefore, we believe that we are justified in speaking of an average rate of erosion over the seventy year period between surveys. The average rate of change for the coast was obtained by drawing a line of best fit through all of the values of erosion rates obtained by us when the points were re-surveyed, (Figure 2). These change have been plotted opposite the geography on Figure 3.

The main cliff section facing the sea is being eroded at a rate of approximately 2.6 feet per year. This erosion becomes less north of Cape Cod Light and finally a point is reached near Pilgrim Lake where the coast is neither building nor cutting. To the north of this point the great Provincetown Hook of loose sands is developed and its coast is growing into the sea. Erosion rates show that Nauset Spit on the south end of our survey was being driven into the marshes at approximately 5 feet per year but we do not think this is a valid figure. At about the time the surveying was being done Nauset Spit was cut by a series of breakthroughs and coastal adjustments were rapid. We have observed no serious bending of this spit in the years following our survey and therefore we assume Nauset Spit must be retreating at the same rate as the cliffs.

VOLUME OF SEDIMENT SUPPLIED BY EROSION AND THE PROFILE OF EROSIOI

Rate of cliff retreat can also be stated in terms of volume because the topography is known, relief having been measured during the surveying. Table I presents the erosion rates in terms of cubic yards of sediment delivered to the sea per year in two categories: 1. for the cliffed section between cliff base and cliff top and 2. for the material eroded from the sea bottom. Cliff base was chosen because it is a point which ordinarily is easily determined and in general on this coast it represents the reach of highest high tide and is therefore a true point on the profile of erosion.

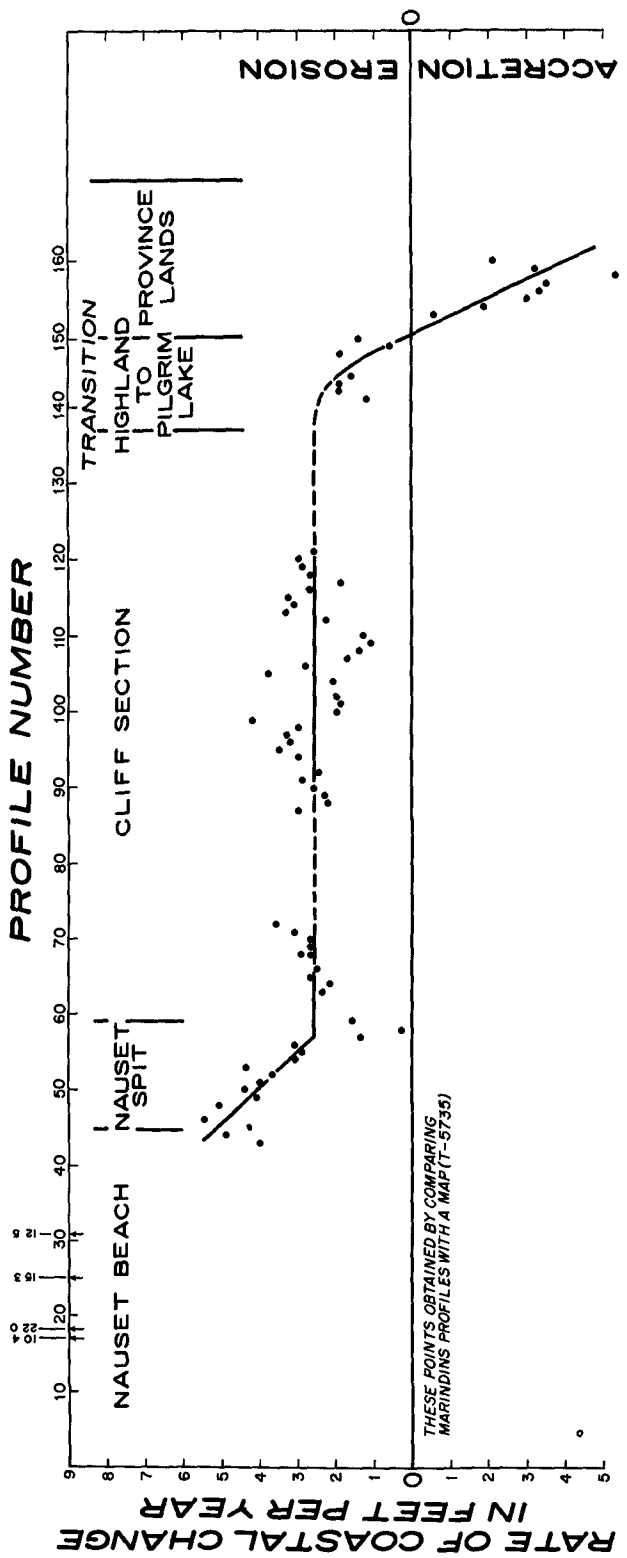

FIG. 2. RATE OF EROSION OF EAST COAST OF CAPE COD DETERMINED BY COMPARING PROFILES MEASURED IN 1887 BY H. MARINDIN AND SAME PROFILES MEASURED IN 1957-1958

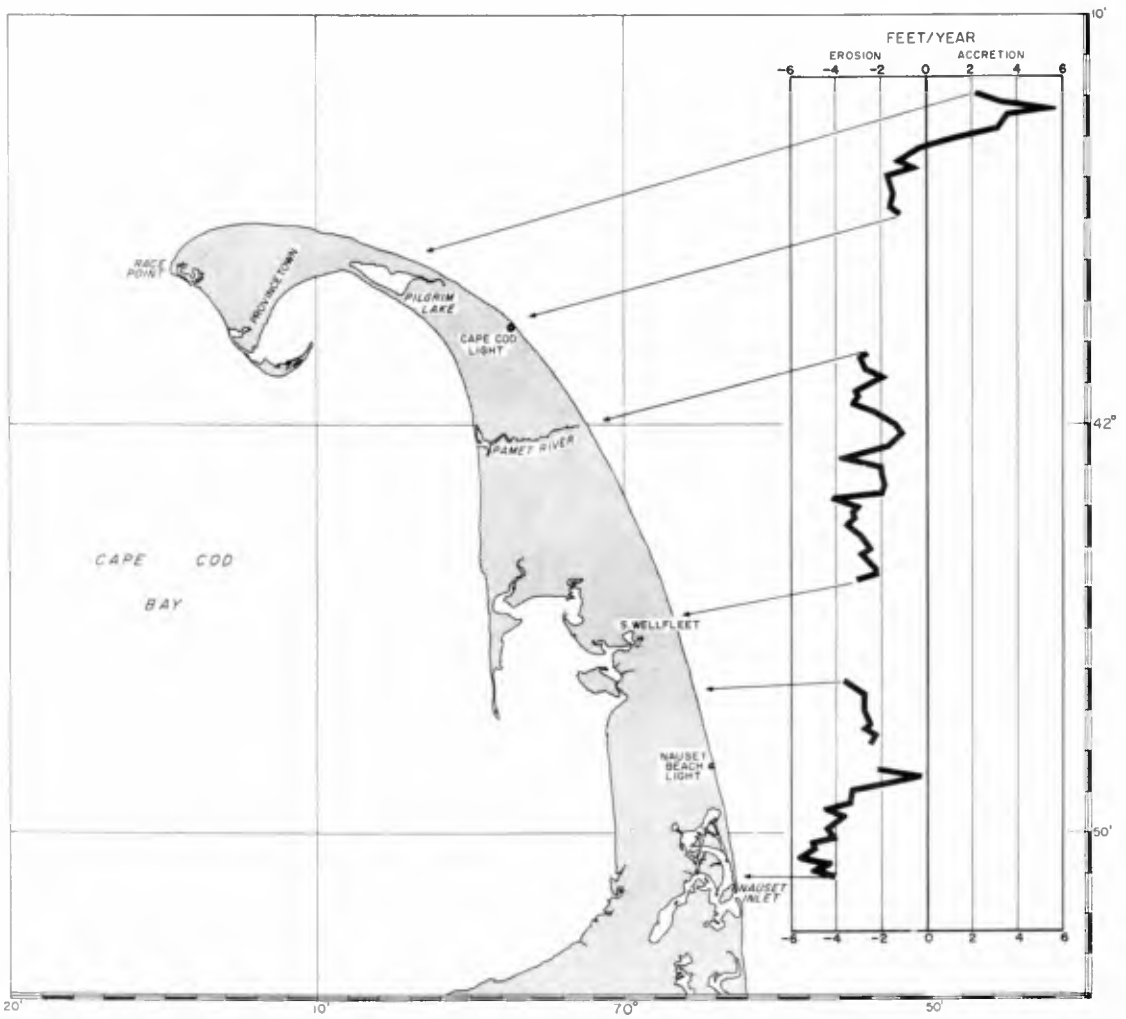

FIG. 3. GEOGRAPHICAL DISTRIBUTION OF RATE OF EROSION: OUTER CAPE COD

Erosion however is also taking place seaward of cliff base and the sediment derived therefrom is likewise available to nourish beaches and bars. In order to estimate the amount of this erosion one must describe the submarine profile of erosion and the dynamics of its shoreward movement. It has been our experience that the relationship of the transient features, beaches and bars, to the profile of erosion here on Cape Cod is that described by Figure 4.

The profile of erosion is fundamentally different from the profile of the sea bottom in several ways. Once a cut has been made on the profile of erosion it is cut forever and simply replacing the loss with loose material does not restore the original condition. The profile is cut and not built, and the sediments exposed along it are composed of the underlying formations be they lithified rock or loose sediment. Only a small fraction of the sediment grains making up this underlying surface are likely to be in hydrodynamic equilibrium with a given sea state, therefore once exposed to water movements strong enough to transport sediment, the grains can be expected to move elsewhere and erosion takes place. The profile of erosion is protected from most of the waves by a sand cover, the beach and bars, but stronger waves are able to shift the sand cover and cut the underlying surface. Erosion also takes place in pulses when over a period of weeks or months the beach or sand cover remains very thin, at which time the underlying glacial drift is cut away by a larger proportion of the waves reaching it. We have observed three such pulses in ten years on Cape Cod when the sand cover was so thin that it afforded little protection against erosion to the underlying sediments. These characteristics lead us to the conclusion that the profile of erosion is in equilibrium with the long term sea state and that it will not change its slope or form unless the average long term sea conditions change. If this be so, then the profile of erosion will translate shoreward without changing its slope, a conclusion already reached by Bruun (1962). Geometrically it means that if one once knows the shape of the profile of erosion and the rate of coastal retreat, he can project the profile either forward or backward in time and either obtain volumes of sediment which will be eroded from beneath the sea or volumes which were eroded in the past. We have used this technique to obtain the volume of sediment made available from the sea bottom to nourish beaches and bars for the past seventy years (Table I).

There are several sources of information which helped us construct the profile of erosion for outer Cape Cod. Parts of the surface of the profile are often visible in three places: (1) the foot of the cliff (2) the toe of the beach to the inner edge of the nearshore bar and (3) the trough area between the nearshore and offshore bar. Sometimes one sees more of the underlying profile when the beach has been temporarily thinned and sometimes one can also find an exposure of the underlying glacial deposits seaward of the offshore bar. We have driven pipes into the underlying glacial deposits in the beach and between the beach and the inner bar. During storms one often sees a band of muddy water between the inner and outer bar where the silts and clays of the underlying glacial deposits are being stirred up. Silts and clays are not found in the sediments of the bars themselves. After some practice one is able to pick the limits of the bars from continuous echo

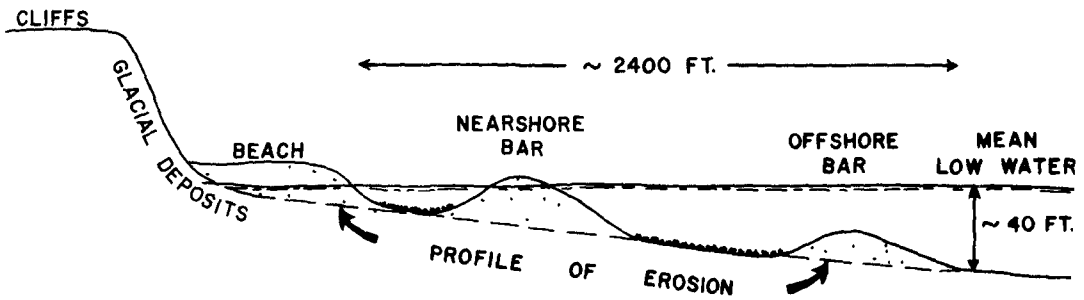

FIG. 4 RELATIONSHIP BETWEEN PROFILE OF EROSION, BOTTOM PROFILE, AND OVERLYING LITTORAL FEATURES

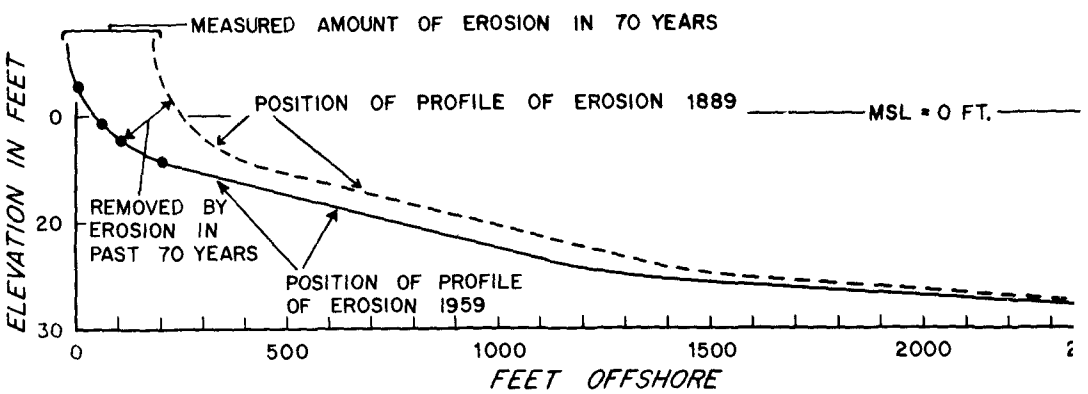

FIG 5 AVERAGE PROFILE OF EROSION FOR OUTER CAPE COD AND ITS POSITION IN 1889

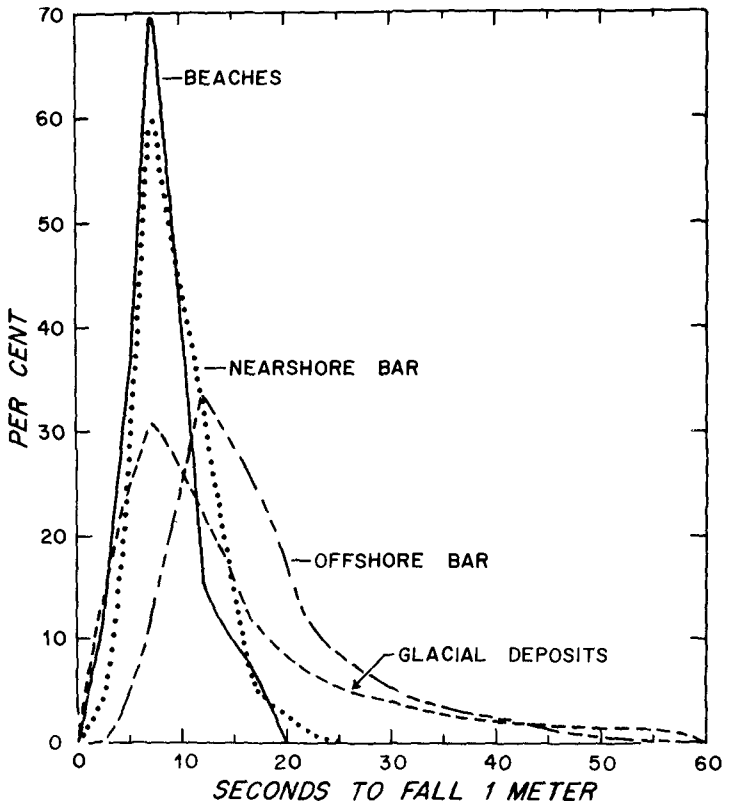

FIG 6. FREQUENCY DISTRIBUTION OF SEDIMENTS REPRESENTING VARIOUS ENVIRONMENTS OF COAST AND SOURCE MATERIAL, GLACIAL DRIFT

TABLE I

Average Yearly Volume of Sediment Supplied to Nourish the Beaches and Bars

	Cubic Yards
Volume eroded from cliffs above high, high water (+14 ft. elevation)	409,740
Volume eroded from below the sea (high, high water +14 ft. to depth of little or no erosion N-40 ft.)	437,892
Total sediment derived from erosion of the 29,400 foot length of coast each year	847,632 Cu. Yds. Per Year

sounding records and check the results against samples taken of the bottom along the same profile. The coarse gravels and cobbles lying on the profile surface are lag deposits.

With these criteria and Figure 4 as guides one can determine the shape of the profile of erosion from measured profiles. We measured hundreds of profiles across these beaches between 1953 and 1962 (Zeigler et al 1959, and Zeigler and Tuttle 1961) and had on some occasions when the beach sand cover was thin and the underlying glacial deposits exposed, established the absolute elevation of points on the profile of erosion (Circle on Figure 5). The more seaward end of the profile of erosion beneath the nearshore and offshore bars was established by drawing a line between the interbar troughs. An average profile of erosion was constructed from such surveys. Inasmuch as we believe that the same profile which existed seventy years ago, had the same geometric shape as the present day profile, we believe we can establish its position by shifting it seaward 182 feet, the average measured amount of coastal retreat in that time (Figure 5). The volume of sediment removed from the sea floor near the coast per unit length of coast per year is therefore the area contained between these two profile lines multiplied by the unit length and divided by seventy years. We found this to be 437,892 cubic yards per year for the portion of the coast under investigation. The dimensions of the profile of erosion thus determined are to some extent subjective at the outer end in spite of the rather substantial field data. On the other hand the control is excellent on the shoreward end. Since we determined the volume of sediment by shifting the entire profile one can see that errors on the seaward end are of little significance and the place where we desire the least error, the shoreward end, is fortunately the place where control is best.

The beaches and bars rest on the eroded surface and one can estimate their volume from the graphical construction by measuring the areas enclosed by the lines defining the features and subsequently multiplying by some length term representing length along the coast.

Because the profiles were taken over a period of several years at all seasons of the year we believe that they are representative of the cycles of change one might expect. The volumes are summarized in Table II.

TABLE II

Volume of Beaches and Bars of Outer Cape Cod between Nauset and Highland (29,400 yar

	Cubic Yards
Beach	5,736,230
Nearshore Bar	8,299,260
Offshore Bar	17,590,020

PER CENT OF ERODED SEDIMENT WHICH NOURISHES EACH ENVIRONMENT

When a cubic yard of material is delivered to these particular beaches it is quickly divided up between the nearshore environments. Very fine sediment is carried offshore into deep water, beyond our zone of interest, very coarse sediment such as gravel and cobbles move to the turbulent step zone at the toe of the beach, or remains as a lag in the interbar trough, the intermediate and coarse sands are delivered to the beach, and nearshore bar and the finer sands to the offshore bar. The material then moves along the shore until it leaves the boundaries of the area under discussion.

Fortunately we are in a position to make a reasonable estimate of the fraction to be assigned to the offshore bar; it turns out that one cannot separate the beaches from the nearshore bars by using the data on hand. Figure 6 gives the frequency distributions of sediment properties with respect to environment. The property measured is fall velocity and it is given in terms of seconds to fall one meter in fresh water. These units were chosen because this is the form in which data are obtained directly from the Woods Hole Rapid Sediment Analyzer (Zeigler, Hayes, and Whitney 1960). The technique is excellent for comparing one sample with another in order to determine a quantitative similarily or dissimilarity.

The degree of unreliability for these comparisons arises mostly from lack of samples and from errors in field sampling. Both of these problems can be corrected somewhat by taking more samples. Field sampling errors in this case arise from natural causes. Glacial deposits, the material from which all nearshore depositional features are derived are exposed in the cliffs and are composed of cross-bedded sands, and silty sands. In some places there is a distinct clay bed (Zeigler, Tuttle, Tasha, Giese 1964) and in many places pebble and cobble beds. Lithology of the cliffs changes laterally in an unpredictable manner. Therefore, to represent the cliff material by a single curve requires a careful analysis of what the cliffs are like. We attempted to overcome the short distance variability of the strata by using trench samples of the entire vertical exposure of the cliffs.

A second field sampling problem arises on the beaches and nearshore bars . Coarse gravel and pebbles tend to concentrate at the toe of the beach but can be spread over the foreshore or part of the bar by some sea states. In other words this material is shared by both environments and changes its position with changing sea state. Fortunately, the number of samples available for bars included four different surveys, two of which were made at times when the bars were visibly more stony, therefore we think this problem of field sampling was somewhat reduced even though the beach samples used did not represent beaches during stony periods and the step zone was unrepresented. The gravel content of the bar should be reliable, leaving the remainder of gravel available for the step zone and times when the gravel is spread over the beach.

If these sampling limitations are not too much of an obstacle, we proceed to analyze th value of our observations. From Figure 6 it is plain that the offshore bar is composed of materials finer than the beach and nearshore bar and that the nearshore bar and beach share sediment in virtually all categories. Thirteen per cent of the glacial material is lost either offshore or by being carried inland by winds, that is, it does not show up in the sediments composing these three environments. Therefore, the frequency distribution for glacial sediments has been recomputed to make the remaining 87 per cent equal to the whole area beneath the curve.

We need to know how much of the glacial sediment goes into each environment. This we estimate by assuming that the curves represent all of the sediment and that none of the coarser material is lost offshore. We further assume that we can divide up the area beneath the curve representing the glacial deposits, by geometric proportioning of the other curves. The fit between the limbs of the curves representing the offshore bar and glacial sediment is not perfect, having a disparity of 7.7 per cent by area. This reflects the fact that the two curves do not have the same skewness and it likewise indicates that this method of approximating the percent of glacial sediment in each environment is subject to uncertainty. Possibly there is loss offshore of some of the finer sands, the 7.7 per cent reflecting this. There is not sufficient difference between the frequency distributions of beaches and bars for the proportioning method to be useful.

It seems to us, therefore that this proportioning method is reasonable for predicting the amount of material which is used to maintain the offshore bars, but that one must combine the beach and nearshore bar as a single hydrodynamic feature in-so-far as residence time is concerned. Results are summarized in Table III.

TABLE III

Per Cent of Glacial Material Eroded from the Cliffs and Bottom which enters each of the Defined Environments.

Beaches plus Nearshore Bars	43.3 per cent
Offshore Bar	36.3 per cent
Lost (Offshore mostly)	20.5 per cent

RESIDENCE TIME

We now have the numbers needed to compute residence time: the volume of the features and the yearly volume of new material added; therefore, reiterating the initial assumption that each of the coastal features, the beaches and bars are neither growing nor diminishing in volume over a long term time base we compute the residence time by simple division as 38.2 years for the beach and nearshore bar taken together and 57.2 years for the offshore bar.

One might use this information in various ways. For example if it becomes necessary to preserve these beaches by artificial nourishment one knows that for every yard of material hauled to the beach (assuming glacial material is taken from one of the many sand pits available) that only 43.3 per cent of each yard will remain on the beaches and bars. Or another way of looking at it; if ever the cliffed section were completely paved by some method to prevent or slow down coastal retreat cutting off approximately one-half of the sand supply, the beaches would disappear completely in 86 years, and probably a lot sooner, or if a harbor of some sort were to be constructed the volume of littoral drift which would have to be handled would be about 680,000 cubic yards per year.

This information is not only useful for applied problems but provides a good boundary for field experiments which would measure the amount of littoral drift by using tracer material. It also provides a tool for estimating the age and rate of growth of some of the large depositional features such as the Provincetown Hook.

ACKNOWLEDGEMENTS

This work was supported in part by grants from The Office of Naval Research under contracts Nonr-1254(00) NR-388-018 from the Geography Branch and ONR contract Nonr 2196(00) NR-083-004 from the Geophysics Branch. We wish to express our thanks to the selectmen of the towns of Provincetown, Truro, Wellfleet, Eastham and Orleans and to many of the local citizens for permitting us to cross private property in pursuance of this work.

Contribution number 1540 from the Woods Hole Oceanographic Institution.

REFERENCES

Bruun, Per, (1962) Sea-level rise as a cause of shore erosion: Jour. of Waterways and Harbors, proceedings Am. Soc. Civil Eng., v. 88, p. 117-130.

Marindin, Henry L., (1889) Encroachment of the sea upon the coast of Cape Cod, Massachusetts, as shown by comparative studies, cross-sections of the shore of Cape Cod between Chatham and Highland Lighthouse: Ann. Report U. S. Coast and Geodetic Survey, 1889, app. 12, p. 403-407, app. 13, p. 409-457.

Marindin, Henry L. (1891) On the changes in the shoreline and anchorage areas of Cape Cod (or Provincetown Harbor) as shown by a comparison of surveys made between 1835, 1867, and 1890; cross-sections of the shore of Cape Cod, Mass., between Cape Cod and the Long Point Lighthouse: Ann. Report U. S. Coast and Geodetic Survey, 1891, app. 8, p. 283-287, app. 9, p. 289-341.

Zeigler, John M., Hayes, Carlyle R., and Tuttle, Sherwood D. (1959) Beach changes during storms on outer Cape Cod, Mass., Jour. Geology, v. 67, p. 318-336.

Zeigler, John M., Whitney, Geoffrey G., and Hayes, Carlyle R. (1960) Woods Hole rapid sediment analyzer, Jour. Sed. Pet., v. 30, p. 490-495.

Zeigler, John M., and Tuttle, Sherwood, D., (1961) Beach changes based on daily measurement of four Cape Cod beaches, Jour. Geol. v. 69, p. 583-599.

Zeigler, John M., Tuttle, Sherwood, D., Tasha, Herman J., and Giese, Graham S. (1964) Pleistocene geology of Outer Cape Cod, Bull. Geol. Soc. Am. v. 76.

Zeigler, John M., Tasha, Herman J., and Giese, Graham S. (1964) Erosion of the cliffs of Outer Cape Cod, Mass., Tables and Graphs, Ref. no. 64.21 Woods Hole Oceanographic Institution, unpublished manuscript.

Chapter 27

A PROJECTION-TYPE SOUNDER

Takeshi Ijima
Dr.Eng. Head, Design Standard Division
Port and Harbor Technical Research Institute
Ministry of Transportation, Yokosuka, Japan

INTRODUCTION

The Depth sounding is the fundamental process for the investigation of sand drift on sandy beach and has been carried out by means of echo-sounders. Although it is necessary to obtain the actual variations of bottom topography under the direct action of strong waves, the data even by the up-to-date method of soundings are limitted to the case of calm sea conditions. Moreover, even in calm seas it is often difficult to measure the depth of water in the surf zone which has remarkable change of bottom topography due to wave action. The author has no information on the data of bottom topography under the direct action of waves on actual beaches in Japan, excepting those of Mr. Fujiki on the coast of Niigata along the Japan Sea, who, however, had measured the bottom profile along one fixed line which was set perpendiculaly to the beach.

At present we have no effective method of measuring the amount of drift sand, and therefore the measurement of dynamical variation of bottom topography is considered to be the possible primary and fundamental approach to the estimation of sand drift on sandy beach without any coast structure and also to be the final method of finding out the similarity law between model test and actual phenomena, through which model test may become a confiderable method of solving the sand drift problem.

In order to observe the dynamical variation of bottom topography by wave action, it is necessary to develope newly any possible method without boat and echo-sounder. This is the purpose of study of projection type sounder.

PRINCIPLE

For the above purpose of field investigation of sand drift, the following conditions should be satisfied.

(i) The observation should be carried out even in ordinary storm conditions, that is, even for the case of waves with heights of 2 or 3 meters and wind speed of 10 or 15 m/sec.

(ii) Bottom topography in the surf zone of remarkable change by wave action should be measured. Therefore, the area within 400 or 500 meters from shore line is to be necessarily observed.

(iii) The accuracy of measurement should be of the order which is sufficient to find out the change of water depth by wave action.

(Iv) Observation should be carried out as easily as possible and also the apparatus should be moved easily on the beach.

As for the methods which are available without any sounding boat and satisfy above conditions, the following three are considered to be possible.

The first is the underwater method, in which a topedo with pressure unit and a rope is to be driven into the sea, stopped and droppec down to the bottom at any required point and then pulled back by rope, measuring the statical water pressure.

The second is the water surface method, where any small boat is tc be used instead of a topedo.

The third is the aerial method, where instead of topedo or self-driving small boat a projectile is to be projected to the required point in the sea. Although any other method may be possible, only the above methods are considered to be practically possible.

In the first method, however, it is difficult to drive the topedo across the surf zone carrying a rope and also it seems to be complicated and difficult to realize from the the points of required horse power and complicated mechanism of the apparatus. The second method seems to have some possibility but it is considered to be difficult for the self-driving small boat to cross surf zone from beach to the sea, keeping any fixed direction.

From above reasons the author adopted and studied on the third method, of which the advantages are such as it is not affected by the sea surface conditions and the projection mechanism is extremely simple. However, the maintenance of conductor cable from breaking by shock of initial discharge and shock pressures which act instantaneously to the pressure unit at the time of discharge and alighting on the water surface become difficult problems.

As for the method of projection, two method may be considered. One is by means of explosive power of gun powder and the other is propulsive power of rocket. At first, the author tried the former because of its simplicity.

The Miroku-Type Rope Projector which is developed recently in Jap is applicable and the simplest one for this purpose. The method of projection is simple as shown in Figure 1. A hollow steel projectile ③ of mm in outside diameter, 40 mm in inside diameter and 820 mm in length is set on a projector ① of 40 mm in outside diameter, gun powder and cartridge case ② are charged and by firing the gun powder the projectile is thrown pulling a nylon rope and a conductor cable ⑤.

The projector is fixed by its basement ④ and a sand bag ⑥ to mai tain the angle of firing of about 35 degree. The weights of the project and projectile are 35 kg and 12.5 kg, respectively. The outside diameter of nylon rope is 3 or 4 mm and breaking strength is 280 kg. When gun pow der of 45 gr in weight is charged, initial velocity of the projectile at the instant of discharge is to be about 120 m/sec and be reached to 500 o 600 meters from the beach. Therefore, if the pressure unit is set on the projectile, variations of statical water pressure due to the change of bottom topography is to be measured by pulling back the projectile to the beach. The successive positions of the pressure unit and the statical water pressure at each position are registered continuously by recorder on the beach. And by each projection a cross-section or profile of botto topography is obtained on the recording paper.

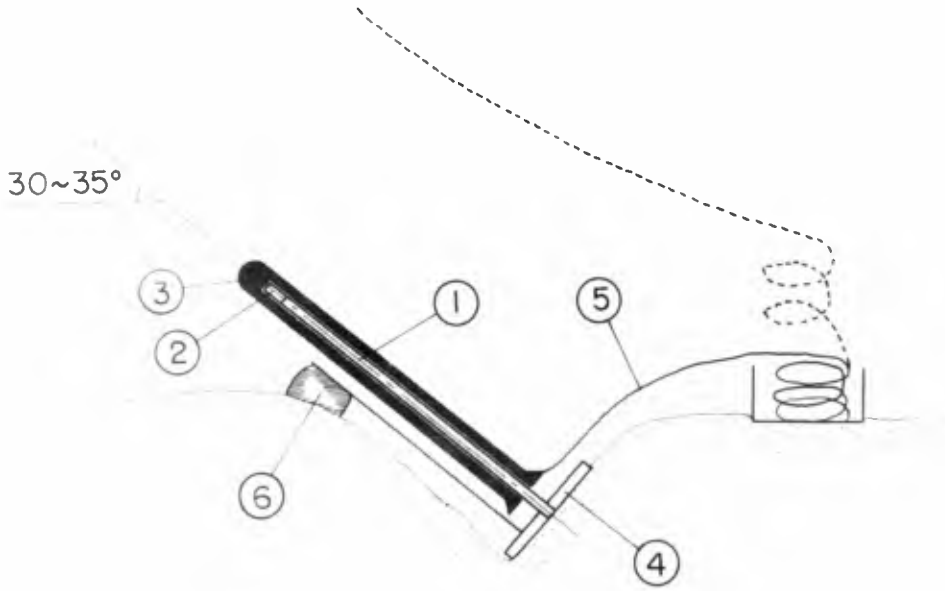

Figure 1 The Outlined Sketch of Rope Projector

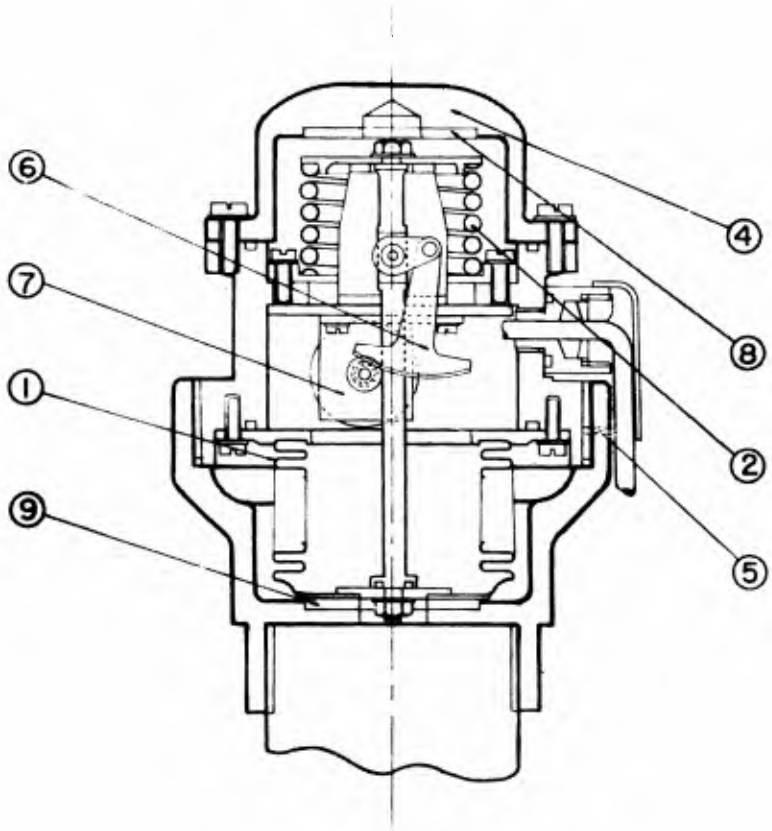

Figure 2 Mechanism of Pressure Unit

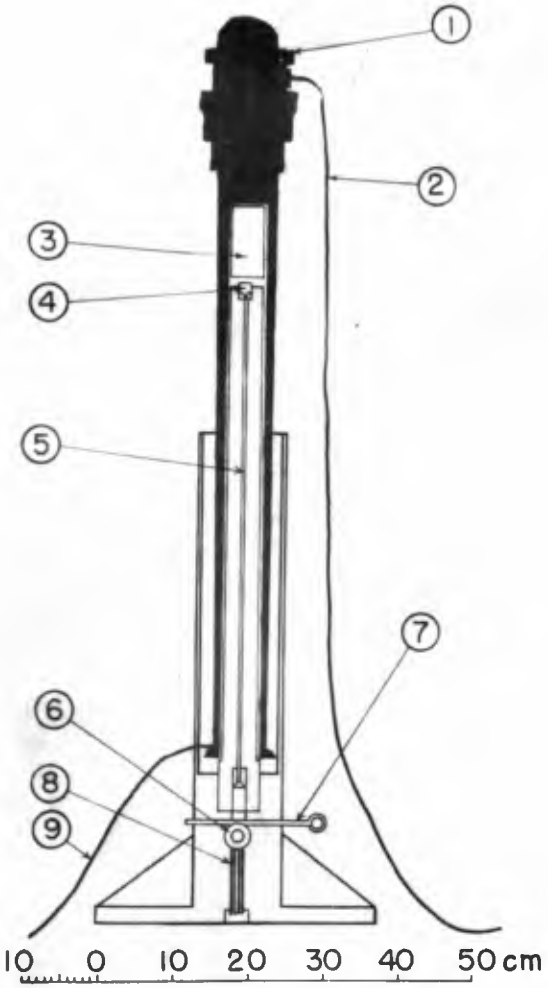

Figure 3 Projectile with Pressure Unit set on Projector

MECHANISM

The most difficult problem for this method is how to meet the shock pressure due to the acceleration at the instant of discharge of the projectile. The maximum acceleration at that instant will mainly depend on the weight of projectile and explosive power of gun powder. In case when the weight of projectile is 12.5 kg, the maximum explosive pressure inside the hollow of projectile due to explosion is said to be about 2000 kg/cm^2 and, therefore, the maximum acceleration of the projectile with the hollow of 40 mm in diameter is estimated to be about 2000 gal.

For the case of such a serious acceleration and for conductor cable with length of 500 or 600 meters, any complicated method cannot be used. Use of strain gage may be possible but the author adopted the mechanical method as shown in Figure 2 and 3, because the use of strain gage has some complicated problems on account of the necessary insulation of conductor cable.

Figure 2 shows the mechanism of pressure unit mainly made of aluminum metal, in which metal bellows ① and spring ② are connected with an axis ③. Inside of the bellows is water-tight with cap ④. When the pressure unit drops down into the sea, water flows into the unit through a small hole ⑤ and pushes the bellows. This water pressure is balanced by spring ② and bellows ①. The amount of compression due to water pressure fluctuation is directly converted into the rotation of sector gear ⑥ and the rotation of potentiometer ⑦, through which pressure fluctuation is changed into the voltage fluctuation. ⑧ and ⑨ are stoppers against shock pressures at the time of discharge and alighting on the water. Total weight of this unit is about 6 kg.

In Figure 3, ① is the pressure unit of Figure 2, ② is conductor cable, ③ the powder case, ④ the cartridge case and ⑤ is gun hammer. For the time of discharge, gun hammer is pulled down by lever ⑥, set by rock key ⑦, and powder and cartridge case are charged, then the projectile with pressure unit is set on the projector. Pulling out the rock key, the gun hammer is pushed out by spring ⑧ and strikes the cartridge case. Then the powder is fired and projectile is thrown out pulling the conductor cable and nylon rope ⑨. A few seconds after discharge, projectile is to reach at given point and drop down to the sea bottom. It is pulled back to the shore by nylon rope, sliding on the bottom and measuring the statical pressure. Recording paper is set to move in connection with the rotation of rope winch so as to be proportional to the displacement of the pressure unit. Thus the pressure record is to be nearly proportional to the cross-section of bottom topography.

EXPERIMENTAL RESULTS

After about 60 test projections, it became evident that the pressure unit in Figure 2 is strong enough against the shock at time of discharge and alighting on the sea, with only neglisible fluctuation of zero point in potentiometer. In case of pulling back the unit, the rope may sometimes be broken by the increasing earth pressure to the buried rope and projectile, especially in crossing the sand ridge in surf zone. In order to avoid this, a pully is prepared on the beach to lift up the

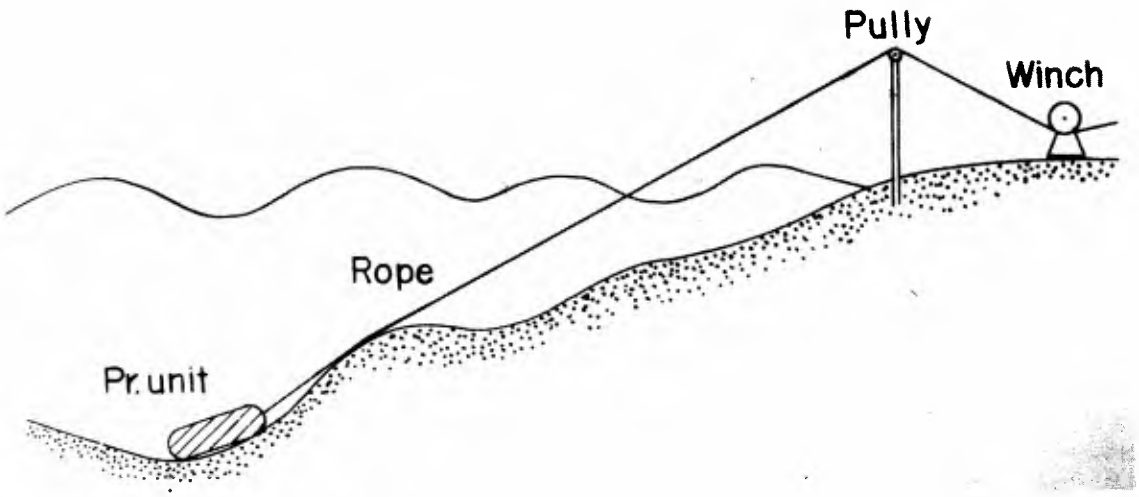

Figure 4 Sketch of Sounding

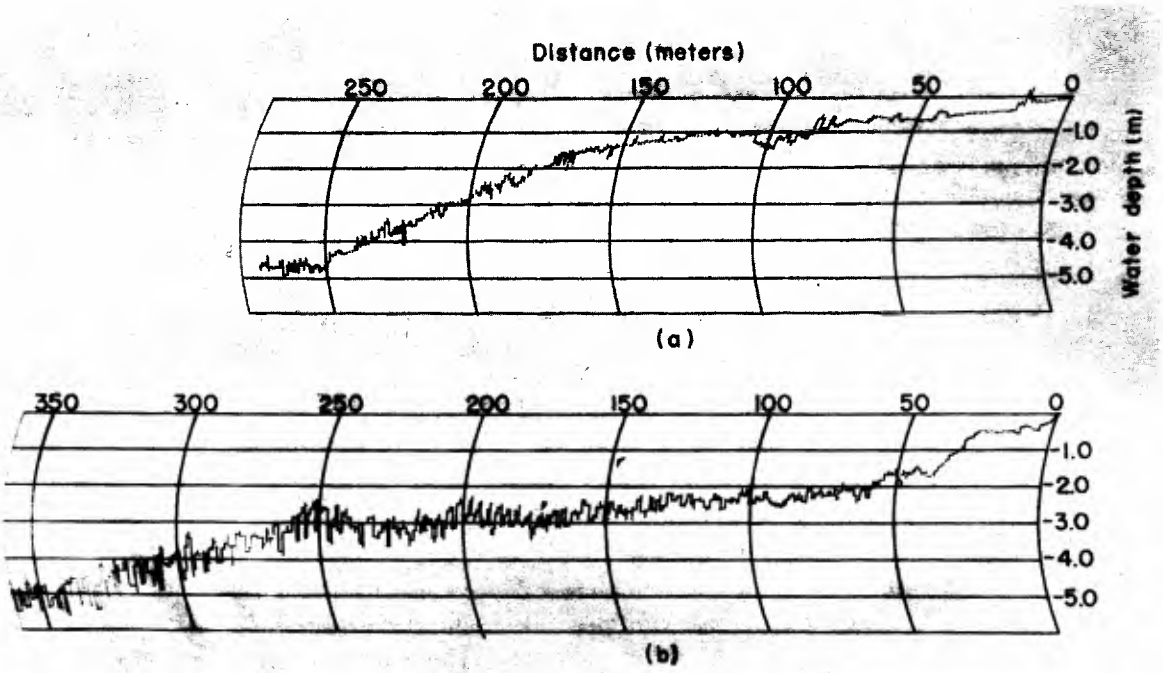

Figure 5 Examples of Records

FIG. 6 Projectile on Beach

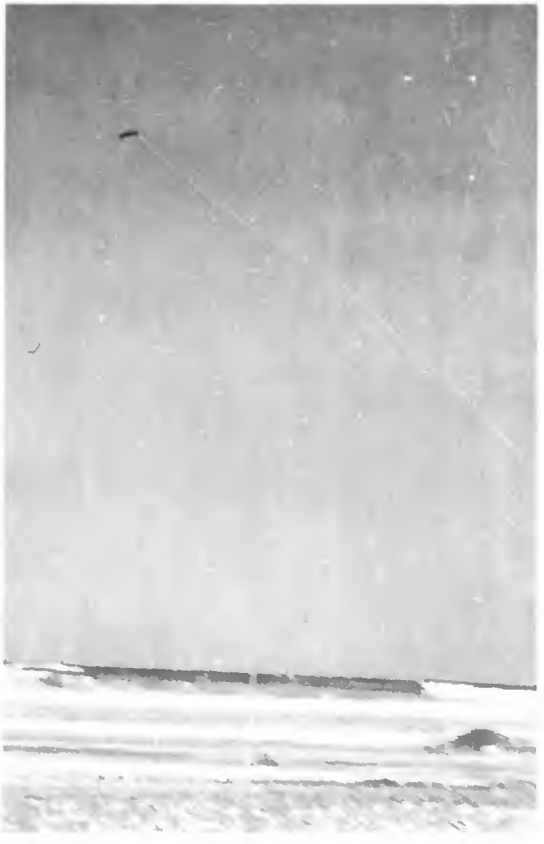

FIG. 7 Flying Projectile with Rope and Cable

rope in height of 2 or 3 meters above the ground as shown in Figure 4. Thus the pulling force to the rope was remarkably decreased.

As for the conductor cable, it became clear that the cable which has one conductor of four copper wires with 0.29 mm in diameter, reinforc by three piano wires with the same diameter and covered with polyethylene was strong enough against the breaking effect of shock at the instant of discharge. In this case, the cable should be initially winded into the shape of hollow cylinder with inside diameter of 12 cm, outside diameter of 20 cm and height of 12 cm, and total length of cable is 600 meters. When gun poeder of 45 gr is charged, the projectile reaches to more than 300 meters from shore line for wind velocity of about 10 m/sec, pulling the rope and cable. The alighting point of the projectile is easily observed using two transit-instruments like as ordinary sounding surveys, and the maximum error of alighting point measurement was expected to be less than 10 meters after several tests by three transit-instruments.

For examples, two typical records are shown in Figure 5, which were obtained on the Kashima-Nada coast of the Pacific Ocean. Figure 5(a is a record on 21st Nov. 1963 and (b) is on 3rd June 1964, in which the ruggedness of recorded curve is due to overlaps of statical water pressur and surface wave pressure fluctuations, so that the middle points of the curve is considered to be the cross-section of bottom topography.

Photograph 1 is the projectile set on projector just before firin and Photograph 2 is the flying projectile pulling a white nylon rope and a black cable just after firing.

REMARKS AND ACKNOWLEDGEMENT

Though it may be desired to increase the alighting distance of th projectile up to 400 or 500 meters, it seems to be somewhat difficult for the present type to cover such distances. The author, however, believes its applicability to the field investigation of sand movement and further data on bottom topography under the direct action of waves will be reported in the near future.

The author expresses his heartfelt thanks to Mr. Y.Suzuki, Mr. Y Abe and Mr. R.Sasage in Wave Laboratory of this Institute for their earnest coorperations to this study.

o

Chapter 23

POSSIBILITY OF HELICOPTER USE IN SOUNDING SURVEY FOR HYDROGRAPHIC PLANS OF MOUTHS NAUTICALLY UNKNOWN

F.C. FONTES and L.M. CASANOVA
Civil Engineers - Chief and Assistant
Mission for the Development and Settlement of the Zambezi
Mozambique - Portugal

SYNOPSIS

Reference is made to the method that it was necessary to resort to for the first complete hydrographic survey of the Cuama mouth on the Zambezi delta, where the plans for the economic development of the Zambezi Valley foresee the need for the establishment of a fluvio-maritime harbour.

This corresponds to the execution of sounding by means of a direct intersection method (shore controlled survey), using heli - copters for the transportation of the echo sounder.

The operational techniques for sounding with helicopters and localization of the points sounded are described, indicating also the equipment and personnel required for such operations.

The results obtained through two hydrographic surveys carried out in 1962 and 1963 are indicated and analysed, examining the technical worth of the method, its efficiency, costs and safety, as compared to the classical sounding methods.

Further, reference is made to the possibilities for improvement offered by the method being described and to the circumstances under which it has been applied, taking into consideration the results obtained during the trial sounding operation.

1. FOREWORD

The Mission for the Development and Settlement of the Zambezi is a technical organization set up by the Portuguese Government to carry out the survey and inventory of the resources to be found in the Zambezi Valley, Mozambique, with a view to the establishment of a program of development for a region of approximately 200,000 squar kilometers.

In view of the necessity to have these studies completed within the shortest possible period this Mission was formed by a series of experts in various fields which in turn were grouped into teams , and provided with the adequate working aids allowing them to attain the Mission's objectives.

Among such working aids, stand out the private fleets of motor vehicles and aircraft (aeroplanes and helicopters) and the necessary workshops for their maintenance.

These teams of experts cover topography, agronomy and forestry, geology and mining prospection, social and economic studies, and hydraulic engineering.

From the latter a working group was detached to the delta zone of the Zambezi river in order to study its fluvio-maritime reach.

1.1 OBJECTIVES OF THE STUDY OF THE FLUVIO-MARITIME REACH OF THE ZAMBEZI RIVER

The planning of the development of the region led to the study of the establishment of a system of transportation for the products which will result from the activities of extraction and transformation, sufficiently economical to make them competitive on the various markets.

The importance of this particular aspect of the studies initiated under the infrastructure plans can be clearly seen, for the majority of those goods will consist of ores or products from their primary transformation which will, as estimated, surpass 3,000,000 metri

tons per year.

As the Zambezi River, owing to its geographical position on the axis of the region to be developed, is the natural outlet for its products, a system of fluvial navigation together with maritime navigation of long and short range, with a harbour at its mouth, was considered under the preliminary plans.

The main purpose of the study of the fluvio-maritime reach consists therefore in the building of an inner harbour on one of the arms of the delta, as near as possible to the sea, accessible to seagoing vessels and not only to coastal navigation as is the case up to now and this under precarious conditions.

1.2 - MAIN STUDIES COMPLETED AND IN COURSE

The Zambezi delta covers approximately 60 km of the coast of Mozambique and includes 7 mouths, of which only three - Pambane, Chinde and Cuama - appear to offer conditions for navigation. The remainder are connected to interior canals with pronounced and progressive silting up and highly developed outer shoals.

The Pambane mouth offers conditions for small draught vessels but its interior canal is excessively narrow, rather shallow , and with no connection into the Zambezi.

The Chinde mouth is still open to coastal navigation but has insufficient depth.

The mouth is unstable, subject to litoral drift and connected to the Zambezi by the Chinde arm, which is very narrow and sinous.

The Cuama mouth is not presently accessible to navigation but historical references show that for a long time it was utilized by all types of vessels. However, even today it appears to be the mouth most suitable for accommodating seagoing vessels. It is in fact joined to the arm connecting it to the Zambezi by areas of width and depth greater than the former and is situated in a neutral zone of litoral drift.

For these reasons, the Chinde and Cuama mouths, and especially

the latter, have been studied in greater detail.

These studies refer mainly to the collection of topographical data for a better planimetric and altimetric knowledge of the part of the delta above low tide water level, drawing up of hydrographic plans of the submerged part, obtention of hydrometric and tidal data, studies of the characteristics of sea and swell waves, and collection and analysis of sedimentation on the interior arms, mouth shoals and shore line.

Based on this data, as well as on that now being collected, studies on scale models are being carried out at the National Laboratory of Civil Engineering, of the terminal reaches of the Cuama and Chinde branches.

Such studies aim at analysing, particularly as far as Cuama is concerned:

- the behaviour of the harbour regarding capacity for maintaining the depth of the access channel between 7.30 to 8.00 meters, under low water level.
- the best location and conditions of shelter for the harbour installations to be situated in the inner part of the Cuama arm;
- the general lines for gauging the Zambezi at its fluvio-maritime reach up to approximately 55 km to the interior of the Cuama mouth.

1.3 - NEED FOR PERIODICAL HYDROGRAPHIC SURVEYS OF THE CUAMA MOUTH - - SOUNDING USING HELICOPTERS

Whereas various hydrographic information on the Chinde mouth has been available since 1883 for owing to its navigability, it has always been possible to sound it using the classical methods, this does not apply to the Cuama mouth which has for one century been unknown to the navigation, seeing that all attempts to have it surveyed with such methods had been unsuccessful.

Back in 1958, and included under the studies of the Zambezi region the Hydrographic Mission of Mozambique was requested to carry

out a complete hydrographic survey of the Cuama mouth, together with those of the other mouths, but this was not possible at the time.

Until the end of 1961 - and after our repeated requests, justified by the advancement of the studies - it was not possible for that Hydrographic Mission to carry out such a survey.

Faced with an increasing need for a hydrographic survey of the Cuama mouth, entirely unknown to today's navigation and the difficulties entailed by its execution according to the experts, the Mission for the Development and Settlement of the Zambezi, in the beginning of 1962, decided to attempt the use of one of its helicopters for the obtention of hydrographic plans of that mouth.

Although a new survey of the Chinde and Cuama mouths with the classical methods, had been programmed for July 1962 by the Hydrographic Mission, in view of the uncertainty of the success of such methods when applied to the Cuama mouth, the Zambezi Mission decided to attempt the use of the helicopter with the method already tested by that time. This was successfully done in April 1962 and made it possible to provide the Hydrographic Mission with a preliminary sketch of the bottom of the mouth in order to enable them to face their survey of the Cuama, to take place in July, no longer as that of an unknown mouth.

The success that met the sounding operations of the mouth using helicopters was confirmed later by the comparison established with the sounding by the classical method that was at last possible to carry out in the course of that same year. Bearing in mind the need for repeating periodically the survey of that mouth, either in connection with scale model under study, or for the examination of its evolution resulting from the newly-built Kariba Dam and the works planned for the Mozambican reach of the Zambezi, the Mission promoted the improvement of the sounding technique making use of helicopters and the repetition of the hydrographic surveys applying this method.

Thus a new survey was carried out in August 1963 and another is under preparation to take place in July 1964.

The description of the sounding techniques applied by the Zam -

bezi Mission using its helicopters, the analysis of the results obtained, and the presentation of the hydrographic plans that it was possible to draw from such surveys, are the object of this paper.

2. SOUNDING TECHNIQUE USING HELICOPTER

2.1 - EQUIPMENT

Before entering the description of the equipment used, it must be pointed out that the method tested and applied in two successive years was entirely executed using solely the equipment and facilities already owned by the Mission. It was necessarily considered as an experiment and because of this there was the preocupation of avoidin the purchase of new equipment during that experimental stage. On th other hand during the stage when the technique was being improved it was not possible to purchase the new equipment that the experien acquired during earlier operations had shown to be useful.

Reference to such equipment, useful for the development and improvement of the method being presented, will be found in the las chapter of this paper.

The following equipment was used for the sounding with heli - copters: one "Kelvin Hughes MS-21" echo sounder whose power transmission and recording units and accessories are mounted inside the helicopter's cabin. The oscillator for out-board use and weighi about 26 kilos hangs from the helicopter hoist. This oscillator i fitted to a buoy which floats on the water surface and thus maintai it approximately 1 ft underwater.

The two pictures of Fig 1 show how the two first mentioned ha been installed inside the helicopter cabin, near the seat of the sounder operator (1a) and the oscillator enveloped by its buoy and hanging from the hoisting cable at the moment it touches the water (1b).

1a.- Recording and power transmission units inside the helicopter's cabin.

1b.- Buoy and oscillator in contact with the water, hanging from the hoist cable.

Fig. 1

Three Wild T-1 theodolites and three S.M.D. high frequency(H. F.) radio-telephones with fixed crystals, set up at three coordinate shore stations.

One A.Ott tide recorder and hydrometric scale mounted on the shore.

Signal buoys scattered over the zone to be sounded and consisting of drums with flags.

One Agusta-Bell 47J helicopter with the following main characteristics of interest for the sounding work:

- Using the hoisting kit and the pneumatic float tubes that permit landing on beaches and alighting on the water surface provided the sea is calm, and taking into consideration the weight of both pilot and fuel, there are about 260 kilos left for the sounder operator and sounding equipment;
- Cruising speed, at sea level, of approximately 135 km/ /hr carrying maximum weight;
- Possibility of installing very high frequency (V.H.F.) radio communications;
- Autonomy of 1:30 hr to 1:55 hr under sounding conditions;
- Stationary flight in ground effect, hovering at 6 m to 8 m from the water surface.

Fig 2 shows a hydrometric scale for recording tide levels (2a) and one of the shore stations where a theodolite and a radio unit and operator are installed (2b).

Fig 3 illustrates the hoisting kit and hanging cable in the helicopter cabin (picture 3a) as well as the helicopter while in flight and lowering the oscillator into the water for the sounding of one point (picture 3b).

2.2 - OPERATING STAFF

The operating staff engaged in the various surveys underwent certain variations but in general it was formed by:

One pilot and one helicopter mechanic, the latter being in

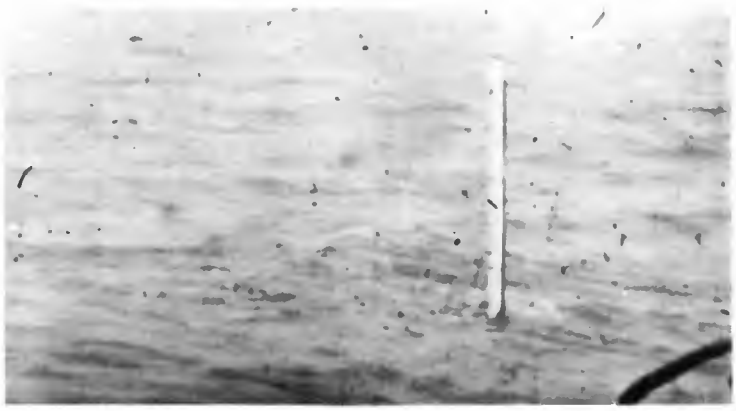

2a.- Hydrometric scale.

2b.- Shore station with theodolite, radio-communications, and its personnel.

Fig. 2

3a.- Pilot and sounder operator while in action inside the helicopter - Hoist and cable.

3b.- Helicopter in flight, showing the oscillator unit hanging from the cable.

Fig. 3

dispensable for the refueling and maintenance of the aircraft, but also acting as radio operator at the shore station. The pilot always cooperates in the planning of the lines to be sounded and, besides flying the helicopter,he operates the hoist and performs the lifting and lowering movements of the oscillator hanging cable.

One sounder operator, normally the technician that plans the sounding lines and whose duties also include the lowering or lifting of the electric cable of the sounder following the movements of the hanging cable activated by the hoist. He controls the whole sounding operation and does the recording of the sounding times and number of points.

Fig 3 and picture 3a show the pilot and the sounder operator in action in the helicopter cabin.

Three surveyors, who must be highly experienced as for each sounding line they have to keep a constant watch, through the theodolite, on the oscillator hanging cable, and about every 35 seconds take readings of the azimuthal angle recording same on the field log. They must also do the plotting of the sounded points at the end of each day's field work.

Fig 2 and picture 2a show a shore station-the one controlling the other two shore stations - where the surveyor instructs the radio operator to transmit to the other surveyors the signal indicating the reading of the azimuthal angle at the moment when the oscillator , lowered from the helicopter, touches the water surface for the sounding of one point.

Finally, and apart from a few workmen, there are the tide recorder and hydrometric scale operator.

2.3 - METHOD OF OPERATION

2.3.1 - Sounding technique

Sounding is carried out point by point, following lines parallel to the wind direction and in a sense contrary to the action of the wind. The distance between the points of each line as well as

between lines is of around 100 meters. However, this distance may be increased for zones of lesser interest and decreased in areas calling for more detailed sounding.

For the sounding of each point the helicopter is kept hovering in ground effect, at about 6 meters from the water level, with the oscillator lowered so as to reach that level, during a period of time long enough for the sounder to record the trough of a wave and the crest of the next one.

At the beginning of each series of lines - their number being conditioned by the autonomy of the aircraft - the oscillator is lowered to a convenient level and remains hanging from the cable (diameter 3/8") activated by the hoist till the end of the line immed_ately preceding the refueling of the helicopter is reached.The pilo operates the hoist as its electrio switch is coupled to the cyclic stick of the helicopter, this controlling the position changes of the angle of the surface determined by the rotation of the main roto blades of the helicopter.

This technique of operation, owing to the outline of the cours followed by the osoillator, might be aptly designated as frog's lea sounding.

Fig 4 shows schematically the technique of operation describe in this and the following paragraphs.

Sounding is carried out following lines parallel to the win direction and in the sense contrary to its action, for two reasons:

- one, to avoid that the wind will throw the helicopter off its course when carrying out the sounding of a line in a certain direction, with the resulting alterations to the sounding plans;
- the other, the fact that sounding is made point by poin and with the helicopter hovering in ground effect, which is onl possible under those conditions.

Sounding is carried out point by point for previous tests ha demonstrated that it is not possible to operate the helicopter continuous horizontal flight when carrying an oscillator of the weight and surface of contact characteristic of the one suppli

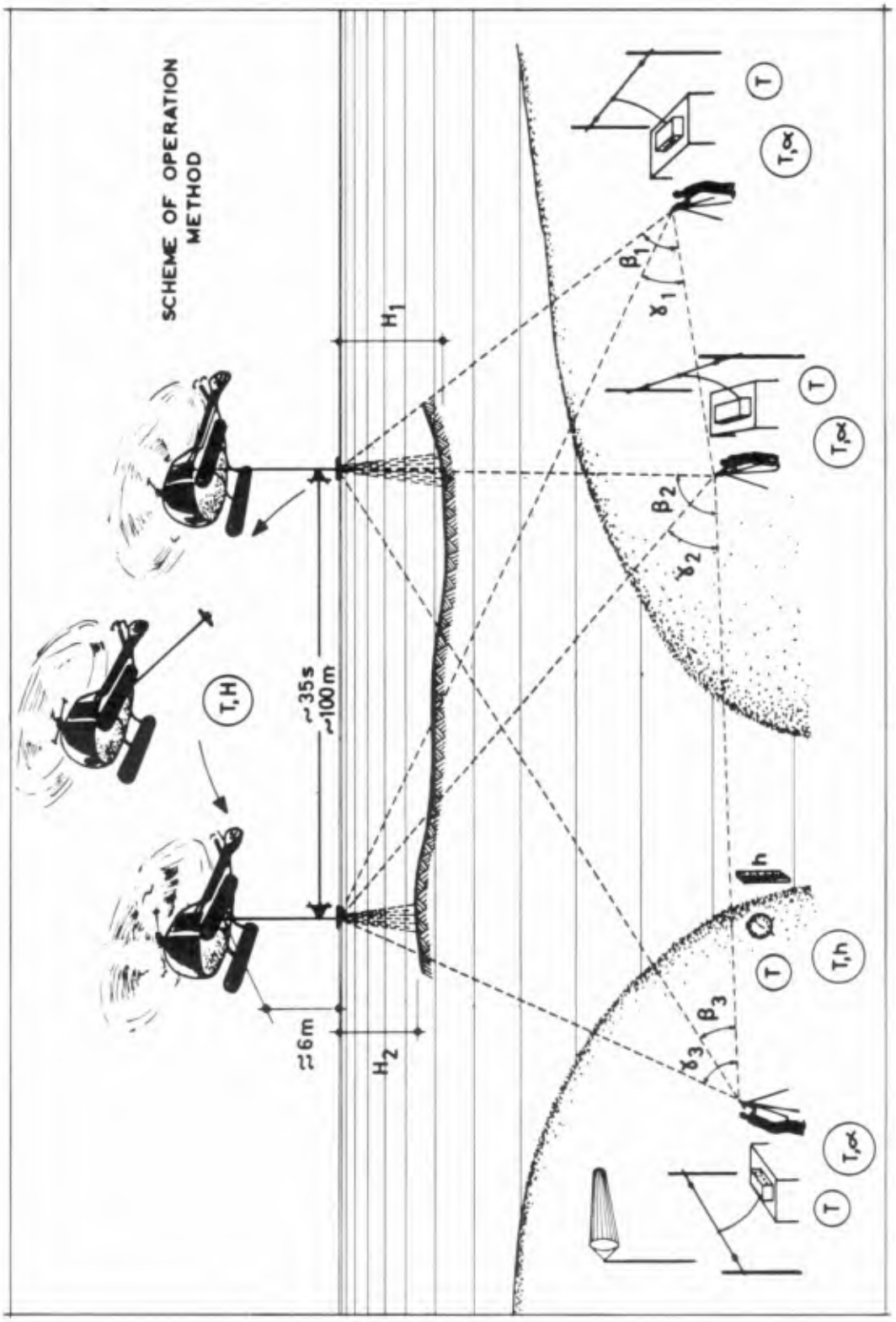
SCHEME OF OPERATION METHOD
T,H
~35s
~100m
≈6m
H1
H2
β1
γ1
β2
γ2
β3
γ3
T
T,α
T,h
h

Fig. 4

with the echo sounder used.

The sounding of each point was carried out with the helicopte hovering at about 6.00 meters above the water level owing to th following:

- firstly, because on account of the equipment used, th work is done just inside the weight limitations for this type c aircraft, and it becomes imperative to benefit from the additional thrust obtained through hovering in ground effect; this groun effect may only be felt up to 8.00 meters above the water surface this at sea level and under the conditions locally prevalent;

- secondly, because the operations were also conditione by the length of the electric cable supplied with the sounder fc connecting the oscillator to the power transmission and recordir units;it would have been necessary to alter its cross section befo replacing it by a longer cable, as by merely increasing the lengt of the existing electric cable the recording of the soundings woul not take place in the recording unit, and it was impossible to ob locally the required electric cable of adequate characteristics.

2.3.2 - Localization of the points sounded

The planimetric location of the points sounded is carried o following the method of direct intersections (shore controlled survey), based on three shore stations set up at coordinate poin on the coast.

In each of these three stations an equal number of surveyo (anglemen) observe, by means of their theodolites, the oscillato hanging cable and all of them read simultaneously the azimuthal angles whilst the oscillator is underwater for the sounding of ea point.

The exact moment for the position reading of the cable (simultaneous) is determined by the surveyor at one of the thre shore stations - the one selected as controlling station - and transmitted by him to the radio operator working by his side whc

in turn immediately instructs the other surveyors, so as to ensure that the reading is taken simultaneously by all three of them.

Fig 2 is a picture of this controlling shore station taken at the moment the surveyor was signalling the radio operator.

The shore stations were set up in accordance with the shape of the shoreline and the layout of the area to be sounded as related to it, for the simultaneous use of three stations as already indicated.

For the case under description a total of only 5 shore stations has been necessary.

Two shore stations for simultaneous observation might be considered sufficient for a reasonable accuracy, but in order to ensure the maximum possible exactitude for the determination of the planimetric location of each point of this sounding survey , three stations were used guaranteeing:

- higher probability of at least two stations recording intersection angles of more than 30 degrees;
- the possibility of checking each point in case of the reading eventually becoming unfeasible at one of the stations , either due to the interposition of any object, operator or radio failure, or to any other reason.

The location of the reading angles is schematically presented under Fig 4.

2.3.3 - Recording and Plotting

The following information is recorded in the course of the sounding and localization operations:

The sounder operator aboard the helicopter inscribes on the sounder graphical records the serial number of each point and its time of execution.

At the reading stations ashore, the surveyors log down the azimuthal angles of each point, their serial numbers and time of execution. The starting angle is previously determined at each

station by the observation of a reference mark (which as a rule is located at the other stations). This starting angle will always be maintained whenever operating at that station, thus enabling each station to determine one scale only, for use when plotting the points sounded.

The water levels are recorded at the hydrometric station at the given time intervals.

The plotting of the points sounded, at the 1:10,000 scale, is made daily, after the sounding work. Once the planimetric location of each point has been determined, the recorded depth is immediately referred to the hydrographic zero adopted, based on the tidal records available.

Fig 5 gives an example of the plotting method, representing only two shore stations in order not to crowd the drawing.

Plotting scales are established for each shore station and marked with the tangents of the angles susceptible of representation in the area to be sounded by each particular station. Once the reading angles of each point are made known the scales obtained with the values of the corresponding tangents, come next, and by setting the rulers the position of a point is then determined.

By using this plotting system, based on the definition of a sole starting angle for each station and placing on the original drawing the scales established at convenient distances from the plotting position of the corresponding stations, it was attempted to make the best possible use of the exactitude allowed by the readings originated at the fixed stations and using theodolites thus giving the plotting the corresponding highest possible degree of accuracy as well.

2.3.4 - Planning the sounding survey

The lines and series of points to be sounded are planned before the start of the field operations. This planning takes place at the work site itself, taking the predominant wind into consideration.

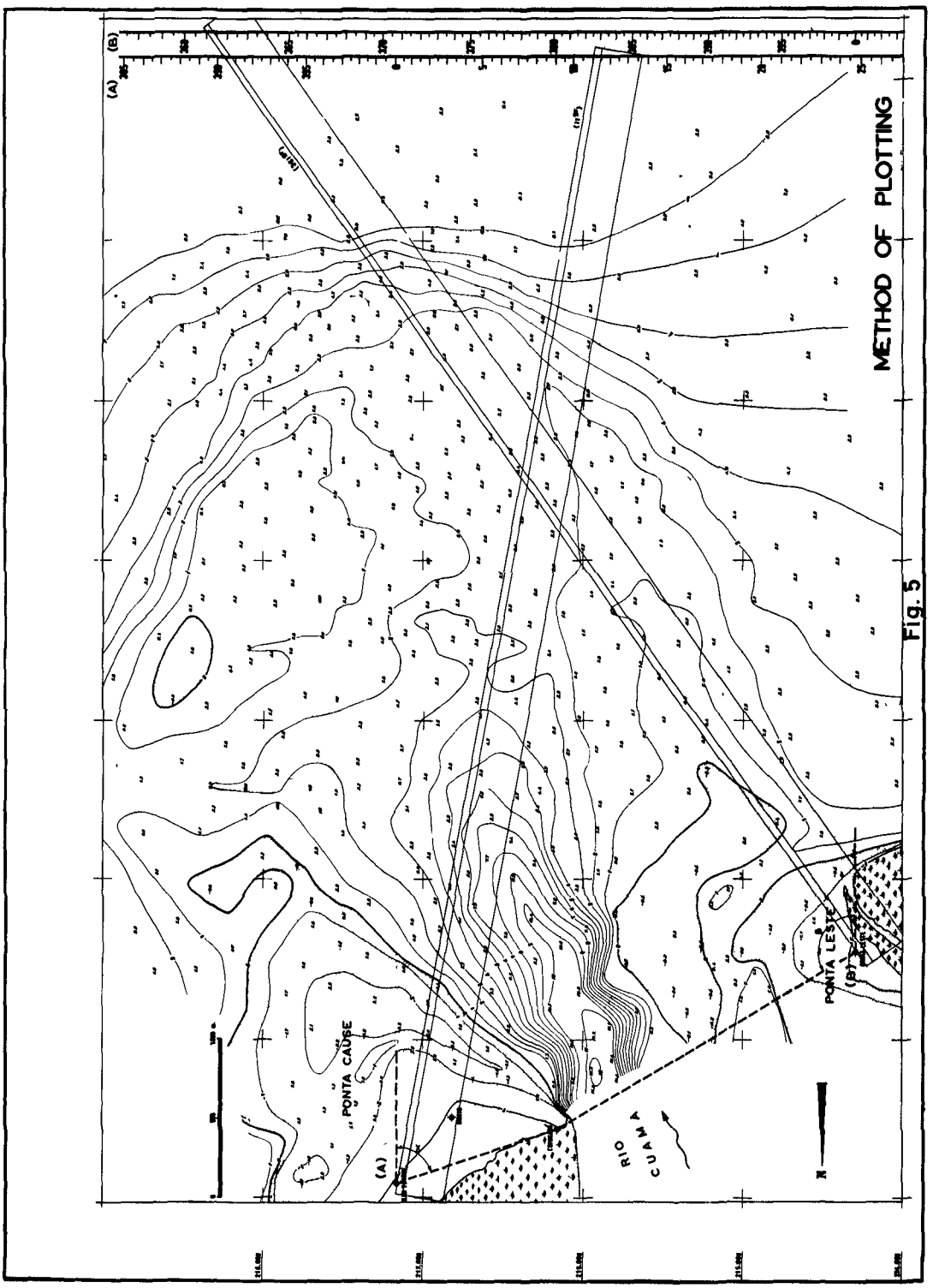
METHOD OF PLOTTING
Fig. 5
PONTA CAUBE
RIO CUAMA
PONTA LESTE
(A)
(B)

Because of these conditions the sounding plan is revised every day, and the fact that the plotting of the points sounded is also done daily makes it possible to correct eventual deviations on the course of the lines and give better coverage to zones that owing to such deviations, or offering greater interest, would require a larger number of sounding points.

During the hydrographic survey carried out in 1963, buoys consisting of drums with flags were used and placed on the zone to be sounded to serve as reference points of the course of the lines for the staff operating aboard the helicopter. It was not always possible to establish such reference points by means of signal lines on the shore, seeing that the work had to be carried out in accordance with the direction and sense of the wind.

This measure has greatly contributed to reducing the operating time and to a better distribution of the points as compared to the hydrographic survey effected in 1962, as indicated under the heading "Results".

2.4 - RESULTS

The first hydrographic survey of the Cuama mouth was carried out in April 1962 using the method under description and took 12 field working days sounding an area of approximately 30 square kilometers and recording around 1,200 points.

The second hydrographic survey took place in August 1963, with improved operation techniques, making it possible to reduce the working time to 6 days for the sounding of the same area, and just about the same number of sounding points were registered.

On the average, to the two hydrographic surveys already effected correspond around 40 sounding points per square kilometer.

Fig 6 and 7 represent, in reduced scale, the above mentioned hydrographic plans with 1-meter equidistant depth contours but it should be pointed out that the final drawing does not show all the

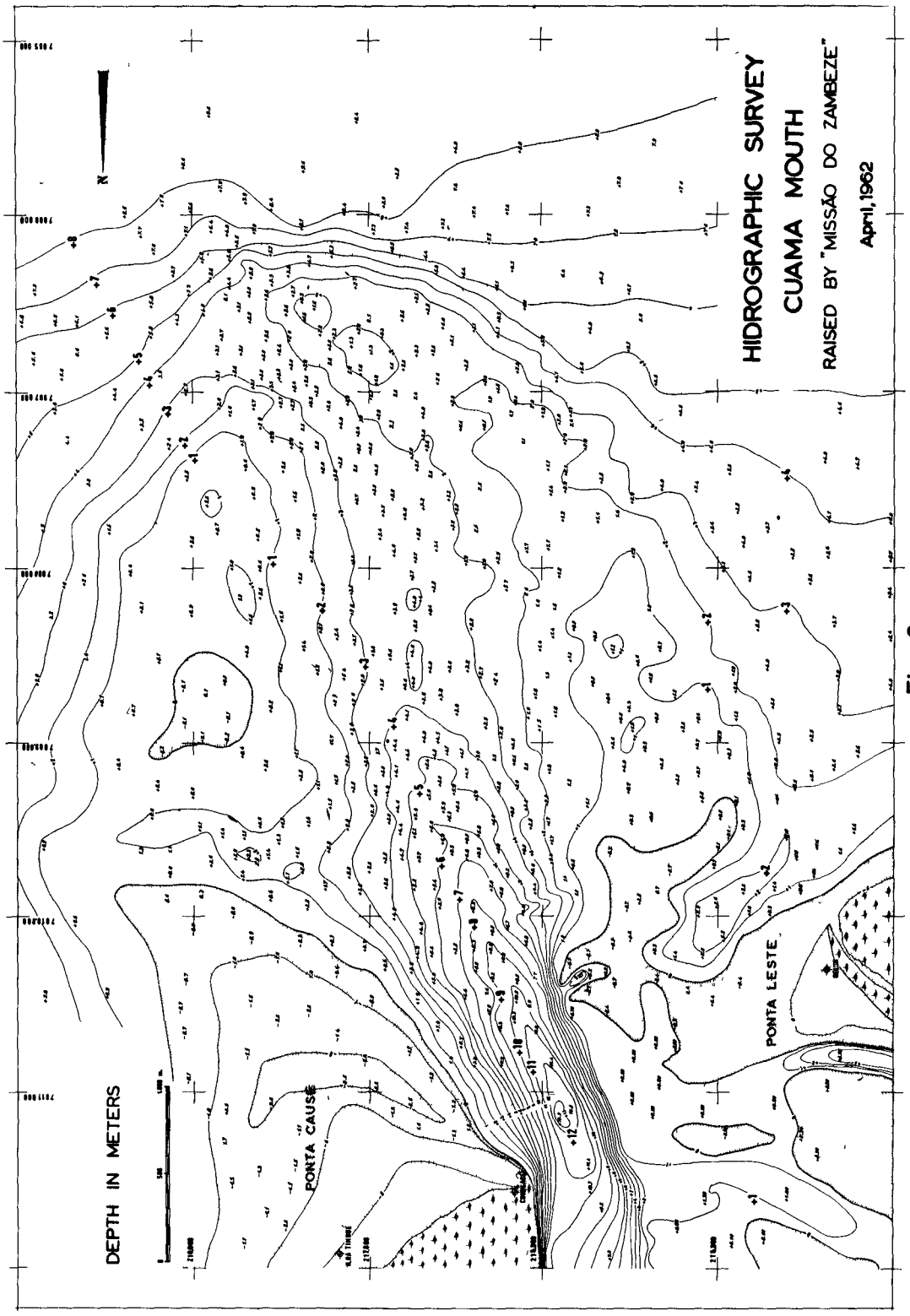
HIDROGRAPHIC SURVEY
CUAMA MOUTH
RAISED BY "MISSÃO DO ZAMBEZE"
April, 1962
DEPTH IN METERS
PONTA CAUSE
PONTA LESTE

Fig. 6

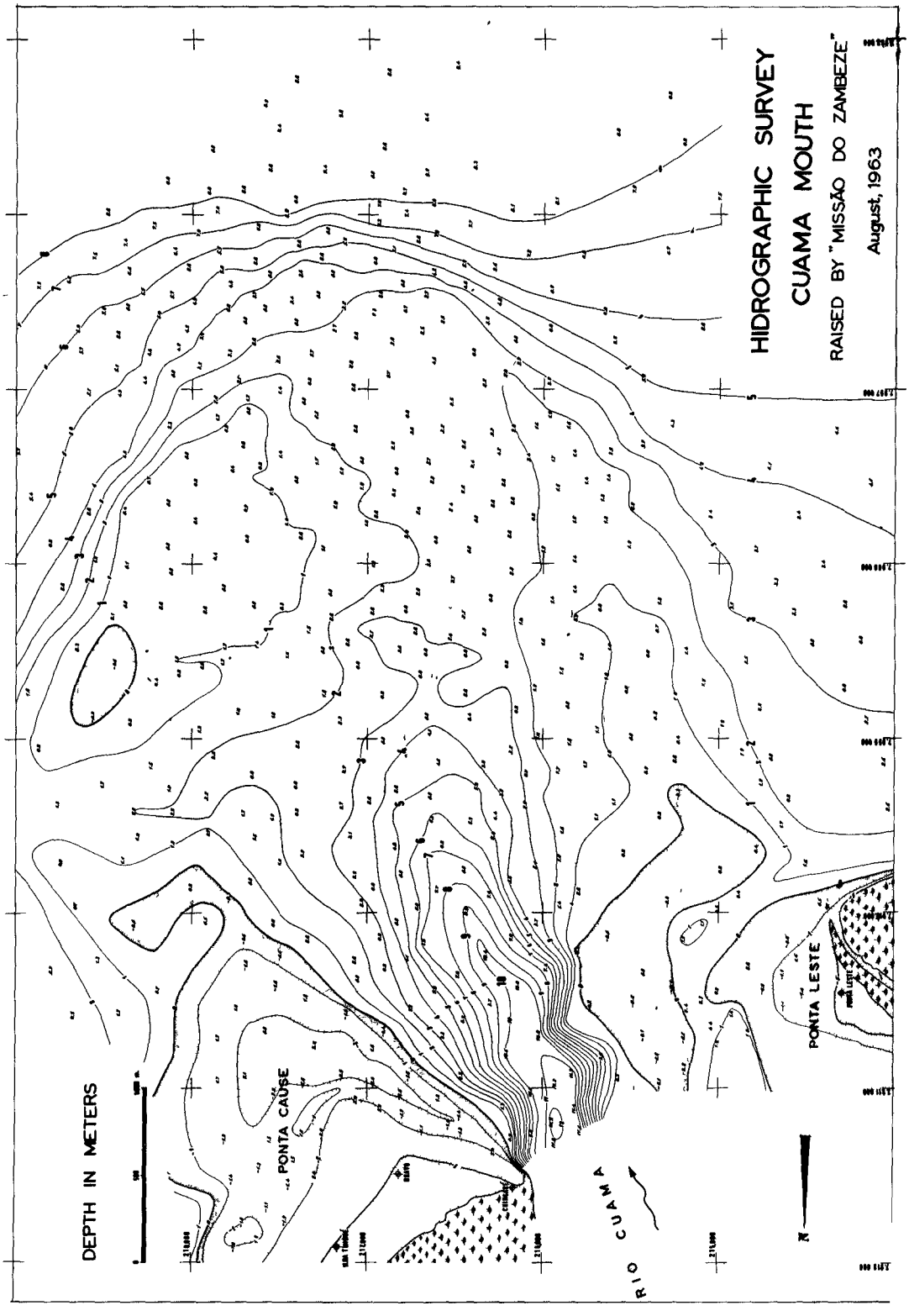
HIDROGRAPHIC SURVEY
CUAMA MOUTH
RAISED BY "MISSÃO DO ZAMBEZE"
August, 1963
DEPTH IN METERS
PONTA CAUSE
PONTA LESTE
RIO CUAMA
N

points sounded, but only those necessary for the correct interpretation of those plans with a distribution as uniform as possible.

3. ANALYSIS OF RESULTS

3.1 - TECHNICAL EFFICIENCY OF THE METHOD

From the examination of the hydrographic plans already obtained, and bearing in mind the attention and care given to the various operations and the comparison established under paragraph 3.5 below, it may be said in connection with the technical worth of the method that:

- The planimetric location of the points sounded is highly accurate.
- The altimetric accuracy appears to be acceptable, seeing that each point always includes the depth recording during at least one trough and one wave crest, for the determination of the average water level; it is granted however that the accuracy attained is nevertheless below the one that would be possible to reach by continuous sounding using the same means of operation.
- It offers the advantage of making it possible to sound shoals and zones non-accessible by boat.
- It allows continuity of operation as it is hardly subject to the sea conditions, which can therefore no longer hinder the access to the work site or the sounding proper.
- It entails reduced inland topographical support, always a lengthy and costly operation.

3.2 - WORKING EFFICIENCY

In order to contribute to the full realization of the technical worth of this method or simply to give a clearer picture of the working efficiency that may be attained through the sounding method described in this paper, the efficiency indexes are being given below and refer to the hydrographic survey carried out in 1963 when improved

operational techniques were applied - made possible by the planning resulting from an earlier experiment and better trained personnel - - resulting in the completion of all field operations at the end of six days only.

- 64 lines of points 100 meters apart approximately were sounded. Though both the length and number of points varied, on the average these represent a length of 1,800 meters and 18 points per line.

- The average sounding time for each point of a line,100 meters apart, was 35 seconds.

- The average sounding time for each point, including the return before starting on a new line, amounted to 59 seconds.

- The average operating time between consecutive refuelings of the aircraft was approximately 1:30 hr, allowing for the execution of 5 lines between each refueling; the average time required for each refueling was of 25 minutes.

- The flight time for the sounding operations, including the time necessary for refueling, averaged 5 hrs.

The number of hours flown per day, including also the displacement of the helicopter to the supporting base of the Delta group located in Chinde and the transportation of operators and equipment on the shore opposite the location of the Cuama camp, goes up to 6:15 hrs.

- Average number of points sounded per day - 200.
- Average area sounded per day - 5 sq.km.
- Average number of points per km2 - 40.

3.3 - COSTS

For a generic appreciation of the worth and interest warranted by this method, and to allow its comparison with other methods and the selection of the procedure to be adopted for sounding, bearing in mind the desired degree of accuracy and the conditions offered by the zone to be sounded, it is also important to refer the costs for the sounding operations using helicopters during the two hydro-

graphic surveys in 1962 and 1963.

Based on the prices for the exploitation of the aircraft fleet belonging to the Zambezi Mission during the period 1958-1963 and including the amortization of the flying equipment, fuel and lubricants, maintenance workshop costs, and flying personnel, the cost per hour of flight of the Augusta-Bell 47J helicopter amounted to 2,640 escudos.

The personnel engaged in the sounding operations - excluding the pilot and the mechanic who have already been included under the price indicated above - and the consumable goods represent an expenditure of 2,450 escudos per day.

Thus, the costs for the hydrographic surveys in question were as follows:

a) In 1962

Considering 12 days' field work and 48.30 hrs of flight - adding to the operating hours the time required to fly between Chinde and Tete where the Zambezi Mission's headquarters are located, and return, the costs amounted to

12 days ×	2,450$00	29,400$00
48.5 hours ×	2,640$00	128,040$00
		157,440$00

b) In 1963

Considering 6 days' field work and 41.30 hrs of flying the helicopter - adding also the return trip referred to above:

6 days ×	2,450$00	14,700$00
41.5 hours ×	2,640$00	109,560$00
		124,260$00

The corresponding average cost per unit thus amounted to:

	Per km2	Per point
1962 Hydrographic Survey	5,258$00	131$00
1963 Hydrographic Survey	4,142$00	104$00

3.4 - SAFETY

Safety depends almost exclusively upon the conditions of maintenance and the guarantees offered by the means of conveyance used and is practically independent from the conditions of the sea.

Transportation being effected by aircraft, subject to very careful and strict maintenance and overhauling rules, the possibilities of engine or other trouble resulting in an accident are therefore very reduced.

But even considering the possibility of an accident occurring, the necessary precautions were taken to reduce the hazards of such an accident being mortal for the occupants of the aircraft by fitting it with pneumatic float tubes.

As subsidiary safety measures, both the pilot and sounder operato wear life jackets and are provided with shark repellent.

The influence of the sea conditions might only be felt if,when sounding zones of surf and high waves - it is pointed out that the helicopter operates at 6 meters above water level - the pilot does not climb high enough to prevent a wave crest from hitting the helicopter float tubes. For this reason, when operating under those circumstances, the concentration and attention demanded from the pilot will evidently be far greater than that demanded from the helmsman of a boat since the first, besides having to watch the conditions of the sea, has to pilot the helicopter, and handle the controls, especially those of the number of rotations, pressure feed unit, and oil temperature in the gear boxes and engine.

In this respect the safety measures adopted forbid the pilot to fly lower than 6 meters when carrying out the sounding operation and to exceed a certain number of flying hours beyond which the resulting tiredness would become dangerous.

3.5 - COMPARISON WITH THE CLASSICAL SOUNDING METHODS

For a better evaluation of the technical worth of the direct

intersection sounding method making use of the helicopter (I), a comparison should be drawn between this and one of the classical sounding methods, amongst which it would seem logical to select the inverse intersections method using the sextant aboard a boat (II), adopted by the Hydrographic Mission of Mozambique for the sounding of the same region.

The information given under paragraph 3, namely that the sounding using helicopters was attempted owing to the uncertainty regarding the feasibility of sounding the Cuama mouth by the classical method aboard boats, and that the sketch of the sounding carried out by helicopter in 1962 permitted that the mouth in question be no longer regarded as entirely unknown at the time the sounding by the classical method took place, give added interest to the choice of this method for comparison purposes.

For a better knowledge of the survey carried out with both methods and corresponding comparison, fig 8 shows the part of the hydrographic survey of the Cuama mouth effected by the Hydrographic Mission in 1962 which corresponds to the zone of that mouth surveyed by the Zambezi Mission. The part represented on Fig 8 is an excerpt of the hydrographic survey already published at the scale of 1:25,000, after reducing it to the same scale used for the surveys represented by fig 6 and 7.

The advantages of method I over method II are considered to be:

- Greater planimetric accuracy;
- Feasibility of sounding in zones hardly accessible or non -accessible by boat and thus possibility of surveying areas with strong swelling and insufficient depth;
- Less dependence upon the sea conditions;
- No need of towers for inland signals;
- Speedier connections between the members of the working team;
- Reduction in the time required for the complete hydrographic survey;
- Reduced operation risks.

The disadvantages presented by method I as compared to method

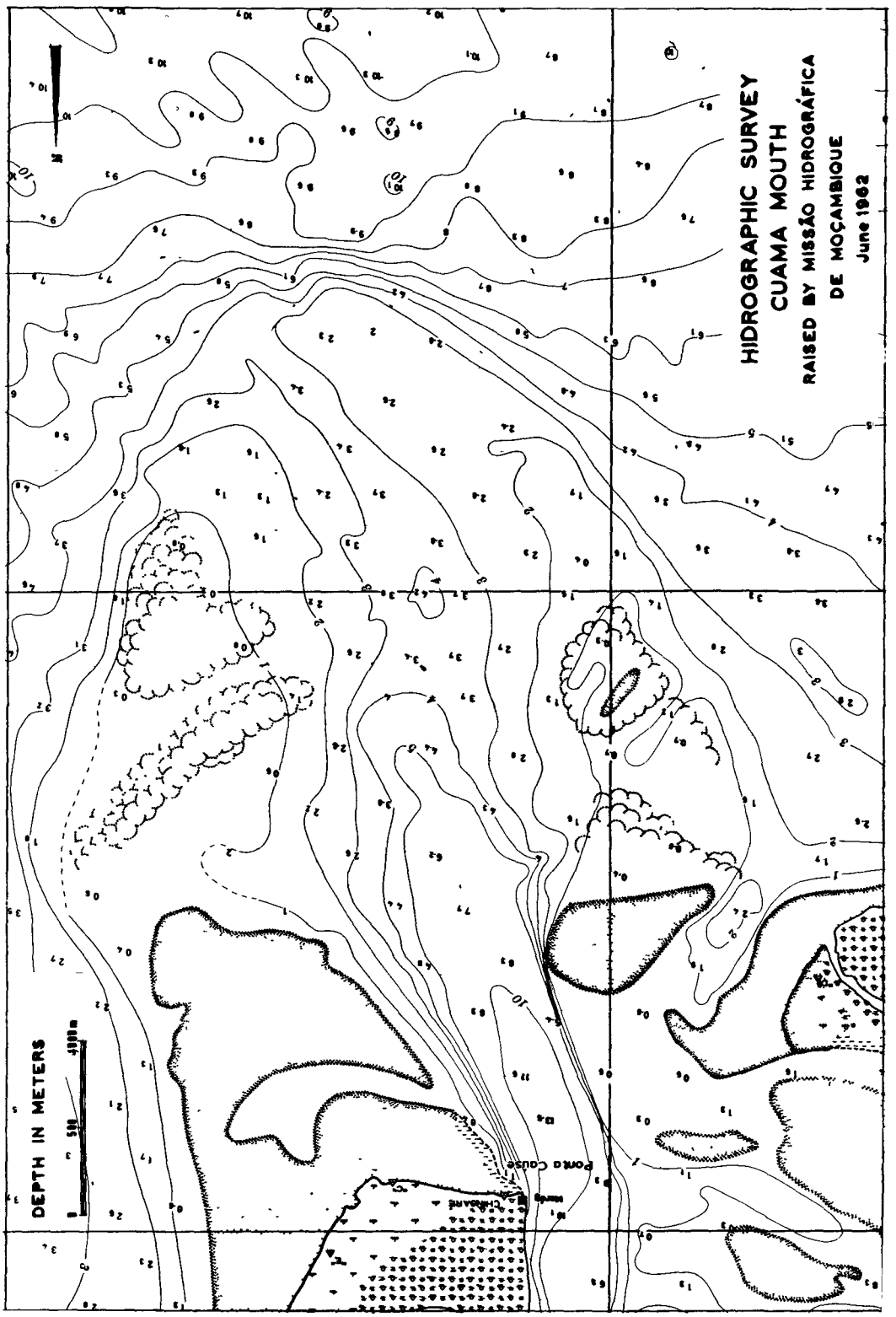
HIDROGRAPHIC SURVEY
CUAMA MOUTH
RAISED BY MISSÃO HIDROGRÁFICA
DE MOÇAMBIQUE
June 1962
DEPTH IN METERS
Ponta Cuase
Chibalane

II, and generally speaking, the inconvenients of the first, will be:

- No possibility of continuous sounding (with the sounder being currently used) and the resulting decrease of altimetric accuracy of the method;

- Operation always conditioned by the direction and sense of the wind, and owing to this conditioning greater difficulties in carrying out a pre-determined sounding net;

- Due to the non-existence of towers for inland signals, necessity of reference points on the zone to be sounded, so as to minimize the above mentioned disadvantage.

It should however be made clear that the method using the helicopter offers possibilities of reducing or even eliminating the main inconveniences, as outlined in the paragraphs below.

It should be further clarified that when establishing such a comparison between the two methods, stating the advantages and dis - advantages of one over the other, there has not been the slightest intention of making the new method appear preferable to the classical one under all circumstances.

The object of this comparison is merely to draw conclusions regarding the value and interest of a method tested and initiated be - cause a classical method appeared inadequate for the sounding of a certain zone, and point out its advantages and disadvantages so that, according to the circumstances, it will be possible to chose the most suitable method for the sounding survey contemplated, taking into consideration the desired degree of accuracy, the working aids available, and the possibilities that the method already tested and now being presented added to the usual sounding methods, with a view to reducing their limitations.

In the case of the Zambezi Mission, the already mentioned need for the periodical repetition of the hydrographic survey of the Cua- ma mouth, the existing conditionings regarding working aids for the application of other methods, the availability of the helicopters , and the cost of the survey using the new method, made its application of undisputable interest for the studies now in course on the Zambe

zi delta.

3.6 - POSSIBILITIES FOR IMPROVEMENT

The possibilities for improvement should fall mainly on the feasibility of:

- equipping the helicopter and the shore stations with V.H.F. radio communications for easier intercommunications;

- carrying out the sounding operations with equipment selected so as to use a light-weight oscillator unit hardly resistant to towing.

It is believed that in this manner it will be possible to reduce the main disadvantages of the method because:

- the first mentioned improvement will allow the starting of the sounding lines at points adequately referred to the lines earlier surveyed and thus with a shorter time of operation ensure a better distribution of the net of points to be sounded; it will also eliminate the need for placing reference points in the zone to be sounded;

- The improvement mentioned second may allow the continuous sounding of each line instead of having to execute it point by point; together with the recommended V.H.F. radio communications, the control of the reading points might be done from the aircraft in the event of continuous sounding.

Lisbon, June 1964.

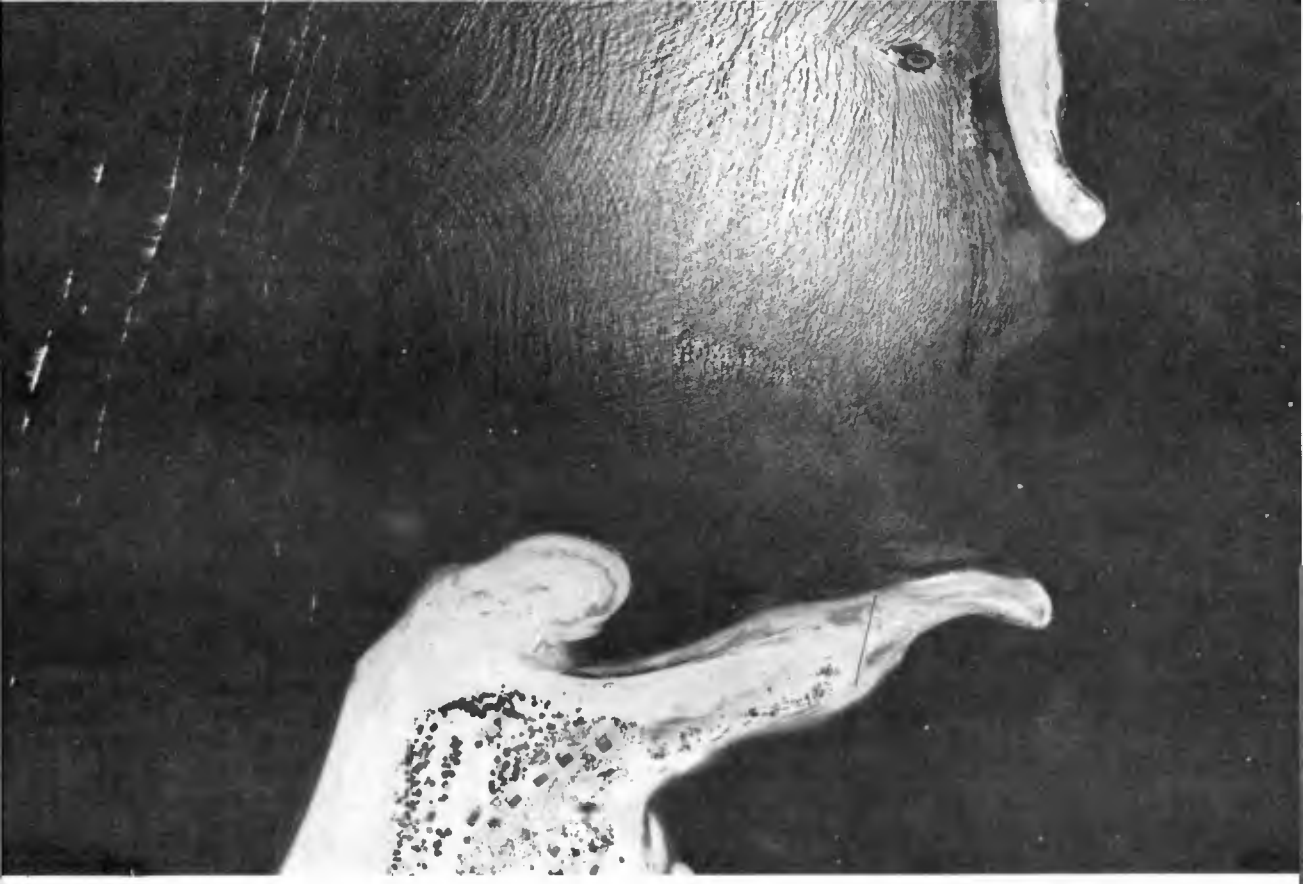

Samba Lagoon Inlet, Angola

Part 3
COASTAL STRUCTURES AND RELATED PROBLEMS

Aveiro Lagoon Inlet, Portugal

Chapter 29

THE DYNAMIC RESPONSE OF OFFSHORE STRUCTURES TO TIME-DEPENDENT FORCES

William S. Gaither, Graduate Student
and
David P. Billington, Professor
Department of Civil Engineering, Princeton University
Princeton, New Jersey

INTRODUCTION

This paper is addressed to the problem of structural behavior in an offshore environment, and the application of a more rigorous analysis for time-dependent forces than is currently used.

Design of pile supported structures subjected to wave forces has, in the past, been treated in two parts: (1) a static analysis based on the loading of a single wave, and (2) a dynamic analysis which sought to determine the resonant frequency by assuming that the structure could be approximated as a single-degree-of-freedom system.(Ref. 4 and 6) The behavior of these structures would be better understood if the dynamic nature of the loading and the many degrees of freedom of the system were included.

A structure which is built in the open ocean is subjected to periodic forces due to wind, waves, floating objects, and due occasionally to machinery mounted on the structure. To resist motion, the structure relies on the stiffness of the elements from which it is built and the restraints of the ocean bottom into which the supporting legs are driven.

Ocean wave forces vary in magnitude, direction, and elevation as they pass through a complete cycle. Figure 1 (b) shows the forces of a wave of length λ passing a simple bent. The legs of the bent, in the plane perpendicular to the wave crest, are spaced at a distance of $\lambda/2$. Leg A is then acted upon by a force to the right while leg B is forced in the opposite direction. If the legs were either an integer number of wave lengths apart, or extremely close together, they would be acted upon by approximately equal wave forces.

Even though the bent is a planar structure waves seldom approach in its plane or perpendicular to its plane. Figure 1 (a) shows the bent in plan with its plane rotated an angle γ from the line of wave crests. Thus the forces on legs A and B are not only unequal and opposite but exert components of force both in the plane of the structure and also out of the plane. To treat this structure realistically it is necessary to formulate an analytic method which can accommodate all the variations in these time-dependent forces.

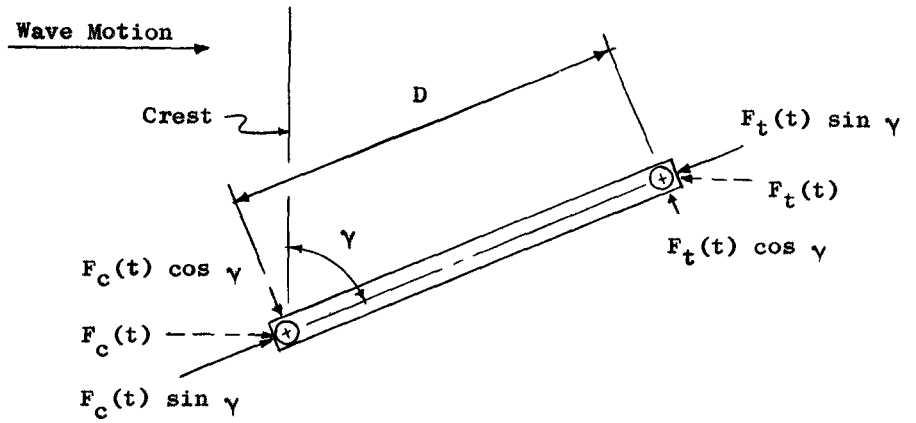

Figure 1 (a) Bent - Plan

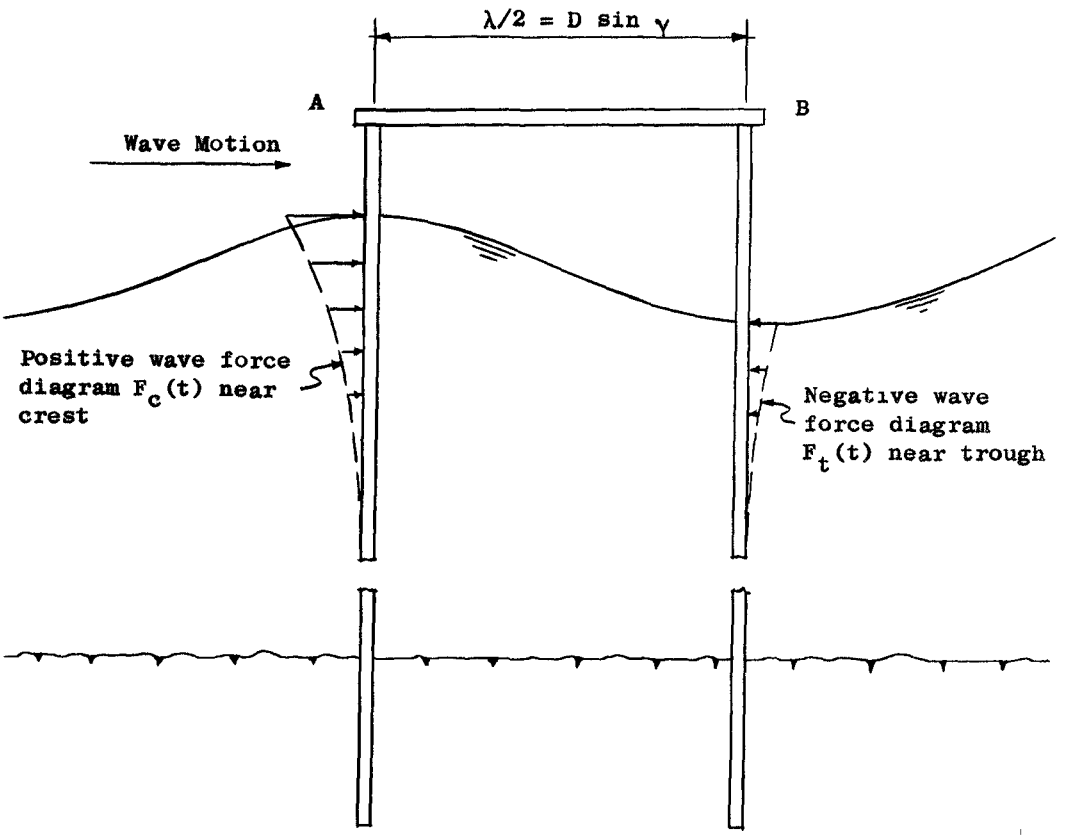

Figure 1 (b) Bent - Elevation

ANALYSIS

For analysis the structural system is idealized as follows: First, the piles are assumed to be driven in the ocean bottom and fixed at a particular elevation. The analytic formulation in no way precludes the application of resisting soil forces as a function of deformation and time. Second, continuous members are assumed to be a series of discrete springs and masses so that a digital computer can be used for the solution.(Ref. 8) Third, the continuous force of a passing wave, represented by a known function of time, is idealized by breaking it into segments of depth L (see Fig. 2 (a)). The resultant of this force segment is denoted by $f_n(t)$.

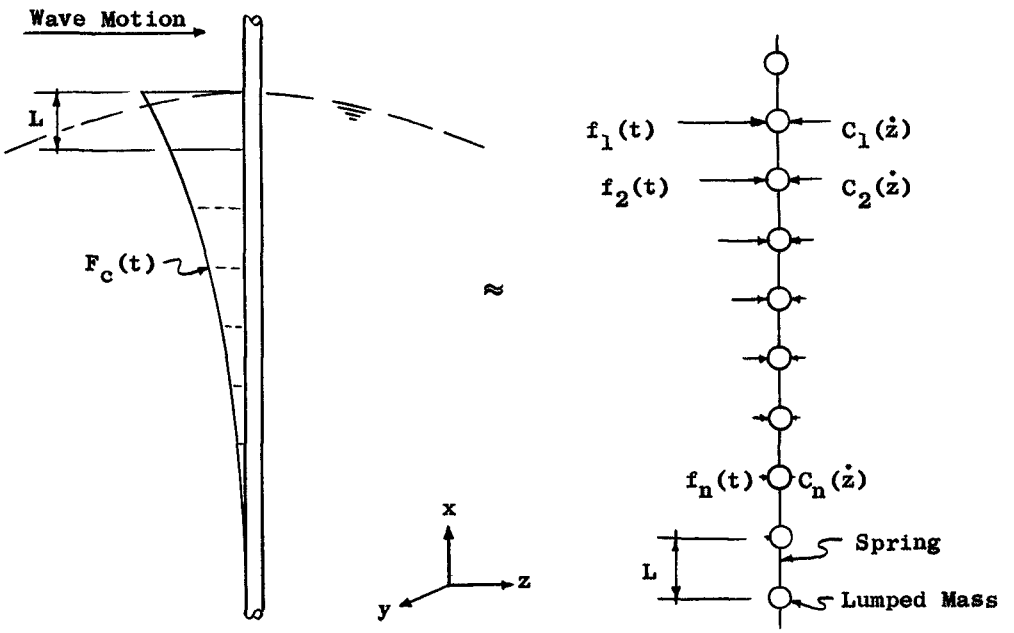

(a) Actual Pile (b) Idealized Pile

Figure 2

Figure 2 (b) shows the idealized pile divided into a series of springs and masses. The distance between masses is also L to correspond to the vertical increment of wave force selected. Acting externally on each mass is the viscous damping force of the water, $C_n(\dot{z})$. Non-linear damping can be included by considering the continuously varying value of C_n as approximated by step values, each of which is constant for a short time. All further reference to beams or piles will assume the lumped mass idealization of Fig. 2 (b).

It is customary for vibrations texts (Ref. 9) to use the coordinate x for the derivation of the equations of motion. To be consistent with later parts of this paper, the coordinate z will be used here.

Further idealizations upon which this analysis is based are: (a) stress is proportional to strain, (b) small deflection theory, (c) all motion is

measured from the position of static equilibrium (P.O.S.E.), and (d) one dimensional analysis.

DIFFERENTIAL EQUATIONS OF MOTION

Figure 3 shows a single-degree-of-freedom system which consists of two basic parts. First, the spring k and dashpot c in parallel are equivalent to the spring of length L in Fig. 2 (b). The dashpot in this location provides a means of expressing structural, or internal, damping. Second, a mass m is damped viscously and also forced by a steady-state periodic function. The need for this second dashpot is to provide a means to apply external viscous damping to the pile as shown in Fig. 2 (b) by $C_n(\dot{z})$. The forcing function P cos Ωt is analogous to $f_n(t)$ of Fig. 2 (b). With each mathematical expression tied to physical reality we may now apply D'Alembert's Principle to Newton's Second Law and write the equation of motion as an equation of static equilibrium for the system of Fig. 3. (Ref. 9)

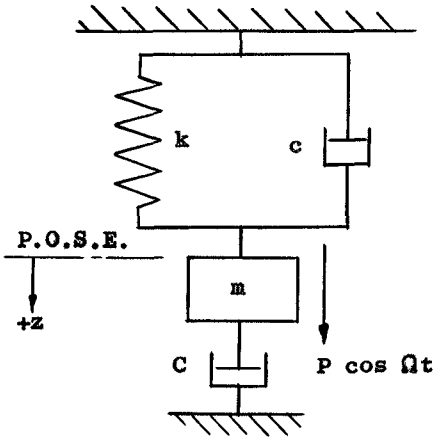

Figure 3 Single-Degree-of-Freedom System with two Viscous Dampers

$$m\ddot{z} + C\dot{z} + c\dot{z} + kz = P \cos \Omega t \tag{1}$$

The forcing expression can be represented for convenience by the real part of the complex function

$$P \cos \Omega t = \mathrm{Re}(P\, e^{j\Omega t}) \tag{2}$$

where $j = \sqrt{-1}$. For the offshore application our interest is focused on the response of the structure to a train of waves of approximately the same period. Mathematically then, we will seek only the steady-state solution to Eq.(1) which is

$$z = \mathrm{Re}(\bar{z}\, e^{j\Omega t}) \tag{3}$$

where the complex amplitude $\bar{z}$ represents the actual amplitude of motion made up of the vector sum of two components, the real and imaginary. For impulse loading (earthquake waves, blasts, or ship berthing) the transient solution could also be included.(Ref. 8) Differentiating Eq. (3) and substituting into Eq. (1), we obtain

$$(-m\Omega^2 + jC\Omega + jc\Omega + k)\bar{z}\, e^{j\Omega t} = P\, e^{j\Omega t}$$

or

$$-m\Omega^2\bar{z} + jC\Omega\bar{z} + jc\Omega\bar{z} + k\bar{z} = P \tag{4}$$

Through the use of complex notation the steady state solution, as given by Eq. (4), is easily obtained and the effect of each term remains apparent.

Structural damping in homogeneous materials may be defined as a function of the forcing frequency Ω such that

$$c = c(\Omega) = k \frac{\epsilon}{\Omega} \tag{5}$$

where k is the spring constant and ϵ is a factor of proportionality which is charateristic of the material.(Ref. 2) By substituting Eq. (5) into Eq. (4) we obtain

$$-m\Omega^2\bar{z} + jC\Omega\bar{z} + jk\epsilon\bar{z} + k\bar{z} = P \tag{6}$$

For analytic convenience the complex modulus $\bar{K}$ for structural damping can be formulated as

$$\bar{K}(\Omega) = k + jek = k(1 + j\epsilon) \tag{7}$$

For example in bending we have a flexibility term of the form $1/k = L^3/6EI$ where the elastic properties are expressed by E, or in the torsional case G. To handle these situations it is convenient to formulate an expression for the complex elastic modulus $\bar{E}$ and the complex shearing modulus G.

$$\bar{E} = E(1 + j\epsilon)$$

and

$$\bar{G} = G(1 + j\epsilon)$$

Where $\bar{E}$ appears in the denominator as cited above, the imaginary portion is then moved to the numerator

$$\frac{1}{\bar{k}} = \frac{L^3}{6E(1 + j\epsilon)I} \frac{(1 - j\epsilon)}{(1 - j\epsilon)} = \frac{L^3(1 - j\epsilon)}{6EI(1 + \epsilon^2)} \tag{8}$$

so that the imaginary part may be separated from the real in the matrix formulation.

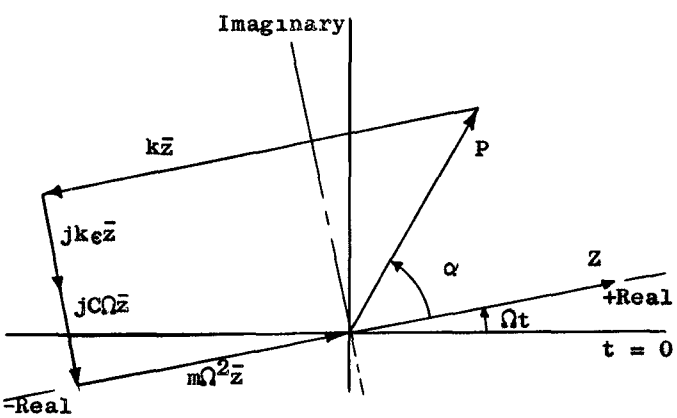

Figure 4 Vector Force Representation of Eq. (6) with Phase Angle $\alpha < 90^o$

Figure 4 shows the vector relationship of the terms of Eq. (6). From the axis t = 0 the entire vector force diagram (an Argand diagram, i.e. any diagram on the complex plane) is rotating at the constant angular velocity Ωt. As the forcing frequency Ω moves toward a resonant frequency of the structure, α approaches 90^o. When $\alpha = 90^o$ the externally applied force is devoted exclusively to opposing damping, both structural and external, while the spring force $k\bar{z}$ is equal

and opposite to the inertia force $m\Omega^2\bar{z}$.

MATRIX FORMULATION

The equations required to describe the motion of each spring and each mass are formulated in matrix notation for concise explanation in this paper, and for systematic manipulation within the program for the digital computer. This section employs three matrix expressions: (1) the state vector, (2) the mass matrix, and (3) the field transfer matrix. The formulation of these types of matrices has been described in detail by Pestel and Leckie.(Ref. 8)

The coordinate system used throughout this paper is shown in Fig. 5 and follows the right-hand rule.

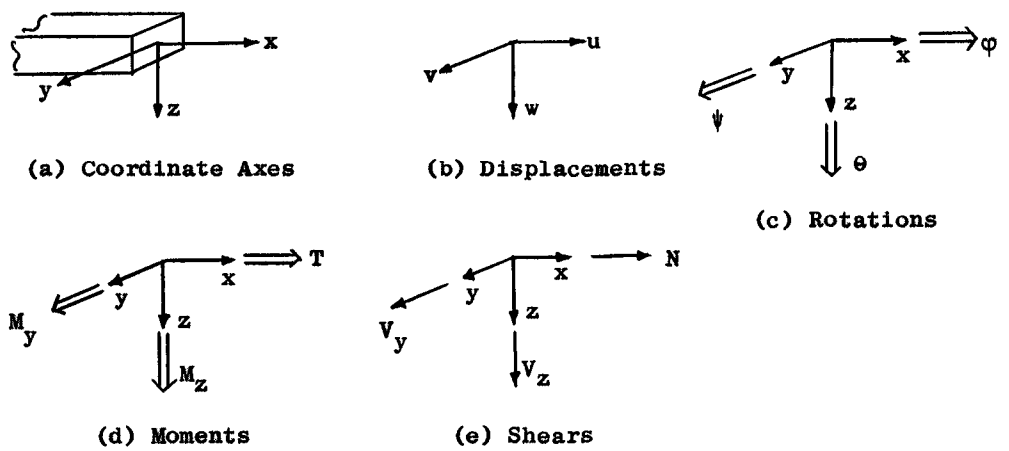

(a) Coordinate Axes (b) Displacements (c) Rotations

(d) Moments (e) Shears

Figure 5 Coordinate System

The centroidal axis, which in the cases studied here is taken always to coincide with the shear center of any member, will be the x-axis as shown in Fig.5 (a).

Equation (6) contains both real and imaginary terms. However, instead of formulating matrices of complex numbers it is possible to partition all matrices in such a way that both real and imaginary terms may be treated as real and still remain separated.(Ref. 7) The following complex multiplication

$$[A][B] = [C]$$

can be written in partitioned form as

$$\left[\begin{array}{c|c} R_A & -I_A \\ \hline I_A & R_A \end{array}\right]\left[\begin{array}{c|c} R_B & -I_B \\ \hline I_B & R_B \end{array}\right] = \left[\begin{array}{c|c} R_AR_B-I_AI_B & -R_AI_B-R_BI_A \\ \hline R_BI_A+R_AI_B & -I_AI_B+R_AR_B \end{array}\right] = \left[\begin{array}{c|c} R_C & -I_C \\ \hline I_C & R_C \end{array}\right] \qquad (9)$$

where R represents real terms and I represents imaginary.

The State Vector The state vector $\{z\}$ is so named because it gives the

displacements and forces at any station along the beam. It is partitioned to separate real and imaginary parts and sub-partitioned to separate displacements and forces. Braces { } are used to denote a vertical column matrix but to use space more efficiently in this paper these will be written horizontally. Brackets [ ] are used for square matrices.

$$\{z\} = \{\underbrace{u\ v\ -w\ \varphi\ \psi\ \theta}_{\text{Generalized Displacements}}\ \underbrace{M_z\ M_y\ T\ V_z\ -V_y\ N}_{\text{Generalized Forces}}\ \underbrace{u\ v\ -w\ \varphi\ \psi\ \theta}_{\text{Generalized Displacements}}\ \underbrace{M_z\ M_y\ T\ V_z\ -V_y\ N}_{\text{Generalized Forces}}\ 1\} \quad (10)$$

Real | Imaginary | Unity

The significance of the unity term will become apparent in the formulation of the mass matrix.

The Mass Matrix Figure 6 shows a section of an arbitrary beam with the superscripts R and L denoting right and left.

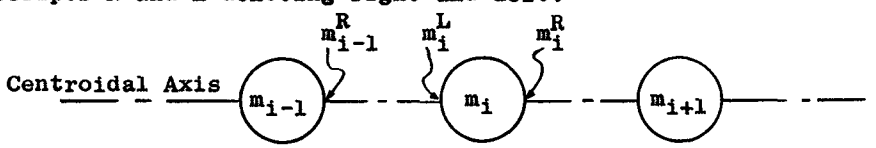

Figure 6 Portion of Arbitrary Beam

In Fig. 7 (a) a free-body diagram of mass m_i in this beam is shown with the forces and displacements in the z-x plane.

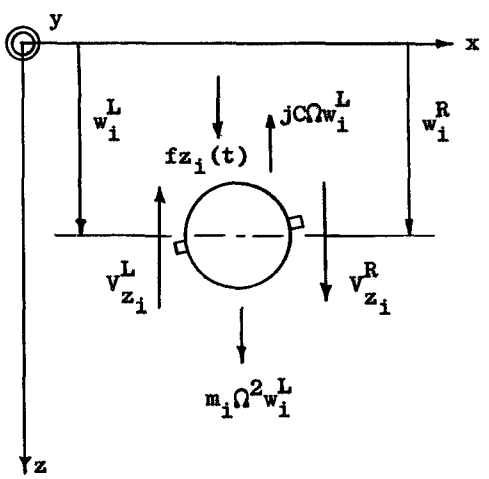

Figure 7 (a) Displacements and Forces - Mass m_i

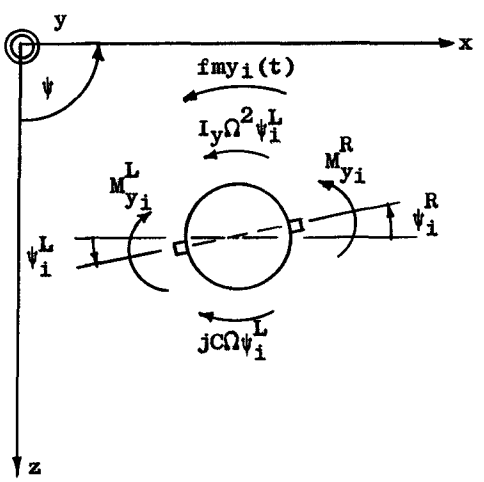

Figure 7 (b) Rotations and Moments - Mass m_i

Since the mass is considered lumped at an infinitesimally small point and is non-deformable, we may write the displacement equation as

$$w_i^R = w_i^L \quad (11)$$

and by summing forces in the z direction

$$V_{z_i}^R + m_i\Omega^2 w_i^L - V_{z_i}^L - j c\Omega w_i^L + f_{z_1}(t) = 0 \tag{12}$$

we recognize three terms from Eq. (6) plus two shear terms.

Figure 7 (b) is a free-body diagram of the same mass m_i as shown in Fig. 7 (a) but showing rotations and moments. The rotation equation is

$$\psi_i^R = \psi_i^L \tag{13}$$

and by summing moments about the y-axis

$$M_{y_i}^R + I_{y_i}\Omega^2 \psi_i^L - M_{y_i}^L - j c\Omega \psi_i^L + f m_{y_i}(t) = 0 \tag{14}$$

where $I_y = \int(x^2 + z^2)dm$ and is called the mass moment of inertia.

By drawing four more free-body diagrams of mass m_i, two in the x-y plane and two in the y-z plane, eight more equations similar to Eqs. (11) through (14) can be written bringing the total to 12. If all equations are solved for the terms at the position to the right of m_1 as shown by m_i^R in Fig. 6, the mass matrix may then be written for mass m_i.

The state vector to the left of m_i is $\{z\}_i^L$ and the state vector to the right is $\{z\}_i^R$, each containing the terms shown in Eq. (10). The 25 x 25 mass matrix [P] is then

$$\{z\}_i^R = \begin{bmatrix} 1 & & 12 & 13 & & 24 & \\ & P_R & & & -P_I & & \\ 12 & & & \text{ith row} & & & \\ 13 & & & & & & \\ & \text{jth col.} & & \rightarrow P_{i,j} & & & 0 \\ & P_I & & & P_R & & \\ 24 & & & & & & \\ 25 & 0 & & 0 & & & 1 \end{bmatrix} \{z\}_1^L \tag{15}$$

The constant term, $fm_{y_i}(t)$ of Eq. (14) is placed in the 25th column of [P]. The coefficient of one, which appears in the state vector of Eq. (10) then has the effect of carrying the forcing function term along in the matrix operations. Table 1 lists the terms of matrix [P].

TABLE 1 Non-Zero Elements in the General Mass Martix Sub-Sections $[P_R]$, $[-P_I]$, and Column 25

P_R(1 thru 12, 1 thru 12) = P_R(13 thru 24, 13 thru 24)

$-P_I$(1 thru 12, 13 thru 24) = P_I(13 thru 24, 1 thru 12)

Row (i)	Col (j)	Term	Col (j)	Term	Col (j)	Term	Col (j)	Term
1	1	1.0						
2	2	1.0						
3	3	1.0						

TABLE 1 (cont.)

Row (i)	Col (j)	Term	Col (j)	Term	Col (j)	Term	Col (j)	Term
4	4	1.0						
5	5	1.0						
6	6	1.0						
7	6	$-I_z\Omega^2$	7	1.0	18	$-C\Omega$	25	$-fm_z(t)$
8	5	$-I_y\Omega^2$	8	1.0	17	$-C\Omega$	25	$-fm_y(t)$
9	4	$-I_x\Omega^2$	9	1.0	16	$-C\Omega$	25	$-fm_x(t)$
10	3	$m\Omega^2$	10	1.0	15	$C\Omega$	25	$-f_z(t)$
11	2	$m\Omega^2$	11	1.0	14	$C\Omega$	25	$f_y(t)$
12	1	$-m\Omega^2$	12	1.0	13	$-C\Omega$	25	$-f_x(t)$

The Field Transfer Matrix The section of beam between points m^R_{i-1} and m^L_i of Fig. 6 represents a spring connector of length L. A free-body dia-

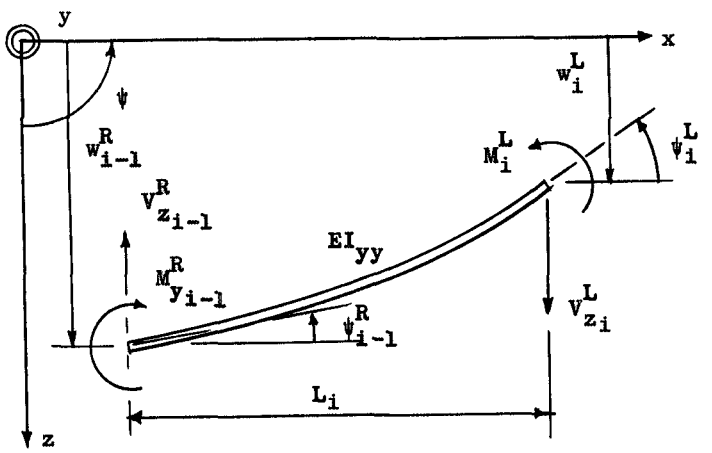

Figure 8 Displacements and Forces; Rotations and Moments

gram of this spring in the z-x plane is shown in Fig. 8 from which the following equations are derived:

$$-w^L_i + w^R_{i-1} - L_i\psi^R_{i-1} - L_i^2M^R_{y_{i-1}}/2EI_{yy_i} - L_i^3V^R_{z_{i-1}}/6EI_{yy_i} = 0 \quad (16)$$

$$\psi^L_i - \psi^R_{i-1} - L_iM^R_{y_{i-1}}/EI_{yy_i} - L_i^2V^R_{z_{i-1}}/2EI_{yy_i} = 0 \quad (17)$$

$$M^L_{y_i} - M^R_{y_{i-1}} - L_iV^R_{z_{i-1}} = 0 \quad (18)$$

$$-V^L_{z_i} - V^R_{z_{i-1}} = 0 \quad (19)$$

Equations (16) and (17) relate the displacements and rotations at one end of the beam to the displacements and rotations at the other. Equation (18) is obtained by summing the moments and Eq. (19) by summing the shears shown in the free-body diagram.

By drawing free-body diagrams of the spring connectors in the x-y and

y-z planes, eight more equations can be written. Solving these equations for the terms to the left of mass m_1, the 25 x 25 field transfer matrix [F] can be written as

$$\{z\}_i^L = \begin{bmatrix} 1 & & 12 & 13 & & 24 & \\ & F_R & & & -F_I & & 0 \\ & & & \text{ith row} & & & \\ 12 & & & & & & \\ 13 & & & \text{jth col.} \rightarrow F_{i,J} & & & \\ & F_I & & & F_R & & 0 \\ 24 & & & & & & \\ 25 & 0 & & 0 & & & 1 \end{bmatrix} \{z\}_{i-1}^R \qquad (20)$$

TABLE 2 (a) Non-Zero Elements in the General Field Matrix, Sub-Section $[F_R]$; F_R(1 thru 12, 1 thru 12) = F_R(13 thru 24, 13 thru 24)

Row (i)	Col (j)	Term	Col (j)	Term	Col (j)	Term	Col (j)	Term
1	1	1.0	12	$L/EA(1+\epsilon^2)$				
2	2	1.0	6	L	7	$L^2/2EI_{zz}(1+\epsilon^2)$	11	$L^3/6EI_{zz}(1+\epsilon^2)$
3	3	1.0	5	L	8	$L^2/2EI_{yy}(1+\epsilon^2)$	10	$L^3/6EI_{yy}(1+\epsilon^2)$
4	4	1.0	9	$L/GJ(1+\epsilon^2)$				
5	5	1.0	8	$L/EI_{yy}(1+\epsilon^2)$	10	$L^2/2EI_{yy}(1+\epsilon^2)$		
6	6	1.0	7	$L/EI_{zz}(1+\epsilon^2)$	11	$L^2/2EI_{zz}(1+\epsilon^2)$		
7	7	1.0	11	L				
8	8	1.0	10	L				
9	9	1.0						
10	10	1.0						
11	11	1.0						
12	12	1.0						

Note:
A = Cross-Sectional Area
J = Moment of Inertia about x-axis
I_{yy} = Moment of Inertia about y-axis
I_{zz} = Moment of Inertia about z-axis

TABLE 2 (b) Non-Zero Elements in the General Field Matrix, Sub-Section $[F_I]$; F_I(13 thru 24, 1 thru 12) = $-[F_I]$(1 thru 12, 13 thru 24)

Row (i)	Col (j)	Term	Col (j)	Term
1	24	$\epsilon L/EA(1+\epsilon^2)$		
2	19	$\epsilon L^2/2EI_{zz}(1+\epsilon^2)$	23	$\epsilon L^3/6EI_{zz}(1+\epsilon^2)$
3	20	$\epsilon L^2/2EI_{yy}(1+\epsilon^2)$	22	$\epsilon L^3/6EI_{yy}(1+\epsilon^2)$
4	21	$\epsilon L/GJ(1+\epsilon^2)$		
5	20	$\epsilon L/EI_{yy}(1+\epsilon^2)$	22	$\epsilon L^2/2EI_{yy}(1+\epsilon^2)$
6	19	$\epsilon L/EI_{zz}(1+\epsilon^2)$	23	$\epsilon L^2/2EI_{zz}(1+\epsilon^2)$

Matrix Formulation for a Single Pile Figure 9 shows a single pile, fixed at the base and free at the upper end. A state vector $\{z\}_A$ may be written for the fixed base and a spring matrix $[F_1]$ for the first spring. The equation which relates the base at A to the lower side of the first mass is

$$\{z\}_1^L = [F_1]\{z\}_A \qquad (21)$$

Similarly the lower side of the first mass may be related to the upper side of the first mass by

$$\{z\}_1^U = [P_1]\{z\}_1^L \tag{22}$$

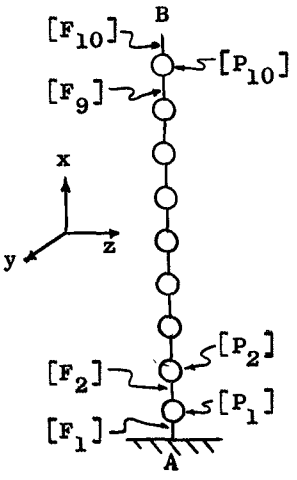

Figure 9 Cantilever Pile Idealized by 9 Lumped Masses

By substituting Eq. (21) into Eq. (22) the upper side of the first mass is related to the fixed base at A by

$$\{z\}_1^U = [P_1][F_1]\{z\}_A \tag{23}$$

This procedure is continued until the top of the pile is related to the base, giving the equation

$$\{z\}_{BA} = [F_{10}][P_9]\text{---}[P_1][F_1]\{z\}_A$$

or

$$\{z\}_{BA} = [AB]\{z\}_A \quad .$$

Corner Transformation Matrix The mathematical model of a simple bent must include a method of transforming displacement and force information from a vertical member to the horizontal bent cap and then back to the second vertical pile. Considering the bent ABCD of Fig. 10 and applying the right-hand-screw rule, the transformation around corner B requires rotation about the y-axis through the angle $\psi = -90^o$. The state vector at the B end of member AB is

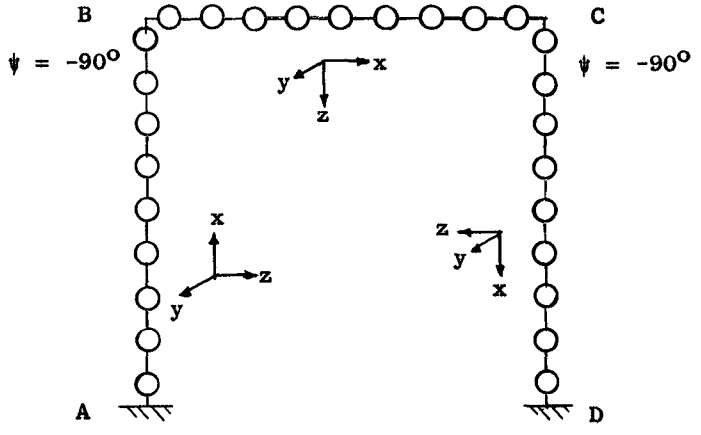

Figure 10 Bent Idealized by 27 Lumped Masses

$\{z\}_{BA}$, the initial state vector in member BC is $\{z\}_{BA}^T$, and the transformation matrix is $[T]$. Therefore,

$$\{z\}_{BA}^T = [T]\{z\}_{AB}$$

which expanded into its partitioned form becomes

$$\{z\}^{T}_{BA} = \left[\begin{array}{c|c|c|c|c} T_1 & 0 & 0 & 0 & 0 \\ \hline 0 & T_2 & 0 & 0 & 0 \\ \hline 0 & 0 & T_1 & 0 & 0 \\ \hline 0 & 0 & 0 & T_2 & 0 \\ \hline 0 & 0 & 0 & 0 & 1 \end{array}\right] \{z\}_{BA} \qquad (24)$$

Submatrix $[T_1]$ transforms displacements and rotations

$$[T_1] = \begin{bmatrix} \cos\psi & 0 & \sin\psi & 0 & 0 & 0 \\ 0 & 1 & 0 & 0 & 0 & 0 \\ -\sin\psi & 0 & \cos\psi & 0 & 0 & 0 \\ 0 & 0 & 0 & \cos\psi & 0 & -\sin\psi \\ 0 & 0 & 0 & 0 & 1 & 0 \\ 0 & 0 & 0 & \sin\psi & 0 & \cos\psi \end{bmatrix}$$

Similarly $[T_2]$ transforms moments and shears

$$[T_2] = \begin{bmatrix} \cos\psi & 0 & \sin\psi & 0 & 0 & 0 \\ 0 & 1 & 0 & 0 & 0 & 0 \\ -\sin\psi & 0 & \cos\psi & 0 & 0 & 0 \\ 0 & 0 & 0 & \cos\psi & 0 & \sin\psi \\ 0 & 0 & 0 & 0 & 1 & 0 \\ 0 & 0 & 0 & -\sin\psi & 0 & \cos\psi \end{bmatrix}$$

Mathematical Model of Bent The bent of Fig. 10 was idealized by assuming nine masses per member, with each mass being allowed six degrees of freedom, or a total of 162 degrees of freedom for the structure. This bent was programmed and is to serve as an analytic and experimental example for the remainder of this paper.

The fixed base of leg A was related to corner B in a single matrix expression. Using Eq. (24) for corners B and C the entire bent can now be formulated in the single equation

$$\{z\}_D = [CD][T][BC][T][AB]\{z\}_A$$

or

$$\{z\}_D = [U]\{z\}_A$$

Expanding Eq. (25) into its partitioned form we obtain

$$\{z\}_D = \left\{\begin{array}{c} d_R \\ \hline p_R \\ \hline d_I \\ \hline p_I \\ \hline 1 \end{array}\right\}_D = \left[\begin{array}{c|c|c|c|c} U_{dRdR} & U_{dRpR} & U_{dRdI} & U_{dRpI} & U_{dR25} \\ \hline U_{pRdR} & U_{pRpR} & U_{pRdI} & U_{pRpI} & U_{pR25} \\ \hline U_{dIdR} & U_{dIpR} & U_{dIdI} & U_{dIpI} & U_{dI25} \\ \hline U_{pIdR} & U_{pIpR} & U_{pIdI} & U_{pIpI} & U_{pI25} \\ \hline 0 & 0 & 0 & 0 & 1 \end{array}\right] \left\{\begin{array}{c} d_R \\ \hline p_R \\ \hline d_I \\ \hline p_I \\ \hline 1 \end{array}\right\}_A \qquad (25)$$

Equation (25) represents a series of 24 simultaneous equations (plus the identity 1 = 1) which can be solved by applying the boundary conditions at points A and D. At these points the displacements and rotations, denoted by d_R for real and d_I for imaginary, are zero due to the assumption of complete fixity, while the moments and shears, p_R and p_I, are unknown. Next, extract from Eq. (25) the submatrices which have not been multiplied by zero displacement or rotation terms of $\{z\}_A$, and which are equated to zero terms of $\{z\}_D$.

$$\begin{Bmatrix} 0 \\ \hline 0 \end{Bmatrix}_D = \left[\begin{array}{c|c} U_{dRpR} & U_{pRpI} \\ \hline U_{dIpR} & U_{dIpI} \end{array}\right] \begin{Bmatrix} p_R \\ \hline p_I \end{Bmatrix}_A + \begin{Bmatrix} U_{dR25} \\ \hline U_{dI25} \end{Bmatrix} \tag{26}$$

The forces p_R and p_I of leg A are found to be

$$\begin{Bmatrix} p_R \\ \hline p_I \end{Bmatrix}_A = \left[\begin{array}{c|c} U_{dRpR} & U_{dRpI} \\ \hline U_{dIpR} & U_{dIpI} \end{array}\right]^{-1} \begin{Bmatrix} -U_{dR25} \\ \hline -U_{dI25} \end{Bmatrix} \tag{27}$$

Electronic Computation The formulation of this analytic method in general terms presupposed its solution by an electronic computer. The matrix operations described above are grouped and written in FORTRAN as general subroutines.(Ref.3) Then a relatively short main program for any specific structure can be made up largely of commands which call subroutines.

In Eq. (23) the state vector for the upper side of mass one of leg AB was expressed in terms of a mass matrix, a spring matrix, and the state vector at A which is now known by Eq. (27). As matrix multiplication proceeds around bent ABCD, a matrix of coefficients is saved at each lumped mass, i.e. $[U_n]$.

$$\{z\}_1^U = [P_1][F_1]\{z\}_A = [U_1]\{z\}_A$$

and

$$\{z\}_2^U = [P_2][F_2][P_1][F_1]\{z\}_A = [U_2]\{z\}_A$$

etc.

By successively retrieving coefficient matrices $[U_1],[U_2],\text{---}[U_n]$ and multiplying by the known state vector $\{z\}_A$, the entire response at each lumped mass may be computed and written out. This means that a numerical value will be computed for each term shown in the state vector of Eq. (10). By paring each real term with its corresponding imaginary term, a complex term may be re-established from which the phase angle α of Figs. 4 and 11 can be computed:

$$\alpha = \arctan \frac{\text{Imaginary Component}}{\text{Real Component}}$$

The analysis of an actual structure would begin with the selection of a frequency range over which the response is of interest. First, the static structural response to the maximum value of the forcing function is obtained by setting $\Omega = \epsilon = 0$. Second, the entire frequency range is traversed in small increments and changes of sign of real terms are noted. Third, at a sign change the response vectors are plotted on the complex

plane, as shown in Fig. 11, to determine the maximum response. The points on the circle, Ω_1 and Ω_2 are found from the incremental approach. By using these two points and the origin, a circle can be constructed, the diameter of which is the value of the maximum response.(Ref. 1) Figure 11 is the plot used to determine the magnitude of the first peak shown in Fig. 12.

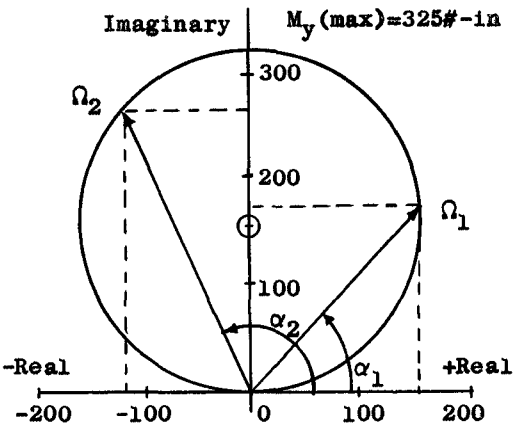

Figure 11 Polar Plot of M_y
Ω = 7.45 cps

The bent ABCD of Fig. 10 was programmed in FORTRAN and run on an IBM 7094 computer.(Ref. 3) A single exciting force of 1.414 pounds was applied to the middle mass of leg AB in the y-z plane at an angle of 45° from the z-axis. This force resolves into 1.0 pound forces concurrent with the y and z axes. The moments M_y, M_z, and T at the base of leg AB were chosen to indicate the structural response through the entire frequency range. Figures 12 and 13 indicate the peaks at which resonant frequencies occur.

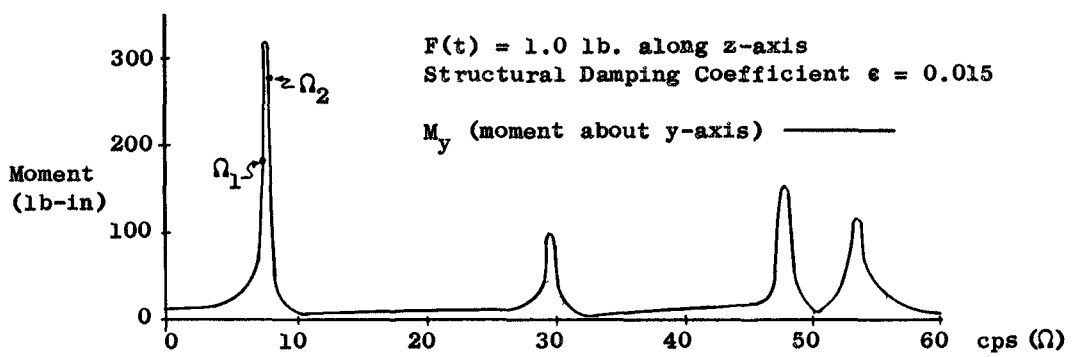

Figure 12 M_y at point A with Forcing at Mid-Height of Leg AB

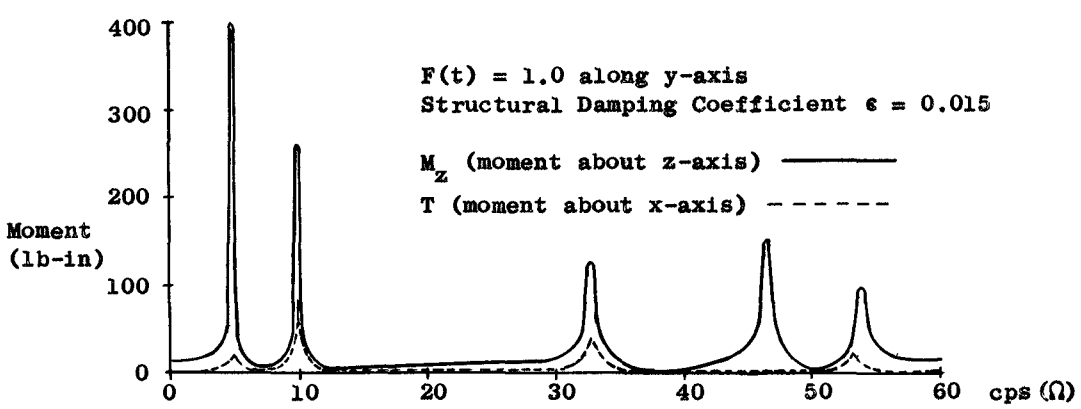

Figure 13 M_z and T at point A with Forcing at Mid-Height of Leg AB

At each resonant peak a characteristic mode shape, or deformed shape of the structure, occurs which can be plotted from the computer output at each lumped mass. The maximum number of resonant frequencies which can be computed is equal to the number of degrees of freedom. Although the bent chosen for illustration was forced by a point load, the mode shapes and resonant frequencies would be similar if a series of point loads, which models a gravity wave function of the same frequency, were applied. The deformed shapes at each resonant frequency for in-plane loading are given by Figs. 14 and for out-of-plane loading by Figs. 15.

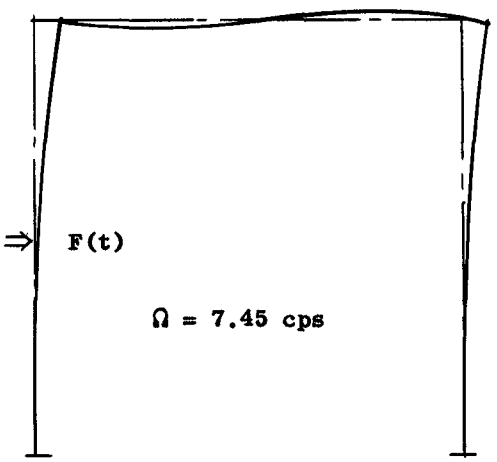

Figure 14 (a) Mode Shape for 1st Resonant Frequency of Structure as a Whole

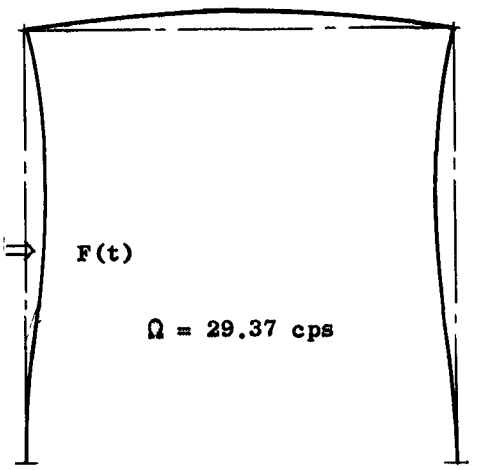

Figure 14 (b) Mode Shape for 2nd Resonant Frequency of Structure as a Whole

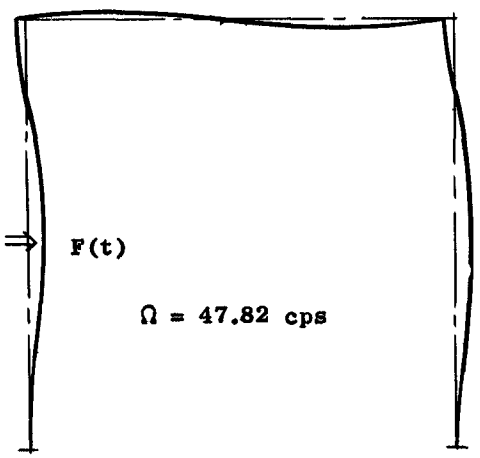

Figure 14 (c) Mode Shape for 3rd Resonant Frequency of Structure as a Whole

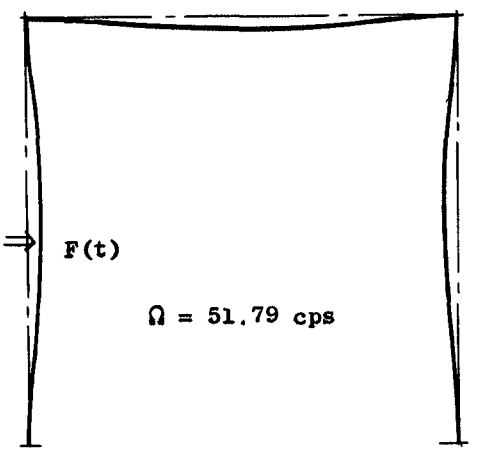

Figure 14 (d) Mode Shape for 4th Resonant Frequency of Structure as a Whole

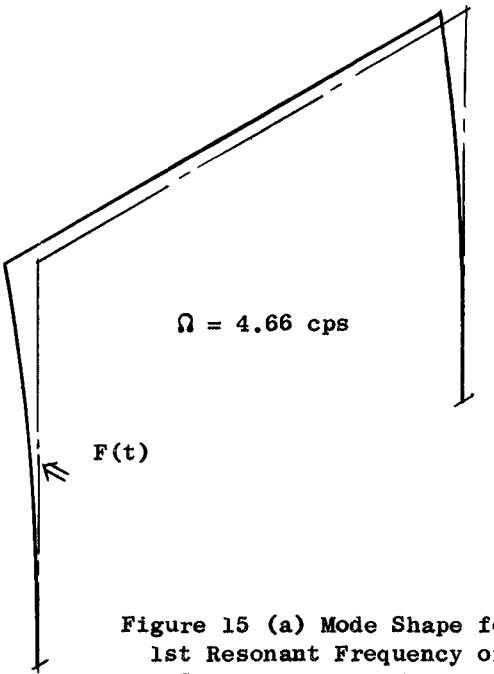

Figure 15 (a) Mode Shape for 1st Resonant Frequency of Structure as a Whole (Out-of-Plane Forcing)

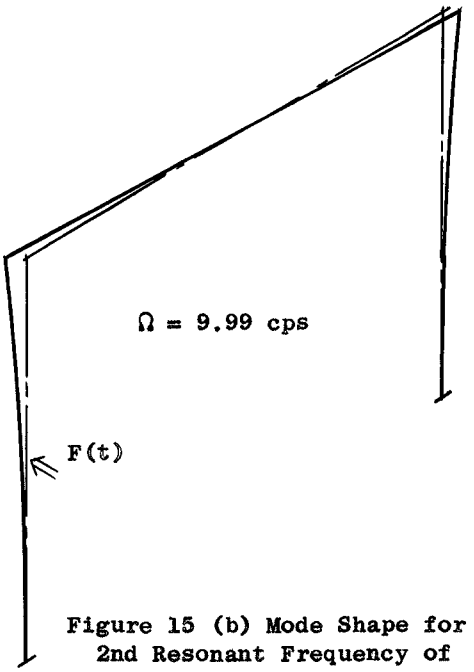

Figure 15 (b) Mode Shape for 2nd Resonant Frequency of Structure as a Whole (Out-of-Plane Forcing)

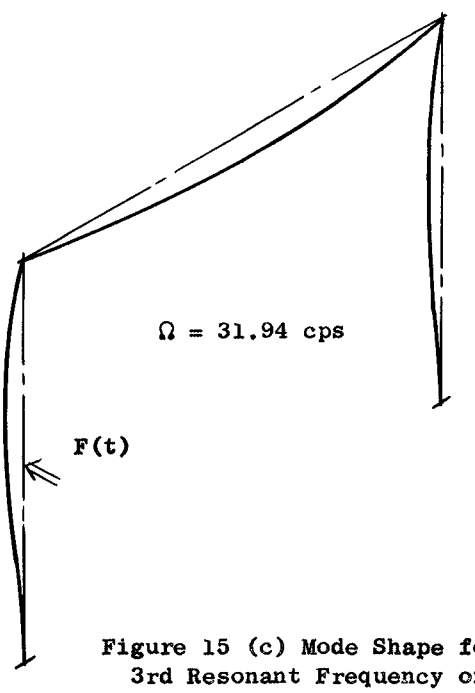

Figure 15 (c) Mode Shape for 3rd Resonant Frequency of Structure as a Whole (Out-of-Plane Forcing)

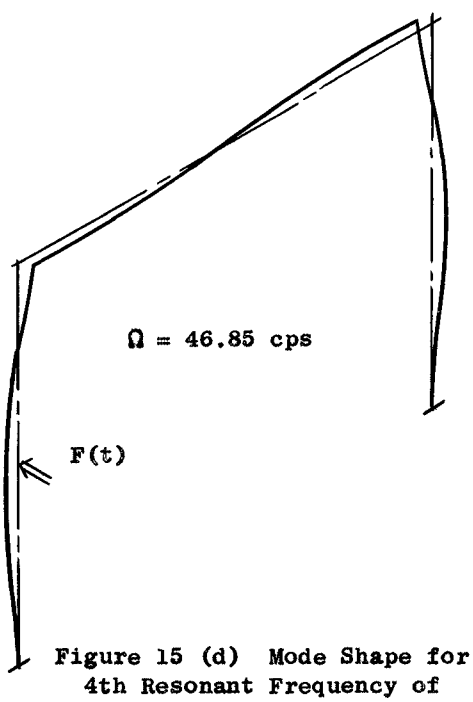

Figure 15 (d) Mode Shape for 4th Resonant Frequency of Structure as a Whole (Out-of-Plane Forcing)

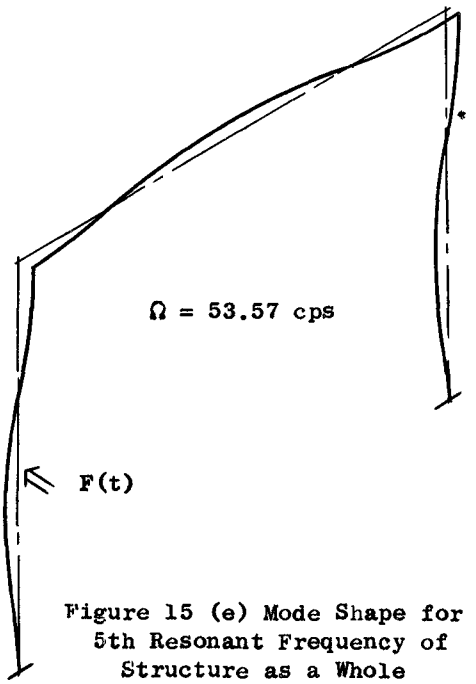

Figure 15 (e) Mode Shape for 5th Resonant Frequency of Structure as a Whole (Out-of-Plane Forcing)

Knowning the mode shapes is of practical significance since the amplitude of resonant deformation is greatest when the forces on each leg are putting energy into the structure. When a bent is deformed in an anti-symmetric mode shape (Figs. 14 (a),(c) and Figs. 15 (b), (d)) forces on legs spaced an integer number of wave lengths apart are mutually reinforcing. Similarly, when a bent is deformed in a symmetric mode shape (Figs. 14 (b),(d) and Figs 15 (a),(c),(e)) forces on legs spaced an integer number of half-wave lengths apart add their effects. (At half-wave lengths the opposing forces are not necessarily at their maximum in all cases.(Ref. 5)) Thus the deformed structures may be thought of in the same light as influence lines for resonant loading.

EXPERIMENTAL VERIFICATION

To test the validity of the analytic formulation a bent was constructed of 3 - 3/8" round steel rods each approximately 36" long. Full penetration welds were used at corners B and C and legs A and D were drilled and welded into a 15" x 1/2" x 4'-0" steel base plate. In-plane and out-of-plane excitation was provided by an electro-magnetic shaker. Force input to the structure was measured by a crystal force gage, from which the signal was minimum at resonance points. The frequency of resonant oscillation was measured by a stroboscopic light which also provided a means of observing mode shapes for comparison with analysis.

TABLE 3 Summary: Calculated vs Experimental Resonant Frequencies

Fig.	In-Plane		Out-of-Plane		High	Low	Std.	Dis-
	Calc. cps	Exp. cps	Calc. cps	Exp. cps	cps	cps	Dev. cps	crep-ancy
14 (a)	7.45	7.35				0.10	0.07	1.4%
14 (b)	29.37	29.27				0.10	0.10	0.4%
14 (c)	47.82	47.43				0.39	0.25	0.8%
14 (d)	51.79	51.80			0.01		0.04	0.0%
15 (a)			4.66	4.62		0.04	0.02	0.9%
15 (b)			9.99	9.82		0.17	0.03	1.7%
15 (c)			31.94	31.75		0.19	0.21	0.5%
15 (d)			46.85	46.26		0.59	0.18	1.3%
15 (e)			53.57	53.58	0.01		0.05	0.0%

Table 3 shows the comparison between calculated and experimental resonant frequencies for the nine modes investigated. The standard deviation was calculated from five experimental readings at each frequency. The discrepancy was computed from the average experimental frequency and the calculated resonant frequency.

COMPARISON TO SINGLE-DEGREE-OF-FREEDOM ANALYSIS

For comparison bent ABCD is assumed to have only one degree of freedom. The idealized structure would consist of an equivalent mass M', supported on a cantilever column. The equivalent mass is made up of the mass of the horizontal member BC and the mass of some portion of the legs, taken for example as 1/3 in Ref. 6.

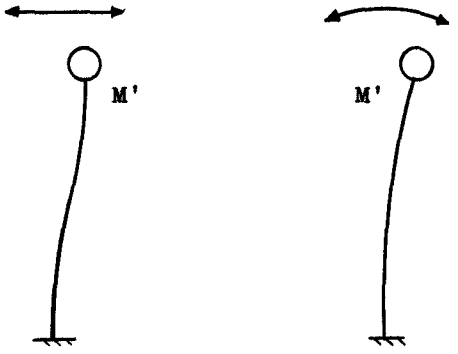

(a) In-Plane Vibration (b) Out-of-Plane Vibration

Figure 16 Bent ABCD Idealized as a Single-Degree-of-Freedom System in Each Plane

If, for in-plane vibration, the equivalent mass be restrained from rotation, the computed natural frequency is 8.87 cps compared to the frequency of 7.45 cps from Table 3, or 19% high.

For out-of-plane vibration both translation and rotation are allowed. This idealization would result in a computed natural frequency of 4.42 cps compared to 4.66 cps from Table 3, or 5% low. Of course no other frequencies can be computed from a single-degree-of-freedom system.

CONCLUSIONS

By the use of a lumped-mass system to describe a structure subjected to wave forces we may (1) apply wave forces of any magnitude, direction, and elevation directly to any part of the structure on which they act, (2) find all resonant frequencies in the range of the waves expected at the site, and (3) compute complete information on deflections, rotations, moments, and shears at all parts of the structure, even at resonance.

Use of the more rigorous analysis presented in this paper removes the three limitations imposed by the single-degree-of-freedom idealization: (1) that wave forces cannot be applied directly to the supporting piles, (2) only one resonant frequency can be obtained, and (3) its accuracy depends on an estimated equivalent mass.

REFERENCES

1. Bisplinghoff, R.L., H. Ashley, and R.L. Halfman, Aeroelasticity. Addison-Wesley Publishing Co, Inc., Reading, Massachusetts, 1955: 860 p.

2. Fraeijs de Veubeke, B.M. Influence of internal damping on aircraft resonance. Manual on Aeroelasticity, v.1, ch.3, North Atlantic Treaty Organization Advisory Group for Aeronautical Research and Development. 1961: 38p.

3. Gaither, W.S. Dynamic analysis of pile-supported offshore structures. Ph.D. Dissertation, Department of Civil Engineering, Princeton University. (Expected date of publication, August, 1964)

4. Harleman, D.R.F., W.C. Nolan, and V.C. Honsinger. Dynamic analysis of offshore structures. Proceedings of VIII Conference on Coastal Engineering, Mexico City. Council on Wave Research, Richmond Field Station, Richmond, California, 1962.

5. Harleman, D.R.F. and R.G. Dean. Interaction of structures and waves. Estuary and Coastline Hydrodynamics, ch.H. Massachusetts Institute of Technology. 33p.

6. Howe, R.J. The design of offshore drilling structures. Publication No. 8, Tech. Services Div., Shell Oil Co., Houston, Texas, 1954: 49p.

7. Lanczos, C. Applied analysis. Prentice-Hall, Inc., Englewood Cliffs, New Jersey, 1956: 539p.

8. Pestel, E.C., and F.A. Leckie. Matrix methods in elastomechanics. McGraw-Hill Book Co., Inc., New York, 1963: 435p.

9. Thompson, W.T. Mechanical vibrations. Prentice-Hall, Inc., Englewood Cliffs, New Jersey, 1953: 252p.

Chapter 30

DUTCH AND FLORIDA PRACTICES ON REVETMENT DESIGN

F. Gerritsen and P. Bruun
Rijkswaterstaat, Holland and University of Florida

INTRODUCTION

In this paper the authors discuss Dutch and Florida practices on revetment design. Instead of presenting two different papers they have preferred to prepare one paper in which basic principles and techniques are emphasized.

DESIGN CRITERIA FOR SEASHORE REVETMENTS

In designing revetments the following factors should be considered:

THE EROSION SITUATION AND THE NEED FOR ARTIFICIAL NOURISHMENT

Before a revetment is to be built the stability conditions of the beach or shore should be carefully evaluated. In some instances the shoreline may be subject to strong periodic variations making it advisable to build the revetment at a certain safe distance from the water line. In other cases, measures against erosion such as groins and artificial nourishment may be necessary before the construction of a revetment is started or in conjunction herewith.

In considering shoreline stability it should be realized that this stability is of dynamic nature. A beach or shore may be stable and still show important seasonal or periodic variations; for this reason the period over which shoreline behavior is studied before the construction of a revetment should be long enough to obtain proper conclusions. A misevaluation of the situation may lead to high cost of repair or even the necessity of complete abandonment of the revetment (1).

In order to arrive at proper data, the area of study should be large enough to determine cyclic coastal processes and to study the influence on the area for which a revetment is considered.

If the pertinent area appears to be subject to gradual erosion, artificial nourishment should be considered. In the last decades experiences on a number of artificial nourishment projects in the United States have shown that this method can be very successful provided the project is carried out with the necessary preparation and know how.

If artificial nourishment is not economically or technically feasible, other measures such as the construction of certain types of groins or - in special cases - the building of a jetty may be justified, but only after a very thorough study of the consequences of such works.

When residential sections or other valuable property are to be protected the revetment may have to be located where it provides the required protection. Situations may occur where occasional bank or dune erosion is restored by natural processes; in such cases the building of a revetment may not be necessary or it should be postponed.

OFFSHORE BEACH PROFILE

In connection with the above section, offshore beach profiles may be indicative of the type of coastal processes that are at stake. In this respect, we may distinguish between sufficiently nourished, undernourished and overnourished offshore profiles(2).

One should particularly be careful if a deep trough is continuously found between the beach and the offshore bar. In this trough, high velocities may occur occasionally thereby adversely affecting beach stability by rapid shoreline fluctuations.

SOIL CONDITIONS

Soil conditions of the beach and foreshore affect littoral drift processes. For the proper choice of material for artificial nourishment, average grain size and grain size distribution of the sand are important.

The permeability (k-value) and the silt content of the soil determine soil condition of the bank or dune. The latter are of importance for the technical design of the structure.

A high degree of permeability facilitates elimination of differences in pore water pressure and is, therefore, beneficial to a high degree of soil stability.

The presence of silt particles reduces the permeability. Thin, horizontal layers of clay prevent water flow in vertical direction. They may, therefore, have an adverse influence on revetment stability.

DESIGN WATER LEVEL

It is a well known fact that during storm and hurricane conditions the water table along the coast line may rise to a level, that is considerably higher than ordinary spring tide conditions.

The problem of extreme high tides has been subject of thorough studies, both in the United States and in Western Europe. The results of these studies can be used as a basis for the design.

A few characteristics may be mentioned here:

The analysis of the height of storm tides on a frequency basis was developed in the Netherlands in 1939 by P. J. Wemelsfelder (3). He showed that for the open Dutch sea coast high tide data plotted in a cumulative frequency diagram presented a linear relationship if a semi-logarithmic diagram was used. Recent studies on Dutch conditions by Wemelsfelder and others (4) have confirmed the applicability of Wemelsfelder's original idea. Although slightly different diagrams were obtained in case all high tide data or a selected group (e.g. associated with dangerous storms) was used the original conception remained the same.

In studying storm tides in Florida (5), it was found that such single linearity for all data could not always be maintained. It appeared that for

the Florida coast high tide data associated with tropical storms (hurricanes) and those associated with regular storms followed different frequency distributions. Treatment of the data was based on the hypothesis that the two groups of data are homogeneous in themselves but nonhomogeneous with respect to one another.

Fig. 1 shows a few selected frequency curves for tide elevations on Florida's East Coast in which the above mentioned characteristics are shown.

The level that is to be selected for the design of a revetment not only depends on the characteristics of the frequency diagram but also on the value of the property that is to be projected.

If large areas of valuable low lying lands are involved design criteria must respect that.

Certain seawalls on the Dutch North Sea coast may be seen as an example of this.

In Holland the Delta dikes are based on a design water level whereby the probability that such level is equaled or exceeded amounts to 1% per century.

Determination of the proper design level is an economic decision problem; an insight into this can be obtained by considering the variation in the coast on costruction and damage (maintenance) that may be expected with an assumed design level. Reference is made to (4) and (5).

The higher the value of the area to be protected, the higher the design water level that is to be chosen as a basis for revetment design.

DESIGN WAVE

The design wave is strongly dependent upon the design water level that has been chosen. The height of the water table and the type of wave conditions constitute two essential boundary conditions for revetment design.

Sometimes one is fortunate enough to have measured wave data in the vicinity of the study area. If the period of wave observation is long enough analysis of the data will provide broad information on wave characteristics from which the design wave can be derived. One should be sure, however, that wave data during storms or hurricanes is included in the recording so as to draw the right conclusions.

Usually it will also be required to consider the changes in wave characteristics that take place during the passage of the waves from the observation post to shore.

Particularly if large shoal areas are to be passed wave height and wave period may be reduced considerably, whereby the height of the tide may play a decisive role.

With respect to wave direction, wave refraction should be considered.

In other instances wave data of the required degree of accuracy may not be available from observations. In such case, computations have to be made

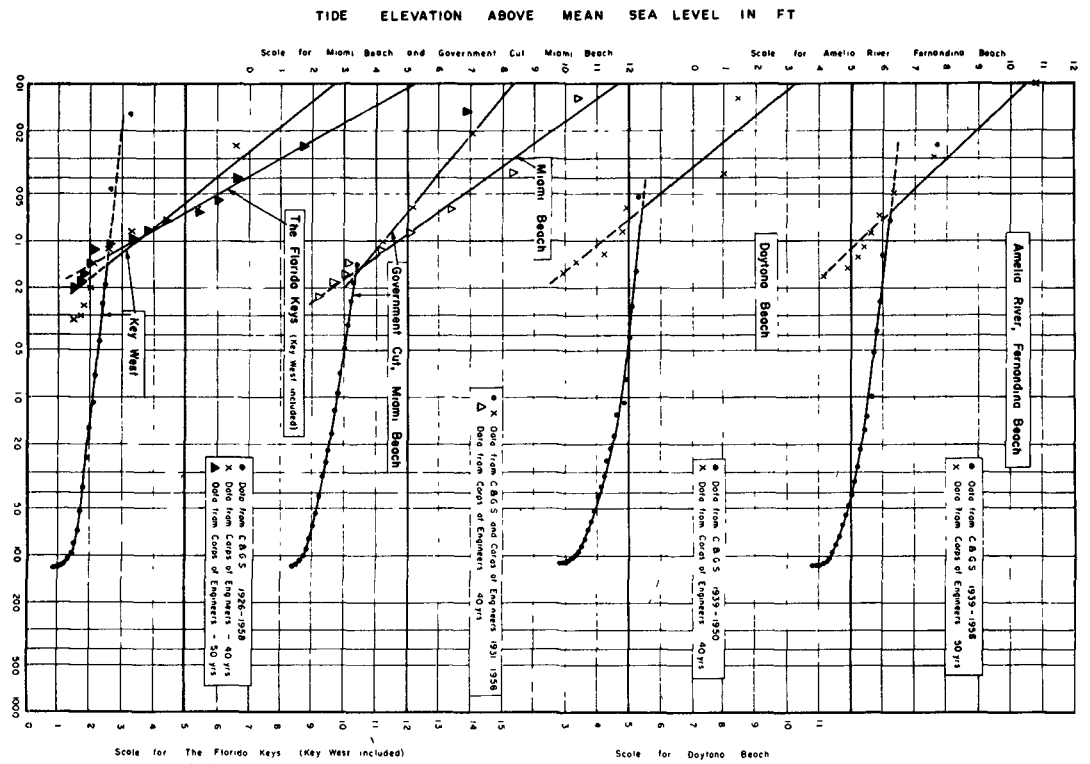

FIG. 1. SELECTED FREQUENCY CURVES FOR FLORIDA'S EAST COAST

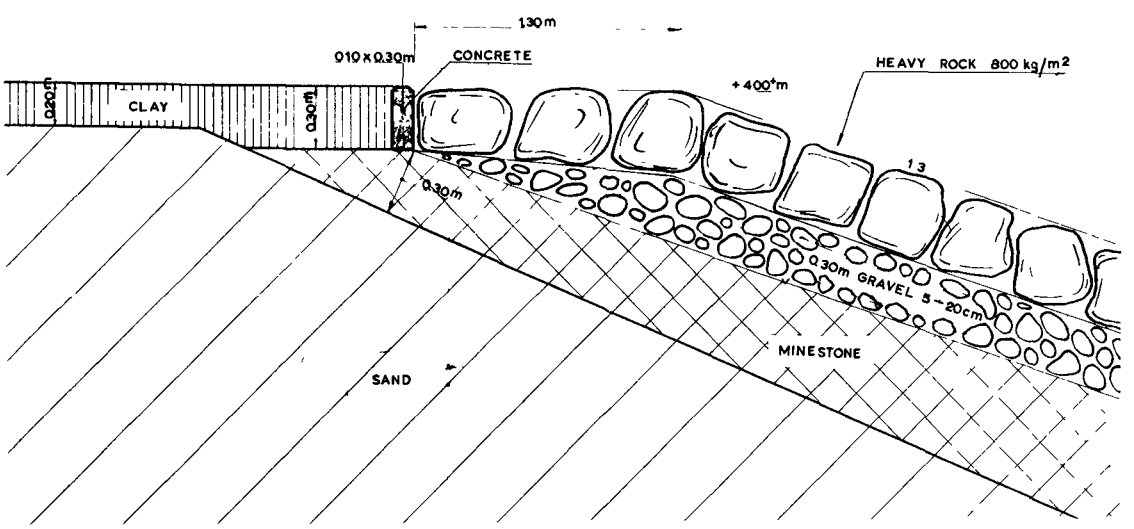

FIG. 2. ROCK REVETMENT WITH FILTER LAYERS OF GRAVEL AND MINESTONE

based on wind and tide data. Reference is made to the studies of Bretschneider (6) and Wilson (7).

For practical design purposes wave analyses can be limited to determining a certain maximum design wave height and period where the wave height is a function of the offshore bottom geometry and deep water wave characteristics. Overtopping may be permitted with a minor frequency only.

Weather observations or computations provide wave data. In both cases, the influence of foreshore configuration on wave characteristics may be considerable, so that approaching waves change direction and may be significantly reduced or increased in height.

WAVE ATTACK, WAVE UPRUSH AND WAVE REFLECTION

Water level and design wave conditions will determine the type of revetment heavy, medium or light - that will be required. From model experiments we may conclude that wave attack is usually heaviest on that part of the slope that lies just below the (average) water table. We cannot exclusively determine, however, what type of blocks (weight, shape) will be required on various parts of the slope: there is still no well established relationship between the characteristics of the waves and the type of construction to be preferred. Conclusions on the type of construction will remain difficult, also in the future, because the strength of a revetment also depends on accuracy of construction, deviations in size of stone or block, width of joints, type of filter, etc

In a few cases, e.g. for asphalt revetment a theoretical evaluation of revetment dimension, in view of given wave condition, is possible (8).

Numerous hydraulic experiments have been carried out on revetments, particularly on wave uprush both in the U.S.A. and in Europe, in later years also in Japan. It has been shown that wave uprush can be reduced by decreasing the outer slope of the revetment, by increasing its permeability or roughness (e.g. by roughness elements of various types) or by the use of a berm. The berm may be gently sloping towards the sea or it may be carried out as a stilling basin sloping towards the backland or backslope. Reference is made to work by Bruun (9) to the studies of the Delft Hydraulics Laboratory (10) and of the Beach Erosion Board (11).

Measures that limit wave uprush usually also limit wave reflection: the smaller the value of the outer slope and the higher the permeability, the lesser also the wave reflection. Heavy backrush may have an adverse influence on the beach in front of the wall and it has been found that roughness elements may be beneficial in limiting erosion at the toe.

On a seashore, economy may often call for simplicity rather than for top performance hydraulically speaking. Complicated block geometry increases costs of manufacturing and placings of blocks. Uprush and backwash may be reduced somewhat but it is cheaper to build the revetment a little higher or to reduce the slope slightly.

If the revetment is not high enough wave uprush may cause overtopping. This may be very dangerous; besides scour and accompanying loss of stability may occur due to saturation of the soil. To prevent this a wave screen may be

helpful for certain conditions. Adequate drainage of the soil behind the revetment is, therefore, indispensable.

HYDRAULIC PRESSURES UNDERNEATH IMPERMEABLE REVETMENTS

Impermeable revetments such as asphalt revetments or bitumen grouted stor pitchings may be subject to hydraulic pressure forces. They are a major factc in the design. During high storm tides of long duration water may enter into the soil behind the revetment and due to a phase difference in water pressure outside and inside the revetment hydraulic pressures may be exerted from withi on the structure. In various cases these forces have been a source of failure and it is, therefore, very essential that these pressure differences be known. Permeability variations in the subsoil and possibly in a pervious toe construc tion will change the magnitude of the lifting forces so that for a good desigr a relatively large number of computations has to be carried out.

For this type of computations an electric analog computer of rather simpl construction can be used (12). It is based on the similarity between Darcy's law (ground water) and Ohm's law (electricity). It consists of a plate conduc in the shape of the dike or seawall. The water storage capacity of the ground is simulated by electric capacitors.

Electric tensions simulate the piesometric level underneath the revetment

DUTCH PRACTICE

Two main types of revetments can be distinguished: permeable and impermea ones.

The permeable types have an "open" surface whereby water may flow into an out of the structure. The impermeable types prevent water to flow through the structure, so that hydraulic pressures may build up behind it. Such pressure forces are important factors in the design.

The permeable types require one or more layers of filter material to reta the soil particles. The filter should be open enough to eliminate hydraulic pressure differences and at the same time dense enough to prevent soil particl from being washed out.

Regarding the permeable or open revetments the following principal types can be considered:

Open filter revetments

Stone pitching

Concrete block revetments

Copper-slag block revetments

Concerning the impermeable types we will distinguish:

Bitumen grouted stone, block or slab revetments

Asphalt revetments

OPEN FILTER REVETMENT

The open filter revetment consists of a few layers of filter material of different size covered by one or more layers of rock or rubble.

Filter characteristics are determined by the fineness of the subsoil on one hand and by the wave forces on the structure on the other hand.

The weight of the individual rock or rubble, forming the top layer has to be in accordance with wave forces to be expected.

From the top layer downward the size and distribution of stone, gravel or sand of various filter layers may rapidly decrease. The requirements of stability are that finer particles do not move into the zones of the bigger ones.

In designing such filters advantage can be taken from filter requirements that are being used for water supply system (13), for which the following general criteria hold:

(a) The material used for the filter must be more pervious than the material of the subsoil in order to avoid excessive hydraulic pressures.

(b) The volume of pores of the filter material must be sufficiently small in order to prevent soil particles to penetrate into and stop up the filter layers.

(c) The thickness of the layer must be big enough to ascertain an adequate grain size distribution across the layer.

Design criteria for filter revetments can never be fully the same; however, a basic indication on the size of the stones or particular on the successive layers may be obtained.

In particular the third requirement will usually not hold for the top layer of heavier stones.

In areas exposed to limited wave action such filter construction may exis of a layer of 6" sand gravel 0.5 - 5 mm, on which a 14" layer gravel 30 - 80 m and covered by basalt rock of 10 - 80 lbs to the amount of 750 lbs per square feet.

Another example of such construction is the use of mine stone (waste material from mines) as filter material (Fig. 2). This structure located in an estuary is exposed to light to heavy waves. The top layer consists of basalt rock of 160 - 400 lbs.

It is interesting to compared Dutch filter revetmentswith similar structures such as applied in Florida.

The basic principles of design are the same. In some Florida structures one or more filter layers have been replaced by synthetic filter sheets.

The weight of the individual blocks of the top layer should be in accordance with wave forces to be expected.

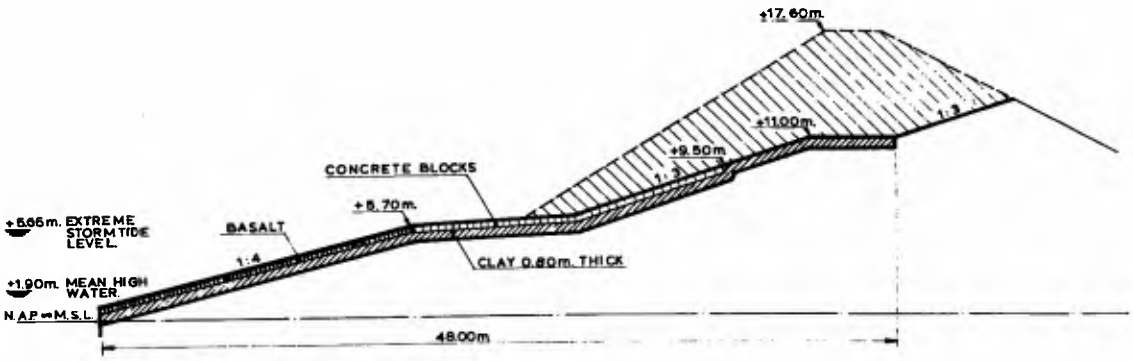

FIG. 3. REVETMENT AT ZOUTELANDE

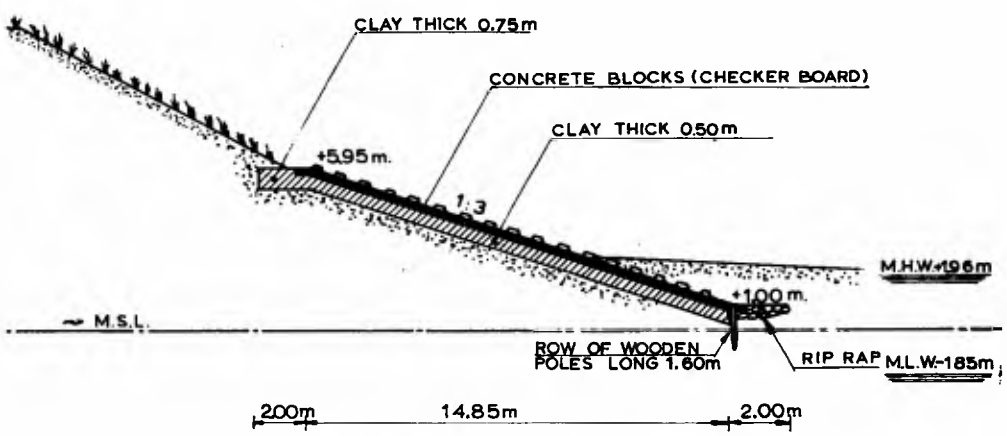

FIG. 4. REVETMENT AT BRESKENS (ZEELAND)

This can be determined by computation or by hydraulic model experiments (16), (17).

STONE PITCHING

Revetments of natural stone have been successfully used in the Netherlands for centuries. A very traditional type is the basalt prism revetment placed on a filter construction. The latter may consist of two layers of brick (on flat side) and a layer of crushed stone or brick. Another filter consists of a layer of crushed brick, well packed, on a straw mat, fixed to the soil. The filter layer also serves to even out differences in length of the individual pieces of rock. In earlier constructions light weight rock has sometimes been used.

An 18" - 24" basalt rock stone pitching forms a very strong revetment which can resist heavy wave action. Small stones are sometimes keyed in between the prisms in order to increase strength of the construction.

Fig. 3 shows a cross section of a recently renewed seawall at Zoutelande in the province of Zeeland. The lower part of this seawall consists of a basalt prism revetment, whereas in the upper part concrete blocks have been used.

In older constructions rows of vertical poles were sometimes erected in the upper part of the slope to act as wave screen and reduce uprush. Such constructions required a great deal of maintenance whereas the efficiency of such devices appeared questionable.

In a number of cases stones of larger size have been used. Compared to a basalt rock stone pitching of the same thickness the use of larger blocks does not seem advantageous since due to the larger surface area hydraulic lifting forces are greater and damage may occur easier. Here the use of a filter between the blocks and the soil is also essential to prevent wash out of soil particles.

CONCRETE BLOCK REVETMENTS

Due to shortage of skilled labor and difficulties with respect to rock supply, stone pitching revetments became too expensive.

At the same time quality of concrete blocks was gradually improving due to improvements in the manufacturing process so that at present concrete blocks of various size and shape are satisfactorily used in coastal protection for a variety of conditions.

The various types are:

(a) rectangular blocks

(b) prismatic blocks

(c) interlocking blocks of different design

(d) blocks with roughness elements of different shape

The strength of a concrete block revetment is considerably increased if a system of interlocking is applied.

Besides the condition that individual blocks cannot easily be lifted from the construction, the shape of the joint also protects the underlying soil or filter from washing out.

In a certain instances concrete blocks have been placed on a layer of clay, without a filter (Fig. 3). This system requires accurate setting and precise dimensions of the blocks so that washout of clay particles through the joints does not occur. If such revetment is frequently attacked by waves, some washout from underneath the blocks may be experienced.

Chances for washout of particles from underneath the blocks are considerably smaller if an adequate filter is used between the blocks and the soil. For this a layer of 5 - 10 mm gravel of, for example, 6" - 8" thickness can be used; the size of the gravel should be small enough to prevent washout of soil particles from underneath and large enough not to pass through the joints between the blocks.

A somewhat larger type of gravel can be used if a synthetic cloth such as Filter-X is placed between the gravel and the sand, permitting that the thickness of the filter layer be cut down.

At the moment experiments are being carried out with different types of filter. In one of the tests the filter consists of broken shell on a mat of straw or reed. The tests also include the use of synthetic filter sheets.

Roughness elements on the blocks, forming a roughness pattern on the slope are beneficial in reducing wave uprush. Extensive investigations by the Delft Hydraulic Laboratory (10) have shown that reduction in run up may be of the order of 20% as compared to a smooth slope. Most effective in this respect are horizontal continuous beams or sleepers, by which a reduction of up to about 50% may be obtained. In order to be effective as a wave run-up reducing system, roughness elements or sleepers are only required on the upper part of the slope. Such elements may also be effective, however, to reduce backrush and when used on the lower part of the slope can be beneficial to prevent scour of the beach in front of the revetment. An example of this is a recently constructed revetment at Breskens (Zeeland) (Fig. 4).

COPPER SLAG-BLOCK REVETMENT

In a few cases use has been made of copper slag-blocks for revetment construction. These blocks have a high specific weight (ab. 2.5) and demonstrate a great resistance against abrasion due to a special surface treatment with rock-split. They are placed on a filter, similar to concrete blocks and perform successfully.

Combined concrete block-copper slag-block revetment was used at the Lauwerszee-works in the northern part of Holland. Block dimensions are 0.20 x 0.20 x 0.33 m.

Concrete blocks of two different heights are used in the upper part of the slope to create extra roughness.

ASPHALT GROUTED REVETMENTS

Maintenance cost of stone pitching was greatly reduced when it became technically and economically feasible to fill the joints with asphalt bitumen. Experiments on this were started in England (Essex) just before the second world war, where asbestos fibers or sometimes sawdust were used in the compound.

A satisfactory grouting mixture consists of a hot mixture of 15-20% asphalt bitumen 80/100, 8% filler and 77-72% sand. The bitumen content depend on grain size and grain size distribution of the sand which is used.

Similarly asphalt grouting can also be used to fill joints between concrete blocks, whereby the upper half of the sides of the block can be recessed so as to form a wedge-formed pouring joint. In Essex standard practice since 1945 has been to use square blocks 12.5 cm thick and 37.5 cm square (14).

It should be realized that asphalt grouting in the joints may change the character of a revetment from a permeable to an impermeable type. In designir such revetment consideration should be given to the possibility of excessive hydraulic pressures as discussed earlier in this paper. Drains, therefore, may he needed and may be placed at the toe. Fig. 5 shows a revetment designec as a dune protection for the North sea coast near Den Helder (province of North-Holland). The lower part of the construction consists of an asphalt grouted basalt rock pitching. The upper part consists of asphalt. At the toe a protective apron below beach level consists of a fascine mattress weigh with rock.

ASPHALT REVETMENTS

After the second world war, asphalt was to an increasing extent used in hydraulic engineering. In revetment design a great many types of constructio were built and tested, whereby the asphalt revetment developed from the test phase to a highly reliable and economic type of protection. Some of its main characteristics and requirements will be mentioned here. The material most commonly used for asphalt revetments is asphalt concrete; due to a large degr of porosity, the use of sand asphalt in earlier revetment design has been proven less satisfactory particularly below high tide level. Sea water and air penetrating into the pores finally lead to destruction of the material. Furthermore, weeds may grow through asphalt and destroy the material.

A second state in the development showed a (thick) layer of sand asphalt covered by a (thin) layer of asphalt concrete. In the tidal zone this was no completely successful. Hydraulic pressures underneath the protection could freely pass through the layer of porous sand asphalt so that the total pressure differences were to be borne by the non-porous layer of asphalt concrete. This layer often proved to be too thin for such pressure forces so that it was lifted from its base. Another weakness was the growth of algae, etc. on asphalt surfaces in the tidal zone, causing desintegration of the asphalt from the surface downward.

In designing asphalt revetments careful consideration should be given to stability conditions of the asphalt (in various parts of the slope) and of the soil underneath as well.

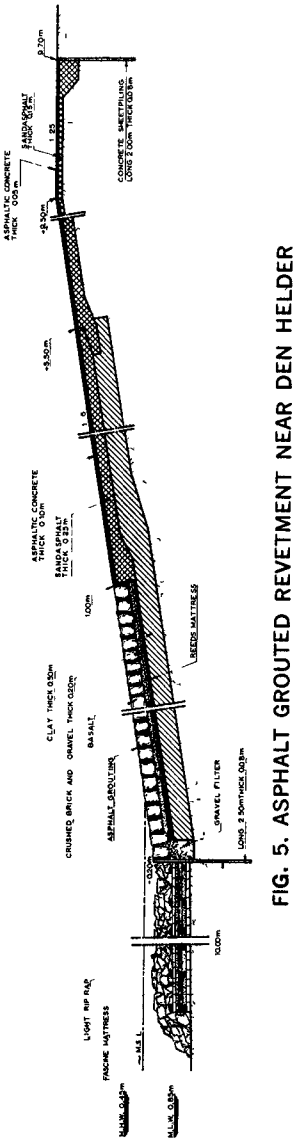

FIG. 5. ASPHALT GROUTED REVETMENT NEAR DEN HELDER

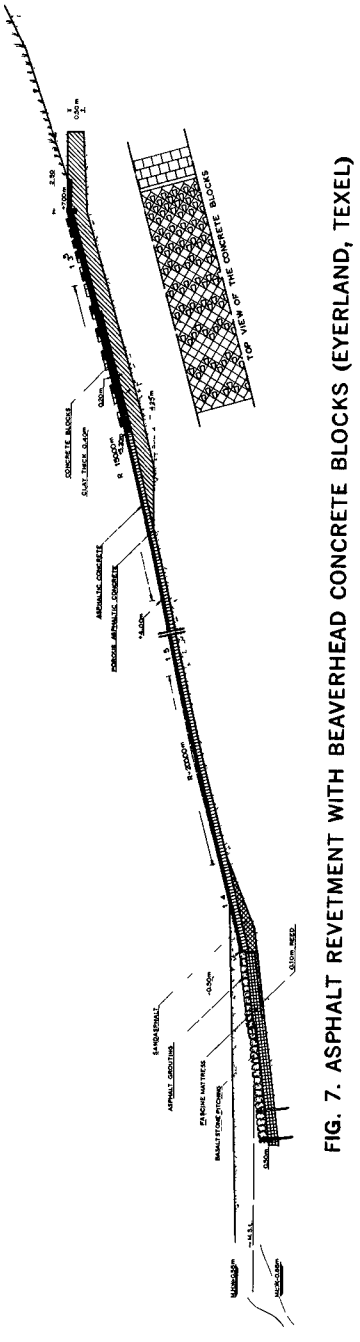

FIG. 7. ASPHALT REVETMENT WITH BEAVERHEAD CONCRETE BLOCKS (EYERLAND, TEXEL)

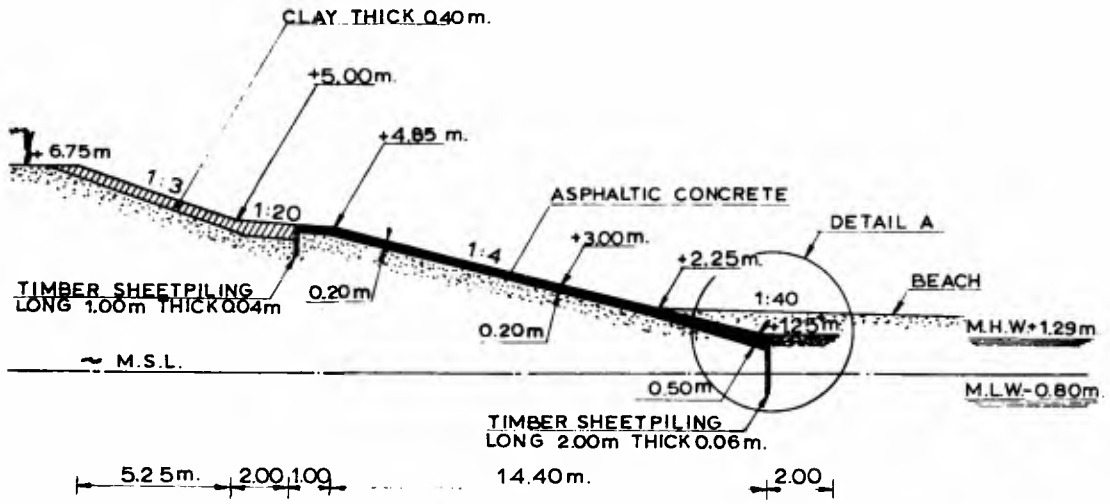

FIG. 6. ASPHALT CONCRETE REVETMENT BUILT IN DELTA AREA

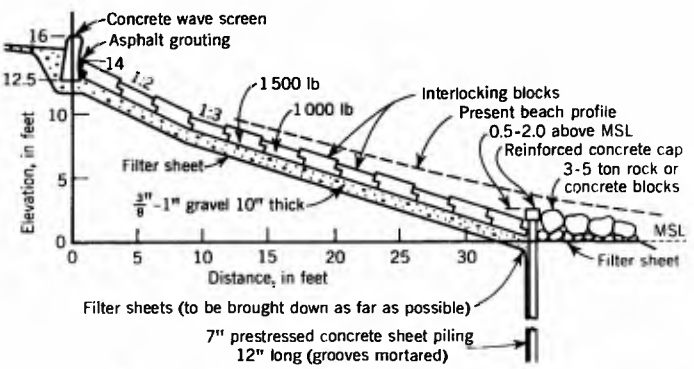

FIG. 9. INTERLOCKING CONCRETE BLOCK ("CHECKER BOARD") REVETMENT, FLA.

FIG. 8. SAND DEPOSITS ON REVETMENT OF FIG. 7 (TEXEL)

At the same time drainage requirements must be carefully evaluated with respect to the type of soil that is to be protected. Two types of asphalt can be used: cold mixtures and hot mixtures. In cold mixtures a "flux" is used to liquefy the mixture; after the flux has evaporated the asphalt becomes solid.

Hot mixtures are obtained in a plant whereby asphalt and aggregates are heated before they are mixed. As a general rule preference is given to the hot asphalt mixture for use in coastal engineering structures. Fig. 6 shows a recently built asphalt revetment in the Delta area. General principles for this design have been the following:

a) The use of asphalt has been limited to elevations above the tidal zone.

b) The asphalt revetment consists of one layer of non-porous asphalt concrete of varying thickness. The mixture consists of:

7% asphalt bitumen 80/100
7% filler
40% graded sand
46% crushed stone (5-15 mm)

The maximum volume of pores is 6%

c) Wave uprush should not destroy the stability of the revetment.

d) The toe consists of a tight wooden sheet piling of 2.00 m length and 0.06 m thickness.

e) A protective apron of light weight rock of about 400 kg/m^2 on polyaethyleen filter cloth secures stability of the toe.

f) A surface treatment is applied consisting of a hot asphalt spray covered by small size gravel.

The asphalt was put on the slope by an automatic device spreading the asphalt in the required thickness on the slope and vibrating it with a special vibrating beam. Fig. 7 shows a revetment on one of the Dutch Wadden Islands. It was constructed on the northern tip of Texel, where erosion of the dunes had been very heavy during a number of years.

The lower part of the revetment consists of an asphalt slope protection; on the upper part concrete blocks, some of them provided with beaverhead shaped roughness elements, have been used.

The pattern of the roughness elements was investigated by hydraulic model tests, so as to find its greatest effectiveness.

The roughness elements proved very successful in working as sand trap for material transported by wind (Fig. 8).

A recently developed asphalt revetment consists of hot asphalt concrete and rock, thoroughly mixed and put on a filter. For the latter a layer of

minestone has been used.

The properties of this type of construction are still being studied. Compared to the asphalt grouted stone revetment, the asphalt rock is cheaper because it contains less bitumen per unit of volume. Other features are a higher permeability and rougher surface. The question of durability is being studied.

AMERICAN PRACTICE WITH SPECIAL REFERENCE TO FLORIDA CONDITIONS

Granite revetments have been built in the United States as rough as well as smooth glacies, but practice has mainly been restricted to areas where granite was easily available as, for example, in the New England States and in the State of California. Granite blocks were carefully placed on gravel filters. Concrete structures of revetment nature, although not always fulfilling the requirement of energy-absorbing ability, are found, for example, in the San Francisco Explanada seawall, in the stepped wall at Corpus Christi, Texas, and in the smooth-faced at Pioneer Point, Maryland. The numerous canal linings and river slope protections in the Mississippi valley are also of revement type. New developments of revetments have taken place in Florida in recent years comprising permeable limestone (local rock) as well as permeable interlocking concrete block designs (15). The former consists of local rock placed on minor rock and gravel which rests on synthetic filter sheets of Poly-Filter X type.

Fig. 9 is cross section of an interlocking block revetment of the type built at Jupiter Island, Fla. All measures refer to this particular location. Figs. 10 and 11 present interesting comparisons between the function of such energy absorbing structure and a vertical wall during a storm situation (March 9-10, 1962). It is clear that the revetment is preserving while the vertical wall is destructive.

This revetment consists of a toe protection of 7 in. reinforced tongue ar groove sheet panels. They are 2½ ft wide and 12 ft long and are capped by reinforced concrete at 0.5 to 2.0 ft above M.S.L. A heavy toe protection of 3-5 t rock (specific weight as high as possible) or of concrete blocks shoul be placed in front resting on filter sheets. If only smaller blocks are avail able, asphalt grouting may be used. Slope protection consists of a 1:3 interlocking block layer, 3' square by 10" thick in two 5" sections with 5" offset on two sides to allow interlocking. In order to provide friction to wave uprush, every second block has a 9" top layer (5" + 4") which increases the total weight from approximately 1,000-1,100 lbs to 1,500-1,600 lbs. These blocks are cast in a continuous pour with no seams. Immediately after the concrete has been poured, a reinforcing rod is placed in the block supported by wooden blocks to be removed later. This allows the dragline hook to be fastened to lift and place the block during construction. Above elevation 10 the slope is 1:2 up to elevation +14' where a concrete wave screen (of varyin design and top elevation) finish the protection upwards. Oversplash behind the wave screen may occur and justifies a gravel filter blanket behind the wave screen. The highest row of blocks is grouted with asphalt where it join the wave screen.

FIG. 10. WAVE ACTION ON VERTICAL (STEEL SHEET PILE) WALL, JUPITER ISLAND, FLA.

FIG. 11. WAVE ACTION ON CHECKER-BOARD REVETMENT, JUPITER ISLAND, FLA.

The interlocking blocks rest on a filter layer consisting of Filter-X with 3/16", 15" steel securing pins provided with our staked "ears" to increase holding power and a ½" diameter metal washer. Overlapping is 8". An 8 to 10" layer of crushed hard rock 3/8-1 in. is placed on the top of the synthetic filter. This filter is carried down behind the toe sheet as deep as practically possible depending upon the permeability of the tongue and groove installation. With double groove panels with proper reliable grouting, this is less important. Florida contractors recommend a minimum depth of 5' below M.S.L. for the filter. Filter sheets are also carried up below and behind the wave screen.

Most important are the returns which often present the weak point of such design. Panels similar to those used for the toe should also be used for the returns. Length of panels may be 12' until halfway up the revetment, then increased to 16' for the remainder of the slope. As a matter of safety against back scours, the returns should be carried well behind the top of the revetment--the actual length depending upon the local situation. The returns should also be lined with filter sheets. The outside of the return should be protected by placing heavy (1-3 t) rubble on filter sheets of the newly invented Poly-Filter X type extending beyond the entire length of the slope. Asphalt grouting and smaller rock may be used too, if necessary.

Under normal conditions, it will be little or no maintenance on such revetment. Minor sinking may occur. During storms damage to toe-protection and return-protection may take place and repairs by replenishments may have to be done. In case breaks should occur in the revetment itself, for example, because a heavy piece of lumber hit the revetment, emergency repairs using filter sheets and rubble are indispensable to avoid that damage spreads to all sides. In a high permeability soil some minor sinking of blocks may take place.

It is obvious that practical and economic considerations will have to be joined in harmony to secure for practical purposes an adequate design. The strongest block is the heaviest and the most expensive one. Special block geometry may decrease uprush height but increase cost of production and construction, etc. So far, the squared checker-board blocks have the advantage of being easy to make and easy to place but uprush height can, needless to say, be decreased by a stepped block. In an estuary boat waves may be important and heavy single wave uprush has to be decreased as much as possible On a seashore, economy may often call for simplicity rather than for top performance hydraulically speaking. The checker-board blocks still seem to have a high grade performance and the best economy but they must be adjusted to meet the local wave and beach situation. Bids on more complex blocks have not justified the use of them as replacement for the squared checker-board block on dune slopes.

REFERENCES

(1) Schijf, J. B. "Generalities on Coastal Processes and Protection", Journal, Waterways and Harbors Division, Proceeding A.S.C.E., March, 1959.

(2) Bruun, P. "Use of Small Scale Experiments with Equilibrium Profiles in Studying Actual Problems and Developing Plans for Coastal Protection' Trans. Amer. Geophys. Union, Vol. 35, No. 3, June, 1954.

(3) Wemelsfelder, P. J. "Wetmatigheden in het optreden van stormvloeden", De Ingenieur, No. 9, 1939.

(4) Report of the Delta Committee. Parts 1 through 6. Final Report and Interim Reports. Staatsdrukkerij- en Uitgeverijbedrijf - 's-Gravenhage, 1960.

(5) Bruun, P.; Chiu, T. Y.; Gerritsen F. and Morgan, W. H. "Storm Tides in Florida as Related to Coastal Topography", Engineering Progress at the University of Florida, Vol. XVI, No. 1, Jan., 1962.

(6) Bretschneider, C. L. "Revision in Wave Forecoasting - Deep and Shallow Water", Coastal Engineering, Council on Wave Research, University of California, Berkeley, Vol. 6, pp 30-67, 1957.

(7) Wilson, B. W. "Deep Water Wave Generations by Moving Wind Systems", Journal, Waterways and Harbors Division, A.S.C.E., New York, Vol. 87, No. WW2, pp. 113-141, May, 1961.

(8) Committee on Impervious Slopes; Progress Report, Rijkswaterstaat, The Netherlands, 1961.

(9) Bruun, P. "Breakwaters for Coastal Protection", XVIIIth Intl. Navigation Congress, Rome, 1953.

(10) Wassing, F. "Model Investigation of Wave Run Up on Dikes Carried Out in the Netherlands During the Past Twenty Years", Coastal Engineering No. VI, Council on Wave Research, University of California, Berkeley, Part IV, pp. 700-714, 1958.

(11) Savage, R. P. "Wave Run Up on Roughned and Permeable Slopes", Proceedings Waterways and Harbors Division, A.S.C.E. New York, Vol. 84, No. WW 3, 38 pp., 1958.

(12) Bischoff van Heemskerck, W. C. "Water Pressures Underneath Asphalt Revetments", Vereniging voor Bitumineuze Werken, The Hague, 1962.

(13) Carlson, E. J. "Gravel Blanket to Prevent Wave Erosion", Journal of the Hydraulics Division, Proceedings, A.S.C.E., Vol. 85, No. HY 5, May 1959.

(14) Asbeck, W. F. van "Bitumen in Hydraulic Engineering," Shell Petroleum Corp. Ltd., London, 1955.

(15) Bruun, P. and Manohar, M. "Coastal Protection for Florida: Development and Design, with Appendix by F. Gerritsen", Engineering Progress at the University of Florida, Vol. XVII, No. 8, August, 1963.

(16) Brandtzaeg, A. "A Simple Mathematical Model of Wave Motion on a Rubble Mound Breakwater Slope", Coastal Engineering No. XIII, Council on Wave Research, University of California, Berkeley, 1963, pp. 444-468.

(17) Hudson, R. Y. "Laboratory Investigations of Rubble Mound Breakwaters", Trans. A.S.C.E., Vol. 126, 1961, Part IV, p. 491.

Chapter 31

WAVE FORCES AGAINST SEA WALL

Masashi Hom-ma and Kiyoshi Horikawa
Department of Civil Engineering, University of Tokyo
Tokyo, Japan

INTRODUCTION

The study concerning the wave forces acting on breakwater has been conducted by numerous scientists and engineers both in field and in laboratory. While few studies have been carried out on the wave forces acting on sea wall which is located inside the surf zone. In this paper are summarized the main results of the experimental studies conducted at the University of Tokyo, Japan, in relation to the subject on the wave forces against a vertical or inclined surface wall located shorewards from the breaking point, and also is proposed an empirical formula of wave pressure distribution on a sea wall on the basis of the experimental data. The computed results obtained by using the above formula are compared with the field data of wave pressure on a vertical wall measured at the Niigata West Coast, Niigata Prefecture, Japan, and also with the experimental data of total wave forces on a vertical wall; the project of the latter is now in progress at the University of Tokyo.

PRESENTATION OF EXPERIMENTAL RESULTS

LABORATORY PROCEDURES

The wave channel which is used for the present studies is 18 m long, 0.6 m high and 0.7 m wide, and a model of sea wall is installed on a gentle uniform slope of 1/15. The face angle of the model is adjustable in a wide range, and six pressure gauges are attached on the surface of model sea wall at different levels to measure simultaneously the time history of pressure working on a sea wall. Fig.1 shows the sensing element of pressure cell which is mainly used for this experiment, and the block diagram of the recording system, by which the fluctuating phenomena of up to 300 cps can be recorded.

PRELIMINARY ANALYSIS

The wave pressure type is generally speaking classified into three, such as the clapotis type, the shock type and the type due to broken waves. Fig.2 shows the classified regions of each wave pressure type mentioned above; the wave steepness ratio in deep water H_o/L_o is taken as the abscissa, and the ratio between the water depth at the foot of vertical sea wall

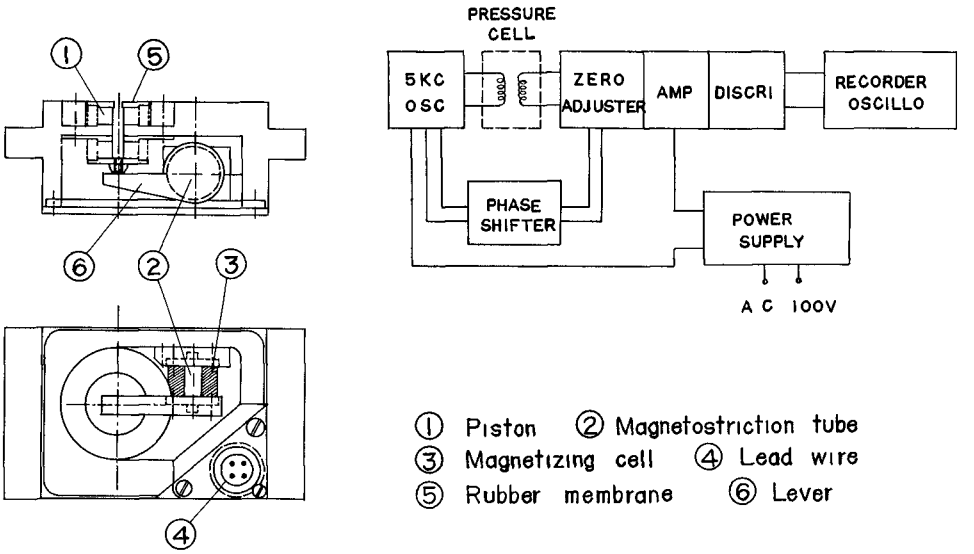

FIG 1 --PRESSURE CELL AND BLOCK DIAGRAM

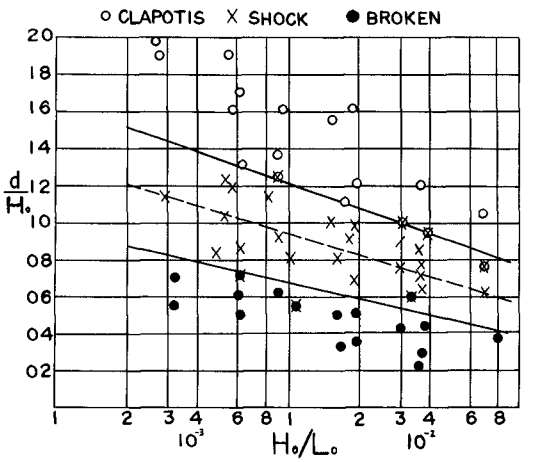

FIG 2 --CLASSIFICATION OF WAVE PRESSURE TYPE

d', and the wave height in deep water H_o as the ordinate after the expression of Rundgren[1] who has taken the case of 1/9.8 beach slope. The authors are mainly concerned with the region of wave pressure due to the broken waves in this paper.

Several samples of wave height reduction of the broken waves as the decrease of water depth is given in Fig.3, from which it is recognized that the average tendency of these data is well expressed by a straight line. The straight line in this figure is introduced from the following assumption; that is, the broken wave holds its critical height determined by the solitary wave theory[2] at each particular water depth. Fig. 4 is the comparison between the hypothetical curves and the field observation data of wave transformation inside the surf zone at the Niigata West Coast obtained by T. Ijima and others[3]. From these results it is indicated that the above assumption is applicable for our present analysis as a first order approximation, hence

$$H = 0.78d \tag{1}$$

where H is the wave height at the depth of water d. As the same rule is shown in Fig.5 the comparison on wave celerity inside the surf zone between the experimental data and the calculated ones by using Eq.(2) which is introduced on the basis of the solitary wave theory combining with Eq.(1)

$$c = \sqrt{g(H + d)} = \sqrt{1.78gd} \tag{2}$$

where c is the wave celerity and g the acceleration of gravity. The agreement is rather good.

PRESSURE DISTRIBUTION ON VERTICAL WALL

According to the careful investigations on the transformation of wave inside the surf zone mentioned above and on the vertical distribution of wave pressure against a vertical sea wall, the following assumptions are introduced:

1) The static pressure works on a vertical wall up to a certain height above still water level h_c, till the bottom of structure.
2) The dynamic pressure distributes simply in a shape of triangle with its maximum pressure intensity at still water level and zero both at the height of h_c above still water level and at bottom.

Fig.6 gives the relationship between the wave pressure intensity at still water level p_1 and the water depth at the foot of sea wall d', while Fig.7 gives the relationship between the additional wave pressure intensity above the static water pressure at the bottom of vertical wall $p_{-d'}$ and d'. By using these data the following Eqs.(3), (4) and (5) are obtained.

$$h_c = 1.2d' \tag{3}$$

$$\begin{aligned} p_1 &= f\rho c^2/2 + \rho gh \\ &= (1.78gd')f\rho/2 + 1.2\rho gd' \\ &= (0.89f + 1.2)\rho gd' \end{aligned} \tag{4}$$

$$f = 1.8 \tag{5}$$

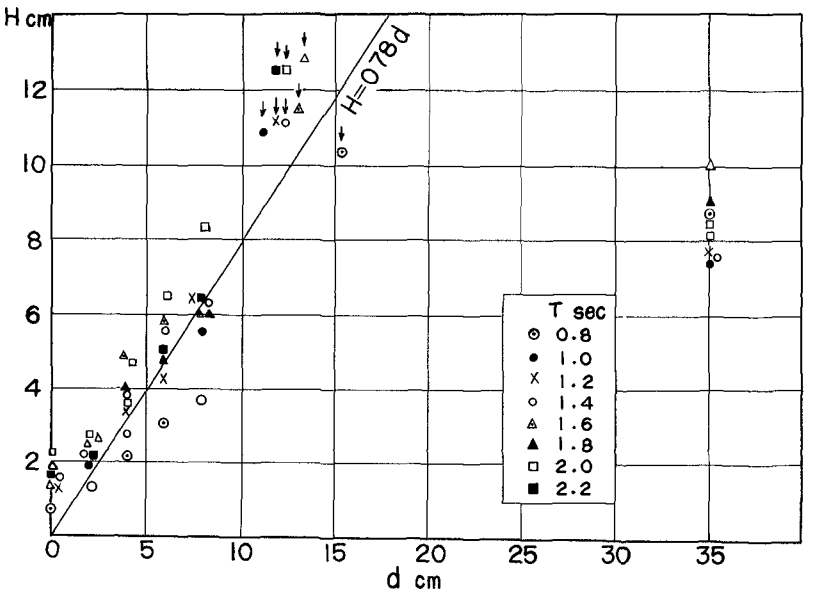

FIG 3 --CHANGE OF WAVE HEIGHT INSIDE SURF ZONE (LABORATORY)

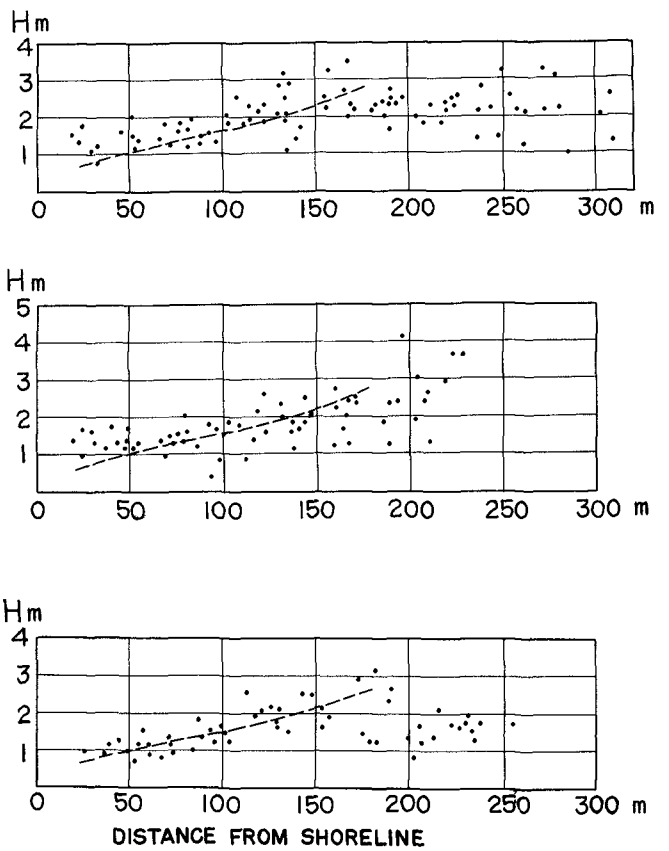

FIG 4 --CHANGE OF WAVE HEIGHT INSIDE SURF ZONE (NIIGATA COAST)

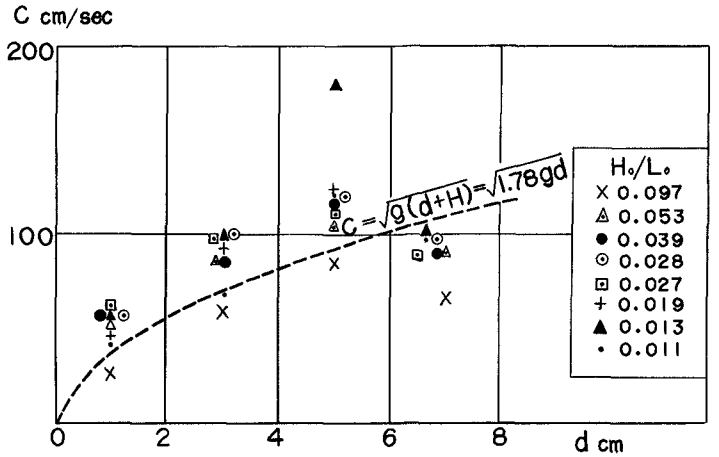

FIG 5 --CHANGE OF WAVE CELERITY INSIDE SURF ZONE (LABORATORY)

FIG 6 --WAVE PRESSURE INTENSITY AT STILL WATER LEVEL

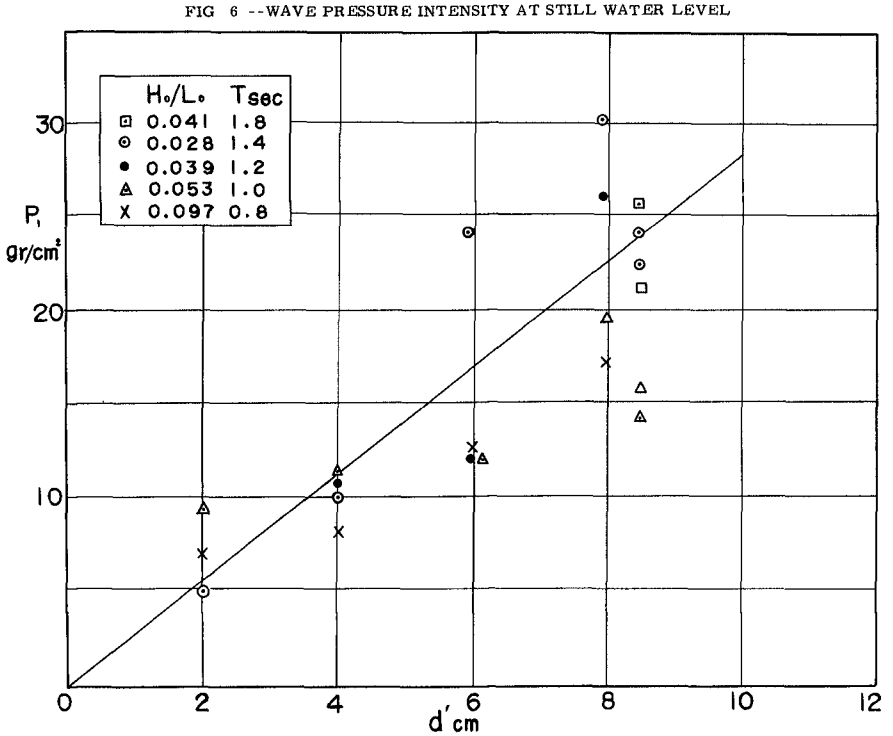

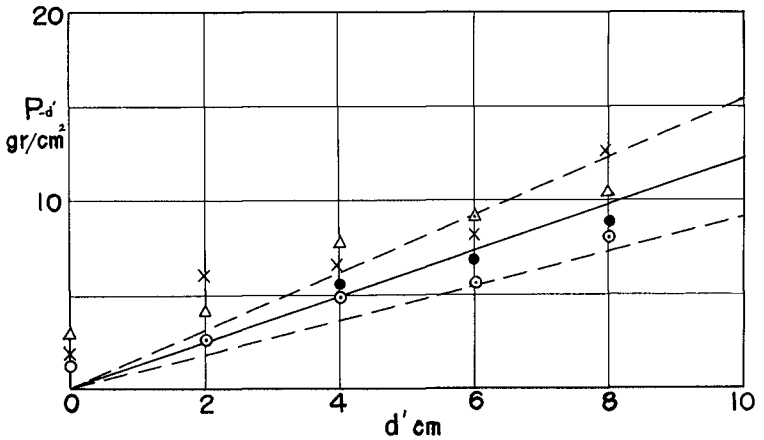

FIG 7 --ADDITIONAL WAVE PRESSURE INTENSITY AT BOTTOM

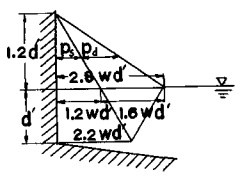

FIG 8

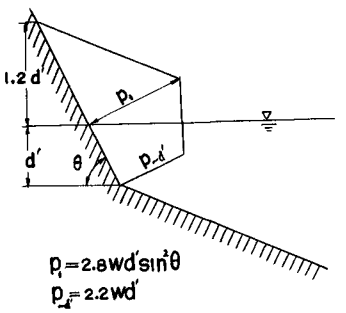

FIG 10

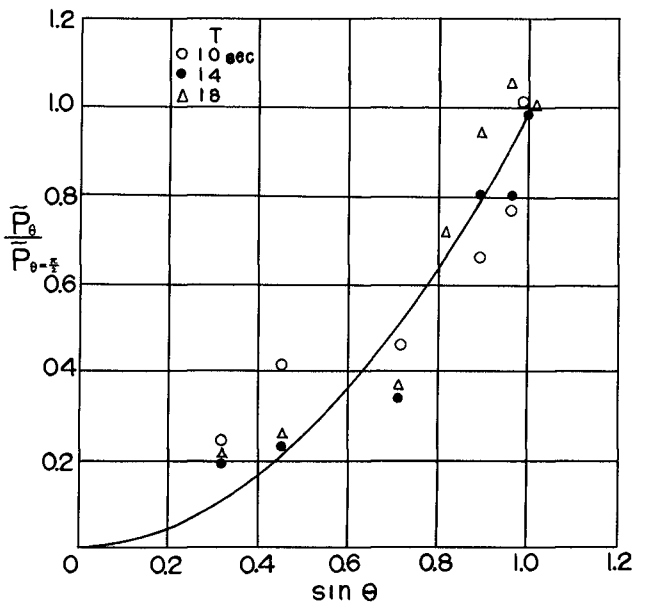

FIG 9 --PRESSURE RATIO AS A FUNCTION OF SLOPE ANGLE

where ρ and g are the density of fluid and the acceleration of gravity respectively. Hence the formula which is applicable for the computation of vertical distribution of wave pressure due to broken waves is expressed as shown in Fig.8.

PRESSURE DISTRIBUTION ON SLOPING WALL

The effect of surface slope angle of sea wall on the intensity of wave pressure is demonstrated in Fig.9, where the ordinate is the ratio of pressure intensity on an inclined slope to that on a vertical wall, $\bar{p}_\theta / \bar{p}_{\theta=\frac{\pi}{2}}$, and the abscissa $\sin\theta$, θ being the angle of slope measured from horizontal plane. The curve shown in this figure is[4),5)]

$$\bar{p}_\theta / \bar{p}_{\theta=\frac{\pi}{2}} = \sin^2\theta \qquad (6)$$

Taking into consideration of the above fact, the previous formula is generalized as shown in Fig.10. Figs.11, 12 and 13 show several examples of the comparison between the experimental data and the calculated curves. The agreement seems to be satisfactory from the engineering point of view. But in the case of very shallow water depth at the foot of structure the discrepancy is large as suggested in Fig.3.

PRESENTATION OF FIELD DATA

TEST PROCEDURES

The field observations of wave pressure against sea wall have been conducted by the engineers at the Niigata Prefectural Government under the instruction of the present authors in order to study the scale effect of model investigations conducted at the University of Tokyo. Fig.14 is a diagram showing the position of three spring type pressure gauges attached on a concrete block which is deposited in front of the actual sea wall; the water depth at the foot of the structure is about 1 m. In a few days during the last winter season the authors attached a sensing element which was almost similar to that in the laboratory instead of the spring type pressure gauge in order to check the characteristics of the two kinds of pressure gauges.

STATISTICAL TREATMENTS

Before extending the discussion about the similarity between the laboratory measurements and the field observation data, we have to consider the way of statistical treatments of the irregularities of wave pressure and wave itself.

The cumulative frequency distribution curves of wave period are shown in Fig.15, from which it may be recognized that the occurrance frequency of the apparent wave period is expressed by the log normal distribution curve. On the other hand the frequency distributions of apparent wave height and wave pressure are well expressed by the Rayleigh distribution curves as

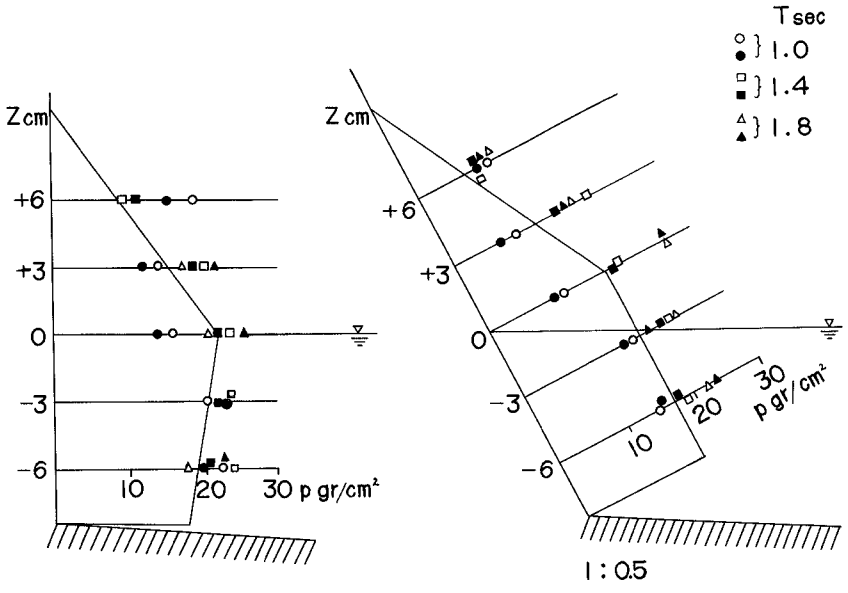
Z cm
+6
+3
0
-3
-6
10
20
30 p gr/cm²
Z cm
+6
+3
0
-3
-6
10
20
30
p gr/cm²
1 : 0.5
T sec
1.0
1.4
1.8

FIG 11

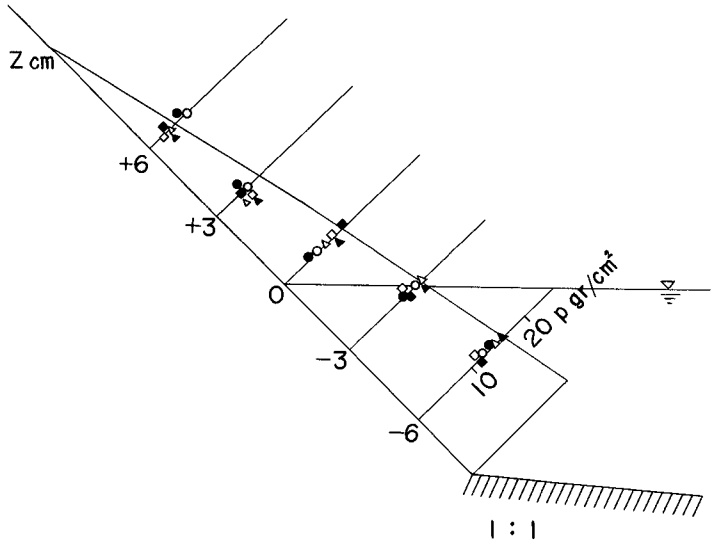
Z cm
+6
+3
0
-3
-6
10
20 p gr/cm²
1 : 1

FIG 12

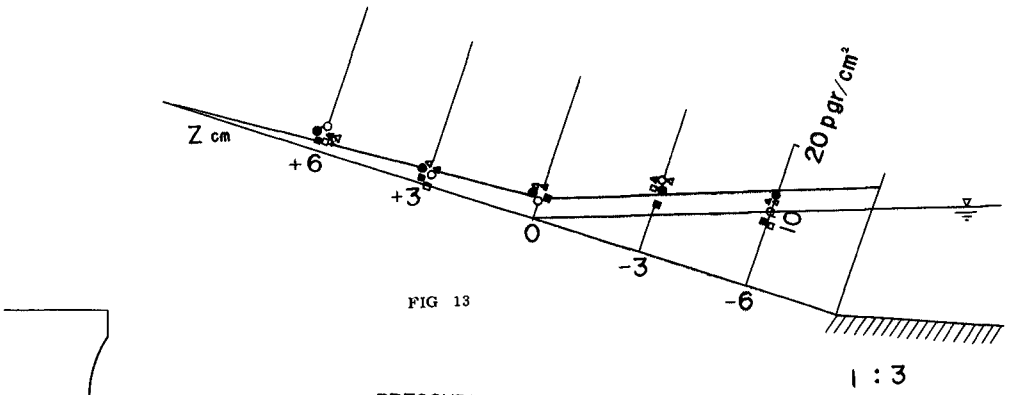

FIG 13

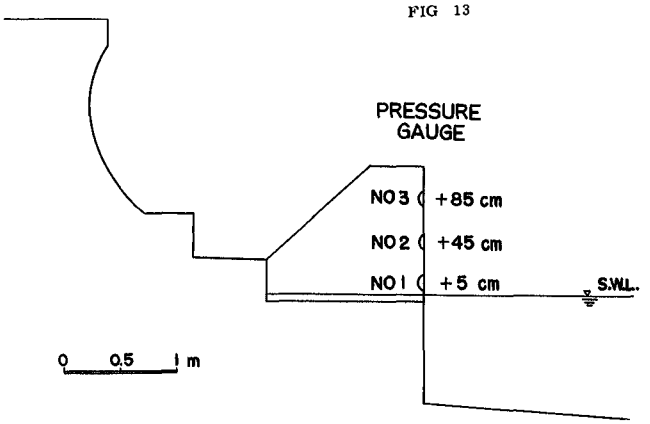

FIG 14 --LOCATION OF WAVE GAUGES (NIIGATA COAST)

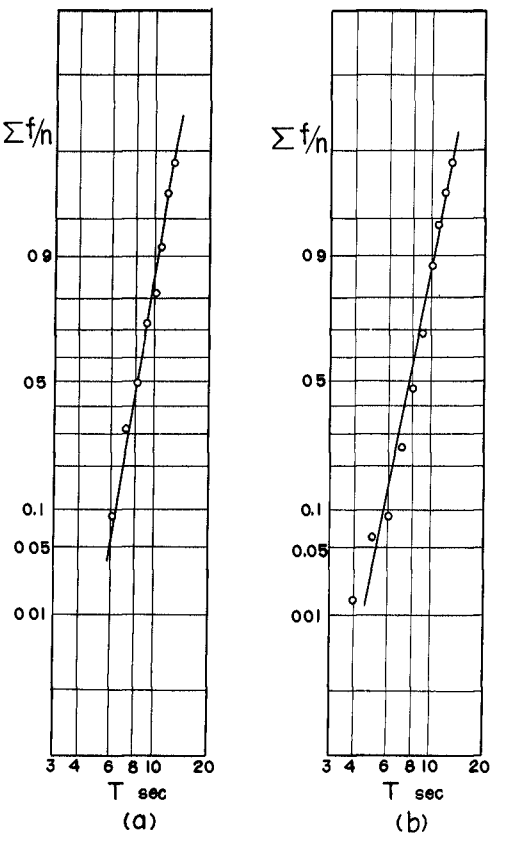

FIG 15 --CUMULATIVE FREQUENCY DISTRIBUTION CURVES OF \
PERIOD

shown in Figs.16, 17, 18 and 19. The data of wave pressure and wave characteristics at 12 m water depth are simultaneously recorded for 10 min at 2 hr interval. Considering the above fact the authors reached the conclusion that the mean values of the highest one third of the samples can be used as a statistical measure of wave characteristics and wave pressure intensity.

ANALYSIS OF DATA

In Fig.20 is given one example of the variation of wave characteristics such as the signigicant wave height $H_{1/3}$ and the significant wave period $T_{1/3}$ and of the statistical values of pressure intensity $p_{1/3}$ recorded by Gauges No.1, 2 and 3 (see Fig.14). By using the available data the relationship between the pressure intensity and wave height is obtained as shown in Fig.21. Unfortunately the wave gauges except No.3 have not working well, hence it seems to be difficult to obtain any comprehensive conclusions. The followings are the tentative ones which should be investigated with care by the further observations in field.

1) The pressure intensity reaches its maximum at certain wave height condition which must be determined by the several factors such as the water depth at the foot of structure and the beach slope in front of the structure. Beyond this wave height, the pressure intensity seems to approach gradually to a certain value. The influence of the wave period on the pressure intensity will be the secondary one. The facts mentioned here have been definitely verified in the laboratory.
2) Comparing the asymptotic values of the wave pressure intensity with the ones estimated by using the empirical formula as shown in Fig.22, we recognize that the both values for p_3 have a satisfactory agreement, but the measured value for p_2 is considerably smaller than the expected one. The main reason of the above discrepancy could be found in the followings; (a) the gauge was not in good order, hence the reliability of this data seems to be poor, and (b) the recording system for the field observation can follow only the relatively low frequency phenomena such as 50 cps because the pen recorder was used.

TOTAL WAVE FORCE MEASUREMENT

TEST PROCEDURES

The authors are now doing another series of experimental studies, the aim of which is to determine the absolute value and the acting point of total wave force against sea wall. In this section the preliminary results of newly established experiment will be reviewed briefly in connection to the previous studies. Fig.23 shows the test procedures; that is, the sensing plate (20 cm wide) is supported by two gauge rings, by

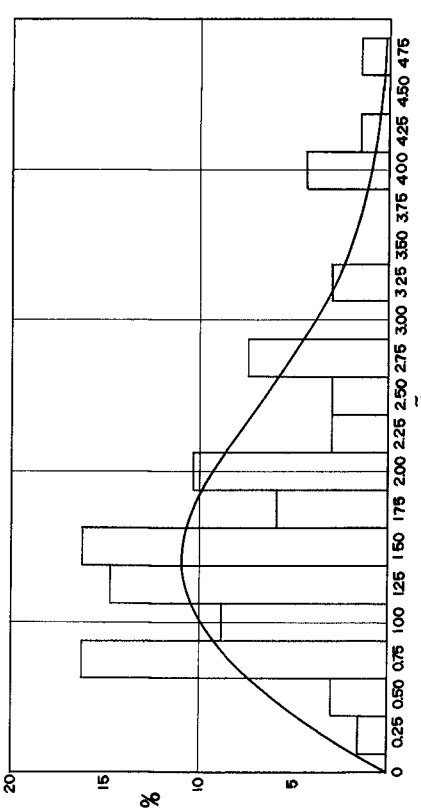

FIG 16 --WAVE HEIGHT DISTRIBUTION

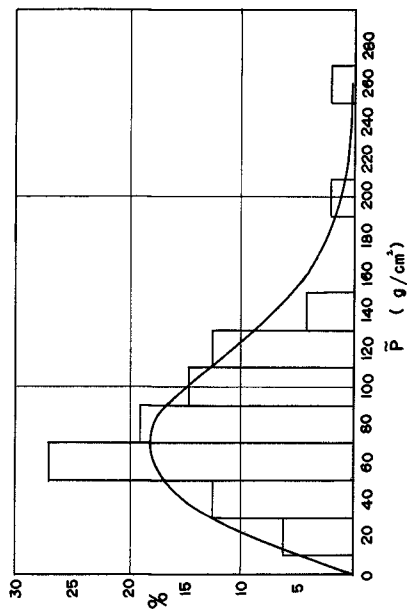

FIG 17 --PRESSURE DISTRIBUTION

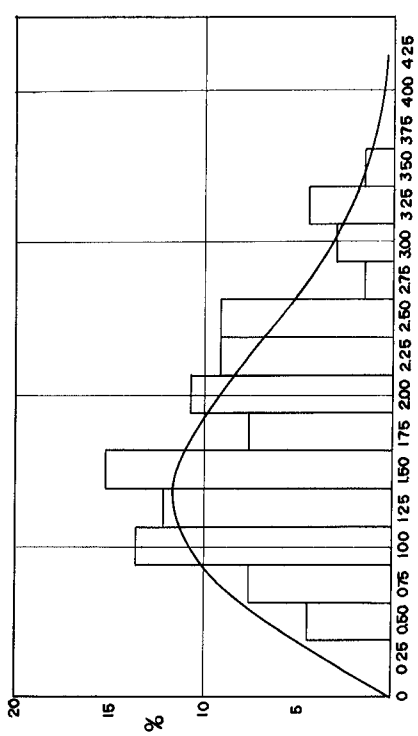

FIG 18 --WAVE HEIGHT DISTRIBUTION

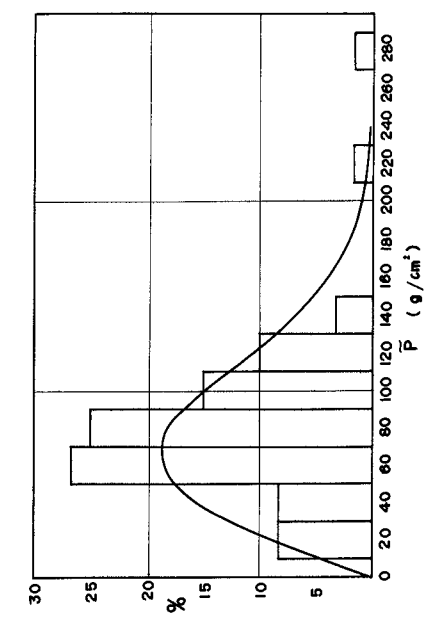

FIG 19 --PRESSURE DISTRIBUTION

Table 1

H cm	T sec	d cm	H /L	d /H	P gr/cm	z * cm	P gr/cm	z * cm
11.9	2.3	6.5	0.015	0.55	125	-2.7	175	-0.8
12.5	2.3		0.015	0.52	119	-2.8		
13.0	2.0		0.021	0.50	196	0.2		
14.0	2.0		0.022	0.47	181	-0.9		
18.3	1.8		0.038	0.36	150	-0.8		
16.3	1.7		0.035	0.40	150	-0.8		
16.1	1.5		0.044	0.40	169	-1.7		
15.9	1.4		0.055	0.41	143	-1.6		
16.7	1.2		0.073	0.39	128	-1.3		
13.8	1.1		0.081	0.47	102	-1.7		
11.6	0.9		0.090	0.56	112	-1.9		

* z, the acting point of total force, is measured upward from still water level.

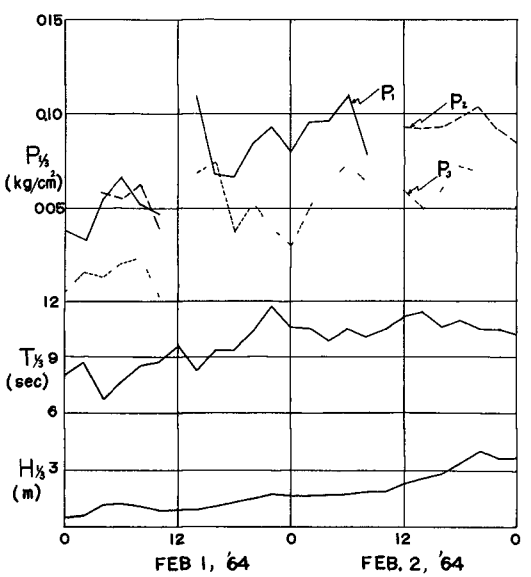

FIG 20 --SAMPLE OF DATA

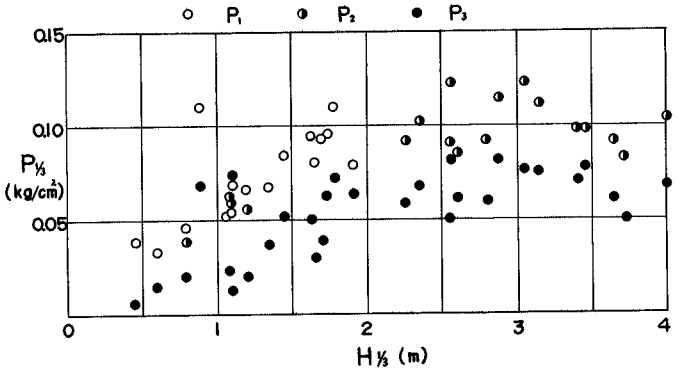

FIG. 21 --PRESSURE VARIATION WITH WAVE HEIGHT

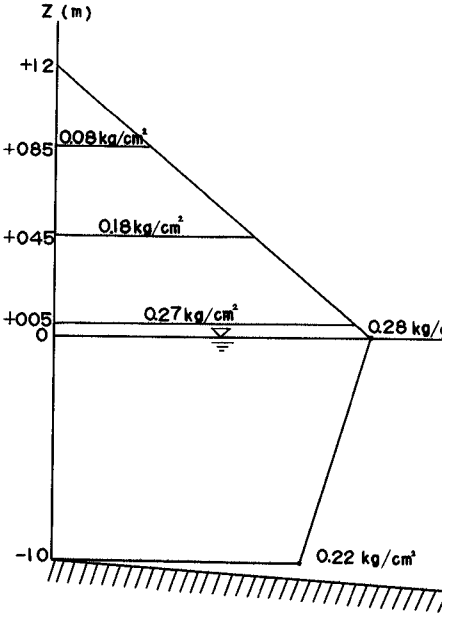

FIG 22 --CALCULATED PRESSURE

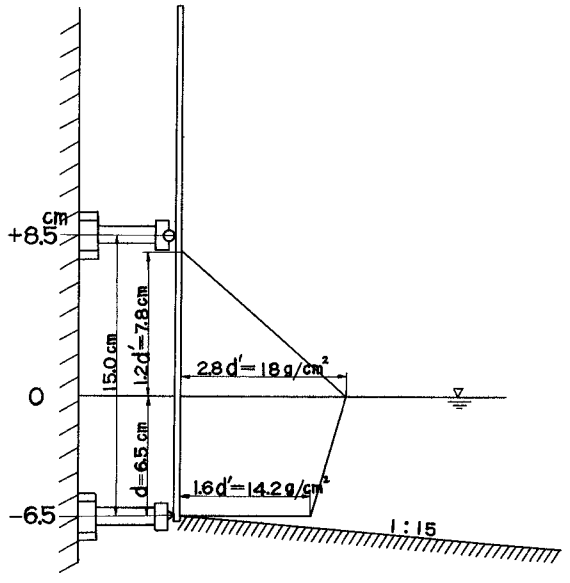

FIG. 23 --TOTAL WAVE FORCE MEASUREMENT

which the fluctuating phenomena of up to 100 cps are measureable.

PRELIMINARY RESULTS

Table 1 gives a part of experimental results, from which it is recognized that the expected conditions of total wave force obtained by using the proposed formula agree fairly well with the measured ones.

ACKNOWLEDGEMENTS

The present studies are partly supported by the scientific research grant of the Ministry of Education, Japan, and also by the research contract between the University of Tokyo and the Niigata Prefectural Government, Japan. In carrying out the series of the present experiments, the authors are indebted to Mr. Naoki Hase, Research Associate of the University of Tokyo, and engineers of the Department of Construction, Niigata Prefecture. The acknowledgement of the authors is also extended to Mr. Shuzo Komori, Graduate Student of the University of Tokyo, who has assisted in the analysis of data and the preparation of the illustrations of this paper.

REFERENCES

1) Rundgren, L. : Water Wave Force, Stockholm, 1958.
2) Munk, W. H. : The Solitary Wave Theory and Its Application to Surf Problems, Ocean Surface Waves, Annals of the New York Academy of Science, Vol.51, Art.3, 1949.
3) Ijima, T., T. Takahashi and K. Nakamura : Wave Characteristics in Surf Zone Observed by Stereophotographic Method, Proc. 3rd Conference on Coastal Engineering in Japan, 1956. (in Japanese)
4) Mitsuyasu, H., N. Hase and A. Shibayama : An Experimental Study of the Pressure of Breaking Waves, Monthly Reports, Transportation Tech. Research Inst., Vol.8, No.2, 1958. (in Japanese)
5) Greslou, L. and J. P. Montaz : Pressure Measurements on an Embankment, Bull. P. I. A. N. C., Vol.III, No.5, 1962.

Chapter 32

INTERLOCKING PRECAST CONCRETE BLOCK SEAWALL

by

Robert A. Jachowski
Chief, Design Branch
U. S. Army Coastal Engineering Research Center
Corps of Engineers, Washington, D. C.

ABSTRACT

As a result of a survey of damage caused by the severe storm of March 1962 which affected the entire east coast of the United States, a new and specially-shaped interlocking concrete block was developed for use in shore protection. This block is designed to be used in a revetment-type seawall that will be both durable and economical as well as reduce wave run-up and overtopping, and scour at its base or toe. A description of model investigations conducted on the interlocking precast concrete block seawall and results therefrom are presented. It is shown that effective shore protection can be designed utilizing these units.

INTRODUCTION

As a result of the severe east coast storm of 5-9 March 1962, a study was made of certain types of structures with a view to low-cost positive means of protecting backshore property from wave action and severe floodin The storm showed that natural features in the form of a wide, high beach berm and a wide belt of sand dunes are the best protection to the backshor area. Rapid increase in population of beach areas has resulted in the leveling of many dune areas by the developers and a loss of this natural protection. In some areas attempts are being made to restore this natural protection by providing wide beach areas by means of artificial beach fill and encouraging the natural rebuilding of the protective dunes by using a system or series of sand fences. In other areas, such as built-up commercial areas along the beach, rebuilding of dunes is virtually impossible because of intensive land development, although wide beaches can be provid by artificial beach fills.

The March 1962 storm also graphically illustrated the limitations of timber bulkheads (as differentiated from seawalls) to withstand the direct forces of severe storm waves. The failure of these bulkheads, which resulted in extensive backshore damage, can be attributed to (1) the loss of the beach fronting the structure which allowed larger waves to break agair the face of the wall and (2) the loss of fill material behind the wall caused by overtopping waves.

For reasons cited above, the need is very apparent for a protective structure which will reduce wave run-up and overtopping, and not induce scour at the seaward toe. During high water stages associated with storms

vertical walls are especially likely to produce conditions which will induce beach scouring. Once this scour has occurred, even ordinary waves break directly against the walls, and the natural rebuilding or accretion of the beach under normal wave and tide conditions is greatly inhibited by the reflected wave. It is well known that a rubble revetment or seawall would be most effective in absorbing wave energy and in reducing wave run-up and overtopping, but this type of structure also introduces a few undesirable features: the first of these is that it limits access to the beach to those areas where suitable stairways across the rough surface of the rubble slope are provided; the second is that it introduces a safety hazard to those people who may cross the rubble slope to the beach and third, it presents an unattractive or non-aesthetic appearance. An interlocking concrete block type of seawall would minimize these undesirable features and was therefore selected for study.

CRITERIA FOR SELECTION OF DESIGN

Primarily, the most important factor of the block design is the interlocking feature, the secondary features are the size and weight of the precast concrete shape. Blocks should be heavy enough, recognizing the interlocking feature, to be stable under design-wave conditions, and yet consideration should be given to the weight for the handling of individual units with small or light crane equipment. Another feature is surface roughness. It is recognized that the greater the surface roughness the greater the reduction in wave run-up, overtopping, backwash and reflection. Other features are those of appearance and utility. The precast concrete wall is more attractive than a rubble slope and provides easy access to the beach anywhere along its length without the need for special ramp areas.

DESIGN CONDITIONS

Basically the interlocking precast concrete block stepped-face seawall is designed in conjunction with a protective beach, the wall being a last line of defense against wave action accompanying severe storm surges. Minor flooding rather than complete destruction of backshore development may occur when protective beach defenses are temporarily eroded away or overtopped. The concrete block seawall as envisioned would extend from the elevation of the crest of the dune seaward on a 1 on 2 slope to mean low water (see Figure 1). The beach fronting the seawall would have to be severely eroded before large storm waves would impinge directly against the seawall. Studies of the March 1962 east coast storm showed that maximum erosion of the beach face (vertical height) could be as great as 8 feet below mean low water for a storm of this magnitude; therefore a cutoff or toe wall is incorporated in the overall design to prevent undermining and failure during severe storms. The sheet pile cutoff wall should extend from the toe of the slope of the wall face to -10 feet MLW as a minimum, or to a greater depth depending on the anticipated depth of scour of the fronting beach during storms in the area where the structure is located. This cutoff wall may be constructed of timber, concrete, or steel sheet piling. Walers and tie backs would be required on the wall in order to prevent its failure from excessive pressure from the backshore side of the wall, that is, the load created by the sand and concrete blocks.

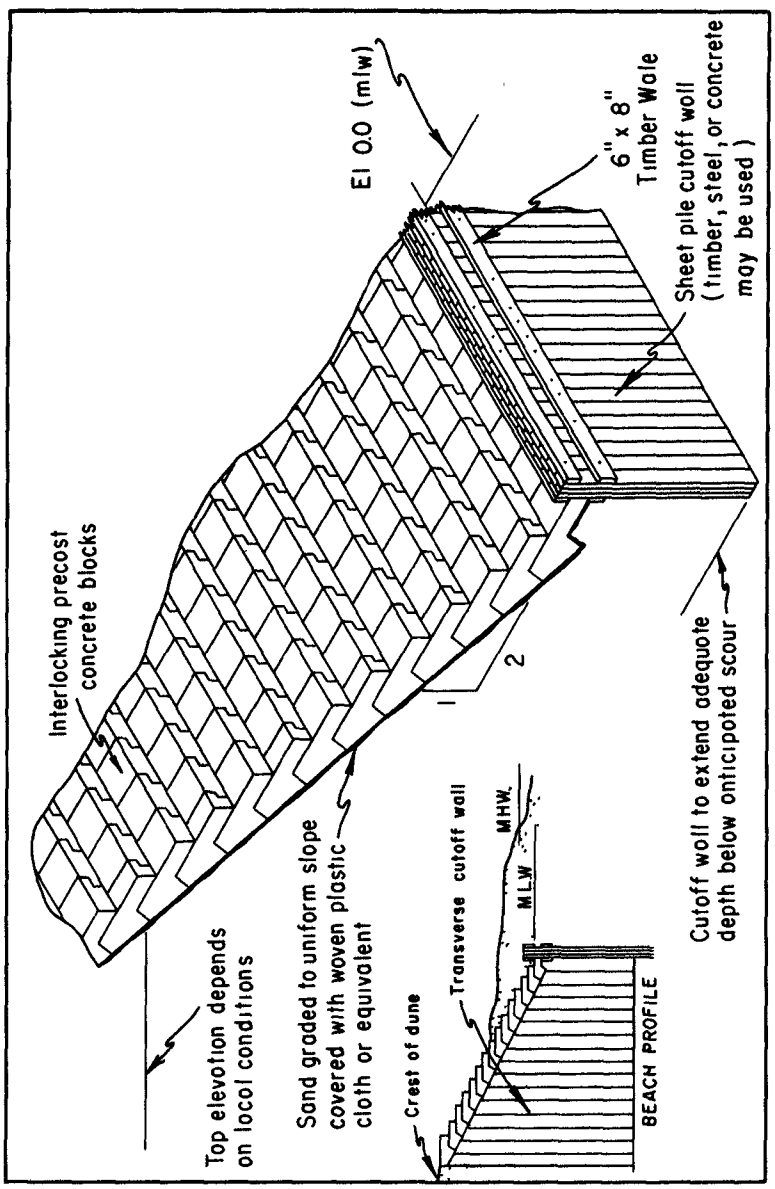

FIGURE 1. STEPPED TYPE INTERLOCKING PRECAST CONCRETE BLOCK SEAWALL

The design wave height (equivalent deep water wave H_o') was selected as 6 feet with a breaking height on the seawall varying from 9.0 to 11.0 feet depending on the wave period and the depth of water immediately seaward.

In any precast concrete block design, consideration of a properly designed underlying filter is of prime importance, for without the filter the sand would be lost through the joints between the blocks. This loss of foundation material can be caused by piping of the sand through the joints due to release of hydrostatic pressures resulting from wave action which in turn can cause undermining and result in failure of the seawall section. One type of filter in use is a plastic (polyvinylidene chloride resin) cloth. This material, woven in a mesh fine enough to be impermeable for sand with average particle diameter of 0.08 mm, has, up to the present, operated satisfactorily as a filter. Properly graded gravel blankets also make satisfactory filters. A combination of the plastic and gravel filter can be used should foundation conditions and hydrostatic pressure relief warrant. Transverse cutoff walls are required to compartment the structure at regular intervals along the shore front thereby minimizing the chance of total failure should one of the compartments become unravelled during sustained damaging wave conditions.

BLOCK DESIGN

The use of interlocking concrete blocks is not a new concept for shore protection. Such blocks have been used extensively both in The Netherlands and England, but only recently has their use obtained any degree of prominence in the United States. Typical blocks, both in Europe and the United States, are generally square slabs with ship-lap type interlocking joints. The types of block considered for this study are shown in Figure 2. Design A, a "waffle" type interlocking block, is designed to lie flat on the surface of the graded slope, and its outer face has alternately raised squares, similar to those on a waffle iron, to provide surface roughness. The joint is of the ship-lap type and provides a mechanical interlock with adjacent blocks. Design B is a step-type inclined-face interlocking block. The name is derived from the fact that after placement the riser face of the step is normal to the slope and thus inclined with the horizontal. The block is interlocked with adjacent blocks by means of ship-lap joints on two sides and by an overlapping projection extending behind the block on which it rests. Design C is a step-type vertical-face block of the same design as the inclined-face block except that the riser face is vertical rather than normal to the slope.

MODEL TESTS

GENERAL

The reaction of waves to a structure and the reaction of the structure to the waves are independent, simultaneously occurring functions to be considered in determining the feasibility of a structure for shore protection. Thus model tests of proposed designs were conducted first to determine which

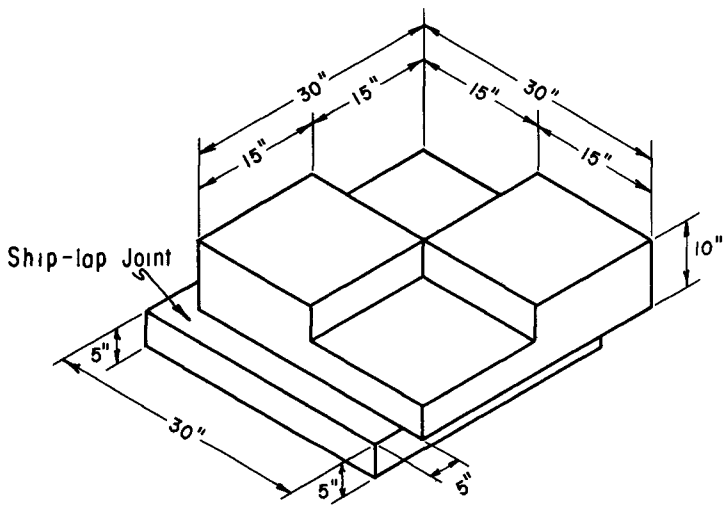

DESIGN-A
WAFFLE TYPE

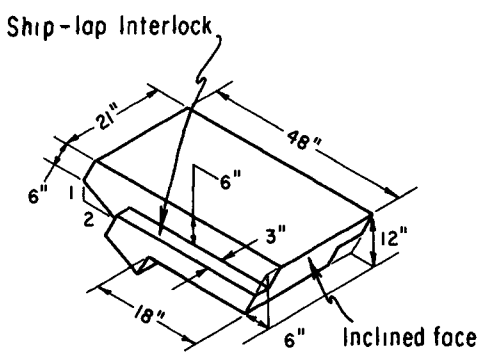

DESIGN-B
INCLINED-FACE

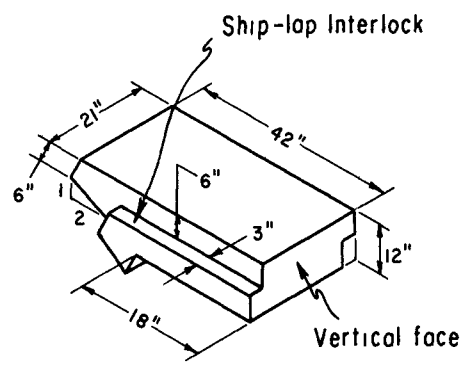

DESIGN-C
VERTICAL-FACE

FIGURE 2. INTERLOCKING PRECAST CONCRETE BLOCK

wall-type most effectively dissipated or absorbed the energy of the waves and second, to determine the stability characteristics of such a structure under the action of waves in order to eventually find the optimum wall design.

WAVE RUN-UP TESTS

The first series of tests on wave run-up were carried out in a wave tank of 72-foot length. Of specific interest was the height above still water to which the waves rose on the structure. Four wooden models were tested in this series, each built to a 1:16 scale. Two stepped-face seawalls, each having a 1 on 2 face slope, were tested, one being a vertical riser stepped-wall and the other an inclined riser stepped-wall but each with identical step height. The riser of the latter was normal to the back slope. The vertical riser stepped-wall was also tested on a 1 on 3 slope. The details of these steps are shown in Figure 2 (DesignC). A "waffle"-type block wall was tested on a 1 on 2 slope. A model of the waffle-type block is shown in Figure 2 (Design A). In addition to testing the four alternative designs under "deep water" conditions, that is, with the toe of the structure extending to the bottom of the wave tank, the inclined riser stepped-seawall on a 1 on 2 slope was tested while fronted by an arbitrarily placed beach representing extreme erosion conditions. This prototype condition is represented in Figure 3. Each model was subjected to a wide range of wave conditions, ranging in prototype height from 0.4 to 10.7 feet and in prototype period from 2.9 seconds to 18.8 seconds. The prototype water depth in the tank was 20 feet at all times.

The results of the run-up tests are presented in Figures 4 through 7. Relative run-up (R/H_o'), or actual run-up (R) (where R = vertical distance) divided by the equivalent deep water wave height (H_o'), is shown as a function of wave steepness (H_o'/T^2), or that is equivalent deep water wave height (H_o') divided by the square of the wave period (T), for constant depth (d/H_o') at the structure's toe, or water depth (d) at the toe of the structure divided by the equivalent deep water wave height (H_o'). The equivalent deep water wave height (H_o') is that deep-water wave height corresponding to the actual wave height (H) at depth (d) which has been corrected for shoaling effect but not for refraction. There was no refraction effect pertinent to these tests. The parameter chosen to represent wave steepness, H_o'/T^2, differs from the true steepness, H_o'/L, by the constant 5.12 through the relationship $L_o = 5.12\ T^2$, where L_o is the deep water wave length. Additional data from smooth seawall tests have been made available and are presented for comparison.

The data as presented allows a comparison to be made of the relative effectiveness of the wall-types for reducing the run-up. It can be seen that the types of relationships obtained for the roughened walls are very similar except for the wall fronted by a beach. For this exception a curve with a "camel's back" shape consistently appears. The first maximum on this curve is associated with the wave that shoals and breaks just on the structure. It is apparent from the data that any form of roughness is far better than none at all from the standpoint of reduced run-up. The difference in run-up between a smooth wall and the least effective roughened wall

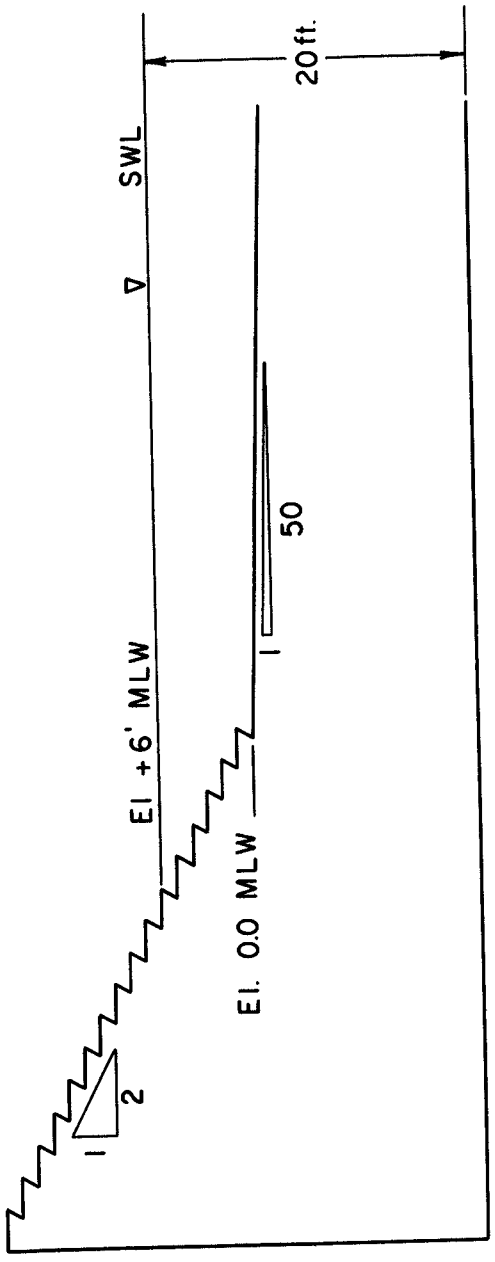

FIGURE 3. PROTOTYPE CONDITION OF RUN-UP TEST-SEAWALL FRONTED BY PARTIALLY ERODED BEACH

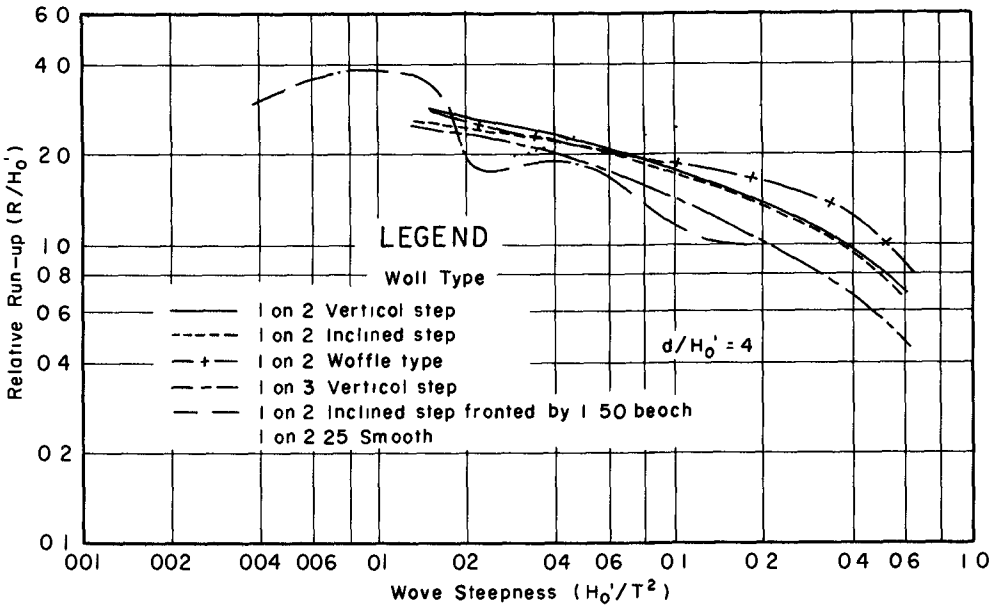

FIGURE 4 RELATIVE RUN-UP (R/H_0') ON ALTERNATE SEAWALL DESIGNS VS WAVE STEEPNESS (H_0'/T^2) FOR CONSTANT STRUCTURE DEPTH (d/H_0')

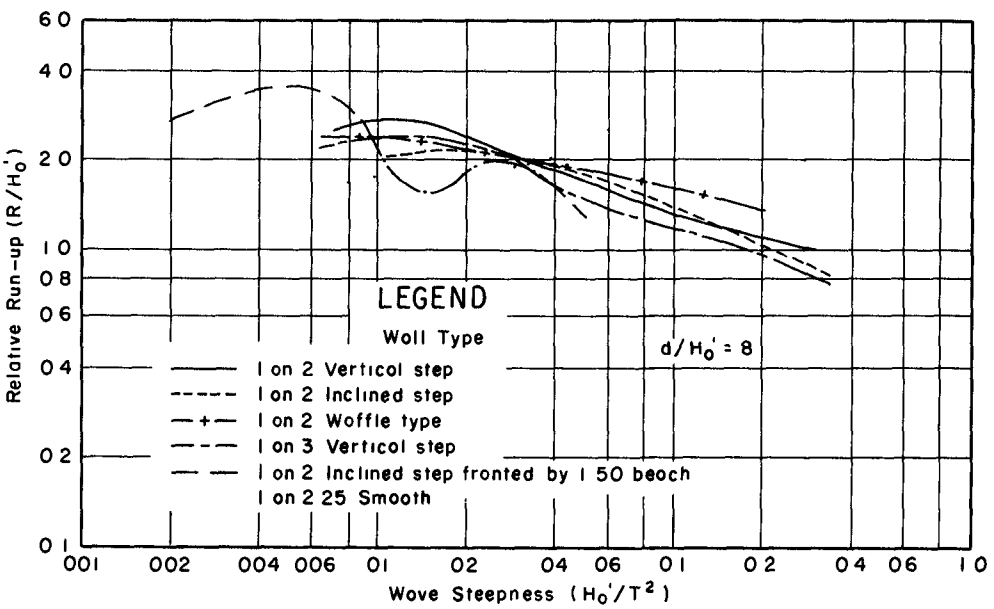

FIGURE 5. RELATIVE RUN-UP (R/H_0') ON ALTERNATE SEAWALL DESIGNS VS WAVE STEEPNESS (H_0'/T^2) FOR CONSTANT STRUCTURE DEPTH (d/H_0')

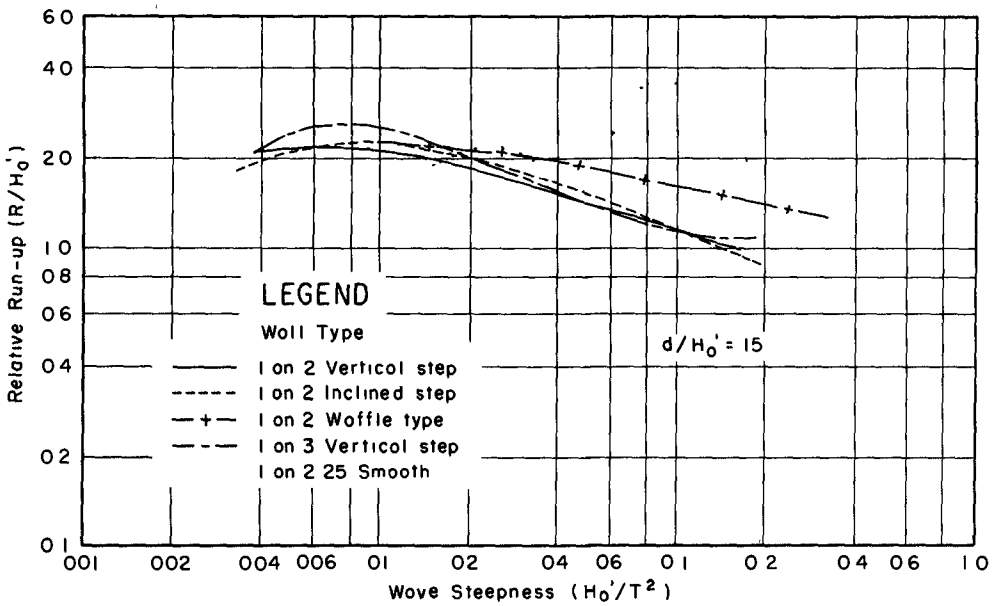

FIGURE 6 RELATIVE RUN-UP (R/H_0') ON ALTERNATE SEAWALL DESIGNS V WAVE STEEPNESS (H_0'/T^2) FOR CONSTANT STRUCTURE DEPTH (d/H_0')

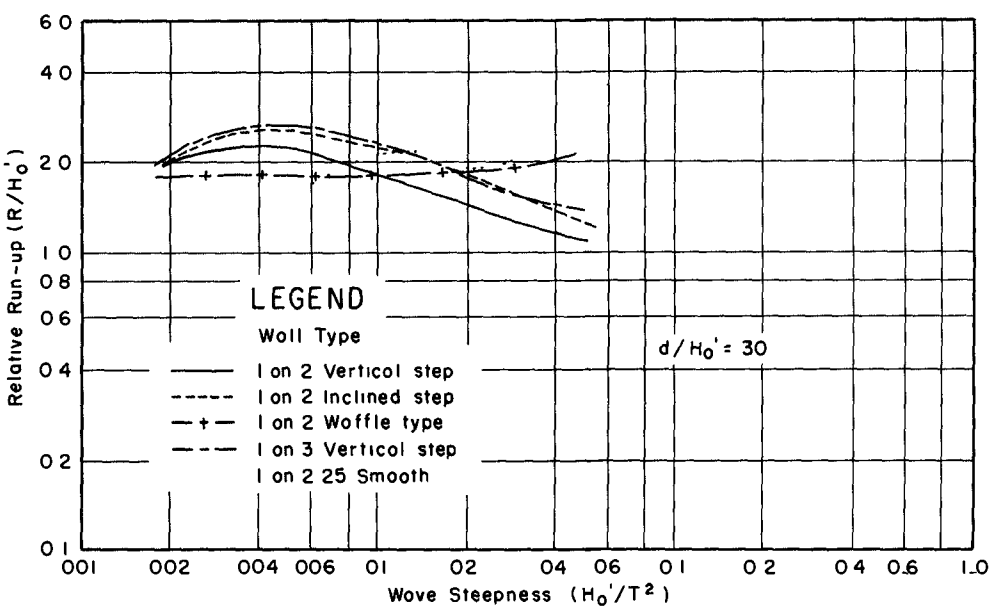

FIGURE 7 RELATIVE RUN-UP (R/H_0') ON ALTERNATE SEAWALL DESIGNS WAVE STEEPNESS (H_0'/T^2) FOR CONSTANT STRUCTURE DEPTH (d/H_0'

is generally much greater than the individual differences between roughened walls. There is, however, a consistent pattern appearing in the comparative data for the roughened walls. The waffle-type block is the least effective design tested for reducing run-up, especially for steeper waves. This is not to say that waffle-type block walls are less effective in dissipating wave energy than stepped-face walls for all conditions of relative face roughness. For these tests only one actual condition of relative roughness for each type of wall was utilized. Little difference in the run-up characteristics on the vertical-riser stepped seawall and the inclined-riser stepped seawall can be seen. There is, however, an indication that the inclined-riser steps might dissipate slightly more wave energy than the vertical-riser steps. This difference, if it exists at all, is quite small. The effect of a flatter wall slope for the wave conditions of major interest is beneficial. For the steep or storm waves, the run-up on the 1 on 3 wall is appreciably less than that on the 1 on 2 wall. If the height of a prototype seawall is a critical factor, then a flatter slope should be used. The flatter slope will, however, increase the number of precast concrete block units required and thereby increase the cost of the wall. The beach in front of the seawall causes the steeper waves to break in front of the structure, thereby dissipating much of their energy before reaching the wall. The data shows that the maximum relative run-up (R/H'_o) on the wall in shallow water is reached by waves that break directly on the structure. Figure 8 indicates the relative run-up vs wave steepness observed during the stability tests at a scale of 1:10; the data actually represent the relative run-up for the beach in its maximum eroded condition and eroded to mean low water at the toe of the wall.

To summarize the run-up tests for the proposed seawall designs, the most effective structure for reducing wave run-up is the stepped-face seawall, possibly with inclined-face block; however, any advantage held by the inclined-face block over the vertical-face block must be slight if it exists at all. The waffle-type is the least effective design for reducing wave run-up. The effect of decreasing the slope of the wall is to decrease the relative run-up (R/H_o') for steep waves. The existence of a beach in front of the wall causes the relative wave run-up to be low except for waves of very low steepness (H_o'/T^2). The maximum wave run-up is reached when waves break directly on the structure. When waves break offshore the wave run-up decreases accordingly. Those run-up tests conducted during the stability tests indicated that the run-up and overtopping were greater for surging waves, as differentiated from plunging waves, at the time of breaking.

STABILITY TESTS

As a result of wave run-up tests, it was determined that the first series of stability tests would be conducted on the inclined-face block seawall. It was recognized that the use of the inclined-face blocks (Figure 2, Design B) presented a conservative test condition in that the inclined faces would be subjected to greater lifting forces than would vertical-face blocks (Figure 2, Design C). The stability test section was constructed as a 1:10 scale model of a typical prototype installation.

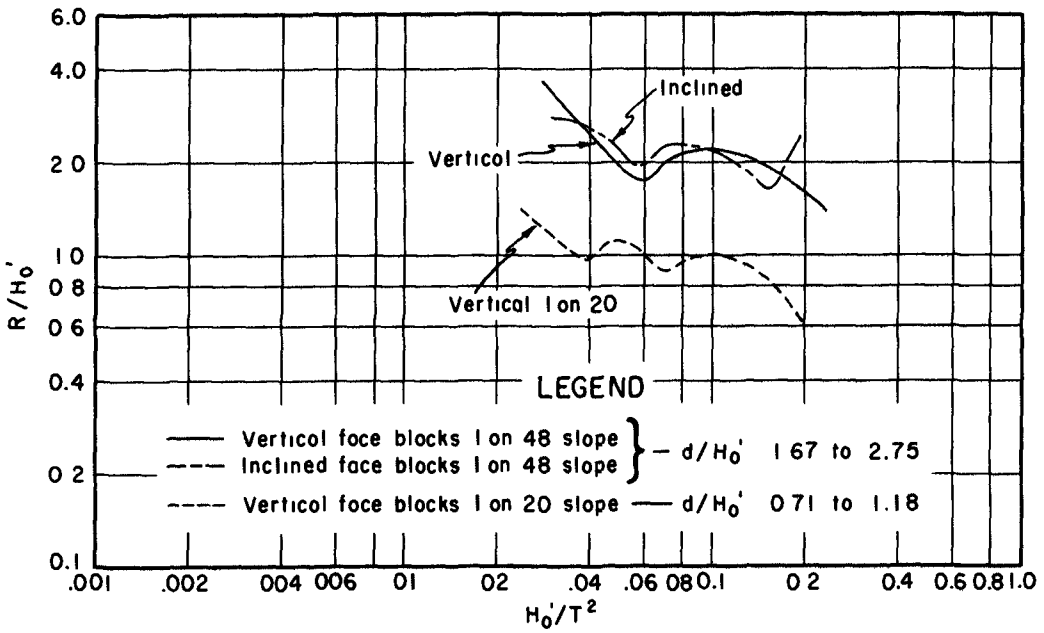

FIGURE 8. WAVE RUN-UP ON CONCRETE BLOCK SEAWALL

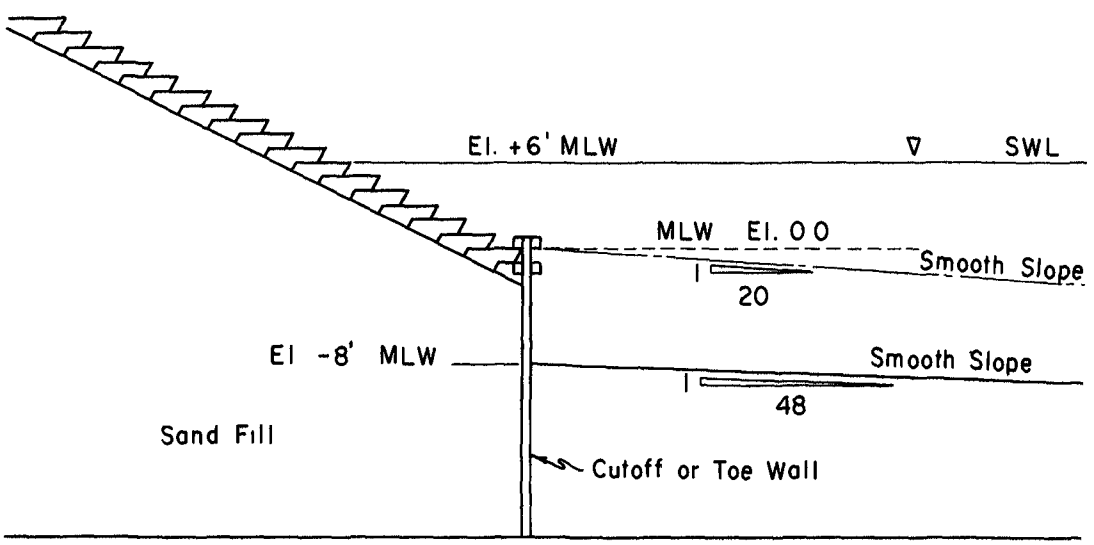

FIGURE 9. PROTOTYPE CONDITIONS OF STABILITY TESTS

The prototype design wave height (H) for this seawall was estimated to be in the order of 6 feet where H equals the wave height unaffected by reflections which would exist at the structure site.

The first series of tests was conducted under the following conditions (see Figure 9): inclined-face blocks (Design B) extending from MLW to El. +23 feet with a beach slope of 1 on 48 fronting the toe wall and scour to El. -8 feet (MLW) (maximum erosion conditions), and a design water level at El. +6 feet (MLW). (All dimensions given are at prototype scale.) A maximum wave height (H) of 8 feet (equivalent deep water wave height, $H_o' = 8.4$ feet or wave height at breaking, $H_b = 13.9$ feet) did not produce any significant displacement of the blocks, even after a (prototype) duration of 10 hours, for a wave period of 7 seconds; however, failure of the inclined-face blocks did occur for a 13-second wave period when wave height (H) was 10.2 feet (or $H_o' = 8.6$ feet, $H_b = 17.6$ feet). The duration of the latter test conditions producing failure of the wall varied from failure after only 1.25 hours to no failure after 10 hours. It thus became apparent that another variable in the test procedure was affecting the duration time to produce wall failure, and this was concluded to be the method of anchoring or restraining the top row of blocks (at El. +23 feet) against displacement by overtopping waves. Looking also at the mode of failure, it was realized that the blocks were being forced up the slope by a succession of plunging or surging waves and the degree of restraint was the prime factor in determining the stability duration for the wall.

A second series of tests was conducted on a combination of vertical-face blocks and inclined-face blocks under the maximum erosion condition (previously designated as -8 feet MLW). The vertical-face blocks were installed to El. 15 feet (above MLW) or 9 feet above design water level and inclined-face blocks from El. 6 feet to 23 feet. In the previous series of tests, the seawall of inclined-face blocks started to fail at El. +8 feet (or 2 feet above the design water level) whereas the combined block seawall failed at the first or lowest row of inclined-face blocks or El. +16 feet. This failure resulted from a 10.2-foot wave height (H) ($H_o' = 8.6$ feet and $H_b = 17.6$ feet) and a 13-second wave period after a duration of 8.4 hours.

The failure at this first or lowest row of inclined-face blocks indicated that these blocks are not as stable as blocks with vertical faces, thus confirming an original concept relative to inclined and vertical-face blocks.

The third series of tests was conducted on the vertical-face blocks under the maximum erosion condition. The vertical-face block seawall was subjected to the following wave conditions which were the maximum capable of being generated by the available equipment.

Wave Period (T)	Wave Height		
	H	H_o'	H_b
7 seconds	8.1	8.4	13.9
10 seconds	7.7	7.2	13.3
13 seconds	10.2	8.6	17.6

The blocks from MLW through El. +23 feet under the maximum wave conditions were completely stable and showed no sign of movement.

The fourth series of tests was conducted on the vertical-face blocks as in the previous series of tests except that the top row, rather than being at El. +23 feet, was lowered to El. +12 feet. The blocks at this lowered elevation were not anchored as in the previous test. The purpose of this series of tests was to determine the wave conditions (height and period) under which the block seawall and specifically the top row would be stable with an extremely eroded beach condition fronting the structure and still water level at El. +6 feet. This condition closely approaches an actual prototype installation without the use of a concrete parapet wall at the top of the slope or any anchoring of the top row of blocks. For an actual prototype installation it is anticipated that some method of anchoring will be used for the top row of blocks, either in the form of a concrete parapet re-entrant-face type wall or a continuous concrete beam.

It was determined that the top row of blocks (El. 12 feet) was stable as no discernible movement occurred for the following wave conditions.

Wave Period (sec)	Wave Height (ft)			Type of breaking wave
T	H	H_o'	H_b	
12.6	6.1	5.2	10.6	Surging
10.0	5.6	5.3	9.8	"
7.0	5.7	6.0	9.8	"
5.7	5.8	6.3	10.1	Plunging

The values obtained for wave height (H) appear to verify the original estimate of a 6-foot design wave.

CONCLUSIONS

It may be concluded from the results of model tests conducted to date on interlocking precast concrete block seawalls that:

a. In addition to wave steepness (H_o'/T^2) the relative wave run-up (R/H_o') is influenced by the following:

1. (d/H_o') relative depth of water at the toe of the structure.

2. The type of block roughness, that is, waffle, inclined-face or vertical-face.

b. The vertical-face blocks are more stable than the inclined-face blocks.

c. The stability number, N_s, (as derived by R. Hudson of the U. S. Army Engineer Waterways Experiment Station, in his rubble-mound stability tests), has a minimum value of 12.8 for these vertical-face blocks, but

this large value is attributed to a great extent to the mechanical interlock of the ship-lap joints.

d. The failure of the concrete block occurs in either of two ways:

1. In the case of the high seawall with the top row of blocks partly restrained, the blocks at or slightly above SWL are forced up the slope by each incident breaking wave, and when sufficient space between individual blocks has been created to render one ship-lap joint ineffective, a gradual dislodging of the blocks in the area of SWL follows.

2. In the case of a low seawall with the top row of blocks unrestrained, the top row is lifted up and displaced by the uprush of the overtopping wave and progressive failure results.

e. The vertical-face blocks can be used to provide a stable structure for incident wave heights greater than 6 feet when adequate restraint or anchoring is provided to the top row of blocks, either in the form of a low parapet wall or a beam.

ACKNOWLEDGMENTS

The data were collected and analysis thereof was made in connection with the general research program of the U. S. Army Coastal Engineering Research Center. Permission of the Chief of Engineers to publish this information is appreciated. Grateful acknowledgment is made to John R. Byerly and Gary A. Hampton for their extensive work on this study. The conclusions reached and presented herein are those of the author and do not necessarily reflect the policy or views of the Corps of Engineers.

REFERENCES

Bruun, Per (1964) Revetment for Coastal Protection; Dock & Harbour Auth.

Jachowski, R. A. and J. R. Byerly (1963) Interim Report on Interlocking Precast Concrete Block Seawall Study; U. S. Army Corps of Engineers, Beach Erosion Board.

Saville, T. Jr. (1953) Wave Run-up on Shore Structures; Proceedings ASCE, Jour. of Waterways and Harbors Division, vol. 82, No. WW2, pp. 720-724.

Thorn, R. B. (1960) The Design of Sea Defence Works; Butterworth Scientific Publication, London.

Chapter 33

THE ECONOMICAL HEIGHTS OF SEA WALLS FOR COAST PROTECTION IN JAPAN

Senri Tsuruta, Dr. Eng.
Head, Hydraurics Division
Port and Harbour Technical Research Institute
Ministry of Transportation, Yokosuka, Japan

Yoshimi Nagao, Dr. Eng.
Chief of Engineer with Special Responsibilities
for Planning and Disaster Prevention
Port and Harbour Bureau, Ministry of Transportation
Tokyo, Japan

Takeshi Ijima, Dr. Eng.
Head, Design Standard Division
Port and Harbour Technical Research Institute
Ministry of Transportation, Yokosuka, Japan

INTRODUCTION

The purpose to construct coast protection works is to protect properties and human lives from the disasters of storm tides, cruel waves, beach erosions, and others. We may expect that the stronger the works are built, the more the disasters will be prevented, but it cost more to strengthen them.

From a view point of national economy, both the construction cost and the amount of damages are regarded as the losses. In general, the amount of damages will be enormous if no protection work is constructed, but the construction cost of protection works to reduce the damages infinitely small will also be enormous. The loss in national economy, or the sum of the damages and the construction cost, will be minimized on some suitable magnitudes of protection works. We deviced a concrete calculation method to decide economical magnitudes of coast protection works, and have applied the method to practical plannings. The paper discusses the fundamental idea of the method and the results of the application.

NATURAL CONDITIONS OF JAPANESE COASTS AND COAST PROTECTION POLICIES

Japan is a country of small islands located at the north-western end of the Pacific Ocean with a very little land being flat and level. She is also a prominent country of industry. Her industry, however, imports most of raw materials from abroad, processes them into manufactured products, and exports them

abroad to get raw materials in return. For these reasons, most of her population and industry are gathered along the coastal areas of low level land. Especialy, the main industrial areas are concentrated on the low land along coasts where good ports and harbors are available.

Since Japan is so frequentry attacked by typhoon, her coasts, especially in low land, often suffer enormous damages by storm tides and waves. The strong waves which are produced by typhoons or winter seasonal-winds cause coastal erosions too. In addition, earthquaks occur so often and the disasters of tsunamis follow the earthquakes in many cases.

Viewed from a point of national economy and stabilization of people's livelihood, the protection of coastal districts from the attack of sea is very important. The measures adopted in Japan in order to protect the coast districts are firstly to prevent the disasters which are caused by storm tides and waves, and secondly to issue a typhoon warning to evacuate and to carry out anti-flood measures in case being attacked by a typhoon. These policies are to be planned and practiced from the view point of national economy.

FUNDAMENTAL IDEAS TO DECIDE ECONOMICAL CROWN HEIGHTS

FUNDAMENTAL IDEA

The damage in the properties along coastal districts are decreased with the enlargement of coast protection works, but the construction cost of the protection works increases at the same time. We have to choose a certain magnitude of structures for the protection works. The most reasonable way of the determination will be to choose such the magnitude that will make the sum of the expected damages and the construction costs at the minimum, because both the damages in properties and the construction costs are the losses in national economy.

In order to find out such the most economical magnitude of structures, the following five informations are necessary:

1) Occurrence frequency curves of storm tide, waves and others.
2) Rates of inundation of inland area under various combinations of the magnitudes of protection works and storm tides.
3) Kinds, amount and distribution of properties in the inland region to be protected.
4) Damage-rate of properties under a certain inundation.
5) Construction cost of protection works estimated for various magnitudes of structures.

The first four informations are required to calculate the expected damages.

PRINCIPLES OF CALCULATION

As a model of calculation the following district is

considered here; the tops of natural banks and/or coastal embankments which surround the entire periphery of the district to be protected are higher than the ordinary high water level, and the natural banks and/or coastal embankments are not destroyed by a storm tide and waves.

In order to calculate the economical magnitude of the coastal embankments and other fascilities to protect the above model district, three fundamental diagrams are to be drawn in the beginning. The first diagram is the estimated damage which the model district with the protection work of a certain crown height will suffer from a storm tide of a given height, such as shown in Fig.1(a). The estimation of the damage can be made from the calculation of overflowing discharge into the district for the given conditions of protection works, storm tide, and wave heights (being assumed as a function of the storm tide only) and the calculation of the inundated depth in the district. The second diagram is the occurrence frequency of the storm tide level shown in Fig.1(b). The third diagram is the construction cost of the protection works as a function of the crown height as illustrated in Fig.1(c).

Then, the variation of expected damages with the possible height of sea level for a certain height h_i of the protection works such as shown in Fig.1(d) is obtained by multiplying the estimated amount of the damages for one sea level of storm tide in Fig.1(a) with the occurrence frequency of that sea level in Fig.1(b). The left-hand side area surrounded with two curves of no protection work and of h_i in Fig.1(d) indicates the expected amount of property protection by the protection works with crown height of h_i. The right-hand side area surrounded with the two curves represents the amount of expected damages yet to occur.

These expected amount of property protection and the amount of expected damages are plotted in Fig.1(e) against the crown height. The construction cost of coast protection works in Fig.1(c) is also re-plotted in Fig.1(e). The expected amount of property protection means the averted amount of expected damage by the construction of the protection works encircling the district entirely with crown height of h_i in comparison with the primary condition of protection work. The amount of expected damage means unprotective amount of damage to be expected even with the protection works of crown height h_i. The sum of the construction cost and the amount of expected damage gives the curve of total loss as shown in Fig.1(e).

The point A in Fig.1(e) is the most right hand side intersection point of the curve of the expected amount of property protection and the curve of construction cost. The value of the abscissa of the intersection point A indicates the highest limit of crown height for the economical construction. In Fig.1-(e), the curve of total loss has a minimum value at the point B (there may be more than two points for the minimum values).

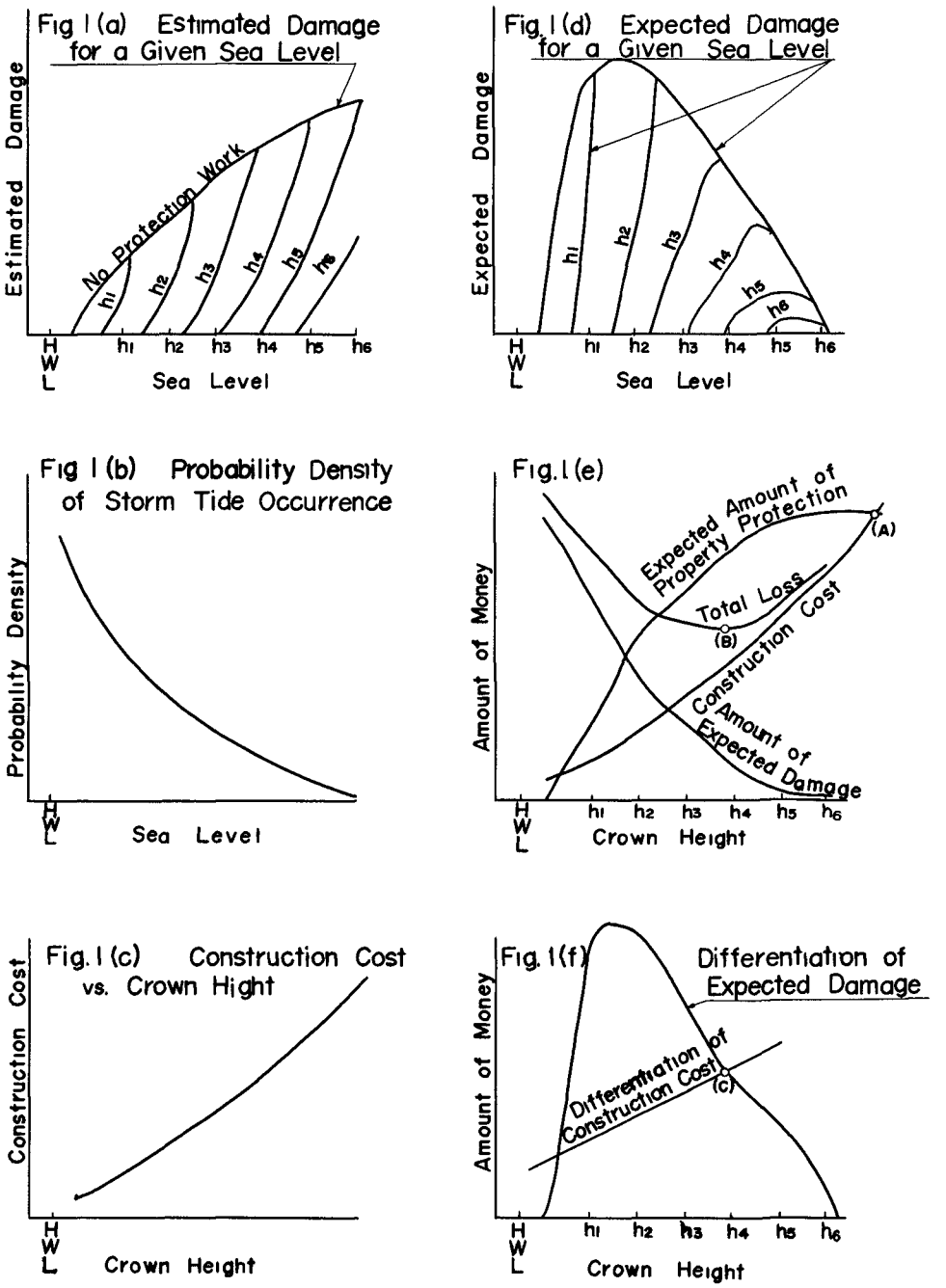

Fig. I Explanation Diagrams for the Calculation of Economical Crown Height

This most economical crown height is determined more accurately as the abscissa of the point C in Fig.1(f); the point C is the intersection of the differentions of the construction cost curve and the expected damage curve.

TIME EFFECTS

The reconstruction period of coast protection works should be decided most economicaly, considering various factors such as construotion cost, primary strength, structural weakening, chemical weakening, external forces to attack the protection works and so on. But such a determination is a difficult task. For this reason the reconstruction period of 50 years has been adopted for all protection works according to the previous practioe. Thus the construction cost and the primary strength are so designed for the protection works as to endure the attack of external forces for 50 years.

In practice, there is a time lag between the investment (construction of coast protection works) and the benefit yielding, and the benefit is expeoted to be yielding during the reconstruction period. Hence the amount of investment and the amount of damages averted should be summed up respeotively from the beginning of the investment to the end of the reconstruction period. But in this case the investment interest and the profits which are produced from the amount of damages averted should be taken into consideration. We have evaluated these investment interest and the profits at the end of the term with the compound interest rates of 7% and 8% a year,respectively.

Since the variation in the properties of the protective region during the reconstruction period must be considerd too, we have assumed that the property will increase with the rate shown in Table 1, every year. In order to simplify the method of calculation for economical magnitude, only one coefficient (I') has been introduoed for the combined effect of interest rate, profit rate and property variation. (This coefficient is also shown in Table 1.) In actual calculations, the construotion costs were multiplied with this over-all coefficient (I') so as to adjust the time effect. With this over-all coefficient (I'), the benefit-cost ratio can be calculated with the following equation.

$$\frac{P_n}{C_n} = \frac{P_n'}{C_o} = \frac{50 P_o}{I' / C_o}$$

where P_n : Amount of expected property protection in the whole period, which is evaluated at the end of reconstruction period with consideration of all time effects.

P_n' : Amount of expected property protection in the whole period, which is evaluated at the beginning point of reconstruction period with consideration of all time

effects.
c_n : Construction cost evaluated at the end of reconstruction period.
c_o : Construction cost.
50: Years of reconstruction period.
p_o : Expected amount of property protection in one year by having coast protection works.

Class of District	Increasing Rate of Property/One Year	(I′)
Established Industrial Districts	5.9 %	1.00
Newly Developing Districts	7.3 %	0.74
Districts with Promising Development Plans	6.1 %	0.96
Other Districts	5.0 %	1.19
Mean of Whole Nation	6.3 %	

Table 1. Increasing Rate of Property Protection and Over-all Coefficient for Time Effect Adjustment, (I′).

The maintenance and administrative expence are not considered explicitly, but they are included in the term of interest rate for the construction cost which is far larger than the formers.

DETAILS OF CALCULATION

OCCURRENCE FREQUENCY OF STORM TIDE LEVEL

The occurrence frequency distributions which have been used for the estimation of high water discharge of river, amount of rainfall and others are the logarithmic normal distribution, the Gumbel's distribution, exponential distribution and others.

As for the storm tide level there are little differences among these distributions in an extent to which observation data are available, but for an extraordinary high tide levels which will occur once in several hundreds to one thousand years, there are considerable differences among these distributions. It is difficult to decide which distribution is the most suitable one for such extraordinary high tide level in Japanese observation data. We have employed the exponential distribution, because it gives a middle value between the values of the logarithmic normal distribution and the Gumbel's distribution and the calculation method of storm tide level by the exponential distribution is simple and easy to be instructed.

Occurrence frequency of storm tide in the exponential distribution - When we found observation data in fairly long term at the planning site or a near-by location which is nearly equal in natural features, we calculated the exceeding occurrence frequency of storm tide level in the one year basis. When we could not find observation data of long period, we estimated the exceeding occurrence frequency in one year by calculating the deviations of sea level with meteorological data (atmospheric pressure, wind velocity and wind direction) and by adding suitable height of astronomical tide to the above deviations with the proper consideration of co-occurrence probability.

We presumed that the exceeding occurrence frequency of storm tide level in one year is expressed by the following exponential equation after Nemelsfelder (1960):

$$m = 10^{\frac{h-h_1}{s}} = e^{\frac{\alpha(h-h_1)}{s}}$$

where m : Exceeding occurrence frequency per one year.
h : Storm tide level.
$\alpha = \log_e 10 = 2.3026$
$s < 0$, $h_1 > 0$: Both are constant, h_1 is such the sea level that its exceeding occurrence frequency per one year is unity.

We calculated the constants, s and h_1, from the observation data or calculated values of storm tide levels by means of the least square s method.

CALCULATION METHOD OF SUBMERSION LEVEL

Modelling of storm tide level variation - We devided the storm tide elevation into astronomical tide and meteorological tide, classifying them according to their regional characteristics The astronomical tides at all obserbation points are classified with diurnal inequality and four major partial-tides. In regards to the meteorological tide, we made a nation-wide investigation of the actual observation data of tidal records for the continuation times of various heights of storm tides at various locations. Both the astronomical and meteorological tides were modeled to isosceles triangles in their time-variations. The continuation times of the astronomical tide were classified regionally and those of the meteorological tides were classified both regionally and by step of tide level (see Table 2). By superposing two models of Table 2 as illustrate in Fig. 2, we can obtain the models of storm tides; the tide model with longer continuation time is taken as the base for the storm tide model. It should be mentioned that these models are applicable only when the crown height or ground height is higher than the astronomical tide level.

Table 2a

Sea Level (Above Datum Level, Meter) / Tipe of Astronomical Tide (Hour) / Classification of Coast Districts		Tipe of Meteorological Tide (Hour) 1.0	1.5	2.0	2.5	3.0	3.5	4.0	4.5	5.0	5.5	6.0	6.5
the Japan Sea	18	18	12										
South Coast of Hokkaido	18	-	-	24									
East Coast of the Pacific Ocean	18	-	-	-	18								
South Coast of the Pacific Ocean (on the East of Cape Irozaki)	18	-	-	24	18								
(on the West of Cape Irozaki)	15	-	-	-	24	18	12						
the Kii Channel	15	-	-	-	24	18	12						
the Bungo Channel	15	-	-	-	-	18	12						
West Coast of Kyushu (Coasts of Open Sea)	12	-	-	-	-	18	18	18					
the Kagoshima Bay	12	-	-	-	-	24							
the Tokyo Bay	15	-	-	-	-	24	18	12	(9)	(9)			
the Ise Bay	12	-	-	-	-	18	12	12	12	(9)	(9)	9	9
the Kinuura Bay	12	-	-	-	-	-	18	12	12	6	(6)	(6)	
the Atsumi Bay	18	-	-	-	18	12	12	9	(6)	(6)	(6)		
the Osaka Bay													
East Part of the Seto Inland Sea (the Harimanada Bay)	15	-	-	-	18	18	12						
(the Hiuchinada Bay and the Western Bays)	12	-	-	-	-	-	-	-	18	18	12	12	

Table 2b

Meteorological Tide / Tipe of Astronomical Tide (Hour) / Classification of Coast Districts		Tipe of Meteorological Tide 0.5	1.0	1.5	2.0	2.5
the Ariake Bay	12	18	18	12	12	12
the Yatsushiro Bay	12	18	18			

Example: Type of 18 hours means a type of storm tide which continuous 18 hours with tidal variation of an isosceles triangle.
( ); Calculated by digital computer

Table 2. Models of Storm Tide

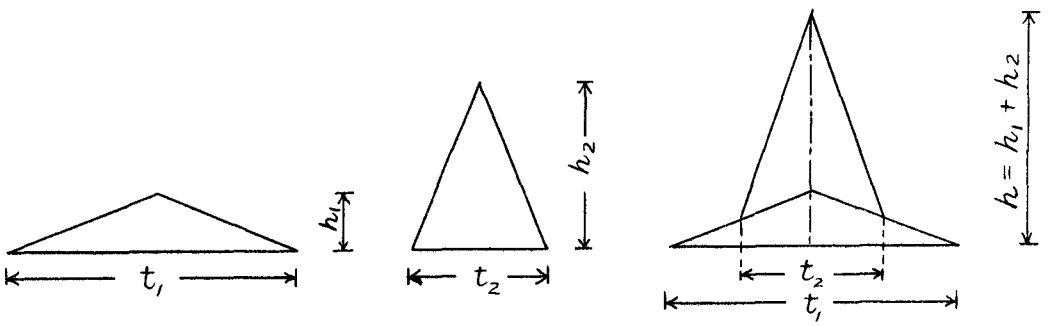

Note: 1. The "sea level" on the Table 2 means h (= $h_1 + h_2$) in Fig.2.
2. In practical calculation, spring rise (HWL - DL) is used as range of astronomical tide.
3. Range of meteorological tide in Table 2a is (h-range of astronomical tide) in Fig.3.
4. Elevation of sea level (above datum level) = elevation of astronomical tide + range of meteorological tide.

Fig.2. Superposing Method of Storm Tide Models.

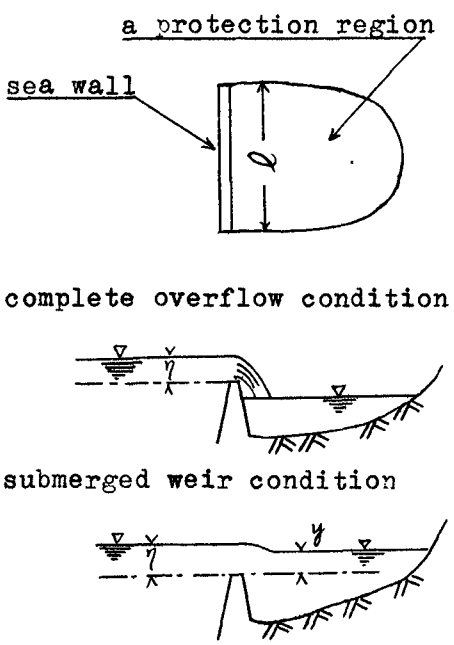

Fig.3. Definition Sketch of Overflow Conditions.

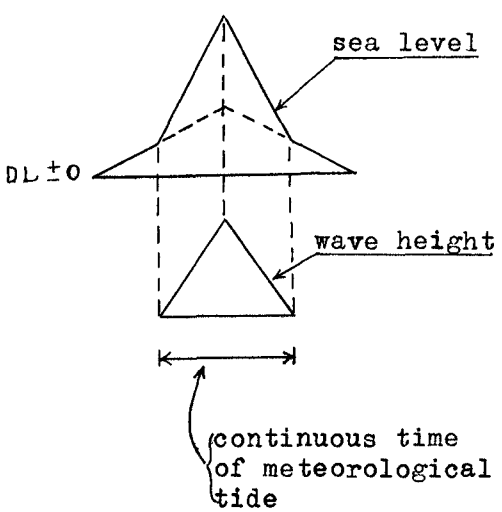

Fig.4. Time Variation of Wave Height.

Calculation method of submersion level - Submersion levels were calculated with the assumption that the submersion quantity of water is calmly stored in the region behind coastal embankments. The submersion quantity was considered to be composed with overflowing discharge which was calculated with the model storm tide level described in the previous paragraph and the overtopping discharge of waves which are accompanied with storm tide.

Quantity of overflow was calculated with the next equations.

(1) Complete overflow condition ($y \leq \frac{2}{3}\eta$)

$$Q = m\sqrt{2g}\,\eta^{\frac{3}{2}}\ell$$

(2) Submerged weir condition ($y \geq \frac{2}{3}\eta$)

$$Q = m'\sqrt{2g(\eta - y)}\,y\,\ell$$

where η: Sea level above crown height (see Fig.3)
y: Inundation level measured upward from crown height.
Q: Quantity of overflow for length per unit time.
ℓ: Length of embankment.
m: Coefficient of overflow for broad weir (theoretical value of m = 0.385 is used).
m': Coefficient of overflow for submerged weir
$m' = 2.6\,m = 2.6 \times 0.385 = 1.0$

Since quantity of overtopping is influenced by many elements such as wave steepness, crown height, site of embankment, type of embankment and others, it is not easy to calculate the quantity in general. But the overtopping quantity can not be neglected in comparison with quantity of overflow. Thus the following method has been adopted to calculate the quantity of overtopping.

1) The wave height varies with respect to time as shown in Fig.4.

2) The quantity of over topping is considered to be stored in the region only when the condition of $H \geq 1.0$ m and $+H \geq R \geq -H$ are satisfied and further the sea level is higher than the ground level of the region behind embankments. R=(crown height - sea level)

3) Quantity of overtopping is calculated by the following equation:

$$q_w = 57.6 \cdot K \cdot H^{\frac{3}{2}} \cdot \ell$$

where q_w : Quantity of overtopping (m^3/min.)
H : Wave height in front of sea wall (m); equal to the equivalent offsea significant height, H_o' for water depth larger than H_o', and equal to water depth for depth smaller than H_o').
K : Coefficient of which value decreases linearly from K=0.25 for R=0 to K=0 for R=±H.

CALCULATION OF DAMAGE AMOUNT

Property in the region to be protected - The calculation has been made for each unit protection region which is a unit of the coast protection plannings. As a rule the protection works of every unit area is independent of each other and complete in its area. Amount of properties in the protective regions were investigated for every step of ground level along storm tide coasts. Unit cost of property was investigated by sample surveys along each coast, then unit cost was applyed to other unit regions along the same coast. Included in the investigations were building, household property, assets of industry, goods in stock, land, outputs of agriculture and industry, public facilities etc.

The data to be used for the investigation were the statistical data prepared by the national government and local self-governing bodys; these data were specified beforhand.

Depth of Submersion (cm) / Kind		0 ~ 49	50 ~ 99	100 ~ 149	150 ~ 199	200 ~ 299	300 ~
House		3	13	28	39	54	67%
House Hold Property		0	27	43	55	69	77
Farm-House, Fishmans House	Properties for Depreciation	0	25	36	45	53	57
	Goods in Stock	0	29	47	61	73	76
Firm, Office and Work	Properties for Depreciation	0	38	44	51	61	74
	Goods in Stock	0	21	40	55	69	74

Note: 1. Submersion depth is measured from ground level.
2. Height of floor above ground level is presumed to be 50 cm.
3. Japanese houses are made of wood in most cases.

Table 3. Damage Ratio of Properties.

Damage ratio of property - The standard damage ratio of property by inundation were determined as shown in Table-3 based on the census-taking data at times of the typhoon Ise Bay and Chilean earthquake tsunami. Damage ratio of property by wave force were also determined from the inspection data at times of various typhoon. In order to evaluate the indirect damages, the number of days on which plants or stores suspend the operation was estimated as shown in Table 4.

Depth of Submersion (cm) / Kind	0 ~ 49	50 ~ 99	100 ~ 149	150 ~
				days
Light Industry	0	16.4	29.3	34.0
Heavy Industry	0	22.3	24.0	29.0
Petro-Chemical Industry	0	19.4	26.7	31.5
Store	0	16.0	39.0	44.0

Note: 1. Submersion depth is measured from the ground level.
2. Period of inundation is presumed to be less than 10 days.

Table 4. Number of days on which plants or stores suspend the operations.

Damage amount of protective region - Damage amount of protective region was the sum of direct and indirect damages. The amount of direct damage was calculated by summing up the number of properties multiplied by the unit costs and damage ratios all over a unit protective region. The amount of indirect damages was calculated by summing up the daily added values of plants and stores multiplyed by the number of days of business suspention.

CONSTRUCTION COST OF COAST PROTECTION WORKS

Standard curves of unit construction cost related to the heights of sea walls were first established for various types of structures after investigating recent designs of coast protection works all over the nation. Then the cost estimate of a particular design section was made at each unit region, and the cost curve drawn parallel to a standard cost curve passing through the point of the construction cost of the particular section was utilized to estimate construction costs of coast protection works with various crown heights.

RESULTS OF INVESTIGATION

With the method described in the preceding sections a nation-wide investigation has been made to calculate the economical crown heights of coast protection works for 81 harbors

with 226 unit regions for storm tide protection. The investigati showed that the investment ratio is greater than unity at 192 uni regions. By constructing the protection works with the economical magnitudes at 192 unit regions, the expected damages in 50 years are estimated to be reduced to the amount of 74 millions dollars from the amount of 44 billions dollars for the case of no protection work. The total construction cost of these magnitudes of protection works is only 400 million dollars. Therefore the overall benefit-cost ratio is nearly 110.

It has been proved that the method presented in this paper is very efficient to decide the magnitude of investment for coast protection works, that the coast protection project in Japan is very productive object of the investment, and that the investment by the government is a very profitable one from a stand point of national economy.

CONCLUDING REMARKS

On the above, we have introduced the fundamental ideas of the concrete calculation method, which was already put into use in Japan, to decide the economical magnitudes of coast protection works, with a few results of the investigations. We have found that the method is effective and appropriate to the practice, and also proved that the coast protection works in Japan is a very benefitial project.

But in this method, the protective effect of the structures against astronomical tide is omitted for the areas where the ground level is lower than the ordinary high water level. We must continue our research to find the calculation method of such the protective effect for astronomical tide (in general, the protective effect for astronomical tide has little influence on the determination of the economical crown height). For the improvement in the accuracy of the present method, it is also necessary to enrich observation data of natural conditions, to make research further on the damage rate of protective property and reconstruction period of coast protection works. It is also necessary to simplify the investigation of the properties in the region behind the protection works in order to apply the present method to a great number of districts.

ACKNOWLEDGEMENTS

The application of the present method to practical plannings were undertaken by the Port and Harbour Bureau of Ministry of Transportation, with the co-operations of Regional Bureaus of Port and Harbour Construction, the Port and Harbour Technical Research Institute, the Meteorological Agency, local self-government bodys and administrators of the ports and harbours concerned. The researches for this method and its development were made possible through the efforts of Messrs. Yoshihisa Kawakami and Hisashi Aono. The authors wish to express

their appreciations for the all members assisted the investigation.

REFERENCES

Gumbell, E. J. "Statistics of Extremes", Columbia University Press, New York, 1958, 375 pp.

Wemelsfelder, P. J. "On the Use of Frequency Curves of Stormfloods", Proceedings, 7th Conference on Coastal Engineering, 1960, pp. 617~632.

Chapter 34

ON OPTIMUM BREAKWATER DESIGN

J. van de Kreeke* and A. Paape**

SUMMARY

A breakwater design is optimum when it results in a structure that meets the requirements at minimum total cost.

The total cost consist of cost of construction, anticipated damage and economic loss due to failure of the structure.

For any type of structure the design wave or load is governed by the condition of minimum total cost. This is worked out for some possible designs for Europoort Harbour, Rotterdam.

The data needed are often insufficient, however, for reasonable assumptions important directives can be obtained especially with respect to ranking of structures of the same type.

DEFINITION OF OPTIMUM DESIGN

Designing the cross section of a breakwater involves deciding upon:
- the type of structure;
- its dimensions.

A criterion has to be established on which the decision can be based, viz. the optimum design is that which results in a structure that meets all the requirements at minimum total cost.

As long as off-shore conditions can only be expressed in terms of statistics any breakwater will suffer damage sooner or later. So the total cost is defined as the cost of construction and the capitalized anticipated expenditure due to damage and economic loss.
For example economic loss is suffered when harbour equipment is damaged or when a harbour fails to function properly as a consequence of failure of the breakwater.

DESIGN CRITERIA

The design criteria are the requirements the structure must satisfy. They depend on:
- the functions the breakwater is expected to fulfil;
- its stability.

* Engineer Hydraulic Division, Service of the Deltaworks, Rijkswaterstaat, The Hague.

** Head Maritime Structures Branch, Delft Hydraulics Laboratory, Delft.

Functions:	Calling for special attention to:
- guiding of currents.	- generally no special requirements as to type of structure.
- attenuation of waves.	- crest height.
- marking of harbour entrance.	- crest height.
- providing a quay.	- crest height and width; harbour-side structure.
- retention of sand.	- inner slope.

Stability. A wave condition or wave load that will just not cause any damage can be determined for any structure. Generally, however, there is a probability that that "design wave" or "design load" as it is called will be exceeded; consequently the fact that damage will be suffered by the structure has to be accepted. If the design wave or design load is small, the cost of construction will be low but the anticipated damage will be great. As the magnitude of the design wave or load increases, the anticipated damage will decrease, due to the decreasing probability that the design conditions will be exceeded. See fig. 1.

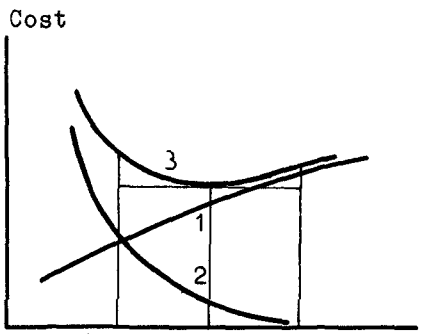

1. cost of construction.
2. capitalized anticipated damage.
3. total cost (= 1 + 2).

Fig. 1. design wave or design load.

According to the foregoing definition of optimum design, the design wave or load must be such that the cost of construction and the capitalized anticipated damage are kept as low as possible. How to determine that minimum is called the "decision problem", which is worked out below.
The following factors are involved:

- the occurrence of various off-shore conditions;
- the relation between off-shore conditions (especially wave conditions) and the behaviour of the structure;
- the relation between the design wave or design load and the cost of construction;
- the relation between off-shore conditions, design wave or design load and anticipated damage.

OUTLINE OF THE "DECISION PROBLEM"

The way in which the above-mentioned information is worked out depends on the type of structure being considered. Two main categories will be dealt with separately:

- monolith structures (caissons, walls built of jointed blocks);

- rubble-mound structures (with cover layers of natural rock and concrete blocks).

THE OCCURRENCE OF VARIOUS OFF-SHORE CONDITIONS

In the following chapter a probability distribution curve of significant wave heights is used to describe wave attack (see specification of H_S below). The probability distribution of H_S can be derived from measurements or estimated from meteorological data by means of the well-known relations between waves, wind and fetch.
Probability distribution curves for the wave forces acting on monolith structures can be derived from the probability distribution curves of H_S combined with wave-force experiments on models.

RELATION BETWEEN OFF-SHORE CONDITIONS AND THE BEHAVIOUR OF THE STRUCTURE

Monolith structures. Wave attack is characterized by a wave force F (or a wave pressure a). The relation between wave forces and off-shore conditions must be established. If the design load F_0 is exceeded, the entire cross section will be displaced (damage to part of the cross section is irrelevant). A relation can be established between displacement x, design load F_0 and actual load F. A certain displacement x_0 is regarded as marking the collapse of the structure. For a structure of a certain type and dimensions (i.e. a known value of F_0) this critical displacement can be related to a wave force F^* by applying the above-mentioned relation between x, F_0 and F. See page 6 . Consequently, the probability of collapse is the probability of force F^* being exceeded, $p(F^*)$.
Summarizing:
$F \leq F_0$, $x = 0$;
$F > F_0$, $x \neq 0$;
$F = F^*$, $x = x_0$.

Rubble-mound structures. In view of the difficulty of determining wave forces the significant wave height H_S is taken as characterizing a wave attack on the structure, provided:

- the term "significant wave height" implies that the actual distributions of wave heights and periods are applied;
- proper allowance is made for the accumulated wave attack with smaller significant wave heights (ref. 8).

Regard for those factors enables us to arrive at a design wave H_{SO} corresponding to a "no damage" criterion. If the design wave H_{SO} is exceeded, displacement of armour units will occur. A relation can be established between the percentage of armour units displaced, the design wave H_{SO}, and actual wave height H_S. Therefore the occurrence of a certain amount of damage can be related to the occurrence of a certain H_S for a structure of a certain type and dimensions (i.e. a known value of H_{SO}).

RELATION BETWEEN COST OF CONSTRUCTION AND DESIGN WAVE OR DESIGN LOAD

Monolith structures. It was assumed in the previous section that the dimensions of the structure could be determined once the design load F_0 was chosen. The cost of construction can be estimated if the dimensions are known. Hence the cost of construction can be expressed

as a function of F_o, $I = f(F_o)$.

Rubble-mound structures. The dimensions are related to the design wave H_{so}; consequently, the cost of construction can be expressed as:
$I = f(H_{so})$.

THE RELATION BETWEEN ANTICIPATED DAMAGE, OFF-SHORE CONDITIONS AND DESIGN WAVE OR DESIGN LOAD

As stated before, with every design wave or load there is a probability of damage occurring to the structure. To determine the amount of anticipated damage it is assumed that an insurance company is willing to insure it against damage. If the company insures a great number of unrelated constant risks, which need not be of the same nature (e.g. all government investment risks), and if the theoretical annual premium is s:
s = probability of damage x the cost of repairing that damage. The same premium would be charged for a single object for an infinite duration, which is (to abandon the insurance model) the average sum spent per year on repairing damage. It seems reasonable to take that premium as the anticipated damage per year.
It should be noted that under constant risk it is assumed that any damage suffered would be repaired immediately.

For monolith structures, partial damage to which is not considered, the anticipated damage per year is:
$s = p(F^*).W$, in which $p(F^*)$ is the probability of force F^* being exceeded in any given year, and W is the cost of repairing when a failure of the structure occurs.

For rubble-mound structures the anticipated damage per year is estimated as follows: For a structure of certain dimensions (i.e. a known value of H_{so}) the occurrence of a certain damage is related to the occurrence of conditions characterized by an H_s (see page 9). If the probability of H_s being exceeded is considered, intervals ΔH_s can be chosen at which a constant amount of damage ΔW may be presumed with reasonable accuracy. Assume the probability of occurrence of waves in the interval ΔH_s in any given year is Δp. The corresponding anticipated annual damage is $\Delta p . \Delta W$. Hence the total anticipated annual damage is:
$s = \sum \Delta p \cdot \Delta W$.

As already stated, the factor W may include economic loss.

The capitalized value of the sum of the "premiums" s depends on the life of the structure. If its life is 100 years or more, the capitalized anticipated damage s is:
$S = \frac{100}{\delta} s^*)$, in which δ is the rate of interest as % per year.

*) If interest is added continuously, the capitalized value (present value) of a sum s to be paid after t years is $e^{-\frac{\delta}{100} t} s$. Consequently, the capitalized value of the sum of the premiums s to be paid for the lifetime T of the structure (sum of all present values) is found to be:
$S = s \int_0^T e^{-\frac{\delta}{100} t} dt$.
For T = 100 years, $S = \frac{100}{\delta} s (1-e^{-\delta}) \approx \frac{100}{\delta} . s$.
For T = 10 years and $\delta = 3.5\%$: $S = \frac{100}{\delta} s (1-e^{-\delta/10}) \approx 0.3 \frac{100}{\delta} . s$.

THE TOTAL COST OF THE STRUCTURE

The total cost of the structure K was defined as the cost of construction I and the capitalized anticipated damage S. Hence: $K = I + S$. With the expressions already established it is then found that for:

Monolith structures: $K = f(F_o) + \frac{100}{\delta} . \rho(F^{**}) . W.$

Rubble-mound structures: $K = f(H_{so}) + \frac{100}{\delta} \sum \Delta\rho . \Delta W.$

THE DESIGN WAVE OR DESIGN LOAD

The design wave or design load is governed by the condition that the cost K shall be as low as possible. It is sometimes possible to determine the minimum values of the expressions for K analytically, but it is usually easier to determine the minimum K_o graphically. This method has the advantage that a good impression is obtained of the function K near its minimum. This is of particular importance with respect to the amount of money "wasted" if the wrong design wave or load is adopted. The latter sum is called the "regret".

The main cause of any error in the value of H_{so} or F_o will be that the K curve itself is wrong, due to inaccuracy of the data. The respective curves K, I and S are generally similar in all cases. The cost of construction increases gradually as H_{so} or F_o increases. See fig. 1. The capitalized damage S, however, decreases rapidly as H_{so} or F_o increases, especially if the decrease in the probability of occurrence of H_{so} or F_o is great. The curve K always has a rapidly decreasing portion on the left of its minimum and a slowly inoreasing portion on the right. Consequently the "regret" is greater for a design wave or load that is too small, than it is for a design wave that is to the same extent too great. See fig. 1. Hence one should be on the safe side when deciding upon a design wave or load.

The method of approach described in the foregoing has been culled from the determination of design levels for the Delta project in the Netherlands (ref. 1, 2 and 7).

The procedure discussed above is worked out for cases embodying optimum values for:

- the dimensions of two monolith struotures;
- the dimensions (weight of stone, slope) of two rubble-mound structures.

Most of the cases were taken from studies carried out on various designs for Europoort Harbour, Rotterdam.
A plan of the harbour is given on page 17.

MONOLITH STRUCTURES

RELATION BETWEEN OFF-SHORE CONDITIONS AND THE BEHAVIOUR OF THE STRUCTURE

The wave forces acting on a monolith structure fall into two main categories:

- quasi-static foroes, defined as forces that fluctuate with the same period as the incident waves (period of about 5-10 sec);
- dynamic or impact forces, defined as forces the duration of

which is short compared with the wave period (for steep barriers a corresponding period of the order of 1 sec*)).

To obtain some idea of the relation between structure displacement and wave force, an approximate and simplified calculation has been made of the positive displacements of a caisson-type breakwater with vertical weather-side front and assuming a sinussoidal load, a friction coefficient f = 0.5 and a non-elastic horizontal bed. The results are given in figure 2 in which the displacement x is given as a function of F/F_0.

If a displacement of the order of one metre is taken as indicating failure of the structure, it appears from figure 2 that for quasi-static loads (period $\geqslant$ 5 sec) the value of F/F_0 always has to be taken as unity, because exceeding force F_0 can easily lead to a displacement of metres. Consequently, the probability of failure is $p(F_0)$. In the case of dynamic forces acting on steep barriers (period in the order of 1 sec) a displacement of about a metre will occur if $F/F_0 \simeq 2$. Adopting a value of $F/F_0 = 2$, however, will generally lead to much greater displacement, because of the accumulated displacement due to forces between F_0 and $2F_0$. So the ratio F/F_0 has to be reduced; $F/F_0 = \alpha$, with $1 < \alpha < 2$. The value of α depends on the probability distribution curve of F and the value of F_0. In this case the probability of failure is $p(\alpha F_0)$.

CAISSON WITH VERTICAL FRONT

Structure. It was concluded from the function criteria, the off-shore conditions and model investigations on wave attenuation that the minimum crest height is M.S.L. + 2 mtrs. Initial calculations showed that in view of the expense and the off-shore conditions concerned the crest height must be kept as low as possible. Hence the crest height is kept at M.S.L. + 2 mtrs. The specific gravity of the caisson with its sand fill is $\gamma = 2.1$ tons per cubic metre. The coefficient of friction is f = 0.5.

A diagram of the structure is given in figure 6.

The occurrence of the off-shore conditions. Both quasi-static and dynamic forces (F_{stat} and F_{dyn}) act on the exposed front of the structure. Probability distribution curves are given in figure 7. They were derived from field measurements and model investigations (see also ref. 6). The wave heights, hence the quasi-static forces are limited by the depth of the water, so for small probabilities the probability distribution curve has the same configuration as that of the water levels. Only H_s = 5.5 mtrs has been taken into account when determining the probability of excess of the dynamic forces. Wave pressures under the caisson are being ignored for the moment.

Relation between off-shore conditions and the behaviour of the structure. See relevant paragraph on page 5 . Assuming for the moment that quasi-static forces and dynamic forces are independent,

*) It should be noted that the duration of overall dynamic forces is often considerably greater than the duration of local pressures.

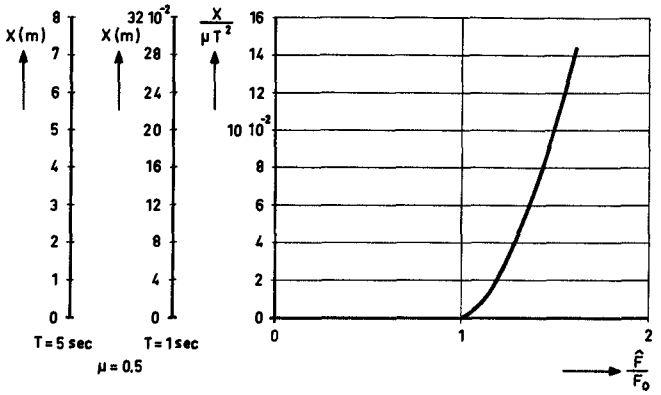

FIG. 2 DISPLACEMENT OF A CAISSON UNDER INFLUENCE OF A SINUSOIDAL FORCE

X = DISPLACEMENT IN m
F(t) = WAVE FORCE = $\hat{F}$ sin ω t
εF(t) = UPLIFT FORCE OUE TO WAVE ACTI
F_0 = DESIGN LOAO
W_{eff} = WEIGHT OF UNIT AT STILL WATER
W = WEIGHT OF UNIT IN AIR
μ = $\frac{W_{eff}}{W}$
f = BOTTOM FRICTION COEFFICIENT = $\frac{1}{2}$
T = PERIOD OF THE WAVE FORCE
ω = ANGULAR FREQUENCY = $\frac{2\pi}{T}$
g = ACCELERATION OF GRAVITY

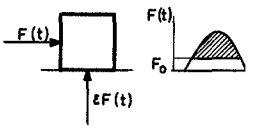

POSITIVE OISPLACEMENT FOUND FRO

$\hat{F}\sin\omega t - f(W_{eff} - \varepsilon\hat{F}\sin\omega t) = \frac{W_{eff}}{\mu g}\frac{d^2x}{dt^2}$

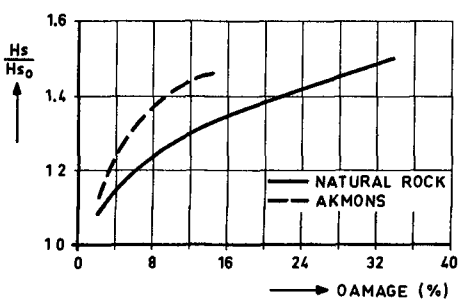

FIG. 3 DAMAGE AS A FUNCTION OF $\frac{Hs}{Hs_0}$

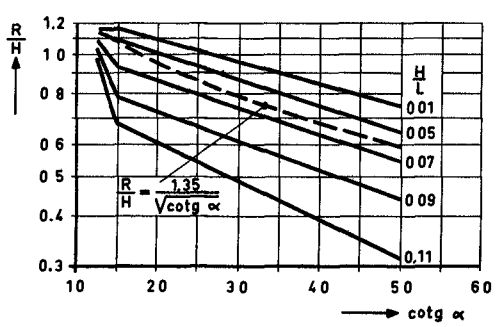

FIG. 4 RELATIVE WAVE RUN UP (AFTER HUDSON)

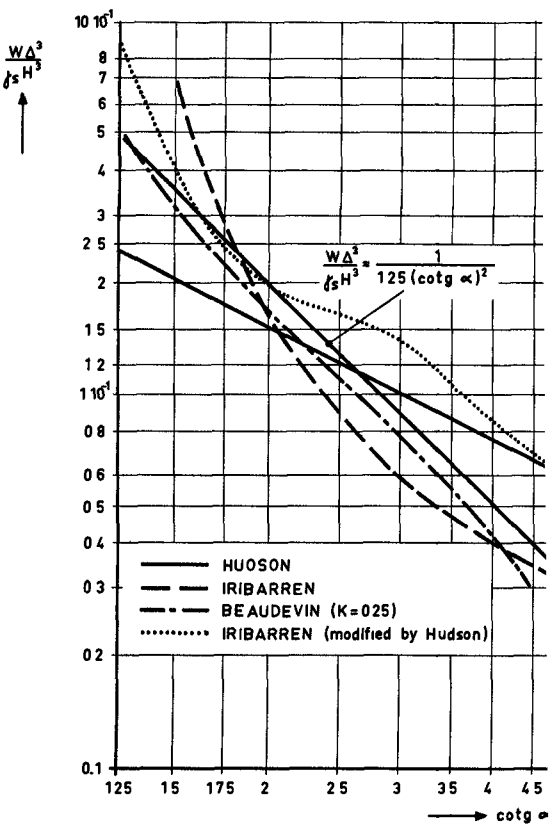

FIG. 5 STABILITY OF NATURAL ROC

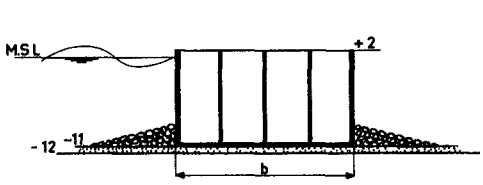

FIG. 6 CAISSON WITH VERTICAL FRONT

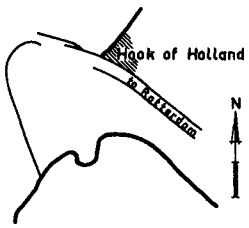

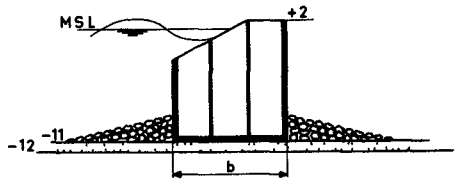

FIG. 9 CAISSON WITH COMPOSITE FRONT

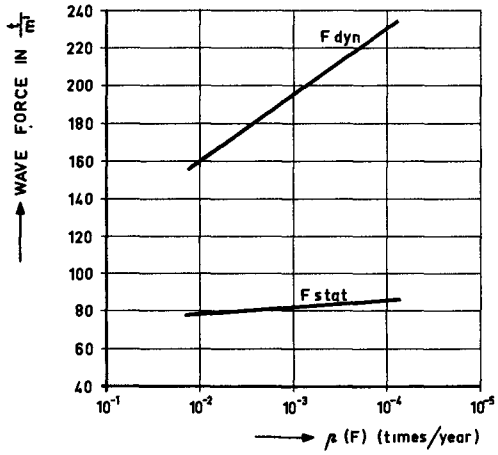

FIG. 7 PROBABILITY OF EXCESS OF F

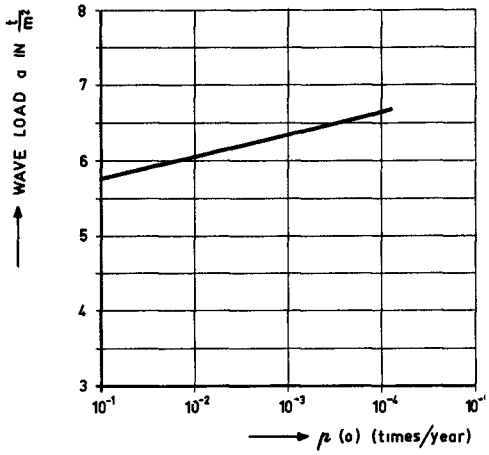

FIG. 10 PROBABILITY OF EXCESS OF σ

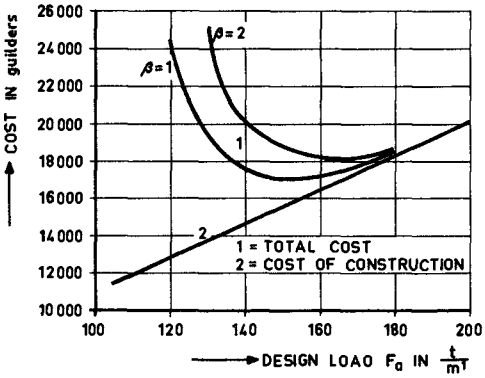

FIG. 8 COST AS A FUNCTION OF F_0

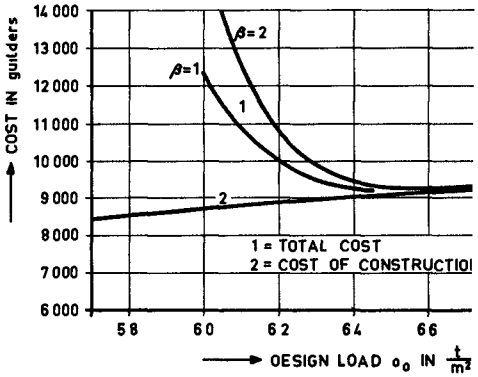

FIG. 11 COST AS A FUNCTION OF σ_0

the probability of failure is:

$$p(\text{failure}) = p(F_{stat}) + p(F_{dyn}).$$

It may be concluded that, for the structure and off-shore conditions considered, a force $F_{dyn} = 1.2\ F_{dyn_o}$ results in a displacement which is fairly representative of the accumulated displacement due to forces $F_{dyn} > F_{dyn_o}$. It is clear from the probability distribution curves that $p(F_{stat})$ is much smaller than $p(1.2\ F_{dyn_o})$ and can be ignored. So dynamic forces only have to be considered and $p(\text{failure}) = p(1.2\ F_{dyn_o})$.

The relation between the required volume of the caisson per metre of exposed front V_{re} and design load F_{dyn_o} is

$$V_{re} = \frac{1}{f(\gamma-1)} F_{dyn_o} = 1.82\ F_{dyn_o} \text{ cub.mtr.}$$

The relation between cost of construction and design load. It is assumed that the cost of construction is a linear function of V, so

$I = AV + B$ in which:

A = Dfl 50 per cub.mtr.

B = Dfl 2000 per cub.mtr. (= cost of toe protection, etc.).

$V = 1.82\ F_{dyn_o}$.

Hence: $I = 91\ F_{dyn_o} + 2000$.

The relation between anticipated damage, off-shore conditions and design load. The capitalized value of the anticipated damage is

$$S = \frac{100}{\delta} p(1.2\ F_{dyn_o}).W$$ (see page 4).

The money per metre weather-side front involved in a failure, W, is assumed to be proportional to the cost of construction.

$W = \beta I$.

From this and the expression for I it follows that

$$S = \frac{100}{\delta} . p(1.2\ F_{dyn_o}).(91\ F_{dyn_o} + 2000).$$

The total cost of the structure, $K = I + S$.

Substitution of the expressions for I and S gives:

$$K = (91\ F_{dyn_o} + 2000).\left\{1 + \frac{100}{\delta} . p(1.2\ F_{dyn_o})\right\} .$$

The values of K and I have been plotted as a function of F_{dyn_o} for $\frac{100}{\delta} = 30$, $\beta = 1$ and $\beta = 2$. See figure 8.

The design load. Dimensions of structure. It is evident from figure 8 that the optimum design load F_{dyn_o} is 150 to 170 tons per metre, depending on the value for β adopted. In view of the difficulty encountered when replacing a single caisson β will generally be greater than unity. For that reason and for the reasons given on page 5. under "Design load", 170 tons per metre has been adopted for F_{dyn_o}. The probability of failure occurring in any given year is $p(1.2\ F_{dyn_o}) = 5.10^{-4}$ or once in 2000 years on an average.

V = 310 cub.mtrs. Hence the width of the caisson $b = \frac{V}{13} = 24$ mtrs.

I = Dfl 17,500.

K = Dfl 17,760 for $\beta = 1$.

K = Dfl 18,020 for $\beta = 2$.

CAISSON WITH COMPOSITE WEATHER-SIDE FRONT

Structure. The upper part of the exposed front of the caisson is inclined, so as to reduce the effect of dynamic forces on its stability. The crest height is determined in the same way as that described for a caisson with vertical front, it is M.S.L. + 2 mtrs. The specific gravity of the caisson with sand fill is $\gamma = 2.1$ tons per cub.mtr. The coefficient of friction is $f = 0.5$. The structure is shown diagrammatically in figure 9.

The occurrence of the off-shore conditions. This type of structure was tested for wave forces by the Coastal Engineering Laboratory at Copenhagen and at the Hydraulics Laboratory at Delft. Those tests and experiments on similar structures showed that:

- When the top of the vertical front is some distance below S.W.L., the dynamic forces on the vertical part are small compaired with the quasi-static forces, so they may be neglected.
- When the crest of the structure is below S.W.L. the quasi-static forces acting on the vertical part result from equally distributed wave pressures. The probability distribution curve for the magnitude of these pressures, a, is given in figure 10. It was derived from field measurements of off-shore conditions and from model tests.
- Both dynamic and quasi-static forces act on the inclined part. The angle of inclination is made equal to the angle of friction between the caisson and its foundation so as to prevent those forces from affecting the caisson's sliding stability.

The wave pressures underneath the caisson are assumed to be linear between the wave pressure at the front and the mean water pressure on the inside.

Relation between off-shore conditions and the behaviour of the structure. See relevant paragraph on page 5 . As only quasi-static forces need be considered: $p(\text{failure}) = p(a_o)$. The relation between the required volume of the caisson per metre of exposed front V_{re} and the design load a_o is:

$$V_{re} = \frac{1}{f}\,\frac{(\text{force on vert. front})}{\gamma - 1} + \frac{\text{force underneath caisson}}{\gamma - 1}$$

or:

$$V_{re} = \frac{a_o\,(13 - \frac{b-4}{2})\frac{1}{f}}{\gamma - 1} + \frac{\frac{1}{2}\,a_o\,b}{\gamma - 1},$$

in which b is the width of the caisson. See fig. 9.
The value of b can be determined from the postulate that the required volume must equal the present volume V_{pr}. The latter is

$$V_{pr} = 13b - \tfrac{1}{4}\,(b-4)^2.$$

The relation between cost of construction and design load. It is assumed that the cost of construction I is a linear function of V.

$I = AV + B$ in which:

$A = \text{Dfl } 50$

B = Dfl 2000 (= cost of toe protection, etc.).
I can be expressed in terms of a_o with the expressions for V_{re} and V_{pr}. See fig. 11.

The relation between anticipated damage, off-shore conditions and design load. The capitalized value of the anticipated damage is:

$$S = \frac{100}{\delta} \rho(a_o).W.$$ See page 4 .

The money per metre weather-side front involved in a failure, W, is assumed to be proportional to the cost of construction I.

$$W = \beta I.$$

From this and the expression for I it follows that

$$S = \frac{100}{\delta} \rho(a_o).(50\ V + 2000),$$

in which V is a function of a_o. See fig. 11.

The total cost of the structure, K = I + S.
Substitution of the expressions for I and S gives:

$$K = (50\ V + 2000).\left\{1 + \frac{100}{\delta}.\rho(a_o)\right\}.$$

The values of K and I have been plotted as a function of a_o for $\frac{100}{\delta} = 30$, $\beta = 1$ and $\beta = 2$. See fig. 11.

The design load. Dimensions of structure. It is clear from figure 11 that the optimum design load $a_o = 6.6$ tons per square metre. The probability of failure occurring in any given year is $1.4\ 10^{-4}$ or once in 7,200 years on an average.
V = 143 cubic mtrs. b = 12.4 mtrs.
I = Dfl 9,150.
K = Dfl 9,190 for $\beta = 1$.
K = Dfl 9,230 for $\beta = 2$.

RUBBLE-MOUND STRUCTURES

RELATION BETWEEN OFF-SHORE CONDITIONS AND BEHAVIOUR OF THE STRUCTURE

So far but little quantitative information has become available on the damage suffered by the structure as a function of off-shore conditions. The experiments carried out mainly concerned initial damage.

With respect to the seaward cover layer, in first approximation the figure 3 for the relation between H_s/H_{so} and the occurrence of damage can be adopted. This relation was derived from tests on models carried out by the Waterways Experiment Station and the Delft Hydraulics Laboratory (ref. 4 and 8). The results should be used with caution. The damage percentages refer to the number of blocks in the area between the crest ($\simeq$ S.W.L. + H_{so}) to S.W.L. - H_{so}. The damage is often found to have occurred in a more restricted area around S.W.L. For that reason and in view of the rapidly increasing damage for damage $> 30\%$ it is assumed that for 30% damage the cover layers will have become displaced locally and that the structure will have collapsed.

Information on wave attack on the crest and inner slope is even

scarcer. It is known, however, that appreciable overtopping can easily cause damage. Two types of structure will be considered in this light:

- If the inner slope is faced with small category blocks, it is assumed that the structure will collapse as soon as there is appreciable overtopping. The wave run-up found by Hudson (ref. 3 and fig. 4) has been adopted as a criterion for overtopping, H being replaced by H_S.
- If the crest and upper part of the inner slope is protected by armour units such as those used for the seaward cover layer, the relation between damage and H_S/H_{SO} is assumed to be the same for small crest heights $h << H_{SO}$ as it is for the seaward cover layer, however, with the restriction that the structure is assumed to collapse at 10% damage. The latter assumption has been made in view of the fact that the damage occurs mainly along the inner crest line. It is stressed once again that these assumptions have not received adequate experimental support.

In the example of a rubble-mound structure with a cover layer of natural rock, the relation between block weight and the angle of the slope must be known. Some existing formulae are given in figure 5. For practical reasons an average curve is assumed in which the block weight is inversely proportional to $\cot g^2 \alpha$, and in which the wave height is H_S, see fig. 5. It is not the intention of the authors to propound a new formula.

RUBBLE-MOUND WITH COVER LAYER OF CONCRETE BLOCKS

Structure. From the function criteria and data on wave heights and water levels (see also ref. 9) it was concluded that the minimum crest height required was M.S.L. + 2 mtrs. This implies that mass overtopping will occur, and that consequently the crest and harbour-side slope will be subject to severe wave attack. The crest would have to be raised to at least M.S.L. + 7 mtrs. to reduce this wave attack, which appeared to be an uneconomical solution in view of the increased cross-sectional area and the relatively expensive core material. Accordingly, the crest height has been kept at M.S.L. + 2 mtrs.

As regards the slope of the structure it can be shown that for the off-shore conditions and prices concerned the steepest possible slope should be adopted. A slope of 1:1.5 was adopted for practical reasons.

The example has been worked out for a cover layer consisting of concrete akmons with a density of ρ = 2800 kilogrammes per cubic metre. A diagrammatic sketch is given in figure 12.

The occurrence of off-shore conditions. The data on wave heights were obtained from wave-recording stations in the North Sea. A probability distribution curve of H_S was derived from the data expressed as the number of storms in which a certain H_S is exceeded. See fig. 13.
For information on the distribution of individual wave heights see ref. 10.

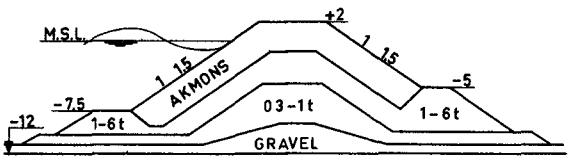

FIG. 12 STRUCTURE WITH COVER LAYER OF CONCRETE BLOCKS

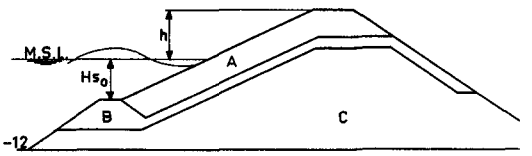

FIG. 15 STRUCTURE WITH COVER LA OF NATURAL ROCK

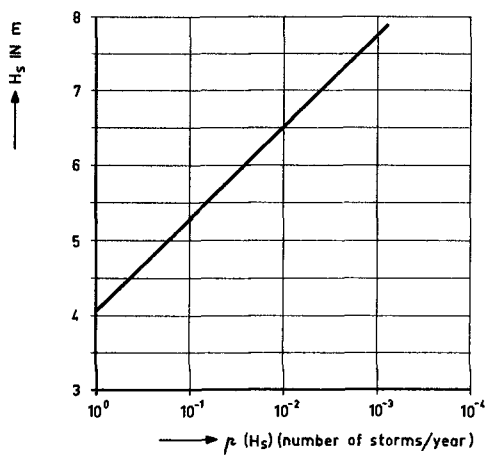

FIG. 13 PROBABILITY OF EXCESS OF H_s

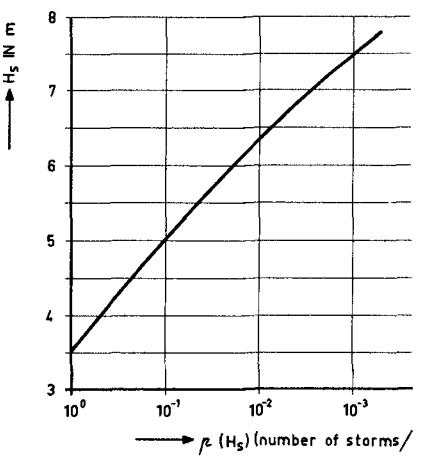

FIG 16 PROBABILITY OF EXCESS OF

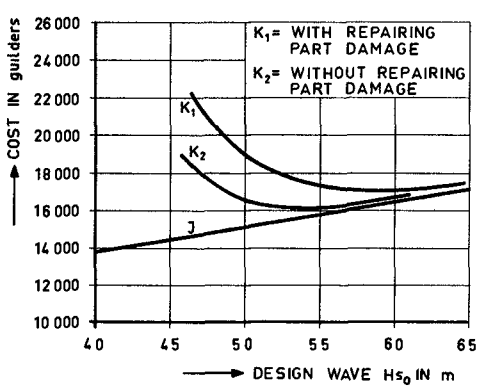

FIG. 14 COST AS A FUNCTION OF H_{s_0}

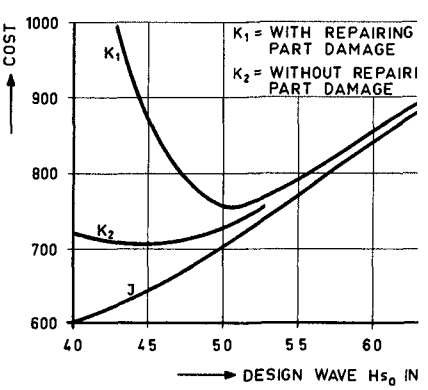

FIG. 17 COST AS A FUNCTION OF H

Relation between off-shore conditions and behaviour of the structure. See relevant paragraph on page 9 . For wave heights exceeding H_{so}, damage occurs as shown in figure 3. Here the percentage of damage refers to the whole concrete cover layer. As mentioned on page 10 it is assumed that the structure will collapse at 10% damage, hence when $H_s/H_{so} = 1.45$, see fig. 3. As regards the relation between the design wave height H_{so} and block weight (akmons), tests on models and data from ref. 8 showed that

$$W = \frac{2.8\ H_{so}^3}{50} \text{ ton (slope 1:1.5; } \rho = 2800 \text{ kilogrammes per cubic metre.)}$$

Relation between cost of construction and design wave. $I = f(H_{so})$. The cost of construction can be divided up into the cost of the concrete cover layers and the cost of the second layers and core. The latter two are independent of the design wave height, and are per metre weather-side front:

79 cub.mtrs.	gravel	Dfl 1580.-
84 " "	rock 0.3-1 t.	" 2270.-
100 " "	rock 1-6 t. (dumped)	" 2700.-
34 " "	" " (by crane)	" 1290.-
		Dfl 7840.-
	wastage 10%	" 780.-
		Dfl 8620.-

The cost of the cover-layers is assumed to be proportional to the total volume of concrete per metre weather-side front, Q.

$Q = CAV^{1/3}$, (ref. 8) in which:

V is the volume of a block: $V = \frac{W}{2.8} = \frac{H_{so}^3}{50}$.

C is a constant; for akmons C = 0.9.

A is the area to be covered per metre: A = 33.

Assuming a wastage of 10% of the blocks during construction, it is seen that:

$Q = 8.8\ H_{so}$.

Concrete costs Dfl 150 per cub.mtr. hence the cost of the cover-layers per metre, I_{cl}, works out at

$I_{cl} = 8.8 \cdot 150 \cdot H_{so} = 1320\ H_{so}$.

Consequently the cost of the structure per metre:

$I = 1320\ H_{so} + 8620$.

Relation between anticipated damage, off-shore conditions and design wave. $S = \frac{100}{\delta} \sum \Delta n\ \Delta W$. See page 4 .

Three intervals for H_s/H_{so} are considered for the occurrence of H_s. The corresponding damage percentages and the probability of occurrence follow from figures 3 and 13. The amount of damage ΔW is assumed to be: percentage of damage x cost of construction of cover-layers x 2. The latter factor 2 has been arbitrarily adopted in view of the fact that the placing of a limited number of blocks later on is more expensive. For a collapse, ΔW is assumed to be equal to the total cost of construction. For various values of H_{so}, Δn and ΔW

are given in Table 1.

As slight partial damage needs not necessarily be repaired*, two cases will be considered:

- the amount of damage when partial damage is repaired;
- the amount of damage when partial damage is not repaired.

For $\frac{100}{\delta} = 30$ the values of s and S are given in Table 2.

The total cost of the structure. K = I + S.
The total cost of the structure for various values of H_{so} is given in table 3. The sums are also given in figure 14 in which I and K have been plotted as a function of H_{so}.

The design wave. Required block weight. In accordance with the minimum total cost criterion the design wave H_{so} is:
H_{so} = 6 mtrs. and H_{so} = 5.5 mtrs. if partial damage is not repaired.

H_{so} (m)	$P(H_{so})$	Probability of failure $P(1.45\ H_{so})$	Block weight W (tons)
6	$2.6\ 10^{-2}$	$1.8\ 10^{-4}$	12
5.5	$6.5\ 10^{-2}$	$7.5\ 10^{-4}$	9

RUBBLE MOUND WITH COVER LAYER OF NATURAL ROCK
Structure. The structure considered has a straight seaward slope in the area of severe wave attack. The cover layers are supported by a hard shoulder and the inclination of its lower slope is 1:1.5, which is assumed to be the steepest slope that is easy to construct. The material available is said to lead to the following conditions:

- the quarry provides certain quantities of various categories of blocks with a clearly defined maximum block weight (W = 7 tons ρ = 2650 kilogrammes per cubic metre).
- the harbour-side slope is protected by smaller blocks than those used for the seaward cover layer, and cannot withstand considerable overtopping (in view of the small percentage of the heaviest blocks).

The stability of the harbour-side slope faced with small blocks depends mainly on the crest height. So increasing the cross-sectional area should be effected by heightening the crest rather than by adopting a gentler harbour-side slope.
The steepest slope that is reasonably easy to construct is assumed to be cotg α = 1.5.

Density of stone and water: ρ_s = 2650 and ρ_w = 1030 kilogrammes per cubic metre, respectively.

* Whether or not repairs shall be carried out is also a matter of personal decision on the part of the one who is responsible for the maintenance of the structure. It is known, however, that a small percentage of damage makes no difference to the effect of successive wave attacks having greater H_s. It would be worth going to the trouble to find out whether that also holds good for appreciable damage, so as to see if repairing such damage would be of any use.

Table 1.

H_{so} (m)	I	I_{cl}	$1 < H_s/H_{so} < 1.3$, n=4%			$1.3 < H_s/H_{so} < 1.45$ n=8%			$H_s/H_{so} \gg 1.45$; collapse		
			Δp	Δ W	$\Delta p . \Delta W$	Δp	Δ W	$\Delta p . \Delta W$	Δp	Δ W	$\Delta p . \Delta W$
4	13900	5280	1.01	420	430	$5.2.10^{-2}$	860	40	$3.8.10^{-2}$	13900	530
5	15220	6600	$1.6.10^{-1}$	530	80	$4.7.10^{-3}$	1060	5	$2.8.10^{-3}$	15220	40
5.5	15900	7280	$6.3.10^{-2}$	580	40	$1.6.10^{-3}$	1160	-	7.10^{-4}	15900	10
6	16540	7920	$2.5.10^{-2}$	630	15	$5.2.10^{-4}$	1260	-	$1.8.10^{-4}$	16540	3

Table 2.

H_{so} (m)	With repairing partial damage		Without repairing partial damage	
	$s = \sum \Delta p \, \Delta W$	$S = \frac{100}{\delta} s$	s	S
4	1000	30000	530	15900
5	125	3750	40	1200
5.5	50	1500	10	300
6	18	540	3	90

Table 3.

H_{so} (m)	With repairing partial damage			Without repairing partial damage	
	I	S	K	S	K
4	13900	30000	43900	15900	29800
5	15220	3750	18970	1200	16420
5.5	15900	1500	17400	300	16200
6	16540	540	17080	90	16630
6.5	17200	100	17300	20	17220

I in guilders.
n = percentage of damage.

Crest width b (in view of block size) b = 5 mtrs.
Height of hard shoulder in seaward cover layer: M.S.L. - H_{so} mtrs.
A diagrammatic sketch is given in figure 15.

The occurrence of off-shore conditions. In this example the wave conditions taken are those found along the south coast of Turkey. A probability distribution curve for H_s is given in figure 16. The water level is constant. The depth is assumed to be 12 mtrs.

Relation between off-shore conditions and behaviour of the structure. The damage to the seaward cover layer for wave heights exceeding H_{so} (see the relevant paragraph on page 9) is given in figure 3, provided that the heaviest layer is extended down to M.S.L. - H_{so} mtrs. It is assumed that the structure will collapse at 30% damage, hence when $H_s = 1.45\ H_{so}$. See fig. 3. In view of the particulars given in figure 4, it is also assumed that critical overtopping (i.e. collapse of the structure) will occur at

$H_s = \frac{h\sqrt{\cot g\alpha}}{1.35}$, in which h is the crest height above M.S.L.

Failure will occur when the critical value for overtopping

$H'_{so} = \frac{h\sqrt{\cot g\alpha}}{1.35}$ or the critical value for the collapse of the seaward cover layer $1.45\ H_{so}$ is exceeded. As the entire cross section is destroyed in both cases, it will always collapse at the smaller of the two values H'_{so} and $1.45\ H_{so}$. Consequently, the optimum design is obtained when $H'_{so} = 1.45\ H_{so}$.
The corresponding crest height is:

$$h = \frac{1.35 \cdot 1.45\ H_{so}}{\sqrt{\cot g\alpha}} = \frac{1.95\ H_{so}}{\sqrt{\cot g\alpha}}$$

The relation between the angle of inclination of the seaward cover layer and the design wave H_{so} for a given block weight W and relative density Δ is:

$$\cot g\alpha = \sqrt{\frac{\gamma_s H_{so}^3}{1.25\,\Delta^3 W}}.$$ See also fig. 5.

Relation between cost of construction and design wave. $I = f(H_{so})$. It is assumed that the breakwater will be built with the aid of floating equipment, the cost of which is practically the same, for all the structures considered. Hence the cost of construction is determined by the quantities of the various categories of rock. The quantities for different values of H_{so} have been worked out, see table 4.

For the sake of simplicity it has been assumed that the prices of all the categories of blocks are the same and equal to the unit. So the cost of construction, I, appears in the last column in table 4.

Relation between anticipated damage, off-shore conditions and design wave. $S = \frac{100}{\delta}\sum \Delta p \cdot \Delta W$.
The capitalized anticipated damage is determined in a manner similar to that in which the akmon cover layer is established. Five intervals

Table 4.

H_{so} (m)	cotg α	h (m)	Vol. of rock in m^3 per m'			Total
			cat. A	cat. B	cat. C	
4	1.55	6.2	77	78	446	601
4.5	1.85	6.3	92	84	470	646
5	2.2	6.4	106	91	505	702
6	2.85	6.7	140	109	594	843
7	3.6	7	182	129	647	958

Table 5.

H_{so} (m)	I	I cat.A	$1 < H_s/H_{so} < 1.2$, n=3%			$1.2 < H_s/H_{so} < 1.3$, n=9%			$1.3 < H_s/H_{so} < 1.4$, n=17%		
			Δn	Δ W	$\Delta n \Delta W$	Δn	Δ W	$\Delta n \Delta W$	Δn	Δ W	$\Delta n \Delta W$
4	601	77	$3.5.10^{-1}$	4.6	1.6	8.10^{-2}	14	1.1	$3.2.10^{-2}$	26	0.8
4.5	646	92	$1.8.10^{-1}$	5.5	1	$2.9.10^{-2}$	16.6	0.5	$1.4.10^{-2}$	31	0.4
5	702	106	8.10^{-2}	6.4	0.5	$1.3.10^{-2}$	19	0.2	$4.2.10^{-3}$	36	0.2
6	843	140	$1.8.10^{-2}$	8.4	0.2	$1.3.10^{-3}$	25	-	4.10^{-4}	48	-
7	958	182	$2.8.10^{-3}$	10.9	-	-	-	-	-	-	-

Table 5.

H_{so} (m)	I	I cat.A	$1.4 < H_s/H_{so} < 1.45$ n=2%			$H_s/H_{so} > 1.45$; collapse		
			Δn	Δ W	$\Delta n \Delta W$	Δn	Δ W	$\Delta n \Delta W$
4	601	77	9.10^{-3}	39	0.4	$2.9.10^{-2}$	601	17.5
4.5	646	92	4.10^{-3}	46	0.2	8.10^{-3}	646	5.2
5	702	106	$1.2.10^{-3}$	53	0.1	$1.6.10^{-3}$	702	1.1
6	843	140	7.10^{-5}	70	-	8.10^{-5}	843	0.1
7	958	182	-	-	-	-	-	-

H_S/H_{SO} are considered. The corresponding percentages of damage follow from figure 3 and refer to category A blocks, see fig. 15. The amount of damage ΔW is assumed to be: damage percentage x cost of cover layers made of category A blocks x 2. For a collapse, ΔW is assumed to be equal to the cost of construction. For various values of H_{SO}, Δn and ΔW are given in table 5. The damage due to the collapse of the structure is also given separately. For $\frac{100}{\delta} = 30$ the values of s and S are given in table 6.

The total cost of the structure. K = I + S.
The total cost of the structure for various values of H_{SO} is given in table 7. The sums are also given in figure 17 in which I and K have been plotted as a function of H_{SO}.

The design wave. Required slope. In accordance with the minimum total cost criterion the design wave H_{SO} is:
H_{SO} = 5.1 mtrs. and H_{SO} = 4.5 mtrs. when partial damage is not repaired.

H_{SO} (m)	$n(H_{SO})$	Probability of failure	Angle of seaward slope
5.1	9.10^{-2}	$1.2\ 10^{-3}$	cotg α = 2.25
4.5	$2.5.10^{-1}$	$7.5\ 10^{-3}$	cotg α = 1.85

CONCLUSIONS

1. The decision on the type of structure and its dimensions can be based on the criterion of minimum total cost.
2. The total cost of a structure can be expressed in terms of design wave or load. To establish this relation there must be known: the off-shore conditions, the behaviour of the structure, the cost of construction and the anticipated damage.
   Although information on this is often insufficient, for reasonable assumptions important directives can be obtained with respect to minimum total cost and corresponding optimum design wave or load.
3. The method is especially of great aid when it concerns ranking of similar structures, as the errors made in costs of construction, damage etc. will in that case affect the results in the same way.
4. The scope of information needed to determine the minimum cost can be used as a bases for future investigations on breakwater design.

REFERENCES

1. W.C. BISCHOFF VAN HEEMSKERCK, Enige beschouwingen over het berekenen van de economische dijkverhoging, waarin opgenomen een berekening voor het gebied van Centraal Holland. Nota Secretariaat Deltacommissie, 1955.

2. D. VAN DANTZIG, Economic decision problems for flood prevention. Econometrica. Vol. 24, No. 3, July 1956.

3. R.Y. HUDSON, Design of quarry-stone cover layers for rubble-mound breakwaters. U.S. Waterways Experiment Station. Research report No. 2-2. Vicksburg, 1958.

Table 6.

H_{so} (m)	With repairing partial damage		Without repairing partial damage	
	$s=\sum \Delta p \cdot \Delta W$	$S = \frac{100}{\delta} s$	s	S
4	21.4	642	3.9	117
4.5	7.3	219	2.1	63
5	1.9	57	0.8	24
6	0.3	9	0.2	6
7	-	-	-	-

Table 7.

H_{so} (m)	I	With repairing partial damage		Without repairing partial damage	
		S	K	S	K
4	601	642	1243	117	718
4.5	646	219	865	63	709
5	702	57	759	24	726
6	843	9	852	6	849
7	958	-	958	-	958

4. R.Y. HUDSON, Laboratory investigation of rubble-mound breakwaters. A.S.C.E. Paper 2171 pp 93-121. New York, 1959.

5. J.E. PRINS, Model investigations of wind-wave forces, Proc. VII Conf. on Coastal Engineering, The Hague, 1960.

6. W.A. VENIS, Determination of wave attack anticipated upon a structure from laboratory and field observations. Proc. VIIth Conf. on Coastal Engineering, The Hague, 1960.

7. DELTACOMMISSIE, Het economisch beslissingsprobleem inzake de beveiliging van Nederland tegen stormvloeden. Rapport Deltacommissie deel 3, bijdrage II.2, September, 1960.

8. A. PAAPE AND A.W. WALTHER, Akmon armour unit for cover layers of rubble-mound breakwaters. Proc. VIIIth Conf. on Coastal Engineering, Mexico, 1962.

9. J.N. SVÅSEK, Correlation between wave height and sea level in a shallow sea. Proc. IXth Conf. on Coastal Engineering, Lisbon, 1964.

10. L.A. KOELÉ AND P.A. DE BRUYN, Statistical distribution of wave heights in correlation with energy-spectrum and water-depth. Proc. IXth Conf. on Coastal Engineering, Lisbon, 1964.

Chapter 35

SEAWARD PROFILE FOR RUBBLE MOUND BREAKWATERS

by

Melville S. Priest
Head of Civil Engineering, Auburn University

Joel W. Pugh
Second Lieutenant, Corps of Engineers, U.S. Army

Rameshwar Singh
Graduate Student, Stanford University

ABSTRACT

For several years, some coastal engineers have been aware that the seaward face of rubble mound breakwaters of the common trapezoidal cross-section is conducive to relatively severe wave action and possible damage to the breakwaters. Further, it has been suggested that a preferable seaward profile would be that composed of three straight lines, with the middle line at a relatively small angle with the horizontal, to form what might be thought of as a broad berm.

In order to arrive at a more realistic knowledge of seaward profiles for which wave intensity and likelihood of breakwater damage are minimal, a laboratory study of shallow-water wave action on rubble breakwaters was initiated at Auburn University. It is hoped that such knowledge will lead to design procedures which will result in (a) less violent wave action, (b) less structural damage, and (c) the possible use of smaller stones.

Thus far, the study has been devoted to shallow-water waves of two types, steep, smooth waves and spilling breakers, acting, with normal incidence, upon breakwaters constructed of various materials and having an initial seaward slope of 1 on $1\frac{1}{2}$.

For each set of conditions, the stable seaward profile was determined. Through dimensional analysis and curve fitting, an effort was made to describe the stable seaward profiles in terms of physical quantities which influence the profiles. It is the authors' belief that the results of this study will be useful in leading to more rational design procedures.

INTRODUCTION

Judging from existing structures, one might say that the conventional cross-section for rubble mound breakwaters is trapezoidal in shape. It is probable that the principal influencing factors in establishing this conventional cross-section were simplicity of construction, initial volume of material, and insufficient knowledge of wave action upon breakwaters. However, it is now known that the seaward

face of the conventional trapezoidal cross-section is not natural to the wave motion and results in relatively violent wave action and the need for extremely large, heavy stones to prevent damage to the structure. In recognition of this problem, a comprehensive study was conducted and reported by Barbe and Beaudevin[1]. Later, it was suggested by Beaudevin[2] that the seaward profile might be designed with a berm, thus reducing the violence of wave action.

Experimental studies by the authors, for shallow-water waves, have resulted in a clearer understanding of the seaward profile which is natural to the breakwater materials and the waves to which they are subjected. To the best of the authors' knowledge, this natural profile has not heretofore been adequately described. For the breakwaters studied in the laboratory, material was moved from the upper part of the seaward profile to the lower part of that profile, without significant change in cross-sectional area of the breakwater. However, practical considerations arising from the steepness of the upper part of the natural profile and from the need to preserve an adequate crest width may require a greater cross-sectional area and volume of material for the breakwater with the natural profile than for the conventional type. But, when one considers the possibility of using smaller stones than those indicated by conventional formulae, there may be instances in which the breakwaters with natural profiles will compare favorably, in an economic sense, with those of conventional profiles.

The continuing study initiated at Auburn University is for the purpose of determining means by which natural seaward profiles of rubble mound breakwaters may be described. The study is concerned with the relationship between particular breakwater materials, stillwater depths, wave characteristics, and profile coordinates for shallow-water waves at normal incidence. The initial phases of the study have been reported in theses by Pugh[3] and Singh[4]. Results of the study are described in generalized terms through dimensionless parameters involving quantities pertinent to the study.

EQUIPMENT

This study was made with facilities in the Hydraulics Laboratory of Auburn University, Auburn, Alabama. The primary item of equipment was a wave basin having an interior length of 44 feet, width of 2 feet, and depth of 2 feet, except for a depression in the vicinity of the generator. The wave generator is of the horizontal-plunger type with a vertical, plane face. Wave frequency is controlled through a variable-speed drive. The wave height is controlled through the setting of a crank arm. The basin is of rectangular cross-section with a horizontal bottom, except for the depression near the generator. A part of one wall in the vicinity of the test section is constructed of glass. A grid system was drawn on the glass to enable determination of coordinates describing the seaward profile of the test section. A hook-point gage was used to determine wave height and stillwater depth.

EXPERIMENTAL PROCEDURE

After the choice of shape, size, and specific gravity of material to be used in the test section had been made, the test section was constructed in the wave basin. The test section was located within that part of the basin having a glass wall along one side and far enough removed from the wave generator that the incident waves could be considered as reasonably stable. The axis of the test section was about 22 feet from the wave generator. Thus far, all test sections have been constructed with seaward faces that were initially plane, with a slope of one vertical on $1\frac{1}{2}$ horizontal. The height of the section was such that there was no significant overtopping. For all tests, the wave period was sufficiently great that each wave was more or less independent, approximating a solitary wave. This condition is considered to be representative of shallow-water waves. The distance between crests was 10 to 12 feet. Two types of waves were studied: smooth waves of such steepness as to be near instability and spilling breakers. After the water level in the basin had been brought to the desired elevation, an approximate setting of the crank arm for desired wave conditions was made and the wave generator operated for a period of time sufficient to make the necessary adjustments in wave height. Then, the seaward face of the test section was reshaped to its initial plane surface. The wave generator was put in operation and allowed to operate until the seaward profile of the test section had become stable. Operation of the generator was then stopped, and coordinates of the seaward profile were determined from the grid system on the glass wall of the basin. The same procedure was repeated for various shapes, sizes, and specific gravities of materials and for various water depths and wave conditions.

Each test section was constructed of a single material. The several test sections were constructed of the following materials:

Material	Specific Gravity	Size (inches)	Shape
Coal	1.30	1 - $1\frac{1}{2}$	Irregular
Granite	2.89	1 - $1\frac{1}{2}$	Irregular
Limestone	2.71	$\frac{1}{2}$ - 3/4 3/4 - 1	Irregular
Concrete	2.26	5/8 $1\frac{1}{4}$	Cube

Coal was included in the study because of its low specific gravity. The greater movement of the coal contributed to a better understanding of the phenomenon through observation and photography and through extension of the range of experimental data. It is not expected that coal would be used as a prototype material.

Limiting values of stillwater depth were 0.5 and 1.10 ft. The value of H/D for which the smooth waves were studied was between 0.4

and 0.5 and the value for which the breaking waves were studied was between 0.6 and 0.7.

ANALYSIS OF DATA

It was observed that the tendency of waves was to move material from the upper portion of the seaward face to the lower portion. This tendency is illustrated in Figure 1. It was found by Pugh[3] that the stable profile intersects the initial plane face at about 0.2 of the still-water depth below the still-water surface. This point was chosen as the origin for subsequent curve fitting. All coordinates determined from the grid system on the glass wall of the basin were converted to coordinates from horizontal and vertical axes through the adopted origin. Physical quantities necessary for describing the stable seaward profile resulting from either a smooth wave or a spilling breaker might be related through dimensionless parameters of the implicit function

$$\phi\left(\frac{x}{D}, \frac{y}{D}, \frac{d}{D}, S, \text{shape}\right) = 0 \quad , \qquad (1)$$

where x and y are coordinates of the profile; D is still-water depth; d is a linear index to size of material; S is specific gravity of the material, and the word shape refers to shape of the unit of material.

Although it was desired to describe the seaward profile through a single functional relation, that has not, as yet, been accomplished. For the shallow water conditions of this study, the lower part of the seaward profile was affected by the presence of the solid boundary of the basin bottom. Also, it is possible that the upper part of the seaward profile was affected, in some instances, by the truncated nature of the crest. It was observed that the part of the profile above the origin usually exhibited different characteristics than the part below the origin. Consequently, it has been expedient to divide the curve fitting into two parts. However, either the upper part or lower part can be described satisfactorily through a power function such as

$$\frac{y}{D} = m\left(\frac{x}{D}\right)^n \qquad (2)$$

where m and n are constant for the upper part or the lower part of any particular profile, but, in general, would depend upon the type of waves and be functions of d/D, S, and shape. For either the upper part or lower part, x/D and y/D will be of like sign. For purposes of curve fitting, Singh[4] treated all measurements from the origin as positive.

For a material of particular specific gravity and unit shape and for a particular type of waves, Singh[4] has suggested that m and n might be expressed satisfactorily through a logarithmic function of d/D such as

$$m \text{ or } n = A \log\left(\frac{d}{D}\right) + B \quad , \qquad (3)$$

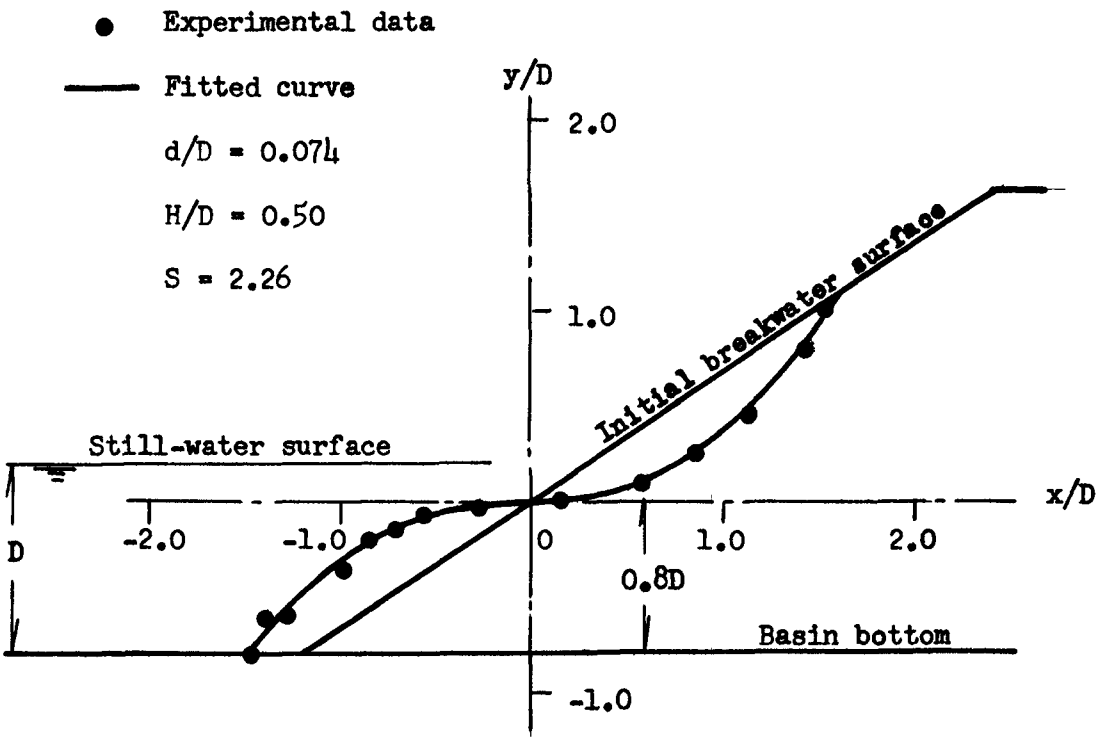

Fig. 1. Seaward profile for steep, smooth waves acting upon a breakwater of concrete cubes

where A and B are constants. In general, the values of A and B would depend upon the type of waves and be functions of specific gravity and unit shape of material. Values of A and B have been tabulated by Singh[4], using the logarithmic base 10.

SUMMARY AND CONCLUSION

It was apparent from the study that the conventional trapezoidal section results in relatively severe wave action coupled with a strong tendency toward movement of material on the seaward face. It was further noted that, after the breakwater material had been moved to form a stable section, the wave action was much less severe and there was no longer any general movement of the material except for very light weight material within a thin zone slightly below still-water surface.

In addition to the observations which have already been stated, Pugh[3] observed that, for particular breakwater material and type of waves, an increase in size of stones resulted in a decrease in volume of material moved and that, for particular size of stones and type of waves, an increase in specific gravity of material resulted in a decrease in the volume of material moved. Singh[4] concluded that, for particular breakwater material and type of waves, the use of cube-shaped units rather than those of irregular shape results in a decrease in volume of material moved.

The study leads to certain design considerations. It is not anticipated that a breakwater would be designed with the expectation that the material would be shifted to a stable section. However, the design could provide for a profile that would be stable for stones which would be more readily moved than those that will actually be used in construction. It seems that it would be practical to design such a section that would be stable for the design incident wave but with smaller stones than would be required by conventional formulae. Although the designer may not be inclined to call for curves such as those resulting from this study, it does seem reasonable to expect that such curves might be used as a guide for a profile composed of appropriate straight lines.

It has been the intent of the authors to point the need for design procedures which will result in a greater degree of compatibility between severe wave action and the rubble breakwater face than is achieved by procedures in common use. Although the study reported herein was limited to conditions which were of primary interest to the authors, such a study can be expanded to include other conditions which are peculiar to some geographical regions. In any event, it is hoped that this paper has served to create an awareness of the shape of the seaward breakwater face as an important design consideration.

REFERENCES

1. Barbe and Beaudevin, Recherches expérimentales sur la stabilité d'une jetée à talus incliné soumise à la houle, La Houille Blanche, June-July 1953.

2. Beaudevin, Stabilité des digues à talus à carapace en vrac, La Houille Blanche, Special A/1955.

3. Pugh, A study of the natural shape of breakwaters, an unpublished thesis presented to Auburn University, December 1962.

4. Singh, A study of the stable cross-section of rubble breakwaters, an unpublished thesis presented to Auburn University, August 1963.

Chapter 36

PRAIA DA VITÓRIA HARBOUR (AZORES) DAMAGES IN THE BREAKWATER DUE TO THE STORM OF 26th - 27th DECEMBER, 1962

José Joaquim Reis de Carvalho
Head, Estuaries and Rivers Division
Laboratório Nacional de Engenharia Civil, Lisboa, Portugal

1 - INTRODUCTION

Praia da Vitória is a harbour in the eastern coast of Terceira, in Azores Islands. These lie in the Nortern Atlantic, between 36° 55' and 39° 43' north latitude and between 26° 46' and 31° 16' west of Greenwich longitude. Terceira island belongs to the central group of islands (fig.1).

The port facilities in Praia da Vitória harbour were constructed with the main purpose of enabling the unloading of liquid fuels, however intense the swell at the entrance of the harbour.

The maritime structures include a rubble mound breakwater about 600 m long, rooted at Ponta do Espírito Santo, and an unloading system, independent from the breakwater and made up of a central hose-handling pier, where tankers can berth, and dolphins to take the mooring lines of the ships. The hose-handling platform and the dolphins are connected with one another and with the shore by means of footbridges (figs. 1 and 3).

2 - DESCRIPTION OF THE BREAKWATER

Given the location of Praia da Vitória harbour in the eastern coast of Terceira and the contour of the island in this zone, the breakwater is free from considerable storm actions, save for NE, E and SE storms. Notice that for the latter direction, S.Miguel and Santa Maria islands restrict the generation of swell, reducing the fetch to a maximum of 120 sea miles. Due to this and to the bottom relief conditions at the southern and the harbour, the breakwater is not subjected to violent actions during SE storms (for a wind of 40 knots, the significant wave height in front of the breakwater does not exceed 4.00 m).

On the other hand, the bottom relief conditions in fron of Ponta de Má Merenda, in the northern area of the harbour give rise to a marked energy dispersion for NE storm and consequently wave height near the breakwater do not exceed 65% o

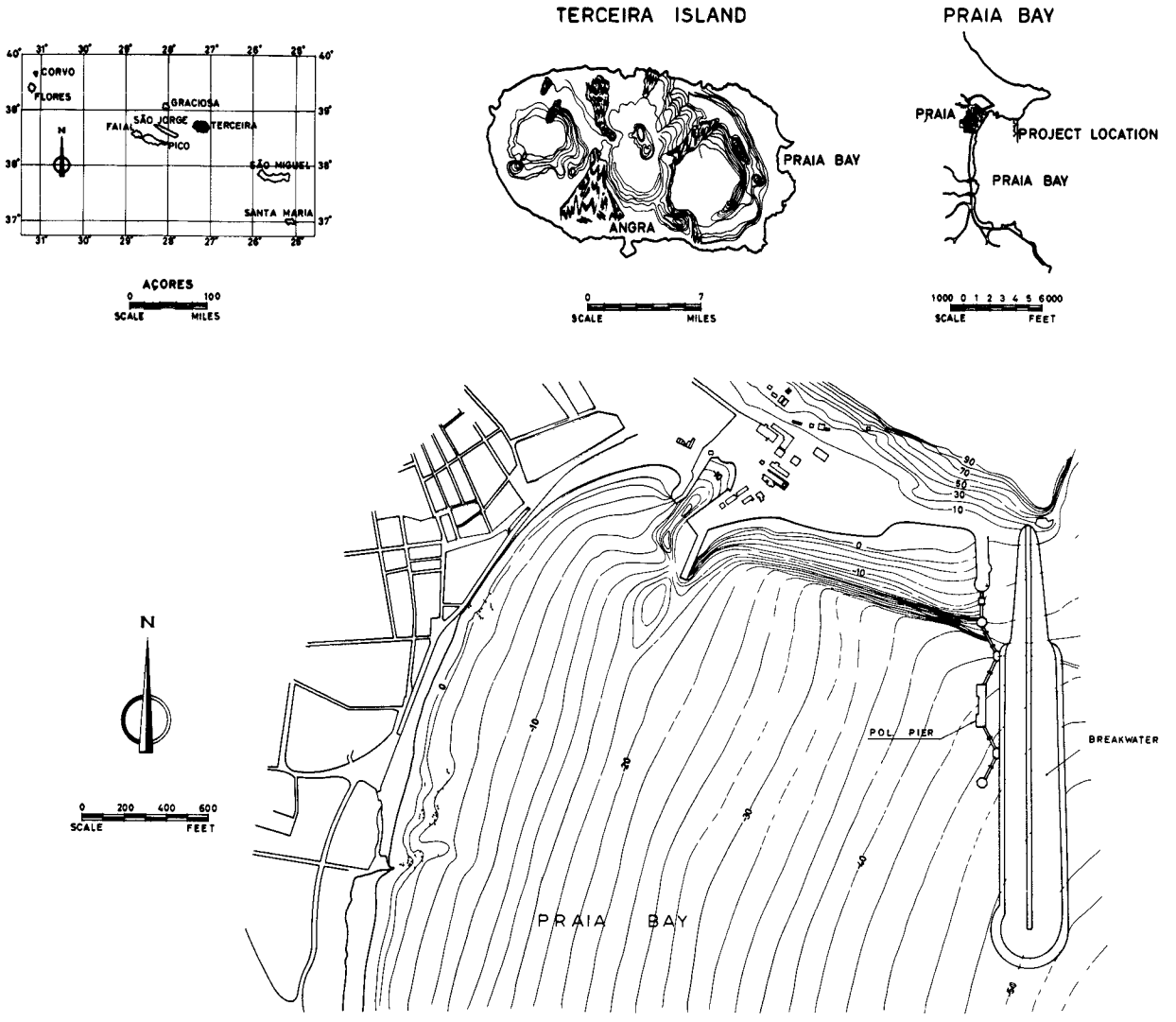

FIG. 1. PRAIA DA VITORIA HARBOR: GENERAL ARRANGEMENT

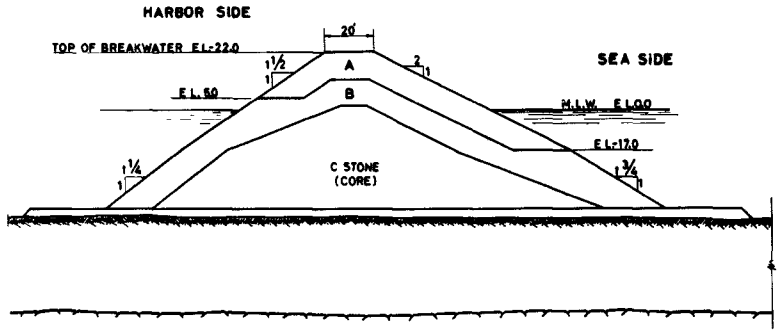

PRELIMINARY TYPICAL SECTION

A	STONE	(ARMOR)	13-15 tons
B	STONE	(ARMOR)	4 - 5 tons

CAST THROUGH STONES

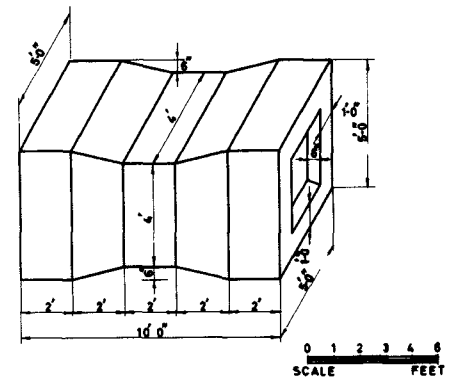

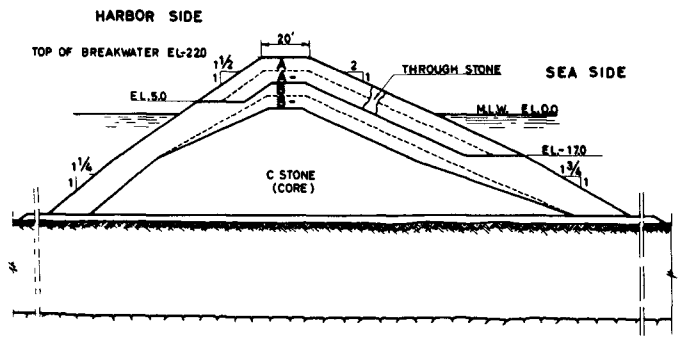

TYPICAL SECTION

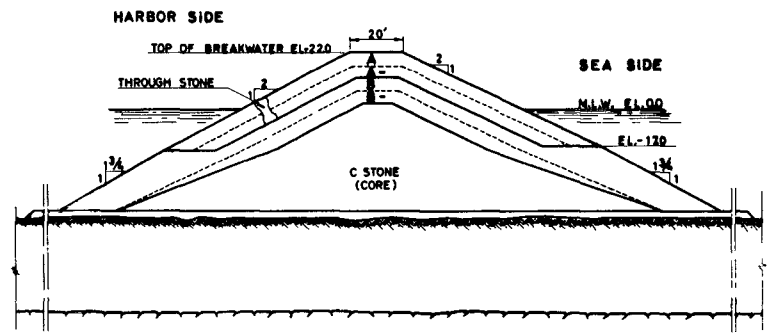

HEAD SECTION

BREAKWATER - STONE SIZES

A	STONE	(ARMOR)	13-15 tons and larger with 50% of stones larger than 14 tons
A-	STONE	(ARMOR)	10-13 tons with 50% of the stones larger than 11 tons
B	STONE	(SECONDARY ARMOR)	4 - 6 tons and larger with 50% of stones larger than 5 tons
B-	STONE	(SECONDARY ARMOR)	2 - 4 tons with 50% of the stones larger than 3 tons

FIG. 3. GENERAL VIEW OF HARBOR

their height offshore.

Thus only storms with about easterly directions offshore can hit the breakwater with full violence.

When the breakwater was being designed, the maximum wave height to be considered was chosen from data from the "Sea and Swell Charts-North Atlantic Ocean", from wind speeds and wind directions recorded at the meteorological post of Lajes airport (Terceira Island) and on values obtained in local observations of swell.

A comparative analysis of the two first sources showed that eastern winds blow during about 20% of the total time with a velocity below 27 knots.

It should be noted at once that, eastern storms being due to eastern winds blowing in the Atlantic area between Azores and the European Continent, it was in this area that the maximum speed of the wind and the extent on which its action could be felt had to be known.

Local observations recorded wave heights of 5.50m during an E storm in November 1955 and waves with estimated heights between 5.50 and 6.00m in February 1956. Nevertheless, these values were not taken into account when the design wave characteristics were chosen. As far as is known the wave-heights in Praia da Vitória harbour in these dates were not checked with values obtained from the synoptic charts.

The wave height for calculating the breakwater was determined by the Sverdrup-Munk method, by means of the charts revised by Bretschneider, for a wind velocity of 27 knots. In these conditions the significant height is about 5.20m and this value was adopted as the maximum for storms with directions between NE and SE offshore. The period arbitrated for this swell was 12 seconds.

3 - PROFILE OF THE BREAKWATER

The profile designed on basis of this maximum wave height consists of a type C stone core (up to 8 000 lbs), covered with E (4-6 short tons) and A (13-15 short tons) armour stones in the zones under the direct action of the waves (fig.2).

It being difficult to obtain in a quarry the required percent

age of A armour stones, the limits between the different stone types were changed so that 10-13 short ton stones were used in the lower layers and 2-4 short ton stones in the secondary armour of the harbour-side slop (fig.2). Tne rockfill has a specific gravity of 174.3 lbs/cuf (2.79 ton/m^3).

Hudson's formula applied at the profile for a wave-height of 5.20m yielded

$$K = \frac{\gamma_r \ H^3}{W \ (S_r - 1)^3 \cot \alpha} = \frac{2.79 \times 5.20^3}{12.7 \times 1.72^3 \times 2} = 3.00$$

This is less than the value recommanded by Hudson, which apparently indicates that the pair of values angle of slope-weight of armour stones was fixed with a certain margin of safety.

Nevertheless the subdivision of armour stone A in two sizes (A, 13-15 and A-10-13 short tons) decreased the safety of the structure as the loss of blocks in the sea-side layer for wave heights above the design values, which is always possible and actually occurred latter on, exposed the lighter layers to the direct action of the waves. For these layers the coefficient K has a value

$$K = \frac{3.0 \times 12.7}{10.43} = 3.65$$

which exceeds the figures recommended by Hudson.

Therefore, due to the changes in armour stone A, the structure had an insufficient margin of safety and a sufficiently prolonged storm, severer than the storm considered in the design, could give rise to the development of a chain destruction phenomenon with serious results, as each layer successively exposed to the action of the sea would be less stable than the preceding one and consequently would be more easily destroyed. This is what actually happened late in December 1962.

In an attempt to obviate the disadvantages of the subdivision of the A armour stone size, it is recommended in the design of the breakwater to use special shaped artificial blocks, cast through stones, placed so as to be included in two armour stone layers. These cast through stones, weighing about 16 short tons, were placed following no special rules, obeying one principle alone, that at least one of every ten A stones placed on the slope in the A stone surface layer must be a through stone.

Notice that, as regards the stability of the slope, the weight of cast through stones exceeds but slightly the weight of the surface layer blocks so that differences between the individual stability of one or other of these stone sizes is not very marked. On the other hand, as each artificial block is surrounded by natural rockfill the stability of the whole is that of its least stable component, notably as the percentage of cast through stones is very small. Their presence therefore contributes but little or nothing at all to the stability of the slope. That was also, in fact, the conclusion drawn from the model tests carried out to investigate the damages in the breakwater.

Three other characteristics of the profile of the breakwater are noteworthy. The first concerns the bottom elevation of the primary cover layer, which in the present case lies 17,0 f below the M.L.W. As in the low water of spring tides the water level can drop about 1,0 m below the M.L.W., the adopted level or (-17!0) does not strictly obey the current requirements and this could lead to suspect that the collapse of the breakwater could have started just in the zone between A and B armour stones The model tests showed that this was not the case however. Additionally, according to Per Anders Hedar's tests, damages in a rubble mound breakwater with a 2/1 slope never occur below an elevation of 0.8 H below S.L.W which confirms the results of the model tests.

In the harbour side the A armour stone cover extends down to level (+5!0), the B armour stone layer being therefore exposed for all the tide levels save the high water spring tide. This solution is not currently adopted when overtopping is possible.

Technical Report nº 4 "Shore Protection Planning and Design" recommends the use of a primary cover layer extending down to the minimum S.W.L. in the harbour side.

It was in the head of the breakwater, however, that the structure deviated more considerable from the currently followed rules. In fact it is generally known that the components of the head of a rubble mound breakwater, as that of Praia da Vitória, are subjected to more intense actions, than the components of the profile, due to the additional effect of the jet generated by the wave breaking in this zone. On the other hand, due to the curvature of the head of the breakwater, the components of the internal sector of the head are less stable than

the components of the remaining sections. Due to the joint action of these effects, heavier elements are required in the head of breakwaters in special inside and between the minimum and the maximum s.w.l. In the case of rubble mound breakwaters, Technical Report nº 4 recommends an increase of weight of about 10% in the head zone.

Hence the conclusion that the head of the breakwater of Praia da Vitória harbour had not the same factor of safety as the other sections. Nevertheless, for the reasons indicated below, the head of the breakwater underwent but slight damages in the internal sector. It should be noted, however, that a decreased strength in the head of a breakwater is extremely dangerous, as any damage in that zone can easily extend to the remaining sections even if these by themselves could resist the storm.

4 - STORM OF 26-27th DECEMBER 1962

Late in December 1962, Azores islands were struck by a violent storm. According to meteorologic data (fig.4) supplied by Serviço Meteorológico Nacional (the Portuguese Weather Bureau), a long depression with its centre over Santa Maria island after the 00.000 hours of 25th December 1962 gave rise to strong east winds in its northern margin. This depression remained in approximately the same position, sometimes with more than one isallobaric nucleus, until after the 27th, although with a reduced influence thereafter.

During period of most marked influence, the depression valley extended from Azores to North Africa, producing east winds of 25-40 knots between the Portuguese coast and Azores.

These particularly unfavourable conditions gave rise to a sufficiently extensive fetch and a duration of the wind producing maximum swell for wind speeds below 40 knots.

Unfortunately the meteorologic records available did not enable to obtain a perfect definition of the field of wind velocities in the fetch. It was only possible to conclude that the velocity of the wind causing the storm was comprised between 30 and 34 knots which, according to Neumann's graphs, amounts to a significant wave-height that could have ranged between 6.50m (30 knots) and 9.00m (34 knots). It should be noted, nevertheless, that the velocity of the east wind, as recorded at the Lages meteorologic post (Terceira Island), did not exceed 25 knots.

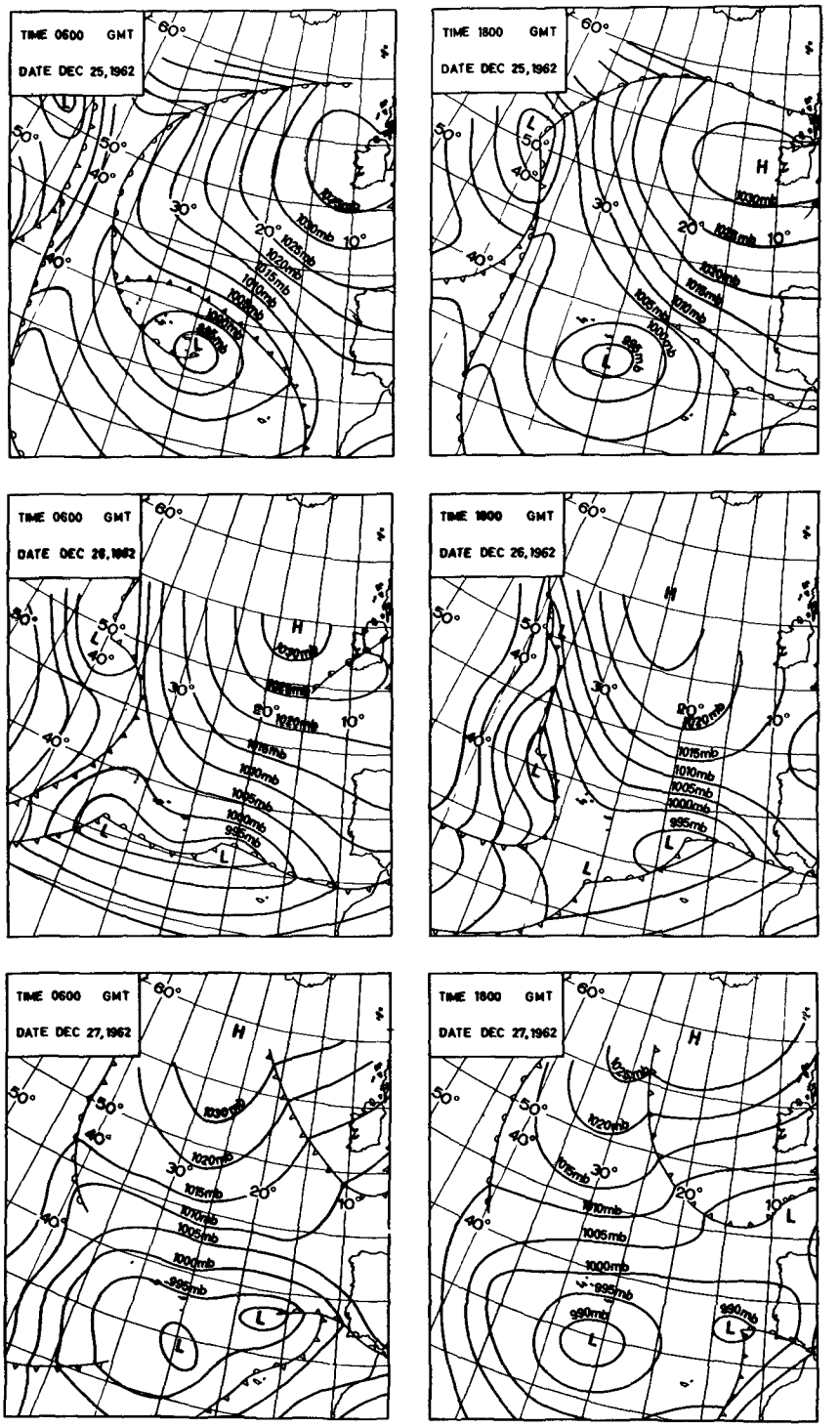

FIG 4 SYNOPTIC MAPS FOR NORTH ATLANTIC OCEAN·
STORM OF DEC 25-27, 1962

According to data supplied by Junta Autónoma do Porto de Angra do Heroismo (Angra do Heroismo Port Authority) (Terceira Island), the breakwater of Praia da Vitória was continously overtopped between the afternoon of 25th December and the morning of the 28th, notably during the high water. In these periods the spray due to the waves overtopping the breakwater reached beyond the tanker-berthing structure itself.

The swell height (amplitude) on the 26th and 27th were calculated by a quick method. The values obtained, average of records during periods of 30-40 minutes, were the following:

Date	Hours (G.M.T)	H meters	Date	Hours (G.M.T)	H meters
12.26th.62	10.00	≃ 8.00	12.27th.62	10.00	≃ 8.70
"	14.00	≃ 8.20	"	15.00	≃ 8.00
"	17.00	≃ 8.70	"	17.00	≃ 8.70

According to the records, individual wave heights did not exceed these mean values by more than 0.90m in each period of observation.

From these values and an analysis, as detailed as possible, of the fields of velocities of the winds blowing in the North Atlantic, it can be concluded that the storm that hit Praia da Vitória should have begun at 00.00 hours of 25th December (G.M.T.). At 12.00 (G.M.T.), the significant height was about 3.00 m, increasing to 6.00 m at 00.00 cours (G.M.T.) of the 26th December. The storm meanwhile grew more violent in this same day, reaching probably its maximum intensity about the 18.00 hours (G.M.T.). Thereafter, swell remained practically constant until about the 18.00 hours (G.M.T.) of the 27th, decreasing then very fast. The period corresponding to the storm was 13 to 14 seconds, in the periods of most violent storm.

5 - DAMAGES. THEIR ANALYSIS

At the date of the storm the breakwater was practically completed save for armour stone A which had still to be placed

between elevations (-12!00) and (-22!0), between the root and the profile 175 metres.

The first signs of damage were observed on the 26th in the morning, consisting in the disappearance of some stones in the submerged zone of profile 335 metres, where armour stones A were being removed and rolled along the profile, disappearing under the water. Surveys carried out after the storm located them at base of the breakwater.

A preliminary conclusion can be drawn from these data. The damages were due to insufficient stability of the sea-side slope and not to overtopping. This would have produced a collapse starting with displacements of stones in the harbour-side slope.

On the night of 26th to 27th, when the storm reached its maximum intensity, the breakwater was particularly hit and damaged. The damages extended to the whole structure and, on the 27th in the morning, a deep breach was visible just near the head, where the storm had ruined the whole profile above elevation (-0.00), attacking even C stones (core).

On the 27th the destruction of the breakwater went on, to such an extent that the overtopping waves, in special in high water, endangered the berthing structure itself, already damaged in the preceding night. Happily the storm abated on the night of 27th to 28th so that no new destructions were observed on the 28th.

The damages undergone by the breakwater during the storm can be summed up as follows (fig.3,5,6,7,8):

- profiles 0 to 176 metres: this section of the breakwater, completed up to elevation (-12'.0), underwent but slight damages at the surface; on the other hand both the sea-side and the harbour-side slopes were covered by a considerable volume of small stones, removed from the coast north of the breakwater;

- profiles 176 to 291 metres: this section remained in good conditions, as the only damages observed were some A armour stones removed from the sea-side slope and some slight settlements at the top; nevertheless, several B armour stones were displaced from the harbour-side slope below elevation (-5'.00),

FIG. 5. VIEWS OF THE DAMAGES

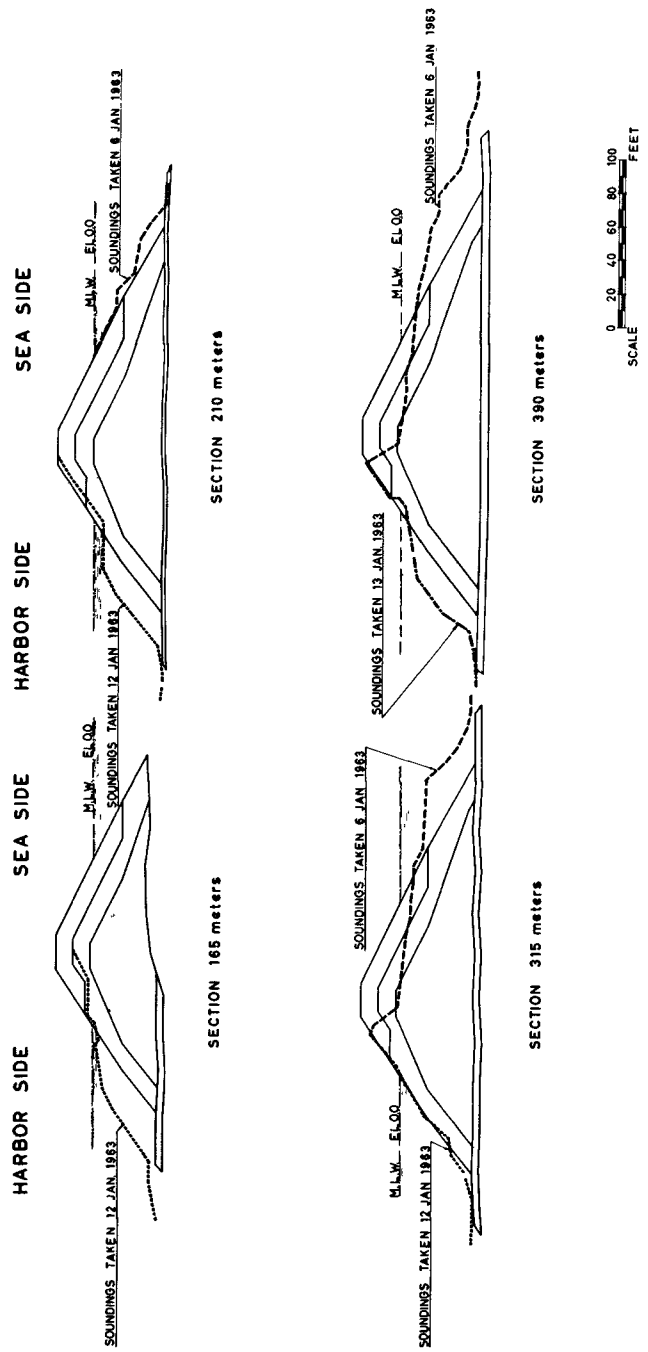

FIG 6 BREAKWATER SECTIONS AFTER STORM

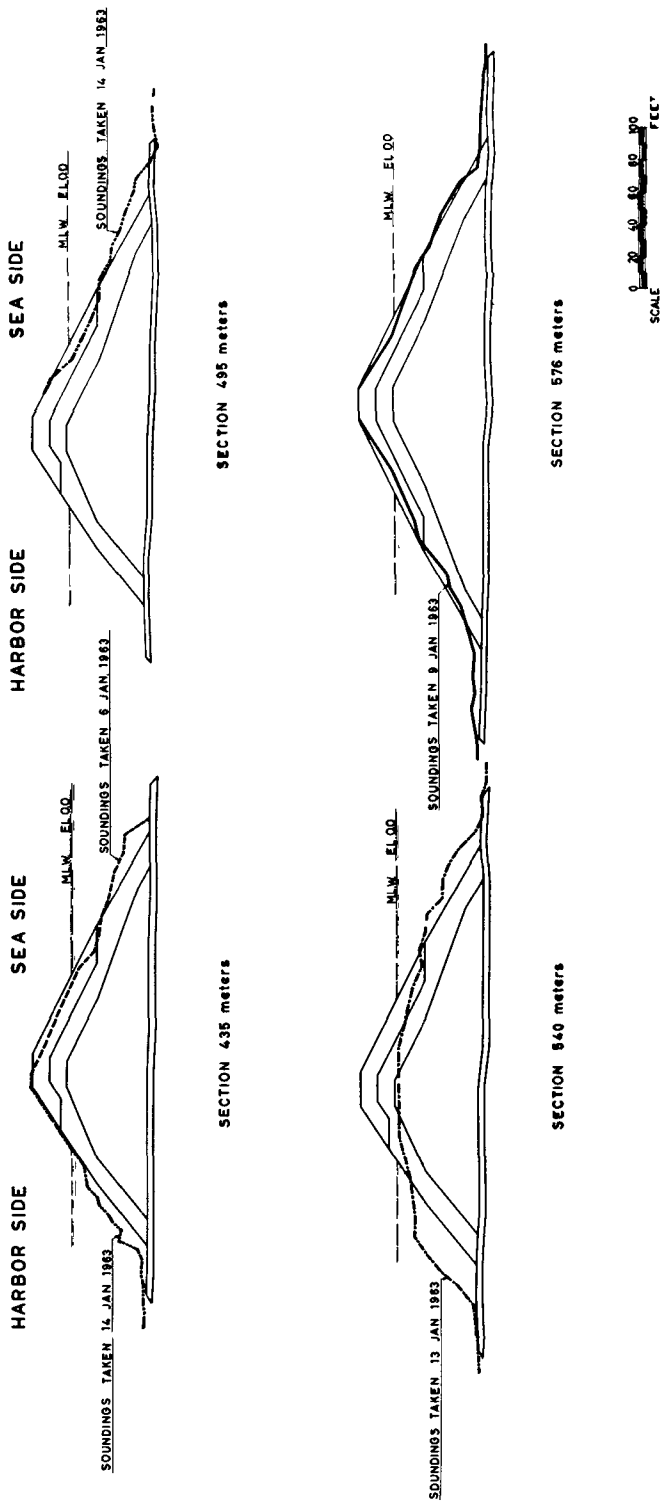

FIG 7 BREAKWATER SECTIONS AFTER STORM

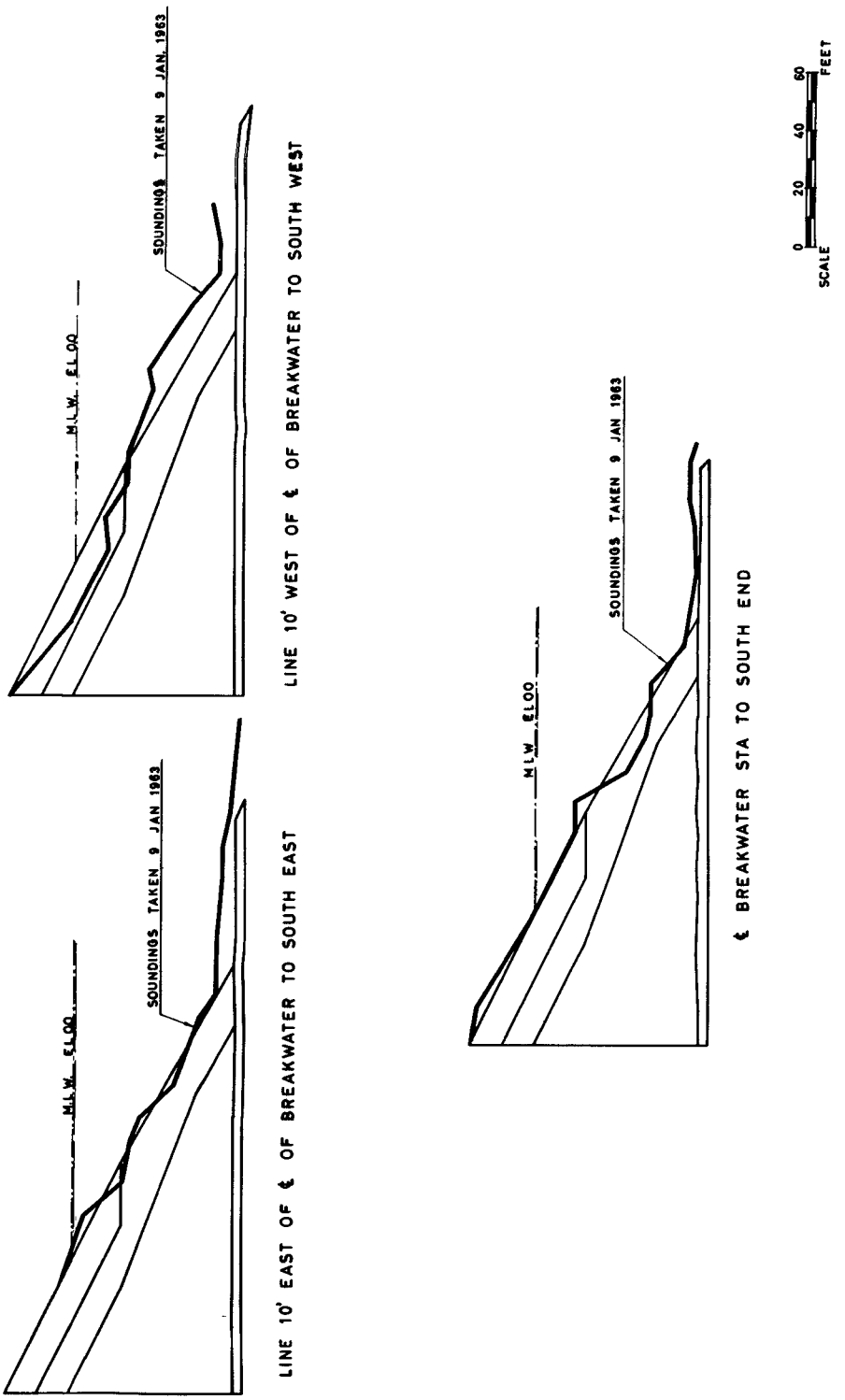

FIG 8 BREAKWATER SECTIONS AFTER STORM

which shows that the overtopping waves had harmful effects on this section;

- profiles 291 to 442 metres: this was one of the most severely hit sections, all the A armour stones of the sea-side slope and the top having been removed, rolling over the sea-side slope to the base of the breakwater, together with the B armour stones placed below; nevertheless, some A armour stones and cast through stones remained in place, although in very precarious equilibrium, in the harbour-side slope: if the storm had persisted somewhat longer, these blocks would also have collapsed and this section of the breakwater would have been razed to a level of about (- 0'.00); the type of damage undergone by this section of the breakwater confirms the observations of the preceding sections, showing that the collapse started in the sea-side slope;

- profiles 442 to 530 metres: this section was less damaged than the former as a length of about 45 metres remained almost intact;

- profiles 530 to 565 metres, this was the section where the most severe damages were observed: the breakwater was razed to elevation (- 0.00);

- profiles 565 to 585 metres (head of the breakwater): this section remained in good conditions as only some stones were removed in the harbour-side slope below the water level, thus confirming our present knowledge on collapse phenomena in the heads of breakwaters.

The first conclusion to be drawn from the preceding analysis of the damages observed along the breakwater, is their extremely irregular distribution: the head remained practically intact, the adjoining section presents a breach, then a length of about 90 metres underwent only slight damages, but just beyond the breakwater was severely hit in an extent of 150 metres.

This extreme irregularity had the advantage, however, of enabling a reconstruction of the evolution of collapse in the visible portion of the breakwater, clearly evinced in the variable extent of the damages indicated above: at first A armour stones were removed, rolling down along the slope; the B armour stone layer thus remained exposed, stones being then also removed to the basis of the slope; finally after, having also removed some

core stones, the waves pushed inside the few remaining blocks still in position in the harbour-side slope, producing a breach in the breakwater similar to the one near the head. It was impossible, however, from the surveys carried out in January 1963 to reconstruct the development of the collapse in the submerged zones, as the stones removed from the upper portion of the breakwater were concentrated at the base.

In the harbour-side slope, overtopping waves displaced some B armour stones alone.

Two factors can have caused this irregular distribution of damages: marked changes of the wave height along the breakwater or variable construction details from zone to zone, evinced by a storm more violent than the one considered in the design.

According to the two wave patterns drawn, one along an eastern direcction offshore and the other with an E-10°-N direction, the sea attack was frontal in the former case, with the following variation of wave-heights along the breakwater: a slight concentration near the root, followed by a slight decrease towards the head, where a marked local decrease is observed notwithstanding a slight concentration of energy in the just preceding section.

For the latter direction, the angle of the sea attack with the structure was small, without any apparent variation of the wave height along the breakwater. The analysis of the (fig. 5) photographs taken during the storm shows that the attack was always practically frontal.

The variation of the wave-height along the breakwater for an east wave offshore explains the absence of damage in the head and the breach in the adjoining profile, but it cannot account for the conditions observed in the remaining portion of the structure, where severely damaged sections alternate with zones practically intact. Apart from the fact that the breakwater was hit by waves higher than the design values and for a long time, these differences have apparently to be ascribed to different constructional methods alone.

6- MODEL TESTS

With a view to clearing up some points of the collapse of the breakwater, it was deemed of great interest to perform some model tests.

These were carried out in a wave channel so that only the case of the standard profile under frontal sea attacks could be considered.

The tests in a 1/50 model concerned first the high water and the low water levels without variations in level and then variations in level alone so as to reproduce local tide conditions.

According to the results of the tests, a reproduction even discontinuous of the tide produces more damages for the same wave heights than one water level alone. That is why the last tests comprised a reproduction of the tide for different values of the wave height.

All these tests showed that the first damages occured for wave-heights of about 6 metres, which confirms that the breakwater was well designed for the wave-heights adopted.

The first damages occurred between the high water and the low water levels, the stones rolling to the base of the slope. Then, as the wave height increased, the damaged zone extended progressively both towards the top and the base. Notice, however, that B armour stones below elevation (-17'.0) were never displaced, although for the highest waves this zone was already covered with A armour stones removed from the upper portion of the breakwater.

The top of the breakwater was not damaged until the wave height reached 7.50 metres.

It follows that the maximum wave-height during the storm should have approximately this value, so that the tests were continued under this wave height for a period of time corresponding to the time during which the most unfavorable swell conditions prevailed in Praia da Vitória.

Notice that, in the harbour-side slope, B armour stones below elevation (-5!00) began to be displaced for wave heights of about 7.00 metres, which confirms that the maximum wave height during the storm was about 7.50 metres. In fact, for higher waves, damages in the harbour-side slope would be much more extensive than those actually observed in Praia da Vitória.

Likewise, damages in the sea-side slope were extraordinarily aggravated by an increase even slight of the wave height,

and when this reached 7.70 metres it produced a breach analogous to the one observed near the head of the breakwater, which therefore can be easily explained by the slight energy concentration disclosed by the wave patterns in that zone of the breakwater.

Although the damages for the maximum wave height of 7.50 metres can be slightly different in the different tests, the very irregular distribution of damages observed could not be explained save by possible differences in constructional details in the different zones of the breakwater, possibly due to the presence in certain zones of A armour stones heavier than those recommended in the project. In fact we are aware through local sources that 20 large tons stones were placed in the breakwater, although their exact location is not known.

7 - CONCLUSIONS

From a joint analysis of the observed damages and of the model tests, the following conclusions can be drawn about the behaviour of the Praia da Vitória breakwater:

- The characteristics of the most violent storm that will act on a maritime structure must be chosen with great care; a deficient estimation can result in serious damages, as in the present case: observation programs with a suitable equipment are recommended; in addition to the probability of occurrence of certain wave-heights, it is also of interest to determine the maximum possible continuous duration of the storm (in the present case, the prolonged action of the storm was a deciding factor in the extent of damages);

- every breakwater design must be checked by model tests in order not only to disclose any deficiency but also to determine the factor of safety of the structure and its behaviour under wave-heights above the design values;

- a very satisfactory agreement having been observed between the damages observed in nature and the results of the model tests, these together with data on sea conditions near the breakwater enable this to be designed so that its total cost is minimum.

The author wishes to thank Mr. Leiria Gomes, Director of "Junta Autónoma do Porto de Angra de Heroísmo" "Angra do Heroismo Port Authority) who kindly supplied the field data without which this paper could not have been written.

REFERENCES

R.Y.Hudson - "Design of quarry-stone cover layers for rubble - mound breakwaters". U.S.Waterways Experiment Station - Research report Nº 2-2 - 1958.
- "Shore protection planning and design" - U.S.Corps of Engineering - Beach Erosion Board - Technical reports Nº 4 - 1961.

P.A.Hedar - "Stability of rock fill breakwaters". Doktorsav - haudlingar vid Chalmers Tekniska Hogskola - Göteborg 1960.

J.van de Kreeke and A.Paape, - "On optimum breakwater design" - Pro.IXth Conf.on Coastal Engineering, Lisboa, 1964.

Chapter 37

COMMUNICATION SUR LA CONSTRUCTION DU PORT DE COTONOU (Dahomey)

P. Sireyjol
Ingénieur en Chef des Ponts et Chaussées
Chef du Service des Ports au
Bureau Central d'Etudes pour les Equipements d'Outre-Mer, Paris

PREAMBULE

Un accord est intervenu en 1959 entre les Gouvernements Français et Dahoméen vue de la construction d'un port en eau profonde sur la côte du Bénin à proximité de ville de Cotonou (République du Dahomey). L'ouvrage en cours de construction est un port gagné sur la mer, en avancée par rapport au rivage, qui a eu pour effet d'inter rompre l'important transit littoral qui s'exerce de l'Ouest à l'Est sur cette côte. travaux commencés en Novembre 1959 sont dès maintenant très avancés. Déjà les pétrol peuvent être reçus dans le port et les navires à marchandises diverses seront reçus quai avant la fin de l'année 1964.

La présente communication porte sur l'incidence très profonde que le phénomèn transit littoral a exercée sur la conception et les conditions d'exécution des diver ouvrages.

I - APERCU SUR LES CONDITIONS NATURELLES EXISTANT DANS LA REGION DU GOLFE DU BENIN

I.1. Type de côte

La côte du Golfe du Bénin est une côte basse et sablonneuse, orientée sensibl ment Est-Ouest. Elle s'aligne sur près de 300 km entre Lomé et Lagos, les deux capi les voisines qui encadrent celle du Dahomey, sans aucun accident de terrain et sans cun pointement rocheux, soit sur le rivage, soit sur l'estran.

La marée étant faible sur cette côte (moins de 2 mètres), les courants côtier sont le plus souvent peu importants. Dans ces conditions, les deux éléments prépond rants qui caractérisent la côte sont constitués, d'une part par la houle, génératri transit littoral, et d'autre part par les embouchures de rivières appelées ici débo lagunaires, en raison de l'important réseau de lagunes qui s'étend le long du litto

I.2. La houle et le transit littoral

Le phénomène dominant des conditions hydrographiques dans la région du Golfe Bénin est celui de la houle. Celle-ci est une houle longue, d'amplitude moyenne rel vement régulière et de direction peu variable. Cette direction moyenne étant inclin par rapport à celle du rivage, il en résulte un transit littoral des sables orienté l'Ouest à l'Est, qui allait être la difficulté essentielle dont on aurait à tenir c pour la construction du port.

De très nombreuses observations de houle ont donc été faites depuis le début des études pour parvenir à une connaissance suffisamment précise de ce phénomène.

En ce qui concerne l'amplitude, cette houle se caractérise par une amplitude qui est le plus souvent comprise entre 1,00 m et 1,50 m. Elle est variable en cours d'année, étant plus faible dans la période de l'été austral (Décembre à Mars), et plus forte au cours de l'hiver austral (Juin à Août). Les zones génératrices de cette houle se trouvent dans les régions fortement ventées de l'hémisphère Sud situées au-delà de 40° de latitude. Les amplitudes moyennes mensuelles telles que nous les avons mesurées, ont été les suivantes pour l'année 1961 :

. Janvier	1,20 m	. Juillet	1,90 m
. Février	1,00 m	. Août	1,70 m
. Mars	0,90 m	. Septembre	1,70 m
. Avril	1,10 m	. Octobre	1,50 m
. Mai	1,10 m	. Novembre	1,60 m
. Juin	1,30 m	. Décembre	1,50 m

En dehors de ces variations saisonnières, existent bien entendu des variations journalières liées, non pas aux vents locaux, mais à l'existence de perturbations traversant des zones génératrices. Il faut remarquer toutefois que ces variations journalières sont beaucoup moins importantes qu'elles ne le sont dans la plupart des mers. C'est ainsi que l'amplitude ne descend pratiquement jamais au-dessous de 0,50 m. Inversement, les houles de tempête ne sont jamais très fortes et nous n'avons jamais mesuré au cours des années d'observations que nous avons effectuées, d'amplitudes supérieures à 4,50 m.

La période de cette houle est généralement longue. Elle ne descent pratiquement jamais au-dessous d'une dizaine de secondes et sa valeur la plus courante est voisine de 12 secondes. Par mauvaise mer, elle croît encore et l'on observe couramment des houles de 15 à 17 secondes.

Cette houle, toujours longue, qui se présente comme un phénomène permanent relativement peu variable, est également quasi constante en direction. Ce paramètre présentait une importance particulière pour les études que nous avions à conduire, car l'obliquité de la houle par rapport à la direction du rivage commande le transit littoral. Nous nous sommes donc attachés avec une rigueur toute spéciale à dresser des statistiques de cette houle par direction. Il n'existe malheureusement pas d'appareil enregistreur permettant d'effectuer une telle mesure. Nous avons donc dû procéder par empirisme, le moyen le plus couramment employé pour observer la direction de la houle consistant à placer une règle rectangulaire de champ sur un plan horizontal et à l'orienter de façon à ce que son arête supérieure se projette suivant les directions des crêtes de houle. Ce procédé très simple est plus précis qu'on pourrait le penser a priori, tout au moins lorsqu'il s'agit de houles régulières et bien formées comme le sont en général les houles du Golfe du Bénin. C'est ainsi que la même mesure effectuée plusieurs fois de suite par des observateurs différents, donne des chiffres assez voisins l'un de l'autre et ne diffère pas en général de plus de deux ou trois degrés.

Ces mesures, effectuées systématiquement depuis l'extrémité du wharf, nous ont permis de connaître les directions des crêtes de houle par des fonds de l'ordre de (-10,00). La construction des plans de houle nous a permis par la suite de déterminer les directions au large. Comme nous l'avons déjà indiqué, ces directions sont peu

variables dans le temps. Fortement groupée autour de la direction moyenne d'origine S Sud-Ouest, cette direction moyenne présentait une obliquité par rapport au rivage d'e viron 18° par fonds (-10,00).

Ainsi que je l'ai déjà indiqué, cette houle toujours assez importante s'attaq avec une obliquité sensible au matériau, extrêmement mobile, qui constitue le rivage doit être à l'origine d'un transit littoral important. Ce transit se situe essentiel ment dans les rouleaux de déferlement de la houle toujours présents sur cette côte, des fonds de l'ordre de 2 à 3 m. Ce phénomène du transit, permanent et extrêmement i portant, ne se traduit pas de façon spectaculaire par des modifications de rivage pu que le sable entraîné par le transit est constamment renouvelé par des apports venan l'Ouest. Il faut, pour le mettre en évidence, un phénomène perturbateur tel que la c truction d'un ouvrage ou la présence d'une épave.

Nous n'avons pu, avant la construction du port, acquérir qu'une idée très gro sière sur l'importance de ce transit littoral, en nous appuyant, soit sur des observ tions occasionnelles rendues possibles par l'échouement de certains navires sur la p ou encore par comparaison entre le transit existant sur des plages soumises à des ho analogues dans la même région.

C'est ainsi que la construction du port d'Abidjan, à quelque 800 km plus à l' a permis de chiffrer autour de 800.000 m3 par an l'importance du transit au droit de port. De même, un chiffre de 700.000 m3 par an a pu être avancé pour Lagos, à 150 km l'Est de Cotonou. Tenant compte de l'ensemble des renseignements que nous avons pu r nir, nous avons seulement pu affirmer avant le début des travaux, que le transit au droit du port de Cotonou devait être compris entre 750.000 et 1.500.000 m3 par an.

I.3. Le débouché lagunaire

La côte basse et rectiligne que nous avons décrite jusqu'ici comme étant cell Dahomey, présente toutefois une particularité dans la région de Cotonou : c'est le c bouché lagunaire. Il existe en effet sur la plus grande partie du rivage du Golfe di nin un important réseau de lagunes intérieures parallèles au rivage et à quelques ki mètres de celui-ci. Ces lagunes n'offrent jamais qu'une profondeur très faible de l' dre le plus souvent de 1 à 3 m. Elles forment néanmoins un vaste plan d'eau qui ne c munique avec la mer qu'en deux endroits. L'une de ces communications se trouve au di même de la ville de Cotonou, l'autre étant dans la région de Lagos. La communicatio réseau lagunaire avec la mer dans la région de Cotonou est constituée par un canal r rel d'environ 5 km de longueur, 300 m de largeur et une profondeur de l'ordre de 3 à Ce canal est le siège de courants de marée provoqués par les variations de niveaux c l'ordre de 1,50 m existant dans la mer devant Cotonou. En outre, l'évacuation des e de pluie donne lieu en période de crue à des courants de chasse relativement import dirigés vers la mer.

Ces deux types de courants : courant de marée et courant d'évacuation des cr tendent à maintenir ouvert le débouché lagunaire qui, par ailleurs, tend à s'ensabl côté mer, du fait du transit littoral. Ces influences contraires conduisaient dans la période antérieure à la construction du Port à un régime variable et plus ou moi cyclique. Au cours de la saison sèche, le transit littoral tendait à fermer le débo lagunaire et il arrivait qu'il y parvienne complètement. On aboutissait alors à une tuation lagune fermée, la totalité des échanges d'eau se faisant alors par le débou permanent de Lagos. Par la suite, à l'occasion d'une crue, le niveau montait suffis

ment dans la lagune pour permettre le franchissement du cordon de sable qui s'était formé pour la séparer de la mer. Ce cordon de sable était alors érodé et l'on aboutissait après quelques heures à une situation lagune ouverte, laquelle pouvait se maintenir pendant quelques mois ou même quelques années. L'ensemble du phénomène présentait donc un caractère cyclique avec une pseudo-période qui était en général comprise entre 1 et 5 années.

Comme je l'ai déjà indiqué, le débouché lagunaire se trouve immédiatement à l'Est de la ville de Cotonou. L'existence de cette ville et celle du wharf qui la dessert jusqu'ici poussaient à construire le port dans la même région. Il allait donc être nécessaire de tenir compte de ce voisinage pour arrêter les grandes lignes du projet.

II - LES OUVRAGES DU PORT - INFLUENCE DU TRANSIT LITTORAL

II.1. Le type du port et ses dispositions d'ensemble

Compte tenu de l'importance du transit littoral qui s'exerce au droit de la vill de Cotonou, 3 types de port pouvaient être envisagés dans cette région pour construire un port gagné sur la mer :

- Port-ilôt construit en mer et n'interrompant pas le transit littoral sur le rivage auquel il aurait été relié par un simple appontement

- Port à transit artificiel de sable. Dans cette solution, le sable dont la construction du port provoque le dépôt à l'Ouest du port, est repris par un matériel de dragage qui le refoule à l'Est du port grâce à des canalisations terrestres

- Enfin, port à accomulation dans lequel la saillie du port par rapport à l'alignement général du rivage est suffisante pour que les matériaux (*) qui se déposent à l'Ouest du port puissent être stockés pendant une longue période sans risquer de pénétrer dans le port ou dans ses accès. (*) du transit littoral

Le Bureau Central d'Etudes pour les Equipements d'Outre-Mer chargé par les deux Gouvernements de la mise au point du projet puis de la Direction des travaux du port, a effectué des études comparatives de ces diverses solutions. Ces études ont comporté l'utilisation de modèles réduits qui ont été construits par le Laboratoire SOGREAH à Grenoble. Elles ont conduit à opter, sans aucune hésitation possible, en faveur de la 3ème d'entre elles, celle du port à accumulation, sur le principe de laquelle reposent les ouvrages qui sont en cours de construction.

Pour nous en tenir aux études des ouvrages qui ont finalement été retenues, nous indiquerons qu'elles ont comporté tout d'abord un modèle sur lequel ont été représentées les évolutions du rivage. On est parti d'une simple plage rectiligne avec son transit littoral. L'échelle des temps sédimentologiques était telle que le transit annuel supposé, égal à 1.500.000 m3 s'écoulait en 20 minutes. La figure n° 2 extraite du rapport faisant suite aux essais, représente les formes successives du rivage côté accumulation et côté érosion, résultant de la construction d'un ouvrage d'arrêt présentant par rapport au rivage une saillie de 1.500 m. Le modèle qui avait été taré pour tenir compte des conditions réalisées à Cotonou, permettait donc de prévoir pour un port présentant par rapport au rivage, une saillie donnée :

- Les quantités de sable pouvant être stockées à l'Ouest du port et le temps pendant lequel le transit serait complètement arrêté,

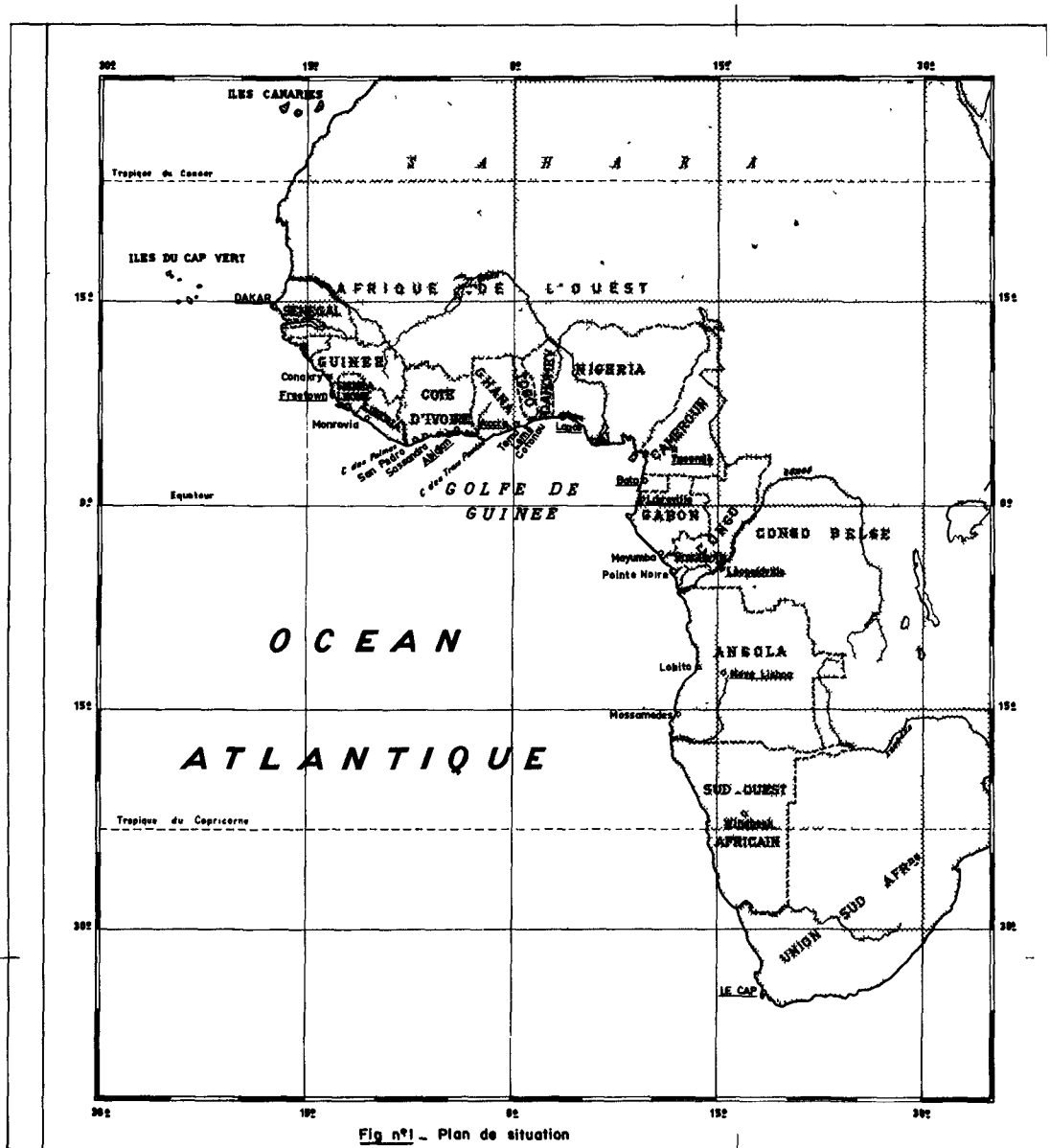

Fig n°1 - Plan de situation

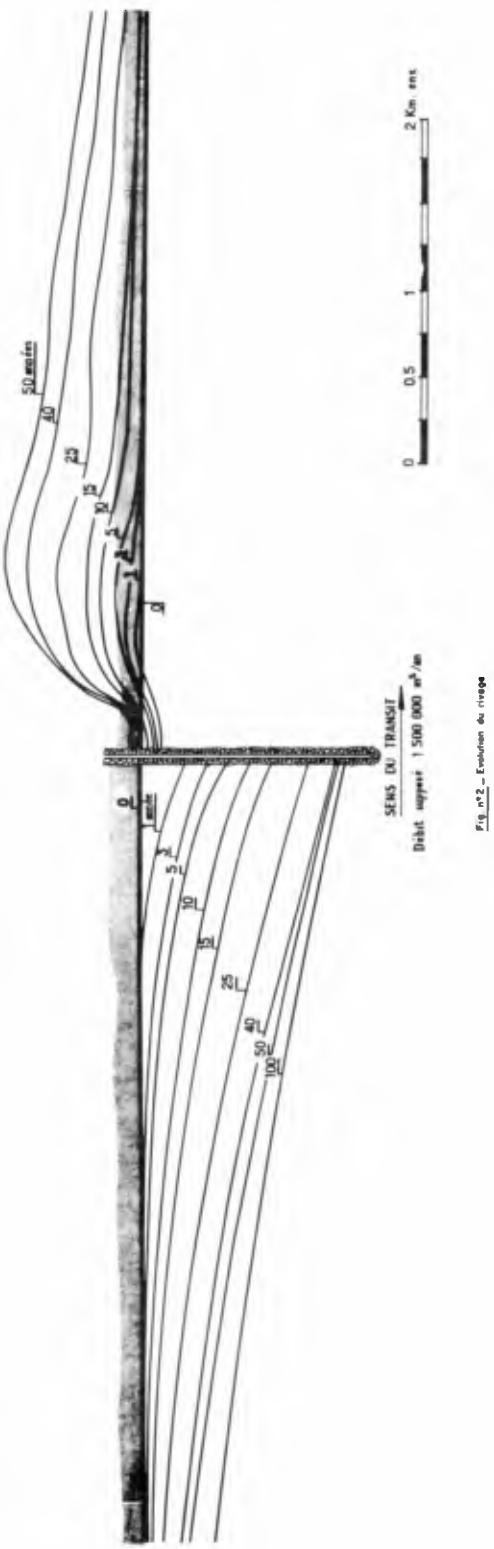

Fig. n°2 - Evolution du rivage

. La courbe du rétablissement progressif du transit à partir du moment où l'ouvrage commencerait à être contourné,

. La forme et la zone des dépôts et des érosions se produisant à l'amont et à l'aval port, etc ...

Tous ces résultats étaient d'ailleurs très voisins de ceux que laisse prévoir théorie élaborée par M. Pelnard-Considère au sujet de ces divers phénomènes.

C'est à partir de ce premier modèle quelque peu théorique, que l'on a pu arrêt les dispositions générales du port qui, dans le projet finalement réalisé, sont celle représentées sur le plan d'ensemble joint (figure n° 3). Ces dispositions comportent sentiellement :

- une jetée Ouest, ouvrage principal de défense contre la houle et d'arrêt des sables Cet ouvrage enraciné au rivage, comporte une branche sensiblement parallèle à celui par fonds voisins de (-12,00) et à 1.000 mètres environ de la côte. Cet ouvrage cor truit principalement en enrochements et tétrapodes comporte toutefois un enracineme constitué par un appontement sur pieux. Nous reviendrons sur ce point.

- une traverse, jetée secondaire destinée à protéger le port contre les clapots de S Est. Cet ouvrage est sur sa plus grande longueur une jetée verticale en palplanches métalliques et accostable par les navires.

- des ouvrages de défense de la côte à l'Est du port.

- enfin, des ouvrages d'accostage comprenant, en 1ère étape, 4 postes à quai pour les marchandises diverses, construits parallèlement au rivage et se prolongeant vers l'Est par les installations du port de pêche. Ces ouvrages épuisent par conséquent possibilités d'accostage offertes par le plan d'eau actuel du port de Cotonou. Il e prévu que les extensions du port de commerce que nécessitera le développement du tr fic seront obtenues en draguant dans l'avenir un nouveau bassin dans les dépôts sableux que l'arrêt du transit littoral ne manquera pas de provoquer à l'Ouest du por

Il n'est pas dans nos intentions de rendre compte, dans le cadre de cette court communication, de l'ensemble des études et des conditions d'exécution des ouvrages qu comporté la construction du port de Cotonou. Nous nous contenterons de signaler les c positions les plus intéressantes qui ont dû être prises pour tenir compte de cet élén essentiel des conditions locales que constituait l'important transit littoral existan dans la région. Nous nous étendrons pour cela sur deux points : les ouvrages de défen à l'Est du port d'une part, et de l'autre l'ordre d'exécution des ouvrages qui conditionnait un ensablement satisfaisant.

II.2. Les ouvrages de défense du rivage

La construction du port extérieur ayant pour effet d'arrêter le transit littor il était prévisible qu'elle entraînerait une certaine érosion de la côte à l'Est du p Le débouché lagunaire se trouvant précisément dans cette région, il était facile de p voir que la tendance à l'obturation du débouché du fait du transit littoral disparaî trait. La situation future postérieure à la construction du port devait donc comporte une ouverture permanente de la lagune.

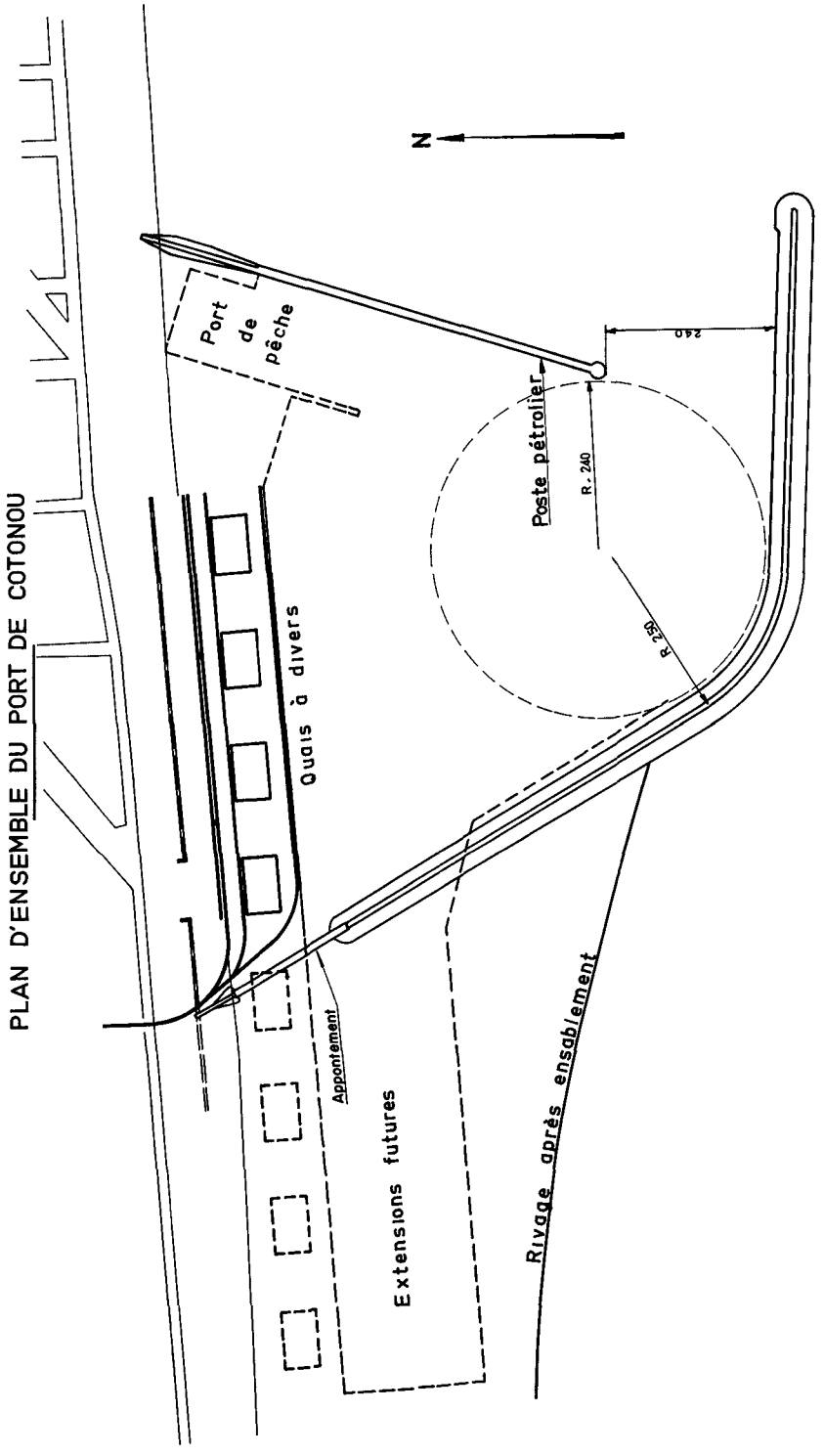
PLAN D'ENSEMBLE DU PORT DE COTONOU
N
Port de pêche
Quais à divers
Appontement
Extensions futures
Rivage après ensablement
Poste pétrolier
R. 240
R. 290
240

Fig n°3

D'un autre côté, la ville de Cotonou étant construite au droit du port, il éta indispensable de prévoir ce que serait exactement l'érosion du rivage, afin de la contrôler et si nécessaire de l'interdire dans les régions vulnérables. Il a été décidé pour ces diverses raisons, de construire un modèle réduit particulier axé sur l'étude des phénomènes d'érosion du rivage, sur l'évolution du débouché lagunaire et sur les ouvrages à prévoir pour protéger les parties vitales du rivage. Ce modèle a été exécu au moment même où commençaient les travaux de construction du port. Son exécution a é relativement délicate dans la mesure où il s'agissait de reproduire des phénomènes variables et relativement peu stables. Le tarage du modèle a été reconnu satisfaisant, lorsqu'on est parvenu à représenter sur le modèle les cycles irréguliers d'ouverture de fermeture de la lagune, en liaison avec les périodes de saison sèche et de saison pluies et celles de fortes houles et de faibles houles.

La mise en place des ouvrages du port sur le modèle a confirmé que la construction du port entraînait immédiatement une ouverture permanente du débouché lagunaire. L'exploitation du modèle a ensuite permis de mettre au point le système d'ouvrages de défense qui a depuis lors été mis en place sur le terrain et qui donne jusqu'ici tout satisfaction. (figure n° 4). Ce système comprend :

a) - Un épi Ouest, ouvrage principal de défense enraciné suivant le prolongeme en mer de la rive Ouest du débouché lagunaire. Cet ouvrage, construit en enrochements, doit atteindre dans sa situation définitive, des fonds de l'ordre de (-6,00). Il joue essentiellement un rôle d'épi, provoquant une accumulation de sable sur la face Ouest, et limitant de ce fait l'érosion du rivage à l'Est de l'enracinement de la traverse. S position a été arrêtée pour protéger de façon absolue l'ensemble du rivage entre l'Es du port et l'Ouest du débouché lagunaire, zone au droit de laquelle se trouve la ville de Cotonou.

Cette position tient également compte de l'existence du wharf qui doit rester exploitable dans la période de construction du port, c'est-à-dire que le rivage au droit de son enracinement ne doit ni s'ensabler, ni s'éroder exagérément. Ces conditi ayant été vérifiées sur le modèle, l'expérience a depuis lors confirmé les résultats modèle sur le terrain.

L'épi Ouest étant construit dans le prolongement de la berge Ouest du débouché lagunaire, il se prolonge le long de celle-ci suivant un ouvrage de protection de ber se terminant à l'intérieur du débouché par un petit épi transversal à ce débouché.

L'effet de cet épi est de déooller les lignes de courant de la berge Ouest qui sans cela, comme l'a montré le modèle et comme il a depuis lors été vérifié en nature auraient tendance à éroder cette berge.

b) - L'ensemble des ouvrages précédents constitue donc une protection du rivag à l'Ouest du débouché. L'érosion doit bien entendu s'étendre également à l'Est. Il se trouve que l'on a ici affaire à des terrains de bien moindre valeur. Comme il n'était pas question de toute façon d'envisager une protection absolue du rivage, on s'est contenté dans cette région de prévoir la construction d'un second épi dit épi Est, en ciné à 2 km environ à l'Est de l'épi Ouest. Ce nouvel épi est d'ailleurs conçu, non p pour provoquer une accumulation de sable, mais simplement pour limiter l'érosion dans cette région. Il constitue en somme un "point dur" qui devra être maintenu sur le riv ge futur. Sa position a été étudiée pour limiter l'érosion dans son voisinage avec la condition impérative que le pont de Cotonou qui franchit le débouché lagunaire un peu

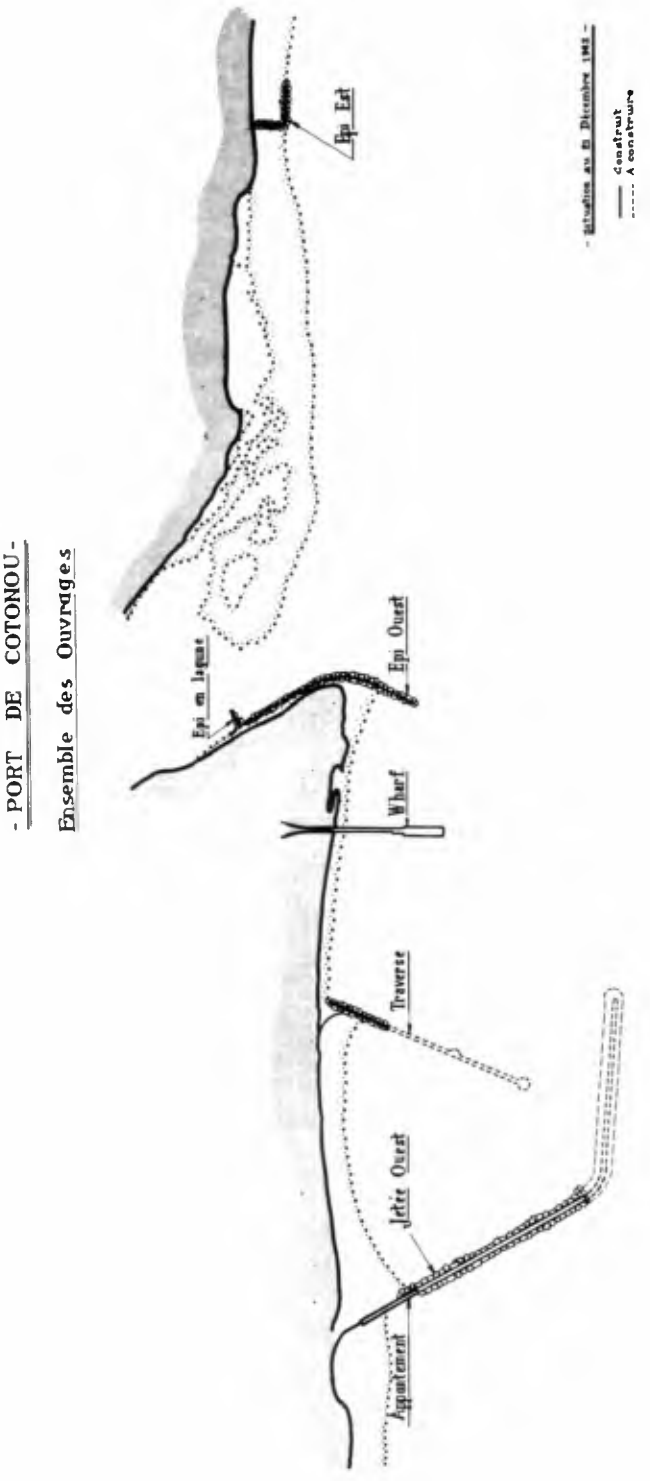
- PORT DE COTONOU -
Ensemble des Ouvrages
Epi Est
Epi en lagune
Epi Ouest
Wharf
Traverse
Jetée Ouest
Appontement
- Situation au 31 Décembre 1963 -
Construit
A construire

Fig. n° 4

amont de la ligne du rivage, ne risque pas d'être menacé dans l'avenir du fait de l'érosion de celui-ci.

Cet ensemble d'ouvrages de défense a été réalisé uniquement en enrochements et nécessité la mise en oeuvre d'environ 100.000 T de matériaux de carrière. Il est probable, vu son comportement au cours des premières années, qu'il suffira pendant assez longtemps à remplir l'office que l'on s'était fixé.

Je signalerai ici une conclusion assez générale qu'il me paraît intéressant de dégager à la suite des essais sur modèle effectués à cette occasion. Il s'agit du type d'ouvrage à reçommander lorsque l'on veut protéger un rivage soumis à un important transit littoral, lorsque ce transit a été arrêté par une cause fortuite. Alors que l'on a l'habitude de construire surtout des épis courts pour les ouvrages de protection du rivage lorsque les conditions dans lesquelles ils se trouvent placés sont voisines de l'équilibre, le modèle nous a montré que dans le cas présent où le transit étant complètement arrêté et où l'on se trouve très éloigné de l'équilibre, les épis courts devenaient inefficaces et la protection ne pouvait être obtenue que par de grands épis atteignant des fonds assez importants pour que le transit ne puisse se produire devant leur musoir.

II.3. Ordre d'exécution des ouvrages en vue de l'obtention d'un ensablement satisfaisant

Le début de la construction, à la cote, de chacun des ouvrages du port, y compris ceux de défense du rivage, a pour effet de perturber la situation antérieure, apparemment stable, caractérisée par un transit littoral constant devant une cote en équilibre. Cette perturbation se traduit par un engraissement à l'Ouest de tout ouvrage en saillie, et par une érosion à l'Est. La prévision exacte de ces phénomènes était évidemment très importante dans le cas du port de Cotonou et elle imposait en fait l'ordre de construction des divers ouvrages. On était en effet tenu à cet égard par les diverses considérations suivantes :

- nécessité d'éviter les érosions importantes au droit de la ville
- nécessité d'éviter l'ensablement du wharf qui devait pouvoir rester en exploitation pendant toute la durée des travaux
- nécessité de provoquer le dépôt dans le port d'une quantité suffisante de sable car le programme des dragages-remblaiements que l'on désirait réaliser était assez fortement déficitaire en matériaux.

Ce dernier impératif conduisait à engager assez rapidement la construction d'une certaine longueur de la traverse destinée à retenir le sable dans la partie Est du port. Mais la mesure essentielle à ce sujet a consisté à remplacer l'ouvrage plein initialement prévu pour l'enracinement de la jetée Ouest par un ouvrage à claire-voie, type appontement. L'efficacité d'un tel ouvrage avait été étudiée sur modèle. Celui-ci avait montré que la construction de l'appontement ne modifiait pas le transport littoral mais qu'au contraire, le début de la construction par fonds, voisin de (-5,00) de la partie en enrochements de la jetée Ouest, provoquait immédiatement une déformation du rivage et déclenchait très vite la formation d'un tombolo. Celui-ci se développe en direction des enrochements provoquant un important ensablement dans le port. Chose curieuse, observée sur le modèle et confirmée par l'expérience, ce tombolo ne va jamais, tout au

moins pendant très longtemps, jusqu'à la coupure complète de la circulation des matériaux entre la plage et les enrochements. Les matériaux de transit continuent à passer à marée haute et vont se déposer dans le port dans la partie à l'abri de la jetée où l'agitation est très réduite.

Ce processus nous a donc permis de faire déposer dans le port une importante quantité de sédiments. Quand nous avons estimé suffisante cette quantité, nous y avons mis un terme par construction d'un petit épi en enrochements au-dessus du tombolo qui s'était formé, au pied même de l'appontement.

Finalement, le calendrier d'exécution des divers ouvrages, sommairement mis au point au début des travaux et rectifié par la suite en fonction des difficultés du chantier et des résultats obtenus dans l'évolution du rivage, a été celui figuré sur le tableau ci-dessous. La colonne de droite de ce tableau mentionne les buts recherchés par l'engagement de chacun des travaux ainsi que les résultats obtenus.

Dates	Travaux	But recherché et observations
13.11.1959	Ordre de service pour début des travaux	
1er semestre 1960	Installation de chantier	
Juin à Août 1960	Battage de l'appontement de la jetée Ouest	Eviter de perturber le transit littoral
Septembre à Décembre 1960	Construction d'un premier élément de l'enracinement de la traverse	Objectif : stocker du sable dans le port
Décembre 1960	Début de construction de la jetée Ouest en enrochements	
Janvier à Avril 1961	Ouvrages de défense en lagune et 1ère tranche de l'épi Ouest (74 m)	Objectif : protéger le rivage entre le débouché lagunaire et le port sans risquer toutefois d'ensabler le wharf
Décembre 1961 Novembre 1962	Achèvement de l'enracinement de la traverse et achèvement de l'épi Ouest	Objectif : éviter le désensablement du port à partir de l'arrêt du transit. Stocker suffisamment de sable entre la traverse et l'épi Ouest pour que le boulevard front de mer ne risque pas d'être attaqué. En fait, ces travaux n'ont pu être exécutés qu'avec un certain retard par manque de moyens de l'Entreprise. Il en est résulté certaines érosions 200 m environ à l'Est de la traverse qui, heureusement, se sont arrêtées à temps

Dates	Travaux	But recherché et observations
Mars - Avril 1962	Cavalier en enrochements sous appontement de la jetée Ouest	Objectif : arrêter le transit pour limiter l'ensablement du p jugé suffisant
Février à Mai 1963	Construction de l'épi Est	Objectif : limiter l'érosion fu ture du rivage à l'Est de la lagune

III - MESURE DU TRANSIT LITTORAL DANS LA REGION DE COTONOU

La construction d'un port à accumulation constitue évidemment une aubaine asse exceptionnelle dont l'ingénieur ne doit pas manquer de profiter pour déterminer de fa précise le transit littoral. Ce n'est toutefois qu'un certain nombre d'années après l construction du port qu'une telle détermination précise pourra être effectuée. Il n'e est pas moins intéressant de regarder les premières conclusions qu'il est possible de tirer des observations faites.

Rappelons tout d'abord que le transit dans la région de Cotonou avait été éva à l'origine de l'étude, à un chiffre compris entre 750.000 et 1.500.000 m3 par an, ce par référence à Lagos et Abidjan où des chiffres de l'ordre de grandeur de 700.000 m avaient été admis.

Les ensablements constatés à Cotonou à l'Ouest de la jetée Ouest dans une pér de 8 mois allant de Février à Novembre 1961 devaient nous donner une première indica- tion. Ces ensablements ont été chiffrés à 300.000 m3 au minimum et portaient sur une période où l'arrêt des sables n'était que très partiel. Le pourcentage stocké à l'Ou de la jetée Ouest, très faible au début de la période, restait encore partiel à la f L'analyse du phénomène permettait seulement de confirmer que le transit annuel devai effectivement être supérieur à 750.000 m3.

Une mesure déjà plus précise peut être déduite de la comparaison des sondages d'Avril et Décembre 1962. La première de ces dates coïncide sensiblement avec l'arrê du transit qui devait résulter de la construction du cordon d'enrochements sous l'ap- pontement de la jetée Ouest. Les deux sondages portent malheureusement sur une zone sez limitée qui couvre seulement 1.000 mètres de front de mer, immédiatement à l'Oue de la jetée Ouest. La quantité de sable déposée dans cette zone au cours de la périod considérée de 8 mois est de 600.000 m3 environ. Au-delà, en direction de l'Ouest de te zone de 1.000 m, on ne dispose que d'un profil en travers tous les kilomètres. Ce profils ne se trouvant pas dans une zone de forte accumulation, leurs variations err tiques sont prépondérantes : ils ne peuvent donc donner aucune indication sur l'impo tance des dépôts à l'Ouest de la zone des 1.000 mètres.

A défaut de ces renseignements essentiels, nous pouvons encore nous donner un idée du volume total sédimenté d'après les considérations suivantes :

a) - Forme du dépôt dans la zone de 1.000 mètres le long de laquelle on dispose de p fils. L'examen de ces profils montre que la section sédimentée ne diminue pas de faç

ENGRAISSEMENT DU RIVAGE A L'OUEST DE LA JETEE W. DU PORT DE COTONOU

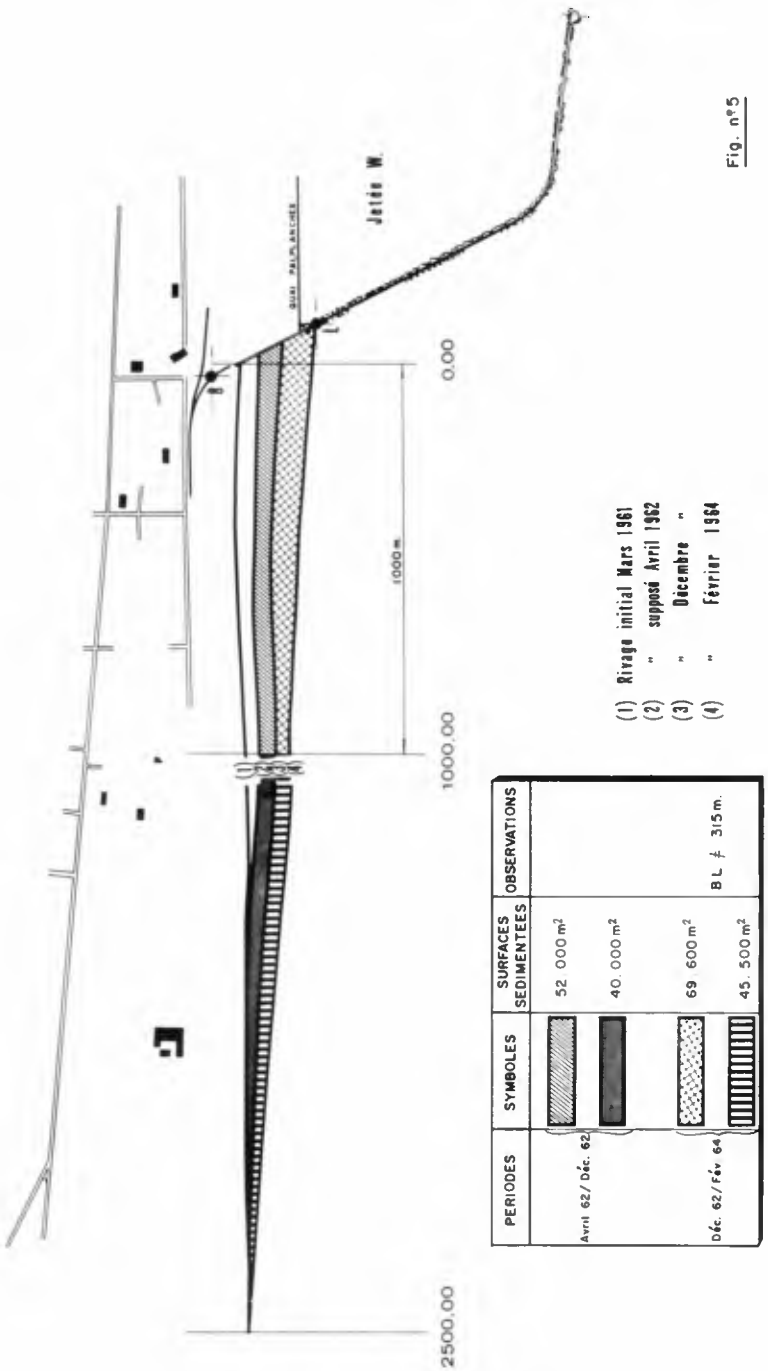

Fig. n°5

considérable entre l'extrémité Est de la zone (contre la jetée Ouest du port) et sa l. mite extrême Ouest. En gros, on peut dire que cette section sédimentée diminue d'un tiers entre l'Est et l'Ouest. Cela signifie que la zone sédimentée s'étend bien au-de de la zone des 1.000 mètres.

b) - Examen des photos aériennes. Cet examen permet de se donner une idée un peu plus précise de l'engraissement du rivage. La superposition d'une photographie verticale a 1/10.000ème prise au début des travaux, avec deux photos identiques prises, l'une en Décembre 1962, et l'autre en Février 1964, nous a permis de tracer le dessin ci-joint (figure n° 5) sur lequel ont été figurés les trois tracés du rivage. Un trait intermé diaire indique ce que pouvait être approximativement ce tracé lors du levé d'Avril 19 qui correspond au début de la période de référence. Il apparaît sur ce dessin que la surface gagnée sur la mer à l'Ouest de la zone étudiée des 1.000 mètres, représente e moyenne 70 % de celle correspondant à la zone étudiée des 1.000 mètres. On serait ain conduit à conclure, à condition que les dépôts en profondeur soient proportionnels, q l'importance totale des dépôts à l'Ouest de la jetée au cours de la période considéré de 8 mois, ont dû être de l'ordre de 1.000.000 m3. L'extrapolation à l'année complète conduirait à retenir provisoirement pour le transit annuel, un chiffre de l'ordre de 1.500.000 m3/an, chiffre qui peut être considéré comme une limite supérieure, étant d né que la période de 8 mois étudiée comprenait la saison des fortes houles.

Un autre calcul peut être fait en admettant que les volumes sédimentés sont pr portionnels aux surfaces gagnées sur la mer, telles qu'elles sont vues sur la photo a rienne. Cette méthode conduit à estimer ainsi qu'il suit le volume sédimenté entre Av 1962 et Février 1964 :

$$600.000 \times \frac{207}{52} = 2.400.000 \text{ m3 environ.}$$

S'agissant d'une période de 22 mois, on voit que le transit ainsi calculé devr dépasser légèrement 1.200.000 m3 par an.

Seuls les nouveaux sondages en cours et de nouvelles observations effectuées a quelques années permettront de préciser davantage ce chiffre.

Liste des figures jointes

Chapter 38

THE STRUCTURAL BEHAVIOUR AND THE SHELTERING EFFICIENCY OF THE SUBMERGED BREAKWATER AT THE ENTRANCE TO THE PORT OF LEIXÕES MAINTENANCE CHARGES AND EFFECTS

Duarte Abecasis
President (retired) of the High Council of Public Works
Lisbon, Portugal

The urgent necessity for providing a system of protective works of the harbour of Leixões with complementary works to improve the poor conditions of the shelter in the basin and to protect ships entering the port became evident in 1934. In fact, the frequency of disaster to trawlers and to other ships within the basin during southwestern gales as well as the very dangerous conditions at the entrance under such gales were incompatible with the increasing economic importance of Oporto and its hinterland.

These bad conditions culminated in the foundering of the 9000 T Dutch steamship "Orania" at anchor in the basin colliding on the 19th December 1934 with the steamship "Luanda" when entering the harbour under severe hurricane.

The construction of the 1000 m long new breakwater was started wit a 15 m wide vertical wall to be set partly on rocky bottom and partly o a sandy bottom. Before leaving the rocky bottom the upper part of the wall was destroyed by a strong gale (Fig. 1). For the advancement of t work the contractor and an official commission recommended the adoption of the Casablanca type of slope work.

For economical reasons and on those of the sure possibility of its conversion into a conventional type of work, would it become convenient it was decided, at the author's suggestion, and after model study at Lausanne School of Engineer's Laboratory, to adopt a new type of submerged work, to replace the unsuccessful vertical type or the type of Casablanca proposed by the contractor (Fig. 2). The section adopted co prised a rubble mound core of stones to 1^T with the crest at level $(-9^m,00)$, and berms of rubble to 4^T, 12 m wide to the sea side and 10 m wide to the port side (Fig. 1).

The top and slopes of the mound were protected by an armour of 90^T concrete blocks with the corners cut for best accommodation. The cost of the work could be reduced to half of that corresponding to the last of these types of breakwaters and its maintenance charge greatly reduce The estimated cost of the works would be reduced from £ 1.770.000 to £ 880.000 and the maintenance charges foreseen reduced from £ 35.400 yearly to £ 2.800 yearly (comparison with the Casablanca type).

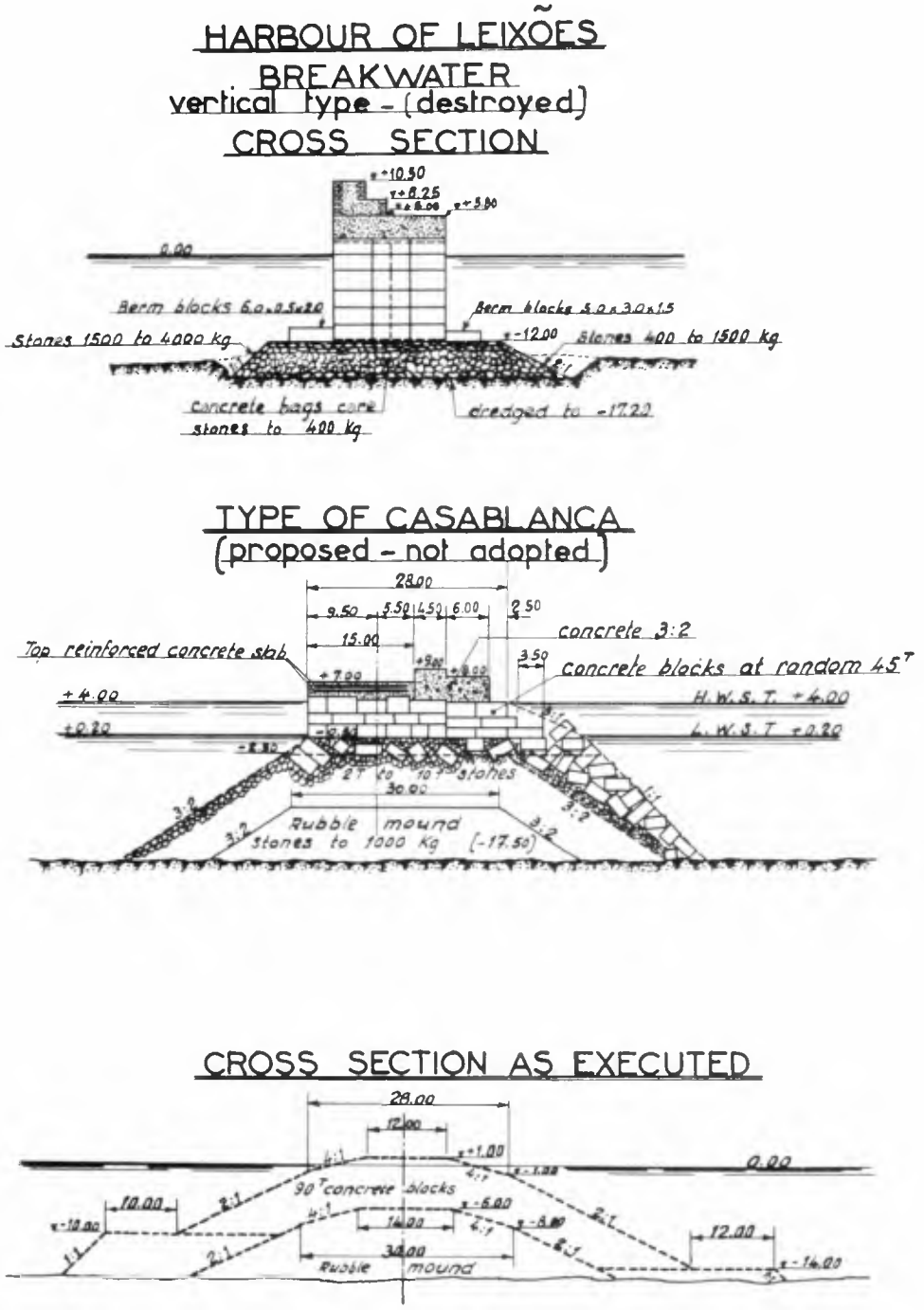
HARBOUR OF LEIXÕES
BREAKWATER
vertical type - (destroyed)
CROSS SECTION
Berm blocks 6.0x3.5x2.0
Stones 1500 to 4000 kg
Berm blocks 5.0x3.0x1.5
Stones 400 to 1500 kg
concrete bags core
stones to 400 kg
dredged to -17.20
TYPE OF CASABLANCA
(proposed - not adopted)
28.00
9.50
5.50
4.50
6.00
2.50
15.00
3.50
concrete 3:2
Top reinforced concrete slab
concrete blocks at random 45°
H.W.S.T. +4.00
L.W.S.T +0.20
+4.00
+0.20
2T to 10T stones
30.00
Rubble mound
stones to 1000 Kg
(-17.50)
CROSS SECTION AS EXECUTED
28.00
12.00
0.00
90T concrete blocks
10.00
14.00
12.00
38.00
Rubble mound

Fig. 1

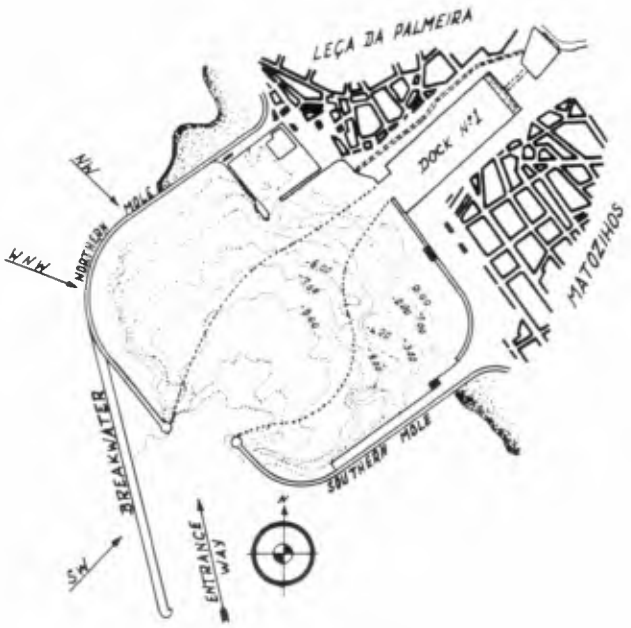

PLAN

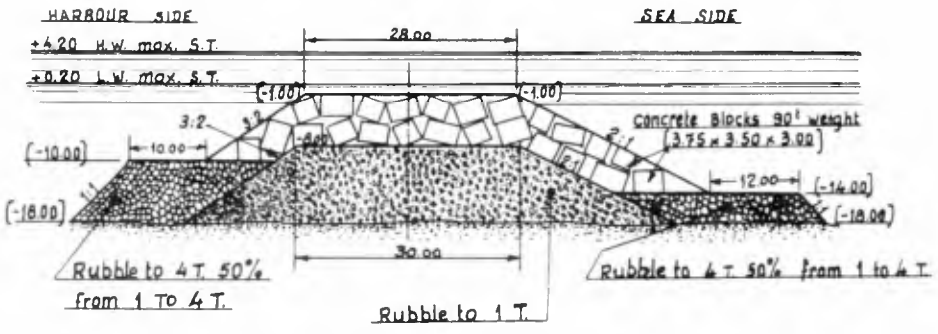

CROSS SECTION

Fig. 2

The maintenance charges were evaluated, for the Casablanca type, by the direct experience reported by the harbour's Authority, and for the type suggested, at Lausanne's Laboratory by a three dimensional model study in a large basin including the total extension of the breakwater (Fig. 2).

In fact, the cost of the first establishment was £ 943.000 and the maintenance charge, during the twenty-five years of the life of the work did not exceed £ 2143 yearly to maintain the crest level increased during the execution to (+ 1^{m},00). The allowance of 10% for sinking of the rubble mound and its revetment of 90 T concrete blocks into the bottom was reduced to less than one-tenth of the provision. The sheltering conditions of the harbour and its entrance were decidedly improved.

Wrecks no longer occurred, and the traffic of the port and fishing were greatly increased (150.000 T goods in 1933 to 2.000.000 T last year).

The maximum waves which were considered in the model study were for gales from the SW to WNW and were 10^{m} in amplitude and 220^{m} in length (prototype).

The works and model study were described in Dock & Harbour Authority, London, July 1939 and Anuário dos Serviços Hidráulicos, Lisbon 1937.

Chapter 39

A GUIDE TO THE DESIGN OF AIR BUBBLERS FOR MELTING ICE

Simon Ince
Hydraulics Section, National Research Council
Ottawa, Canada

INTRODUCTION

The use of air bubblers for maintaining ice-free areas in lakes and in the sea has been reported abundantly in the technical literature. This author (1962) reported his observations on two air bubbler installations in the Canadian Arctic to the Eighth International Conference on Coastal Engineering.

The results of these investigations were, at that time, still inconclusive. Today, some of the mystery is resolved and it is the author's opinion that the existence of a heat reserve is the answer to the problem. Based on this premise, an attempt is made here to develop some guide lines for the proper utilization of this thermal reserve.

AIR BUBBLER SYSTEMS

A review of the literature and evaluation of experiments and observations bring out the following salient points.

1. PREVENTION OF ICE-COVER FORMATION

To prevent ice formation the operation of the air bubbler must begin before freeze-up. If a large thermal reserve due to stratification exists, then the upward transport and mixing of the warmer strata supplies to the surface layers water above its freezing point and compensates for the heat losses to the atmosphere. The size of the ice-free area depends - aside from atmospheric conditions - upon the temperature structure of the water, the quantity of water transported to the surface, the mixing in the vertical plume and the temperature and velocity decay of the surface current.

If there is insufficient thermal reserve to compensate for heat losses, the system may still work to a limited extent, provided there is enough turbulence created on the surface to prevent the formation of a solid ice cover. The heat losses in this case are compensated by the formation of frazil ice, each gram of which liberates upon freezing its latent heat of fusion. The frazil particles are carried away by the currents and deposited on the underside of the adjacent ice sheets. The principles involved in this process are the same in fresh or sea water.

2. MELTING OF AN EXISTING ICE COVER

The melting of an ice cover when a large thermal reserve exists is a function of the flow factors outlined in the previous section. If there is insufficient thermal reserve within the range of influence of the air bubblers, only a limited amount of ice can be removed from the underside of the cover. There are reports, however, that by using underwater pumps, under certain conditions it is possible to "erode" the sea ice by the mechanical action of abrasion rather than melt it by thermal energy. The disturbing part of these claims is that the efficiency of the system is reported to be much greater than 100 percent, i.e. the energy input is smaller than that required to melt the volume of ice. This is undoubtedly an area which will require more research. Based on reports of the operation of this pump, it is the opinion of this author that two factors might have contributed to the success of the operation.

(a) There must have been in the region a small thermal reserve not detected by conventional oceanographic instruments. With the very large amounts of water circulated by the pump this may have been sufficient to honeycomb the ice cover and cause its disintegration.

(b) The experiments were conducted in relatively mild weather (about 0°C) at which time the strength of sea ice had decreased considerably, thus contributing to the rapid decay.

SOME APPROXIMATE RULES FOR THE DESIGN OF AIR-BUBBLER SYSTEMS

On the premise that ice removal is due to thermal effects, an attempt will be made to give simple working rules for the practicing engineer, to guide him in the efficient design of air bubbler installations.

The hydrodynamics of bubble curtains in homogeneous water has been studied quite extensively. For the practicing engineer the results of Bulson (1961) and Abraham and Burgh (1964) are most useful.

In summary and referring to Figure 1, the following relationships are found to be valid within reasonable limits.

(a) The maximum horizontal velocity V_o occurs approximately at a distance $x = d/2$ (1)

(b) $V_o = 1.2\,(g \cdot q_a)^{1/3}$ (2)

(c) $b = d/4$ (3)

where

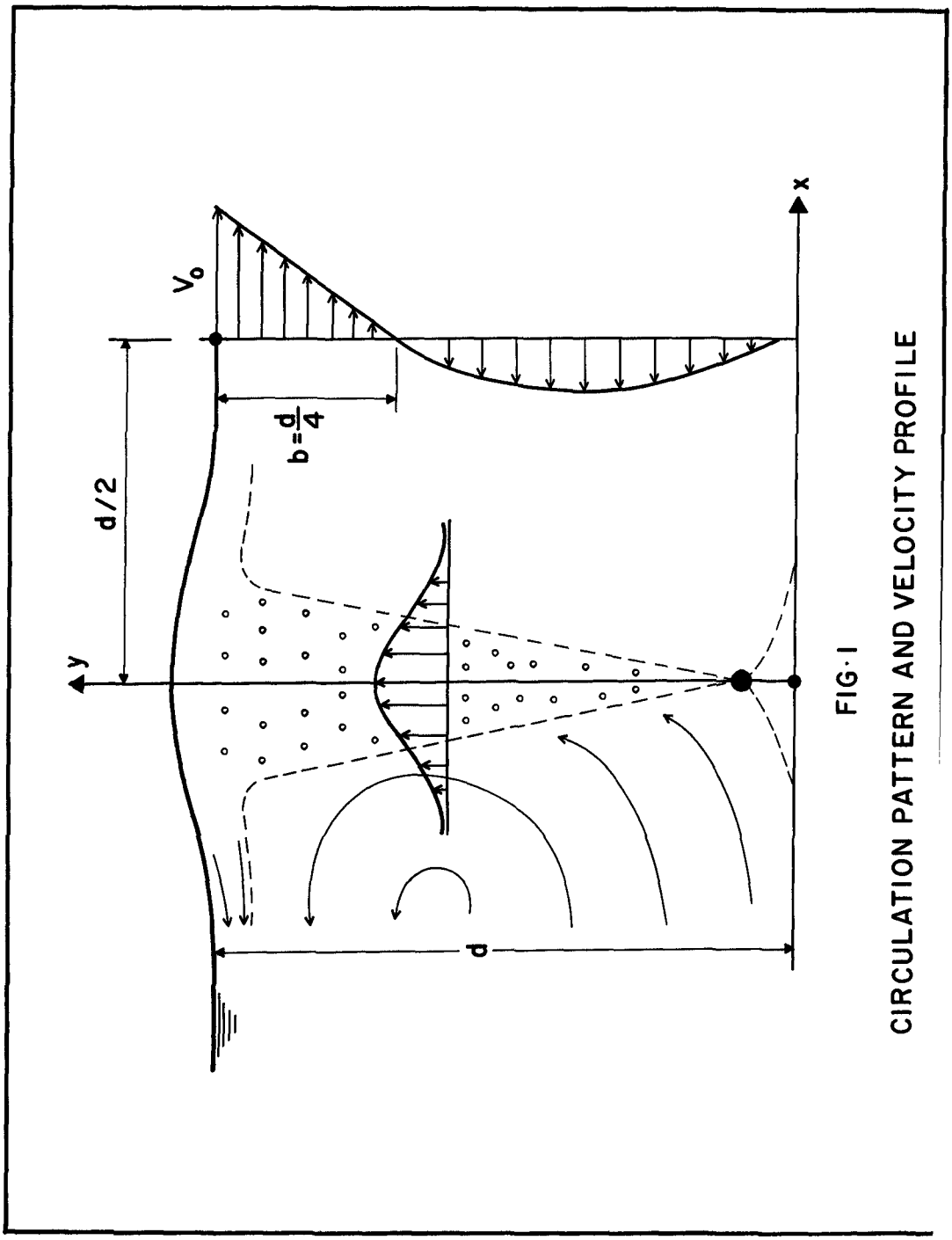

FIG·1 CIRCULATION PATTERN AND VELOCITY PROFILE

d = depth of water

q_a = rate of air flow per unit length of manifold measured at atmospheric pressure

g = acceleration of gravity

b = thickness of horizontal jet at $x = \frac{d}{2}$.

The author has plotted the decay of the surface velocity, given by Bulson and Abraham, in dimensionless form in Figure 2, and has obtained the relationship

$$\frac{V}{V_o} = 1.5 \left(\frac{x}{b}\right)^{-0.50} \qquad (4)$$

In view of the scatter of the experimental points and because in stratified fluids the surface jet tends to plunge and be effective only up to a limited distance, this simple relationship seems for the present sufficiently accurate.

The horizontal jet under an ice cover has, of course, the velocity distribution shown in Figure 3, but it can be reasonably assumed that the decay of the maximum velocity follows the same law.

The effect of the bubbler's orifice size on the maximum velocity has also been investigated and found to have no significant influence. Porous pipes do increase V_o by about 10 percent but are impracticable because of the higher air pressures required. For practical purposes simple square-edged orifices of 1/8" to 1/16" diameter are recommended.

The effect of orifice spacing has not been studied extensively but it was observed that for the same air flow a large number of smaller orifices spaced closely together were more effective than larger orifices spaced widely apart.

HEAT TRANSFER THROUGH THE ICE

The transfer of heat from the horizontal jet to the ice cover is at best a most complicated problem. By making some very rough assumptions, however, it may be possible to arrive at conclusions which may be of help in designing air bubbler installations.

As a first approximation, it is possible to consider the horizontal flow induced by the air bubbler as a form of two-dimensional wall-jet, where the jet velocity V_j is replaced by V_o , and jet thickness a by b .

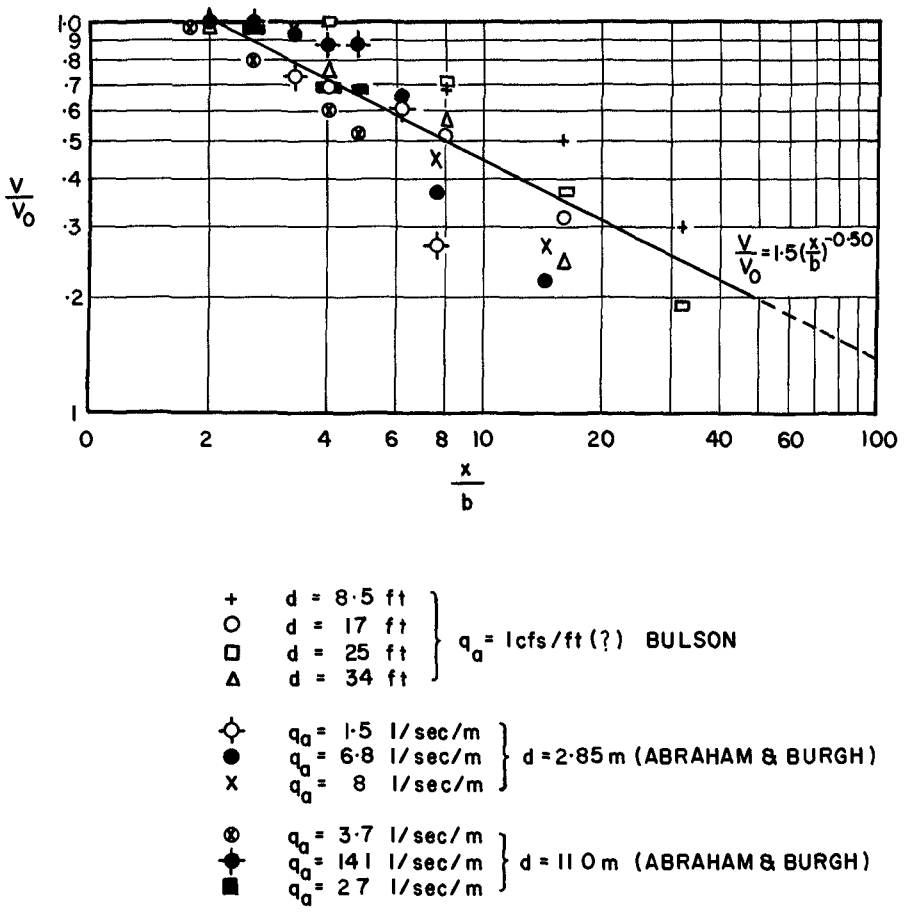

FIG·2

DIMENSIONLESS PLOT OF DECAY
OF MAXIMUM HORIZONTAL VELOCITY

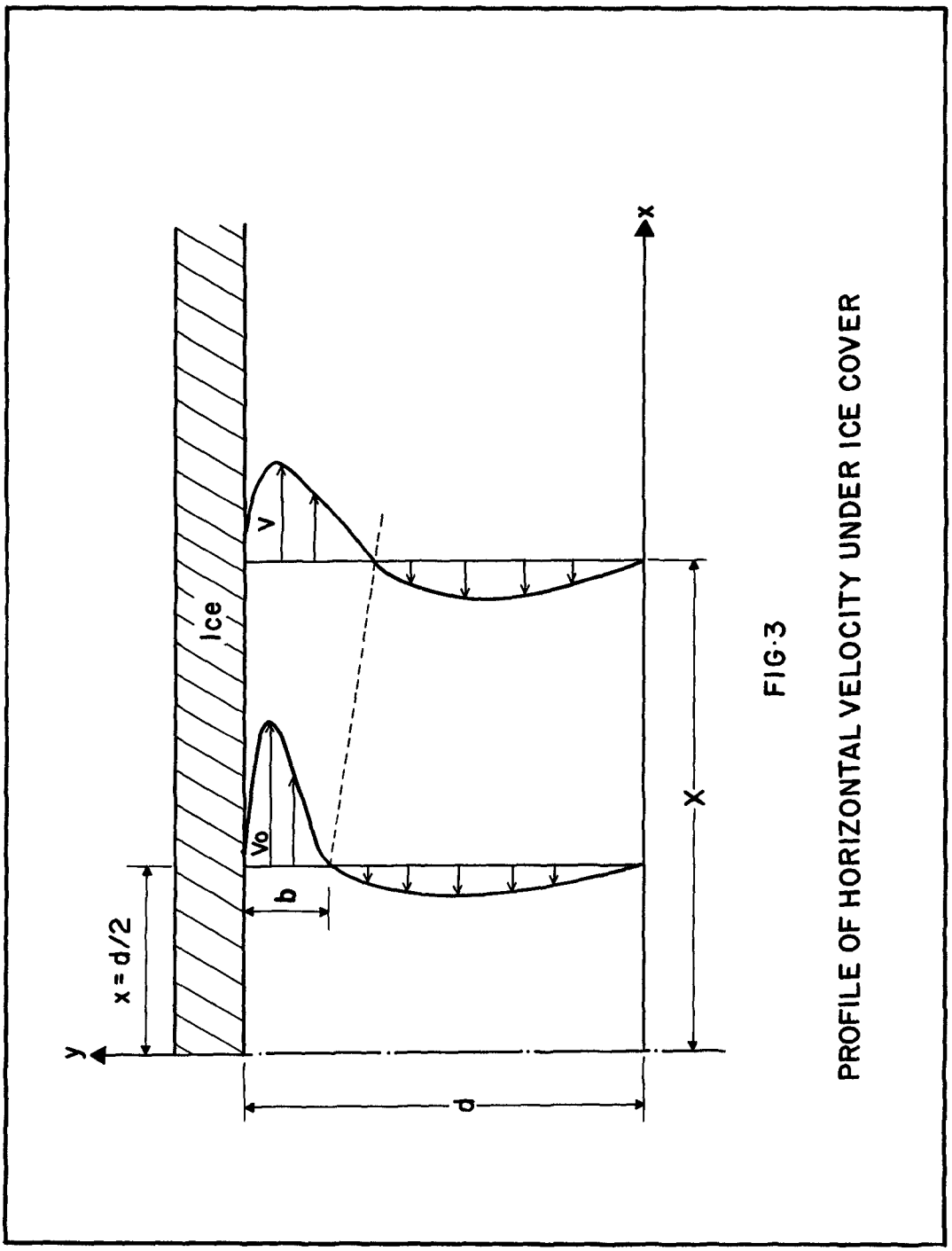

FIG·3

PROFILE OF HORIZONTAL VELOCITY UNDER ICE COVER

Comparing the horizontal velocity decay function of air bubblers with that of wall-jets,

$$\frac{V}{V_j} = 3\left(\frac{x}{a}\right)^{-0.5} \qquad (5)$$

given by Sigalla (1958), it is seen that the analogy does not appear far-fetched.

In the absence of further experimental data on air bubblers, it seems reasonable for a first approximation to use for our application temperature variation and shear distribution functions obtained experimentally for wall-jets.

Sigalla (1958) reports $\theta = 3 \cdot \left(\frac{a}{x}\right)^{1/2}$ (6)

Here $\theta = (T_1 - T_o)/(T_j - T_o)$

where T_1 = maximum temperature at any position along the wall,

T_o = ambient temperature,

T_j = temperature at nozzle exit.

In the case of air bubblers, T_j would correspond to the temperature of the horizontal current at $x = d/2$.

For the skin friction, Sigalla reports the relationship

$$C_f = \tau_o/\tfrac{1}{2}\rho V^2 = 0.0865/\left(\frac{Vx}{\nu}\right)^{0.2} \quad \text{for} \quad \frac{x}{a} > 30 \; . \qquad (7)$$

Assuming for our case,

$$C_f = 0.1/\left(\frac{Vx}{\nu}\right)^{0.2} \quad \text{for} \quad \frac{x}{b} > 2 \; , \qquad (8)$$

we can make use of the relationship derived by Sidorov (1957) for heat transfer by the turbulent horizontal jet to the lower surface of the ice,

$$N = \tfrac{1}{2} C_f R P_r^{1/3} \qquad (9)$$

Here,

N = Nusselt number = $q\,x/k\,(T_1 - T_s)$

R = Reynolds number = $\frac{Vx}{\nu}$

P_r = Prandtl number = $C_p \mu/k$

where

q = local rate of heat transfer

k = thermal conductivity of water evaluated at a temperature of $\frac{1}{2}(T_1 + T_s)$

T_s = temperature of wall surface

ν = kinematic viscosity of water

μ = dynamic viscosity of water

C_p = specific heat of water

V = maximum velocity at point x .

The Prandtl number for water at 32°F is 13.6. It is convenient to assume it constant for all applications where the temperatures are close to this value.

Substituting into equation (9) the value of C_f from (8) and that of V from (4), we get

$$N = 0.94 \left(\frac{V_o x}{\nu}\right)^{0.8} \left(\frac{b}{x}\right)^{0.4} \qquad (10)$$

and hence,

$$\frac{q\,x}{k\,(T_1 - T_s)} = 0.94 \left(\frac{V_o x}{\nu}\right)^{0.8} \left(\frac{b}{x}\right)^{0.4} \qquad (11)$$

With the help of the relationships (1), (2), (3), (6) and (11), a more rational design of air bubblers can be accomplished than has been possible up to now.

A very simple example may illustrate the new approach.

Consider the water-temperature structure in a lake, shown in Figure 4.

It is desired to melt the ice at $x = 20$ m. within 24 hours after installation of the air bubbler. This requires, on the average, a heat supply

$$q_1 = 0.05 \text{ cal/cm}^2\text{/sec.}$$

Assuming the heat losses to the atmosphere to be,

$$q_2 = 0.0112 \text{ cal/cm}^2\text{/sec. } (3600 \text{ BTU/ft}^2\text{/day})$$

the total heat to be supplied is,

$$q = q_1 + q_2 = 0.0612 \text{ cal/cm}^2\text{/sec.}$$

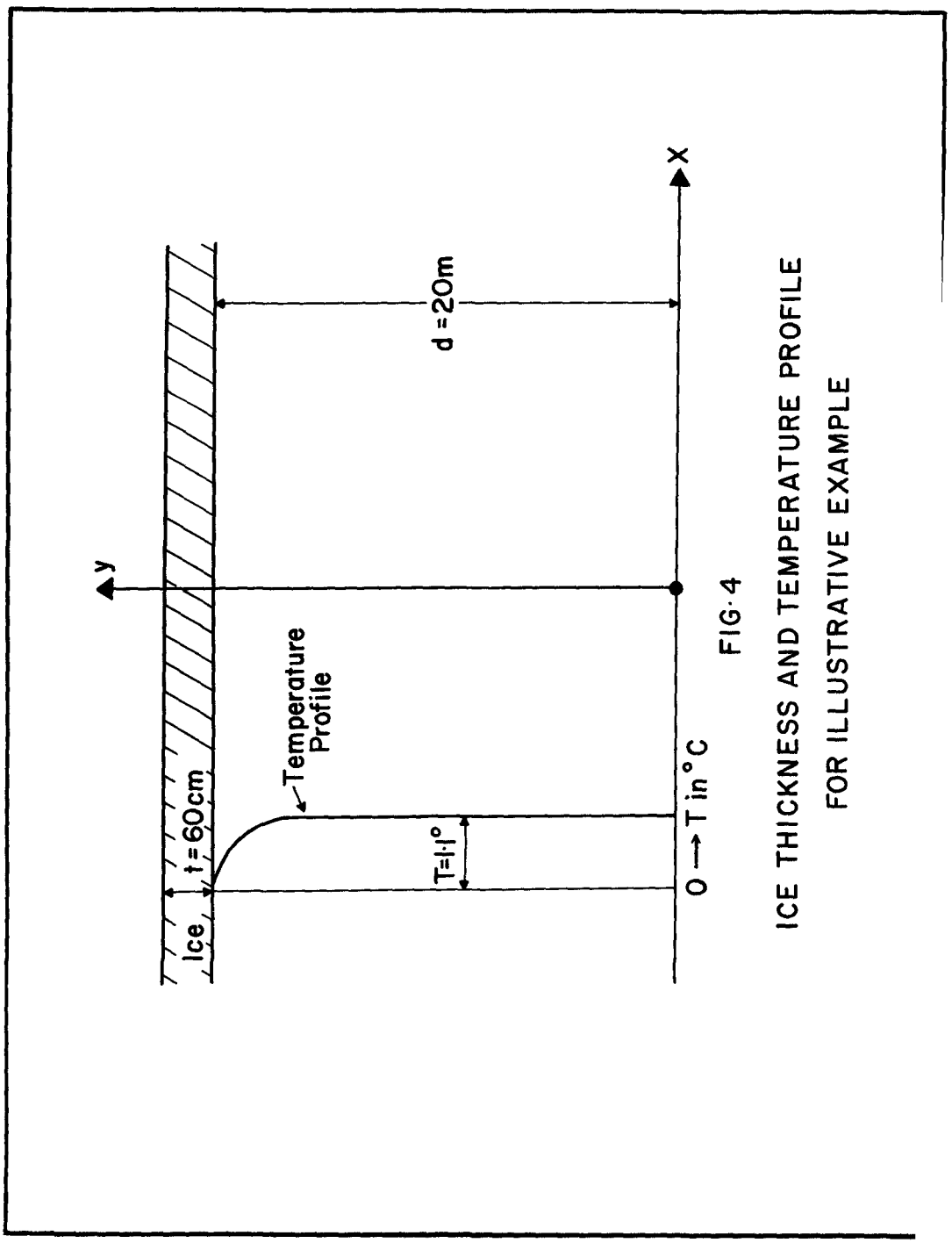

FIG·4

ICE THICKNESS AND TEMPERATURE PROFILE FOR ILLUSTRATIVE EXAMPLE

If the bubbler is to be installed at the bottom (d = 20 m.), it seems reasonable to assume that the temperature of the horizontal jet at $x = d/2$ will be approximately $T_1 = 1°C$. Conveniently, $T_s = 0$.

With $q = 0.0612$ cal/cm^2/sec.

$x = 2000$ cm.

$k = 0.00133$ cal/sec.cm/°C.

$T_1 - T_s = 1°C$.

$\upsilon = 1.86 \cdot 10^{-2}$ cm^2/sec.

$b = \frac{d}{4} = 500$ cm.

equation (11) yields $V_o = 32$ cm/sec.

From equation (2), $q_a = 1920$ cm^3/sec/m.

The energy per second available in the air leaving the manifold, assuming isothermal conditions and an air pressure just sufficient to overcome the static head, is given by

$$E_A = \gamma_w H_o q_a \ln \left(1 + \frac{d}{H_o}\right)$$

where γ_w = specific weight of water

H_o = atmospheric pressure in cm. of water.

Substitution of values yields,

$E_A = 207$ watts/m.

For the same conditions, if the manifold is suspended at a depth of 10 m,

$b = \frac{d}{4} = 250$ cm,

and we get

$V_o = 45$ cm/sec., $q_a = 5460 \frac{\text{cm}^3}{\text{sec}}$/m,

and $E_A = 373$ watts/m.

CONCLUSIONS

The paper is an attempt to put on a more rational basis the design of air bubblers for melting the ice cover and maintaining ice-free areas in lakes and in the sea. Since there is not sufficient experimental data to support the validity of some of the relationships used from the wall-jet analogy, caution should be exercised in putting too much

faith in exact numerical results. Nevertheless, it is believed that the procedure outlined above might be useful in estimating the order of magnitude of the air supply and power requirements, once information is available about the atmospheric and oceanic or limnologic environment.

REFERENCES

Ince, S. (1962). Winter regime of a tidal inlet in the Arctic and the use of air bubblers for the protection of wharf structures: Eighth International Conference on Coastal Engineering, Mexico, pp. 521-532.

Bulson, P. S. (1961). Currents produced by an air curtain in deep water: The Dock and Harbour Authority, May, pp. 15-22.

Abraham, G. and Burgh, P.v.d. (1964). Pneumatic reduction of salt intrusion through locks: Proc. Am. Soc. Civil Engrs., vol. 90, No. HY1, January 1964, part 1, pp. 83-119.

Sigalla, A. (1958). Experimental data on turbulent wall jets: Aircraft Engineering, vol. 30, pp. 131-134.

Sidorov, A. (1957). The relation of surface friction and heat transfer: Soviet Physics, vol. 2, No. 3, pp. 499-504.

Praia daVitoria, Azores

Part 4

COASTAL ENGINEERING PROBLEMS

Figueira daFoz, Portugal

Chapter 40

PRINCE HENRY THE NAVIGATOR AND THE KNOWLEDGE OF THE COASTS

A. Teixeira da Mota
(Portuguese Navy)
Director, Secção de Lisboa do Agrupamento de Estudos de Cartografia Antiga (Junta de Investigações do Ultramar)

BEGINNINGS AND EVOLUTION OF NAUTICAL SCIENCE

When, under the strong impulse of Prince Henry, Portuguese maritime discoveries began, in the dawn of the XVth Century, methods of navigation were still those of coastal and estimated navigation and resulted mostly from the progress made in the XIIIth Century. During that period the knowledge of geometry of ancient Greece had spread widely and the mariner's compass had been adopted on board the Mediterranean ships. These innovations had the following consequences:

a) Rutters: to the former indication of the principal characteristics of the coasts, particularly as regards to ports and bars, and of the distance between the most remarkable accidents, was from now on added the indication of the magnetic azimuths between these accidents.

b) Nautical charts: the nautical chart, nonexistent in Europe, was created at that time.

The chart was mainly a simple graphic representation of the rutters, the coast being drawn according to magnetic azimuths, without longitude or latitude scales and with one sole distance scale for all the area comprised in the chart. At first only the coasts of the Mediterranean were drawn, then the Atlantic coast of Europe from Denmark to the British Isles and the coast of Africa up to Cape Bojador, as well as those of Madeira and the Canary Islands.

It was these types of rutters and charts that the Portuguese began to spread also to other zones when they started their maritime discoveries in the time of Prince Henry. But they soon proved insufficient to face new conditions and needs.

Actually, the regime of winds of the North Atlantic forced ships to swing far out towards the northwest on their way from Africa to Europe and thus the Azores were discovered in 1427 and the oriental side of the Sargasso Sea before 1448. The methods of estimated navigation currently used in those days became insufficient for the sailors who had to spend several weeks at the open sea, away from the coast. This gave rise to astronomic navigation and to the development of studies on oceanography and magnetism.

It is unnecessary to describe here the evolution processed in that century, it being enough to refer the progress attained around 1500:

a) Determination of latitude at sea by means of the North Star.

b) Determination of latitude at sea by means of the observation of the meridian height of the sun.

c) Knowledge of the regime of winds and currents of the North Atlantic.

d) Discovery of magnetic declination and its variation in space.

Thanks to new knowledge and techniques, maritime discoveries were extended to all the oceans and this had its effects on rutters and nautical charts, wich now comprised much wider areas. The drawing and description of coasts also improved considerably. And it is this extension and progress that are described below.

IMPROVEMENT AND EXTENSION OF THE DESCRIPTION AND REPRESENTATION OF THE COASTS

EXTENSION

The French historian Gernez wrote the following about this subject:

"Si on examine une des meilleures cartes portugaises du milieu du 16^{e} siècle, celle qu'André Homem fit à Anvers en 1559, on constate que, à l'époque où cette carte fut tracée, soit 124 ans après que Gil Eanes eût, le premier, dépassé le cap Bojador (1434), les marins portugais avaient levé toutes les côtes de l'Afrique (y compris Madagascar), une grande longueur de côtes de l'Asie et des îles de la Malaisie, et les côtes du Brésil, et cela d'une façon relativement exacte. Ce levé hydrographique de plus de 27.000 km. de côtes africaines (Madagascar comprise), de plus de 21.000 km. de côtes asiatiques, de plus de 5.000 km. de côtes des îles malaises, de plus de 7.000 km. de côtes brésiliennes - soit, en tout, de plus de 60.000 km. de côtes, a donc été exécuté en moins de 124 ans, soit une moyenne de plus de 480 km. de côtes levées par an.

"L'ensemble de ces levés hydrographiques constitue donc un travail formidable qui, à cause des difficultés de toute nature rencontrées - faibles navires, équipages trop souvent malades et toujours mal nourris, luttes avec les indigènes aux points de relâche, grossièreté des instruments d'observation employés - est réellement unique dans l'histoire mondiale et mérite d'être admiré sans réserve par les marins de toutes les nations".

The same as with charts, rutters also began to cover a much wider range of coasts, although the increase was not so considerable as in the charts.

PROGRESS IN THE DRAWING

It is still Gernez who says:

"Quand on compare les oeuvres des grands cartographes italiens du 15^{e} siècle avec les cartes nautiques portugaises, on constate une différence entre le dessin des côtes exécuté par les Italiens et le dessin portugais. Tandis que les Italiens représentaient la côte d'une façon presque schématique, en forme d'arcs de cercles plus ou moins courbes présentant souvent en leurs milieux une coupure ressemblant à l'embouchure de quelque fleuve, les Portugais arrivèrent à donner au dessin de la côte un tracé plus conforme à la véritable forme des côtes. Ou remarque encore, sur les cartes portugaises, de représentations un peu schématiques, comme celles des embouchures de rivières, qui sont figurés relativement étroites, mais avec un élar-

gissement un peu en amont de l'embouchure; mais on peut dire que, en général, le tracé de la côte devient plus conforme à la nature".

LATITUDE SCALE

Besides this improvement in the drawing of charts, a new element, also introduced by the Portuguese, increased considerably the accuracy of the reproduction of coast in nautical charts: the scale of latitudes.

Once sailors had found the means of determining latitude at sea (which they did in the middle of the XVIth Century with a mean error of 1/6 of a degree) it became necessary to reform the traditional nautical chart, wich was drawn only according to estimated distances and magnetic courses, as the position of ships determined by astronomic methods ceased to be correct in relation to the coastline. To obtain agreement the drawing must be based on the corresponding determinations of latitude, and, if possible, with greater accuracy than at sea.

About the year of 1485, king John II sent José Vizinho, Duarte Pacheco Pereira and other cosmographers to Africa to determine the latitudes of numerous points on the coast, with a view to reforming the traditional nautical charts. This was the first time that a group of scientists and technical men were sent on a study mission to make new hydrographic surveys by working on land and sea, and it is yet another thing in which the Portuguese were the beginners.

And thus the scale of latitudes was introduced in nautical charts, which, together with the fleur-de-lis as the symbol of the north, are two Portuguese innovations still used.

When the Portuguese reached the Indian Ocean they found there a nautical science based on astronomical observations, with the determination of star heights on their meridian passage, but the Orientals did not have real nautical charts. The nautical chart based on compass courses and on astronomical latitudes - this latter case being a Portuguese innovation - was the great symbol of the superiority of the European sailors and the basic instrument for their expansion in the seas all the world over.

Likewise Portuguese started recording the new data - the latitude of coastal points - on the rutters, what rendered them far more accurate.

MAGNETIC DECLINATION

It was the Portuguese, and not Columbus, as many people erroneously believe, that discovered the phenomenon of magnetic declination and its variation in space. In the early XVIth Century they were already aware of the great values of the magnetic declination in Newfoundland and in the South Atlantic, as well as they knew the agonic lines then passing near Azores and in South Africa. In the XVIth Century they carried out a large number of magnetic observations in the Atlantic and the Indian Ocean.

The knowledge of the magnetic declination, its variation in space and in time (this last instance was noticed in the beginning of the XVIIth Century) brought about a progressive need for new hy-

drographic surveys where true courses and not magnetic ones were used, in order to correct prior influences of the magnetic declination on the drawing of coasts. This correction, carried on through numerous doubts, took a long time to be fully perfomed, and Portuguese also played an important part in it.

A similar improvement was made on the rutters, where true azymuth replaced magnetic ones and the local values of magnetic declination were indicated.

The first observation of the deviation of the mariner's needle on board (Moçambique, 1538) as well as the finding out of local magnetic anomalies (Chaul and Bacaim, 1538) were also due to a Portuguese, D. João de Castro.

In this way, the nautical chart, and therefore the representation of the coasts, were much improved.

COASTAL VIEWS ON THE COASTLINE

It is also on Portuguese works - D. João de Castro's rutters (1538-1542) - that an important progress in the field of the representation of coasts was made for the first time.

It is the drawing of coastal views as seen from the sea, the basis of this drawing following the coastline on the hydrographic plans.

This practice, that is no more currently used, quickly passed to the Dutch and afterwards to other peoples, and was a feature of the nautic cartography of the XVIIth and XVIIIth Centuries.

Nowadays, coastal views are given independently of the coastline, but , in that time, such a representation helped to secure a bet ter knowledge of the coasts.

SOUNDINGS

The origin of the numerical record of soundings in nautical cartography is not plain. It is usually said that they appear, for the first time, on Dutch charts of Western Europe, in the last quarter of the XVIth Century. Nevertheless, on a set of charts owed to the Portuguese cartographer Bartolomeu Velho and dated from 1561, some soundings can already be seen near Newfoundland. Although this seems to be their most ancient appearance on dated charts that were known up to the present, we cannot assure, however, that the record of soundings is a Portuguese invention, since the soundings could have been already entered on other charts that were lost.

Anyway, Portuguese were amoung the first who used such an improvement, which also represented an important step in the study of the coasts.

TIDES

When the Portuguese started their maritime discoveries, the usual sailing directions gave already some guidance with reference to the characteristics of tides in the various European harbours.

On the new rutters for the coasts they discovered, the Portuguese followed the same methods and successively recorded the va-

lues of tides in accordance with the observations they carried out.

SPREADINGS OUT OF NEW NAUTICAL AND HYDROGRAPHICAL METHODS

It was not only through their own discoveries that Portuguese contributed to the progress of the representation and knowledge of coasts. All the Atlantic peoples from Western Europe that threw themselves into overseas undertakings after the Portuguese - the Spaniards, the French, the Dutch and the English - fully adopted the new nautical and cartographic methods created by the Portuguse. Therefore also their maritime expansion brought about an extension and progress in the representation and knowledge of the coasts.

The spreading out of the new techniques was due to direct translations from Portuguese originals (or from Spanish works based on them), to the use and reproduction of Portuguese charts or to the services of numerous Portuguese pilots and cosmographers in other countries. Among these men, many bound their name to the history of the discoveries and of the cartography, such as João Dias Solis, Fernão de Magalhães, João Rodrigues Cabrilho, Estêvão Gomes, Diogo Ribeiro, Duarte Barbosa, Pedro Fernandes de Queirós, João Baptista Lavanha, João Afonso Francês, André Homem and Bartolomeu Velho.

Through the abundant documentation of that period, it is often possible to follow the efforts of authorities of several countries - specially of Spain and of France - with a view to secure the services of skilled Portuguese pilots and cartographers, and also the measures taken by Portuguese rulers against that aim.

Likewise, Portuguese cartography strongly influenced that of several countries in the XVth and the XVIth Centuries as regards the representation of coasts.

Numerous Portuguese rutters were widely used and translated in other countries too, a better knowledge of the coasts of recently discovered regions becoming thus more general.

To end up with, and as we do not wish to indicate only those Portuguese influences, it may be useful pointing out that the ancient Portuguese cartography and rutters can still be of practical interest today inasmuch as they supply data enabling to understand the evolution of some coastal phenomena. Two examples will be given for evidence.

In his "Tratado Breve dos Rios da Guiné de Cabo Verde" (1594), André Álvares de Almada said that bore was met at Rio da Furna (perhaps the now called R. Kapatchez in the Republic of Guinea). Today the phenomenon is no more observed in that region, from what we can infer that the coast underwent some alteration.

On several Portuguese charts of the beginning of the XVIIth Century the island of Luanda appears quite more distant from the continent in the south side than at present. Rutters and other contemporary documents show that ships could take this way for entering the harbour, what is no more possible long since.

A careful analysis of ancient charts and rutters will surely provide a large number of examples of coastal evolution. There-

fore it seems useful that in the different countries a collaboration in this domain could be established between the modern scientists and the historians working on ancient cartography.

REFERENCES

Gernez, D. (1940). Importance de l'oeuvre hidrographique et de l'oeuvre cartographique des portugais au 15e et au 16e siècles: Congresso do Mundo Português - Memórias, vol. III, pp. 487-504.

Mota, A. Teixeira da (1962). A evolução da ciência náutica durante os séculos XV-XVI na cartografia portuguesa da época: Memórias da Academia das Ciências de Lisboa - Classe de Letras, vol. VII, pp. 247-66.

Chapter 41

THE ASH WEDNESDAY EAST COAST STORM, MARCH 5-8, 1962
A HINDCAST OF EVENTS, CAUSES, AND EFFECTS

Charles L. Bretschneider
Director, Washington Office
National Engineering Science Co.
Washington, D. C.

ABSTRACT

Hindcasts were made for winds, waves and tides for several east coast locations for the storm of 5-8 March 1962. A limited amount of recorded data and a considerable amount of other observations were available from near-by and remote stations. The data were analyzed for correlation or "calibration" purposes in order to improve the "state of the art" of wave and storm surge hindcasting for locations where recorded data were not available. Wind records were analyzed to obtain sustained wind speeds, average gust factors, and probability distribution of gust factors. Isobaric patterns were used to determine sustained wind speeds over the water fetch for deep and shallow water waves and storm surge hindcasts. Wave run-up calculations were made to determine the wave activity on the beach and the dunes and were used to estimate the probable rate of beach erosion and dune evolution. The off-water wind speeds were modified to determine wind speeds over the beach and over the top of the dunes. Finally, by summarizing the time-history of the various meteorological, oceanographic, and coastal engineering events, a very interesting scientific and engineering evaluation of the causes and effects can be made.

INTRODUCTION

The Ash Wednesday East Coast Storm, 5-8 March 1962, was perhaps the most severe storm of the century along the east coast of the United States. It occurred during spring tide conditions, and as a result produced near-record-breaking high tides enabling large waves to attack the shoreline and cause extensive beach erosion, and combined with exceptionally high winds caused a tremendous amount of property damage along the Atlantic coast from Long Island, New York, to Cape Hatteras, North Carolina. The effects of the storm even reached northern Florida where swell greater than 12 seconds was a record observed for the first time. In many cases the dunes were moved back 20 to 40 feet or more. Figure 1 shows the areas of interest along the east coast of the United States.

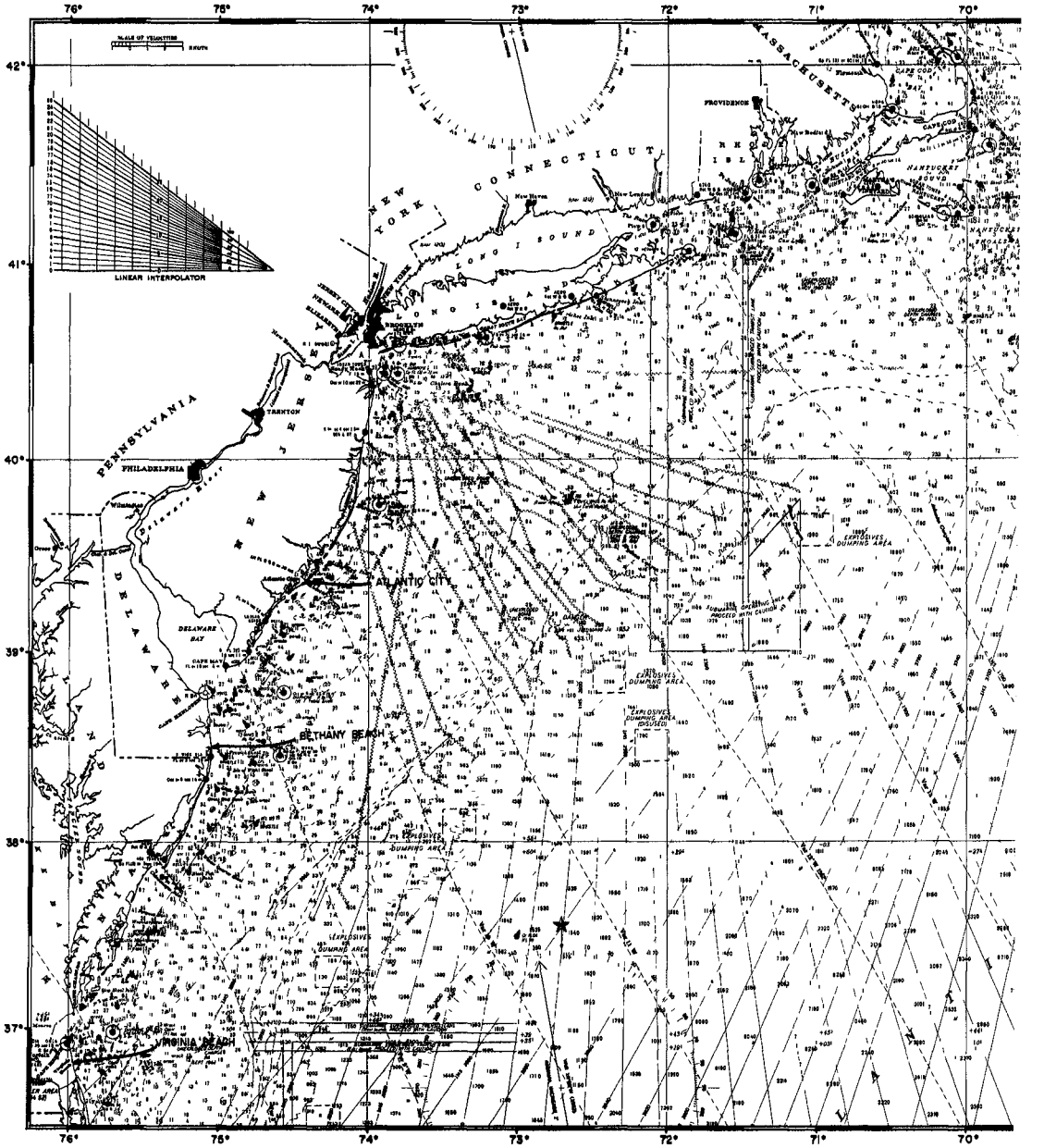

FIG. 1.--LOCATION MAP, EAST COAST OF UNITED STATES

The storm persisted through four to five high tide cycles, a situation which never before had been recorded. As compared to a hurricane, this storm can be considered greater in damage potential because a hurricane affects a much shorter reach of coastline at any particular time and usually lasts through only one high tide cycle at a particular location. Furthermore, in a hurricane the high tides usually precede the highest winds whereas in a steady-state type northeast storm the highest winds usually precede, and may last through, the highest tides.

Two particular areas were investigated in detail and a third qualitatively by use of hindcast techniques. The location of Atlantic City, New Jersey (Ventnor, N. J. to be exact) was investigated by Bretschneider and Collins (1963), and South Bethany, Delaware, was investigated by Bretschneider, Le Mehaute, and Allen (1963). The coast of Virginia was investigated qualitatively. In all cases the detailed hindcasts were correlated with available data.

The winds and tides in the area were comparatively well recorded giving a complete picture of the wind and water levels near the coast. The only actual waves recorded were for the early part of the storm at the Beach Erosion Board's wave gauge on the Steel Pier at Atlantic City, N. J. The gauge became inoperative on the second day due to power failure when a part of the Pier was destroyed by a drifting barge or ship. The U. S. Coast and Geodetic Survey tide recorder, also near the end of Steel Pier, operated throughout the storm since no outside power source was required. A number of Coast Guard lightships observed and logged wind and wave data. These wave data are for moderate water depths on the continental shelf and are not applicable to the shallower surf zone depths along the coastline.

The extent of damage caused by this storm has been summarized previously by O'Brien and Johnson (1962). The storm even affected shipping to a great extent. Some ships actually lost distance when navigating into the wind and waves.

This paper represents a hindcast of the causes and effects of the great northeast storm of 5-8 March 1962. Included in the hindcast are deep water waves; waves and tides over the continental shelf and in the surf zone; and wind, tides, waves, wave run-up and erosion over the beach and the dunes. In some respects this paper is more or less a case history study, and a test of hindcasting techniques. It should be apparent from this report that there are certain interesting aspects requiring further research.

THE PROBLEM

The problem is best defined in terms of a general problem coupled with individual local problems. The general problem pertains to the determination of wind, waves and swell, and tides from deep water to breaking wave or surf zone, and if more-or-less average physical coastal features are assumed, the general study can be extended from the surf zone to the coastline over the beach and dunes to the limits of the flooding. The local studies include any deviations from the general study as might be required for an engineering evaluation of the timing and causes of damage, whether wind or water or a combination of both. The type of engineering evaluation depends on whether the structure is a pier extending into the sea, a coastal bulkhead, a dune, or a building on top of or behind the dune, etc.

Specifically the problem consists of the determination of the time-history of many events. The following steps are generally considered important:

1. Analyze past weather maps for the particular storm of interest to determine wind and wind stress diagrams.

2. Analyze all other available data pertinent to the area of interest such as wind, tide, storm surge, waves, wave run-up, high water marks, beach and dune erosion, etc.

3. Hindcast deep water wave heights and periods and compare, where possible, with existing data.

4. Determine the normal or predicted tide using the appropriate tide tables.

5. Hindcast storm surge and compare with existing data, where possible.

6. Hindcast wave heights and periods over the continental shelf taking into account the combined effects of bottom friction, wave refraction, wind generation, and compare with existing data, where possible.

7. Hindcast the breaking wave heights and periods and depths of breaking waves in the surf zone coincident with total tides.

8. Hindcast wave heights and periods at the coastline coincident with the total tides.

9. Hindcast wave run-up on the beach, berm and dunes.

10. Hindcast the beach and berm erosion and dune evolution.

11. Hindcast the sustained winds and peak gusts along the coastline.

12. Hindcast the sustained winds and peak gusts over the dunes for the area of interest

13. Compute wave and wind pressures and forces for the type of structure being affected.

14. Analyze in detail each particular structure of interest subjected to all or some of the factors hindcasted above.

15. Based on all the available information, hindcast data and observed and/or recorded data, determine the most probable cause or causes and time of damage and/or destruction of various structures.

The above step-by-step procedure appears to be relatively straight-forward and somewhat idealistic. Depending upon the available facts, each particular problem can impose difficulties of various degrees. However, when the problem as a whole is finally analyzed in terms of good engineering judgment, then the many inherent difficulties are minimized and very sound conclusions can be drawn. Perhaps one of the most important reminders is that there must be coherence from location to location. Eyewitness accounts from people possessing no particular self-interest are a consolation to the accuracy of the hindcasts. Although the consistancies between reliable eyewitness accounts and a hindcast have a definite role in establishing the factual causes of damage during the storm, eyewitness accounts during the storm should not be considered as scientific data to be used in the calibration of the hindcast techniques.

AVAILABLE DATA

In order to perform the hindcast study, various sources of data must be investigated and the data must be studied. Important for this study were the following:

1. The official U. S. Weather Bureau maps, Northern Hemisphere charts, at 6-hourly intervals, 5-8 March 1962, were used to determine sustained wind speeds and direction over the water fetch. Figure 2 gives a typical example of the component of wind speed resulting in maximum wave generation, and figure 3 gives a typical example of the average wind stress diagrams resulting in maximum storm surge generation off the east coast.

2. The official U. S. Coast and Geodetic Survey recorded tide data for various locations along the east coast of the United States were used to determine the increase in total water depth during the storm. This information is of value to hindcast total water depths where recordings were not available. Figure 4, reproduced from Harris (1963), gives the storm surge hydrographs measured at various locations along the east coast. Figure 5, also reproduced from Harris (1963), shows high water marks which were indicative of wave set-up, and also maximum probable wave run-up.

3. The U. S. Coast and Geodetic Survey Tide Tables for 1962 were used to determine the normal predicted tides, sometimes called the astronomical tides. Neglecting the second order effects, the storm surge is obtained by subtracting the predicted tide from the recorded tide.

4. The Beach Erosion Board's analysis of the wave record for Atlantic City Steel Pier, 5-6 March 1962, was used to check the accuracy of wave hindcasts in shallow water near the coast, mean low water depth of about 17 feet. (The wave gauge became inoperative after 0400 GMT on 6 March 1962.)

5. The official U. S. Weather Bureau records and logs for various land stations near the coast were used to determine relations between average gust speeds and 1-minute average sustained wind speed, and were also used to determine the probability distribution of gust factors. The 1-minute average is the average of the last 1-minute of a 15-minute period, and the gust is the peak wind during the same 15-minute period.

6. Wind and wave data logged by U. S. Coast Guard lightships and other vessels at sea were used to check wind and wave hindcasts. The winds reported by ships at sea represent an average wind speed, and gusts are not normally reported. The waves are average of the maximum observed and are probably close to the significant wave.

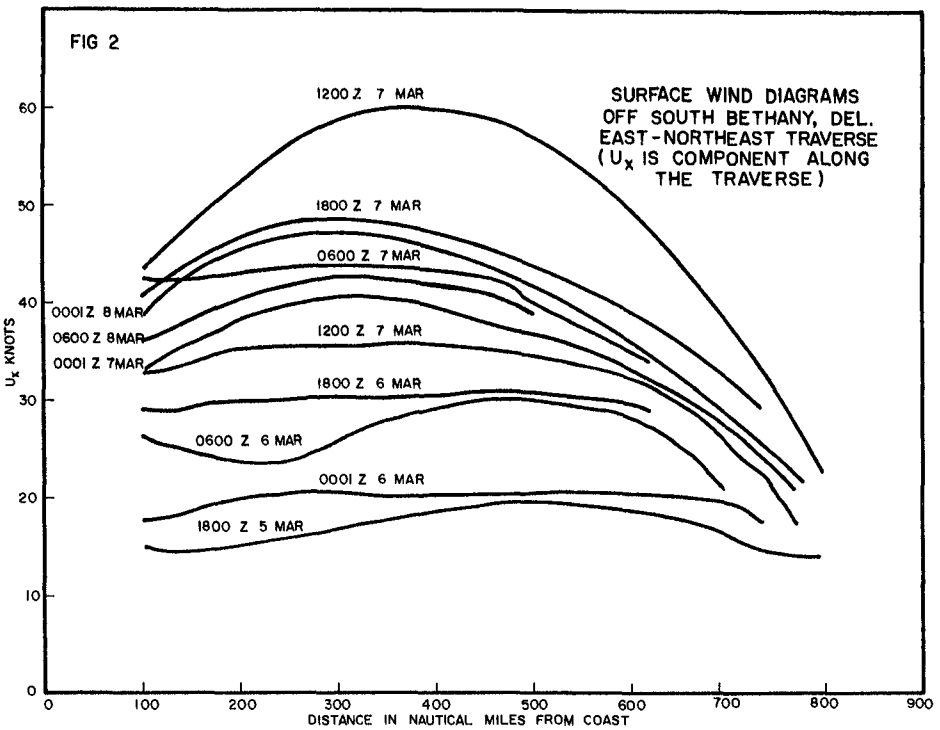
FIG 2
SURFACE WIND DIAGRAMS
OFF SOUTH BETHANY, DEL.
EAST-NORTHEAST TRAVERSE
(Ux IS COMPONENT ALONG
THE TRAVERSE)
1200 Z 7 MAR
1800 Z 7 MAR
0600 Z 7 MAR
0001 Z 8 MAR
0600 Z 8 MAR
0001 Z 7 MAR
1200 Z 7 MAR
1800 Z 6 MAR
0600 Z 6 MAR
0001 Z 6 MAR
1800 Z 5 MAR
Ux KNOTS
0
10
20
30
40
50
60
0
100
200
300
400
500
600
700
800
900
DISTANCE IN NAUTICAL MILES FROM COAST

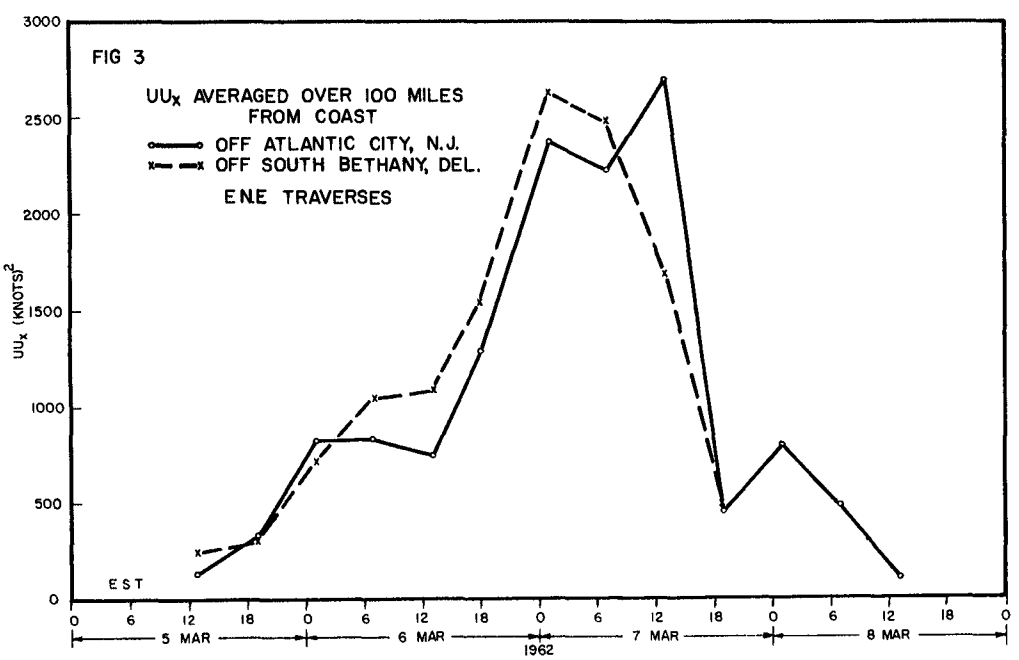
FIG 3
UUx AVERAGED OVER 100 MILES
FROM COAST
OFF ATLANTIC CITY, N.J.
OFF SOUTH BETHANY, DEL.
ENE TRAVERSES
UUx (KNOTS)2
0
500
1000
1500
2000
2500
3000
EST
0
6
12
18
0
6
12
18
0
6
12
18
0
6
12
18
0
5 MAR
6 MAR
7 MAR
8 MAR
1962

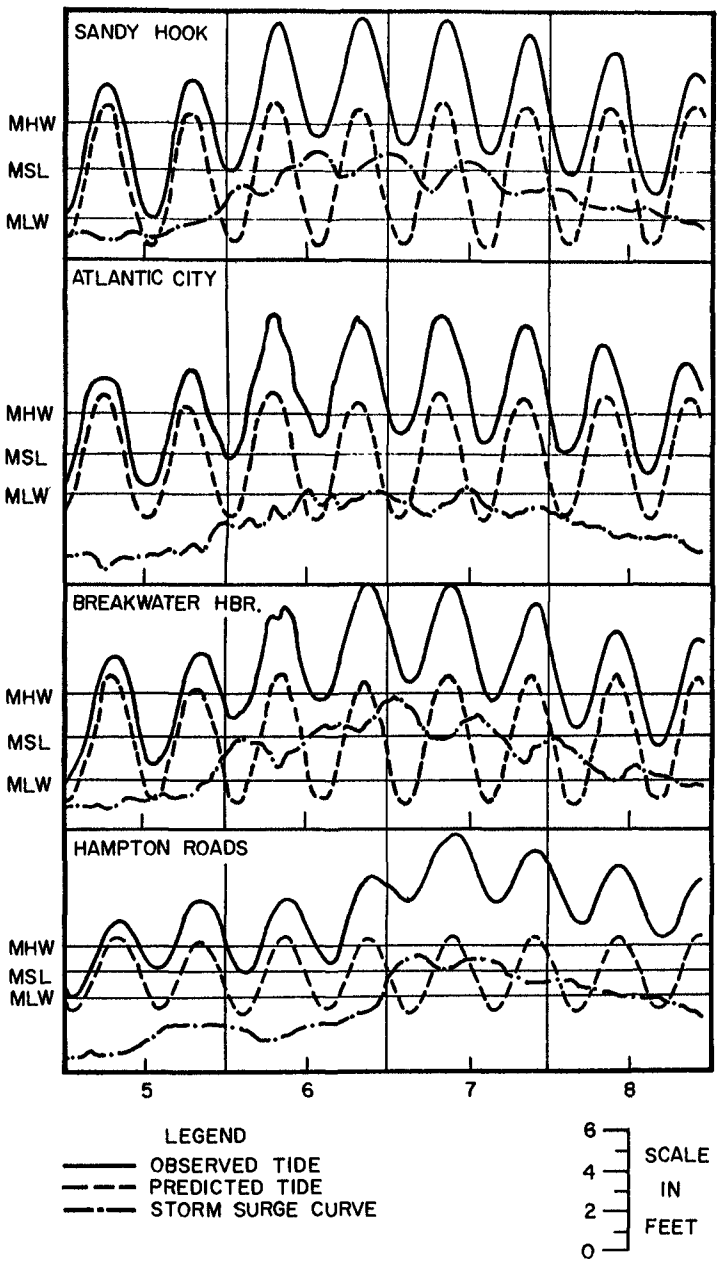

FIG. 4 OBSERVED TIDE, PREDICTED TIDE AND STORM SURGE, FOR SELECTED STATIONS MARCH 5-8, 1962. (AFTER HARRIS, 1963)

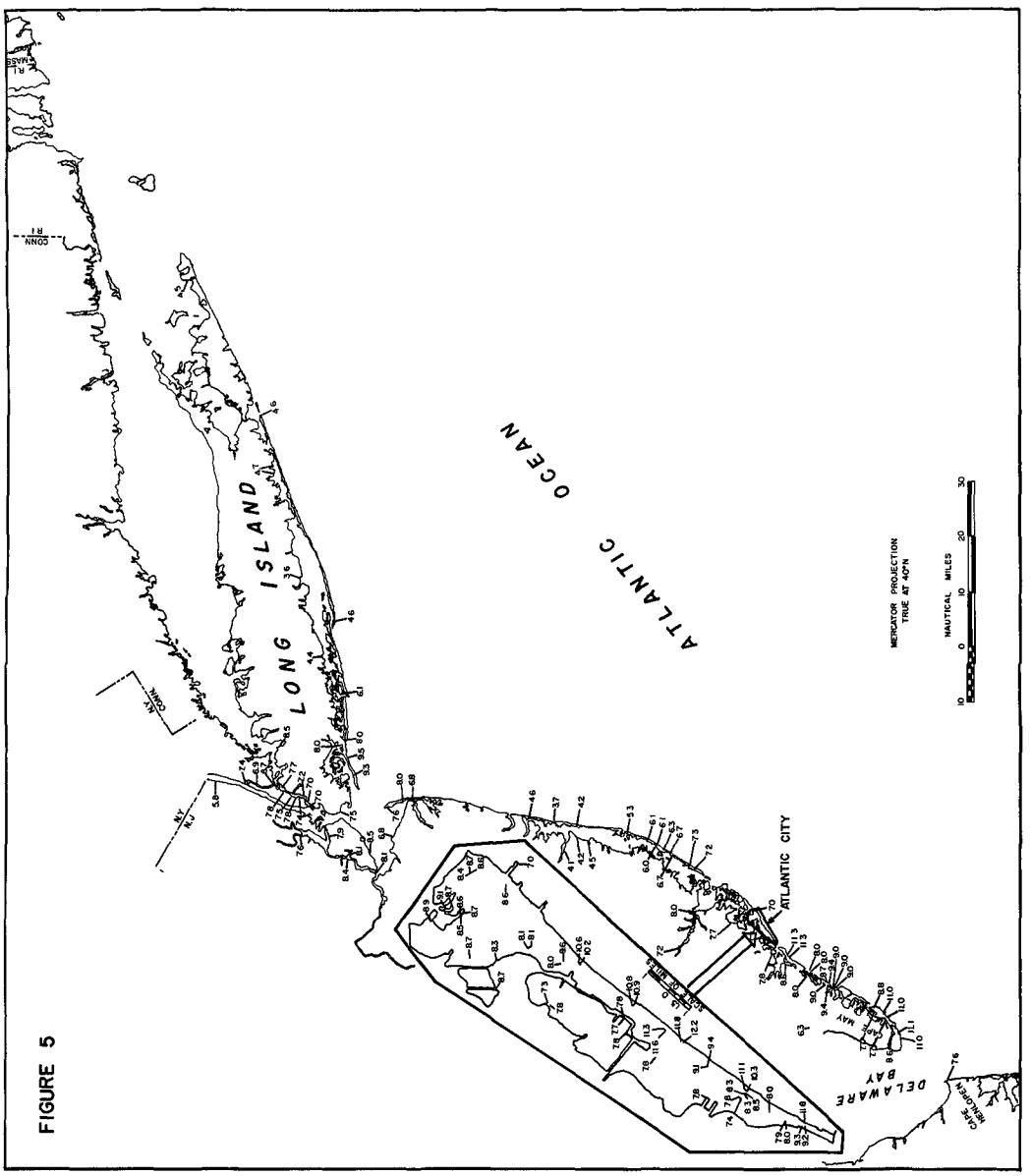

FIGURE 5

HIGH WATER MARKS FOR THE EARLY MARCH STORM, 1962 (REDRAFTED FROM HARRIS, 1963)

7. The U. S. Coast and Geodetic Survey hydrographic charts for the year 1954 were used to obtain the bottom profiles from deep water, over the continental shelf, through the surf zone, to the coastline. Figure 6 shows typical bottom profiles for various locations off the east coast of the United States, representative of the year 1954. Other sources of information were consulted in order to estimate the more recent changes near the coastline.

8. The U. S. Army Engineer District "Beach Erosion Control Survey Report, Kitts Hummock to Fenwick Island, Delaware," was used to obtain details of beach and dune profiles and soil conditions for the Delaware coast as of the year 1954. This report was also of use to hindcast the average change in bottom contours and the coastline after 1954 based on the corresponding changes prior to 1954. Some of this information also appears in House Document 216, 85th Congress, 1958. Figure 7 represents typical average dune and beach profiles prior to and after the 1962 storm.

9. The U. S. Army Engineer District post-storm survey and flood reports were used to examine the extent of flooding, beach and dune erosion, and the general extent of damage. This included three reports: "Post-Flood Report, Coastal Storm of 6-7 March 1962, Southern New Jersey and Delaware," prepared by the U. S. Army Engineer District, Philadelphia, December 1962; "The March 1962 Storm along the Coast of Maryland," prepared by the U. S. Army Enginee District, Baltimore, November 1962; "The March 1962 Storm on the Coast of Virginia," prepared by the U. S. Army Engineer District, Norfolk, August 1962.

10. Hearings before the Sub-Committee on Oceanography, 87th Congress, April 4, 1962, on "Improvement of Storm Forecasting Procedures," were examined for certain information and various degrees of opinions pertaining to the 6-8 March 1962 east coast storm.

11. The U. S. Army Engineer District Report, "Revised Report on Cooperative Beach Erosion Control Study for Atlantic City, N. J.," June 1962 (unpublished), was used to obtain the beach profiles at Ventnor, N. J. before and after the storm. Figure 8 is based on this report.

12. Estimates of beach and dune erosion along the Delaware coast were obtained from the Beach Erosion Board. Typical of this information is Figure 9.

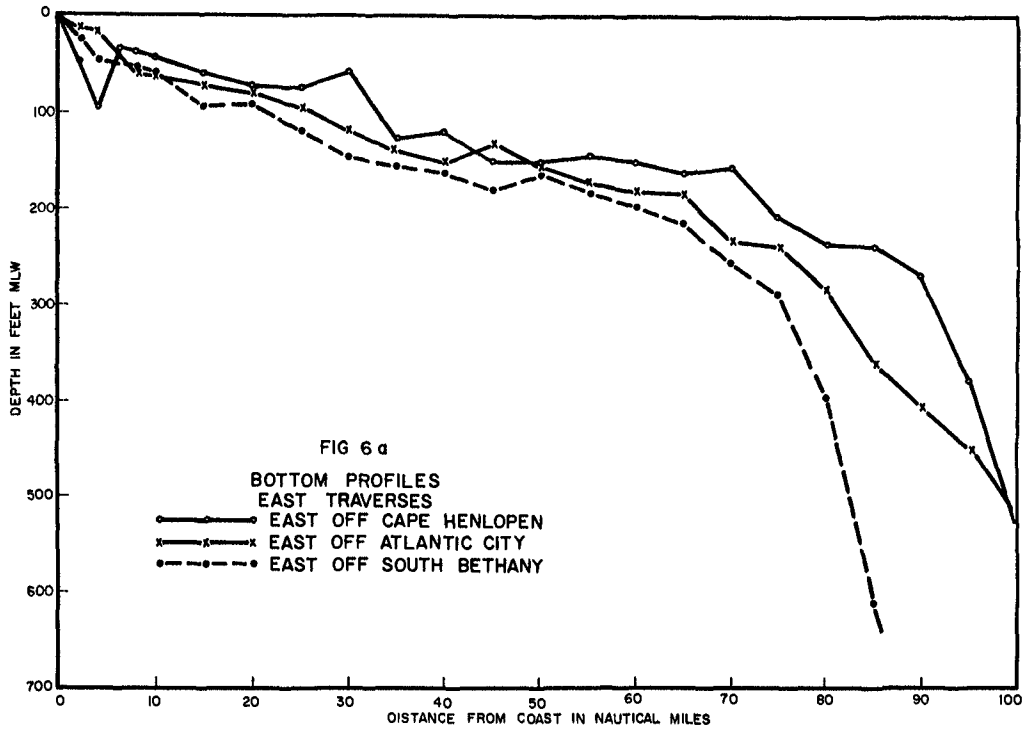
DEPTH IN FEET MLW
0
100
200
300
400
500
600
700
0
10
20
30
40
50
60
70
80
90
100
DISTANCE FROM COAST IN NAUTICAL MILES
FIG 6 a
BOTTOM PROFILES
EAST TRAVERSES
EAST OFF CAPE HENLOPEN
EAST OFF ATLANTIC CITY
EAST OFF SOUTH BETHANY

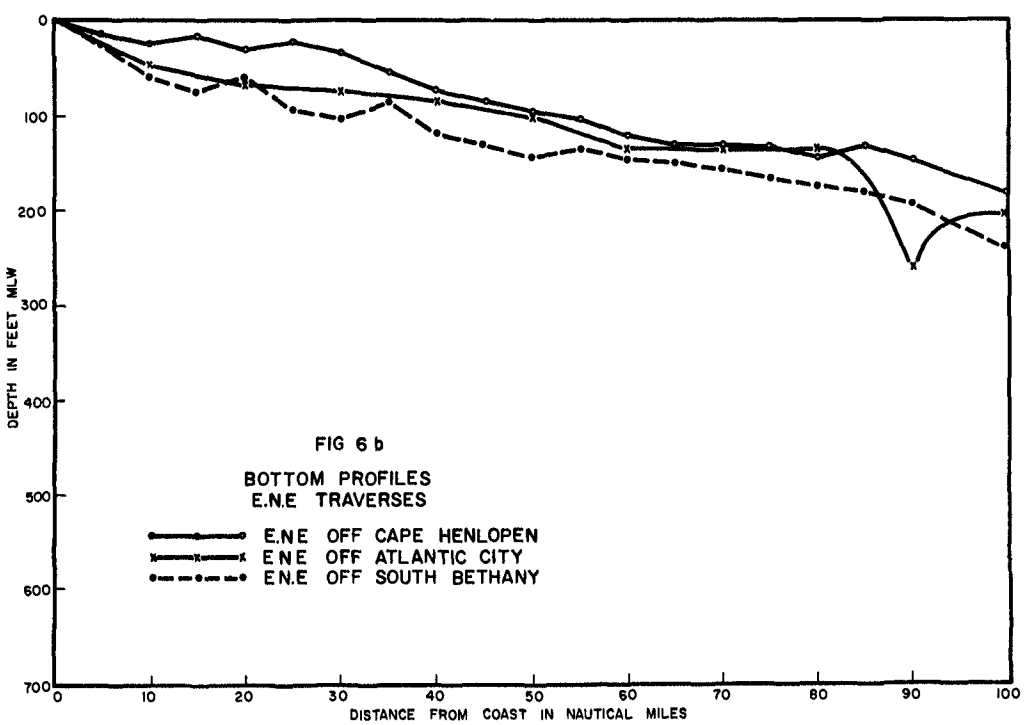
DEPTH IN FEET MLW
0
100
200
300
400
500
600
700
0
10
20
30
40
50
60
70
80
90
100
DISTANCE FROM COAST IN NAUTICAL MILES
FIG 6 b
BOTTOM PROFILES
E.N.E TRAVERSES
E.N.E OFF CAPE HENLOPEN
E N E OFF ATLANTIC CITY
E.N.E OFF SOUTH BETHANY

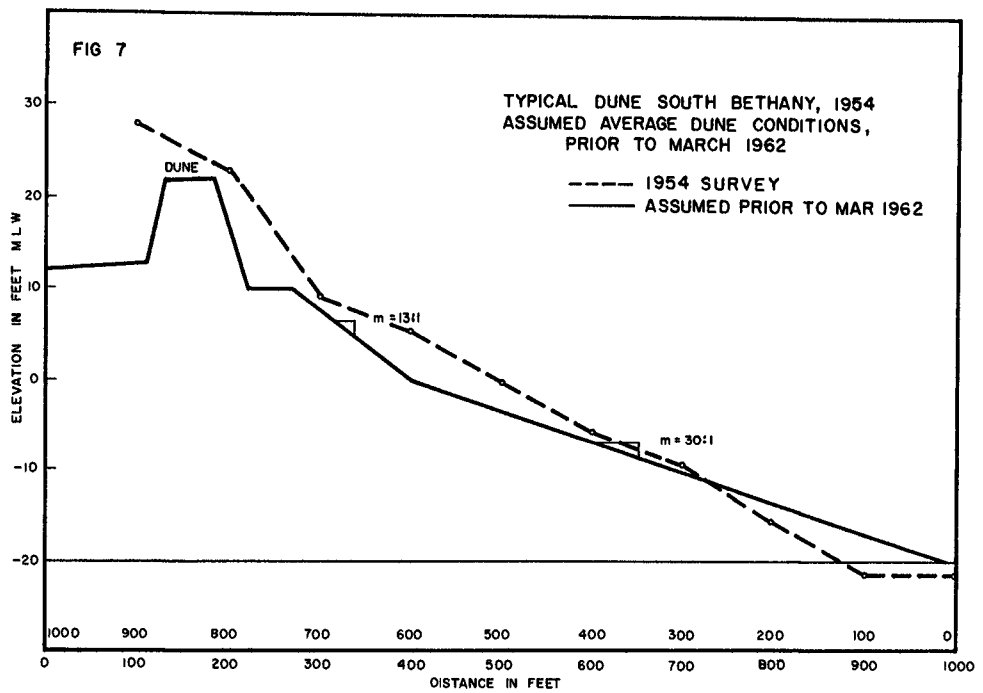

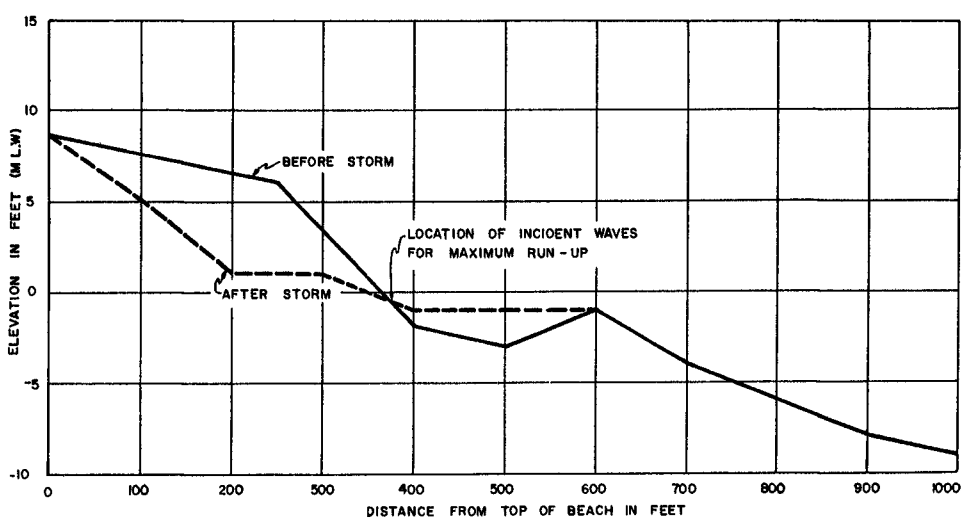

FIGURE 8 BEACH PROFILES AT VENTNOR, BEFORE AND AFTER STORM OF MARCH 1962

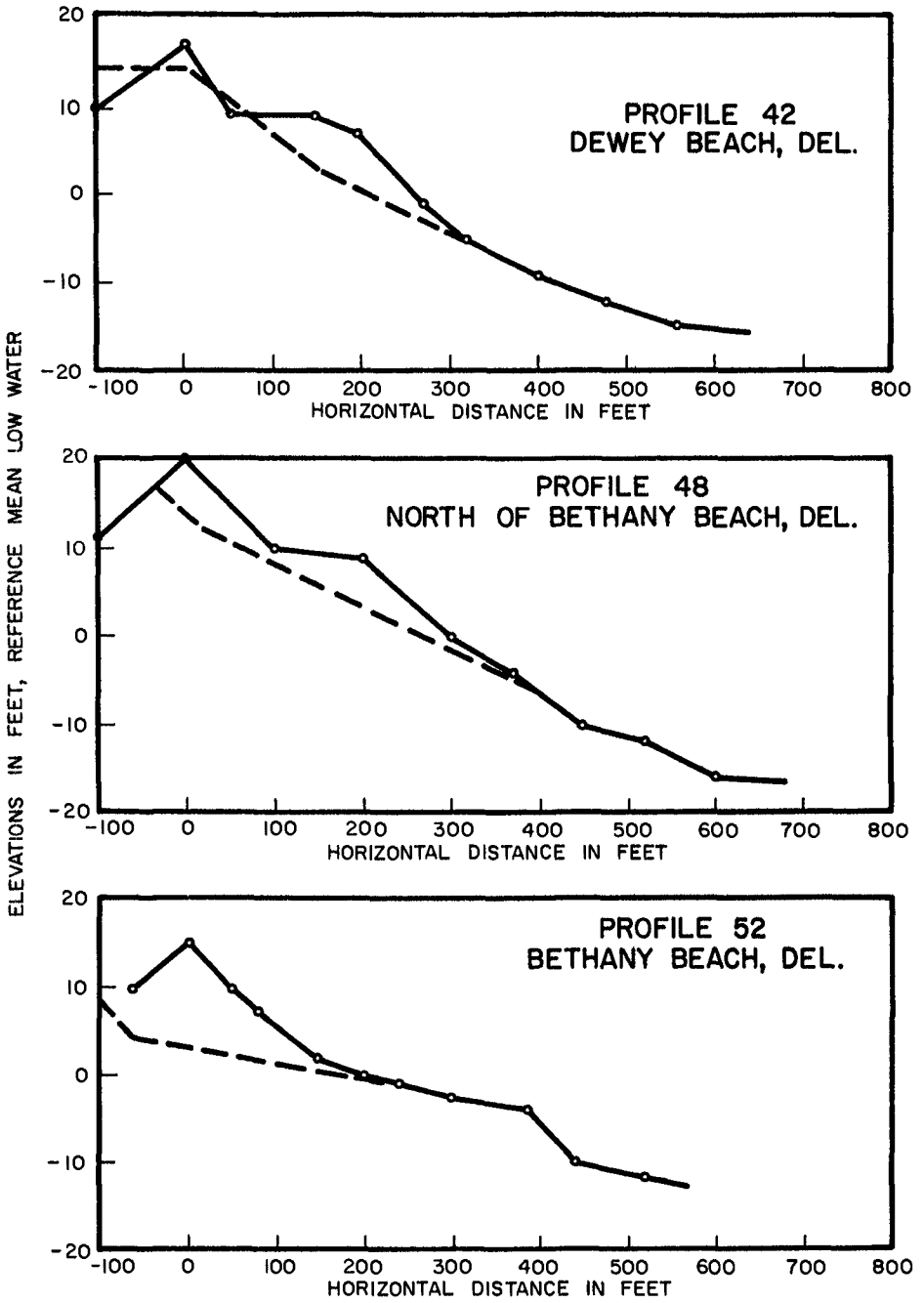

FIG. 9 TYPICAL BEACH PROFILES FOR DEL. COAST (BEFORE AND AFTER STORM)

13. Various U. S. Weather Bureau publications (given in the references at the end of this paper) were used for supplemental data.

14. Numerous U. S. Coast and Geodetic Survey aerial photographs of the coastline before and after the storm were used to estimate the extent of flooding and erosion. Figure 10 shows typical photgraphs taken before and after the storm.

15. Numerous storm reports, including many photographs published by various newspapers, were used with great interest. References to this material are given at the end of this paper.

16. Supplemental data and text material, given in the references, were used to support the interpretations and conclusions of the study. For example, an analysis of winds for Hurricane Carla, 1961, was made in order to verify the relationships of gust speed to wind speed for high winds for coastal and inland stations. This information aids in the conclusion for various relationships established for the east coast storm, and is consistent with the relationships found in literature for other storms.

17. Data on model tests by Ning Chien, et. al. (1951) were investigated to determine the behavior of wind over various shaped objects. Also of particular interest were the results of a very elaborate field experiment by Landsberg (1942) along the west coast of Lake Michigan, which included relationships for the vertical distribution of winds over the beach and over a typical Michigan sand dune.

AVAILABLE THEORY AND PROCEDURES

When making wind, wave, tide and wave run-up hindcasts, it is necessary to use selected theories and procedures, coupled with any reliable available data, and the hindcast procedures may be altered accordingly. In some respects the formulations may be considered more or less semi-theoretical or semi-empirical. Regardless of the terminology, the theory and procedures used must be of sound engineering judgment. For this particular study the following determinations were included.

1. Over-water wind speeds were computed from the pressure gradients obtained from the U. S. Weather Bureau maps, using the procedures outlined in Beach Erosion Board Technical Report No. 4 (BEB T. R. 4), "Shore Protection Planning and Design" (revised ed., 1961).

AERIAL PHOTOGRAPH - 1962

FIGURE 10A DUNES - 1954

1 2 3 3 2

BEFORE AFTER

FIGURE 10 B SOUTH BETHANY, DELAWARE

Winds were also estimated by averaging the observed wind speeds which were entered on the weather charts. Both the computed winds and the winds averaged from the observations represent a 10 to 15 minute average sustained wind at 10 meters above the water surface, such as those defined by the U. S. Weather Bureau (Goodyear, 1963, for example). Figure 11 shows typical 1-minute average winds based on the wind data from weather maps for Ventnor, N.J. The mean of 1-minute average peak wind speeds is equal to about 1.15 to 1.25 times the 10-minute average. The variability of several-minute average to computed 10- to 15-minute average is demonstrated in figure 12, reproduced from Goodyear (1963).

2. The total tides -- storm surge plus normal predicted astronomical tide -- were calculated according to the procedures given by Bretschneider (1958) in "Engineering Aspects of Hurricane Surge." In addition, wave set-up on the beach was estimated according to the material and data presented by Saville (1961) and Longuet-Higgins (1963). The important consideration is the instructions on calibration, taking into account the available recorded tide data. Figure 13 shows the results for storm tide hindcasts off the New Jersey and Delaware coasts. Figure 14 accounts for wave set-up on the beach based on wave height hindcasts obtained later in this paper.

3. Deep water waves were hindcast according to the methods proposed by Bretschneider (1958). The significant waves were hindcast and compared with the available data from ship reports, and were also compared with the wave contours presented by Cooperman and Rosendall (1962). Some of this information is given by O'Brien and Johnson (1963). In addition, deep water wave spectra were hindcast, but were used only for calculations to determine the wave spectra in shallow water. Figure 15 and 16 are the results of deep water wave hindcasts for Ventnor City, N.J. and South Bethany, Delaware, respectively.

4. Wave hindcasts were made for the continental shelf and the surf zone, taking into account the combined effects of deep water waves propagated shoreward, wave refraction, wave energy loss due to bottom friction, and the regeneration of waves by wind in shallow water. The procedures for modification of wave spectra over the continental shelf, given by Bretschneider (1962), have been extended to take into account the wind regeneration of wind waves in shallow water. Hindcasts over the continental shelf were compared with the available data from ship reports. Figure 17 shows the results of wave hindcasts over the

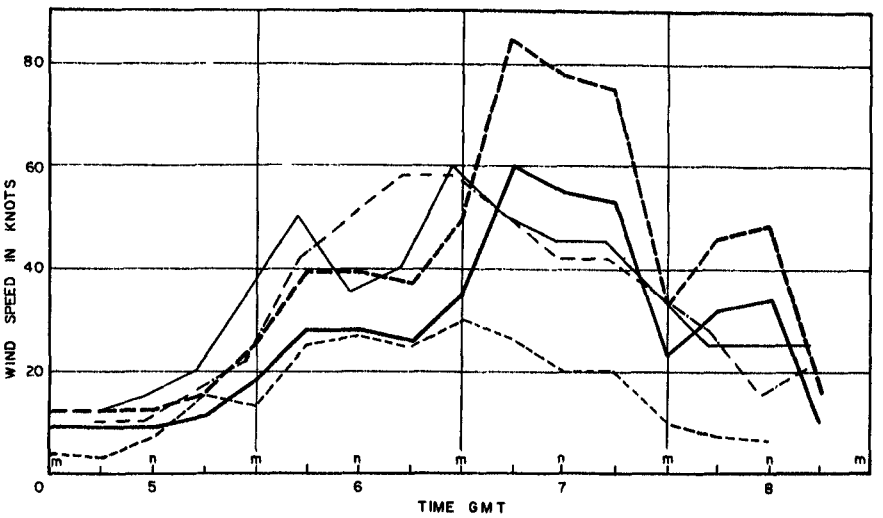

FIGURE II WINDS AND GUSTS DURING STORM, MARCH 1962

VENTNOR CITY, SYNOPTIC CHARTS
VENTNOR CITY, GUSTS (CALCULATEO)
BARNEGAT LIGHTSHIP
FIVE FATHOM LIGHTSHIP
ATLANTIC CITY, NATIONAL AVIATION EXPERIMENTAL CENTER

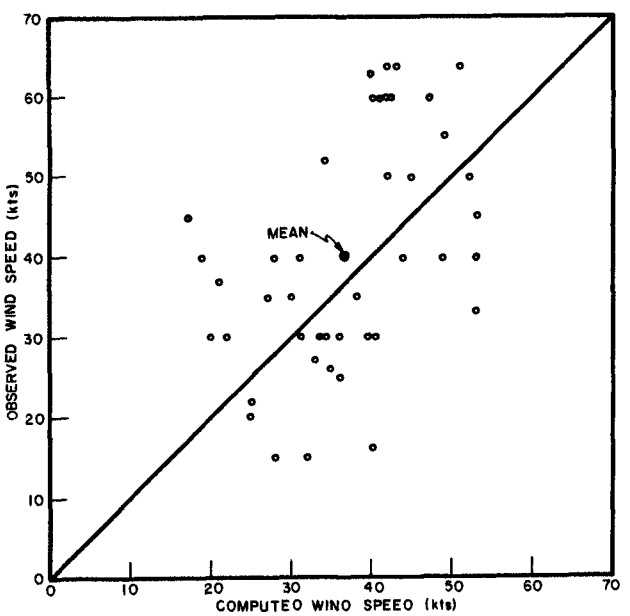

FIG.12- COMPUTED vs OBSERVED SURFACE WIND SPEED FOR 43 RANDOMLY SELECTED POINTS (AFTER GOODYEAR, 1963)

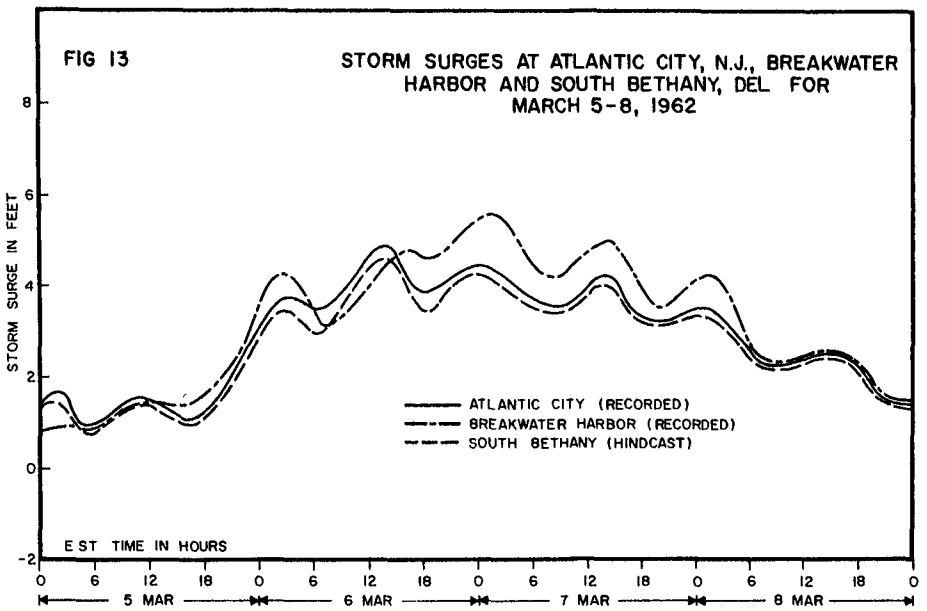
FIG 13
STORM SURGES AT ATLANTIC CITY, N.J., BREAKWATER HARBOR AND SOUTH BETHANY, DEL FOR MARCH 5-8, 1962
STORM SURGE IN FEET
8
6
4
2
0
-2
ATLANTIC CITY (RECORDED)
BREAKWATER HARBOR (RECORDED)
SOUTH BETHANY (HINDCAST)
EST TIME IN HOURS
0 6 12 18 0 6 12 18 0 6 12 18 0 6 12 18 0
5 MAR
6 MAR
7 MAR
8 MAR

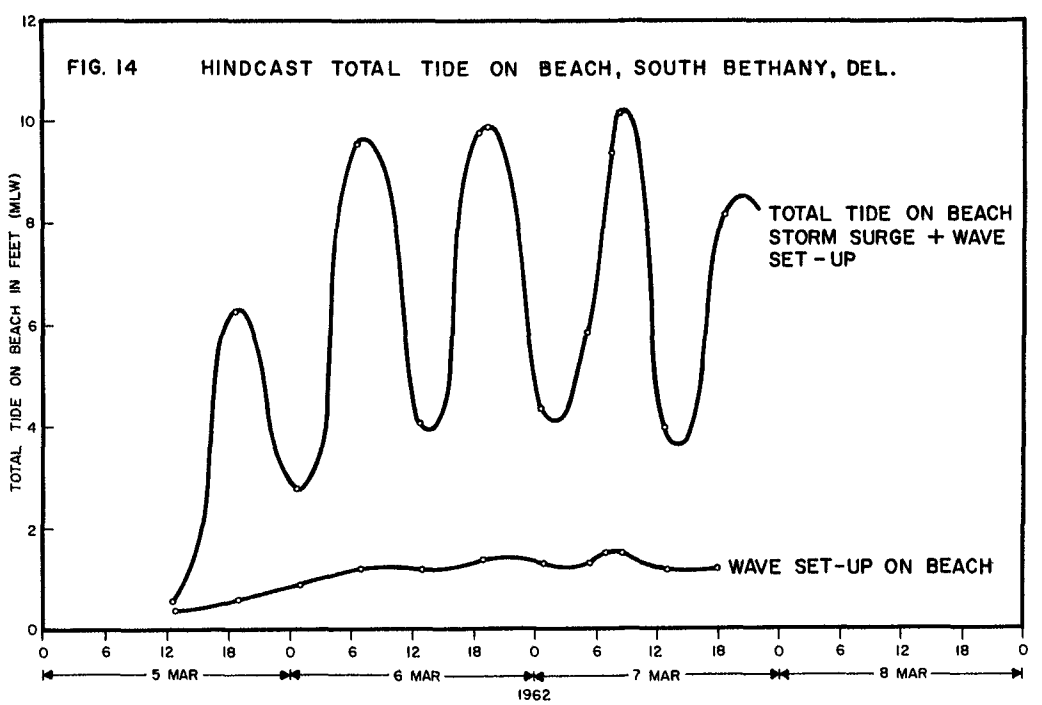
FIG. 14 HINDCAST TOTAL TIDE ON BEACH, SOUTH BETHANY, DEL.
TOTAL TIDE ON BEACH IN FEET (MLW)
12
10
8
6
4
2
0
TOTAL TIDE ON BEACH
STORM SURGE + WAVE
SET - UP
WAVE SET-UP ON BEACH
0 6 12 18 0 6 12 18 0 6 12 18 0 6 12 18 0
5 MAR
6 MAR
7 MAR
8 MAR
1962

FIG. 15 DEEP WATER WAVE HINDCASTS E.N.E. OFF NEW JERSEY COAST

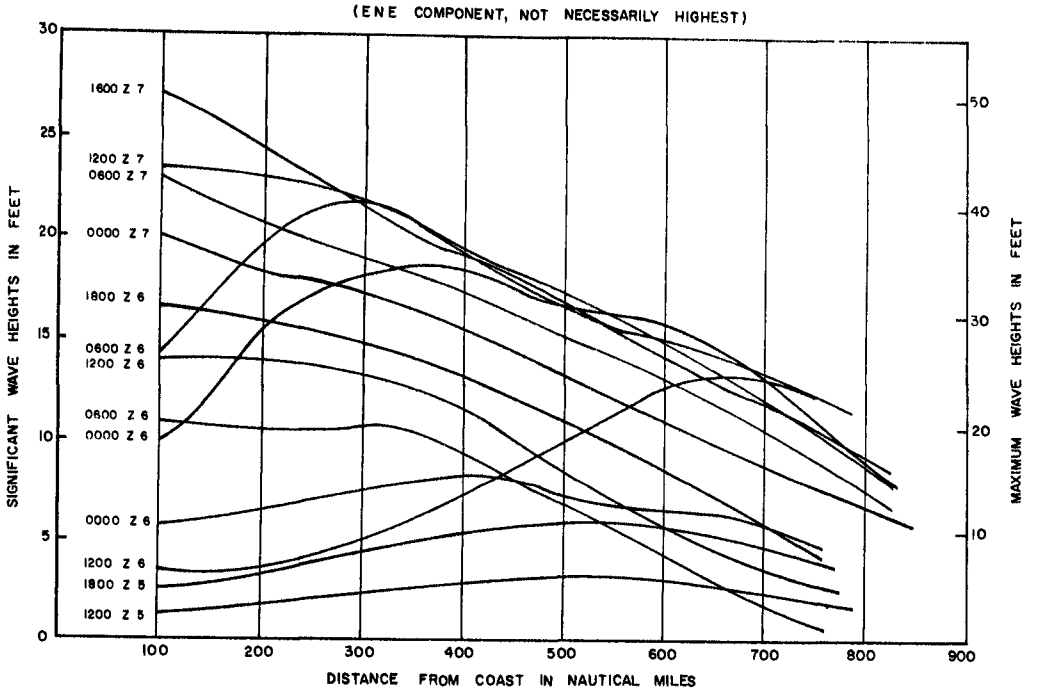

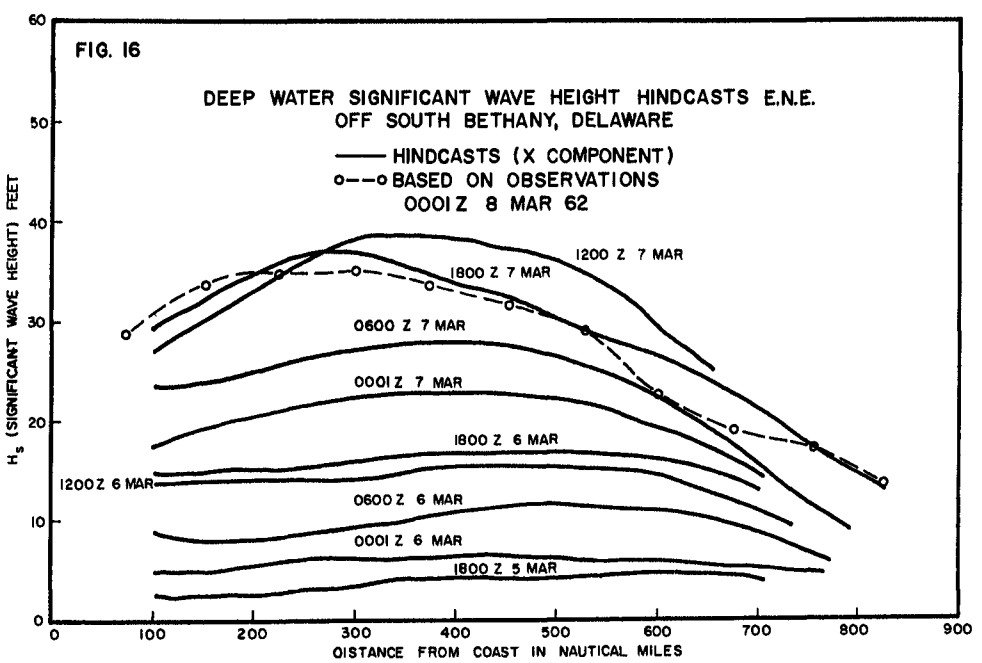

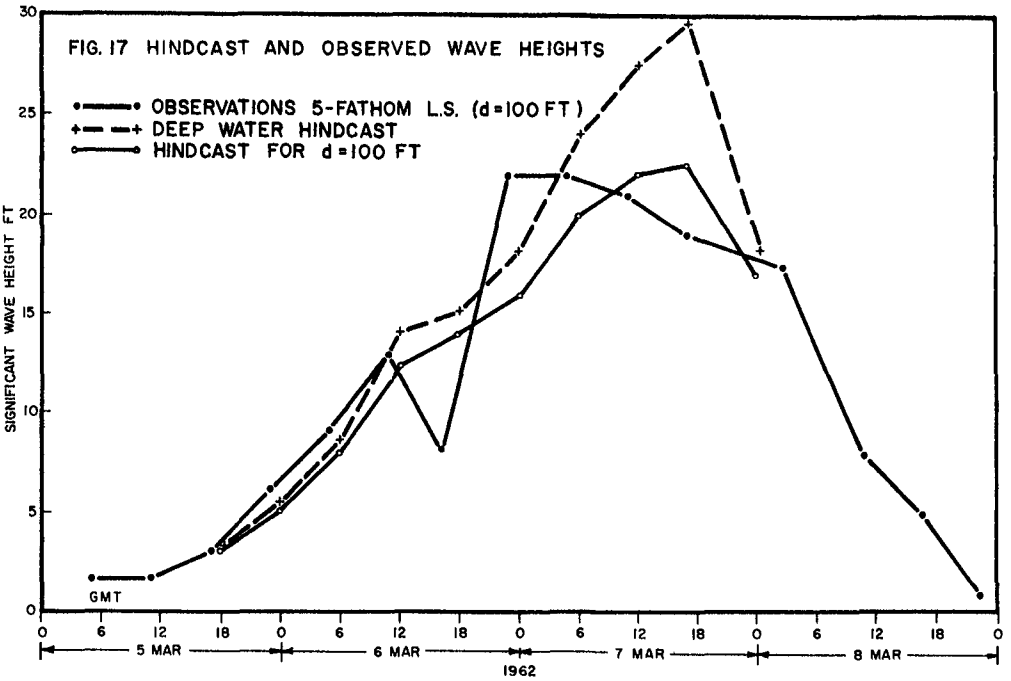
FIG. 17 HINDCAST AND OBSERVED WAVE HEIGHTS
OBSERVATIONS 5-FATHOM L.S. (d=100 FT)
DEEP WATER HINDCAST
HINDCAST FOR d=100 FT
SIGNIFICANT WAVE HEIGHT FT
GMT
5 MAR
6 MAR
7 MAR
8 MAR
1962

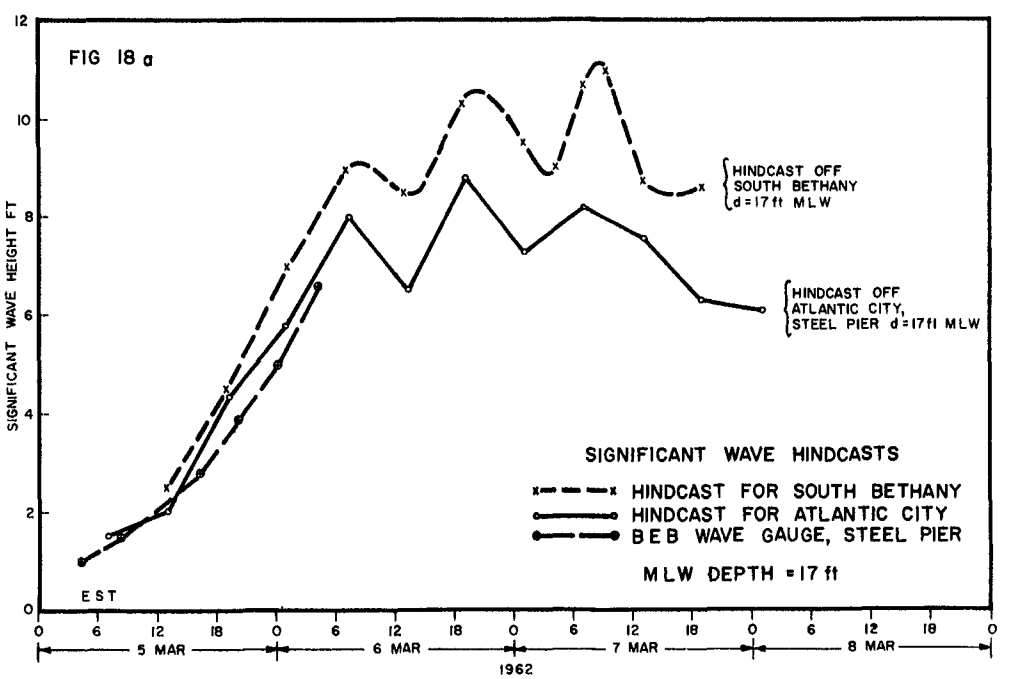
FIG 18 a
HINDCAST OFF SOUTH BETHANY d=17 ft MLW
HINDCAST OFF ATLANTIC CITY, STEEL PIER d=17 ft MLW
SIGNIFICANT WAVE HINDCASTS
HINDCAST FOR SOUTH BETHANY
HINDCAST FOR ATLANTIC CITY
BEB WAVE GAUGE, STEEL PIER
MLW DEPTH = 17 ft
SIGNIFICANT WAVE HEIGHT FT
EST
5 MAR
6 MAR
7 MAR
8 MAR
1962

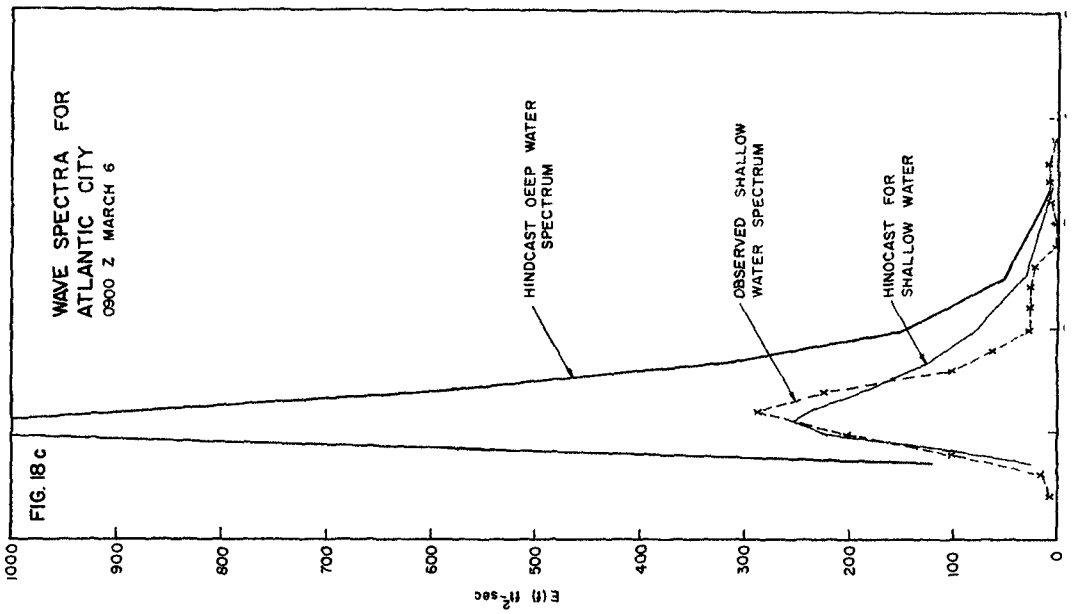
FIG. 18c
WAVE SPECTRA FOR ATLANTIC CITY
0900 Z MARCH 6
HINDCAST OEEP WATER SPECTRUM
OBSERVED SHALLOW WATER SPECTRUM
HINOCAST FOR SHALLOW WATER
E (f) ft²-sec
1000
900
800
700
600
500
400
300
200
100
0

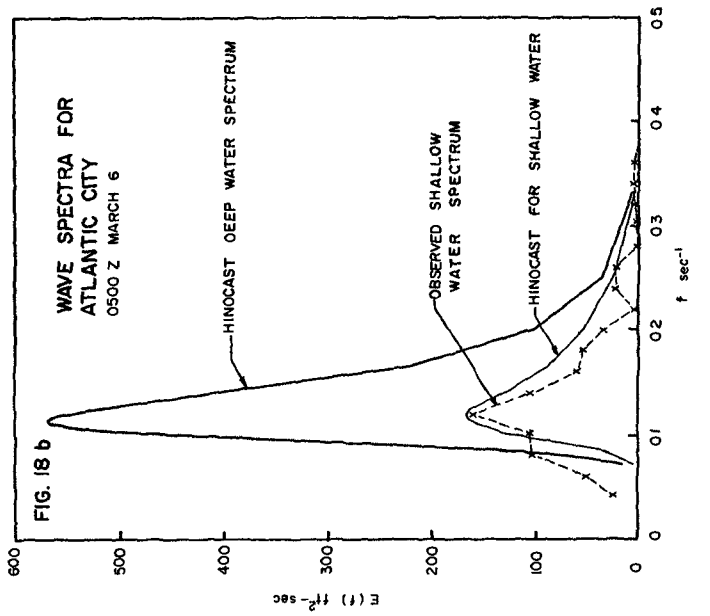
FIG. 18b
WAVE SPECTRA FOR ATLANTIC CITY
0500 Z MARCH 6
HINOCAST OEEP WATER SPECTRUM
OBSERVED SHALLOW WATER SPECTRUM
HINOCAST FOR SHALLOW WATER
E (f) ft²-sec
600
500
400
300
200
100
0
0
01
02
03
04
05
f sec⁻¹

continental shelf compared with the data reported by the Five Fathom Lightship in 100 feet of water depth off the coast of Delaware. The hindcasts in shallow water were compared with the data recorded at Atlantic City Steel Pier. Figure 18 shows the results of wave hindcasts and recorded data in shallow water at Atlantic City Steel Pier, mean low water depth of 17 feet. The periodic increase in wave height is an indication of change in total water depth as a function of tide and not as a change in storm intensity. Figure 18 also shows the results of hindcasts of the wave spectrum for several periods of time. The recorded wave data for Atlantic City were also used to calculate the wave spectra according to the simplified method proposed by Bretschneider (1961).

5. The breaking wave zone was determined for the water depth and individual breaking wave heights according to the breaking wave index criteria as given by Bretschneider (1958). Because a spectrum of wave heights and periods exists, the breaking waves occur over a broad zone instead of a single line of breakers. These conditions should result in a spectrum of breaking depths. In the present study the first most probable maximum wave breaks first at a far distance from the coast, followed by all other waves breaking shoreward from this first point of breaking. Eventually the smallest waves break on the beach. Because the total tide is a function of time, depending upon the twice-daily normal predicted tides, the breaking wave zone moves seaward and shoreward, alternating with time. Figure 19 shows a typical example of how the point of breaking moves in and out from the coastline as a function of time.

6. The wave run-up calculations were made according to the procedures of Saville (1958), taking into account the composite slope techniques. For these calculations average conditions (see figure 7) were assumed to consist of a 20-foot high dune above mean low water, the slope of the dune as 1-foot horizontal and 3-foot drop to the berm at 10 feet above mean low water. The berm was 50 feet wide, followed by a beach slope of 1 foot on 13 to the coastline, and a bottom slope of 1 foot on 30 to the minus 20-foot contour, and a gradual slope to the minus 100-foot contour. Figure 20 shows the results of wave run-up calculations for the typical composite slope given in figure 7.

Waves which arrived at the 20-foot mean low water contour result in essentially the same maximum wave run-up as those waves which break at the coastline during high tides. The spectrum of wave run-up was determined according go the Rayleigh distribution, suggested by Saville (1962). The most probable maximum wave run-up

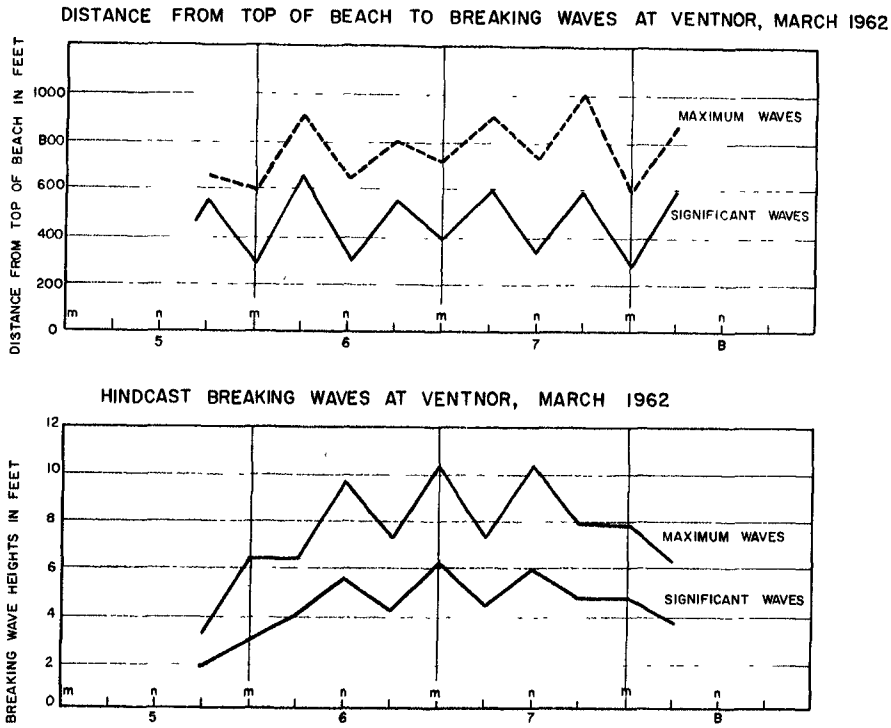

FIG 19 HINDCASTS FOR BREAKING WAVE HEIGHTS AND LOCATIONS

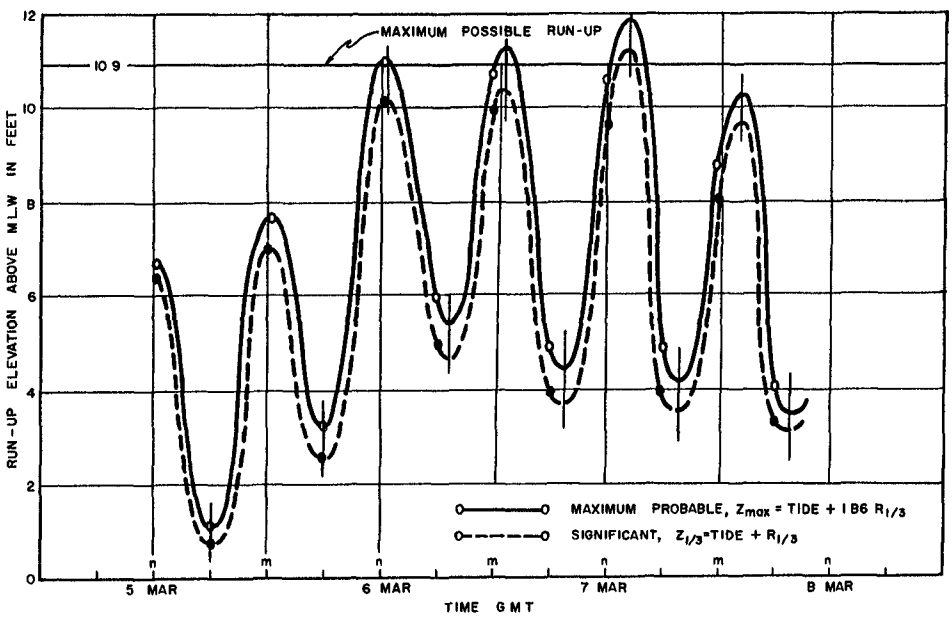

FIGURE 20a WAVE RUN-UP ON THE BEACH AT VENTNOR, NJ

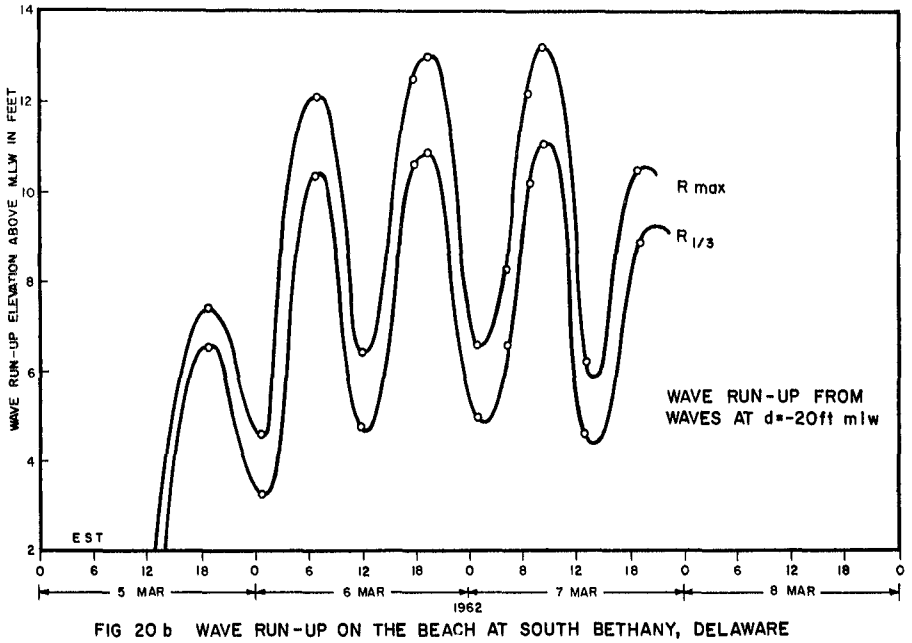

FIG 20 b WAVE RUN-UP ON THE BEACH AT SOUTH BETHANY, DELAWARE

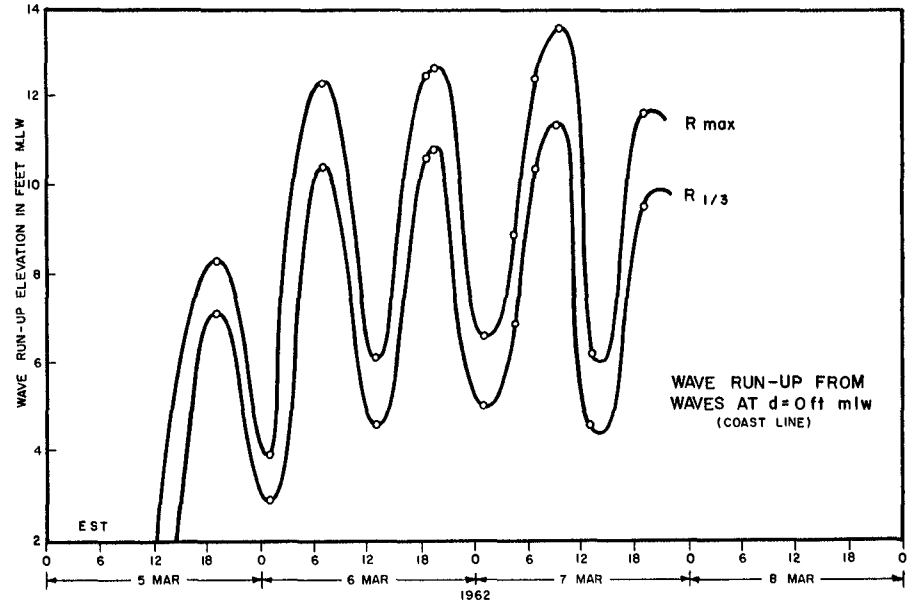

FIG 20 c WAVE RUN-UP ON THE BEACH AT SOUTH BETHANY, DELAWARE

was compared with the high water marks reported by Harris (1963) and also given in the U. S. Army Engineer District Post-Storm Survey Reports. Calculations also show that during the final phases of the storm the maximum probable wave run-up was very close to the maximum possible wave run-up governed only by the maximum possible wave height as a function of total water depth.

7. The beach, berm, and dune activity can be defined in terms of the relative wave energy reaching above 10 feet mean low water elevation. Local observers have stated that the erosion of the dune was a gradual process. No previous theory or available data exist in regard to the rate of dune erosion. It might be postulated that the rate of erosion for an average dune can be related to the relative wave energy reaching above 10 feet mean low water. The exact nature of erosion of a factual dune will depend upon deviations from the average dune, such as height, width, type and amount of grass cover, etc. The U. S. Army Engineers Post-Storm Survey Reports state that in some areas along the east coast the dunes were moved back 20 to 40 feet or more along the Virginia coast. Wave and wave run-up calculations were essentially the same for New Jersey, Delaware and Virginia.

One method for estimating the rate of dune erosion is to assume as a first approximation that the cumulative erosion is proportional to the cumulative wave energy reaching above 10 feet mean low water. Probably more erosion takes place during a falling tide when the erosion forces are aided by the hydrostatic pressure directed outward from the dune and less erosion during a rising tide when the erosion forces are opposed by the hydrostatic pressure directed into the dune. For this particular study it appears that the average dune corresponding to figure 7 has a width of 40 feet, corresponding to 100 percent wave energy erosion. Other considerations remaining the same, wider dunes would not be breached, whereas narrower dunes would have been destroyed prior to the end of the last high tide. Figure 21 shows histograms of wave energy (arbitrary scale in feet squared) and percent cumulative energy as a function of time for waves reaching above 10 feet mean low water.

8. Winds, which were hindcast over water at the coastline, were adjusted to off-water winds over the beach. The appropriate reduction factors can be estimated based on the data obtained by the U. S. Army Engineers from the Lake Okeechobee, Florida, experiments and summarized by Meyers (1954) in the U. S. Weather Bureau Hydrometeorological Report No. 32. The reduction factor varies between

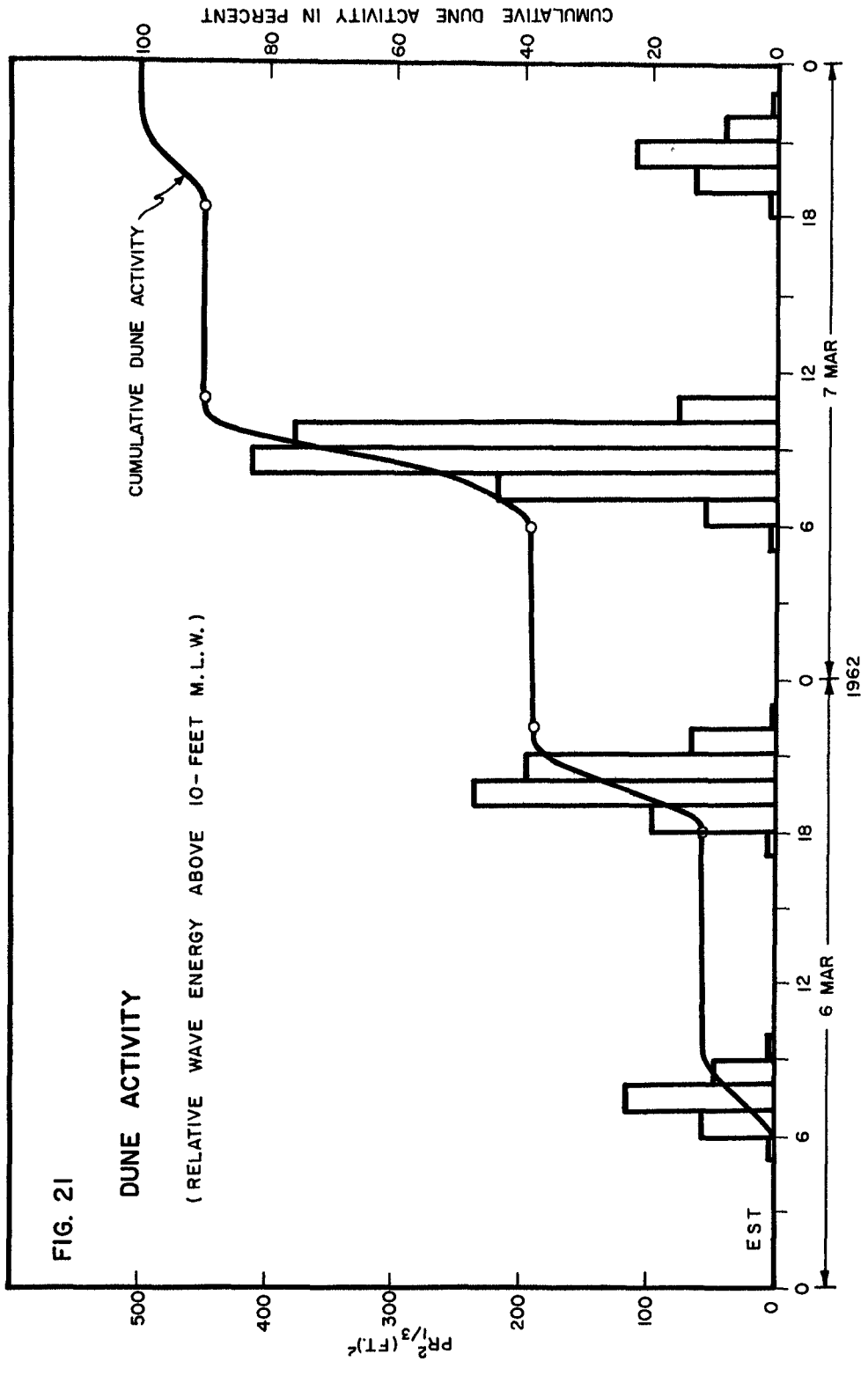
CUMULATIVE DUNE ACTIVITY IN PERCENT
100
80
60
40
20
0
CUMULATIVE DUNE ACTIVITY
DUNE ACTIVITY
(RELATIVE WAVE ENERGY ABOVE 10-FEET M.L.W.)
$PR^2_{1/3}$ (FT)^4
500
400
300
200
100
0
EST
0
6
12
18
0
6 MAR
6
12
18
0
7 MAR
1962

FIG. 21

1.0 and 0.9, depending upon the distance from the coast. In a U. S. Weather Bureau report Graham and Nunn (1959) recommend using a gradual reduction factor from 1.0 to 0.9 over the first two miles from the coast. Ten-minute average wind speeds over the beach of South Bethany, Delaware, were calculated from the over-water wind speeds using a reduction factor of 0.9. The 1-minute average peak winds are 1.15 times the 1-minute average.

9. The vertical distribution of wind speed above the water and above the beach were estimated in accordance with the 1/7th power law; that is:

$$U_Z = U_{10} (Z/10)^{1/7} \qquad (1)$$

where U_Z is the wind speed at elevation Z meters above the surface, and U_{10} is the wind speed at 10 meters above the surface. The above formula seems applicable above wet sandy beaches as well as above water surfaces. For example, the data by Sheppard (1958) follows very nearly the 1/7th power law for velocity distribution over water, and the experiments of Landsberg (1942) follow very nearly the 1/7th power law for velocity distribution over a Michigan beach.

10. Wind gust speeds were investigated using the U. S. Weather Bureau data for the East Coast Storm and for Hurricane Carla, 1961. Except for low wind speeds, linear relationships were found between gust speed and wind speed. These results were also in agreement with other data given in the literature (Huss, 1946, for example). Numerous results on gust factors are also summarized in the U. S. Air Force Handbook of Geophysics (1961).

A summary of gust factors is given in Table 1. In this table U_{max} and G_{max} respectively are the maximum values during the storm of the 1-minute average and the peak gust, which do not necessarily occur during the same 15-minute period of time. $\overline{U}$ and $\overline{G}$ are respectively the average of the 1-minute average sustained wind and the average of the corresponding peak gusts.

Figure 22 shows typical results of gust determinations for the east coast storm and figure 25 is based on hurricane Carla. The analysis was made by averaging gust speeds for 3-knot intervals and the corresponding averages of the 1-minute average sustained wind

TABLE 1

SUMMARY OF GUST FACTORS

EAST COAST STORM, MARCH 6-8, 1962

Station	U_{max} Knots	G_{max} Knots	G_{max}/U_{max} U_{max}	$\overline{U}$ Knots	$\overline{G}$ Knots	$\overline{G}/\overline{U}$
Dover, Del.	35	49	1.40	18.5	27.6	1.49
Salisbury, Md.	35	47	1.34	20.4	31.7	1.55
Atlantic City, N. J.	38	49	1.29	25.0	36.3	1.45
Nantucket, Mass.	44	60	1.37	29.8	41.9	1.41
AVERAGE			1.35			1.47

HURRICANE CARLA, 1961

Station	U_{max} Knots	G_{max} Knots	G_{max}/U_{max} U_{max}	$\overline{U}$ Knots	$\overline{G}$ Knots	$\overline{G}/\overline{U}$
Port Arthur, Tex.	34	47	1.38	25.5	34.8	1.37
Galveston, Tex.	52	75	1.44	36.5	50.6	1.38
Victoria, Tex.	87	130	1.50	37.2	49.1	1.32
Houston, Tex.	45	67	1.49	25.1	37.3	1.48
Corpus Christi, Tex.	55	75	1.36	31.5	44.0	1.40
Freeport, Tex.	73	100	1.37	48.2	66.9	1.39
AVERAGE			1.42			1.41

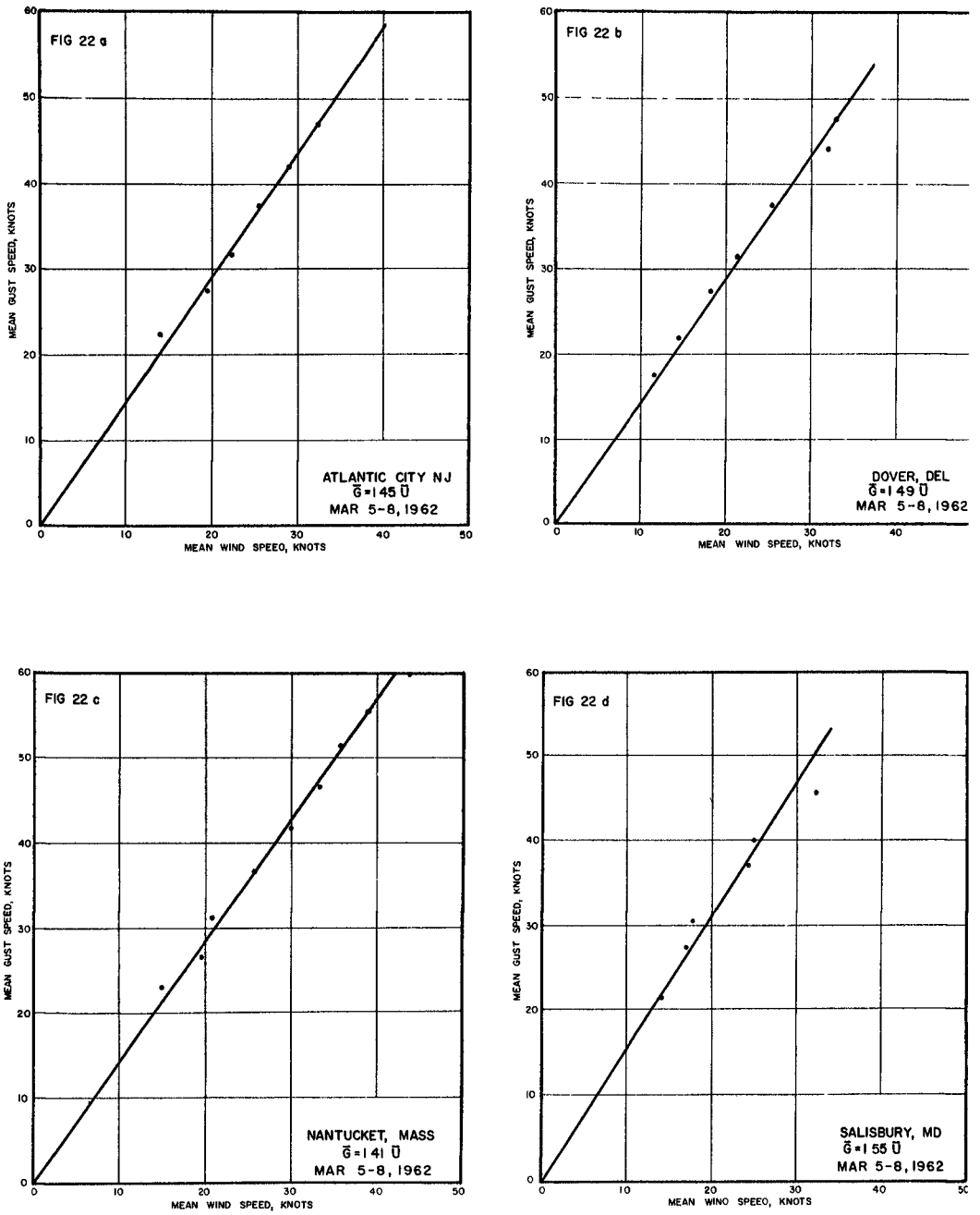

FIG. 22. --AVG. GUST SPEEDS VS. AVG. 1-MIN AVG. WIND SPEEDS FOR EAST COAST STATIONS

speed. Figure 23 shows histograms of gust factors and figure 24 the cumulative probability distribution of gust factors for the east coast storm. The data for hurricane Carla reduces to similar relationships.

The vertical distributions of gust speed above the land were estimated in accordance with the 1/12th power law as obtained from the results of Sherlock (1953) and Deacon (1955); that is:

$$G_Z = G_{10} (Z/10)^{1/12} \qquad (2)$$

where G_Z is the average gust speed at elevation Z and G_{10} is the average gust speed at 10 meters above the surface.

11. Sustained wind speeds and gust speeds will be greater over the top of the dunes than at the coastline. This follows from the fact that the flow is convergent, and the principle of continuity and Bernoulli's equation must apply, and the air can be treated as incompressible fluid. Unfortunately no data are available for this particular storm to determine the exact flow of air over the dunes. However, it must be expected that there is a considerable increase in wind speed over the top of a dune, similar to that associated with the flow of air over any type of obstacle. (Ning Chien, et. al., 1951)

Sutton (1953) states that the inviscid fluid theory (potential flow) gives a first approximation to the solution of the problem of finding the increase in horizontal velocity caused by a half-parabolic ridge. In fluid mechanics (Rouse, 1938, for example), it can be found, based on experiments, that there is a considerable increase in speed for incompressible flow over a half-cylinder and a vertical wall. This is also true for high Reynolds numbers, even though separation of the flow takes place on the back side of the obstacle. In the present study it is only of interest to consider the incident face of the dune where convergent flow exists and separation of the flow does not exist. Therefore, except for the small laminar boundary layer, potential theory can be applied. In this respect one must also take into account the vertical velocity distribution, which otherwise is normally assumed to be constant for potential theory.

For demonstration purposes, one can assume that a dune has the shape of a half-cylinder, an ellipse, a parabola, or a vertical flat plate. For example, it can be found in Lamb (1945), or more easily in Valentine (1959), that for potential flow the increase in

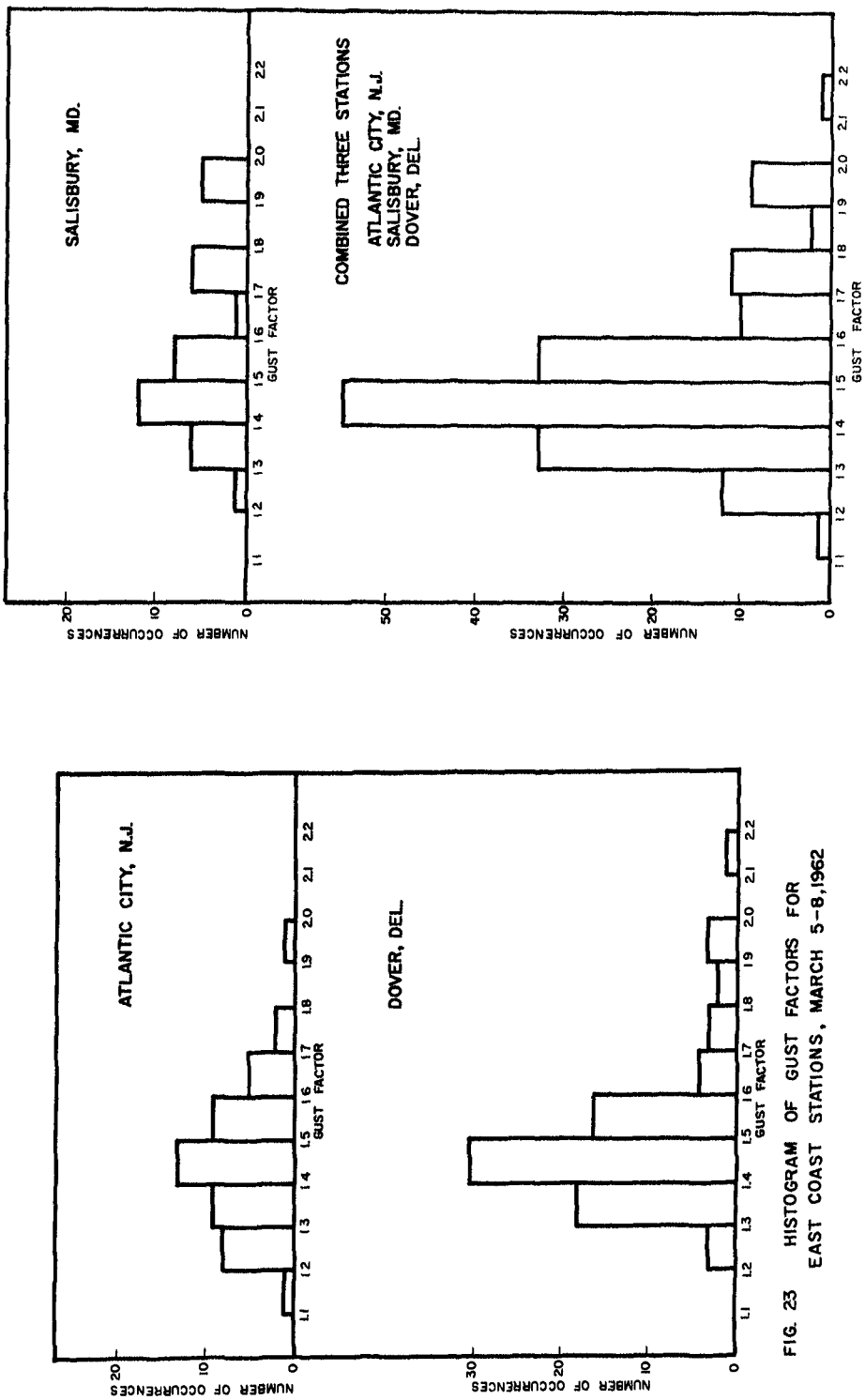

FIG. 23 HISTOGRAM OF GUST FACTORS FOR EAST COAST STATIONS, MARCH 5-8, 1962

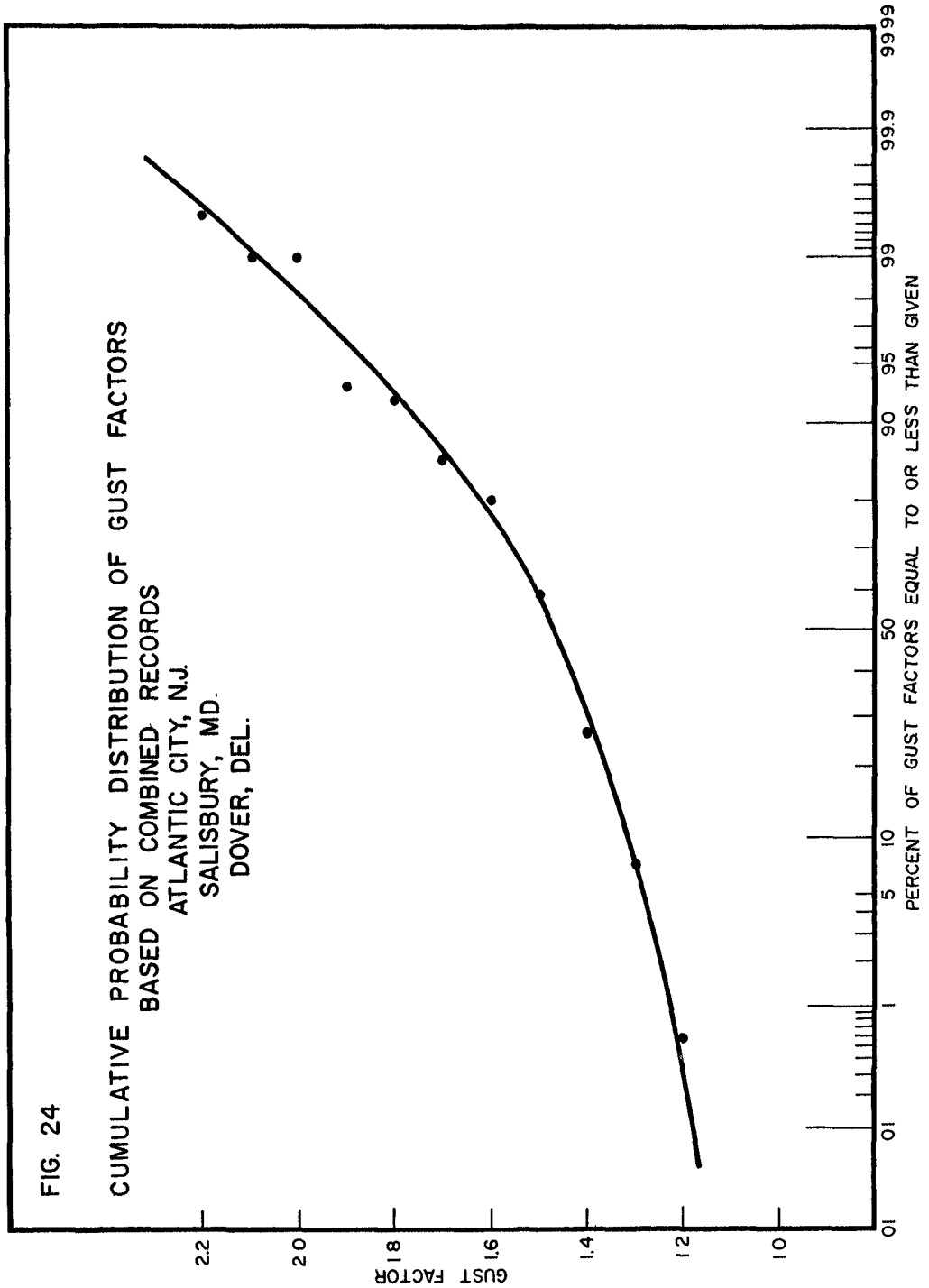
FIG. 24
CUMULATIVE PROBABILITY DISTRIBUTION OF GUST FACTORS
BASED ON COMBINED RECORDS
ATLANTIC CITY, N.J.
SALISBURY, MD.
DOVER, DEL.
GUST FACTOR
2.2
2.0
1.8
1.6
1.4
1.2
1.0
.01
.1
1
5
10
50
90
95
99
99.9
99.99
PERCENT OF GUST FACTORS EQUAL TO OR LESS THAN GIVEN

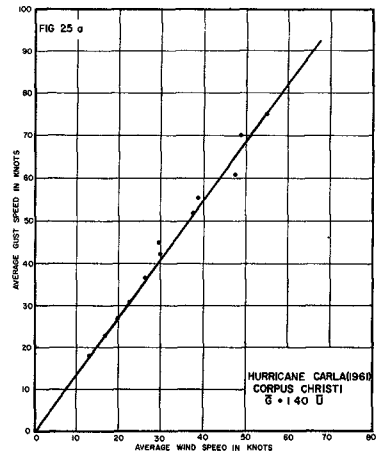

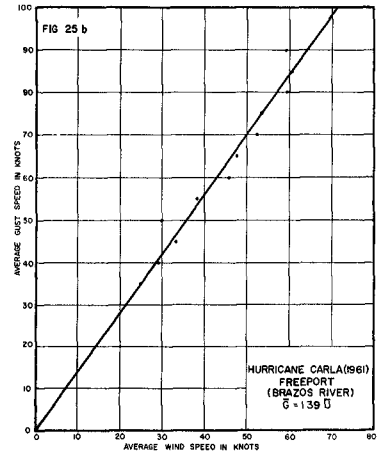

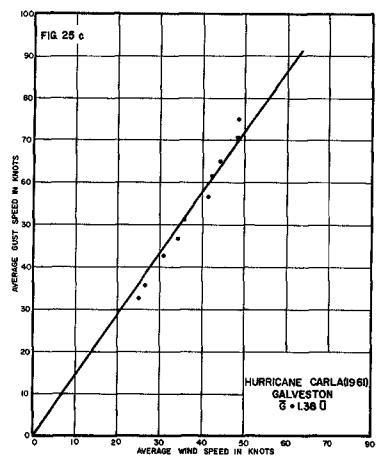

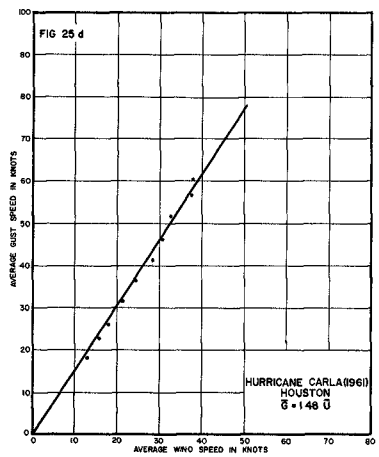

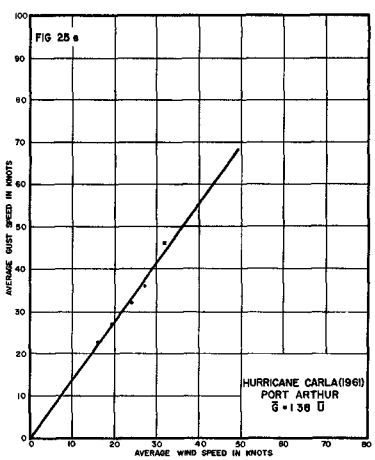

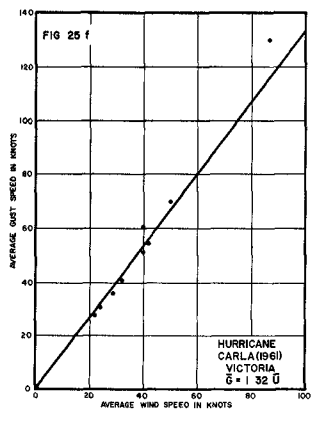

FIG. 25.--AVG. GUST SPEEDS VS. AVG. 1-MIN AVG. WIND SPEEDS FOR HURRICANE CARLA, 1961

horizontal wind speed over a half-cylinder (wind perpendicular to the dune) is given by:

$$U = U_\infty \left[1 + h^2 \frac{y^2 + x^2}{(y^2 + x^2)^2} \right] \quad (3)$$

where U is the wind speed above the dune; h is the height of the dune; x is the horizontal distance measured from the center of the dune; y is the vertical distance measured upward from ground level in absence of the dune, and U_∞ is the horizontal wind speed in absence of the dune. Figure 26 is based on the solution of equation 3 in non-dimensional form.

Of immediate interest in this study is the maximum horizontal wind speed in the vertical plane which occurs at $x = 0$, and referencing the coordinate system from the top of the dune, let $y = Z + h$, whence for a half-cylinder dune:

$$U = U_\infty \left[1 + \left(\frac{h}{Z + h} \right)^2 \right] \quad (4)$$

Similarly, for a vertical flat plate dune one obtains

$$U = U_\infty \left[\frac{Z + h}{\sqrt{(Z + h)^2 - h^2}} \right] \quad (5)$$

Either of the above equations can be used to estimate a first approximation to the solution of the maximum wind speeds over the top of the dunes. Because of friction and turbulence, the incident wind speed U_∞ is not constant with elevation and a second approximation can be obtained by replacing U_∞ with U as a function of elevation Z. It will be convenient to refer all elevations measured upward from the free surface streamline instead of from a horizontal plane; i.e. $Z = 0$ all along the beach from the coastline to the toe of the dune, up the face of the dune to the top of the dune. Assuming that continuity is approximately satisfied and that additional frictional losses in the convergent flow are negligible from the beach to the top of the dune, then the second approximation can be estimated by replacing U_∞ in the above equations with U_Z from equation 1, whence for a half-cylinder dune

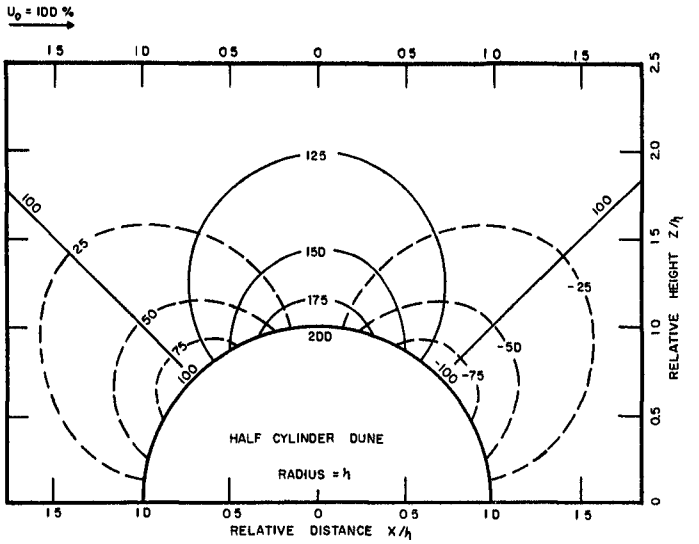

FIG 26 VERTICAL AND HORIZONTAL WIND SPEED COMPONENTS FOR IDEALIZED FLOW

SOLID LINES ARE HORIZONTAL COMPONENTS IN PERCENT OF U_0
DASH LINES ARE VERTICAL COMPONENTS IN PERCENT OF U_0
U_0 = 100 PERCENT AWAY FROM DUNES
POSITIVE SIGN ON VERTICAL COMPONENT IS UP
NEGATIVE SION INDICATES DOWNDRAFT

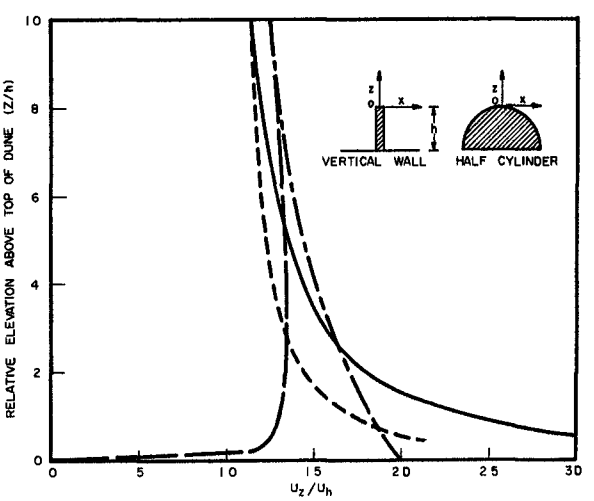

FIG 27— DEMONSTRATION OF INCREASE IN WIND SPEED OVER TOP OF A DUNE

VERTICAL WALL POTENTIAL THEORY
HALF CYLINDER POTENTIAL THEORY
VERTICAL WALL MODIFIED FLOW
HALF CYLINDER MODIFIED FLOW

$$U_Z = U_h \left(\frac{Z}{h}\right)^{1/7} \left[1 + \left(\frac{h}{Z+h}\right)^2\right] \quad (6)$$

and for a vertical flat plate dune

$$U_Z = U_h \left(\frac{Z}{h}\right)^{1/7} \left[\frac{Z+h}{\sqrt{(Z+h)^2 - h^2}}\right] \quad (7)$$

Landsberg (1942) conducted an elaborate experiment on "The Structure of Wind Over a Sand Dune." The vertical and horizontal distributions of winds were investigated over a typical Michigan dune near Stevensville, Michigan. The dune was a so-called "blow-out" that had been cut through an older chain of grown-over dunes. The measurements were made where the dune had been cut above 100 feet below the level of the grown-over portion of the dune. The "blow-out" formed a fairly narrow channel about 75 feet wide at the base, which was at an elevation of about 80 feet above the level of Lake Michigan. The channeling effect of the front slope and the two ridges to either side of the blow created much higher velocities nearer the ground than elsewhere. Over the top of the "blow-out" the velocities were practically uniform from 1/2 to 10 meters.

In the analysis of the data Landsberg (1942) used the logarithmic vertical distribution of wind speed given by the following equation

$$U_Z = 2.5\sqrt{\tau/\rho}\ \ln Z/Z_o = 2.5\sqrt{\tau/\rho}\ \ln\left[\frac{Z}{h} \cdot \frac{h}{Z_o}\right] \quad (8)$$

where τ is the shear stress, ρ is the density, and Z_o is the friction length parameter. The height of the dune h is introduced in the present paper.

From the data of Landsberg for winds over the beach, $Z_o = 0.155$ cm and $U = 2.8$ meters per second in 1 meters height, and over the top of the "blow-out" $Z_o = 0.09$ cm and $U = 4.2$ meters per second in 1 meters height, representing a 50 percent increase in wind speed in 1 meters height.

Figure 27 represents the solution of equations 4, 5, 6 and 7 in non-dimensional form. The increase in wind speed over the

top of the dunes determined from equations 6 and 7 is in reasonable agreement with the measurements made by Landsberg, allowing for the fact that the theoretical dunes and the actual Michigan dune are not necessarily in similitude.

The ratio of the average wind speed over the top 5 or 10 feet of the dune to the average wind speed in absence of the dune is called the average "dune factor". The general conclusion is that the average dune factor for a 10 to 20 foot high dune is between 1.35 and 1.45. Since the gust factor varies between 1.35 and 1.45, it is probable that the combined gust and dune factor is on the order of 2.0. Without the dune, 50 percent of the gust factors (see figure 24) will be as high as 1.45, and only 2 percent of the gust factors will be as high as 2.0. For a dune factor of 1.35 times a gust factor of $1.45 \cong 2.0$, one might expect that about 50 percent of the gust speeds over the top of the dune will be on the order of twice the incident 1-minute average wind speeds over the beach. This presumes that the dune and gust factors can be combined linearly.

Since the pressures acting on an object vary as the square of the wind speed, and since the dune factor is on the order of 1.35 to 1.45, the pressures acting against a house on top of the dune should be about twice that of a similar house located some distance ahead of or behind the dune.

SUMMARY

The material presented in this paper represents a hindcast of events during the March 6-8, 1962, storm along the east coast of the United States. Specifically the hindcasts include (1) deep water waves, waves over the continental shelf, waves in shallow water, and waves at the coastline; (2) total tide, including normal predicted tide, storm surge and wave set-up; (3) wave run-up on the beach and an estimation of beach berm and dune erosion; (4) wind speeds over water, over the beach, and over the top of the dunes. The hindcasts were checked with available data for the storm. Numerous sources of information on the storm were available to improve the accuracy of the "state of the art" in forecasting. Theory was required for various aspects of the problem for which little or no data were available.

The summary of this study leads to a time-history of the many events stated above. Figure 28 presents a brief summary of the more important determinations. This includes the normal predicted tide obtained from the tide tables; the total tide which includes the storm surge, the wave run-up of the maximum waves, the cumulative

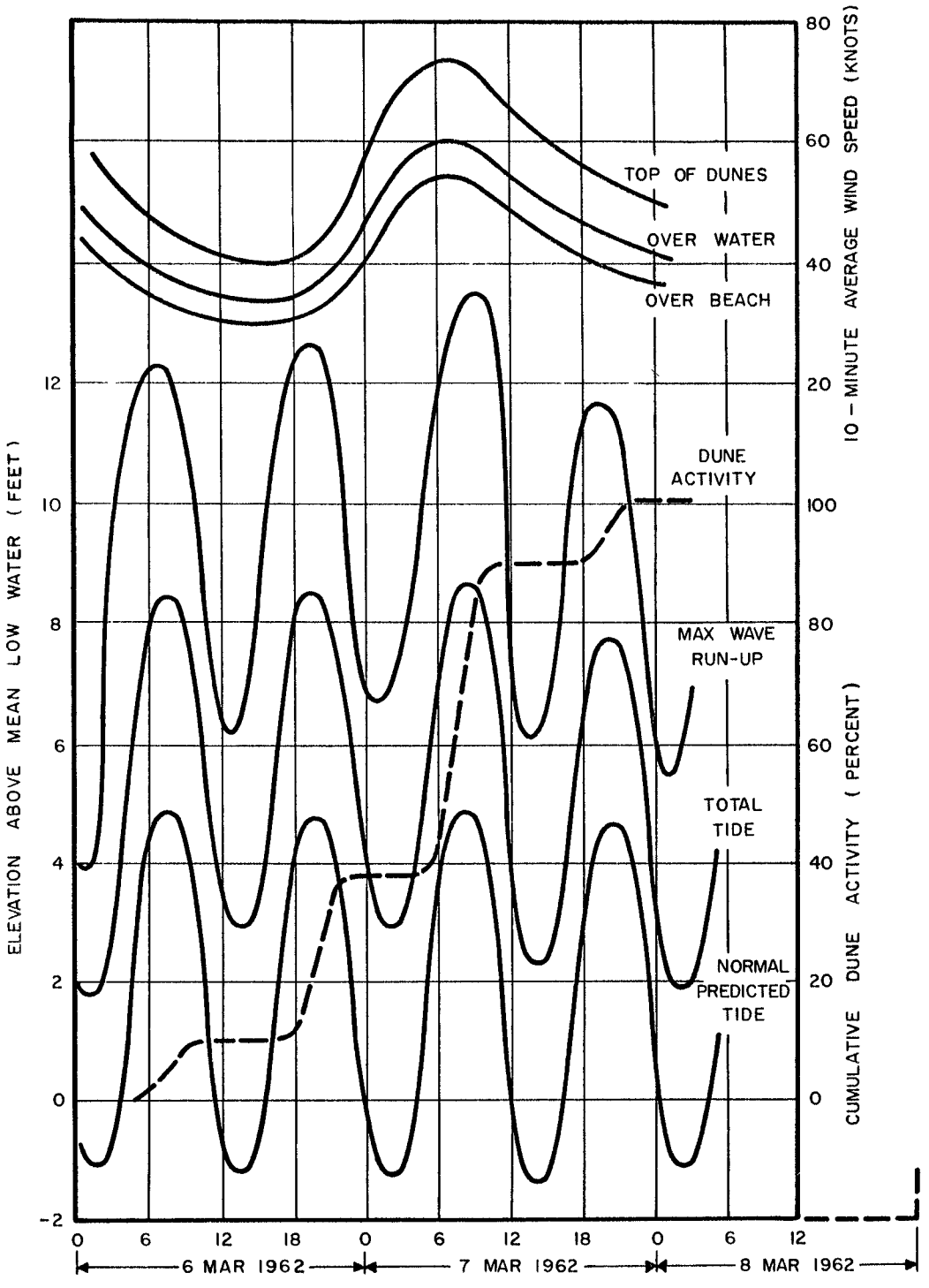

FIG. 28 TIME-HISTORY SUMMARY OF WIND, TIDES, WAVE RUN-UP AND DUNE ACTIVITY

presentation of estimated dune activity, and wind speeds over water, over the beach, and over the top of the dunes.

The over-water winds and winds over the beach are referenced to the 10-meter elevation. The winds over the dunes are averaged over the top 5 or 10 feet above the crown of the dune and are calculated to be about 1.35 times the incident wind speed. All winds represent the standard 10-minute average sustained wind speed. The peak one-minute average wind speeds average about 1.15 times the 10-minute average. The peak gusts are given approximately by 1.45 times the peak one-minute average wind speed.

The so-called "calibrated methods" for hindcasting were quite suitable for the present storm conditions. It is not necessarily recommended that these same methods be applied to some other factual storm or a design storm of different orientation direction and speed of wind, and direction and forward translation of the storm.

The state of the art of wave and storm surge hindcasting and forecasting is being advanced considerably by taking advantage of the data of both the east coast storm and hurricane Carla, as well as data from other storms along the Gulf coast and the east coast of the United States.

ACKNOWLEDGEMENTS

This paper represents a condensation of a number of reports pertaining to the east coast storm of 6-8 March 1962. Much of the work pertaining to the New Jersey coast was supported by the U. S. Naval Civil Engineering Laboratory under Contract No. NBy-32235. Much of the work pertaining to the Delaware coast was supported by more than 40 citizens of the Delaware Beach Rehabilitation Association under a letter agreement with Brookhart, Becker and Dorsey. The work performed pertaining to additional work beyond the requirements of the above contracts, including the work on wave spectra concepts and the drafting of this paper, was performed under contract with the Office of Naval Research under Contract No. Nonr-4177(00). Otherwise this paper could not have been documented. Of particular appreciation are numerous photographs and documents furnished by Mr. Garnett D. Horner, White House correspondent for the Washington Star. Appreciation is also extended to Mr. Louis Allen for his interpretation of wind speeds over the South Bethany, Delaware beaches. Those at NESCO who have contributed to this work include, among others, Dr. Bernard Le Mehaute, Dr. J. Ian Collins, Mr. Raymond Hurt and Prof. Raymond Fox.

REFERENCES

Bretschneider, C. L. (1958). "Engineering Aspects of Hurricane Surge." Proc., Tech. Conf. on Hurricanes, American Meteorological Society, Miami Beach, Florida

Bretschneider, C. L. (1958). "Selection of Design Wave for Offshore Structures." Trans., ASCE, Vol. 125, Part I, 1960, pp. 338-416.

Bretschneider, C. L. (1961). "A One-Dimensional Gravity Wave Spectrum." Ocean Wave Spectra, Prentice-Hall, pp. 41-65. (1963)

Bretschneider, C. L. (1962). "Modification of Wave Spectra on the Continental Shelf and in the Surf Zone." Proc., VIIIth Conference on Coastal Engineering, pp. 17-33.

Bretschneider, C. L., B. J. Le Mehaute, and Louis Allen (1963). "Oceanographic, Meteorological and Coastal Engineering Evaluation of the March 1962 East Coast Storm along the South Bethany, Delaware Coast Area." National Engineering Science Co. Tech. Report, SN-96.

Bretschneider, C. L. and J. I. Collins (1963). "Winds, Waves, Tides and Wave Run-up at Ventnor, New Jersey, during the Storm of March 5-8, 1962." National Engineering Science Co. Tech. Report, SN-138.

Chien, Ning, Y. Feng, H. Wang, and T. Siao (1951). "Wind Tunnel Studies of Pressure Distribution on Elementary Building Forms." Iowa Institute of Hydraulic Research, State Univ. of Iowa.

Cooperman, A. I. and H.E. Rosendall (1962). "Great Atlantic Coast Storm, 1962." Mariners Weather Log, U. S. Weather Bureau, May, 1962.

Deacon, E. L. (1955). "Gust Variation with Height up to 150 m." Quarterly Journal, Royal Meteorological Soc., Vol. 81, p. 562.

Graham, H. E. and D. E. Nunn (1959). "Meteorological Considerations Pertinent to Standard Project Hurricane, Atlantic and Gulf Coasts of the United States." National Hurricane Research Proj. Rpt. No. 33, U. S. Weather Bureau.

Goodyear, Hugo V. (1963). "Reconstructed Surface Wind Field for the East Coast Storm of March 6-8, 1962." Paper presented at the 1963 Annual Meeting of the American Meteorological Society.

Harris, D. Lee (1963). "Coastal Flooding by the Storm of March 5-7, 1962." Paper presented at the 1963 Annual Meeting of the American Meteorological Society.

Huss, P. O. (1946). "Relation between Gusts and Average Winds for Housing Load Determination." DGAI Report No. 140, Univ. of Akron, Ohio.

Lamb, H. (1932). Hydrodynamics. Dover Publications, 6th Ed.

Landsberg, H. (1942). "The Structure of the Wind Over a Sand Dune." Trans., American Geophysicaion Union.

Landsberg, H. and N. Allen Riley (1943). "Wind Influences on the Transportation of Sand Over a Michigan Sand Dune." Proc., Second Hydraulics Conf., Bulletin No. 27, Univ of Iowa Studies in Engineering.

Longuet-Higgins, M. S. and R. W. Stewart (1963). "A Note on Wave Set-up." Journal of Marine Research, Vol. 21, No. 1, pp. 4-10.

Meyers, V. A. (1954). "Characteristics of United States Hurricanes Pertinent to Levee Design for Lake Okeechobee, Florida." Hydrometeorological Rpt. No. 32, U. S. Weather Bureau.

O'Brien, M. P. and J. W. Johnson (1963). "The March 1962 Storm on the Atlantic Coast of the United States." Proc., VIIIth Conf. on Coastal Engineering, pp. 555-562.

"Pictorial Report of Delaware's Great Storm of March 1962." (1962). Published by the Delaware State News, Dover, Delaware.

Rouse, H. (1938). Fluid Mechanics for Hydraulic Engineers, McGraw-Hil

Saville, Thorndike, Jr. (1958). "Wave Run-up on Composite Slopes." Proc., VIth Conf. on Coastal Engineering.

Saville, Thorndike, Jr. (1961). "Experimental Determination of Wave Set-up." Proc., Second Tech. Conf. on Hurricanes, Nat. Hurricane Research Project Report No. 55, pp. 242-252.

Saville, Thorndike, Jr. (1962). "An Approximation of the Wave Run-up Frequency Distribution." Proc., VIIIth Conf. on Coastal Engineering, pp. 48-59.

Sheppard, P. A. (1958). "Transfer Across the Earth's Surface and Through the Air Above." Quarterly Journal, Royal Meteorological Society, 84, pp. 205-224.

Sherlock, R. H. (1953). "Variation of Wind Velocity, Gusts with Height." Trans., ASCE, Vol. 118A, 463, Paper No. 2553.

"Shore Protection Planning and Design." (1961). Beach Erosion Board T. R. 4, U. S. Army Corps of Engineers.

Sutton, O. G. (1953). Micrometeorology. McGraw Hill.

"The Storm of '62." Sussex Printing Corp., Seaford, Del., April 1962.

"The Storm of the Century." (1962). Published by the Baltimore Sun, Baltimore, Md.

Valentine, H. R. (1959). Applied Hydrodynamics. Butterworth's Scientific Publications, London.

Chapter 42

HURRICANE STUDIES FOR NARRAGANSETT BAY

John B. McAleer
Chief, Hurricane Unit, New England Division
U. S. Army Corps of Engineers, Waltham, Mass.

ABSTRACT

Hurricane flooding has emerged as one of the major coastal engineering problems of the Atlantic and Gulf Coast areas of the United States. Engineering and scientific investigations have been made to determine the fundamental mechanics of the hurricane surges that cause inundation of coastal areas and to develop practical and economical protection. Mathematical models and large hydraulic models were used for the Narragansett Bay studies of two major projects.

The discussions presented herein are limited to the hydraulic studies of barriers at the mouth of the bay, known as the Lower Bay Barri Plan, and a brief description of this plan and the Fox Point Hurricane Barrier which is now under construction.

INTRODUCTION

Hurricane tidal surges generated in the Atlantic Ocean have flooded Narragansett Bay areas of Rhode Island and Massachusetts 10 to 1⁴ feet above normal tide levels, and caused extensive inundation of business and residential properties. A map of the bay is given in Figure 1. Flood damages of about $100 million occurred in the September 1938 hurricane a again in the August 1954 hurricane. Loss of life was 110 in 1938 but only 1(in 1954 owing mainly to better warnings. The ocean surges travel with th hurricane at speeds of 30 to 50 miles an hour, then build up in height as they cross the Continental Shelf and flow into bays and estuaries. Althoug records of occasional great hurricanes go back to 1635, it is the recent di astrous hurricanes that have attracted attention to the problem.

HURRICANE CHARACTERISTICS

Tracks of selected hurricanes are shown on Figure 2. Major storms have followed the coastline striking inland west of Rhode Island th placing Narragansett Bay in the dangerous north-east quadrant of the stor

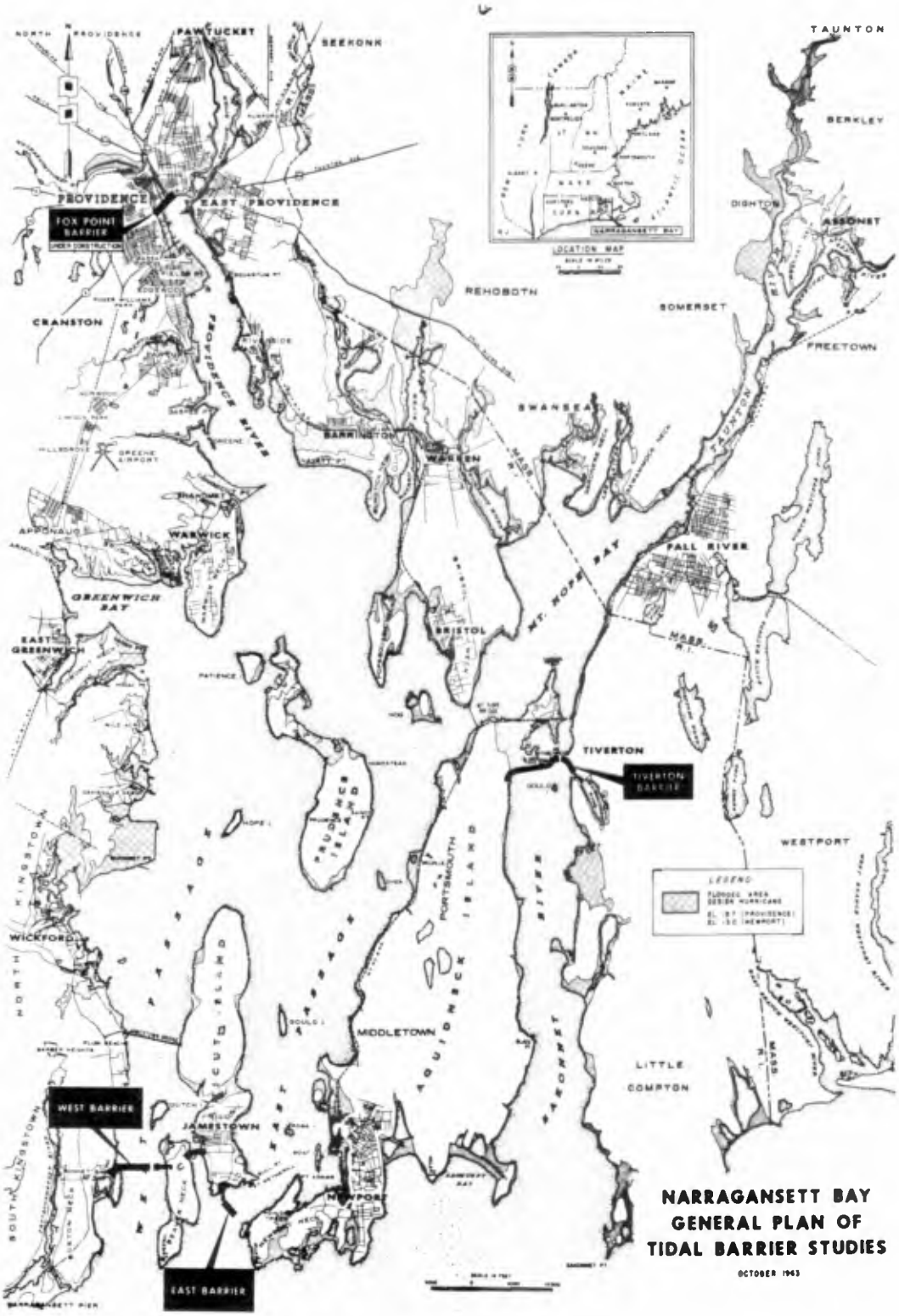
PAWTUCKET
SEEKONK
TAUNTON
BERKLEY
PROVIDENCE
EAST PROVIDENCE
FOX POINT BARRIER
UNDER CONSTRUCTION
DIGHTON
ASSONET
LOCATION MAP
REHOBOTH
SOMERSET
CRANSTON
FREETOWN
PROVIDENCE RIVER
SWANSEA
BARRINGTON
WARREN
GREENE AIRPORT
APPONAUG
WARWICK
FALL RIVER
GREENWICH BAY
MT. HOPE BAY
EAST GREENWICH
BRISTOL
PATIENCE
TIVERTON
TIVERTON BARRIER
WESTPORT
LEGEND
PROPOSED AREA DESIGN HURRICANE
EL. 87 (PROVIDENCE)
EL. 50 (NEWPORT)
PRUDENCE ISLAND
PORTSMOUTH
ISLAND
SAKONNET RIVER
WICKFORD
NORTH KINGSTOWN
CONANICUT ISLAND
AQUIDNECK ISLAND
MIDDLETOWN
LITTLE COMPTON
WEST BARRIER
JAMESTOWN
NEWPORT
SOUTH KINGSTOWN
EAST BARRIER
NARRAGANSETT BAY
GENERAL PLAN OF
TIDAL BARRIER STUDIES
OCTOBER 1963

Fig. 1

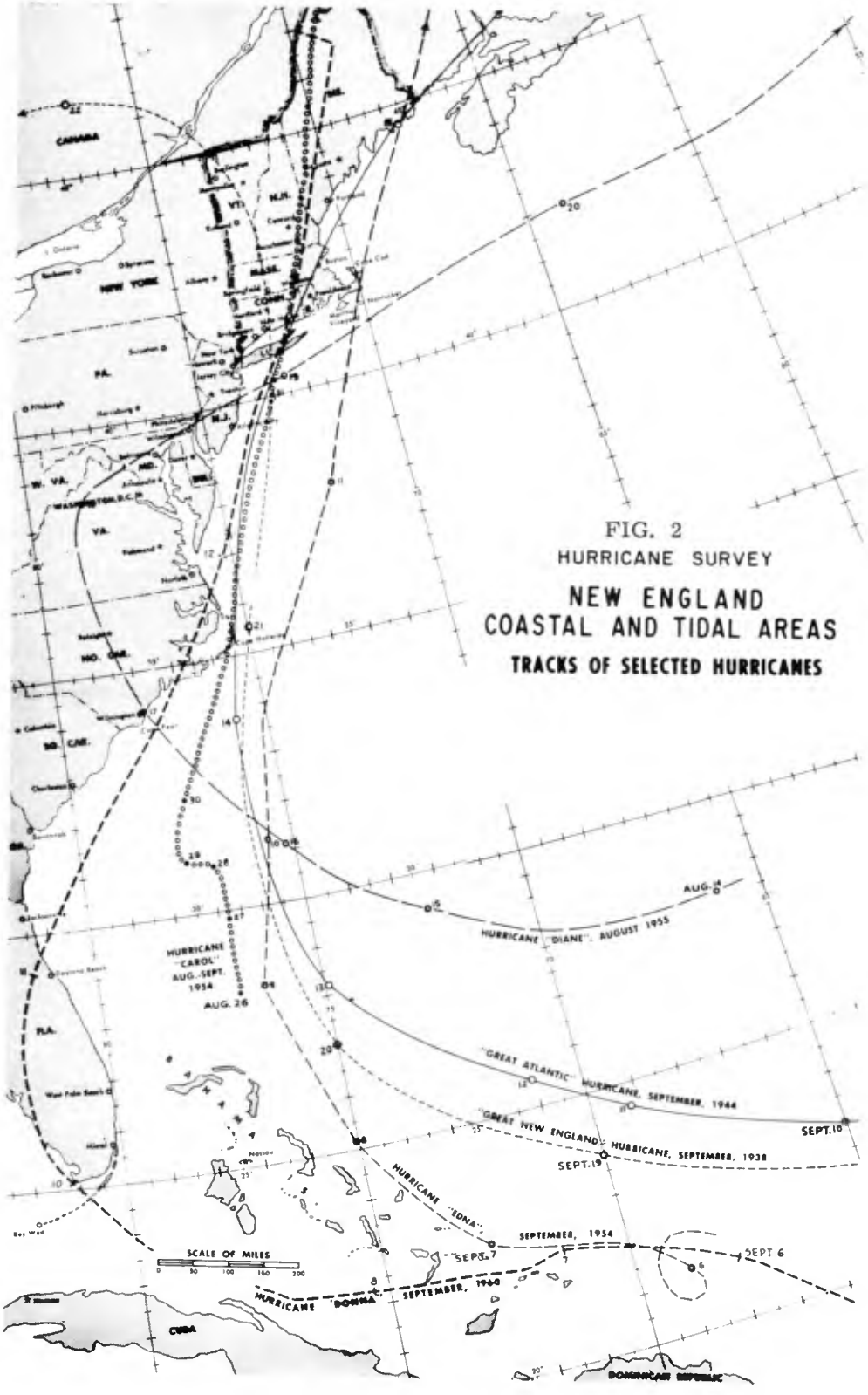

FIG. 2
HURRICANE SURVEY
NEW ENGLAND
COASTAL AND TIDAL AREAS
TRACKS OF SELECTED HURRICANES

Also important are the fast movement and short duration of the great hurricanes on the northeast coast in contrast to the slower storm movement farthe south.

The result is that a storm reported stalled or moving slowly along the South Atlantic coast may accelerate and strike Narragansett Bay 8 or 10 hours later; or it may completely miss the area and pass harmlessly out to sea. Forecasting, warning and evacuation of people from flood areas becomes extremely difficult under these conditions and there are bound to be many false alarms.

Maximum sustained winds in the great hurricanes have been generally above 75 miles per hour in the Narragansett Bay area, with 1-minute velocities of about 90 miles per hour and gusts recorded above 125 miles per hour. Minimum barometric pressures were recorded at about 28.50 inches of mercury (964.8 millibars). Significant wave heights in the bay entrances were about 25 feet, with 11 second period and waves within the bay areas were reported up to 9 feet in height with 7 second period.

SCOPE OF INVESTIGATIONS

As this was one of the first major hurricane studies in the United States, extensive engineering and scientific investigations were made over a 9-year period by the U. S. Army Corps of Engineers and many private and public agencies, including the Corps' Coastal Engineering Research Center and Waterways Experiment Station; other Federal agencies such as the Weather Bureau, Coast & Geodetic Survey, Public Health Service, Fish & Wildlife Service; and universities, including the Texas Agricultural & Mechanical Research Foundation, University of Rhode Island Oceanographic Department, and Massachusetts Institute of Technology. The purpose of these studies were: (1) to secure data on the behavior and frequency of hurricanes; (2) to determine the fundamental mechanics of hurricane surges and determine improved forecasting and warning methods, and (3) to develop practical and economical protection of life and property.

The investigations in Narragansett Bay included hydrographic and oceanographic investigations for hurricane and normal conditions as a basis for the studies by hydraulic models and mathematical models. Engineering studies and field investigations were made of 15 plans of protection.

FLOOD CONTROL

BARRIERS ACROSS THE ENTRANCES TO THE BAY

A plan of rockfill barriers, with large ungated navigation openings across the three entrances to Narragansett Bay, has been studied by hydraul model and computation methods. It was determined that satisfactory flood control, with reduction of 6 to 7 feet in flood levels over the 120 square mile bay area could be obtained by construction of barriers. The ungated navigation openings into the bay would have a total area of 122,000 square feet, whi is 23 percent of the waterway area of the natural openings into the bay.

STUDIES OF HURRICANE SURGES

Historical records show 2 to 5 great hurricanes in each century since 1635 when the country was settled. Although 70 hurricanes have been recorded since 1900 as crossing or threatening the area, of which 13 caused major flooding in Narragansett Bay, reliable data are available on only a fe hurricanes. (1) Studies of hurricane windfields and associated rainfall have been made of recent hurricanes and of maximum probable hurricanes by the Weather Bureau (2) (3). Using this wind data, the offshore surges were reproduced by Reid (4) in mathematical model studies. Surges within Narragansett Bay were reproduced in hydraulic models. Analytical methods were used to check model results and calculate local wind set-up effects.

FLOOD CONTROL EFFECT

The 1938 hurricane surge at the Newport entrance to the bay (Ea Passage) and the flood control effect of the barriers is shown in Figure 3. will be noted that without barriers most of the rise to 10.8 feet mean sea le occurs in 2 hours and the entire surge has a duration of 6 to 8 hours. With barriers, the opening into the bay would be reduced from their natural 532,000 square feet to 122,000 square feet. The rate of rise is limited by the smaller openings and flood levels are reduced over the bay area.

Next considering the bay as a whole, profiles of flood levels, frc the mouth of the bay to the head of the bay at Providence are given in Figur 4 for the 1938 hurricane, with and without the Lower Bay Barriers. The ir crease in levels towards the head of the bay is caused by the combination o wind set-up and the dynamic effect of the surge, which builds up in much th same manner that the normal tide range increases towards the head of the bay.

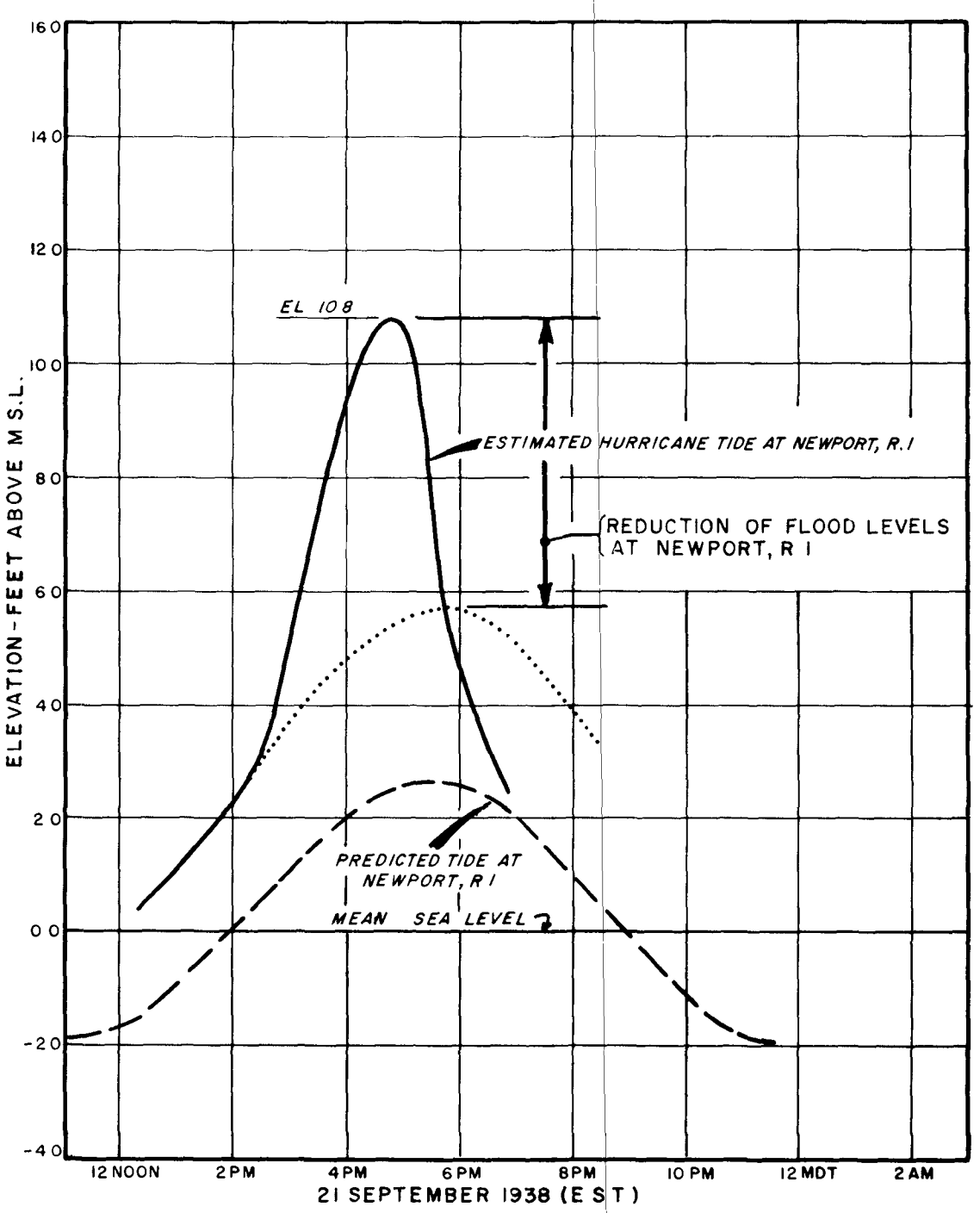

FIG. 3 NARRAGANSETT BAY, R.I.

EFFECT OF HURRICANE BARRIERS ON FLOOD LEVELS
SEPT. 1938 FLOOD AT NEWPORT

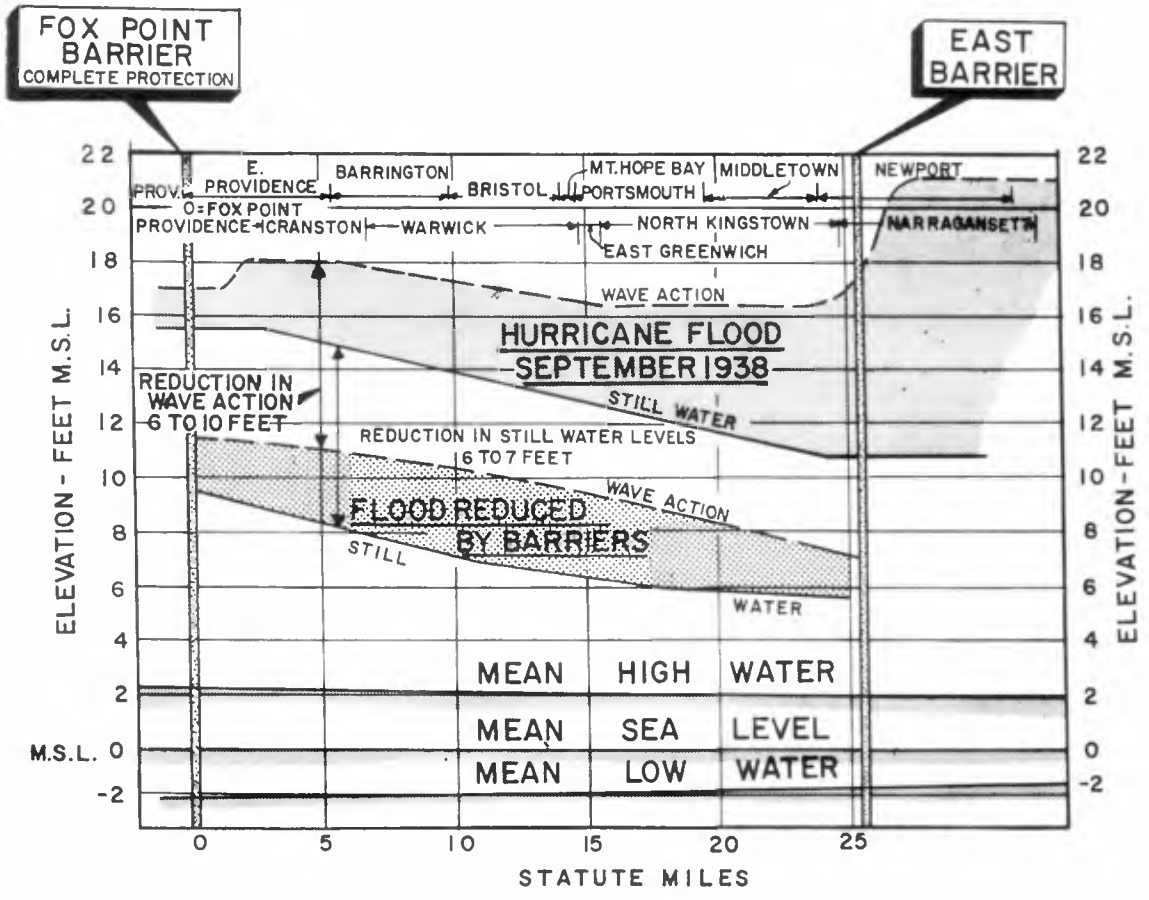

FIG. 4

HURRICANE FLOOD LEVELS

NARRAGANSETT BAY HURRICANE PROTECTION

DETERMINATION OF FLOOD EFFECTS

Navigation openings of various sizes were investigated. Openings were selected as large as practicable while retaining satisfactory flood reductions. The sequence of study was as follows:

(1) Hurricane Windfields. Charts of wind velocity, direction, barometer, and rate of travel were prepared by the Weather Bureau.

(2) Offshore Surge. Mathematical model studies were made by Reid (4) (5) employing the method of characteristics to reproduce floods of record and maximum probable floods. Storm track and speed were varied to determine the most severe conditions.

(3) Storm Surge at bay entrance. Observed for floods of record an computed for maximum probable hurricane.

(4) Storm Surge in Narragansett Bay. Observed levels for floods of record (1). Hydraulic model tests at Waterways Experiment Station (6) (7) reproduced floods of record and established maximum probable hurricane. This gave dynamic buildup within the bay, without local wind effects. Wind set-up was calculated in method outlined by Coastal Engineering Research Center (8), and added to the results of the model studies. Independent mathematical model studies were made by Reid (5).

(5) Flood Control Effect within Narragansett Bay.

(a) Determined from Waterways Experiment Station model tests without local wind effects. Wind set-up calculated as in (3) above.

(b) Independent mathematical routings were made using the discharge characteristics of the navigation openings determined in hydraulic model tests, as described below, and storage of water in the 120 square mile bay area (1).

(6) Inflow of water from wave overtopping. The extra flow of hurricane waters into the bay area from storm waves overtopping the barriers was calculated by the method of Saville (8). Waves were determined from the hurricane windfields furnished by Weather Bureau (2) using method of Bretschneider (9).

(7) Inflow from fresh water runoff. The additional water flowing into the bay during the hurricane surge period was determined from rainfall associated with hurricanes by Weather Bureau (3). Unit hydrographs were prepared of local runoff and river flood flow.

EFFECT ON OCEANOGRAPHY OF BAY

A basic consideration in the design of Lower Bay Barriers was to avoid changing the normal conditions in the bay, insofar as possible, because of the important recreational use and natural resources value of the area for commercial and sport fishing.

The normal tides and currents were first reproduced in the hydraulic model of Narragansett Bay. In later tests tidal interchange, mixing, salinity, stratification and sedimentation were reproduced for natural conditions and with the barriers over a period of 600 tidal cycles (10) (11).

Opening sizes were varied to determine effect on the natural tide. It was found that with openings totaling about one-third of their natural area there would be no reduction in the tidal prism or levels. Sluice gates, closed in hurricane periods, would provide the increase in area for the normal tidal interchange. Narragansett Bay is a partly mixed estuary as river flow is small and stratification occurs only in the upper bay areas. The Lower Bay and entrance areas are well mixed. With full tidal interchange the barrier would not be expected to change the natural salinity, stratification, temperature and sedimentation to increase the pollution problem, or to adversely affect finfish and shellfish. Extensive studies have been made of pollution and fishery effects by the U. S. Public Health Service (13) and U. S. Fish and Wildlife Service (14) assisted by other agencies.

EFFECT OF OPENINGS ON NORMAL TIDE RANGE

Barrier plans with openings varying from 63,000 square feet to 172,000 square feet were investigated (11). The reductions in the present mean tide range of 3.6 feet at the Newport entrance, plotted against area of openings are given in Figure 5, as determined from the model tests and routings described in paragraph (5) (b) above, and in the section on Hydraulic Design and Navigation Openings. It will be noted that an opening of about 125,000 square feet is critical. If the openings are smaller than the critical area the tide range is reduced. For larger openings the tide range is not significantly affected and the recommended plan with 172,000 square feet would not change the present normal tide range. Sluice gates in the East

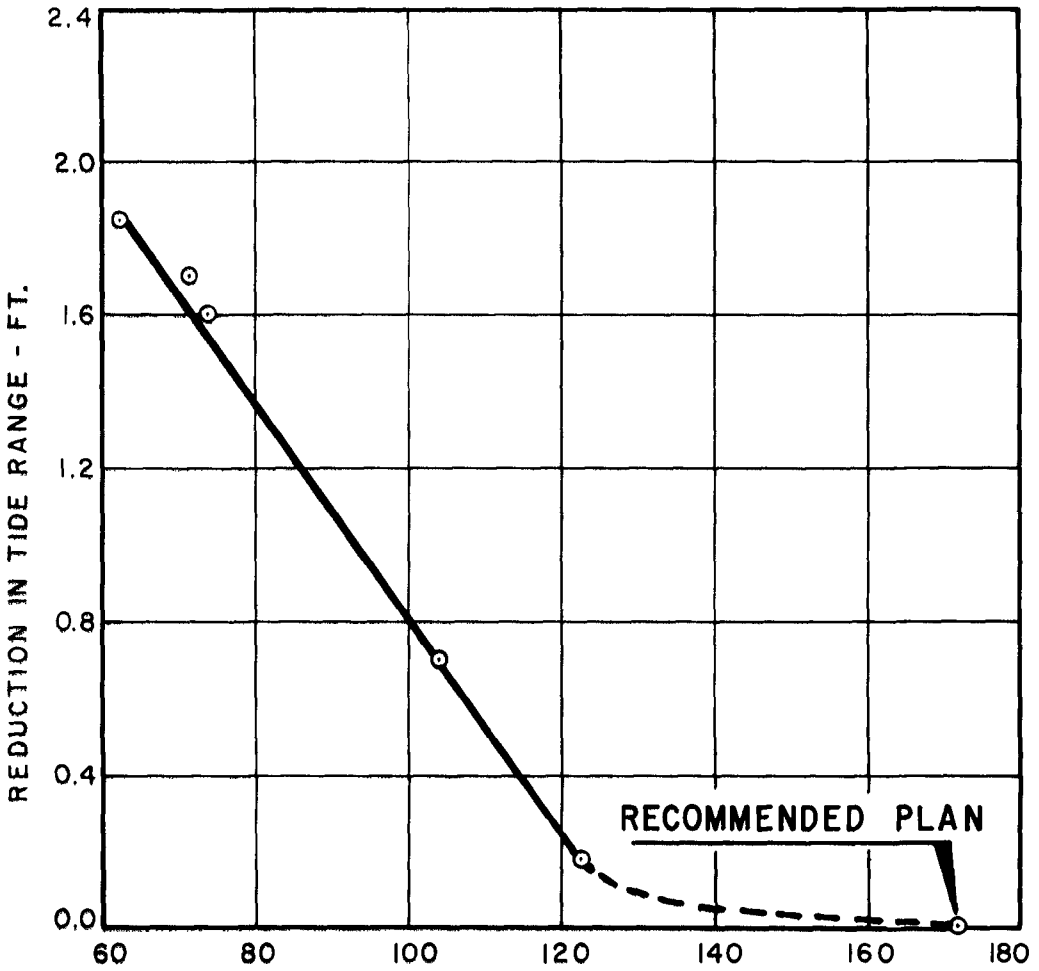

FIG. 5

NARRAGANSETT BAY, R.I.

REDUCTION IN MEAN TIDE RANGE OF BAY

and West Passages would provide the additional 50,000 square feet of openi over the 122,000 square feet in the three navigation openings.

EFFECT ON NORMAL TIDES AND CURRENTS

Tides at the entrance to Narragansett are semi-diurnal with two approximately equal tides having a period of 12 hours 40 minutes. It is a stationary type tidal wave with tide range increasing from 3.6 feet at the mouth to 4.6 feet at Providence, 25 miles away, where high water occurs only 10 minutes later than at the mouth. The tidal currents and levels are sensitive to offshore and local meteorological conditions.

Although the selected plan with 172,000 square feet of openings would not change the normal tidal range it would cause the phase of the bay tide to lag the ocean tide about 15 minutes as shown in Figure 6. As a resu the maximum currents in the East Passage would be increased from 1.5 to about 3.0 knots for a mean tide, as shown in Figure 7.

EFFECT ON SALINITY AND TIDAL MIXING

At present the entrance and lower half of the bay are well mixed by tidal currents with very nearly constant salinity from the surface to the maximum bottom depth of 170 feet in the East Passage, as shown in Figure In the upper bay and river areas stratification is apparent with surface sal of about 22 parts per thousand dropping to 8 parts per thousand during the spring runoff season as illustrated by the salinity graphs for present condi in the Providence River.

For the bay as a whole the ratio of fresh water runoff (per tidal cycle) to the tidal prism is small with an average of about 1 to 150.

As the selected barrier plan will provide full tidal interchange, good vertical mixing will continue to be produced by tidal currents becaus the water is nearly constant density from surface to bottom. Flume tests show full vertical mixing at the East Barrier site although the sill, at elev tion -60, will be about 100 feet above the bottom. For the other passages t sill of the navigation openings is near the natural bottom.

It is not anticipated that the normal salinity, mixing and flushin conditions would be changed by the barrier plan. However, detailed hydr lic tests of the final plan with sluice gates have not been made in the bay model during the present survey report study.

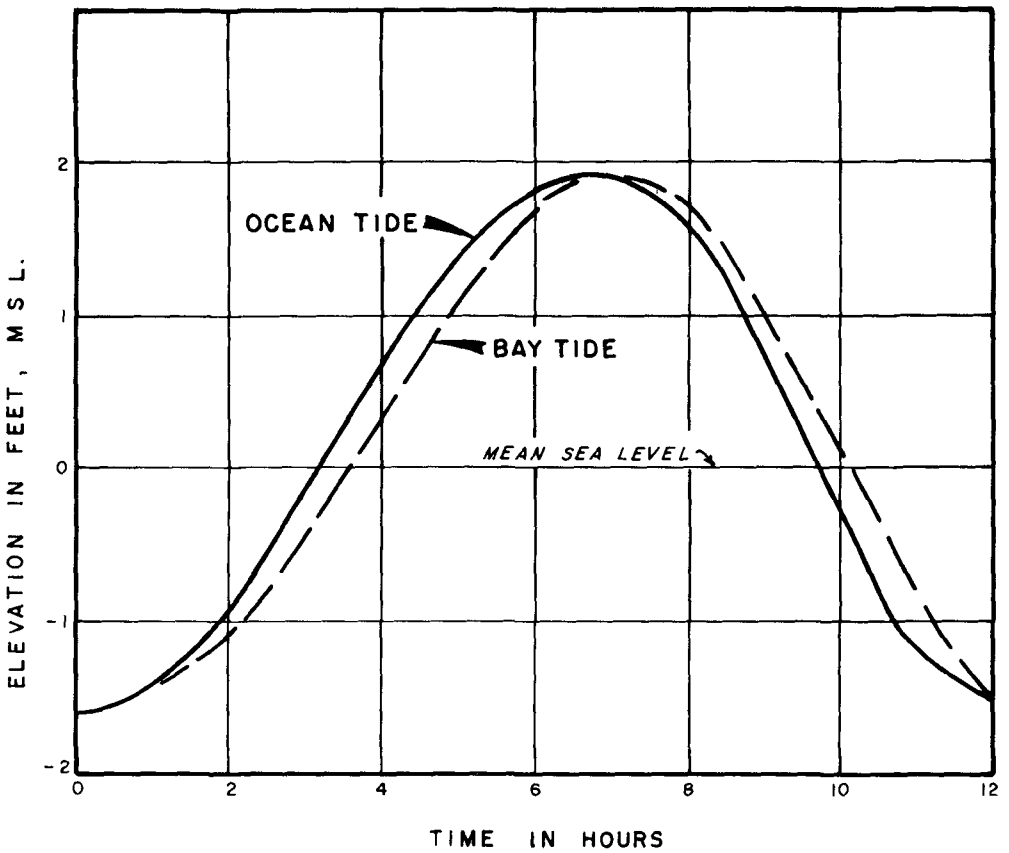

NOTE

MEAN TIDE
EAST AND WEST PASSAGES

FIG. 6

NARRAGANSETT BAY, R.I.

EFFECT OF HURRICANE BARRIERS ON TIDE LEVELS

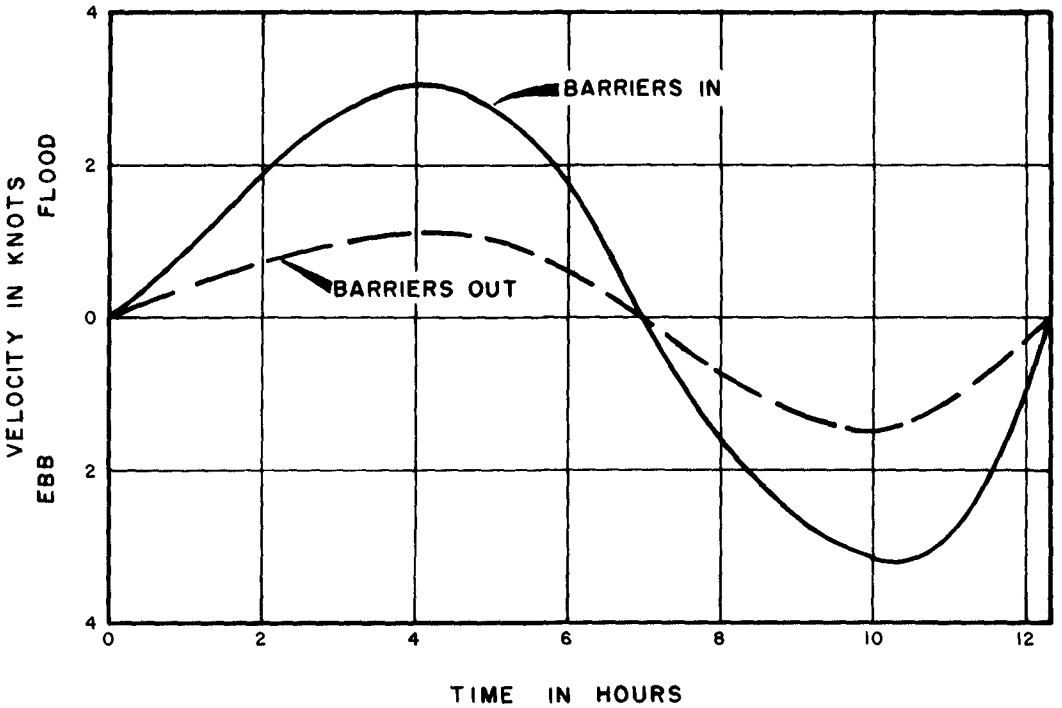

NOTE.
CURRENTS IN THE EAST PASSAGE FOR A MEAN TIDE

FIG. 7

NARRAGANSETT BAY, R.I.

EFFECT OF HURRICANE BARRIERS ON TIDAL CURRENTS

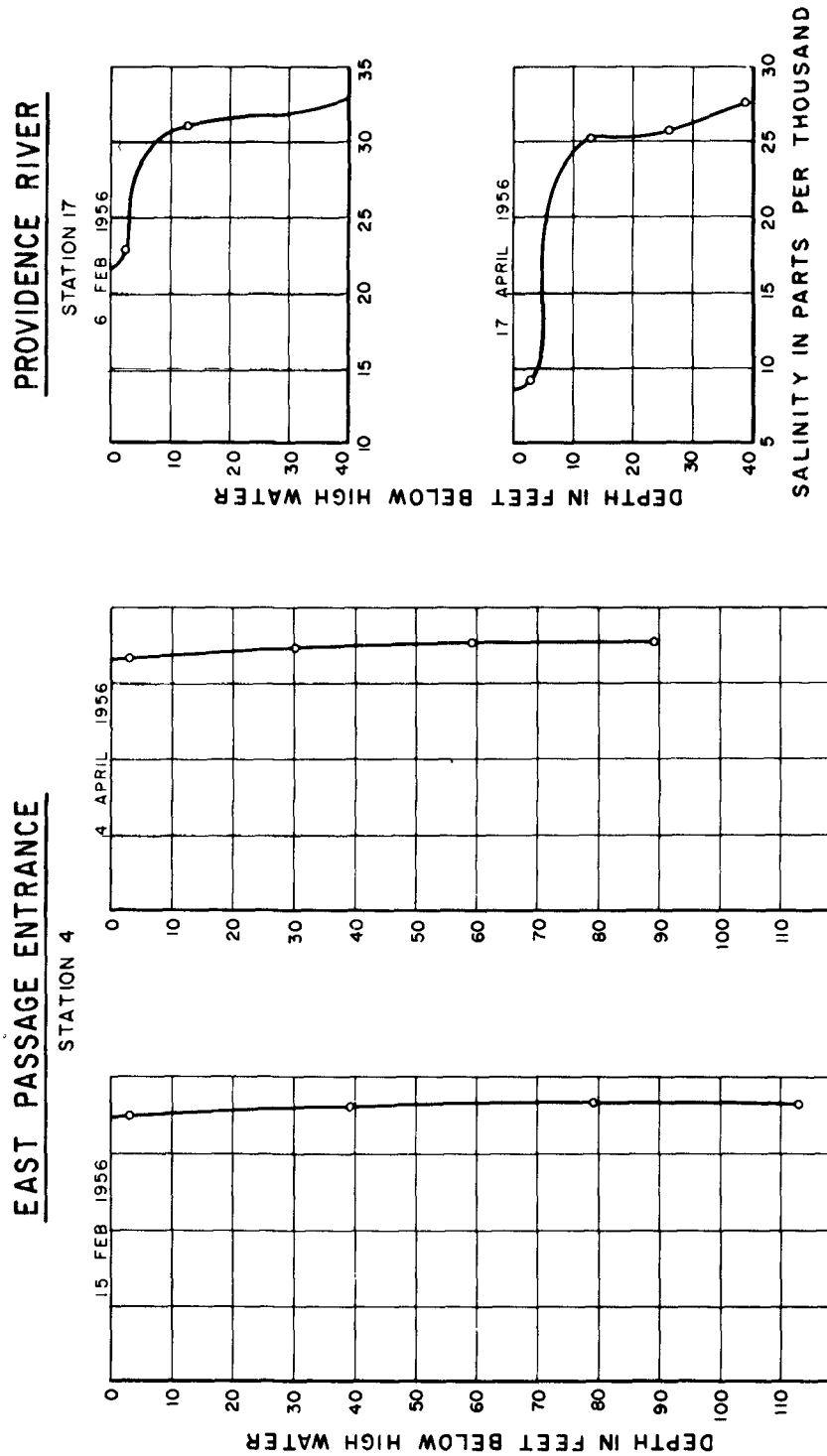

FIG. 8 NARRAGANSETT BAY, R.I. OBSERVED SALINITY

HYDRAULIC DESIGN OF NAVIGATION OPENINGS

The navigation openings studied included broad-crested and sharp crested weirs of varying sizes and different abutment configurations. The objective was to design openings (1) that would give parallel flow for normal navigation conditions (low head and low velocity), and (2) restrict the flow c abnormal tides and hurricane surges into the bay (sluice gates closed). Th are conflicting requirements.

The adopted design for the principal navigation opening, 1,720 fe x 60 feet in the East Passage, provided rounded abutments to obtain a satis factory current pattern for navigation and a sharp-crested weir type of sill in order to obtain effective flood control.

Extensive model tests were made of ship operations in the East Passage. A 1 to 150 scale model of an 1,100-foot long vessel was used in the hyc lic model of the East Passage to simulate present conditions with the barri The present mean tide current of about 1.5 knots would be increased to abo 3 knots by the barriers, as shown in Figure 7. For strong running tides (spring tide) the present maximum current of 2 knots would be increased tc about 4 knots for a maximum ebb and flood in the immediate vicinity of the barriers (sluice gates open).

DISCHARGE CHARACTERISTICS

The discharge characteristics of the navigation opening in the pr posed hurricane barrier for the East Passage were investigated by means both sectional and 3-dimensional models. Two sectional models reproduci the barrier at scales of 1:50 and 1:150 were used to determine the effect of approach depth, roughness of the barrier, model scale and weir design on the discharge characteristics of the structure for steady flow conditions. discharge characteristics of plans for both flood and ebb flows were determined with the 1:150 scale, undistorted, 3-dimensional model for the East Passage entrance.

As expected, the discharge capacity of the structure was greate with a deeper depth of approach. The roughness of the barrier due to the cover stone increased the discharge capacity of the navigation opening by reducing the effect of a contractive sill 10 feet high by 10 feet wide located on the oceanside of the weir crest. The model scale was found to have no significant effect on the discharge characteristics of the barrier. Tests revealed that the barrier surmounted by the 10 by 10-foot contractive sill v almost as effective as a 40-foot high vertical sill in contracting flood flow

The tests showed that discharge characteristics of navigation openings were highly sensitive to the design of sill and abutments. Good flood control demandsthe lowest practicable coefficient of discharge and this is normally associated with high contraction and high energy loss which can readily lead to a meandering jet with large eddies and unstable flow conditions. On the other hand if the transitions are rounded and eased to improve navigation conditions flood control effectiveness diminishes as the coefficient of discharge increases and little energy is lost.

The solution was the use of the contractive sills which formed a sharp-crested weir with high vertical contraction and dissipation of energy in vertical eddies which do not affect the steering of a vessel. These were combined with rounded abutments to give a smooth flow pattern in the horizontal plane.

The coefficient of discharge for representative weir sections that were tested (12) are shown in Figure 9. For the proposed plan the C is about 0.9 for flood and 1.0 for ebb flows, using the basic equation:

$$Q = CA\sqrt{2g\ h}$$

where the terms used in the equation are defined as follows:

Q - total discharge in cfs

C - submerged flow discharge coefficient

A - cross-sectional area of navigation opening with reference to tailwater elevation (00.0 mlw) above weir crest in sq. ft.

h - differential between total energy of approach channel flow and depth of tailwater with reference to weir crest in ft. (H-h)

g - acceleration due to gravity in ft/sec^2

The mathematical routings for normal tides and for hurricane surges were predicated on storage in the 120 square mile area above the barriers and the above equations. The computations gave a good check on the test results of the bay model.

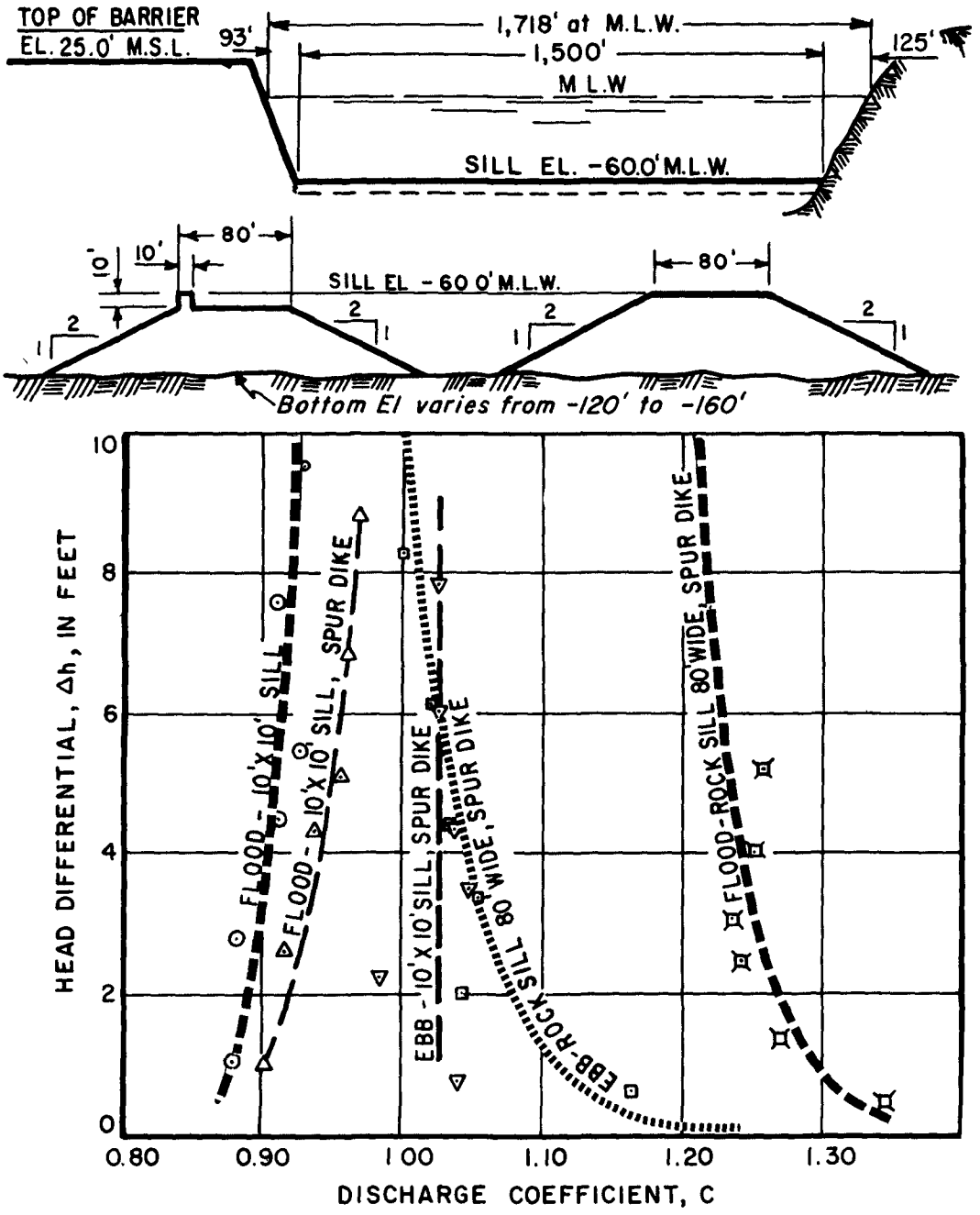

FIG. 9 NARRAGANSETT BAY, R.I.
DISCHARGE COEFFICIENTS
EAST BARRIER NAVIGATION OPENING

NAVIGATION

Navigation currents in the barrier openings were investigated for plans with openings varying from 63,000 square feet to the 172,000 square fee total of the recommended plan, with sluice gates open. Estimated maximum current at strength of flood or ebb, for a spring tide, are given in Figure 10. It will be noted that increasing the openings from 122,000 square feet to 172,0 square feet by adding the sluice gates reduces currents about 30 percent, whi substantially improves navigation conditions. This is particularly important for recreational boating which is a major factor in the Narragansett Bay area. The maximum current velocities in the East Passage and West Passage, estimated at about 4 knots in a spring tide and about 3 knots in a mean tide would be confined to the immediate vicinity of the barriers. Figure 7 shows the variation of currents over the tide cycle. Although currents at the navigation openings would be strong, small recreational craft and fishing boats regularly use waterways on the East and West Coasts of the United States where stronge currents occur. Flood protection would be afforded for many dock and anchor age areas and marine facilities along the shoreline of the bay.

The East Passage model was also used to demonstrate navigation conditions in the vicinity of the East Barrier before and after construction of the proposed barrier, using a model ship having a prototype length of 1,100 feet.

(1) Normal conditions. Tests were made using the model ship whic satisfactorily transited the passage in both directions at speeds of 15, 10 and 7 knots.

At an engine speed of $7\frac{1}{2}$ knots the ground speed of the vessel over the barrier was slow, without the sluice gates, because the vessel must buck the 4 knot current and also to climb the gentle slope to the higher pool level. There was no control problem with parallel flow normal to the axis of the barrier.

With sluice gates open, navigation conditions and maximum currents are considerably improved; operation was satisfactory.

(2) Gale conditions. Waves 11 feet in height had little effect on a large ship. Some protection was afforded by the barriers. Windage on the vessel moving at low speed was very important -- with or without barrier. Engine speeds used were the same as for normal conditions. Operation was satisfactory.

(3) Hurricane conditions. Navigation during hurricane conditions of current, 25-foot high waves, and 70 knot winds were simulated using vess speeds of 20 and 15 knots. The present maximum flood current of 5 knots would be increased to 11.5 knots with barrier, and the present maximum hurricane ebb current of 9.5 knots would be about the same with the barrier in place. Model operation under these conditions (which may in nature include low visibility) is difficult but can be accomplished either with or witho the barrier. It is definitely an emergency operation (sluice gates closed).

PROJECT STUDIES

Planning and design studies include hydraulic, . structural design and economic analyses for the Fox Point Hurricane Barrier at the head of tl bay and the Lower Bay Barriers at the entrance (15) (16).

FOX POINT HURRICANE BARRIER

One of the first hurricane flood control structures to be built in this country, the Fox Point Barrier is now under construction. It will affo protection to the commercial and business section of downtown Providence against a design hurricane tide of 20.5 feet above mean sea level, which is 4.8 feet higher than the maximum flood on record. The barrier was desigr as a dam across the Providence River. Figure 1 gives the location of the p ject, and Figure 11 shows the layout.

The central structure is a concrete gravity dam about 680 feet lo with its top 25 feet above mean sea level. In the east section of the main barrier three 40-foot wide tainter gates will pass normal river and tidal fl These gates will generally be in a raised position to permit the passage of small boats and barges. When closed, the gates will prevent entry of tidal flood waters from Narragansett Bay.

The western section of the barrier includes a large pumping station to discharge the flood runoff of the Providence River when the gates a closed during hurricane emergencies. Intake gates at the pumping station permit the entrance of water to a cooling water canal along the west side o the river leading to large steam electric plants upstream of the barrier.

Dikes on either side of the main dam tie in to high ground so as prevent flanking by flood waters; each dike is about 800 feet long, 10 to 15 feet high, and composed of rolled earth faced by armor stone to protect against wave action. Steel swing gates are provided at street crossings, t be closed during hurricanes. The top elevation of 25 feet for the barrier

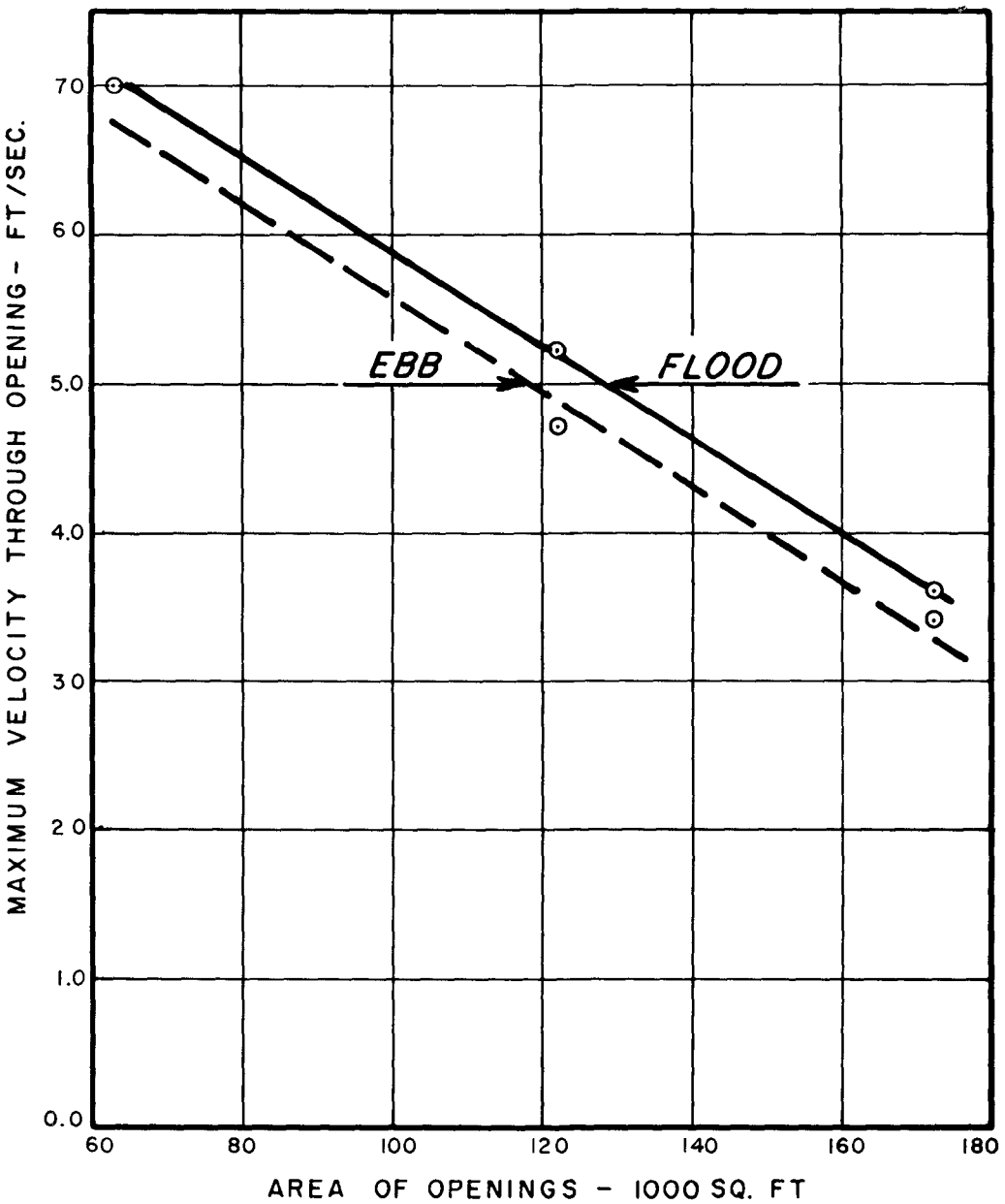

FIG. 10 NARRAGANSETT BAY, R.I.

VELOCITIES THROUGH BARRIER OPENINGS
SPRING TIDE

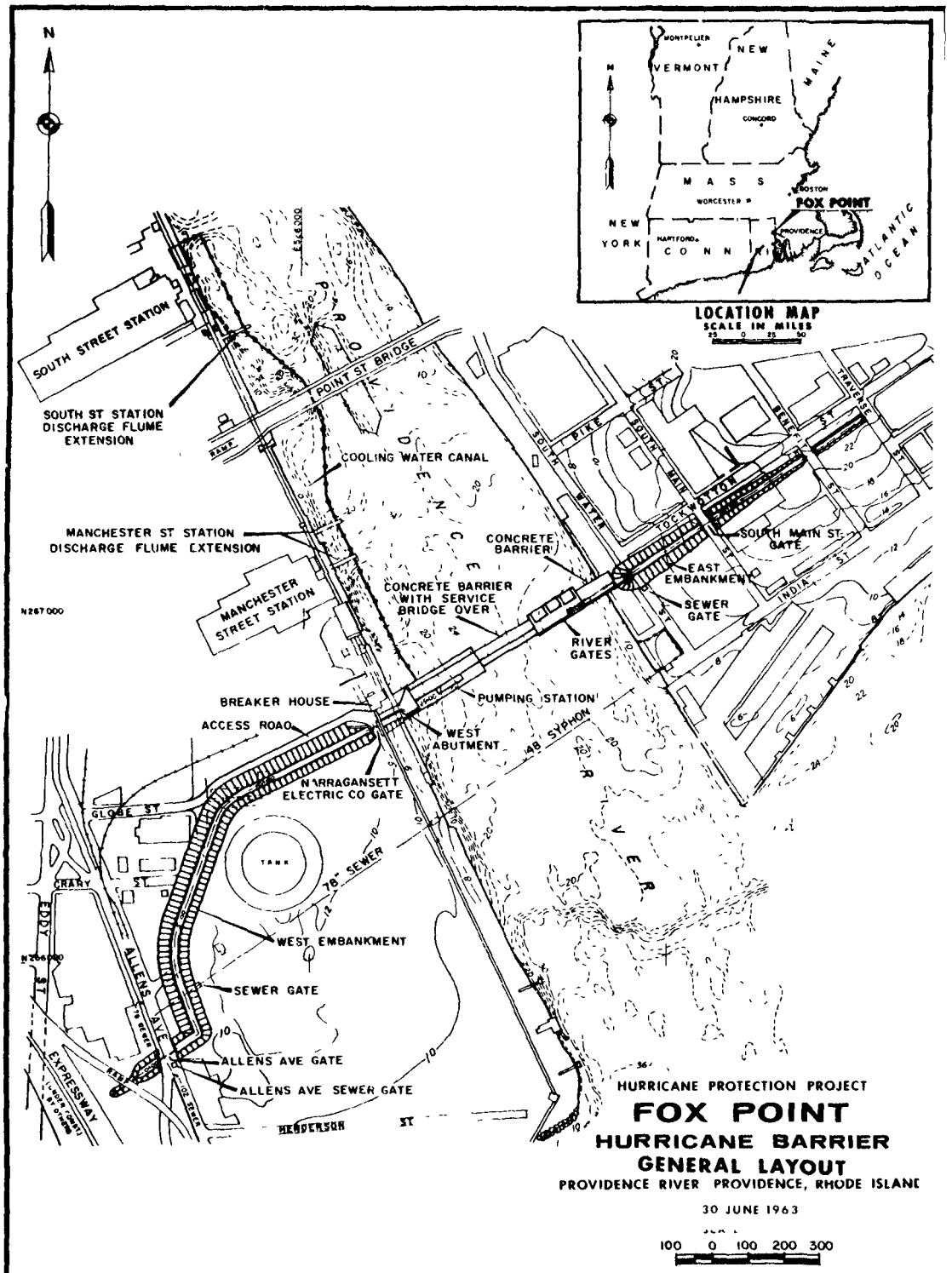
N
LOCATION MAP
SCALE IN MILES
VERMONT
NEW HAMPSHIRE
MAINE
MASS
NEW YORK
CONN
BOSTON
WORCESTER
FOX POINT
PROVIDENCE
HARTFORD
ATLANTIC OCEAN
SOUTH STREET STATION
SOUTH ST STATION DISCHARGE FLUME EXTENSION
POINT ST BRIDGE
COOLING WATER CANAL
MANCHESTER ST STATION DISCHARGE FLUME EXTENSION
MANCHESTER STREET STATION
CONCRETE BARRIER
CONCRETE BARRIER WITH SERVICE BRIDGE OVER
SOUTH MAIN ST GATE
EAST EMBANKMENT
SEWER GATE
RIVER GATES
PUMPING STATION
BREAKER HOUSE
ACCESS ROAD
WEST ABUTMENT
48" SYPHON
NARRAGANSETT ELECTRIC CO GATE
GLOBE ST
TANK
78" SEWER
WEST EMBANKMENT
SEWER GATE
ALLENS AVE GATE
ALLENS AVE SEWER GATE
EXPRESSWAY
HENDERSON ST
PROVIDENCE RIVER
HURRICANE PROTECTION PROJECT
FOX POINT
HURRICANE BARRIER
GENERAL LAYOUT
PROVIDENCE RIVER PROVIDENCE, RHODE ISLAND
30 JUNE 1963
100 0 100 200 300

FIG. 11

will contain the calculated waves of the design storm for the fetch of the Providence River fronting the barrier. Rock facing will effectively dissipate breaking wave forces on the front of the dikes, while rear faces are riprapped for protection against the moderate overtopping flow of maximum waves. The concrete structures in the river are in relatively deep water so that the waves will not break and only wave runup has been provided for.

The tainter gates will pass a major river flood and prevent back-up into the city streets during normal tides. In the event of a hurricane tide the gates will be closed and the five 109-inch pumps of the pumping station will go into action. These pumps have a design capacity of 7,000 cfs at 20-foot head which is adequate for any flood of record and for the maximum runoff of a transposed 1938 hurricane rainfall. The pumps would maintain the Providence River pool upstream of the barrier near mean sea level elevation. Sewers passing through the barrier will be gated and flow will be bypassed into the river upstream of the barrier in hurricane tide periods.

Foundation conditions include glacial till at elevation 80 feet below mean sea level, generally overlain by two layers of silt separated by a 10-foot sand-gravel layer. The upper silt layer was removed in the river section and replaced with sand fill; all river section structures will be supported by steel piling driven to till. The river sections are being constructed in the dry using cellular cofferdams.

The estimated cost of the Fox Point project is about $18,000,000, of which the non-Federal share is 30 percent. Local costs are being shared, two-thirds by the City of Providence, and one-third by the State of Rhode Island. Upon completion the project will be turned over to the local authorities for maintenance and operation. The project would prevent flood damages of about $40 million in a recurrence of the 1938 hurricane.

LOWER BAY BARRIER PLAN

After consideration of numerous plans proposed by local interests involving 25 different sites, the specific locations of the barriers were selected after (1) extensive hydraulic model tests, (2) economic studies of alternative sites and structures, and (3) the evaluation of navigation conditions. Figure 1 shows the location of the structures. The plan of protection includes a system of three massive rock barriers with ungated openings large enough to meet navigation needs but small enough to control the entrance of hurricane tidal surges into the bay area. The component structures are described in more detail below.

The East Barrier would consist of a massive rockfill barrier acr the East Passage from Castle Hill to Fort Wetherill and provide for an unga navigation opening 1,718 feet wide at mean low water, and 1,500 feet wide at depth of 60 feet below mean low water; and 40 sluice gates 25 feet wide x 27. feet high. The maximum water depth near the barrier in the East Passage 200 feet. See Figure 12.

The West Barrier would consist of a massive rockfill barrier acr the West Passage at Bonnet Shores, with an ungated navigation opening 520 wide at mean low water, and 400 feet wide at a depth of 40 feet below mean water; and 40 sluice gates 25 feet wide x 27.5 feet high. The maximum wat depth at the barrier site is 60 feet.

The Tiverton Barrier would cross the third opening into the Narr gansett and Mt. Hope Bay area with an earthfill armored structure across t Sakonnet River providing for an ungated navigation opening 166 feet wide at mean low water, and 100 feet wide at a depth of 20 feet below mean low wate flanked by beach raising, widening and back-up dikes.

Dikes to complete the closure would include road raising combin with beach raising and widening at Mackerel Cove and dikes across the low lands at Bonnet shores and Castle Hill.

The present plan provides for substantially larger navigation ope ings and more effective tidal interchange than the original 1956 proposal wh had a total waterway area of about 63,000 square feet in the three navigatio openings. The larger navigation openings provide 122,000 square feet of op ing, and the sluice gates another 50,000 square feet for a total of 172,000 square feet open during normal tidal conditions.

Effect of Barriers on Natural Resources. A three year study of the fishery problems was made by the U. S. Fish and Wildlife Service, ass ted by the University of Rhode Island, the Rhode Island Fish and Game Dep ment, and other agencies (14). The problems of pollution and water quality effects were the subject of a two year study by the U. S. Public Health Ser (13) assisted by the University of Rhode Island and the Rhode Island Health Department. In both instances it was concluded that the Lower Bay Barrie would have very little effect on present conditions within the Bay. The effe of the barriers on navigation conditions has already been discussed.

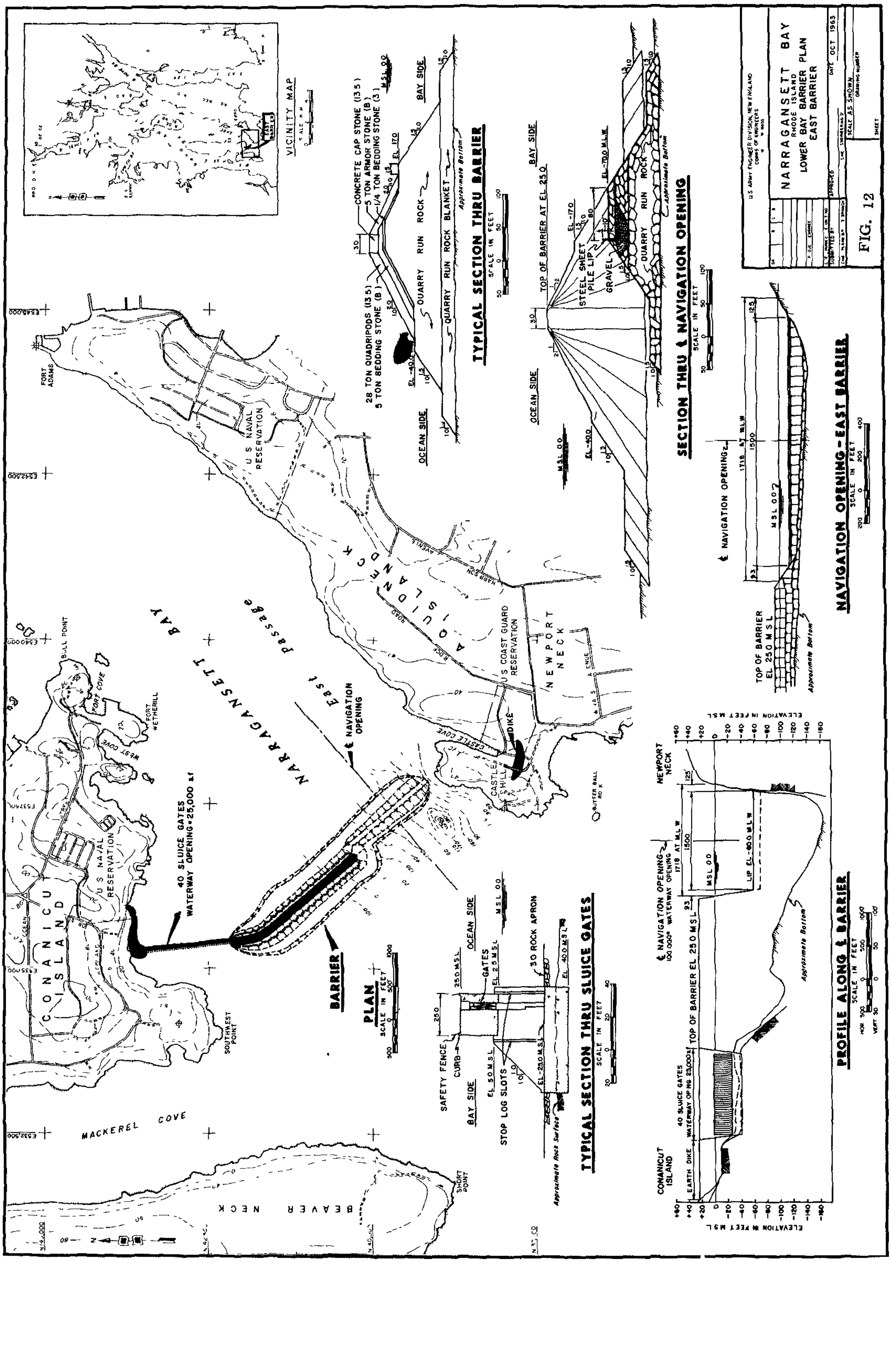
US ARMY ENGINEER DIVISION, NEW ENGLAND
CORPS OF ENGINEERS
NARRAGANSETT BAY
RHODE ISLAND
LOWER BAY BARRIER PLAN
EAST BARRIER
DATE OCT 1963
SCALE AS SHOWN
VICINITY MAP
TYPICAL SECTION THRU BARRIER
CONCRETE CAP STONE (13.5)
5 TON ARMOR STONE (B)
1/4 TON BEDDING STONE (3)
28 TON QUADRIPODS (13.5)
5 TON BEDDING STONE (B)
QUARRY RUN ROCK
QUARRY RUN ROCK BLANKET
Approximate Bottom
OCEAN SIDE
BAY SIDE
SCALE IN FEET
SECTION THRU ℄ NAVIGATION OPENING
TOP OF BARRIER AT EL 25.0
STEEL SHEET PILE LIP
GRAVEL
NAVIGATION OPENING-EAST BARRIER
TOP OF BARRIER EL 25.0 M.S.L.
℄ NAVIGATION OPENING
PROFILE ALONG ℄ BARRIER
CONANICUT ISLAND
EARTH DIKE
40 SLUICE GATES
NEWPORT NECK
ELEVATION IN FEET M.S.L.
TYPICAL SECTION THRU SLUICE GATES
SAFETY FENCE
CURB
STOP LOG SLOTS
GATES
30 ROCK APRON
Approximate Rock Surface
PLAN
BARRIER
40 SLUICE GATES
WATERWAY OPENING = 25,000 s.f.
NARRAGANSETT BAY
East Passage
℄ NAVIGATION OPENING
CONANICUT ISLAND
U.S. NAVAL RESERVATION
FORT WETHERILL
BULL POINT
SOUTHWEST POINT
MACKEREL COVE
BEAVER NECK
SHORT POINT
FORT ADAMS
U.S. NAVAL RESERVATION
AQUIDNECK ISLAND
U.S. COAST GUARD RESERVATION
NEWPORT NECK
CASTLE HILL
CASTLE COVE
DIKE
BUTTER BALL ROCK

FIG. 12

Present Status. Studies are being completed for the system of Lower Bay Hurricane Barriers which would reduce flood levels 6 to 7 feet over the 120 square mile bay area. More than 90 percent of the design floo damages of $126,000,000 in the area below the Fox Point Barrier would b prevented. The estimated cost of the plan is about $90,000,000. A survey report is being prepared by the Army Engineers for submission to the Unit States Congress.

ACKNOWLEDGMENTS

This study is being made by the U. S. Army Engineer Division, New England, under the direction of Brigadier General Peter C. Hyzer. Tl author extends appreciation to Mr. Henry B. Simmons and the staff of the Waterways Experiment Station; also to Mr. Joseph Caldwell and the staff of the Coastal Engineering Research Center and the many participating agenci and individuals for their invaluable assistance.

REFERENCES

1. U.S. Army Engineer Report (1957) Interim Report on Hurricane Survey, Narragansett Bay, Rhode Island and Massachusetts: printed as HD 2 1st Session, 85th U.S. Congress.

2. U.S. Weather Bureau (1956 to 1960). Unpublished memoranda of the Hydrometeorological Section, Washington, D. C.

3. U. S. Weather Bureau (1956). Rainfall Associated with Hurricanes: National Hurricane Research Project, Report No. 3 by R. W. Schone and S. Malonsky. Washington, D. C.

4. Reid, R. O. (1956). Approximate Response of Water Level on a Slopin Shelf to Wind Fetch which moves directly Toward Shore: Beach Eros Board Technical Memorandum No. 83, U.S. Army Corps of Enginee Washington, D. C.

5. Reid, R. O. (1960). Numerical Evaluation of Surges and Tides in Narr gansett Bay: The Agricultural and Mechanical College of Texas, College Station, Texas.

6. Waterways Experiment Station (1957). Protection of Narragansett Bay Hurricane Tides, by H. B. Simmons: Interim Report, U. S. Army (of Engineers.

7. Waterways Experiment Station (1964). Unpublished Report On Hydraulic Model Investigation, Narragansett Bay, by H. B. Simmons: U. S. Army Corps of Engineers.

8. Coastal Engineering Research Center (Beach Erosion Board) 1961: Technical Report No. 4, U. S. Army Corps of Engineers.

9. Bretschneider, C. L. (1958). Revisions in Wave Forecasting, Deep and Shallow Water: Coastal Engineering Proceedings, 6th Conference.

10. Waterways Experiment Station (1959). Effects of Lower Bay Barriers on Salinities, Shoaling and Pollution in Narragansett Bay, by H. B. Simmons and W. H. Bobb, U. S. Army Corps of Engineers.

11. Waterways Experiment Station (1964). Unpublished Report on Hydraulic Model Tests, as in (10) above: U. S. Army Corps of Engineers, Vicksburg, Mississippi.

12. Waterways Experiment Station (1964). Discharge Characteristics of Hurricane Barrier, East Passage, Narragansett Bay, Rhode Island: Unpublished report, U. S. Army Corps of Engineers.

13. U. S. Public Health Service (1960). Effects of Proposed Hurricane Barriers on Water Quality of Narragansett Bay: U. S. Department of Health, Education and Welfare, Region I, Boston, Mass.

14. U. S. Fish and Wildlife Service (1959). Hurricane Damage Control, Narragansett Bay and Vicinity, Rhode Island and Massachusetts - A Detailed Report on Fishery Resources: U. S. Department of the Interior, Washington, D. C.

15. McAleer, J. B. and Scott, P. J. A. (1958). Hurricane Protection in New England: Journal of the Boston Society of Civil Engineers, April 1958.

16. McAleer, J. B. and Townsend, G. E. (1958). Hurricane Protection Planning in New England: Journal of Hydraulics Division, American Society of Civil Engineers, August 1958.

Chapter 43

NUMERICAL PREDICTION ON TYPHOON TIDE IN TOKYO BAY

Takeshi Ito, Mikio Hino
Central Research Institute of Electric Power Industry
Komae-cho, Kitatama-gun, Tokyo, Japan

Jiro Watanabe, Kazuko Hino
Mitsubishi Atomic Power Industries Inc.
Ōtemachi, Chiyoda-ku, Tokyo, Japan

ABSTRACT

The paper discusses firstly mathematical problems on the numerical calculation of storm surges. The partial differential equations of motion adopted here take into account the Coriolis force and the non-linear terms such as the inertial terms and a quadratic form of bottom friction. As a result, special care must be taken in order to obtain stable forms of finite-difference equations. It is shown that inadequate forms accumulate errors to cause divergence of the step by step calculations. A set of stable forms of the finite-difference equations of motion and continuity has been derived.

Sometimes, it is convenient to divide the numerical integration region into two or more sub-regions, the mesh-dimensions of which are not equal. A method is described to calculate both regions by one procedure.

Japan coasts were frequently damaged by severe storm surges (Typhoon Tides). To protect the metropolitan area from storm surges, a proposal has been made to construct a dike across Tokyo Bay. A numerical calculation has been made by means of IBM 7090 to estimate for several opening width of the proposed dike its effects on the reduction of surges. Interactions between daily tides (astronomical tide) and surges are also discussed.

INTRODUCTION

A rapid development of the industrial activities is now going on in the urban districts of Japan, especially in the metropolitan area around Tokyo Bay. The expected increase of the urbanization and industrial activities will ask for improvement of traffic conditions and for remodeling of the metropolitan centre and its through ways. From this point of view, a proposal has been made by the Council for Industry Planning to construct a dike (of length about 18 km) across the central part of Tokyo Bay, which connects the over-crowded area of Tokyo, Kawasaki and Yokohama on the west side to the developing industrial area on the other side of the bay.

On the other hand, Japanese coasts have been frequently damaged by severe storm surges (Typhoon tides or TAKASHIO in Japanese). To protect the metropolitan area from storm surges, the proposed dike is expected to be also effective, probably reducing the typhoon water level. Thus, it would seem that there will be a chance of killing two birds with one stone

Here, care must be taken in that the dike is not situated on the entrance of the bay but on the central part. A check on the effectiveness of the two positions for reduction of storm surges has already been made to conclude that the central position is superior to the other.

Two reports Miyazaki (1961), Unoki and Isozaki (1962) have been published on the numerical prediction of the typhoon tides and of the effectiveness of the proposed dike. A precise and comprehensive numerical calculation by means of IBM 7090 is presented in this paper. Numerical integrations in the earlier ones were limited within the bay (north region above Kurihama). Two openings for navigation, each of 500 m, were situated on east and west ends of the dike. The openings have been removed in our calculation to the centre of the dike according to the recommendation by P. Ph. Jansen and J.J. Dronkers (1962). In order to give more precise boundary conditions the region of numerical integration has been extended, about nine times in area, to the outer part of the bay into the Pacific Ocean where the depth is a thousand meter or more.

In these calculations, great difficulties are encounted because we can no more neglect as usually done the non-linear inertial terms at the opening. Further computational problems are experienced by introduction of the Coriolis force and a quadratic form of bottom friction which in the earlier computations is approximated by a linear form. These will be discussed as the stability problem of the finite-difference equations.

Sometimes, it is convenient to divide the numerical integration region into two or more sub-regions, the mesh dimensions of which are not equal. In this computation, the integration area has been extended from Tokyo Bay(about 1000 km^2) to the outer region (about 9000 km^2). A method is described to calculate the two regions by one procedure.

MATHEMATICAL PROBLEMS

FUNDAMENTAL EQUATIONS AND BOUNDARY CONDITIONS

The hydrodynamic equations of motion and continuity in two-dimension are represented, with use of the volume of water transported in unit time across vertical section of unit width between the free surface and the bottom, by

$$\frac{\partial M}{\partial t}+\frac{M}{(h+\zeta)}\frac{\partial M}{\partial x}+\frac{N}{(h+\zeta)}\frac{\partial M}{\partial y}=-g(h+\zeta)\frac{\partial(\zeta-\zeta_o)}{\partial x}+fN-\frac{\tau_b^{(x)}}{\rho_W}+\frac{\tau_s^{(x)}}{\rho_W} \tag{1}$$

$$\frac{\partial N}{\partial t}+\frac{M}{(h+\zeta)}\frac{\partial N}{\partial x}+\frac{N}{(h+\zeta)}\frac{\partial N}{\partial y}=-g(h+\zeta)\frac{\partial(\zeta-\zeta_o)}{\partial y}-fM-\frac{\tau_b^{(y)}}{\rho_W}+\frac{\tau_s^{(y)}}{\rho_W} \tag{2}$$

$$\frac{\partial \zeta}{\partial t}=-\left(\frac{\partial M}{\partial x}+\frac{\partial N}{\partial y}\right) \tag{3}$$

where t = time coordinate
x, y = coordinate system (x = east, y = north direction)
U, V = velocity components taken as means in vertical line, in x and y direction respectively
$M = UH$
$N = VH$
$H = h + \zeta$
h = mean water depth
ζ = elevation above mean sea-level
$\zeta_0 = \Delta p/\rho_w g$
Δp = atmospheric pressure drop
$f = 2\omega \sin\varphi$, Coriolis parameter
ω = angular speed of the rotation of the earth
φ = latitude
g = acceleration of gravity
ρ_w = specific weight of water

External forces, τ_s (wind stress), τ_b (bottom friction) and ζ_0 are given by

$$\vec{\tau}_s = \rho_a \gamma^2 \, |W| W \qquad (\rho_a \gamma^2 = 32 \times 10^{-6}) \tag{4}$$

$$\vec{\tau}_b = \rho_w \gamma^2 \, |V| V - \kappa_s \vec{\tau}_s \tag{5}$$

$$\zeta_0 = \frac{a}{\rho_w g} \left\{ 1 + \left(\frac{r}{r_0}\right)^2 \right\}^{-\frac{1}{2}} \tag{6}$$

where the wind velocity W is represented by eqs. (7) and (8)

$$W_y = C_1 U_x \exp\left(-\frac{r\pi}{5 \times 10^7}\right) - \frac{C_2 f}{2} \left[-1 + \sqrt{1 + \frac{4a}{\rho_a f^2} \cdot \frac{1}{r_0^2 \left\{1 + \left(\frac{r}{r_0}\right)^2\right\}^{\frac{3}{2}}}} \right] \tag{7}$$
$$(0.500x + 0.866y)$$

$$W_y = C_1 U_y \exp\left(-\frac{r\pi}{5 \times 10^7}\right) - \frac{C_2 f}{2} \left[-1 + \sqrt{1 + \frac{4a}{\rho_a f^2} \cdot \frac{1}{r_0^2 \left\{1 + \left(\frac{r}{r_0}\right)^2\right\}^{\frac{3}{2}}}} \right] \tag{8}$$
$$(0.866x - 0.500y)$$

r = distance from the centre of a tropical cyclone (typhoon)
a, r_0 = constants referred to the intensity and range of typhoon, respectively
U_x, U_y = speed of center of typhoon
C_1, C_2 = constants
$V = U + iV$

Equation (6) is an empirical formula by Fujita giving atmospheric pressure drop due to cyclone. Eqs. (7) and (8) are derived from eq. (6).

Boundary conditions are given as follows: On natural coastal lines,

there exists no mass transport, M = N = 0. Also the mass transport perpendicular to the axis of the dike is zero. Elevations of water level on boundaries in the Pacific Ocean are given equal to the sum of the water-level rises due to the atmospheric pressure drop (ζ_0) and the astronomical or daily tides (ζ_*); $\zeta = \zeta_0 + \zeta_*$.

STABILITY OF FINITE-DIFFERENCE EQUATION

To carry out the numerical integration, the hydrodynamic equations are to be reduced to the finite difference forms. It is well known that for numerical stability of successive calculations a relationship between the space-difference $\triangle s$ and the time-difference $\triangle t$ should be satisfied such as

$$\frac{\Delta s}{\Delta t} \geq \sqrt{2gh_{max}} \tag{9}$$

This is the so-called "Courant-Friedrichs-Lewy criterion." One should use such small time-steps that the above condition is well fulfilled.

Besides of this, a complicated problem is provoked when non-linear terms such as a quadratic form of bottom friction and the inertial terms are taken into account.

One way to investigate the numerical stability is an numerical experiments to decide what forms of the innumerable finite-difference versions are stable. Shuman (1962), with a numerical experience of one-dimensional model, showed that the semi-momentum and the filtered factor forms exhibited no significant instability.

However, in our case, the change of the inertial term, especially at the opening, is so local that neither of the finite-difference forms recommended by Shuman was available.

Therefore, the stability problems were investigated as described in the followings

In order to clarify the logic, we will discuss the stable finite-difference forms of three elementary types of partial differential equations.

a) Firstly, the simple differential equation (10) will be treated.

$$\frac{dM}{dt} = aM + f(t) \tag{10}$$

Denoting $(M)_{t=n\Delta t}$ by M^n, equation (10) can be reduced to equation (11),

$$(M^{n+1} - M^{n-1})/2\triangle t = aM^n + f(n) \tag{11}$$

A vector defined by $X^n = (M^n, M^{n-1})$ is transformed into a vector $X^{n+1} = (M^{n+1}, M^n)$ through a linear operator R

$$R = \begin{pmatrix} 2a\triangle t & 1 \\ 1 & 0 \end{pmatrix} \tag{12}$$

The eigenvalue λ of the operator R is given by

$$\lambda = a\triangle t \pm \sqrt{a^2\triangle t^2 + 1} \tag{13}$$

For $a < 0$, λ becomes $|\lambda| > 1$. Thus, the finite-difference equation (11) is always unstable for $a < 0$. A stable finite-difference form is obtained

by replacing the term aM^n in eq.(11) by $a(M^{n+1}+M^{n-1})/2$ as demonstrated in the next section.

b) Next, the partial differential equations which include the Coriolis force and the bottom friction of quadratic form will be treated,

$$\frac{\partial M}{\partial t} = fN - eM\sqrt{M^2+N^2} + C_1 \tag{14}$$

$$\frac{\partial N}{\partial t} = -fM - eN\sqrt{M^2+N^2} + C_2 \ . \tag{15}$$

$$(M = M_o , N = N_o \quad at \quad t = t_o)$$

It will easily be seen from the result of a)that eqs. (14) and (15) should not be reduced as

$$\frac{M^{n+1}-M^{n-1}}{2\triangle t} = fN^n - \{ e\sqrt{(M^n)^2+(N^n)^2}\ \}M^n + C_1 \ . \tag{16}$$

However, the following forms, eqs. (17) and (18) may be shown to be stable,

$$\frac{M^{n+1}-M^{n-1}}{2\Delta t} = fN^n - \frac{e}{2}(M^{n+1}+M^{n-1})\sqrt{(M^n)^2+(N^n)^2} + C_1 \tag{17}$$

$$\frac{N^{n+1}-N^{n-1}}{2\triangle t} = -fM^n - \frac{e}{2}(N^{n+1}+N^{n-1})\sqrt{(M^n)^2+(N^n)^2} + C_2 \ . \tag{18}$$

Here, transformations as follows are introduced,

$$\left.\begin{aligned} \alpha &= \frac{1-e\Delta t\sqrt{(M^n)^2+(N^n)^2}}{1+e\Delta t\sqrt{(M^n)^2+(N^n)^2}} \ ; \ \beta = \frac{2f\Delta t}{1+e\Delta t\sqrt{(M^n)^2+(N^n)^2}} \\ \gamma_1 &= \frac{2C_1\Delta t}{1+e\Delta t\sqrt{(M^n)^2+(N^n)^2}} \ ; \ \gamma_2 = \frac{2C_2\Delta t}{1+e\Delta t\sqrt{(M^n)^2+(N^n)^2}} \end{aligned}\right\} \tag{19}$$

Considering the fact that the divergence of step-by-step calculations due to instability grows within a few decade of steps the factors α, β, γ_1, and γ_2 may be treated as constants.
Equations (17) and (18) are represented as

$$M^{n+1} = \alpha M^{n-1} + \beta M^n + \gamma_1 \tag{20}$$

$$N^{n+1} = \alpha N^{n-1} - \beta M^n + \gamma_2 \tag{21}$$

Furthermore, they can be rewritten using the matrix expression,

$$X_1 = \begin{bmatrix} M^{1-1} \\ N^{1-1} \\ M^1 \\ N^1 \end{bmatrix} \ , \ Y = \begin{bmatrix} 0 \\ 0 \\ \gamma_1 \\ \gamma_2 \end{bmatrix} \ ; \ R = \begin{bmatrix} 0 & 0 & 1 & 0 \\ 0 & 0 & 0 & 1 \\ \alpha & 0 & 0 & \beta \\ 0 & \alpha & -\beta & 0 \end{bmatrix} \tag{22}$$

$$X_{n+1} = RX_n + Y \ . \tag{23}$$

By repetition, eq. (23) reduces to

$$X_{n+1} = R^n X_1 + (R^{n-1} + R^{n-2} + \cdots + R^2 + R + E)\,Y \tag{24}$$

where E means the unit matrix of four dimensions. Therefore, the stability condition for the finite difference equation is given such that the absolute values of all roots of secular equation (25)

$$|\lambda E - R| = (\lambda^2 - \alpha)^2 + \beta^2\lambda^2 = 0 \tag{25}$$

should be smaller than unity or at the most one of the roots may be equal to unity but it should not be double roots. Because $0<\beta \ll \alpha<1$, eigenvalues λ of the determinant R ($|\lambda|^2 = \alpha$) are smaller than unity. As a consequence, the finite-difference equations of the form eqs. (17) and (18) are shown to be stable.

c) Two finite difference versions of the inertial term abreviated as eq. (27) are considered,

$$\frac{\partial u}{\partial t} = -u\frac{\partial u}{\partial x} + f(t,x)\ (0<x<1,\ u(0)=u(1)=0) \tag{26}$$

$$\text{(I)}\quad \frac{u_i^{n+1}-u_i^n}{\Delta t} = -\overline{u_i^n}\,\frac{(u_{i+1}^n - u_{i-1}^n)}{2\Delta x} + f_i^n \tag{27}$$

$$\text{(II)}\quad \frac{u_i^{n+1}-u_i^n}{\Delta t} = -\overline{u_i^n}\,\frac{(u_{i+1}^n - u_i^n)}{\Delta x} + f_i^n \qquad (\overline{u_i^n} \le 0) \tag{28}$$

$$\frac{u_i^{n+1}-u_i^n}{\Delta t} = -\overline{u_i^n}\,\frac{(u_i^n - u_{i-1}^n)}{\Delta x} + f_i^n \qquad (\overline{u_i^n} \ge 0) \tag{29}$$

where suffix i refers to a mesh-point and n to a time-step

Let $r = -\overline{u_i^n}\,\Delta t/\Delta x$, $V_i = u_i^{n+1}$ and $u_i = u_i^n$. A (n-1)-dimensional vector $\vec{u} = (u_1, u_2, \cdots, u_{n-1})$ is transformed to a vector $\vec{V} = (v_1, v_2, \cdots, u_{n-1})$ through operators R_I (for eq. (27)), R_{II} (for eq. (28)) and R_{II}' (for eq. (29)),

$$\text{(I)}\quad R_I : v_i = u_i + \frac{r}{2}(u_{i+1} - u_{i-1})\ (i=1, 2, \cdots, N-1) \tag{30}$$

$$\text{(II)}\quad R_{II} : v_i = (1-r)u_i + ru_{i+1} \qquad (r>0) \tag{31}$$

$$R_{II}' : v_i = (1+r)u_i - ru_{i-1} \qquad (r<0) \tag{32}$$

where matrices are represented by

$$R_I = \begin{bmatrix} 1 & r/2 & & & 0 \\ -r/2 & 1 & r/2 & & \\ & -r/2 & 1 & r/2 & \\ & & \ddots & \ddots & \ddots \\ & & & -r/2 & 1 & r/2 \\ 0 & & & & r/2 & 1 \end{bmatrix} \tag{33}$$

$$R_{II} = \begin{bmatrix} 1-r & r & & & \\ 0 & 1-r & r & & \\ & 0 & 1-r & r & \\ & & \ddots & \ddots & \ddots \\ & & & 0 & 1-r & r \\ & & & & 0 & 1-r \end{bmatrix} \qquad R_{II}' = \begin{bmatrix} 1-r & 0 & & & \\ -r & 1-r & 0 & & \\ & -r & 1-r & 0 & \\ & & \ddots & \ddots & \ddots \\ & & & -r & 1-r & 0 \\ & & & & -r & 1-r \end{bmatrix} \tag{34}$$

Eigenvalues of the matrix R_I are sum of eigenvalues of the matrix $S = R_I - E$ and 1. While, the matrix S being skew-symmetric, eigenvalues are purely immaginary Therefore, the absolute value of eigenvalues of R_I is always greater than unity. The finite-difference of (27) cannot be stable.

Whereas, eigenvalues of R_{II} and R_{II}' are $(1 - r)$ $(r \geq 0)$ and $(1 + r)$ $(r \leq 0)$, respectively. Thus, eqs. (28) and (29) are numerically stable.

In fact, our earlier calculations showed that the finite-difference form of the bottom friction and the Coriolis force such as

$$\frac{M^{n+1} - M^{n-1}}{2\Delta t} = fN^n - \{ g \sqrt{(M^n)^2 + (N^n)^2} \} \cdot M^n + C$$

produced the divergence of step by step calculation. Also, the finite-difference forms of the inertial terms such as

$$-\frac{N_{J,k}^n}{(h+\zeta)} \quad \frac{N_{J,k+1}^n - N_{J,k-1}^n}{2\Delta s} \quad \text{or} \quad -\frac{N_{J,k}^{n+1} + N_{J,k}^n}{2(h+\zeta)} \cdot \frac{N_{J,k+1}^n - N_{J,k-1}^n}{2\Delta s}$$

were very unstable yielding the divergence of numerical solution

Finally, from the above mentioned discussions, a set of stable finite-difference equations is derived.

$$M_{J,k}^{n+2} = \frac{1}{[1 + \frac{c}{2} d(x,y) \sqrt{(M_{J,k}^n)^2 + (N_{J,k}^n)^2}]} [M_{J,k}^n - a(x,y) \{ \zeta_{J+1,k}^{n+1} - \zeta_{0\,J-1,k}^{n+1} - \zeta_{J-1,k}^{n+1} + \zeta_{0\,J+1,k}^{n+1} \} + bN_{J,k}^{n+1} - \frac{c}{2} \{ d(x,y) M_{J,k}^n \sqrt{(M_{J,k}^n)^2 + (N_{J,k}^n)^2} - 3\tau_{s\,J,k}^{(x)\,n} \} - I_{11} - I_{12}] \tag{35}$$

where

$$I_{11} \begin{cases} = f(x,y) M_{J,k}^n \{ M_{J,k}^n - M_{J-1,k}^n \} & (M_{J,k}^n \geq 0) \\ = f(x,y) M_{J,k}^n \{ M_{J+1,k}^n - M_{J,k}^n \} & (M_{J,k}^n < 0) \end{cases} \tag{35a}$$

$$I_{12} \begin{cases} = f(x,y) N_{J,k}^n \{ M_{J,k}^n - M_{J,k-1}^n \} & (M_{J,k}^n \geq 0) \\ = f(x,y) N_{J,k}^n \{ M_{J,k+1}^n - M_{J,k}^n \} & (N_{J,k}^n < 0) \end{cases} \tag{35b}$$

$$N_{J,k}^{n+2} = \frac{1}{[1 + \frac{c}{2} d(x,y) \sqrt{(M_{J,k}^n)^2 + (N_{J,k}^n)^2}]} [N_{J,k}^n - a(x,y) \{ \zeta_{J,k+1}^{n+1} - \zeta_{0J,k-1}^{n+1} - \zeta_{J,k-1}^{n+1} + \zeta_{0J,k-1}^{n+1} \} - bM_{J,k}^{n+1} - \frac{c}{2} \{ d(x,y) N_{J,k}^n \sqrt{(M_{J,k}^n)^2 + (N_{J,k}^n)^2} - 3\tau_{J,k}^{s(x)} \} - I_{21} - I_{22}] \tag{36}$$

where

$$I_{21} \begin{cases} = f(x,y) M_{J,k}^n \{ N_{J,k}^n - N_{J-1,k}^n \} & (M_{J,k}^n \geq 0) \\ = f(x,y) M_{J,k}^n \{ N_{J+1,k}^n - N_{J,k}^n \} & (M_{J,k}^n < 0) \end{cases} \tag{36a}$$

$$I_{22}\begin{cases} =f(x,y)N^{n}_{j,k}\{N^{n}_{j,k}-N^{n}_{j,k-1}\} & (N^{n}_{j,k}\geq 0) \\ =f(x,y)N^{n}_{j,k}\{N^{n}_{j,k+1}-N^{n}_{j,k}\} & (N^{n}_{j,k}<0) \end{cases} \tag{36b}$$

$$\zeta^{n+3}_{j,k}=\zeta^{n+1}_{j,k}-\Theta\{M^{n+2}_{j+1,k}-M^{n+2}_{j-1,k}+N^{n+2}_{j,k+1}-N^{n+2}_{j,k-1}\} \tag{37}$$

At the opening point (m, n), the value $N_{m,n}(=V_{m,n}(h+\zeta))$ is replaced by $N^{*}_{m,n}$, denoting an opening width by ℓ

$$N^{*}_{m,n}=\frac{\ell}{2\Delta s}N_{m,n}\ . \tag{38}$$

Coefficients in the above equations are given below,

$$a(x,y)=g(h+\zeta)\Delta t/\Delta s \qquad b=4\omega(\sin\varphi)\Delta t=2f\Delta t$$
$$c=2\Delta t/\rho_w \qquad d(x,y)=\gamma_b^2\rho_w/(h+\zeta)^2$$
$$e=\Delta t/\Delta s \qquad f(x,y)=2\Delta t/(h+\zeta)\Delta s$$

where $a(x,y)$, $d(x,y)$ and $f(x,y)$ may be computed every n-th time-step (in our case every 20 min = $40\Delta t$), because they vary very slowly.

The variables thus computed must be smoothed by adding a certain proportion of the mean value computed from the four surrounding points after completion of n-th time-step, to obtain a probale value, e.g.

$$(M^{n}_{j,k})=\alpha M^{n}_{j,k}+\frac{1-\alpha}{4}(M^{n}_{j+1,k}+M^{n}_{j-1,k}+M^{n}_{j,k+1}+M^{n}_{j,k+1}) \tag{39}$$
$$(0\leq\alpha\leq 1)$$

For economy of the computation time, the discharge fluxes, M and N have been calculated every odd time step, and the elevation ζ every even time step. Likewise, the grid points for M, N and ζ were arranged alternatively, i.e. the values of M and N were determined on grid points where water depths are assigned in Fig. 1, the values of ζ on grid points where depths are not written.

CONNECTION OF SUBREGIONS

In our study of the Typhoon tide prediction, the numerical integration region was inevitably divided into two regions (Fig. 1). Because the water depths differ greatly between the inside and the outside of the entrance of the bay, the stability condition for grid dimensions, eq. (9), requires entirely different grid width for each of the two regions. In such a case, usual prediction precedures are too much cumbersome. Firstly, a rough calculation is made either for both regions with the same rough grid as the outer or only for the outer region neglecting the smaller one, to obtain the change of the water level at the entrance of the bay-the boundary condition for the second calculation. Using the values of ζ at the entrance thus determined as input data, the second precise computation may be carried out for the very interested region with finer grid width.

In order to complete the calculation by one procedure, the two regions are to be overlapped at the neck of the bay. Grid points B, C, D and E in Fig. 2 stand in common for both regions. (In Fig. 2, circles show points for M and N, crosses for ζ). The values of M and N at D as

a grid point of the outer subregion are decided as mean values at points on X - Y determined by calculation in the inner subregion On the other hand, the values of ζ on B - C to be used as boundary condition for the inner are chosen equal to that at E determined from the outer region. The values of ζ on X" - Y" may be obtained from values of M and N in the inner region one time-step before. Thus, ζ on X' - Y' may be determined as mean of four surrounding points on B - C and X" - Y".

NUMERICAL CALCULATION

MODEL OF TYPHOON

Before a series of detailed numerical calculations, reliability of prediction procedures was checked by comparison of a record of an observed surge (caused by Typhoon No 5821) with calculation. Considerably good agreement between them was confirmed. (Fig. 3 is an example of comparisons.)

A model of typhoon was chosen as that which caused the severest damages ever experienced in Japan, named the Ise-Bay Typhoon. The typhoon was assumed to proceed northwards along the course parallel to axis of the bay about 40 km west of Tokyo with speed of 73 km/hr (A-course in Fig. 4). Subsidarily, two other courses (named E- and I-course) were also investigated. In the earlier study, several courses parallel to them were compared to decide the worst ones. Course A coincides with that of a typhoon (attacked on Oct. 1, 1917) which caused the severest damages on coast of the ba

Constants used in this study are as follows:

Typhoon : $a = 7 \times 10^4$ (dyne/cm^2), $a/\rho_w g = 71.5$ (cm), $r_0 = 7.5 \times 10^6$ (cm), $\zeta_o = 1.028 \times 10^3$ (cm), $V = 2.02 \times 10^3$ (cm/sec) (speed of Typhoon), $\rho_a = 1.293 \times 10^{-3}$ (gr/cm^3), $C_1 \approx 4/7$, $C_2 \approx 0.6$

Grid : $\Delta s = 1.5 \times 10^5$ (cm) (for the inner region) and 6×10^5 (cm) (for the outer region), $\Delta t = 30$ (sec),

External faces : $\gamma^2 \rho_a = 3.2 \times 10^{-6}$ (gr/cm^3), $\gamma_b^2 \rho_w = 2.6 \times 10^{-3}$, $k = 0.5$.

EFFECT OF DIKE ON REDUCTION OF SURGES

The opening of the dike should preferablly be wide from the standpoint of navigation. On the other hand, the effects of the dike on the reduction of surges will be increased with decrease in the opening width. Here, we must determine the most preferable opening width to suffice both requirements.

A series of computations has been carried out for different opening widths, i.e. for a) the present state (no dike), for the central opening with length b) 2000 m, c) 1000 m, d) 1000 m (with shallow opening depth: Hop = 21 m) and e) 500 m and for f) two openings each 500 m at both ends of the dike.

In these calculations, the Coriolis force and the quadratic type of bottom friction are considered at every grid point. However, the inertial term is considered only at the opening where it becomes exceedingly predominant. An alternative of the inertial-term method is to make use of discharge coefficient due to contraction ($V_{m,n} = \pm K\sqrt{2g\,|\zeta_{m,n+1} - \zeta_{m,n-1}|}$) Both the methods have been shown to give the same results [Unoki and Isozaki (1962)] . Fig. 5 shows comprehensively results of computations for the course A, illustrating the reduction of maximum surge elevation with decreasing opening width. The time variations of elevations with

progress of the typhoon are given in Fig. 6. Fig. 7 is graphs of contour lines (in cm) every one hour. A peak water level at Chiba occurs at 8 h 20 m.

Figs. 8 and 9 give results for the courses E and I respectively.

For typhoons along the course-A, empirical relations, eq. (40), between the maximum water level inside the dike and the opening area have been obtained as shown in Fig. 10,

$$\zeta_{max} = a + m \log A \quad (1.3 \times 10^4 \ m^2 \leq A \leq 5.5 \times 10^4 \ m^2) . \qquad (40)$$

where A means the cross sectional area of opening, a constant m is almost independent of the position of observation,while a in eq. (40) is a constant dependent on position. The location of openings has almost no direct influence on the effect of the dike. It should be noticed that there results no appreciable increase in peak water level in the outside of the dike. In some cases, the maximum water levels in the outside rather decrease slightly.

DAILY TIDE AND DISCHARGE VELOCITY AT THE OPENING

Numerical calculation of the astronomical tide (the semi-diurnal M_2 tide) for the present state has been compared with the estimated in Fig. 11, showing a remarkably good agreement between them. In order to protect the dike from erosion and to secure the safety of navigation, the maximum discharge velocity at the opening should not exceed some limit.

A model of spring tide which is composed of 13 components has been assumed to estimate the maximum discharge velocity. It amounts to 1.9 m/sec and 2.0 m/sec for opening (length 1000 m) with depths of 28 m and 21 m, respectively. (Fig. 12)

INTERACTION BETWEEN DAILY TIDE AND TYPHOON TIDE

As far as the above treatments are concerned, we considered only the water level rise due to tropical cyclones In practice, the catastrophic damages have been experienced when peak storm surges superposed on high tidal level. Superposition of both phenomena may be allowed in the cases where effects of non-linear terms are negligible. However, in our study of the dike across the Bay, the inertial terms govern so strictly the liquid motion that we can no more admit the superposition.

Because the motivation of tidal motion is given at the boundary of integration region, the stationary movement of tide can be attained after about 36 hours from the beginning (Fig. 11). As a consequence, it needs very long computation time to obtain exact solutions of the problem of superposition.

Figs. 13 and 14 are supplied to demonstrate that the superposition of daily tide and typhoon tide overestimates surge elevations. In these computations, the peak of storm surge is chosen to occur just at high tidal level.

The amounts of reduction in maximum surge elevation within the dike are far increased as a result of interaction. Thus, the construction of dike is extremely effective.

For the outside of the dike, superposition may be admitted.

Maximum velocity at the opening is given to be 3.25 m/sec (width 1000 m, depth 28 m). (Fig. 12b)

EFFECT OF TYPHOON SPEED AND WIND STRESS

Storm surges are affected by a number of factors. Of course, topography is a governing factor. It is a point of practical interest how speed of storm affects the water level rise. In the case of Tokyo Bay, the point has been thoroughly investigated by S. Unoki and I. Isozaki (1962). They concluded from a series of numerical calculations that the speed of Typhoon has no significant effect within the range of speed from 40 km/h to 80 km/h. This is surprising because the average velocity of long waves propagating the bay is about 55 - 60 km/h. There exist no resonance phenomenon in the region limited by a boundary.

Relative contribution of the atmospheric pressure drop and the wind stress is also an interesting problem. Numerical experiments by us for Tokyo Bay (without the dike, the typhoon model A) show that both have the same order of effects (Fig. 15). Of course, in the outer part the effect of atmospheric pressure drop is far predominant over the wind stress (see the curve for Kurihama).

Acknowledgement

The authors are greatly indebted to Dr. S. Unoki, Meteorological Research Institute of Japan, for his valuable advice.

REFERENCES

Ito, T., Watanabe, J., Hino, K. and Hino, M. (1963): Some remarks on numerical prediction of typhoon tide, Proc. 8th Conference on Hydraulic Research, Japan, Japan Soc. Civil Eng.

Ito, T., Hino, M. and Hino, K. (1964): Summary report: Numerical calculations on the effects of the dike across Tokyo Bay on reduction of typhoon tides, Report No.300, Sangyo Keikaku Kaigi (Council for Industry Planning).

Jansen, P. Ph. and Dronkers, J.J. (1962): Memorandum on dike construction as a part of a masterplan for Tokyo Bay. Sangyo Keikaku Kaigi (Council for Industry Planning)

Miyazaki, M. (1961): Chapters 4, 5 and 6 in "Numerical calculations of typhoon tide and counter plans as a part of Neo Tokyo Plan", Sangyo Keikaku Kaigi (Council for Industry Planning).

Sangyo Keikaku Kaigi (Council for Industry Planning) (1961): Recommendations on construction of a dike across Tokyo Bay as a resolution of typhoon tide and traffic problems.

Shuman, F.G. (1962): Numerical experiments with primitive equations. Proc. International Symposium on Numerical Weather Prediction in Tokyo, Nov. 7-13, 1960.

Unoki, S. and Isozaki, I. (1962a): On some results of numerical experiments on typhoon tide. Proc. of 9th Conference on Coastal Engineering, Japan, Japan Soc. Civil Eng.

Unoki, S. and Isozaki, I. (1962b): Comment on numerical calculation of velocity at an opening of dike, ibid. A translated text of the above two papers entitled "On the effect of a dike with openings on the storm surge caused by a typhoon" is collected in Coastal Engineering in Japan, VI (1963).

Welander, P. (1961): Numerical prediction of storm surges.
Advances in Geophysics, vol. 8, Academic Press.

CAPTIONS

Fig. 1. The grid points used in the calculation. Numbers on mesh point mean water depth where discharge fluxes are determined

Fig. 2. Overlapping of two regions. Circles represent grid points where discharge fluxes are to be determined, while crosses correspond to points for water level.

Fig. 3. An example of comparison between observed and calculated storm surges.

Fig. 4. Three typical courses of typhoon. Numbered circles show position of typhoon center every one hour.

Fig. 5. Summary representation of calculated maximum surge elevations on the coast caused by the hypothetical Ise-Bay Typhoon along the A-course.

Fig. 6. Predictions of water levels at various point on coast of Tokyo Bay, showing effects of the dike opening on the reduction of surges

Fig. 7. Contour lines of sea level elevations (in cm) by the Ise-Bay Typhoon along course-A.

Fig. 8. Maximum surge elevations at various points caused by the Ise-Bay Typhoon along course-E.

Fig. 9. Maximum surge elevations caused by the Ise-Bay Typhoon along course-I.

Fig. 10. Empirical relationships between maximum surge elevations at points within the inner part of the dike and the cross sectional area of opening.

Fig. 11. Comparisons of the calculated semi-diurnal M_2 tide with the estimated (at Tokyo and Yokohama).

Fig. 12. Tidal velocity at the opening (calculated results).

Fig. 13. Predictions of water levels at various points, when storm surge occurs at high tidal level.

Fig. 14. Summary representation of maximum surge elevation when surge superposes on high tidal level. Linear superposition of daily tide and storm surge overestimates the maximum when the proposed dike is constructed.

Fig. 15. Relative contribution of atmospheric pressure drop and wind stress. The solid lines represent total effect, the dashed lines the atmospheric pressure effect. The calculation has been made for present state (no dike) with the hypothetical Ise-Bay-Typhoon along course-A.

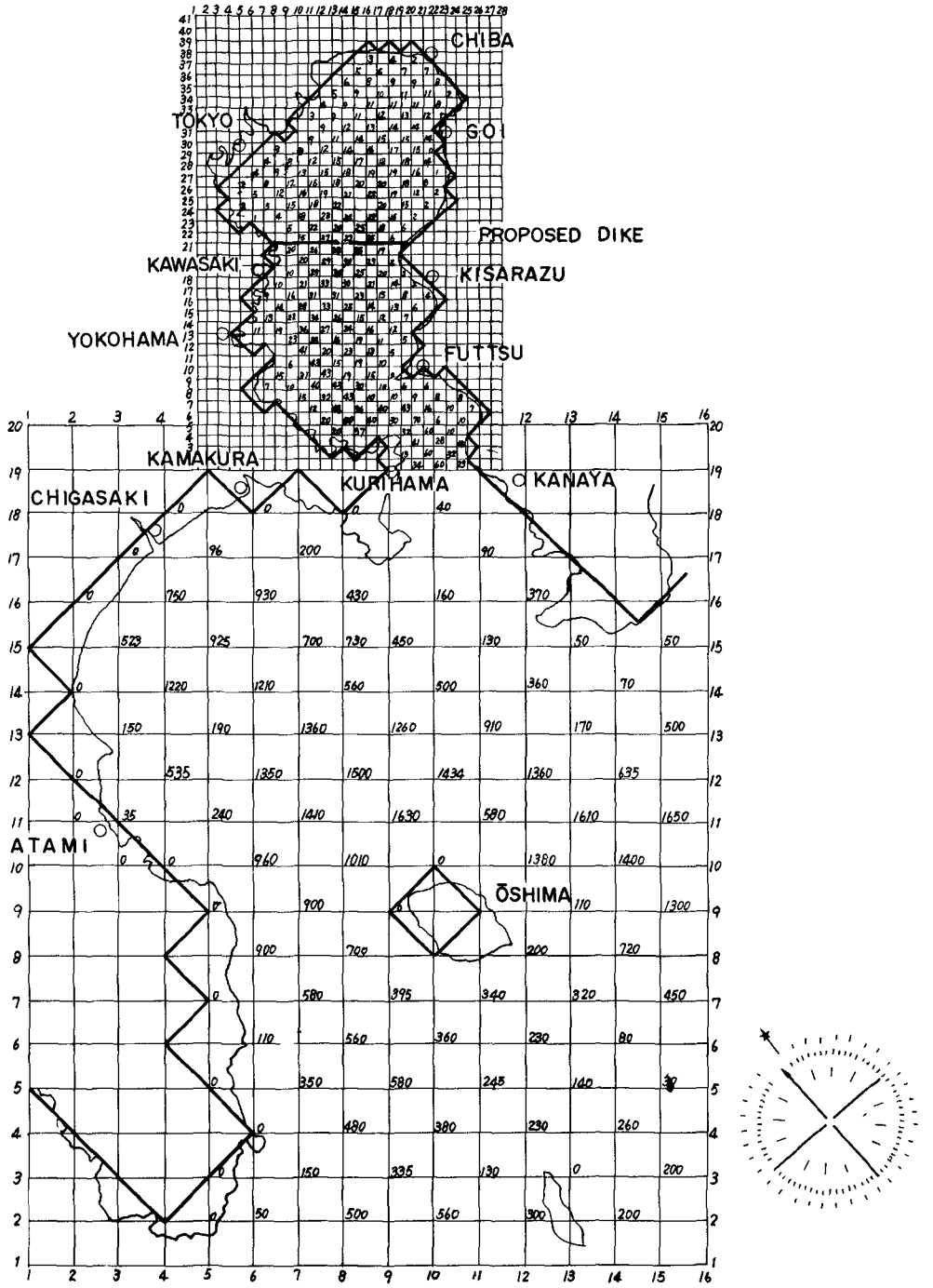
CHIBA
TOKYO
GOI
PROPOSED DIKE
KAWASAKI
KISARAZU
YOKOHAMA
FUTTSU
KAMAKURA
KURIHAMA
KANAYA
CHIGASAKI
ATAMI
ŌSHIMA

FIG - 1

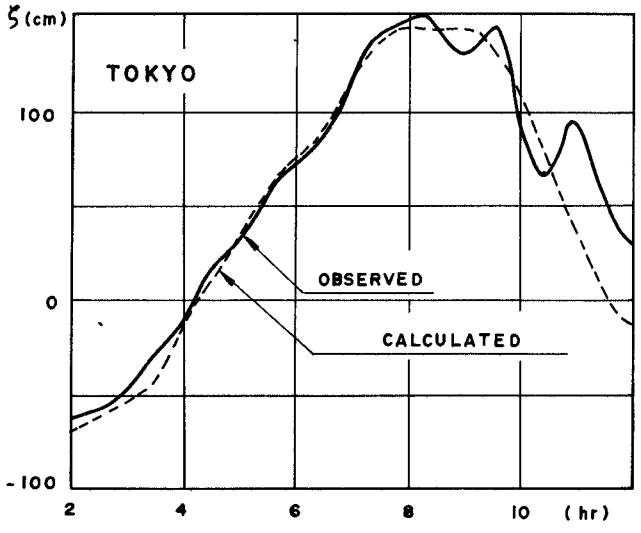
ζ (cm)
TOKYO
100
0
-100
OBSERVED
CALCULATED
2
4
6
8
10
(hr)

FIG - 2

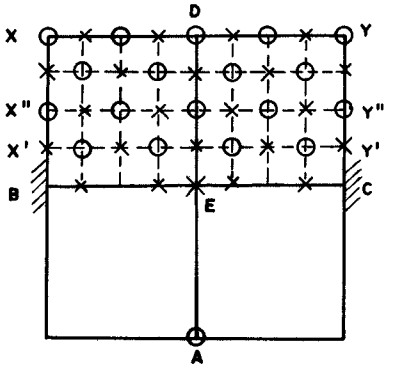
D
X
Y
X"
Y"
X'
Y'
B
C
E
A

FIG - 3

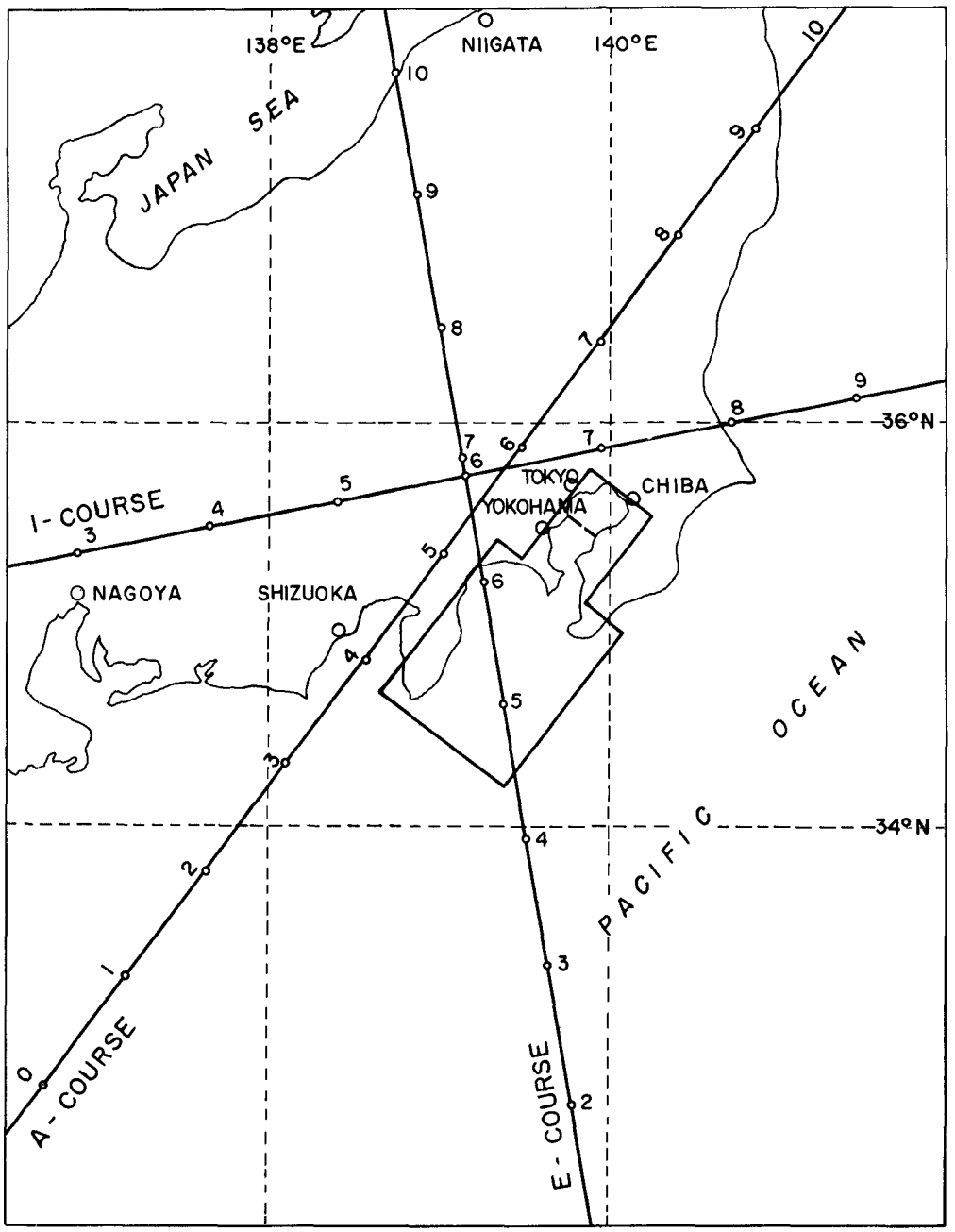
138°E
NIIGATA
140°E
JAPAN SEA
36°N
34°N
I-COURSE
A-COURSE
E-COURSE
TOKYO
YOKOHAMA
CHIBA
NAGOYA
SHIZUOKA
PACIFIC OCEAN

FIG - 4

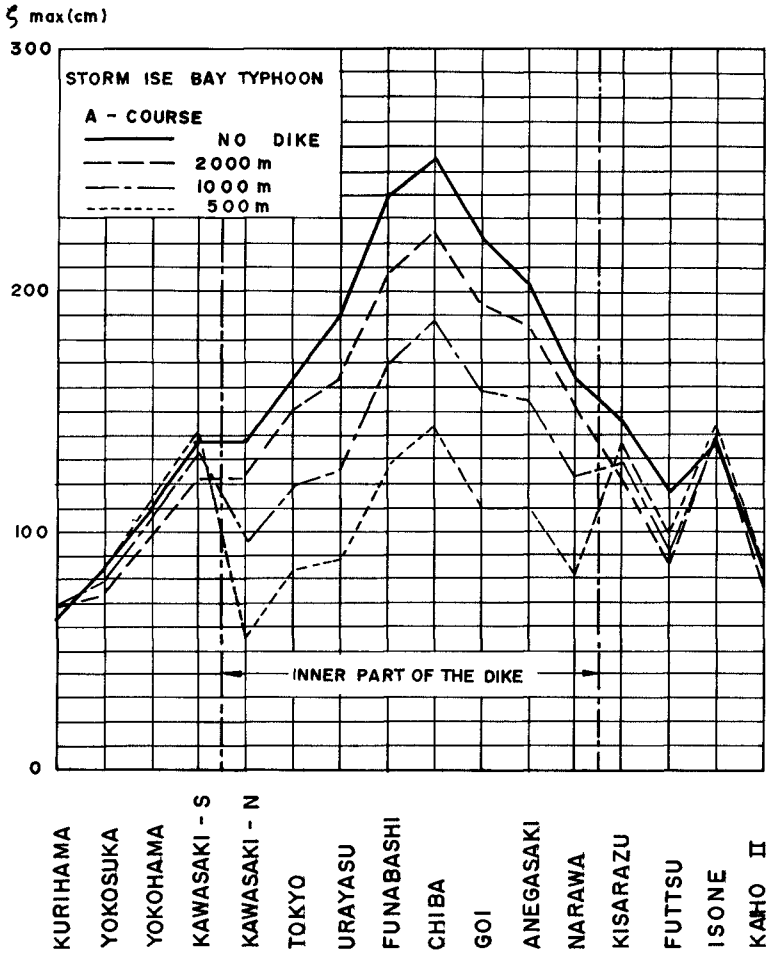
ζ max(cm)
300
200
100
0
STORM ISE BAY TYPHOON
A - COURSE
NO DIKE
2000 m
1000 m
500 m
INNER PART OF THE DIKE
KURIHAMA
YOKOSUKA
YOKOHAMA
KAWASAKI - S
KAWASAKI - N
TOKYO
URAYASU
FUNABASHI
CHIBA
GOI
ANEGASAKI
NARAWA
KISARAZU
FUTTSU
ISONE
KAHO II

FIG - 5

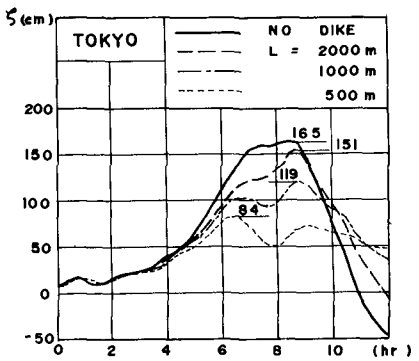
TOKYO
NO DIKE
L = 2000 m
1000 m
500 m
165
151
119
84
ζ(cm)
(hr)

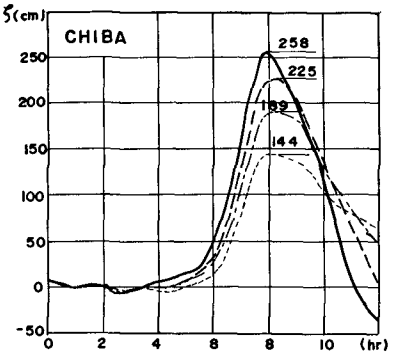
CHIBA
258
225
192
144
ζ(cm)
(hr)

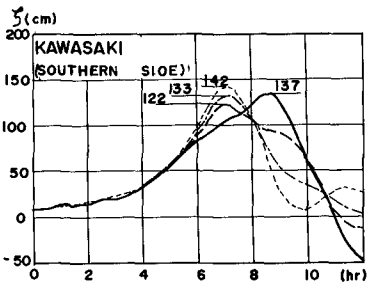
KAWASAKI
(SOUTHERN SIDE)
142
133
122
137
ζ(cm)
(hr)

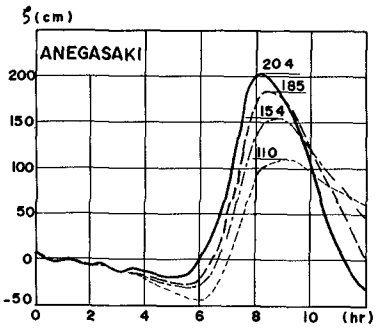
ANEGASAKI
204
185
154
110
ζ(cm)
(hr)

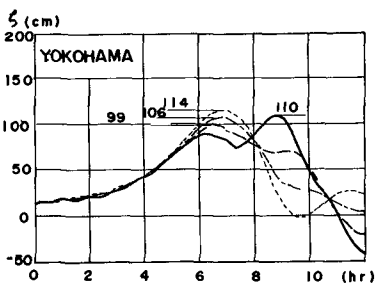
YOKOHAMA
99
106
114
110
ζ(cm)
(hr)

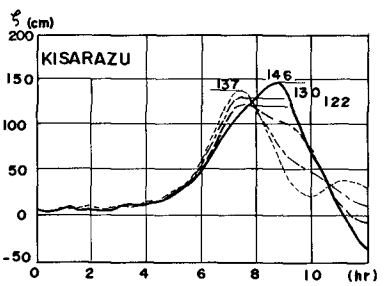
KISARAZU
137
146
130
122
ζ(cm)
(hr)

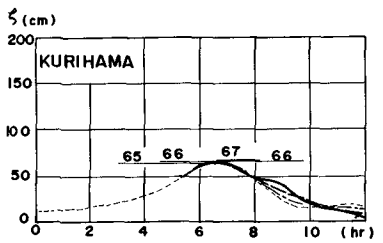
KURIHAMA
65
66
67
66
ζ(cm)
(hr)

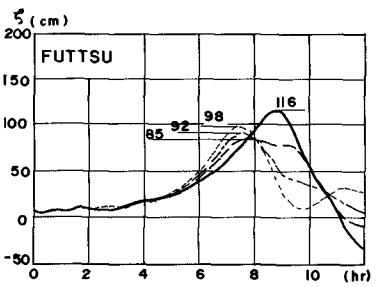
FUTTSU
85
92
98
116
ζ(cm)
(hr)

FIG - 6

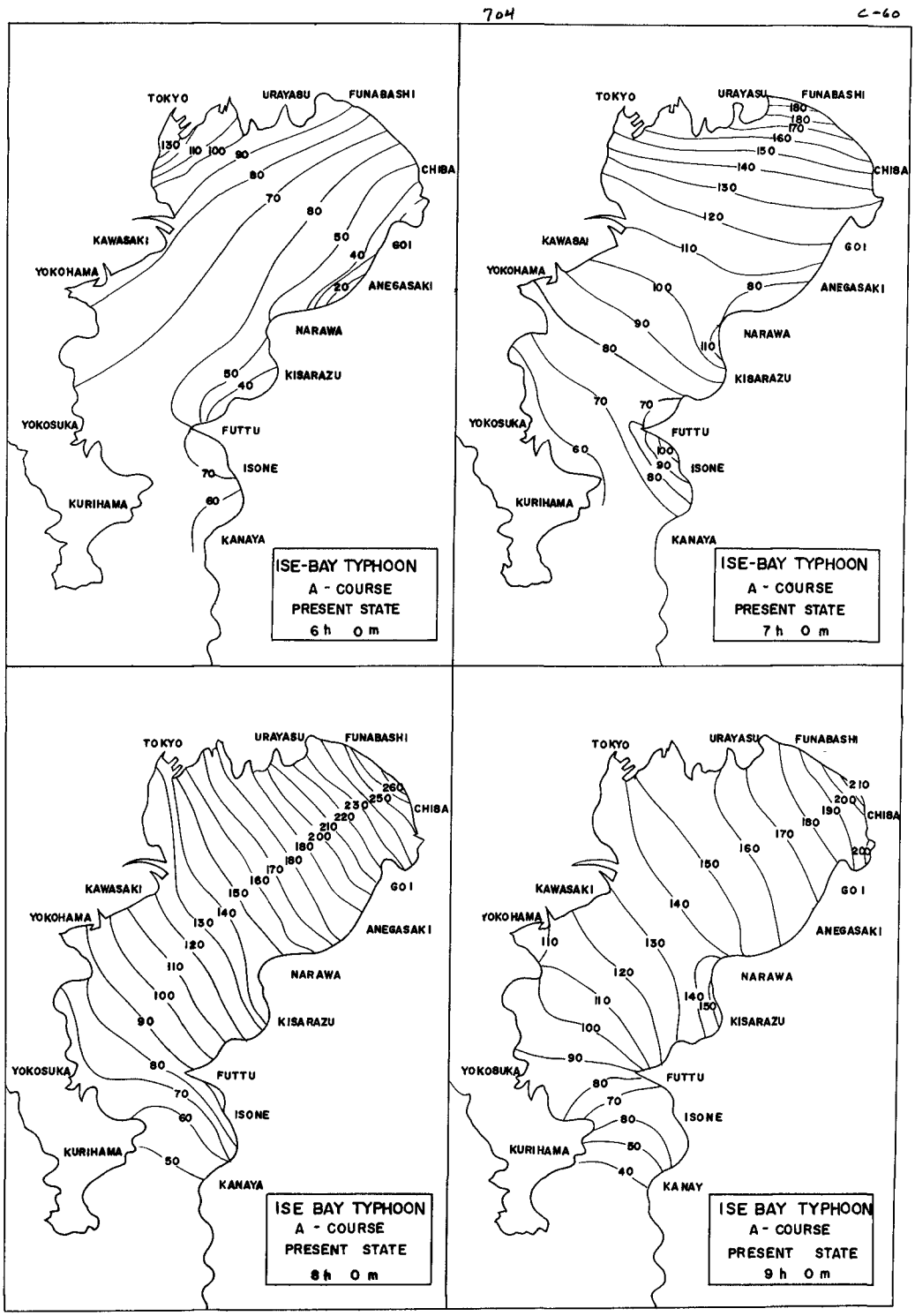
704
C-60
TOKYO
URAYASU
FUNABASHI
CHIBA
KAWASAKI
YOKOHAMA
GOI
ANEGASAKI
NARAWA
KISARAZU
YOKOSUKA
FUTTU
ISONE
KURIHAMA
KANAYA
ISE-BAY TYPHOON
A - COURSE
PRESENT STATE
6 h 0 m
ISE-BAY TYPHOON
A - COURSE
PRESENT STATE
7 h 0 m
ISE BAY TYPHOON
A - COURSE
PRESENT STATE
8 h 0 m
ISE BAY TYPHOON
A - COURSE
PRESENT STATE
9 h 0 m

FIG 7 (a)

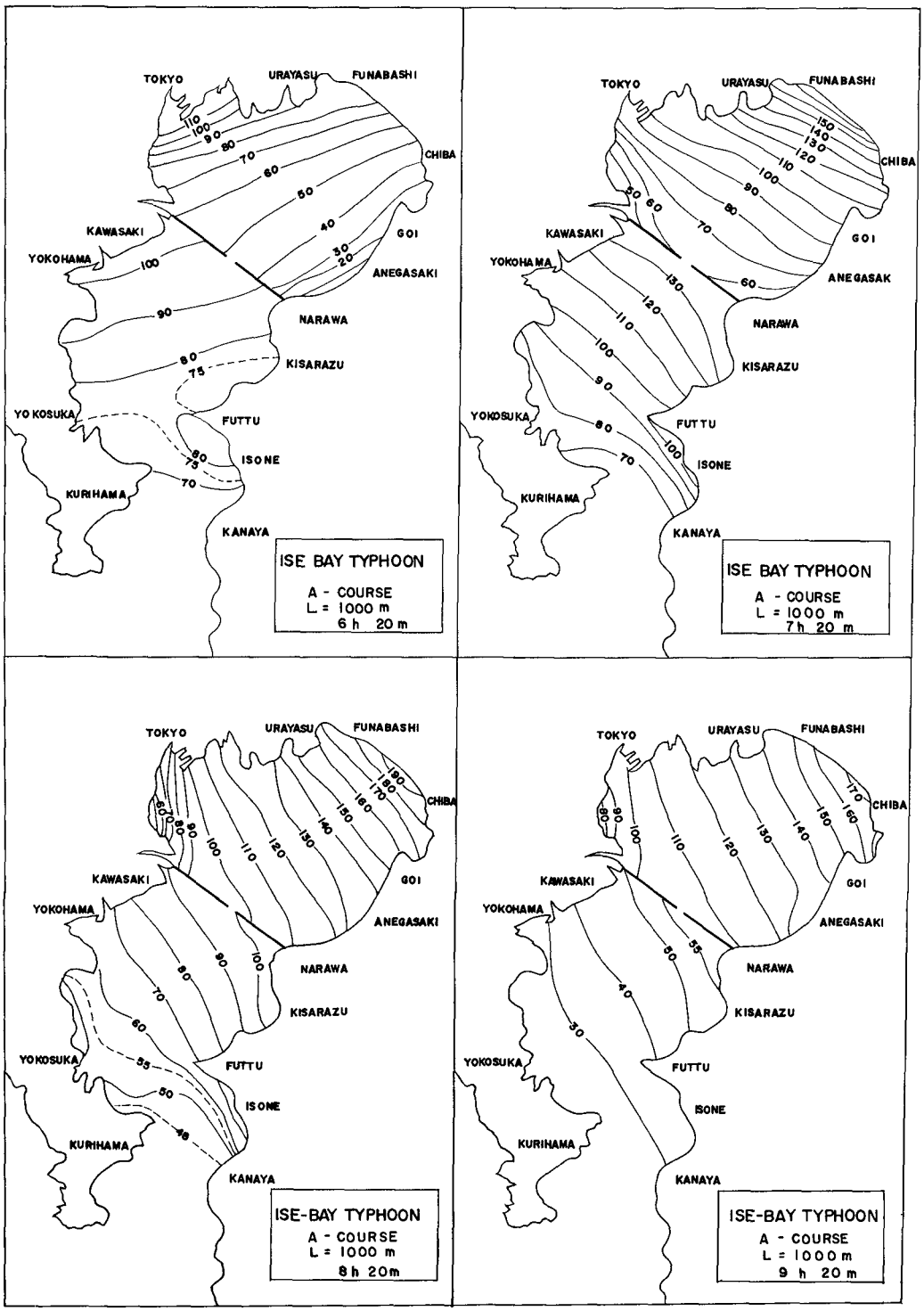
TOKYO
URAYASU
FUNABASHI
CHIBA
GOI
ANEGASAKI
NARAWA
KISARAZU
FUTTU
ISONE
KANAYA
KURIHAMA
YOKOSUKA
KAWASAKI
YOKOHAMA
ISE BAY TYPHOON
A - COURSE
L = 1000 m
6 h 20 m
ISE BAY TYPHOON
A - COURSE
L = 1000 m
7h 20 m
ISE-BAY TYPHOON
A - COURSE
L = 1000 m
8h 20m
ISE-BAY TYPHOON
A - COURSE
L = 1000 m
9 h 20 m

FIG - 7 (b)

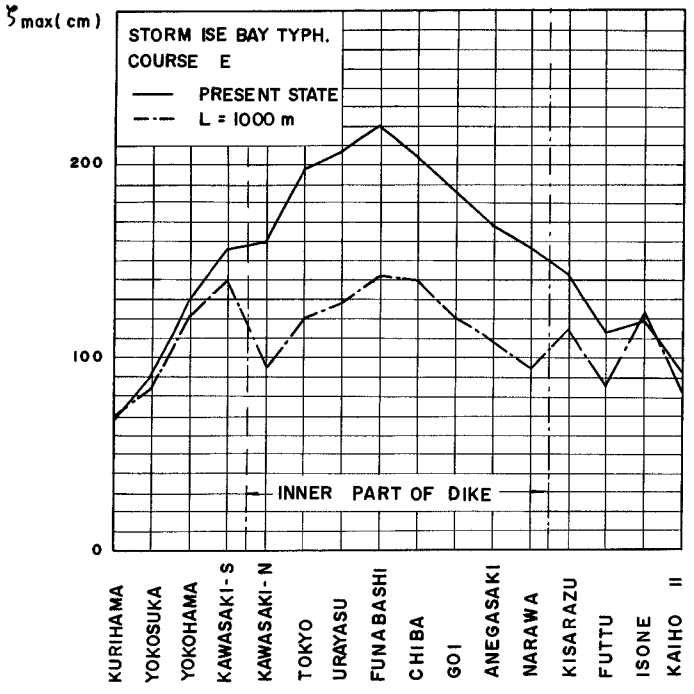
ζmax(cm)
STORM ISE BAY TYPH.
COURSE E
PRESENT STATE
L = 1000 m
200
100
0
INNER PART OF DIKE
KURIHAMA
YOKOSUKA
YOKOHAMA
KAWASAKI-S
KAWASAKI-N
TOKYO
URAYASU
FUNABASHI
CHIBA
GOI
ANEGASAKI
NARAWA
KISARAZU
FUTTU
ISONE
KAIHO II

FIG 8

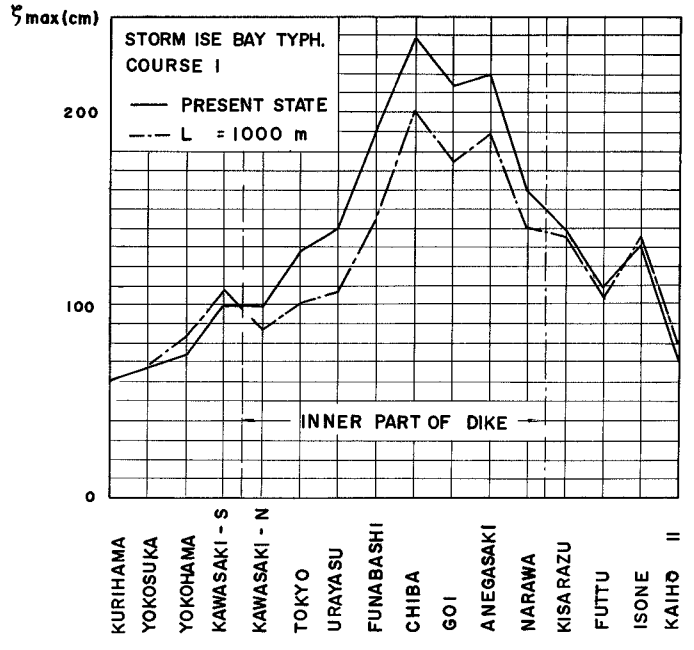
ζmax(cm)
STORM ISE BAY TYPH.
COURSE I
PRESENT STATE
L = 1000 m
200
100
0
INNER PART OF DIKE
KURIHAMA
YOKOSUKA
YOKOHAMA
KAWASAKI-S
KAWASAKI-N
TOKYO
URAYASU
FUNABASHI
CHIBA
GOI
ANEGASAKI
NARAWA
KISARAZU
FUTTU
ISONE
KAIHO II

FIG 9

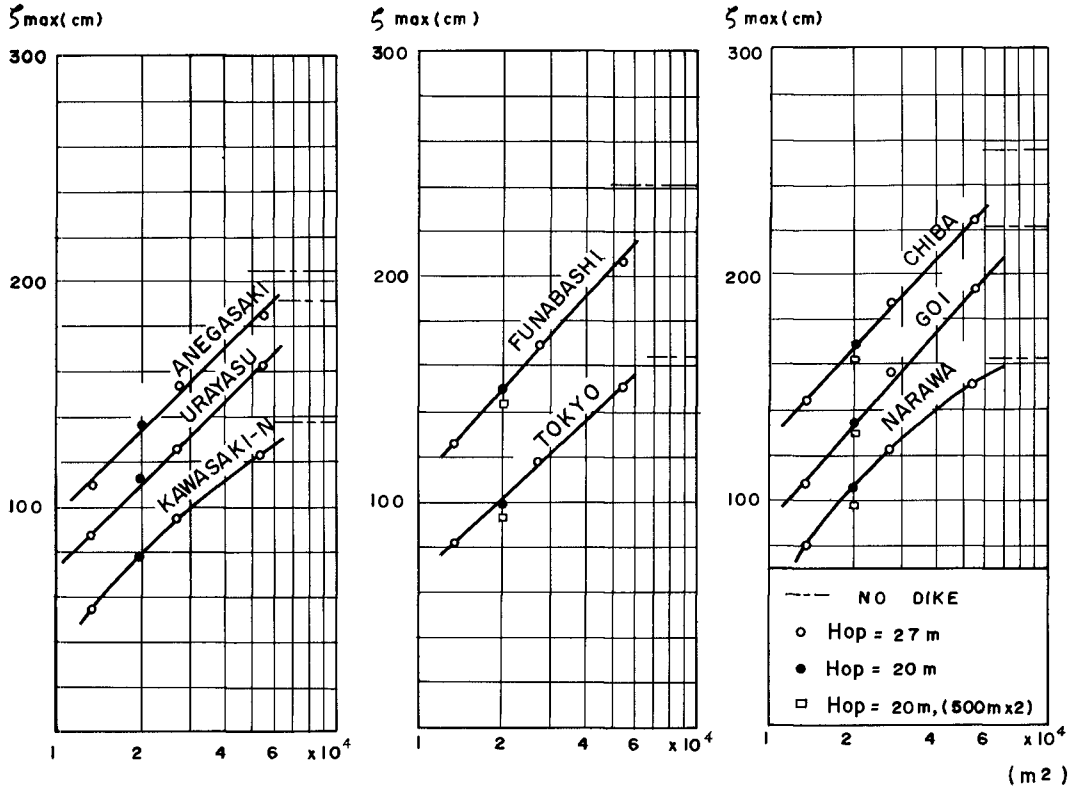
ζmax(cm)
300
200
100
ANEGASAKI
URAYASU
KAWASAKI-N
1
2
4
6
x10⁴
ζ max(cm)
FUNABASHI
TOKYO
CHIBA
GOI
NARAWA
NO DIKE
Hop = 27 m
Hop = 20 m
Hop = 20m,(500mx2)
(m2)

FIG - 10

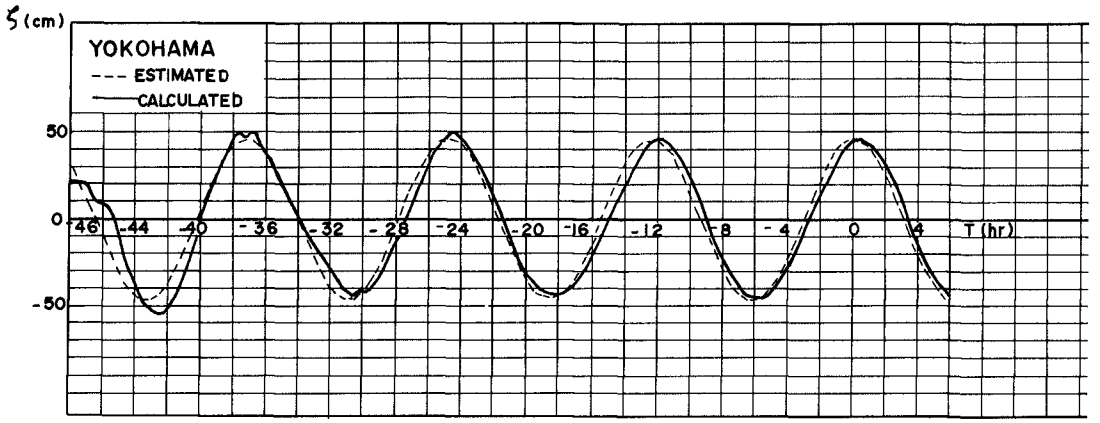
ζ (cm)
YOKOHAMA
--- ESTIMATED
——CALCULATED
50
0
-50
-46
-44
-40
-36
-32
-28
-24
-20
-16
-12
-8
-4
0
4
T (hr)

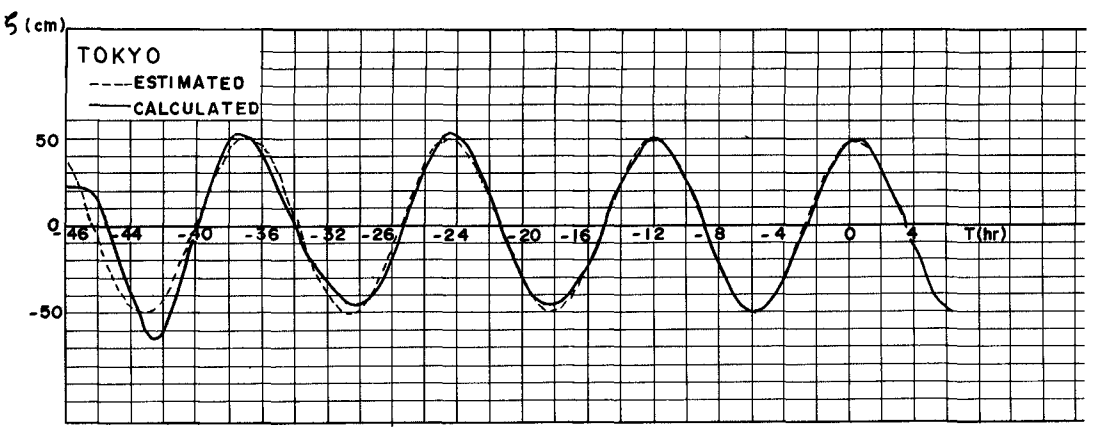
ζ (cm)
TOKYO
----ESTIMATED
——CALCULATED
50
0
-50
-46
-44
-40
-36
-32
-26
-24
-20
-16
-12
-8
-4
0
4
T(hr)

FIG - 11

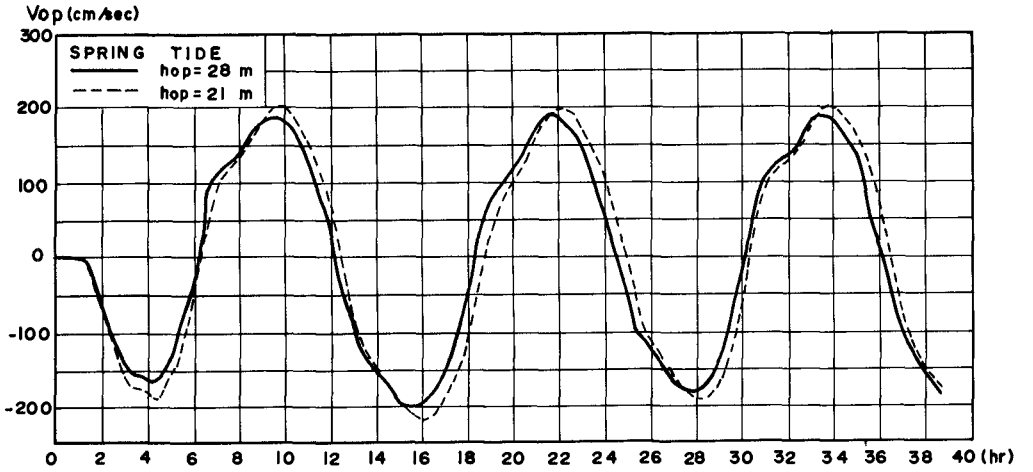
Vop (cm/sec)
SPRING TIDE
hop = 28 m
hop = 21 m
300
200
100
0
-100
-200
0 2 4 6 8 10 12 14 16 18 20 22 24 26 28 30 32 34 36 38 40 (hr)

(a)

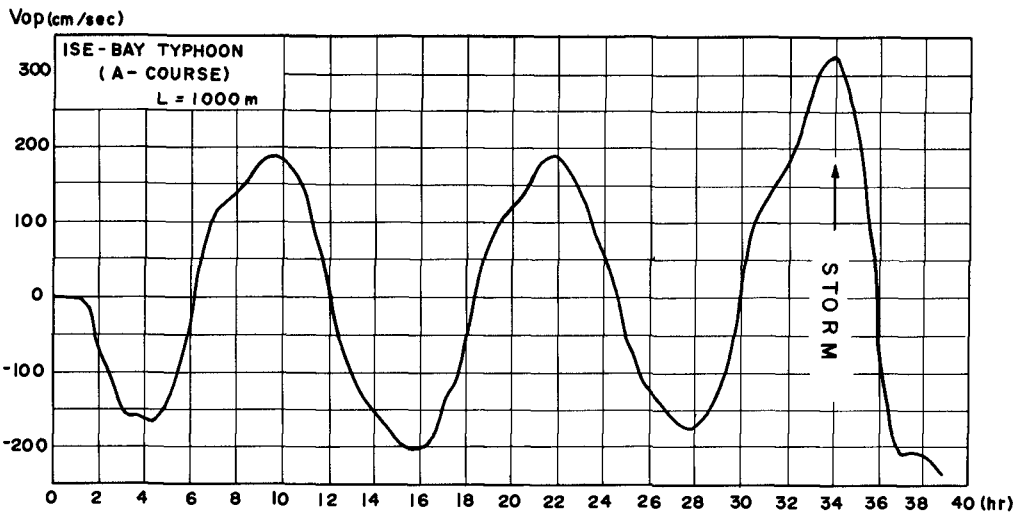
Vop (cm/sec)
ISE-BAY TYPHOON
(A-COURSE)
L = 1000 m
300
200
100
0
-100
-200
STORM
0 2 4 6 8 10 12 14 16 18 20 22 24 26 28 30 32 34 36 38 40 (hr)

(b)

FIG - 12

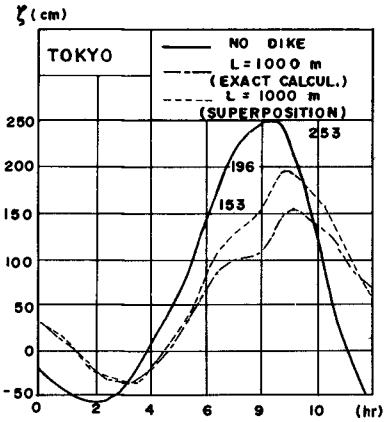
ζ (cm)
TOKYO
NO DIKE
L=1000 m
(EXACT CALCUL.)
L = 1000 m
(SUPERPOSITION)
253
196
153
(hr)

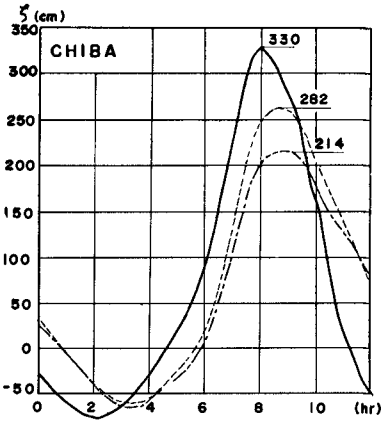
ζ (cm)
CHIBA
330
282
214
(hr)

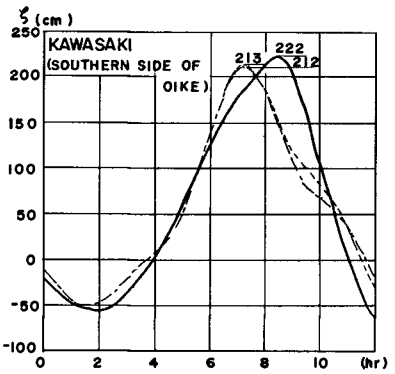
ζ (cm)
KAWASAKI
(SOUTHERN SIDE OF DIKE)
213
222
212
(hr)

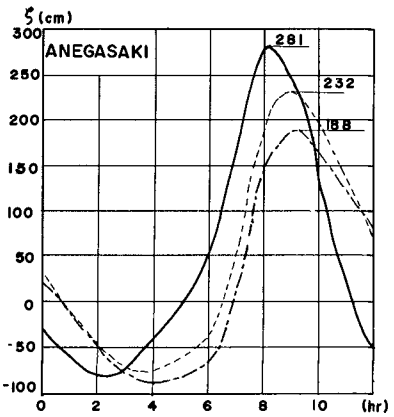
ζ (cm)
ANEGASAKI
281
232
188
(hr)

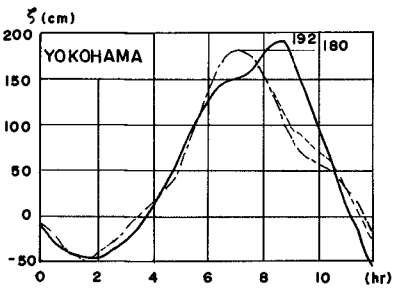
ζ (cm)
YOKOHAMA
192
180
(hr)

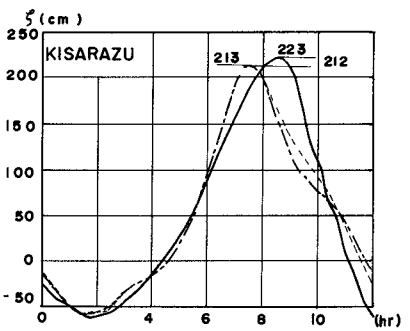
ζ (cm)
KISARAZU
213
223
212
(hr)

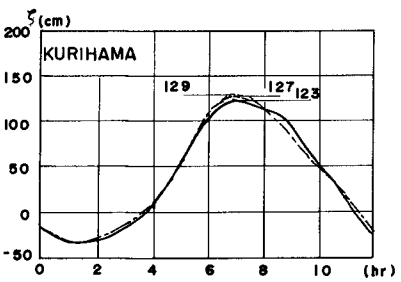
ζ (cm)
KURIHAMA
129
127
123
(hr)

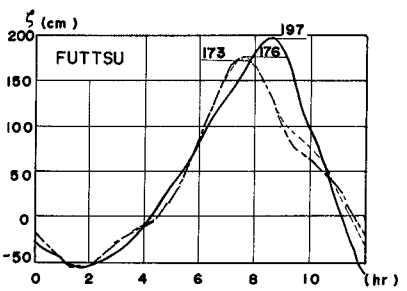
ζ (cm)
FUTTSU
197
173
176
(hr)

FIG - 13

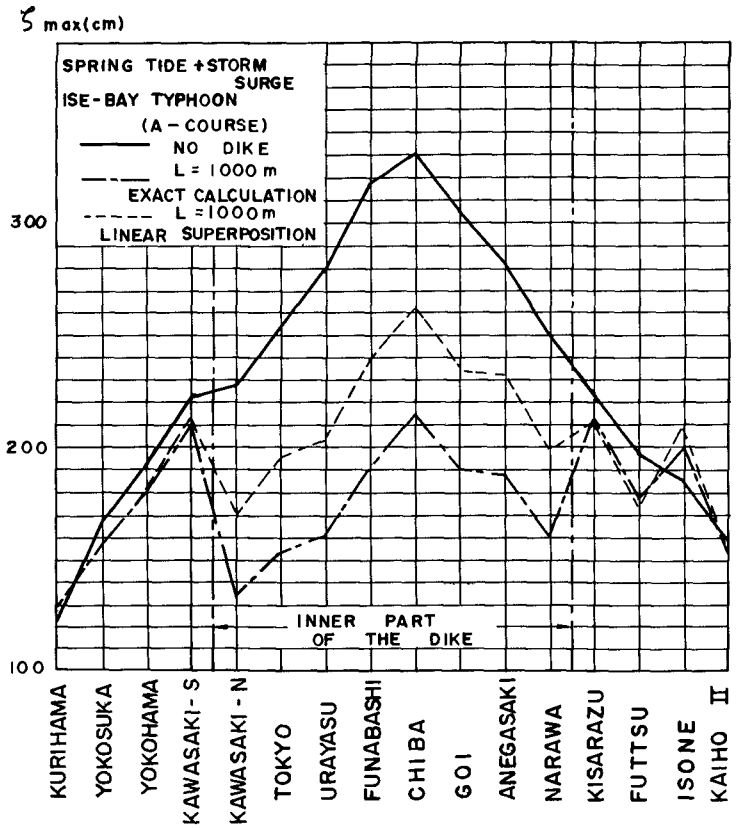
ζ max(cm)
SPRING TIDE + STORM SURGE
ISE-BAY TYPHOON
(A-COURSE)
NO DIKE
L = 1000 m
EXACT CALCULATION
L = 1000 m
LINEAR SUPERPOSITION
300
200
100
INNER PART OF THE DIKE
KURIHAMA
YOKOSUKA
YOKOHAMA
KAWASAKI-S
KAWASAKI-N
TOKYO
URAYASU
FUNABASHI
CHIBA
GOI
ANEGASAKI
NARAWA
KISARAZU
FUTTSU
ISONE
KAIHO II

FIG-14

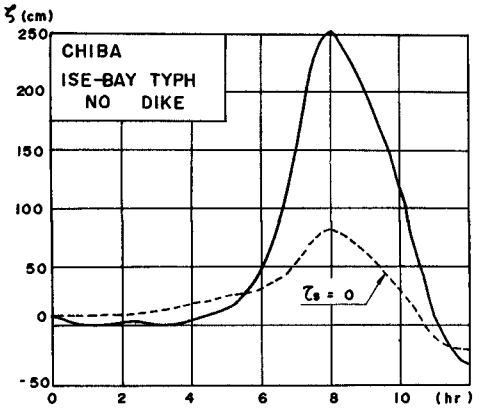
ζ (cm)
250
200
150
100
50
0
-50
CHIBA
ISE-BAY TYPH
NO DIKE
τs = 0
0
2
4
6
8
10
(hr)

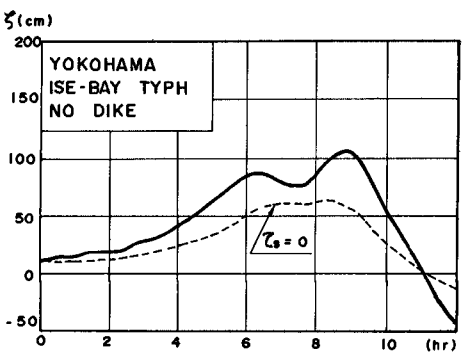
ζ (cm)
200
150
100
50
0
-50
YOKOHAMA
ISE-BAY TYPH
NO DIKE
τs = 0
0
2
4
6
8
10
(hr)

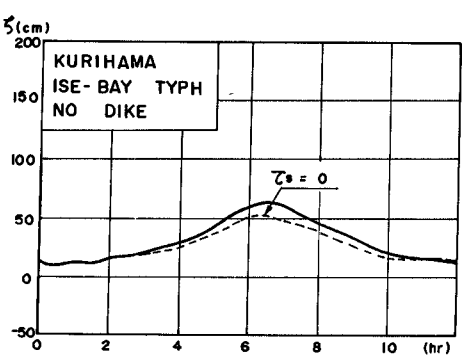
ζ (cm)
200
150
100
50
0
-50
KURIHAMA
ISE-BAY TYPH
NO DIKE
τs = 0
0
2
4
6
8
10
(hr)

FIG - 15

Chapter 44

ON THE DESIGN OF SMALL CRAFT HARBORS

Charles E. Lee
Assistant Chief, Hydraulic Design Branch
Department of the Army, Washington, D. C.

INTRODUCTION

There is little useable, up-to-date written data on the design of small craft harbors. That which has been written does not in general fit the needs of today's crowded marinas. Therefore, we are pioneering a new phase of coastal engineering, one that needs the cooperation of both scientist and engineers, of private practice, university and government. To develop these needs, we must have specialization, as today's research, development, and design is too complex for any one individual to be expert in all. In larger organizations, such as government, three specializations must be developed. It is necessary that all of us in coastal engineering realize and admit this. Therefore, in this introduction the delineation of the responsibilities of these specialties are discussed.

The designer must go to the shore, evaluate the needs of the area, conceive the works that will accomplish the needs, relate to the researcher where his lack of understanding lies and therefore the areas where research is needed. The researcher must then go to the laboratory and to the basic mathematical relationships and establish the relationship of one factor to another. The designer must then take these relationships to the drawing board and devise the structures to furnish a useable harbor. The relationship between the designer and the researcher must be initimate with each having full confidence in the other. Each of these takes long experience, training, and direction of thought that is peculiar to his calling. However, most frequently one in his specific knowledge feels that he can better do the job of the other. Here is often perpetrated a mistake that is severely injurous to the general public. A designer cannot be developed by reading literature, doing laboratory experiments, and discussing design with field personnel, even with frequent visits to the sites. A designer is developed by consultation with the scientist, or researcher, living with the on-site problems, and bearing full responsibility for the designs he devises by living with his projects. A scientist or a research engineer is developed by love of delving into the unknown, logically relating one factor of truth to another, starting with idealized conditions completely unrelated to actual conditions, then developing coefficients to compensate for the irregularities of nature until a procedure is developed that the designer, with his long experience with actual conditions, can utilize in the development of a project. Rarely is both specialties inherent in one man. Therefore, grave errors are made by giving principal research responsibilities to a designer or principal design responsibilities to a researcher.

In a large organization, such as the Corps of Engineers, there must be, in between these two, another type of specialist who must be trained and experienced in both research and design, but basically be a designer. He must be technically aware and appreciative of the skills, problems, and needs of the researcher and provide the direction of the research. He must also be aware of the problems and skills of the designer and provide the guidance in techniques for him. He must remain intimate with the work of the researcher and designer and, with their advice and cooperation, assure that all facets are investigated fully and, based on his design knowledge, give proper weight and impetus to each factor. He must take sole responsibility that findings are ready for application and that they apply to the specific requirements of the project site. Recognizing the limits of the research and the many other variables in nature, he must assure that the findings are used in proper perspective in the design. Success in research and in design is dependent on development of these three types of personnel. Each is a full time venture and delegation of the responsibility of one to the other can only result in chaos.

PROBLEMS

In the United States earlier small craft harbors were constructed to provide for swing-line mooring rather than the more convenient marina type construction. With this type of mooring, the boats could swing and face the on-coming waves directly and could withstand greater wave heights without damage. As small boating increased, space became too small for the number of boats, and it became necessary to use marinas to obtain a greater population density of boats. The type of person interested in boating also changed. With these changes, came the need for greater convenience of access. In addition to that, there also became a greater number of boaters who were unskilled in the handling of their crafts. All this combined, required a smaller wave height, smaller currents, and the elimination of surge in recreational craft harbors.

To fulfill the need of the greater number of crafts, larger harbors were designed. With the larger harbors came greater problems. These larger harbors also required the greatest utilization of area to economically justify their cost. This required increased use of vertical wall wave protection, which reflects rather than absorbs the energy which enters the harbor. Naturally with larger areas of reflective surface, there is a greater capability for the development of resonance. The combination of these reflected waves may reach heights several times that of the impinging wave. This is one cause of great problems in mooring and in the stability of the mooring facilities. Short period waves have little effect on the deeper draft ships, but by slapping against the bottoms of the shallow draft boats and the floating mooring facilities causes racking by quickly lifting them and allowing them to fall.

Studies have been undertaken under Corps of Engineers contract by the California Institute of Technology to determine the effect of various wave characteristics on small boats of various dimensions. This study will also investigate the effect of basin shape on the response to waves of various characteristics. These studies have not been completed, therefore,

present criteria for maximum allowable wave height is based generally on the knowledge of small boat operators and the opinions of those closely connected with small craft harbors. It is generally considered that wave heights in recreational craft harbors should be reduced to one foot or less. This is often very difficult when it is considered that wave energy varies as the wave height squared.

When there is a large variation in the direction of the approach of the waves, it may be very difficult or impossible to provide a suitable width of entrance to the harbor and to reduce the wave heights to less than one foot. In this connection, methods must be employed to reduce the wave height after it enters the harbor but before it endangers the craft within the harbor. One method of accomplishing this is by the utilization of wave absorbers. Although there are several such structures in operation, there has been no distinct design criteria developed.

Upon the development of the larger small craft harbors, many unanticipated problems arose. It is considered that these problems can best be discussed by specific examples. The harbors to be discussed are at Marina del Rey, Redondo Beach, and Half Moon Bay, California, and were concerned with short period waves.

MARINA DEL REY

One of the most complex problems experienced to date is that of Marina del Rey, a small craft harbor located in Santa Monica Bay, about 15 miles west of Los Angeles, California. This harbor is exposed to wind waves, both sea and swell, generated from all deep water directions between west-northwest and south-southwest. The limiting directions are determined by Point Conception and Point Dume to the west-northwest, and Santa Catalina Island and Point Vicente to the south-southwest. The harbor was designed in 1954-55 and was one of the first attempts to establish a large marina for the protection of small craft, with an entrance exposed to a severe wave climate. Plate 1 shows the layout of the harbor.

At the time of design of this harbor, our knowledge of oceanographic phenomena was not sufficiently advanced to forecast the conditions which resulted. Upon the opening of the harbor, it was found that resonance occurred in the basins and that the height of the waves entering through the entrance channel were more than doubled in various basins. Reduction of the width of the 1000-foot wide entrance channel to reduce the energy input was not desirable because of the great number of craft, over 8,000, to be based in the harbor. Basin B was the most critical area of resonance with basins A and H following closely. It was unfortunate that the first development was undertaken in Basin B, and that it was severely damaged during the first storm after construction. It was necessary to transfer boats and remove floats until temporary protective works were undertaken.

The unforeseen wave heights and surge caused severe damage to both craft moored in the basins and to the mooring facilities themselves. It was clear that improved conditions must be provided for suitable functioning

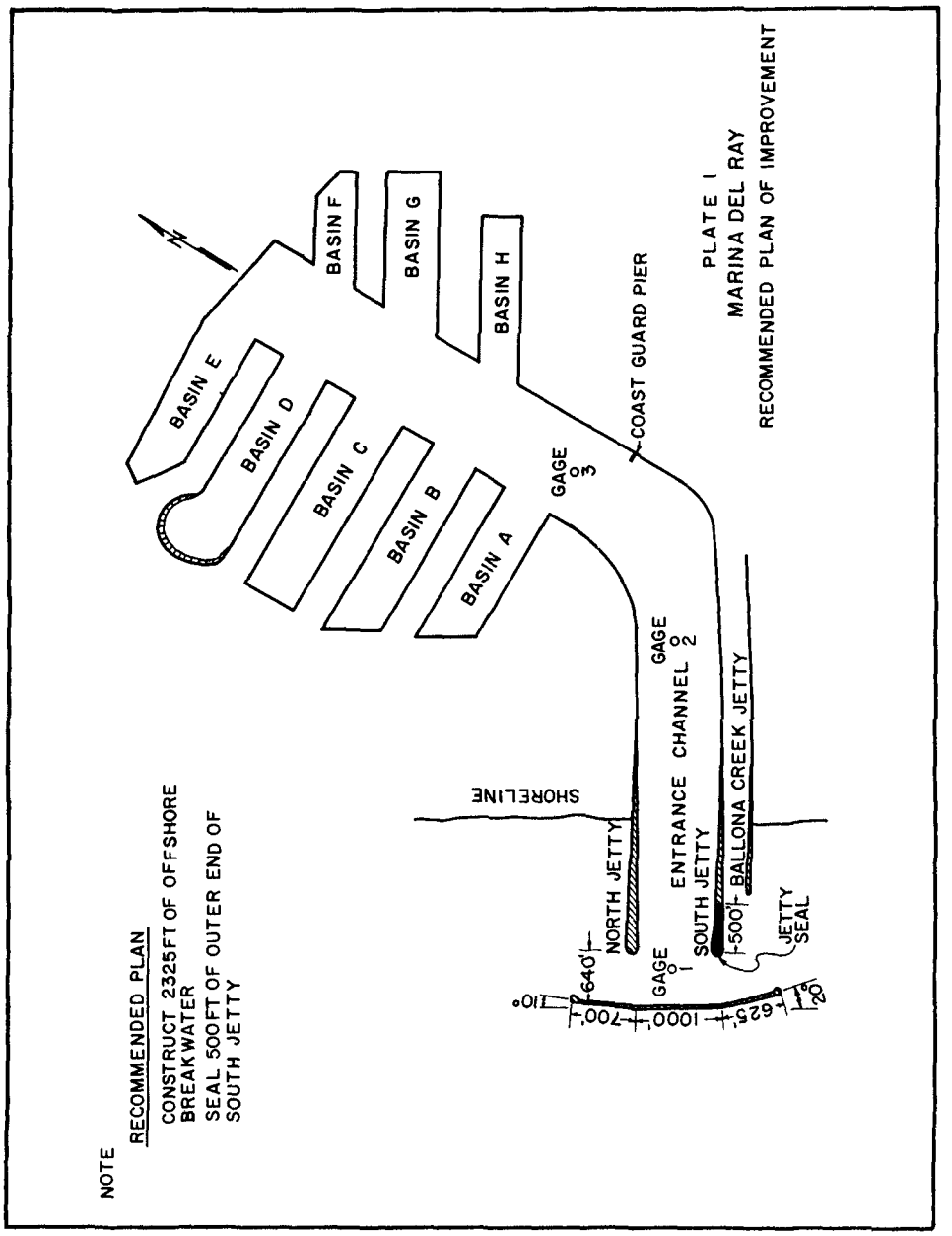
PLATE I
MARINA DEL RAY
RECOMMENDED PLAN OF IMPROVEMENT
BASIN A
BASIN B
BASIN C
BASIN D
BASIN E
BASIN F
BASIN G
BASIN H
COAST GUARD PIER
GAGE 3
GAGE 2
GAGE 1
ENTRANCE CHANNEL
NORTH JETTY
SOUTH JETTY
BALLONA CREEK JETTY
JETTY SEAL
SHORELINE
640'
700'
1000'
625'
500'
10°
20°
NOTE
RECOMMENDED PLAN
CONSTRUCT 2325FT OF OFFSHORE BREAKWATER
SEAL 500FT OF OUTER END OF SOUTH JETTY

of the harbor. One of the principal factors requiring consideration in the design of such an improvement is the determination of the height, period, and direction of travel of the design wave. Since actual wave observations were not available for this purpose, statistical hindcast studies were used to predict the characteristics of the waves that would attack the proposed breakwater. From the statistical study, considering the effects of shoaling and refraction, a design wave 16 feet in height, with a 13-second period approaching from a deep water azimuth of 260°, was selected.

To determine the most efficient plan of improvement, a hydraulic model study was undertaken at the U. S. Army Engineer Waterways Experiment Station at Vicksburg, Mississippi. The selection of a geometrically undistorted model to a linear scale of 1:75 was based on model bottom friction effects, the absolute size of waves to be produced, available shelter area, characteristics of the apparatus, and cost. The model was constructed of concrete and reproduced to scale the existing prototype harbor and the contours of Santa Monica Bay adjacent to the harbor. Sufficient area of Santa Monica Bay was included to permit generation of waves and wave front patterns from the different directions selected for testing. The model waves were generated by a 40-foot long plunger-type wave-machine mounted on casters to permit flexibility in direction for generation. Wave heights were measured by wave rods and were recorded on chart paper of a six-channel electrically operated oscillograph.

Model tests were conducted of a rubble-mound wave absorber installed along the east side of the main channel, of a wave refraction plan, several different offshore breakwater arrangements, and 38 different combinations of these components. The model study determined that a breakwater 2,325 feet long, as shown on Plate 1, or a combination of absorber in the main channel together with constriction of the entrances to the various basins, would reduce wave action in the marina to a satisfactory level. After considering all factors, such as loss in revenue and lease adjustment, it was concluded that the breakwater plan was the most desirable improvement. The construction of the recommended breakwater should prevent approximately 95 percent of the wave energy from entering the harbor.

Elements of the selected plan consists of an offshore breakwater, totaling 2,330 feet in length, located 640 feet seaward of the ends of the existing jetties, and made up in three sections, a center section 1,000 feet long with a top elevation at +22 feet, MLLW; a northerly section 700 feet long to elevation +22 feet; and a southerly section, 630 feet long to elevation +17 feet. To prevent excessive transmission of energy through the existing southerly jetty, it will also be sealed for distance of about 1,000 feet from its outer end. This sealing will make it impervious to about elevation +8 feet, MLLW.

It is planned to accomplish the sealing as at Mission Bay, California. This was accomplished through two-inch diameter intrusion holes drilled 12 feet apart on center to a depth of 14 feet below the top of the existing jetty, which is the top of the existing core. As the drill used for this

purpose has to drop through voids and encounter wiggling and sloping surfaces, a percussion drill was specified in lieu of a rotary drill. Grout containing a mixture of sand, cement, clay, calcium chloride and water was introduced to the voids through a pipe under gravity flow. The pipe was withdrawn at such a rate as to build grout cones. The spacing of the grout entry holes are of such a distance as to produce intersections of the grout cones thus formed to a height 8 feet above the top of the core.

The breakwater is under construction at the present time. It is of layered construction with a core of graded stone ranging in size from 20 pounds to 1 ton. It is considered that the core will form a dense, compact, impervious mound with a top elevation ranging from 7 to 12 feet above MLLW, depending on requirements. The armor stone will be select quarrystone with a specific gravity of at least 2.56. The minimum size and gradation varies but in general no armor stone will weigh less than 10 tons and the 50 percent size will not be less than 13 to 16 tons. Size requirement to withstand the wave force was calculated by the Hudson equation and is substantiated by successful structures in the area.

To temporarily alleviate the condition, until the permanent breakwater construction could be accomplished, Los Angeles County Division of Small Craft Harbors constructed constricting works in the entrance channel just seaward of the bend. This consisted of two steel sheet pile walls, with batters, which overlapped a 300 foot wide entrance. The constriction reduced the wave energy reaching the basins to tolerable proportions and allowed sufficient entrance width for the small amount of development. However, as previously mentioned, removal of the temporary works is necessary before complete development of the harbor is realized. The temporary works will be removed in increments, after completion of the breakwater, and the effect of the removal of each increment observed before removal of the next.

REDONDO BEACH-KING HARBOR

Redondo Beach-King Harbor is located about 6½ miles south of Marina del Rey and, therefore, is subject to very similar wave climate. The harbor was protected by two rubble-mound breakwaters, approximately 4,985 feet in total length with the crest elevation of 14' above MLLW. The inner harbor consists of three boat basins inclosed by moles with revetted slopes. The basins are dredged to depths ranging from 8-12 feet below MLLW. The harbor is designed to provide berthing for approximately 1,350 small craft and for land storage facilities for about 150 boats. See Plate 2.

The breakwater was constructed with an impervious core up to elevation -10 feet. Above the core, armor stones weighing about 13 tons were placed to a crest elevation of +14 feet. As the structure above elevation -10 was constructed entirely of the large armor stones, excessive wave energy permeated through the interstices of the structure. During intense storms overtopping occurred. The combination of the overtopping and energy transmission through the structure caused severe damage to boats and their facilities during the winter of 1962-63. It is considered that during the time of design, the knowledge of wave phenomena was not advanced and that inadequate

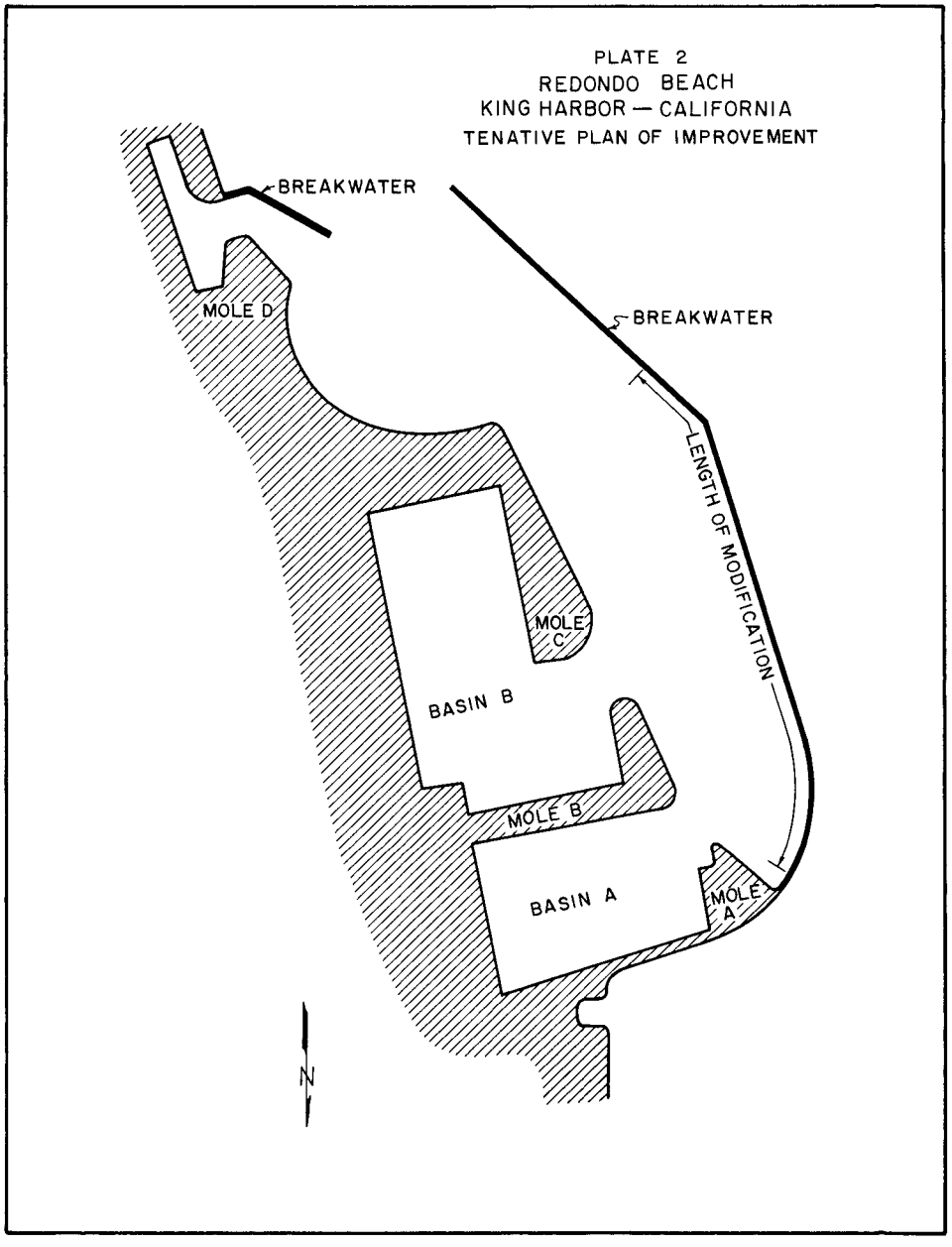
PLATE 2
REDONDO BEACH
KING HARBOR — CALIFORNIA
TENATIVE PLAN OF IMPROVEMENT
BREAKWATER
BREAKWATER
MOLE D
LENGTH OF MODIFICATION
MOLE C
BASIN B
MOLE B
BASIN A
MOLE A
N

knowledge of the actual characteristics of the waves impinging on the harbor, the degree of energy transferred through the voids, and the degree of wave reformation resulting from overtopping were not fully considered. Design of a modification included hydraulic model study, which was accomplished during the fall of 1963.

The model tests were made at the Coastal Engineering Research Center in two phases. Initially tests were made at a 1 to 50 scale in a small wave flume, 96 feet long, 1.5 feet wide, 2 feet deep. In this tank, a wide variation of plans were investigated and the less effective eliminated. Favorable appearing plans were further tested at a scale of 1 to 5 in the large wave tank, which is 635 feet long, 15 feet wide, and 20 feet deep. The investigation program consisted of stability, overtopping, and wave reformation tests using various wave periods. Wave heights of 10 and 17 feet at the structure and tide elevations of 5.5 feet (MHHW) and +7 feet (MHHW plus storm setup). The model tests indicated that: (1) a seaward slope of 1 on 2 is stable, (2) a harborside slope of 1-1/4 on 1, or steeper, is not stable, (3) placing a layer of core material to elevation +9 on the harborside and covering it with B stone and cover stone provides a stable slope, (4) placing the core too high does not allow sufficient porosity and weight to hold the sections. When the core is too high, the upper portion of the new layer collapses en masse as a slide, and (5) with a slope of 1 on 2 with a top elevation of +22, the overtopping was decreased to the degree that the height of the regenerated waves were within a tolerable range.

The plan of improvement devised consisted of impervious layer placed on the harborside of the structure to an elevation of 9 feet above MLLW, as shown on Plate 3. This was covered by armor stone to prevent damage during severe storms. The model indicated that with the initial structure approximately 1.5 to 3 percent of the incident wave energy passed through and over the breakwater at a tide of 0 feet MLLW, and approximately 16 to 21 percent of the incident wave energy passed through and over the breakwater at a tide of +7 feet. It is estimated that the modified plan will reduce the wave energy passing through the breakwater to about one percent at mean higher high tide, with a 17 foot incident wave. The resulting reformed wave would be about 1.7 feet high.

The purpose of the proposed breakwater improvement is to reduce the height of waves entering Basins 1 and 2 to 2 feet or less. This is no greater than the height local winds can generate in the harbor entrance channels. Although it is not part of its purpose, the improvement also reduces the wave energy arriving at the faces of Moles B and C. A detailed analysis of the wave heights arriving at the basins and moles show that waves of this height result with a storm of design magnitude occurring at mean higher high tide. This would have an approximate frequency of occurrence of 5 years. The heights are summarized as follows:

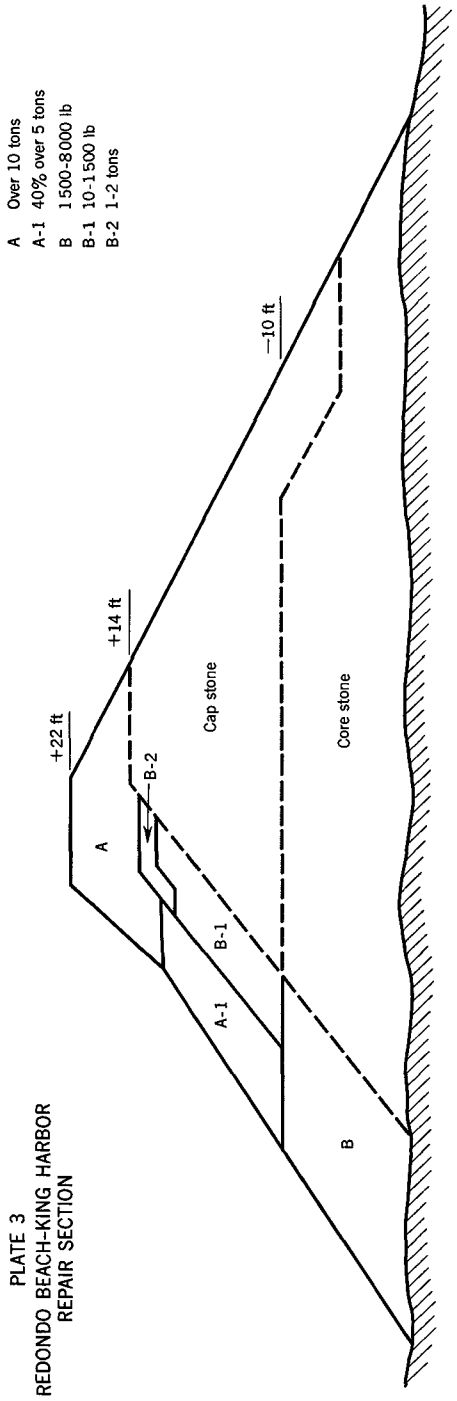

PLATE 3
REDONDO BEACH-KING HARBOR
REPAIR SECTION

Wave height at mouth of Basins 1 and 2.....2 feet or less
Wave height at mouth of Basin 3.....about 3½ feet
Wave height along Mole B.....2 feet
Wave height along Mole C.....2 to 6 feet
Wave height along Mole D.....about 10 feet
Wave height between Mole C and D.....about 7 to 10 feet

The wave heights given for Basins 1 and 2 and Moles B and C are considered to be reliable estimates of the worst wave conditions which are likely to occur. Those heights given for Basin 3, Mole D, and the reach between Moles C and D are somewhat questionable because of the simplifying assumptions and approximations which are necessary to facilitate analysis.

HALF MOON BAY

The case of Half Moon Bay Harbor is presented to describe a different type of problem. At Half Moon Bay, the energy was entering through the entrance, and was not properly attenuated for small boat harbor requirements. This project is located about 20 miles south of the entrance to San Francisco Bay, California. The harbor is protected by two rubble-mound breakwaters, the westerly one being about 2620 feet long, and the companion easterly breakwater about 4420 feet long. The navigation entrance is 600 feet wide. Half Moon Bay is exposed to waves approaching from directions between west and south-southeast. Deep water waves from the west and west-southwest are of greater magnitude as they range to a maximum of about 21 feet. Analysis of the wave data showed that significant waves, ranging from 9 to 12 feet in height, occur in the navigation entrance for more than 100 hours each year. Model tests data indicate that waves greater than two feet occur along the bulkhead line of the inner harbor from five to twenty percent of the time.

The waves travel through the entrance and, according to their direction of approach, severely effect different sections of the harbor. The principa public piers are located directly opposite the opening, and severe agitation occurs there under most directions of severe wave approach. Due to the natur of the problem, it was determined that a hydraulic model study would be required to devise a suitable plan of protection. An undistorted linear scale of 1 to 100 was selected, after consideration of such factors as: (a) the required depth of water in the model to prevent appreciable frictional resistance and surface tension effects, (b) absolute size of model waves, (c) available shelter space, (d) available wave generating and measuring apparatus, (e) cost of construction, and (f) model operation convenience. The model was constructed of concrete and the breakwaters were constructed of graded stone to simulate different degrees of porosity and wave absorbing characteristics of the rubble-mound breakwaters. The model covered an area of about 13,000 square feet approximating 4.7 square miles in the prototype. The model waves were generated by a vertical bulkhead type wave machine, which was 60 feet long and mounted on casters so it could be positioned for any required direction of wave approach. Analyses of the model data indicated that an angular extension to the west breakwater provided the best overall protection. The extension 1050 feet long would reduce the average wave heights along the inner bulkhead line to about 1.5 feet during the design storm.

The model data has now been presented to the design engineers, who will review the efficiency of each plan tested, and make the final selection of the project modification that will best suit the requirements of this specific harbor.

RESEARCH

There is a need for much research in the area of small craft harbor design. The Corps of Engineers has initiated several research programs to help devise suitable design criteria. However, research is time consuming; and there will probably be many mistakes made in the future before the design criteria is developed to the stage that we can confidently anticipate all problems. As mentioned previously, one of the research programs that is vital to small boat harbor design is the study of the design of wave absorbers and their effect on wave action in harbors. The initial phase of this study will be (1) Conducting critical review and preparing a summary of the theoretical and experimental aspect of: (a) natural sand beaches, (b) wave traps and resonators, and (c) rubble-mound absorbers in the form of a simple mound backed by an impervious vertical wall. The transmission of waves through rubble-mound breakwater type of absorber will also be investigated. (2) Showing by specific examples how the findings from the literature review can be adapted to actual situations. (3) Making a special theoretical investigation on the feasibility of using rubble-mound or other pervious construction for the absorbing of wave energy entering the harbors. (4) Preparing a review of scale-effects related to wave absorbers for both long and short period waves and proposing a solution or outline of an experimental investigation to evaluate or correct the scale effect. The initial study will be followed by an analytical and model study to determine actual design criteria for various combinations of wave characteristics and water levels and to fill the gaps in existing data. The Corps of Engineers is planning to use wave absorbers in connection with breakwater protection in at least three small boat harbors which are now being considered by Congress for authorization. It is felt that much additional information will be available in a short period of time on this subject. One rubble-mound wave absorber that appears successful in protection of a small craft harbor is that at Oceanside, California. The small craft basin and the absorber are shown on Plate 4. The absorber is of saw-tooth design with varying slopes on the teeth.

The second contract aimed specifically at the solution of small craft harbor problems is underway at the California Institute of Technology at Pasadena, California, entitled "Wave Induced Oscillations of Small Moored Vessels". Serious ship and dock damage can be caused by wave induced oscillations of moored vessels. The ship and its mooring system constitute a mechanical system capable of response characteristics analagous to a simple spring-mass combination, so that the ship can experience resonant oscillations significantly amplifying the motions and restraining forces.

The specific aim of the research is to investigate theoretically and experimentally the response of prismatic bodies moored to floating platforms under the action of standing and progressive waves. Later phases of the

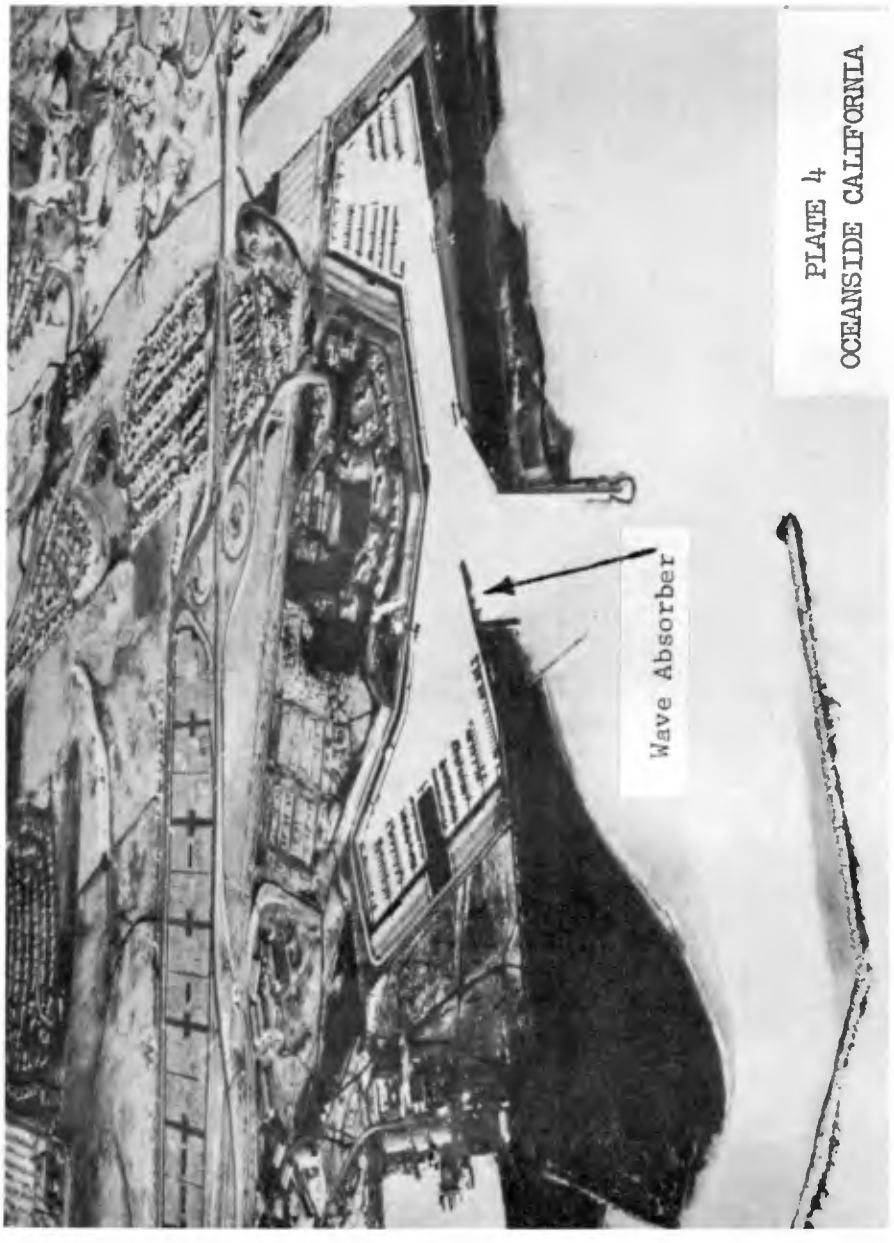

PLATE 4
OCEANSIDE CALIFORNIA

study would be concerned with the harbor oscillations which create this problem; the major attention being devoted to the response characteristics of complex harbor shapes to wave induced surging.

The Corps of Engineers is involved in many types of research effecting small boat harbor design. It is planned to increase the scope and accelerate the completion of these studies.

MODEL STUDIES

Our present knowledge of the phenomena that occurs when a wave enters a small craft harbor makes it necessary that most of our small boat harbor designs be supplemented by a hydraulic model study. At the present time, it appears necessary to simulate the actual conditions of the site in order to fully anticipate wave travel, attenuation and reflection within the confines of the harbor. It is hoped that research programs will soon yield sufficient general design criteria that some model tests may be eliminated. However, it is assumed that for the more complex problems, specific project model studies will be required for some time in the future.

CONCLUSIONS

More research and study is necessary before effective small craft harbor design criteria is developed. Some of this research is underway, but much additional must be planned and initiated in the near future. Specific harbor cases, such as the three discussed herein, give some data on which to proceed. Case histories should be given detailed analysis for proper guidance of future research programs.

Chapter 45

COASTAL ENGINEERING RESEARCH ON THE GREAT LAKES

L. Bajorunas

U. S. Lake Survey, Corps of Engineers
Detroit, Michigan

ABSTRACT

Collection and study of field data relative to coastal engineering is underway for the following problems: wind over the lakes and its relationship with wind recorded on land; wave characteristics and effect of wind and environment; water level disturbances and mathematical relationship with acting forces; currents in harbors and factors affecting them; littoral transport.

INTRODUCTION

The problems of coastal engineering on the Great Lakes are rather similar to the problems on oceans since the lakes act in many aspects as oceans due to their large size, Fig. 1. However, there are distinct differences between these lakes and oceans. The water itself is different: the Great Lakes contain quite pure fresh water. These lakes also are generally covered by ice each winter for two to four months during which time coastal processes are greatly reduced. The water levels are subject to significant fluctuation; it is known that at high lake levels, the shore erosion is much more active than at low levels; however, it is possible that at low levels (as at present) conditions for high erosion are created by moving the offshore sand bars deeper into the lakes. Not much data is available on the waves in the Great Lakes. It is believed that wave characteristics are different from those of ocean waves due to limited area of generation and the absence of significant swells.

For any kind of oceanographic research, the lakes offer a large variety of conditions. The causative factors are more easily measurable and the costs of research in many instances are much lower than in salt water. It is not surprising that the Great Lakes have been suggested as a proving ground to test theories and to develop and test new instruments and data transmission equipment for both fresh and salt water research.

The research of the Great Lakes is gaining impetus due to the increasing population in their basins in both the United States and Canada, and with the accelerated use of their waters for a variety of purposes. Many universities, state and provincial agencies, and the federal governments of both countries are engaged in research activities.

Through its Research Division, the United States Lake Survey, an agency of U. S. Army Corps of Engineers, is conducting research in the fields of hydrology of the lakes, lake water characteristics, water

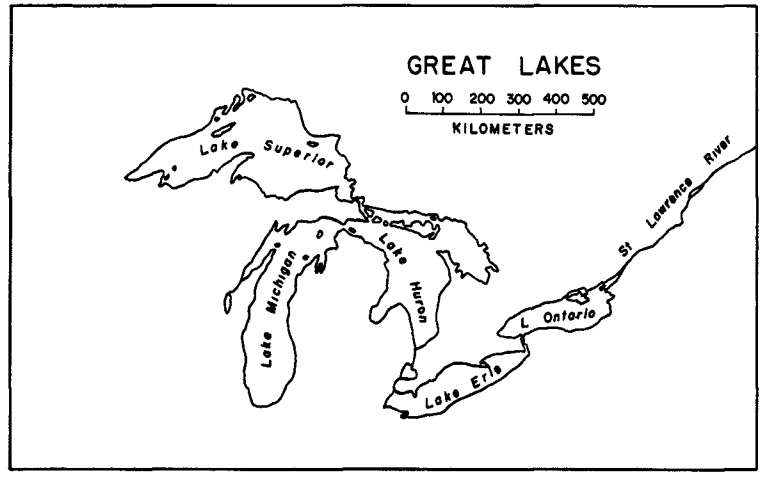

Fig. 1 Outline of the Great Lakes.

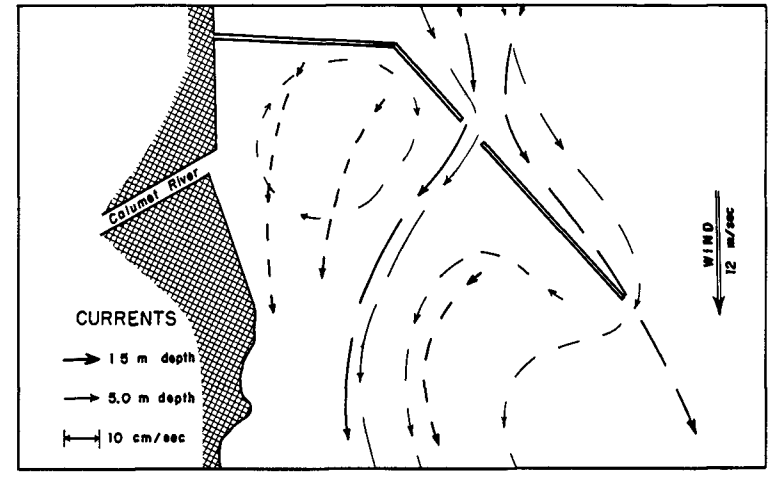

Fig 2 Currents in Calumet Harbor.

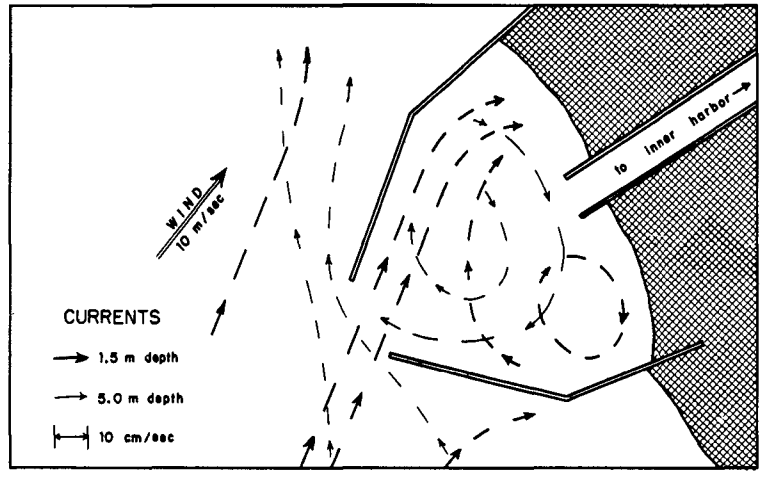

Fig 3 Currents in Muskegon Harbor

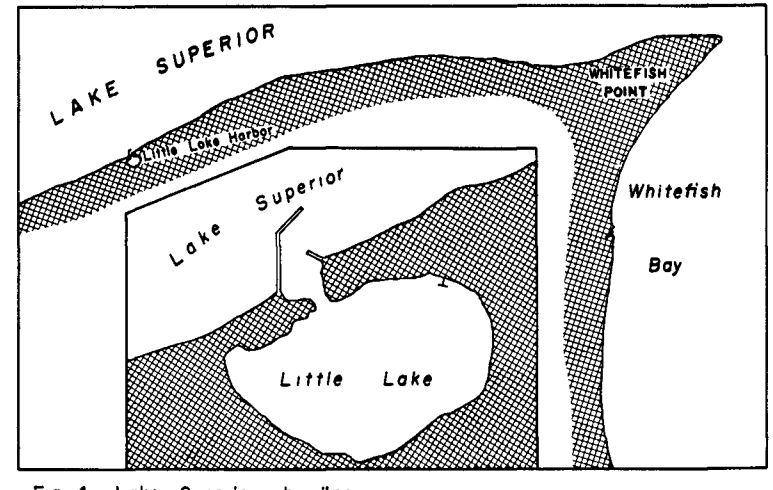

Fig 4. Lake Superior shoreline

motion, shore processes, and ice and snow problems. In this paper, the coastal engineering phases of both the on-going research and the near-future planned research will be discussed.

OVERWATER WIND

The research on overwater wind is conducted in two categories: one to explore the relationship between the wind recorded on shore near the lake with the wind recorded over the lake, and the other to explore the energy transfer from air to water and reverse. The recording of wind speed and direction is being done at weather stations all around the Great Lakes and the records are available for the past sixty years. By comparison with records of overwater winds from vessels having wind recorders on board, it was found that the overwater winds generally have much higher speeds than those recorded by land stations. However, a high variation was observed, depending on the time of day or season. For example, at the same wind speed on land, the recorded overwater wind is about thirty per cent faster during the fall months than during the spring months. Investigation is aimed toward determining if the energy transfer from air to water is subject to similar variation and what factors affect it. The results will improve understanding of the relationship between wind and waves or wind and tides.

To accomplish this investigation, two stations are operated in Lake Michigan which record overwater wind speed and direction, along with many other factors. The first, a tower, was placed in 15 m deep water, 1.6 km from shore near Muskegon. This tower, extending 16 m into the air, supports cup anemometers at the 3, 4, 6, 10 and 16 meter levels. Additional anemometers are placed at 0.5, 1.0, 1.5, and 2.0 meter levels when wave conditions permit. Data are being transmitted to shore and recorded on magnetic tape. The 9 anemometers give good profiles of low winds, and the upper 5 instruments record conditions during storms. Besides the wind profiles, the other recorded factors are: air temperature and humidity profiles, water temperature profile, water current speed and direction, water level, wave height and period, precipitation, water albedo, and exchange of radiation. The University of Michigan and the U. S. Weather Bureau participate in these investigations.

The other wind installation is on South Manitou Island, a small island in the northeastern part of Lake Michigan. The instrumentation at this installation is more simple than that on the tower; however, it has the advantage that it stays in operation year round, while the tower must be removed before winter and reinstalled in the spring. A small wooden platform near the island was also erected to support the instruments recording water level and temperature, and to test the effect of the island on overwater winds.

LAKE WAVES

At the present time, nine wave gages are in operation in lakes Erie, Michigan, and Superior. Their purpose is to collect data for the statistical determination of lake wave spectra and to correlate wave

characteristics with wind speed, duration, and lake bottom geometry. Of these nine wave gages, four have pressure cells for the sensing unit. The pressure cells do not properly depict the smaller waves; however, they are easy to mount on submerged tripods, require only low power supply, and are not affected by icing. The other type of sensing unit is the step resistance gage developed by the Coastal Engineering Research Center of the Corps of Engineers. This gage is being used for the installations near harbor entrances where shallow water allows fairly easy installation. Comparison is being made of the two sensors to establish accuracy limits for the pressure cell.

In remote regions of Lake Superior where commercial electric power is not available, sensors of the relay type are used. They are more expensive, but their power demand is much smaller than that of the step resistance unit. A thermoelectric generator of 15 watt capacity having 12 VDC proved to be a very handy power supply under these conditions, with no maintenance problems and a minimum supply of liquified propane gas for fuel. In the near future an inertial-type wave sensor will be procured and used for investigations of waves further away from shore to establish the environmental effects on wave growth and propagation.

Extensive investigations were made on the methods of recording the waves. From the several choices (paper chart, paper tape, magnetic tape), the magnetic tape was selected as the basic recording method. Waves in analog form are continuously recorded on magnetic tape at a speed of 1.2 cm per min on a reel that lasts for about four weeks. In the office, an osciloscope is connected to a tape recorder for visual inspection of the record and for selection of portions of the record for wave analysis.

Up to the present time no studies have been made of the wave records that have been collected. A brief analysis indicates that the Great Lakes act more like oceans than inland reservoirs. Heights exceeding 2.5 meters and periods of 10 seconds were recorded during the first two months of operation of the gages. There is some indication that the fetch effect on wave formation is less pronounced than that generally employed by some wave forecasting schemes.

WATER LEVEL DISTURBANCES

Shifts of water mass by wind and by variation of barometric pressure raise some portions of lake levels and lower others, although the mean level in the lake remains the same. These disturbances, called wind tides, surges, or seiches, are of importance to coastal engineering problems because they require more height for the shore protection structures and occasionally create strong currents. Lake Erie is widely known for having the largest disturbances of this kind. Wind-caused water setups on Erie have been recorded exceeding 4 meters in height. The extreme displacement of Lake Erie water is attributed to both the lake's shallow depth and its length lying in the direction of prevailing winds. All the other lakes have similar phenomena and, although not as frequent or as pronounced as on Lake Erie, they are occasionally severe.

The investigations aiming to derive physical laws and mathematical models for such disturbances and their propagation into harbors are made by the Lake Survey in conjunction with data being collected by the Public Health Service. The Public Health Service operates buoy stations to measure wind speed and direction, air and water temperature, and water velocity at several depths. The Lake Survey is making detailed water level recordings at shore stations and at several points in the lake. During 1963 the main effort was directed to Lake Michigan, where 22 water level recorders, 31 buoys, one tower and one island station were in operation. This year the emphasis was shifted to Lake Erie and later will be extended to Lake Ontario.

HARBOR CURRENTS

The initial purpose of these investigations was to collect information on the existence of currents in harbors, and their magnitude and persistence. Due to lack of significant astronomical tides in the lakes, it was believed that only a few exposed harbors have significant water movement inside the harbor. However, surveys have indicated measurable currents in all the harbors measured. The next step in this research is to derive a mathematical model establishing relationships between acting forces and water movement, and closely depicting the observations. Such a mathematical model would allow forecasting the effects of proposed harbor modifications without going through the expensive and time-consuming testing procedure on a physical model.

During the summer of 1963, four harbors in Lake Michigan were instrumented and the water movement traced. At the present time similar surveys are underway in two harbors of Lake Erie. Instrumentation consists of recorders to make continuous records of wind speed and direction, barometric pressure, wave height and period, water level, water temperature, and direction and speed of water movement. A Savonius rotor is used to sense the speed and a vane for direction. Some of the current measurements are recorded on film with readings at 20-minute intervals. Such current recorders remain submerged for six weeks, at which time the film must be removed and a new roll inserted. There is no indication if the instrument is operating properly while submerged, which is the disadvantage of such an instrument. When a submerged instrument stops, all subsequent records are lost. This year improved meters were added, which transmit the water speed and direction by submerged cables to recorders on shore.

The continuous recordings of the current meters are supplemented by tracings of the water movement at several depths inside and outside the harbor. Drogues adjustable for different depths are used for these tracings, and a survey lasts for 3 to 6 weeks. Also rhodomine dyes were tested for this purpose, releasing them between prior established markers and photographing movement. Plans are underway to survey currents by stereo photography as soon as an airplane and a camera equipped with a wide-angle lens is available. The vertical distribution of water velocity is measured by Price current meters.

Samples of harbor current surveys are shown in Figs. 2 and 3. In Calumet Harbor near Chicago, a strong current caused by 12 m/s wind from the north crosses the harbor and flushes it. The fresh lake water removes the polluted water which enters the harbor from Calumet River. In Muskegon Harbor, the current structure is quite complex. Note that the current measured at a 5 m depth crosses the entrance to the inner harbor against the wind.

LITTORAL TRANSPORT

Data are being collected at the present time for establishment of the relationships between energy and movement of shore materials and their characteristics. For this task a reach was selected on the southern shore of Lake Superior, between Little Lake and Whitefish Point, Fig. 4. Due to its exposed location to the predominantly northwest winds, this reach has quite a large movement of shore material, with the net movement from west to east. A small harbor was recently constructed at Little Lake, which produced at least a temporary check point for the sediment movement. Another natural check point is at Whitefish Point, where the shoreline turns sharply southward. These sites are now the subject of detailed surveys.

Two towers placed in water 5 m deep are each equipped with a wind speed and direction recorder, a relay-type wave gage with magnetic tape recorder, and a water-level recorder. One pressure cell for deep-water waves was placed on a submerged tripod in water 15 meters deep. In the breaker zone, at 1.5 m depth, two tripods are used for ducted-type current meters and direction sensors, with shore-based strip chart recorders. All these instruments are in continuous operation.

Periodic topographic surveys are made for establishing the rate of sediment deposition or removal. These surveys consist of measurements of bottom elevations at preselected locations marked by plastic rods inserted into the bottom along sixteen ranges at each site. Also, sediment samples are taken for preliminary analysis on shore and for detailed physical analysis in the laboratory. The following sediment characteristics will be determined: phi mean diameter, sorting coefficient, kurtosis, and skewness.

Data collection is restricted by ice to the open-water season, which in this northern region is rather short. It is planned to make resurvey of the sites next spring, although the effect of ice cover on energy transfer will make the problem much more involved.

FUTURE OUTLOOK

The present program for coastal engineering research in the lakes is oriented toward immediately useful results. Of necessity, applied research will continue to have higher priority over basic research. However, research progress is limited until there is a better understanding of the basic fundamentals and relationships.

In the research on waves, work will be expanded in the study of the shape of lake waves as a function of length, steepness, and propagation speed. Charts will be prepared indicating the wave characteristics in each of the lakes. Work is also planned on investigations of the interrelationship between lakes and rivers. The water in the outflow rivers is extremely clear, except during storms when the lakes supply shore material to outflow rivers, causing detrimental effects on water quality and silting of navigation channels and water intakes. Tracer techniques are planned for study of the movement of material from lakes to rivers. Further research will include the energy transfer from air to water and reverse, and the distribution of energy in the waves.

Chapter 46

ANALYSIS OF THE RESPONSE OF OFFSHORE-MOORED SHIPS TO WAVES

Jan J. Leendertse*
The RAND Corporation
Santa Monica, California

INTRODUCTION

A vessel moored at sea will experience complicated series of translational and rotational oscillations due to sea waves. These motions can be considered as the summation of six components, three translational and three rotational.

In the presently available analyses of motions of unmoored ships, differential equations can be written for each mode of movement. Unfortunately, motions in one of these modes are coupled to motions of other modes, and the analysis becomes rather complicated. Generally, the problem is simplified by neglecting some of the coupling effects and by specifying the position of the vessel in the wave system.

This study develops and analyzes a model for a moored ship restrained by mooring lines, using the presently available mathematical models for the free ship and the force-displacement relationship of the cable-holding points on the ship.

The coupled movement (three degrees of freedom) in a vertical plane through the longitudinal axis of the vessel and the generated mooring-line forces are considered in detail. The general case of six degrees of freedom in arbitrary heading is discussed briefly in general terms.

MOTIONS OF AN UNRESTRAINED VESSEL IN HARMONIC WAVES

Referring to the analyses by Weinblum and St. Denis (1950), the movement of a vessel unrestrained by mooring lines in harmonic waves may be expressed with certain approximations by the second-order linear differential equation

$$M_{ss} \frac{ds^2}{dt^2} + N_{ss} \frac{ds}{dt} + K_{ss} s + R_t = \bar{AF}^s_{ex} e^{j\omega t} \qquad (1)$$

The first subscript of the mass, damping, and stiffness coefficients refers to the considered force or moment equation; the second subscript, to the mode of movement to which the coefficient belongs (see Appendix for symbols). The first term on the left in Eq. (1) represents the inertia force; the second term represents the damping force; the third term is the restoring force; and the fourth term is the force due to other modes of movement. The term on the right expresses the periodic force of the waves.

*This research is sponsored by the United States Air Force under Project RAND. This is an abridgment of RAND Memorandum RM-3368-PR. The views, conclusions, and recommendations expressed herein do not necessarily reflect the official views or policies of the United States Air Force.

Extensive literature is available concerning the calculations of the mass and damping coefficients for a ship of particular dimensions and the periodic wave force. Weinblum and St. Denis (1950), and Korvin-Kroukovsky (1961), particularly, present readily applicable data for calculating these coefficients and the wave forces. However, in many instances it will be necessary to obtain these coefficients from model tests. It is noted here that the magnitude of the wave force depends on the direction of the ship to the waves.

Information about the coupling of the different modes of movement is limited, and only a few incidental cases have been investigated; for example the coupled heave and pitch by Korvin-Kroukovsky and Jacobs (1957). Weinblum and St. Denis neglect the coupling in their analyses of ship motion, and in this study, the coupling term will also be neglected initially.

For the unrestrained ship, the restoring forces and moments in the different modes are caused by the displacement of the ship from the position of rest; if the ship is moored, the forces in the mooring line will, of course, cause additional restoring forces and moments.

MOORING-LINE CHARACTERISTICS

The forces exerted on a ship or vessel by mooring it with a long single chain or cable that has an embedded anchor at its other end are functions of the weight of the chain or line and the location of the holding point in the ship relative to the anchor. If it is assumed that the cable is lying partly on a flat bottom as in (a) of Fig. 1, then the horizontal and the vertical forces on the ship are nonlinear functions of the horizontal and vertical displacement. Based on the analyses of single mooring lines by use of catenary equations, (b) of Fig. 1 presents the total tension and its horizontal and vertical components as a function of the displacement in nondimensional parameters.

In a particular condition of the mooring chain, for example, as presented in (a) of Fig. 1, a rectangular-coordinate system is fixed to this point, with the x-axis horizontal and z-axis vertical. For small displacements around the holding point (o,o) the horizontal and the vertical components of the force in the chain at this point may be assumed to be linear with the displacement and may be expressed by

$$H_{(x,z)} = H_{(o,o)} + ax + bz \tag{2}$$

$$V_{(x,z)} = V_{(o,o)} + cx + dz \tag{3}$$

The coefficients a, b, c, and d can be obtained directly from Fig. 2, which is based upon an analysis of the catenary equations. It will be noted that $b < a$ and $d < c$.

If a chain with a sinker is used, the forces can again be expressed by Eqs. (2) and (3), but the calculation of the coefficients becomes cumbersome.

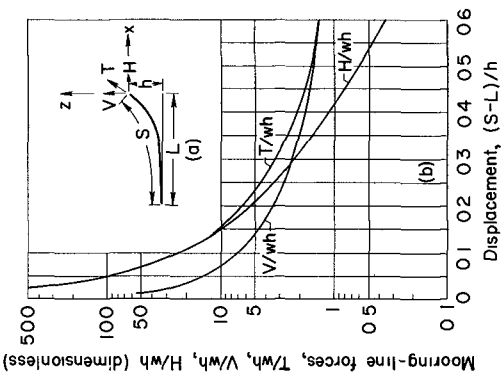

FIG 1 NONDIMENSIONAL REPRESENTATION OF MOORING-LINE FORCES AS FUNCTION OF DISPLACEMENTS

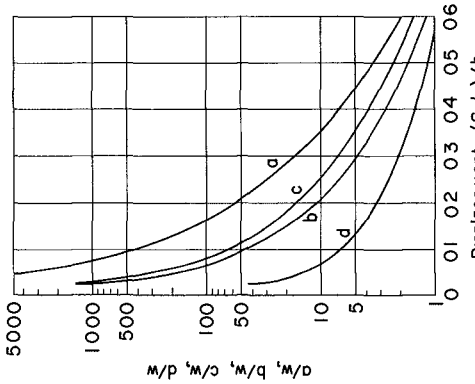

FIG 2 LINEAR COEFFICIENTS FOR SMALL DISPLACEMENT OF HOLDING POINT

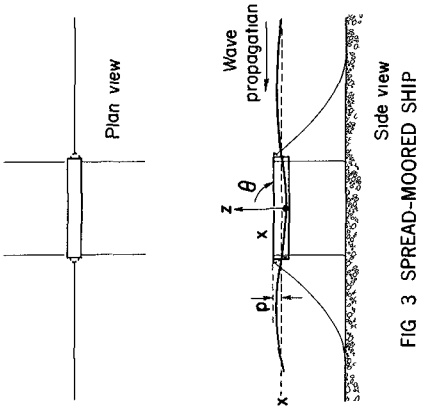

FIG 3 SPREAD-MOORED SHIP

SPREAD-MOORED SHIP

Spread-mooring is used presently in the oil industry for mooring tender-barges near offshore drilling platforms. The layout of a simple mooring is represented in Fig. 3. It is assumed that the waves approach the ship head-on. Initially, it is assumed that the ship is subjected to uniform waves; later on, the effect of irregular waves will be introduced.

The ship's motions in the plane considered involve surging, heaving, and pitching. For the unrestrained (free-floating) ship, surge does not have important effects on the heave and pitch and consequently may be considered uncoupled. In the case of the moored ship, however, coupling will enter into the system due to the mooring lines. For example, the position of the bow, which is determined by heave and pitch, influences the horizontal component of the mooring-line force, and hence the surge.

Referring to Eq. (1), Weinblum and St. Denis (1950), and Wilson (1959) the linearized equation of motion in surge for the center of gravity of the unrestrained ship, compared to a fixed coordinate system taken in the cente of the ship in still water, takes the form

$$M_{xx}\ddot{x} + N_{xx}\dot{x} = A\bar{F}^{x}_{ex}\, e^{j\omega t} \tag{4}$$

where

$M_{xx} = M + M'_x$ = virtual mass of the ship in x direction

M = mass of ship

M'_x = added mass in x direction

Generally, the drag is small and may be neglected. However, in some cases, moored crafts may be built specially for mooring purposes, and in that case, no emphasis may be placed on towing or propulsion characteristic Then, N_{xx} (damping coefficient) is not necessarily small, and estimates of values may be obtained from the propulsion characteristics and a linearization process as developed by Havelock (described in Ref. 1) for the heaving motion. For the time being, the drag term will be maintained, being important even when small in cases of a resonance condition.

In addition to the inertia and drag forces, a restraining force exists for the moored vessel, and the equation of motion becomes

$$M_{xx}\ddot{x} + N_{xx}\dot{x} + F_h = A\bar{F}^{x}_{ex}\, e^{j\omega t} \tag{5}$$

where F_h is the resultant horizontal component of the restoring force of the mooring cables. With reference to Eqs. (2) and (3), taking the direction of the x-axis toward the left in the direction of wave propagation, the horizontal force of the left cable is

$$H_{(x,z)_{stern}} = H_{(o,o)_{stern}} - a(x - p\theta) + b(z + L\theta) \tag{6}$$

and for the cable on the upstream side

$$H_{(x,z)_{bow}} = - H_{(o,o)_{bow}} - a(x - p\theta) - b(z - L\theta) \tag{7}$$

The other four mooring lines have no significant component in the x direction. Consequently, the total restoring force is

$$- F_h = - 2ax + 2(bL = ap)\theta \tag{8}$$

Thus, Eq. (5) becomes

$$M_{xx}\ddot{x} + N_{xx}\dot{x} + 2ax - 2(bL + ap)\theta = A\overline{F}^{x}_{ex}\, e^{j\omega t} \tag{9}$$

Introducing the stiffness coefficients

$$K_{xx} = 2a \tag{10}$$

and

$$K_{x\theta} = - 2(bL + ap) \tag{11}$$

Eq. (9) becomes

$$M_{xx}\ddot{x} + N_{xx}\dot{x} + K_{xx}x + K_{x\theta}\theta = A\overline{F}^{x}_{ex}\, e^{j\omega t} \tag{12}$$

In this analysis, following the presentation by Kriloff (1898), Weinblum and St. Denis (1950), and Wilson (1959), the coupling effects as induced on the free-floating ship are neglected. Tests on ship models and computation of coupled and uncoupled motions indicated that neglecting the coupling terms is of minor significance for the pitching motion but is more important for the heaving motions. As will appear, since the effects of heave on the mooring-line forces are relatively minor compared with those of pitch, neglecting these coupling terms in the motion equation of the free-floating ship seems justified and simplifies the analysis significantly.

For the moored ship, the heaving motion is influenced by the restoring force of the chains. The restoring force F_v for the bow and stern chains can be calculated from the vertical mooring-line force

$$V_{(x,z)_{stern}} = - V_{(o,o)_{stern}} + c(x - p\theta) - d(z + L\theta) \tag{13}$$

$$V_{(x,z)_{bow}} = - V_{(o,o)_{bow}} - c(x + p\theta) - d(z - L\theta) \tag{14}$$

Addition of Eq. (13) and Eq. (14) gives

$$F_v = - V_{(o,o)_{stern}} - V_{(o,o)_{bow}} - 2dz \tag{15}$$

The constant forces $V_{(o,o)_{stern}} + V_{(o,o)_{bow}}$ act downward on the ship and increase its displacement. Generally, this increase is very small and may be neglected. Consequently, the stiffness coefficient in heave for the

moored ship becomes

$$K_{zz} = \left(\rho g A_s + 2d\right)z \tag{16}$$

where A_s is the horizontal cross-sectional area of a ship at the still-water surface. The first term on the right side of Eq. (16) represents the vertical force due to the displaced bolume of water; the second term, the force due to the mooring lines on the bow and stern of the vessel.

The coefficient d appears to be very small compared with $\rho g A_s$, and consequently the bow and stern mooring lines have an insignificant effect on the heaving motion. Likewise, the other mooring lines already neglected in Eq. (16) have no effect on the heaving motion.

Following Eq. (1), the equation of motion in pitch of a free-floating vessel may be written, if coupling with other modes of movement is neglected as

$$M_{\theta\theta}\ddot{\theta} + N_{\theta\theta}\dot{\theta} + K_{\theta\theta}\theta = A\bar{F}^{\theta}_{ex}\, e^{j\omega t} \tag{17}$$

where

$$K_{\theta\theta} = \rho g J_{\gamma}$$

The restoring moment ($K_{\theta\theta}\theta$) of the free-floating ship is increased when the ship is moored.

The total moment of the vertical components of the bow and stern line is

$$M_v = -(L - p\theta)\, V_{(x,z)_{stern}} + (L + p\theta)\, V_{(x,z)_{bow}} \tag{18}$$

$$= 2cLx = 2cpL\theta - 2dL^2\theta$$

$$+ p\theta \left(V_{(o,o)_{stern}} + V_{(o,o)_{bow}}\right) + 2dz \tag{19}$$

The moments due to the horizontal forces in the stern and bow lines are

$$M_h = -(p + L\theta)\, H_{(x,z)_{stern}} + (p - L\theta)\, H_{(x,z)_{bow}} \tag{20}$$

$$= +2apx - 2ap^2\theta - 2pbL\theta$$

$$- L\theta \left(H_{(o,o)_{stern}} + H_{(o,o)_{bow}}\right) - 2bzL\theta \tag{21}$$

the moments due to vertical forces in the mooring lines perpendicular to the long axis of the ship are

$$M_p = 4\left(d_1 L^2 + pV_{(o,o)_p} + pd_1 z\right)\theta \tag{22}$$

where

d_1 = coefficient determining the influence of the vertical movement

Neglecting the higher-order terms, the resultant moment due to all mooring-line forces is

$$M_h + M_v + M_p = 2(ap + cL)\,x - \Big[2ap^2 + 2(b + c)pL + \Big(H_{(o,o)_{stern}} + H_{(o,o)_{bow}} + 2dL + 4d_1L\Big)L - \Big(V_{(o,o)_{stern}} + V_{(o,o)_{bow}} + 4\,V_{(o,o)_p}\Big)p\Big]\,\theta \tag{23}$$

Consequently, the total restoring moment is a function of x and θ, and the equation of motion may be written

$$M_{\theta\theta}\ddot{\theta} + N_{\theta\theta}\dot{\theta} + K_{\theta\theta}\theta + K_{\theta x}x = A\overline{F}^{\theta}_{ex}\, e^{j\omega t} \tag{24}$$

where

$$K_{\theta\theta} = pgJ_\gamma + \Big[2ap^2 + 2(b + c)pL + \Big(H_{(o,o)_{stern}} + H_{(o,o)_{bow}} + 2dL + 4d_1L\Big)L - \Big(V_{(o,o)_{stern}} + V_{(o,o)_{bow}} + 4\,V_{(o,o)_p}\Big)p\Big] \tag{25}$$

$$K_{\theta x} = -\,2(cL + ap) \tag{26}$$

Thus, the three equations of motion are

$$M_{xx}\ddot{x} + N_{xx}\dot{x} + K_{xx}x + K_{x\theta}\theta = A\overline{F}^{x}_{ex}\, e^{j\omega t} \tag{27}$$

$$M_{\theta\theta}\ddot{\theta} + N_{\theta\theta}\dot{\theta} + K_{\theta\theta}\theta + K_{\theta x}x = A\overline{F}^{\theta}_{ex}\, e^{j\omega t} \tag{28}$$

$$M_{zz}\ddot{z} + N_{zz}\dot{z} + K_{zz}z = A\overline{F}^{z}_{ex}\, e^{j\omega t} \tag{29}$$

It will be noticed that Eqs. (27) and (28) are coupled. Anticipating a solution

$$x = \overline{A}\, e^{j\omega t} \qquad \theta = \overline{B}\, e^{j\omega t} \tag{30)(31}$$

Where $\overline{A}$ and $\overline{B}$ are complex quantities, then

$$\dot{x} = j\omega\overline{A}\, e^{j\omega t} \qquad \ddot{x} = -\omega^2\,\overline{A}\, e^{j\omega t} \tag{32)(33}$$

$$\dot{\theta} = j\omega\overline{B}\, e^{j\omega t} \qquad \ddot{\theta} = -\omega^2\,\overline{B}\, e^{j\omega t} \tag{34)(35}$$

Introducing these complex quantities in place of the real quantities in Eqs. (27) and (28) gives

$$\Big(-\omega^2 M_{xx} + j\omega N_{xx} + K_{xx}\Big)\,\overline{A} + K_{x\theta}\overline{B} = A\overline{F}^{x}_{ex} \tag{36}$$

$$K_{\theta x}\bar{A} + \left(-\omega^2 M_{\theta\theta} + j\omega N_{\theta\theta} + K_{\theta\theta}\right)\bar{B} = A\bar{F}^{\theta}_{ex} \tag{37}$$

We now introduce the impedances

$$\bar{Z}_{xx} = -\omega^2 M_{xx} + j\omega N_{xx} + K_{xx} \tag{38}$$

and

$$\bar{Z}_{\theta\theta} = -\omega^2 M_{\theta\theta} + j\omega N_{\theta\theta} + K_{\theta\theta} \tag{39}$$

which simplifies Eqs. (36) and (37) to

$$\bar{Z}_{xx}\bar{A} + K_{x\theta}\bar{B} = A\bar{F}^{x}_{ex} \tag{40}$$

$$K_{\theta x}\bar{A} + Z_{\theta\theta}\bar{B} = A\bar{F}^{\theta}_{ex} \tag{41}$$

Solving for $\bar{A}$ and $\bar{B}$ gives

$$\bar{A} = \frac{\begin{vmatrix} \bar{F}^{x}_{ex} & K_{x\theta} \\ \bar{F}^{\theta}_{ex} & \bar{Z}_{\theta\theta} \end{vmatrix}}{\begin{vmatrix} \bar{Z}_{xx} & K_{x\theta} \\ K_{\theta x} & \bar{Z}_{\theta\theta} \end{vmatrix}} A \qquad \text{and} \qquad \bar{B} = \frac{\begin{vmatrix} \bar{Z}_{xx} & \bar{F}^{x}_{ex} \\ K_{\theta x} & \bar{F}^{\theta}_{ex} \end{vmatrix}}{\begin{vmatrix} \bar{Z}_{xx} & K_{x\theta} \\ K_{\theta x} & Z_{\theta\theta} \end{vmatrix}} A \tag{42)(43}$$

by which amplitudes and phase lags with the exciting periodic waves can be calculated.

For the vertical motion, a complex solution is anticipated

$$z = \bar{C}e^{j\omega t} \tag{44}$$

where $\bar{C}$ is a complex quantity. Following the method for x and θ, we obtain

$$\bar{Z}_{zz}\bar{C} = A\bar{F}^{z}_{ex} \tag{45}$$

where

$$\bar{Z}_{zz} = -\omega^2 M_{zz} + j\omega N_{zz} + K_{zz} \tag{46}$$

Thus

$$\overline{C} = \frac{\overline{F}^{z}_{ex}}{\overline{Z}_{z}} A \tag{47}$$

The fluctuations in the mooring cables may now be determined. For example, rewriting Eq. (6)

$$H_{(x,z)_{stern}} = H_{(o,o)_{stern}} - ax + (ap + bL)\theta + bz$$

If we introduce the following expression for the force fluctuation in the mooring cable, which is a function of wave amplitude and frequency

$$H_{stern}(A,\omega) = - ax + (ap + bL)\theta + bz \tag{48}$$

then

$$H_{stern}(A,\omega) = Re\left[- a\overline{A} + (ap + bL)\overline{B} + b\overline{C}\right]Ae^{j\omega t} \tag{49}$$

In many instances, the term $K_{x\theta}$ in Eq. (40) is very small compared to $\overline{Z}_{xx}$, and $K_{\theta x}$ in Eq. (41) is very small compared to $\overline{Z}_{\theta\theta}$. Then the pitch and surge of the moored ship are essentially uncoupled, and

$$\overline{A} \approx \frac{\overline{F}^{x}_{ex}}{\overline{Z}_{xx}} A \tag{50}$$

$$\overline{B} \approx \frac{\overline{F}^{\theta}_{ex}}{\overline{Z}_{\theta\theta}} \tag{51}$$

The coupling is important, however, for the resonance movement in surge, which is generally not significantly damped, and in that case Eqs. (42) and (43) have to be used.

If coupled motion for the free-floating ship in pitch and heave are important--for example, for a ship with the center of mass not approximately in the middle of the ship as described by Korvin-Kroukovsky (1961)--the equation of motion of this vessel when moored becomes

$$M_{xx}\ddot{x} + N_{xx}\dot{x} + K_{xx}x + K_{x\theta}\theta = A\overline{F}^{x}_{ex}\, e^{j\omega t} \tag{52}$$

$$K_{\theta x}x + M_{\theta\theta}\ddot{\theta} + N_{\theta\theta}\dot{\theta} + K_{\theta\theta}\theta + M_{\theta z}\ddot{z} + N_{\theta z}\dot{z} + K_{\theta z}z = A\overline{F}^{\theta}_{ex}\, e^{j\omega t} \tag{53}$$

$$M_{z\theta}\ddot{\theta} + N_{z\theta}\dot{\theta} + K_{z\theta}\theta + M_{zz}z + N_{zz}\dot{z} + K_{zz}z = A\overline{F}^{z}_{ex}\, e^{j\omega t} \tag{54}$$

or using the mechanical impedances $\overline{Z}_{\theta z}$ and $\overline{Z}_{z\theta}$, similarly $\overline{Z}_{xx}$ as in Eq. (38) the equations of motion may be expressed:

$$\overline{Z}_{xx}\,\overline{A} + K_{x\theta}\,\overline{B} = A\overline{F}^{x}_{ex} \tag{55}$$

$$K_{\theta x}\,\bar{A} + \bar{Z}_{\theta\theta}\,\bar{B} + Z_{\theta z}\,\bar{C} = A\bar{F}^{\theta}_{ex} \tag{56}$$

$$\bar{Z}_{z\theta}\,\bar{B} + \bar{Z}_{zz}\,\bar{C} = A\bar{F}^{z}_{ex} \tag{57}$$

This set of linear equations may be solved by using Cramer's rule, writing for the determinant of the system

$$\Delta = \begin{vmatrix} \bar{Z}_{xx} & K_{x\theta} & 0 \\ K_{\theta x} & \bar{Z}_{\theta\theta} & \bar{Z}_{\theta z} \\ 0 & \bar{Z}_{z\theta} & Z_{zz} \end{vmatrix} \tag{58}$$

The unique solutions are given by

$$\bar{A} = \frac{\Delta_x}{\Delta} A \qquad \bar{B} = \frac{\Delta_\theta}{\Delta} A \qquad \bar{C} = \frac{\Delta_z}{\Delta} A \tag{59)(60)(61}$$

where Δ_x, Δ_θ, Δ_z are the determinant forms obtained by replacing the elemen of the first, second, or third columns, respectively, of Eq. (58) by $\bar{F}^{x}_{ex}$, $\bar{F}^{\theta}_{ex}$, $\bar{F}^{z}_{ex}$.

For a unit wave amplitude, the complex numbers $\bar{A}$, $\bar{B}$, and $\bar{C}$, which are frequenty dependent, are generally called complex response operators and written as $T_{x\eta}(\omega)$, $T_{\theta\eta}(\omega)$, and $T_{z\eta}(\omega)$. The real part of these complex oper tors is that part of the response,which is in phase or 180 deg out of phase with the wave and often indicated as $c_{x\eta}(\omega)$, $c_{\theta\eta}(\omega)$, and $c_{z\eta}(\omega)$. The imaginary part of the complex operators is that part which is 90 deg or 270 deg out of phase with the wave and is indicated as $q_{x\eta}(\omega)$, $q_{\theta\eta}(\omega)$, and $q_{z\eta}(\omega)$ (see Korvin-Kroukovsky (1961).

SHIP MOORED BY BUOYS WITH UNIFORM WAVES HEAD-ON

The equations of motion for a ship using mooring buoys can be derived in a fashion similar to that for the ship using mooring cables only. In this case, the motions of the buoys have to be considered in addition to the motions of the ship.

Considering a mooring configuration in Fig. 4, it will be noted that the relative vertical motions between the buoys and the ship will induce small horizontal displacements between the buoys and the ship, thus relatively small force fluctuations in the lines between ship and buoy. Consequently, the heaving and pitching motions of the ship are considered as of no importance to the forces in these lines. This is naturally not the case for the heaving motions of the buoys.

Assuming again a linear relationship between forces and movements, and neglecting the pitching of the buoys, the equations of motion for waves with this height of the system neglecting damping in surge become

$$M_{1_{xx}}\ddot{x}_i + N_{1_{xx}}\dot{x} + a\,x_1 + K_1\,(x_1 - x_2) - b\,z_1 = \bar{F}^{x}_{1_{ex}}\,e^{j\omega t} \tag{62}$$

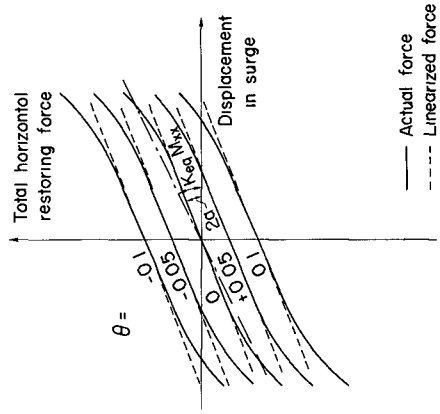

FIG 5 TYPICAL PLOT FOR HORIZONTAL RESTORING FORCE VERSUS DISPLACEMENT FOR DIFFERENT PITCH ANGLES

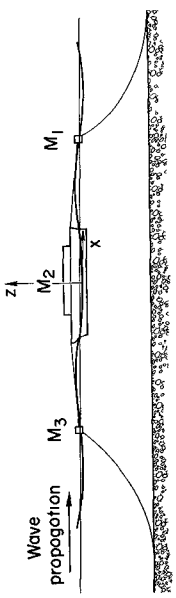

FIG 4 BUOY MOORING

$$M_{2_{xx}} \ddot{x}_2 + K_1 (x_2 - x_1) + K_2 (x_2 - x_3) = \overline{F}^x_{2_{ex}} e^{j\omega t} \tag{63}$$

$$M_{3_{xx}} \ddot{x}_3 + N_{3_{xx}} \dot{x} + K_2 (x_3 - x_2) + a x_3 + b z_3 = \overline{F}^x_{3_{ex}} e^{j\omega t} \tag{64}$$

$$M_{1_{zz}} \ddot{z}_1 + N_{1_{zz}} \dot{z} + \left[\rho g (2 L_1 B_1) + d\right] z_1 - c x_1 = \overline{F}^z_{1_{ex}} e^{j\omega t} \tag{65}$$

$$M_{3_{zz}} \ddot{z}_3 + N_{3_{zz}} \dot{z} + \left[\rho g (2 L_3 B_3) + d\right] z_3 + c x_3 = \overline{F}^z_{2_{ex}} e^{j\omega t} \tag{66}$$

In many instances, in mooring with buoys, the connection between the ship and buoy is made with a cable that is relatively light in comparison with the heavy chains used on the buoys. If these cables are placed in high tension, the horizontal movements of the buoys and the ship are practically the same, and it may be assumed that $x_1 = x_2 = x_3$. Then Eqs. (62) through (66) reduce to

$$\left(M_{1_{xx}} + M_{2_{xx}} + M_{3_{xx}}\right) \ddot{x} + \left(N_{1_{xx}} + N_{2_{xx}}\right) \dot{x} + 2ax - bz_1 + bz_3 = \left(\overline{F}^x_{1_{ex}} + \overline{F}^x_{2_{ex}} + \overline{F}^x_{3_{ex}}\right) e^{j\omega t} \tag{67}$$

$$M_{1_{xx}} \ddot{z}_1 + N_{1_{zz}} \dot{z}_1 + \left[\rho g (A_\pi) + d\right] z_1 - cx = \overline{F}^z_{1_{ex}} e^{j\omega t} \tag{68}$$

$$M_{3_{zz}} \ddot{z}_3 + N_{3_{zz}} \dot{z}_3 + \left[\rho g (A_\pi) + d\right] z_3 + cx = \overline{F}^z_{2_{ex}} e^{j\omega t} \tag{69}$$

In Eq. (67), the virtual masses of the buoys are small compared with the mass of the ship, and also the horizontal wave forces are small compared with the wave force acting on the ship; consequently, the effects of the buoys in this horizontal movement of the ship may be neglected. Generally, the natural frequency in heave of the buoys is higher than the frequencies of the waves, thus the terms $M\ddot{z}$ and $N\dot{z}$ are small compared with the term $\left[\rho g(2LB) + d\right]$ and may be neglected in our initial investigation of the ship's movement. Disregarding the above-mentioned terms, introduction of Eqs. (68) and (69) into Eq. (67) gives

$$M_{2_{xx}} \ddot{x} + \left(N_{1_{xx}} + N_{2_{xx}}\right) \dot{x} + \left\{2a - \frac{2bc}{(\rho g A_\pi + d)}\right\} x = \left(+ \frac{b}{(\rho g A_\pi + d)} \overline{F}^z_{1_{ex}} - \frac{b}{(\rho g A_\pi + d)} \overline{F}^z_{3_{ex}} + \overline{F}^x_{2_{ex}}\right) e^{j\omega t} \tag{70}$$

This result is important, since in principle it enables the design of a mooring which, at the resonance frequency

$$\omega_{o_x} = \left[\frac{2a - \frac{2bc}{\rho g A_{\pi} + d}}{M_{2_{xx}}}\right]^{1/2} \tag{71}$$

the excitation term on the right side of Eq. (70) becomes small by proper placement of the buoys.

SPREAD-MOORED SHIP IN LONG-CRESTED IRREGULAR WAVES

It appears that the actual wave condition in the ocean can best be represented by use of the model of a random process as derived by Neumann and described by Pierson, Neumann, and James (1960). Statistical values such as average wave height are given, not values of the environment as a function of time. The sea is taken as a summation of a large number (or as an integral of an infinite number) of uniform wave trains, each with different amplitudes and directions superimposed in random phase. The profiles of the individual waves are assumed to be sine curves according to Airy's Theory (Johnson (1951)).

Techniques are available to predict the amplitudes of the waves and their distribution over the frequency range from wind velocity, wind duration, and the fetch. Generally, the result can be presented in the form of a wave spectrum, which is the distribution of the mean squares of the wave amplitudes in a given increment of the frequency (spectral density) over the wave frequencies.

In the following analysis, it is assumed that the waves are unidirectional and meet the ship or submerged vessel head on. This case is realistic, as it represents the crafts moored in swell.

Following the work by St. Denis and Pierson (1953), the relation between the spectral density of wave and ship responses is given by

$$S_r(\omega) = S_w(\omega)\left[T(\omega)\right]^2 \tag{72}$$

where

$S_r(\omega)$ = spectral density of the response in a particular variable (displacement, strain, etc.)

$S_w(\omega)$ = spectral density of the wave

$T(\omega)$ = ratio of response in a particular variable to wave amplitude (complex frequency factor)

If the spectrum of the waves if given, the spectrum of the response can be calculated by Eq. (70). The mean square of the response is then given by

$$\sigma^2 = \int_o^{\omega} S_r(\omega)\,d\omega = \int_o^{\omega} S_w(\omega)\left[T(\omega)\right]^2 d\omega \tag{73}$$

It has been shown by Longuet-Higgins (1952) that for a relatively narrow band of wave frequencies, such as is the case with swells being assumed

here, the probability distribution of the wave amplitudes tends to be Gaussian if the frequency factor has nonzero values in the range of wave frequencies. Consequently, it may be expected that the probability distribution of the response amplitudes is also Gaussian.

Longuet-Higgins calculated important statistical relationships for the narrow-frequency spectrum, which were consequently tabulated by Pierson, Neumann, and James (1960); for example

$$R_{av} = 1.25\,\sigma \qquad \text{(Average response amplitude)}$$

$$R_{1/3} = 2.0\,\sigma \qquad \text{(Average response amplitude of the 1/3 highest responses equals significant response amplitude)}$$

In many instances, the response spectrum may not be considered to be narrow, and the expected number (M_α) of maxima of the response per unit time exceeding the value of the response $R(t) = \alpha$ can be expressed after Bendat (1958) as

$$M_\alpha = \frac{1}{2\pi}\left(\frac{E\left[R'(t)^2\right]}{\sigma^2}\right)^{1/2} e^{\left(\frac{-\alpha^2}{2\sigma^2}\right)} \tag{74}$$

where

$$E\left[R'(t)^2\right] = \int_0^\infty \omega^2 S_w \left[T(\omega)\right]^2 d\omega \tag{75}$$

Thus, this presentation introduces the probability concept into the calculation of movements and cable stresses.

EFFECT OF THE NONLINEAR MOORING-LINE FORCES

In the analyses of the response, it has been assumed that the restoring forces of the cables are linear with the displacement by use of Eqs. (2) and (3). This assumption will introduce certain errors in the calculated response and the mooring-line forces.

Considering the spread-moored ship, it has been seen that the pitch and surge are coupled because of the bow and stern mooring lines.

If the total horizontal restoring force of a system is plotted as a function of the horizontal displacement for different pitch angles, a graph of the type presented in Fig. 5 will be obtained. In this graph the linearization calculated by Eqs. (2) and (3) is also plotted.

The nonlinearity of the total restoring force is much smaller than that of the individual cables.

It will be seen from such graphs that force-displacement curves for different pitch angles are essentially parallel for equal distances over the expected range of pitch angles.

It is assumed that movements in surge extend into the nonlinear range. The horizontal restoring force may now be written, following the procedures of Crandall (1961), by extending the linear Eq. (8)

$$F_h = 2a\left[x + \epsilon g(x)\right] - 2(bL + ap)\theta \tag{76}$$

where

ϵ = small parameter modifying the nonlinear function
$g(x)$ = odd single-valued power function of x

The values ϵ and $g(x)$ are chosen in such a manner that for zero pitch angle, Eq. (76) is identical with the force-displacement curve obtained by use of calculations of the catenary equations.

The coupled equations of motion in surge and pitch for the ship in irregular waves can now be written by introducing the nonlinearity in Eq. (27).

$$\ddot{x} + \frac{N_{xx}}{M_{xx}}\dot{x} + \frac{2a}{M_{xx}}\left[x + \epsilon g(x)\right] + \frac{K_{x\theta}\theta}{M_{xx}} = I_x(t) \tag{77}$$

$$\ddot{\theta} + \frac{N_{\theta\theta}}{M_{\theta\theta}}\dot{\theta} + \frac{K_{\theta\theta}}{M_{\theta\theta}}\theta + \frac{K_{\theta x}\theta}{M_{\theta\theta}} = I_\theta(t) \tag{78}$$

where $I_x(t)$ and $I_\theta(t)$ are random functions, both derived from the wave spectrum.

Equation (77) may be rewritten by introducing the equivalent linear stiffness coefficient K_{eq}

$$\ddot{x} + 2\alpha\dot{x} + K_{eq}x + k_{x\theta}\theta = I_x(t) + \Xi \tag{79}$$

where

$$\Xi = \left(K_{eq} - \omega_{o_x}^2\right)x - \epsilon\omega_{o_x}^2 g(x) \tag{80}$$

$$\omega_{o_x}^2 = 2a/M_{xx} \tag{81}$$

Assuming that Ξ is zero, the mean square response of the system to an irregular sea with a particular spectrum is found by Eq. (73)

$$\bar{\sigma}_x^2 = \int_o^\infty S_w(\omega)\left[T(\omega)\right]^2 d\omega \tag{82}$$

The spectral density $S_w(\omega)$ is given from the assumed sea condition, and the square of the absolute value of the complex-frequency factor $\left[T(\omega)\right]^2$ is obtained from Eq. (42)

$$\left[T_{x,\eta}(\omega)\right]^2 = \left| \frac{\begin{vmatrix} \bar{F}^x_{ex} & K_{x\theta} \\ \bar{F}^\theta_{ex} & \bar{Z}_{\theta\theta} \end{vmatrix}}{\begin{vmatrix} \bar{Z}_{xx} & K_{x\theta} \\ K_{\theta x} & \bar{Z}_{\theta\theta} \end{vmatrix}} \right|^2 \tag{83}$$

where

$$\bar{Z}_{xx} = -\omega^2 M_{xx} + j\omega N_{xx} + M_{xx} K_{eq} \tag{84}$$

Introducing Eqs. (83) and (84) into Eq. (82)

$$\bar{\sigma}_x^2 = G\, f\left(K_{eq}\right) \tag{85}$$

for small variation of K_{eq} from $\omega_{o_x}^2$, Eq. (85) may be expressed

$$\bar{\sigma}_x^2 = G_w \left[1 + \gamma\left(K_{eq} - \omega_{o_x}^2\right)\right] \tag{86}$$

where $G_w = \bar{\sigma}_o^2$ = spectral energy of the response for $\epsilon = o$

$$\gamma = \frac{d\, f\left(K_{eq}\right)}{d\, K_{eq}} \text{ at } K_{eq} = \omega_{o_x}^2 \tag{87}$$

In the analysis with Eqs. (82) through (86) it was assumed that the remainder function Ξ equals zero, which is naturally not the case; Ξ is again a stationary random process just like $I_x(t)$ and depends on the value of the equivalent stiffness coefficient. A measure of its value is its expected mean square $E\left[\Xi^2\right]$

The mean square of the remainder function Ξ can be expressed by use of Eq. (80)

$$E\left[\Xi^2\right] = K_{eq}^2\, E\left[x^2\right] - 2K_{eq}\omega_o^2 E\left[x^2 + \epsilon x g(x)\right] + \omega_o^4 E\left[\left\{x + \epsilon g(x)\right\}^2\right] \tag{88}$$

This will be a minimum for fixing K_{eq} when

$$\frac{d\left(E\left[\Xi^2\right]\right)}{dK_{eq}} = 0 \tag{89}$$

which results in

$$K_{eq} = \omega_{o_x}^2 \left(1 + \epsilon \frac{E\left[xg(x) \right]}{E\left[x^2 \right]} \right) \tag{90}$$

Inserting Eq. (90) into Eq. (86) results in

$$\frac{\bar{\sigma}_x^{-2}}{\bar{\sigma}_o^{-2}} = 1 + \gamma \omega_{o_x}^2 \epsilon \frac{E\left[xg(x) \right]}{E\left[x^2 \right]} \tag{91}$$

The probability density of a random variable Y with zero mean value is

$$f(Y) = \frac{1}{\sigma\sqrt{2\pi}} e^{-Y^2/2\sigma^2} \tag{92}$$

where σ = standard deviation.

The expectation value $E\left[xg(x) \right]$ in Eq. (91) is for the nonlinear system, which would require knowing the response of the nonlinear system. Fortunately, the term in Eq. (91) is to be multiplied by the small parameter ϵ, and the expectation value $E\left[xg(x) \right]$ of the linear system instead of the nonlinear system will induce errors of the second order.

Consequently

$$\frac{\bar{\sigma}_x^{-2}}{\bar{\sigma}_o^{-2}} = 1 + \frac{\gamma \epsilon \omega_{o_x}^2}{\sqrt{2\pi}\, \bar{\sigma}_o^3} \int_{-\infty}^{+\infty} xg(x) e^{-x^2/2\sigma_o^2} dx \tag{93}$$

by which the effect of the linearization can be investigated. The term γ may be positive or negative.

DISCUSSION

The mathematical models presented here have shortcomings. The most important one is the assumed linear relationship between the restoring forces and the displacement of the ship. The effect of the nonlinearity of the mooring lines in the surge motion, which is particularly affected by the nonlinearity, was investigated in detail in the previous section of this paper, and a method was presented for calculating the ratio of the mean square of the nonlinear response and the linear response.

Naturally, the methods of analyzing the response of the moored ship has the limitations that are imposed on the analysis of a free-floating vessel, and the direct force-displacement relationship established in the section about mooring-line characteristics limits the method to mooring in a few hundred feet depth as only to that depth are the dynamic effects on the mooring line considered small.

Unfortunately, no experimental data are available in the literature to check the analysis in detail. A paper (Wiegel (1958)) describing model tests performed at the University of California presents no detailed information concerning the important characteristics of the vessel and its moorings, but by selecting a mooring with about the same characteristics in surge, one can obtain good agreement between experimental and calculated values of the response of an 880-ton vessel (Figs. 6 and 7 by Leendertse (1963)).

The design of moorings by using the formulas of this paper can be expedited considerably by graphical representation of the exciting forces and the impedances.

Since the impedance concept is introduced in the calculating of the responses, the procedures used for electrical circuit design and the design of servomechanisms appears to be a powerful tool for the numerical calculation of responses. Graphical representation of exciting forces and the impedances by use of complex plane diagrams enhances the understanding of the complicated phase relationship between waves and responses (Chestnut (1951)).

In practically all cases, the surge response of the vessel is the main contributor to high forces in the mooring lines. This is caused by the fact that very limited damping is available in this mode of movement. In principle, a reduction of the surge response is possible by two methods: namely, by increasing the damping or by mismatching the natural frequency in surge with the main range of frequencies of wave excitations. The application of the first method is limited because it is difficult. In an incidental case, surge movements have been limited by the introduction of damping devices in the mooring lines. Since wind and currents, whose effects are not discussed here, impose certain requirements on the mooring-line tensions, the applicability of the second method is often also limited.

In the previous sections of this paper, a few relatively simple but realistic cases where the ship was moored in the longitudinal plane of symmetry were considered. Mooring lines in directions other than the main axis will introduce coupling between many more modes of movement than is studied in this paper.

Weinblum and St. Denis (1950), in their now classical paper, presented a method for calculating the uncoupled motions of an unrestrained ship in its six degrees of freedom in regular waves with arbitrary heading. This work has been expanded by Pierson and St. Denis (1953) for the movement in irregular waves with a directional spectrum.

If the motions of the free-floating ship are considered uncoupled, the same ship in a moored condition will have coupled motions due to the mooring lines. For an arbitrary mooring, for example, the linearized equation of motion in surge becomes

$$M_{xx}\ddot{x} + N_{xx}\dot{x} + K_{xx}x + K_{xy}y + K_{xz}z + K_{x\theta}\theta + K_{x\psi}\psi + K_{x\varphi}\varphi = \overline{F}^{x}_{ex}\, Ae^{j\omega t} \tag{94}$$

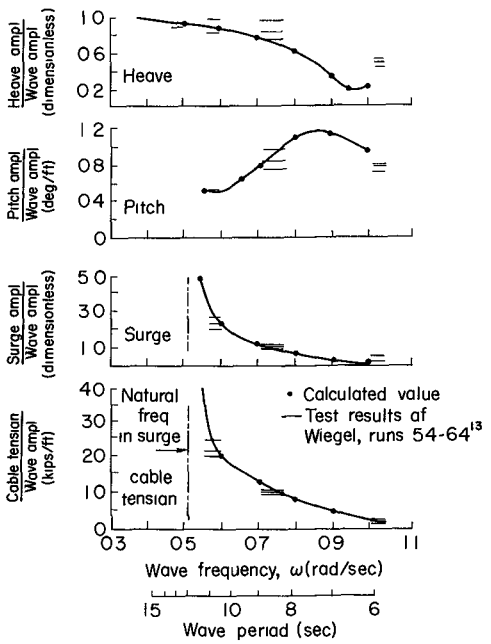

FIG 6 EXPERIMENTAL AND CALCULATED VALUES OF RESPONSE OF AN 880-TON VESSEL

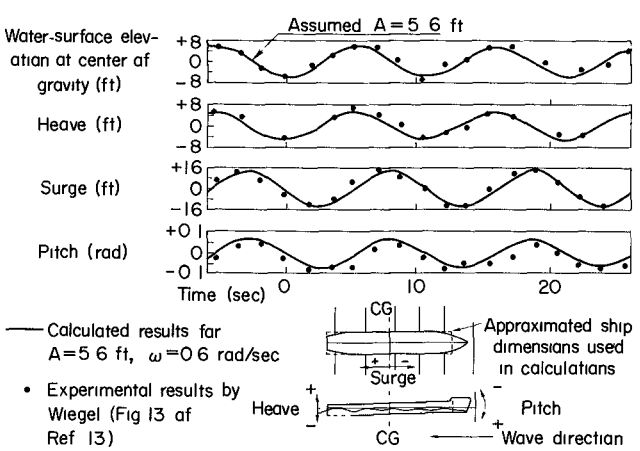

FIG 7 COMPARISON BETWEEN CALCULATED AND MEASURED RESPONSES OF A MOORED SHIP IN UNIFORM WAVES

The equations of motion in the other modes are similar, and the solution of response operators follows the pattern of Eqs. (52) to (61). The coefficients K_{xy}, K_{xz}, etc., depend on the mooring lines and can be calculated in a manner similar to that for the spread-moored ship in waves head-on (e.g., Eqs. (6) through (8)).

The procedure for the investigation of the nonlinear effects is not limited to unidirectional waves. For a directional wave spectrum, containing only energy in two quadrants such as the directional Neumann wind wave spectrum, Eq. (82) becomes

$$\bar{\sigma}_x^2 = \int_0^{\infty} \int_{-\pi/2}^{+\pi/2} S(\omega,\beta) \left| T(\omega,\beta - \chi) \right|^2 d\beta \, d\omega \qquad (95)$$

where

β = angle between direction of wave propagation and the coordinate system of the ship

χ = angle between center of the directional wave spectrum and the coordinate system of the ship

The directional complex response operators in Eq. (95) is calculated by use of Eq. (83) if one takes into account that the excitations F_{ex}^{x} and F_{ex}^{θ} are functions of the wave angle. The procedure in this section for nonlinear effects is otherwise generally valid.

In cases where the response operator of the linearized system is peaked within the frequency range of the maximum wave amplitudes, the gamma (γ) coefficient in Eq. (86) will be small and consequently the effect of the linearization used upon expectation values of the nonlinear response amplitudes will be very small.

REFERENCES

Weinblum, Georg, and Manley St. Denis (1950). On the Motions of Ships at Sea: Trans. SNAME, vol. 58, pp. 184-231.

Korvin-Kroukovsky, B. V. (1961). Theory of Seakeeping: Society of Naval Architects and Marine Engineers, New York.

Korvin-Kroukovsky, B. V., and Winnifred R. Jacobs (1957). Pitching and Heaving Motions of a Ship in Regular Waves: Trans. SNAME, vol. 65, pp. 590-632.

Wilson, Dr. Basil W. (1959). The Energy Problem in the Mooring of Ships Exposed to Waves: Perm. Int. Assoc. of Nav. Congresses Bull. No. 50.

Kriloff, A. (1898). A General Theory of the Oscillations of a Ship on Waves, and On Stresses Experienced by a Ship in a Seaway: INA, vol. 40, pp. 135-212.

Weinblum, Georg (1954). Progress of Theoretical Investigations of Ship Motions in a Seaway: Ships and Waves, pp. 129-159.

Pierson, Williard J., Gerhard Neumann, and Richard W. James (1960). Observing and Forecasting Ocean Waves: Hydrographic Office Pub. 603.

Wiegel, R. L., and J. W. Johnson (1951). Elements of Wave Theory: Proc. of the First Conf. on Coastal Engineering, Council on Wave Research, Berkeley, California.

St. Denis, Manley, and Willard J. Pierson, Jr. (1953). On the Motions of Ships in Confused Seas: Trans. SNAME, vol. 61, pp. 280-357.

Longuet-Higgins, M. S. (1952). On the Statistical Distribution of the Heights of Sea Waves: J. Mar. Res., vol. 11, pp. 245-266.

Bendat, Julius S. (1958). Principles and Applications of Random Noise Theory: John Wiley and Sons, New York, pp. 130-133.

Crandall, Stephen (1961). Random Vibrations of Systems with Non-Linear Restoring Forces: Massachusetts Institute of Technology, AFOSR 708,

Wiegel, R. L. (1958). Model Studies of the Dynamics of an LSM Moored in Waves: Proc. of Sixth Conf. on Coastal Engineering, Council on Wave Research, Berkeley, California.

Leendertse, J. J. (1963). Analysis of the Response of Moored Surface and Subsurface Vessels to Ocean Waves: The RAND Corporation, RM-3368-PR, Santa Monica, California.

Chestnut, Harold, and Robert W. Mayer (1951). Servomechanism and Regulating System Design: J. Wiley and Sons, New York.

APPENDIX

A = wave amplitude

A_s = horizontal cross-sectional area of a ship at the still water surface

A_π = horizontal cross-sectional area of a buoy at the still water surface

$\overline{A}$ = complex value of the movement in surge for a wave with unit height

a,b,c,d = coefficients in linearized mooring-line equations

$\overline{B}$ = complex value of the movement in pitch for a wave with unit height

$\overline{C}$ = complex value of the movement in heave for a wave with unit height

d_1 = coefficient in linearized mooring-line equations

E = expectation value

F_n = resultant horizontal component of the restoring forces of the mooring cables

$\overline{F}^s_{ex}$ = complex value of the exciting force or moment in the s mode of movement for a wave of unit height

$f()$ = function

$\overline{f}^{s}_{ex}$ = complex value of the exciting force or moment per unit mass

G = spectral energy of the response for $\epsilon = o$

g = acceleration of gravity

$g(x)$ = odd-single valued power function of x

$H_{(o,o)}$ = horizontal force at the holding point (o,o)

$H_{(x,z)}$ = horizontal force at the holding point (x,z)

h = vertical distance between the holding point of a mooring line and the sea bottom

$I_x(t)$ = random (force) function, derived from the wave spectrum

$I_\theta(t)$ = random (moment) function, derived from the wave spectrum

Jy = inertia moment of the horizontal cross-sectional area of a ship around the y axis

K_{eq} = equivalent linear stiffness coefficient

$K_{s\tau}$ = stiffness coefficient in force equation of the s mode for the movement in the τ mode

k_{st} = stiffness coefficient per unit of mass

L = half-length of a ship

M_h = total moment of the horizontal components of the bow and stern lines

M_p = total moment due to the vertical forces in the mooring lines perpendicular to the long axis of the ship

$M_{s\tau}$ = virtual mass or mass inertia moment in the force on moment equation of the s mode for the movement in the τ mode

M_v = total moment of the vertical component of the bow and stern lines

M_α = expected number of maxima of the response per unit time exceeding the value of the response $R(t) = \alpha$

$M_{1_{xx}}$ = virtual mass in the x movement

$M_{2_{xx}}$ = virtual mass in the x movement

$M_{3_{xx}}$ = virtual mass in the x movement

M'' = added mass

$N_{s\tau}$ = linearized damping term in the force equation of the s mode for movement in the τ mode

p = vertical distance between the holding points of a mooring line and the mass center of the ship

R_{av} = average response amplitude

R_t = periodic force due to other modes of movement

$R(t)$ = response amplitude

$R_{1/3}$ = average response amplitude of the 1/3 highest responses (i.e., of the highest third of all amplitudes)

S = total length of a mooring line

$S_w(\omega)$ = spectral density of the response in a particular variable

s = general indication for mode of movement

T = total force in a mooring line

$T(\omega)$ = ratio of response in a particular variable to wave amplitude (complex frequency factor)

$\left[T(\omega)\right]^2$ = square of the absolute value of the complex frequency factor

t = time

$V_{(o,o)}$ = vertical force in a mooring line at the holding point o

$V_{(o,o)_p}$ = vertical component of the force in the mooring lines perpendicular to the long axis of the vessel

$V_{(x,z)}$ = vertical force in a mooring line at the holding point (x,z)

w = net weight of a mooring line per unit length

x,y,z = Cartesian co-ordinate axes

Y = random variable with zero mean value

$\bar{Z}_{ss} = -\omega^2 M_{ss} + j\omega N_{zz} + K_{zz}$ (impedance)

α = a value of the response

β = angle between direction of wave propagation and the co-ordinate system of the ship

γ = coefficient = $\dfrac{df(K_{eq})}{dK_{eq}}$

ϵ = small parameter modifying the nonlinear function

θ = pitch angle

Ξ = remainder function (Eq. 79)

σ = root mean square

σ_o = root mean square of the response of the assumed linear system in surge

σ_x = root mean square of the response of the nonlinear system in surge

τ = general indication for mode of movement (used only as a subscript)

φ = angle of roll

χ = angle between center line of the directional wave spectrum and the co-ordinate system of the ship

ω = wave frequency

ω_{o_s} = natural frequency in the s mode

Chapter 47

SEA TESTS OF A SPREAD-MOORED LANDING CRAFT

J.T. O'Brien and B.J. Muga

Engineers, U.S. Naval Civil Engineering Laboratory, Bureau of Yards and Docks, Department of the Navy, Port Hueneme, California

ABSTRACT

Sea tests of motion and mooring force were conducted on an LST (Landing Ship Tank) of about 4400 long tons displacement. The LST was spread-moored by six 2-1/16 inch and one 1-1/4 inch (port breast) stud-link chains in simple catenary configuration in about 45 feet of water in the open Gulf of Mexico about 65 air miles south of New Orleans, Louisiana. Water-level variations at a single location, ship rotations and accelerations, mooring force, and wind were measured in sea states of 2 and 4. Three recordings of 38, 62, 67 minutes duration were analyzed, using time-series techniques to provide apparent amplitude-response operators for all of the ship's motions and seven mooring chains. Theoretical prediction of the operators using long crested regular waves was made also. In longitudinal plane, theory predicts motions 1/3 to 4 times and chain tensions 1/4 to 9 times those measured. The most probable maximum-motion amplitude responses in sea state 4 are found to be 1.7, 1.1, and 1.7 feet, respectively, in surge, sway and heave, and 3.4 and 0.5 degrees, respectively in pitch and yaw. Roll was measured only in sea-state 2 with a corresponding maximum of 2.1 degrees. Maximum wave-induced chain tensions in kips were: 85.1 and 48.0 in port and starboard bow chains respectively; 10.6 (sea state 2) and 19.7 in port and starboard breast chains; 13.9 and 4.3 in port and starboard quarter chains (sea state 2) and 9.7 in stem chain. Total tension in port bow chain was 116.1 kips (85.1 plus initial tension of 31.0 kips). Chain response operators vary directly with initial tension, whic complicates design.

It is concluded that: (i) moor was unbalanced, i.e., port bow chain took most of load; (ii) chains loaded lightly, e.g., maximum wave induced tension was 116 kips compared to new proof load of 300 kips for the particular chain, the port bow; (iii) water level should be measured at more than one point; (iv) discouragement over differences is balanced by encouragement over agreements between measurements and theoretical prediction of motion and chain tension; (v) toward improvement: Theory needs extension to include short crested waves and barge types; (vi) initial tension unique to problem of mooring design; (vii) propulsion devices may be needed toward maintaining design initial tension, especially in storm; (viii) if directional spectra had been measured and if theory involving short crested waves had been available and used, then discrepancies between observation and theory likely would have been less.

INTRODUCTION

As the need to operate from fixed platforms floating at the sea surface at points beyond the continental shelf boundaries increases due to dictates of National defense, economic forces and scientific requirements, ways to hold these platforms in position when subjected to the forces of wind, wave, and current have to be developed.

One way to hold such a platform in position is to power it, continually sense its position, and continually apply power to maintain it on station.

A second way is to moor the platform by means of anchor and lines. Systems using conventional and even stake pile anchors and heavy anchor chains are very common. They have been employed in water of varying depth to moor a number of different kinds of platforms.

In high wave and strong winds, platforms moored in this way are subject to forces and motions of a complex nature. In turn, the mooring chains experience tensions that are much greater than those experienced under calm conditions. Such platforms have, in fact, broken their mooring chains and been lost or damaged.

The failure of the anchor chains can be due to the imposition of forces beyond their design capability or to the gradual deterioration of the chain in a marine environment. In either case, the nature of the forces applied to the chain needs to be investigated theoretically and compared with measurements.

Also the nature of the motions of the moored platform due to the forces of wind and wave needs to be investigated as a measure of the kinds of work that can be done on such a platform.

A platform restrained by mooring chains in the two horizontal directions will seek an equilibrium position in which the chains, hung from the platform in the form of a catenary, when displaced from this equilibrium position by the force of the wind on the "sail" area of the platform and by the effects of waves and currents, exert forces (of the nature of spring constants) in surge, sway, and yaw. These tend to restore the platform to its equilibrium position. These restoring forces have to be added to the equations that describe the motions of the platform.

As a simple case, the restoring forces can be treated as linear, but, especially for extreme motions that may occur, these forces may be non-linear depending on terms of the form $(k_1 + k_2 (x)^2)x$ where x is the displacement in surge, and k_1 and k_2 are constants reflecting particular chain properties. Due to coupling with the other motion components, the analysis of the non-linear problem appears to be difficult. Some analytical and theoretical success has been achieved with the linear

model.

The other complicating effect in this problem is the nature of the applied excitations. The wind, being turbulent, exerts a mean force on the platform and a fluctuating component with periods that are more than 30-minutes on down through 10-minutes, 5-minutes, 1-minute, 30-seconds, and so on. The waves, in turn, contain periods ranging from 20 seconds on down.

Both the wind and the waves can be represented by stationary random processes that oscillate about certain mean values and that grow and shrink from oscillation to oscillation. The application of random process theory to the problem of the moored platform is essential toward understanding its behavior.

However, and this is the rub, the extreme values that occur in random process theory are the least well-documented aspect of the theory and depend on probability concepts that are the most subject to criticism. In particular, the non-linear and not well-understood model of the moored system needs to be analyzed when the motions are extreme.

Despite these difficulties, some progress has been made in gathering and analyzing the data pertinent to the behavior of moored systems and in developing a theory to explain and interpret the data. It is the purpose of this paper to present the highlights of the results of tests of a particular system and to point out where theoretical and observational improvements can be obtained. It is based on the report to the U.S. Naval Civil Engineering Laboratory by O'Brien and Muga (1964).

THE SHIP AND ITS INSTRUMENTATION

THE SHIP

The craft studied is a landing ship tank (LST CLASS 542) modified to serve as a tender for an offshore drilling platform about 30 feet forward of her bow. The owners, the Califomia Company, designate the craft as S-23. It has a length of 319 feet at the waterline, an extreme moulded breadth of 50 feet, a draft of 12 feet, and a displacement of 4420 long tons. Other characteristics are given in Table I.

The craft (Figure 1) was spread-moored in 45 feet of water in the open Gulf of Mexico, at about N 29-01-42 W 90-09-18, approximately 65 air miles south of New Orleans, Louisiana, by six 2-1/16 and one 1-1/4 inch stud-link chains with proof breaking loads when new of 300 and 185 kips, respectively. Their length varied from approximately 440 feet at the port bow to 1, 140 feet at the quarter (Figure 2) as shown in Table II, which lists the results of on-site measurements. These were difficult and required about three weeks of work by a large crew, including a three man team of divers.

The port bow chain (No. 2) was anchored to a 10,000 pound conventional anchor. The remaining six chains were anchored to stake piles. In addition, a 10,000 pound conventional anchor helped to hold the stern chain (No. 6).

The craft was displaced analytically in the longitudinal and transverse directions, i.e., in surge and sway respectively. The resulting change in chain tensions were calculated and resolved in proper components to provide values for restoring force of 20.0 kips per foot in surge (k_x), 12.7 kips per foot in sway, (k_y) and 5.62 kip-feet per degree of the yaw (k_ψ), as shown in Table I. The chains were considered ineffective against heave, pitch, and roll.

DATA PICKUPS

A total of seventeen measurements were made simultaneously as a function of time on 3 September, namely: water level variation (wave) at one point; wind speed and direction; ship acceleration in surge, sway, and heave at bow and sway and heave at stem; roll and pitch; tension in all seven chains (Figure 1). On 23 March, roll, pitch and tension, in three of the chains (#1, 5, and 7) were not measured due to malfunctioning of the pickups.

Water level variation (wave) was measured at a point approximately 30 feet forward from the bow of the craft by means of a vertical staff of the resistance type. Electrical type water level sensors, similar to sparkplugs, were fastened to the staff at one half foot intervals in the vertical from about -10 to+20 feet mean water level; their shorting on contact with water was sensed through a proper electrical circuit.

Table I. Characteristics of LST (S-23), Class 542

Length (ft):	
overall	327.8
at water-line	318.6
between perpendiculars	316.0
Breadth, B, extreme molded, (ft)	50.0
Draft, D, (ft)	12
Depth, h, molded, at midships, (ft)	25.16
Water Depth, d, (ft)	45
Displacement, long tons	4,420
Mass, M, lbs-sec^2/ft^4 (slug)	307,478
A_s surface area at water-line (3rd deck), (ft^2)	14,887
Free period of oscillation (seconds/cycle): *surge = 24.6; *sway = 31.1	
roll	6.8
*pitch	3.3 to 4.4
*heave	5.1
BG, Vertical distance between CG and CB (ft)	5.9
OG, Vertical distance from free surface to CG (ft)	0.2
GM, Metaccentric height (ft)	11.8
CG, Center of gravity (ft):	
aft fwd perpendicular	171.6
above keel	12.2
I_{x_T}, virtual moment of inertia about x-axis (including added moment of inertia) (slug-ft^2)	1.38×10^8
I_y, ship's moment of inertia about y-axis (slug-ft^2)	1.97×10^9
I_z, ship's moment of inertia about z-axis (slug-ft^2)	2.020×10^9
ξ_s, coordinate of aft-most point at water-line (center-of-gravity coordinate system), (ft)	-155.3
ξ_b, coordinate of fore-most point at water-line (center-of-gravity coordinate system), (ft)	163.3
Restoring force:	
surge, k_x, kips/foot	20.0
sway, k_y, kips/foot	12.7
yaw, k_ψ, kip-feet/degree	5.62

*calculated.

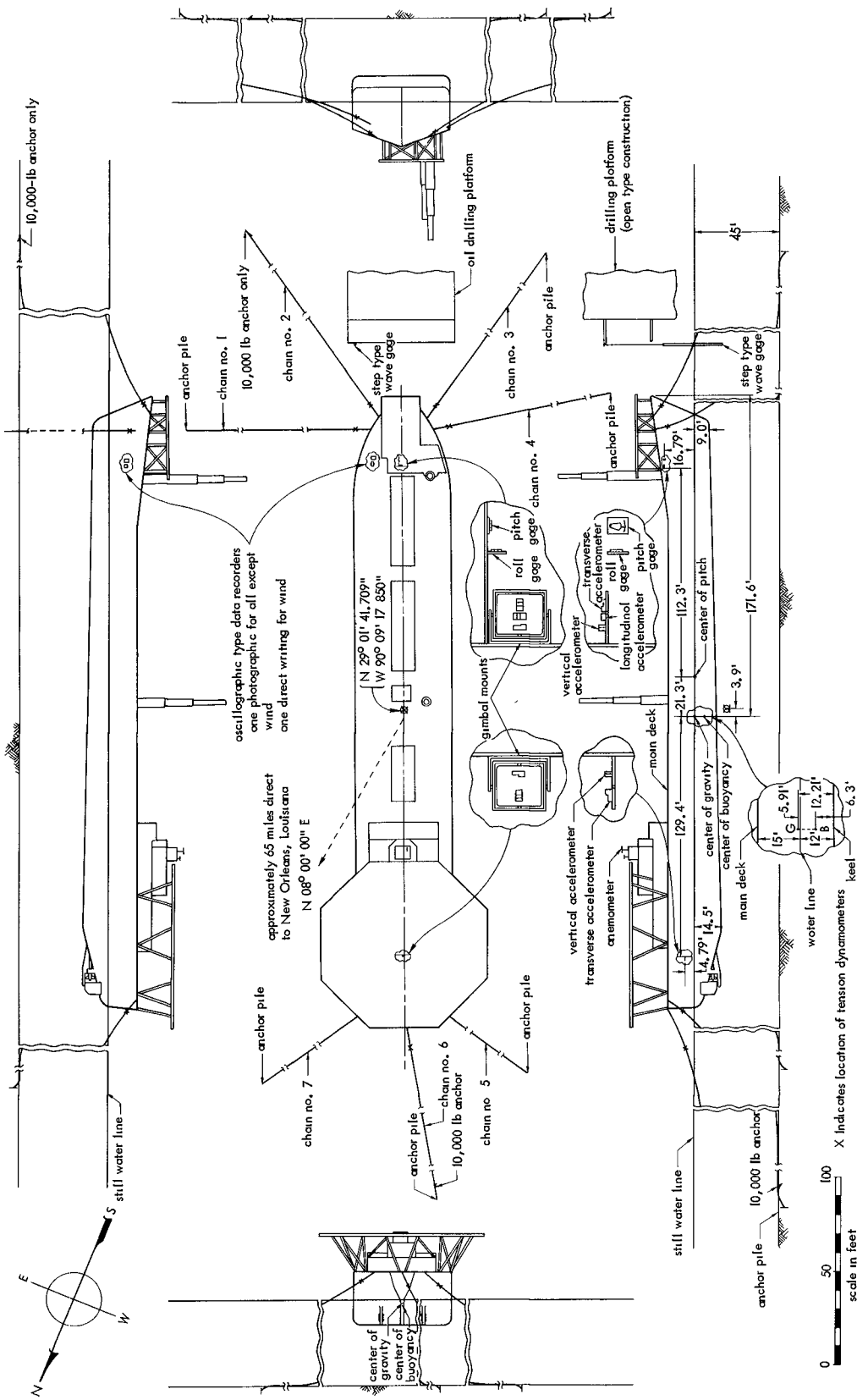

Figure 1 LST as moored and instrumented.

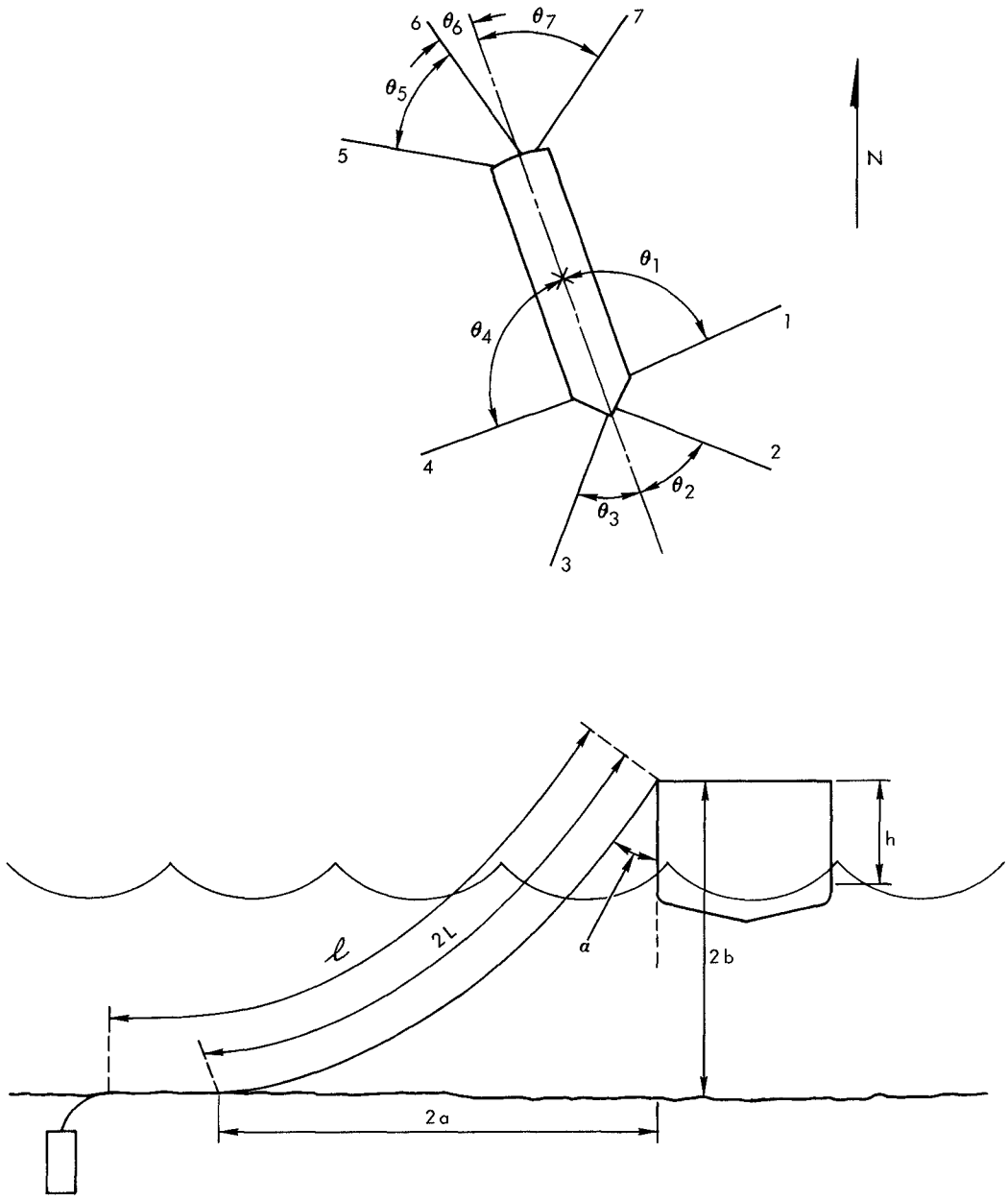

Figure 2 Convention used to describe mooring chain geometry. (See Table II for actual dimensions and tensions.)

Table II. Characteristics of LST Moorings
(See Figure 3 for explanation of symbols)

Chain No.	Chain Position	2b (feet)	h (feet)	s (feet)	ℓ (feet)	2L (feet)	2a (feet)	α (deg.)	θ (deg.)	Initial Tension			
										Equilibrium (kips)	23 March AM (kips)	23 March PM (kips)	3 Sept (kips)
1	Port Breast	35.7	10.0	910.5	915.4	174.8	169.9	24.7	87.25	6.0	---	---	10.8
2	Port Bow	63.0	21.0	430.7	438.8	328.1	320.0	20.6	35.00	31.1	31.0	30.6	34.6
3	Starboard Bow	71.6	23.0	598.3	609.1	321.0	310.2	23.9	34.78	26.4	30.2	30.7	28.3
4	Starboard Breast	66.0	20.5	868.4	884.0	191.0	175.4	37.2	87.53	10.8	17.7	17.8	6.6
5	Starboard Quarter	51.0	17.5	971.4	981.6	173.7	163.5	32.6	51.92	11.2	---	---	12.2
6	Stern	57.7	18.0	817.1	824.3	312.7	305.5	22.2	11.0	30.6	7.4	7.6	24.1
7	Port Quarter	54.0	17.0	1132.4	1140.8	233.5	224.7	26.6	53.97	18.6	---	---	21.5

Note: (1) Values for 2b through θ are for the equilibrium condition; they are assumed to reflect those for 23 March and 3 September to a significant accuracy.

(2) All chains are stud-link. No. 1 is 1-1/4 inch; all others are 2-1/16 inch.

A conventional torque type recording selsyn-type anemograph was used to measure wind speed and direction. Both the direction vane and the speed cups were located on the bridge of the ship, approximately 40 feet above the water surface or 25 feet above the main deck.

Ship acceleration was measured by gimbal mounted linear accelerometers with sensitivity of about 0.001 G as installed on the longitudinal axis of the ship; three 112.3 feet forward of the C.G. for measurements in respectively surge, sway, and heave directions; two about 129.4 feet aft of the C.G. for measurements in respectively sway and heave directions.

Separate conventional pendulum type inclinometers were used to measure roll and pitch.

Chain tension was measured by means of a four wire strain gage bridge, cemented to a standard link in each of the seven chains. The vertical inclination of the link was not recorded; however, it was measured manually periodically.

All pickups were part of separate energized electrical circuits such that pick-up response was sensed by the deflection of a galvanometer, and this deflection suitably recorded by means of a photographic type oscillograph at relatively low paper speeds, i.e., 13.2 inches per minute on 23 March and 2.75 inches per minute on 3 September. The exception was the wind velocity pickup, whose output was recorded by a direct writing oscillograph, which was part of the anemograph.

The velocity of the surface currents was measured periodically with a propeller type meter and also with floats. In general, these measurements were difficult and not always successful.

MEASUREMENTS MADE

GENERAL

Figure 3 is a facsimile of four minutes duration, taken from an oscillogram on 3 September. It is typical of the total of about 100 hours of measurements made in 1958. The highly embroidered profile for water level is reflected in that of the responses. Water level was recorded as a series of equivalent one-half foot steps on the original oscillogram; they have been rendered as a continuous line on the facsimile.

Note the low frequency component of about 39 seconds period (0.17 radians per second) in the chain response, particularly for numbers 2, 3, and 7, as excited by a beam-on wave of this period.

Wind velocity was measured continuously with all other quantities and recorded on a conventional type anemogram.

MEASUREMENTS SELECTED FOR ANALYSIS

Three continuous records of measurement, during which a stationary random process was assumed to exist, were selected for analysis: 38 minutes in the morning of 23 March (1146 to 1223 CST), 62 minutes in the afternoon of 23 March (1225 to 1326 CST), and 67 minutes on 3 September (1200 to 1306 CST).

As noted under "Data Pickups," the 3 September data contains output from seventeen different pickups; that for 23 March is less data from the inoperative roll, pitch and three chain tension pickups (#1, 5, 7).

The measurements of wind velocity, although complete, were only scanned since, although the wind displaced the craft from its equilibrium position, it was not high enough to interfere significantly with the response of the craft to waves, which was the main concern of the study.

To permit machine analysis, the height of each pickup trace above a base line was read at intervals of one-second and recorded as punches (data points) on standard machine type cards; specifically: 2281 and 3721 points for 23 March and 4021 points for 3 September.

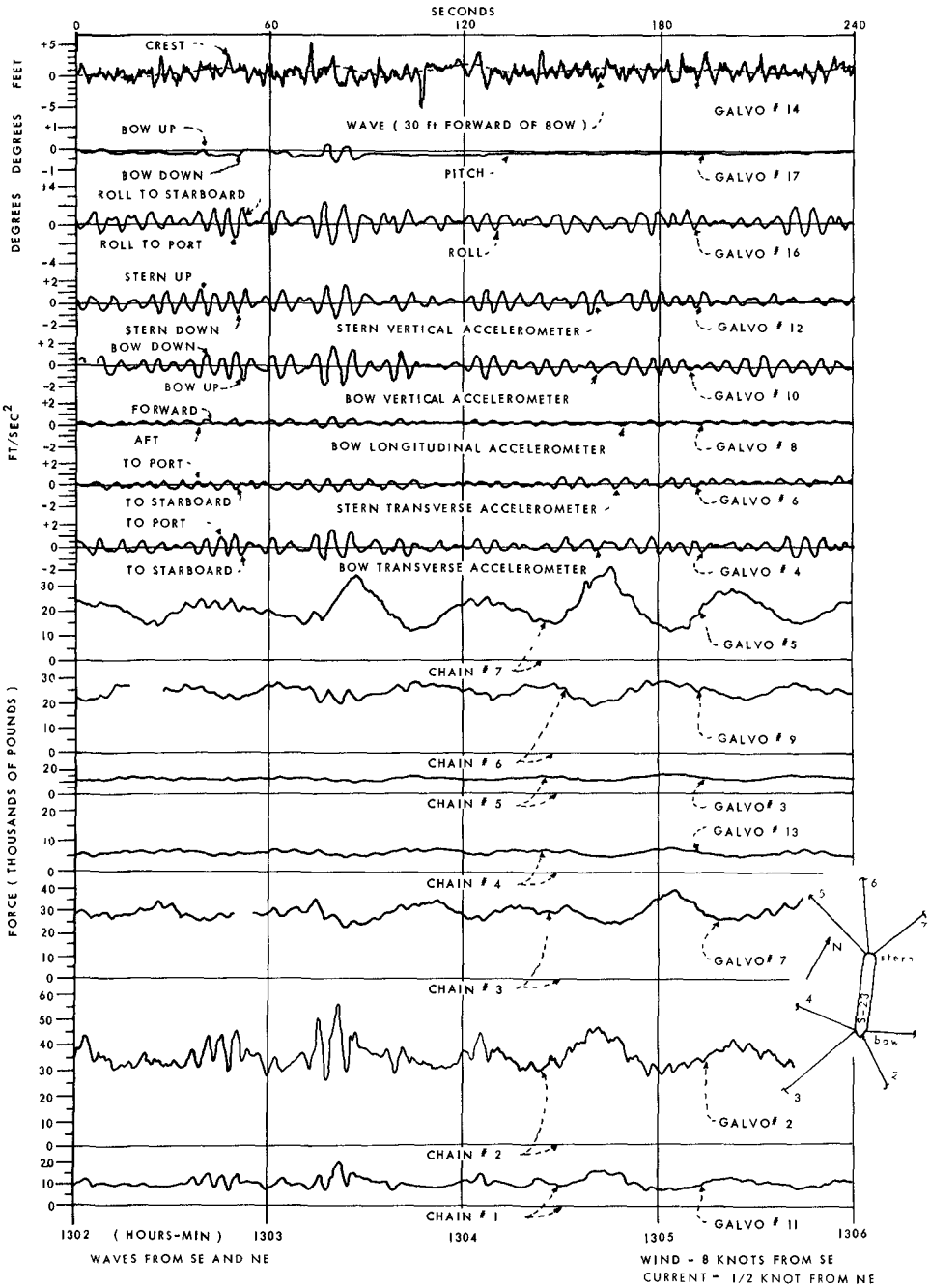

Figure 3 Facsimile of oscillogram for 3 September, 1302 to 1306 CST.

METHODS OF ANALYSIS

The analysis of measurements as complex as those obtained in this study (Figure 2) would have been improbable if not impossible a few years ago. However, due to the pioneer work of Pierson (1952), based on the earlier work of Blackman and Tukey (1958) in electrical engineering, and applied by Canham, et. al. (1963), among others, to seakeeping trials, the analysis technique now is nearly routine, albeit tedious. Therefore, only a very general explanation of it is given here.

The time-series technique forms the basis for the analysis. A stationary random process is assumed over a period of sensible duration. All answers obtained are statistical in nature with the attendant variability. The principle of linear superposition is used as a device for breaking down the complex records of excitation (sea state), mooring force, and ship response into simple elements. The irregular excitations and responses are regarded as the approximate sum of a number of regular sinusoidal components in a random phase relationship.

By use of correlation functions and transforms, the energy in the irregular wave record is isolated into particular magnitudes (square of the amplitude (A) of water level, motion or force) in particular frequency (ω) bands. These two quantities are used to plot a diagram known as the "energy spectrum" specifically (A^2/ω) versus ω.

For a particular frequency, the ratio of the response ordinate to the excitation ordinate gives an ordinate on a diagram known as the "response amplitude operator." For the sea tests such as these, the response operator tends to provide a check on the rigor of the sea measurements since it can also be obtained experimentally in the laboratory with a reduced scale model and also theoretically where, in both cases, regular long-crested waves are used.

The phase of one motion relative to another is obtained by comparing the recorded amplitude of one motion to that of the other by use of cross spectral analysis technique.

The quantity, which indicates the departure of the field measurements from those predicted by experiments and theories based on long-crested waves, is termed "coherency." This measures the ratio of that part of two signals having a definite phase relationship to the total power in the two signals.

For spectra and cross spectra, the coherency is related to the correlation coefficient of the records after passing them through the equivalent of a band-pass filter to study a particular narrow filter range.

A value of coherency equal to, or near, unity provides a confirmation of the linearity of the relationship between two particular motions within the frequency

range analyzed, and of essentially long-crested wave action on the system. If the data are believed to be accurate, and digitization and computations are carefully checked, then coherencies less than one are a measure of the short crestedness of the forcing waves.

Finally, the degree to which the true value is approximated by an estimate is defined by "confidence limits" as computed from familiar probability theory.

By use of the area (E) under the energy spectrum, termed the variance, important statistical predictions can be made on the basis of a Rayleigh distribution and information contained in Longuet-Higgins (1952). For example, $\sqrt{E}$ multiplied by the following factors gives the following amplitudes: 0.707 for the most frequent; 0.886 for the average; 1.416 for average of highest one-third; 1.800 for average of highest one-tenth. The factor for the most probable maximum is not so straightforward. It is necessary to first determine the average number of oscillations in a particular record and thereby to determine the average period. The number of oscillations in the record is then computed and this number applied to the proper curve in Longuet-Higgins (1952) to obtain the factor by which $\sqrt{E}$ is multiplied in order to obtain the value of the most probable maximum. This factor differed for each of the three test records, namely: 2.60 and 2.67 on AM and PM 23 March respectively and 2.72 on 3 September. The values in Table 5 are based on all of these factors, using the values of the variances as given.

Sorting indicates that the excitation and response amplitudes tend to have a Rayleigh distribution. This is more the case for wave amplitudes than for the chain tensions as is apparent from comparing the results in Tables 4 and 5 for sorting and variance type prediction, respectively.

Even if it had been possible to measure the directional spread of the wave energy, it would not have been possible to obtain the response operators from response measurements since particular motions could not be related to waves from a particular direction. However, since some insight into these important operators was desired, a uni-directional wave system was assumed so that by use of measurements of water level at a single point and of the analytical techniques outlined previously, it was possible to obtain a quantity termed "apparent response amplitude operator." The adjective "apparent" is dropped hereinafter. Yawing of the vessel as well as the directional effects are contained in this somewhat crude operator.

Heave, surge, sway and yaw were not measured directly. Rather, they were deduced along with pitch from acceleration measurements using the technique described by Cartwright (1957) and also O'Brien and Muga (1963). Pitch was also measured directly along with roll on one day: 3 September. Acceleration measurements pertinent to roll were not made, unfortunately.

Simple harmonic motion was assumed for both excitation and response, e.g., acceleration was divided by the square of the pertinent frequency to obtain displacement.

Table III. Frequency of Peak-Response Energy and Corresponding Amplitude (To obtain corresponding chain tension add the initial tensions given in Table II)

	Frequency (ω) (raps)			Period (T) (spc)			Amplitude			
	23 March		3 Sept	23 March		3 Sept	23 March		3 Sept	
	AM	PM		AM	PM		AM	PM		Units
Surge	0.60	0.66	0.75	10.5	9.5	8.4	1.22	1.45	0.25	feet
Heave	0.60	0.57	1.07	10.5	11.0	5.9	0.89	1.03	0.31	feet
Pitch	0.63	0.63	1.01	10.0	10.0	6.2	2.2	2.3	0.31	degrees
Pitch Measurement			0.97			6.5			0.31	degrees
Sway	0.88	0.85	0.94	7.1	7.4	6.7	0.84	0.78	0.53	feet
Yaw	0.60	0.63	0.63	10.5	10.0	10.0	0.35	0.31	0.24	degrees
Roll			0.94			6.7			0.92	degrees
Water Level	0.66	0.66	1.04	9.5	9.5	6.0	3.43	3.75	1.41	feet
Chain Nos:										
1			0.16			39.3			1.3	kips
			1.20			5.7			not definable	
2	0.16	0.16	0.16	39.3	39.3	36.0	5.3	5.4	2.6	kips
	0.63	0.66	0.97	10.0	9.5	6.5	7.2	8.9	3.1	kips
3	0.22	0.19	0.16	28.6	33.1	39.2	4.45	3.5	2.0	kips
	0.63	0.66	1.04	10.0	9.5	6.0	7.95	8.15	1.45	kips
4	0.16	0.16	0.16	39.3	39.3	39.3	1.37	1.37	0.45	kips
	0.63	0.63	1.01	10.0	10.0	6.2	4.60	4.43	1.35	kips
5			0.16			36.0			1.0	kips
			1.20			5.7			not definable	
6	0.19	0.19	0.25	33.1	33.1	25.1	1.73	1.65	1.73	kips
	0.63	0.66	1.01	10.0	9.5	6.2	2.10	2.15	1.2	kips
7			0.16			39.3			3.9	kips
			1.20			5.7			not definable	

Table IV. Amplitudes From Sorting

1	2	3	4	5	6	7
	Most Frequent	Average	Average Of Highest 1/3	Average Of Highest 1/10	1/2 of Maximum Double Amplitude	Maximum Single Amplitude
Chain 1 (kips):						
3 Sept	1.5	1.6	2.9	3.8	6.5	10.6
Chain 2 (kips):						
23 Mar AM	9.5	8.8	14.8	23.5	54.0	85.1
23 Mar PM	10.5	9.0	15.0	21.1	32.5	58.4
3 Sept	2.5	3.2	5.7	8.0	16.5	22.9
Chain 3 (kips):						
23 Mar AM	3.8	6.2	11.4	17.4	29.5	44.5
23 Mar PM	3.8	6.6	11.3	15.1	23.5	29.8
3 Sept	1.5	1.7	3.2	4.3	7.0	10.6
Chain 4 (kips):						
23 Mar AM	2.5	3.3	5.5	7.9	13.5	19.7
23 Mar PM	2.8	3.3	5.5	7.0	10.0	13.8
3 Sept	0.3	0.3	0.6	1.1	2.5	4.7
Chain 5 (kips):						
3 Sept	0.5	0.5	1.1	1.7	2.5	4.3
Chain 6 (kips):						
23 Mar AM	1.8	1.9	3.2	4.0	6.5	9.9
23 Mar PM	1.8	2.0	3.1	3.5	5.5	9.8
3 Sept	1.3	1.4	2.3	3.1	4.5	5.0
Chain 7 (kips):						
3 Sept	1.8	2.4	5.0	6.8	11.0	13.9
Water Level (feet):						
23 Mar AM	1.8	2.6	4.4	5.8	8.0	9.5
23 Mar PM	1.8	2.6	4.3	5.8	7.8	9.0
3 Sept	1.3	1.1	1.7	2.0	4.5	5.0
Roll (degrees):						
3 Sept	0.6	0.7	1.1	1.5	2.1	2.1
Pitch (degrees):						

Table V. Amplitudes Obtained from Spectral Variance

1	2 Limits Lower (raps)	2 Limits Upper (raps)	3 E	4 $\sqrt{E}$	5 Most Frequent	6 Average	7 Average Of Highest 1/3	8 Average Of Highest 1/10	9 Most Probable Value of Maximum
Water Wave (feet):									
23 Mar AM	0.44	1.88	5.50	2.35	1.66	2.08	3.32	4.22	6.11
23 Mar PM	0.44	1.80	5.57	2.36	1.66	2.09	3.34	4.25	6.30
3 Sept	0.44	1.80	1.10	1.05	0.74	0.93	1.49	1.89	2.86
Surge (feet):									
23 Mar AM	0.50	1.57	0.44	0.66	0.47	0.59	0.93	1.19	1.72
23 Mar PM	0.50	1.57	0.59	0.77	0.54	0.68	1.09	1.38	1.58
3 Sept	0.50	1.57	0.02	0.15	0.11	0.14	0.22	0.28	0.41
Heave (feet):									
23 Mar AM	0.44	1.57	0.34	0.58	0.41	0.51	0.82	1.04	1.51
23 Mar PM	0.44	1.57	0.45	0.67	0.47	0.59	0.94	1.20	1.79
3 Sept	0.70	1.57	0.04	0.19	0.13	0.17	0.26	0.34	0.52
Pitch, measured (degrees):									
3 Sept	0.44	1.57	0.03	0.18	0.13	0.16	0.26	0.33	0.49
Pitch, derived (degrees):									
23 Mar AM	0.44	1.57	1.37	1.17	0.83	1.04	1.66	2.11	3.04
23 Mar PM	0.44	1.57	1.64	1.28	0.91	1.13	1.81	2.31	3.42
3 Sept	0.44	1.57	0.03	0.18	0.13	0.16	0.26	0.33	0.49
Sway (feet):									
23 Mar AM	0.69	1.57	0.19	0.43	0.31	0.38	0.61	0.78	1.12
23 Mar PM	0.69	1.57	0.17	0.41	0.29	0.37	0.59	0.74	1.09
3 Sept	0.82	1.57	0.10	0.32	0.23	0.28	0.45	0.58	0.87
Yaw (degrees):									
23 Mar AM	0.44	1.88	0.03	0.18	0.13	0.16	0.26	0.33	0.47
23 Mar PM	0.44	1.88	0.05	0.23	0.16	0.20	0.32	0.41	0.61
3 Sept	0.44	1.88	0.02	0.13	0.09	0.12	0.18	0.23	0.35
Roll (degrees):									
3 Sept	0.63	2.51	0.62	0.79	0.56	0.70	1.11	1.42	2.15

Units: (a) Column 3 is square of underscored unit in Column 1.
(b) Columns 4 through 9 are the same as underscored unit in Column 1.
For example, "feet" in Column 1 gives "feet^2" in Column 3, but "feet" in columns 4 through 9.

Table V. Amplitudes Obtained from Spectral Variance (Cont)

1	2		3	4	5	6	7	8	9	
	Limits Lower (raps)	Upper (raps)	E (kips squared)	$\sqrt{E}$ (kips)	Most Frequent (kips)	Average (kips)	Average Of Highest 1/3 (kips)	Average Of Highest 1/10 (kips)	Most Probable Value of Maximum By Frequency (kips)	Total (kips)
Chain 1:										
3 Sept	0.00	0.63	1.57	1.25	0.89	1.11	1.77	2.26	3.25	
3 Sept	0.63	1.57	1.10	1.05	0.74	0.93	1.49	1.89	2.80	
Chain 2:										
23 Mar AM	0.00	0.41	27.30	5.22	3.69	4.63	7.40	9.40	13.57	21.11
23 Mar PM	0.00	0.44	28.30	5.32	3.76	4.71	7.53	9.58	14.20	21.76
3 Sept	0.00	0.63	6.45	2.54	1.80	2.25	3.60	4.57	6.91	9.36
Chain 2:										
23 Mar AM	0.41	1.88	38.60	6.21	4.39	5.50	8.80	11.18	16.15	
23 Mar PM	0.44	1.88	38.10	6.17	4.36	5.47	8.74	11.11	16.48	
3 Sept	0.63	2.20	5.35	2.31	1.64	2.05	3.28	4.16	6.28	
Chain 3:										
23 Mar AM	0.00	0.47	12.55	3.54	2.50	3.14	5.02	6.38	9.20	15.44
23 Mar PM	0.00	0.47	10.50	3.24	2.29	2.87	4.59	5.83	8.65	15.86
3 Sept	0.00	0.63	3.93	1.98	1.40	1.76	2.81	3.57	5.39	5.82
Chain 3:										
23 Mar AM	0.47	1.88	22.70	4.76	3.37	4.22	6.75	8.58	12.38	
23 Mar PM	0.47	1.88	24.80	4.98	3.52	4.41	7.05	8.96	13.30	
3 Sept	0.63	2.20	0.63	0.79	0.56	0.70	1.12	1.43	2.15	
Chain 4:										
23 Mar AM	0.00	0.41	1.96	1.40	0.99	1.24	1.98	2.52	3.64	7.67
23 Mar PM	0.00	0.41	1.96	1.40	0.99	1.24	1.98	2.52	3.74	7.88
3 Sept	0.00	0.63	0.31	0.56	0.39	0.49	0.79	1.00	1.52	3.40
Chain 4:										
23 Mar AM	0.41	1.88	6.75	2.60	1.84	2.30	3.68	4.68	6.76	
23 Mar PM	0.41	1.88	6.75	2.60	1.84	2.30	3.68	4.68	6.94	
3 Sept	0.63	1.88	1.26	1.12	0.79	0.99	1.59	2.02	3.05	
Chain 5:										
3 Sept	0.00	0.63	0.70	0.84	0.59	0.74	1.18	1.51	2.28	
						0.79	1.26	1.60	2.42	

Table V. Amplitudes Obtained from Spectral Variance (Cont)

1	2		3	4	5	6	7	8	9	
	Limits		E	$\sqrt{E}$	Most		Average	Average	Most Probable Value of Maximum	
	Lower (raps)	Upper (raps)	(kips squared)	(kips)	Frequent (kips)	Average (kips)	Of Highest 1/3 (kips)	Of Highest 1/10 (kips)	By Frequency (kips)	Total (kips)
Chain 6:										
23 Mar AM	0.00	0.41	2.20	1.48	1.05	1.31	2.10	2.67	3.85	5.25
23 Mar PM	0.00	0.41	1.89	1.37	0.97	1.22	1.95	2.47	3.66	5.18
3 Sept	0.00	0.63	2.20	1.48	1.05	1.31	2.10	2.67	4.03	4.41
Chain 6:										
23 Mar AM	0.41	1.88	1.89	1.37	0.97	1.22	1.95	2.47	3.56	
23 Mar PM	0.41	1.88	1.89	1.37	0.97	1.22	1.95	2.47	3.66	
3 Sept	0.63	1.88	0.42	0.65	0.46	0.57	0.92	1.17	1.77	
Chain 7.										
3 Sept	0.00	0.63	8.95	2.99	2.12	2.65	4.24	5.38	8.13	
3 Sept	0.63	1.88	0.94	0.97	0.69	0.86	1.37	1.75	2.64	

Frequency (ω) is expressed in radians per second abbriviated as raps; period (T) is expressed in seconds per cycle abbreviated as spc; $\omega = 2\pi/T$.

The digitized measurements were manipulated in a high-speed computer to provide a seemingly endless stream of answers, of which a few of the more important are presented herein.

EXCITATION

HIGH FREQUENCY WAVES

These were wind generated with peak frequency of 0.66 raps on 23 March and 1.04 raps on 3 September (Figure 4 and Table 3). Both spectra seem conventional with variance (area under the spectrum) of 5.6 ft.^{2} on 23 March and 1.1 ft.^{2} on 3 September. These indicate to sea states of 4 and 2 respectively.

Distribution of amplitudes was obtained by sorting and by predicting from the spectral variance as outlined in Method of Analysis. Results (Table 4 and 5) indicate that amplitudes from sorting are 1.1 to 1.5 times those predicted. This of course detracts from the neatness of the value of the variance type prediction. It could be due to: Improper pickup performance; lack of Rayleigh amplitude distribution; and errors in data analysis.

LOW FREQUENCY WAVES

Although a beam-on seiche of about 39 seconds period was present, as deduced from chain response, the water level pickup with sensors at 1/2 foot intervals in the vertical did not sense it, at least consistently. Hence, its amplitude is assumed to have been less than 1/4 foot.

WIND AND CURRENTS

Winds on 23 March were generally from 135 - 146 degrees azimuth at 20 to 24 knots with gusts to 28 knots and from 113 - 135 degrees on 3 September with gusts to 24 knots where bow on winds are from 159 degrees. Currents on both days are considered to have had negligible dynamic effect. Along with winds they tended only to displace the ship from its position of static equilibrium and hence to alter the initial tension in the mooring chains.

RESPONSE

GENERAL

Response (Figures 4, 5 and 6) like excitation, was in two frequency bands; a

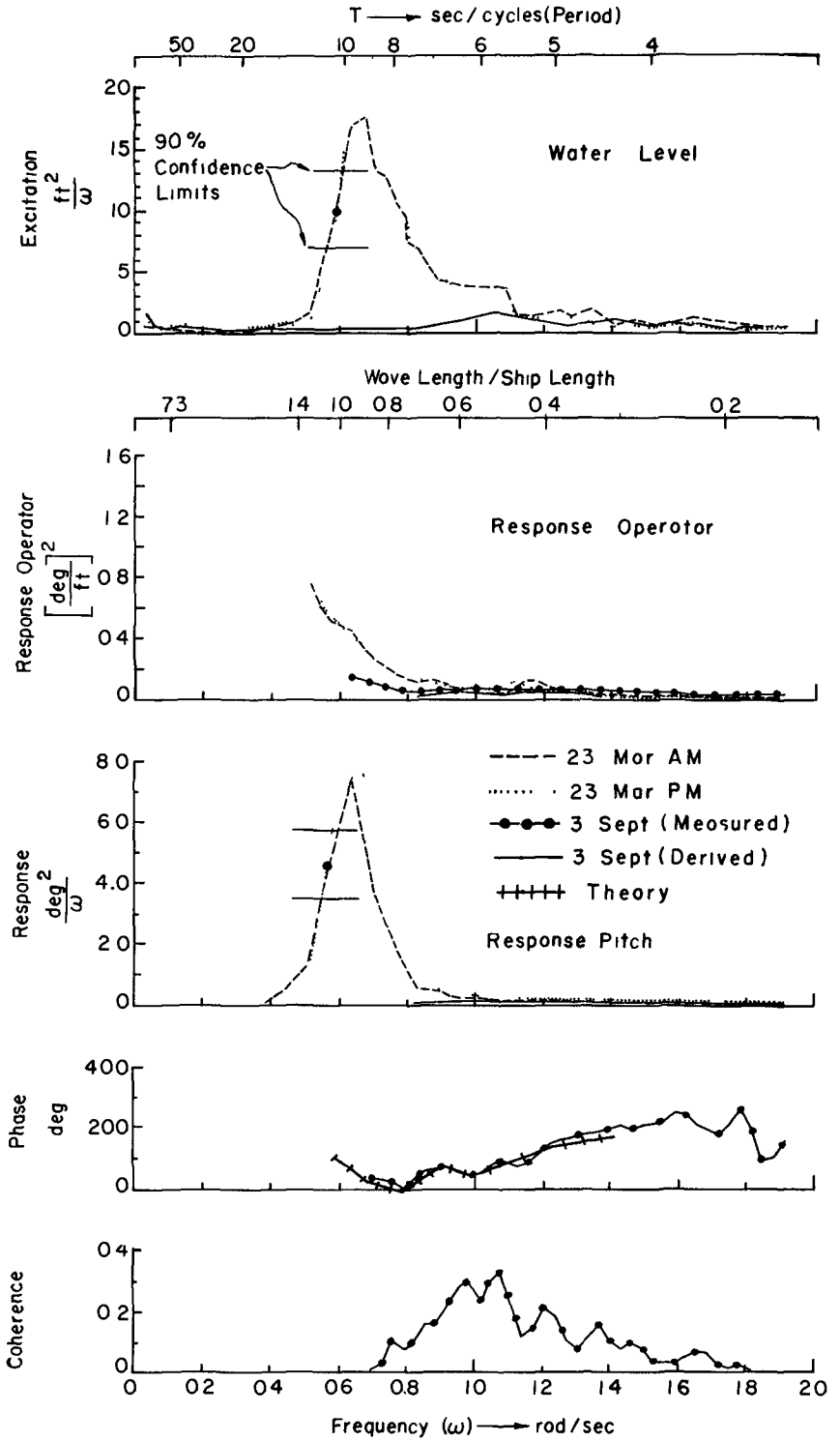

Figure 4 Water level versus pitch. In the range 1.0 to 2.0 radians per sec the response as measured direct and as derived from acceleration measurements are sensibly the same; therefore, the former is not shown. The phase convention is: Pitch bow up lags water level (wave) crest up.

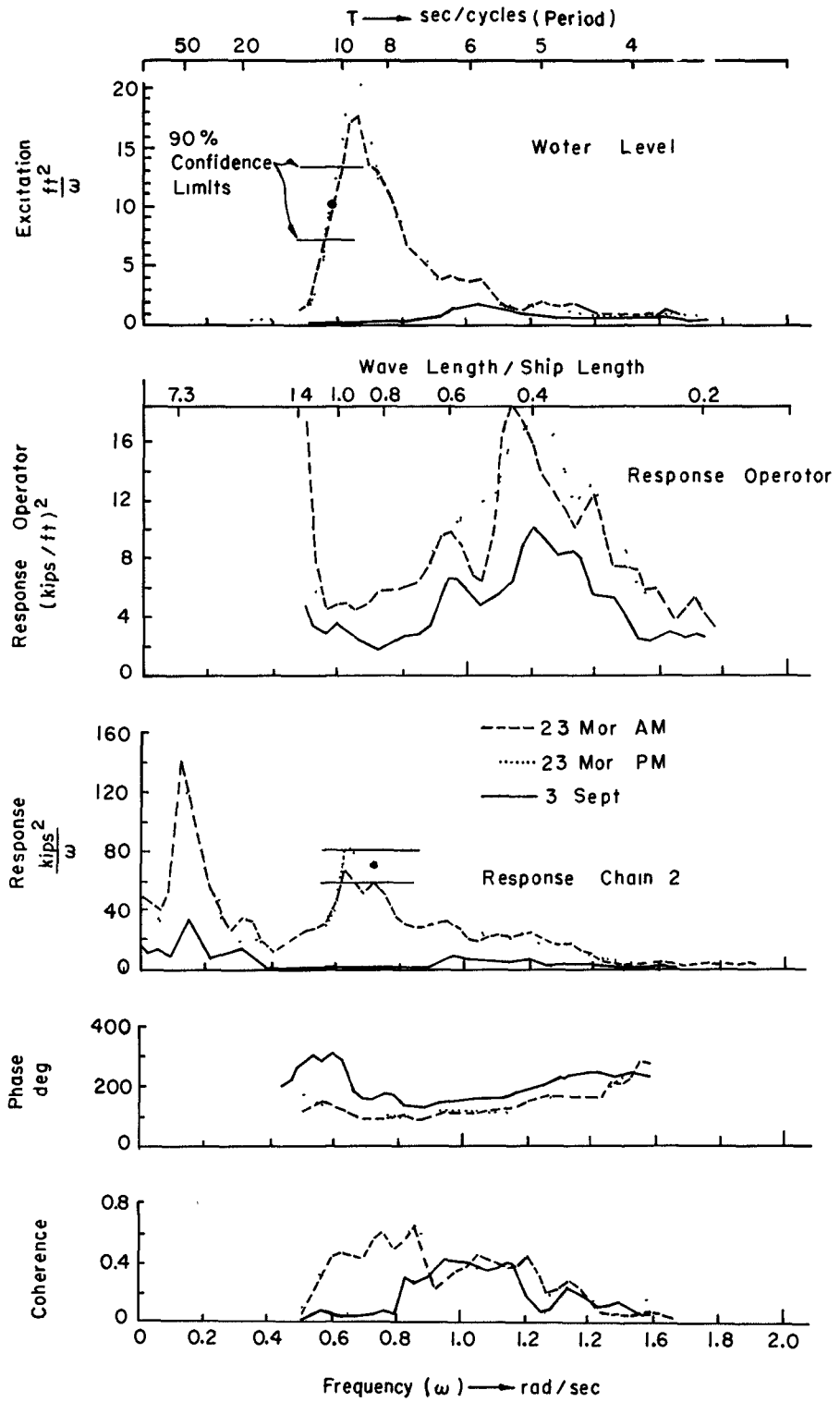

Figure 5 Water level versus tension in the port bow chain (No. 2). The phase convention is: Tension increase lags water level (wave) crest up.

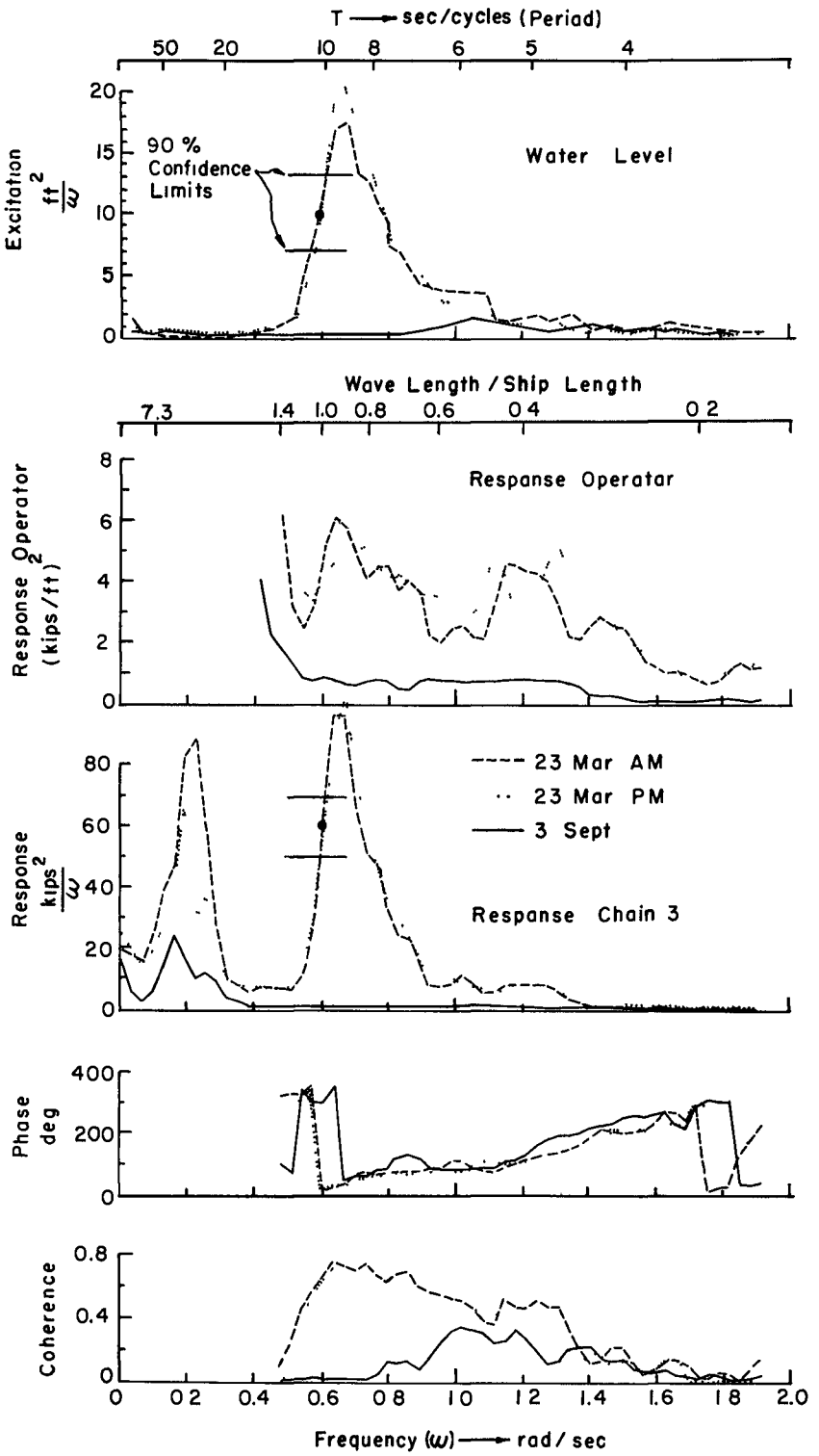

Figure 6 Water level versus tension in starboard bow-chain (No. 3). The phase convention is: Tension increase lags water level (wave) crest up.

high one due to wind wave excitation of from 0.50 to 1.28 raps frequency (12.6 to 4.9 spc period) as sensed by all pickups; a low one, due to unexpected seiche action of from 0.16 to 0.19 raps (39.1 to 32.1 spc) as sensed only by the chain tension pick-ups. The latter was a happy accident.

It likely is feasible to calculate motion of a moored ship from measurements of tension induced in its moorings. However, in the case of these tests, such calculations were considered much too tedious. Thus, low frequency ship motion, although likely considerable, is not accounted for.

There was ship response in all six degrees of freedom; that in the longitudinal plane was more evident.

Phase angle, relative to the excitation (wave) was obtained for all responses over a considerable frequency range; however, only those for pitch and the bow chains are presented (Figures 4, 5, and 6).

LONGITUDINAL MOTIONS

Values for surge, heave and pitch as predicted from the spectral variance are tabulated in Table 5. Note that the most probable maximum amplitude for the three periods was: 1.7 feet surge and heave and 3.4 degree pitch. These are slight motions but sufficient to induce noticeable changes in chain tensions.

LATERAL MOTIONS

In the high frequency range, the lateral motions were much less than the longitudinal. The most probable maximum was 1.1 feet sway and 0.5 degrees yaw (Table 5). The equivalent for roll on 3 September was 2.1 degrees; however, this is not likely a maximum for the three periods since the roll on 23 March was likely higher.

The high frequency lateral motions are the result of the directional nature of the short-crested nearly bow on waves. For example, in commenting on the roll of a ship in head-seas and symmetrically oriented relative to the encounter spectrum of short-crested waves, Pierson (1957) writes:

> " . . . . The oncoming apparent waves will at one time be high on the port side and at another be high on the starboard side causing the vessel to roll first one way and then the other for the same apparent wave form . . . . "

He implies that the coherencies will be near zero in head seas between the following, water level variation and roll; heave and pitch; and pitch and roll. This was found to be the case in these tests; for example, the coherency between water level and roll was found to be 0 to 0.3 on 3 September.

As mentioned, the ship motions excited by the low frequency beam on wave was not sensed. They were likely high especially in surge. Some idea of their magnitude could be obtained from an analysis of the changes in chain tension at this frequency; however, this would be tedious and very time-consuming.

CHAIN TENSIONS

Note in Table 5 that the significant and most probable maximum change in tension, as predicted using the spectral variance, are 8.8 and 21.8 kips respectively. Both were in the port-bow chain (#2). Responses at high and low frequencies were of comparable magnitudes.

However, these do not agree with those obtained by sorting (Table 4) where comparable values of 14.8 and 54.0 kips were found (The maximum single amplitude was 85.1 kips and that in the port-bow chain). Generally, it appears that sorting gives amplitudes 1.5 to 2.5 times those predicted from the spectral variance. The reasons are the same as those given for similar disagreements noted for the high frequency waves.

Sorting within the two frequency bands, rather than overall, as in Table 4, is of course feasible and might provide a better basis for checking variance type prediction. It would not of course change the value of the overall maximum.

The wave induced tensions do not seem alarming when considered relative to the new chain proof load. This is 185 kips for the single light chain (#3) and 300 kips for the rest, compared to the maximum total tension of 116.1 kips, i.e., 85.1 kips maximum wave induced amplitude plus 31.0 kips initial tension, as measured in the heavy port chain (#2) on 23 March A.M. (Table 4).

Of course, it is not obvious that all chains could have withstood even their new proof load, no less their ultimate, due to deterioration by, for example, corrosion and fatigue and without parting due to poor connections of the chain to anchor and ship. Therefore, during storm, new proof load could be small consolation to the captain charged with the safety of the ship. He might understandably tend to drop the moorings and take to the sea unfettered when his seaman's eye seemed to sense critical chain tensions. This tendency existed and one of the objectives of these tests was to quantify the seaman's eye toward keeping the ship on station longer in higher seas and thereby, to reduce the down time on the bow-on oil drilling rig which the ship served.

RESPONSE AMPLITUDE OPERATORS FROM MEASUREMENTS

GENERAL

This operator was developed from the measured data by operations at successive frequencies (ω) over the full spectral range as follows: The amplitude of the response spectrum (ft^2 or deg^2 or $kips^2/\omega$) was divided by amplitude of the excitation spectrum (ft^2/ω) to obtain the corresponding amplitude of the response amplitude operator (ft^2 or deg^2 or $kips^2/ft^2$). Linearity between excitation and response and long-crested waves were assumed in all cases. That these assumptions were not realized fully is discussed in the concluding part of this chapter.

When linearity exists, the operator is a powerful design tool for it is apparent that it can be used generally to predict response from excitation and of course, excitation from response, e.g., wave spectrum from the response of a buoy.

Because of their importance, the analysis of the test results was directed mainly to obtaining these operators so as hopefully to predict ship response at sea states higher than those encountered in the tests and also to compare the operators with those predicted by theory since of course this is the ultimate design tool. Operations derived from model tests were not available.

LONGITUDINAL MOTION OPERATORS

These are shown in Figures 7 and 8 where it is apparent that the amplitude of surge and heave decreases with increased frequency as would be expected. The pitch operators tend to peak at about 0.7 raps frequency or about where wave length equals ship length. Thereafter, they decrease with increased frequency. Operators derived from the three separate sets of measurements agree fairly well, although less so at the lower frequencies, especially for heave (Figure 7). A curve eyeballed through them is likely adequate for engineering design.

LATERAL MOTION OPERATORS

These were determined but are not presented here. As mentioned under "Response," they are the result of the directional nature of the short-crested nearly bow-on waves. Roll and yaw amplitudes did not exceed 1.0 and 0.1 degrees per foot of wave amplitude respectively over the most of the significant frequency range of 0.5 and 1.6 raps. Sway showed a notable peak of about 0.4 feet/foot at about 0.9 raps (7.0 spc) on the 23 March operator. That from the 3 September measurements was generally 1-1/2 to 3 times higher.

CHAIN TENSION OPERATORS

All operators have a peak at about 1.25 and 0.16 raps frequency. The equivalent periods are 5.0 and 39.3 seconds per cycle and wave length/ship length ratios

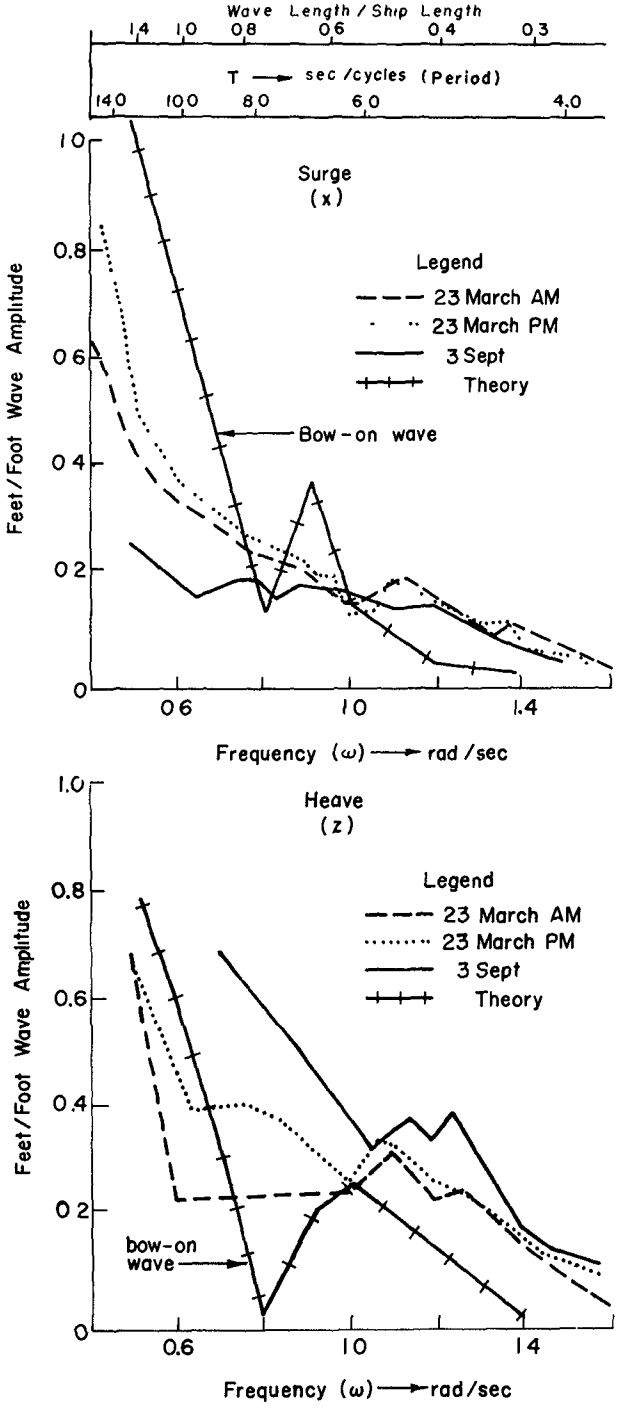

Figure 7. Response amplitude operator for surge and heave.

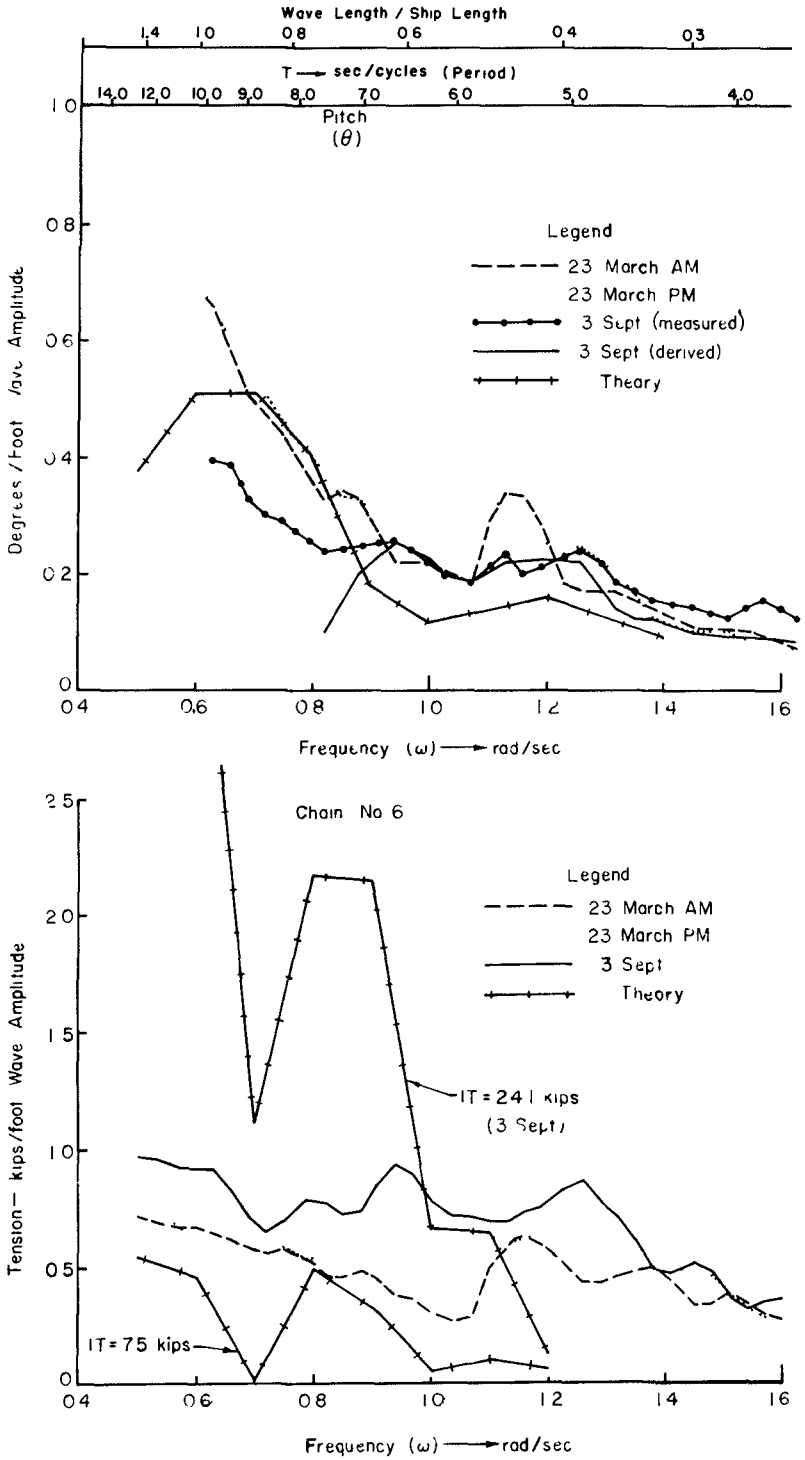

Figure 8. Response amplitude operator for pitch and stern chain (#6).

0.4 and 4.6 respectively.

The high frequency peak is that predicted for the surge of the unmoored ship by Wilson (1959 Equation 21). The low frequency peak is close to the calculated resonant frequency in surge of 0.25 raps.

The two bow chains dominated with that on the port the greater; the other five chains served mainly to keep the ship from fishtailing significantly. For example, at 1.25 raps, the change of tension in kips per foot of wave amplitude is: 4.5 and 2.2 for the port and starboard bow chains respectively (#2 and #3); 1.4 and 1.5 for port and starboard breast chains (#1 and #4); 1.0 and 0.3 for the port and starboard quarter chains (#7 and #5) and 0.7 for the stem chain (#6).

The non-linear nature of the spring restoring force, i.e., the tension-displacement relation for the mooring chain-in-catenary configuration, is apparent in the operators for those chains for which measurements were made on the two days, i.e., the stem cabin (#6); the starboard breast chain (#4) and the two port chains (#2 and #3) in Figures 8, 9, and 10, respectively. That is, generally for a given chain and wave the change in tension varies directly with the initial tension. The exception is the important port bow chain (#2) where, to spoil an apparently sound generality, the reverse is true, e.g., the greater changes in tension occur on 23 March when the chain had a lower initial tension, 31.1 kips, than on 3 September with 34.6 kips, although the difference is obviously not great (Figure 10).

It is satisfying to note that the pairs of operators derived from measurements made on both AM and PM on 23 March for chains #2, 3, 4 and 6 are significantly the same since the respective initial tensions are sensibly equal (Table 2 and Figures 8, 9, 10).

RESPONSE OPERATORS FROM THEORY

GENERAL

The model used in these theoretical predictions consisted of the ship with zero forward speed, spread-moored by four mooring lines. Two lines were attached forward and two aft, representing the seven actual chains. The model was situated in a windless, currentless sea, 45 feet deep, and exposed to regular long crested sinusoidal waves of unit amplitude with fixed frequency and heading of either bow-on or beam-on. Waves with circular frequencies of from 0.5 to 1.4 radians per second (raps) were considered. These are equivalent to waves with periods of 12.5 to 4.5 seconds per cycle (spc) or 530 feet to 100 feet in length, in water 45 feet deep on the ship 319 feet long at the water line.

The theory used is a modification of the deep water theory used by Kaplan and Putz (1962). Specifically, the proper shallow water wavelength is imposed on the deep water theory, and the change in the orbital velocity pattern from circular, as in deep water, to elliptical, as in shallow water, is neglected. The rigorous shallow water wave theory was not used since the amount of computation required was considered excessive.

The craft had the usual 6 degrees of freedom; 3 translational (surge, sway and heave) and 3 rotational (roll, pitch and yaw).

BASIC ASSUMPTION

The basic assumption is that of linearity. Specifically, it is assumed that in the absence of excitation, the ship motion can be described in terms of homogeneous, second-order, linear, differential equations with time as the independent variable. An excitation term is added to the homogeneous equations as a "right-hand-side term" which, in the present case, is sinusoidal. In accordance with linear theory, it is assumed that there is no coupling between the variables in the two planes of motion; that is, those longitudinally in heave, pitch and surge, and those laterally in sway, yaw, and roll. However, the longitudinal motions are coupled with each other and, similarly, the lateral motions are coupled with each other.

A fundamental analytical tool in carrying out the prediction is the slender-body theory. Essentially, this theory makes the assumption that, for an elongated body where a transverse dimension is small compared to its length, the fluid flow at any cross-section is independent of the flow at any other section; therefore, the flow problem is reduced to a two-dimensional problem in the transverse plane. The force is found by integrating the pressure over the length of the body.

Equations are formulated by the balance of inertial, damping, restoring, exciting, and coupling forces and moments. Hydrodynamic and hydrostatic fluid effects, together with body inertia and mooring influences, are included in the analysis.

INERTIAL FORCES

The forces exerted by the ship in accelerating the surrounding water give rise to equal and opposite forces by the water on the ship. These are termed inertial forces and, correspondingly, inertial moments. Since they are proportional to acceleration, they are usually expressed in terms of a fictitious added mass. The total inertia force has components in all three directions of translation and rotation.

DAMPING FORCES

Damping forces involve the dissipation of energy and are due to wave generation, viscosity and eddy-making. Except in the case of roll, damping due to wave generation only is considered in this study. Total damping force, like inertia force, has components in all three directions of translation and rotation.

HYDROSTATIC RESTORING FORCES

These forces are due to the buoyancy effect arising from static displacements. Total hydrostatic restoring force has a component only in the vertical, or heave direction. The hydrostatic restoring moment has components only in the roll and pitch directions.

MOORING RESTORING FORCES

This additional restoring force has been added, in the case of the landing craft under analysis, in addition to the hydrostatic restoring force which is always present in the case of a craft in water. The mooring restoring force is effective only in surge, sway and yaw. While it is present in the three remaining modes (heave, pitch, and roll), it is never significant in relation to the hydrostatic restoring forces. Mooring restoring force is assumed to be a linear function of displacement in surge and sway as well as yaw. The assumption of linearity is a proper one for the small displacements encountered during the sea tests; however, for large displacements, linearity is not assumed.

EXCITATION FORCES

Excitation forces could also be called wave forces, since they represent the waves which excite the ship motion and which give rise to all the preceding forces. They are sinusoidal in nature, and have components in all three directions of translation and rotation, although some of these components vanish at certain headings of the craft.

EQUATIONS OF MOTION

The following five forces, as explained above, are considered in the analysis, namely; inertial, damping, excitation and restoring force. In the latter, the hydrostatic and mooring forces are combined. On the basis of these five items, six equations of motion, one for each degree of freedom, are written as follows:

$$m\ddot{x} = F_x^i + F_x^d + F_x^m + F_x^w \qquad \text{(surge)} \qquad (1)$$

$$m\ddot{y} = F_y^i + F_y^d + F_y^m + F_y^w \qquad \text{(sway)} \qquad (2)$$

$$m\ddot{z} = F_z^i + F_z^d + F_z^h + F_z^w \qquad \text{(heave)} \qquad (3)$$

$$I_x\ddot{\varphi} = M_\varphi^i + M_\varphi^d + M_\varphi^h + M_\varphi^w \qquad \text{(roll)} \qquad (4)$$

$$I_y\ddot{\theta} = M_\theta^i + M_\theta^d + M_\theta^h + M_\theta^w \qquad \text{(pitch)} \qquad (5)$$

$$I_z\ddot{\Psi} = M_\Psi^i + M_\Psi^d + M_\Psi^m + M_\Psi^w \qquad \text{(yaw)} \qquad (6)$$

where m = mass of the ship
F = force
M = moment
with superscripts on the F's and M's indicating components, and subscripts indicating the type of force or moment, according to the following notation:

i = inertial
d = damping
h = hydrostatic restoring
m = mooring restoring
w = wave
x = surge
y = sway
z = heave
φ = roll angle
θ = pitch angle
Ψ = yaw angle

Acceleration is indicated by the superscript (••) above the motion symbol; for example $\ddot{x}$, etc.

Equations of motions consist of linear combinations of terms which vary in time and are proportional to acceleration, velocity and displacements; the latter included those which vary sinusoidally and are connected with the wave term which excites the system. Each of these contains certain coefficients which must be evaluated.

SHIP MOTION OPERATORS

By considerable effort, mainly due to the difficulty of determining the coefficients simultaneous equations for the longitudinal motion were evolved in the form of a 3 by 5 matrix. By inverting this matrix, solutions for motions in three degrees of freedom are obtained. The same procedure is followed in the case of the lateral motions. By varying the value of the exciting frequency, responses are calculated in the form of amplitude of motion for a unit amplitude excitation. When these responses are expressed as a function of frequency they are known as "response operators." They were computed for both the lateral and longitudinal motions with the latter shown in Figures 7 and 8. The phase relationship of the motion to the wave was calculated for all motions but is presented only in the case of pitch (Figure 4).

There is surge and pitch only in head seas (Figure 7 - 8); also, at frequencies greater than about 1.2 raps (5.24 seconds period), the motion in both modes is relatively small. Both beam-on and head-on waves produce noticeable heave. In head seas, heave becomes relatively small (Figure 7) at frequencies greater than 1.2 raps (5.24 seconds period). In beam seas, t heave slightly exceeds the amplitude of the incident wave, up to about 0.8 raps; after this, it decreases relatively slowly to about 0.3 of the amplitude of the incident wave at 1.4 raps. The magnification of the heave is puzzling, but seems to be explainable by the equations used, if not physically.

Consistent with linear theory, there is sway, yaw and roll, only in beam-on waves. The sway up to about 0.9 raps is slightly greater than the amplitude of the incident wave. After 0.9 raps, the sway decreases slowly to about 0.4, the amplitude of the incident wave at 1.4 raps. The roll in beam-on waves peaks at about 0.9 raps raps (5.2 degrees per foot) and then decreases to about 1.90 degrees at 1.2 raps. The yaw in beam seas attains 0.15 radians at about 1.2 raps.

RESPONSE AMPLITUDE OPERATORS FROM THEORY

CHAIN TENSION OPERATORS

Motion of ship end of chain in longitudinal plane. This point is designated by subscript "c" and located at a distance "ℓ" forward or aft of the C.G. as measured along the center line. The previously calculated phase angle (ϵ) and maximum amplitude of surge (X) and heave (Z) of the C.G. and pitch (θ) about the C.G. were used in the equation for simple harmonic motion, e.g., surge of point "c" is

$$X_c = X \cos(\omega t + \epsilon_1) \quad \ldots\ldots(7)$$

The heave of the point is a combination of the effect of heave and pitch at the C.G., i.e.,

$$Z_c = Z \cos(\omega t \ \epsilon_2) + \ell\theta \cos(\omega t + \epsilon_3) \quad \ldots\ldots(8)$$

By suitable trigonometric manipulation, Equation (8) can be written as:

$$Z_c = (A+B)^{\frac{1}{2}} \cos(\omega t + \tan^{-1}(B/A)) \quad \ldots\ldots(9)$$

where $A = Z \cos \epsilon_2 + \ell\theta \cos \epsilon_3$

$B = Z \sin \epsilon_2 + \ell\theta \sin \epsilon_3$

At a given frequency, previously calculated maximum values of surge, heave and pitch due to waves of unit amplitude with their respective phase angles are substituted into Equations (7) and (9) at various times (t) from 0 to T (wave period) sufficient to plot the closed path of the point in the X - Z plane. It will be elliptical, i.e., a Lissajou figure with the point of initial tension at the center of the figure.

Change of tension due to the movement of the ship end of the chain, as it oscillated in the Lissajou figure in the longitudinal plane, was calculated using the Table 2 chain geometry and the equations of the catenary given by O'Brien and Kuchenreuther (1958). The maximum change in tension was determined thereby and plotted as a function of frequency to form the response amplitude operators given in Figures 8 through 11.

As with the motion operators, the change in tension is low at frequencies greater than about 1.2 raps.

Note, particularly in Figures 8 and 9, that the amplitude of the operator varies directly with the magnitude of the initial chain tension, as discussed under the Operators derived from measurements. This is due to the non-linear relationship between tension and geometry for a chain in a catenary configuration.

Thus, a chain tension operator derived for one initial tension cannot be expected to agree with one derived for another initial tension. This, of course, limits seriously the usefulness of chain tension operators in design.

However, for small ship motions and chains with normal sag, of the order of those

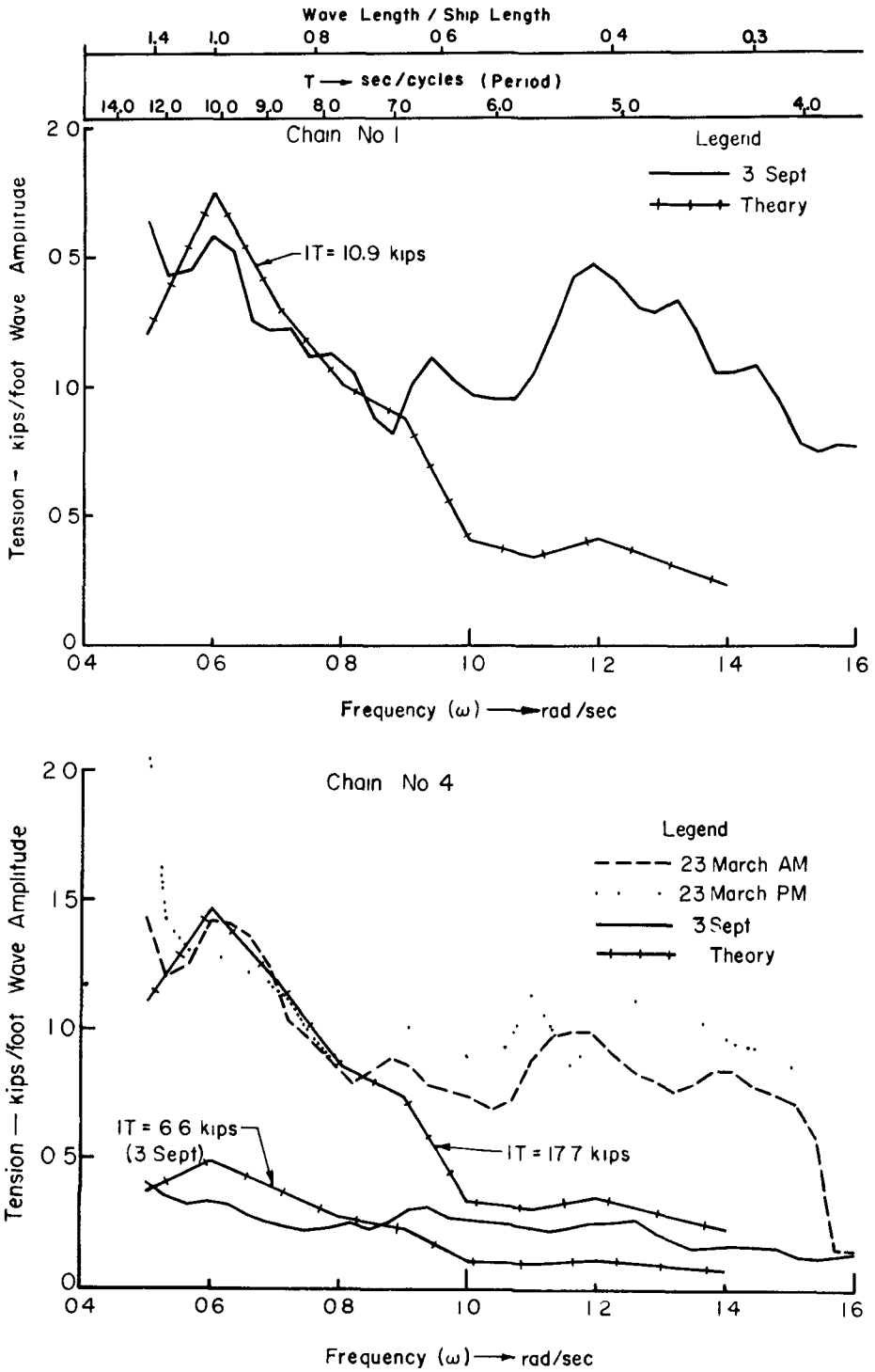

Figure 9. Response amplitude operator for port and starboard breast chains (#1 and #4).

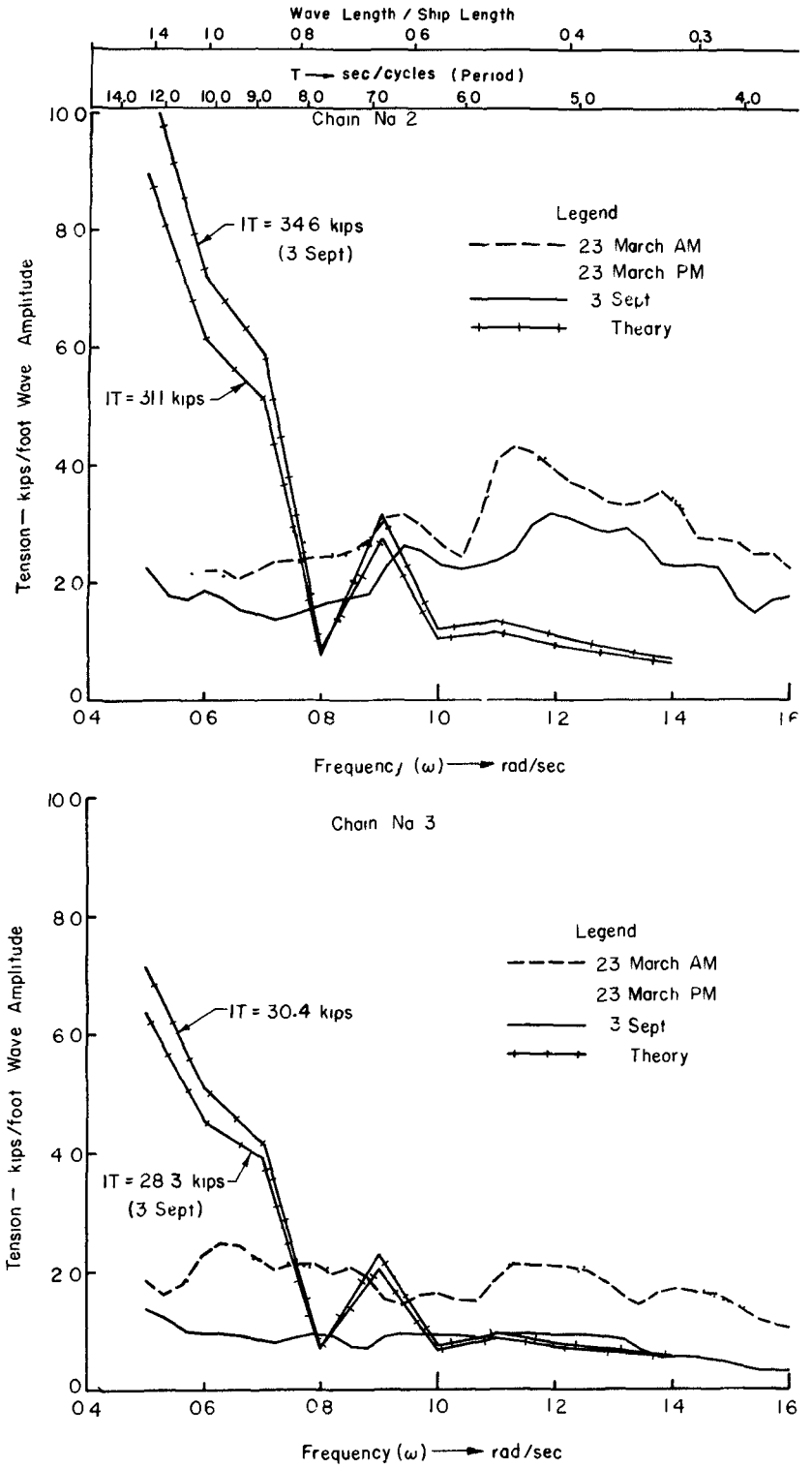

Figure 10. Response amplitude operator for port and starboard bow chains (#2 and #3).

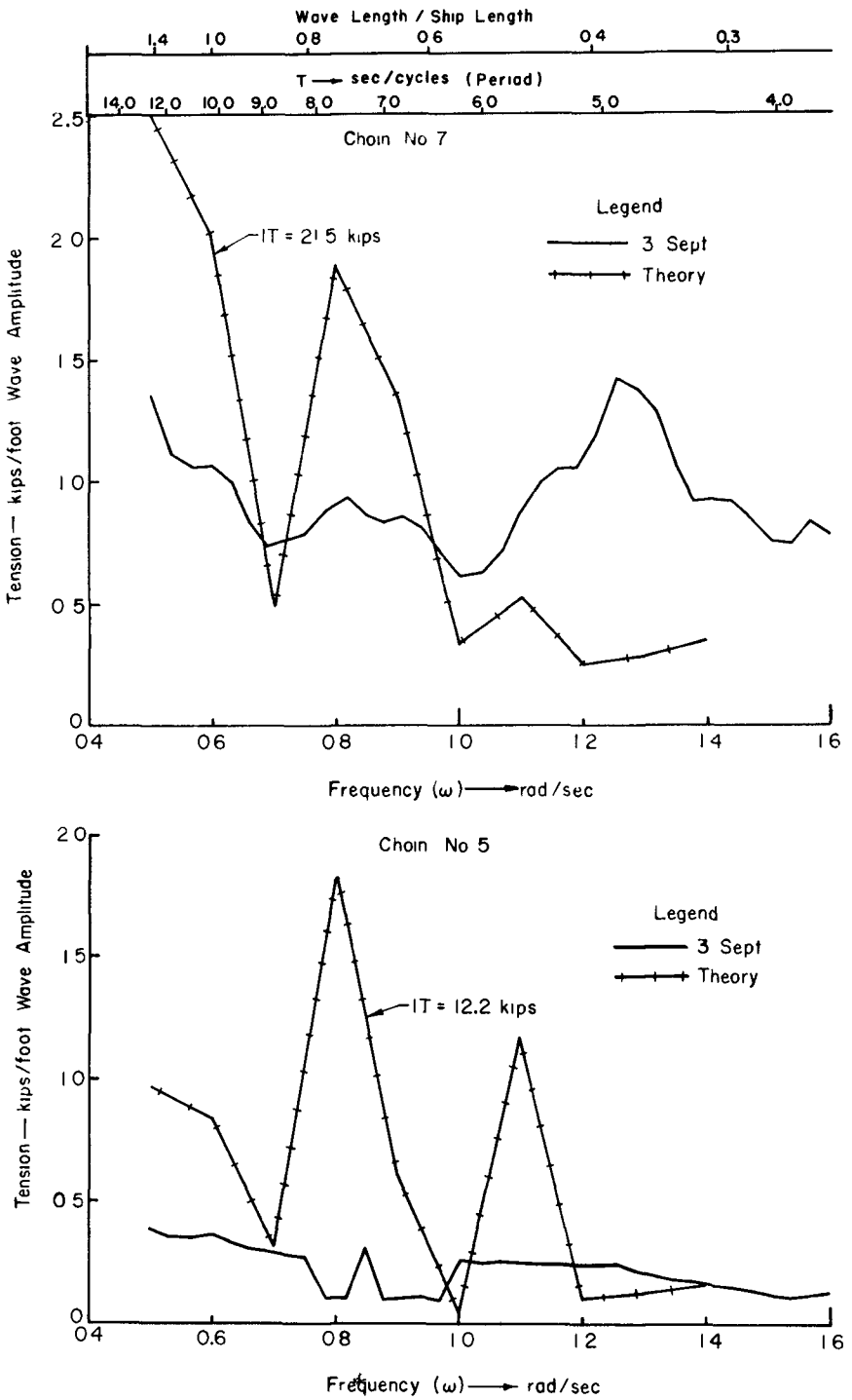

Figure 11. Response amplitude operator for port and starboard quarter chains (#7 and #5).

encountered in these tests, the tension-displacement relationship (restoring force) for a given initial tension may be considered to be sensibly linear for design purposes. Hence, ship motion calculations made on this basis, as in the preceding paragraphs, may be considered meaningful, although strictly the pertinent motion operators so derived, i.e., surge, sway and yaw, are subject to the same initial tension limitation as the chain tension operators.

COMPARISON OF EXPERIMENTALLY AND THEORETICALLY DERIVED OPERATORS

LONGITUDINAL SHIP MOTIONS OPERATORS

In the frequency range of 0.5 to 1.4 raps, the agreement is worst at the lower frequencies where theory predicts 3/4 to 4 times measurement. It is best near 1.0 raps where this factor is 3/4 to 1 and somewhat poorer at 1.4 raps in that theory predicts 4/3 to 3/4 or measurement (Figures 7 and 8).

The agreement in the case of pitch is relatively good with theory predicting about 1/2 to 4/3 of measurement. It is not nearly as good in surge and heave where theory predicts 1/3 to 4 times measurement and in one exceptional case 12 times measurement (heave of 0.8 raps, Figure 7).

LATERAL SHIP MOTION OPERATORS

There is no basis for comparison here since the measurements reflect response due to short crested bow-on waves while the theory used for bow-on waves assumes zero response in the lateral plane.

CHAIN TENSION OPERATORS

Generally the agreement is best in the middle frequencies, i.e., 0.8 to 1.0 raps with the glaring exception of the quarter chains (Figures 9, 10, and 11).

Overall, there is better agreement in the breast chains (#1 and #4) with prediction about 1/2 measurement and to a lesser extent in the bow chains (#2 and #3) with prediction about 1/4 to 3 times measurement than for the quarter chains (#7 and #5) with prediction 1/4 to a fantastic 9 times measurement (at 0.8 raps in the starboard quarter).

The stem chain (#6) deserves special comment since its initial tension was markedly different on the two days, i.e., 7.5 kips on 23 March and 24.1 kips on 3 September. Here the agreement was very poor on both days at the lower frequencies, e.g., at 0.5 raps theory predicted 3/2 to 4 times measurement. However, in the middle and high frequencies the agreement was better with these factors varying from 1/4 to 1.

PHASE AND COHERENCY

LONGITUDINAL SHIP MOTION

Pitch bow-up lagged water level crest from about 0 degrees at 0.7 raps to about 150 degrees at 1.2 raps based on the only available direct measurements in this plane, e.g., those on 3 September. Theoretical predictions agree rather well (Figure 4).

Phase, for surge and heave, were not determined from the pertinent acceleration measurement; the task would have been tedious, although not difficult. Theory indicates that surge-aft lagged water level crest by about 180 degrees at less than 0.7 raps and by 150 degrees at greater than 0.9 raps; in between the phase lag dropped to 0 degrees at 0.8 raps. Heave-up lagged water level crest by about 80 degrees at 0.9 raps then gradually increased to 150 degrees at 1.2 raps.

Heave and pitch had similar phase patterns over 0.5 to 1.2 raps with the pitch lags lower by about 40 degrees. At about 0.6 and 1.2 raps, they were in phase at about 80 and 150 degrees lag, respectively.

Coherency between excitation (wave) and response, is an experimentally derived quantity, and hence available only for pitch. It is low generally being 0 at 0.7 and 1.8 raps with peak of 0.3 at 1.1 raps (Figure 4).

LATERAL SHIP MOTIONS

The only pertinent phase and coherency information is for roll, since that was the only lateral motion measured directly. Roll port-up lagged water level crest in degrees as follows: 200 at 0.6 raps; 100 at 0.7 raps; 300 at 1.4 raps. As mentioned under Response, the roll motion in this frequency range is due to the short-crested nature of the bow-on waves; hence, the phase calculated for beam-on waves is not pertinent.

Coherency between water level and roll was low, being 0 at about 0.6 and 1.8 raps and with peak of 0.3 at about 1.1 raps.

CHAIN TENSION

In the range 0.6 to 1.4 raps an increase in chain tension lagged water level crest by the following degrees: 100 to 180 for bow chains (#2 and #3); 50 to 250 for the breast chains (#1 and #4); 180 to 450 or 90 lead for the quarter chains (#7 and #5) and 100 to 360 for stern chain (#6). All in all, there was an exasperating lack of harmony in the phase behavior of the chains, particularly since they were fastened to a sensibly rigid body, although the patterns for surge and the starboard bow (#3) and stern (#6) chains appear to be sensibly similar.

Coherency of chain tension with water level was rather low at about 0 to 0.75 for all chains. The peak on 23 March was at about 0.70 raps and on 3 September at 1.0 raps.

SUMMARY

GENERAL

Sorting generally gave amplitudes of excitation and response which were 1.1 to 2.5 times those predicted from the spectral variance.

EXCITATION

1. Sea state was 4 on 23 March and 2 on 3 September.

2. Two wave systems were operative. One was wind-generated from about bow-on with significant amplitude of about 4.4 feet and peak response at 9.5 seconds period on 23 March and 1.7 feet and peak response at 6.0 seconds period on 3 September. The other was a seiche, apparently, beam-on, with significant amplitude of about 1/4 foot and period of about 39.3 seconds.

3. Maximum single wave amplitude measured was 9.5 feet on 23 March and 5.0 feet on 3 September.

4. Winds were from about bow-on at 14 to 24 knots on both days.

5. Currents were negligible.

RESPONSE

1. Response was greater on 23 March.

2. Significant amplitude (average of highest one-third) of ship motion did not exceed: 1.1 feet surge; 0.9 feet heave; 1.8 degrees pitch; 0.6 feet sway; 0.3 degrees yaw; and 1.1 degrees roll (3 September only).

3. Significant amplitude of wave-induced chain tension in kips did not exceed 15.0 for bow chains (#2 and #3); 5.5 for breast chains (#1 and #4); 5.0 for quarter chains (#7 and #5) with measurements for 3 September only; and 3.2 for stern chain (#6).

4. The maximum wave-induced tension in kips measured in each of the seven chains was: 85.1 and 48.0 in port and starboard bow chains respectively; 10.6

(3 September) and 19.7 in port and starboard breast chains; 13.9 and 4.3 in port and starboard quarter chains both on 3 September; and 9.7 in the stern chain. To obtain total tension add the initial tensions in Table 2 to the above, e.g., the maximum total tension in the port bow chain was 85.1 plus 31.0 or 116.1 kips. New proof load in the port breast chain is 185 kips; it is 300 kips for all the others.

RESPONSE AMPLITUDE OPERATORS FOR SHIP MOTION

1. Those for surge, and heave decreased with increased frequency; pitch tends to peak at about 0.7 raps(about 9.0 spc period) or where wave length equals ship length.

2. In the range 0.6 to 1.6 raps motions per foot of wave amplitude as derived from acceleration measurements did not exceed 0.4 feet surge; 0.5 feet heave; 0.7 degrees pitch; 1.0 degrees sway; 0.1 degrees yaw; 1.0 degrees roll (direct measurement). Sway shows peak of 0.4 feet/foot, 0.9 raps, 23 March.

3. In the longitudinal plane, linear bow-on wave theory predicts motions 1/3 to 4 of those obtained from measurements. In one exceptional case this factor is 12 (heave at 0.8 raps).

4. Ship motion in lateral plane, i.e., sway, yaw, roll, in the high frequency range, is the result of the directional nature of the short crested nearly bow-on waves. The ship motion theory used with those waves assumes no response in the lateral plane. Thus, there is no basis for comparing measurements with theoretical prediction.

RESPONSE AMPLITUDE OPERATORS FOR CHAIN TENSION

1. All operators show a peak at 1.25 radians per second (raps) frequency or 5.0 seconds per cycle (spc) period and 0.16 raps (39.3 spc).

2. The two bow chains dominate, e.g., change of tension in kips/foot wave amplitude at 1.25 raps is: 4.5 and 2.2 for port and starboard bow chains, respectively; about 1.5 for both breast chains; 1.0 and 0.3 for port and starboard quarter chains, respectively; and 0.7 for stern chain.

3. Theoretical prediction (made only in high frequency range) generally is not good, i.e., prediction 1/4 to 3 times measurement in the bow chains; 1/2 in breast; 1/4 to 9 in the quarter, and 1/4 to 3/2 in the stern chain.

4. The amplitude of the operators varies directly with the magnitude of the initial chain tension due to the non-linear relationship between tension and geometry for the chain-in-catenary configuration used in the tests. Thus, operators derived for one initial tension do not agree with those derived for another.

PHASE AND COHERENCY

Longitudinal ship motions

1. In the range 0.7 to 1.2 raps, the following lagged water level crest in degrees by: pitch bow-up, 150; surge-aft, 150 - 180; and heave, 80 - 150. All three were in phase at about 1.2 raps at about 150 degrees lag.

2. Coherency between water level and motion was low, being 0 at both 0.7 and 1.8 raps with peak of 0.3 at 1.1 raps.

Lateral ship motion

1. Roll information only available. Roll-port-up lagged water level crest by 100 - 300 degrees in the range 0.6 to 1.4 raps.

2. Coherency was low being 0 at both 0.6 and 1.8 raps with peak of 0.3 at 1.1 raps.

Chain tension

1. In range 0.6 to 1.4 raps increased tension lagged water level crest in degrees by: 100 - 150 bow chains; 50 - 250 breast chains; 180 - 450 (90 lead) quarter chains; 100 - 360 stem chain. Disharmony is noted.

2. Coherency was low at 0 to peak of 0.75 on 23 March.

CONCLUSIONS

1. The moor was unbalanced in that the bow chains, particularly the port, tended to take the bulk of the load.

2. Even in sea-state 4, the maximum total tension in the lines, 116 kips in the port bow chain, is considered low relative to the new proof load of 300 kips for the chain concerned. It is realized that this margin needs to be large toward combating corrosion and fatigue excitations in addition to those of wind, wave, and current.

3. Water level variations should be measured at more than one point in ocean tests such as these, so as to permit definition of the directional wave spectrum. Measurements at some three to six points about the platform would be required; a single instrumented buoy of the type described by Cartwright (1964) could be used instead.

4. Discouragement over the extreme differences between theoretical prediction and measurements found in these tests is balanced by encouragement over agreements.

5. Toward improvements, the fairly well-established theory for motion of unmoored ships as used herein, needs to be extended to short crested waves and to moored platforms of relatively broad beam, including those of odd shape, such as barges. It needs to include dealing with short crested waves and the difficult problem of providing properly for damping and initial tension. The latter is unique to the problem. It is dependent on the whims of the wind and current which tend to alter the attitude and position of the platform and hence the tension in the lines fastened to it. The prediction of initial tension during storm is most demanding. However, unless this can be done, it will not be feasible to predict the motion and mooring tensions properly, either by theory or model tests.

6. Propulsion devices controlled by read-out of tension in key moorings may be necessary toward realization of the design initial tensions in the prototype. Also non-catenary line configurations may be necessary, e.g., lines so buoyed as to hang in straight lines, so as to provide a linear type spring of constant initial tension.

7. If the directional properties of the waves had been measured (Directional spectra) and if a theory involving short crested waves had been available and used, then the discrepancies between observations and theory likely would have been less.

ACKNOWLEDGEMENTS

The late D. I. Kuchenreuther supervised and participated in the making of the bulk of the measurements, and was assisted by F.E. Nelson and R. K. VanSlyke. He also made preliminary analysis of the measurements. R. E. Jones was responsible for much of the design of the data collection system and for its installation at the site. All of these were members of the NCEL staff at the time of the study.

Mr. C. A. Besse, of the California Company, New Orleans, Louisiana, and his staff, provided outstanding technical and logistical support in, for example, the underwater measurements of the chain length.

Special acknowledgement is extended to W. J. Pierson, Jr., Ph.D., of New York University, for his aid and instruction in the analysis and to John Roberts of NCEL for his computation of the response operators for the ship motions.

Permission from the U.S. Naval Civil Engineering Laboratory, Port Hueneme, California of the Bureau of Yards and Docks of the U.S. Navy to present this Paper is gratefully acknowledged.

REFERENCES

1. Blackman, R.B. and Tukey, J.W. (1958) "The Measurement of the Power Spectra from Point of View of Communications Engineering," Dover Publications, Inc., New York, 1958.

2. Canham, H.J.S., Cartwright, D.E., Goodrich, G.J., Hogben, N. (1963) "Seakeeping Trials on O.W.S. Weather Reporter," Trans. Royal Inst. of Naval Architects, 1963.

3. Cartwright, D.E. (1957) "On the Vertical Motions of a Ship in Sea Waves," Proc. Symp. on "Behavior of Ships in a Seaway" Vol. i, Netherlands Ship Model Basin; Wageningen, Netherlands, September 1957.

4. Cartwright, D.E. and Smith, N.D. (1964) Proc. Symp. on "Buoy Techniques for Obtaining Directional Wave Spectra," Marine Technology Society, 1964.

5. Kaplan, P. and Putz, R.R. (1962) "Motions of a Moored Construction Type Barge in Irregular Waves & Their Influence on Construction Operation," Marine Advisers, Inc. contract NBy-32206 with NCEL, August 1962.

6. Longuet-Higgins, M.S. (1952) "On the Statistical Distribution of Heights of Sea-Waves," J. of Marine Research, Vol. XI, No. 3, pp. 245 - 266, August 1962.

7. O'Brien, J.T. and Kuchenreuther, D.I. (1958) "Free Oscillation in Surge and Sway of a Moored Floating Dry Dock," Chapter 52 from "Proceedings of Sixth Conference on Coastal Engineering," Council on Wave Research, The Engineering Foundation, 1958.

8. O'Brien, J.T. and Muga, B.J. (1963) "Sea Tests of a Swing-Moored Aircraft Carrier" Technical Report 251, U.S. Naval Civil Engineering Laboratory, Port Hueneme, California, September 1963.

9. O'Brien, J.T. and Muga, B.J. (1964) "Sea Tests on a Spread-Moored Landing Craft" Technical Report 268, U.S. Naval Civil Engineering Laboratory, June 1964.

10. Wilson, B.W. (1958) "The Energy Problem in the Mooring of Ships Exposed to Waves," Pro. Conf. on Berthing and Cargo Handling in Exposed Locations, Princeton University, October 1958.

Chapter 48

RESONANCE CONDITIONS IN Nº.1 DOCK OF LUANDA HARBOUR

Fernando Manzanares Abecasis
Research Engineer, Head, Hydraulics Department
Laboratório Nacional de Engenharia Civil, Lisboa, Portugal

1. OBJECT OF THE PAPER

About 900 m of berth length arranged around a single pier are at present available in the port of Luanda.

Due to the constant increase of traffic through the port, the "Brigada de Estudos do Porto de Luanda" (Brigade of Studies of the Luanda Harbour) decided to prepare a general plan of extension of the port facilities. The extension planned comprises the construction of a new pier, which together with the existing one will delimit a triangular dock - dock nº.1 —, and of a series of rectangular basins between the new dock and the area of S. Pedro da Barra fortress (fig.1).

The danger of possible resonance phenomena and the fact that this problem can be dealt with before construction begins, led the Brigade to undertake a detailed analysis of it before taking decisions on the extension works of the port. This analysis comprised three stages:

a) Observation in nature of long-period waves in Luanda bay.

b) Analytic study of the behaviour of the planned docks under the action of possible long-period waves.

c) Experimental study in model of the same phenomenon.

The author, as consulting engineer of the Brigade of Studies, programmed observations a) and analysed their results, performed the analytic study b) [1] , [2] , [3] and, as head of the Hydraulic Department of Laboratório Nacional de Engenharia Civil, planned, supervised and interpreted the model studies (1). These concerned dock nº 1 alone because, on one hand, this is the structure whose construction will begin first and, on the

(1) - These model tests were directed by Mr. J. Pires Castanho

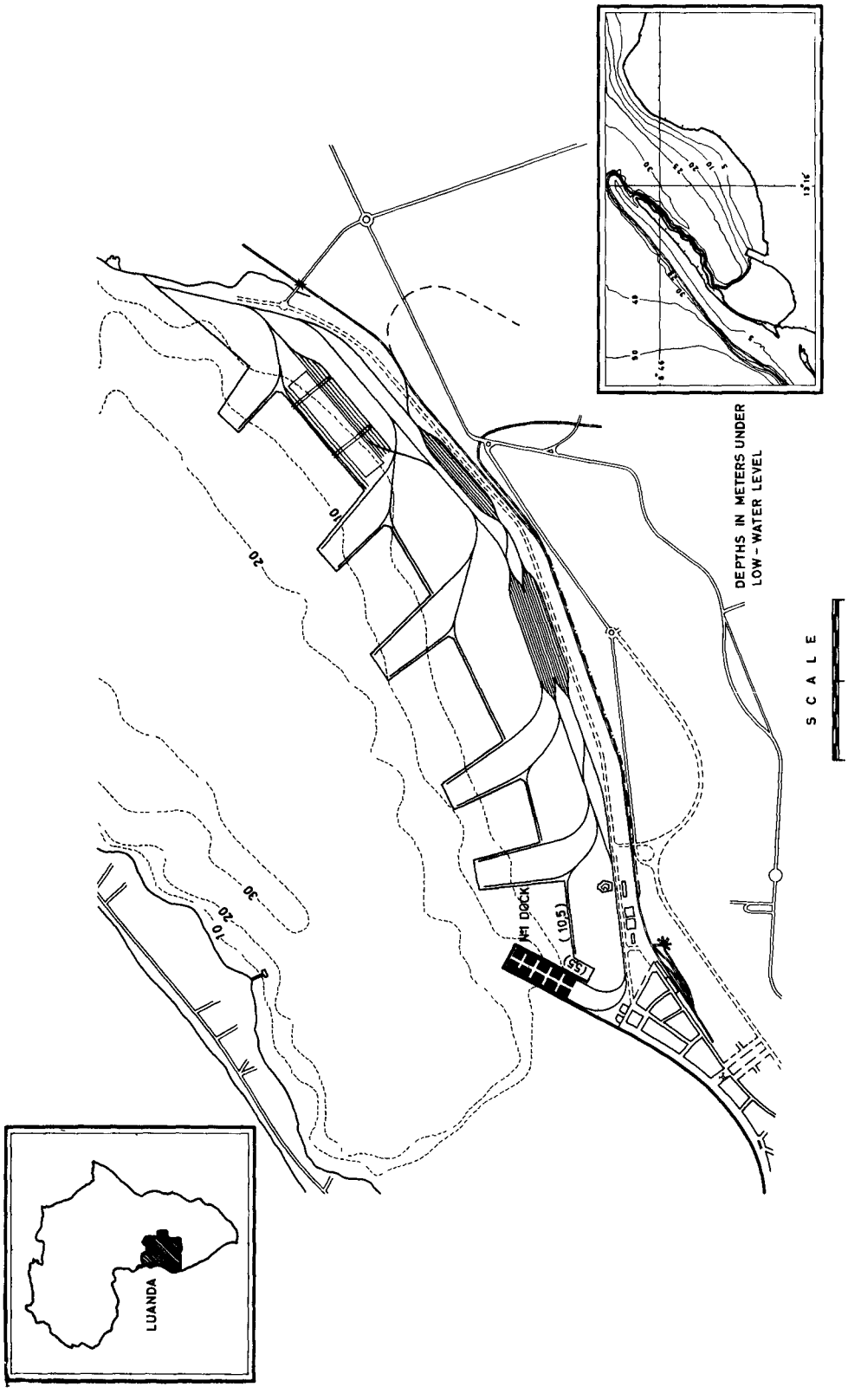

FIG 1 --LOCATION MAP AND PLAN OF ENLARGEMENT OF LUANDA HARBOR

other, due to its shape, the conclusions of the analytic study about this dock are to be viewed with great reservations.

In the present paper the author presents the results of the studies in reference on dock nº 1, seeking in special to compare the results of the analytic study and of the model tests, stressing agreements and differences, trying to explain the latter and drawing conclusions applicable in practical cases.

2 - OBSERVATIONS IN NATURE

2.1 - Observations carried out in 1958 - Quick rotation tide recorders were installed after 1959, so that their records were not available for the first analytic studies. This lack was made good by means of a standard rotation tide recorder installed in the pier of Departamento Marítimo (fig.2). The supplied data concern the period between 4th December 1957 and 1st January 1959.

These tide records, to a scale of time of 1 mm≃2 min and of heights of 1:20, were analysed by direct observation methods as follows: whenever a certain regularity was observed in the distances between peaks of recorded curves, the time during which this regularity lasted was determined and by dividing this time by the number of intervals between peaks, the wave period was obtained. The amplitude was not taken into account as it remained fairly uniform between 6 and 9 cm. The last figure was rarely exceeded, the maximum recorded value being about 20 cm.

The results of this analysis are indicated in Table 1 which lists the times during which the waves, classified according to their periods in classes of 10 s, were observed; the cumulated times during which waves with periods inside a certain interval were observed are then determined. Then the percentages of durations in each class and of cumulated durations are calculated, both for the total time of observation (565 920 minutes) and the time during which regular long-period waves lasted (28 844 minutes). These data enable two histograms and two cumulated frequency curves to be plotted for the two total durations indicated above (fig. 3 and 4).

According to the histograms, the long-period waves most frequent in Luanda harbour range from 130 to 140 seconds (30 per cent of the recorded values), followed by those between 140 and 150 seconds and between 110 and 120 seconds. The first cu

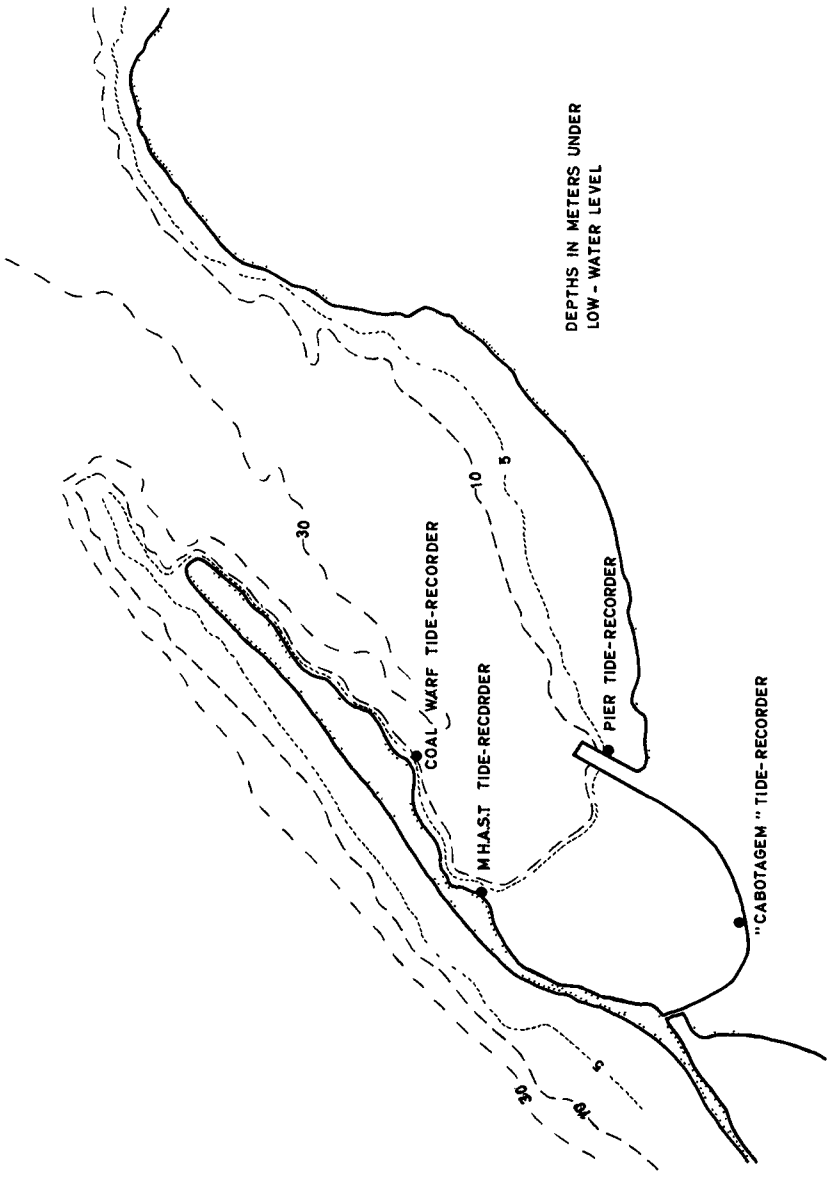

FIG. 2. --LOCATION OF TIDE-RECORDERS

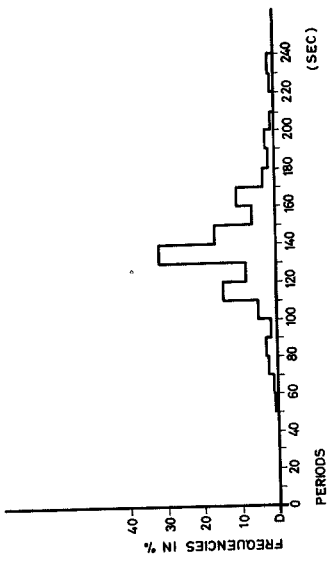

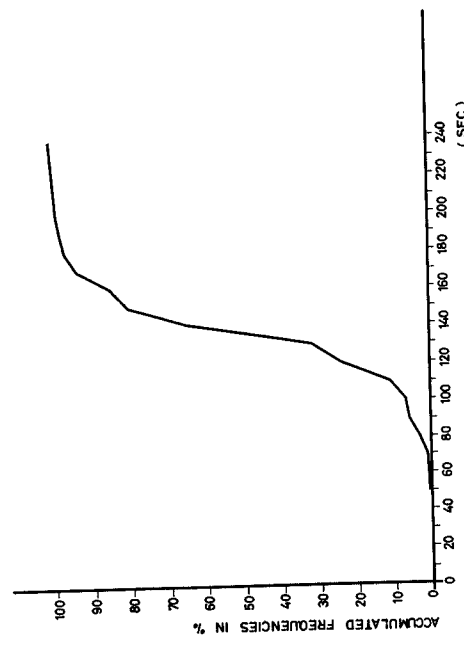

FIG 4 --OBSERVATIONS OF 1958 HISTOGRAM AND CUMULATED CURVE OF OBSERVED PERIODS IN % OF TIME OF POSSIBILITY OF ANALYSIS OF LONG PERIOD WAVES IN RECORDS

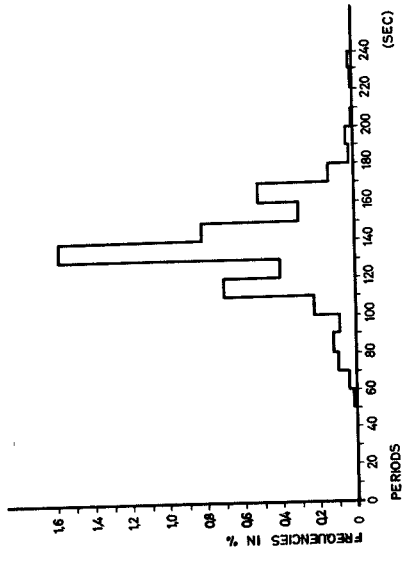

FIG. 3 --OBSERVATIONS OF 1958 HISTOGRAM AND CUMULATED CURVE OF OBSERVED PERIODS IN % OF TOTAL OBSERVATION TIME

TABLE 1

10-sec period ranges	Observation times (min)	Cumulated times (min)	Percentage with respect to		Percentage of cumulated times with respect to	
			28 844m	565 920m	28 844m	565 920m
41 to 50 s						
51 to 60 s	76	76	0.26	0.013	0.26	0.013
61 to 70 s	164	240	0.57	0.028	0.83	0.041
71 to 80 s	660	900	2.29	0.116	3.12	0.157
81 to 90 s	692	1 592	2.40	0.122	5.52	0.279
91 to 100 s	418	2 010	1.45	0.073	6.97	0.352
101 to 110 s	1 282	3 292	4.44	0.226	11.41	0.578
111 to 120 s	3 946	7 238	13.68	0.697	25.09	1.275
121 to 130 s	2 262	9 500	7.84	0.399	32.93	1.674
131 to 140 s	8 934	18 434	30.97	1.578	63.90	3.252
141 to 150 s	4 588	23 022	15.90	0.810	79.80	4.062
151 to 160 s	1 650	24 672	5.72	0.291	85.50	4.353
161 to 170 s	2 756	27 428	9.55	0.486	95.07	4.839
171 to 180 s	802	28 230	2.78	0.141	97.85	4.980
181 to 190 s	198	28 428	0.69	0.034	98.54	5.014
191 to 200 s	278	28 706	0.96	0.049	99.50	5.063
201 to 210 s	28	28 734	0.10	0.004	99.60	5.067
211 to 220 s	-	28 734	-	-	99.60	5.067
221 to 230 s	42	28 776	0.16	0.007	99.76	5.074
231 to 240 s	68	28 844	0.24	0.012	100.00	5.086

mulated frequency curve shows that 90 per cent of the observed periods are concentrated in the interval 100-170 sec.

It should be noted however that:

a) It is very likely, from the general look of the tide records, that waves of long period in Luanda bay have been more frequent than the preceding results seem to show but, due to the scale of the records and the apparenthy irregular distribution of peaks, their presence could not be analysed.

b) As said, the amplitude of the oscillations recorded by the tide-recorders do not exceed a few centimeters, as a rule, but in three exceptional cases amplitudes of 15-20 cm (with periods of 130-160 sec) were recorded. It is noteworthy that long-period waves with periods of the same order of magnitude were observed on the same occasions at Lobito, 400 km to the south, and also that the external regular normal-period waves of the swell type had a small amplitude (0.40 to 0.60 m).

2.2 - The observations of 1960 - Two quick-rotation tide recorders installed in Luanda bay were observed during several months: one in the cabotage quay (to be called hereafter "cabotage-tide recorder") and another in the eastern portion of the pier (to be called "pier tide recorder"). A standard rotation tide recorder was installed in the coal wharf (fig.2). The location of the two quick rotation tide recorders was chosen bearing in mind two basic requirements: first to avoid disturbances due to waves generated by local winds or by the frequent passage of ships nearly; second to avoid sites likely to lie in nodal zones of possible long-period stationary oscillating systems which, in that case, would not be recorded.

The results obtained show that the position of the "cabotage tide-recorder" was not very favourable as regards the former requirement which rendered more difficult the analysis of the records; on the other hand the location of the pier tide-recorder proved excellent in this connexion.

The pier tide-recorder started operating on the 19th March 1960, the cabotage tide recorder on the 5th April 1960 and the coal wharf tide recorder on the 31st December 1959. The tide records used in the study concern a period of time from the dates above up to 28th June 1960.

Experience showed that due to the time scale chosen, the

coal wharf tide records were not worthwhile using as they could yield reliable data on the amplitudes alone.

The other two tide records were on the contrary excellent: the scale of time was 1 mm ≃ 17.15 seconds and of height 1.5. Yet, due no doubt to the preceding reasons, the values of the pier tide recorder were much clearer than those of the cabotage tide-recorder (fig.5), and so they alone were used in the analysis of long-period waves in the harbour.

The cabotage tide-records were used merely for comparison of periods and amplitudes notably in the case of marked oscillations in the pier tide-records. The results obtained in the coal wharf served only for comparison of amplitudes.

2.3 - Analysis of the tide records - As precedingly explained, long-period waves in Luanda bay and their frequency were studied on basis of the values of the pier tide-record alone, between 19th March and 28th June 1960, i.e. about 100 days.

The records were carefully analysed all the time save for some short periods in which this proved impossible due to gaps or superpositions in the records.

The indicated period was deemed sufficiently significant as neither trends for concentration of long-period waves in certain epochs nor deviations of the results of the analysis with respect to the results of 2.1 were observed.

The records were studied according to the rules indicated above.

The results obtained are presented in Table 2, as a list of the times during which were observed long-period waves classified in 10-s intervals.

The same table contains the cumulated times during which waves with periods inside certain intervals were observed and the percentages of duration of each class and of the cumulated durations with respect to both the total time of observation (about 2,400 hours = 8 640 000 seconds) and the time during which regular long period waves were observed (3 976 528 seconds).

Two histograms and two cumulated frequency curves with

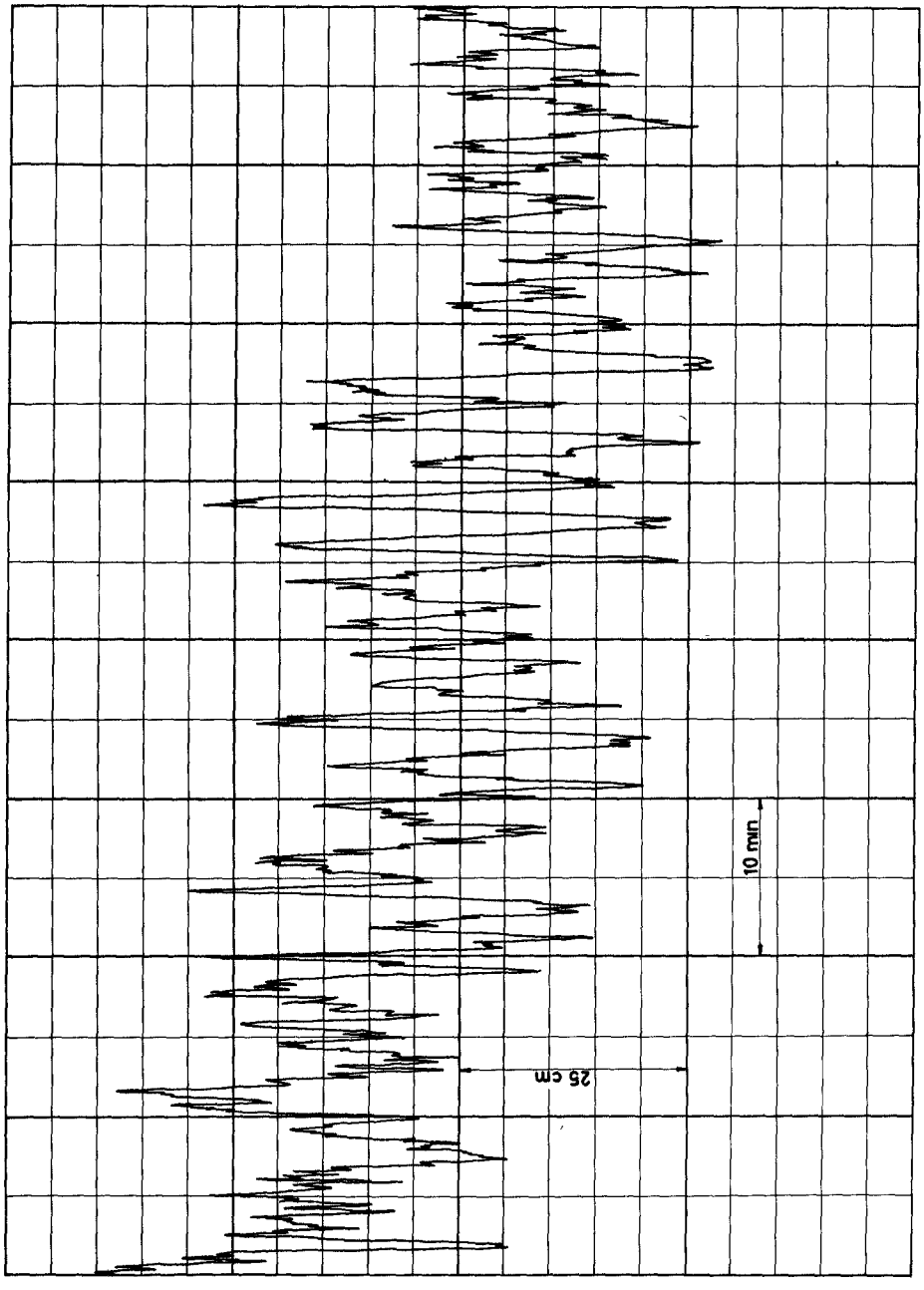

FIG. 5 -- EXAMPLE OF RECORDS OBTAINED IN PIER QUICK-ROTATION TIDE-RECORDER

TABLE 2

10-sec period ranges	Observation times (sec)	Cumulated times (sec)	Percentage with respect to		Percentage of cumulated times with respect to	
			3 976 528 sec	8 640 000sec	3 976 528 sec	8 640 000 sec
31- 40	720	720	0.02	0.008	0.02	0.008
41- 50	7 013	7 733	0.18	0.081	0.19	0.089
51- 60	52 547	60 280	1.32	0.609	1.52	0.698
61- 70	86 559	146 839	2.18	1.002	3.69	1.700
71- 80	172 003	318 842	4.32	1.992	8.02	3.692
81- 90	209 743	528 585	5.27	2.429	13.29	6.121
91-100	289 692	818 277	7.28	3.356	20.60	9.477
101-110	379 242	1 197 519	9.54	4.393	30.11	13.870
111-120	496 036	1 693 555	12.47	5.745	42.59	19.615
121-130	639 672	2 333 227	16.09	7.409	58.67	27.024
131-140	587 064	2 920 291	14.80	6.800	73.44	33.824
141-150	551 777	3 472 068	13.90	6.391	87.31	40.215
151-160	311 420	3 783 488	7.83	3.607	95.14	43.822
161-170	84 485	3 867 973	2.12	0.979	97.27	44.801
171-180	31 930	3 899 903	0.80	0.370	98.07	45.171
181-190	17 184	3 917 087	0.43	0.199	98.50	45.370
191-200	7 666	3 924 753	0.19	0.089	98.70	45.459
201-210	806	3 925 559	0.02	0.009	98.72	45.468
211-220	4 255	3 929 814	0.11	0.049	98.82	45.517
221-230	2 022	3 931 836	0.05	0.023	98.87	45.540
231-240	25 761	3 957 597	0.65	0.299	99.52	45.839
321-330	2 948	3 960 545	0.07	0.034	99.60	45.873
361-370	1 097	3 961 642	0.03	0.013	99.62	45.886
381-390	1 560	3 963 202	0.04	0.018	99.66	45.904
441-450	2 211	3 965 413	0.06	0.025	99.72	45.929
451-460	9 041	3 974 454	0.20	0.105	99.95	46.054
511-520	2 074	3 976 528	0.05	0.024	100.00	46.058

respect to the above-mentioned total durations were plotted on basis of these data (figs.6 to 9).The curve of observed values in 1958 (see 2.1) was superposed to the last cumulated curve.

A comparison of the records of the two rapid rotation tide recorders shows that:

a) As said, the pier tide records are much smoother and clearer than the cabotage tide records; the location of the former recorder seems excellent.

b) The wave-periods recorded in both instruments are approximately the same, although occasionally somewhat imprecise in the cabotage tide-recorder.

c) When absent in one tide-recorder,long-period waves are also absent in the other.

d) As a rule, amplitudes are larger in the pier tide-recorder. Thus, for instance, amplitudes were maximum (0.60m) in the pier tide-recorder on the 19th June 1960, whereas they did not exceed 0,35m in the cabotage tide-recorder that same day.The simultaneous maximum amplitude value in the coal wharf tide-recorder was 0.40m. These facts show that amplitudes increase in the area of the pier tide-recorder. At first sight this could apparently be ascribed to resonance but a careful analysis of the phenomenon shows it to be due to a mere concentration of energy in the funnel-shaped zone where the pier tide-recorder was installed, as selectivity for certain periods is not observed.

A comparison of the values observed in 1958 and in 1960 shows that:

a) Long-period waves in Luanda bay are much more frequent than the analysis of the 1958 records would indicate.

Thus, whereas long-period waves could be clearly detected in the former in no more than 5% of the total observation time due to the scales used, these same waves were observed during about 46% of the time in the 1960 records.

b) A remarkable agreement is observed between the results of 1958 and 1960, in spite of a slight deviation towards the shortest periods. The most frequent periods ranged from 120 to 130 seconds (from 130 to 140 seconds in the 1958 results), fol

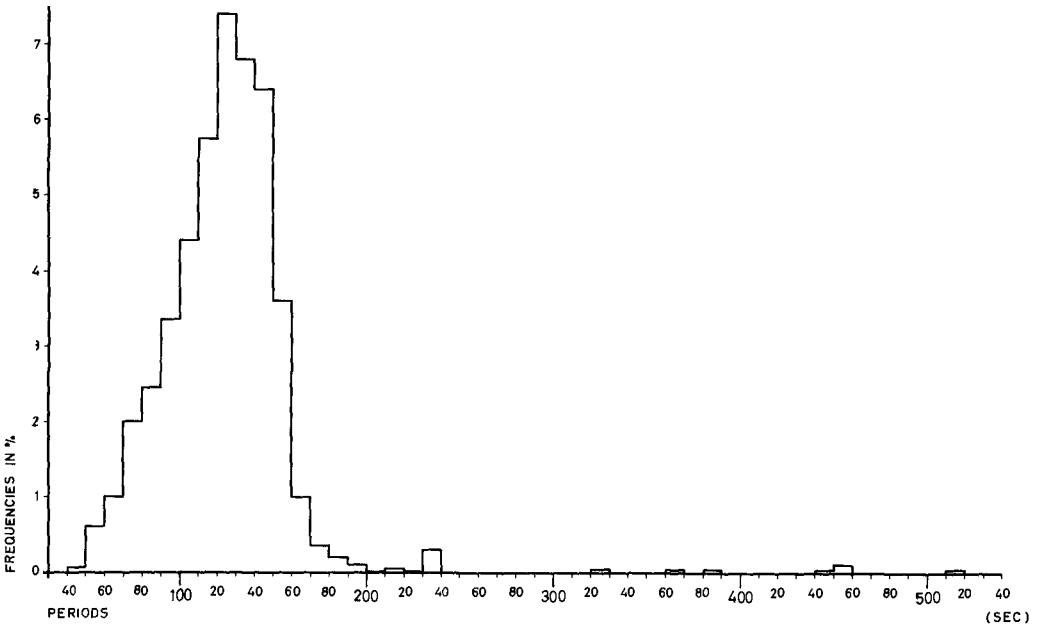

FIG 6 --OBSERVATIONS OF 1960 HISTOGRAM OF OBSERVED PERIODS IN % OF TOTAL OBSERVED TIME

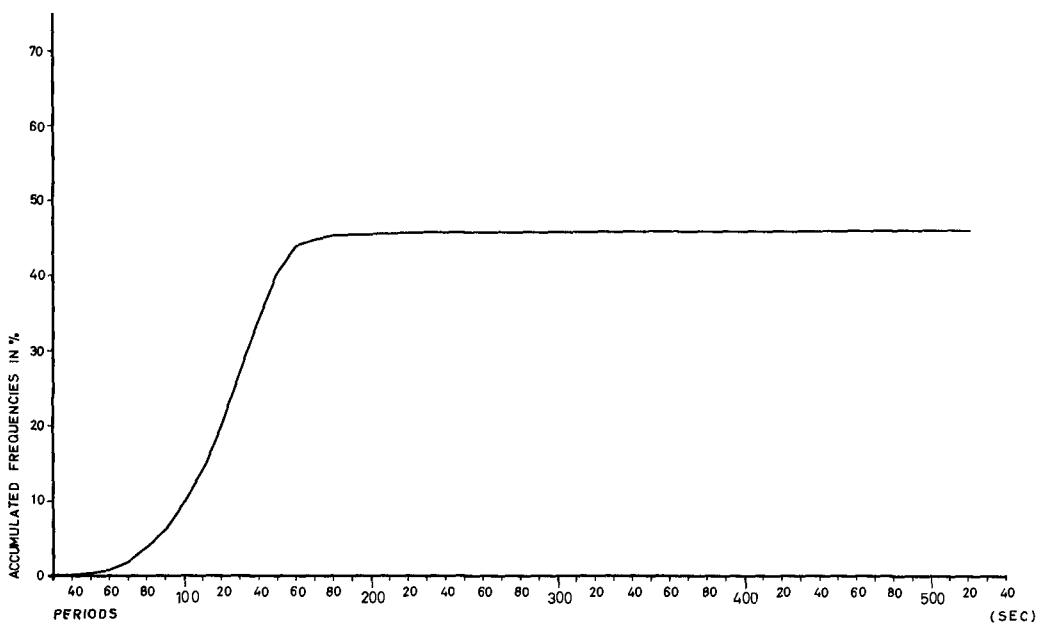

FIG 7 --OBSERVATIONS OF 1960 CUMULATED CURVE OF OBSERVED PERIODS IN % OF TOTAL OBSERVATION TIME

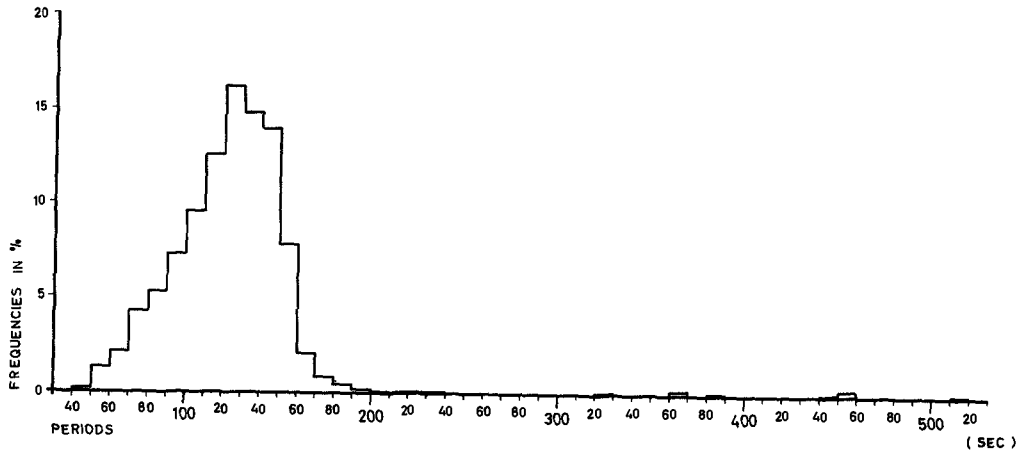

FIG 8. --OBSERVATIONS OF 1960 HISTOGRAM OF OBSERVED PERIODS IN % OF TIME OF POSSIBILITY OF ANALYSIS OF LONG PERIOD WAVES IN RECORDS

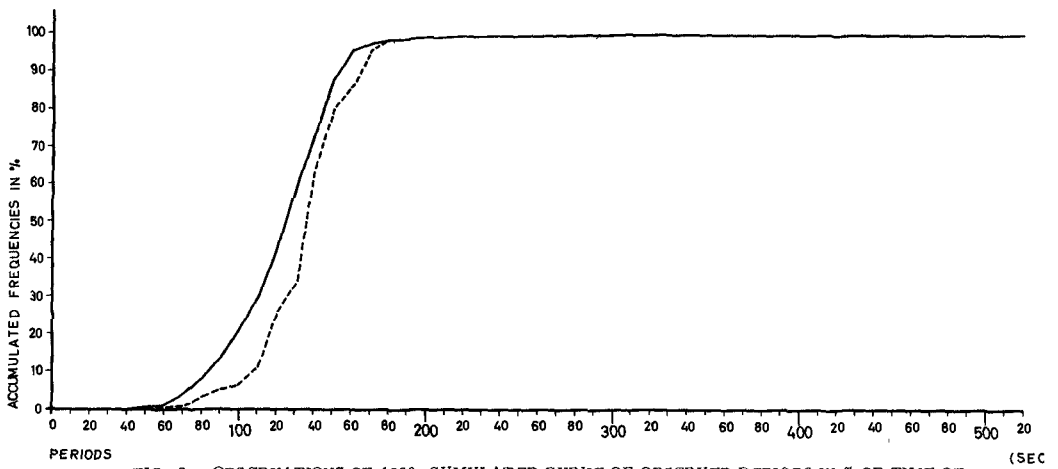

FIG. 9 --OBSERVATIONS OF 1960 CUMULATED CURVE OF OBSERVED PERIODS IN % OF TIME OF POSSIBILITY OF ANALYSIS OF LONG PERIOD WAVES IN RECORDS

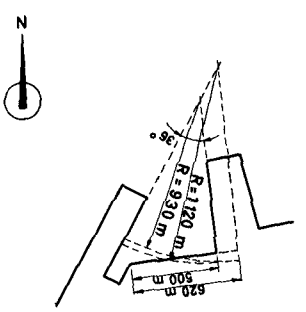

FIG 10. --SOLUTIONS O and I

lowed by those between 130 and 140 seconds and between 140 and 150 seconds. According to the cumulated frequency curve, 90% of the periods (between the 5% and the 95% ordinates) range from 74 to 160 seconds.

3 - ANALYTIC PREDICTIONS

3.1 - Solution 0 - As indicated above, although analytic studies were performed for all the docks, the results presented concern nº 1 dock alone, because on one hand only this one was tested in model so far and, on the other, the remaining docks being rectangular, no difficulties arose in connexion with the analytic calculation of their natural periods of oscillation.

The solution proposed by "Brigada de Estudos do Porto de Luanda", for nº 1 dock, presented in fig.10, will be called solution 0. When the analytic study presented below was carried out, only the 1958 observations in nature were available .

Given the irregular shape of the dock, an accurate analytic study of its resonant conditions was not feasible. Nevertheless, the dock could be roughly assimilated to a constant-depth solid, sector-shaped in plan. The natural period of oscillation of basins with this shape is given by the expression (see [4], [5]):

$$T = \frac{2\pi}{\sqrt{gK \text{ th } Kh}} ,$$

where h is the depth of the basin and K is a coefficient depending on the shape of the basin that can be obtained as follows.

Let us denote by θ the angle at the center of the sector and by R its radius.

Let us consider

$$n = \frac{\pi}{\theta}$$

The values of the coefficient K in the expression above are the results of the division by R of the roots of the derivatives of the Bessel functions of 0, n, 2n, 3n, ... order.

In the present case, $\theta = \frac{\pi}{5}$, $R = 920$ m and $h = 11,5$*.

Consequently

$$n = \frac{\pi}{\theta} = 5$$

and the roots of the derivatives of Bessel functions $J_o, J_5, J_{10} \cdots$ equal to KR were the unknowns from which the values of K could be obtained.

The zeroes of functions $J'_o(x)$ are:

$x_1 = 3.8317$
$x_2 = 7.0156$
$x_3 = 10.1735$
$x_4 = 13.3237$
$x_5 = 16.4706$

Those of function $J'_5(x)$ are:

$x_1 = 6.415$
$x_2 = 10.520$
$x_3 = 13.985$
$x_4 = 17.310$

For lack of tabulated values, only the order of magnitude of the zeroes of $J'_{10}(x)$ could be determined

$x_1 = 12$
$x_2 = 16.5$

---

* - The bottom of the dock lying at a depth (-10.5m) and the maximum range of the tide being about 1.5m, the study was performed for a constant depth of 11.5m, roughly corresponding to the mean level depth.

The values of K corresponding to the zeroes of $J'_o(x)$ are:

$$K_1 = 0.004120$$
$$K_2 = 0.007544$$
$$K_3 = 0.010939$$
$$K_4 = 0.014327$$
$$K_5 = 0.017710$$

The corresponding periods of resonance are:

$$T_1 = \underline{143} \text{ seconds}$$
$$T_2 = \underline{79} \quad "$$
$$T_3 = \underline{54} \quad "$$
$$T_4 = 41 \quad "$$
$$T_5 = 34 \quad "$$

To the values of $x = \underline{KR}$ of about 13 there correspond periods of resonance of about 40 seconds, of no interest in the case in reference, and so only the roots x_1 and x_2 of $J'_5(x)$ were taken into account. The corresponding natural periods of oscillation are:

$$T_1 = \underline{86} \text{ seconds}$$
$$T_2 = 47 \text{ seconds}$$

The fundamental period of oscillation of the basin (143 seconds) falls within a range of periods somewhat frequent in Luanda bay, so that the dimensions of the basin were considered unsuitable.

3.2 - Solution I - In order to prepare recomendations on how to change the characteristics of the dock, the following data were considered according to the directions of "Brigada de Estudos do Porto de Luanda":

- The bottom of the dock should remain at a depth of (-10.5) ;

- the location of the end quay should remain unchanged although its length could be altered;

- even if displaced, the western quay in the second pier should remain perpendicular to the above mentioned end quay;

- it was desirable that neither the length of the end quay (500m) nor the free width of the entrance to the dock were diminished.

Thus the only possible change was an eastward displacement of the second pier, which amounted to maintaining the angle at the center (and therefore n), increasing the radius of the sector and consequently the fundamental period of resonance of the basin. Another consequence to be taken into account, nevertheless, was that the period of oscillation corresponding to the first root of $J'_5(x)$ was also increased and so it was advisable to avoid for it values falling in the range of frequently observed wave periods in Luanda bay.

In order to determine dimensions of the basin enabling this disadvantage to be avoided, the radius of the sector was chosen so that

$$T = \frac{2\pi}{\sqrt{g\ K\ \text{th}\ K\ h}} \geqslant 175 \text{ seconds},$$

as oscillation periods exceeding this value are very seldom observed in Luanda.

The equation above, apparently difficult to solve due to the presence of the transcendent function th Kh, can be simplified taking into account that the values of Kh of interest in this case are very small, and consequently it is possible to take

$$\text{th } Kh = Kh$$

up to the fourth decimal place. The equation then becomes

$$\frac{2\pi}{K\sqrt{g\ h}} \geqslant 175,$$

from which

$$K \leqslant \frac{6.28}{175 \times 10.60}$$

Now the value x=KR corresponding to the fundamental oscillation period is, as indicated

$$K\ R = 3.8317$$

whence

$$R \geqslant 1,120\ m$$

Thus a radius of 1,120 m would be required for the sector, in order to ensure a fundamental period of oscillation of 175 sec.

It was first advisable to determine the period of oscillation corresponding to this radius for the first root of $J'_5(x)$ which, as is known, is x = 6.415 = KR.

The value of K is:

$$K = \frac{6.405}{1,120} = 0.005728$$

and the corresponding period:

$$T = \frac{2\pi}{\sqrt{g\ K\ th\ Kh}} = 103 \text{ seconds}$$

falls within a range of infrequent periods in Luanda bay and so is aceptable, above all bearing in mind that this is not the fundamental oscillation.

A radius of 1,120 m for the sector implied for the southern quay of nº 1 dock a length of 620 m, i.e. more 120 m than the planned value. These characteristics, recommended for nº 1 dock, gave rise to solution I.

3.3 - Solution III - Meanwhile "Brigada de Estudos do Porto de Luanda", on basis of the first model tests of solution I, prepared solution III (presented in fig.11) that, whilè maintaining the general shape of solution I, eliminated the small rectangular dock which, according to the experimental studies, proved very harmful.

Before testing this solution in model, its resonance conditions were investigated in an analytic study briefly presented below.

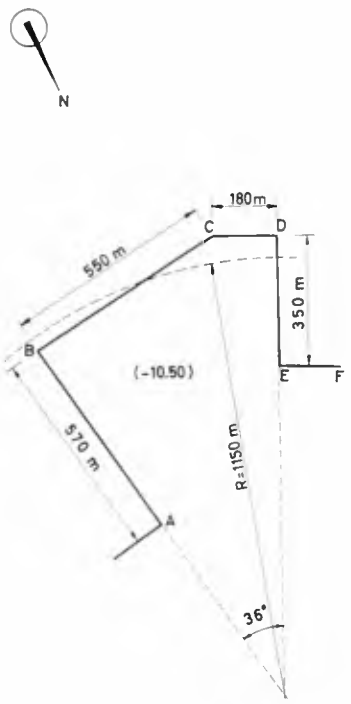

FIG. 11. --SOLUTION III

FIG. 12. VIEW OF MODEL

The basic data of solution III were:

$$R = 1{,}150 \text{ m} \qquad \theta = 36^{\circ}$$

The periods of natural oscillation corresponding to the zeroes of the derivatives of the Bessel function are:

	x = KR	$T = \frac{2\pi}{\sqrt{gK \text{ th } Kh}}$
$J'_o(x)$	3.8317	177 seg
	7.0156	97 "
	10.1735	67 "
	13.3237	51 "
	16.4706	41 "
$J'_5(x)$	6.415	106 "
	10.520	65 "
	13.985	49 "

The result of the analytic study was deemed satisfactory as no period of natural oscillation of solution III was contained in the range of most frequent periods in Luanda bay - 105 to 175 sec.

4 - MODEL TESTS: 1st stage

4.1 - General - A detailed description or discussion of the experimental conditions in which these tests were carried out being outside the scope of the present paper, the only indication given about them is that the scales of the model were 1/400 in plan and 1/200 in height (fig.12).

The coeficient of amplification of the response curves obtained in the tests is the ratio of the maximum amplitude observed inside the dock to the mean amplitude in the neighbourhood of the entrance.

The tide records of 1960 were already available when the model tests were carried out. So, although the analytic study was based on the observations of 1958, the response curves obtained in the tests are superposed to the histograms of the periods determined in the observations of 1960.

4.2 - Model test of solution I - The response curve obtained in the model test of solution I is presented in fig.13, superposed on the histogram of the periods of the tide records of

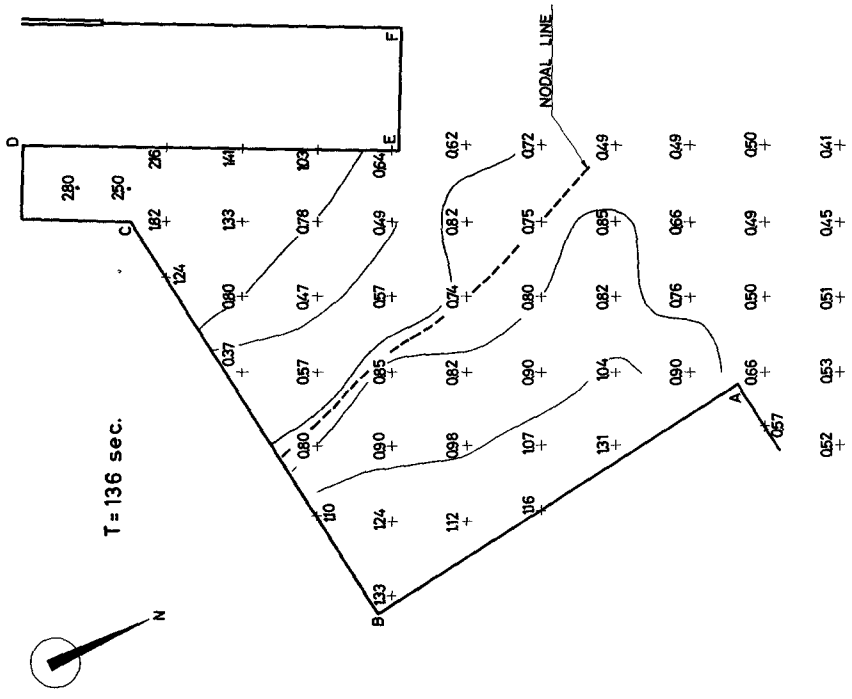

FIG. 14 --RESONANT OSCILLATION OF SOLUTION I T = 136 SEC

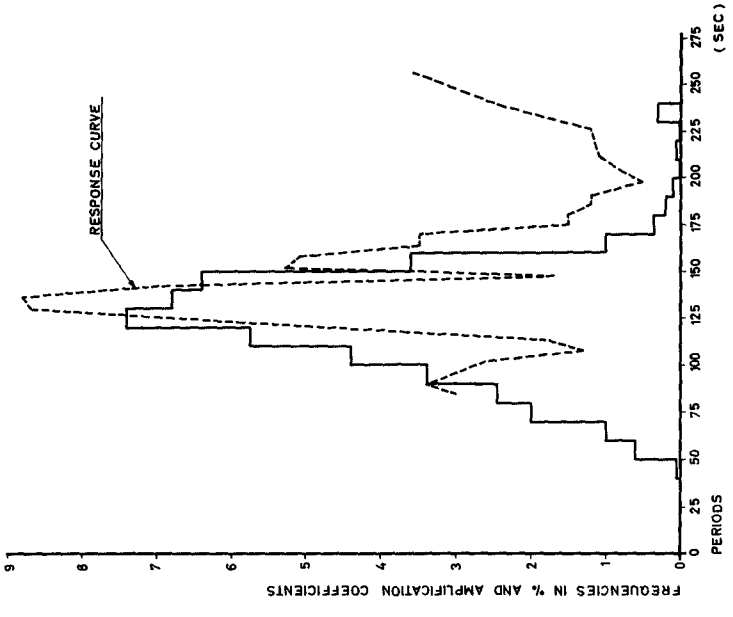

FIG 13 --RESPONSE CURVE OF SOLUTION I

1960. As shown, contrary to the predictions of the analytic study, according to which no period of oscillation between 103 and 170 sec. would be present in the harbour, the maximum amplification occurred for a period of 136 seconds (with a band of periods above and below where amplification remained considerable). According to fig.14, in which the amplitudes at the different points and the lines of equal amplitude are indicated, this resonance corresponded to a one-node oscillation between the area of the small rectangular dock and quay AB.

The tests also showed that, independently of resonance, the rectangular dock had the worst possible effects on the water movement in nº 1 dock. In fact the entrance to the dock lay in an area where the existant pier (DE) would meet quay BC. The increased amplitudes thus generated together with the strong inflow due to the rectangular dock gave rise to extremely strong currents which, on being reflected inside the dock, originated alternate water movements, not only near the entrance to the rectangular dock but also everywhere in nº 1 dock, in special along quay BC. Fig.14 shows the extremely rough conditions inside the rectangular dock. It is noteworthy that this same phenomenon took place even for non-resonant oscillations in nº 1 dock. On the other hand, when the rectangular dock was closed in the model, the alternate water movements along quay BC were considerably reduced.

A first and obvious conclusion of these tests is the need to eliminate the rectangular dock and that was why "Brigada de Estudos do Porto de Luanda", as indicated above, presented solution III (fig.11).

4.3 - Model test of solution III - The response curve obtained in this test (fig.15) presented 4 more or less marked peaks with periods of 56, 96, 108 and 136 sec. in the period range of interest, each corresponding no doubt to a different resonance mode. The three latter periods fall in a range of very frequent periods in Luanda bay.

Curves of equal amplitude for periods of 96, 108 and 136 seconds are presented in figs. 16, 17 and 18.

Solution III proved much better than solution I. In addition to the elimination of the above-mentioned disturbances due to the small rectangular dock, the coefficients of amplification were appreciably reduced, assuming acceptable values (the "coefficient

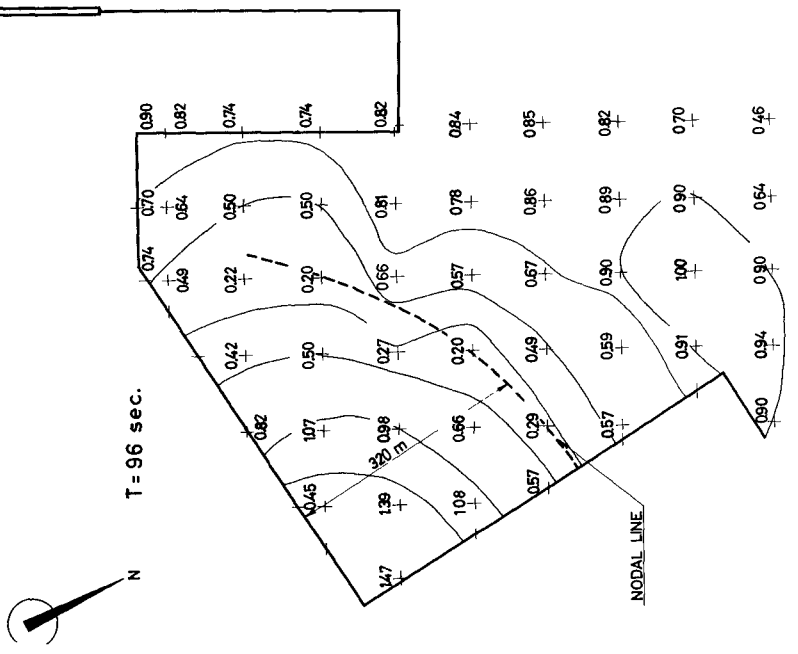

FIG 16 --RESONANT OSCILLATION OF SOLUTION III T = 96 SEC

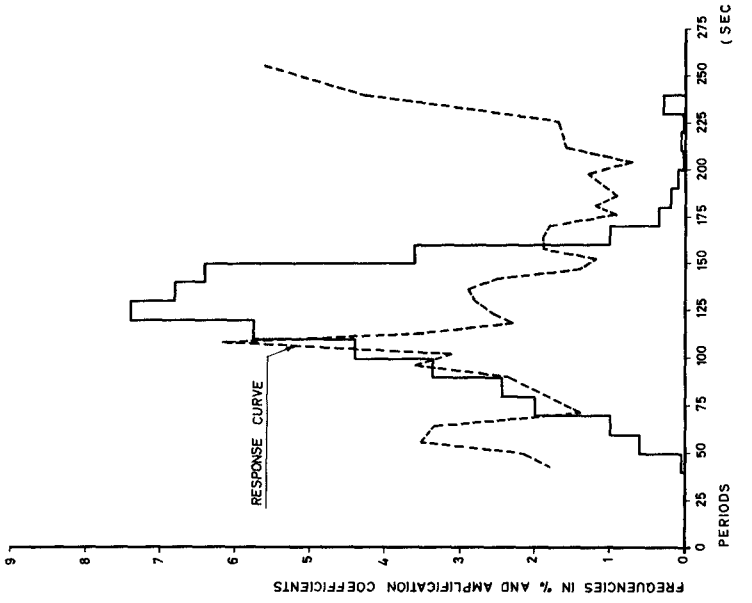

FIG 15 --RESPONSE CURVE OF SOLUTION III

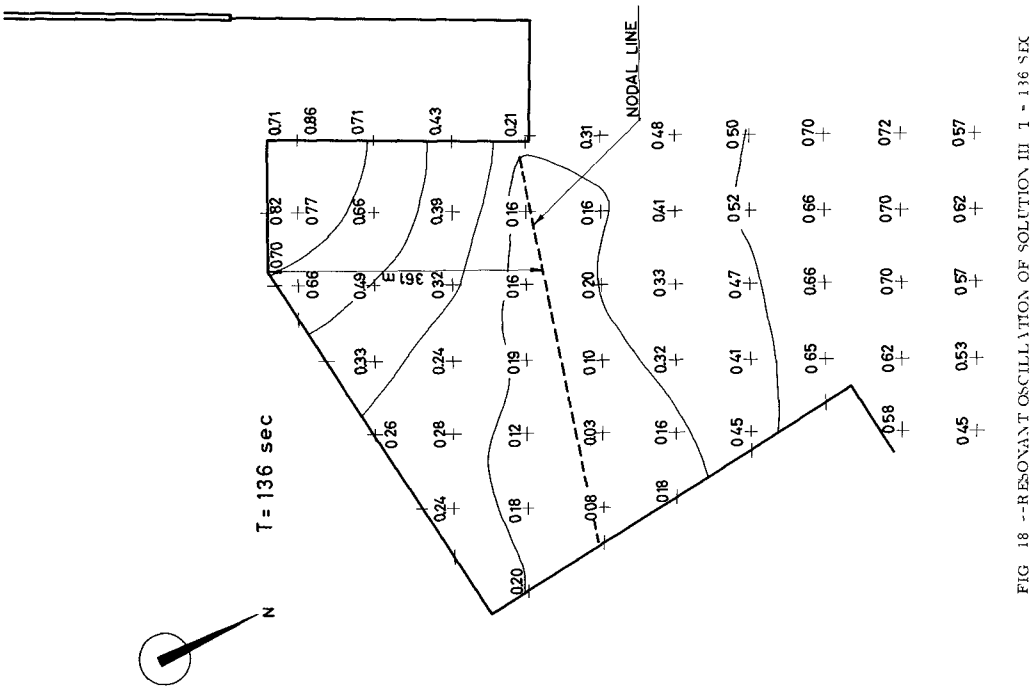

FIG 18 --RESONANT OSCILLATION OF SOLUTION III T = 136 SEC

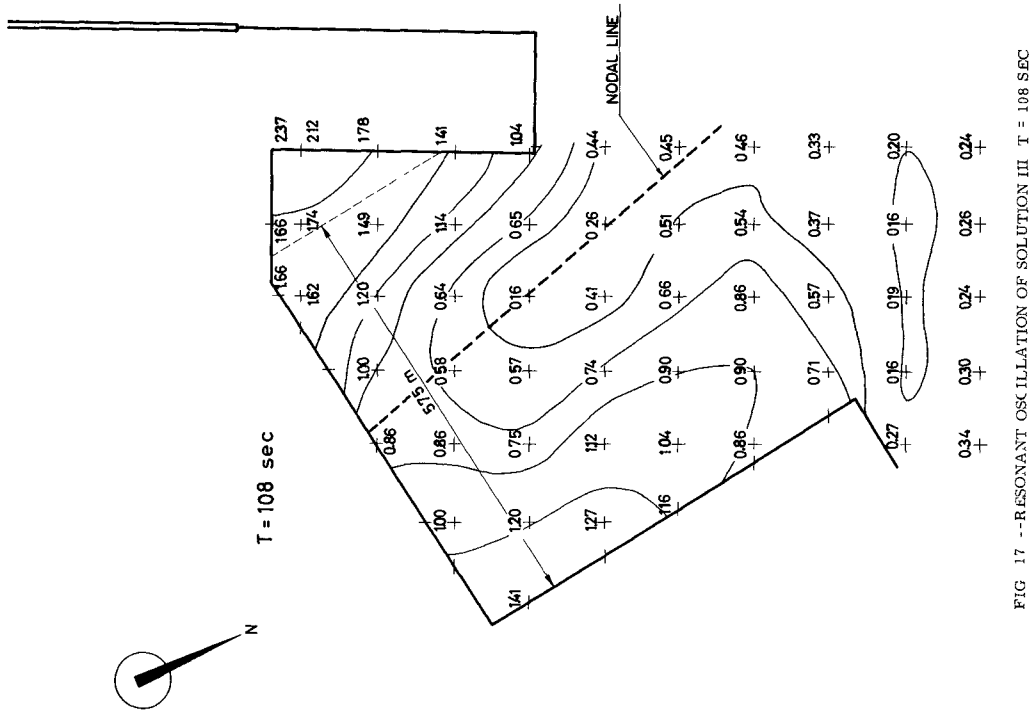

FIG 17 --RESONANT OSCILLATION OF SOLUTION III T = 108 SEC

of amplification" was defined as the ratio of the maximum internal amplitude to the mean external amplitude). Nevertheless, as some periods of resonance corresponded to waves frequently occurring in Luanda bay, the shape of nº 1 dock had to be changed.

5 - COMPARISON AND ANALYSIS OF THE RESULTS OBTAINED

5.1 - Comparison of analytic and experimental results-As shown in figs. 13 and 15, the analytic predictions were not confirmed by the tests, notably as regards solution I, possibly on account of the disturbances due to the small rectangular dock. On one hand the response curve displayed peaks for periods non-predicted in the analytic study, whereas for some predicted resonance periods moderate amplification coefficients were obtained. Only for solution III, in which deviations are slighter, peaks of the response curve for periods approaching the predicted values could be obtained. Thus, resonance had been predicted for periods of 97 and 106 seconds and the response curve displayed peaks for 96 and 108 seconds; in the zone of 49, 51, 65, 67 seconds, where resonance phenomenon were anticipated, considerably high amplification coefficients and a peak for 56 seconds were obtained. On the contrary, for the period of 77 seconds, where resonance had been predicted, the response curve presented a minimum.

The deviations just described should be ascribed to the non-validity of assimilating the dock to a sector.

5.2 - Interpretation of the experimental results - A careful analysis of the equal amplitude curves (figs. 16, 17, 18) is extremely useful for the interpretation of the experimental results.

Thus, according to fig.16, the oscillation with a period of 96 seconds corresponds to a quarter-wave-length oscillation in an open basin with respect to the larger quay at the end of the dock the nodal line is removed slightly more than a quarter-wave-length from this quay. In fact the wave length for a period of 96 seconds is

$$L = CT = \sqrt{gh} \times T = \sqrt{9.8 \times 11.5} \times 96 = 1{,}020 \text{ m}$$

and

$$\frac{L}{4} = 255 \text{ m}$$

The oscillation of 108 seconds (fig.17) corresponds to a half--wave-length oscillation in a closed basin between the new pier and a line near the angle of the present pier with the new quay. In fact the wave length is now

$$L = CT = \sqrt{g\ h} \times T = \sqrt{9.8 \times 11,5} \times 108 = 1,150 \text{ m}$$

and

$$\frac{L}{2} = 575 \text{ m},$$

that is the distance between the two lines.

The oscillation of 136 sec.(fig.18) corresponds to a quarter-wave-length oscillation in an open basin with respect to the smaller quay at the end of the dock, a line parallel to the quay through the end of the present pier behaving roughly as the entrance to the dock. In fact, the wave length for a period of 136 seconds is

$$L = CT = \sqrt{9.8 \times 11.5} \times 136 = 1,446 \text{ m}$$

and

$$\frac{L}{4} = 361 \text{ m},$$

which is sensibly the distance between the quay and the above--mentioned line.

Finally, the 56 sec oscillation, whose equal-amplitude curves are not presented due to their minor interest, proved to be a binodal oscillation, with nodal lines roughly parallel to the large quay at the end of the dock. This oscillation was neglected for the following reasons:

a) It was a binodal oscillation, which in itself at once made it of minor importance as it tended to be damped much faster than uninodal oscillations.

b) its amplification coefficient was not high;

c) its period fell in an interval of very rare periods in Luanda bay.

6 - SOLUTION IV AND ITS EXPERIMENTAL STUDY

6.1 - Solution IV - From the foregoing and from an analysis of the shape of nº 1 dock (fig.19) it is clear that distances d_1, d_2, d_3 conditioned resonances corresponding to the periods of 136, 108 and 96 seconds respectively. So it was decided to investigate how to change these distances so as to obtain a satisfactory solution.

It was proved that some advantages could be derived from a change in d_1. In fact, its value gives rise to a quarter-wave-length resonance which, although slight, corresponds to a very frequent period (136 seconds) in Luanda bay. The problem nevertheless was difficult to solve. In fact, for this resonance to fall in the period range of 170 seconds, comparatively rare in the bay, distance d_1 should obey the condition

$$L = 4\, d_1 = \sqrt{g\, h} \times T = \sqrt{9.8 \times 11{,}5} \times 170 = 1{,}800 \text{ m}$$

and

$$d_1 = 450 \text{ m}$$

This value had the disadvantage of extending the present pier, eliminating its end quay and giving rise to a resonance with a period of 96 seconds (with a higher amplification coefficient), therefore in the range of the most frequent wave periods in Luanda bay.

In order to solve the problem by means of a resonance in the low periods (about 60 seconds), which are infrequent, it would be necessary to have

$$L = 4\, d_1 = \sqrt{gh} \times T = \sqrt{9.8 \times 11{,}5} \times 60 = 638 \text{ m}$$

and

$$d_1 = 159 \text{ m},$$

which is obviously unacceptable.

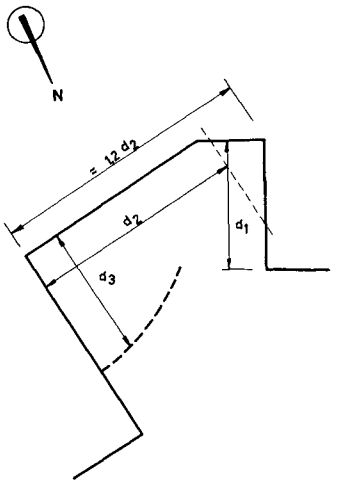

FIG 19 -DISTANCES COMMANDING RESONANT OSCILLATIONS

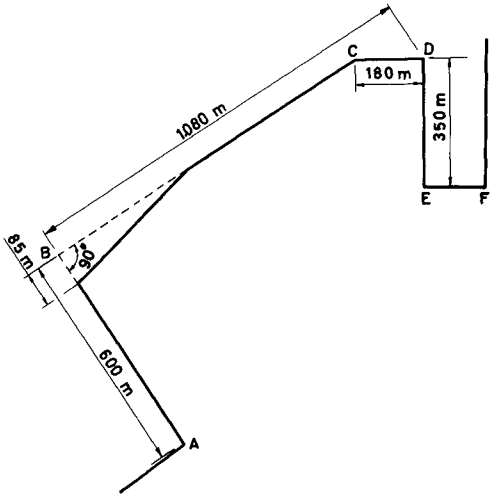

FIG 2- --SOLUTION IV

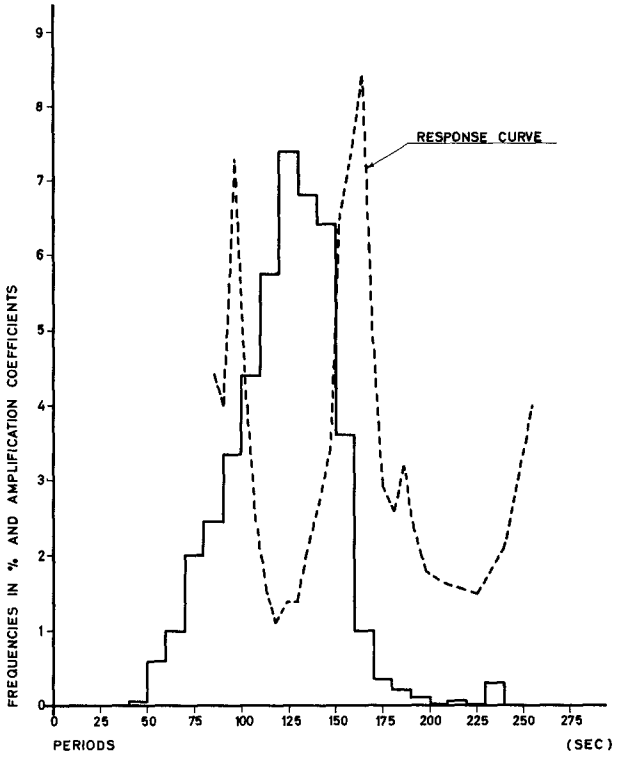

FIG 21 --RESPONSE CURVE OF SOLUTION IV

Nevertheless, given its small amplification coefficient that probably could be further reduced by the increase of distance d_2 (which, as will be seen below, was necessary for other reasons), this resonance did not seem very dangerous.

Distance d_2 had to be changed so that the corresponding half-wave-length resonance, that was marked, would fall in an infrequent period. This could be done by decreasing or increasing d_2 and consequently the corresponding resonance period. In the former case, reducing the resonance period to 70 seconds, which is an infrequent period, d_2 should be such that:

$$L = 2\, d_2 = \sqrt{gh} \times T = \sqrt{9.8 \times 11,5} \times 70 = 742 \text{ m}$$

and

$$d_2 = 371 \text{ m}$$

This value was deemed unacceptable as it would reduce too much both the length of the end quay and the entrance width. It was thus necessary to increase d_2, so as to obtain a resonance period of about 170 seconds. Consequently:

$$L = 2\, d_2 = \sqrt{gh} \times T = \sqrt{9.8 \times 11,5} \times 170 = 1,800 \text{ m}$$

and

$$d_2 = 900 \text{ m}; \quad 1.2\, d_2 = 1,080 \text{ m}$$

Therefore d_2 had to be increased by about 320 m.

As for distance d_3, it gave rise to a not very marked quarter-wave-length resonance with a period of 96 seconds which is not very frequent. Nevertheless only a short reduction of d_3, and consequently of d_1 connected with it, was advantageous.

The foregoing reasons led to solution IV presented in fig. 20. The angle of the end quay was suggested by "Brigada de Estudos do Porto de Luanda".

6.2 - Model test of solution IV - The model test of solution IV yielded the response curve presented in fig. 21 that displays two comparatively marked peaks. One, for a period of 165

seconds, is due to the half-wave-length resonance between quays AB and DE that had been predicted for a period of about 170 seconds; the other, with a period of 96 seconds, corresponds to the first harmonic of the former. In fact, the equal-amplitude curves (fig.22, 23) show that in the former case two lines of maxima (loop lines) are generated near the quay walls and a node line roughly in the middle dock; in the latter case the oscillation is binodal with two loop lines near the quays and another roughly in the middle dock.

The quarter-wave-length oscillation of solution III were not conspicuous in solution IV, probably due to the increased width of the dock entrance and the reduced ratio of its cross dimension (distances d_1 or d_3) to its length (distance d_2).

The superposition of the response curve on the histogram of long-period waves observed in Luanda (fig.21) shows a shift between the peaks of both graphs, which means that the probabilities of resonance are minimum. The peak in the uninodal oscillation corresponds to a very small frequency of the long-period waves; as for the binodal oscillation, its frequency is slightly higher but anyhow this is always less dangerous than the fundamental oscillation. For all these reasons, solution IV was considered as satisfactory.

7 - CONCLUSIONS

In addition to enabling the determination of a suitable shape for nº 1 dock of Luanda port, we believe that from the studies presented the following general conclusions of practical interest can be drawn:

a) Special care is required when choosing the location of quick rotation tide recorders for long-period waves. It is necessary not only to prefer locations in or near loop zones for all the periods but also to avoid at all costs the disturbing influences of normal waves coming from the open sea or locally generated by the wind or ships passing nearby. Without these precautions the interpretation of the obtained results will be very difficult.

b) In the analytic study of oscillations in an irregular shaped basin, an extreme prudence is recommended in the assimilation of the basin to another with simpler geometric shapes making an analytic study possible.

c) The consideration of half-wave length and one-quarter

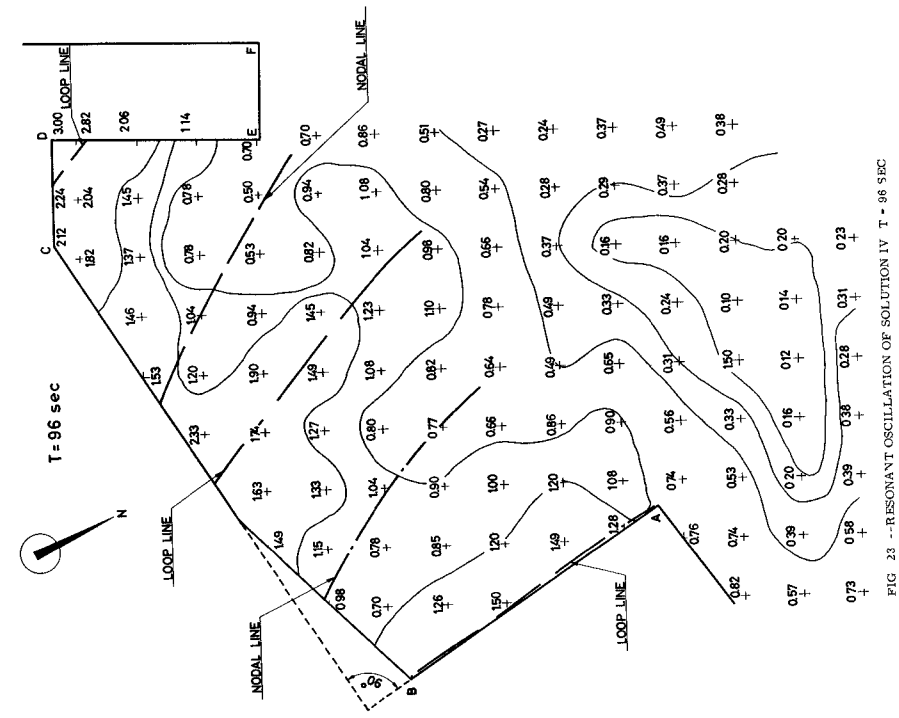

FIG 23 --RESONANT OSCILLATION OF SOLUTION IV T = 96 SEC

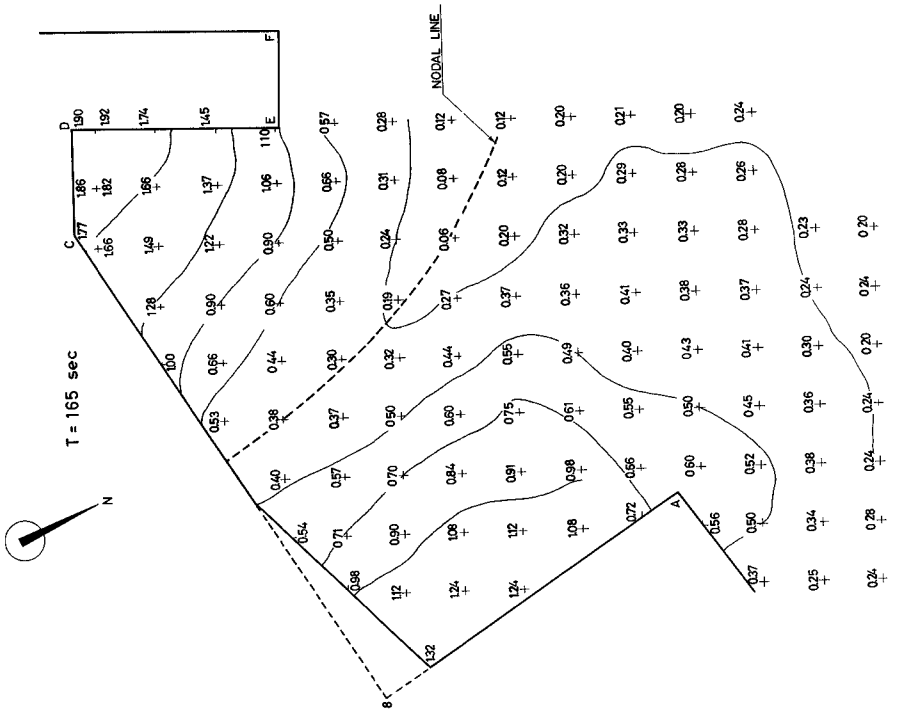

FIG 22 --RESONANT OSCILLATION OF SOLUTION IV T = 165 SEC

wave length oscillations and their harmonics between roughly regular reflecting surfaces can be very useful when predicting oscillation conditions in an irregular shaped basin.

d) The presence of small docks near loop zones is extremely harmful as regards oscillations in a wider space.

e) The intensity of one-quarter wave length oscillations is substantially reduced when the opening increases. The latter conclusion, in fact, agrees with others obtained by analytic or experimental means [6], [7] .

REFERENCES

[1] Abecasis, F.M. - "Consulta de Hidráulica Marítima para a Brigada de Estudos do Porto de Luanda" - 1st rep., 1960 e 3rd rep., 1961 (unpublished).

[2] Abecasis, F.M. - "2ª Consulta Hidráulica Marítima para a Brigada de Estudos do Porto de Luanda" - 1st rep., 1961 (unpublished).

[3] Abecasis, F.M. - "Estudo do problema das ondulações de longo período na ampliação do porto de Luanda", Técnica, nº. 303, 1960.

[4] Lamb, H. - "Hydrodynamics" Cambridge University Press 6th edition, pag. 284 following.

[5] Le Mehauté, B. - "Agitation dans les ports", l'Ingénieur (Canadá) Winter 1958.

[6] Biesel et Le Mehauté - "Mouvements de résonance à deux dimensions dans une enceinte sous l'action d'ondes incidentes" La Houille Blanche nº 3 - 1956.

[7] Ippen and Goda - "Wave induced oscillations in harbors; the solution for a rectangular harbor connected to the open-sea" MIT. Hydrodynamics Laboratory. Report nº 59 1963.

Chapter 49

POTENTIALS OF TIDAL POWER ON THE NORTH ATLANTIC COAST IN CANADA AND UNITED STATES

Jan T. Laba

Asst. Professor, Dept. of Civil Engineering
University of Windsor, Windsor, Ontario, Canada.

In this paper the most suitable locations for erection of tidal power plants on the North Atlantic Coast are reviewed and classified in respect to the possible pool arrangement. The harnessing of the tides to produce power in various lay-outs is described. Due to the limited length of this paper, it was only possible to discuss and compare the power output from two proposed tidal power projects, Passamaquoddy Bay and Shepody Bay, and also to discuss some auxiliary power sources to supplement the varying output of tidal power. The tide producing forces and the effect of the coastline on the tide height is also briefly introduced.

TIDES

The principal movements of the ocean may be divided into three classes: ordinary or wind waves, ocean currents and tidal movements. The essential feature of any tidal movements is, as the name applies, its periodicy, which distinguishes it from the others.

Tides and tidal currents are the vertical and horizontal water movements which occur in response to the periodic tide-raising forces of the moon and sun. Tidal movements are periodic vertical oscillations above and below mean sea level. Tidal currents are periodic horizontal oscillations over a fixed point on the earth's surface, or in open waters, an elliptical movement around a fixed point. The periods of these oscillations are identical to those of the forces to which they respond, i.e. the rotation of the earth on its axis, the revolution of the moon about the earth and the revolution of the earth about the sun.

At the beginning of the period, the magnitude of the force increases from zero to a maximum in a positive direction, then diminishes to zero and increases to a maximum in the negative direction, and thence back to zero to end the period. Each of the periodic forces undergoes some modifications with changes in astronomical conditions. The length of the period varies only slightly but there are large variations in the magnitude of the forces.

The principal tide-raising forces fall into two groups those with a period of about half a day, which are termed semidiurnal forces: and those with a period of about a day, known as diurnal forces.

One of the principal semidiurnal forces is the lunar tide-raising force, with a period of half a lunar day (about 12h 25m). The magnitude of this force varies with the distance of the moon from the earth, being increased by about 20 per cent when the moon is in perigee and decreased by that amount when it is in apogee. The other principal semidiurnal force is the solar force, with a period of half a solar day (about 12h 00m). The magnitude of this force varies with the position of the earth in its orbit around the sun. It is increased by about 27 per cent at each equinox, decreased by about 32 per cent at the June solstice and decreased by about 22 per cent at the December solstice.

One of the principal diurnal forces is a combined lunar and solar (luni-solar) force. This force varies both with the distance of the moon from the earth and with the position of the earth in its orbit around the sun. The force is increased at perigee and decreased at apogee by about 13 per cent and is increased at the solstices and decreased at the equinoxes by about 33 per cent. The other principal diurnal force is purely lunar force, whose period is related to both the lunar and sidereal days. This force is increased when the moon is in perigee, and decreased when it is in apogee by about 20 per cent. (Ref 1).

Figure 1, greatly simplified, indicates how the two principal semidiurnal forces vary with the position of the moon in its orbit around the earth. When the moon is new or full, the range of the tides is considerably greater than the average. They are called spring tides, and are produced by combined tide-raising forces of the moon and sun. When the moon is either in first or third quarter, the tide-producing forces of the moon and sun are in opposition to each other, producing the neap tides with the smallest range.

Tidal energy cannot be harnessed wherever it presents itself, as in the open sea. However, the reflection of the tidal movements on the continental plateau, and the incidental resonances greatly amplifying the tide's height (up to 25 times), create the possibility for their energy to be harnessed.

The height of the tide is not only affected by the moon and sun, but to a large degree by the coastline. On the coast the range is usually greater, the oscillations of the ocean waters tend to grow higher as they run into shallow water. In shallow water the tidal waves move slowly, so that the time of high water could differ widely at stations only a few miles apart, but the period will be exactly that of the impressed force.

In the Gulf of Maine for example, where the continental shelf drops down towards the deep areas of the Atlantic Ocean,

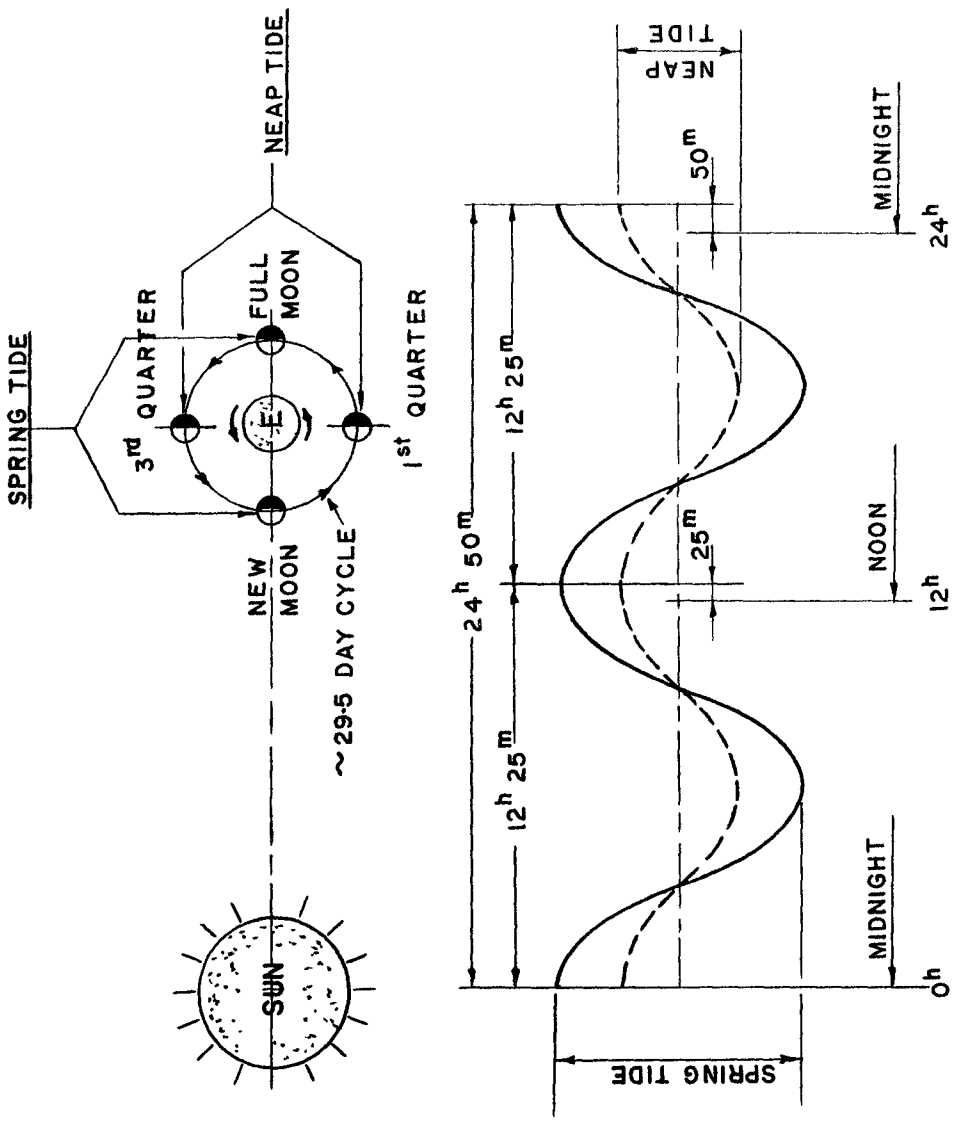

Fig. 1 Moon's Phases and Tidal Cycle.

the tides are amplified by the configuration of the shore line and the bottom of the ocean. Also, where configuration of the coast forces the tide into a corner, or where the natural period of oscillation of the water in a bay or gulf is nearly the same as that of the tides, the height becomes very great. The above conditions exist at the head of the Bay of Fundy where the mean range of spring tides is 50 ft, one of the greatest in the world, and also in the Hudson Strait.

The advantages of a tidal power plant are that the tides remain independent of the atmospheric movements, except for the amplitude which could be affected by the latter. Tides can also be predicted for many years to come and produce power unaffected by droughts, floods, ice jams or silting which usually decreases the output and limits the life of the hydroelectric plants.

The existing disadvantage of the tides as a source of energy is that the tides follow the lunar day of 24 hours and 50 minutes, rather than the solar day of 24 hours. This 50 minute daily lag has a great influence on the economics of tidal power. Since power output varies with the tides, tidal power is completely out of phase with the normal patterns of the daily use of electricity. Therefore, as a general rule the tidal plant should be supplemented by an auxiliary plant during the period of low generation.

POSSIBLE LOCATIONS FOR THE TIDAL POWER PLANTS ON THE NORTH ATLANTIC COAST

There are three main requirements governing the selection of a suitable location for a tidal power plant. The first requirement is the economic justification for such a project in a chosen area and distance to the possible present and future markets for the produced energy. The second and third requirements are: sufficient height of tides and favourable configuration of the shore line. The higher the tide range, the larger the amount of energy that could be produced. A shore line having a number of natural bays and estuaries creates an ideal location for a tidal power scheme, since this will allow the engineers to build artificial pools with a minimum length of enclosing dams, thus making the project more economical.

A study of the tide heights on the North Atlantic coast indicates that the tide range increases along the United States coastline from south to north, reaching the following average tide heights: in Newport 3.5 ft, in the gulf of Maine about 10 ft, and in Cobscook Bay between the United States and Canada 18 ft. In the Bay of Fundy along the New Brunswick coast, the tide range steadily increases towards the head of the bay, reaching at St. John 20.5 ft, and at the inlet of Chignecto Bay to Cumberland Basin 35 ft. Along the Nova Scotia

shore the process is repeated and the average tide height at Burntcoat Head (Minas Basin) is 41.5 ft, at Digby 21 ft, at Yarmouth 7.5 ft and at Cape Sable 7 ft (See Fig 2).

Along the Atlantic coast of Nova Scotia, Gulf of St. Lawrence, Newfoundland and Labrador, the average range of the tides is rather small and varies from a few feet to a maximum not exceeding 10 ft. However, at the entrance to the Hudson Strait at the head of Frobisher Bay, the range of the largest semidiurnal tides is 40 ft, and 50 ft in Ungava Bay.

From the above, it seems that the Bay of Fundy area offers the best possibilities for the development of tidal energy on the North Atlantic coast.

The following are the most suitable locations for erecting a tidal power plant in the Bay of Fundy area:

(1) On the border between the United States and Canada, the configuration of the shore line creates two large bays; they are Cobscook Bay and Passamaquoddy Bay with the St. Croix River estuary. A number of islands located close to the shore at the inlets to the above mentioned bays create an ideal location for a tidal power plant. Although the average tide range is only 18 ft, the place itself offers large possibilites and flexibilities to produce a continuous supply of power, using more than one pool system.

(2) At the head of Chignecto Bay where the average tide range is 35 ft, two bays, Shepody Bay with the Petitcodiac River estuary and Cumberland Basin create the prospect of a very promising tidal power project. In view of the economi aspects, this two-pool project would be superior to the previously mentioned Passamaquoddy project in dependable power supply and amount of energy generated per year.

(3) The next possible place would be Minas Basin where the height of the tides is the highest in the world, the average being over 40 ft. The barrage could be built at the entrance to the basin, cutting off a large volume of water at high ti and a large amount of energy could be produced. This projec could be a typical one-pool scheme (one or two-way operating plant), but could not produce alone a continuous supply of power.

(4) Another two places where energy from tides could be produced are located along the shores of Nova Scotia, They are St. Mary Bay and Annapolis Basin, where the average tide height reaches 21 ft. These two bays could also be develope into two separate single pool schemes, but much smaller than those previously mentioned.

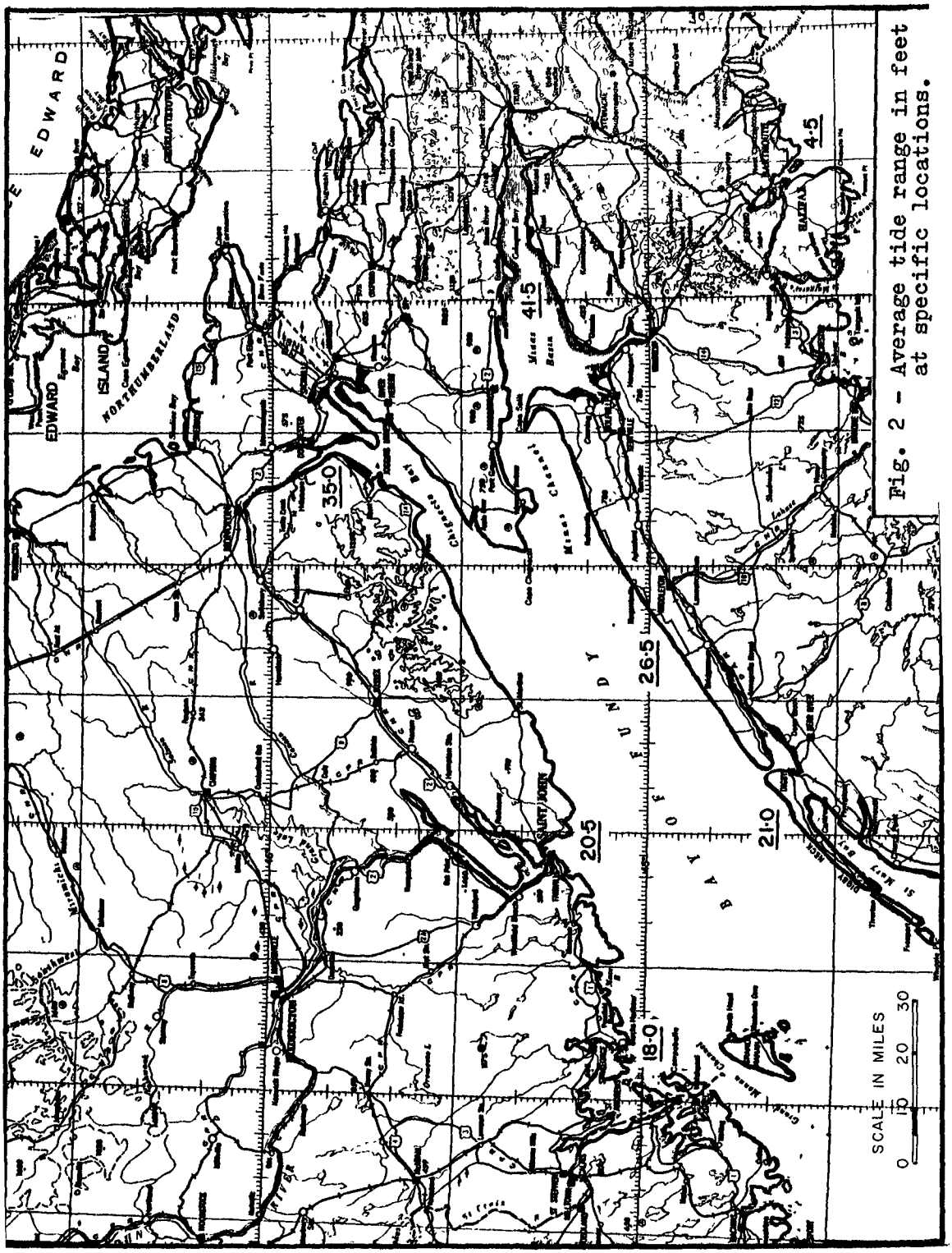

Fig. 2 - Average tide range in feet at specific locations.

POWER FROM TIDES

Tidal hydroelectric power similar to river hydro power, can be obtained by the flow of water from higher to lower levels through hydraulic turbines. Dams, gates, and powerhouses are needed for tidal projects as for a power project on a river. Other factors such as a rapidly varying head and problems of salt water corrosion must also be considered. A tidal power project may be arranged in many different ways, and these are described in the following.

A single pool equipped with turbines and gates can be created by building a barrage enclosing an estuary or bay. The pool can be filled during high tide and the potential energy of the water can be utilized when the pool is emptied at low tide. This is known as the single high pool emptying cycle. Alternatively, the pool may be emptied at low tide and receive discharge through the turbines from the ocean at high tide. In this case, the layout is known as a single low pool. These two cases are sometimes refered to as one-way operating tidal power plants.

Using a single pool layout, with turbines generating power from flow in either direction, the energy can be produced during both the filling and the emptying of the pool. Such a layout is known as a two-way operating plant or single-mean-pool arrangement.

If a selected site offers certain topographical characteristics, two separate pools equipped with emptying and filling gates may be used. One pool will be filled at the high tide and the other emptied at low tide, with the high pool discharging through the turbines into the low pool. This arrangement can be called a two-pool layout.

INTERNATIONAL TIDAL POWER PLANT

A few suitable sites for the location of the tidal power plant have already been described. Let us first conside the St. Croix River estuary with Passamaquoddy Bay and Cobscoc Bay. This project includes 100 square miles of Passamaquoddy Bay and 40 square miles of Cobscook Bay. (The 100 square miles represents pool area at an elevation of 6 ft above m.s.l. and the 40 square miles at elevation of 5 ft below m.s.l.). This would involve both New Brunswick (Canada) and Maine (U.S.A.) interests and therefore would be an internatiór al project. The range of tides in the above mentioned areas at the site of the proposed project, varies from a minimum of 11.3 ft at neap tide to a maximum of 25.7 ft at spring tide, averaging 18.0 ft. On the average, during each tidal cycle approximately 70 billion cubic feet of water enters and leave: both bays.

A design including both bays in one project would be

more advantageous than the separate development of either bay by each nation. Independent separate projects would involve international complications concerning navigation, fish, wild life and other aspects.

PRELIMINARY CALCULATION OF THE POWER OUTPUT

Before the most suitable layout of a tidal power arrangement for this area can be chosen, let us consider the possible energy production from a few layouts. The purpose of this investigation is to compare the theoretical power outputs obtainable from different layouts. Some assumptions will be required to simplify the actual complicated problem.

The calculations will be carried out for an average tide height of 18 ft. The equation of the tide wave oscillation will be assumed to be:

$$y = z \cos \frac{2\pi}{T} t$$

where: amplitude $z = 9$ ft
period $T = 12\text{hr.}25\text{min.}$
variable t = time

The generated power will be expressed as a function of the average discharge through the turbines, and the average area of the pool or pools (160 sq miles) will be assumed to remain constant in the range of the tides. Also, the minimum required operational head for the turbines will be taken as 6 ft.

Single pool, one-way operating plant - In considering a one-way operating tidal power plant (Fig 3), built to trap water at high tide and discharge to the ocean at low tide, (high pool layout), four separate operating phases can be recognized:

(1) A waiting phase (A-B), when turbines are stopped and filling gates are closed.

(2) An energy production phase (B-C), when the turbines are operating and the gates are closed. In this layout the turbines are producing power operating under a head which is always in the same direction - from the pool to the ocean.

(3) A waiting phase (C-D), with the gates closed and the turbines stopped, after the generating head decreases below its minimum required value.

(4) A filling phase (D-A), when the turbines are stopped and the filling gates open. The tide is rising and the water flows from the ocean to the pool.

Figure 3, indicates that the pool is filled during high

LEGEND

----- Operation without pumping.

– —·· Operation with pumping.

T = Turbines

G = Gates.

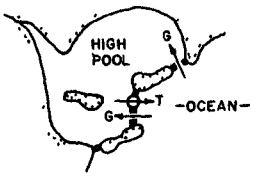

SCHEMATIC LAYOUT

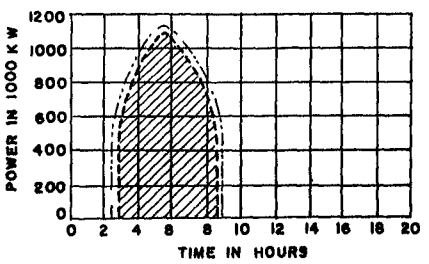

POWER OUTPUT

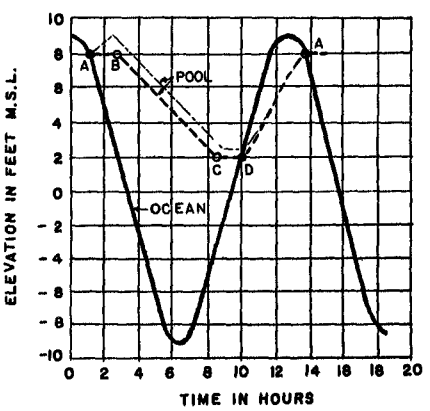

POOL ELEVATIONS

Fig. 3 - Single-Pool Layout. One-way operating plant.

tide up to 8 ft above m.s.l. As soon as the head from the pool to the ocean is large enough, power is generated during each tide cycle, over a period of 5.74 hours, in which the water level in the pool will drop 6 ft. No power is generated during the pool filling on the high tide.

In all the following tables, generated power indicated was calculated on the assumption of 88 per cent average efficiency of the power plants. Table I shows a relationship between time, operational head and theoretically generated power for a one-way operating plant.

TABLE I

Time t (hr)	Water Level in pool (ft)	Operational head (ft)	Generated power (kW)
2.66	+ 8.00	6.00	514,000
4.00	+ 6.59	10.51	904,000
5.75	+ 4.78	13.53	1,160,000
7.50	+ 2.92	10.10	865,000
8.40	+ 2.00	6.00	514,000

Note: water level in respect to m.s.l. and the first peak of high water occurs at t = 0 hours.

The total energy produced during the complete tidal cycle will be 5,150,000 kW-hr, and the next production phase will start after the waiting period of 6.68 hours.

If energy from outside sources is available, it would be advantageous for the above project to use turbines that also operate as pumps. Immediately after the filling gates are closed, the water level in the pool could be raised further by pumping at low head and increase the generating head for the following production phase. The energy gained in the power generating cycle would be larger than the energy used for pumping.

Single pool two-way operating plant - A single mean pool could be created by using turbines which can generate power from flow in either direction. It would operate as a high pool during low tides, and as a low pool during high tides, see Fig 4, where the mean pool is filled and drained respectively to ± 2 ft. This arrangement results in two separate generating periods and six operating phases can be recognized.

(1) A waiting phase (A-B). Generation can start as soon as the minimum head is available. If energy for pumping from outside sources is available, the water level in the

pool could be raised further. (The energy gained in both generating cycles will exceed the energy used for pumping at low head, adding to the benefit of the project).

(2) An energy production phase (B-C), with the water flowing through the turbines from the pool towards the ocean. Generation will continue until sufficient water volume has been evacuated from the pool and the generating head decreased to its minimum required value.

(3) An emptying phase (C-D). By stopping all turbines and opening all gates, the water within the pool can be rapidly evacuated at the time of the low tide.

(4) A waiting phase (D-E), when the turbines are stopped and the gates are closed. Generation can start as soon as the minimum required generating head between the ocean and the pool is available. This period in relation to the tide could occur sooner if a reverse pumping operation would be available to lower the water level in the pool.

(5) The energy production phase (E-F). As the tide continues to rise, generation takes place until sufficient water has flowed into the pool to destroy minimum generating head.

(6) A filling phase (F-A), when the turbines are stopped and the gates are opened. As the high tide begins to drop down the water flows from the ocean to the pool, until both water levels are the same.

The required minimum operational head of 6 ft will occur in the pool 4.02 hours after high water and the power generation period will last 3.53 hours, and during this time the water level in the pool will drop 3 ft. Then the water from the pool will drain through the gates or turbines which could be changed to orifices bringing the water level down to 2 ft below m.s.l.

The reverse process will start again at $t = 10.23$ hours, but this time water from the ocean will flow to the pool through the turbines generating power again for 3.53 hours, and then the gates will be opened, or the turbines changed to orifices and the cycle will be repeated.

Table II shows a relationship between time, operational head and generated power for a two-way operating plant.

TABLE II

Time t (hr)	Water Level in pool (ft)	Operational head (ft)	Generated power (kW)
2.66	+ 2.00	0.00	0
4.02	+ 2.00	6.00	418,000
5.84	+ 0.46	9.31	650,000
7.55	- 1.00	6.00	418,000
8.87	- 2.00	0.00	0
10.23	Reverse operation will start		

The total developed energy in two generating periods during a complete tidal cycle will be about 3,800,000 kW-hr. Since the average pool level is about the same as mean sea level, the generating head is considerably less than for a high pool arrangement; because of this, total generated power for the mean-pool plan is less than for the previous layout by 26 per cent, but the waiting period between energy production phases will decrease to 2.68 hours, compared with 6.68 hours for a one-way operating plant.

Two-pool arrangement - The disadvantage of intermittent generation can be overcome by the simple two-pool plan illustrated in Fig 5. The high pool, having an area of 100 square miles is filled during high tide through one set of gates, and the low pool having an area of 40 square miles emptied during low tide through a separate set of gates. Since one pool is operated at a high level and the other at a low level, conventional turbines which permit flow in one direction can be used. The two-pool plan produces a varying but continuous supply of power.

To compare this operation with the previously described one-pool arrangement, let us assume that maximum water level in the high pool will reach 8 ft. Then during a period of 9.54 hours, the water level in the high pool will drop 3 ft and the filling gates for the high pool will be open at time t = 10.47 hours, as the high water is approaching. The filling process will take 2.88 hours, and the water level will again reach 8 ft at the time t = 13.35 hours after the first high water which occured at t = 0 hours.

The low pool having 2.5 times smaller area will drain its water volume at low tide to the lowest level (8.5 ft below m.s.l.) and then the emptying gates will be closed. In line with our previous assumption introducing the average discharge, there will be a continuous and constant flow rate of water from high to low pool, and the water level in the low pool will increase 2.5 times faster than it decreases in the high pool. This will last for 8.95 hours and at t = 15.85 hours, the water level in the

LEGEND

A-B , Power units generating. Filling gates closed.

B-A , Power units generating. Filling gates opened.

C-D , Emptying gates opened.

D-C , Emptying gates closed.

T = Turbines.

FG = Filling gates.

EG = Emptying gates.

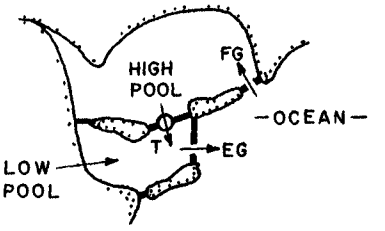

SCHEMATIC LAYOUT

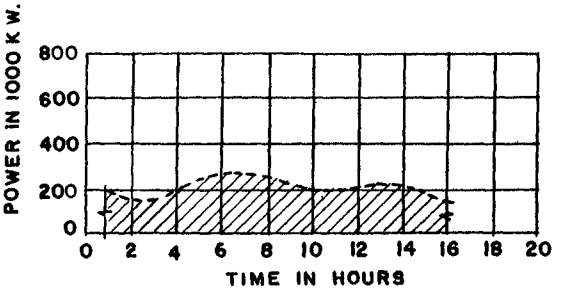

POWER OUTPUT

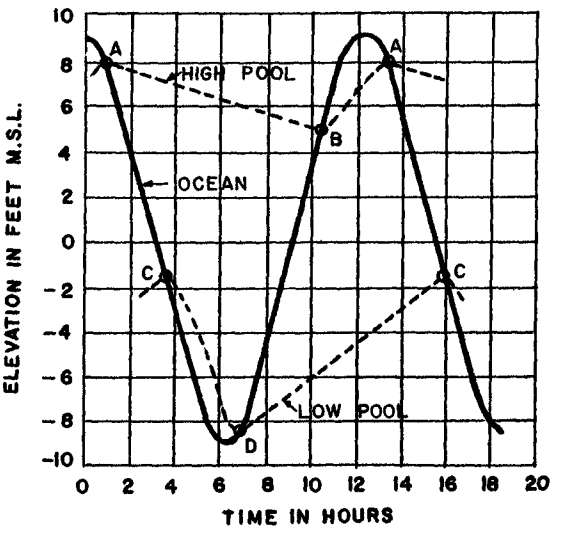

POOL ELEVATIONS

Fig. 5 - Two-Pool Layout.

low pool will reach its peak, 1.5 ft below m.s.l.

Table III shows relationship between time, operational head and generating power for the two-pool arrangement.

TABLE III

Time t (hr)	High Pool level (ft)	Low Pool level (ft)	Operational head (ft)	Generated power (kW)
0.93	+ 8.00	- 3.42	11.42	211,000
3.43	+ 7.21	- 1.50	8.71	161,000
6.89	+ 6.12	- 8.50	14.62	270,000
10.47	+ 5.00	- 5.68	10.68	196,000
13.35	+ 8.00	- 3.42	11.42	211,000
15.85	+ 7.21	- 1.50	8.71	161,000

Since the high pool level in the above is always above m.s.l. and the low pool is always below, and the difference between these two levels is creating operational head for the turbines which never drops below the minimum required head of 6 ft, a continuous supply of power is produced. During one complete tidal cycle energy equal to 2,680,000 kW-hr is produced.

Conclusion - From the above investigation of energy production from the average tide height (18 ft), it is evident that the single high pool will produce during one complete tidal cycle 1.92 times more energy and the single mean pool plan 1.42 times more energy than the two-pool system. However, the single pool layout with a one or two-way operating plant has the disadvantage of producing an intermittent power supply, because no power can be generated without sufficient difference between the levels of the pool and the ocean. Even with additional features such as auxiliary gates and pumps, a single pool would not be able to deliver on its own, an uninterrupted power supply to the network.

The above disadvantage is overcome by a two-pool plan which generates varying but continuous amounts of power. Furthermore, this layout could also deliver at any required time a sizable amount of energy, (independent of the water level in the ocean) after the operational water levels in both pools were obtained and the gates were closed.

As a continuous supply of power seems to be a very important factor in the development of the Canadian Maritimes, the two-pool system appears to be the most attractive, and will be discussed in detail.

PROPOSED TWO-POOL LAYOUT

Figure 6, shows one of the possible layouts which include Passamaquoddy Bay as the high pool and Cobscook Bay as the low, with a powerhouse located on Moose Island, north west from Eastport. The narrowest part of the island would be excavated to provide the headrace for the powerhouse. The location of the tidal power project and the general arrangement of the selected layout is shown on Fig 6, where the arrows indicate the direction of the flow. With 34 generating units rated at 10,000 kW each, operated at about 6 per cent above rated capacity for short periods during spring tides, the output of the tidal power plant would range from 73,000 to 360,000 kW. Average energy generation would be 1,890 million kW-hr a year.

About 36,000 linear feet of tidal dams will be required, which could be composed of clay core supported by flanking dumped-rock fills.

The proposed plan calls for 100 filling gates, 50 in Letite Passage and 50 at Deer Island Point. North east from Indian Island 67 emptying gates, and 5 more at Quoddy Roads similar to the filling gates but set at a lower elevation would be needed to empty the lower pool. A vertical lift gate 30 ft x 30 ft, (completely submerged), set in the venturi throat, with rounded rectangular entrance (1,600 sq ft would be recommended for this project as the venturi throat permits maximum discharge for a given gate area.

Four navigational locks would be required for this project. Two locks to pass fishing vessels, one in the passage between McMaster and Pendleton Islands, and the second at Quoddy Roads. Another two bigger locks, one at Head Harbour Passage and the second at Western Passage north at Eastport would pass large seagoing vessels.

The topography of the selected area permits many different arrangements of the components of a two-pool project. Cobscook Bay has much flatter shores in the tide range than Passamaquoddy Bay; for this reason the area and also the volume of the tidal pools would be larger if Cobscook Bay would be used as the high pool and Passamaquoddy as the low, this could produce more energy than the proposed layout. An important advantage of the proposed plan over Cobscook Bay high pool plan is that all Passamaquoddy Bay and Western Passage would be in the upper pool where the water surface would vary between el + 2.81 ft and + 11.85 ft instead of the present maximum variation between el ± 12.85 ft in respect to m.s.l. In consequence, the navigation and harbour depths for ports in Canada and U.S.A. would be improved. The now existing controlling navigational depth at St. Stephen, New Brunswick, would change from 7 ft at mean lc

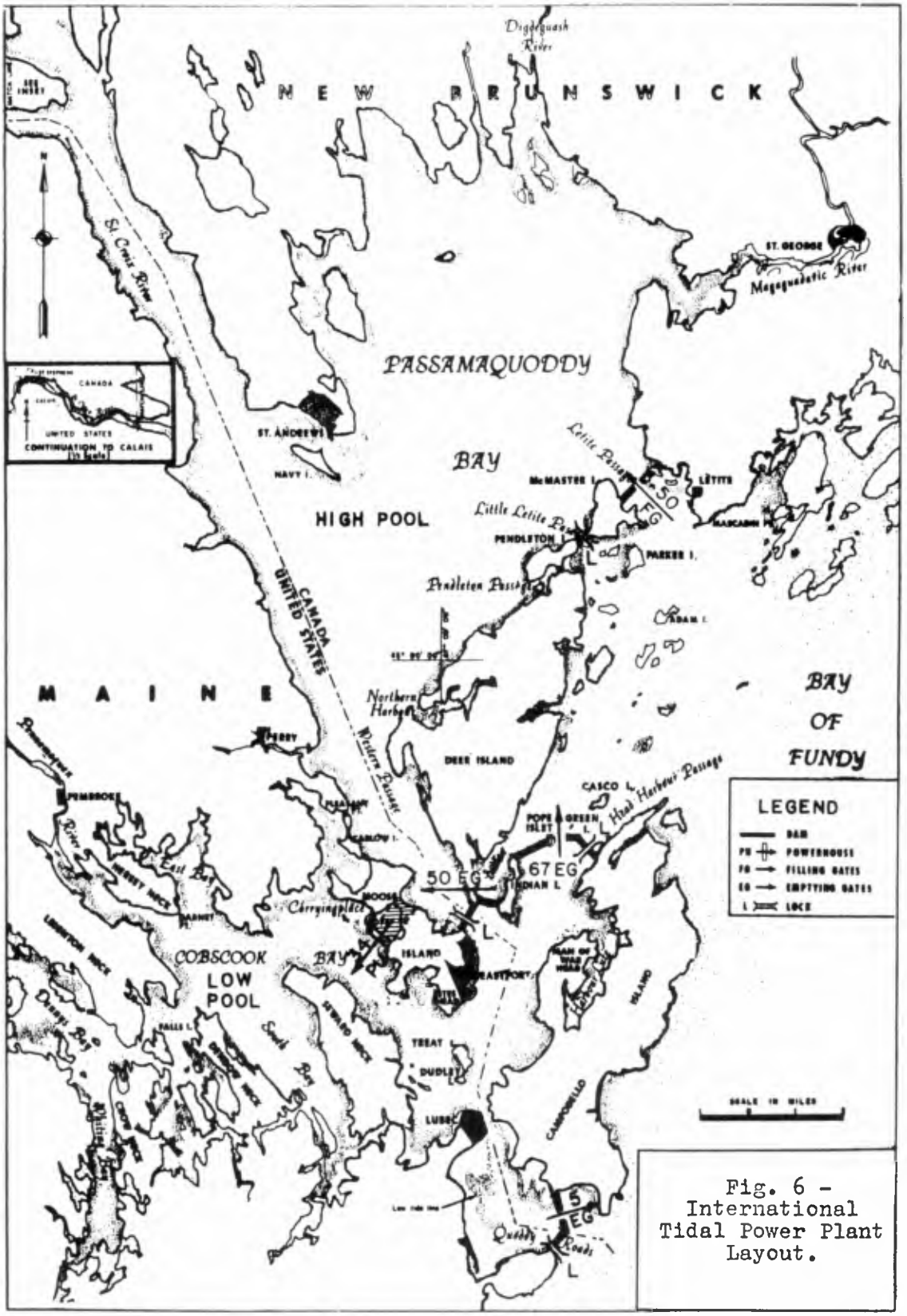

Fig. 6 - International Tidal Power Plant Layout.

tide, to about 22 ft at mean low stage of the high pool. For this reason, Passamaquoddy Bay as the high pool is the most attractive project.

Power output - Figure 7, illustrates typical tidal plant operation where the power output of the selected two-pool layout would vary with ebb and flood of the tides.

Table IV shows momentary tidal power output during the maximum and minimum tides:

TABLE IV

	Max. Generated Power (kW)	Min. Generated Power (kW)
Maximum tide	402,000	258,000
Minimum tide	122,000	73,000

The above figures were derived on the assumption that the highest spring tide and the smallest neap tide were preceded and followed by tides having on the average 1 ft smaller or larger amplitude respectively. If these conditions would not exist and the smallest neap tides appeared one after another, the minimum momentary output of the tidal plant would be reduced to 65,000 kW. In conclusion, the International Tidal Power Plant would have installed capacity of 340,000 kW, and operate slightly above rated capacity for short periods during spring tides.

Turbines - The generating units previously mentioned would be comprised of large European Kaplan turbines, and due to the low and variable operating head, the turbines would be connected to generators with the relatively low rating of 10,000 kW. The average generating head for the turbines would be about 11 ft, normal (operating) speed 40 r.p.m. and a runner discharge diameter of 24 ft.

INTERPROVINCIAL TIDAL POWER PLANT

A very promising Canadian tidal power project could be created by combined use of Shepody Bay and Cumberland Basin, located at the head of the Bay of Fundy, between the provinces of New Brunswick and Nova Scotia.

Shepody Bay, with an approximate area of 75 square miles could be used as the high pool, which also would improve navigation on the Petitcodiac River. Cumberland Basin with an area equal to 50 square miles (after some improvements), could be used as the low pool.

Figure 8 shows the proposed Interprovincial Tidal Power Project layout. At the entrance to Shepody Bay 140

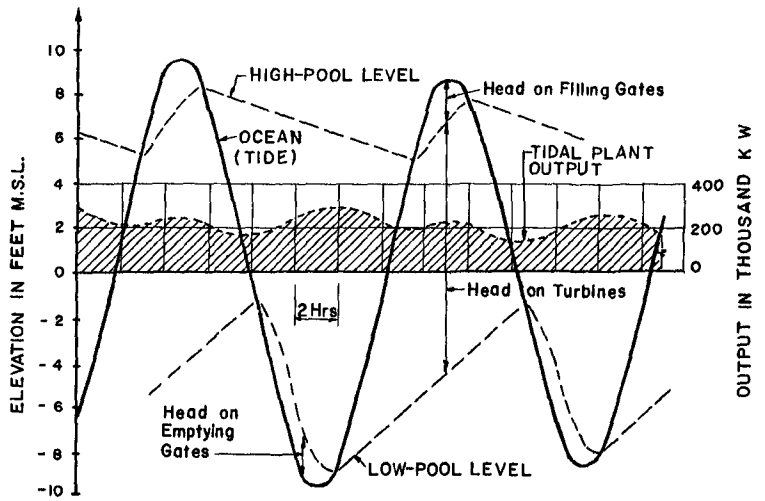

Fig. 7 - Typical International Tidal Plant Operation.

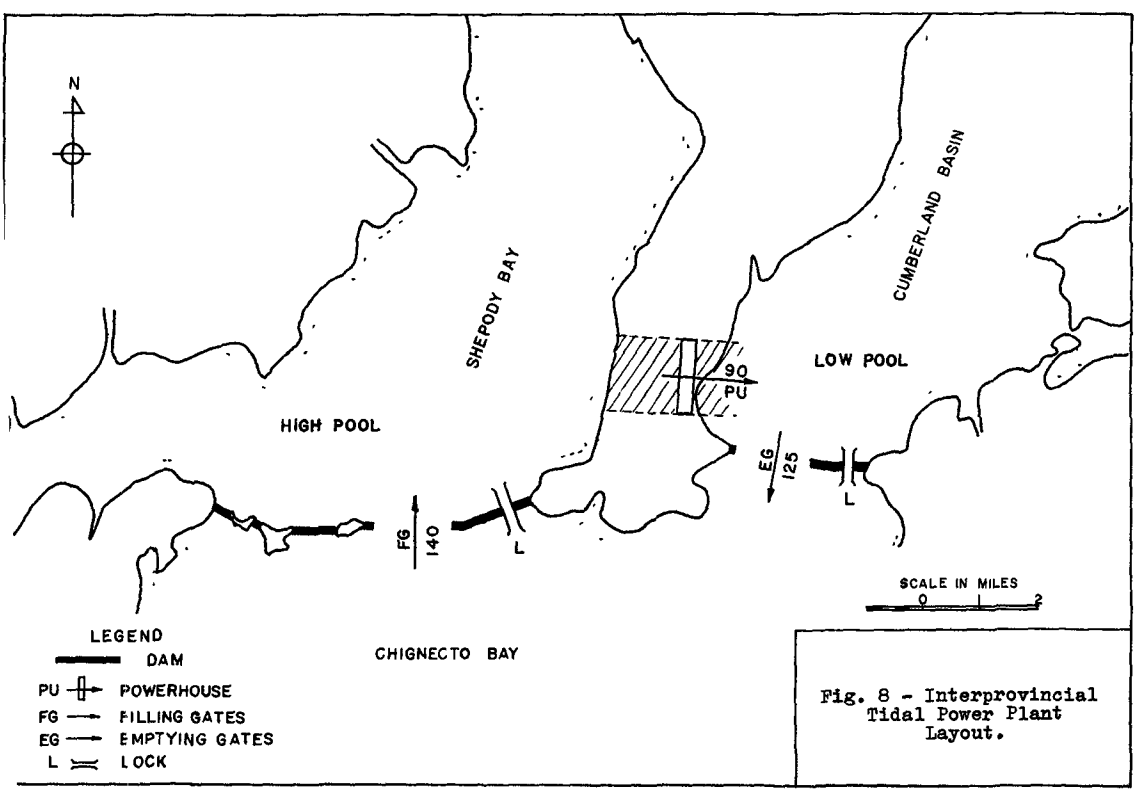

Fig. 8 - Interprovincial Tidal Power Plant Layout.

filling gates and one navigation lock to pass seagoing vessels would be located. A smaller lock to pass fishing vessels and also 125 emptying gates would be located at the entrance to Cumberland Basin. The filling and emptying gates would be the same shape and size as previously described for the Passamaquoddy Tidal Power Project.

The best location for the power house would be at the narrowest point of the peninsula, separating two pools at Peck's Cove, with an excavated area for the head and tailrace. With 90 generating units rated at 10,000 kW each, operated at 6 per cent above rated capacity for short periods during spring tides, the output of the tidal power plant would range from 272,000 kW to 954,000 kW. Average energy generation would be about 5,670 million kW-hr a year.

Height of tides - At Cape Hopewell in the lower reaches of Petitcodiac River (Shepody Bay), the largest tides rise and fall to about 24 ft above and below m.s.l. Further north in Petitcodiac and Memramcook estuaries, the tides range from 21 ft at neap (lowest) tide to over 51 ft at spring (highest) tides.

Maximum tide height for the above project will be assumed as 49 ft, average height 35 ft, and minimum tide height of 21 ft.

Two-pool arrangement - To produce a continuous supply of power, a two-pool plan must be selected. Economic efficiency of the whole project will depend on the proper selection of the flow-rate from high to low pool and also on the number of gates installed.

Figure 9, shows typical operation and power output for a proposed Interprovincial Power Plant, using the average tide height of 35 ft.

The filling gates will be closed when water level in the high pool reaches its maximum level of + 16.5 ft at time t = 0.67 hr after high water. The water level in the high pool will drop 6 ft in 9.87 hr, and at t = 10.54 hr the filling gates will be open again.

The low pool having a smaller area will drain its water volume at low tide to the lowest level - 17.0 ft, and then the emptying gates will be closed. As there is a continuous and constant flow-rate of water from the high to the low pool, the water level in the low pool will increase approximately 1.5 times faster than it decreases in the high pool. This will last for 9.85 hr and at t = 16.52 hr, the water in the low pool will reach its highest level, and then the emptying gates will be opened. With an assumed average efficiency of the power plant of 88 per cent, the total energ

LEGEND

A-B , Power units generating. Filling gates closed.

B-A , Power units generating. Filling gates opened.

C-D , Emptying gates opened.

D-C , Emptying gates closed.

T = Turbines.

FG = Filling gates.

EG = Emptying gates.

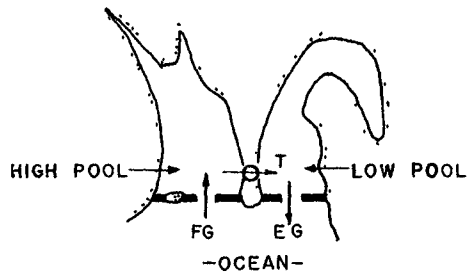

SCHEMATIC LAYOUT

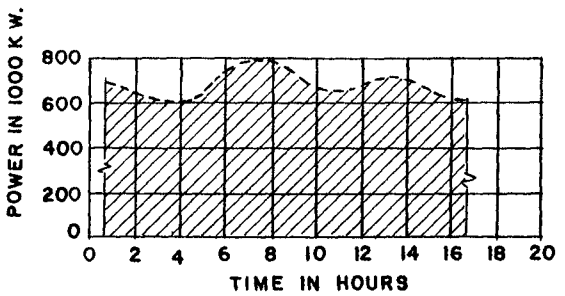

POWER OUTPUT

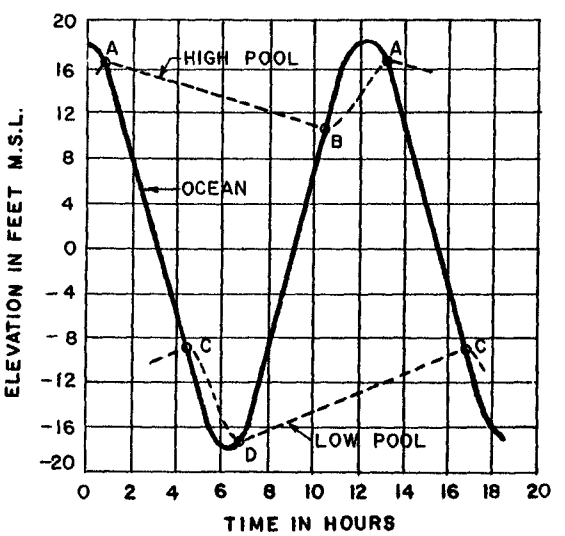

POOL ELEVATIONS

Fig. 9 - Interprovincial Tidal Power Plant output from the average tide height.

produced during the complete tidal cycle will be 8,300,000 kW-hr.

Table V shows momentary tidal power output during the maximum and minimum tides:

TABLE V

	Max. Generated Power (kW)	Min. Generated Power (kW)
Maximum tide	1,180,000	870,000
Minimum tide	342,000	272,000

The above figures were derived on the assumption that the highest spring tide and the lowest neap tide were preceded and followed by tides having, on the average, 2 ft smaller or larger amplitudes respectively.

Turbines - Since the purpose of this paper is only to compare tidal power output of each tidal plant, the turbines used in this case were assumed as before to be European Kaplans, with an average power generating head of 25 ft normal (operating) speed of 90 r.p.m. and a runner discharge diameter of 15 ft.

COMPARISON OF INTERPROVINCIAL AND INTERNATIONAL TIDAL POWER PLANTS

From the preceding discussion, the superiority of the Interprovincial (Shepody Bay) Tidal Power Plant over the International (Passamaquoddy Bay) can be expressed as follow

(1) The dependable firm power supply would be 3.73 times higher.

(2) The average energy generated per year would be 3 times more.

(3) The ratio of the high pool area to the low pool area is closer to unity, which creates a more economical operating plant.

(4) The average design head for selection of the turbines is 25 ft, as compared with 11 ft in the case of the International Tidal Power Plant; this will permit the use of smaller sized turbines to produce the same amount of power i.e. 10,000 kW per turbine.

(5) Only two navigation locks will be required to pass sea-going and fishing vessels.

(6) As the higher tides in Shepody Bay have greater powe

producing potential, the number of filling and emptying gates indicated on Fig 8, could be reduced if desirable for economical or other reasons. The amount of energy produced by the above project could still compare favourably with Passamaquoddy Bay.

Comparison of tidal power output with normal load pattern - Figure 10, shows the output of the two previously discussed tidal power projects compared with the typical load curve for a period of one week. In this particular case, maximum power output for both plants occured Sunday after midnight and minimum power output occured the following Saturday before midnight. The load curve shown has a total annual energy of 8,450 million kW-hr and a load factor of 60 per cent. It represents the combined utility loads of Maine and New Brunswick expected in about the year 1975. (Ref 2).

In New Brunswick alone, with the present population of 615,000, the energy requirements of the utility market are estimated at 1,220 million kW-hr for 1965, and at 2,240 million kW-hr for 1975. The corresponding peak demand will be 260,000 and 455,000 kW. The load factor is expected to increase from the present 52.3 to 56.5 per cent in 1975. (Ref 2).

AUXILIARY POWER PROJECTS

Each tide will fill the upper pool of the tidal project regardless of the amount of water used to generate energy in the preceding cycle. Water left unused would be wasted; therefore, power must be generated from each tide before the next tide occurs or it will be lost.

It was mentioned previously, that the tides follow closely the gravitational pull of the moon as it circles the earth at varying distances, once every lunar day (24h 50m). Due to existing difference between the lunar and solar day, the high and low waters will occur 50 minutes later each day. On the other hand, the use of electricity follows the pattern of a 24-hour solar day, following the nature of demand, the work and play habits of consumers. This 50-minute daily time lag could be directly responsible for the maximum power demand occuring during the time of minimum tidal power production, and also for minimum demand during the maximum tidal power generation.

For load carrying purposes, power from the tidal project is limited to the amount it can furnish under the most adverse conditions, which will be 73,000 kW for the International Tidal Power Project and 272,000 kW for the Interprovincial. All output in excess of this amount is not dependable for serving loads and would have value only as non-firm energy. Since this excess is large, it should be

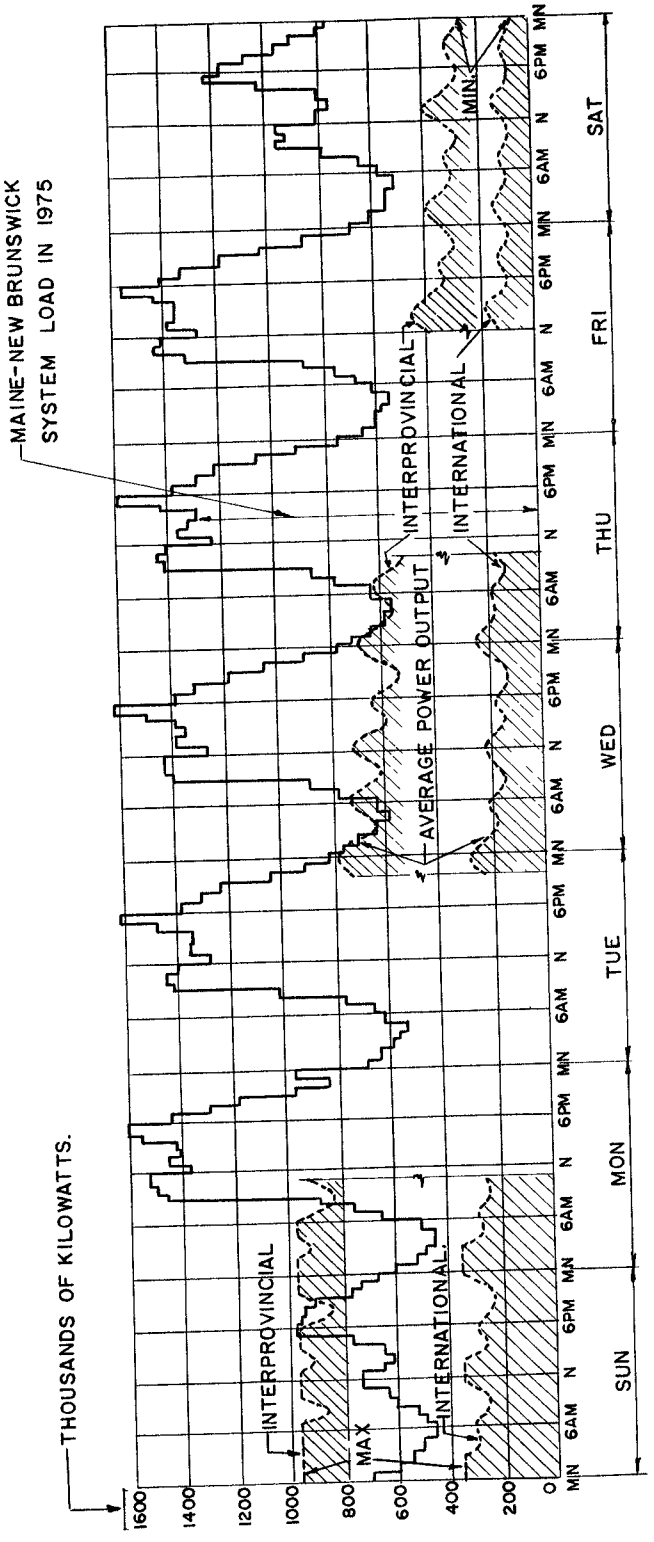

Fig. 10 - Load pattern showing maximum, average and minimum output from the Interprovincial and International Tidal Power Plants.

firmed by an auxiliary source of power to make it dependable for serving loads.

Firming of the tidal power output - The tidal power plant should be supplemented by an auxiliary plant during the period of low generation to increase the dependable power supply. Also in the case when combined output of both sources will supply only a portion of the required system load, the auxiliary source of energy should firm the tidal power output in such a way that the pattern of the remaining load would be acceptable to the other generating plants of the system. The power output could also be combined with one or more hydroelectric, nuclear, steam or combustion power plants. The combined energy obtained from the above sources should form a pattern similar to the required load curve.

In the areas where water storage could be provided, it would be possible to firm the tidal power output by pumping water to the storage reservoir at times of high tidal energy output, and then use the stored water to generate power during low tidal power output. This continuously repeated process of generating and pumping could regulate the tidal power output to deliver the required amount of power to the network. This type of operation however, will result in the loss of a certain amount of energy consumed by pumping and other losses in the system.

FINDINGS OF THE INTERNATIONAL JOINT COMMISSION

In 1961, The International Joint Commission, a six man board, with equal U.S.A. and Canadian representation, stated that the International Tidal Project could work if tied to a St. John plant. One of their proposed layouts, similar to the one shown on Fig 6, could deliver the net average annual energy of 1,843 million kW-hr, with installed capacity of 300,000 kW and power output varying from 345,000 kW to 95,000 kW (dependable 98 per cent only). The construction cost of the tidal plant alone would be close to $500 million.

(1) Among a number of river hydroelectric sites examined, Rankin Rapids on the upper St. John River in Maine, was selected by the commission as the best source of auxiliary power. The Rankin Rapids project could provide 2.8 million acre-feet of usable storage capacity. If the output of the tidal power project would be combined with all of the capacity and energy available at Rankin Rapids (460,000 kW dependable, and 1,220 million kW-hr) it would provide a total dependable capacity of 550,000 kW and an average annual generation of 3,063 million kW-hr.

Assuming an equal division of power output and of first costs between U.S.A. and Canada, construction of the

tidal power project with all of Rankin Rapids as auxiliary plant is not an economically justified project for Canada.

(2) As a possible alternative plan of development, Rankin Rapids could be constructed initially with 200,000 kW of dependable capacity to carry part of the load in the State of Maine. An additional 260,000 kW of dependable capacity would also be provided as an auxiliary power supply for the tidal project. Energy thus borrowed from the Rankin Rapids project when using the "incremental capacity" would be repaid when tidal output is greater than the load. In this way, Rankin Rapids and the tidal project would provide 355,000 kW dependable capacity and 1,843 million kW-hr of average generation without a serious effect on the basic Rankin project (200,000 kW and 1,220 million kW-hr).

(3) Tidal power could also be supplemented by pumped storage, located on the Digdeguash River near the outlet into Passamaquoddy Bay east of St Andrews. This pumped storage plant could increase dependable capacity of the tidal plant by 228,000 kW. The average annual generation however, would decrease to 1,759 million kW-hr.

In conclusion, the International Commission stated that power rates would not be competitive if Canada and the U.S.A. built the tidal project together. Canadian interest rates would be higher, because of differences in interest rates existing in the two countries, and because of different values of alternative power. Assuming a 50-year amortization period and initial cost equally divided, the cost of power for alternative plan (2) would be 11.5 mills per kW-hr for U.S.A. and 15.8 mills for Canada, and this would not be economical at the present time (Ref 2).

In the summer of 1963, the late President Kennedy approved a modified plan of a low interest project entirely financed by the U.S.A. As the two-pool system could hold its power until it is needed, the Passamaquoddy project could operate for one hour, twice a day to take peak lunch and dinner power loads. The tidal project could also be tied to a hydroelectric plant at Rankin Rapids, and the combined peak period operation of the two plants would be 1,250,000 kW to meet the 5 to 6 p.m. greatest power demand period of the New England - Maritime Provinces area. This project would cost over $1 billion, and the Province of New Brunswick would receive a share of the power at cost price.

CONCLUSION

All plans concerning the future of the International Tidal Power Project (Passamaquoddy Bay) are unpopular among some Canadian officials. The reasons could be economic as well as political, but there still exists a very important

factor which should not be overlooked. Shepody Bay and Cumberland Basin (at the head of the Bay of Fundy) with much higher tides, offers more potential and therefore should be given first consideration. If natural resources are not going to be considered as the most important factor, but political and national aspects only, the International Project may remain only as a dream and a toy for politicians.

Another challenge to the proposed Canadian - U.S.A. partnership in the development of the Passamaquoddy Bay Tidal Power scheme is created by Minas Basin which has the highest tides in the world. With an area over three times larger than Passamaquoddy and Cobscook Bays combined, and with the average tide height exceeding 40 ft, and a narrow channel connecting the basin to the Bay of Fundy, this creates a very inviting prospect for harnessing of the tides. It is beyond the scope of this paper to arrive at any definite conclusion regarding the possible amount of harnessable energy produced by this project, but on the average, during each tidal cycle, approximately 500 billion cubic feet of water enters and leaves Minas Basin, compared with 70 billion for Passamaquoddy and Cobscook Bays combined.

In view of the preceding discussion, and that the erection of the International Tidal Project as proposed by U.S.A. authorities would take about 15 years, it is the author's belief that a plan on a larger scale should be prepared first. This plan should include the possible development and combined utilization of all available tidal potentials of the entire area of the Bay of Fundy, including a larger number of Canadian Provinces, also a greater area of the U.S.A. Only such a plan would be beneficial to all interested parties.

REFERENCES

(1) Canadian Hydrographic Service (1955 - 1963), Atlantic Coast Tide and Current Tables, Ottawa.

(2) The International Joint Commision United States and Canada (April 1961), Report on the International Passamaquoddy Tidal Power Project, Washington - Ottawa.

Chapter 50

ON THE PROCESS OF CHANGE FROM SALT WATER TO FRESH WATER BY EFFECTIVE CONTROL OF OUTLET GATES FOR A LAKE OR RIVER DISCHARGING TO THE SEA

Isao Minami[1)]

1. SUMMARY

In previous studies, the mechanisms for changing salt water lake to fresh water were analysed by Dr. Jansen[2)] and Okuda[1)]. But in these theories, the effectiveness of the structure of the outlet gate and its control for salinity had not been considered. For this reason, the above studies are not precise enough to estimate the necessary time required for changing salt water to fresh water in the actual sea-reclamation planing. The author has proposed a new method to calculate the necessary time. In this paper the mechanism of transport of salinity in water is also considered.

2. INTRODUCTION

In general the lake with a narrow opening at the sea side has vertically stratified salinity distribution. The upper water contains little salinity, but the lower water near the bed has much salinity and high density. The mechanism of transport of salinity in stratified turbulent flow must be applied to the water exploitation plan for the change from salt water lake to fresh.

Fig. 1 shows an example of the lake that is separated by the gate from the outer sea. At the gate, the outflow velocity must have greater value than the flow in velocity which is produced by the water density difference between seaside and lake.

1) Associate Professor, Agricultural Engineering, Kyoto Univ. Kyoto Japan

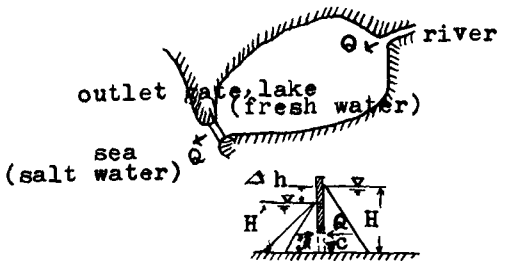

Fig.1

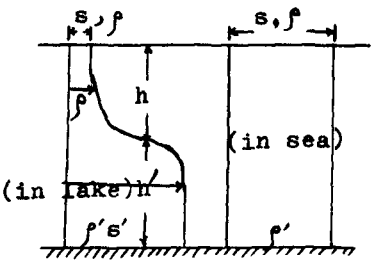

Fig.2

The progress of change from salt water to fresh water could be classified as follows;

1st step: The salt water goes out to the sea through the lower part of the gate. In this case, the salt water exiting near the gate plate in the lake will be almost entirely diminished. But the salt water below the elevation of the sill of gate cannot diminish so fast because of its vertical density difference.

2nd step; The salinity will go out with discharge by vertical mixing from lower salt water and this is strengthened by wind force or flowing upper water. But in these types of mixing, the salt content mixed with upper fresh water would be negligiblly small. These phenomena are seen in the lake having deeper parts than the elevation of the sill of outlet gate.

3rd step; The salinity in the soil will go into upper water from its void.

We must take into consideration the above three hydraulic steps in planning, and precise analysis of diffusion or movement of salt water must be effectively used for reclamation planning.

3. GATE EQUATIONS

In Fig.1, to flush out the salinity from the lake by the gate management, the critical difference of water elevation must exist between the outer sea and the inner lake as follows:

$$\Delta h > \frac{\rho' - \rho}{\rho} H' \qquad (1)$$

At the sluice in Fig.2, the lost salinity mixed with discharge from sluice are supplied by the movement of salinity in the lake. At the upper open gate, as Fig.3a, the salinity out flow is smaller than that lower the open gate. Therefore, the time necessary to change the salty lake to fresh is surely dependent on the structure of

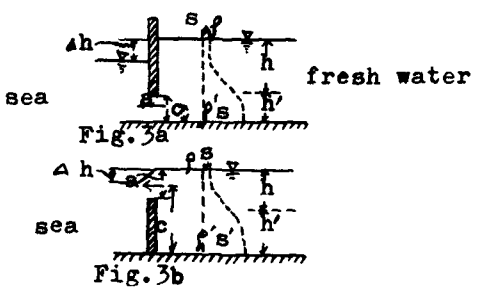

Fig.3a

Fig.3b

the gate and its management. At the upper open gate, the mechanism of vertical transport of salinity in the lake is an important control factor. At the lower open gate, the mechanism of horizontal transport of salinity is most important. In small discharge the horizontal transport of salinity by the density action is larger than the vertical transport.

The discharge from the outlet gate is calculated by the next equation by Dr. Kuwano.

$$Q = C_1 B a \sqrt{2g\Delta h} \qquad (2)$$

$$C_1 = \frac{2}{3} C \frac{\Delta h}{2a} \left\{ \left(1 - \frac{\varepsilon h - \Delta h}{\Delta h}\right)^{3/2} - \left[1 - \frac{\varepsilon(a + h' + \Delta h)}{\Delta h}\right]^{3/2} \right\}, \quad \varepsilon = \frac{\rho' - \rho}{\rho}$$

The salinity mixed in the discharge can be written as follows due to dimensional theory:

$$\rho_g = \rho + K C^{\alpha_1} h^{\alpha_2} h'^{\alpha_3} a^{\alpha_4} g^{\alpha_5} g^{\alpha_6} (\rho' - \rho)^{\alpha_7}$$

To determine the index. $\alpha_1, \alpha_2, \alpha_3, \alpha_4, \alpha_5, \alpha_6, \alpha_7$, the author performed the experiment in the laboratory. Fig.4 shows the model of the outlet gate.

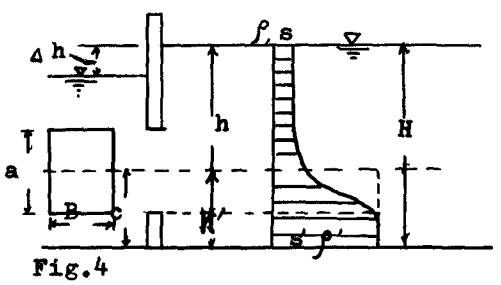

Fig.4

The dimensions of all hydraulic factors are as follows:

$[\rho] = ML^{-3}$
$[C] = L$
$[h] = L$
$[h'] = L$
$[a] = L$
$[g] = L^2T^{-1}$
$[\rho' - \rho] = ML^{-3}$
$[g] = LT^{-2}$

The dimension equation is

$$ML^{-3} = K[L]^{\alpha_1}[L]^{\alpha_2}[L]^{\alpha_3}[L]^{\alpha_4}[L^2T^{-1}]^{\alpha_5}[ML^{-3}]^{\alpha_6}[LT^{-2}]^{\alpha_7} \qquad (3)$$

about the dimension M $\quad 1 = \alpha_7$

about the dimension L $\quad -3 = \alpha_1 + \alpha_2 + \alpha_3 + \alpha_4 + 2\alpha_5 - 3\alpha_6 + \alpha_7$

about the dimension T $\quad 0 = -\alpha_5 - 2\alpha_7$

By dimensional analysis, the next equation is given:

$$\rho_g = \rho + K(\rho'-\rho)\left(\frac{h}{C}\right)^{\alpha_1}\left(\frac{\rho'}{C}\right)^{\alpha_2}\left(\frac{q}{C}\right)^{\alpha_3}\left(\frac{H^2g}{q^2}\right)^{\alpha_4} \tag{4}$$

By the data from experiment, we can decide the value of index as follows:

$$\rho_g = \rho + 0.2793(\rho'-\rho)\left(\frac{h}{C}\right)^{-0.00101}\left(\frac{\rho'}{C}\right)^{0.0361}\left(\frac{q}{C}\right)^{-0.00304}\left(\frac{H^2g}{q^2}\right)^{+0.000231} \tag{5}$$

By the equation (5), we can calculate the salinity of discharge flowing through the gate.

In the above equation (5), the relation between density and salinity was given as follows:[3]

$$\rho = 1 + \frac{1}{1000}(-0.069 + 1.4768\,Cl - 0.00157\,Cl^2 + 0.0000398\,Cl^3) \tag{6}$$

4. STABILITY OF BOUNDARY LAYER IN THE ESTUARY

The vertical distribution of salinity of lake water in the estuary has the following characteristics, namely upper fresh water and lower salty water exist as Fig.5, and in boundary of two layers the spring layer of salinity is developed. To know the stability of the boundary layer or diffusion from the lower water, we used Richardson's number. But Richardson's number is not so convenient to calculate because it demands a gradient of density and velocity that is difficult to know.

Therefore, we should modify Richardson's number as follows:

$$R_i = \frac{\frac{1}{\rho}\frac{\partial \rho}{\partial z}}{\left(\frac{\partial u}{\partial z}\right)^2} \tag{7}$$

$$R_{im} = \frac{g(\rho'-\rho)h}{\rho U^2}$$

$$\Delta\rho = \rho'-\rho, \quad \Delta z = h, \quad \Delta U = u'-u$$

This number is useful because the shape of vertical distribution of salinity has always a typical style, as Fig. 5, and the depth of the upper layer is generally about 3m to 5m, and the value of density is 1,000--1,025.

When the modified Richardson's number has the relation,

$$R_{im} > 1 \tag{8}$$

the boundary layer is stable, but when thenumber has the relation,

$$R_{im} < 1 \qquad (9)$$

the boundary layer is not so stable.

In stable conditions, the vertical diffusion of salinity from lower salt water is very small, but in unstable conditions, the diffusion is actively developed by the wind or flowing water.

1. Stability of boundary layer against the wind.

The modified Richardson's number is deduced by the following equation:

$$R_{im} = \frac{C_f g(\rho' - \rho)h}{\tau_a} \qquad (10)$$

$$\tau_a = 2.6\times10^{-3}\rho_a W^2, \quad \rho_a = 1.25\times10^{-3}$$

In equation (10), resistant coefficient c_f is taken as follows:

$$C_f \fallingdotseq 0.001 \qquad (11)$$

These data were given by the observation of Nakauma[7] in Simane Prefecture in Japan. Fig. 6 shows the modified Richardson's number of the boundary layer during February 1964.

(The depth of boundary layer was during 5m or 3m from water suface)

Fig.6

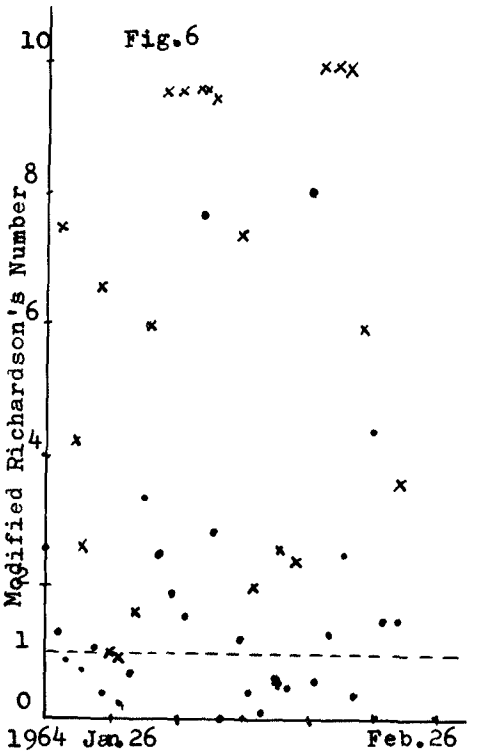

In Fig. 6, about few days per month, the modified Richardson's number was smaller than 1, and the other day it was larger than 1. This shows that the vertical diffusion exists only in strong windy days. In calm days, the vertical diffusion is very small.

Now we can show the value of c_f against the difference of density.

Table 1.

$\rho' - \rho$	C_f
0.001	0.00375
0.002	0.00106
0.003	0.00072
0.004	0.00088
0.005	0.00086
0.013	0.00068

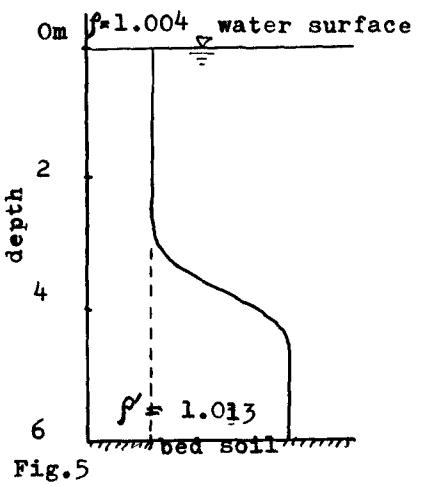

Fig.5

2. Stability of boundary layer due to flow of upper fresh water.

The stability of boundary layer is given by modified Richardson's number as follows:

$$R_{im} = \frac{\frac{1}{\rho}\frac{\Delta\rho}{\Delta z}}{\left(\frac{\Delta U}{\Delta z}\right)^2} = \frac{1}{\rho}\frac{g(\rho'-\rho)h}{U^2} \qquad (12)$$

If the Richardson's number is larger than 1, the boundary layer is stable and in the case of $R_{im} < 1$, the boundary layer is unstable and mixing between upper water and lower water is actively progressed.

5. HORIZONTAL TRANSPORT OF SALINITY IN STRATIFIED TURBULENT FLOW

The horizontal transport of salinity in the stratified flow is shown in Fig. 7. If the loss of salinity is produced in a part lower than the elevation of the boundary layer near the gate, the lost salinity will be supplied from the neighbour by the velocity of the internal wave. In general, the sudden loss of salinity makes the local deformation of equi-salinity line on the horizontal plane as Fig. 7. The discontinuous deformation of the equi-salinity line will propagate as internal wave and by this movement the transport of salinity is completed in horizontal direction. Then the value of the horizontal transport of salinity is calculated by tne next equation:

$$S = (S'-S)(h'-h_2')\sqrt{\frac{gh_2'h'}{h+h'}\frac{\rho'-\rho}{\rho}} \qquad (13)$$

If the out flow discharge is very large, the internal equi-salinity line would be much deformed near the gate surface, but the water surface would not be so deformed. In this mechanism of horizontal transport of salinity, fluctuation velocity is not important and the transport energy is supplied by density difference in the water. The critical transport velocity of salinity is given by the next equation:

$$S = (S'-S)h'\sqrt{\frac{gh'}{\rho}\frac{\rho'-\rho}{\rho}} \qquad (14)$$

But these phenomena are only seen when there is small discharge. In the case of large discharge, the upper layer would be mixed with lower water.

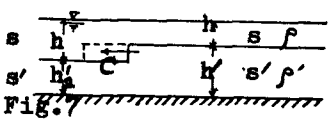

Fig. 7

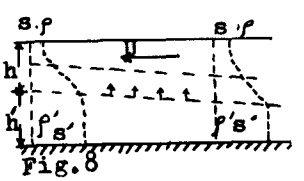

Fig. 8

6. VERTICAL TRANSPORT OF MOMENTUM IN STRATIFIED TURBULENT FLOW

The vertical eddy viscosity in stratified turbulent flow is a function of Richardson's number. η_0 is eddy viscosity when there is no stratified turbulent flow, but the eddy viscosity η would be changed by salinity distribution as the next equation[8] shows:

$$\eta = \eta_0 (1 + e Ri)^{-1/2} \qquad (15)$$

Namely the vertical transport of momentum is given as follows in unit time and unit area:

$$\tau = \eta \frac{\partial u}{\partial z} = \eta_0 (1 + e Ri)^{-1/2} \frac{\partial u}{\partial z} \qquad (16)$$

Fig. 9 shows the above relation coincides with experimental results. The value of index$(-\frac{1}{2})$ and e are decided by experiment. The turbulent diffusion coefficient in no salinity flow is shown as follows:

$$\eta_0 = 1.8 \times 10^4 \text{ cm}^2/\text{s}$$
$$\eta_0 = 1.2 \cdot 10^4 \text{ cm}^2/\text{s} \quad \text{(Okuda)} \qquad (17)$$

At the vertical section;

$$= 0.01 L^{4/3} \text{ cm}^2/\text{s} \quad \text{(H.Stommel)} \qquad (18)$$

But we can estimate the eddy viscosity from the **folllow equations;**

$$\eta_0 = \frac{K h \sqrt{g h i}}{6} \qquad (19) \quad \text{(by water flow)}$$

$$\eta_0 = 1.02 W^3 \qquad W < 6 \text{ m/s} \quad \text{(Thordde, 1914)}$$

$$\eta_0 = 4.3 W^2 \qquad W > 6 \text{ m/s} \qquad (20) \quad \text{(by wind velocity)}$$
(Ekman, 1905)

By Munk's ,by other's and by the author's experiments, the following value is deduced.

$$e = 8 - 13 \qquad (21)$$

But in this paper, the author used the modified Richardson's number expressed as equation (7) and (10). If the modified Richardson's number is used, the transport of momentum is given as follows:

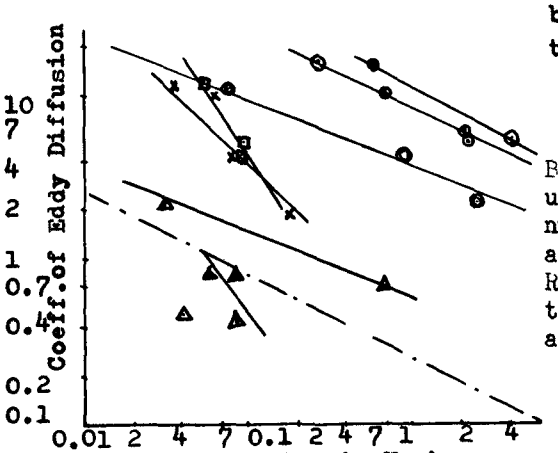

Fig.9

$$\tau = \eta_0 (1 + e' R_{im})^{-\frac{1}{2}} \frac{\partial u}{\partial z} \quad [8] \qquad (22)$$

7. VERTICAL TRANSPORT OF SALINITY IN THE TURBULENT FLOW

The coefficient of vertical eddy diffusion and diffused salinity is also a function of Richardson's number and Fig. 10 shows that the tendency of equation (23) coincides with experimental results.

$$\eta_s = \eta_0 (1 + b R_i)^{-3/2} \quad [8] \qquad (23)$$

(i) by flowing water

If we use the modified Richardson's number, the vertical transport of salinity in stratified turbulent flow is shown as follows:

$$S = \eta_s \frac{dS}{dz} = \eta_0 (1 + b_m R_{im})^{-3/2} \frac{\partial S}{\partial z} \quad [8] \qquad (24)$$

In upper equations, the writer used the modified Richardson's number instead of Ri and the constant bm is decided by the experiment.

$$b_m \fallingdotseq 10 \qquad (25)$$

(ii) by wind action

$$S = \eta_0 (1 + b_{mw} R_{im})^{-3/2} \frac{\partial S}{\partial z} \qquad (26)$$

In equation (26), the modified Richardson's number must be used.

$b_{mw} \fallingdotseq 10000$

This is deduced from field survey of Nakaumi.[7] Then the value of η_0 was calculated by Thordde[3] equation.

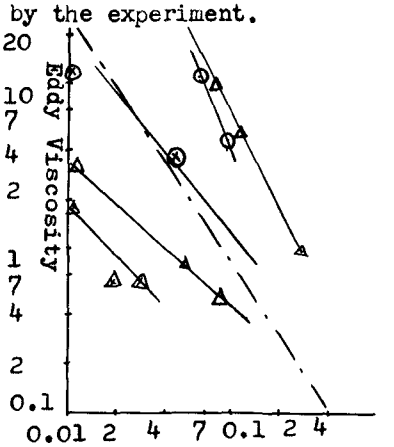

Fig.10 Modified Richardson'

8. THE CALCULATION OF LONGITUDINAL ELEVATION OF THE BOUNDARY LAYER

To know the vertical salinity distribution, the elevation of the boundary must be calculated for all discharge. In hydraulics, the shape of that boundary is called the salt wedge. The elevation of the salt wedge is a very important factor in understanding the progress of fresh water from salt water. The salt wedge may be calculated by following equations: The following equations are deduced by Prof. Dr. Schönfeld.[5]

The momentum equation are

$$-i+\frac{\partial h}{\partial x}+\frac{\partial h'}{\partial x}+\alpha\frac{\partial}{\partial x}\left(\frac{u^2}{2g}\right)+\frac{1}{g}\frac{\partial u}{\partial t}+i_f=0$$
$$-i'+(1-\varepsilon)\frac{\partial h}{\partial x}+\frac{\partial h'}{\partial x}+\alpha\frac{\partial}{\partial x}\left(\frac{u^2}{2g}\right)+\frac{1}{g}\frac{\partial u'}{\partial t}+i_f'=0 \quad (27)$$

The continious equations of discharge are

$$\frac{\partial h}{\partial t}+u\frac{\partial h}{\partial x}+h\frac{\partial u}{\partial x}=0$$
$$\frac{\partial h'}{\partial t}+u'\frac{\partial h'}{\partial x}+h'\frac{\partial u'}{\partial x}=0 \quad (28)$$

These equations are modified as follows:

$$\frac{dh}{dx}=\frac{1}{\phi(\omega)}\left[\left(1-\frac{u'|u'|}{gh'}\right)\left\{i-\frac{f_i}{2gh}(u-u')|u-u'|\right\}-\left\{i-\frac{f_i'}{2gh'}u'|u'|-\frac{f_2'}{2gh'}(u-u')|u-u'|\right\}\right]$$
$$\frac{dh'}{dx}=\frac{1}{\phi(\omega)}\left[\left(1-\frac{u|u|}{gh'}\right)\left\{i-\frac{f_2'}{2gh'}u|u|+\frac{f_i'}{2gh'}(u-u')|u-u'|\right\}-(1-\varepsilon)\left\{i-\frac{f_i}{2gh}(u-u')|u-u'|\right\}\right] \quad (29)$$

$$\phi(\omega)=\frac{u^2}{gh}\frac{u'^2}{gh'}-\frac{u^2}{gh}-\frac{u'^2}{gh'}+\varepsilon \quad (30)$$

If we assume the values for salt wedge as follows:

$$u'=0, \qquad f_i=0.01$$
$$\varepsilon=\frac{\rho'-\rho}{\rho}=0.025 \quad (31)$$

We can write equation (29) as follows.

$$\frac{dh}{dx}=f$$
$$\frac{dh}{dx}=g \quad (32)$$

In the equations (32) the values of f and g are calculated for many values of depth of fresh water, depth of salt water and velocity of upper fresh water. Table 2. shows the value of f and g. By the Table 2, we can calculate the salt wedge and the elevation of water surface as follows.

(i) The simplest calculation method

$$x=x_0+\Delta x$$
$$h=h_0+\Delta h=h_0+f\cdot\Delta x$$
$$h'=h_0'+\Delta h'=h_0'+g\cdot\Delta x \quad (33)$$

Table 2 The values of f and g .

h	h	u	i=0.00005		i=0.0001		i=0.000133		i=0.0002	
			f_i=0.01		f_i=0.01		f_i=0.01		f_i=0.01	
m	m	m/s	f	g	f	g	f	g	f	g
2.5	6	1.5	+000973	-0.00393	+0 00973	-0 00387	+0.00973	-0.00392	+0 00973	-0.00391
		1.1	+0.01434	-0 00576	+0 01434	-0.00581	T0 01434	-0 00576	+0 01434	-0.00576
		0.8	+0 16485	-0.06675	+0.16485	-0.07053	+0.16485	-0.06675	+0.16485	-0.06675
		0.5	-0 00489	+0 00207	-0 00489	+0 00249	-0 00489	+0.00212	-0 00487	+0.00221
		0.3	-0 00122	+0 00059	-0.00122	+0.00092	-0 00122	+0.00059	-0 00122	+0 00059
		0.05	-0.000029	+0.00011	-0.000029	+0.00041	-0.000029	+0 00014	-0.000029	+0.00021
2.5	5	1.5	+001031	-0.00338	+0.01031	-0 00329	+0 01031	-0.00338	+0.01031	-0.00336
		1.1	+001519	-0.00494	+0 01519	-0 00494	+0 01519	-0 00494	+0 01518	-0 00499
		0.8	+0 17455	-0.05710	+0 17455	-0.06029	+0 17454	-0 05709	+0 17454	-0 05790
		0.5	-0 00517	+0 00178	-0 00517	+0.00218	-0 00519	+0 00183	-0 00517	+0.00191
		0.3	-0.00129	-0 00052	-0 00129	+0 00084	-0.00129	+0.00052	-0.00127	+0 00052
		0.05	-0.000031	+0.00011	-0.000031	+0.00041	-0.000031	+0 00014	-0 000031	+0.00021
2.5	4	1.5	+0.01116	-0 00260	+0.01116	-0 00296	+0 01116	-0 00259	+0.01116	-0 00255
		1.1	+001645	-0 00372	+0.01645	-0 00364	+0.01645	-0.00372	+0 01645	-0.00372
		0.8	+0 18909	-0.04269	+0.18909	-0 04500	+0.18909	-0.04269	+0.18909	-0 04268
		0.5	-0 00560	+0 00135	-0.00560	+0 00172	-0 00560	+0.00139	-0 05600	+0.00147
		0.3	-0.00139	+0 00041	-0 00139	+0.000 73	-0.00140	+0.00041	-0.00139	+0.00041
		0.05	-0 000033	+0.000011	-0.000033	+0.00041	-0.000033	+0.00014	-0.000033	+0.00021
2.5	3	1.5	+0 01259	-0.00137	+0 01259	-0 00133	+0.01257	-0.00131	+0.01250	-0 00126
		1.1	+0 01856	-0.00172	+0 01856	-0 00152	+0.01856	-0.00172	+0 01856	-0.00172
		0.8	+0 21333	-0.01888	+0.21333	-0.01974	+0.21333	-0.01888	+0.21333	-0 01888
		0.5	-0.00632	+0.00057	-0 00632	+0 00062	-0.00632	+0.00066	-0.00632	+0.00074
		0.3	-0 00158	+0.00023	-0 00157	+0.00054	-0.00158	+0.00023	-0.00157	+0.00023
		0.05	-0.000038	+0.000053	-0.000038	+0.00010	-0.000038	+0.00014	-0.000037	+0.00020
2.5	2	1.5	+0.01546	+0.00097	+0.01546	+0.00104	+0.01546	+0.00108	+0.01546	+0.00117
		1.1	+0 02278	+0 00215	+0.02278	+0 00261	+0 02278	+0.00215	+0.02278	+0.00215
		0.8	+0 26182	+0.02793	+0.26182	+0 02998	+0.26182	+0.02793	+0 26182	+0.02990
		0.5	-0.00776	-0.00085	-0 00776	-0 00081	-0.00776	-0.00078	-0.00776	-0.00093
		0.3	-0 00194	-0 00019	-0.00194	+0 00015	-0.00194	-0.00014	-0.00194	-0.00014
		0.05	-0.000046	+0.000054	-0.000046	+0.00009	-0.000046	+0.00013	-0.000046	+0.00019
2.5	1	1.5	+0.02405	+0.00669	+0.02405	+0.00689	+0.02405	+0.00694	+0.02405	+0.00705
		1.1	+0.03544	+0.01272	+0.03544	+0.01393	+0.03544	+0.01272	+0.03544	+0.01272
		0.8	+0.40727	+0.16205	+0 40727	+0.17282	+0.40727	+0.16205	+0.40727	+0.16205
		0.5	-0.01207	-0.00504	-0.01207	-0.00504	-0.01207	-0.00504	-0.01207	-0.00505
		0.3	-0.00301	-0.00122	-0.00301	-0 00099	-0.00301	-0.00122	-0.00301	-0.00122
		0.05	-0.000072	+0.000018	-0.000072	+0.000068	-0.000072	+0.00010	-0.000072	+0.00017

(ii) By Runge - Kutter's method

$$x = x_0 + \Delta x, \qquad h = h_0 + k, \qquad h' = h_0' + l \tag{34}$$

$$k = \frac{1}{6}(k_1 + 2k_2 + 2k_3 + k_4)$$

$$\begin{cases} k_1 = f(x_0, h_0, h_0')\Delta x \\ k_2 = f(x_0 + \frac{\Delta x}{2}, h_0 + \frac{k_1}{2}, h_0' + \frac{l_1}{2})\Delta x \\ k_3 = f(x_0 + \frac{\Delta x}{2}, h_0 + \frac{k_2}{2}, h_0' + \frac{l_2}{2})\Delta x \\ k_4 = f(x_0 + \Delta x, h_0 + k_3, h_0' + l_3)\Delta x \end{cases}$$

$$l = \frac{1}{6}(l_1 + 2l_2 + 2l_3 + l_4)$$

$$\begin{cases} l_1 = g(x_0, h_0, h_0')\Delta x \\ l_2 = g(x_0 + \frac{\Delta x}{2}, h_0 + \frac{k_1}{2}, h_0' + \frac{l_1}{2})\Delta x \\ l_3 = g(x_0 + \frac{\Delta x}{2}, h_0 + \frac{k_2}{2}, h_0' + \frac{l_2}{2})\Delta x \\ l_4 = g(x_0 + \Delta x, h_0 + k_3, h_0' + l_3)\Delta x \end{cases}$$

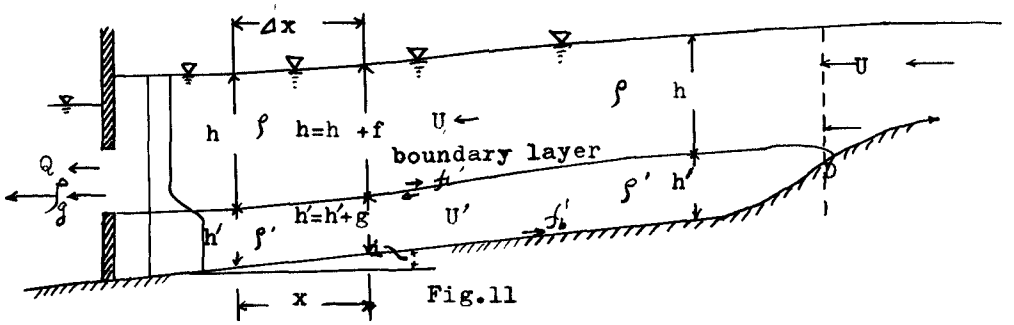

Fig.11

In the place furtner from the salt wedge front D in Fig. 11, the flowing water will directly contact the soil surface and the salinity has vertically constant value. The point D is given by the front of the salt wedge. But in the case of small water velocity of the upper water, the elevation of point D is nearly equal to the elevation of the sill surface of the gate. But in actually, the wind velocity is also an important factor in deciding the elevation of the boundary layers.

9. THE EQUATION OF THE CHANGE OF SALINITY OF THE LAKE IN THE ESTUARY

The fundamental differential equation is given by Prof. Jansen.[2] But in this equation the value of the ratio r between outflow salinity and original salinity is not exactly considered.

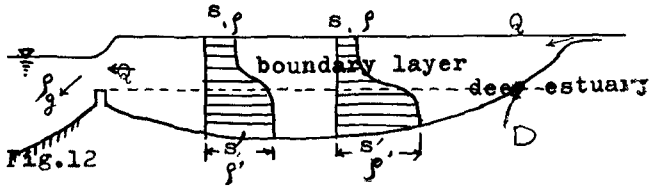

Fig.12

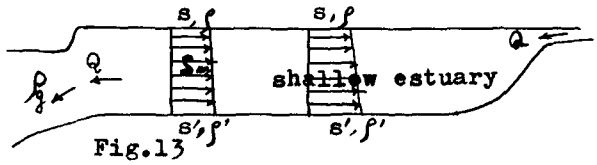

Fig.13

In the case of r=const., the solution is given by Prof. Jansen's equation as follows:

$$S = \frac{a}{r} + (S_0 - \frac{a}{r})\, e^{-\frac{rQ}{U}t} \qquad (35)$$

$$r = \frac{S}{Sm}.$$

After these studies Prof. Okuda[1] assumed the next equation for the value of r, $r = 1 - k\,(Sm - a)$

(36)

and the solution of the salinity in the estuary is given as follows:

$$S = \frac{\frac{c}{P} - a\, e^{\frac{PQ}{U}t}}{c - e^{\frac{PQ}{U}t}} \qquad (37)$$

where

$$P = 1 - ka$$

$$c = \frac{kS_0 - ka}{kS_0 - 1} \qquad (38)$$

In Fig. 12 and Fig. 13, we can understand that these equations are only effective for the shallow lake as Fig. 13. When the elevation of the sill of the gate is higher than the bed of lake, the equations (35) and (37) are not so effective.

The above two equations are not so precise because of following reasons:

(i) There are no equations to calculate the value of r.

(ii) They neglect the density effect against the eddy diffusion coefficient. The vertical salinity distribution changes the modified Richardson's number and this also changes the diffusion of salinity.

(iii) They neglect the vertical diffusion from the lower salty water.

(iv) They don't consider the effectiveness of the structure of the outlet gate and its control.

10. LONGITUDINAL SALINITY DISTRIBUTION IN THE UPPER WATER BEING ON THE BOUNDARY LAYERS

The salinity mixed the upper fresh water may be calculated by the equations below: In this case the coefficient of vertical turbulent diffusion is calculated by the next equations.

$$\eta = \eta_0 (1 + a_m R_{im})^{-1/2} \tag{39}$$

$$\eta_s = \eta_0 (1 + b_m R_{im})^{-3/2} \tag{40}$$

where

$$R_{im} = \frac{g(\rho' - \rho)h}{u^2} \quad \text{(for water flow)} \tag{41}$$

$$R_{im} = \frac{C_f(\rho' - \rho)gh}{\tau_a} \quad \text{(for wind action)} \tag{42}.$$

Because the shape of vertical salinity distribution has the same form below the water surface in the lake, the above equations would have practical use. Namely, the fresh water is sitting on the boundary layer between fresh water and salt water. In the part below the boundary layer, there is salt water and its salinity is an almost constant value.

(1) AT THE SALINITY MIXED IN FRESH WATER FROM LOWER SALT WATER

If there is a flow of upper fresh water, salinity is diffused from the lower salt part only very slightly. Then the salinity of the upper water is changed from the mouth of the river to the outlet gate as Fig. 14,

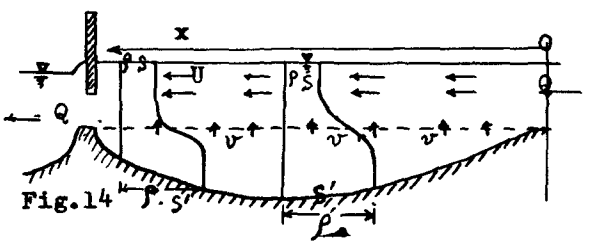

Fig.14

The differencial equations of the change of salinity are led as follows:

$$u\frac{ds}{dx} = \eta_s \frac{d^2S}{dx^2} + \frac{\eta_s}{h}\left(\frac{ds}{dz}\right) \qquad (43)$$

$$u\frac{ds}{dx} = \eta_0 (1 + b_m R_{im})^{-3/2} \frac{d^2S}{dx^2} + \frac{\eta_s}{h^2}(S'-S) \qquad (44)$$

The boundary equations are:

$$\begin{aligned} x &= 0, \quad S = 0 \\ x &= l, \quad S = S_0 \end{aligned} \qquad (45)$$

From the upper boundary condition, we can deduce the next equation of salinity.

$$S = S_0\left\{1 - \frac{e^{\alpha x}\sin h\beta(l-x)}{\sin h\beta l}\right\} \qquad (46)$$

where,

$$\alpha = \frac{u}{2\eta_s}, \qquad \beta = \frac{\sqrt{u^2 + 4\eta_s^2/h}}{2\eta_s} \qquad (47)$$

(2) FUNDAMENTAL DIFFUSION EQUATION FROM SOIL

The fundamental differencial equation is led as follows:

If these conditions occur, that is, the mean velocity U is const., mean water depth h is const., and turbulent coefficient of diffusion η is constant, then, the equation of diffusion of salinity is given as follows by Okuda[1]

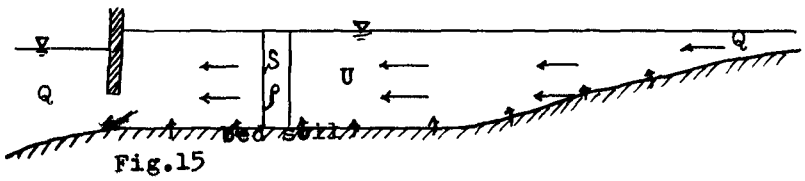

Fig.15

$$u\frac{ds}{dx} = \eta_s \frac{d^2s}{dx^2} + \frac{k}{h^2}(s'-s) \qquad (48)$$

The boundary condition of differential equations are shown as follows.

$$\begin{aligned} x &= 0, \quad s = 0 \\ x &= \ell, \quad s = s_0 \end{aligned} \qquad (49)$$

By the boundary condition, we can deduce the solution as follows:

$$s = s_0\left\{1 - \frac{e^{\alpha x}\sinh\beta(\ell-x)}{\sinh\beta\ell}\right\} \qquad (50)$$

where

$$\alpha = \frac{u}{2\eta_s} \qquad (51) \qquad \beta = \frac{\sqrt{u^2+4\eta_s k/h}}{2\eta_s} \qquad (52)$$

11. THE CHANGE OF THE SALINITY IN DEEP ESTUARY NEAR THE OUTLET GATE

If the outlet gate is open at the lower part, and the modified Richardson's Number in the lake is larger than 1, the required time to replace old salt water with fresh water is calculated as follows.

1st step

The outflow salinity through the gate is calculated by equation (5).

$$\Delta s \sim \rho_g Q = \Delta V \cdot \Delta\rho$$
$$\Delta V = h \cdot A_m \qquad (53)$$

We can assume the following important facts by the field survey and experiments of salinity distribution:

(i) The boundary layer exists on the same level as the sill of gate. (at the start of calculation)

(ii) The decrease of salinity happens only in the upper region of the boundary layer in the deep estuary.

If the vertical salinity distribution and discharge from the outlet of the gate are given, the outflow salinity mixed in the discharge is calculated by the equation (5).

The decreased salinity of the lake is given as follows:

$$\rho - \Delta\rho = \frac{\rho_g Q}{h \cdot A_m} \qquad (54)$$

The sunk depth of the boundary layer is calculated by the next equation:

$$\Delta h' = \frac{\Delta \rho \cdot h}{\rho'} \qquad (55)$$

2nd step

We must modify the salinity distribution of the upper layer by the following method:

$\rho = \rho + \Delta\rho$, $\rho' = \rho'$

But if the elevation of the boundary layer is lower than the elevation of the sill surface, the escape of salinity from the estuary is very difficult. This calculation method was verified by the following experiment as Fig. 16:

3rd step

We must modify the salinity distribution by wind action by equation (26).

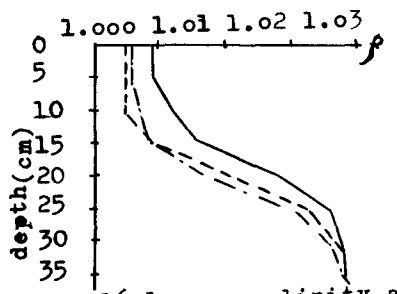

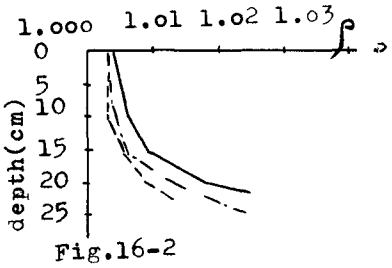

Fig.16-2

Fig.16-1 -----salinity after 60 min.
-.-.-.salinity after 30 min.
——— original salinity distribution

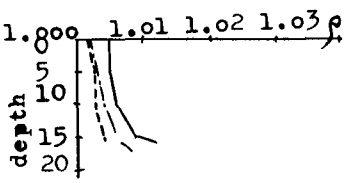

4th step

We must calculate the salinity in the discharge by equation (5) and return to the 1st step.

12. MODEL TEST OF ISAHAYA SEA RECLAMATION PLAN

The author made the model of Isahaya bay in Fig. 21. The bay opens to Nagasaki bay through the gate. The hydraulics factors of the model are as follows:

Mean sea water elevation	± 0 cm
Amplitude of water surface	± 3.5 cm
Salinity in Nagasaki Bay	$\rho' = 1.025$
The elevation of sill of the outlet gate	-18 cm
The effective total width of the outlet gate	10 cm

The structure of the outlet gate and V-H, A-H curve of Nagasaki bay are given by Fig. 18 and Fig. 21. Fig. 16 shows the changing process of vertical salinity distribution in the pool inner the embankment. In this experiment, the discharge from the outlet gate was 200 cm^3/s. Before the reclamation works in Isahaya bay, the distribution of salinity had the same value in vertical directions. This shows that there was intense mixing by wind friction on the sea surface and tidal actions of total amplitude of 3 m. But after the reclamation works, the wave in the pool would be very small and the vertical distribution of salinity would abruptly change at the same elevation as the sill. The upper fresh water would have a density about $\rho = 1.002$ and the salt water would have a density about $\rho' = 1.020$.

To chase out the salinity by the outlet gate, we must constantly operate the gate on the condition that the difference of water surface between outer sea and inner pool has the value of equation (1). In this case the salinity distribution in the pool will change as Fig. 16 and has stratified salinity distribution. In this case the boundary line between fresh water and salt water has the elevation nearly equal to the height of the sill of the outlet gate. This is first step for making the change in salinity. In the 2nd step, the salinity lower than the spring layer or in the bed soil would be transported by mixing with fresh water flow. If the strong wind blows on the sea, the salinity of the fresh water will increase and the depth of the spring layer will be deep.

In the sea reclamation, the most important factor is to make the elevation of the boundary layer deep. The method to make the boundary layer deep is shown as follows:

(a) The gate must work to flow out the flooding discharge.

(b) The gate must work to flow out the salinity from the deepest part of the gate on the embankment. To accomplish the above, we must open the lowest part of the gate. As an example in Fig. 17, it is best to make the one deep gate for chase out the high salinity water.

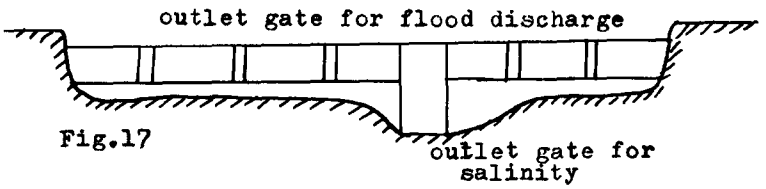

Fig.17

If the elevation of the boundary layer is sufficiently deep, at the strong wind or flooding flow, we can constantly gain fresh water from the lake.

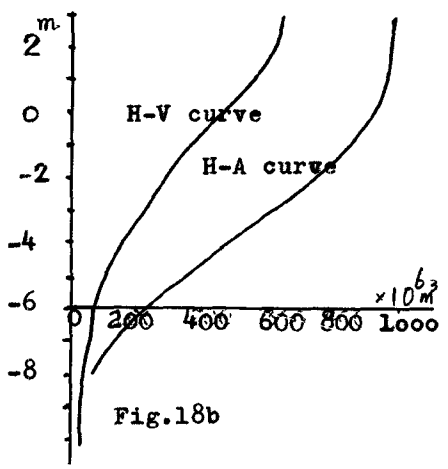

Fig.18b

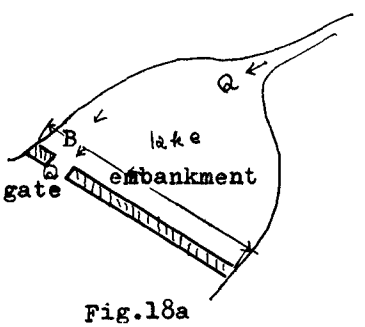

Fig.18a

13. EXAMPLE

Initial conditions

$h = 8\ m$, $\rho = 1.025$, $B = 300\ m$, $\Delta t = 0.432 \times 10^6\ sec$,
$h' = 4\ m$, $\rho' = 1.025$, $C = 0.8$, $Q = 580.8\ m^3/s$,
$c = 4.25\ m$, $\rho_g = 1.025$, $2g = 19.6\ m/s$, $B_l = 5000\ m$,
$a = 0.5\ m$, $\Delta h = 0.3\ m$,

1st step in calculation,

elevation of boundary layer ($\fallingdotseq$ elevation of sill) $-8.0\ m$

salinity out flow through the gate

$S = Q(\rho_g - 1) = 5808(1.025 - 1) = 14.52\ ton$

water volume existing on the boundary layer(in Fig.18)

$\Delta V = (655 - 90)\,10^6 = 565 \times 10^6\ m^3$

lost salinity from the upper region

$\Delta\rho = \frac{14.52}{565 \times 10^6}\Delta t = 0.01105$

modification of vertical salinity distribution

$\rho = 1.025 - 0.01105 = 1.01395$

$\rho' = 1.025$

water velocity of upper region

$u = Q/A = 580.8/8 \times 5000 = 0.014452\ m/s$

modified Richardson's Number

$R_{im} = \frac{(\rho' - \rho)hg}{u^2} = \frac{(1.025 - 1.01395)\,8 \times 9.8}{(0.014452)^2} = 4196$

salinity mixed into upper fresh water

$\Delta\rho = \eta_0 (1 + 10 R_{im})^{-\frac{3}{2}} \frac{(\rho' - \rho)}{h}$

$\eta_0 = \frac{\kappa h \sqrt{ghi}}{6}$

gradient of water surface(by Manning equation)

$i = \left(\frac{un}{h^{2/3}}\right)^2 = \left(\frac{0.014452 \times 0.01}{8^{2/3}}\right)^2 = 0.363 \times 10^{-8}$

$\eta_0 = \frac{0.4 \times 8 \times \sqrt{9.8 \times 8 \times 0.363 \times 10^{-8}}}{6} = 2.843 \times 10^{-4}$

$\rho = 0.000\,2843\,(1 + 10 * 4196)^{-\frac{3}{2}} \frac{0.01105}{8} \times 0.432 \times 10^6 \div 0$

$\rho = 1.01395$

$\rho' = 1.025$

mixing by the wind velocity

$\tau_a = 2.6 \times 10^3 \times 1.25 \times 10^{-3} W^2 = 11.7 \times 10^{-6}\ ton/m$

modified Richardson's Number

$R_{im} = \frac{C_4(\rho' - \rho)hg}{\tau_a} = \frac{0.002(0.01105) \times 9.8 \times 8}{11.7 \times 10^{-6}} = 14.808$

$\eta_0 = 1.02 \times 6^3 = 220.32$

$\Delta\rho = \eta_0 (1 + 10000 R_{im})^{-\frac{3}{2}} \frac{\rho' - \rho}{\rho} = 220.32\,(1 + 10000 \times 14.808)^{-\frac{3}{2}} \frac{0.01105}{\rho} \times 0.432 \times 10^6 = 0.0028$

$\rho = 1.01395 + 0.0023 = 1.01625$

$\rho' = 1.025$

$\delta h_l = \frac{0.0023 \times 8}{0.025} = 0.736\ m$

$h' = 8 + 0.736 = 8.736\ m$ (elevation of boundary layer)

2nd step in calculation

The outgoing salinity through the gate is calculated through the next equation.

$$\rho_g = \rho + 0.2793(\rho' - \rho)\left(\frac{h}{C}\right)^{-0.00101}\left(\frac{h'}{C}\right)^{0.0361}\left(\frac{a}{C}\right)^{-0.00304}\left(\frac{H^2 g}{g^2}\right)^{0.000231}$$

$H = 8+4 = 12\,m$, $C = 4.25\,m$, $h' = 3.264\,m$

$\rho' = 1.025$, $a = 0.5\,m$, $g = \frac{580.8}{300} \approx 1.936\ m^3/s/m$

$\rho = 1.01625$, $h = 8.736\,m$

$$\rho_g = 1.01625 + 0.2793(1.025 - 1.01625)\left(\frac{8.736}{4.25}\right)^{-0.00101}\left(\frac{3.264}{4.25}\right)^{0.0361}\left(\frac{0.5}{4.25}\right)^{-0.00304}\left(\frac{12^2 \times 9.8}{1.936^2}\right)^{0.000231}$$

$$= 1.01899$$

Return to the calculation of the 1st step.

14. SYMBOLS

Δh; critical difference of water surface between lake and sea,
ρ; water density of the upper region,
ρ'; water density of the lower region,
s; salinity of the upper region,
s; salinity of the lower region,
h; water depth of the upper region,
h; water depth of the lower region,
k; experimental constant,
Q; total discharge through the gate,
q; discharge through the gate of unit width,
g; acceleration of the gravity,
a; open height on the sill,
s; salinity mixed in discharge outgoing through the gate,
ρ_g; density of the water of discharge outgoing through the gate,
u; water velocity in horizontal direction,
z; vertical coordinate,
x; horizontal coordinate,
t; time,
η; eddy viscosity,
η_0; eddy viscosity which is no salinity,
η_s; eddy coefficient of diffusion,
κ; Karman's constant,
i; gradient of the water surface,
c; velocity of the internal wave,
α; constant of momentum distribution,
f_i'; resistant coefficient between upper fresh water and lower salt water,
f_b; resistant coefficient between salt water and soil,
ΔV; water volume of the lake,

r;ratio of salinity in discharge against lake,
H;total water depth of a lake,
H';the water depth of the sea,
C;discharge constant,
B;width of the outlet gate,
B_1;width of the lake,
c;height of the center of the open part ,
Cl;content of the chlorinity,
Ri;Richardson's Number,
Rim;Modified Richardson's Number,
u';velocity of salt water,
c_a;coefficient of resistance by wind velocity,
τ_a;shesring force acting on the sea surface by the wind,
ρ_a;density of the air,
L;water depth,
w;wind velocity,
e;experimental constant,
e';experimental constant (Modified Richardson's Number),
b;experimental constant,
bm;experimental const.(water flow),
bmw;experimental const.(wind),
i_f ,i'_f ;constant for resistant,
f_b ,f_b ;resistant constant,
a ;salinity ratio in flow in discharge,
S. ;original salinity in the lake,
k;molecular diffusion coefficient,
Am;area of the lake at the optional elevation,
$\Delta h'$;sunk depth of boundary layer by the vertical diffusion of salinity

15.BIBLIOGRAPHY

1.Okuda ;On the salinity distribution of salinity in the Kozima-bay. Report of the Conference on High-Tide of Chugoku.1958,Japan.
2.Pr.Jansen;On the sea reclamation of Japan. Japan Bureau of Agriculture and Forest.1954.
3.Sverdrup,Jahnson and Fleming; The Oceans,1959.
4.Isao Minami;On the transport of salinity in the stratified turbulent flow,Proceeding of the 12th Japan National Congress for Appl.Mech.,1962.
5.J.C.Schönheld,J.B.Schijf;Theoretical consideration on the motion of salt water,Proc. of Minesota International Hydraulic Convention,1953.
6.Sadami Kuwano;On the discharge constant of the gate in the density current,Journal of Japan Agricultural Engineering,Vol.5, 1962.
7.Isao Minami;Jun Hukuma;The effect of the wind for salinity distribution,Report No.1,Dept of Agricultural Engineering,Kyoto University,Japan,1963.
8.H.Munk andR.Anderson; Notes on a Theory of the Thermocline, Journal of Marine Research, Vol.VII,1948.

Chapter 51

ON THE SHEAR STRESS AT THE INTERFACE AND ITS EFFECTS IN THE STRATIFIED FLOW

Toshio Iwasaki, Eng.D.
Professor of Civil Engineering
Tohoku University
Sendai, Japan

At the moderate velocity of the pure water which lies on the quiet salt water stable internal waves appear at the interfac in the stratified flow, and these waves will break and violated surface will arise if the velocity of the pure water may be increased. In this phase of phenomena the shear stress at the interface has the most important part. However observed values of this shear stress have not been reported in the systematic style.

Experiments have been conducted in our laboratory since 1960. Some theoretical considerations could be served to get an empirical equation on the interfacial shear using experimental results and data presented by other researchers. This equation was as follows;

$$k_f = 3.940 \psi^{-0.8356} \qquad (1)$$

in which k_f is a coefficient of the internal shear stress τ_s and is expressed as $\tau_s / \rho_1 u_o^2$ where ρ_1 is the density of the upper layer, u_o is the velocity and ψ is $(Fr')^2 Re'$.

Free turbulent flow can be assumed to develope at the interface from the contact point of two layers. Owing to turbulence, Pure water was partly mixed with salt water at rest. Weak flow was induced in the lower layer and the zone of influence was developed downstream. Velocity and density distributions in both layers were derived theoretically following the methods of Tollmien and using the two dimensional convective diffusion equation, and were compared to the experimental values. Good coincidence was acquired.

The theory showed the zone of influence in the pure water diverged more pronouncedly and interfacial velocity decreased if the value of k_f was large, when curves of the velocity distribution had the remarkable gradient. However the diverging rate in the salt water was nearly constant for different values of k_f. For flow at the lower value of ψ which was rather stable, theory showed the inverse flow in the salt water which was verified by experiments. In the case at the higher value of ψ, such reverse flow did not exist. And intermediate value of ψ gave no solution for the salt layer which was caused presumably by the interfacial instability.

The density distribution in the lower transient zone was nearly linear in the ordinary density difference. In the extreme case of the remarkable density difference, the density came near asymptotically to that of the upper layer.

INTRODUCTION

At an estuary, in case of weak mixing the pure water flow quietly over the stational salt water building up the stratified flow. The shape of the interface can be calculated if the shear stresses along the interface and along the riverbed can be reasonably estimated.

In 1949, Keulegan described phenomena around this interface very clearly. When the relative velocity between the two layers is small, the flow is laminar. However when this velocity is increased up to the formation of ridges and waves, the flow becomes turbulent.[1] This shows the shear stress at the interface is closely related to the interfacial waves in case of turbulent flow. In 1959, Bata derived formulae on frictional resistance at the interface employing the boundary layer theory.[2] It was the flow established on which he treatec but in the ordinary flumes in laboratories such established flow can be hardly realized and flow is usually non-established. This may be assumed the case also in the real flow.

In this paper another approach is tried to express the internal shear stress using some semi-theoretical considerations and the flow in the zone of establishment is analyzed making use of the theory of free turbulence originated by Tollmien and of the convective-diffusion equation.

The theory presented herin may be considered casting some light upon phenomena in the stratified flow.

THE COEFFICIENTS OF THE SHEARING STRESS AT THE INTERFACE

Keulegan defined the number θ as the criterion of the interfacial instability in the stratified flow which was

$$\theta = (\nu_2 g \Delta\rho / \rho_1)^{1/3} / u_0 \qquad (1)$$

in which u was the relative velocity, ρ_1 was the density of the upper fluid, $\Delta\rho$ was the density difference, ν_2 was the kinetic viscosity of the lower layer and g was the accerelation of gravity.

Then following expressions hold;

$$\psi = \frac{1}{\theta^3} = (F_2')^2 \cdot R_2 = \frac{16}{s} \cdot \frac{\lambda_2}{\lambda_1} \qquad (2)$$

$$\lambda_1 = \frac{8\pi\nu_2}{s} \frac{\omega}{(u_0-\omega)^2}\Big|_{\omega=\frac{u_0}{2}} \qquad (3)$$

$$\lambda_2 = \frac{\pi u_0^2}{g'} \qquad (4)$$

ψ is introduced for the sake of convenience. F_2' is the internal Froude number $u_o/\sqrt{g'd_2}$, R_2 is the internal Reynolds number $u_o d_2/\nu_2$ in which d_2 is the depth of the lower layer. s is the sheltering coefficient and ω is the wave celerity on the interface. And g' is the reduced gravitational accerelation.

After Keulegan we can easily define λ_1 as the wave length of the stable internal waves in the viscous stratified flow and λ_2 as that in the irrotational stratified flow.

In turbulent flow, the critical value of θ is nearly equal to 0.018. So the critical value of ψ is 170, and if we assume s as 0.274 following Jeffereys,[3] the ratio λ_2/λ_1 is nearly equal to 3.00 which suggests the wave energy in the viscous flow is much smaller than that in the potential flow. When the value ψ becomes larger, the internal waves are beggining to break and energy must be consumed in this breaking. Internal shear stress is that which cause energy loss. So, the coefficient k_f which is $\tau_s/\rho_1 u_o$ must also be correlated with the ψ number.

In fig.1, data are plotted from experiments conducted in the Hydraulic Laboratory of Tohoku University since 1960, from experiments by Dr.T.Hamada[4] and from observations in River Ishikari.[5]

The relation between k_f and ψ is given as follows;

$$k_f = 3.940\,\psi^{-0.8356} \qquad (5)$$

and certifies the assumption mentioned above.

TURBULENT DIFFUSION IN THE STRATIFIED FLOW

When the pure water with density ρ_1 flows over the still salt water with density ρ_2, there must take place momentum exchange by turbulent diffusion both in pure and salt water. In fig.2, zones of influence are assumed as lines OB and OC. Then the horizontal velocity on the line OB is equal to u_o, the incident velocity of the pure water and that on the line OC is equal to zero. In the region between OB and OC, velocity varies gradually, but the density is rather constant in the region between OA and OB and varies in the region between OB and OC. This is because transfered water is easily diffused in the pure water flowing with the finite velocity u_o but is not so easily diffused in the salt water which is stable.

In this connection we can assume as;

$$\tau = \rho_1 l^2 \left|\frac{du}{dy}\right|^2 \qquad (6)$$

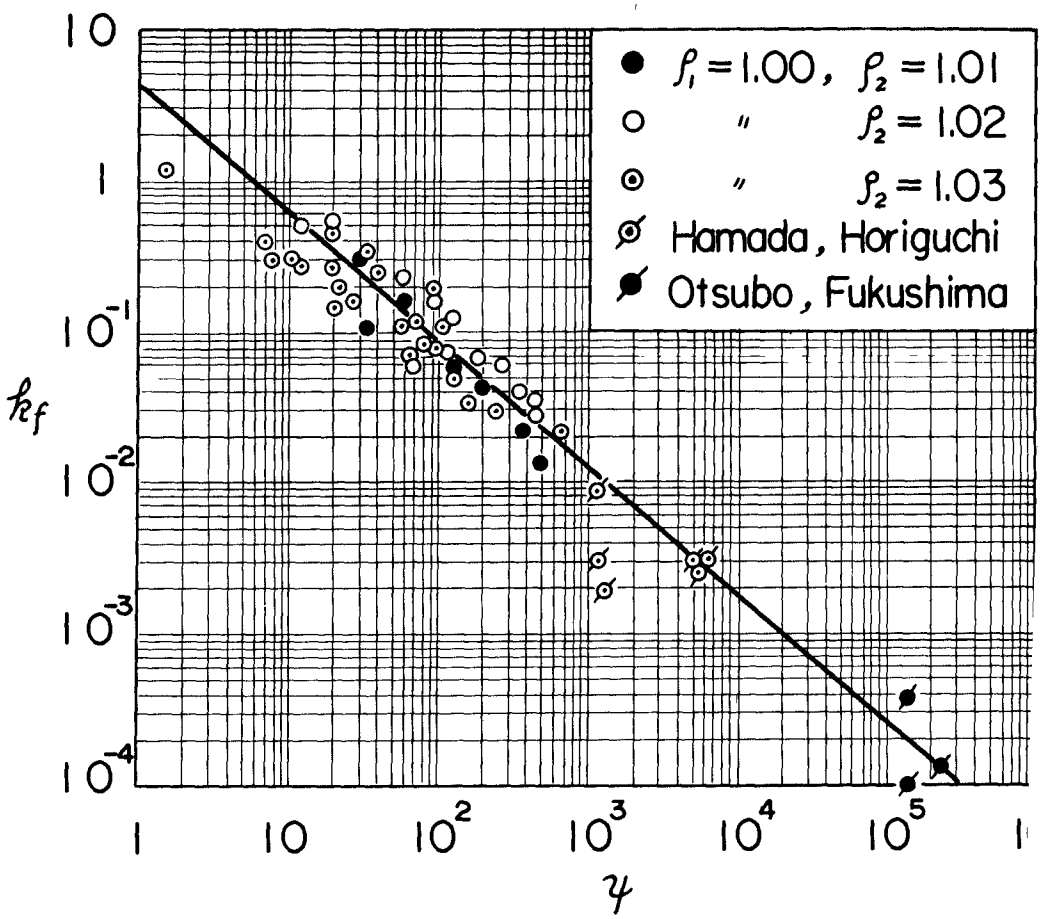

Fig.1. Relationship between k_f and ψ.

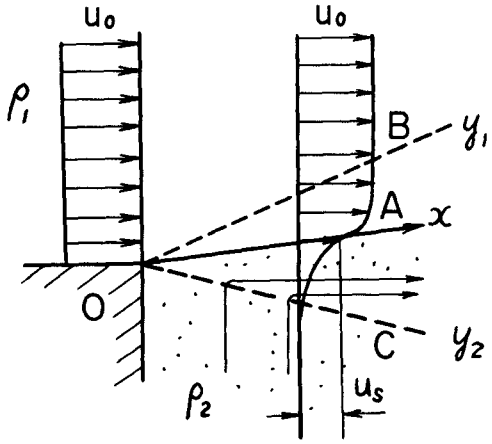

Fig.2. Illustration of the turbulent diffusion in the stratified flow.

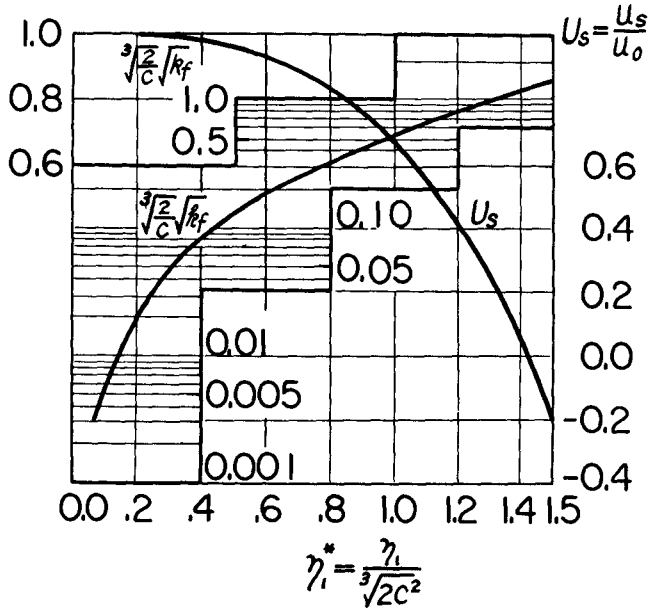

Fig.3. Relationship between U_s, $\eta_1^*=\frac{\eta_1}{\sqrt[3]{2c^2}}$ and $\sqrt[3]{\frac{2}{c}}\sqrt{k_f}$.

where l is the Prandtl's mixing length and is assumed proportio to the horizontal distance from the point of contact O, that is $l=cx$ in which c is constant.

FREE TURBULENT FLOW IN THE ZONE OF AOB

The equation of motion is

$$u\frac{\partial u}{\partial x}+v\frac{\partial u}{\partial y}=\frac{1}{\rho}\frac{\partial \tau}{\partial y} \tag{7}$$

Now we put

$$U=\frac{u}{u_0}=f\left(\frac{y}{x}\right)=f(\eta)=F'(\eta) \tag{8}$$

as Tollmien in which y is taken vertical to the interface OA.[6] The stream function ψ is,

$$\psi=\int f\left(\frac{y}{x}\right)dy=x\int f(\eta)\,d\eta=xF(\eta) \tag{9}$$

$$\therefore V=\frac{v}{u_0}=-\frac{\partial f}{\partial x}=-F(\eta)+\eta F'(\eta) \tag{10}$$

Then eq. (7) can be rewritten as;

$$F+2c^2F'''=0 \tag{11}$$

in which we take $F''\neq 0$.

Boundary conditions are as follows;

$$\begin{aligned} &\text{at } \eta=\eta_1, \quad F(\eta_1)=\eta_1,\ F'(\eta_1)=1,\ F''(\eta_1)=0\\ &\text{at } \eta=0, \quad F'(0)=\frac{u_s}{u_0}=U_s,\ F''(0)=\frac{\sqrt{k_1}}{c} \end{aligned} \tag{12}$$

in which u_s is the velocity at OA.

Now we put $\eta^*=\frac{\eta}{\sqrt[3]{2c^2}}$, then eq.(11) can be reduced to

$$F+\frac{d^3F}{d\eta^{*3}}=0 \tag{13}$$

and the boundary conditions are

$$\begin{aligned} &\text{at } \eta^*=\frac{\eta_1}{\sqrt[3]{2c^2}}, \quad F(\eta^*)=\sqrt[3]{2c^2}\,\eta_1^*,\ F'(\eta^*)=\sqrt[3]{2c^2},\ F''(\eta^*)=0\\ &\text{at } \eta^*=0, \quad F'(0)=\sqrt[3]{2c^2}\cdot U_s,\ F''(0)=\sqrt[3]{4c}\sqrt{k_1} \end{aligned} \tag{14}$$

From (13) and (14), we can get

$$F=Ae^{-\eta^*}+Be^{\frac{\eta^*}{2}}\cos\frac{\sqrt{3}}{2}\eta^*+Ce^{\frac{\eta^*}{2}}\sin\frac{\sqrt{3}}{2}\eta^* \tag{15}$$

and

$$U=\frac{u}{u_0}=-Ae^{-\eta^*}+\frac{1}{2}(B+\sqrt{3}C)e^{\frac{\eta^*}{2}}\cos\frac{\sqrt{3}}{2}\eta^*-\frac{1}{2}(\sqrt{3}B-C)e^{\frac{\eta^*}{2}}\sin\frac{\sqrt{3}}{2}\eta^* \tag{16}$$

where,

$$A = \alpha e^{\eta_1^*}(\eta_1^* - 1)$$
$$\beta = \alpha e^{-\eta_1^*}[(1+2\eta_1^*)E_c - \sqrt{3}E_s]$$
$$C = \alpha e^{-\eta_1^*}[\sqrt{3}E_c + (1+2\eta_1^*)E_s] \qquad (17)$$
$$E_c = e^{\frac{\eta_1^*}{2}}\cos\frac{\sqrt{3}}{2}\eta_1^*, \quad E_s = e^{\frac{\eta_1^*}{2}}\sin\frac{\sqrt{3}}{2}\eta_1^*, \quad \eta_1^* = \eta/\sqrt[3]{2c^2}$$
$$\alpha = 1/3\cdot\sqrt[3]{2c^2}.$$

FREE TURBULENT FLOW IN THE ZONE OF AOC

In the zone of AOC, the density varied gradually. Then we must take ρ in eq.(7) as a variable.

If we assume eq.(8) also hold in this zone, we can get from eq.(6) as,

$$\frac{1}{u_0^2}\frac{\partial\tau}{\partial y} = \frac{c^2F''}{x}(F''\rho' + 2F'''\rho) \qquad (18)$$

in which, $\rho' = d\rho/d\eta$.

Then from eq.(7), we can derive

$$F + 2c^2F''' + c^2\frac{\rho'}{\rho}F'' = 0 \qquad (19)$$

and the boundary conditions are

$$\begin{aligned} &\text{at} \quad \eta = 0, && F'(0) = U_S, && F''(0) = \sqrt{k_t}/c \\ &\text{at} \quad \eta = \eta_2, && F'(\eta_2) = 0, && F''(\eta_2) = 0 \end{aligned} \qquad (20)$$

in which η_2 denotes the lower boundary OC.

The two-dimensional convective diffusion equation is,

$$u\frac{\partial S}{\partial x} + v\frac{\partial S}{\partial y} = \frac{\partial}{\partial x}\left(E_x\frac{\partial S}{\partial x}\right) + \frac{\partial}{\partial y}\left(E_y\frac{\partial S}{\partial y}\right) \qquad (21)$$

where s is the salinity and E_x and E_y are the coefficients of horizontal and vertical eddy diffusivity.respectively. In turbulent flow, molecular diffusivity is negligible and eddy diffusivity is predominant. So, we can assume E_x and E_y as $c^2x^2(\partial u/\partial y)$ as eddy viscosity.

The density ρ and the salinity s are related by;

$$\rho = \rho_1(1 + as) \qquad (22)$$

And if we take ρ as a function of η like u, the following equation can be reduced from eq.(21),

$$\frac{\rho''}{\rho'} = -\frac{1}{F''}\left[F''' + \frac{1}{c^2}\cdot\frac{\eta}{1+\eta^2}\cdot F'\right] \qquad (23)$$

From eq.(19)

$$p = -\frac{\rho}{c^2F''}(F + 2c^2F''') \qquad (24)$$

in which $p = \frac{d\rho}{d\eta} = \rho'$. And if we differentiate it, we get

$$\frac{dp}{d\rho} = -\frac{1}{c^2 F''}\left(F + 2c^2 F'''\right) \tag{25}$$

As $\rho''/\rho' = dp/d\rho$, from (23) and (24)

$$\frac{1}{c^2}\left(F + 2c^2 F'''\right) = F''' + \frac{1}{c^2}\frac{\eta}{1+\eta^2}F'$$

$$c^2 F''' + F'\frac{\eta}{1+\eta^2} + F = 0 \tag{26}$$

If we put $\bar{\eta}^* = \frac{\eta}{\sqrt[3]{c^2}}$ (27), then eq.(26) can be reduced to,

$$\frac{d^3 F}{d\bar{\eta}^{*3}} + \frac{\bar{\eta}^*}{1 + c^{4/3}\bar{\eta}^{*2}}\frac{dF}{d\bar{\eta}^*} + F = 0 \tag{28}$$

The boundary conditions (20) are reduced to,

$$\text{at } \bar{\eta}^* = 0,\ \frac{dF}{d\bar{\eta}^*} = \sqrt[3]{c^2}\,U_s,\ \frac{d^2F}{d\bar{\eta}^{*2}} = \sqrt[3]{c}\sqrt{kf}$$

$$\text{at } \bar{\eta}^* = \bar{\eta}_2^* = \frac{\eta_2}{\sqrt[3]{c^2}},\ \frac{dF}{d\bar{\eta}^*} = 0,\ \frac{d^2F}{d\bar{\eta}_*^2} = 0 \tag{29}$$

If we assume F as the power series of $\bar{\eta}^*$, and if we define its coefficients by (28) and (29), we can get its solution as;

$$F = A_0 + A_1\bar{\eta}^* + A_2\bar{\eta}^{*2} - \frac{A_0}{6}\bar{\eta}^{*3} - \frac{A_1}{12}\bar{\eta}^{*4} - \frac{A_2}{20}\bar{\eta}^{*5} \tag{30}$$

in which

$$A_0 = \frac{K(24+4Y+Y^2)}{4\bar{\eta}_2^*(6+Y)},\ A_1 = U^*,\ A_2 = \frac{K}{2},\ U^* = \sqrt[3]{c^2}\,U_s$$

$$K = \sqrt[3]{c}\sqrt{kf},\ Y = (\bar{\eta}_2^*)^3 \tag{31}$$

and

$$\frac{u}{u_0} = U = \frac{dF}{d\eta} = \frac{1}{\sqrt[3]{c^2}}\cdot\frac{dF}{d\bar{\eta}^*}$$

$$= U_s\left(1 + W\eta^* - \frac{1}{\sqrt[3]{4}}W f(Y)(\eta^*)^2 - \frac{2}{3}(\eta^*)^3 - \frac{W}{4}(\eta^*)^4\right) \tag{32}$$

$$W = \frac{1}{U_s}\sqrt[3]{\frac{2}{c}}\sqrt{kf},\quad f(Y) = \frac{24+4Y+Y^2}{4\bar{\eta}_2^*(6+Y)} = \frac{24+4Y+Y^2}{4\sqrt[3]{2}(6+Y)\eta_2^*}$$

$$Y = (\bar{\eta}_2^*)^3 = 2(\eta_2^*)^3 \tag{33}$$

in which we use the relation of $\bar{\eta}^* = \sqrt[3]{2}\,\eta^* = \frac{\eta}{\sqrt[3]{c^2}}$ for it may be convenience that equations (16) and (32) have either the same independent variable.

THE EFFECTS OF k_f UPON THE INTERFACIAL VELOCITY AND BOUNDARIES OF MIXING ZONES

From eq.(14), the non-dimensional interfacial velocity can be written as;

$$U_s = \frac{1}{\sqrt[3]{2C^2}} F'(0) \tag{34}$$

Using eq.(15) and (17), eq.(34) is reduced to;

$$U_s = \frac{u_s}{u_o} = \frac{1}{6\alpha}(-2A + B + \sqrt{3}\,C) \tag{35}$$

Also from eq.(14),

$$\sqrt[3]{4C}\sqrt{k_f} = F''(0) \tag{36}$$

And this equation can be rewritten as

$$\sqrt[3]{4C}\sqrt{k_f} = A - \frac{B}{2} + \frac{\sqrt{3}}{2}C \tag{37}$$

in these equations, A,B,C and α are expressed in eq.(17).

In fig.3, the relationship between U_s and η_1^* is given in the normal scale. And that between $\sqrt[3]{\frac{2}{c}}\sqrt{k_f}$ and η_1^* is given in the semi-logarithmic scale. It is shown that if k_f becomes large, the upper zone of mixing diverges more rapidly because η_1 is the ratio of the value y at the upper boundary OB and the distance x from the point of contact.

The interfacial velocity U_s decreases when the coefficient of the shear stress increases.

Following Tollmien, we may assume the value c as 0.0174. The critical value of ψ is 170 as cited above. Then, from eq.(5) k_f is 0.055. And from fig.3 the critical value of η_1^* can be given as 1.40. In this case the value U_s is zero, and in case of the value $\sqrt[3]{\frac{2}{c}}\sqrt{k_f}$ lower than 1.14, U_s is negative as in fig.3, which is meaningless from the physical aspect and also substantiates the critical condition stated by Keulegan.

Using eq.(30) the following relation can be derived from eq.(29);

$$\frac{U_s}{\sqrt[3]{\frac{2}{c}}\sqrt{k_f}} = -\frac{3}{4}\cdot\frac{4+\gamma}{6+\gamma}\cdot\eta_2^* \quad ; \quad \gamma = 2(\eta_2^*)^3 \tag{38}$$

where $\eta_2^* = \eta_2 / \sqrt[3]{2c^2}$ and η_2 is the ratio of the value y at the lower boundary OC and x. As expressed in fig.4, we know

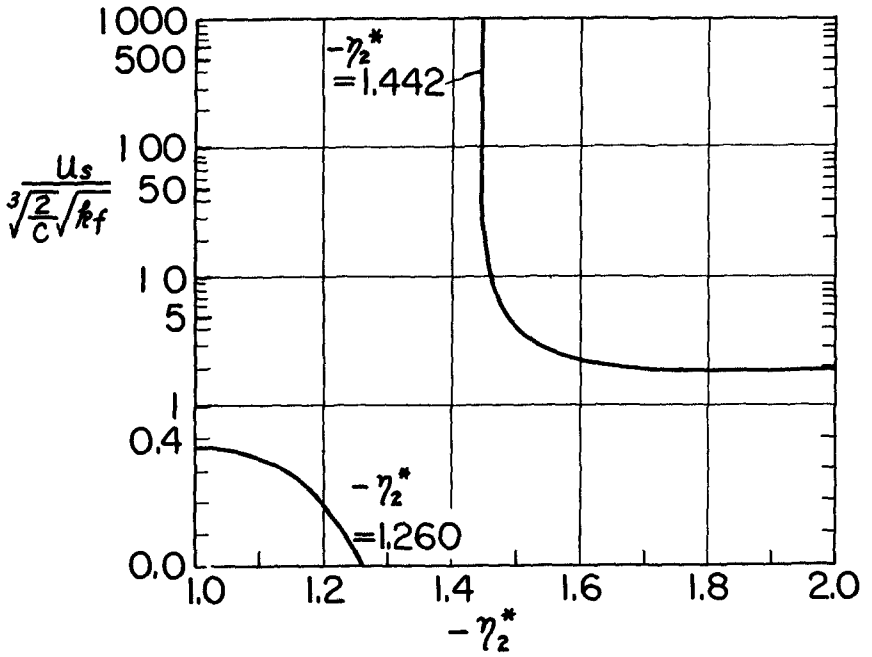

Fig.4. Relationship between $\frac{U_s}{\sqrt[3]{\frac{2}{c}}\sqrt{k_f}}$ and $-\eta_2^*$.

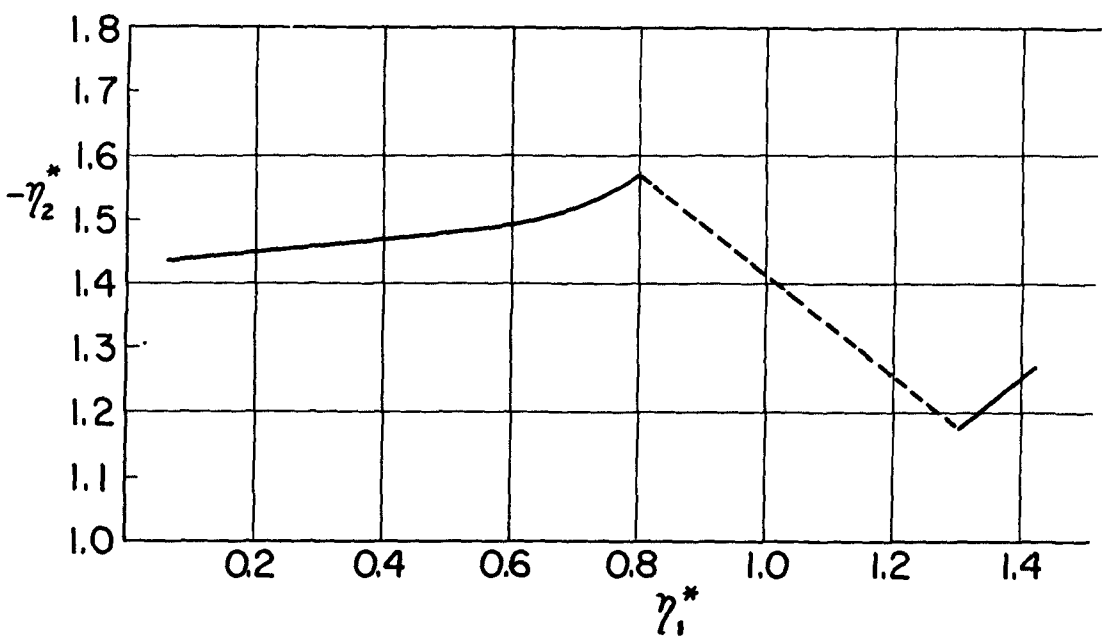

Fig.5. Relationship between η_1^* and $-\eta_2^*$.

that no real solution of the lower boundary can be given for the values of $u_s / \sqrt[3]{\frac{2}{c}\sqrt{k_f}}$ between 0.368 and 1.792.

From fig.3, values of U_s and $\sqrt[3]{\frac{2}{c}\sqrt{k_f}}$ can be taken for any value of η_1^* and their ratio gives the related value of η_2^* in fig.4. Fig.5 shows the relationship between η_1^* and η_2^* thus acquired. In which, the dotted line shows the region where no solution can be given for the lower boundary as cited above. And also it is shown that there is no solution for the value of η_1^* higher than 1.40.

VELOCITY DISTRIBUTIONS IN THE ZONES OF INFLUENCE

In fig.6, the velocity distributions are presented from eq.(16) and (32). The ordinates is taken for η^* / η_1^*, so the velocity at the interface is shown at the horizontal axis. Four curves are shown. The curve for k_f=0.055 which is critical as cited above shows the remarkable gradient of the velocity distribution in the pure water and a reverse flow in the salt water which is the phenomenon that has been observed frequently in the small scale flume. The curve for k_f=0.01 presents no solution in the velocity field of the lower layer. The curve for 0.001 of the value of k_f is an example for the large scale flume and the fourth curve is for k_f=0.0001 which is observed in the real estuaries.[5] In these cases there happens no reverse flow and the zone of influence in the lower layer spreads remarkably in contrast to that in the upper layer which has also been observed in an estuary.

DENSITY DISTRIBUTIONS IN THE ZONES OF INFLUENCE

From eqs.(24) and (25), we get;

$$\frac{p}{\rho} = \frac{dp}{d\rho} \tag{39}$$

then we can deduce,

$$\rho = \kappa e^{c\eta} \tag{40}$$

and the boundary conditions are

$$\text{at } \eta = 0,\ \rho = \rho_0\ ;\ \text{at } \eta = \eta_2,\ \rho = \rho_0 (1+\varepsilon) \tag{41}$$

then from (40) and (41), we can derive as;

$$1 + \alpha\varepsilon = (1+\varepsilon)^{\eta/\eta_2}$$

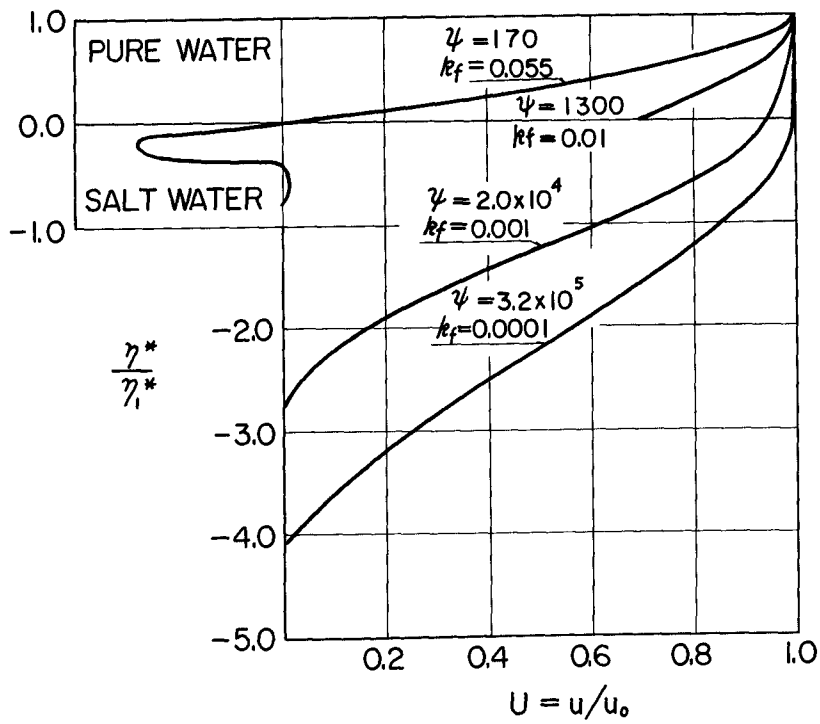

Fig.6. Velocity distributions in the zones of influence.

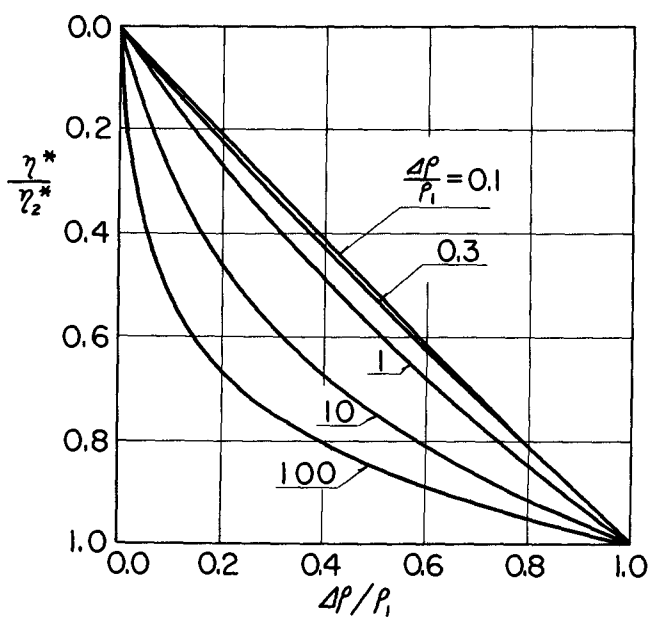

Fig.7. Density distributions in the lower zones of influence.

in which $\alpha = \rho - \rho_1 / \rho_2 - \rho_1$.

Fig.7 shows the density distributions in the lower zones. For the values of $\Delta\rho / \rho_1$ between 0.1 and 0.3, which are popular cases for the estuary, curves are nearly linear. However if $\Delta\rho / \rho_1$ should be as large as 10 or 100, density distributio might deviate remarkably from the linear one.

CONCLUSIONS

In comparison with experiments conducted in the Hydraulic Laboratory in Tohoku University, the relation between $\sqrt[3]{\frac{2}{c}}\sqrt{k_f}$ and U_s is reasonably hold and lower zone of influence was not distinctly recognized in the experiments in cases of $U_s / \sqrt[3]{\frac{2}{c}}\sqrt{k_f}$ between 0.513 and 1.420, which substantiated the above theory, if we assume c as 0.174.

However values of η_i^* derived from this theory were seemec to be rather high compared to the actual one. And in the experiments the density distributions had minute wavy configurations over the linearized appearance. The eddy diffusivity must be observed in detail for horizontal or vertical direction.

However the theory presented herin seemed to cast much light upon phenomena in the stratified flow.

ACKNOWLEDGEMENT

The auther wishes to acknowledge his appreciation to Professor T. Kataoka of Iwate University for his precise execution of experiments as a visiting professor and to staffs of Hydraulic Laboratory of Tohoku University for their efforts in the experiments.

REFERENCES

1. Keulegan,G.H.(1949). Interfacial instability and mixing in stratified flow: Jour. Research Nat. Bur. Stand, vol.43,p487, RP2040

2. Bata,G.L.(1959). Frictional resistance at the interface of density currents: Proc. 8th Congress-Montreal, I.A.H.R. 12-C

3. Jeffereys,H.(1925)(1926). On the formation of water waves by wind: Proc. Roy. Soc. London A ,vol.107 and 110

4. Hamada,T.(1960). On the behaviour of the salt wedge: Proc. 7th Conf. Jap. Coast. Eng.,p.163(in Japanese)

5. Otsbo,K. and Fukushima,H.(1959). Density currents in a river mouth with a small tidal range: Proc. 8th Congress-Montreal,I.A.H.R. 4-C

6. Tollmien,W.(1926). Berechnung turbulenter Ausbreitungsvorgänge: Z.a.M.M.,Bd. 6,p.468

Chapter 52

STORM CONDITIONS AND VEGETATION IN EQUILIBRIUM OF REEF ISLANDS

D.R. Stoddart

Department of Geography
Cambridge, England

The study of reef islands on the British Honduras coast before and after a major hurricane in 1961 demonstrated the critical significance of vegetation in determining whether storm action is mainly erosional or aggradational. Man-induced vegetation change in this area has led to major storms becoming primarily destructive, and this change can be related to the recent history of the islands. Instability resulting from continued interference with natural vegetation will have serious consequences for the economic use and even future existence of the islands; such use will best be regulated by allowing natural regeneration of vegetation in shelter belts along the most exposed shores of islands.

NATURE OF REEF ISLANDS

Detrital reef islands are of two major types: sand cays and sand-shingle cays. Sand cays consist of coral grit, algal, shell and other organic sediments in the size range 0-2 ϕ, accumulated on a reef flat under the action of refracted waves. The point of accumulation is a function of wave approach and characteristics, and of reef geometry and depth. On small patch reefs and at gaps in linear reefs, sand cays normally develop on the leeward side of the reef flat. Sand-shingle cays develop primarily because of the lodgment on reef flats, of coral and mollusc shingle in the size range -5 to -10 ϕ, median -8 ϕ, with subsequent accumulation of sand-size sediments to leeward. Lodgment may take place either under the action of refracted waves on patch reefs or at reef gaps, or on exposed linear reefs as unrefracted waves dissipate energy when crossing the reef flat. The point of sedimentation will again depend on local wave characteristics and reef morphology.

Islands of these types have been investigated off the coast of British Honduras, Central America, where a 130-mile long barrier reef and three atolls give widely varying conditions of reef island formation. The reefs are aligned north-south, transverse to the dominant Northeast Trades and wave trains, and tides are negligible (less than 2 ft.). With essentially unidirectional waves and no tidal complications, the nature of above-water sedimentation is essentially a function of (a) local exposure to waves, largely a matter of protection by windward reefs; and (b) local reef morphology, in particular width and depth of the reef flat. Under these conditions, initially formed sand and sand-shingle islands may rise to a height of 3 ft. above still water level under the action of wave run-up. Such islands may then be colonised by

vegetation, and the sediments subject to local diagenesis, either by cay sandstone formation above high water level, or by intertidal beachrock formation.

Detailed mapping of islands on the British Honduras reefs in 1959-61 showed considerable areal variations in island topography and sediment composition. On the exposed eastern reefs, sand-shingle cays reach a maximum height of 10 ft. above sea level on Lighthouse and Glover's Reefs. On more protected reefs (Turneffe Islands, southern barrier reef), islands do not exceed 5 ft. in maximum elevation, with less coarse seaward shingle ridges. Along the central barrier reef, protected by the atolls to windward, islands lack shingle and are less than 5 ft. in height. On protected shoal areas within the barrier and Turneffe lagoons, colonisation by Rhizophora mangle and Avicennia germinans has led to island formation and the entrapment in more exposed areas of sand on their windward sides.

EFFECT OF HURRICANE HATTIE

Mapping of these islands was completed in August 1961. On October 30-31 1961 Hurricane Hattie crossed diagonally over the centre of the reef area (figure 1), with a minimum recorded pressure of 27.4 inches, winds gusting to over 200 m.p.h., and a storm surge extending on the mainland coast to about 30 miles north and 15 miles south of the storm centre, with a maximum amplitude of 15 ft. Wave action associated with the hurricane was greatest to the north of the storm track: initial easterly swell was followed late on 30 October by wind-driven northerly then easterly seas, travelling directly across the Caribbean towards the transverse atoll and barrier reefs. South of the storm track, initial easterly swells were followed by southeast, south and southwest seas with the passage of the storm. In the reef area these were generated in shallow water with restricted fetch, in areas where the storm surge was less significant: hence they were much less destructive than seas to the north of the storm track. Distinction must be made between sea and wave action, therefore, which varied in intensity on each side of the storm, and wind action, which was more symmetrically zoned in intensity north and south of the storm track. As a result, damage in the reef area varied both with dominant process and location:

(a) submarine changes and damage to living reef by waves was catastrophic to the north of the storm track for a distance of 30 miles from the centre, but much less important to the south.

(b) wave action on reef islands was greatest to the north of the storm track, but much less to the south, decreasing with distance from the storm centre.

(c) wind action on reef islands was greatest near the storm

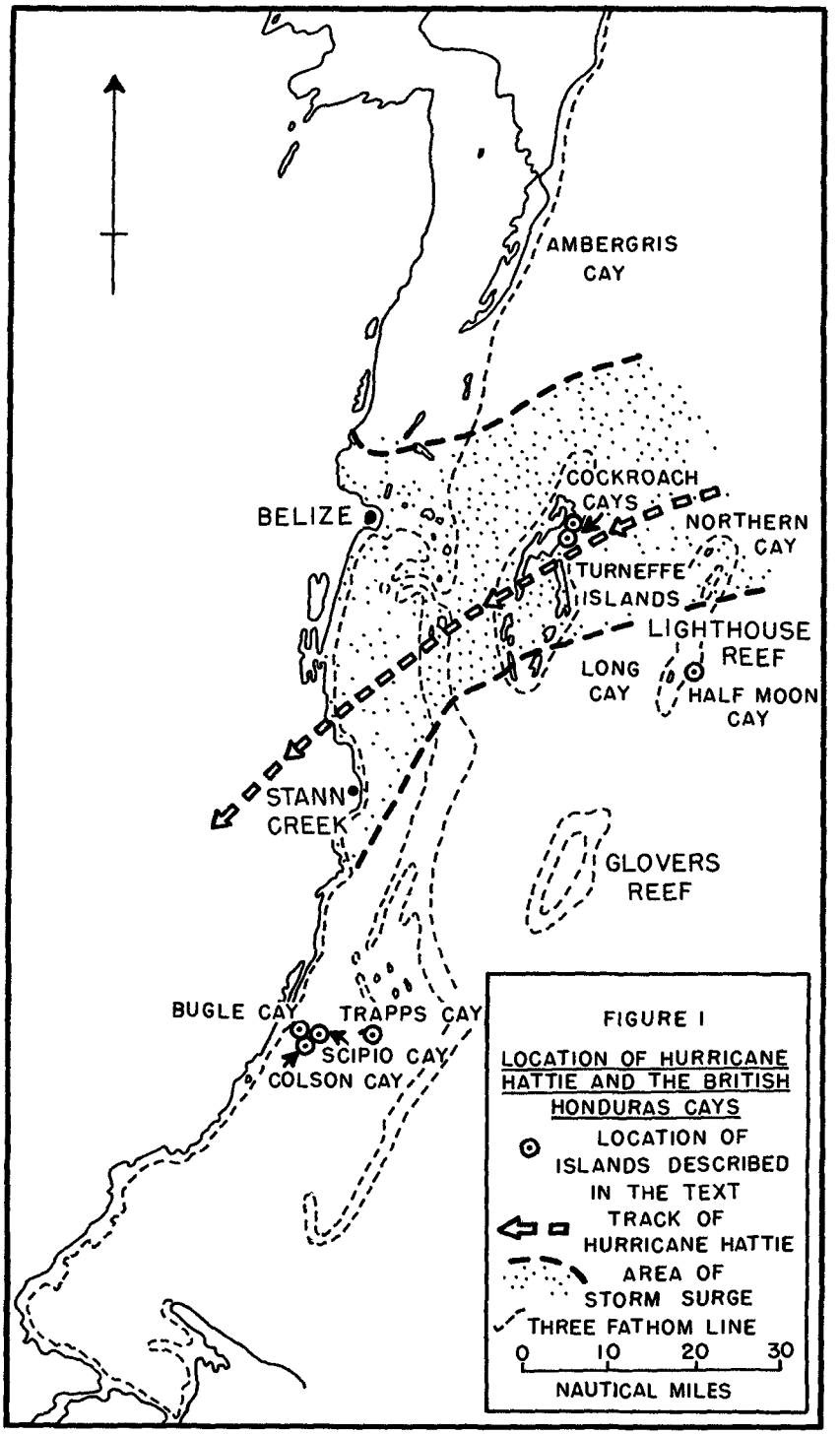
AMBERGRIS CAY
COCKROACH CAYS
BELIZE
NORTHERN CAY
TURNEFFE ISLANDS
LIGHTHOUSE REEF
LONG CAY
HALF MOON CAY
STANN CREEK
GLOVERS REEF
BUGLE CAY
TRAPPS CAY
SCIPIO CAY
COLSON CAY
FIGURE I
LOCATION OF HURRICANE HATTIE AND THE BRITISH HONDURAS CAYS
LOCATION OF ISLANDS DESCRIBED IN THE TEXT
TRACK OF HURRICANE HATTIE
AREA OF STORM SURGE
THREE FATHOM LINE
0 10 20 30
NAUTICAL MILES

TABLE I

ROLE OF VEGETATION COVER IN HURRICANE EFFECTS ON REEF ISLANDS DURING HURRICANE HATTIE, 1961

VEGETATION TYPE / HURRICANE EFFECT	(A) NATURAL VEGETATION	(B) COCONUTS WITH REGENERATED THICKET	(C) COCONUTS WITH LOW UNDERGROWTH	(D) COCONUTS WITH NO UNDERGROWTH	(E) SMALL ISLAND WITH SMALL VEGETATION THICKET	(F) UNVEGETATED
DISAPPEARANCE	-	-	-	2	10	7
MAJOR SURFACE SAND-STRIPPING & CHANNEL-CUTTING	-	2	3	17	-	-
MAJOR BEACH RETREAT	-	3	-	10	-	-
MARGINAL AGGRADATION	15	9	-	-	-	-

NUMBERS REFER TO INDIVIDUAL ISLANDS IN EACH VEGETATION & DAMAGE CLASS

centre, decreasing symmetrically both to north and south.

Because of the extreme conditions, no quantitative data are available on wave conditions during the passage of the storm: all available data has been collated elsewhere (Stoddart, 1963).

Within this framework of storm conditions, changes on detrital reef islands varied greatly, but remapping of all damaged islands in 1962 demonstrated regularities. Reef islands vary in size, shape, height, composition, and vegetation cover. Erosional effects due to waves were of two main types: first, peripheral backwearing of shorelines, both on sand and shingle beaches, leading to undermining and removal of surface vegetation, and in some cases followed by deposition of fresh sediment on the eroded shore; and second, surface stripping of sand and scouring of channels and holes by overtopping water, with attendant vegetation damage. Within 40 miles of the storm centre, the first type, peripheral beach erosion, was universal, and to some extent is only a more extreme case of the annual shoreline readjustments following winter storms of "northers". The incidence of surficial erosion was much more limited, and was restricted to islands where overtopping by the sea gave wave action access to island interiors. Clearly, this occurred most often on low islands; on islands narrow transverse to the direction of water movement; and on islands exposed to most intense sea conditions, particularly those within the high storm surge zone, where smaller cays were overtopped by up to 10 ft. of water. Hence, on the larger islands, such as Ambergris Cay, Long Cay (Lighthouse Reef), and Northern Cay (Lighthouse Reef), in spite of shoreline readjustments of up to 50 yards, gross topographic changes were minor, and damage in the interiors was restricted to felling of trees by wind. Conversely, on small islands, easily overtopped, erosion could be catastrophic over the whole cay surface, and in several cases led to the complete disappearance of the cay.

VEGETATION AND HURRICANE CHANGES

Mapping disclosed, however, one further critical variable limiting hurricane effects, which is best demonstrated by reference to examples.

In the southern barrier reef lagoon , off Placencia, 30 miles south of the storm centre, there are numerous small sand cays on individual patch reefs. Most of these islands consist of peripheral sand beach ridges with interior *Avicennia* marsh. Vegetation on the beach ridges consists of a dense thicket of *Chrinax*, *Cordia* and coconuts. The pattern of damage at Scipio, Solson, Owen, Trapp's and Cary Cays was similar: beach retreat and minor cliffing, with local destruction of vegetation, on the weather side, followed by deposition of fresh shingle both on the old beach ridge crest and as a low carpet to seaward of the eroded cliff. The fresh crest shingle was banked against and partly buried the palm

thicket and ground vegetation, had a maximum thickness of about 3 feet, and presented a steep slope to landward. On neighbouring Bugle Cay, however, in other respects topographically similar, the original vegetation had been cleared for a lighthouse station and coconut plantation, with no undergrowth. In spite of distance from the storm centre the sea overtopped the island and wave action took place across the whole cay surface. Shore retreat averaged 10-20 yards, much more than on vegetated islands, surface sand was stripped and trees disappeared, and all houses were destroyed. Sediment deposition was restricted to shoal water on the leeward side of the island, and no fresh shingle accumulated along the seaward beach ridge.

Similar, if more spectacular effects, were seen at Half Moon Cay, 20 miles south of the storm centre, on the exposed eastern reef of Lighthouse Reef atoll. Half Moon Cay (Figure 2) is a sand-shingle island 1100 yards long, with shingle ridges along its south and northeast shores, reaching a maximum height of 10 ft. above sea level. Comparison of contour maps made in 1961 and 1962 gives a detailed picture of hurricane changes. Vegetation distribution is again significant. The western half of the island in 1961 was covered with a thicket of Cordia sebestena, Bursera simaruba, Ficus, Neea and coconuts; the eastern half had been cleared of natural vegetation, mostly since 1927, and in 1961 carried tall coconuts, largely without ground vegetation. Before the hurricane the thicket-covered west end of the cay consisted of a seaward shingle ridge, declining in height from 9 ft. to 3 ft. above sea level from east to west, with attendant decrease in shingle calibre; Cordia formed a dense hedge along the ridge crest. Lagoonward of the crest the surface was flat, built of coarse coral grit and rotten shingle, and covered with dense vegetation. The eastern half of the cay, under coconuts, was almost entirely sand, the seaward beach crest rising mostly to more than 8 ft., and locally to 10 ft. above sea level. During the hurricane, in addition to considerable wind damage to vegetation, changes resulting from south to southwest seas took the following forms:

(a) on the sand area under coconuts: the seaward beach retreated up to 20 yards, and the crest elevations were lowered at least 3 ft. and in places up to 7 ft. The area back of the crest suffered surface sand stripping, with some channelling on the narrower part of the cay.

(b) on the western vegetated sector, the seaward ridge crest was pushed about 25 yards landward and nearshore vegetation was uprooted and destroyed. The dense vegetation thicket, however, acting as a baffle against the waves, served as a massive sediment trap for coral blocks, shingle and sand. In place of the former graded sediment distribution and decline in crest height from east to west, fresh sediment has been piled against the vegetation barrier to a height

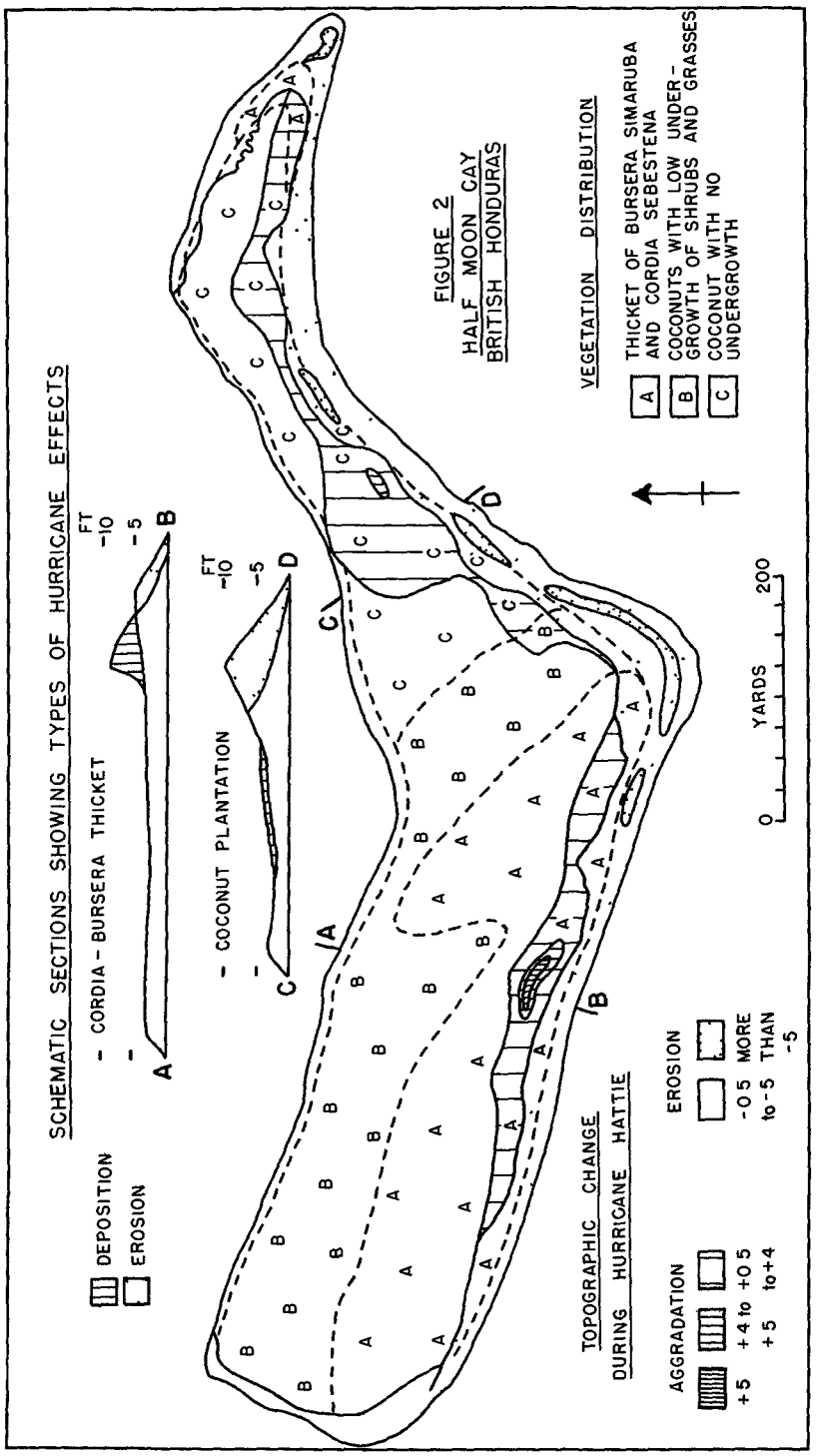

FIGURE 2
HALF MOON CAY
BRITISH HONDURAS

of 8 ft. above sea level for most of its length, and in one place to 10 ft. The inner edge of the fresh sediment is marked by a sharp break of slope.

Thus, where the natural vegetation had been replaced by coconuts before the storm, erosion and beach retreat led to net vertical decreases in height of 3-7 ft.; whereas where natural vegetation remained, banking of storm sediments against the vegetation hedge led to net vertical increases in height of 1-5 ft.

The Half Moon Cay case is best documented, but throughout the reef area affected by the hurricane the same pattern is seen. For example, north of the hurricane track, on the east-facing reef of Turneffe Islands, one island in the Cockroach Group (Cockroach Cay) had been cleared for coconuts. During the hurricane all the vegetation disappeared, and surface sediments were scoured out over the whole island surface to depths of 1-2 ft., with no corresponding above-water deposition. Smaller, lower islands a few yards away, which retained their natural vegetation of Bursera, Cordia and Thrinax, suffered slight marginal erosion but massive deposition of fresh shingle against the vegetation hedge (as at Pelican Cay). Comparative pre- and post-hurricane maps for most of the storm-affected islands have been published elsewhere (Stoddart, 1963), and provide further evidence on the significance of vegetation cover in affecting the nature of hurricane effects.

SUMMARY OF CHANGES

From these data we conclude that:

(1) on islands with natural littoral thicket, or with coconut thicket with dense naturally regenerated undergrowth, both within and outside the surge zone, debris-laden storm waves are incompetent to destroy more than an outer fringe of vegetation, and massive deposition of sand and shingle from storm waves occurs at the margins of the thicket.

(2) on islands planted to coconuts, especially with no undergrowth, and particularly within the storm surge zone, trees are readily removed, either by direct wind and wave action, or by erosion of the substrate by waves. Destruction of the vegetation removes any obstacle to storm waves, which may cause general beach retreat, surface sand stripping and channel-cutting, and in extreme cases total erosion of the island.

(3) on mangrove islands the mangrove was defoliated during the storm but not uprooted. Since these islands are located in sheltered areas remote from zones of active sediment production, however, little aggradation followed. These islands are not further considered here.

On islands in the first category, it is immaterial whether

vegetation mortality is immediate or delayed: the major point is that vegetation retained its root-hold and remained in the position of growth, and this prevented the passage of sediment-laden storm water. Table 1 summarises types of physiographic change for all islands studied, in terms of six categories of vegetation cover, and clearly demonstrates the importance of vegetation type in controlling the pattern of storm effects.

A MODEL OF REEF ISLAND FORMATION

These data have important implications for the morphology, structure, history and equilibrium conditions of reef islands generally. A model of island evolution suggested by the British Honduras cases will be briefly stated, and then related to known history of the islands and to outstanding problems of island morphology.

The conditions necessary for the accumulation of detrital reef sediments have already been stated in outline as functions of wave characteristics, reef depth and geometry, and source and nature of sediment supply. A full statement would also include effects of tides and tide and wind-induced currents. Such conditions are clearly competent to account for the formation of embryonic "sand-bores" or small unvegetated detrital islands of reef areas, which are typically of variable topography, location and size, and often of intermittent life. Such patches are stabilised by vegetation growth through a series of successional stages to climax, and secondarily by diagenesis of loose clastic sediments. Sandbores, however, rarely if ever exceed 3 ft. in height, whereas cays, depending on exposure, may reach 10 ft. It is suggested here that the climax vegetation of reef islands, by its dense structure and root system, forms a natural protection against storm waves, and that further, once such vegetation is established, it acts during violent storms as a sediment trap, leading to net increase in height of the land surface. In 1961 storm sediments were thus built to a height of 10 ft. above sea level at Half Moon Cay, a height equal to that of any other island on the reefs before the storm. In the reef island ecosystem, therefore, vegetation and sediment accumulation are complexly interlocked: without the sediment-trapping function of the natural vegetation, islands could not be built to heights of more than 3-5 ft. above sea level without relative shifts of sea level. High-standing islands are thus in complex equilibrium with marine processes, with vegetation as a critical control during major storms. If the vegetation is removed from any island, this equilibrium is disturbed. Sediment is no longer trapped from storm waters, which cause considerable marginal and surficial erosion leading to net decrease in surface height and even to disappearance or fragmentation of the island. When natural vegetation is removed, it is normally replaced by coconut plantations, which (a) have an open structure easily penetrated by seawater; (b) frequently have no ground vegetation, exposing the surface to stripping and channelling; and

(c) have a dense but shallow (12-18 inches) root mat easily undermined by marginal sand sapping. Hence, in any given area subject to catastrophic storms, islands with natural vegetation will tend to increase in height during storm action and thus become progressively less subject to catastrophic damage, while those under coconuts will tend to be eroded and destroyed.

IMPLICATIONS OF THE GENERAL MODEL

Some implications of this model may now be explored. First, the change from aggradation to erosion must date from the replacement of natural vegetation by coconuts. In British Honduras coconuts are a post-Columbian introduction. They were first noted by Uring in 1720, but according to a sketch of Half Moon Cay in 1829 were still few in number. They apparently increased during the eighteenth century (Speer, 1765; Jefferys, 1775), but chiefly with the growth of the coconut export industry in the period 1850-1930. At Half Moon Cay most of the trees date from the 1920's. The vegetation change, therefore, has largely taken place within the last century. Apart from maps by Speer and Jefferys, the first detailed charts of the reefs date from the Admiralty surveys in the 1830's, since which time approximately twenty islands have disappeared on these reefs (Figure 3). Many others have undergone erosion, especially on their seaward shores. Almost all islands described in 1760-1830 as being covered with bushes or thicket are now planted with coconuts, and those within the storm area suffered severe damage in 1961. There is no evidence of islands becoming established as vegetated cays during this same period. Concurrently with the widespread replacement of natural vegetation by coconuts, therefore, there has been a large scale disappearance of formerly vegetated islands, in a period when (since 1787) there have been 21 recorded hurricanes, 14 of them since 1900.

The proposed model also provides a simple explanation for the height of reef islands. As shown elsewhere (Stoddart, 1962a) there is no evidence in the area of raised reefs, raised beachrock, or raised beaches indicating Holocene high stands of sea level, said to be widespread in the Indo-Pacific reef province. No such high stands have been found in detailed studies in the Gulf Coast area of the U.S.A. (Shepard, 1961), and it would therefore be unwise to call upon postulated high stands of the sea to explain anomalously high sediment accumulation on reef islands. The 1961 hurricane data indicate clearly that such high accumulation can take place during storms under certain vegetation conditions, to heights equal to those so far recorded on the reefs.

Island accumulation by this mechanism will result in distinctive island structures, characterised by a succession of soil and root horizons dipping seaward and overlain by thick but narrow and variable bands of fresh sediment, generally coarse and poorly sorted.

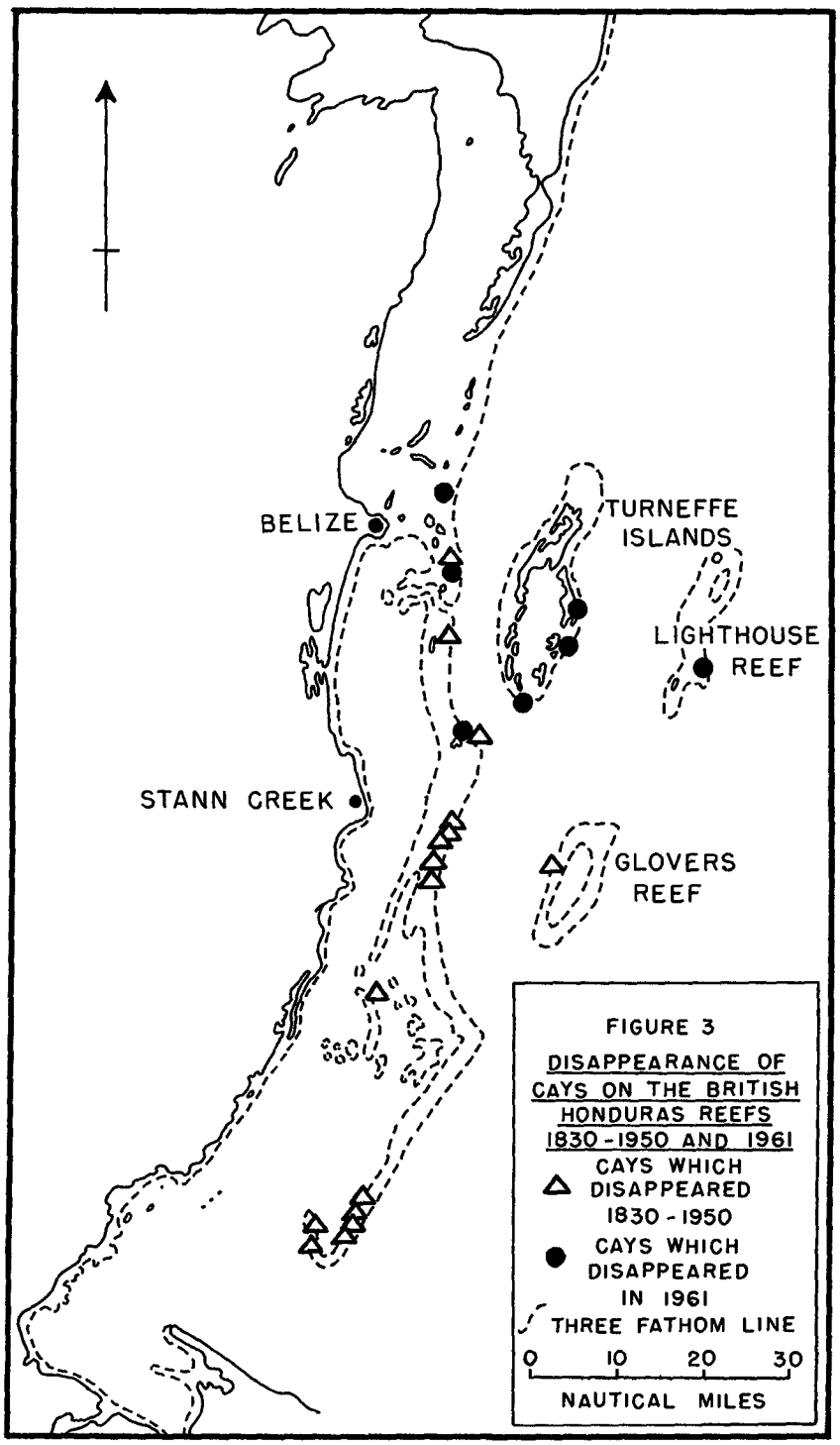
BELIZE
TURNEFFE ISLANDS
LIGHTHOUSE REEF
STANN CREEK
GLOVERS REEF
FIGURE 3
DISAPPEARANCE OF CAYS ON THE BRITISH HONDURAS REEFS 1830-1950 AND 1961
CAYS WHICH DISAPPEARED 1830-1950
CAYS WHICH DISAPPEARED IN 1961
THREE FATHOM LINE
0 10 20 30
NAUTICAL MILES

Such structures could easily be demonstrated on cay margins following the 1961 hurricane, but was not further verified by trenching. However, trenching on Jaluit Atoll, Marshall Islands, following Typhoon Ophelia in 1958 revealed sequences of soil horizons buried by later sediments (McKee, 1959; Blumenstock, 1961), and similar structures are reported from Ifaluk Atoll, Caroline Islands (Tracey, Abbott and Arnow, 1961). Acceptance of the present model involves two further structural implications:

(1) that island structures will differ (a) in islands still covered by dense natural vegetation, (b) in those where natural vegetation has been recently replaced, and (c) in those where coconuts have been established for many centuries. In the Caribbean the vegetation change has been relatively recent, whereas reef islands in the Indo-Pacific may have been planted to coconuts for a very long time. The history of the origin and spread of the coconut is significant here.

(2) that island structure and topography will differ on islands exposed to tropical storms from those in areas where such storms do not occur. Information on reef islands, however, is at present rather sparse: a useful location to test this suggestion would be the atolls of the Maldive and Laccadive groups, the southern parts of which are not affected by tropical storms, while the northern parts are (Oldham, 1895; Sewell, 1935).

IMMEDIATE PROSPECT

Apart from the general applicability of the model relating storm conditions, vegetation type and sedimentation, there is the question of the long-term stability of the British Honduras cays. The evidence indicates quite clearly that conversion to coconuts has disturbed the reef island equilibrium, often with catastrophic results. There are two major motives in removing natural vegetation on these cays: first, the economic return from the coconut plantations, which has been most important up to 1960; and second, the provision of tourist amenities in developing the islands as holiday and fishing resorts, which is likely to become more important in the future. In this context natural vegetation has no scenic attraction and harbours rats, iguanas and insects. With the increasing frequency of major storms on this coast since 1945 it is unlikely that capital will again be available for coconut replanting and clearing on any large scale on the reef islands; indeed, there is a distinct possibility that in some cases natural vegetation will return and the old equilibrium be re-established. On the other hand the attraction of tourists is a Government policy which has few other outlets apart from the coastal reefs and islands: mechanised vegetation clearance has already taken place on one of the larger islands near Belize. If this continues in such a drastic form, involving clearance more complete than that in the transition from natural vegetation to coconut plantation, the instability of reef

islands under storm conditions will be accentuated. With present hurricane frequency and magnitude, unrestrained clearing will inevitably lead to catastrophic erosion and disappearance of reef islands, and to major damage to any capital installations. Both tourist development programmes and new coconut plantations could safeguard island stability by a shelter belt policy of allowing natural regeneration of vegetation along the exposed and windward sides of cays. It is, of course, impossible to safeguard against wind effects on buildings and trees during hurricanes, but such marginal shelter belts would at least give protection against erosion by overtopping storm waves at times of high surge. Further work would be required on resistance to uprooting of local trees, but indications are that the dominants of natural littoral thicket are well adapted to resist storm action. Unless such measures are adopted, capital investment on reef islands is likely to be unrewarding.

From the physiographic point of view, reef islands present a useful indication of the limitations of frequency-magnitude studies of process, in the interpretation of topographic forms, and of the role of vegetation in effecting equilibrium between material and process. The conclusions reached here are those demonstrated by the changes during the 1961 hurricane in British Honduras, and subsequent work may indicate whether they are of more than local application.

REFERENCES

Blumenstock, D.I., editor. (1961). A report on typhoon effects upon Jaluit Atoll: Atoll Research Bulletin, No. 75, pp. 1-105.

Jefferys, T. (1775). The Bay of Honduras. In: The West India Atlas, or A general description of the West Indies. London.

McKee, E.D. (1959). Storm sediments on a Pacific atoll: Journal of Sedimentary Petrology, vol. 29, pp. 354-364.

Oldham, C.F. (1895). Natural history notes from H.M. marine survey steamer 'Investigator'. 1. The topography of the Arabian Sea in the neighbourhood of the Laccadives. 2. The physical features of some of the Laccadive Islands with suggestions as to their mode of formation: Journal of the Asiatic Society of Bengal, vol. 64, pp. 1-14.

Sewell, R.B.S. (1935). Studies on coral and coral formations in Indian waters: Memoirs of the Royal Asiatic Society of Bengal, vol. 9, pp. 461-540.

Shepard, F.P. (1960). Rise of sea level along Northwest Gulf of Mexico: In: F.P. Shepard, F.B. Phleger and Tj. H. van Andel, editors: Recent sediments, Northwest Gulf of Mexico. Tulsa, pp. 338-344.

Speer, J.S. (1765). The West-India Pilot: London.

Stoddart, D.R. (1962a). Three Caribbean atolls: Turneffe Islands, Lighthouse Reef, and Glover's Reef, British Honduras: Atoll Research Bulletin, No. 87, pp. 1-151.

Stoddart, D.R. (1962b). Catastrophic storm effects on the British Honduras reefs and cays: Nature, vol. 196, pp. 512-515.

Stoddart, D.R. (1963). Effects of Hurricane Hattie on the British Honduras reefs and cays, October 30-31, 1961: Atoll Research Bulletin, No. 95, pp. 1-142.

Tracey, J.I., Jr., Abbott, D.P., and Arnow, T. (1961). Natural history of Ifaluk atoll: physical environment: Bernice P. Bishop Museum Bulletin, No. 222, pp. 1-75.

Chapter 53

LAKE NYASA PORTUGUESE COAST AND ITS SEDIMENTS

João T. Pacheco

Geologist, Junta de Investigações
do Ultramar, Lisboa, Portugal.

INTRODUCTION

On the course of geological work in the Lake Nyasa region, several observations were made on coastal features and beach sediments which allowed some preliminary conclusions to be drawn on sedimentary and coastal processes active in the lake shore.

The purpose of this paper is to present these conclusions together with the data on which they are based.

GENERAL INFORMATION

GEOGRAPHY

Lake Nyasa is the southern and easternmost of the African Great Lakes and is situated between parallels 9° 30' and 14° 30' S and meridians 34° and 35° E Gw. It is elongated, about 580 km long by 15 to 90 km wide, and roughly oriented N-S. It covers an area of some 30,860 km^2 and is rather deep, with depths in excess of 700 m.

Its coasts and waters belong to three politically different territories, Tanganyika, Nyasaland and the Portuguese Province of Mozambique.

The lake drainage basin, although generally narrow, is wider in the western side where it shows an average width of about 100 km. In the Portuguese (Mozambique) sector it is a very narrow strip, 275 km long and from 10 to 45 km wide.

GEOLOGY

The lake occupies a great depression of tectonic origin integrated in the big African Rift Valley.

The older geological formations of the area are the Precambrian highly metamorphosed sediments and associated intrusives, that form the basement complex, upon which later sediments were deposited. The first of these were Karroo continental sediments which began accumulating during Permian times. They are made up of sandstone and shale with subordinate tillite, marl and coal beds. Karroo sediments continued being deposited until early Jurassio times, when

general uplift of the basement stopped sedimentation and started an erosional cycle from which a great Jurassio peneplain resulted. Large scale tectonic movements, at the close of the Triassic period, resulted in the faulting down of several blocks topped by Karroo sediments into more resistant basement rocks, which offered some protection against dennudation, allowing part of the Karroo sediments to be preserved to this day. Later, in the beginning of the Cretaceous, the basement subsided again and more sediments were deposited over the area. From then on, more stable conditions prevailed with widespread further dennudation which culminated at Miocene and resulted in almost total erosion of the Cretaceous formations of which only a few remnants are found today.

The large scale Rift faulting that resulted in successive drops along the present lake coastline, forming the lake basin, began then. During the Tertiary and the Pleistocene, faulting continued, bringing eventually the lake to its present level (Dixey, F., 1941).

On the Mozambique sector of the lake drainage basin the predominant outcropping formation is the basement complex. Its lithology varies widely. Highly metamorphosed rocks, gneisses, migmatites, granulites, etc. dominate, but granitio and basic intrusions also occur. Karroo sediments outcrop as a narrow strip oriented NE-SW reaching the lake shore about the middle of the Portuguese section of the coast (Fig. 1). Among Karroo sediments shale and sandstone are the main types (Borges, A. et al., 1953).

HYDROLOGY, HYDROGRAPHY AND METEOROLOGY

The lake gets all its water from the rain that fall on its drainage basin. The amount of this varies considerably both in space and time. Figures available for average annual rainfall range from about 2,800 mm to less than 635 mm (Pyke, J. G., 1958). On the other hand, for a given place, annual rainfall may vary from less than 60% of average (dry years) to more than 200% (wet years).

About 85% of annual rainfall corresponds to a wet season of 4 months, December to March. November, April and May are transitional months during which an additional 12% falls. June to October are the dry months.

Intensity of rainfall is usually high and can be extreme. Maximum intensity recorded was 152 mm in one hour (Pyke, J. G., 1958)

Rain water falling on the drainage basin,not retained by vegetation or ground, runs to the lake in numerous small rivers and streams. These, in the major part of the Portuguese section, only flow during and immediately after rainstorms, as could be expected from the high rainfall intensity and steep topography already mentioned. Only where the basin beoomes wider as in the extreme south and, specially, on the Karroo formations, are rivers better develo-

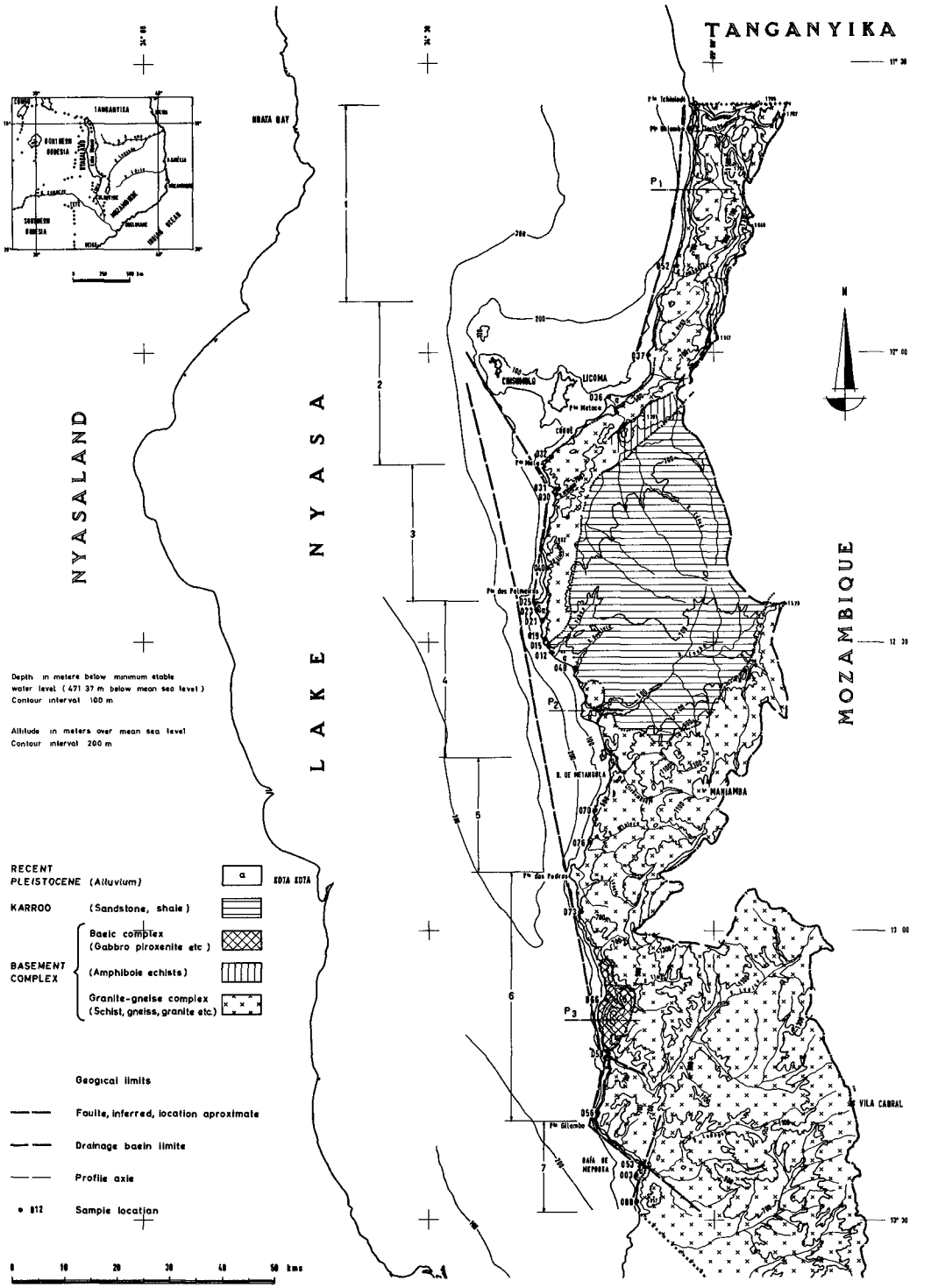
TANGANYIKA
NYASALAND
MOZAMBIQUE
LAKE NYASA
NKATA BAY
LICOMA
MANIAMBA
VILA CABRAL
KOTA KOTA
N
Depth in meters below minimum etable water level (471 37 m below mean sea level)
Contour interval 100 m
Altitude in meters over mean sea level
Contour interval 200 m
RECENT
PLEISTOCENE (Alluvium)
KARROO (Sandstone, shale)
BASEMENT COMPLEX
Basic complex (Gabbro piroxenite etc)
(Amphibole echists)
Granite-gneiss complex (Schist, gneiss, granite etc.)
Geogical limits
Faulte, inferred, location aproximate
Drainage basin limite
Profile axie
Sample location
0 10 20 30 40 50 kms

FIG 1

ped but, even these, barely flow during the dry season.

Lake water is lost by evaporation at an average annual rate of about 1,700 mm, and also, in a minor proportion, by discharge into the Zambeze through the Shire River that flows from the suthern end of the lake.

The lake water level depends mostly on rainfall and evaporation and,so, it shows an annual variation, that averages 1.10 m but can be as high as 1.80 m, with a maximum in May and a minimum in December (Instituto Hidrográfico, 1963). This variation is superimposed on a long term one whose law is still obscure but might be related to the Shire River discharge, which shows great variability, or to long term rainfall trends. Anyway, it is known that since 1850 the lake mean level dropped steadily, perhaps some 4 m, until 1914. From then, the lake rose about 4.5 m to reach a maximum in 1937 and, since then, has fluctuated within 3 m below this level although not yet having exceeded it (Pyke, J. G., 1958).

The dominant winds on the lake are from the South, West and Northwest. Northwest wind is the strongest but South wind dominates for longer periods. It is also a strong wind, specially from June to August, reaching as much as 50 km/h and blowing normally for 3 to 5 days, sometimes for 10 consecutive days. West and Northwest winds can rise a strong sea while blowing but, due to absence of an appreciable fetch, this soon dies, as quickly as the wind falls. South wind has much better fetch, the whole length of the lake, and as it blows frequently for long periods, rises a stronger sea, as high as 3 m, that dies slowly many hours after the wind (Instituto Hidrográfico, 1963).

No currents of any appreciable strength have been detected on the lake. If they exist, they are certainly weak, perhaps temporary and related to the wind. Also, no preceptible tides are observed and this is certainly due to the unfavourable form and dimensions of the lake (Instituto Hidrográfico, 1963).

COASTAL MORPHOLOGY

The coastline is, at least in its major part, shaped by faulting. This was accomplished rather recently in geological time and sub-aerial erosion has, as a rule, not yet had time to erase the characteristic topography. As a result the coastline shows a zigzag pattern, and profiles normal to it usually display steep slopes. In the Portuguese section the main exception to this rule is found in the area where the soft Karroo sediments reach the lake shore. These have been extensively eroded and give a low coastline, as shown in Fig. 2, profile 2.

Most of the coast is rocky, as could be expected, but many beaches are nevertheless found. Their distribution was investigated in the Portuguese sector of the coast which, for descriptive purposes, can be divided into 7 sections, as depioted in Fig. 1:

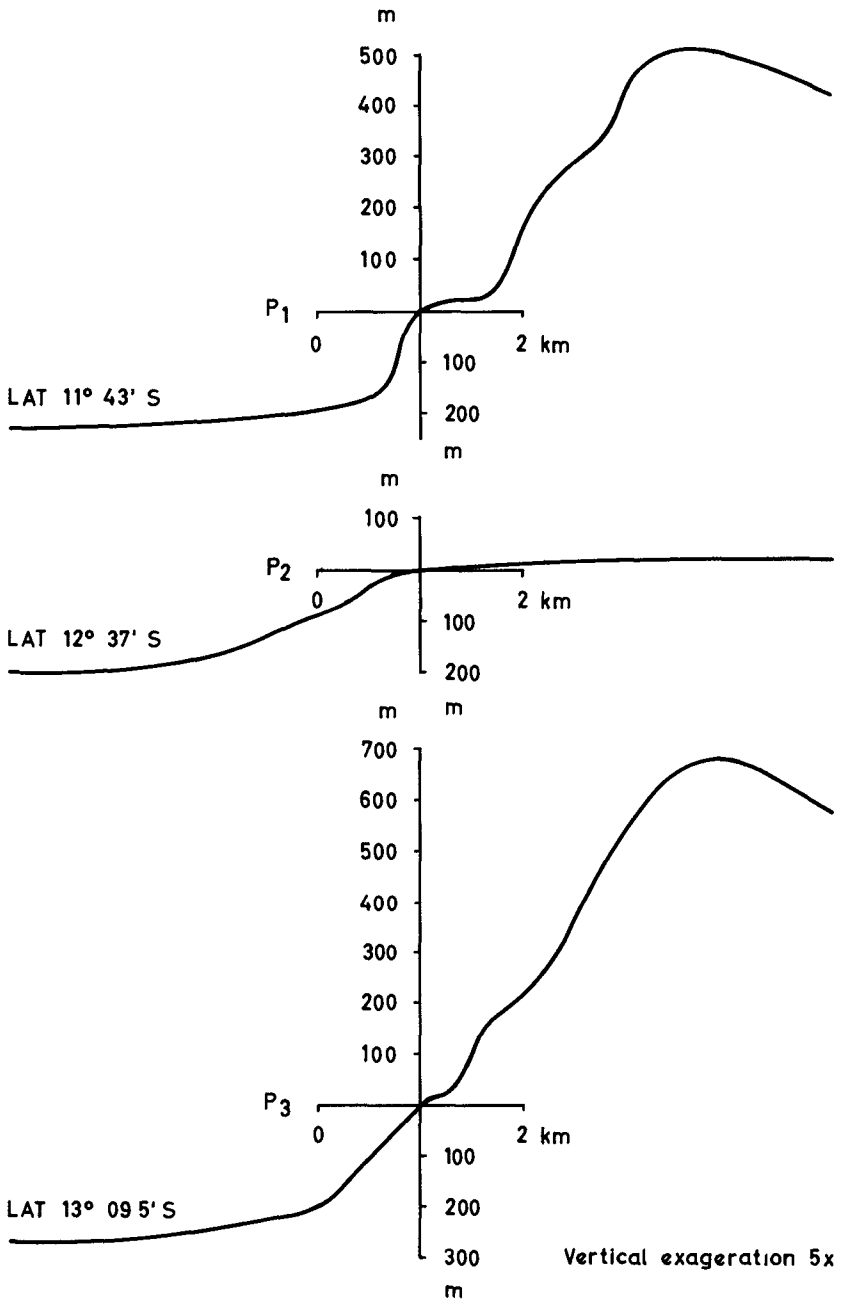
m
500
400
300
200
100
P1
0
2 km
100
200
m
LAT 11° 43' S
m
100
P2
0
2 km
100
200
m
LAT 12° 37' S
m
m
700
600
500
400
300
200
100
P3
0
2 km
100
200
300
m
LAT 13° 09 5' S
Vertical exageration 5x

FIG. 2

Section 1 - From the northern border to Point Messule, oriented aproximately N-S,is mostly rocky with very steep offshore slopes.

Section 2 - From Point Messule to Point Mala, oriented NE-SW, shows predominance of beaches, and has not so steep offshore slopes, as it is on the border of the platform from which Licoma and Chissumulo Islands rise.

Section 3 - From Point Mala to Palmeiras' Point, oriented N-S, predominantly rocky, and with steep offshore slopes.

Section 4 - From Palmeiras' Point to Metangula Peninsula, oriented NW-SE, with beaches dominating largely (rock only showing at a few scattered points), and very gentle offshore slopes.

Section 5 - From Metangula to Pedras' Point,oriented NNE-SSW, with beaohes alternating with rocky coast in about equal amounts and offshore slopes gradually increasing southward.

Section 6 - From Pedras' Point to Point Gilambo, with a N-S trend but arching slightly, with the oonvex side landward, showing dominance of rooky coast although some relatively large beaohes occur its southern limit. Offshore slopes begin steep, become gentler around the middle of the section, and then increase again.

Section 7 - From Point Gilambo to the southern border, shows a NW-SE trend and is predominantly rocky,with offshore slopes deoreasing to the South.

As can be seen, the coast shows an alternanoe of rocky and beachy stretohes, with beaches dominating generally on sections protected from South wind wave aotion. The only exception is section 4, which shows high dominance of beaches, although oriented NW-SE and thus well exposed to the waves coming from the South. This is due, no doubt, to its relation to the Karroo formations (Fig. 1) which,being much softer than normal basement rocks, supply much more beach material.

On sections described as predominantly rocky some beaches also occur. These are generally situated at the bottom of bays and coves, but many are found projecting from the coast, at the mouth of streams bording deltas that result from the accumulation of material brought by these.

Sand spits, allways showing a northward drift of sedimentary material, are sometimes found along section 4, some of them at the tip of the largest deltas. Quite often, these spits are well developed and isolate small lagoons.

SEDIMENTOLOGY

Beach material is usually fine to medium sand,but in qui-

te a few instances it contains a rather high proportion of poorly rounded gravel. Cumulative curves of this sands (Fig. 3) often show two modes, one between 1ϕ and 2ϕ (0.50 to 0.25 mm) and another at -3ϕ to -1ϕ (8 to 2 mm), implying mixture of at least two different types of material. This correlates well with field observation that suggested mixing of wave transported sand with runoff transported sediments.

Sorting varies considerably, also as a result of mixing. Sand of beaches totally derived from the accumulation of material transported by longshore drift show very good sorting with a grain size distribution closely aproximating lognormality (samples 021,078, 081, Fig. 3). On beaches where mixing has occurred, sorting can be extremely poor as a result of considerable amounts of coarser and finer material having been added to the longshore drift transported sand (samples 056,066,Fig. 3).

Mineralogically,beach sands are detrital quartz sands with considerable amounts of feldspar and heavy minerals, these last beeing frequently concentrated in localized zones of the beaches. Sometimes a small amount of organogenic carbonate material is found, as shell fragments, but it never makes more than about 1% of the sand.

Heavy mineral composition was investigated in detail in order to obtain data on provenance and tranportation of beach material. Techniques used included detailed fractionation of samples obtained from the heavy mineral concentration zones,both by electromagnetic and heavy liquid separation, followed by mineral counts on selected fractions. Other fractions were only examined for qualitative mineral composition.

On the whole it was found that almost all samples showed quartz, alkali feldspar, acid plagioclase, red garnet, hornblende, epidote, sphene and opaque minerals (magnetite,hematite,ilmenite) in variable amounts, while basic feldspar, bronzite, staurotide, biotite, muscovite, monazite, diopside, zircon, kyanite, sillimanite and andalusite could be used to define mineral provinces by its presence or absence.

Along those sections of the coast where beaches dominate and offshore slopes are gentle, the mineral content of beach sands could, in many instances, be traced to the rocks outcropping on the drainage areas of rivers reaching the lake in the close proximity,or just to the South of the beaches. This clearly demonstrates a northward longshore drift, probably due to South wind wave action. As an example we can take section 4 where the Karroo formations reach the lake (Fig. 1). These relatively soft rocks furnish abundant beach material, as is shown by the large deltas at the mouth of rivers draining the area, mineralogically characterised by the presence of monazite and zircon (also epidote and garnet in well rounded grains). In beach sands monazite and zircon can be found from the southern limit of the Karroo formations, over the northern one, well into section 3 (Fig. 4). They reappear later, north of Cobué River mouth, in section

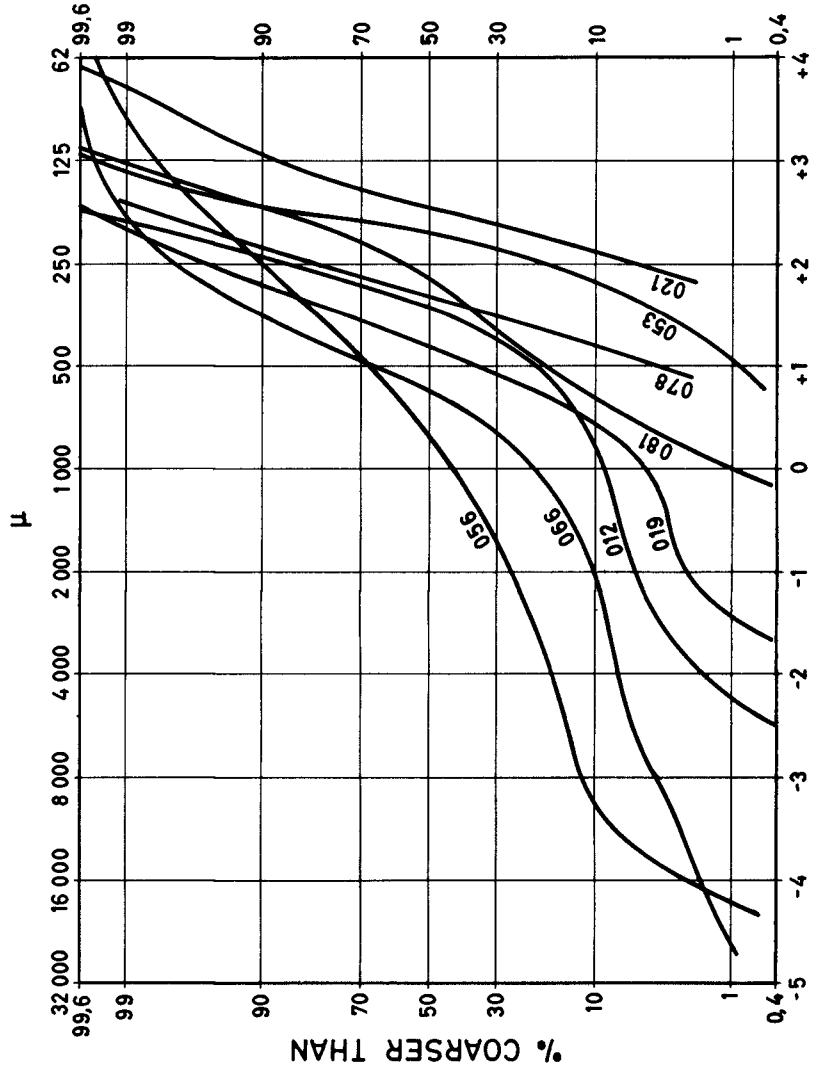
μ
62
125
250
500
1 000
2 000
4 000
8 000
16 000
32 000
99,6
99
90
70
50
30
10
1
0,4
% COARSER THAN
ø
+4
+3
+2
+1
0
-1
-2
-3
-4
-5
021
053
078
081
056
090
012
010

FIG. 3

2, due to this river having the major part of its drainage basin in the Karroo, although it reaches the lake out of it. Northward from there, monazite and zircon can be followed for the rest of section 2, and all of section 1. It must be noted, however, that monazite and zircon also show, although in small amounts, in beaches just south of Cobué River, suggesting a temporary reversal of longshore drift direction, probably due to Northwest wind wave action to which section 2 is particularly exposed.

On rocky sections of the coast, generally with steep offshore slopes, evidence of a northward longshore drift was also found whenever the mineral content of river alluvium and of beaches to the North and South of the river mouth, was investigated. Nevertheless, in these sections longshore drift seems to be, generally, more limited, probably due to quick loss of sand to the depths of the lake. Even, in some instances, although conditions were favourable, no indication of any longshore drift could be at all found. This happened, for instance, in section 6 where a small gabro-diorite intrusion outcropps in the middle of the regional granite-gneiss complex, reaching the lake shore (Fig. 1). This is reflected by the presence of abundant bronzite and labradorite grains on the beaches along the intrusion (Fig. 4). Samples taken north and south of the intrusion limits failed to show any of these minerals, suggesting that longshore drift, along this section, is very small or even absent.

As has been said, heavy minerals often show concentrated as patches of dark sand in localized zones of the beach surface. Their distribution was also investigated in depth and it was found that they formed mor or less regular strata a few centimeters thick, alternating with light coloured sand layers, generally many times thicker, revealling a well defined layered beach structure.

A typical beach profile (Fig. 5) shows a lakeward dipping more or less flat foreshore limited on the lake side by a foreshore step, and landwards by a beach scarp. Behind this scarp there is usually a berm that either dies against the first mountain slopes or merges into an alluvial plain. Foreshore slope varies widely being steepest on beaches of rocky sections with steep offshore slopes, and gentlest on large beaches bording deltas. Sometimes a double berm is found and this is thought to be related to an old and higher maximum level of the lake waters.

Heavy mineral concentrations visible on the beach surface are usually localized at the foreshore step and beach scarp crests (Fig. 5). They were often observed while being built up on the foreshore step by wave action. Small breakers lapp gently up the step depositing its charge as they lose speed. Backwash, being no so powerfull as much of the water sinks into the sand, picks up mostly the lighter material leaving the heavy grains behind.

CONCLUSIONS

The following conclusions are to be considered as preli-

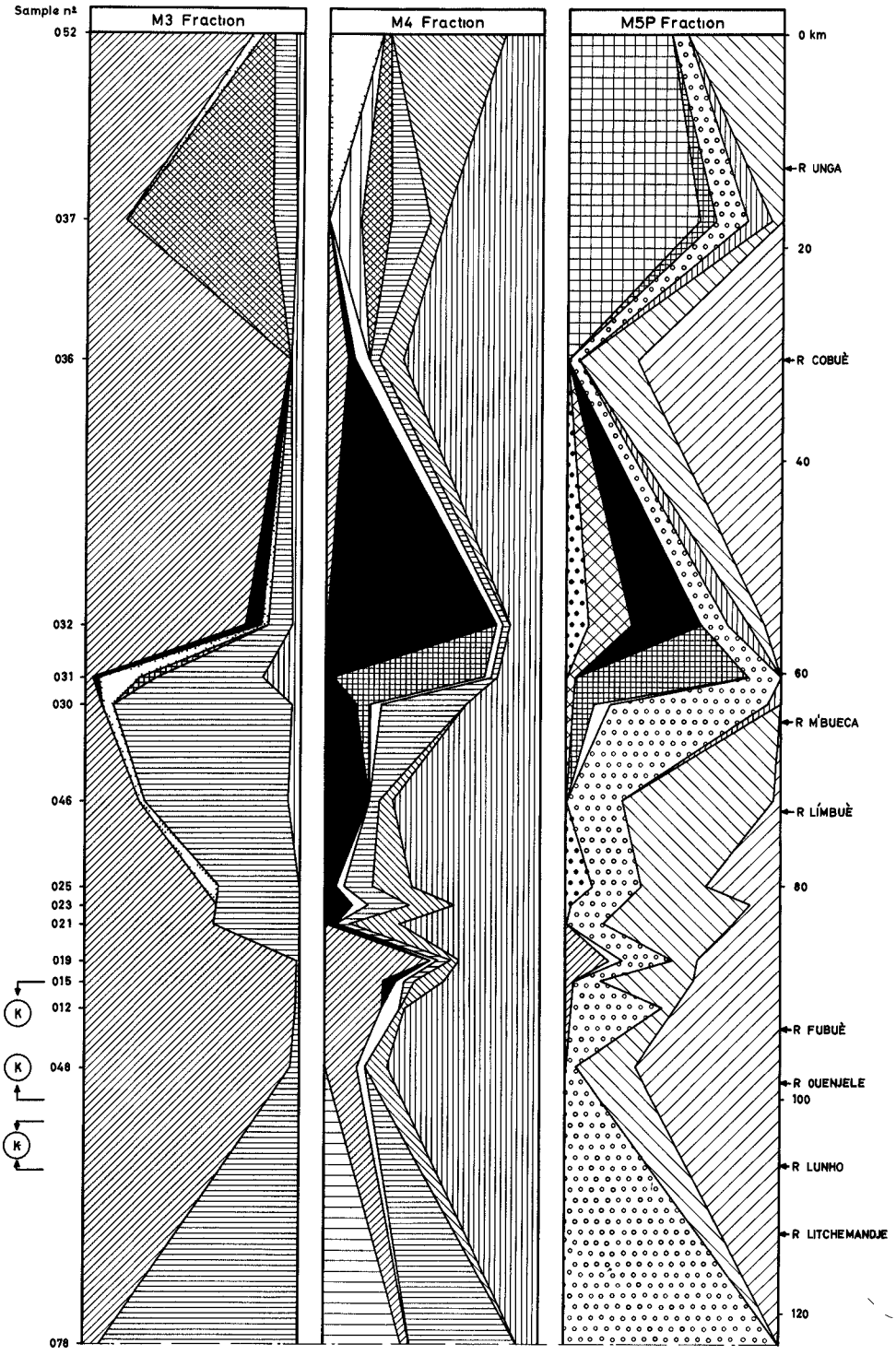
Sample nº
M3 Fraction
M4 Fraction
M5P Fraction
052
037
036
032
031
030
046
025
023
021
019
015
012
048
078
K
K
K
0 km
R UNGA
20
R COBUÈ
40
60
R M'BUECA
R LÍMBUÈ
80
R FUBUÈ
R OUENJELE
100
R LUNHO
R LITCHEMANDJE
120

FIG. 4

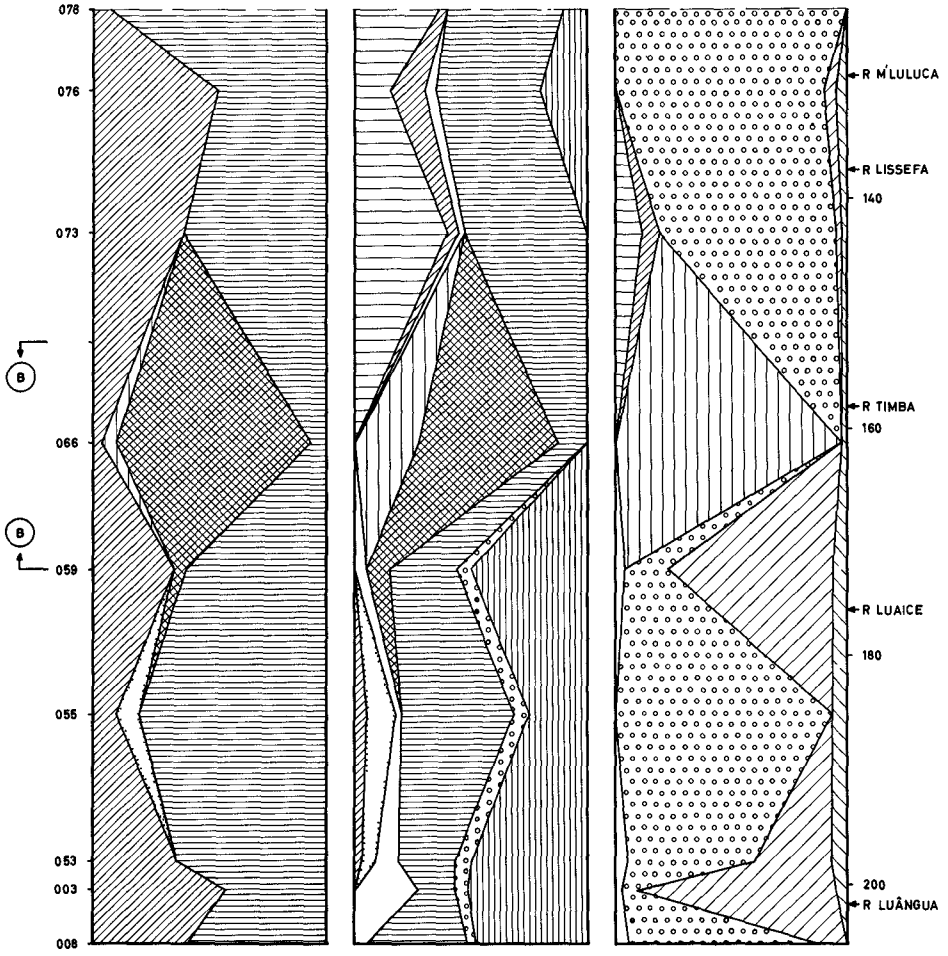

LEGEND

EPIOOTE
HORNBLENOE
GARNET
MONAZITE
STAUROTIOE
BIOTITE
MUSCOVITE
BRONZITE
LABRADORITE
DIOPSIDE
OTHERS
ZIRCON
RUTILE
SILLIMANITE
KYANITE
SPHENE
ANDALUSITE
K
K
KARROO LIMITS
B
B
BASIC INSTRUSION LIMITS

FIG 4 (CONT)

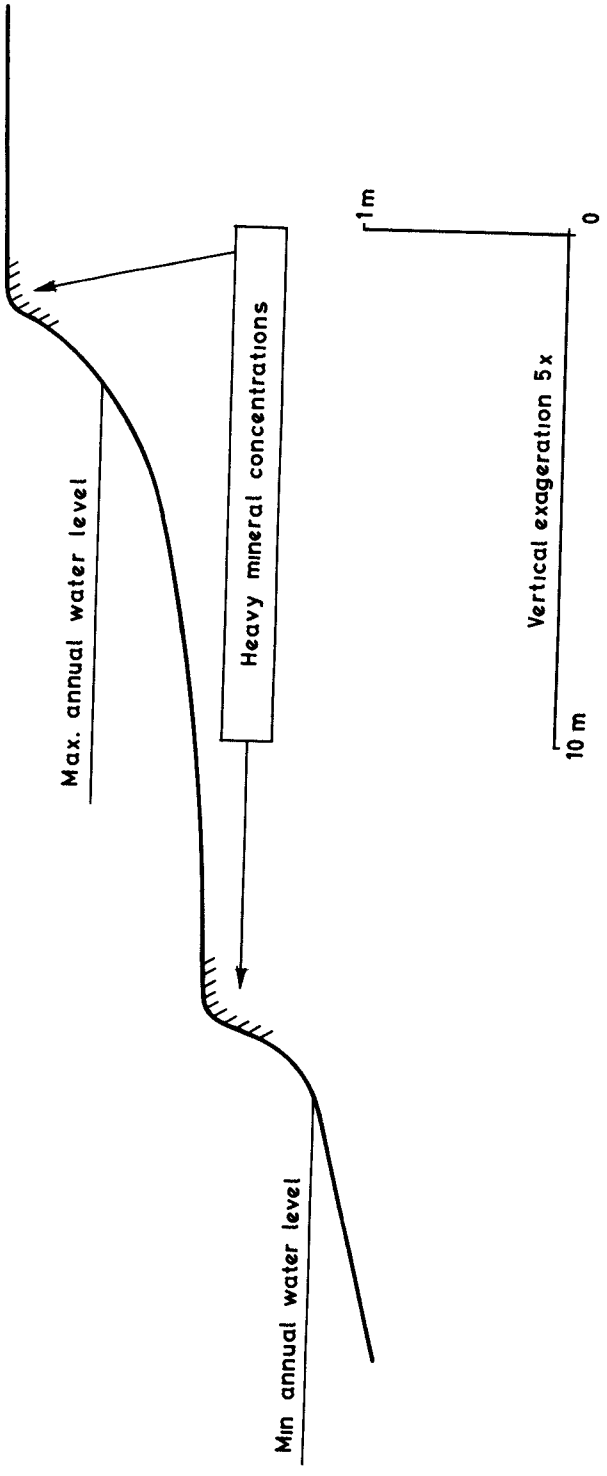
Max. annual water level
Heavy mineral concentrations
Min annual water level
1m
0
Vertical exageration 5x
10 m

FIG. 5

minary. They apply only to the Portuguese section of the lake coast and should not be generalised to the rest of the lake without further research.

1 - Although the shoreline is generally rocky, this is mostly a result of the tectonic origin of the lake basin,and the beaches and deltas that develop locally along it show sediment supply to the shore to be, on the whole, higher than sediment loss to the bottom of the lake, i. e.,sedimentation prevails over erosion.

In fact, high rainfall rate and intensity, as well as topographic conditions (also a result of faulted tectonics), concur to a high rate of sub-aerial erosion on the drainage basin and hence to a high sediment supply to the lake shore.

On the other hand, erosive capacity of the lake waters is low. Most of the beach material is brought to the lake during and immediately after the short rainy season by the streams and rivers,and large accumulations of sediments build up at the mouths of these. From then on, sediments start being eroded and moved alongshore by the waves but, as water level soon begins to fall, most material is left behind, out of reach of the waves. When the rains come again and the lake level rises, extensive erosion of last season deposits neces sarily occurs, but this seems to be overcompensated by the arrival of fresh material since definite indications of beach accreation can be found along the whole shore.

2 - Longshore drift is, on the whole, in a northward direction, as shown by the variation of beach sand mineralogy along the shore and by the sand spits found on some sections of the coast. This direction must be the result of South wind wave action. There are indications that temporarily andor locally this direction can be reversed, probably due to Northwest wind wave aotion, but net transport is allways to the North.

Distance of transportation alongshore, as also shown by the variation of beach sand mineralogy, seems to be generally limited and conditioned by the steepness of the offshore slopes. Along most of the sections, since they have steep slopes, sand must be lost to the depths at an high rate, thus resulting a generally short distance of transportation. Longer distance transportation is only found along the few seotions with gentler offshore slopes.

3 - Favourable conditions for the local accumulation of sediments as beaches seem to be, by order of importance, high supply of sedimentary material, gentle offshore slopes (which may depend on sediment supply or tectonics) and protection from South wind wave action.

ACKNOWLEDGMENTS

Thanks are due to the Instituto Hidrográfico in general and, specially, to the staff of the Missão Hidrográfica de Moçambique

which made the hydrographic survey of the Portuguese sector of the lake, for the valuable help received during field work.

We are also indebted to the Instituto de Investigação Cientifica de Moçambique, for partly financing this investigation.

Finally, we wish to thank our colleague Luis M. de Castro, for his help on the preparation of this paper.

REFERENCES

Borges, A., et al. (1953). Contribuição para o Reconhecimento do Karroo Português do Lago Niassa : Bol. Serv. Indust. Geol. Prov. Moçambique, vol.12, Lourenço Marques.

Dixey, F. (1941). The Nyasa Rift Valley : S. A. Geog. Journ., vol.23.

Pyke, J. G. (1958). Northern Nyasaland; A Regional Geographical Study with Special Reference to Hydrology and Hydrography:Water Development Department of Nyasaland.

Instituto Hidrográfico (1963). Roteiro da Costa Portuguesa do Lago Niassa : Ministérios da Marinha e do Ultramar, Lisboa.

FIGURE CAPTIONS

Fig. 1 - General geological and teotonic sketch of the Portuguese section of Lake Nyasa drainage basin, with location of the samples mentioned in the text. P_1 to P_3 refer to profiles shown on Fig. 2. The division of the coast in sections 1 to 7 follows the description given in the text.

Fig. 2 - Profiles more or less normal to the lake shore, showing typical steepness of inshore and offshore slopes (P_1 and P_3), and the very different character of the coast where the Karroo formation reaches the lake shore (P_2).

Fig. 3 - Cumulative curves of typical beach sediments. These are generally mixtures of well sorted, wave transported, medium to fine sand (e. g.,samples 078 and 021) with poorly sorted material deposited directly on the beach by runoff.

Fig. 4 - Variation of beach sand mineralogy along the coast. Mineralogio composition was determined quantitatively only on 3 of the fractions in which the samples were split by means of electromagnetic and heavy liquid separation.

Fig. 5 - Typical beach profile, showing the most common locations of surface heavy mineral concentrations.